FZM-4625
17 MAY 1966
NAS-7-100

A STUDY OF

JUPITER FLYBY MISSIONS

FINAL TECHNICAL REPORT

GENERAL DYNAMICS
Fort Worth Division

FZM-4625
17 MAY 1966

FINAL TECHNICAL REPORT

OF

A STUDY OF JUPITER FLYBY MISSIONS

Prepared for

The Jet Propulsion Laboratory
California Institute of Technology
Pasadena, California

on

JPL Contract No. 951285

NAS-7-100

GENERAL DYNAMICS
Fort Worth Division

F O R E W O R D

This document is the Final Technical Report on a Study of Jupiter Flyby Missions. The study was conducted by the Fort Worth Division of General Dynamics for the Jet Propulsion Laboratory of the California Institute of Technology on JPL Contract No. 951285, a subcontract under the National Aeronautics and Space Administration prime contract NAS7-100. An earlier report on this study, the Mid-Term Technical Progress Report (FZM-4572), is completely susperseded by this document.

A C K N O W L E D G E M E N T S

Listed below are the personnel of the Fort Worth Division of General Dynamics who made primary contributions in the technical areas indicated:

L. E. Hove	Project Leader
G. F. Gibson	Spacecraft System Integration and Structural, Mechanical, and Configuration Design
B. J. Csaszar	Configuration Design
J. C. Redmond	Science Subsystem Definition
B. A. Sodek	Science Subsystem Definition
S. W. Wilson	Mission Analysis
M. C. Poteet	Trajectory Analysis
E. R. Conrad	Communications Subsystem Studies
H. A. Shubert	Spacecraft Antenna Studies
C. D. Campbell	Data Management Subsystem Studies
M. B. Veal	Navigation & Guidance and Spacecraft Control Subsystem Studies
B. J. Ward	Spacecraft Control Subsystem Studies
C. W. Heller	Spacecraft Computer and Sequencer Studies
G. P. Breaux	Attitude Control Studies
J. A. McCabe	Propulsion Subsystem Studies
J. S. Turner	Electrical Power Subsystem Studies
R. A. Knezek	Thermal Control Studies
D. E. Croy	Thermal Control Studies
J. J. Tierney	Radiation Protection Studies
J. B. Eggen	Radiation Protection Studies
J. H. Lewis	Radiation Protection Studies
L. E. Heyduck	Meteoroid Penetration Protection Studies
R. J. Allen	Subsystems Reliability Studies and Probability of Mission Success Evaluations
H. R. Darby	Development Requirements Evaluations
G. K. Abel	Development Requirements Evaluations
G. G. Tharp	Cost Analyses
H. F. Coble	Cost Analyses

Professor Harlan J. Smith, Head of the Department of Astronomy at The University of Texas, contributed to the study in the role of consultant on Science Subsystem Definition.

Mr. K. H. Fishback of the Jet Propulsion Laboratory monitored the study and provided technical assistance in all study areas.

TABLE OF CONTENTS

		Page
FOREWORD		iii
ACKNOWLEDGEMENTS		iv
SECTION 1	INTRODUCTION	1-1
1.1	Definition of Task	1-1
1.2	Constraints	1-2
1.3	Technical Approach	1-3
1.3.1	Mission Planning	1-3
1.3.2	Spacecraft Systems Design and Analysis	1-5
1.3.3	Spacecraft Concept Evaluation	1-5
1.4	Design Philosophy	1-5
1.4.1	Spin Stabilization	1-6
1.4.2	Three-Axis Stabilization	1-9
1.5	Summary of Results	1-13
SECTION 2	MISSION PLANNING	2-1
2.1	Science Subsystem Definition	2-1
2.1.1	Summary of Observations of the Planet Jupiter	2-1
2.1.2	Magnetic Field Measurements	2-4
2.1.3	The Detection of Charged Particles in Interplanetary and Planetary Regions	2-7
2.1.4	Solar Plasma Measurements	2-18
2.1.5	Cosmic Dust Measurements	2-20
2.1.6	Television	2-23
2.1.7	Photometric, Radiometric and Spectrometric Measurements	2-28
2.1.8	Ranging and Radio Experiments	2-31
2.1.9	Miscellaneous	2-35
2.1.10	Scientific Instrument Characteristics	2-36
2.1.11	Typical Mission Payloads	2-36
2.1.12	References	2-42

TABLE OF CONTENTS (Continued)

		Page
2.2	Energy Requirements and General Trajectory Characteristics	2-43
2.2.1	Launch Window Definition	2-43
2.2.2	Arrival Date Corrections	2-47
2.2.3	Mission Planning Charts	2-47
2.2.4	Conclusions	2-60
2.2.5	References	2-61
2.3	Launch Vehicle Evaluation	2-62
2.3.1	Basic Payload Capabilities	2-62
2.3.2	Payload Capabilities for Jupiter Missions	2-67
2.3.3	References	2-67
2.4	Detailed Mission Profile Analysis	2-81
2.4.1	Two-Body Trajectory Data	2-81
2.4.2	Numerically Integrated Trajectory Data	2-88
2.4.3	Reference	2-95
SECTION 3	SPACECRAFT SYSTEMS DESIGN AND ANALYSIS	3-1
3.1	Communications	3-1
3.1.1	Functional Requirements	3-1
3.1.2	Identification of Trade-offs	3-2
3.1.3	Conclusions	3-17
3.1.4	References	3-22
3.2	Data Management	3-23
3.2.1	Functional Requirements	3-24
3.2.2	Possible Concepts	3-25
3.2.3	Analyses	3-26
3.2.4	Results	3-36
3.2.5	Conclusions	3-39
3.2.6	References	3-39

TABLE OF CONTENTS (Continued)

		Page
3.3	Spacecraft Control	3-41
3.3.1	Spacecraft Control Operations	3-42
3.3.2	Design of the Central Computer and Sequencer	3-45
3.3.3	Design of the Attitude Control Electronics	3-47
3.3.4	Theory of Attitude Determination	3-49
3.4	Navigation and Guidance	3-53
3.4.1	The Guidance Requirement	3-53
3.4.2	Performance Analysis	3-54
3.4.3	Guidance Analysis	3-57
3.4.4	Self-Contained Terminal Navigation	3-60
3.5	Attitude Control	3-65
3.5.1	Configuration Concepts	3-65
3.5.2	Nominal Trajectory Characteristics	3-67
3.5.3	Considerations for Spin-Stabilization	3-69
3.5.4	Considerations for Three-Axis Stabilization	3-74
3.5.5	Design Data for Gas Jet System	3-79
3.5.6	Design Data for Reaction Wheel System	3-81
3.5.7	Use of Solar Torque for Control Purposes	3-83
3.5.8	Analysis of Example Case	3-86
3.5.9	Conclusions	3-94
3.6	Propulsion	3-96
3.6.1	Midcourse Propulsion Subsystem	3-96
3.6.2	Attitude Control Propulsion Subsystem	3-107
3.7	Auxiliary Electric Power	3-120
3.7.1	Scope and Requirements	3-120
3.7.2	Raw Power Generation	3-120
3.7.3	Power Management System	3-131
3.7.4	Energy Storage	3-137
3.7.5	Recommended Configuration	3-139
3.7.6	References	3-140

TABLE OF CONTENTS (Continued)

		Page
3.8	Thermal Control	3-142
3.8.1	Component Thermal Control Requirements	3-142
3.8.2	Mission Considerations	3-142
3.8.3	Design Considerations	3-145
3.8.4	Equipment Bus Thermal Control Concepts	3-150
3.8.5	Conclusions and Recommendations	3-157
3.8.6	Reference	3-158
3.9	Radiation Protection	3-159
3.9.1	Description of the Radiation Environments	3-159
3.9.2	Radiation Effects on Vehicle Equipment	3-178
3.9.3	RTG Safety Considerations	3-197
3.9.4	Conclusions and Recommendations	3-198
3.9.5	References	3-200
3.10	Meteoroid Penetration Protection	3-203
3.10.1	Basic Relationships	3-203
3.10.2	Meteoroid Environments	3-205
3.10.3	Parametric Analysis	3-210
3.10.4	Design Approach	3-213
3.10.5	References	3-215
3.11	Spacecraft Configuration	3-217
3.11.1	Launch Vehicle Constraints	3-217
3.11.2	Trajectory Constraints	3-218
3.11.3	Spacecraft System Integration	3-219
3.11.4	References	3-227
3.12	Structural and Mechanical Design	3-228
3.12.1	Structural Systems	3-228
3.12.2	Mechanical Systems	3-330
3.12.3	Weight Estimation	3-332

TABLE OF CONTENTS (Continued)

		Page
3.13	Subsystems Reliability	3-234
3.13.1	Subsystem Predicted Reliability	3-234
3.13.2	Subsystems Reliability Analyses	3-235
SECTION 4	SPACECRAFT CONCEPT EVALUATION	4-1
4.1	Mission Performance Analysis	4-1
4.2	Probability of Mission Success	4-2
4.2.1	Approach	4-2
4.2.2	Discussion of Results	4-3
4.3	Development Requirements	4-5
4.3.1	Special Test and Mission Vehicle Requirements	4-6
4.3.2	Radioisotope Thermoelectric Generator Development	4-6
4.3.3	Science Subsystem	4-13
4.3.4	Program Implementation Network and Schedule Preparation	4-16
4.3.5	References	4-23
4.4	Cost Analysis	4-24
4.4.1	Subsystem Cost Methodology	4-24
4.4.2	Nonsubsystem Cost Estimating Relationships	4-28
4.4.3	Operational Cost Methodology	4-30
4.4.4	Reference	4-33
SECTION 5	SPACECRAFT DESIGN CONCEPTS	5-1
5.1	Spacecraft Design Concept A	5-1
5.1.1	Design Summary	5-1
5.1.2	System Design Information	5-5
5.1.3	Mission Performance	5-30

TABLE OF CONTENTS (Continued)

		Page
5.1.4	Probability of Mission Success	5-32
5.1.5	Development Requirements	5-34
5.1.6	Cost Results	5-34
5.2	Spacecraft Design Concept B	5-40
5.2.1	Design Summary	5-40
5.2.2	System Design Information	5-44
5.2.3	Mission Performance	5-65
5.2.4	Probability of Mission Success	5-67
5.2.5	Development Requirements	5-69
5.2.6	Cost Results	5-69
5.3	Spacecraft Design Concept C	5-75
5.3.1	Design Summary	5-75
5.3.2	System Design Information	5-79
5.3.3	Mission Performance	5-95
5.3.4	Probability of Mission Success	5-99
5.3.5	Development Requirements	5-100
5.3.6	Cost Results	5-100
5.4	Spacecraft Design Concept D	5-106
5.4.1	Design Summary	5-106
5.4.2	System Design Information	5-110
5.4.3	Mission Performance	5-135
5.4.4	Probability of Mission Success	5-139
5.4.5	Development Requirements	5-140
5.4.6	Cost Results	5-143
5.4.7	References	5-146
APPENDIX A -	MISSION MAPS	A-1
APPENDIX B -	PRECISION TRACKING DATA	B-1
APPENDIX C -	METEOROID DAMAGE TO SPACECRAFT ANTENNAS	C-1
APPENDIX D -	PARAMETRIC ANALYSIS OF THE BASIC HYDRAZINE PROPULSION SUBSYSTEM	D-1
APPENDIX E -	PARAMETRIC ANALYSIS OF A COLD GAS ATTITUDE CONTROL PROPULSION SUBSYSTEM	E-1

L I S T O F F I G U R E S

Figure	Title	Page
1.3-1	Technical Approach	1-4
1.4-1	Design Alternatives for Spin-Stabilization	1-7
1.4-2	Design Alternatives for Three-Axis Stabilization	1-10
2.2-1	Launch Window Definition	2-44
2.2-2	Injection Energy as a Function of Window Width	2-44
2.2-3	Typical Launch Corridor	2-46
2.2-4	Jupiter Arrival Date Corrections	2-46
2.2-5	Mission Planning Chart, 1973 Launch	2-48
2.2-6	Mission Planning Chart, 1974 Launch	2-49
2.2-7	Mission Planning Chart, 1975 Launch	2-50
2.2-8	Mission Planning Chart, 1976 Launch	2-51
2.2-9	Mission Planning Chart, 1977 Launch	2-52
2.2-10	Mission Planning Chart, 1978 Launch	2-53
2.2-11	Mission Planning Chart, 1979 Launch	2-54
2.2-12	Mission Planning Chart, 1980 Launch	2-55
2.2-13	Range of Preferred Arrival Conditions	2-57
2.3-1	Summary of Launch Vehicle Payload Capability	2-63
2.3-2	Payload Curve Adjustments	2-65
2.3-3	Payload vs Flight Time, 1973 Launch	2-68
2.3-4	Payload vs Flight Time, 1974 Launch	2-69

LIST OF FIGURES (Continued)

Figure	Title	Page
2.3-5	Payload vs Flight Time, 1975 Launch	2-70
2.3-6	Payload vs Flight Time, 1976 Launch	2-71
2.3-7	Payload vs Flight Time, 1977 Launch	2-72
2.3-8	Payload vs Flight Time, 1978 Launch	2-73
2.3-9	Payload vs Flight Time, 1979 Launch	2-74
2.3-10	Payload vs Flight Time, 1980 Launch	2-75
2.3-11	Jupiter Mission Payload Capability, Saturn V/Centaur	2-76
2.3-12	Jupiter Mission Payload Capability, Saturn V	2-77
2.3-13	Jupiter Mission Payload Capability, Saturn IB/Centaur/HEKS	2-78
2.3-14	Jupiter Mission Payload Capability, Titan IIICx/Centaur	2-79
2.3-15	Jupiter Mission Payload Capability, Atlas SLV3x/Centaur/HEKS	2-80
2.4-1	Geocentric Distance vs Time, Typical Departure Trajectories	2-82
2.4-2	Heliocentric Geometry, Typical 500-Day Mission	2-83
2.4-3	Communication Parameters History, Spin-Stabilized Spacecraft, 1976 500-Day Mission	2-84
2.4-4	Communication Parameters History, Spin-Stabilized Spacecraft, 1974 600-Day Mission	2-85
2.4-5	Communications Summary, Spin-Stabilized Spacecraft, 1974 600-Day Mission	2-86

LIST OF FIGURES (Continued)

Figure	Title	Page
2.4-6	Jovicentric Distance vs Time, Typical Encounter Trajectories	2-87
2.4-7	Geometry of Typical Encounter Trajectories	2-88
2.4-8	Encounter Parameters Targeting Chart, 582-Day Flight	2-89
2.4-9	Encounter Parameters Targeting Chart, 498-Day Flight	2-90
2.4-10	Encounter Parameters Targeting Chart, 413-Day Flight	2-91
2.4-11	Post Encounter Parameters Targeting Chart, 582-Day Flight	2-92
2.4-12	Post Encounter Parameters Targeting Chart, 498-Day Flight	2-93
2.4-13	Post Encounter Parameters Targeting Chart, 413-Day Flight	2-94
2.4-14	Trajectory No. 582A: Heliocentric Geometry	2-96
2.4-15	Trajectory No. 582A: Heliocentric Distance vs Time	2-96
2.4-16	Trajectory No. 582A: Heliocentric Latitude vs Time	2-97
2.4-17	Trajectory No. 582A: Canopus Cone Angle vs Time	2-97
2.4-18	Trajectory No. 582A: Geocentric Declination vs Time	2-98
2.4-19	Trajectory No. 582A: Geocentric Distance vs Time	2-98

LIST OF FIGURES (Continued)

Figure	Title	Page
2.4-20	Trajectory No. 582A: Earth Cone vs Clock Angle	2-99
2.4-21	Trajectory No. 498A, B, & C: Heliocentric Geometry	2-100
2.4-22	Trajectory No. 298A, B, & C: Heliocentric Distance vs Time	2-100
2.4-23	Trajectory No. 498A, B, & C: Heliocentric Latitude vs Time	2-101
2.4-24	Trajectory No. 498A, B, & C: Canopus Cone Angle vs Time	2-101
2.4-25	Trajectory No. 498A, B, & C: Geocentric Declination vs Time	2-102
2.4-26	Trajectory No. 498A, B, & C: Geocentric Distance vs Time	2-102
2.4-27	Trajectory No. 498A, B, & C: Earth Cone vs Clock Angle	2-103
3.1-1	Communications Interfaces	3-2
3.1-2	Communications Subsystem Trade-Offs	3-3
3.1-3	Gain of Antennas with Toroidal Patterns	3-5
3.1-4	Antenna Pointing Accuracy	3-15
3.1-5	Earth-Sun Position	3-15
3.1-6	PSK Transmission Chart	3-16
3.1-7	Doppler Rate at Encounter with Jupiter	3-18
3.1.8	Typical Communications Subsystem	3-20

LIST OF FIGURES (Continued)

Figure	Title	Page
3.2-1	Data Management Subsystem	3-23
3.2-2	Fan Data Compression Technique	3-28
3.2-3	Zero Order Interpolator Data Compression Technique	3-29
3.2-4	Quantile Data Compression Technique	3-29
3.2-5	Stop-Scan Edge Detector Data Compression Technique	3-30
3.2-6	Data Storage Element	3-32
3.2-7	Data Encoder Element	3-34
3.2-8	Ground Telemetry Demodulator	3-35
3.2-9	Command Decoder Subelement	3-37
3.2-10	Command Word Format	3-38
3.3-1	Typical Mechanization-Central Computer and Sequencer	3-46
3.3-2	Typical Attitude Control Electronics	3-48
3.3-3	Determination of Spacecraft Heliocentric Attitude	3-51
3.4-1	Injection and Vernier Correction Geometry	3-55
3.4-2	Terminal Maneuver Geometry	3-56
3.4-3	State Estimation Flow Diagram	3-62
3.4-4	Self Contained Terminal Navigation (Sixteen Observations Per Day)	3-64
3.4-5	Self Contained Terminal Navigation (Thirty-Two Observations Per Day)	3-64

LIST OF FIGURES (Continued)

Figure	Title	Page
3.5-1	Orbit Radius and Solar Pressure	3-68
3.5-2	Solar Aspect Angle for Earth Orientation	3-69
3.5-3	Meteoroid Approach Conditions	3-70
3.5-4	Spin-Rate Limitations	3-71
3.5-5	Spin-Axis Precession Due to Solar Pressure	3-73
3.5-6	Allowable Moment - Area Unbalance	3-73
3.5-7	Torque Due to Solar Pressure	3-75
3.5-8	Integrated Angular Momentum Due to Solar Pressure	3-76
3.5-9	Angular Impulse Due to Meteoroid Impact	3-78
3.5-10	Limit-Cycle Characteristics	3-80
3.5-11	Reaction Wheel Design Data	3-82
3.5-12	Stability Contribution of Fixed Solar Vanes	3-84
3.5-13	Block Diagram for Control System Utilizing Solar Vanes	3-85
3.6-1	Schematic Diagram of the Basic Hydrazine Subsystem	3-98
3.6-2	Weight of Hydrazine Required vs Total Propulsion Subsystem Weight	3-105
3.6-3	Spherical Tank Diameter vs Weight of Hydrazine Required	3-106
3.6-4	Propulsion Subsystem Weight vs Payload Weight	3-109
3.6-5	Propulsion System Weight vs Payload Weight	3-110
3.6-6	Propulsion Subsystem Weight vs Payload Weight	3-111

LIST OF FIGURES (Continued)

Figure	Title	Page
3.6-7	Propulsion System Concepts for Spacecraft Attitude Control	3-112
3.6-8	Schematic Diagram of Cold Gas Propulsion Subsystem - Configuration A	3-114
3.6-9	Schematic Diagram of Cold Gas Propulsion Subsystem - Configuration B	3-114
3.6-10	Attitude Control Subsystem Weight vs Total Impulse Required	3-118
3.7-1	Requirement Schedule and AEC Programs	3-121
3.7-2	Thermocouple Theoretical Loss Analysis Diagram	3-123
3.7-3	Theoretical Efficiency Comparison of Pb-Te & Si-Ge Couple Material	3-124
3.7-4	Thermocouple Interconnections	3-129
3.7-5	Thermocouple Failure Effects	3-130
3.7-6	Systems Configurations	3-132
3.7-7	McMurray-Bedford Inverter Circuit	3-134
3.7-8	Electric Power System Schematic Diagram	3-135
3.8-1	Mission Characteristics	3-144
3.8-2	Controlled Heat Absorption from RTG	3-148
3.8-3	Estimated Louver Performance	3-149
3.8-4	Thermal Control of Extended Components	3-150
3.8-5	Effect of Coating Properties on Thermal Control of Isothermal Module	3-152

LIST OF FIGURES (Continued)

Figure	Title	Page
3.8-6	Effect of Solar Distance on Thermal Control of Isothermal Module Design with No Sidewall Insulation	3-153
3.8-7	Effect of Solar Distance on Thermal Control of Isothermal Module Design with Sidewall Insulation	3-153
3.8-8	Effect of Deviation from Nominal Value of Emissivity on Heat Balance	3-154
3.8-9	Effect of Deviation from Nominal Value of Solar Absorptivity on Solar Heating	3-154
3.9-1	Integral Spectra of Galatic Cosmic Radiation	3-160
3.9-2	Energy Spectrum of a Severe Nonrelativistic Flare	3-162
3.9-3	Energy Spectrum of a Typical Relativistic Flare	3-163
3.9-4	Solar Flare/Sunspot Correlation	3-164
3.9-5	Earth Trapped Radiation	3-166
3.9-6	Integrated Electron Flux Vs Energy	3-170
3.9-7	Integrated Electron Flux Vs Jupiter Radii (= 1.02)	3-171
3.9-8	Integrated Electron Flux Vs Jupiter Radii (= 2)	3-172
3.9-9	Jupiter Trapped Radiation Iso-Flux Map	3-173
3.9-10	Neutron Attenuation Factors (6 Mev Neutrons)	3-176
3.9-11	Neutron Attenuation Factors (2 Mev Neutrons)	3-177
3.9-12	Gamma Ray Attenuation Factors	3-178
3.9-13	RTG Approximate Neutron Spectrum	3-179
3.9-14	Ionization Curve	3-192

LIST OF FIGURES (Continued)

Figure	Title	Page
3.10-1	Meteoroid Velocity Determination	3-206
3.10-2	Summary of Meteoroid Environment	3-210
3.10-3	Meteoroid Penetrations of Aluminum Sheet for Near-Earth Region	3-211
3.10-4	Meteoroid Penetrations of Aluminum Sheet for Interplanetary Region	3-211
3.10-5	Meteoroid Penetrations of Aluminum Sheet for Asteroidal Region (Nominal)	3-212
3.10-6	Meteoroid Penetrations of Aluminum Sheet for Asteroidal Region (Worst Case)	3-212
3.10-7	Meteoroid Penetrations of Aluminum Sheet for Near-Jupiter Region	3-213
3.11-1	Spacecraft-to-Adapter Interface Requirements	3-218
3.11-2	Typical Encounter Geometries, 0^{o} Inclination	3-220
3.11-3	Typical Encounter Geometries, 90^{o} Inclination	3-221
3.11-4	Typical Encounter Geometries, 45^{o} Inclination	3-222
3.11-5	Directional Antenna - Spacecraft Location Alternatives	3-224
3.11-6	Effect of RTG Location on Stability of Spin Stabilized Spacecraft	3-225
3.12-1	Extension Device for Providing Sensor - Spacecraft Separation	3-231
3.12-2	Structural/Mechanical System Weight	3-233
3.13-1	Reliability Block Diagram and Equipment MTBF's for a Series Communication Subsystem Configuration	3-236

LIST OF FIGURES (Continued)

Figure	Title	Page
3.13-2	Reliability Block Diagram for Three Communication Subsystem Configurations with Redundancies	3-237
3.13-3	Reliability Block Diagram and Subelement MTBF's for the Series Data Encoder Element	3-238
3.13-4	Reliability Block Diagram for Three Configurations of the Data Encoder Element	3-239
3.13-5	Reliability Block Diagram and Subelement MTBF's for the Command Detector and Decoder Element	3-240
3.13-6	Reliability Block Diagram and Subelement MTBF's for the Combined Data Automation Element	3-241
3.13-7	Reliability Block Diagram and Subelement MTBF's for a Two Section Data Element	3-242
3.13-8	Reliability Block Diagram, Equipment MTBF's, and Equipment Operating Times for Spacecraft Control Subsystem Concept One	3-243
3.13-9	Reliability Block Diagram of Central Computer and Sequencer	3-244
3.13-10	Reliability Block Diagram, Equipment MTBF's, and Equipment Operating Times for Spacecraft Control Subsystem Concept Two	3-244
3.13-11	Reliability Block Diagram, Equipment MTBF's, and Equipment Operating Times for Spacecraft Subsystem Concept Three	3-245
3.13-12	Reliability Block Diagram and Equipment Probabilities of the Single Cold Gas Attitude Control Subsystem	3-246
3.13-13	Reliability Block Diagram and Equipment Probability for Dual Cold Gas Attitude Control Subsystem One	3-246
3.13-14	Reliability Block Diagram for Dual Cold Gas Attitude Control Subsystem Two	3-247

LIST OF FIGURES (Continued)

Figure	Title	Page
3.13-15	Reliability Block Diagram and Reliabilities for Two Attitude Control Tank Configurations	3-248
3.13-16	Reliability Block Diagram and Equipment Probabilities for the Propulsion Subsystem	3-249
3.13-17	Control Squib Configurations for the Propulsion Subsystem	3-249
3.13-18	Regulator Configuration for the Propulsion Subsystem	3-249
3.13-19	Reliability Block Diagram and Equipment MTBF's for Electrical Power Subsystem	3-250
4.3-1	Pu 238 Production	4-9
4.3-2	RTG Development Time Estimates	4-12
4.3-3	Program Implementation Network	4-17
4.4-1	Science Subsystem Costs	4-25
4.4-2	Pu 238 Decay Rate	4-27
4.4-3	Electrical Power Subsystem Costs	4-27
4.4-4	Communications and Data Management Subsystem Costs	4-27
4.4-5	CC&S and Attitude Control Electronics Costs	4-27
4.4-6	Structure Subsystem Costs	4-29
4.4-7	Midcourse Propulsion Subsystem Costs	4-29
4.4-8	Cold Gas Attitude Control Propulsion Subsystem Costs	4-29
4.4-9	Other Nonrecurring Costs	4-29

LIST OF FIGURES (Continued)

Figure	Title	Page
4.4-10	Spacecraft Assembly and Checkout Costs	4-31
4.4-11	RTG Fuel Costs	4-31
4.4-12	Spacecraft Operational Support Costs	4-32
5.1-1	Spacecraft Design Concept A	5-2
5.1-2	Design Concept A - Data Automation Element	5-12
5.1-3	Design Concept A - Meteoroid Penetrations vs Aluminum Sheet Thickness	5-27
5.1-4	Design Concept A - Mission Performance Envelope	5-31
5.1-5	Design Concept A - Launch Vehicle Mission Performance Summary Chart	5-33
5.1-6	Design Concept A - Time Line Chart	5-37
5.1-7	Design Concept A - Schedule Confidence	5-37
5.2-1	Spacecraft Design Concept B	5-41
5.2-2	Antenna Positioning Example - 1976, 600-Day Mission	5-45
5.2-3	Antenna Positioning Example - 1975, 600-Day Mission	5-46
5.2-4	Antenna Positioning Example - 1974, 600-Day Mission	5-46
5.2-5	Design Concept B - Data Automation Element	5-57
5.2-6A	Meteoroid Impact Conditions	5-61
5.2-6B	Design Concept B - Meteoroid Penetrations vs Aluminum Sheet Thickness	5-61

LIST OF FIGURES (Continued)

Figure	Title	Page
5.2-7	Design Concept B - Mission Performance Envelope	5-66
5.2-8	Design Concept B - Launch Vehicle Mission Performance Summary Chart	5-68
5.2-9	Design Concept B - Time Line Chart	5-72
5.2-10	Design Concept B - Schedule Confidence	5-72
5.3-1	Spacecraft Design Concept C	5-78
5.3-2	Design Concept C - Data Automation Element	5-84
5.3-3	Design Concept C - Meteoroid Penetrations vs Aluminum Sheet Thickness	5-93
5.3-4	Design Concept C - Mission Performance Envelope	5-97
5.3-5	Design Concept C - Launch Vehicle Mission Performance Summary Chart	5-98
5.3-6	Design Concept C - Time Line Chart	5-103
5.3-7	Design Concept C - Schedule Confidence	5-103
5.4-1	Spacecraft Design Concept D	5-107
5.4-2	Design Concept D Data Encoder and Data Storage Element Interface	5-114
5.4-3	Design Concept D - Meteoroid Penetrations vs Aluminum Sheet Thickness	5-132
5.4-4	Design Concept D - Mission Performance Envelope	5-136
5.4-5	Design Concept D - Launch Vehicle Mission Performance Summary Chart I	5-137
5.4-6	Design Concept D - Launch Vehicle Mission Performance Summary Chart II	5-138

LIST OF FIGURES (Continued)

Figure	Title	Page
5.4-7	Design Concept D - Time Line Chart	5-140
5.4-8	Design Concept D - Schedule Confidence	5-143
A-1	Injection Energy and Asymptote Declination Mission Map, 1973 Launch	A-2
A-2	Injection Energy and Asymptote Declination Mission Map, 1974 Launch	A-3
A-3	Injection Energy and Asymptote Declination Mission Map, 1975 Launch	A-4
A-4	Injection Energy and Asymptote Declination Mission Map, 1976 Launch	A-5
A-5	Injection Energy and Asymptote Declination Mission Map, 1977 Launch	A-6
A-6	Injection Energy and Asymptote Declination Mission Map, 1978 Launch	A-7
A-7	Injection Energy and Asymptote Declination Mission Map, 1979 Launch	A-8
A-8	Injection Energy and Asymptote Declination Mission Map, 1980 Launch	A-9
A-9	Hyperbolic Excess Speed Mission Map, 1973 Launch	A-10
A-10	Hyperbolic Excess Speed Mission Map, 1974 Launch	A-11
A-11	Hyperbolic Excess Speed Mission Map, 1975 Launch	A-12
A-12	Hyperbolic Excess Speed Mission Map, 1976 Launch	A-13
A-13	Hyperbolic Excess Speed Mission Map, 1977 Launch	A-14

LIST OF FIGURES (Continued)

Figure	Title	Page
A-14	Hyperbolic Excess Speed Mission Map, 1978 Launch	A-15
A-15	Hyperbolic Excess Speed Mission Map, 1979 Launch	A-16
A-16	Hyperbolic Excess Speed Mission Map, 1980 Launch	A-17
B-1	582-Day Flight Targeting Chart: Time in CPJ $< 10^{o}$ Zone	B-2
B-2	582-Day Flight Targeting Chart: Time in SPJ $< 10^{o}$ Zone	B-3
B-3	582-Day Flight Targeting Chart: Time in SPJ $\leq 0^{o}$ Zone	B-4
B-4	582-Day Flight Targeting Chart: Time in EPJ $\leq 0^{o}$ Zone	B-5
B-5	582-Day Flight Targeting Chart: Solar Immersion and Emersion Latitudes	B-6
B-6	582-Day Flight Targeting Chart: Earth Immersion and Emersion Latitudes	B-7
B-7	582-Day Flight Targeting Chart: Eccentricity and Inclination of PEH Trajectory	B-8
B-8	582-Day Flight Targeting Chart: Perihelion and Aphelion Distances of PEH Trajectory	B-9
B-9	498-Day Flight Targeting Chart: Time in CPJ $< 10^{o}$ Zone	B-10
B-10	498-Day Flight Targeting Chart: Time in SPJ $\leq 10^{o}$ Zone	B-11
B-11	498-Day Flight Targeting Chart: Time in SPJ $\leq 0^{o}$ Zone	B-12

LIST OF FIGURES (Continued)

Figure	Title	Page
B-12	498-Day Flight Targeting Chart: Time in EPJ $\leq 0^{o}$ Zone	B-13
B-13	498-Day Flight Targeting Chart: Solar Immersion and Emersion Latitudes	B-14
B-14	498-Day Flight Targeting Chart: Earth Immersion and Emersion Latitudes	B-15
B-15	498-Day Flight Targeting Chart: Eccentricity and Inclination of PEH Trajectory	B-16
B-16	498-Day Flight Targeting Chart: Perihelion and Aphelion Distances of PEH Trajectory	B-17
B-17	413-Day Flight Targeting Chart: Time in CPJ $\leq 10^{o}$ Zone and Time in SPJ $\leq 10^{o}$ Zone	B-18
B-18	413-Day Flight Targeting Chart: Time in SPJ $\leq 0^{o}$ Zone and Time in EPJ $\leq 0^{o}$ Zone	B-19
B-19	413-Day Flight Targeting Chart: Solar Immersion and Emersion Latitudes	B-20
B-20	413-Day Flight Targeting Chart: Earth Immersion and Emersion Latitude	B-21
B-21	413-Day Flight Targeting Chart: Eccentricity and Inclination of PEH Trajectory	B-22
B-22	413-Day Flight Targeting Chart: Perihelion and Aphelion Distances of PEH Trajectory	B-23
D-1	Ratio of Hydrazine Tank Weight to Hydrazine Volume Versus Ullage Factor	D-5

LIST OF TABLES

Number	Title	Page
2.1-1	Orbital and Physical Characteristics of Jupiter	2-2
2.1-2	Energy Ranges of Corpuscular Radiation	2-8
2.1-3	Energy Response of Energetic Particle Detector	2-15
2.1-4	Intervals of Particle Energy	2-17
2.1-5	Television I	2-26
2.1-6	Television II	2-27
2.1-7	Scientific Instrument Characteristics	2-37
2.1-8	Scientific Experiment Packages	2-40
2.3-1	Payload Decrements	2-66
2.3-2	C_3 Decrements	2-66
3.1-1	DSIF Assumed Characteristics	3-8
3.1-2	Spacecraft Assumed Characteristics	3-9
3.1-3	Low Data Rate Modulation Comparison	3-13
3.6-1	Weight Breakdown of Subsystem Fixed Hardware	3-103
3.6-2	Midcourse Correction Propulsion Subsystem - Nomenclature and Equation	3-104
3.6-3	Design Data	3-108
3.6-4	Attitude Control Propulsion Subsystem - Nomenclature and Equation Summary	3-117
3.6-5	Attitude Control Propulsion Subsystem - Sizing Design Data	3-119

LIST OF TABLES (cont'd)

Number	Title	Page
3.7-1	60-, 80-, and 120-Watt RTG Geometry	3-127
3.7-2	Battery System Characteristics	3-138
3.8-1	Potential Modular Group Arrangement of Components	3-156
3.9-1	Characteristics of UO_2	3-174
3.9-2	Effects of Proton Irradiation on the Reflectivity of Thermal Control Coatings	3-181
3.9-3	Effects of 1.2 Mev Electrons on the Transmission of Some Optical Materials	3-185
3.9-4	Detector Characteristics and Nuclear Properties	3-194
3.13-1	Mean-Time-Between Failures for Scientific Instruments	3-251
4.3-1	Summary of Spacecraft Hardware Requirements	4-7
4.3-2	RTG Thermal Watt Requirements for 240 and 280 Electrical Watt Power System	4-8
4.3-3	Scientific Instrument State-of-the-Art	4-14
4.3-4	Abbreviations Used on Figure 4.3-3	4-18
4.4-1	Launch Vehicle Costs	4-33
5.1-1	Sequence of Significant Flight Events For Spacecraft Design Concept A	5-3
5.1-2	Spacecraft Design Concept A - Weight Summary	5-5
5.1-3	Design Concept A - Gain-Loss Chart	5-6
5.1-4	Design Concept A - Antenna and Information Rate Schedule	5-7

LIST OF TABLES (Cont'd)

Number	Title	Page
5.1-5	Design Concept A - Communications Subsystem Weight	5-8
5.1-6	Design Concept A - Anticipated Data Bit Rates	5-9
5.1-7	Design Concept A - Data Management Subsystem Weight	5-14
5.1-8	Design Concept A - Control Subsystem Weight	5-17
5.1-9	Design Concept A - Midcourse Propulsion Subsystem Weight	5-21
5.1-10	Design Concept A - Electric Power Loads	5-22
5.1-11	Design Concept A - Electric Power Subsystem Weight	5-23
5.1-12	Design Concept A - Thermal Control Information	5-24
5.1-13	Design Concept A - Meteoroid Protection Analysis Data	5-26
5.1-14	Design Concept A - Equipment MTBF	5-29
5.1-15	Design Concept A - Probability of Mission Success	5-32
5.1-16	Design Concept A - Subsystems Probability of Mission Success	5-32
5.1-17	Design Concept A - PERT III Input Activity Time Estimates	5-35
5.1-18	Design Concept A - PERT III Event Schedule Report	5-36
5.1-19	Design Concept A - Summary of Program Costs	5-38
5.1-20	Design Concept A - Recurring Spacecraft Costs for Two Flights	5-39
5.1-21	Design Concept A - Cost Increment For a Third Flight	5-39

LIST OF TABLES (cont'd)

Number	Title	Page
5.2-1	Sequence of Significant Flight Events For Spacecraft Design Concept B	5-42
5.2-2	Spacecraft Design Concept B - Weight Summary	5-44
5.2-3	Design Concept B - Gain-Loss Chart	5-47
5.2-4	Design Concept B - Antenna and Information Rate Schedule	5-47
5.2-5	Design Concept B - Communications Subsystem Weight	5-48
5.2-6	Design Concept B - Anticipated Data Bit Rates	5-49
5.2-7	Design Concept B - Data Management Subsystem Weight	5-52
5.2-8	Design Concept B - Control Subsystem Weight	5-55
5.2-9	Design Concept B - Midcourse Propulsion Subsystem Weight	5-56
5.2-10	Design Concept B - Electric Power Loads	5-57
5.2-11	Design Concept B - Electric Power Subsystem Weight	5-58
5.2-12	Design Concept B - Thermal Control Information	5-59
5.2-13	Design Concept B - Meteoroid Protection Analysis Data	5-60
5.2-14	Design Concept B - Equipment MTBF	5-64
5.2-15	Design Concept B - Probability of Mission Success	5-67
5.2-16	Design Concept B - Subsystems Probability of Mission Success	5-67
5.2-17	Design Concept B - PERT III Input Activity Time Estimates	5-70

LIST OF TABLES (cont'd)

Number	Title	Page
5.2-18	Design Concept B - PERT III Event Schedule Report	5-71
5.2-19	Design Concept B - Summary of Program Costs	5-73
5.2-20	Design Concept B - Recurring Spacecraft Costs for Two Flights	5-74
5.2-21	Design Concept B - Cost Increment For a Third Flight	5-74
5.3-1	Sequence of Significant Flight Events For Spacecraft Design Concept C	5-77
5.3-2	Spacecraft Design Concept C - Weight Summary	5-78
5.3-3	Design Concept C - Gain-Loss Chart	5-80
5.3-4	Design Concept C - Antenna and Information Rate Schedule	5-81
5.3-5	Design Concept C - Communications Subsystem Weight	5-81
5.3-6	Design Concept C - Anticipated Data Bit Rates	5-83
5.3-7	Design Concept C - Data Management Subsystem Weight	5-85
5.3-8	Design Concept C - Control Subsystem Weight	5-86
5.3-9	Design Concept C - Midcourse Propulsion Subsystem Weight	5-87
5.3-10	Design Concept C - Electric Power Loads	5-88
5.3-11	Design Concept C - Electric Power Subsystem Weight	5-89
5.3-12	Design Concept C - Thermal Control Information	5-90

LIST OF TABLES (cont'd)

Number	Title	Page
5.3-13	Design Concept C - Meteoroid Protection Analysis Data	5-92
5.3-14	Design Concept C - Equipment MTBF	5-95
5.3-15	Design Concept C - Probability of Mission Success	5-99
5.3-16	Design Concept C - Subsystems Probability of Mission Success	5-100
5.3-17	Design Concept C - PERT III Input Activity Time Estimates	5-101
5.3-18	Design Concept C - PERT III Event Schedule Report	5-102
5.3-19	Design Concept C - Summary of Program Costs	5-104
5.3-20	Design Concept C - Recurring Spacecraft Costs for Two Flights	5-105
5.3-21	Design Concept C - Cost Increment For a Third Flight	5-105
5.4-1	Sequence of Significant Flight Events For Spacecraft Design Concept D	5-107
5.4-2	Spacecraft Design Concept D - Weight Summary	5-109
5.4-3	Design Concept D - Gain-Loss Chart	5-111
5.4-4	Design Concept D - Antenna and Information Rate Schedule	5-112
5.4-5	Design Concept D - Communications Subsystem Weight	5-112
5.4-6	Design Concept D - Anticipated Data Bit Rates	5-115

LIST OF TABLES (cont'd)

Number	Title	Page
5.4-7	Design Concept D - Data Management Subsystem Weight	5-116
5.4-8	Design Concept D - Control Subsystem Weight	5-125
5.4-9	Design Concept D - Midcourse Propulsion Subsystem Weight	5-126
5.4-10	Design Concept D - Electric Power Loads	5-127
5.4-11	Design Concept D - Electric Power Subsystem Weight	5-128
5.4-12	Design Concept D - Thermal Control Information	5-130
5.4-13	Design Concept D - Meteoroid Protection Analysis Data	5-131
5.4-14	Design Concept D - Equipment MTBF	5-134
5.4-15	Design Concept D - Probability of Mission Success	5-139
5.4-16	Design Concept D - Subsystems Probability of Mission Success	5-140
5.4-17	Design Concept D - PERT III Input Activity Time Estimates	5-141
5.4-18	Design Concept D - PERT III Event Schedule Report	5-142
5.4-19	Design Concept D - Summary of Program Costs	5-144
5.4-20	Design Concept D - Recurring Spacecraft Costs for Two Flights	5-145
5.4-21	Design Concept D - Cost Increment For a Third Flight	5-145

SECTION 1

INTRODUCTION

This document is the final report on the work accomplished during a study of Jupiter flyby missions which was conducted for the Jet Propulsion Laboratory by the Fort Worth Division of General Dynamics. An earlier report on this study, the Mid-Term Technical Progress Report (FZM-4572), is completely superseded by this document.

The report is presented in four technical sections: (1) Mission Planning, (2) Spacecraft Systems Design and Analyses, (3) Spacecraft Concept Evaluation, and (4) Spacecraft Design Concepts. The first three sections are devoted to the general analyses which are the bases for the material presented in the fourth section, i.e., conceptual designs of spacecraft to perform flyby missions to Jupiter.

Hereinafter, the tasks, constraints, and technical approach are delineated, and their relationship to the overall study is indicated. A discussion of the design philosophy employed in the study is also included. The study results are summarized in subsection 1.5.

1.1 DEFINITION OF TASK

The objective of the study as it is described in the Jet Propulsion Laboratory Statement of Work No. 1285, 25 May 1965, is to

> ... perform a feasibility study to develop spacecraft design concepts for a 'flyby' mission of the planet Jupiter. The study shall consider a range of alternate design concepts for accomplishing the successive mission objectives listed below within the applicable design constraints:
>
> (1) Interplanetary and planetary measurements of the spatial distribution of particles and fields. Measurements shall include but not necessarily be limited to: (i) magnetic fields; (ii) solar plasma; (iii) dust and micrometeorites; (and) (iv) ionized radiation. The trapped radiation belts of Jupiter are considered a special case of particle and field measurements and shall be presented relative to the design complexity required for their measurement.
>
> (2) Measurements of the planetary atmosphere of Jupiter which shall include but not necessarily be limited to: (i) composition (and) (ii) temperature and pressure.

(3) Measurements of the physical properties of Jupiter which shall include but not necessarily be limited to: (i) observation of the cloud cover and possibly gross features of the Jovian terrain.

The specific tasks to be completed during the course of the study are described in the subject Statement of Work as follows:

(1) Develop the conceptual designs for spacecraft systems for each of the (mission) objectives listed ... above by accomplishing the following: (i) establish the functional requirements for spacecraft systems to perform the mission; (ii) forecast the applicable state-of-the-art for the time period considered; (iii) perform design trade-offs as a basis of the rationale employed for design selection; (iv) synthesize the appropriate system concepts; (v) identify the problem areas and indicate approaches to their solution; (and) (vi) review the system concepts in terms of the Mariner Mars '64 spacecraft system design.

(2) Provide a description for each of the systems developed ... above, which shall include, but not necessarily be limited to, the following: (i) system block diagrams; (ii) operational sequences; (iii) expected performance characteristics and design reliabilities; (and) (iv) weight and power estimates.

(3) Provide estimates of schedule, cost, and probability of success, including success of partial missions, for each of the systems developed ... above, and indicate the trade-offs involved.

1.2 CONSTRAINTS

The constraints which have been observed in the study are indicated in the listing below. The first and third items are quotations from the Jet Propulsion Laboratory Statement of Work No. 1285, and the source of the second item is indicated therein.

(1) Mission accomplishment shall be during the 1973 through 1980 time period. State-of-the-art applicability for design concepts evolved by this study shall consider development lead-time requirements for the time period of interest.

(2) Missions shall be compatible with at least one of the following launch vehicles: (i) Atlas SLV3x/Centaur/HEKS; (ii) Titan IIICx/Centaur; (iii) Saturn IB/Centaur/HEKS; (iv) Saturn V; and (v) Saturn V/Centaur. The performance and physical characteristics of these vehicles to be used by this study shall be as described in the Jet Propulsion Laboratory Technical Direction Memorandum No. 1, Contract 951285, 7 January 1966.

(3) Compatibility with the Deep Space Instrumentation Facility (DSIF), as described in the Jet Propulsion Laboratory Technical Memorandum 33-83, Revision 1, dated 24 April 1964 (shall be maintained).

1.3 TECHNICAL APPROACH

The technical approach which was formulated by General Dynamics and followed in order to meet the objectives and to perform the tasks outlined in subsection 1.1 is illustrated in Figure 1.3-1. First, all aspects of a Jupiter flyby mission relative to launch vehicle requirements, scientific accomplishment, and spacecraft performance were examined. Subsequently, spacecraft systems which are capable of carrying out selected groups of mission objectives were designed. In the final phase of the study, each spacecraft concept was evaluated in terms of its mission capabilities and the ramifications of its implementation. The study approach shown in Figure 1.3-1 was based on the interpretation of the study objectives and tasks discussed below. This brief discussion of study objectives and tasks is intended to complement the study task description in subsection 1.1.

1.3.1 Mission Planning

The Mission Planning phase was designed to supply the information required for spacecraft design. The primary objectives were (1) to describe possible scientific requirements in the Science Subsystem Definition task, and (2) to determine mission performance requirements in the Mission Analysis task.

The definition of science subsystems was accomplished by considering as candidate experiments all interplanetary and planetary experiments which (1) have been previously established as feasible in existing literature, (2) satisfy one or more of the mission objectives outlined in subsection 1.1, and (3) are applicable to a Jupiter flyby mission. Each of these experiments was described in terms of the required instrumentation and the associated requirements for the various spacecraft subsystems. From these experiments, several "packages" were made up which are representative of different levels of scientific capability. These experiment packages were selected to provide design points for spacecraft subsystem studies.

The Mission Analysis task was directed toward the identification of characteristics of Earth-Jupiter heliocentric, ballistic transfer trajectories in order (1) to support spacecraft design studies, and (2) to evaluate launch vehicle payload capabilities. In keeping with the constraints listed in subsection 1.2, this work was limited to launch dates in the 1973-1980 time period and to the Atlas SLV3x/Centaur/HEKS, Titan IIICx/Centaur, Saturn IB/Centaur/HEKS, Saturn V, and Saturn V/Centaur launch vehicles. Jupiter encounter trajectories were analyzed in detail to provide

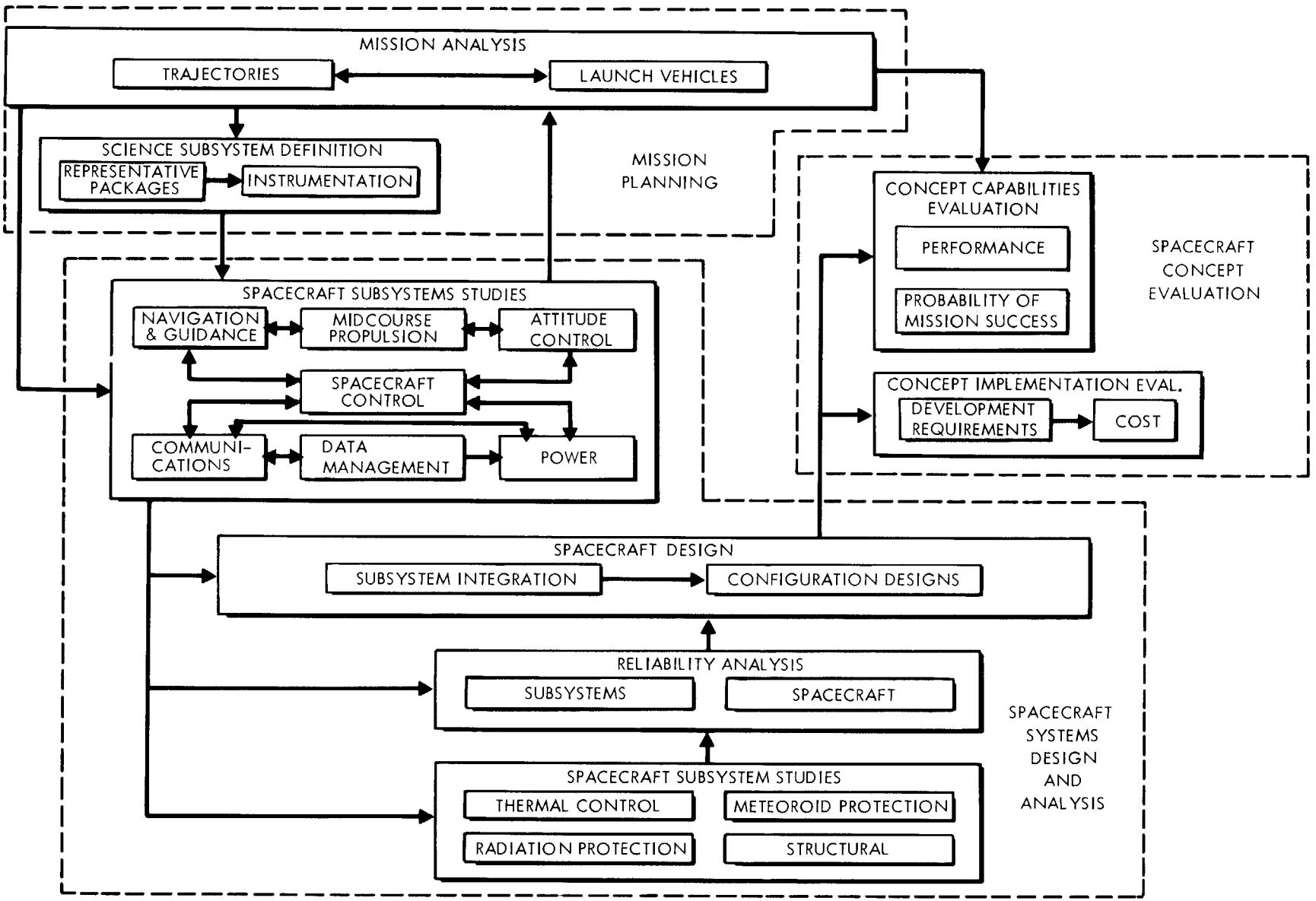
MISSION ANALYSIS
TRAJECTORIES
LAUNCH VEHICLES
SCIENCE SUBSYSTEM DEFINITION
REPRESENTATIVE PACKAGES
INSTRUMENTATION
MISSION PLANNING
CONCEPT CAPABILITIES EVALUATION
PERFORMANCE
PROBABILITY OF MISSION SUCCESS
SPACECRAFT CONCEPT EVALUATION
CONCEPT IMPLEMENTATION EVAL.
DEVELOPMENT REQUIREMENTS
COST
SPACECRAFT SUBSYSTEMS STUDIES
NAVIGATION & GUIDANCE
MIDCOURSE PROPULSION
ATTITUDE CONTROL
SPACECRAFT CONTROL
COMMUNI-CATIONS
DATA MANAGEMENT
POWER
SPACECRAFT DESIGN
SUBSYSTEM INTEGRATION
CONFIGURATION DESIGNS
RELIABILITY ANALYSIS
SUBSYSTEMS
SPACECRAFT
SPACECRAFT SUBSYSTEM STUDIES
THERMAL CONTROL
METEOROID PROTECTION
RADIATION PROTECTION
STRUCTURAL
SPACECRAFT SYSTEMS DESIGN AND ANALYSIS

FIGURE I.3-1

data pertinent to subsystems design and "aim point" selection. Post-encounter trajectories were also considered in terms of their effect on aim point selection.

1.3.2 Spacecraft Systems Design and Analysis

The Spacecraft Systems Design and Analysis phase entailed the establishment of a design iteration loop which resulted in spacecraft design concepts based on mission objectives and requirements defined in the Mission Planning Phase. The study tasks included Spacecraft Subsystems Studies, Reliability Analysis, and Spacecraft Design.

Spacecraft Subsystem Studies were conducted on each of the various subsystems which together comprise a complete spacecraft. Studies in the following technological areas were required: (1) communications, (2) navigation and control, (3) data management, (4) spacecraft control, (5) midcourse propulsion, (6) attitude control, (7) power, (8) thermal control. (9) radiation protection, (10) meteoroid protection, and (11) structural and mechanical provisions.

The effort in the Reliability Analysis was directed toward estimating and enhancing reliability at the subsystems level and, finally, at the integrated spacecraft level. Although it was treated as a separate study effort, the Reliability Analysis task was an integral part both of the Spacecraft Subsystems Studies and the Spacecraft Design tasks.

The task in Spacecraft Design was to integrate selected subsystem design concepts into spacecraft design concepts. Configuration designs for these concepts were then determined.

1.3.3 Spacecraft Concept Evaluation

In the third phase, Spacecraft Concept Evaluation, the spacecraft design concepts resulting from the second study phase were considered in terms of mission capability and implementation requirements. Specifically, this work entailed the evaluation of mission performance characteristics, the probability of mission success, development requirements, and cost. In each case, the task was basically one of combining the appropriate results of mission and subsystems studies in order to obtain information related to an integrated spacecraft. The results of these studies served as a basis for an evaluation of the merits of each concept, not as a means of selecting one spacecraft design concept rather than another.

1.4 DESIGN PHILOSOPHY

In performing the Jupiter Flyby Mission Study, it has sometimes been necessary to choose an approach to spacecraft design without recourse to extensive analyses. Such choices have often

been based on design philosophies, and the more important of these philosophies are outlined in detail in this subsection.

The primary guideline employed in conducting the study was the requirement to "consider a range of alternate design concepts." In consequence, spacecraft designs which represent scientific capabilities ranging from "minimal" to "full" were considered. From the studies of scientific missions for Jupiter flyby spacecraft, it was determined that three more or less distinct levels of scientific capability can be identified. The spacecraft requirements associated with these levels were used as starting points in spacecraft design.

Next, the various spacecraft design approaches were examined. It became apparent that the basic choice among design approaches was that stemming from the method of spacecraft stabilization, i.e., the choice between spin and three-axis stabilization. Although from the standpoint of planetary scientific investigations a spin-stabilized spacecraft is not the optimum vehicle, it was considered necessary to include a spin-stabilized spacecraft in the range of alternate design concepts to be considered in the study because of advantages that possibly could be realized in other areas.

By combining the three levels of scientific capability and the two approaches to stabilization, and by taking the scope of the study into consideration, four basic spacecraft concepts were selected to serve as the basis for conceptual designs: (1) a spin-stabilized spacecraft with a science complement compatible with the stabilization mode, (2) a three-axis-stabilized spacecraft exhibiting a minimal scientific capability, (3) a three-axis-stabilized spacecraft to support an intermediate science package, and (4) a three-axis-stabilized spacecraft with a full scientific capability. These are referred to in this report as Spacecraft Design Concepts A, B, C, and D, respectively.

After the four basic design philosophies were established, it was necessary to develop a design approach for each of the four selected concepts. In the following subsections, the philosophies and the manner in which they were evolved are described.

1.4.1 Spin Stabilization

A spin-stabilized spacecraft is of interest in this study for reasons of spacecraft simplicity. The long flight times associated with Jupiter flyby missions indicate the definite need for highly reliable spacecraft, and simplicity is tantamount to achieving high reliability. An attempt is made in Figure 1.4-1 to indicate the more feasible of the many design alternatives associated with spin stabilization. The alternatives and the ultimate choices of design philosophy made in the case of Spacecraft Design Concept A are discussed below.

The planetary scientific capability of a spin-stabilized spacecraft is limited to measurements of particles and fields unless some form of stabilized platform is established at Jupiter

DESIGN ALTERNATIVES FOR SPIN-STABILIZATION

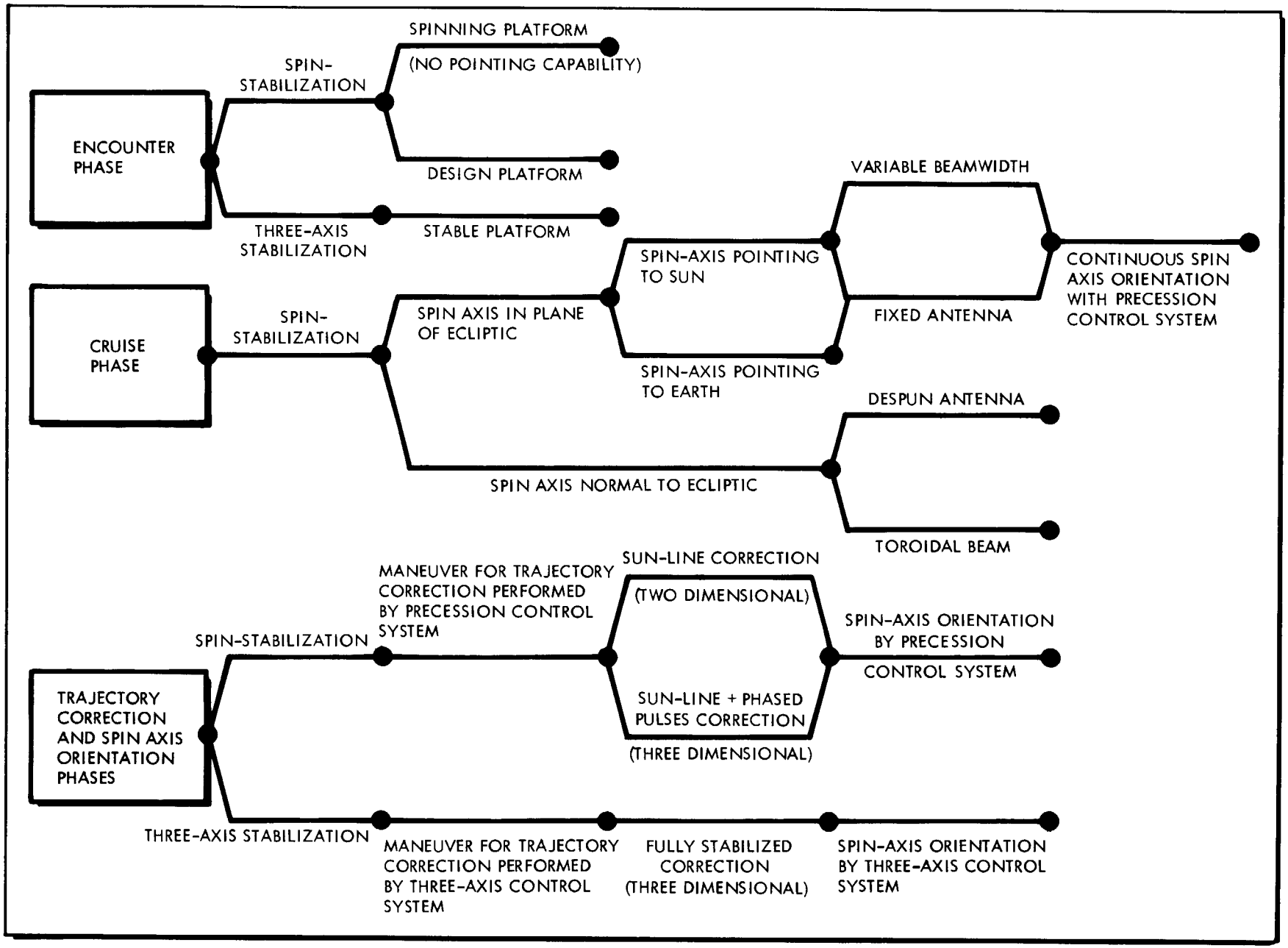

FIGURE 1.4-1

encounter. The provision of such a platform is contrary to the design philosophy of simplicity; therefore, Concept A is considered to be spin-stabilized from the time of initial spin-up to its end-of-life.

Since the planetary scientific capability of the spin-stabilized spacecraft is somewhat limited, the design philosophy can be established more completely. Specifically, the cost of the spacecraft should be low; little or no advanced development should be required; and the spacecraft should be compatible with an inexpensive launch vehicle.

The method of spin stabilization employed on deep-space probes during cruise definitely affects the spacecraft-to-Earth communications capability. For communication distances as great as those experienced by Jupiter flyby spacecraft, a highly directional spacecraft communications antenna is desirable. To implement this type of antenna, a means must be provided to point the antenna in a specified direction. One method is to orient the spin-axis in the plane of the ecliptic so that it either continuously points toward the Sun or continuously points toward the Earth. In the former case, the antenna must utilize a rather large beamwidth in order for spacecraft-to-Earth communications to be continuous throughout the mission. The latter case allows a very high gain antenna to be used; however, the implementation of the Earth-pointing orientation entails substantial increase in complexity. In either case, the spin-axis must be continuously reoriented by an active precession control system, and an additional degree of complexity contrary to the original design philosophy is required. For this reason, the two concepts were not considered further in the evolution of Design Concept A.

The other methods of implementing spacecraft-to-Earth communications with spin stabilization involve the use of antennas which are based on a spin-axis which is essentially perpendicular to the ecliptic plane. The two primary types of antennas for this application are despun antennas and toroidal-beam-pattern antennas. The use of despun antennas offers the possibility of higher gains; however, they are relatively undeveloped, and thus they were eliminated from further consideration for Concept A. Consequently, a toroidal-beam antenna, with the associated spin-axis orientation normal to the ecliptic, is employed for spacecraft-to-Earth communications for Design Concept A.

In the study of navigation and guidance, it was determined that a trajectory correction for a Jupiter flyby mission is very desirable regardless of the simplicity of the scientific complement. The planetary data which could be gained without a trajectory correction do not appear to be significant. Thus, it was determined that Concept A should be capable of performing a midcourse correction. In this case, one of the design alternatives is (1) to spin the spacecraft immediately following separation from the

launch vehicle, (2) to orient the spacecraft spin-axis properly by means of some form of precession control system, and then (3) to perform a trajectory correction while the spacecraft is spinning. The last event is accomplished either by a Sun-line correction or by a Sun-line correction in conjunction with a series of phased pulses. The precession control system is state-of-the-art; however, both of the methods of trajectory correction are at present undeveloped.

The other design possibility is to include in the design a complete three-axis attitude control system such as the one used on Mariner IV. This method of attitude control is employed after separation and through the midcourse correction. It is also used to orient the spacecraft spin-axis precisely prior to spin-up and after the midcourse maneuver. Because the use of this system does not result in spacecraft physical characteristics which are substantially different from those associated with the systems discussed in the above paragraph, and because the method is definitely state-of-the-art, it was chosen for Design Concept A.

In summary, Spacecraft Design Concept A is spin-stabilized throughout the cruise and encounter mission phases with the spin axis oriented approximately normal to the ecliptic. The spacecraft is three-axis stabilized for the initial phases of the mission. During this time, a three-dimensional trajectory correction is made, and the spin axis is properly oriented prior to spin-up.

1.4.2 Three-Axis Stabilization

The three spacecraft design concepts utilizing three-axis stabilization which are described in this report are all characterized by essentially the same general design approach. There are, however, several design alternatives which were seriously considered for incorporation in one or more of the spacecraft. The aggregate of these alternate approaches is depicted by Figure 1.4-2. In the following paragraphs, these approaches are discussed, and the design philosophy followed in the case of each of the three-axis stabilized spacecraft is indicated.

The possible design choice of a two-axis stabilized spacecraft with the roll rate simply nulled by viewing the relative motion of the spacecraft with respect to stars is not depicted in Figure 1.4-2. Although the use of this concept affords a degree of simplicity in attitude control electronics which is greater than that of the fully stabilized vehicle, it also entails a penalty, or even an incapability, in pointing a communications antenna, in pointing scientific sensors at Jupiter, and in performing a trajectory correction. On the other hand, the fully stabilized spacecraft approach is state-of-the-art, and although it is based on a more sophisticated design philosophy,

DESIGN ALTERNATIVES FOR THREE-AXIS STABILIZATION

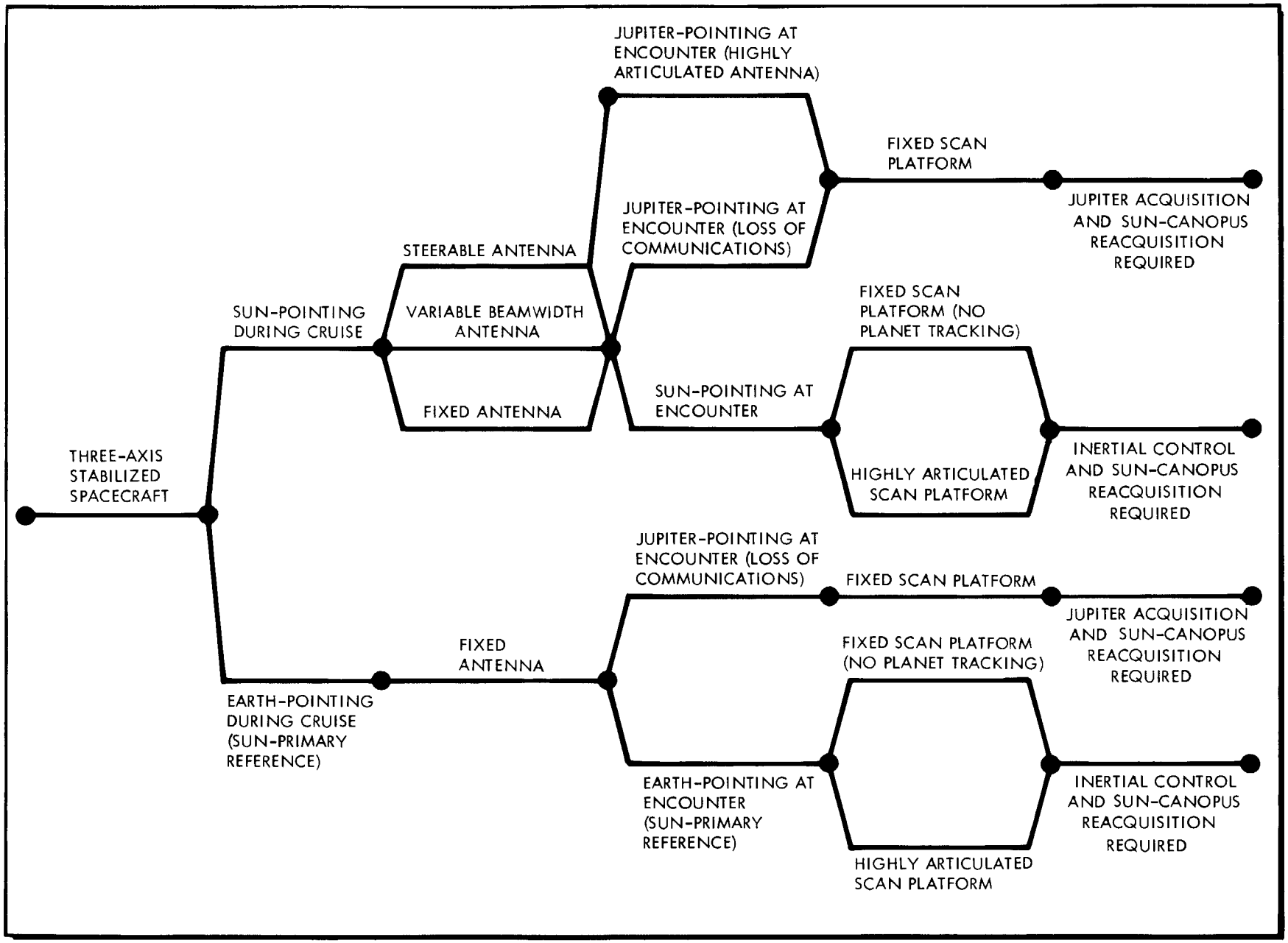

FIGURE 1.4-2

it is indicated that there is sufficient justification for using this approach because of the capability attainable in terms of mission performance.

As shown in Figure 1.4-2, there is a design alternative in the selection of the orientation of the body-fixed spacecraft axes during the cruise phase of the mission, i.e., the choice of continuously pointing one axis at the Sun or continuously tracking the position of the Earth with one axis. The advantage of the latter is that a body-fixed, high gain communications antenna can be incorporated into the spacecraft design. The attendant disadvantage is that a high degree of angular motion must be provided in the Sun and star sensors (particularly the star tracker) even to allow the spacecraft one degree of freedom of movement.

In the Sun-pointing spacecraft approach, three antenna concepts can be employed. The first is a body-fixed communications antenna. The use of this design approach dictates a very wide beam antenna in order to allow spacecraft-to-Earth communications during at least a major portion of the cruise phase. The second antenna concept is also body-fixed to the spacecraft, but it incorporates a variable beamwidth, or beam spoiling, feature to provide the large beamwidth necessary during the cruise phase and the high gain required at extreme communications distances. At present, such an antenna with suitable performance has not been developed. The third antenna design approach related to a Sun-pointing spacecraft is an antenna which is either mechanically or electronically steered. The mechanically steered rather than the electrically steered antenna was selected for purposes of this study because of the relative simplicity and more advanced stage of development of the former.

In consequence, a choice exists among the following four antenna concepts: (1) body-fixed, Earth-pointing, (2) body-fixed, Sun-pointing, (3) body-fixed, variable beamwidth, and (4) mechanically steered. The variable beamwidth antenna was eliminated on the basis of its stage of development. Also, it was determined that by adding just one degree of freedom of movement to an antenna, the resulting possible bit rates are at least four times larger than those which are possible with a body-fixed, Sun-pointing antenna. This reason was considered to be sufficient for eliminating the body-fixed Sun-pointing antenna as a possible design approach. The choice between pointing the spacecraft at the Earth or steering the antenna relative to the spacecraft was made in favor of the steerable antenna because of its relative simplicity of implementation in comparison with implementing the steerable spacecraft concept.

A major design philosophy also had to be established in regard to the attitude orientation mode of the spacecraft at encounter. In selecting an appropriate design approach, the influence of the characteristics of Jupiter encounter trajectories were very

important; e.g., the planet occludes both the Sun and Canopus as seen from the spacecraft under most expected approach conditions, and the large mass of Jupiter results in encounter hyperbolas which are quite pronounced. The choice of design approach is also dependent on the design philosophy associated with the communications antennas (see Figure 1.4-2).

Basically, there are two possible modes for use in Jupiter encounter orientation. In one, the spacecraft continues in the Sun-pointing attitude employed during the cruise phase. In the other, it is reoriented to the local Jupiter vertical in order to use Jupiter as a primary reference.

An important design alternative is associated with the latter case. It stems from the question of whether to retain spacecraft-to-Earth communications during the encounter (except for the period of Earth occultation by Jupiter). If spacecraft-to-Earth communications are to be maintained, the communications antenna must be capable of turning through an angle of approximately 270 degrees at a fairly rapid angular rate. As a result, stringent requirements are imposed both on the spacecraft configuration and the steering mechanism.

One solution to this problem is to suspend communications during the encounter portion of the mission. The science complements for three-axis stabilized spacecraft are such that enough data will be gathered at encounter to require a data storage capability. Therefore, the suspension of all communications during encounter results in only a slight increase in data storage requirements; the spacecraft itself will be relatively unaffected. The disadvantages of this concept are the loss of tracking data and an occultation experiment and the undesirable psychological effect of not being in contact with the spacecraft during this critical phase.

The mode of encounter orientation affects the selection of the platform from which planetary scientific sensors are pointed. In the case of the Sun-pointing attitude at encounter, it is possible to use an essentially fixed scan platform such as that used on Mariner IV. However, if the scientific instruments dictate pointing requirements other than those associated with a simple pass across the face of the planet, a scan platform with approximately 270 degrees of motion in one degree of freedom and approximately 30 degrees of motion in another degree of freedom is necessary to accommodate such requirements. On the other hand, the use of a fixed-scan platform in connection with a Jupiter-pointing attitude is obviously possible.

In determining the desirability of the various spacecraft orientation concepts during the encounter phase, the modes of spacecraft operation and spacecraft maneuvers required during encounter are major considerations. For the Sun-pointing

attitude, inertial control is used during occultation of the primary attitude references. After the occultation periods, these references must be reacquired, but this probably will not constitute a major maneuver.

In the case of the Jupiter-pointing attitude, the spacecraft must acquire this attitude prior to beginning the encounter phase. The acquisition can be accomplished without a major maneuver; i.e., Jupiter is acquired at some distance from the planet simply by turning on a properly placed planet sensor and Jupiter is then made the primary attitude reference without an acquisition maneuver. However, after the encounter period, the spacecraft must reacquire the Sun and Canopus. Since the spacecraft has turned through approximately a 270 degree angle, the reacquisition of these references constitutes a major maneuver. The reacquisition must be successfully accomplished in order to play back the data taken during encounter; thus, this maneuver is very critical.

After the advantages and disadvantages of the various encounter orientation modes were considered and evaluated, the Sun-pointing orientation with inertial control during Sun and Canopus occultations was selected for incorporation into the three-axis stabilized spacecraft design concepts synthesized in this study. The choice of scan platform and communications antenna characteristics varies as a function of the scientific complement associated with the individual spacecraft design concepts.

1.5 SUMMARY OF RESULTS

The results of this study indicate that a flyby mission to the planet Jupiter is definitely feasible during the 1973-1980 time period. In determining this feasibility, the general characteristics of Jupiter missions were surveyed in terms of scientific objectives and trajectory considerations. Subsequently, spacecraft subsystem designs which are applicable to a Jupiter flyby spacecraft and compatible with the various scientific and mission performance requirements were evolved.

The subsystems were integrated into four spacecraft design concepts which represent a range of alternate concepts. The four spacecraft were individually evaluated in terms of launch vehicle requirements, probability of mission success, development requirements, and program costs.

A design summary of each of the four spacecraft design concepts is included at the beginning of subsections 5.1, 5.2, 5.3, and 5.4 of Section 5, "Spacecraft Design Concepts."

SECTION 2

MISSION PLANNING

In this section, the studies devoted to scientific endeavors, the trajectories, and the launch vehicles applicable to flyby missions to Jupiter are described. To a large degree, the results of these studies are indicative of the performance requirements for Jupiter flyby spacecraft.

2.1 SCIENCE SUBSYSTEM DEFINITION

As a part of the present study of flyby missions to Jupiter, a spectrum of scientific experiments has been defined in order to derive estimates of the engineering requirements and constraints imposed by the science payload on other spacecraft systems. Although the actual definition of the science payloads to be used in a mission of this type will be determined by NASA and NASA advisors at a later date, it is necessary to define relatively realistic approximations at the present time so that the effects of the science package on the other study parameters can be evaluated with reasonable confidence in their validity.

The following subsections contain descriptions of the physical phenomena to be studied, as dictated by the mission objectives identified in subsection 1.1, and the scientific investigations required to pursue such objectives. The characteristics of the instruments necessary to perform these investigations are described in both narrative and tabular form. To provide design points for spacecraft design, several instrument groupings are defined as possible mission payloads.

2.1.1 Summary of Observations of the Planet Jupiter

The orbital and physical characteristics of Jupiter have been determined from astronomical observations of the planet and its satellites. Some of these characteristics which are summarized in Table 2.1-1 are known with a fair degree of accuracy, e.g., the orbital period and the planetary mass. Others, such as the rotation rate of the solid planetary surface or the planetary flattening, are only approximate because Jupiter is obscured by cloud layers of indefinite thickness and no actual planetary surface is observed.

Table 2.1-1 ORBITAL AND PHYSICAL CHARACTERISTICS OF JUPITER

Distance, Jupiter to Sun (max.)	817×10^6 km (508×10^6 miles)
Distance, Jupiter to Sun (min.)	740×10^6 km (460×10^6 miles)
Distance, Jupiter to Earth (max.)	967×10^6 km (601×10^6 miles)
Distance, Jupiter to Earth (min.)	591×10^6 km (367×10^6 miles)
Angular Diameter, From Earth (max.)	50 sec
Angular Diameter, From Earth (min.)	31 sec
Eccentricity of Orbit	0.0484
Inclination of Orbit to Ecliptic	1.03 deg
Inclination of Equator to Orbital Plane	3.01 deg
Orbital Period (sidereal)	11.86 years
Orbital Period (synodic from Earth)	399 days
Average Orbital Velocity	13.1 km (8.12 miles) per sec
Radius (average), R_j	69×10^3 km (43×10^3 miles)
Mass	1.902×10^{27} kg
Average Density	1.35 gms/cm^3
Gravitational Acceleration at Poles	26.0 meters (85.2 feet) per sec per sec
Escape Velocity	61 km (38 miles) per sec
Rotation Period	9 hr 55 min

All of the information concerning Jupiter has been gathered from visual observations, spectroscopic determinations in the visible and infrared, and detections of radio emission. These three regions of the spectrum can be observed from Earth, but the data obtained from these regions is probably related only to the upper levels of the atmosphere on Jupiter. More extensive measurements of the electromagnetic radiation in the ultraviolet and infrared portions of the spectrum could profitably be made above the atmosphere of the Earth.

The albedo of Jupiter is relatively high, about 0.4, and its angular diameter is relatively large, 31 to 50 seconds; therefore, the planet is easily seen. When the disc of Jupiter is observed by use of a telescope, it appears to be obviously flattened, and significant limb darkening is seen. Jupiter exhibits a number of alternate light and dark bands running parallel to the equator. The light-colored, yellowish regions are called zones, and the dark-colored bands are referred to as belts. The belts have been observed as being dark gray or brown, and occasional regions in these belts as blue, dark green, or red. A broad equatorial zone is bounded by north and south tropical belts which are followed by north and south tropical zones. There are then a temperate belt, a temperate zone, another temperate belt, and finally a polar region in each hemisphere.

The bands, which are believed to be clouds in the middle levels of the Jovian atmosphere, are quite irregular in their appearance. The temporary and variable nature of such features indicates that movements are taking place within the cloud system that surrounds the planet.

Most of the markings on Jupiter change fairly quickly. There are, however, some of a more permanent nature, lasting from periods of months to many years. One of the most striking is the Great Red Spot which lies mainly in the south tropical zone. It is an oval area, extending approximately 45,000 kilometers in length and 13,000 kilometers in width. The visibility varies in an irregular manner; at times the Red Spot is faintly pink, but there have been periods of one to three years when it has had a definite red color.

The nature of the cloud bands, of the Red Spot, and of other apparent markings is still the subject of considerable speculation.

The spectrum of the planet Jupiter has been extensively studied in the visible and infrared regions. Positive identifications of methane (CH_4), ammonia (NH_3), and the hydrogen molecule (H_2) have been made. The abundances of these and other possible constituents of the atmosphere are not well known.

Experiments involving the occultation of σ Arietis have been used to derive an atmospheric mean molecular weight of $\mu = 3.3 \pm 0.5$. Such a low value indicates that the bulk of the atmosphere is composed of hydrogen and helium. In most theoretical determinations of the Jovian atmosphere, neon and argon are also considered present.

Powerful radio emissions have been detected from Jupiter. The radiation falls into three wavelength regions: the centimeter region, the decimeter region, and the decameter region. In the first region, the radiation is believed to be mostly thermal; in the latter two, nonthermal.

The radiation from Jupiter in the decimeter region has been studied in the range from 10 to 68 centimeters. This radiation, which is characterized by long-term variations, is emitted continuously. The most satisfactory explanation of this radiation is that it is emitted by high-energy electrons spiraling around the lines of force of the Jovian magnetic field. The electrons responsible for the emission are trapped in radiation belts similar to the Van Allen zone in the Earth's magnetic field. The observations could be accounted for by synchrotron radiation if the strength of the magnetic field of Jupiter in the emitting region is on the order of 10 gauss. The

main emission appears to come from the equatorial regions of Jupiter at distances from about 1.5 to 3.0 planetary radii.

The third type of radio-frequency emission from Jupiter is in the decameter range from 10 to 30 meters. The emission occurs in bursts. These bursts, which last a second or so, are generally observed in groups lasting for 5 or 10 minutes and occurring continually over a period of a few hours. There is as yet no satisfactory explanation of Jupiter's decameter radiation. Several theories have been proposed to explain this emission. The emission exhibits several of the characteristics associated with lightning on Earth, but the energy from Jupiter is on the order of a billion times greater. There is some evidence that the radiation is of the cyclotron type originating high in the Jovian atmosphere. Another possibility is that the bursts are caused by plasma oscillations in a Jovian ionosphere.

2.1.2 Magnetic Field Measurements

The strong magnetic field of Jupiter offers an interesting opportunity for investigation. The existence of a strong field has been inferred from the examination of the nonthermal radio emission from Jupiter, as discussed in the preceding section. The most plausible description of the magnetic field of Jupiter presently available is that the major part of the planetary field is caused by a dipole component aligned at an angle of about 10 degrees to the axis of rotation. The sense of the dipole moment is believed to be opposite to that of the Earth.

Jupiter is a large and rapidly rotating planet. Large-scale fluid or atmospheric motions are observed on the surface. If convective fluid motions occur in the core, a hydrodynamic dynamo may operate to produce a magnetic field. Accurate measurements of the magnitude and orientation of the Jovian magnetic field would contribute to a quantitative refinement of the dynamo theory.

The intensity and the spatial distribution of a planet's magnetic field control a number of important phenomena. The size and shape of the cavity in the solar wind containing the magnetosphere of a planet is determined by the deflection of the plasma flow by the planet's magnetic field. The energy distribution of energetic particles incident on a planet is also controlled by the planet's magnetic field. Many of the phenomena related to magnetic storms and auroras on Earth are related to the geomagnetic field. The latitude of maximum occurrence of auroras on the Earth is apparently determined by the outer boundary of the region of trapped radiation in the Earth's magnetosphere. Particles that enter the atmosphere to produce auroras are either accelerated within the magnetosphere or are injected into the magnetosphere from the solar plasma.

Knowledge of the distribution and variation of the magnetic fields of planets permits useful inferences concerning their interiors. For example, studies of geomagnetic data have shown that (1) motions of material are probably going on within the Earth; consequently the existence of a fluid core is suggested; (2) changing electric currents and winds in the upper atmosphere induce changing earth currents; consequently, the electrical conductivity of the Earth's crust is indicated; (3) parts of the Earth have different structures, i.e., mineral deposits, ocean floors, etc.; and (4) the field is self-maintained. Similar results should be obtained from measurements of the Jovian magnetic field.

A planetary magnetic field causes a transition region to exist between interplanetary space and the region close to the planet. In the generally accepted theories which are supported by a few measurements of the geomagnetic field at tens of Earth radii, the existence of a characteristic transition region called the magnetopause is predicted. This magnetopause separates the planetary field from the ionized component of the interplanetary medium. The planetary magnetic field is confined to a tear-drop shaped cavity inside the interplanetary gas.

An estimate of the extent of Jupiter's magnetosphere can be made in the following way. If Jupiter were not rotating, and if the flow of the solar wind were laminar at Jupiter's orbit, then the magnetospheric envelope would be tear-drop shaped, with a stagnation point at the front. If an inverse square dependence upon distance is assumed, the energy density of the solar wind at the orbit of Jupiter is about 1/25 that at the orbit of Earth. Then, if the magnetic field near Jupiter's surface at the equator is in the vicinity of 20 gauss, the distance of the stagnation point from the center of the planet is 60 R_j, where R_j indicates a distance of one Jovian radius.

Actually, however, the rotation of the field must exert a great influence on the boundary location. If the solar-wind velocity is disregarded and it is assumed that Jupiter is rotating in a sea of stationary plasma, the plasma will possess an apparent circulatory motion relative to the field. At the magnetospheric boundary, the apparent kinetic energy density of the plasma must be approximately equal to the magnetic energy density:

$$\frac{R}{R_j} = \left(\frac{H_e}{\omega R_j}\right)^{1/4} (4\pi n m_p)^{-1/8}$$

where R is the approximate distance from the center of the planet to the magnetospheric boundary in the equatorial plane; H_e is the equatorial magnetic field at the Jovian surface; is the angular velocity of rotation; n is the number density of protons; and m_p is the mass of a proton.

If n at Jupiter's orbit = .4 cm^{-3}, then

$$R \approx 50R_j$$

Although the actual situation is much more complicated, such an estimate seems reasonable.

The great strength of the Jovian magnetic field and the flyby trajectory should enable such measurements to be made at points well inside the magnetopause. Such measurements would be used to determine the geographic and altitude dependence of the undisturbed planetary field. It might then be possible to infer the multipolarity of the source and its orientation with respect to the planetary rotation axis.

A second objective set for a magnetometer experiment is the measurement of the interplanetary magnetic field. Preliminary measurements beyond the magnetopause of the Earth indicate that, approximately 20 percent of the time, magnetically quiet conditions prevail in the steady interplanetary field of approximately 3 gamma. Accurate measurements of this field will contribute to our understanding of the dynamics of the solar system. It will also be possible to study the long-period fluctuations in the interplanetary magnetic field. These data could lead to important information about solar disturbances and about the existence of hydromagnetic waves or magnetized plasmas in interplanetary space and to estimates of the kinetic energy density of the interplanetary plasma.

Ideally, a space magnetometer would be used to measure the magnitude and orientation of the magnetic field vector with an absolute accuracy of a fraction of 1 gamma. It would be used to provide measurements over a range in field magnitude between about 10 gauss near the Jovian surface to 1 gamma (10^{-5} gauss) in interplanetary space and to record fluctuations of the vector field over a frequency range between zero and several thousand cycles per second. This instrument would be light-weight, exhibit low power consumption, and be unaffected by shock, vibration, and extremes of temperature. Unfortunately, like most utopian designs, none of the instruments presently available meets all of these specifications. The magnetometers which seem most suited for use in a Jupiter flyby mission are the helium, rubidium, or cesium vapor-type magnetometers.

The physical principle underlying the operation of the helium magnetometer involves the transparency of a plasma of metastable helium atoms to a beam of resonant radiation at 1.083 μ wavelength and the dependency of this transparency on magnetic fields. Although this type of magnetometer is very accurate and stable, it has a relatively low dynamic range and, as such, its application is limited for a Jupiter flyby mission since it must be used with another instrument.

A self-oscillating rubidium or cesium vapor magnetometer, may be developed which is capable of operating over the entire range of magnetic field encountered. Such a development is within the present state of the art if internal electronic switching is used. An instrument of this type may operate in a range of from 3 to 30,000 gammas with an accuracy of about 0.1 gamma and in a range of 0.25 to 10 gauss with an accuracy of about 20 gammas.

One objection to the use of this type of magnetometer is that the self-oscillation continues only under optimum conditions of vapor pressure temperature, 25° to 45°C; consequently, environmental temperature control within these limits is required.

Although it may become apparent that the advantages inherent in using a single instrument outweigh the present advantages of using two instruments (such as better accuracy), for purposes of this study two magnetometers, i.e., two separate sensors sharing a common electronics package, will be utilized in the scientific definition.

The electronics package may be mounted in the main part of the spacecraft. It would weigh about 5.0 pounds and require about 7.0 watts of power. The two sensing elements would weigh 1.5 pounds each.

In order to minimize the magnetic background from the spacecraft and its components, each of the two magnetometer sensors should be placed at an extreme extension of the spacecraft. As a general rule, the background field should be less than 0.5 gamma; consequently, every component placed on the payload should be magnetically checked and shielded if necessary. If absolutely necessary, highly coercive magnets may be appropriately located in the main body of the spacecraft to cancel the spacecraft field at the magnetometer.

2.1.3 The Detection of Charged Particles in Interplanetary and Planetary Regions

During a Jovian flyby mission, high-energy radiation will be measured over a relatively long time and over significantly varying spatial coordinates. These two features will allow the

collection of information useful for understanding the nature, origin, and behavior of such radiation. An approximate classification of the energy ranges of corpuscular radiation is presented in Table 2.1-2. The extension and propagation of solar coronal material, i.e., the solar wind, would consist of ions and electrons exhibiting energies less than 30 keV, the mean thermal energy of the Sun.

Table 2.1-2 ENERGY RANGES OF CORPUSCULAR RADIATION

EXTRA - GALACTIC COSMIC RAYS	
Nucleonic	$>10^{17}$ eV
GALACTIC COSMIC RAYS	
Nucleonic	10^{7} - 10^{16} eV
Electronic	$>10^{5}$ eV
SOLAR COSMIC RAYS	
Nucleonic	$>10^{12}$ eV
Electronic	10^{3} - 10^{7} eV
TERRESTIAL RADIATION BELTS	
Nucleonic	10^{3} - 10^{9} eV
Electronic	10^{3} - 10^{7} eV
JOVIAN RADIATION BELTS	
Nucleonic	10^{6} - 10^{9} eV
Electronic	10^{6} - 10^{8} eV
TERRESTIAL AURORAE	
Electronic	10^{3} - 10^{5} eV
JOVIAN AURORAE (?)	
Electronic	10^{4} - 10^{6} eV

Much of the electromagnetic radiation and most of the particles emitted by the Sun and other sources never reach the surface of the Earth (or Jupiter) because of the protection of the atmosphere and magnetic field. Although the mechanisms of the trapping of charged particles are not well understood, extensive radiation belts around the Earth are believed to be caused by the interaction between the upper atmosphere of the Earth, the geomagnetic field, and the incoming corpuscular radiation. These trapped charged particles spiral back and forth along the lines of force of the magnetic field. The particles are predominantly, and perhaps exclusively, protons and electrons. From an analysis of radio emission from Jupiter, two radiation belts have been inferred. One is centered at a distance of 1.5 planetary radii from the center of Jupiter. The other extends from about 2 to at least 3.5 planetocentric radii. The most reasonable estimate is that the latter belt consists mostly of electrons with energies in the range of 1 to 10 MeV. Measurements of energy spectra in the Jovian radiation belts would provide a fruitful source of information in itself and also be applicable to still unresolved questions concerning the terrestrial radiation belts.

The corpuscular radiation, which is probably a source of the planetary radiation belts, is of primary interest in interplanetary space. Throughout the universe, certain physical processes result in the formation, ionization, and acceleration of matter. The motion of these charged particles results in the formation of magnetic and electric fields. The further interaction of these moving particles with other magnetic and electric fields results in their further acceleration. Consequently, there exists a whole continuum of charged particles which exhibit energies from thermal to at least 10^{21} eV and nuclear structures from that of hydrogen (single protons) to that of heavier materials (at least iron).

Galactic cosmic rays are those particles which are accelerated outside of our solar system and arrive with energies greater than about 10 MeV per nucleon. The features of galactic cosmic rays which are most easily investigated are (1) their energy and charge spectra and (2) the changes of their characteristics with time.

The Sun is also a source of cosmic rays. When a solar flare occurs, a tongue of high-energy particles erupts from the Sun's surface. The charged particles drag along the lines of the solar magnetic field which become frozen into the cloud. As the force lines become distended, they lose their strength. The field is still strong enough, however, to cause a partial

screening of that portion of the solar system containing the Earth from the galactic cosmic rays.

The composition of the primary cosmic radiation striking the top of the Earth's atmosphere is approximately 85 percent hydrogen; 12 percent helium; 1 percent in the carbon, nitrogen, and oxygen group; 0.25 percent in the lithium, beryllium, and boron group; and 0.25 percent in the neon and heavier groups. The flux of nuclei in the Li, Be, B, and C-N-O and heavier groups is greater than would be expected from present estimates of stellar abundances. There are practically no data on the primary cosmic-ray electrons and positrons. Further measurements would help to differentiate solar and extrasolar abundances.

It appears reasonable to assume that the flux of cosmic rays incident on the solar system is constant. In the vicinity of Earth, however, large modulations are observed, and they appear to be controlled by solar activity. The two most important types of modulation are the 11-year variation and the Forbush decrease. It was first noted by Forbush that the cosmic-ray intensity varied inversely with the solar activity corresponding to an 11-year cycle. Forbush also observed the rapid worldwide decreases in cosmic-ray intensity associated with some types of solar magnetic flares.

The modulation effects are interpreted as being caused by large-scale variations of the solar magnetic field. Increases of the magnetic field strength near the Earth result in the deflection of the lower energy particles before they penetrate this field. This interplanetary field arises from two sources. A relatively steady magnetic field is the result of the streaming plasma from the Sun. The Forbush decreases are caused by somewhat more localized fields generated as a result of large solar flares.

Cosmic rays play a major role in the physical processes taking place in the Universe. The energy density of galactic cosmic rays is of the same order of magnitude as the kinetic energy of interstellar matter and the magnetic energy density in interstellar space.

One of the most fundamental questions to be answered by future exploration of interplanetary space is that of the galactic cosmic ray flux in interstellar space. It is now believed that these cosmic rays play a significant role in the dynamics of the universe, and a knowledge of their flux is required to construct a more realistic cosmological model.

In connection with the physics of the Sun and the circumsolar space, it will be interesting to determine (1) the conditions required for the propagation of galactic cosmic rays within the limits of the Solar System and (2) the mechanisms which are responsible for the generation, composition, and conditions of propagation of solar cosmic rays.

A cosmic-ray detector, i.e., a charged-particle detector, will be used

1. To monitor solar, galactic, and extragalactic cosmic rays in interplanetary space and provide data for the study of their angular distribution, energy spectra, and time histories.

2. To search for magnetically trapped particles in the vicinity of Jupiter and provide data for estimates of their spatial distribution, energy spectra, and identity.

3. To provide similar information concerning the Van Allen belts, if desired.

Estimates of the charge spectra and chemical composition would also be desirable, but these estimates could perhaps be obtained from circumterrestrial or lunar experiments.

2.1.3.1 Particle Detectors

A large number of physical techniques are required for the detection and analysis of the extreme energy scale of corpuscular radiation. The most efficient of terrestrial detectors, such as nuclear emulsion or electrostatic-magnetic analyzers, are ruled out because of weight limitations. Three basic types of detectors are under consideration:crystal, solid-state, and gas ionizing. The use of a combination of these types would cover the range of energies indicated in Table 2.1-2.

In all particle detectors, the interaction between a sample (with associated electronics) and an incoming particle is used as the basis of detection. The Čerenkov counter depends on the production of Čerenkov radiation by the passage of relativistic particles through a dielectric medium. Some variation of the particle-energy threshold is made possible by the choice of the gas or liquid used as a sample. This detector, as well as other detectors, is usually used in a coincidence arrangement with one or more particle detectors to limit both the kinds of particles detected and their energy range. Such packages, which also restrict the physical path of detected particles, are called telescopes.

A similar detector, the scintillation counter, depends on the production of fluorescent radiation (which can be monitored by photomultipliers) by passing high-energy particles through a suitably chosen crystal. Again, when a choice is made from a number of organic or inorganic crystals, variations in energy thresholds can be attained.

A relatively simply instrument which contains a gold-silicon (Au - Si) surface barrier detector is available for measuring protons. The sensitive elements of such a solid-state detector are thin wafers of high-resistivity silicon with a very thin film of gold evaporated on the front surface. A space-charge region extends from the Au - Si interface into the bulk of the silicon. The thickness of this region is adjusted (by adjusting the potential difference across the wafer) to approximate equality with a particular proton energy range. A charged particle incident on the detector will penetrate the thin gold film and produce electron-hole pairs as it passes through the space-charge region. The liberated ion pairs are swiftly swept apart by the high electric field in the space-charge region; this action results in a measurable voltage pulse proportional to the amount of energy lost by the particle in passing through the sample.

A similar device is the semiconductor detector which is a small crystal of photoconductive cadmium sulfide (CdS). The sensitive element is approximately 2 millimeters square and between 0.1 and 0.3 millimeter thick. The electrical conductivity of such a sample is proportional to the rate of the deposition of energy of ionization in the crystal. If a constant voltage is applied, the current flow through the crystal can be calibrated in terms of energy flux.

A Neher-type ionization chamber consists of a spherical volume of argon gas contained by a thin steel wall. This detector is used to measure the ionization produced in the argon by all naturally occurring ionizing particles: those produced by secondary particles generated in the spacecraft which can penetrate the chamber walls, and those caused by secondary particles generated in the ion-chamber walls and gas. The flux of particles or current passing through the gas is easily measured and correlated with an ionizing particle.

In the Geiger-Muller counter, the ionizing power of nuclear radiations is also used as a basis for particle detection. Extensive variation in relations between response and detected particles are made possible through the use of various geometries, shielding, and kinds of wall material.

Each type of radiation detector discussed above can, over a large range, be adjusted to a minimum-threshold level of energy. The use of any radiation detecting instruments on a Jovian mission would involve two or more similar or dissimilar instruments in a coincidence telescope arrangement. Such an arrangement will serve to control the energy ranges accepted and to discriminate quite effectively against gamma rays from the Radioisotope-Thermalelectric-Generator (RTG). The radiation from the RTG should pass at large angles to the axis of any telescope so that electrons produced by the large gamma ray flux will not be counted. Consequently, in the presently considered spacecraft design concepts, the sensors would be mounted on the main body of the spacecraft. Shielding would be required for a non-telescoping detector, either by using absorbing material or by placing the detector at safe distance from the RTG units. Because of the microsecond coincidence times in the associated electronics, the flux produced by the RTG will be negligible in comparison with the expected planetary and interplanetary flux. Especially high fluxes of gamma rays and neutrons from the RTG could be kept from the sensors by absorbers in the vicinity of the detectors. The effects of the RTG in the science subsystem are described further in subsection 3.9.

2.1.3.2 Energetic Particle Detector

In the case of planetary investigations, the energy range of most interest would comprise the regime of magnetically trapped particles, i.e., a few keV to a few MeV. Detectors which are operated in this area would also yield information on the space and time variation of galactic and solar cosmic rays in interplanetary space.

The "Trapped Radiation Detector" designed by Van Allen and used on Ranger and Mariner flights is an extremely useful and versatile instrument. A typical package for use in the measurement of energetic particles contains a system of five detectors. Herein, it is designated as the "Energetic Particle Detector." The following discussion is derived from the experiment as used on Mariner IV, but it can be regarded as representative of the particle detector in a Jupiter flyby mission.

Three of the detectors, called A, B, and C, are Geiger-Muller end-window counters which measure the total number of charged particles passing through their sensitive volumes. The sensitive volume of each tube is shielded so that low-energy particles can enter only by passing through the window at the end of each tube. Only higher-energy particles can penetrate from other directions. If an allowance is made for the non-directional counting of higher energy particles, a directional measurement of the low-energy particles can be made.

The other two detectors, D_1 and D_2, are essentially one unit, a silicon surface barrier diode. The detector is virtually insensitive to electrons of any energy. Through amplitude discrimination in the associated electronics, two levels of proton energy discrimination are recognized.

A representative range of such an instrument is presented in Table 2.1-3. Within limits, shielding could be used to vary the listed operating regions.

In order to determine proper in-flight operation, the solid-state detector is equipped with a source of 5.5 MeV alpha particles. The counting rate of each of the three Geiger tubes is the sum of the rates caused by galactic cosmic rays, electrons, x-rays, protons, alpha particles, and other particles, which pass through their collimators; and, in some cases, by sidewall penetrations. Combinations of data from this system provide information on absolute intensities, particle identification, energy spectra, and angular distributions. In favorable cases, particle identification is conclusive.

The five particle detectors of this experiment are combined in one package of a total weight of 2.5 pounds. The power required to operate the system is 0.4 watt. There are 4 sensors mounted on a magnesium chassis. Detector A will be constructed so that (1) the look-angle axis is directed at a 135-degree angle to the probe-Sun line, (2) the full-look angle will be 60 degrees, and (3) no payload structure will obscure its conical field of view. In Detectors B, C, and D, the look-angle axis will be directed at a 70-degree angle to the probe-Sun line, the full-look angle will be 60 degrees, and no payload structure will obscure their conical field of view. The counters must be protected from direct sunlight during the trip.

A radiation detector could be made up of a group of instruments different from those listed above. As a general rule, on earlier missions, the use of Geiger-Muller (G-M) tubes rather than the more sophisticated solid-state telescope coincidence detectors or the very heavy Čerenkov or scintillation counters would be preferred. The G-M tubes offer the advantage of counting all energetic particles above a certain minimum-threshold energy. Solid-state detectors are usually sensitive only to protons in a rather narrow energy range. A further advantage of G-M counters is that they recover quickly after being saturated by radiation. The major disadvantage of G-M tubes is their lack of energy resolution. This defect can be partly overcome by choosing combinations of ionization tubes and Cd-Si detectors.

By pointing identical detectors in different directions, directional information about the detected radiation can be obtained. A telescope arrangement with a coincidence counting circuit, such as D_1 and D_2 above, could incorporate Geiger-Muller tubes to provide discrimination against RTG-produced background radiation.

Table 2.1-3 ENERGY RESPONSE OF ENERGETIC PARTICLE DETECTOR

Detector		Energy (MeV)
G-M Tubes		
A	Electrons	0.04
	Protons	0.50
B	Electrons	0.04
	Protons	0.50
C	Electrons	0.13
	Protons	3.00
Solid State Detectors		
D_1	Protons	0.5- 11.0
D_2	Protons	0.9- 4.0

2.1.3.3 Ion Chamber

Another particle detector system used on Mariner vehicles consists of an ionization chamber, a Geiger-Muller tube, and associated electronics. This system is used to detect and measure the average omnidirectional flux of corpuscular radiation between Earth and Jupiter by determining the average specific ionization caused by this flux. It is also intended for the measurements of trapped particles in the vicinity of Jupiter.

Both the ionization chamber and the G-M tube detect particles of the same energy, i.e., electrons of energy greater than 0.5 MeV, and alpha particles of energy greater than 40 MeV. Both sensors have omnidirectional sensitivity.

The Ion Chamber unit weighs 2.6 pounds. The power required is 0.5 watt. The bit rate is 20 bits per sample. The two sensors should be mounted as close together as possible so that they receive a similar radiation flux. In order that the main body of the spacecraft subtend the minimum solid angle with regard to the detector, this unit should be mounted on a boom away from the main chassis.

Because of the large, sensitive volume of the ion chamber, it is especially susceptible to background radiation from which spurious counts are produced. Such counts could be produced by the radiation from the Radioisotope-Thermalelectric-Generator (RTG). Local shielding of the ion chamber could be provided by covering the sensitive surface area of the chamber, but the energy threshold of the detector would thereby be raised. A more suitable solution can be obtained by extending the chamber from the spacecraft body or designing it to measure fluxes so large that the background radiation from the RTG would be negligible and spurious counts would not be registered.

2.1.3.4 High-Energy Proton Directional Monitor

The high-energy proton directional monitor has been proposed for obtaining information regarding the temporal, spatial, and directional variations in galactic cosmic ray flux. A Čerenkov or scintillation counter would be used to measure the fluxes of particles which exhibit energy greater than 1 BeV.

The sensing units consist of four conical receptors; each unit is provided with a look angle of 60 degrees. While the location of this package is not critical, it must be mounted in such a way that the view of each sensor is not obstructed by the spacecraft.

The size of this unit has been estimated to be 3 by 4 by 4 inches. The weight is 4 pounds. The power required is 0.5 watt. Data handling is quite similar to that of the charged-particle telescope described below; however, the bit rate is 60 bits per sample. The reliability of Čerenkov and scintillation counters would probably ensure that no in-flight calibration is required.

2.1.3.5 Cosmic-Ray Spectrum Analyzer

The cosmic-ray spectrum analyzer is designed to be used in the study of the energy region of primary interest in the case of solar and galactic cosmic rays. The energy range would include 1 to 400 MeV protons. The objective of such an experiment is to determine the intensity and flux gradient of charged particles in interplanetary space as functions of nuclear species and time. In order to measure the mass, energy, and charge of high-energy particles, improved versions of integrating and differential Čerenkov counters of the type used in Russian satellites would have to be developed.

An estimate of the design characteristics of such an instrument has been made by Professor Simpson of the University of Chicago. The general design of the experimental package

would be similar to that of the High-Energy Proton Directional Monitor. The 4 sensors of 60-degree look angle must be appropriately mounted. For the case of the Mariner B spacecraft, this cosmic-ray spectrum analyzer was to be 6 by 6 by 18 inches, the weight being 18 pounds. The power required is 2.0 watts. Data would be received at a rate of 70 bits per sample.

2.1.3.6 Medium-Energy Proton Directional Monitor

The medium-energy proton directional monitor is intended as a secondary detector to back up both investigations of cosmic rays and measurement to planetary radiation belts. The design range is intended for the measurement of particles of energy 10 to 30 MeV, but it can be easily extended to 3 to 50 MeV. The geometry and location requirements are identical to those of the Cosmic-Ray Spectrum Analyzer. The size of such an instrument, proposed for a Mariner B spaceflight, is 4 by 4 by 5 inches, the weight being 3 pounds and the power requirement 1.0 watt. Data would be taken at a rate of 60 bits per sample.

2.1.3.7 Charged-Particle Telescope

The charged-particle telescope was on board the Mariner IV and functioned according to design specifications. This unit consists of three Au-Si, surface barrier detectors, together with aluminum and platinum absorbers. Two circular detectors, D_1 and D_2, have surface areas of 2.4 square centimeters. The area of detector D_3 is 5 square centimeters. In detectors D_1 and D_2, an acceptance cone angle of 40 degrees is provided for the charged particles that are arriving. The geometrical factor provided for D_3 is determined by the exact location of a necessary temperature control fin.

The counting rates of charged particles fall into three intervals of particle energy. The ranges are listed in Table 2.1-4.

Table 2.1-4 INTERVALS OF PARTICLE ENERGY

	1	2	3
Protons	15-80 MeV	15-80 MeV	80-190 MeV
Electrons	.18-.35 MeV	none	none
Alphas	2-60 MeV	60-320 MeV	320 MeV

The instrument is able to separate protons from alpha particles. The complete package weighs 2.6 pounds; 0.6 watt is needed for operation. The average information-bit rate for this experiment

is 40 bits per sample. At periodic intervals, the instrument is switched to a "calibrate" mode in order to check the performance of individual detectors.

The charged particle telescope must be mounted so that a 60-degree opening angle with apex at the front detector is not obstructed in its view of space when it is pointed away from the Sun. Within this cone angle lies the 40-degree opening angle of the telescope. The package must be electrically isolated from the spacecraft chassis except for a single wire into the DAS. In the case of Mariner IV, a mechanical envelope was used to provide a circular hole in the frame so that a thermal radiating shield could maintain a low temperature for the telescope.

2.1.3.8 Triple-Coincidence Cosmic-Ray Telescopes

A similar but more versatile instrument has been flown successfully on Explorer VI and Pioneer V. This radiation detector consists of an assembly of seven proportional-counter tubes. Six of the counters are grouped in a concentric ring around the seventh counter; the outer counters are connected in two adjacent groups of three to form two triple-coincidence telescopes.

The high-energy unit has a threshold of 75 MeV for the case of a triple-coincidence count caused by protons and a threshold for the case of electrons of 13 MeV. The threshold for detection of electrons through their bremsstrahlung radiation is approximately 200 keV. The thresholds for particle detection by means of the low-energy telescope are approximately 10 MeV for the case of protons and 0.5 MeV for the case of electrons.

The total weight of the coincidence telescopes is 9 pounds and the total power requirement is 0.5 watt. Two telescopes are placed so that their axes are normal to the probe-Sun line in such a way that particles incident from the general direction of the Sun can be seen by both high- and low-energy telescopes.

2.1.4 Solar Plasma Measurements

In addition to the solar cosmic rays produced by large flares, a number of lower-energy charged particles are continuously given off by the sun. This production of plasma is essentially a hydrodynamic expansion of the solar corona. This stream of particles is termed the solar wind. An important effect of the solar plasma is the distortion of the shape of the geomagnetic cavity within which the Earth is located. This

boundary is a rather sharply defined surface separating the region within which the Earth's magnetic field exerts primary control over the particle motion from the interplanetary region. A similar transition region should occur in the vicinity of Jupiter. This region would be one of the primary targets to be observed by means of a solar plasma detector.

The interplanetary plasma, which is the solar wind, consists of ionized hydrogen and helium whose energies range from a few keV to hundreds of keV. The flux decreases as the distance from the sun increases; probably as $1/r^2$.

Outside the magnetopause, the main field of the Sun, rather than the trapped field of the plasma, is dominant. The solar wind carries part of the solar field with it and stretches out the lines so that they are very nearly radial in the vicinity of the Earth. A more accurate picture is given by consideration of an Archimedean spiral, which results from the fact that the field lines are carried around by the rotation of the Sun. This is analogous to a rotating lawn sprinkler, which squirts water out radially, but makes a spiral pattern in the air at any instant of time. It may be that the solar wind is not smooth and regular, but turbulent; in which case the magnetic field lines trapped within it will become distorted. This phenomenon should occur at some large distance from the Sun, probably well beyond the orbit of Earth. The time and space variation of the solar plasma between Earth and Jupiter would help to differentiate between several theories of solar wind propagation.

The solar plasma experiment is designed to measure the flux and energy spectrum of the positively charged components of streams of solar plasma. The plasma flux measured by Pioneer V, Mariner II, and IMP in the vicinity of 1 AU averaged about 10^8 ions per square centimeter-second; however, this value fluctuates one or two orders of magnitude. This value corresponds to an electrical current density of only 1.6×10^{-11} ampere per square centimeter. At 5 AU, currents would be expected to be lower by an order of magnitude; when the total current is divided into several angle and energy channels, individual currents (which are another order of magnitude below this level) could be expected. The instruments developed for use in Mariner II and Mariner IV exhibit a threshold sensitivity of 10^{-13} ampere per square centimeter. This value should be extended one or two orders of magnitude for the case of a flyby mission to Jupiter.

The plasma analyzer used on the Mariner IV was designed to sample the plasma energy spectrum from 10 eV to 10 keV. This probe consists of a solar-oriented electrostatic particle-energy analyzer which selects the desired particles; a Faraday cup that collects the charge of the particles which traverse

the electrostatic field; an electrometer circuit for measuring the current caused by this collected charge; and a high-voltage generating system, which consists of a programmer and a sweep amplifier and is used to apply a sequence of voltages to the analyzer plates.

The entire experiment is mounted on the main chassis of the spacecraft; the entrance end of the analyzer plates is extended and pointed toward the Sun. The weight of the unit is estimated to be about 7 pounds. The power required is 2.5 watts.

2.1.5 Cosmic Dust Measurements

A knowledge of the spatial and temporal density of cosmic dust between the Earth and Jupiter (particularly in the asteroidal and near-Jupiter regions) is of great importance, both for understanding the sources and dynamics of these interplanetary particles and for the design of future manned and unmanned spacecraft and equipment.

An understanding of the nature, origin, and dynamics of the cosmic dust in interplanetary space is helpful in formulating any theory of the origin and evolution of the solar system. There are at least four possible sources for these particles:

1. The disintegration of comets
2. The collisional fragmentation of larger solid bodies, such as the Moon, the asteroids, or other planetoids
3. Interstellar particles which move through the solar system
4. Primordial particles remaining from the formation process of the solar system.

Prior to space exploration, small solid extraterrestrial masses had been observed by recovering and examining meteors and meteoritic dust which penetrated the Earth's atmosphere; by visual and radar observations of meteor trails; and by measurements of the zodiacal light, gegenschein, and solar corona. With the advent of space flight, direct measurements of the dust were conducted by means of space probes. These initial studies revealed a higher concentration of very small particles in the vicinity of the Earth than had been predicted from the earlier studies. In addition, the existence of particle "streams" was indicated. Concentrations of cosmic dust (of the very small particles) are thought to be dispersed by the Poynting-Robertson and other drag effects, as well as by the cumulative effects of small differences in the orbital

elements of the individual particles. Any large concentration of particles such as the "streams" should therefore be of relatively recent origin.

Measurement of the dust in interplanetary space, outside of the Earth-Moon system, has been relatively limited. In Mariner II, a crystal microphone detector measured only two impacts on its interplanetary trip to Venus. This unit was capable of measuring particles with a momentum down to about 7×10^{-4} dyne-second (or to a mass of 1.4×10^{-10} grams if a relative velocity of 50×10^{5} centimeters per second is assumed). The flux was thus calculated to be 6×10^{-6} particles per square meter-second-steradian. Mariner IV was capable of measuring particles with a momentum of at least 6×10^{-5} dyne per second. The data taken by means of this probe, which included over two hundred impacts, indicated an increase in the flux level with an increase in heliocentric distance from the Earth to a maximum of 3.3×10^{-4} particles per square meter-second-steradian at a distance of 1.36 to 1.43 AU from the sun to 1.8×10^{-4} particles per square meter-second-steradian in the vicinity of Mars.

The trajectory to Jupiter will extend a distance from the sun of about 5 1/2 AU, will involve a path through the asteroid belt, and will pass near to the planet, probably within the orbits of its moons. Present data are insufficient to predict what flux levels or average particle sizes will be encountered.

The cumulative influx rate of the micrometeoroids, as a function of particle mass, has been observed near the Earth to increase logarithmically with decreasing particle size down to the Poynting-Robertson limit of about 10^{-11} gram. Whether or not this relation, combined with the Mariner data, can be extrapolated to define the micrometeoroid environment of the asteroid belt and the Jupiter environs is not certain. It may well be that there is a higher relative concentration, especially of the larger particle sizes in the asteroidal region between Mars and Jupiter, than between Earth and Mars.

To date, most of the measurements of micrometeoroids have been made by means of a piezoelectric crystal microphone detector. Upon impact, the output of the microphone is proportional to the momentum of the impacting particle (except at extremely high velocities). Thus, if a velocity for the particle is assumed, its mass may be calculated. In another type of detector, a photomultiplier device is used to measure the light flash of an impact. This instrument, which is also used to measure a mass-velocity combination (energy), is capable of measuring a much smaller mass than the microphone detector, but it is not as simple in operation nor as reliable.

There are other types of detectors which have been used or proposed, but they probably would not be as suitable for the first Jupiter mission. A possible exception may be devices similar to those used on Explorer XVI to observe the larger particles.

In addition to the mass-velocity combination measurements, other information relevant to the particles would be useful; these include mass and velocity alone, penetrating and cratering ability, electrostatic charge, and composition and other physical properties. While instruments capable of performing these measurements will eventually be developed, a proven device is suggested for use in this study.

A suitable cosmic dust detector is one similar to the instrument used on the Mariner IV spacecraft. An advantage to using this instrument is that the data from the two probes would then be directly comparable. This device detects the impact of cosmic dust particles upon a sensor plate. This sensor is an aluminum plate .030 inch thick. A crystal acoustical transducer that yields a signal amplitude proportional to the momentum of the particle is bonded to one side of this plate. The sensor plate is coated on both sides with a dielectric material. A thin film of aluminum is then deposited over this dielectric. The combination of impact plate, dielectric, and aluminum film forms a penetration detection capacitor. When a static potential is connected across the capacitor, an impact will produce a voltage pulse across a connecting resistor. The films are over an order of magnitude more sensitive than the microphone; consequently, their primary function is to indicate the direction of the impacting particle and to detect particle hits below the microphone threshold.

The instrument would be in continuous operation throughout the duration of the mission. It is calibrated in flight, at time periods on the order of one day, by means of an acoustical transducer. Upon receipt of a command, the transducer imparts a mechanical shock to the input plate, producing an output from the detector microphone.

The plate is a bidirectional sensor. The particular plate on the Mariner IV was 22 by 22 centimeters and weighed 0.5 pound. The sensor may be mounted anywhere to provide approximately a π-steradian view (in the Mariner IV it was attached to the electronics chassis in the main part of the spacecraft). The total weight of sensor and associated electronics is 2.5 pounds. The power required is 0.2 watt. One side should look into the plane of the ecliptic (or the plane containing the Earth and Jupiter) in direct motion, and the other side should look into the same plane in retrograde motion.

2.1.6 Television

The obvious advantage of receiving pictures of Jupiter taken by a television camera in a near passage of the planet is an increase in the spatial resolution over that presently available from the Earth. What is not obvious, however, is the actual utility of such pictures.

At the present time, the maximum resolution of surface features on Jupiter, obtainable with large-aperture telescopes on the surface of the Earth, is close to 1000 kilometers. Therefore, only the grossest features, such as the latitude banding and the red spot, are discernable. Since the Earth-based resolution of the large telescopes is limited by the atmosphere, telescopes placed in Earth orbit will allow an increase in the resolution. In the case of a diffraction-limited Earth-orbit telescope with an aperture of 40 inches, the resolution is about one-tenth of a second of arc, or approximately 200 to 300 kilometers at the surface of Jupiter.

It is difficult to predict what detailed information an increased spatial resolution will yield in terms of the data presently available on Jupiter. It is known that Jupiter is cloud-covered, yet these cloud systems are not featureless. Even in terms of the present data, it is possible to surmise, in general, what an increased resolution may yield about several of the visible features.

With a resolution of the order of several tens of kilometers, the fine structure of the features presently observed could be detected. The red spot, for example, may be seen to be characterized by smaller features, a knowledge of which would allow a better explanation of the spot's origin and existence, or the boundaries between the various latitude bands may be examined to establish their fine structure.

In addition, the pictures may provide information regarding the meteorology of the outer Jovian atmosphere. Cyclonic and anti-cyclonic-type features may be visible, and their size and distribution may be indicative of the dynamics of the meteorological processes operating on the planet.

With a resolution ranging from a few kilometers down to a few hundred meters, it may be possible to determine the fine structure of the upper cloud layers in order to establish whether Jupiter's atmosphere is the convective adiabatic or stratospheric isothermal-layer type. Thus, information about the presence of an internal source of heat in the planet would be derived.

While the inspection of the light side of the planetary surface is the most important phase of the television camera mission, there are other observations that would yield useful information. A view of one of the Galilean satellites may provide information concerning the nature of its surface and the presence or absence of an atmosphere. On the dark side of the planet, the presence of large thunderstorms may be indicated by flashes of lightning that would be visible to the camera. Observations of the number and extent of these flashes would yield information concerning the nature and dynamics of the atmosphere. Near the limb of the planet, aurora may be seen, especially within about ten to thirty degrees of the magnetic poles.

In addition to the resolution discussed above, the importance of areal coverage must also be included in the consideration of gathering information by television pictures. The area covered must be sufficient to allow interpretation of the individual specific features or parts of such features observed as they are related to the larger features. Thus, if a requirement is warranted for obtaining an order of magnitude increase in the resolution over an Earth-orbit telescope, this increase must be so effected that the fine structure observed can be interpreted in terms of the larger structure to which it is related.

The trade-offs between resolution and area covered are difficult to establish, but a general assumption of an order of magnitude increase in resolution to be used with two orders of magnitude decrease in areal coverage (actually one order of magnitude decrease in the radius of the areal coverage) is considered adequate for the purposes of this study. Thus, if the resolution of 200 to 300 kilometers is obtained of the whole planetary disc, a resolution of 20 to 30 kilometers is dependent on obtaining a picture (or composite of more than one picture) covering at least one-tenth of the planetary diameter. An apparently attractive, optional method of combining areal coverage with high resolution is to use an auxillary lens on the camera that would permit the taking of wide angle views intermixed every few frames with the high-resolution pictures. This type of data gathering would allow the orientation of the high-resolution pictures on the planetary surface.

For planning purposes, a general-purpose television camera with an angle of view of 1.5 degrees, a raster of 400 lines per frame, and thirty-two shades of gray is conceived. The pictures would be taken in overlapping triplets through three spectrally separated filters (e.g., 3000-5000-8000Å). A special constraint in using filters is to insure that their spectral response does not change appreciably or by an unknown amount as a result of

exposure to the space and planetary radiation environment. The television package weighs 15 pounds, and 10 watts of power are required for operation. The approximate size is 4 by 4 by 10 inches.

Table 2.1-5 contains a list of the areas covered and the spatial resolutions for several distances from the planet in terms of the general-purpose camera specifications described above. The use of this general-purpose camera in a representative mission may be examined by considering a flyby of Jupiter with a closest approach of one-half of a planetary radius, a passage of thirty degrees from the south pole and a program of taking fifty pictures at one-minute intervals, starting at a planetocentric distance of two and one-third Jovian radii. The slant range of the picture series for a fixed-scan camera will vary from about 160,000 to 50,000 kilometers from the visible planetary surface. The resolution and areal coverage attained may be estimated from Table 2.1-5. It should be noted that this sequence will include some pictures of the dark side of the planet. The camera system may be roughly calibrated by taking pictures of free space prior or after the planetary encounter.

This mission may be considered to be representative and may be used in the considerations of mission planning and data handling. However, the actual spectrum of possibilities of various cameras, trajectories, and data handling capabilities is much more involved than is indicated in this description of a single mission. More complicated situations may be envisioned for the larger payloads when use will be made of more than one camera.

A television package consisting of two cameras, one for large areal coverage and one for high resolution, is described below:

Camera I - Raster of 1000 lines per frame
Angle of view of 10 degrees
Thirty-two shades of gray

Camera II- Raster of 400 lines per frame
Angle of view of 1 degree
Thirty-two shades of gray.

The pictures are so oriented that the area covered in pictures taken by Camera II are in known locations within the area covered by the pictures taken by Camera I.

Table 2.1-5 TELEVISION I

Distance from Center of Jupiter (Jupiter Radii)	Distance from Visible Surface of Jupiter (km)	Area Covered* (km on a side)	Max. Theoretical Spatial Resolution* (km)
11.0	700,000	18,300	90
5.0	280,000	7,300	37
4.0	210,000	5,500	27
3.5	175,000	4,600	23
3.0	140,000	3,700	18
2.5	105,000	2,800	14
2.0	70,000	1,800	9
1.8	56,000	1,500	7
1.5	35,000	900	5
1.3	21,000	600	3
1.1	7,000	180	1

* On a plane surface normal to the pointing direction of the camera.

The area covered and the resolution of these cameras for various distances from the planet are given in Table 2.1-6. The weight of this television package is taken as 30 pounds, and 20 watts of power are required for operation. The size is approximately 5 by 7 by 14 inches.

This camera package is considered for use on maximum capability missions.

A constraint relative to all of the cameras is that they must be mounted on the spacecraft in such a location that no light is reflected from any part of the spacecraft into the cameras.

Table 2.1-6 TELEVISION II

Distance from Center of Jupiter (Jupiter Radii)	Distance from Visible Surface of Jupiter (km)	Area Covered* (km on a side)	Max. Theoretical Spatial Resolution* (km)
	Camera I		
11.0	700,000	114,000	228
5.0	280,000	48,200	96
4.0	210,000	36,200	72
3.5	175,000	30,200	60
3.0	140,000	24,200	48
2.5	105,000	18,200	36
2.0	70,000	12,000	24
1.8	56,000	9,600	19
1.5	35,000	6,000	12
1.3	21,000	3,600	7
1.1	7,000	1,200	2
	Camera II		
11.0	700,000	12,200	60
5.0	280,000	4,900	24
4.0	210,000	3,700	18
3.5	175,000	3,100	16
3.0	140,000	2,400	12
2.5	105,000	1,800	9
2.0	70,000	1,200	6
1.8	56,000	980	5
1.5	35,000	610	3
1.3	21,000	370	2
1.1	7,000	120	0.6

* On a plane surface normal to the pointing direction of the camera.

2.1.7 Photometric, Radiometric, and Spectrometric Measurements

Photometric, radiometric, and spectrometric measurements made in a flyby mission of Jupiter have three distinct advantages over those made from the surface of the Earth. These advantages are (1) access to the entire Jovian phase angle; (2) freedom from the absorbing atmospheric envelope surrounding the Earth; and (3) an increase in the spatial resolution of measurements at the planetary surface (and also the greater angle subtended by the planet, which enables the use of a greater amount of energy flux available at the detector).

If the same comparison is made between measurements made in a flyby mission and an Earth-orbit location, it is seen that (1) the resolution advantage is reduced by about an order of magnitude (however, in the case of weak sources, the increase in energy flux may be significant); (2) the advantage of freedom from the absorbing envelope is nearly eliminated; and (3) the advantage of access to the entire Jovian phase angle is retained.

In establishing a scientific payload for a Jupiter flyby at the present time, a decision is necessary regarding the assumption that astronomical Earth orbit measurements will be possible at or before the time period for the flyby mission. Because of mission complexity and long duration, it will be assumed, for the purposes of this study, that higher priority will be given to experiments which can be performed to best advantage only on a mission to Jupiter instead of those which can be accomplished from or near the Earth. Therefore, experiments will be assigned a higher relative importance when they involve (1) the view of locations on the planet that are inaccessible to near-Earth observations or (2) the use of a high spatial resolution.

2.1.7.1 Photometers

A photometer to measure the relative brightness reflected from Jupiter at various phase angles would allow a determination of the phase function for the planet $I(\alpha)/I(o) = \emptyset(\alpha)$. A relatively simple instrument could be used in a limited payload that would merely sample the brightness at a frequency near the solar maximum of around 5000Å at five-degree intervals around the planet. A slight modification to this experiment will include a filter wheel to look in a wide spectral region and also to make polarimetric measurements, thus allowing the definition of the polarimetric phase curve. A filter wheel with filters centered on wavelengths of 3000, 5000, 7000, and 9000 angstroms and two polarizers would provide suitable data.

It is envisioned that a simple instrument to measure only the brightness variation would weigh 2.0 pounds, would require 1.5 watts, and would provide a data output of 30 bits-per-sample. With an increased capability of sampling at several wavelengths and measuring polarization, the instrument would weigh 6.0 pounds, would require 5.0 watts, and would provide a data output of 120 bits-per-sample. These instruments, as with the TV system, will not yield reliable data if light is reflected from any part of the spacecraft into the sensing element. To aid in obtaining an accurate calibration of the data and to provide relative qualitative compositional information across a larger portion of the disk, the photometer would be programmed to scan the planet perpendicular to the flight path in addition to the traverse along the flight path during the measurements. This perpendicular scanning action is important to the calibration of the total intensity measured, because the photometer integrates what it sees within its field of view. Thus, if there are variations within the field of view, an average value will be taken. Because the solid angle of view is constant and the distance from the visible planetary surface changes, that portion of the planet viewed by the photometer decreases as the probe gets closer to the planet. Although this will complicate the interpretation of the data, it is difficult to avoid. The use of a variable focal length lens would probably create more problems than it would solve.

An in-flight calibration of the instrument will have to be made at least twice, once prior to and once after the actual measurements. The calibration will require looking at a very stable internal radiation source (a Čerenkov source is suitable) through each of the filter wheels. Another method of calibration would be to look at a star of known brightness. In order to obtain really useful data, the measurements would have to be accurate to within one percent, or a few tenths of one percent would be especially desirable.

2.1.7.2 Radiometers

A radiometer may be used to measure the temperature distribution of the planet on both the light and dark sides. In addition to a general survey at various phase angles, specific locations on the surface could be examined. An especially interesting locale would be that in the vicinity of the poles where the clouds might be thin enough to permit the observation of the solid surface.

A single- or dual-channel instrument used in a mapping mode would provide significant information relative to compositional lateral distributions. A multichannel device, with wavelengths centered at absorption bands of ammonia and water and at wavelengths between, including the emission around the radiation

temperature peak, would yield important data concerning composition, compositional abundances, and vertical compositional distributions.

A four-channel radiometer, as suggested in Reference 2.1-1, to measure the radiation at 4, 8, 13, and 20 microns is appropriate to the subject mission. The instrument would weigh 28 pounds, would require 6 watts of power, and the antenna would be about 30 centimeters in diameter. There would be a data output of 40 bits-per-reading. If a reading is made once every five minutes starting three hours prior to perijove, once every minute one hour prior to and continuing until one hour after perijove, and then again every five minutes to three hours after perijove, sufficient data should be provided for this measurement. The instrument would be calibrated after each measurement by reference to an internal noise source.

An infra-red radiometer may be used to measure the thermal emission from the planet, and also to derive some information about the composition of the atmosphere. Although this instrument is somewhat redundant to the microwave radiometer, such redundancy is desirable on an extended mission. Mapping of the surface at at least two wavelengths would aid in the study of the unexplained radiation leak. A view near the poles is also suggested. A two-channel instrument operating at 10 to 20 microns is satisfactory. Such an instrument would weigh about 5 pounds, require 3 watts of power, and would have a data output of 20 bits-per-reading. The readings would be taken in the same schedule as given for the microwave radiometer. The instrument would in fact be mounted with the microwave radiometer antenna.

2.1.7.3 Spectrometers

An infra-red spectrometer should also be considered for use in obtaining data relevant to the planetary compositions and composition abundances. The device would operate in the region from approximately 5 to 30 microns, with a resolution of one micron. This range would allow scanning over bands of methane, ammonia, and water, and viewing of the spectral region of interest in order to obtain a better understanding of the nature of the unexplained thermal radiation leak. An instrument of this type would weigh about 16 pounds, require 5 watts of power, and have a data output of 5000 bits-per-scan and a scan rate of one per five or ten minutes. The instrument will start operation three hours prior to encounter and continue for three hours after encounter. It would take approximately one minute to complete one scan. A thermoelectric device or equivalent appears satisfactory for cooling the detector.

An ultra-violet-to-visible spectrometer may also be considered for the detection of minor constutuents of the Jovian atmosphere. A frequency range of 1000 to 6000 Å with a spectral resolution of 10 Å would be adequate. The instrument weighs 20 pounds and requires 10 watts. A bit rate of 10^4 bits per scan which would start at a distance of four planetary radii prior to encounter and continue until four planetary radii after encounter is planned with readings taken every 5 to 10 minutes.

2.1.8 Ranging and Radio Experiments

Experiments involving the normal range-tracking required in any Jovian mission can be used to extend the scientific capability of the spacecraft. Measurement of the time-delay effect made possible by the precise tracking of a Jovian probe could provide data that would be helpful in evaluations of competing theories of general relativity. An occultation experiment, similar to the one performed with the Mariner IV spacecraft, could be performed in the Jupiter flyby mission to obtain data relevant to the structure of the Jovian atmosphere and ionosphere.

Additional experiments could be performed by using radar and radio frequencies and equipment (1) to detect low-level emission, (2) to probe the Jovian atmosphere, and (3) to locate more precisely the sites of strong radio emissions.

2.1.8.1 General Relativity Experiments

It should be possible to perform a test (or tests) of general relativity with a Jupiter probe. It should be noted, however, that methods for the evaluation of relativistic effects are not well defined in general relativity theory, and that models for curved and flat spacetime must exist before any "relativistic effects" can be delineated.

The most promising as well as the newest test for employment with a Jupiter probe appears to be the measurement of the time-delay effect. This test was proposed originally by Muhleman and Richley (Jet Propulsion Laboratory Space Programs Summary No. 37-29) in a form that required radar tracking of Venus from the Earth. The use of a probe launched from Earth would yield better results, in one sense, because the mass and other characteristics of the probe would be known. Further, the plot of its locus relative to the Earth would include points near the Earth where the relativistic time delay would be completely negligible. Moreover, the uncertainty in the speed of light owing to experimental error in measurement would have the least effect in resolving the location of the probe.

Thus, it is indicated that despite the "concealing" effects resulting from the uncertainty in the local speed of light, the uncertainty in planetary positions, and dispersion of the plasma around the Sun, the time-delay effect should be observable (Reference 2.1-5).

If enough measurements are made so that the orbit of the probe around the Sun is determined, then the non-linearity of the relativistic time delay will appear in a distortion of the Keplerian orbit if mapped in flat space. If by correcting the orbit for the relativistic time delay, as well as dispersive effects of the media, the orbit is changed into a better approximation of an ellipse (or really the nearly elliptical orbit of the solar many-body problem), it can be concluded that space is not flat or the Newtonian gravitational theory is invalid.

If a tracking station on the Earth is used to trace the orbit of the probe, the dispersive effects of the solar atmosphere and interplanetary media on the signal must be calculated and the mapping corrected to account for them. If two signals, separated in frequency, are used, then the corrections for plasma dispersion can be made more accurately than might be warranted on the basis of data on the plasma density because the effect is dependent upon the frequency.

Other tests of general relativity, such as the red shift, light deflection, and perihelion precession, could be undertaken with a Jupiter probe, but the results would probably not be as satisfactory as those for the time-delay test. To perform a red shift test, the signal transponder and frequency shifter on the spacecraft would have to be extremely stable. Performance of a light deflection test would be difficult because of problems in separating the deflections due to the gravitational field and those due to changes in refractive index. In the case of the perihelion test, special trajectories would be required.

2.1.8.2 S-Band Occultation Experiment

In order to investigate the upper atmosphere of Jupiter by means of an occultation experiment, a trajectory must be chosen so that the spacecraft will pass behind the planet, as seen from Earth. The tracking signal will then pass through the Jovian atmosphere. The variations in the signal should provide information about a number of characteristics of the Jovian atmosphere and ionosphere. Those which have been indicated by Kliore, et al (Reference 2.1-6) are described in the following listing:

1. The electron density profile of the ionospheric layer (or layers).

2. The refractivity profile of the neutral atmosphere, from about 100 km above the cloud tops down to a point at which the atmospheric attenuation prevents radio reception. It is extremely unlikely that the latter point would be near the Jovian surface, if there is a surface.

3. The position, thickness, and perhaps the composition of the top cloud layer (or layers). It should be possible to distinguish at least between water crystals, ammonia crystals, solid hydrocarbons, or dust.

4. The mean molecular weight, if the temperature of the cloud tops is known. Such information will indicate a limit of the possible composition of the atmosphere.

The requirements for a successful occultation are as follows:

1. A trajectory which passes behind Jupiter, as seen from the Earth. A nominal aim point (and accompanying error ellipse) which will lie within the Earth occultation region will be required.

2. Sufficient down-link communication power to allow significant probing of the atmosphere. The strength of the radio-tracking signal should be great enough to penetrate the Jovian atmosphere to a depth of several scale heights. Such a capability would require a communication margin of 20 to 30 db to enable some atmospheric attenuation to be overcome.

3. Suitable receiving equipment, capable of following wide variations of frequency at a high rate during occultation. There is a possibility that the rate of change of the Doppler shift may be so great that standard DSIF equipment could not maintain a "lock-on" of the tracking signal. (Such a failure would affect the flight mechanics experiments as well as the S-band occultation experiment.) Because of the high Doppler shift rate resulting from a passage close to Jupiter, special DSIF equipment or special trajectory constraints might be required. The requirements are discussed in subsection 3.1.

Additionally, other possible areas of difficulty must be investigated before a satisfactory evaluation of a Jovian occultation experiment can be made. These include

1. Effects of vapors and particulate matter in the Jovian atmosphere.

2. Diffraction effects from large, dense irregularities in the atmosphere (Fresnel Diffraction).

3. Effects of atmospheric electrical activity. Layers of high electron density could cause ducting of the signals.

4. The value of performing "received power" measurements at the spacecraft. The use of higher communications margins in spacecraft receivers must be weighed against any major modifications required in proposed spacecraft to incorporate such receivers.

On the basis of the state of knowledge of the Jovian atmosphere and the efficacy of the scientific payload experimental list, an occultation experiment is advisable at the present time only if it can be performed with minor modifications of the receiving equipment and minor changes in the spacecraft mission definition.

2.1.8.3 Planetary Radio and Radar

A bistatic radar may be used (at a frequency above about 40 Mcs.) to measure the radar-scattering function at various phase angles. This measurement may also be made in interplanetary space to obtain information on the absolute electron density. One operational program that is envisioned involves an instrument with a weight of 15 pounds, a power requirement of 8 watts, a bit rate of 30 bits-per-sample, and which can be used to take samples every three minutes starting at three planetary radii from the surface prior to encounter and continuing to three planetary radii from the surface after encounter.

A null radio seeker may be used to determine the location of particular radio sources and may provide information relevant to the nature of the source of the electromagnetic disturbances. An instrument of about 5 pounds with a power requirement of 2 watts, a data rate of 50 bits-per-sample. A directional antenna would have to be gimbled to move in any direction across the planetary disc.

A radio experiment designed to search for possible emission at low flux levels would provide information that would augment that available from measurements from the Earth. Measurements made in the decimeter wavelength region would be desirable. A representative instrument would weigh about 5 pounds, require 4 watts of power, and provide a data output of 50 bits-per-sample during its program operation of three hours prior to encounter to three hours after encounter.

A radar altimeter may be used to obtain information about the planetary structure. Reflection off the solid planetary surface may be obtained with a wavelength of about one-half to one meter. Longer wavelengths reflections would be from the ionosphere, while shorter wavelengths would be affected by molecular absorption in the atmosphere. The instrument would weigh about 25 pounds, require about 10 watts of power, and provide a data rate of 50 bits-per-sample. An operational program of taking measurements every five minutes from three hours prior to encounter to three hours after encounter would be satisfactory. The antenna would have to point at the planet during the measurements.

2.1.9 Miscellaneous

In addition to the information obtained from the scientific instruments defined in the preceding sections, there are other means by which information may be generated. These are described in the following paragraphs:

1. The normal measurement of the position of the spacecraft as a function of time will yield data relevant to a more accurate determination of the orbital and gravitational parameters of Jupiter, (and probably the solar system, by a better determination of the astronomical unit). Increased accuracy in the values of the Jovian mass and second gravitational harmonic should result from the measurement of the spacecraft's hyperbolic orbit about the planet.

2. The feasibility of releasing a probe into the Jovian atmosphere should be examined. The capability of such a probe to yield direct, quantitative data may outweigh the problems involved in its operation. This probe could contain a mass spectrometer to give information about the relative compositional abundances of the planet. In particular, a determination of the relative abundance of deuterium would be especially valuable in providing information concerning the origin and history of the solar system and the universe. Determination of the existence and abundance of deuterium at Jupiter would aid in establishing whether or not this isotope had its origin as a remnant of the primordial atmosphere or is the result of a secondary nuclear process, as is probably the case for the Earth. Jupiter, unlike the Earth, is massive enough to retain its hydrogen and is large enough to have the element present in a relatively undiluted abundance. The relative abundance of deuterium may thus be indicative of the nuclear reactions involved in the very early formation of the

universe. A probe into the Jovian atmosphere could also measure such parameters as pressure, temperature, density, electric charge, and others.

It may be possible, although its feasibility is uncertain at the present time, to use an interferometer spectrometer that would scan a small wavelength region at a very high resolution to look for lines of HD, NH_2D, or CH_3D. This might be an optional method of detecting deuterium in the Jovian atmosphere.

3. Using Jupiter to provide a turnaround so that the spacecraft would follow an out-of-the-ecliptic trajectory after planetary encounter would allow the continuation of the interplanetary measurements in a region of the solar system different from that encountered on the inbound path.

4. There should be at the same time as the Jupiter mission an Earth-orbiting satellite to gather radiation data similar to that obtained by the Jupiter spacecraft. This second satellite would allow a wide spatial separation in the data-gathering points and would yield information about the dynamics of these radiations as they propagate through the solar system.

2.1.10 Scientific Instrument Characteristics

In Table 2.1-7, the physical characteristics of the instruments necessary to perform the suggested scientific experiments are outlined.

2.1.11 Typical Mission Payloads

Typical scientific mission payloads ranging from a minimum instrument complement to a "full" package are represented in Table 2.1-8. The full experiment list represents a wide spectrum of investigations and would be expected to yield a relatively complete picture of the planet for the flyby mission. It is possible, however, that the individual instruments could be expanded in size and scope thus increasing the full payload size. It is suggested that, if a substantial increase in payload weight is available, it could best be utilized in putting the vehicle in an orbit around Jupiter rather than adding additional scientific payload weight.

Intermediate science packages are made of loosely ordered selections ranging between the minimal and full science complement. The Minimal Scientific Experiment Package includes

Table 2.1-7 SCIENTIFIC INSTRUMENT CHARACTERISTICS
(Sheet 1)

Instrument	Weight (lbs)	Size (inches)	Power (Watts)	Data Requirements	Calibration	Location	Operating Regime	Special Considerations
Magnetometer	electronics 5.0 Two-sensor: 1.5 each	electronics 4 x 4 x 6 Two-sensor: 13 dia spheres	7.0	30 bits/ sample	on-off pulse from DAS	Sensor as far from bus as possible	Planetary & Inter-planetary	Remant magnetic field of bus should be reduced to a fraction of a gamma at the sensor. Temperature range of sensor 30 to 55°C.
Energetic Particle Detector	2.5	electronics: 3 x 5 x 6 sensor: Four-5 x 1 dia.	0.4	50 bits/ sample	Internal Alpha Source	On bus, sensors exposed	Planetary & Inter-planetary	Sensors point in plane normal to Sun-probe line. Basic instrument of type used on Mariner IV.
High Energy Proton Directional Monitor	4.0	electronics 3 x 4 x 4 sensor: Four-5 x 1 dia.	0.6	60 bits/ sample		Sensors extend out of package on bus	Inter-planetary	Energy response variable over a wide range. Sensors not to point toward Sun.
Medium Energy Proton Directional Monitor	3.0	electronics 4 x 4 x 5 sensor: Four-5 x 1 dia.	1.0	60 bits/ sample	Pulses from DAS	Sensors extend out of package on bus	Inter-planetary & Planetary	Sensors not to point toward Sun
Ion Chamber	3.0	5 x 10 x 13	0.5	20 bits/ sample		On boom three feet from bus	Planetary & Inter-planetary	Basic instrument of type used on Mariner IV
Plasma Probe	7.0	6 x 8 x 8	2.5	10 bits/ sample	Pulse from DAS	On bus, sensor exposed		Sensor to look toward Sun approximately 10 degrees above Sun-prove line
Cosmic Ray Spectrum Analyzer	18.0	electronics: 6 x 6 x 18 sensor: Four-5 x 1 dia.	2.0	70 bits/ sample	Internal Source	Sensors extend out of package on bus.	Inter-planetary & Planetary	Sensors not to point toward Sun
Infrared Radiometer	5.0	4 x 6 x 6	3.0	20 bits/ sample	Internal Source	Antenna looks at Jupiter	Planetary	

Table 2.1-7 SCIENTIFIC INSTRUMENT CHARACTERISTICS
(Sheet 2)

Instrument	Weight (lbs)	Size (inches)	Power (Watts)	Data Requirements	Calibration	Location	Operating Regime	Special Considerations
Microwave Radiometer	28	6 x 10 x 14	6	40 bits/scan	Internal noise source	Antenna to look at and scan planet, electronics in bus	Planetary	Antenna is about 12 inches in diameter. Must only see planet (and reference horns if used)
Infrared Spectrometer	16	10 x 12 x 14	5	5000 bits/ scan	Internal comparison source spectra	Electronics in bus. Sensor to look at planet	Planetary	
UV-Visible Spectrometer	20	10 x 13 x 16	10	10,000 bits/scan	Internal comparison source spectra	Electro-nics in bus. Sensor to look at planet	Planetary	Cannot tolerate sunlight into instrument at any time, scattered light during measurements
Bistatic Radar	15	6 x 6 x 12	10	30 bits/ sample		Antenna visible to Earth and Jupiter	Planetary (Possibly Inter-planetary)	
Null Radio Seeker	5	4 x 6 x 6	2	50 bits/ sample		Direction-al antenna looks at Jupiter	Planetary	
Radio Noise Detector	5	4 x 6 x 6	4	50 bits/ sample		Antenna looks at Jupiter	Planetary	
Radar Altimeter	25	6 x 10 x 12	10	50 bits/ sample		Antenna looks at Jupiter	Planetary	

Table 2.1-7 SCIENTIFIC INSTRUMENT CHARACTERISTICS
(Sheet 3)

Instrument	Weight (lbs)	Size (inches)	Power (Watts)	Data Requirements	Calibration	Location	Operating Regime	Special Considerations
Triple Coincidence Cosmic Ray Telescope	9.0	electronics: 2 x 6 x 6 Sensor: 5 x 3.5 dia.	0.5	110 bits/ sample		On bus, Sensor Exposed	Inter-planetary & Planetary	Axis of Sensor normal to Sun-probe line. Similar to instrument on Explorer VI
Charged Particle Telescope	3.0	2 x 6 x 6	0.6	40 bits/ sample	Internal Alpha Source	On bus, Sensor exposed	Inter-planetary & Planetary	Sensor to look away from Sun. Similar to instrument on Mariner IV
Cosmic Dust Detector	2.5	electronics: sensor: 1 x 22 x 22	0.2	8 bits/ sample	One known acoustic pulse per day	Sensor plate perpendicular to ecliptic plane	Inter-planetary & Planetary	Similar to instrument on Mariner IV
Television I	15	4 x 4 x 10	10	calculated from camera description	Pictures of free spaces	On scanning platform on bus	Planetary	Must not have scattered light into instruments
Television II	30	5 x 7 x 14	20	calculated from camera description	Pictures of free space	On scanning platform on bus	Planetary	Must not have scattered light into the instrument
Visible Photometer	2.0	2 x 3 x 6	1.5	30 bits/ sample	Standard brightness source	On scanning platform on bus	Planetary	Cannot have scattered light into instrument
Expanded Photometer	6.0	4 x 5 x 6	5.0	120 bits/ sample	Standard brightness source	On scanning platform on bus	Planetary	Cannot have scattered light into instrument

Table 2.1-8 SCIENTIFIC EXPERIMENT PACKAGES
(Sheet 1)

Full Scientific Experiment Package

Instrument	Weight	Power
Extended Magnetometer	8.0 lbs.	7.0 watts
Energetic Particle Detector	2.5	0.4
Cosmic Dust Detector	2.5	0.2
Expanded Photometer	6.0	5.0
TV Camera (TV-II)	30.0	20.0
Plasma Probe	7.0	2.5
Microwave Radiometer	28.0	6.0
Infrared Radiometer	5.0	3.0
Ion Chamber	3.0	0.5
Infrared Spectrometer	16.0	5.0
High Energy Proton Directional Monitor	4.0	0.6
Cosmic Ray Spectrum Analyzer	18.0	2.0
UV - Visible Spectrometer	20.0	10.0
Medium Energy Proton Directional Monitor	3.0	1.0
Bistatic Radar	15.0	8.0
Radio Noise Detector	5.0	2.0
Null Radio Seeker	5.0	2.0
Radar Altimeter	25.0	10.0
	203.0 lbs.	85.2 watts

Intermediate Scientific Experiment Package - 1

Instrument	Weight	Power
Extended Magnetometer	8.0 lbs.	7.0 watts
Energetic Particle Detector	2.5	0.4
Cosmic Dust Detector	2.5	0.2
Expanded Photometer	6.0	5.0
TV Camera (TV-I)	15.0	10.0
Plasma Probe	7.0	2.5
Microwave Radiometer	28.0	6.0
Infrared Radiometer	5.0	3.0
Ion Chamber	3.0	0.5
Infrared Spectrometer	16.0	5.0
High Energy Proton Directional Monitor	4.0	0.6
Cosmic Ray Spectrum Analyzer	18.0	2.0
	115.0 lbs.	42.2 watts

Table 2.1-8 SCIENTIFIC EXPERIMENT PACKAGES
(Sheet 2)

Intermediate Scientific Experiment Package - 2

Instrument	Weight	Power
Extended Magnetometer	8.0 lbs.	7.0 watts
Energetic Particle Detector	2.5	0.4
Cosmic Dust Detector	2.5	0.2
Expanded Photometer	6.0	5.0
TV Camera (TV-I)	15.0	10.0
Plasma Probe	7.0	2.5
Microwave Radiometer	28.0	6.0
Infrared Radiometer	5.0	3.0
Ion Chamber	3.0	0.5
	77.0 lbs.	34.6 watts

Minimal Scientific Experiment Package

Instrument	Weight	Power
Extended Magnetometer	8 lbs.	7 watts
Energetic Particle Detector	2.5	0.4
Cosmic Dust Detector	2.5	0.2
Visible Photometer	2.0	1.5
TV Camera (TV-I)	15.0	10.0
Plasma Probe	7.0	2.5
	37 lbs.	21.6 watts

Spin-Stabilized Spacecraft Experiment Package

Instrument	Weight	Power
Extended Magnetometer	8 lbs.	7 watts
Energetic Particle Detector	2.5	0.4
Cosmic Dust Detector	2.5	0.2
	13 lbs.	7.6 watts

instruments whose use would be most advantageous in view of the increase in spatial resolution and planetary phase availability afforded by a Jovian flyby mission (refer to Table 3.1-8). The results of a study of the meteorology, fine structure, and basic thermal character of the Jovian atmosphere will be much less ambiguous if a television camera is used. For example, the data obtained from scanning regions of the spectrum other than the visible cannot be interpreted as readily as photographs of the visible.

The smallest scientific package, listed as the last item in Table 2.1-8, is representative of a payload that could be employed in a spin-stabilized spacecraft whose relatively high spin rate precludes an opportunity to scan the planet. The use of instruments on this list offers an excellent means of obtaining design data for later probes.

2.1.12 References

Numerous articles and reports relative to the scientific investigations of Jupiter were utilized in this report; however, a complete list is not being included. There were some references that were used extensively in defining the descriptions of the scientific instruments in this report. These are listed below:

2.1-1 "Survey of a Jovian Mission," Report No. M-1, Astro Sciences Center of Illinois Institute of Technology Research Institute, March 1964.

2.1-2 "Jupiter - Advanced Planetary Probe, Scientific Objectives and Typical Experiments," R. G. Brereton, Jet Propulsion Laboratory

2.1-3 "Mariner C Reference Information for Future Mission Studies," Jet Propulsion Laboratory Engineering Planning Document No. 296, 15 April 1965.

2.1-4 "Design Data Information System," Jet Propulsion Laboratory, 1 October 1965.

2.1-5 "Evaluation of the Time-Delay Test of General Relativity," G. H. Brigman, Fort Worth Division, General Dynamics Report ERR-FW-432, 29 September 1965.

2.1-6 "An S-Band Occultation Experiment for the 1967 Venus Mission," A. Kliore, D. L. Cain, and G. S. Levy, Jet Propulsion Laboratory and S. I. Rasool, Goddard Spaceflight Center.

2.2 ENERGY REQUIREMENTS AND GENERAL TRAJECTORY CHARACTERISTICS

The basic sources of information regarding energy requirements and general trajectory characteristics are the mission maps presented in Appendix A. In addition, guidance sensitivity parameters were obtained from heliocentric conic trajectory data supplied by JPL. Data from these sources have been summarized in charts which are designed to aid the mission planner in the analysis of mission requirements. The methods used, the results obtained, and the conclusions reached in this process of summarizing mission characteristics are discussed in following paragraphs.

2.2.1 Launch Window Definition

The injection energy requirements and other characteristics of interplanetary missions are influenced by the ground rules for selecting launch windows. Since one of the primary objectives of mission analysis is to determine the relationship between flight time and the injection energy required for the mission, it would seem logical for this purpose to use fixed-flight-time windows of the type illustrated in Figure 2.2-1. The determination of energy requirements for such windows over a selected range of flight times would define a curve of energy requirement versus flight time. However, if flight time is held constant as the launch date is delayed, the time of arrival at Jupiter must also be delayed. In the areas of spacecraft design and mission operations, there are significant advantages in holding the encounter date constant for any launch date within the window. A number of important mission parameters, such as communication distance at encounter time, arrival hyperbolic excess velocity, size of the guidance error ellipse, etc., are either uniquely determined by the arrival date, or else they remain more nearly constant if the arrival date is held fixed than if the flight time is held fixed. For these reasons, fixed-arrival-date windows have been used for the purpose of defining mission requirements. Arrival dates themselves are of little interest to spacecraft designers, and mission requirements, although determined on the basis of arrival date, are commonly identified by reference to a characteristic flight time. The characteristic flight time used for this purpose is the mean flight time within the appropriate window. Actual flight times within the window differ from the characteristic

LAUNCH WINDOW DEFINITION

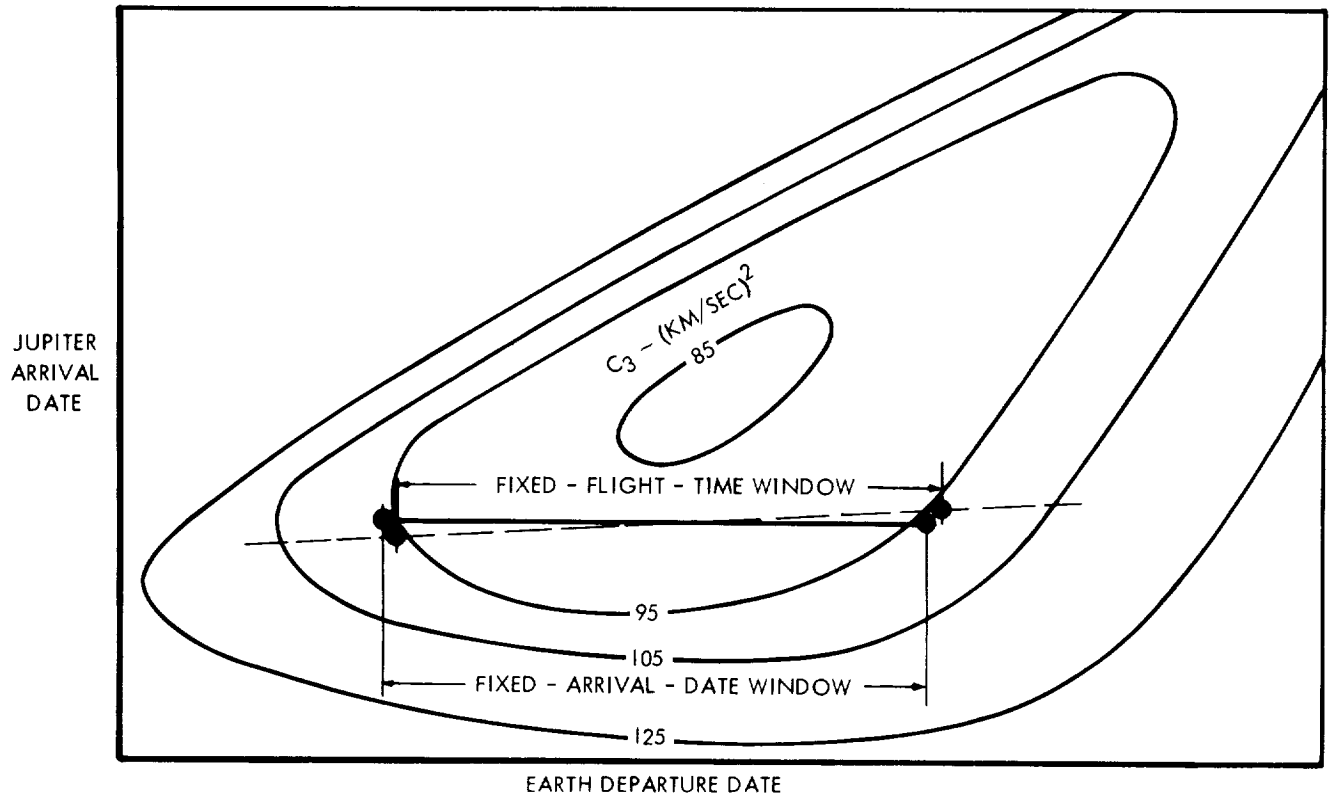

FIG. 2.2-1

INJECTION ENERGY AS A FUNCTION OF WINDOW WIDTH

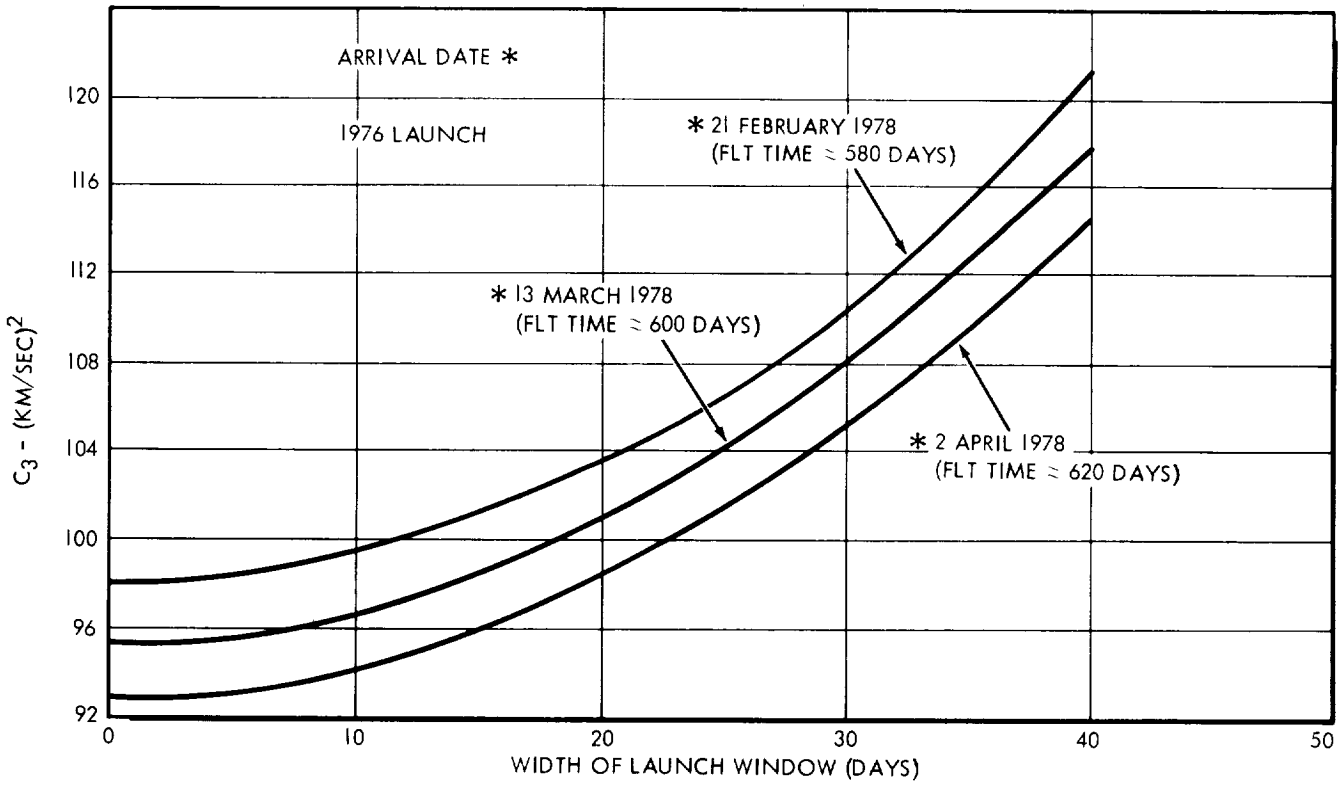

FIG. 2.2-2

flight time by as much as half the window width, but such variations are relatively small when compared to the overall flight time itself.

As illustrated in Figure 2.2-2, the injection energy requirement is strongly dependent on the width of the launch window. A nominal width of 20 days was selected for defining mission requirements in this study. This is somewhat less than the width normally considered desirable for, say, Mars and Venus missions. However, injection energy "valleys" for Jupiter missions are considerably narrower than comparable valleys for Venus and Mars. Because Jupiter's synodic period (i.e., the interval between launch opportunities) is only about half as long as the synodic period of Mars, the narrower window width is considered justifiable.

Another launch-window ground rule which has a significant effect on mission requirements in some launch years is the stipulation that the declination of the departure asymptote must fall within the range of ± 36 degrees for all nominal trajectories. This restriction was imposed in line with an overall policy of conservatism which is believed to be desirable in a feasibility study of this nature. Assuming a minimum acceptable daily lift-out window of approximately an hour, plus 36 degrees and minus 36 degrees represent the approximate limiting values of asymptote declination which can be realized (without an orbital plane change) by a launch from Cape Kennedy within the normal firing sector of 90- to 114-degree launch azimuths. Orbit determination during the first few days after injection into the interplanetary trajectory is another factor which was considered before selecting the asymptote declination limits. If the magnitude of the declination of the asymptote were very much greater than 36 degrees, DSIF stations in only one hemisphere (northern or southern) could be used to track the spacecraft during this critical period. Since a spread of tracking-station latitudes is desirable for accurate orbit determination, such a situation should be avioded if possible.

A launch "corridor", defined by the loci of launch-window boundary points, is shown in Figure 2.2-3. Although the figure is entitled "Typical Launch Corridor", the corridor is not typical in the sense that in most launch years the 36-degree asymptote declination constraint does not cause the corridor to swerve so drastically away from the minimum-energy region as indicated.

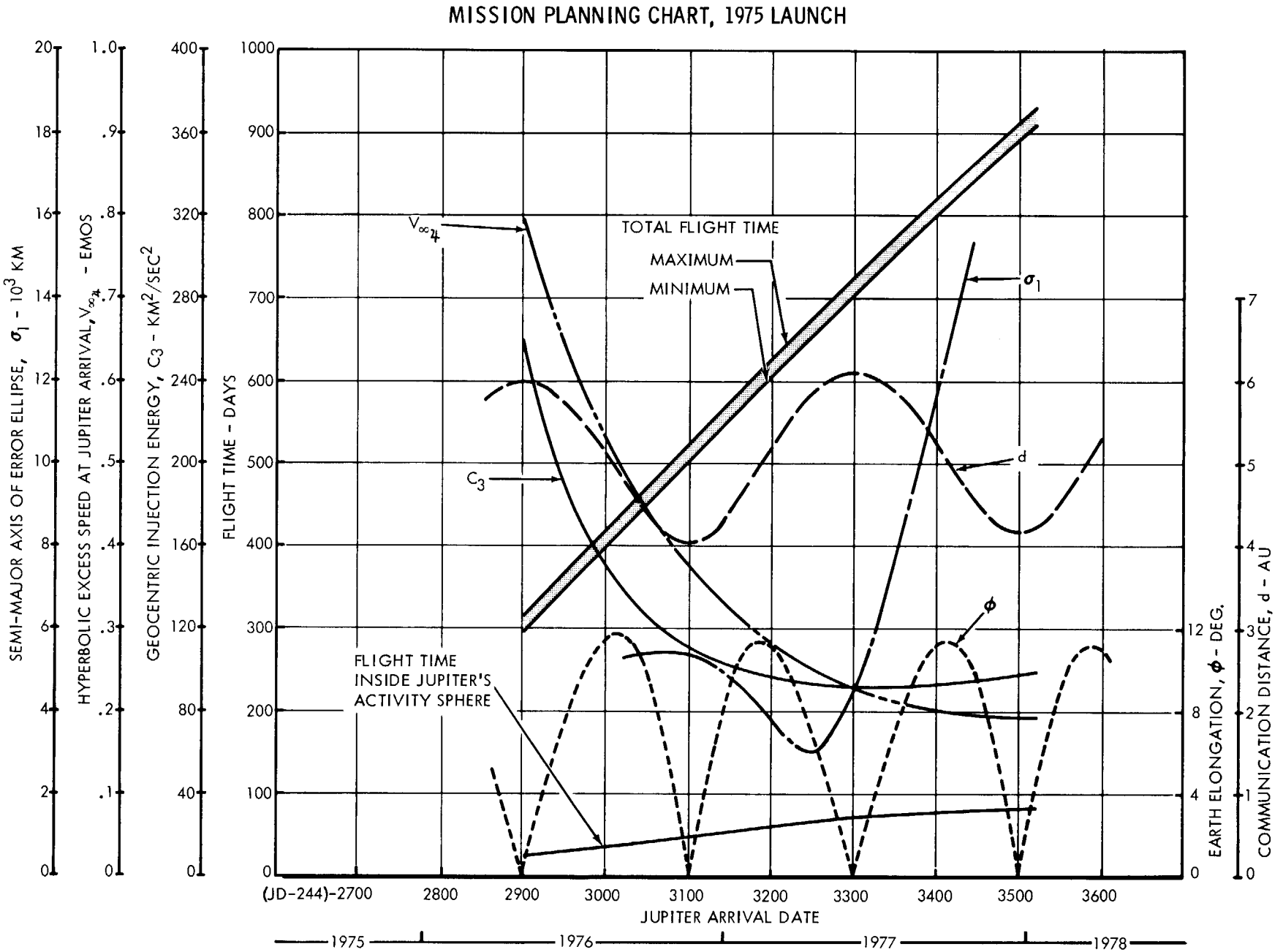
MISSION PLANNING CHART, 1975 LAUNCH
SEMI-MAJOR AXIS OF ERROR ELLIPSE, σ_1 - 10^3 KM
HYPERBOLIC EXCESS SPEED AT JUPITER ARRIVAL, V_{∞_4} - EMOS
GEOCENTRIC INJECTION ENERGY, C_3 - KM^2/SEC^2
FLIGHT TIME - DAYS
EARTH ELONGATION, ϕ - DEG.
COMMUNICATION DISTANCE, d - AU
V_{∞_4}
TOTAL FLIGHT TIME
MAXIMUM
MINIMUM
σ_1
C_3
d
ϕ
FLIGHT TIME INSIDE JUPITER'S ACTIVITY SPHERE
(JD-244)-2700
JUPITER ARRIVAL DATE
1975
1976
1977
1978

FIGURE 2.2-7

flight time by as much as half the window width, but such variations are relatively small when compared to the overall flight time itself.

As illustrated in Figure 2.2-2, the injection energy requirement is strongly dependent on the width of the launch window. A nominal width of 20 days was selected for defining mission requirements in this study. This is somewhat less than the width normally considered desirable for, say, Mars and Venus missions. However, injection energy "valleys" for Jupiter missions are considerably narrower than comparable valleys for Venus and Mars. Because Jupiter's synodic period (i.e., the interval between launch opportunities) is only about half as long as the synodic period of Mars, the narrower window width is considered justifiable.

Another launch-window ground rule which has a significant effect on mission requirements in some launch years is the stipulation that the declination of the departure asymptote must fall within the range of ± 36 degrees for all nominal trajectories. This restriction was imposed in line with an overall policy of conservatism which is believed to be desirable in a feasibility study of this nature. Assuming a minimum acceptable daily lift-out window of approximately an hour, plus 36 degrees and minus 36 degrees represent the approximate limiting values of asymptote declination which can be realized (without an orbital plane change) by a launch from Cape Kennedy within the normal firing sector of 90- to 114-degree launch azimuths. Orbit determination during the first few days after injection into the interplanetary trajectory is another factor which was considered before selecting the asymptote declination limits. If the magnitude of the declination of the asymptote were very much greater than 36 degrees, DSIF stations in only one hemisphere (northern or southern) could be used to track the spacecraft during this critical period. Since a spread of tracking-station latitudes is desirable for accurate orbit determination, such a situation should be avioded if possible.

A launch "corridor", defined by the loci of launch-window boundary points, is shown in Figure 2.2-3. Although the figure is entitled "Typical Launch Corridor", the corridor is not typical in the sense that in most launch years the 36-degree asymptote declination constraint does not cause the corridor to swerve so drastically away from the minimum-energy region as indicated.

TYPICAL LAUNCH CORRIDOR

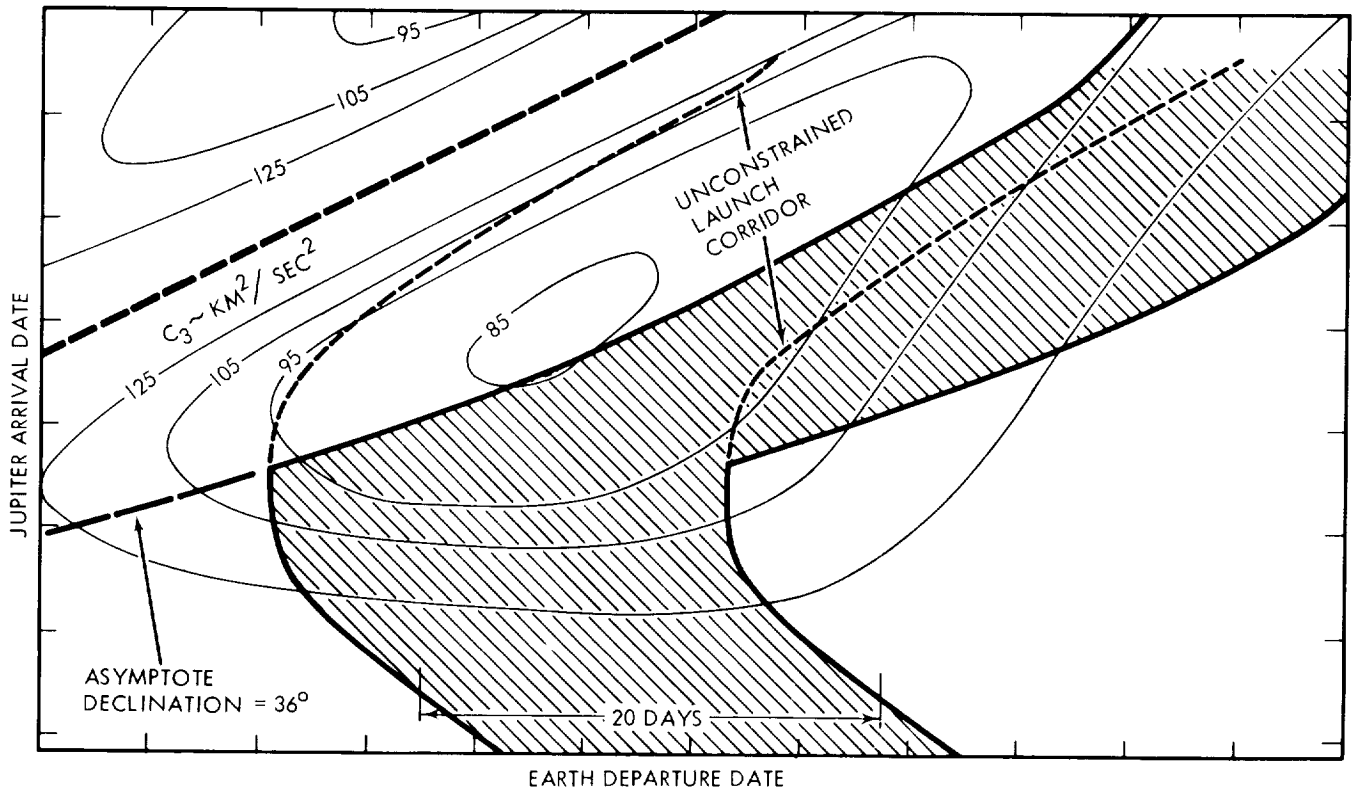

FIGURE 2.2-3

JUPITER ARRIVAL DATE CORRECTIONS

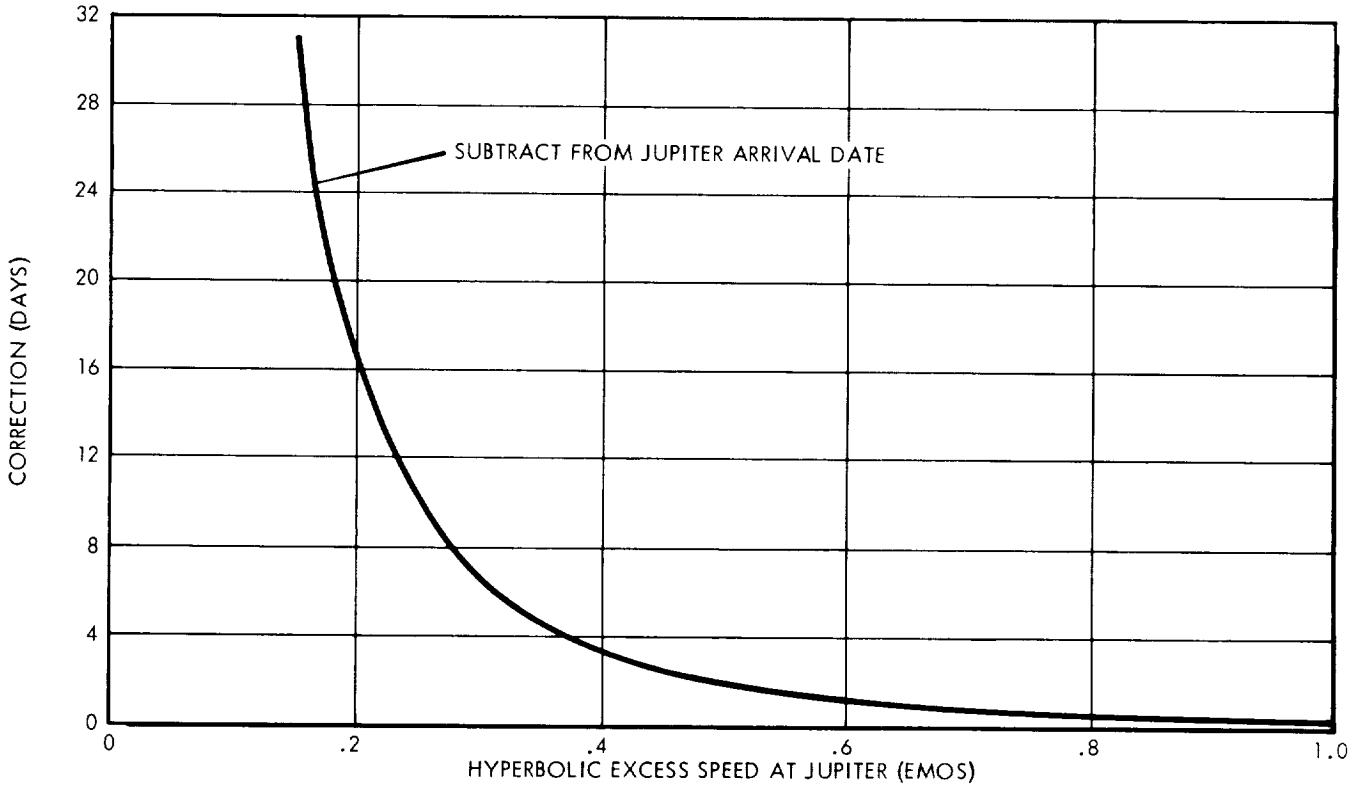

FIGURE 2.2-4

2.2.2 Arrival Date Corrections

The departure and arrival dates and flight times associated with heliocentric conic two-body trajectory computations are somewhat erroneous because the gravitational acceleration of the spacecraft caused by the planetary fields is ignored. The effect of Earth's gravity field is comparatively small, and the few hours error in departure date can be ignored for most purposes of mission analysis. However, Jupiter's gravity field is sufficiently strong to cause flight-time errors as great as 20 days. Essentially all of the flight-time error is built up within Jupiter's activity sphere, i.e., the volume of space in which Jupiter is the dominant gravitational body rather than the Sun.

The correction curve shown in Figure 2.2-4 was used to adjust the arrival dates and flight times associated with heliocentric conic data before they were incorporated in the mission planning charts which are discussed in paragraph 2.2.3. The corrections were computed by taking the difference between the "linear" flight time within Jupiter's activity sphere (i.e., the radius of the activity sphere divided by the appropriate hyperbolic excess speed) and the two-body hyperbolic flight time from the boundary of the activity sphere to perijove. For this purpose, the perijove altitude was taken to be one-tenth of Jupiter's surface radius. After adjustment, helicocentric conic arrival dates and flight times are accurate to within about 10 percent of the applied correction (i.e., to within ± 2 days or better), provided perijove altitude does not exceed about 10 planet radii.

2.2.3 Mission Planning Charts

Mission planning charts applicable to each of the launch opportunities between 1973 and 1980 are shown in Figures 2.2-5 through 2.2-12. In these charts several important mission parameters are plotted as functions of arrival date.

2.2.3.1 Arrival Hyperbolic Excess Speeds

As previously stated, the heliocentric conic flight times and arrival dates appearing in these charts have been adjusted to account for Jupiter's gravitational attraction. For the purpose of making these adjustments, the hyperbolic excess speed at Jupiter on any given arrival date was taken to be equal to its mean value for the appropriate 20-day constant-arrival-date launch window. The curves of the mean hyperbolic excess arrival speed are shown on each of the charts.

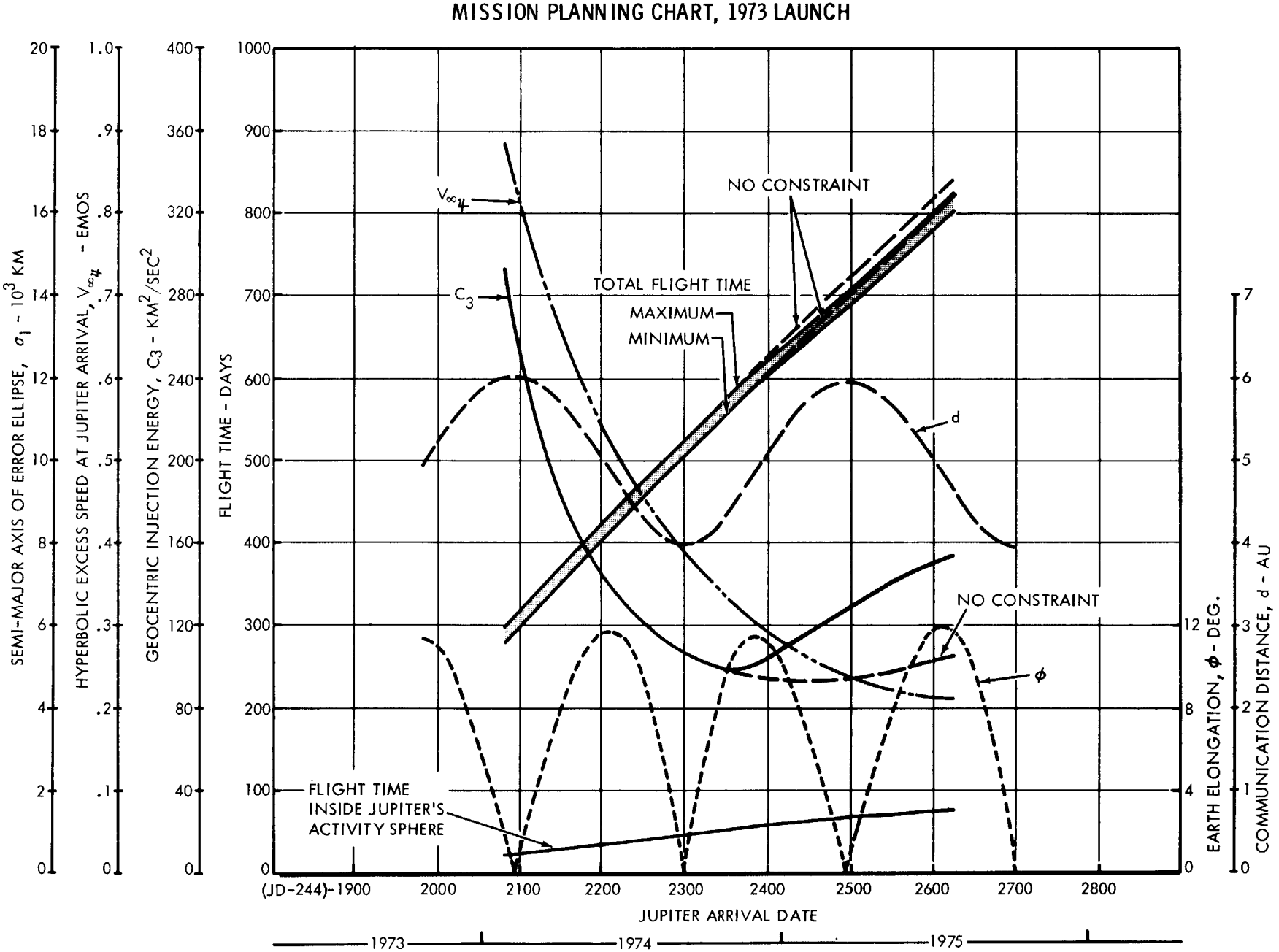
MISSION PLANNING CHART, 1973 LAUNCH
SEMI-MAJOR AXIS OF ERROR ELLIPSE, σ_1 - 10^3 KM
HYPERBOLIC EXCESS SPEED AT JUPITER ARRIVAL, V_{∞_4} - EMOS
GEOCENTRIC INJECTION ENERGY, C_3 - KM^2/SEC^2
FLIGHT TIME - DAYS
EARTH ELONGATION, ϕ - DEG.
COMMUNICATION DISTANCE, d - AU
V_{∞_4}
C_3
NO CONSTRAINT
TOTAL FLIGHT TIME
MAXIMUM
MINIMUM
d
NO CONSTRAINT
ϕ
FLIGHT TIME INSIDE JUPITER'S ACTIVITY SPHERE
(JD-244)-1900
JUPITER ARRIVAL DATE
1973
1974
1975

FIGURE 2.2-5

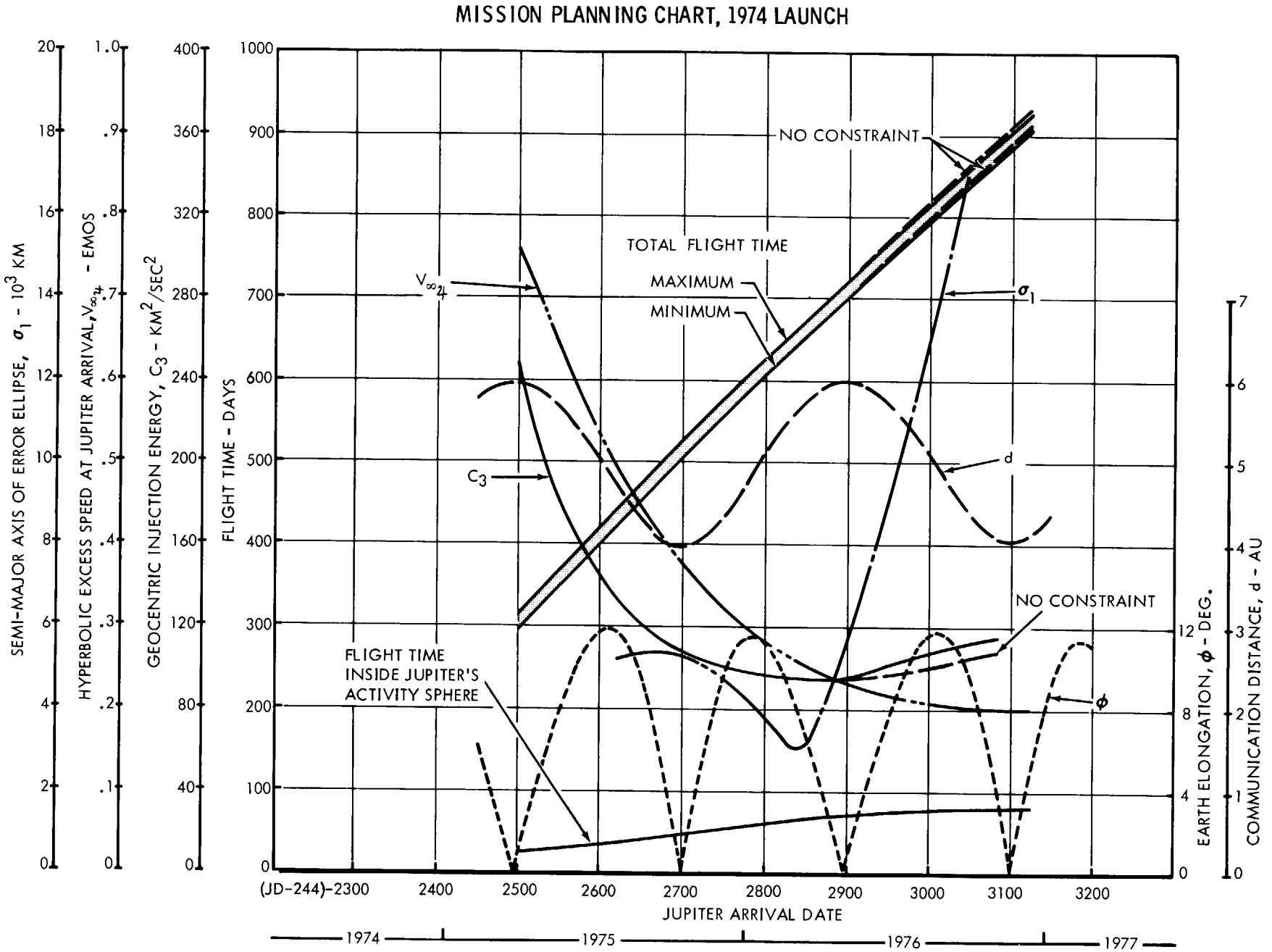
MISSION PLANNING CHART, 1974 LAUNCH
SEMI-MAJOR AXIS OF ERROR ELLIPSE, σ_1 - 10^3 KM
HYPERBOLIC EXCESS SPEED AT JUPITER ARRIVAL, V_{∞_4} - EMOS
GEOCENTRIC INJECTION ENERGY, C_3 - KM^2/SEC^2
FLIGHT TIME - DAYS
EARTH ELONGATION, ϕ - DEG.
COMMUNICATION DISTANCE, d - AU
NO CONSTRAINT
TOTAL FLIGHT TIME
MAXIMUM
MINIMUM
V_{∞_4}
C_3
σ_1
d
ϕ
NO CONSTRAINT
FLIGHT TIME INSIDE JUPITER'S ACTIVITY SPHERE
(JD-244)-2300
JUPITER ARRIVAL DATE
1974
1975
1976
1977

FIGURE 2.2-6

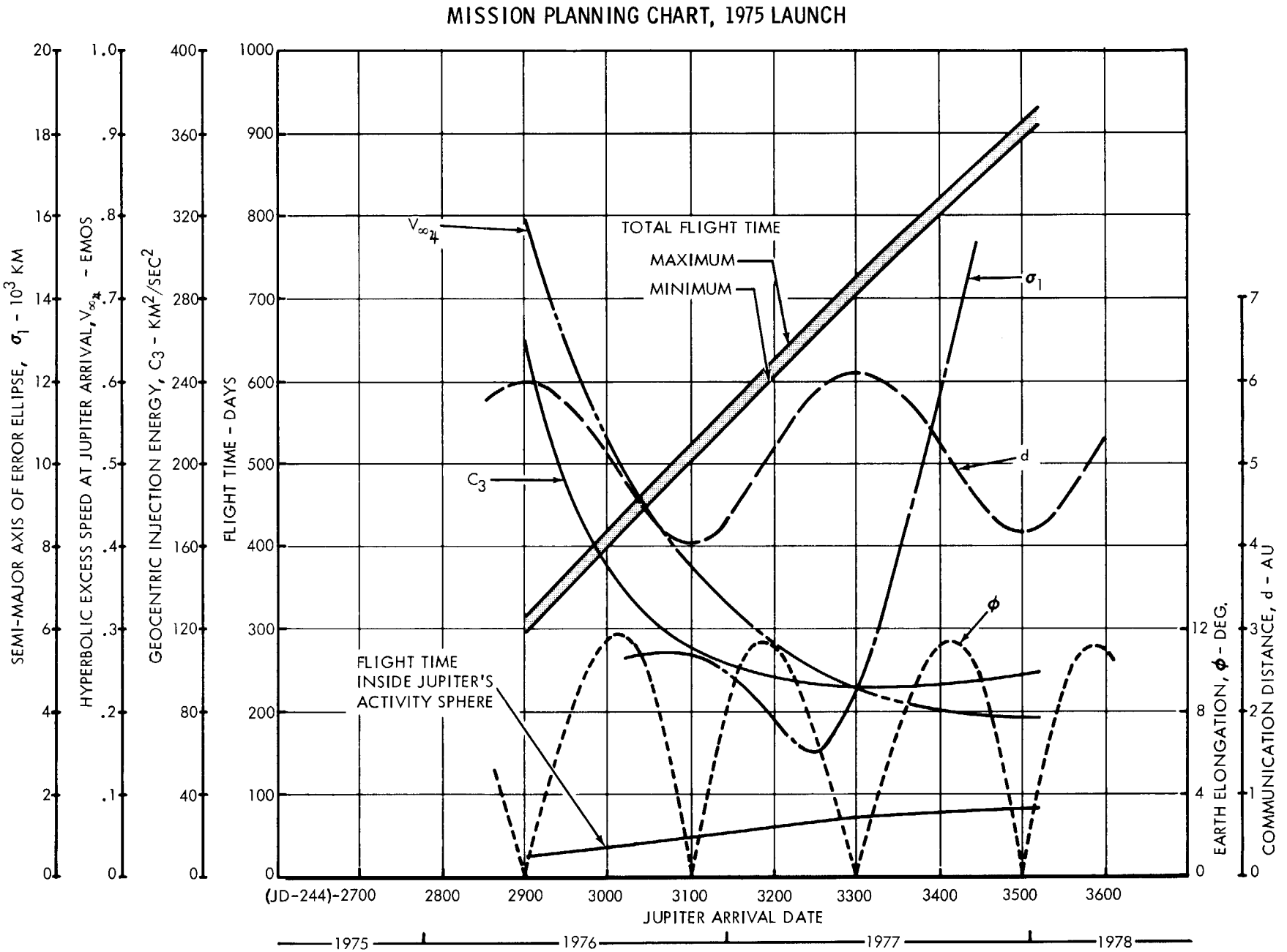
MISSION PLANNING CHART, 1975 LAUNCH
SEMI-MAJOR AXIS OF ERROR ELLIPSE, σ_1 - 10^3 KM
HYPERBOLIC EXCESS SPEED AT JUPITER ARRIVAL, V_{∞_4} - EMOS
GEOCENTRIC INJECTION ENERGY, C_3 - KM^2/SEC^2
FLIGHT TIME - DAYS
EARTH ELONGATION, ϕ - DEG.
COMMUNICATION DISTANCE, d - AU
V_{∞_4}
TOTAL FLIGHT TIME
MAXIMUM
MINIMUM
σ_1
C_3
d
ϕ
FLIGHT TIME INSIDE JUPITER'S ACTIVITY SPHERE
(JD-244)-2700
JUPITER ARRIVAL DATE
1975
1976
1977
1978

FIGURE 2.2-7

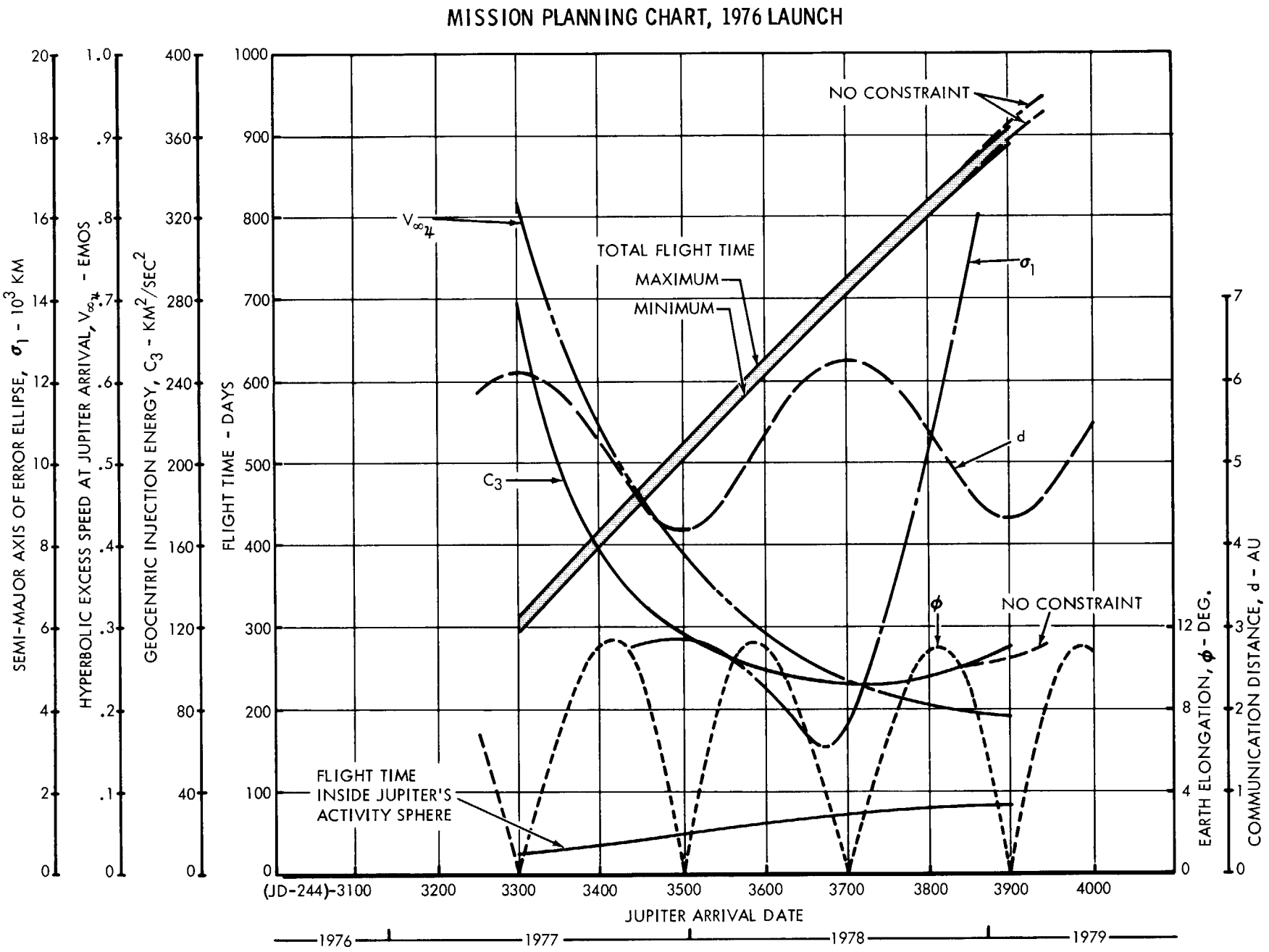
MISSION PLANNING CHART, 1976 LAUNCH
SEMI-MAJOR AXIS OF ERROR ELLIPSE, σ_1 - 10^3 KM
HYPERBOLIC EXCESS SPEED AT JUPITER ARRIVAL, V_{∞_4} - EMOS
GEOCENTRIC INJECTION ENERGY, C_3 - KM^2/SEC^2
FLIGHT TIME - DAYS
EARTH ELONGATION, ϕ - DEG.
COMMUNICATION DISTANCE, d - AU
NO CONSTRAINT
V_{∞_4}
TOTAL FLIGHT TIME
MAXIMUM
MINIMUM
σ_1
d
C_3
ϕ
NO CONSTRAINT
FLIGHT TIME
INSIDE JUPITER'S
ACTIVITY SPHERE
(JD-244)-3100
JUPITER ARRIVAL DATE
1976
1977
1978
1979

FIGURE 2.2-8

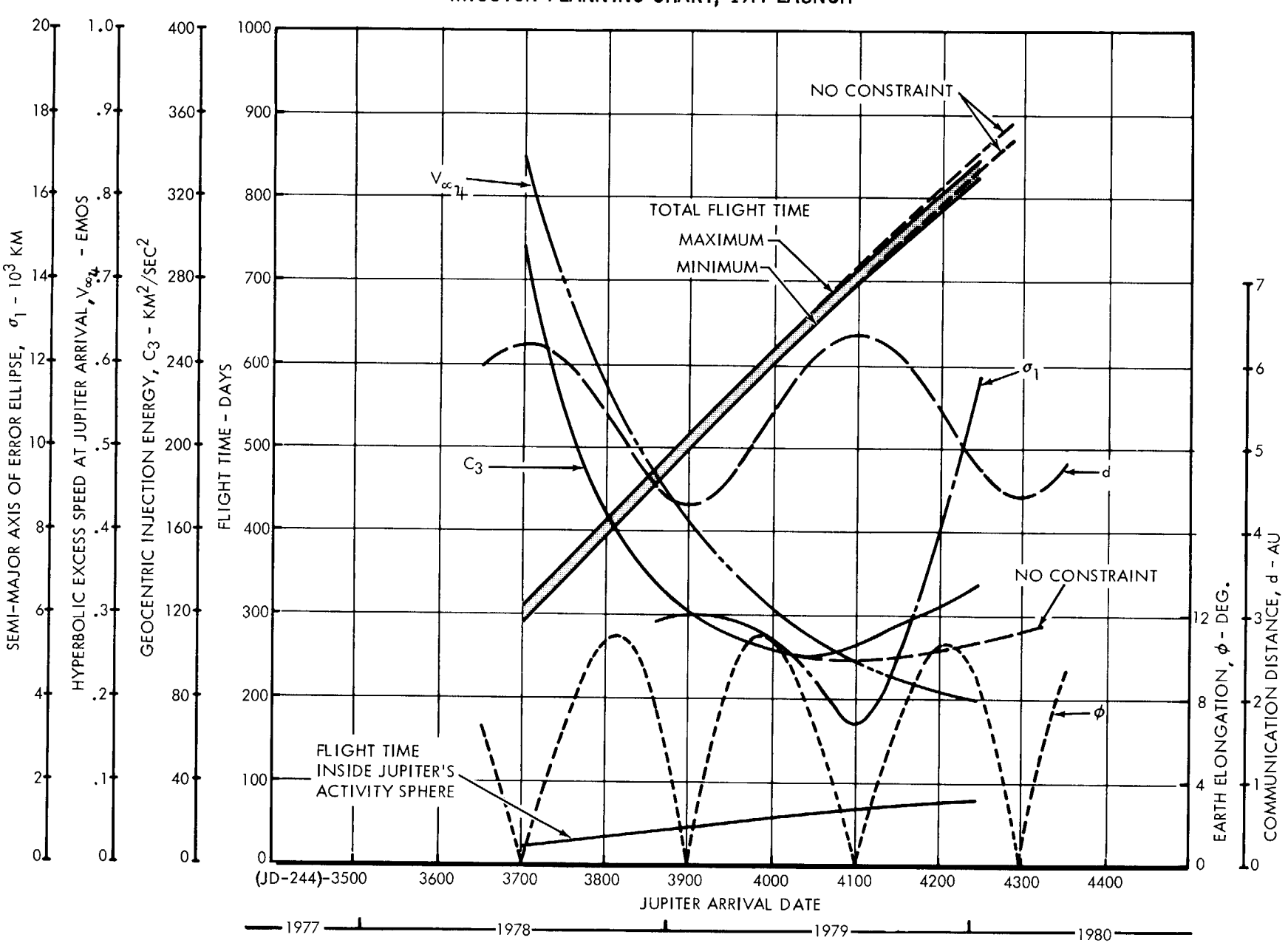
MISSION PLANNING CHART, 1977 LAUNCH
SEMI-MAJOR AXIS OF ERROR ELLIPSE, σ_1 - 10^3 KM
HYPERBOLIC EXCESS SPEED AT JUPITER ARRIVAL, V_{∞_4} - EMOS
GEOCENTRIC INJECTION ENERGY, C_3 - KM^2/SEC^2
FLIGHT TIME - DAYS
EARTH ELONGATION, ϕ - DEG.
COMMUNICATION DISTANCE, d - AU
NO CONSTRAINT
V_{∞_4}
TOTAL FLIGHT TIME
MAXIMUM
MINIMUM
σ_1
C_3
d
NO CONSTRAINT
ϕ
FLIGHT TIME INSIDE JUPITER'S ACTIVITY SPHERE
(JD-244)-3500
JUPITER ARRIVAL DATE
1977
1978
1979
1980

FIGURE 2.2-9

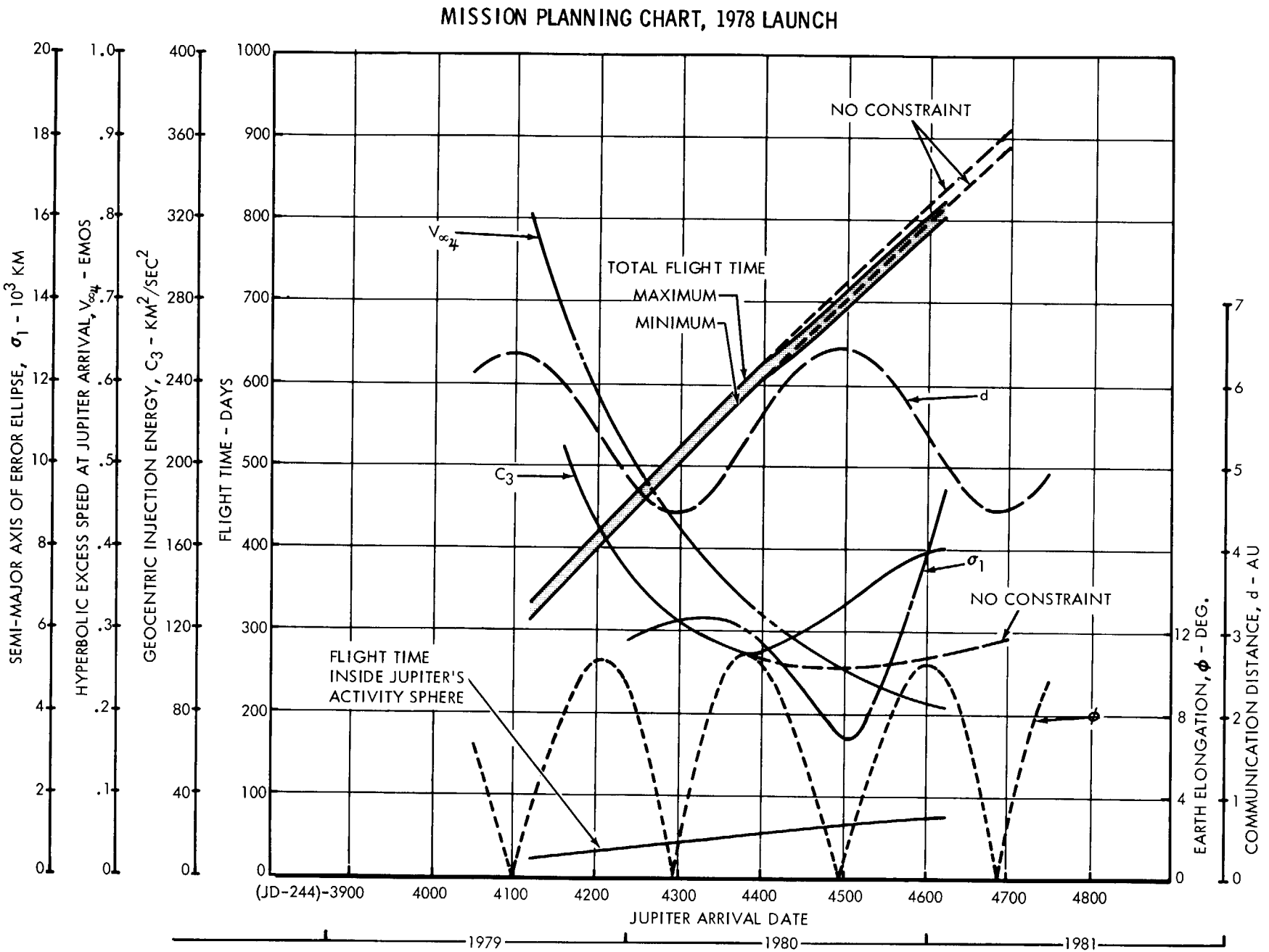
MISSION PLANNING CHART, 1978 LAUNCH
SEMI-MAJOR AXIS OF ERROR ELLIPSE, σ_1 - 10^3 KM
HYPERBOLIC EXCESS SPEED AT JUPITER ARRIVAL, V_{∞_4} - EMOS
GEOCENTRIC INJECTION ENERGY, C_3 - KM^2/SEC^2
FLIGHT TIME - DAYS
EARTH ELONGATION, ϕ - DEG.
COMMUNICATION DISTANCE, d - AU
NO CONSTRAINT
V_{∞_4}
TOTAL FLIGHT TIME
MAXIMUM
MINIMUM
d
C_3
σ_1
NO CONSTRAINT
FLIGHT TIME
INSIDE JUPITER'S
ACTIVITY SPHERE
ϕ
(JD-244)-3900
JUPITER ARRIVAL DATE
1979
1980
1981

FIGURE 2.2-10

MISSION PLANNING CHART, 1979 LAUNCH

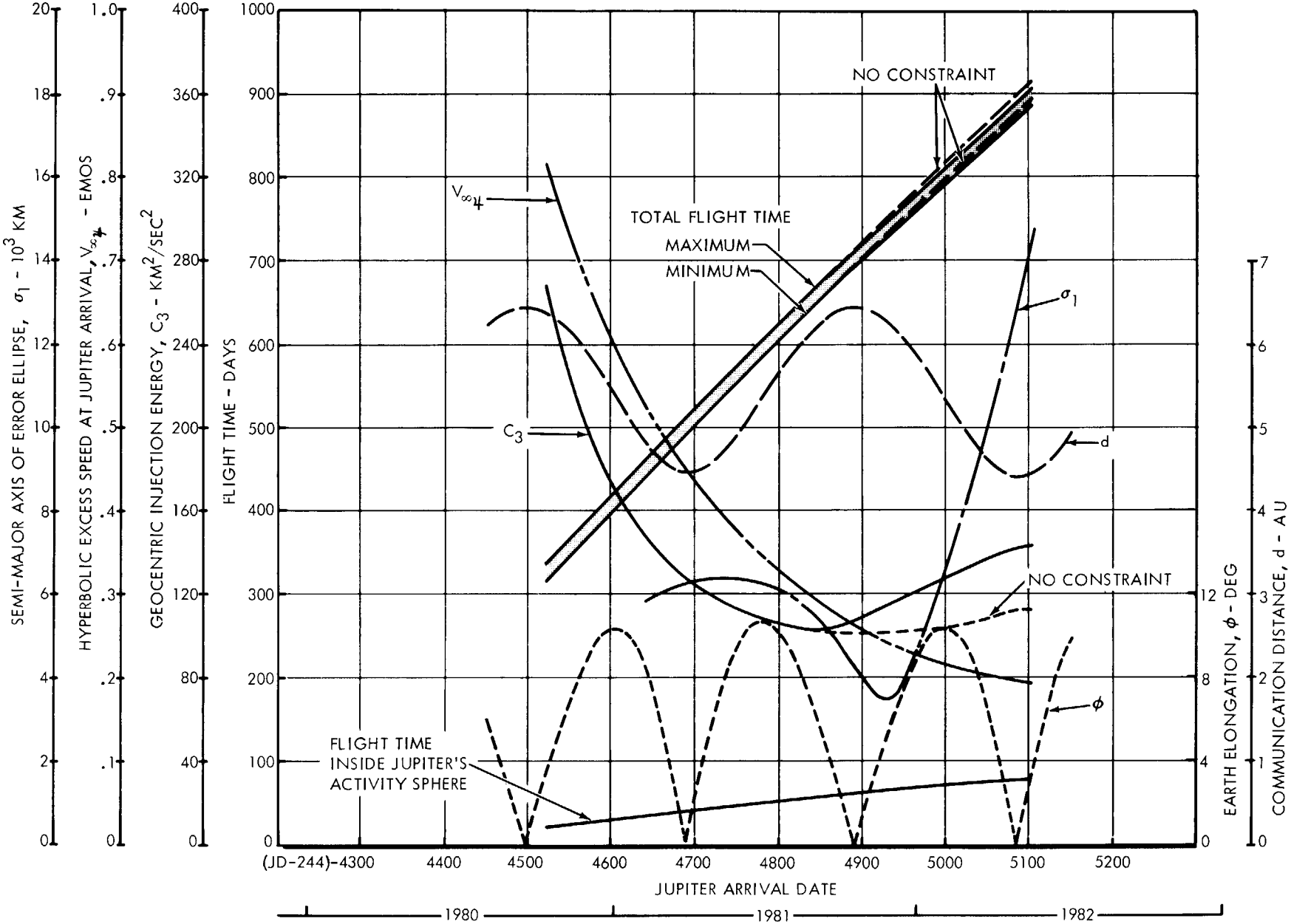

FIGURE 2.2-11

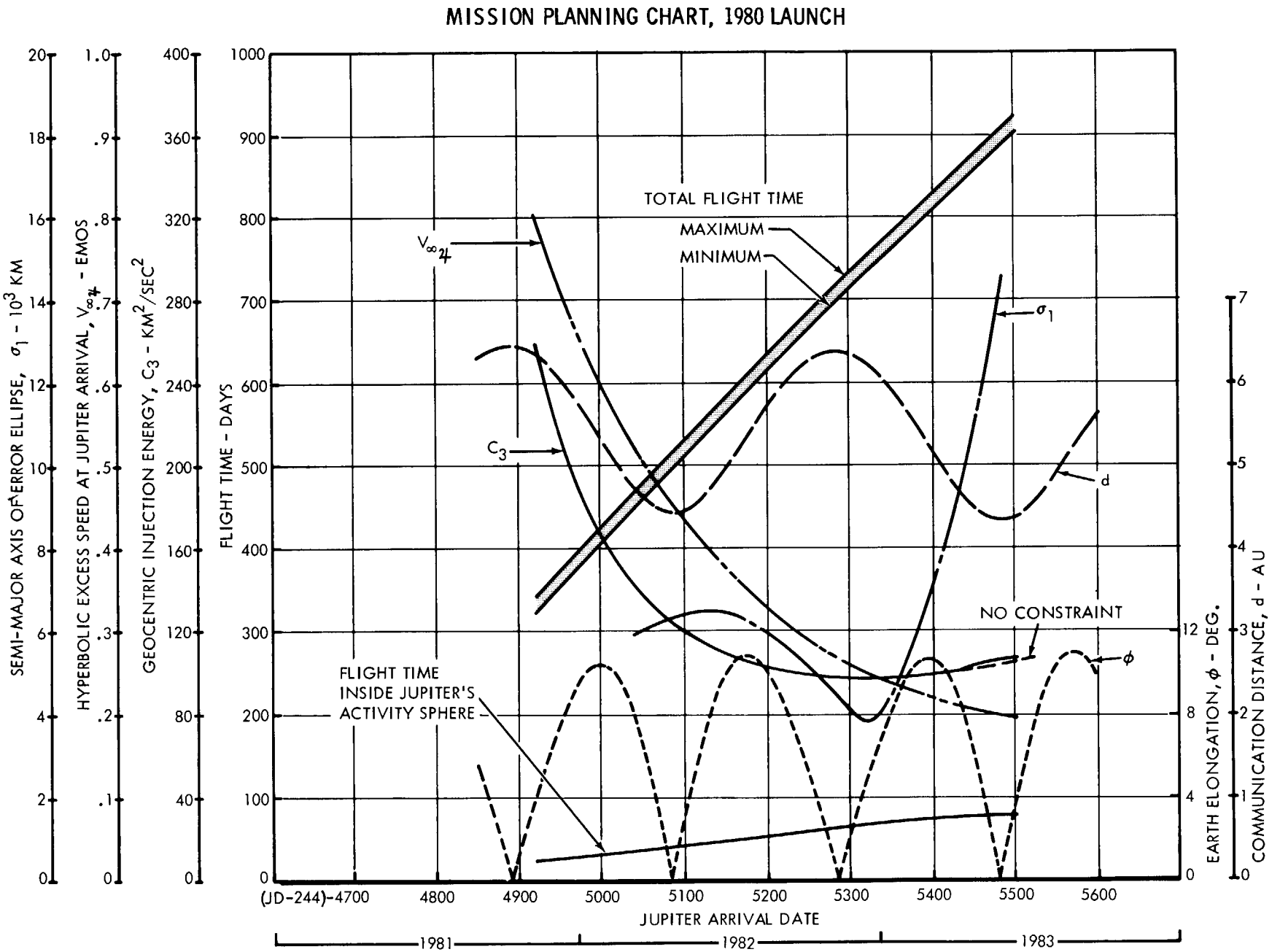
MISSION PLANNING CHART, 1980 LAUNCH
SEMI-MAJOR AXIS OF ERROR ELLIPSE, σ_1 - 10^3 KM
HYPERBOLIC EXCESS SPEED AT JUPITER ARRIVAL, V_{∞_4} - EMOS
GEOCENTRIC INJECTION ENERGY, C_3 - KM^2/SEC^2
FLIGHT TIME - DAYS
EARTH ELONGATION, ϕ - DEG.
COMMUNICATION DISTANCE, d - AU
TOTAL FLIGHT TIME
MAXIMUM
MINIMUM
V_{∞_4}
C_3
σ_1
d
ϕ
NO CONSTRAINT
FLIGHT TIME INSIDE JUPITER'S ACTIVITY SPHERE
(JD-244)-4700
JUPITER ARRIVAL DATE
1981
1982
1983

FIGURE 2.2-12

2.2.3.2 Flight Time Curves

The distance between the two (minimum and maximum) total flight time curves corresponds to the 20-day width of the launch windows which was stipulated for the purpose of defining mission requirements. The curve showing flight time inside Jupiter's activity sphere at the bottom of each chart reflects the two-body hyperbolic flight time from the activity sphere boundary to perijove at an altitude of 0.1 planet radii.

2.2.3.3 Communication Distance and Earth Elongation Angle

The helicocentric configuration of the planets on the arrival date is defined by the communication distance, d, and the Earth elongation, $\emptyset$. The communication distance is the distance between the planets and the Earth elongation angle is the angular separation between Earth and the Sun, as seen from Jupiter. Conjunctions and oppositions of Jupiter are defined by maxima and minima respectively in the communication distance curve. These two types of events are accompanied and more sharply defined by local minima in the Earth elongation curve. Local maxima occur in the Earth elongation curve approximately 90 days before and after each opposition. The maximum Earth elongation just prior to opposition corresponds to a western quadrature of Jupiter, while the maximum immediately following opposition corresponds to an eastern quadrature. The relative positions of the planets at quadrature and opposition are shown in Figure 2.2-13.

Arrival at Jupiter on an opposition date is usually most desirable from the standpoint of radio tracking and communication for the simple reason that the communication distance is minimal. However, there may be situations in which arrival near the date of western or eastern quadrature would be more favorable for communication. For instance, a possible design concept for a minimal-capability spacecraft involves spin-stabilization for attitude control with the directional antenna beam aligned along the spin axis. The transmission of planetary encounter data to Earth would be accomplished by pointing the spacecraft spin vector at the time of spinup in the direction in inertial space where the Earth would appear at the time of encounter. For such a spacecraft, arrival on or near a date of quadrature would maximize the time period available for transmission of encounter data because the angular coordinates of Earth in inertial space (as seen from a spacecraft in the near vicinity of Jupiter) would be changing at a minimal rate.

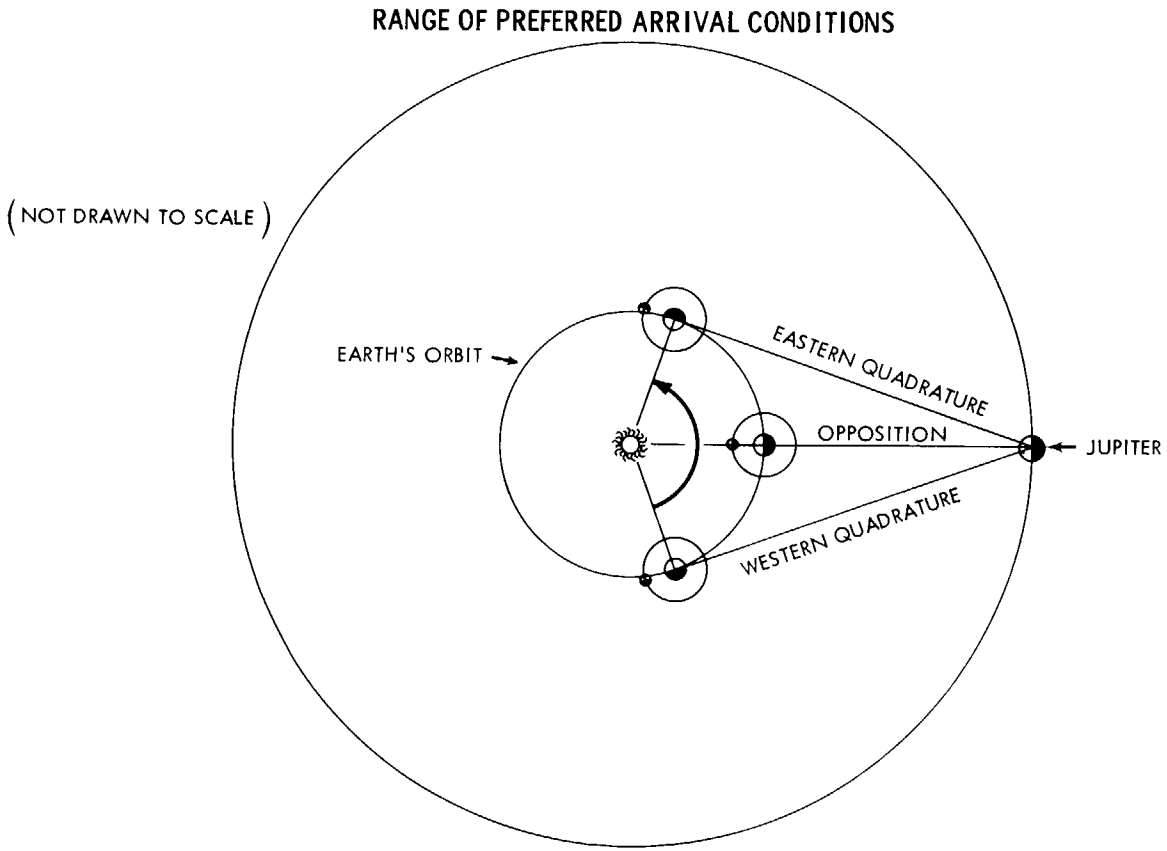
RANGE OF PREFERRED ARRIVAL CONDITIONS
(NOT DRAWN TO SCALE)
EARTH'S ORBIT
EASTERN QUADRATURE
OPPOSITION
JUPITER
WESTERN QUADRATURE

FIGURE 2.2-13

Another mission-planning aspect related to the communication-distance and Earth-elongation curves is concerned with Earth-based optical telescopic observation of the target planet. The correlation of data received from the spacecraft with concurrently obtained Earth-based data would almost certainly improve the scientific value of the mission. Again, arrival on an opposition date would be most favorable for these purposes. This is ture not only because the distance between planets is minimal at opposition, but also (and possibly of greater significiance) because Jupiter rises at sunset, transits the local meridian at midnight, and sets at dawn; thus, the daily observation period is maximized, and optimum viewing conditions are provided. From the standpoint of concurrent optical observation of Jupiter, arrival before the date of western quadrature would be highly undesirable because the planet would transit the local meridian during daylight hours, and less than half the nighttime hours would be available for observation.

One other mission-planning consideration which is related to the Earth-elongation curves in Figures 2.2-5 through 2-2-12 should be mentioned. The Earth elongation angle is equal to the angular separation of the conical (almost cylindrical) Earth-occultation and Sun-occultation zones in jovicentric space. If scientific, operational, and/or environmental considerations relevant to a particular mission should require, for instance, that the spacecraft pass through one of these occultation zones and avoid the other (as in the Mariner 1964 mission), it would have to arrive on a date when the Earth elongation angle is significantly different from zero.

2.2.3.4 Guidance Sensitivity Curves

The σ_1 curves in Figures 2.2-6 through 2.2-12 (the data for the 1973 launch opportunity had not been received when the illustrations were prepared) which show the relationship between guidance sensitivity and arrival date are particularly significant for mission planning. The variable σ_1 is the length of the semi-major axis of the arrival position error ellipse which would result from a 0.1 meter per second spherically-distributed random velocity error in the execution of a guidance correction maneuver. The guidance correction maneuver is assumed to occur a few days after injection, and the gravitational effect of Jupiter is ignored in the computation of the arrival error ellipse. The focussing effect of Jupiter's gravity field reduces the position error at perijove to something

on the order of one-half to one-fourth of the magnitude of σ_1. The arrival position error is proportional to the midcourse execution velocity error, therefore an appropriate factor should be used to obtain arrival errors for a spacecraft guidance system whose execution accuracy is different than 0.1 meter per second.

The σ_1 values shown in the mission planning charts are the maximum values within the appropriate 20-day launch windows, and they were obtained from heliocentric conic trajectory data supplied by JPL. The minimum value of σ_1 occurs for arrival dates ranging from approximately 50 days before to 50 days after a conjunction of jupiter with corresponding flight times ranging from 650 to 750 days depending on the launch year. The position error increases quite rapidly for longer flight times; whereas, in the case of shorter flight times, the increase is more moderate and reaches a local maximum value less than twice as great as the minimum.

2.2.3.5 Geocentric Injection Energy

The single most important mission-planning parameter is the required injection energy, because it determines the payload capability of the launch vehicle for the mission. The geocentric injection energy C_3 is equal to the square of the departure hyperbolic excess speed, and actually corresponds to twice the Earth-relative kinetic energy per unit mass of the spacecraft when it is an "infinite" distance from Earth. The injection energy curves shown in Figures 2.2-5 through 2.2-12 reflect the maximum values of C_3 within the appropriate 20-day launch windows. Only data for Type I heliocentric trajectories (having heliocentric transfer angles smaller than 180 degrees) are contained in these mission planning charts. This is in line with the results of earlier studies (Reference 2.2-1) which revealed that the reduction in C_3 which can be realized in some launch years by using Type II trajectories (having transfer angles greater than 180 degrees) is comparatively small in relation to the required increase in flight time.

In all of the mission planning charts, injection energy requirements for unconstrained launch windows are shown for reference. Notable examples of the effect of the previously-described 36-degree asymptote declination constraint on injection energy requirements can be seen in the mission planning charts for the 1973 and the 1978 launch periods (Figures 2.2-5 and 2.2-10. The greatest difference in minimum C_3 for constrained

and unconstrained injection energy curves occurs in 1978, where the miminum-C_3 penalty is about 7 percent (i.e., 7 km^2/sec^2). The 36-degree declination constraint never causes a penalty for flight times shorter than 575 days.

Optimum flight times based on minimum injection energy requirement range from 575 to 750 days, depending on the launch year. For flight times shorter than about 400 days, the injection energy requirements increase very rapidly beyond the reasonable capabilities of chemically-propelled launch vehicles. The payload capabilities of 5 possible launch vehicles for Jupiter missions, based on the injection energy requirements shown in Figures 2.2-5 through 2.2-12, are discussed in subsection 2.3.

2.2.4 Conclusions

On the basis of the results of the investigation of energy requirements and general trajectory characteristics of Jupiter flyby missions discussed in the preceding paragraphs, the following major conclusions have been reached:

1. Assuming a 20-day launch window is needed, the nominal interplanetary flight time required to realize the minimum injection energy for Type I trajectories is never longer than 750 days.

2. If good guidance accuracy is to be realized, interplanetary flight time should never exceed 800 days. If flight times are held below 700 days, the arrival position error will never be greater than twice the minimum value possible.

3. The use of chemically-propelled launch vehicles on missions with flight times shorter than 400 days will probably not be feasible.

4. From the standpoint of (a) radio tracking and communication, and (b) concurrent Earth-based optical observation of Jupiter, preferred arrival dates range from approximately 90 days before to 90 days after an opposition date (between the dates of western and eastern quadrature).

5. For a given launch year, there is only one 180-day arrival period which conforms to the conditions described in conclusion (4) and which also falls within the flight time limits described in conclusions (1), (2), and (3). The center of this arrival period is the date of the second opposition of Jupiter following the spacecraft's departure from Earth. The nominal interplanetary flight time for arrival on this opposition date is approximately 510 days. The nominal flight time for arrival on the date of western quadrature immediately preceding this opposition is about 420 days. The nominal flight time for arrival on the date of eastern quadrature immediately following this opposition is about 600 days.

6. In the case of missions arriving at perijove within the 180-day period described inconclusion (5), the stipulation that the departure asypmptote declination must lie in the range of $\pm$36 degrees has no effect on mission requirements in any launch year studies, except 1973. The effect of the declination constraint in 1973 is minimal, causing only a slight increase in injection energy requirement for flights between 575 and 600 days duration.

2.2.5 References

2.2-1 Wilson, S. W. Jr., et al., "Preliminary Analysis of One-Way Ballistic Flyby and Caputre Missions to Jupiter", General Dynamics Corporation, Fort Worth Division, MR-FS-36, 11 November 1964.

2.3 LAUNCH VEHICLE EVALUATION

The payload capabilities of 5 launch vehicles were evaluated in relation to the energy requirements for Jupiter Flyby missions. The following vehicles were specified by JPL:

1. Saturn V/Centaur
2. Saturn V
3. Saturn IB/Centaur/HEKS
4. Titan IIICx/Centaur
5. Atlas SLV3x/Centaur/HEKS.

A sixth vehicle, Atlas SLV3x/Centaur (without the high energy kick stage, HEKS) was determined to have no potential for a Jupiter mission early in the study and was considered no further.

2.3.1 Basic Payload Capabilities

The basic payload capabilities of the subject vehicles were defined by JPL in the form of curves of gross payload (including spacecraft adapter and aerodynamic fairing) versus C_3 attainable with a 90-degree launch azimuth on the Eastern Test Range (ETR). These curves were contained in a guideline document (Reference 2.3-1) in which it was pointed out that the indicated capabilities did not represent those of current vehicle configurations or of configurations currently being developed but that they represented the performance capabilities which would be technically feasible by the 1970-1980 time period with appropriate uprating and development programs. In this light, the payload data should be considered acceptable for long-range mission planning and conceptual design studies, but not necessarily so for other purposes.

The launch vehicle gross payload curves in Reference 2.3-1 were adjusted to reflect performance capabilities that were more compatible with the probable operational modes and constraints associated with Jupiter flyby missions. Specifically, two adjustments were made (1) to account for the net payload decrement caused by carrying the mass of the payload aerodynamic fairing to 350,000 feet, and (2) to account for the injection energy decrement resulting from an ETR launch azimuth of 114 rather than 90 degrees. The adjusted curves for all 5 launch vehicles are shown in Figure 2.3-1.

SUMMARY OF LAUNCH VEHICLE PAYLOAD CAPABILITY

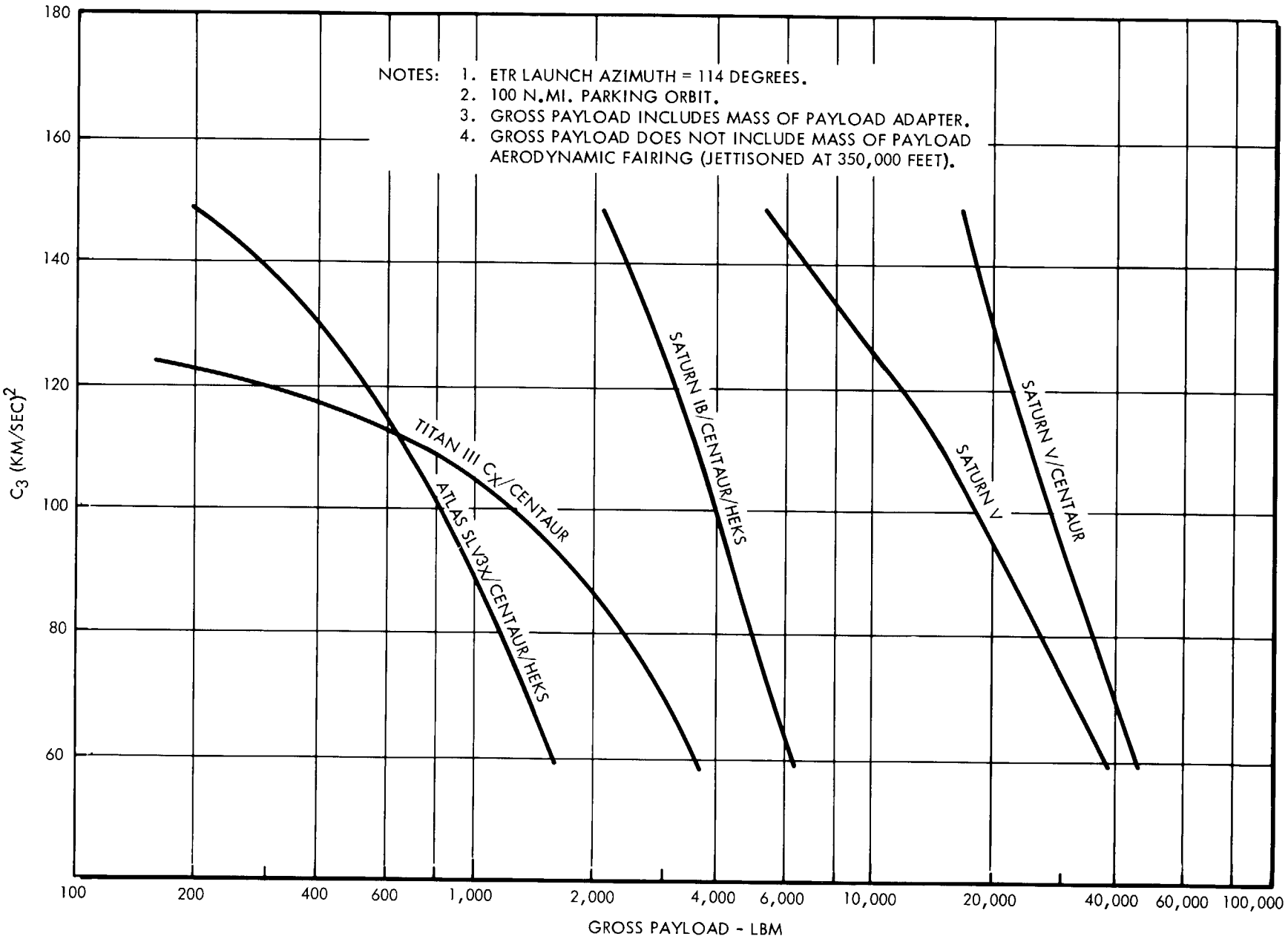

FIGURE 2.3-1

In Reference 2.3-1, it is stated that if the payload aerodynamic fairing is jettisoned at 350,000 feet (during ascent to the parking orbit), the interplanetary injection payload values shown in the curves in Reference 2.3-1 should be reduced by 10 percent of the actual fairing mass W_F. If the fairing is jettisoned in the parking orbit or after interplanetary injection, payloads should be decremented by 0.4 W_F or 1.0 W_F, respectively. Since aerodynamic effects are negligible above 350,000 feet, there appear to be only two plausible reasons for retaining the payload fairing beyond this point: (1) for thermal and meteoroid protection during the parking orbit coast and/or interplanetary injection phases, or (2) as an auxiliary load path for thrust acceleration loads. In view of the significant payload mass penalties involved in retaining the fairing, and the relatively short period (less than 2 hours) spent in the parking orbit as compared to the length of the interplanetary flight (several hundred days), retention of the fairing for thermal or meteoroid protection does not appear desirable.

Although a more thorough structural analysis is in order after launch vehicle/payload selections have been made, retention of the fairing for structural reasons does not appear to be a likely necessity. In the case of Saturn vehicles in which a Centaur stage is used, it is stated in Reference 2.3-1 that the load from the spacecraft and the HEKS (High Energy Kick Stage), when used, should be shared "approximately equally" between the fairing and the Centaur stage (i.e., about half of the load should be routed around Centaur, via the fairing, to the SIVB stage) during the boost phase of the trajectory. A check of thrust acceleration histories for typical Saturn IB/Centaur and Saturn V/Centaur boost trajectories indicates that the maximum acceleration experienced between 350,000 feet and SIVB burnout ranges from 50 to 67 percent of the peak acceleration which occurs below 350,000 feet. Therefore, jettisoning the fairing at 350,000 feet should not impose a much greater maximum load on Centaur than would result if the fairing were retained until final burnout of the SIVB stage. On the Atlas and Titan vehicles, there is no available load path around Centaur (i.e. all of the load from fairing, spacecraft, and kick stage must be routed through Centaur during the entire boost trajectory); hence, retention of the payload fairing on these vehicles above 350,000 feet would not be desirable from the structural standpoint.

Adjustment of the data in Reference 2.3-1 to a launch azimuth of 114 degrees was accomplished in line with the conservative overall policy which was adopted for the definition of launch vehicle capabilities for Jupiter missions. The 114 degree azimuth is the most severe azimuth from the standpoint of payload degradation due to non-Easterly launches within the normal ETR firing sector of

90 to 114 degrees. To assure maximum utilization of existing range facilities, only those interplanetary transfer trajectories which can be attained with the limits of the normal ETR firing sector were considered acceptable for the purpose of defining mission requirements. The effect of this constraint is to rule out any interplanetary transfer requiring a departure asymptote declination outside the range of $\pm$ 36 degrees. Therefore, when the geocentric injection energy C_3 required for a heliocentric trajectory which satisfies the cited asymptote declination constraint is used to find an allowable spacecraft-plus-adapter mass from the adjusted curves, the launch vehicle can be counted on to deliver the indicated payload (with some reserve in most cases).

Figure 2.3-2 schematically illustrates the procedure which was followed in the adjustment of the payload curves. In line with the previous discussion, the payload decrement ΔW_λ was taken to be 10 percent of the estimated payload fairing mass given in Reference 2.3-1. The ΔW_λ values (constant for a given launch vehicle) are given in Table 2.3-1.

PAYLOAD CURVE ADJUSTMENTS

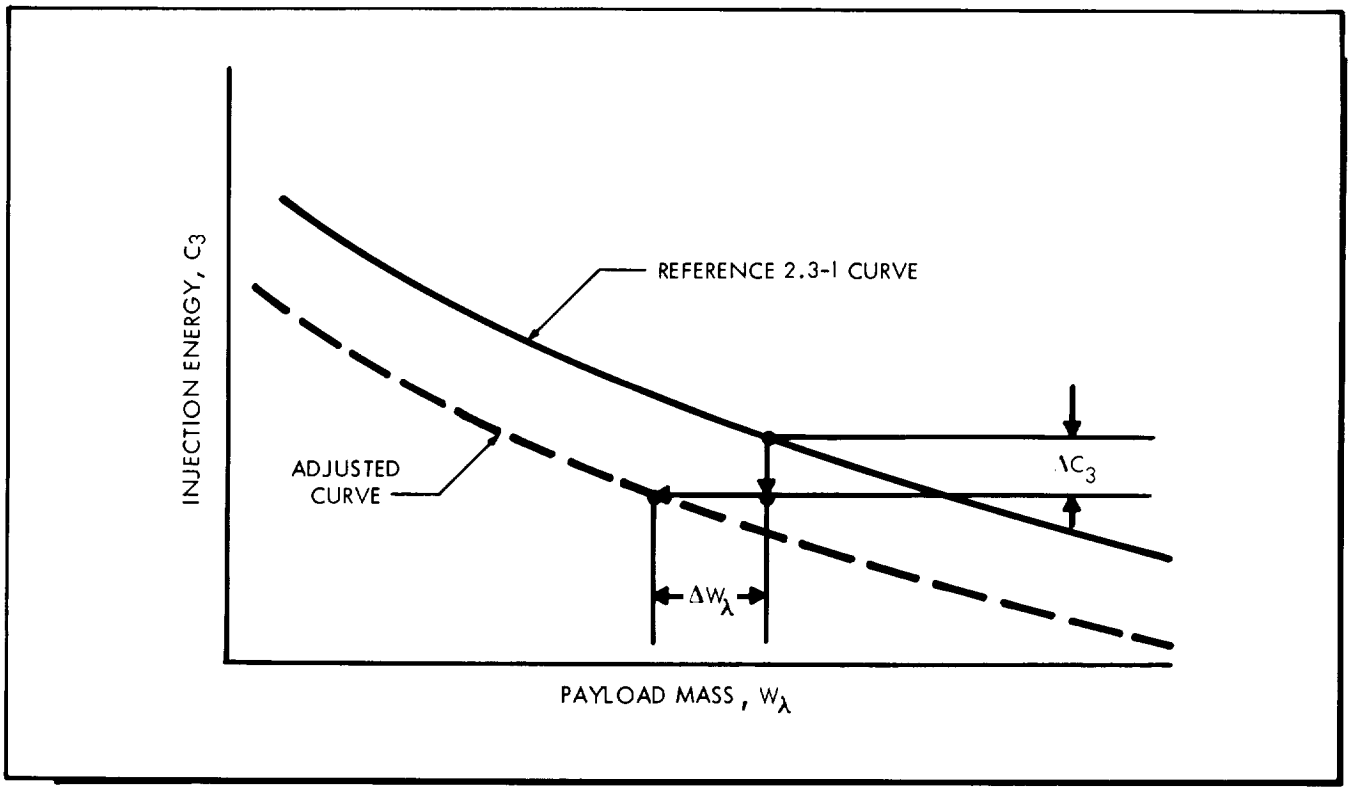

FIG. 2.3-2

Table 2.3-1 PAYLOAD DECREMENTS

Launch Vehicle	ΔW_λ (lbm)
Saturn V/Centaur	330
Saturn V	750
Saturn IB/Centaur/HEKS	260
Titan IIICx/Centaur	185
Atlas SLV3x/Centaur/HEKS	152

The injection energy decrements ΔC_3 were obtained by subtracting 36.6 meters per second (the difference between the components of Earth rotational velocity in the launch trajectory planes for ETR launch azimuths of 90 and 114 degrees) from the injection velocity required for the original value of C_3. Injection was assumed to occur at a geocentric distance of 8000 kilometers. Specifically, the equation

$$\Delta C_3 = C_3 - \left[\left(\sqrt{99.6508 + C_3} - .0366 \right)^2 - 99.6508 \right]$$

was used. The constant, 99.6508, is the square of the escape speed (in units of km/sec) at a distance of 8000 kilometers from the center of the Earth. The resulting values of ΔC_3 are shown in Table 2.3-2.

Table 2.3-2 C_3 DECREMENTS

C_3 $(km/sec)^2$	ΔC_3 $(km/sec)^2$
60	0.92
70	0.95
80	0.98
90	1.01
100	1.03
110	1.06
120	1.08
130	1.11
140	1.13
150	1.17

The method used to adjust the payload curves to account for the 114 degree launch azimuth is admittedly crude and may be somewhat in error. Point checks of actual payload decrements due to non-easterly launches in the case of a similar launch vehicle indicate

that the ΔC_3 values possibly should be greater by a factor of two. Doubling the injection energy decrement would shift all the adjusted payload curves downward by about 1.0 km^2/sec^2. The effective payload decrement resulting from such an additional shift would be less than 4 percent in all cases except for payloads smaller than 1600 lbm on the Titan IIICx/Centaur and smaller than 350 lbm on the Atlas SLV3x/Centaur/HEKS launch vehicle.

2.3.2 Payload Capabilities for Jupiter Missions

In Figures 2.3-3 through 2.3-10, the payload capability of each launch vehicle is shown as a function of flight time for each launch opportunity between 1973 and 1980. The flight times shown in these figures are mean values for 20-day-fixed arrival-date launch windows; therefore, the actual flight time within any launch window represented by a point on one of these curves varies by $\pm$10 days from the indicated value. The C_3 requirements which define the payload capability for a given vehicle and flight time were taken from the mission planning charts which were discussed in paragraph 2.2.3. It is noteworthy that, although Titan IIICx/Centaur always has a greater maximum payload capability in any given launch year, below a certain flight time the Atlas SLV3x/Centaur/HEKS can deliver a greater payload. The break-even flight time varies from 490 to 565 days, depending on the launch year.

In Figures 2.3-11 through 2.3-15, payload capability as a function of flight time is summarized with respect to launch vehicle rather than launch year. It is not surprising that the payload capabilities of Sature V/Centaur and Saturn IB/Centaur/HEKS, since they are rather efficient 4-stage vehicles, are relatively insensitive to variations in flight time and launch year. The Titan IIICx/Centaur is most sensitive to such variations, while Saturn V and Atlas SLV3x/Centaur/HEKS exhibit a moderate degree of sensitivity.

2.3.3 References

2.3-1 Technical Direction Memorandum No. 1, Contract 951285, 7 January 1966.

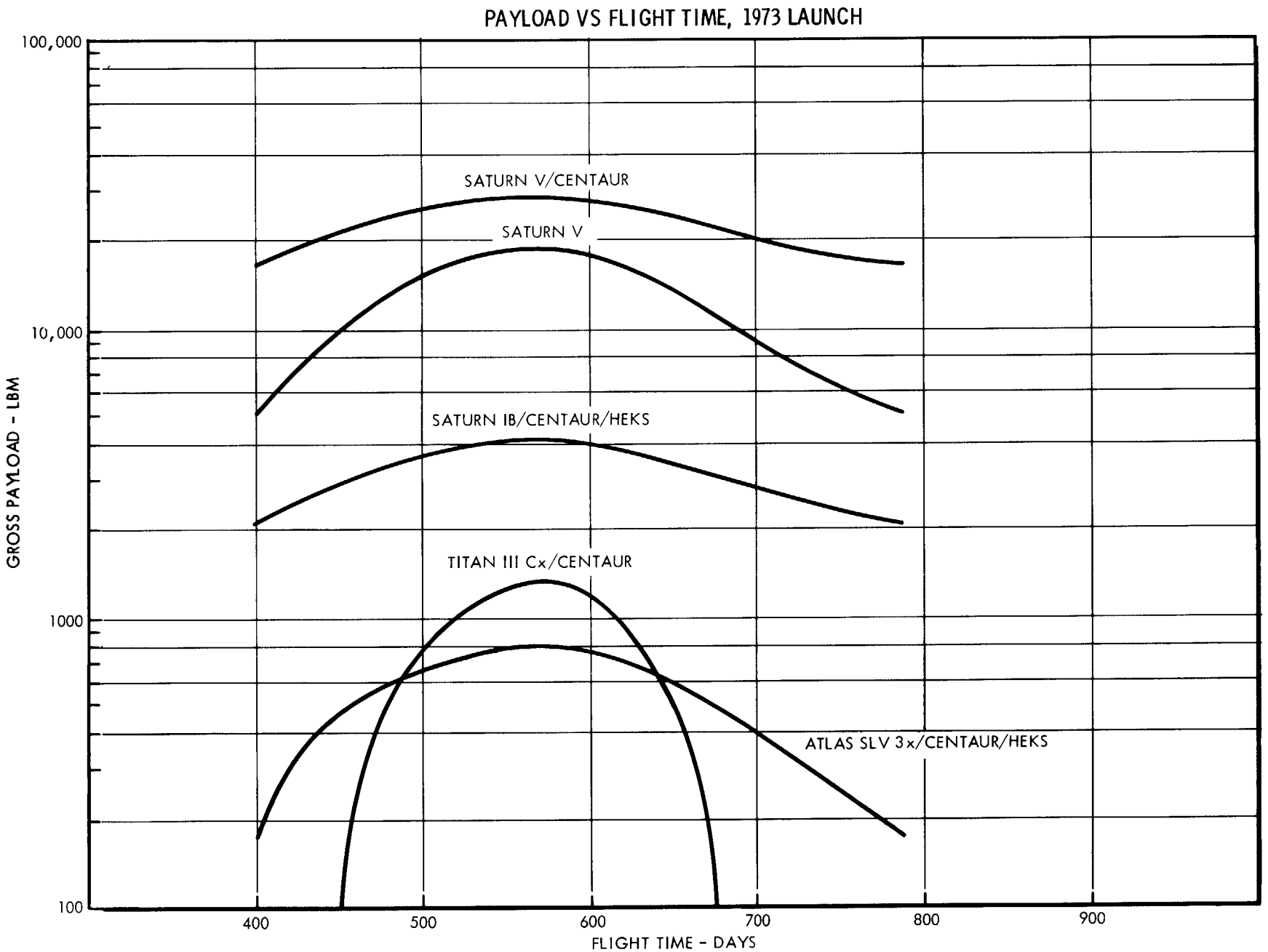
PAYLOAD VS FLIGHT TIME, 1973 LAUNCH
100,000
10,000
1000
100
GROSS PAYLOAD - LBM
SATURN V/CENTAUR
SATURN V
SATURN IB/CENTAUR/HEKS
TITAN III Cx/CENTAUR
ATLAS SLV 3x/CENTAUR/HEKS
400
500
600
700
800
900
FLIGHT TIME - DAYS

FIGURE 2.3-3

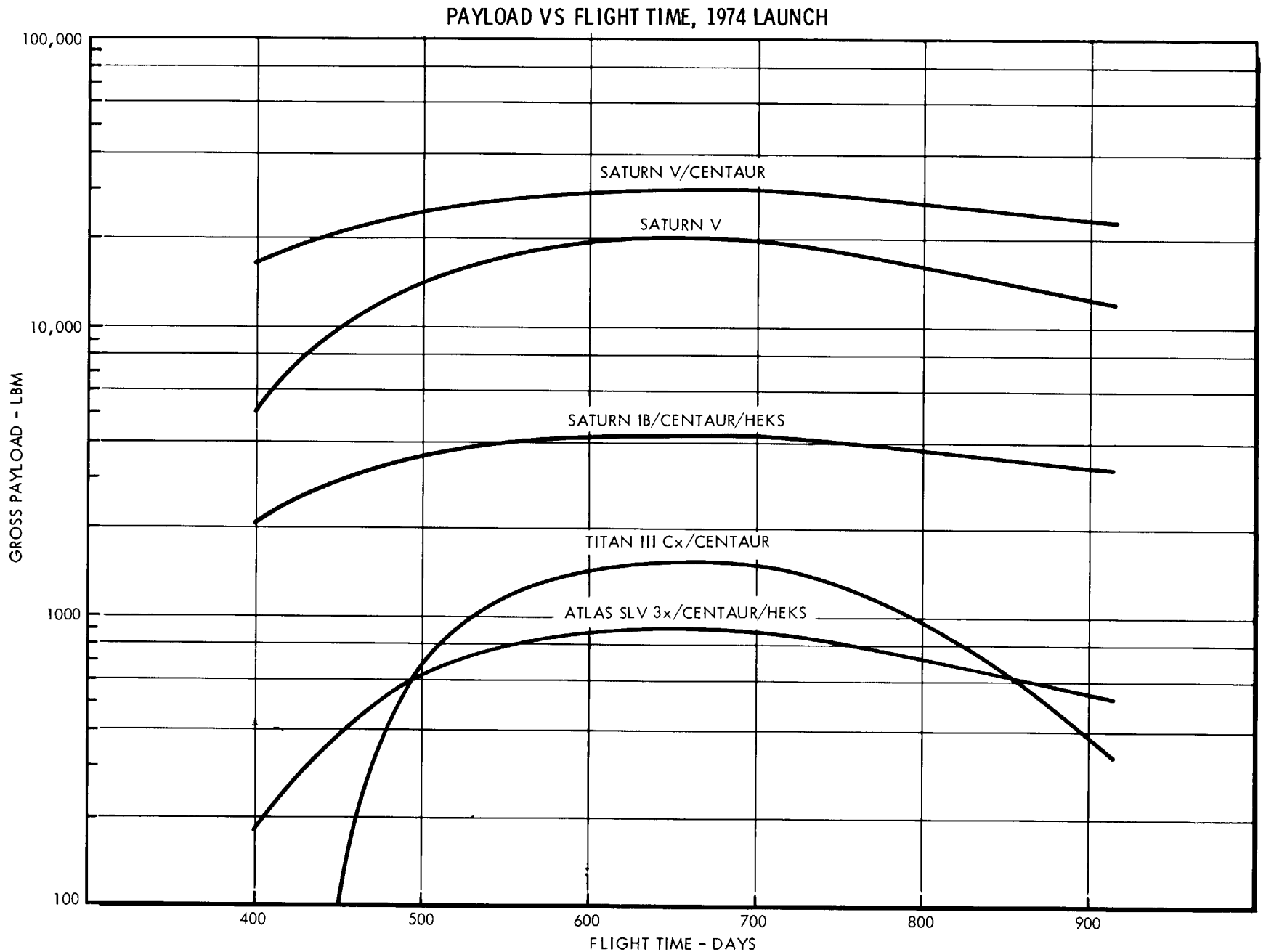
PAYLOAD VS FLIGHT TIME, 1974 LAUNCH
100,000
10,000
1000
100
GROSS PAYLOAD - LBM
SATURN V/CENTAUR
SATURN V
SATURN IB/CENTAUR/HEKS
TITAN III Cx/CENTAUR
ATLAS SLV 3x/CENTAUR/HEKS
400
500
600
700
800
900
FLIGHT TIME - DAYS

FIGURE 2.3-4

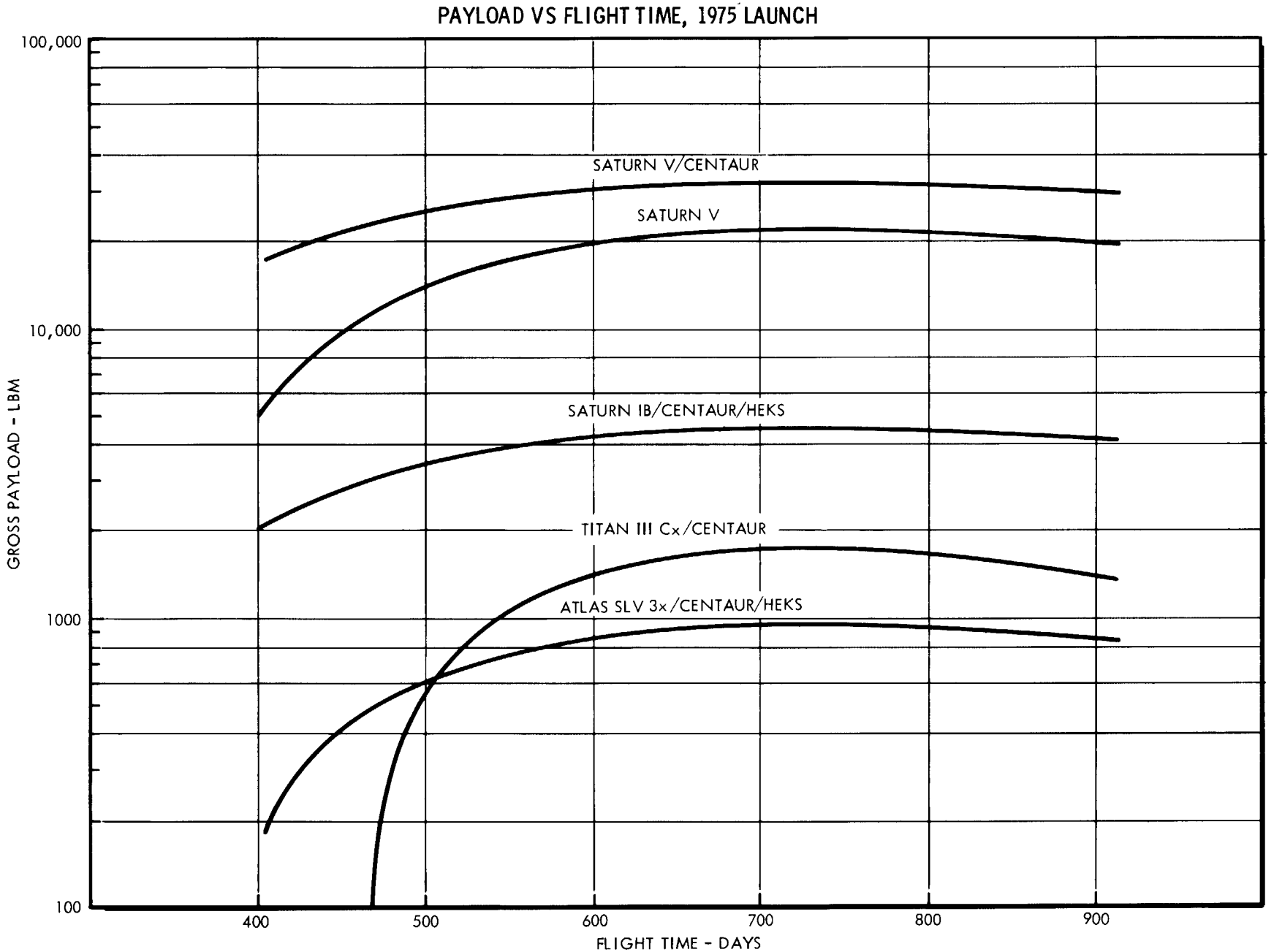
PAYLOAD VS FLIGHT TIME, 1975 LAUNCH
100,000
10,000
1000
100
GROSS PAYLOAD - LBM
SATURN V/CENTAUR
SATURN V
SATURN IB/CENTAUR/HEKS
TITAN III Cx/CENTAUR
ATLAS SLV 3x/CENTAUR/HEKS
400
500
600
700
800
900
FLIGHT TIME - DAYS

FIGURE 2.3-5

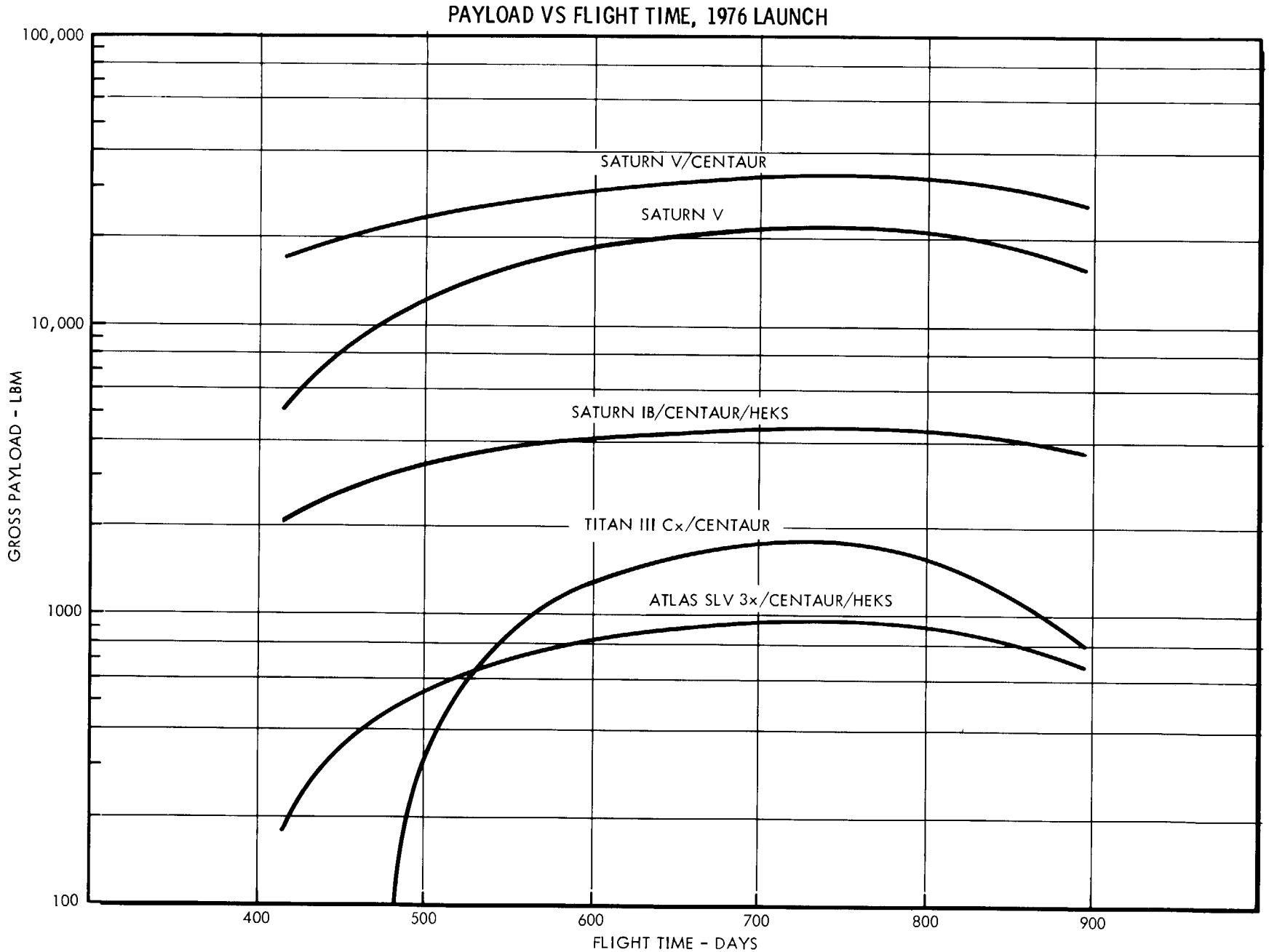
PAYLOAD VS FLIGHT TIME, 1976 LAUNCH
100,000
10,000
1000
100
GROSS PAYLOAD - LBM
SATURN V/CENTAUR
SATURN V
SATURN IB/CENTAUR/HEKS
TITAN III Cx/CENTAUR
ATLAS SLV 3x/CENTAUR/HEKS
400
500
600
700
800
900
FLIGHT TIME - DAYS

FIGURE 2.3-6

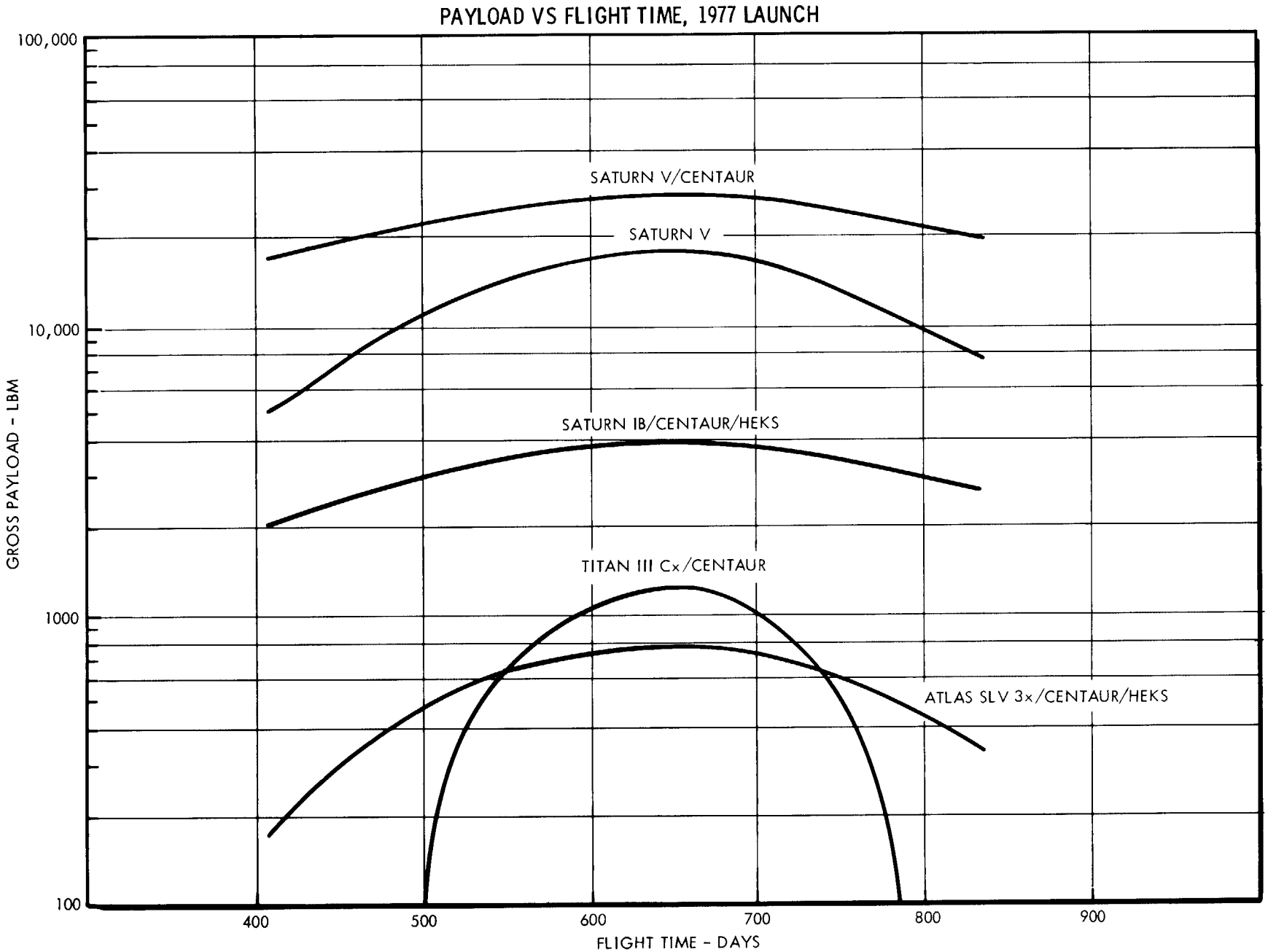
PAYLOAD VS FLIGHT TIME, 1977 LAUNCH
100,000
10,000
1000
100
GROSS PAYLOAD - LBM
SATURN V/CENTAUR
SATURN V
SATURN IB/CENTAUR/HEKS
TITAN III Cx/CENTAUR
ATLAS SLV 3x/CENTAUR/HEKS
400
500
600
700
800
900
FLIGHT TIME - DAYS

FIGURE 2.3-7

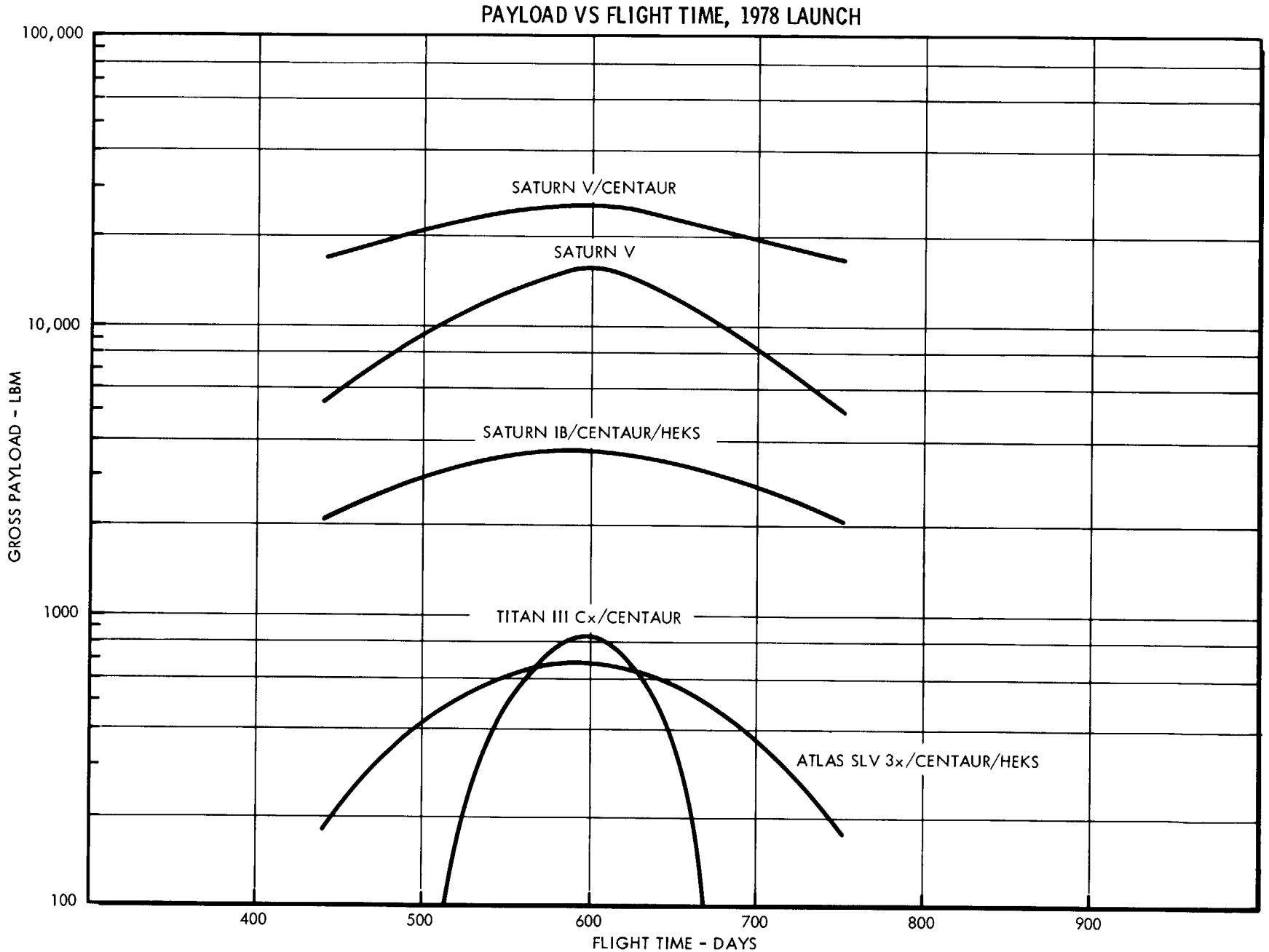
PAYLOAD VS FLIGHT TIME, 1978 LAUNCH
100,000
10,000
1000
100
GROSS PAYLOAD - LBM
SATURN V/CENTAUR
SATURN V
SATURN IB/CENTAUR/HEKS
TITAN III Cx/CENTAUR
ATLAS SLV 3x/CENTAUR/HEKS
400
500
600
700
800
900
FLIGHT TIME - DAYS

FIGURE 2.3-8

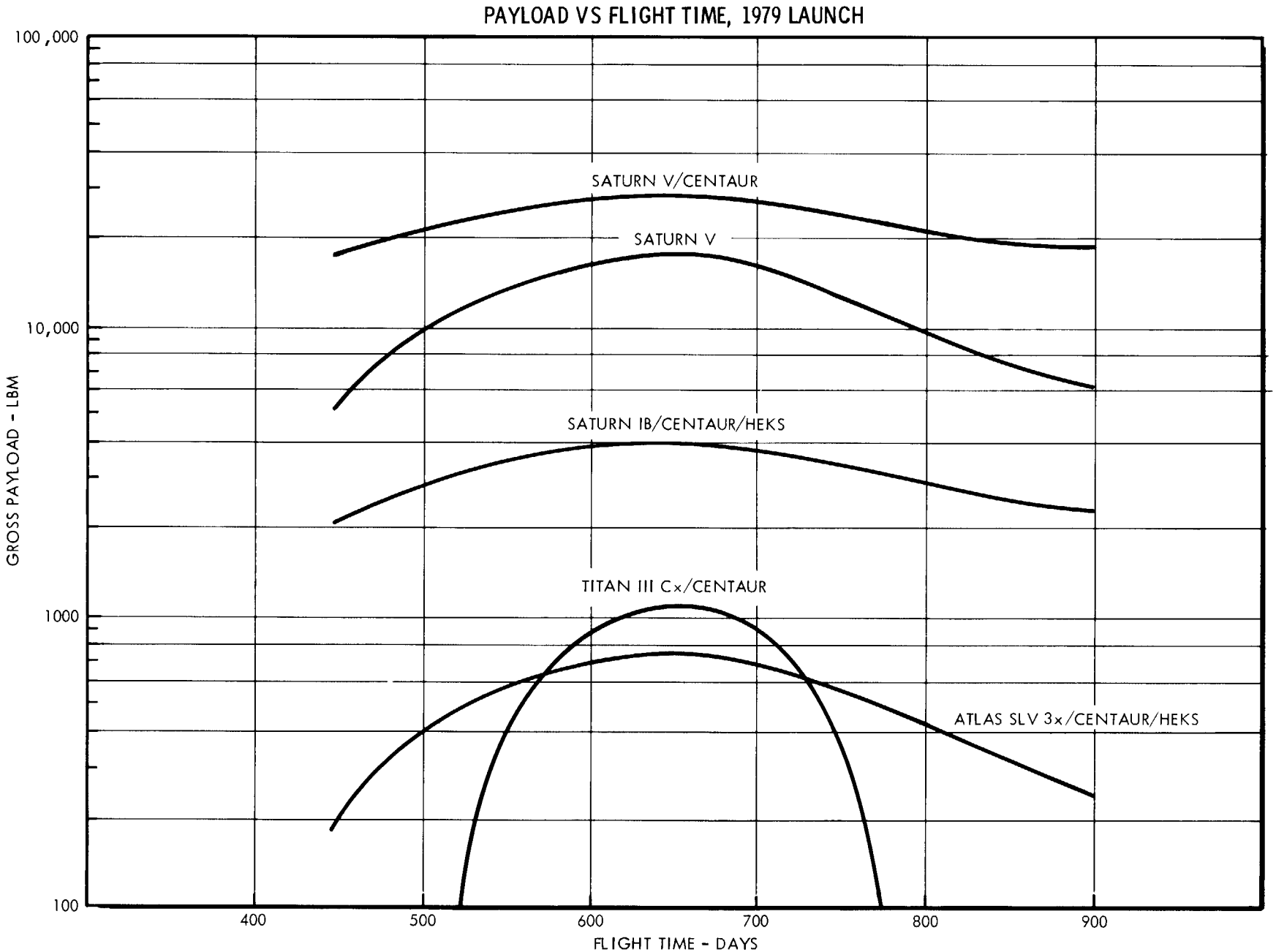
PAYLOAD VS FLIGHT TIME, 1979 LAUNCH
100,000
10,000
1000
100
GROSS PAYLOAD - LBM
SATURN V/CENTAUR
SATURN V
SATURN IB/CENTAUR/HEKS
TITAN III Cx/CENTAUR
ATLAS SLV 3x/CENTAUR/HEKS
400
500
600
700
800
900
FLIGHT TIME - DAYS

FIGURE 2.3-9

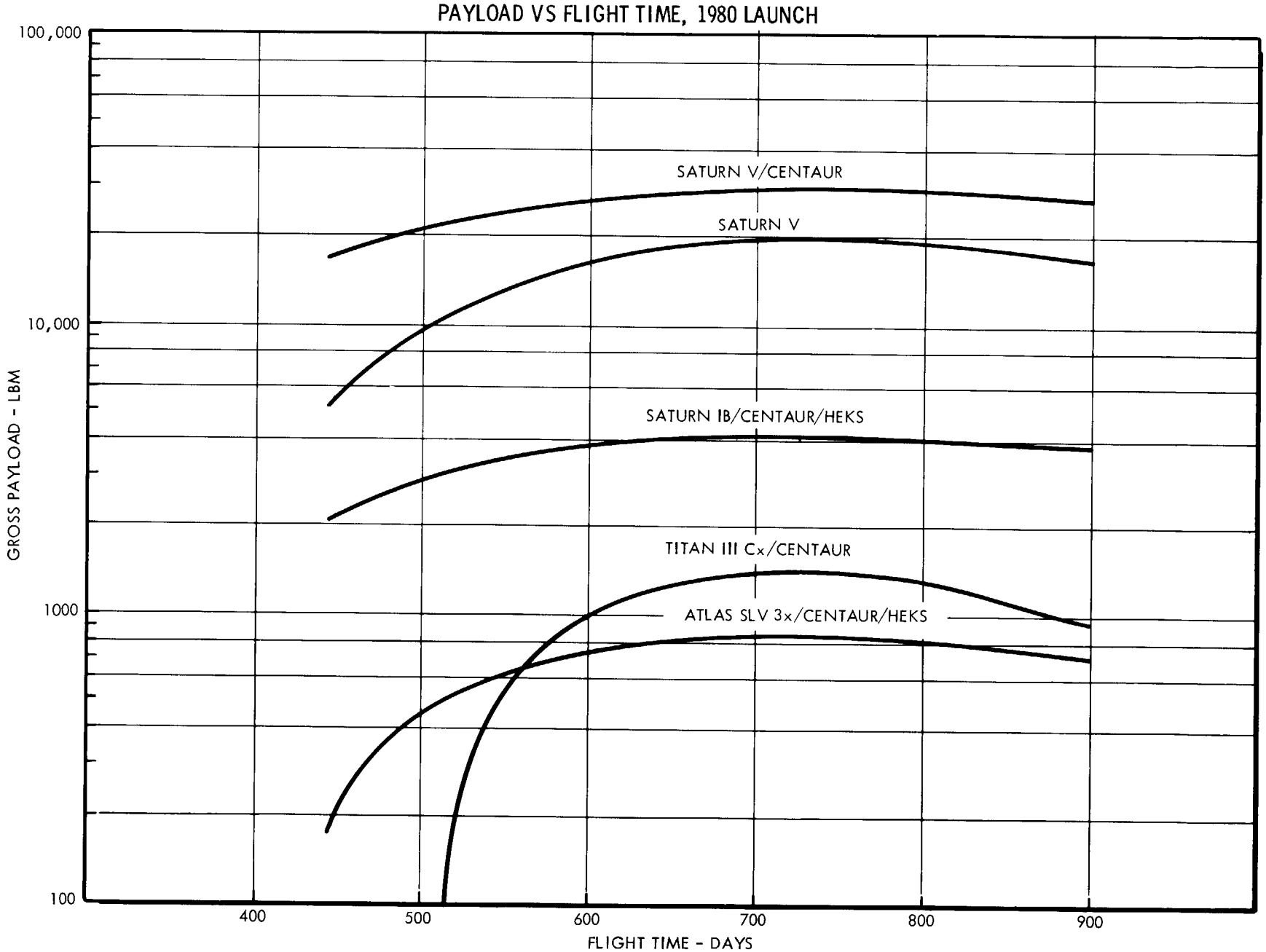
PAYLOAD VS FLIGHT TIME, 1980 LAUNCH
100,000
10,000
1000
100
GROSS PAYLOAD - LBM
SATURN V/CENTAUR
SATURN V
SATURN IB/CENTAUR/HEKS
TITAN III Cx/CENTAUR
ATLAS SLV 3x/CENTAUR/HEKS
400
500
600
700
800
900
FLIGHT TIME - DAYS

FIGURE 2.3-10

JUPITER MISSION PAYLOAD CAPABILITY, SATURN V/CENTAUR

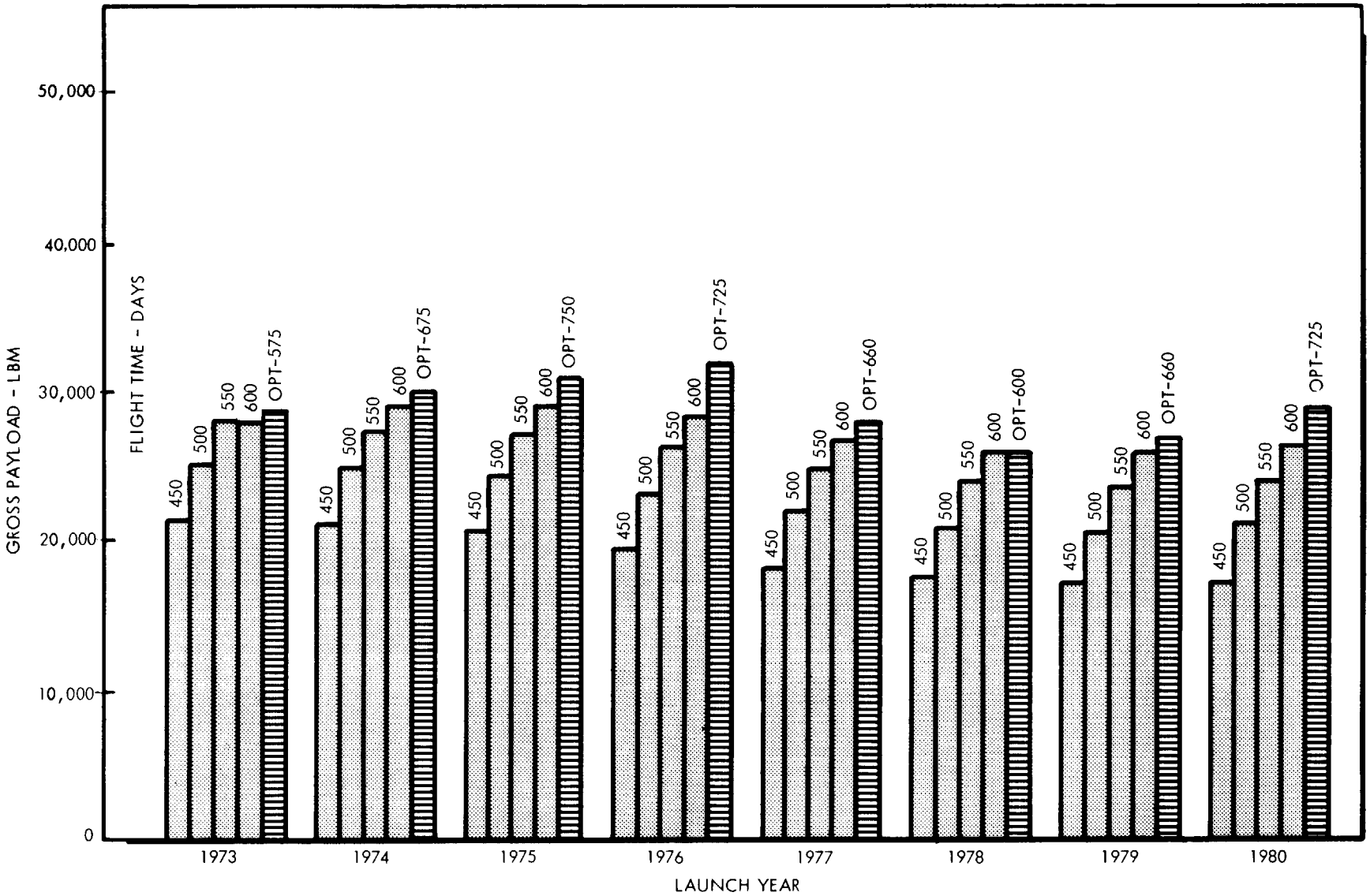

FIGURE 2.3-11

JUPITER MISSION PAYLOAD CAPABILITY, SATURN V

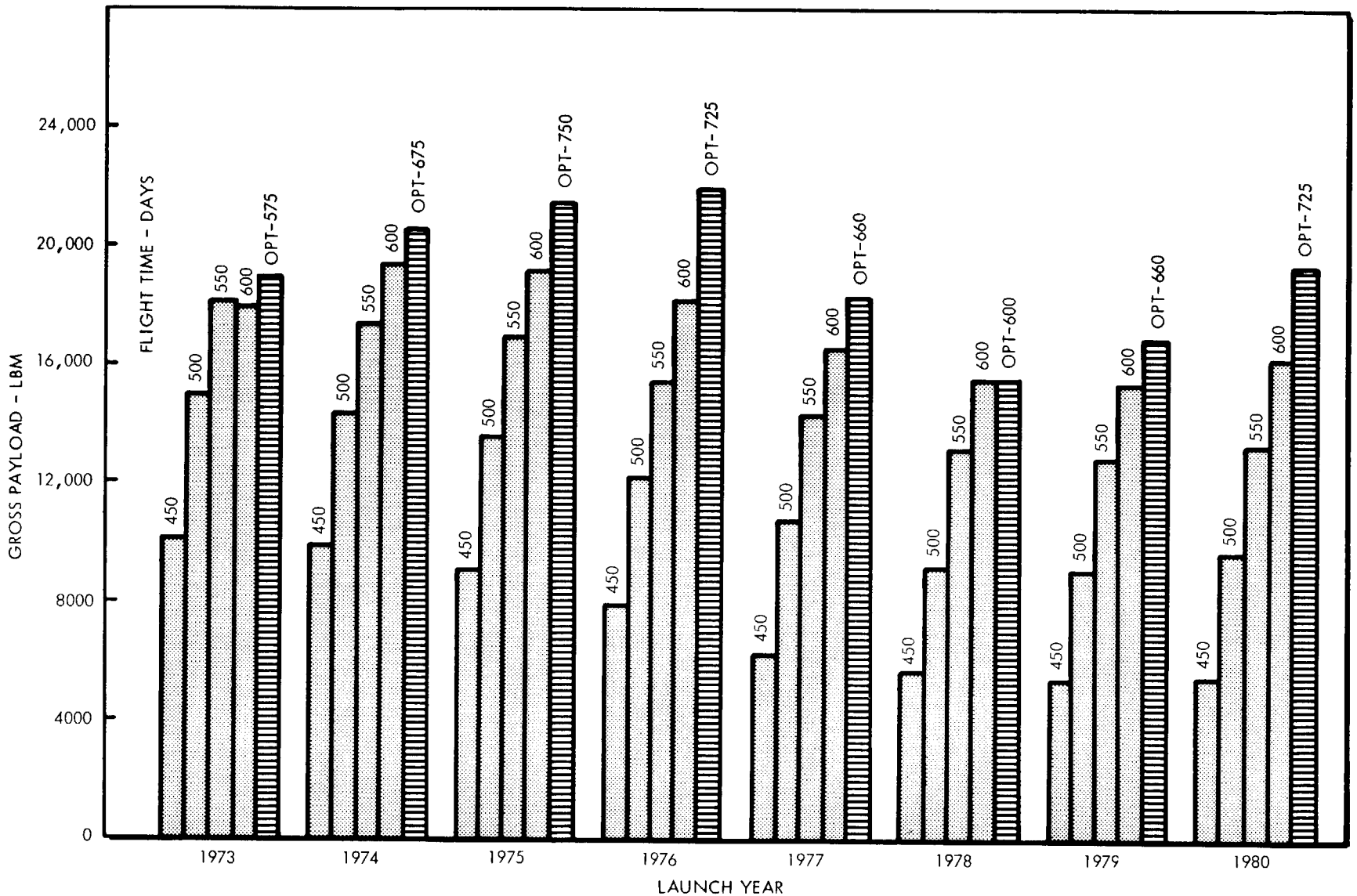

FIGURE 2.3-12

JUPITER MISSION PAYLOAD CAPABILITY, SATURN IB/CENTAUR/HEKS

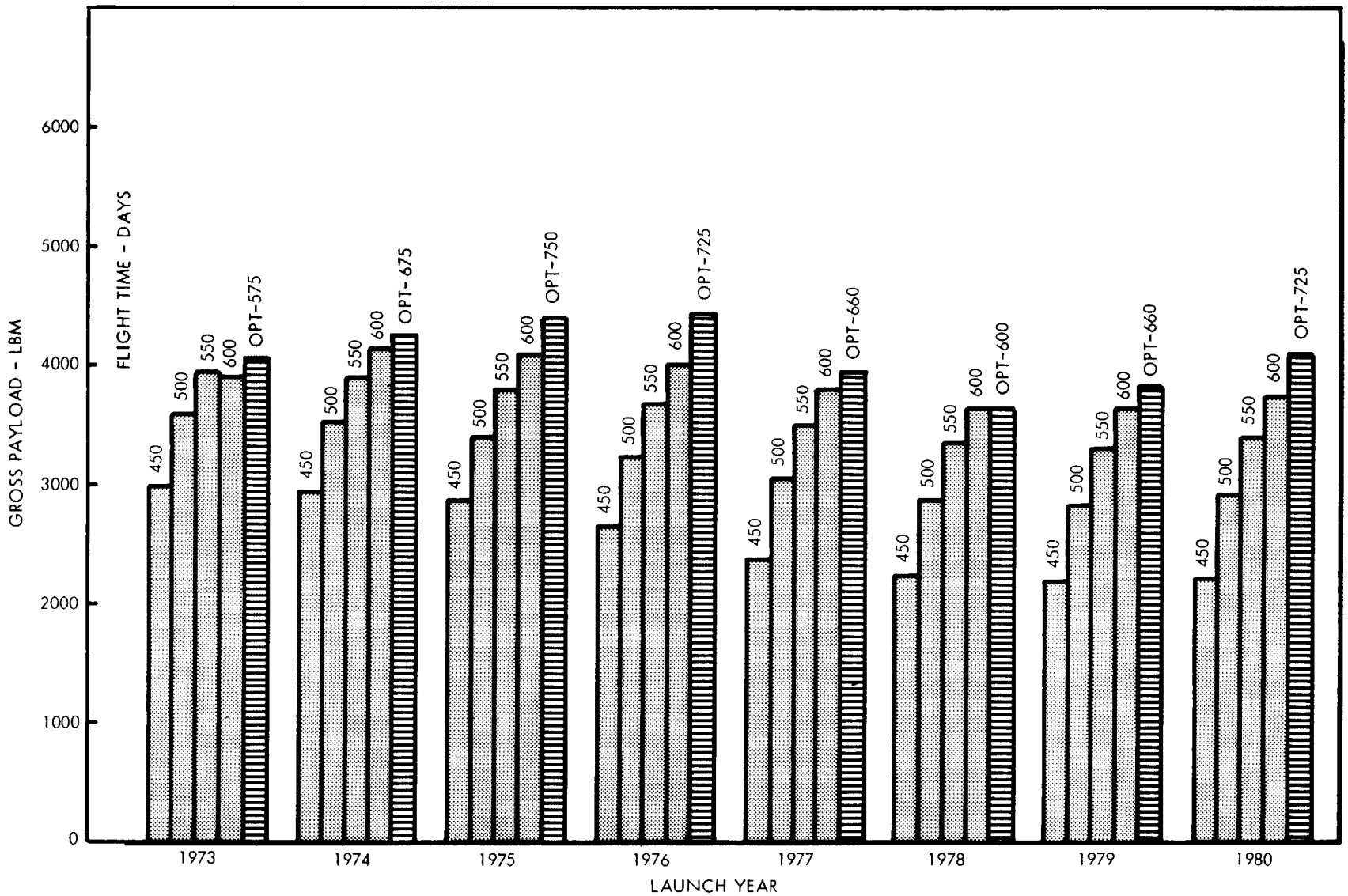

FIGURE 2.3-13

JUPITER MISSION PAYLOAD CAPABILITY, TITAN IIICx/CENTAUR

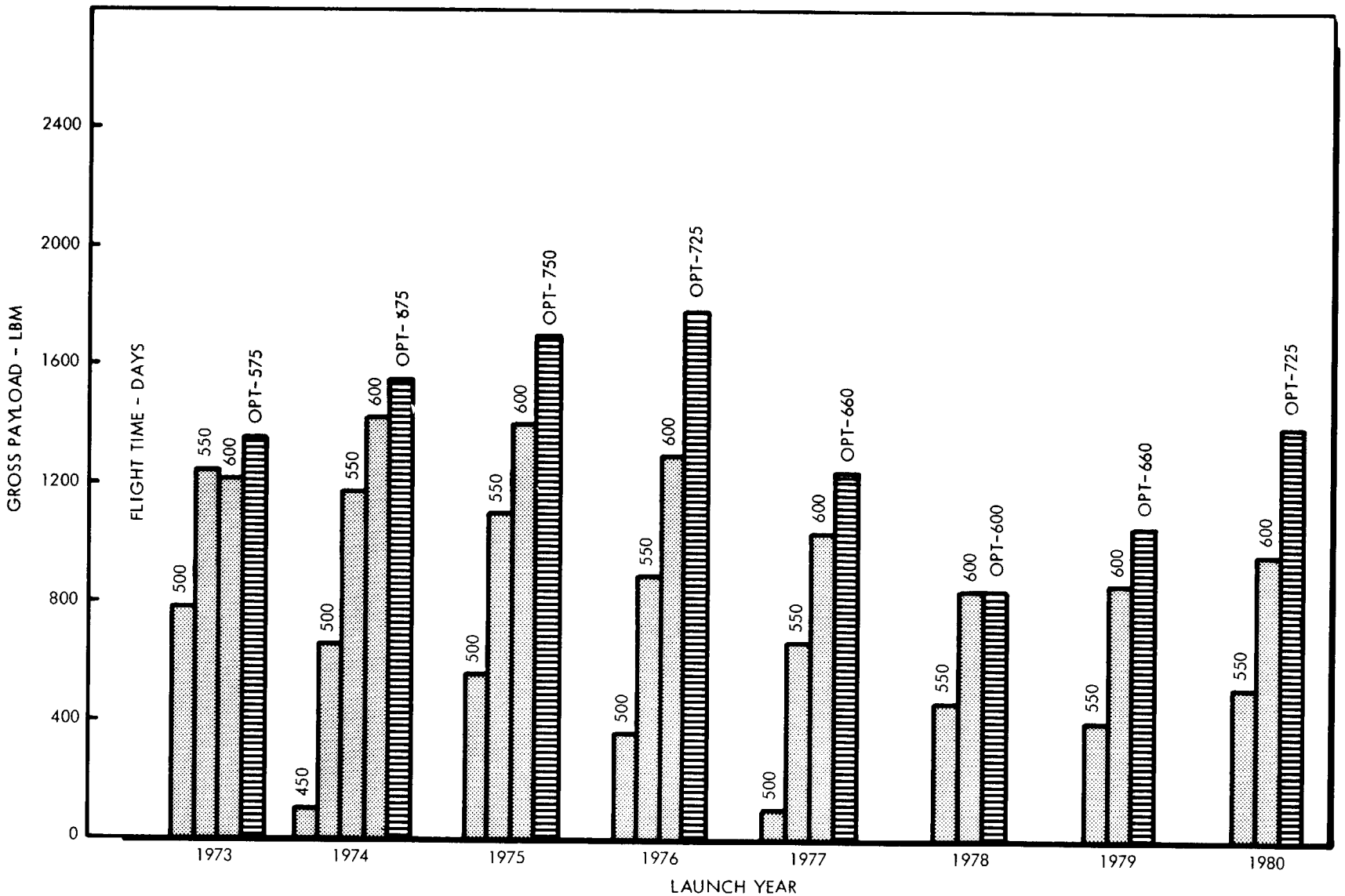

FIGURE 2.3-14

JUPITER MISSION PAYLOAD CAPABILITY, ATLAS SLV3x/CENTAUR/HEKS

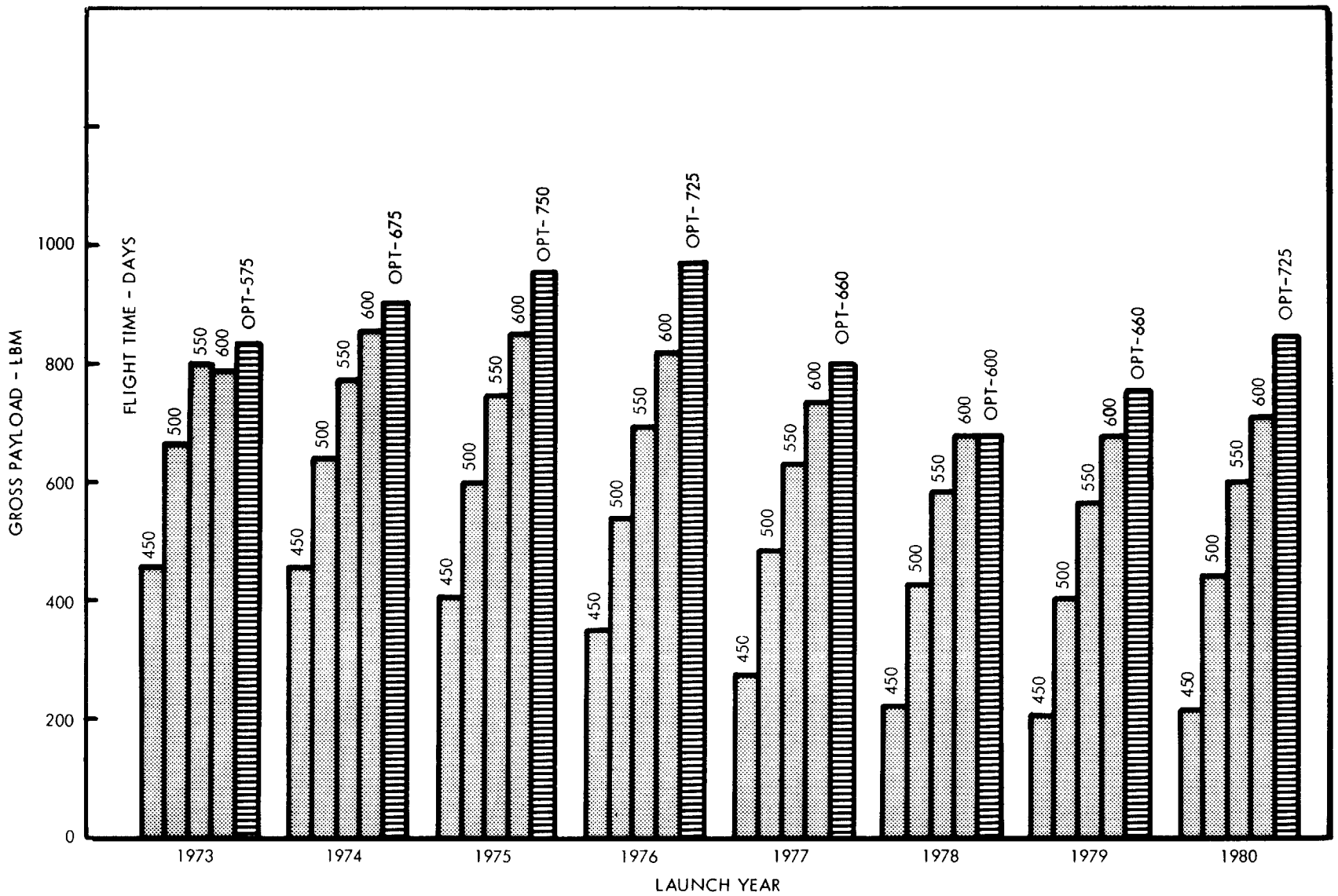

FIGURE 2.3-15

2.4 DETAILED MISSION PROFILE ANALYSIS

The detailed mission profile analysis has been conducted to obtain histories of environmental data, pointing angles, and similar design data for use in the subsystem design studies and to determine the effects of targeting alternatives on overall flight path characteristics. Mission profile characteristics were defined (1) by the use of simple two-body trajectory approximations and (2) by the use of very accurate numerical integrations of the differential equations of motion.

2.4.1 Two-Body Trajectory Data

For the purpose of making two-body trajectory computations and analyses, the overall flight profile was divided into four phases: (1) Earth departure, (2) outbound heliocentric, (3) encounter, and (4) post-encounter. Within each of these phases, the particular trajectory approximation and analysis method most appropriate to the phase was utilized.

2.4.1.1 Earth Departure Phase

Curves of geocentric distance versus time for typical Earth-departure hyperbolas are shown in Figure 2.4-1. The time required for the spacecraft to reach the boundary of Earth's activity sphere ($\approx$ 925,000 kilometers) is typically on the order of one day for Jupiter missions, as compared to approximately three days for Mars and Venus missions. Assuming comparable DSIF tracking configurations, this means that, on a Jupiter mission, only about one-third as much close-in tracking data is available prior to the execution of the first guidance correction maneuver. However, according to heliocentric conic trajectory data supplied by the Jet Propulsion Laboratory, the contribution of orbit determination errors to the arrival position error ellipse is roughly an order of magnitude smaller than the contribution of a nominal 0.1 meter per second execution error in the maneuver itself. Therefore, orbit determination accuracy during the departure (geocentric) phase of the mission does not appear to present a problem.

2.4.1.2 Outbound Heliocentric Phase

Two-body heliocentric trajectory data on a number of representative Earth-Jupiter transfers were complied (Reference 2.4-1) for use in the subsystem design studies. The heliocentric geometry of a representative trajectory is shown in Figure 2.4-2.

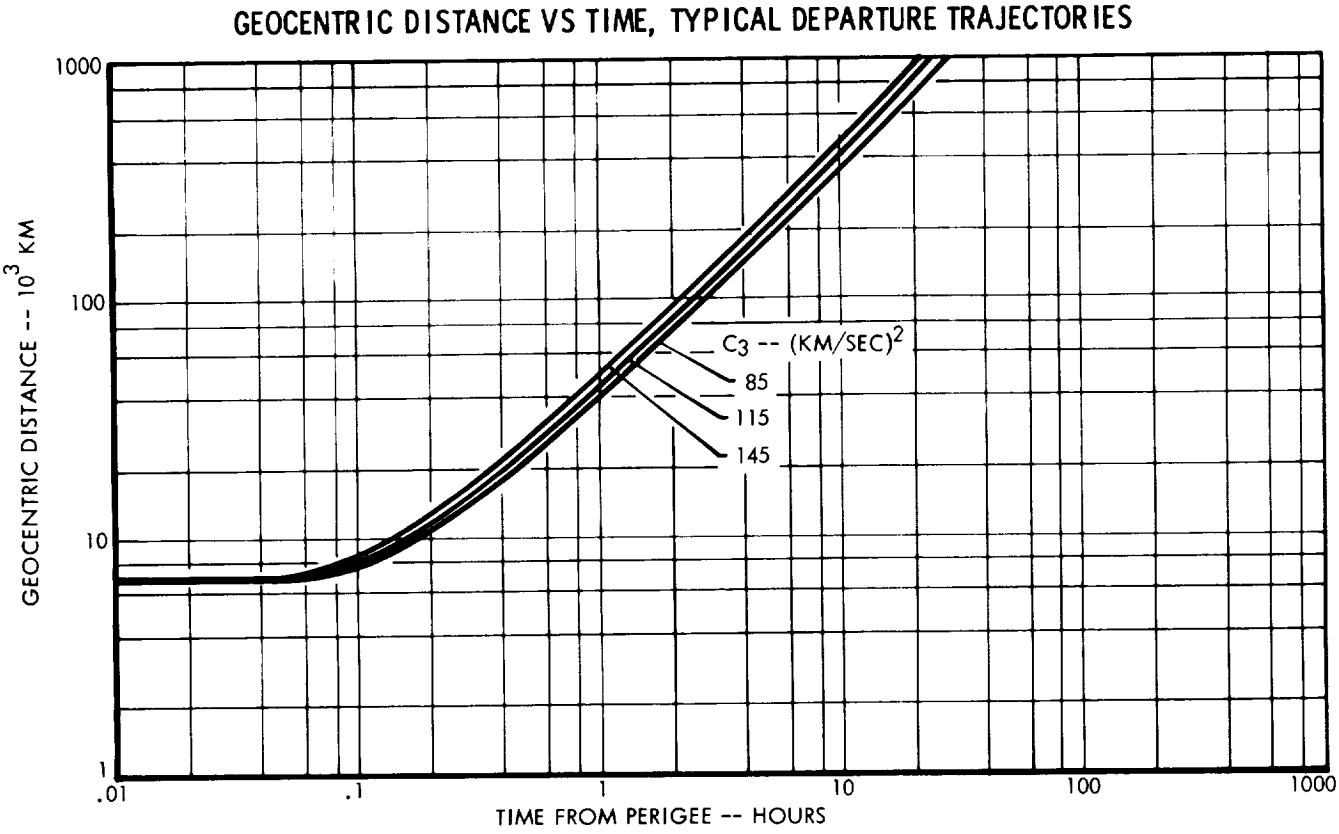

FIGURE 2.4-1

In addition to the heliocentric and geocentric coordinates of the spacecraft, the referenced report contains spacecraft-centered coordinates (relative to a Mariner-type Sun-Canopus reference system) of Earth and Jupiter at 10-day intervals, as well as the spacecraft-relative speed and impact direction of "average" meteroids.

Of particular interest are the histories of communication distance and Earth's out-of-beam-plane angle (Figures 2.4-3 through 2.4-5). These histories are applicable to a spin stability of spacecraft whose spin axis is approximately normal to the ecliptic. They are used to investigate the feasibility of communication with such a spacecraft. In this particular design concept, a toroidal beam antenna is utilized for long-distance communication. Therefore, the Earth (as seen from the spacecraft) must be located within a fraction of a degree of the antenna beam plane (normal to the spin axis). In order to demonstrate antenna feasibility, is is necessary to show that a direction in inertial space can be found such that the spacecraft's spin vector is properly oriented during the major portion of the mission.

HELIOCENTRIC GEOMETRY, TYPICAL 500-DAY MISSION

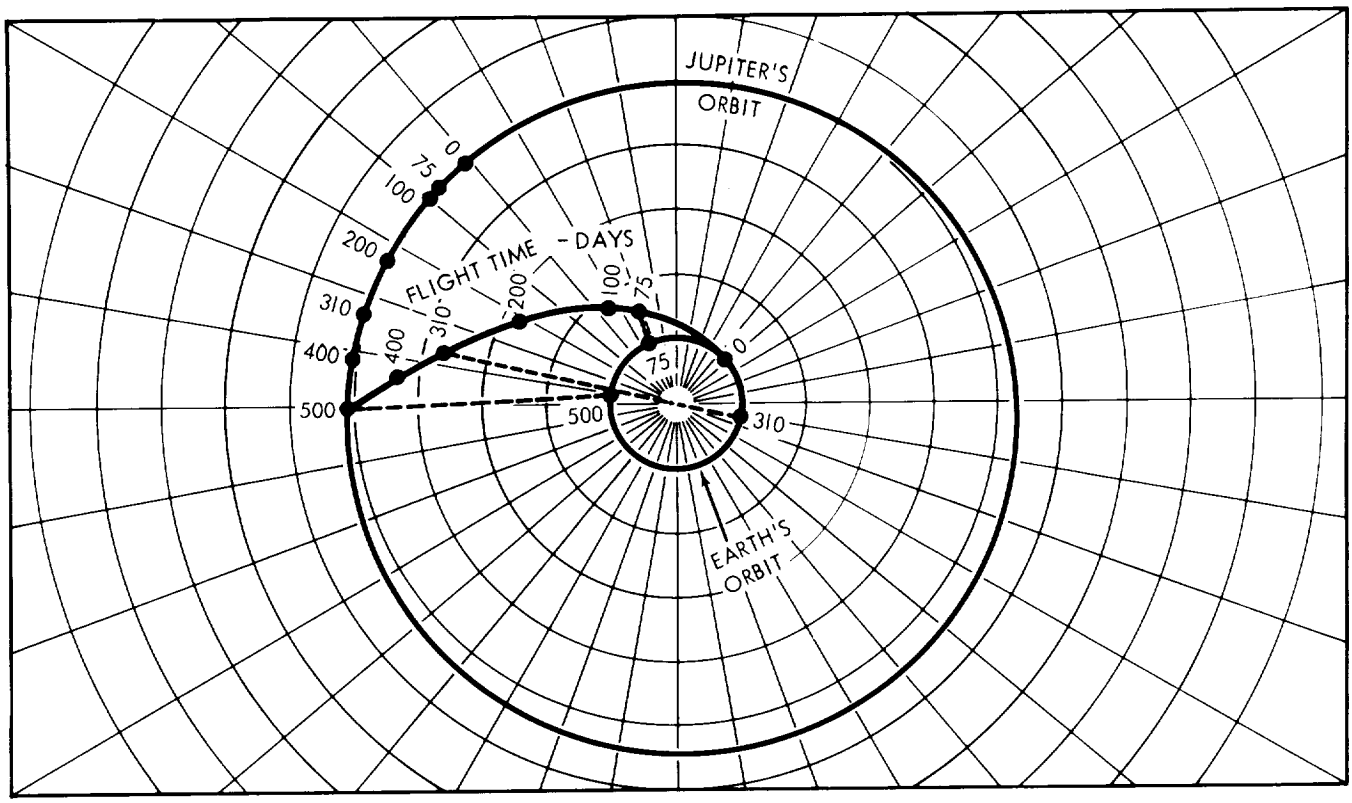

FIGURE 2.4-2

The figures cited demonstrate that such a concept is geometrically feasible. One of the primary disadvantages of this concept is that the choice of jovicentric encounter trajectories is essentially limited to equatorial passages. This latter restriction is necessary if the communication link is to be maintained during the post-encounter phase of the mission.

2.4.1.3 Encounter Phase

In Figure 2.4-6, jovicentric distance is shown as a function of time for representative encounter hyperbolas. For the purpose of demonstrating the three-dimensional aspects of the encounter phase of the mission, relatively crude but effective three-dimensional models -- of which Figure 2.4-7 is a two-dimensional representation -- were prepared for typical approach conditions. These models have proved very helpful in visualizing the available alternatives with respect to the planet-relative orientation of the encounter trajectory.

The available alternatives in the area of encounter trajectory characteristics are more clearly defined in Figures 2.4-8 through 2.4-10. The targeting charts for the 582-day,

COMMUNICATION PARAMETERS HISTORY, SPIN-STABILIZED SPACECRAFT, 1976 500-DAY MISSION

(ANTENNA BEAM PLANE NORMAL TO SPIN AXIS)

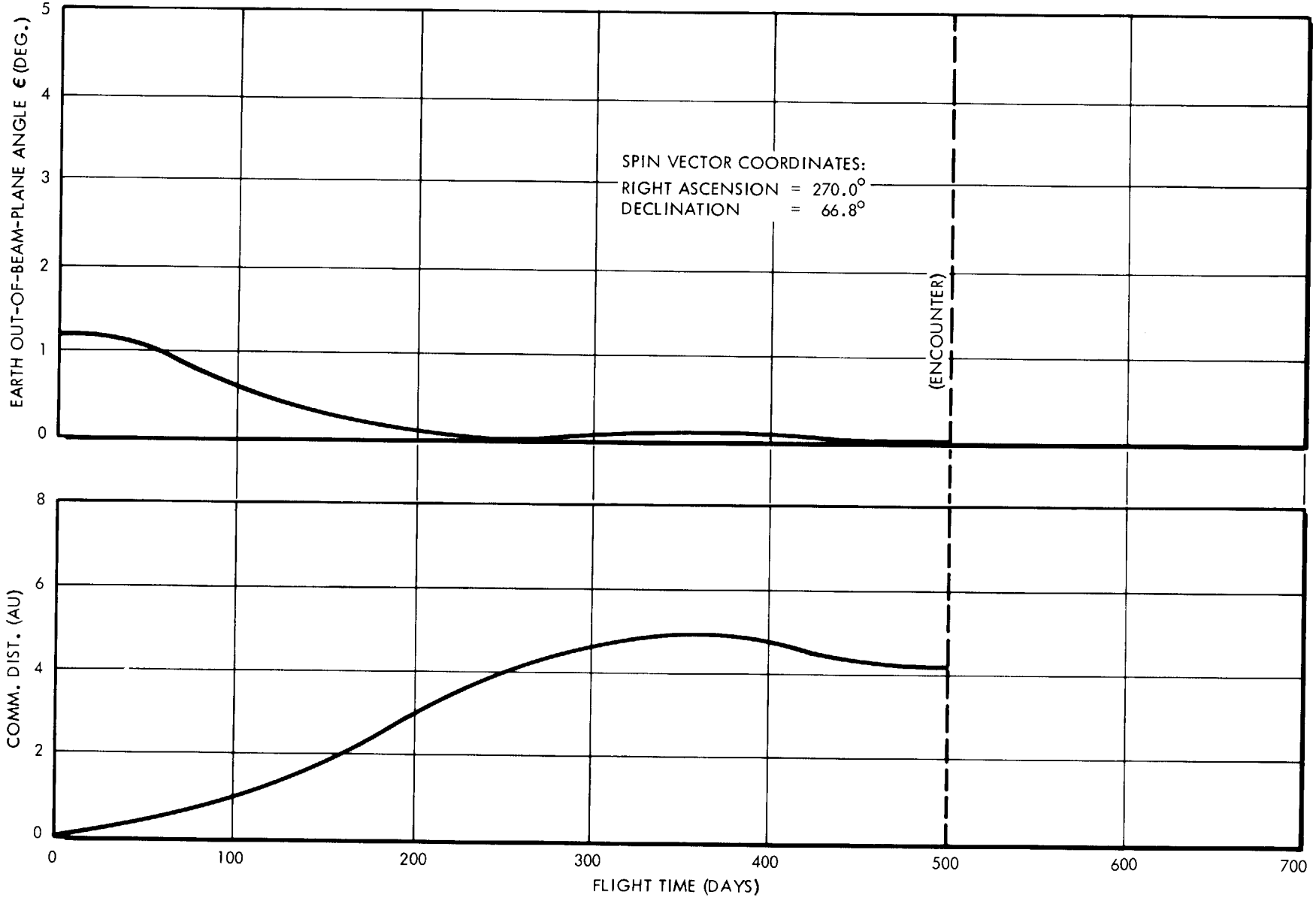

FIGURE 2.4-3

COMMUNICATION PARAMETERS HISTORY, SPIN-STABILIZED SPACECRAFT, 1974 600-DAY MISSION

(ANTENNA BEAM PLANE NORMAL TO SPIN AXIS)

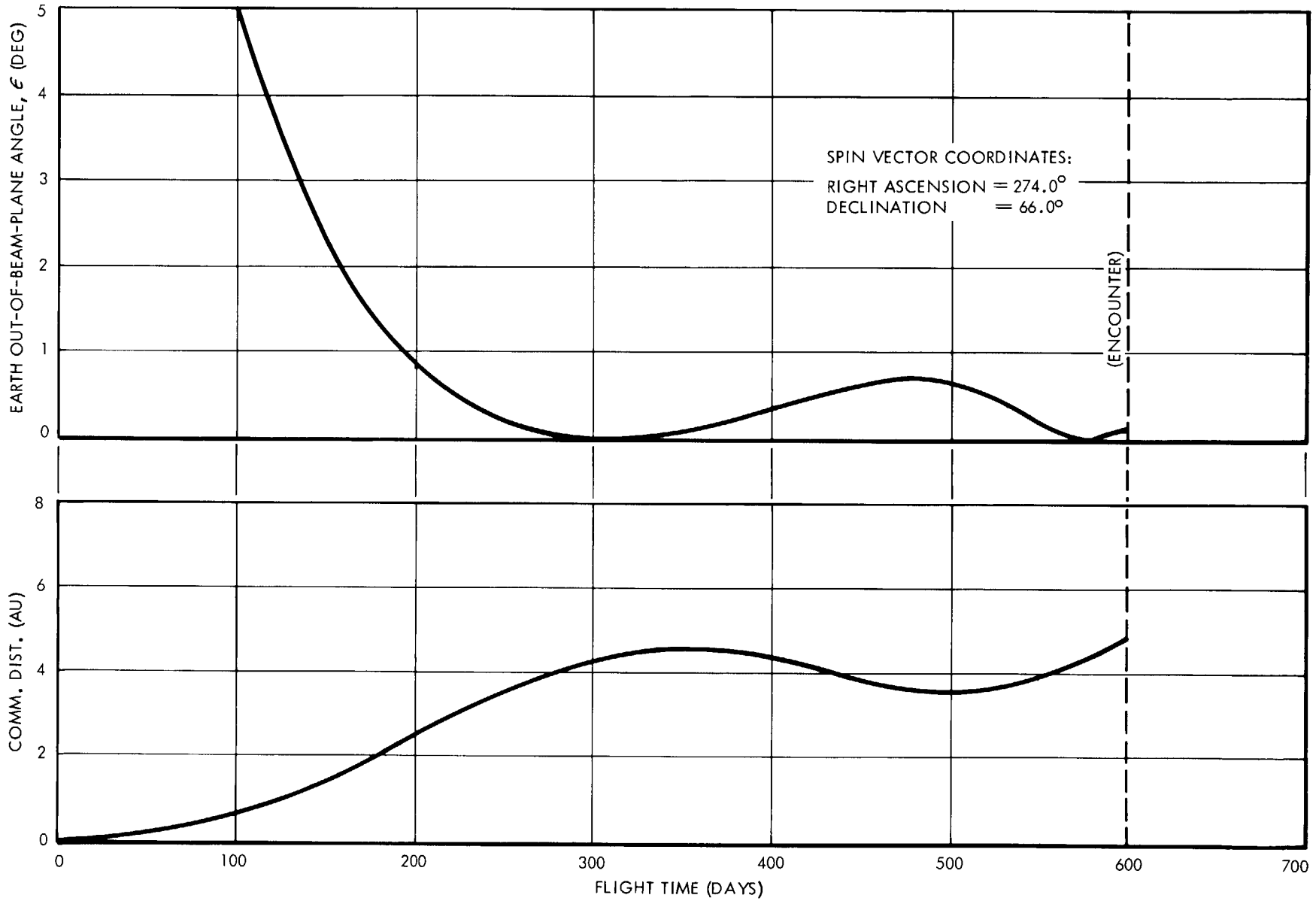

FIGURE 2.4-4

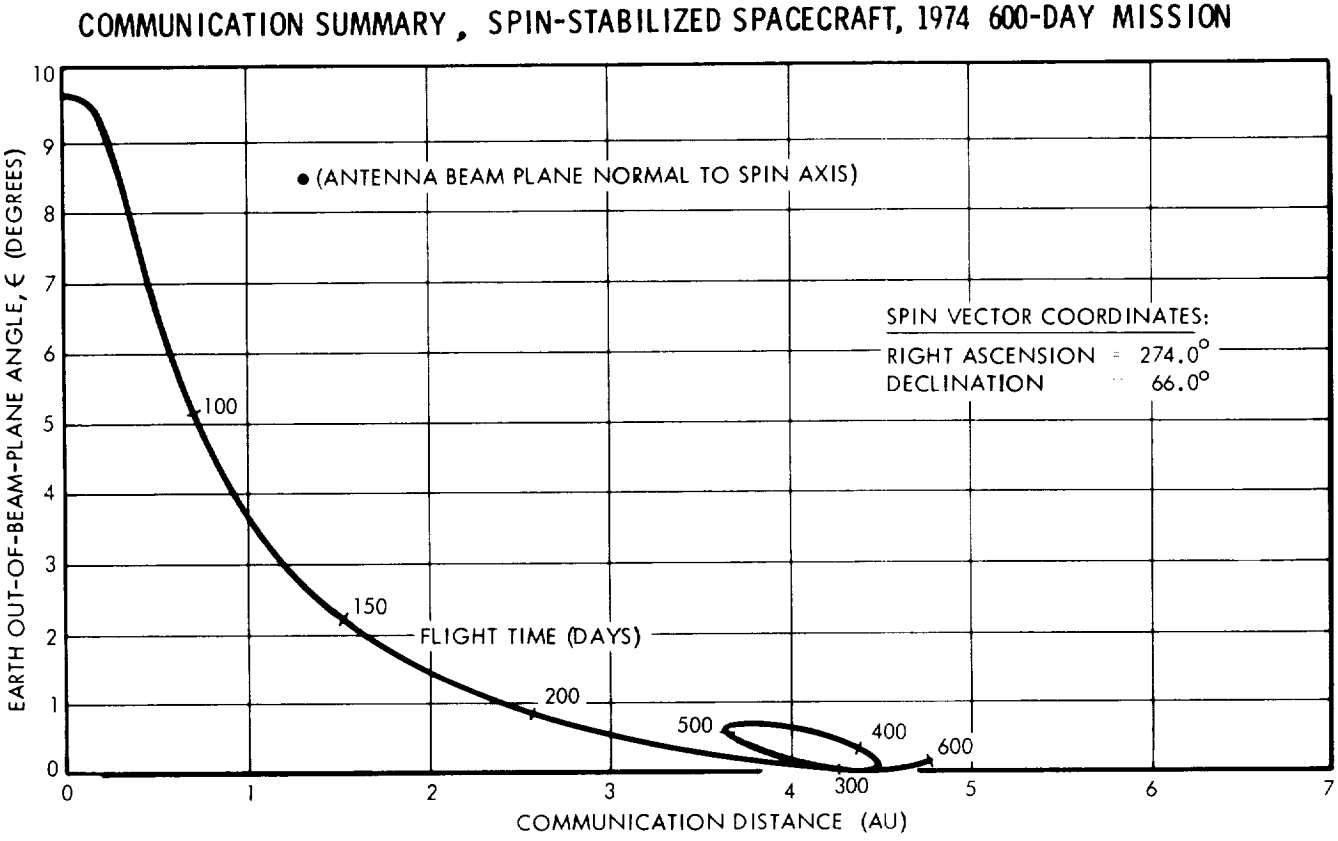

FIGURE 2.4-5

498-day, and 413-day flights correspond to arrival very near the dates of eastern quadrature, opposition, and western quadrature, in that order. (These conditions are not exact because the arrival dates are adjusted to obtain a difference of 180 degrees in the geocentric positions of Jupiter and the Moon on the date of perijove passage). In each case the launch occurs near the optimal departure date of the 1976 opportunity.

The targeting charts shown here are summaries of the data contained in Appendix B. The charts shown in the appendix contain more detailed information including the time interval spent within Earth and solar occultation zones and the immersion and emersion latitudes for Earth and solar occultations. As pointed out in Appendix B, these data are based on a spherical model of Jupiter and should therefore be regarded as only approximate.

The aiming-point coordinates of trajectories 582A, 498A, 498B, and 498C are identified in Figures 2.4-8 and 2.4-9. These trajectories were numerically integrated from injection to about 500 days after encounter, and the results of these integrations are presented graphically in subsection 2.4.2.

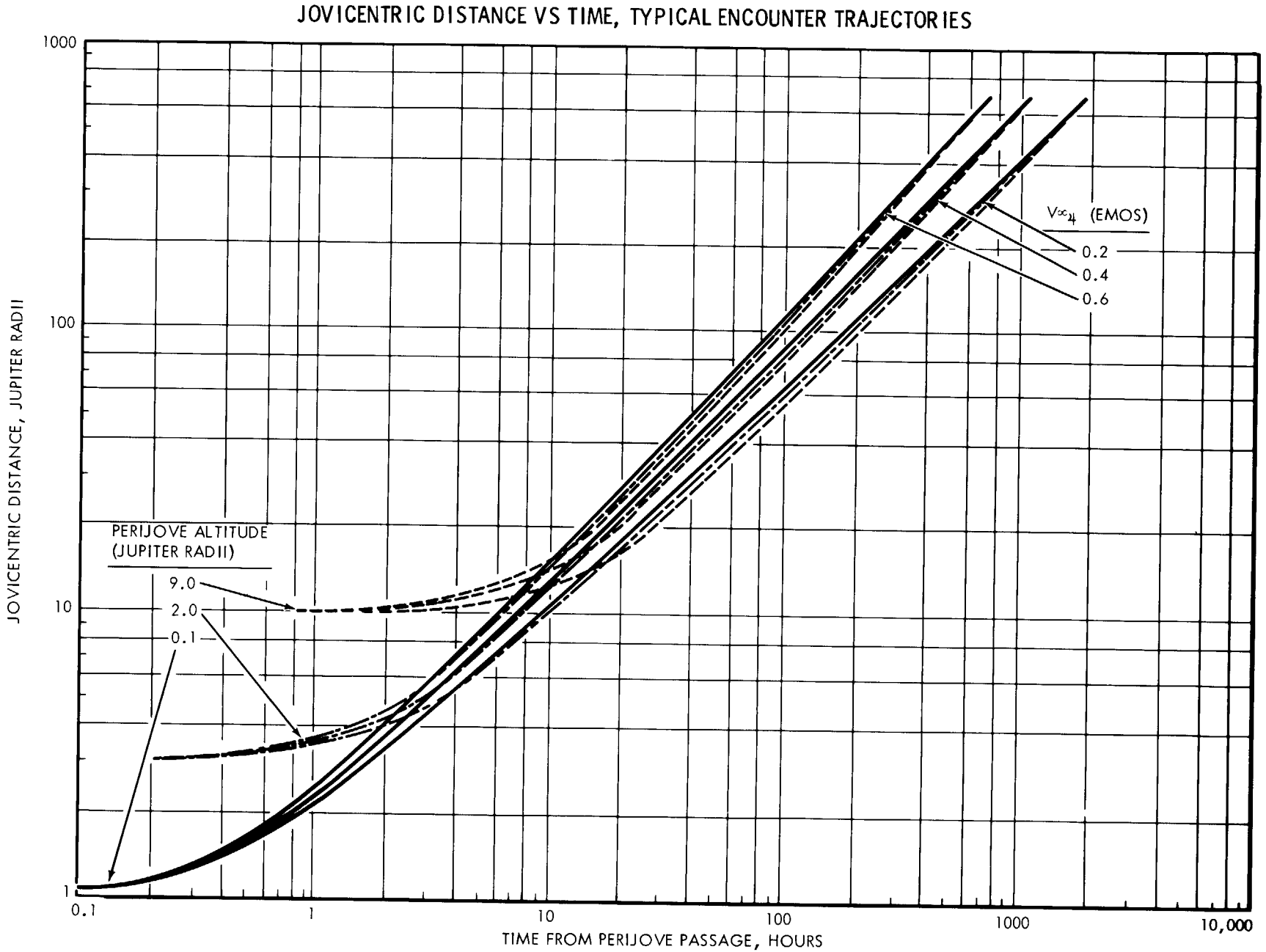
JOVICENTRIC DISTANCE VS TIME, TYPICAL ENCOUNTER TRAJECTORIES
JOVICENTRIC DISTANCE, JUPITER RADII
1000
100
10
1
0.1
1
10
100
1000
10,000
TIME FROM PERIJOVE PASSAGE, HOURS
V_{∞_4} (EMOS)
0.2
0.4
0.6
PERIJOVE ALTITUDE
(JUPITER RADII)
9.0
2.0
0.1

FIGURE 2.4-6

GEOMETRY OF TYPICAL ENCOUNTER TRAJECTORIES

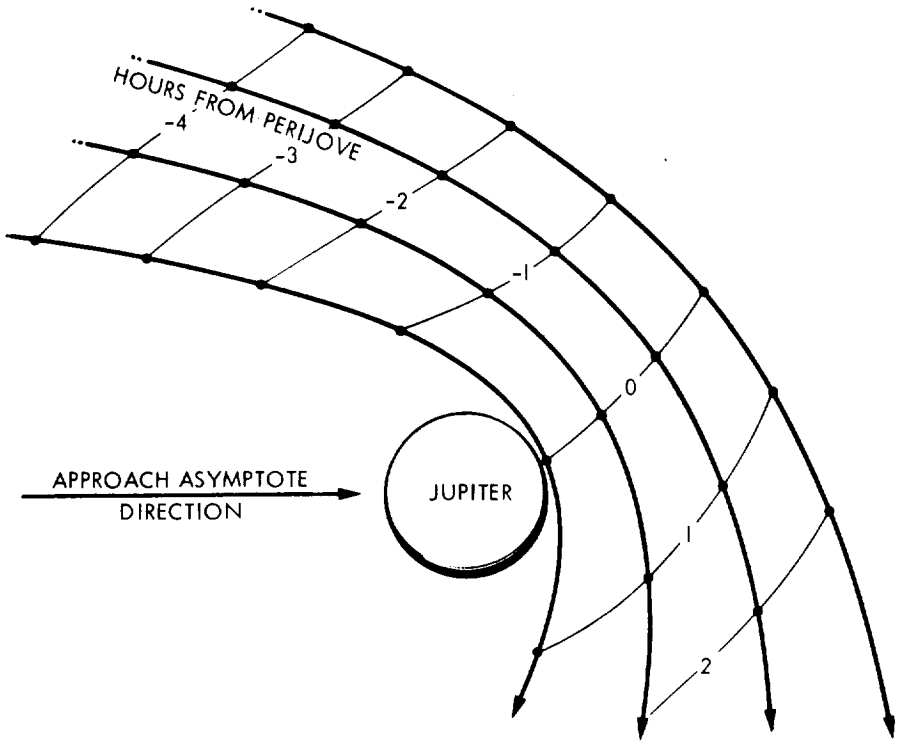

FIGURE 2.4-7

2.4.1.4 Post-Encounter Phase

Some of the more pertinent characteristics of post-encounter heliocentric trajectories attainable with the 582-day, 498-day, and 413-day flights are summarized in Figures 2.4-11 through 2.4-13. The heliocentric retrograde and solar impact regions of Figure 2.4-13 are particularly interesting. More detailed data are presented in Appendix B.

As in the previous targeting charts, the aiming points for the numerically integrated trajectories designated 582A, 498A, 498B, and 498C are those shown in Figures 2.4-11 and 2.4-12. Post-encounter histories of these trajectories are contained in subsection 2.4.2.

2.4.2 Numerically Integrated Trajectory Data

Selected trajectory profiles have been integrated numerically with the Jet Propulsion Laboratory's Trajectory Monitor System (Fort Worth Division Procedure No. Y72). The purposes of the Y72 runs were (1) to verify the two-body approximations previously discussed and (2) to obtain certain spacecraft design data which this computer procedure is uniquely capable of generating.

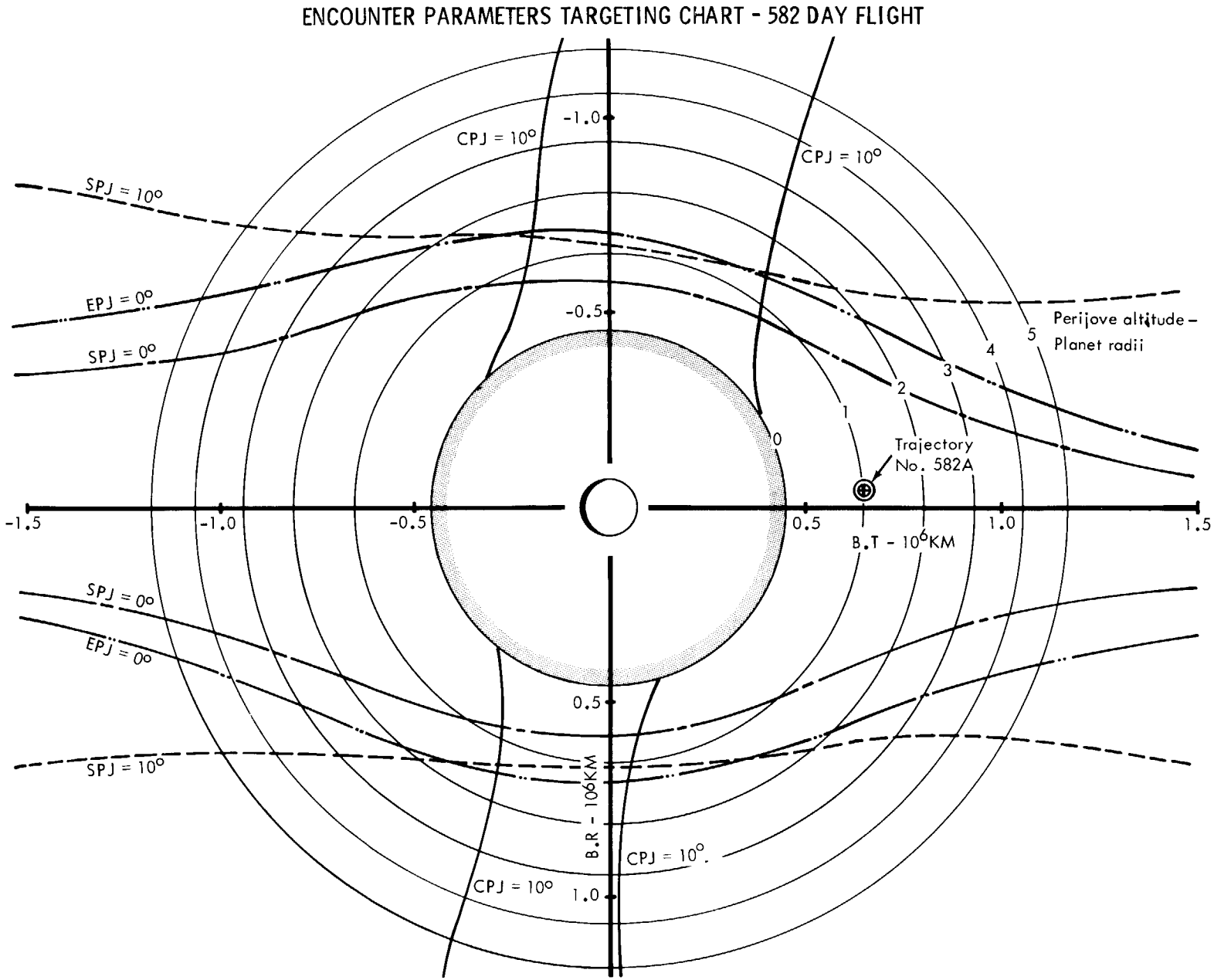
ENCOUNTER PARAMETERS TARGETING CHART - 582 DAY FLIGHT
CPJ = 10°
CPJ = 10°
SPJ = 10°
EPJ = 0°
SPJ = 0°
-1.0
-0.5
Perijove altitude – Planet radii
5
4
3
2
1
0
Trajectory No. 582A
-1.5
-1.0
-0.5
0.5
1.0
1.5
B.T - 10⁶KM
SPJ = 0°
EPJ = 0°
SPJ = 10°
0.5
B.R - 10⁶KM
CPJ = 10°
CPJ = 10°
1.0

FIG. 2.4-8

ENCOUNTER PARAMETERS TARGETING CHART - 498 DAY FLIGHT

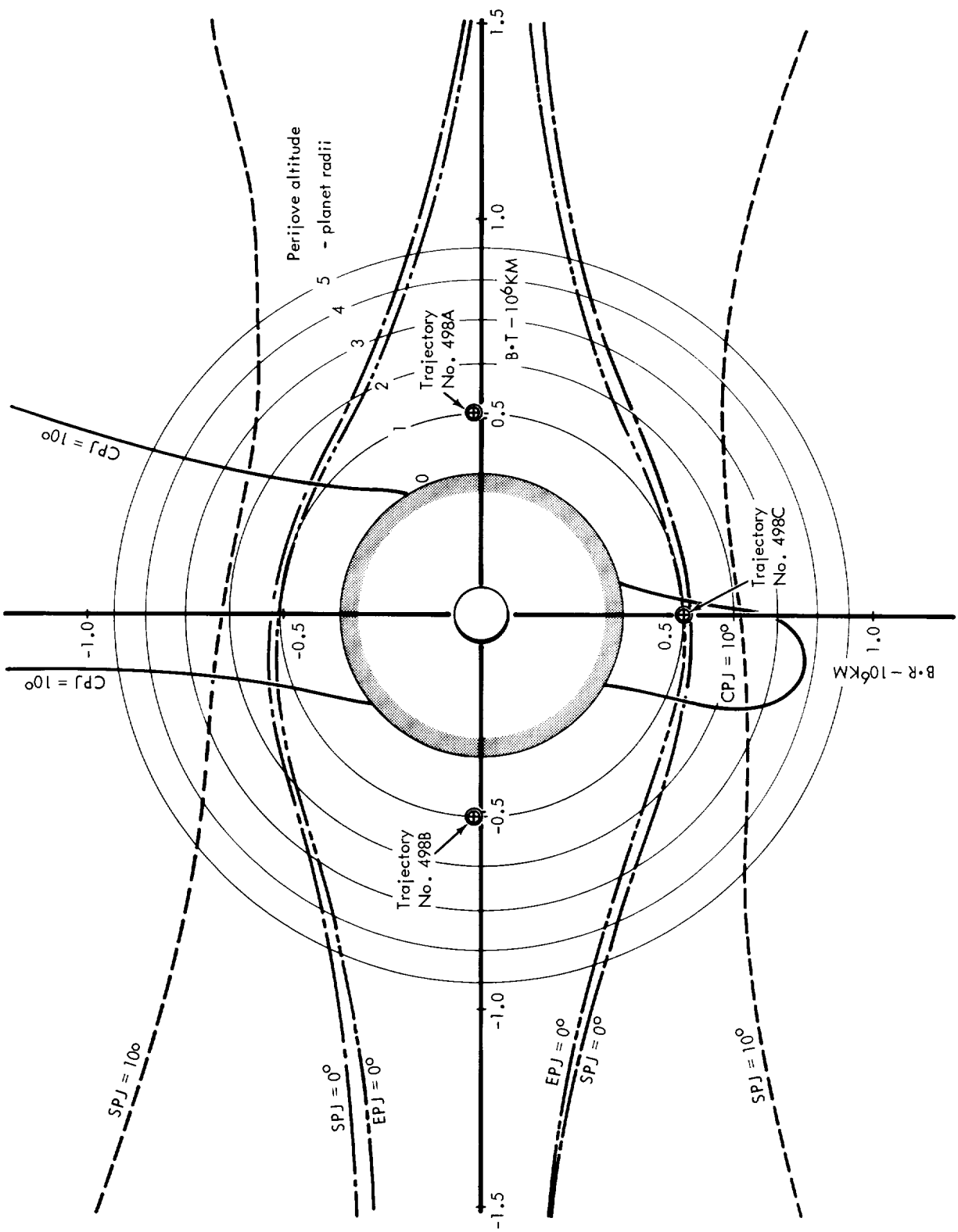

FIG. 2.4-9

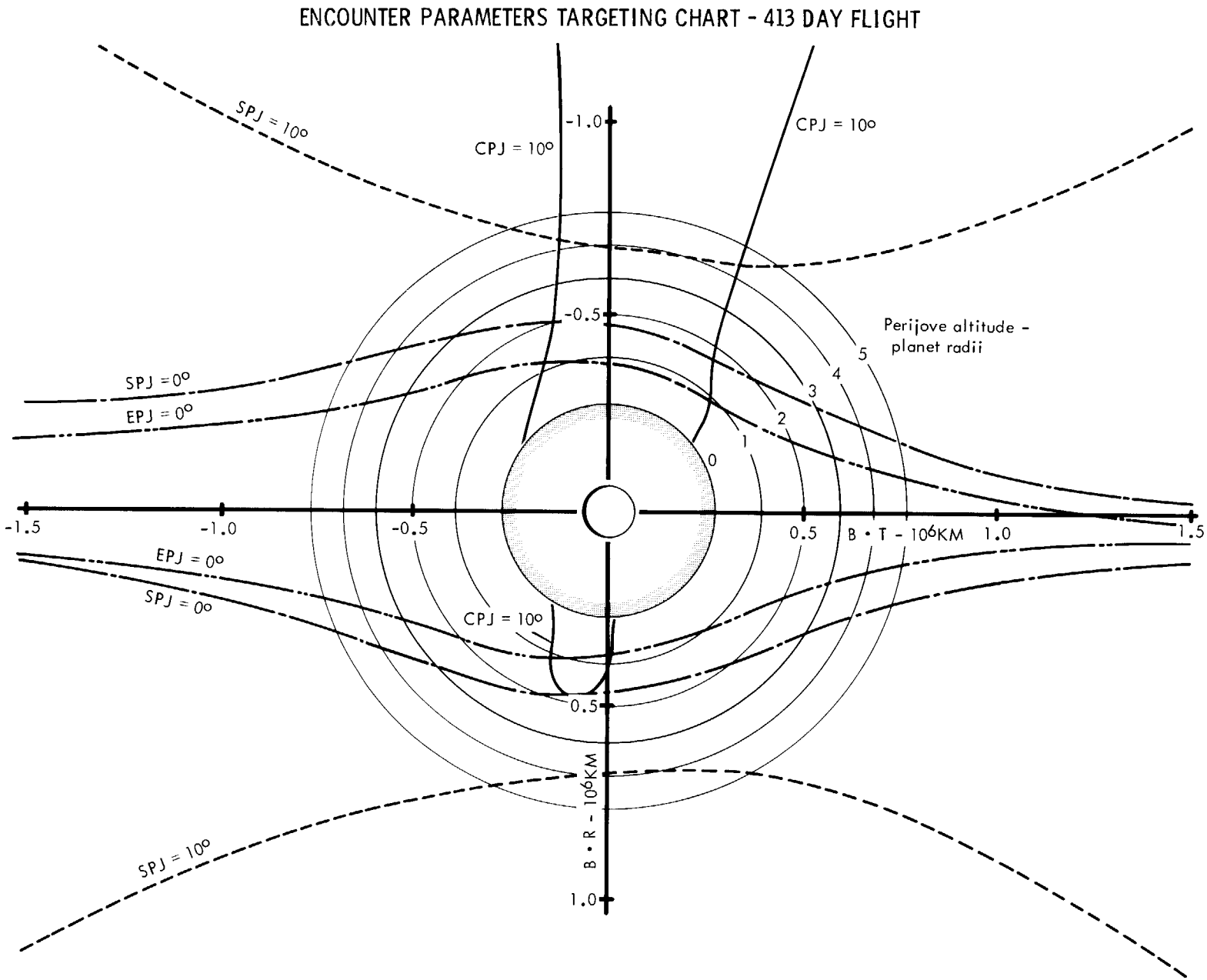
ENCOUNTER PARAMETERS TARGETING CHART - 413 DAY FLIGHT
SPJ = 10°
CPJ = 10°
CPJ = 10°
-1.0
-0.5
Perijove altitude - planet radii
5
4
3
2
1
0
SPJ = 0°
EPJ = 0°
-1.5
-1.0
-0.5
0.5
B • T - 10⁶KM
1.0
1.5
EPJ = 0°
SPJ = 0°
CPJ = 10°
0.5
B • R - 10⁶KM
SPJ = 10°
1.0

FIGURE 2.4-10

POST-ENCOUNTER PARAMETERS TARGETING CHART - 582 DAY FLIGHT

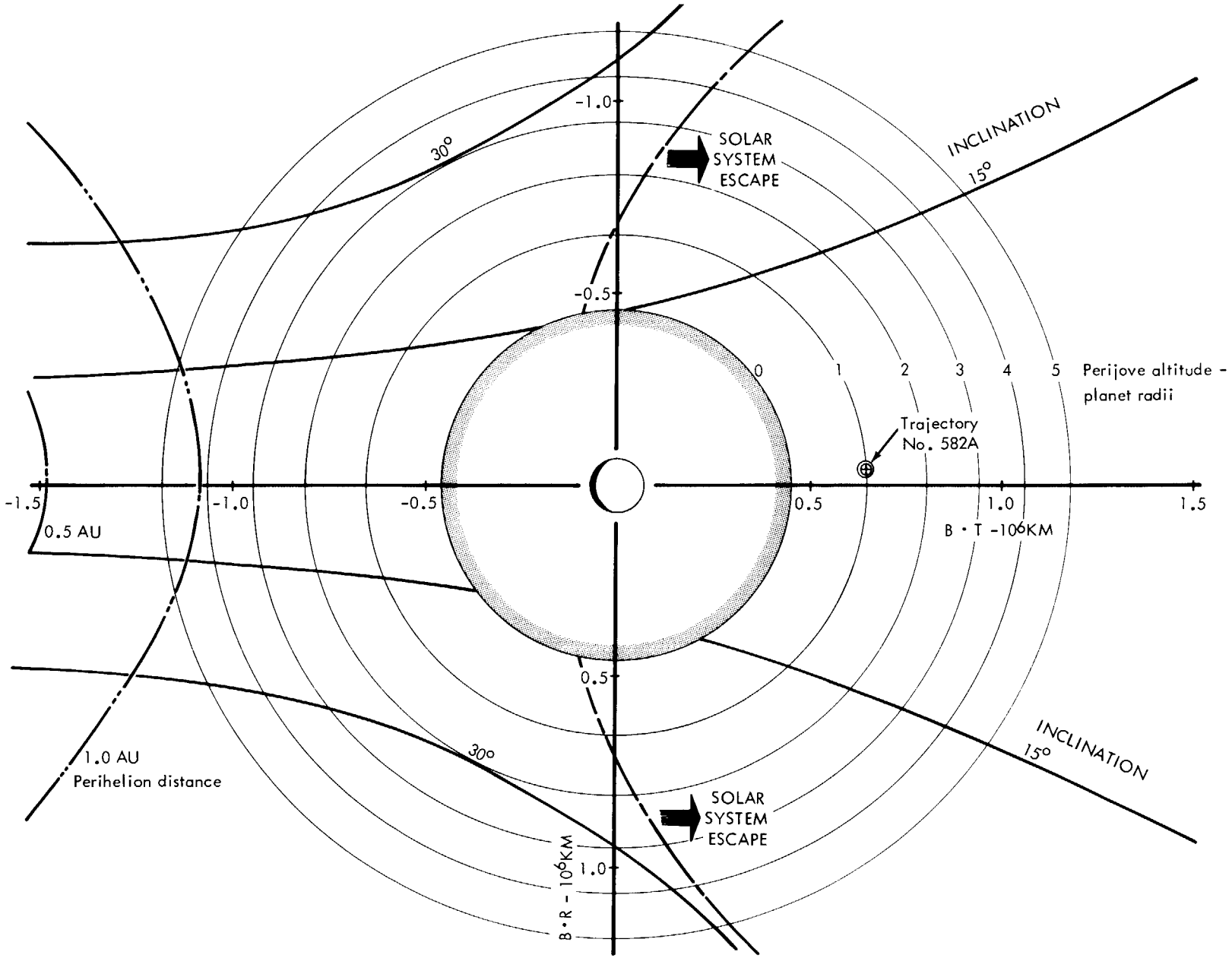

FIGURE 2.4-11

POST-ENCOUNTER PARAMETERS TARGETING CHART - 498 DAY FLIGHT

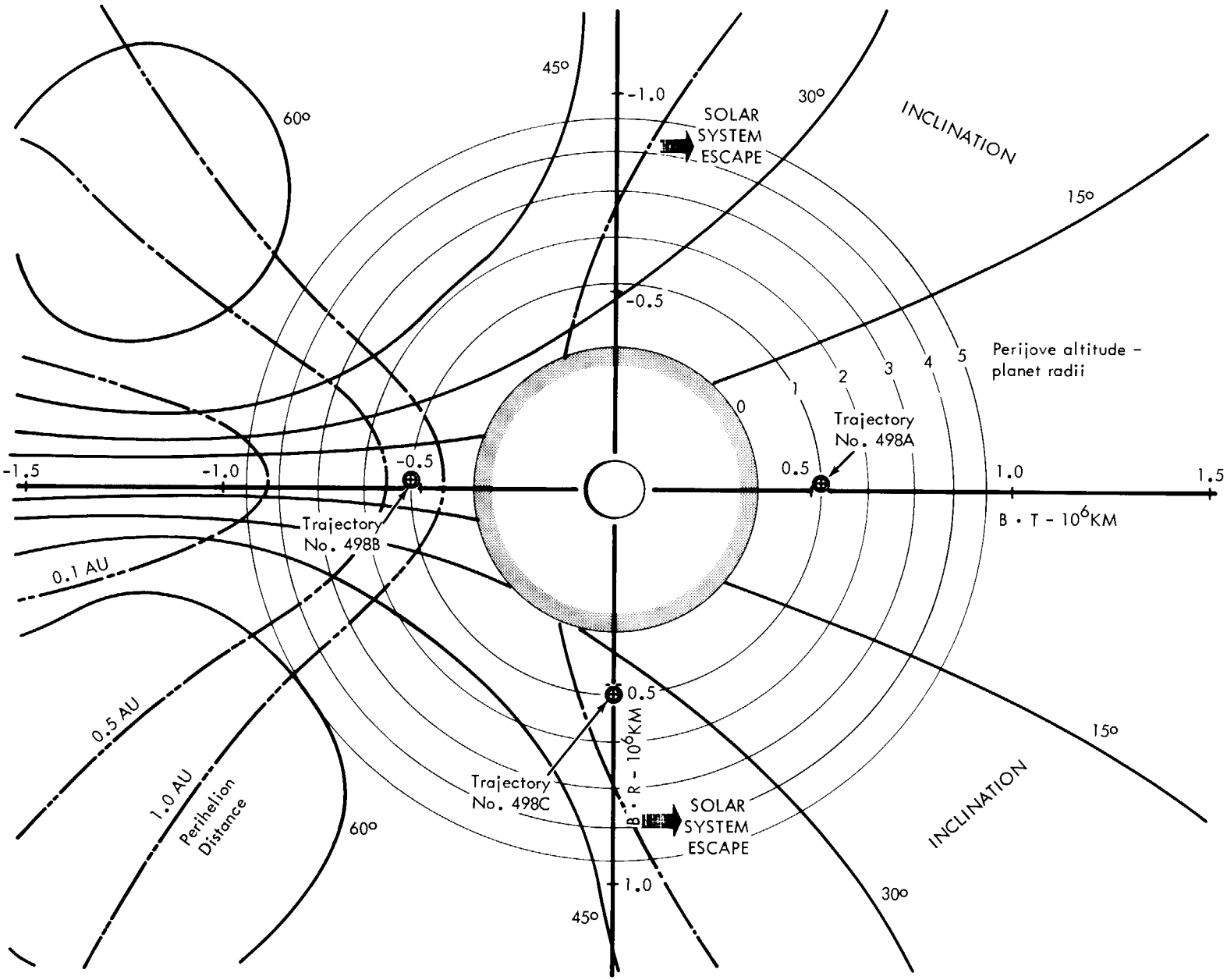

FIG. 2.4-12

POST-ENCOUNTER PARAMETERS TARGETING CHART - 413 DAY FLIGHT

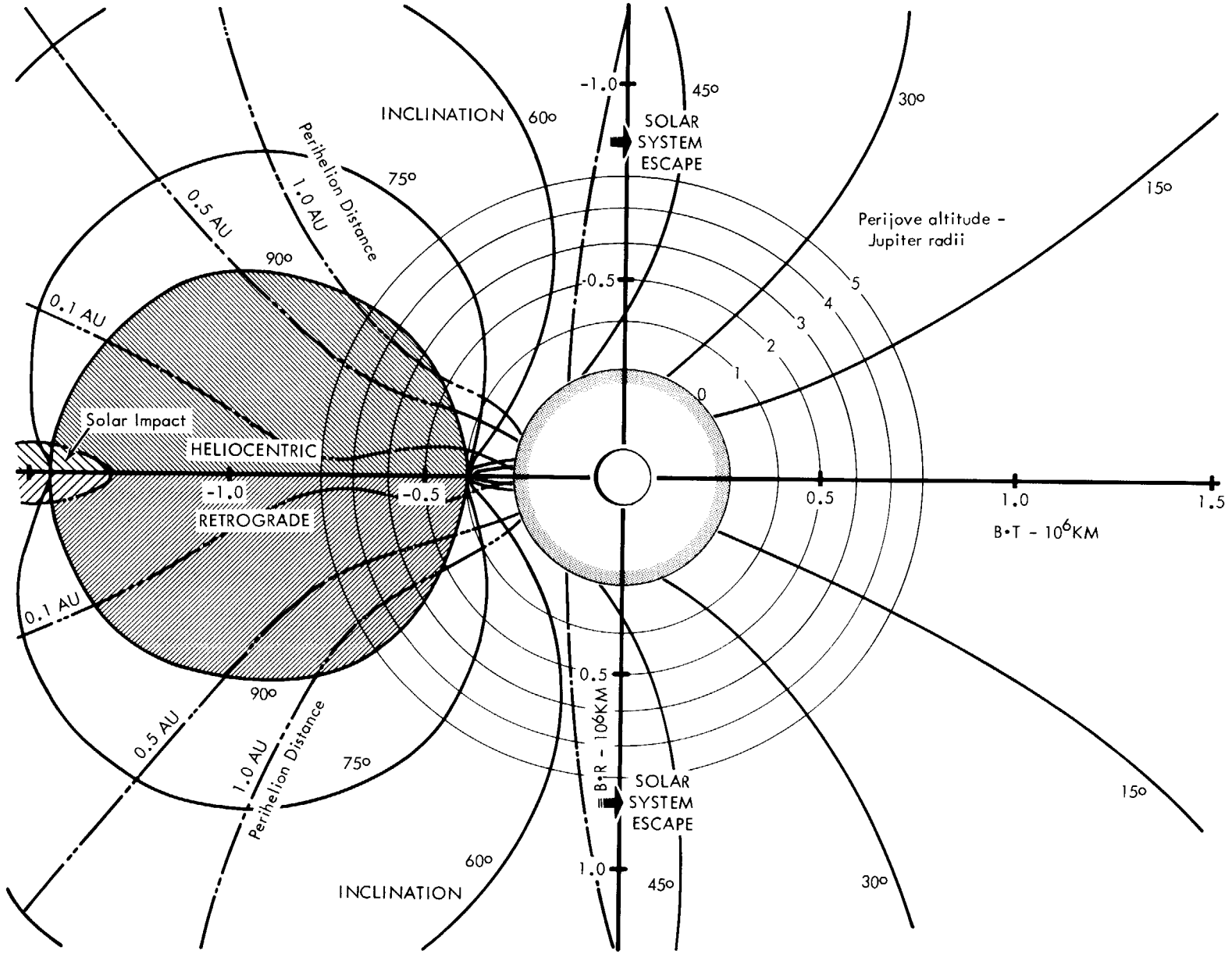

FIGURE 2.4-13

Histories of selected flight and spacecraft design parameters of the 582A trajectory are shown in Figures 2.4-14 through 2.4-20. Similar histories for the 498A, B, and C trajectories are shown in Figures 2.4-21 through 2.4-27. These illustrations are essentially self-explanatory. Clearly shown in Figures 2.4-21 through 2.4-23, are the great perturbative influence of Jupiter and the wide range of post-encounter flight path alternatives that are inherent in a Jupiter flyby mission.

2.4.3 Reference

2.4.1 Wilson, S. W., Jr., "Earth-Jupiter Haliocentric Transfer Trajectory Data," General Dynamics Corporation, Fort Worth Division, MR-A-2001, 13 December 1965.

TRAJECTORY NO. 582A: HELIOCENTRIC GEOMETRY

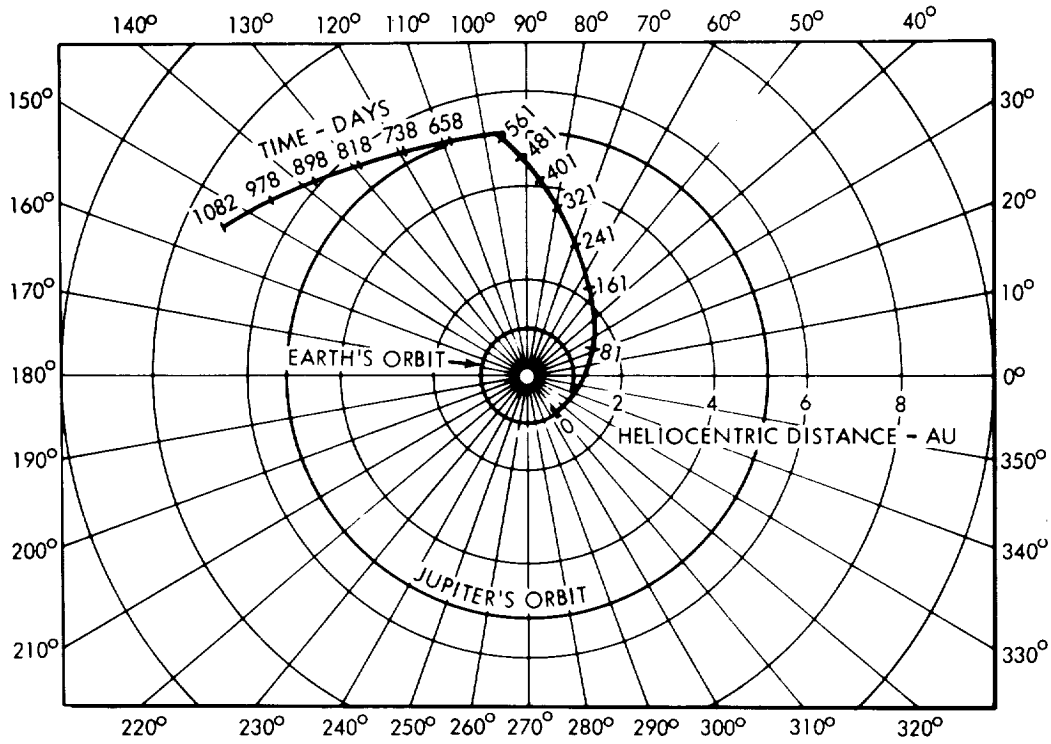

FIGURE 2.4-14

TRAJECTORY NO. 582A: HELIOCENTRIC DISTANCE VS. TIME

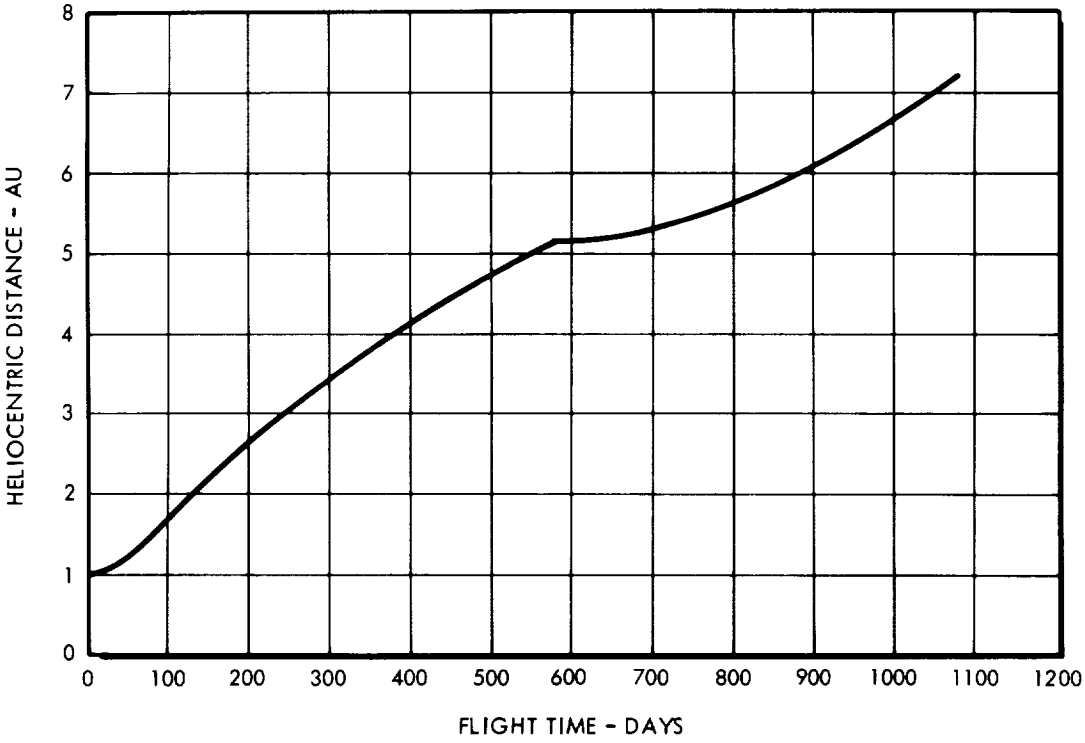

FIGURE 2.4-15

TRAJECTORY NO. 582A: HELIOCENTRIC LATITUDE VS. TIME

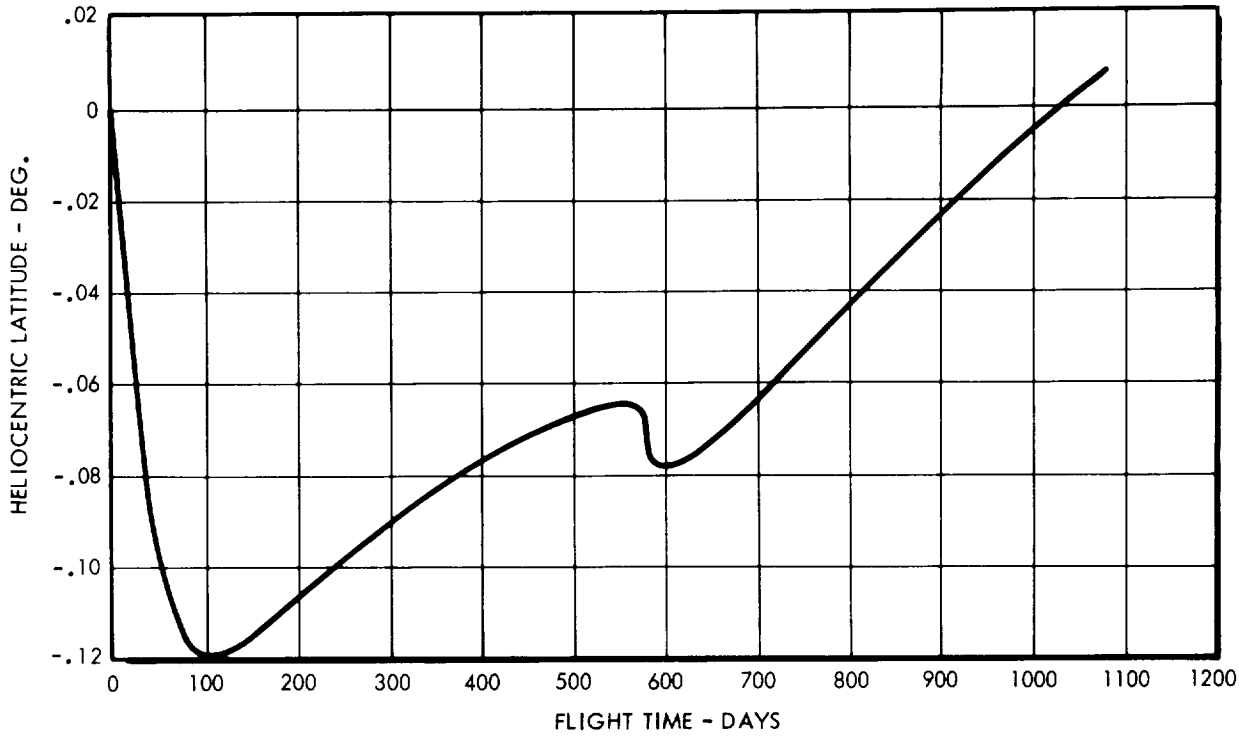

FIGURE 2.4-16

TRAJECTORY NO. 582A: CANOPUS CONE ANGLE VS TIME

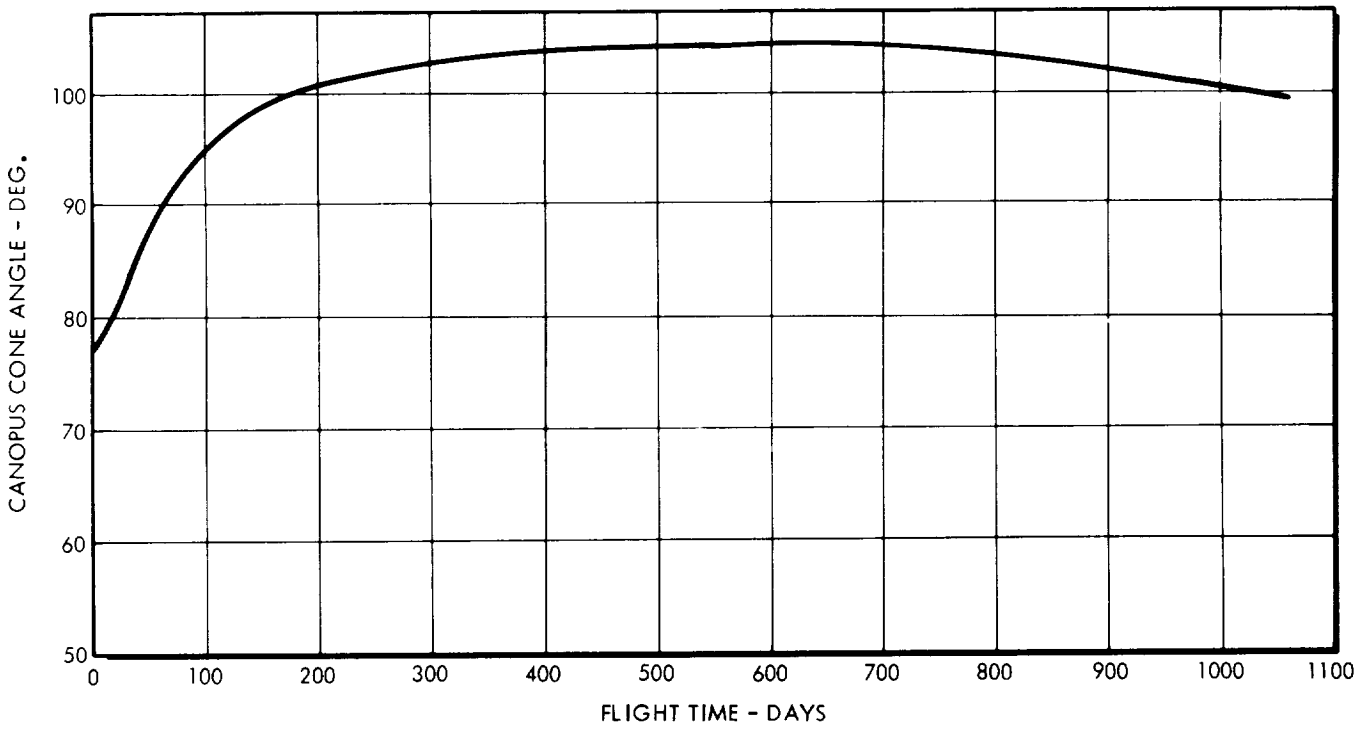

FIGURE 2.4-17

TRAJECTORY NO. 582A: GEOCENTRIC DECLINATION VS. TIME

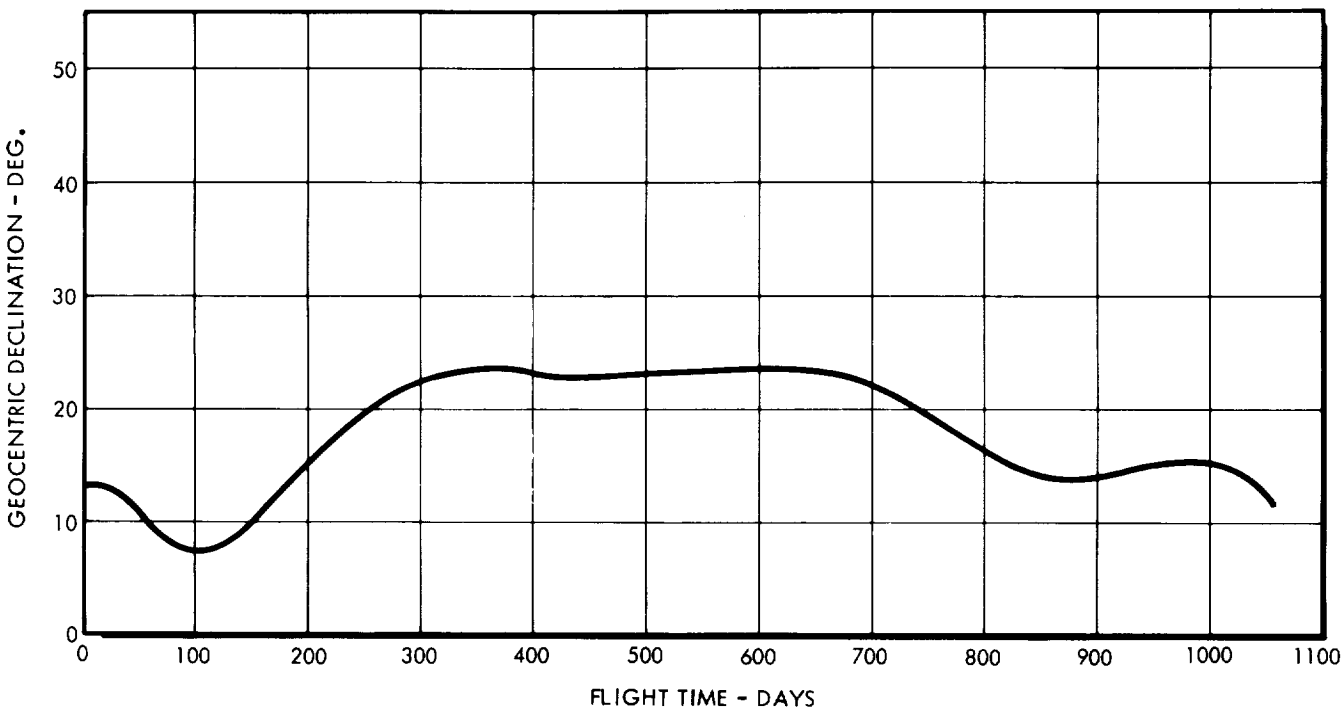

FIGURE 2.4-18

TRAJECTORY NO. 582A: GEOCENTRIC DISTANCE VS. TIME

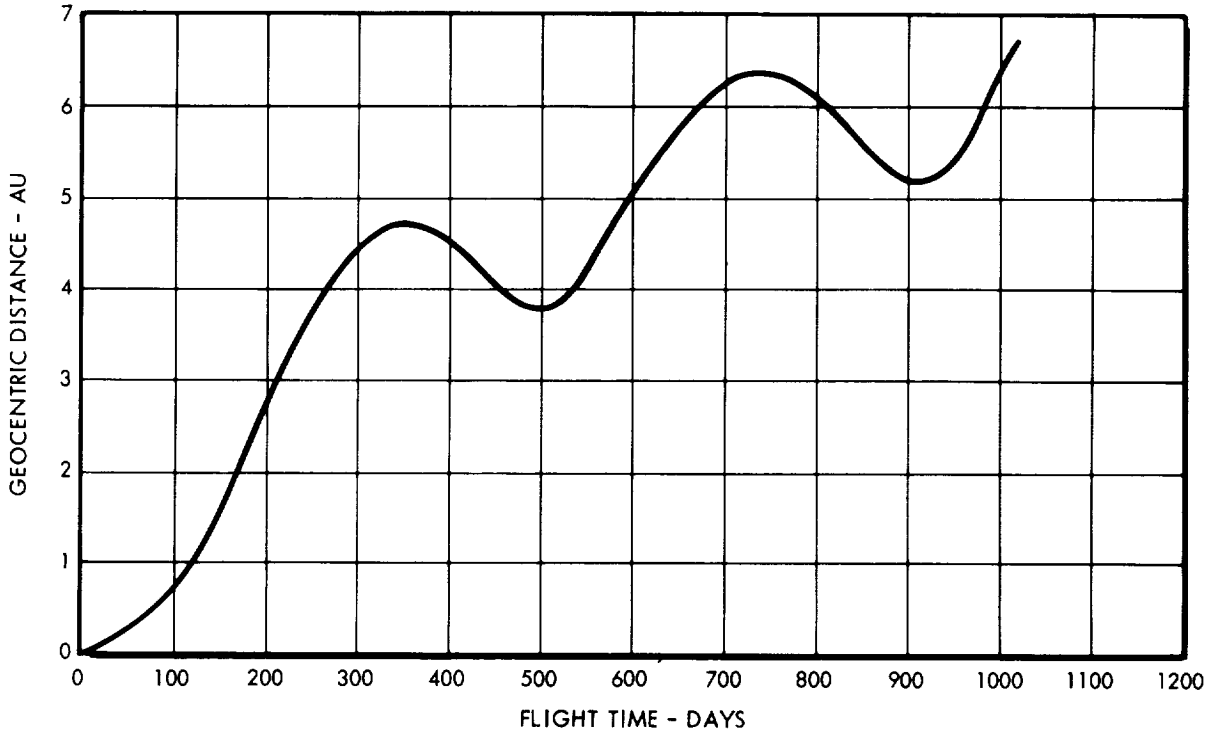

FIGURE 2.4-19

TRAJECTORY NO. 582A: EARTH CONE VS. CLOCK ANGLE

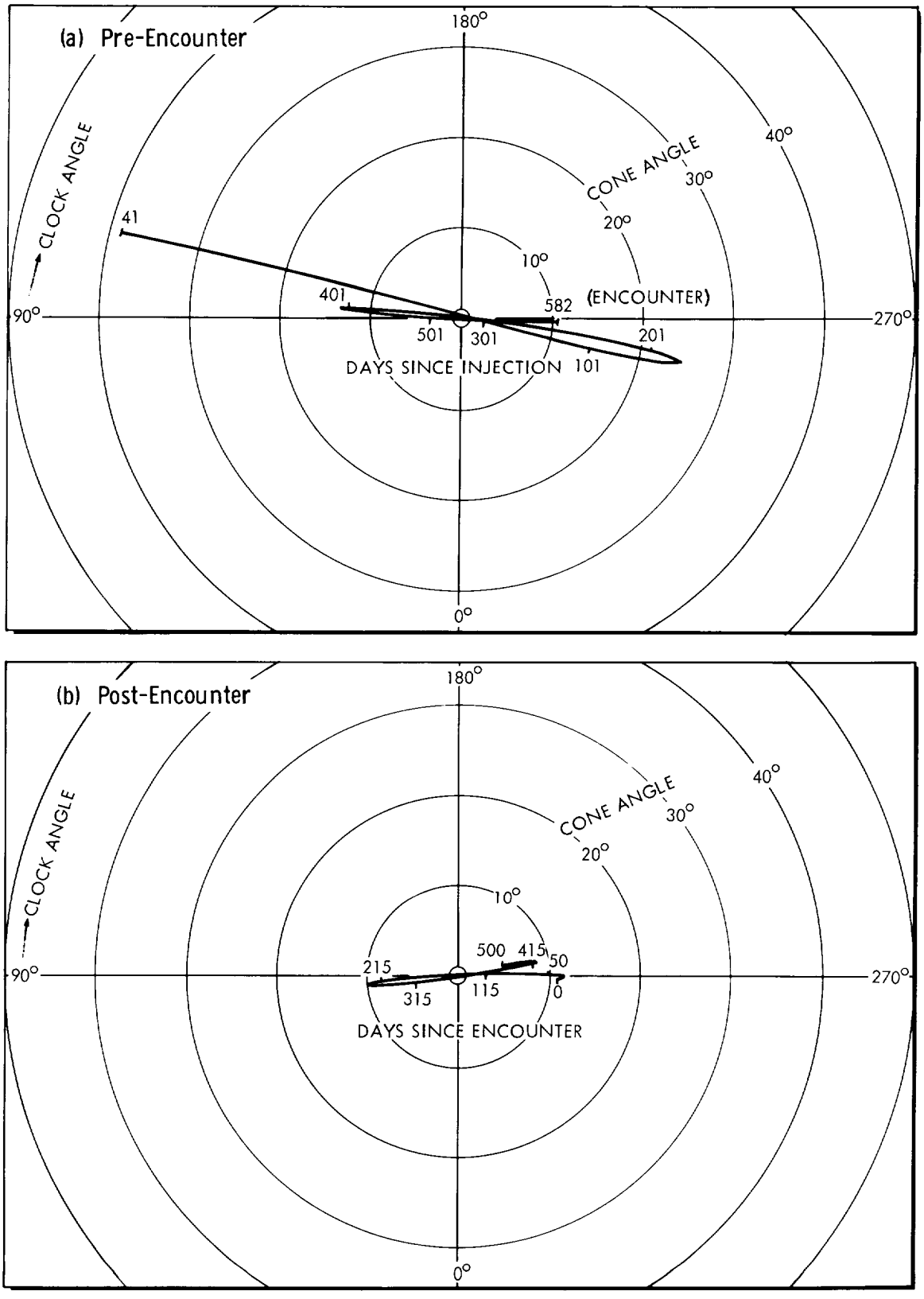

FIGURE 2.4-20

TRAJECTORY NO. 498 A, B, & C: HELIOCENTRIC GEOMETRY

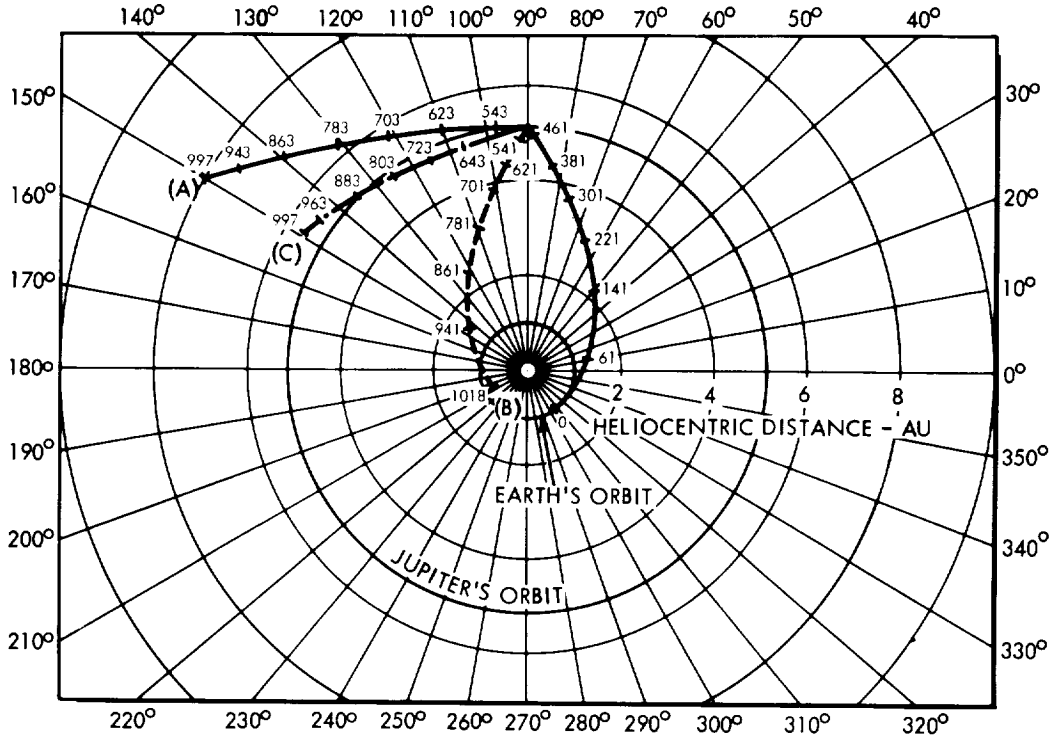

FIGURE 2.4-21

TRAJECTORY NO. 498A, B, & C: HELIOCENTRIC DISTANCE VS. TIME

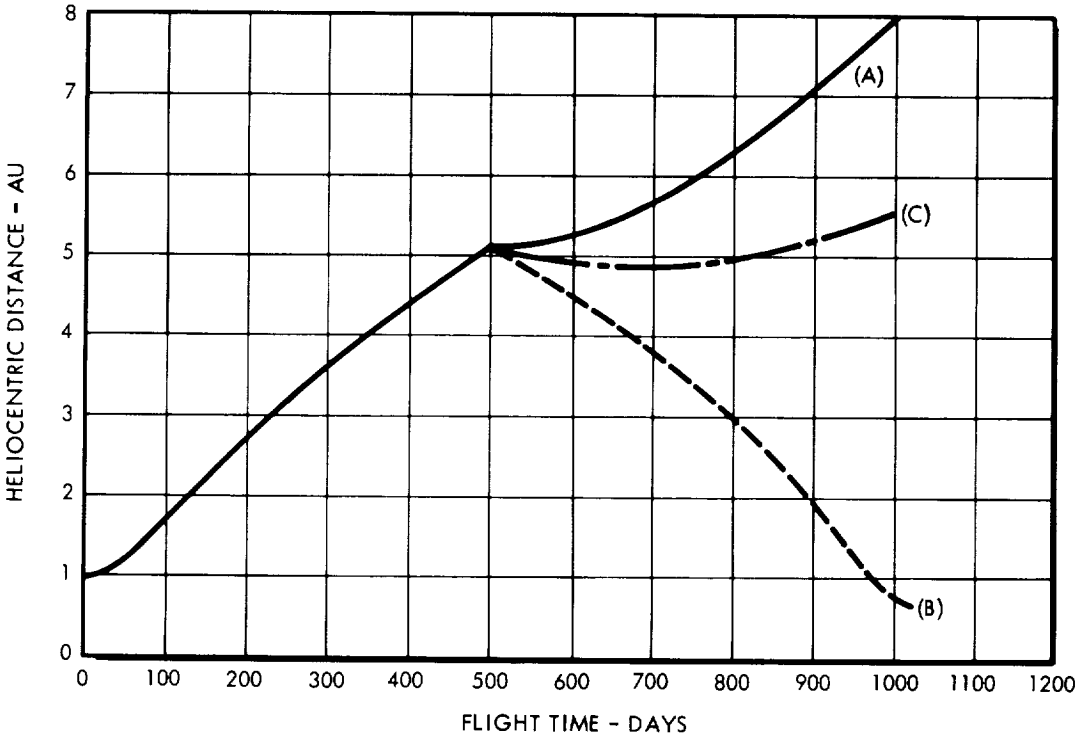

FIGURE 2.4-22

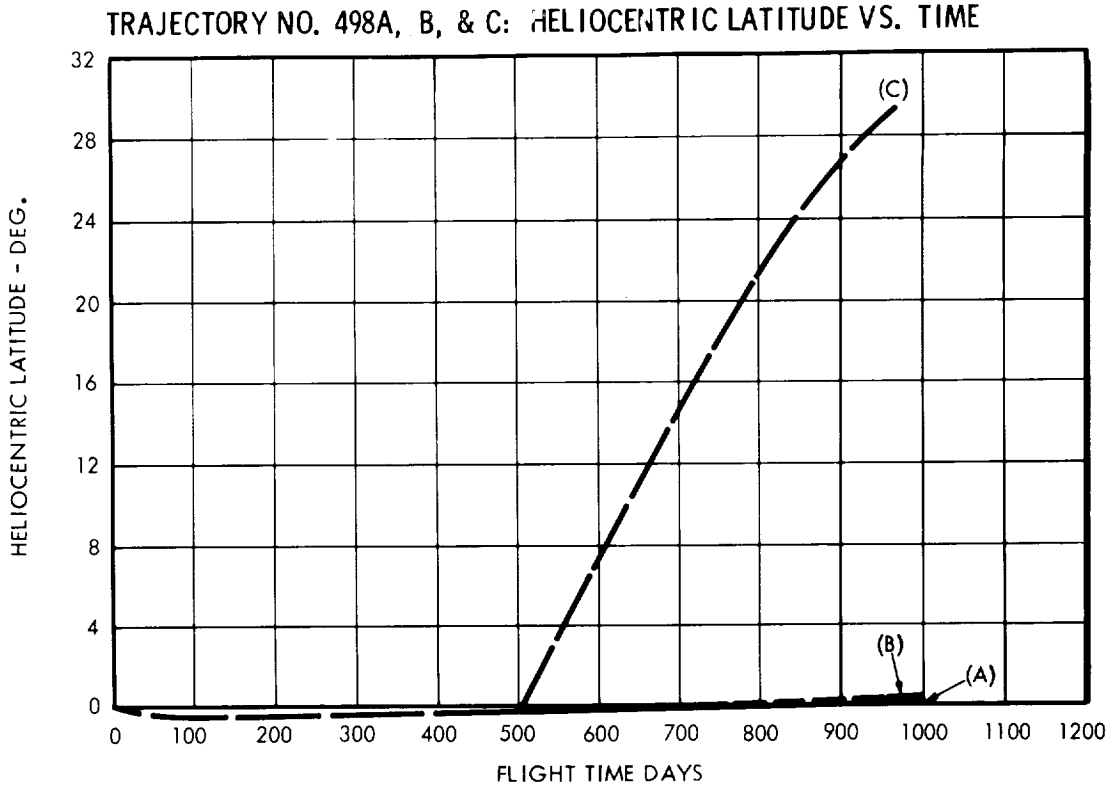

FIGURE 2.4-23

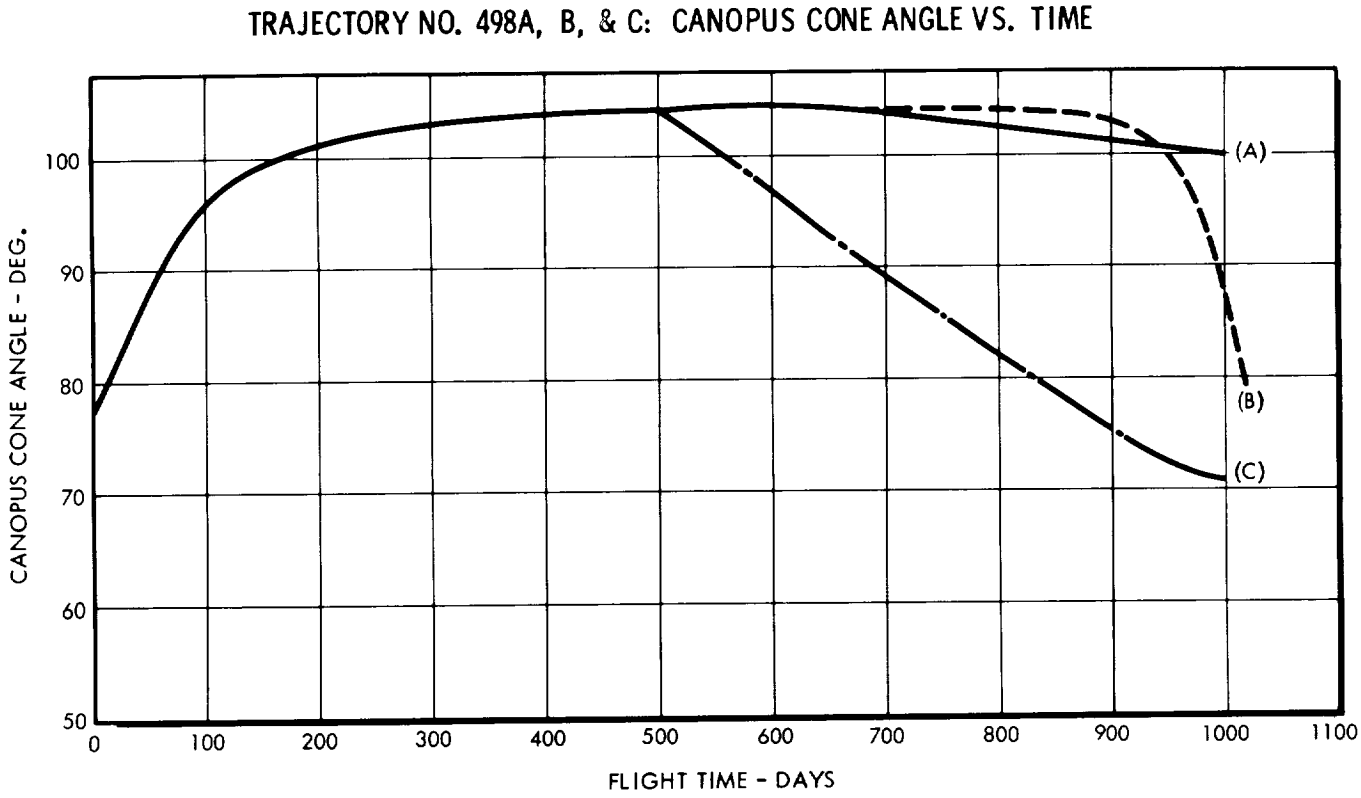

FIGURE 2.4-24

TRAJECTORY NO. 498A, B, & C: GEOCENTRIC DECLINATION VS TIME

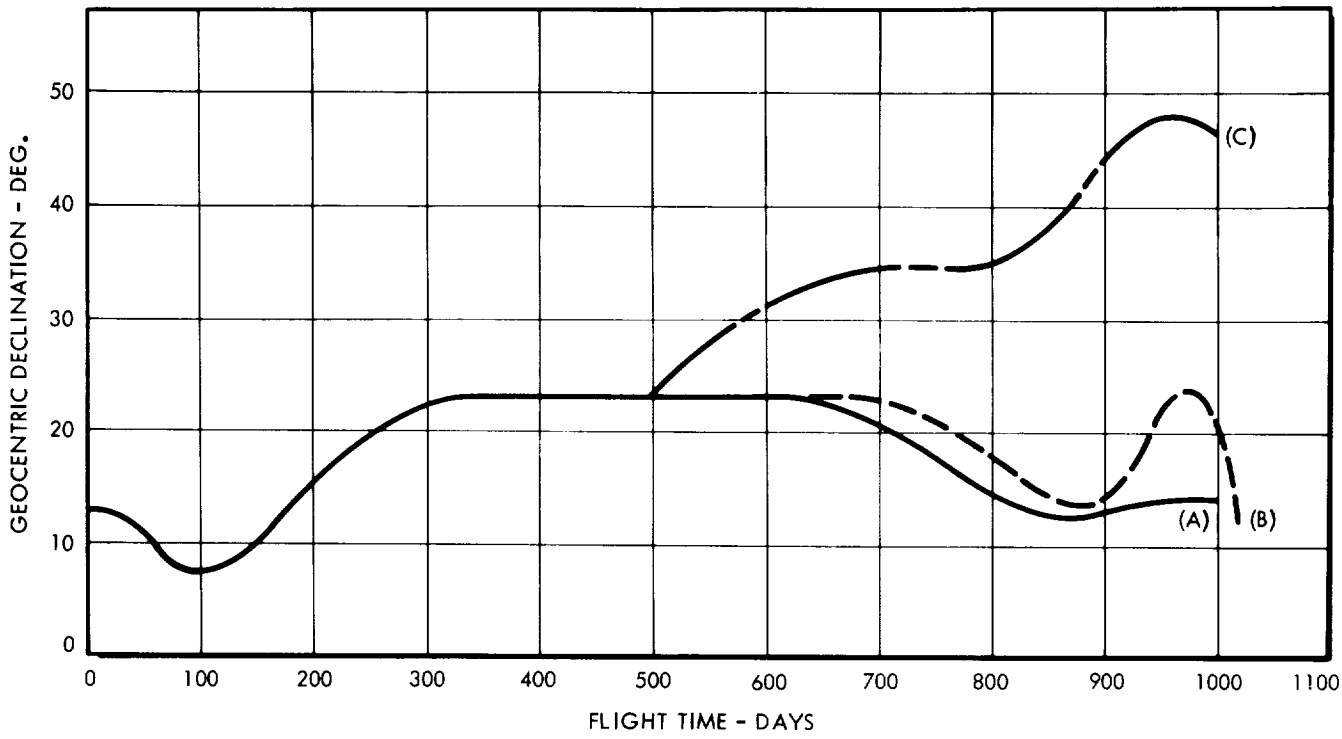

FIGURE 2.4-25

TRAJECTORY NO. 498A, B, & C: GEOCENTRIC DISTANCE VS. TIME

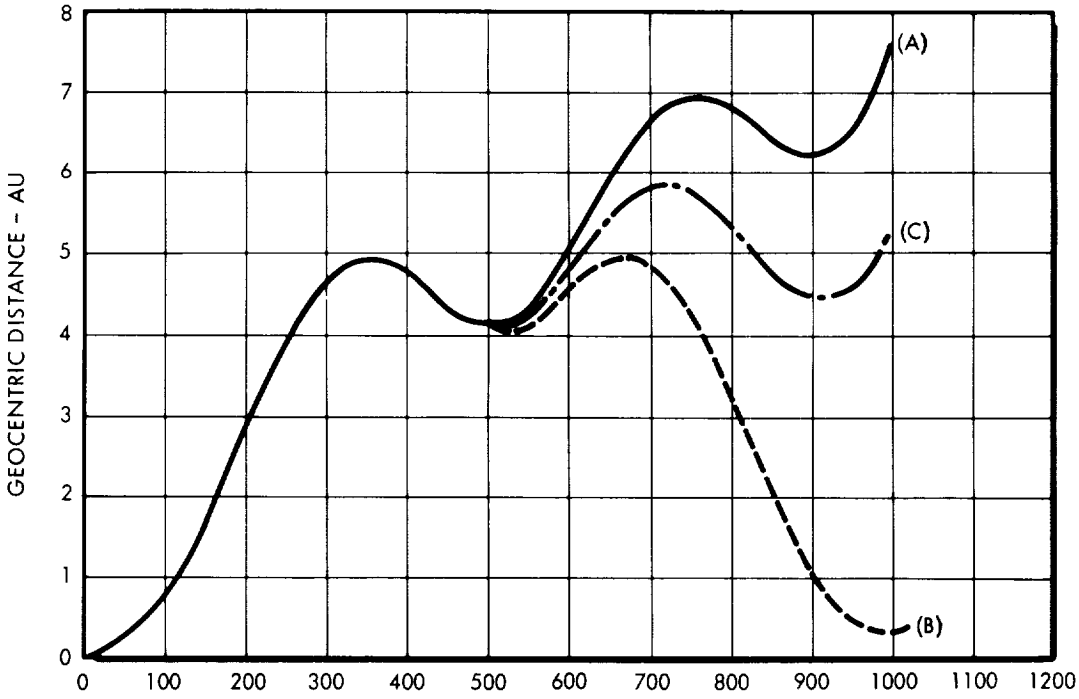

FIGURE 2.4-26

TRAJECTORY NO. 498A, B, & C: EARTH CONE VS. CLOCK ANGLE

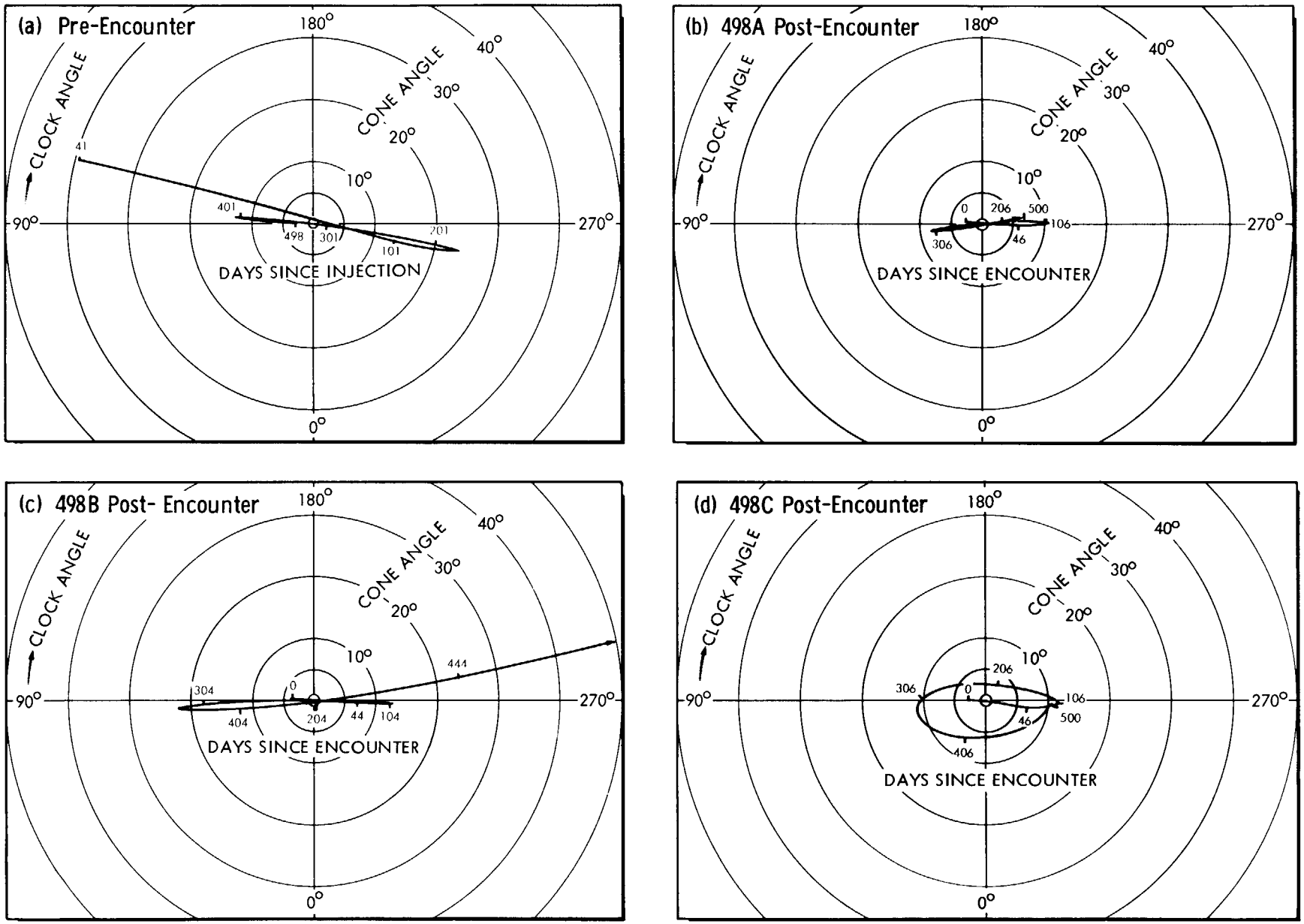

FIGURE 2.4-27

SECTION 3

SPACECRAFT SYSTEMS DESIGN AND ANALYSIS

This section contains a description of the general aspects of the design and analysis of spacecraft subsystems which are intended to perform flyby missions of Jupiter. Analyses have been made with regard to (1) communications, (2) data management, (3) spacecraft control, (4) navigation and guidance, (5) attitude control, (6) propulsion, (7) electrical power, (8) thermal control, (9) radiation protection, (10) meteoroid protection, (11) structure, (12) mechanical design and configuration, and (13) reliability. The section is arranged so that these topics are presented in this order.

3.1 COMMUNICATIONS

3.1.1 Functional Requirements

3.1.1.1 Basic Communications Requirements

The communications subsystem will be used to perform four basic functions: (1) transmission to Earth of scientific data gathered by the spacecraft; (2) transmission to Earth of engineering data, i.e., the condition of the spacecraft and its functions; (3) reception of command signals from Earth to direct the spacecraft and its subsystems to perform certain functions; and (4) retransmission of ranging interrogations to provide range information to Earth. The communications subsystem, which will be used to accomplish these functions, will be considered as being composed of four components: (1) the antenna, (2) the receiver, (3) the transmitter, and (4) the modulator. The modulator can be considered as a part of the transmitter; but since it is used to add information to the radio signal returned to Earth, it will be considered as a separate subsystem component. In order to maintain proper communications with Earth, the communications subsystem must receive an adequate signal from Earth, receive data from the data management subsystem, modulate an RF signal by use of the data, amplify the modulated signal to the necessary power level, and transmit this signal to Earth through a properly oriented antenna.

3.1.1.2 Interfaces

A simple block diagram of the interfaces between the communications subsystem and other spacecraft subsystems is shown in Figure 3.1-1. The signal flow between the communications subsystem and other subsystems is as follows:

1. Data management provides communications with conditioned data at the proper information rate and in terms of a time schedule suitable for input to the modulator.

2. Communications provides data management with signals suitable for processing the communications engineering data.

3. Communications provides command and control with demodulated command signals received from DSIF.

4. Command and control provides communications with an antenna-positioning signal, if applicable.

5. Electrical power is provided by the power subsystem.

COMMUNICATIONS INTERFACES

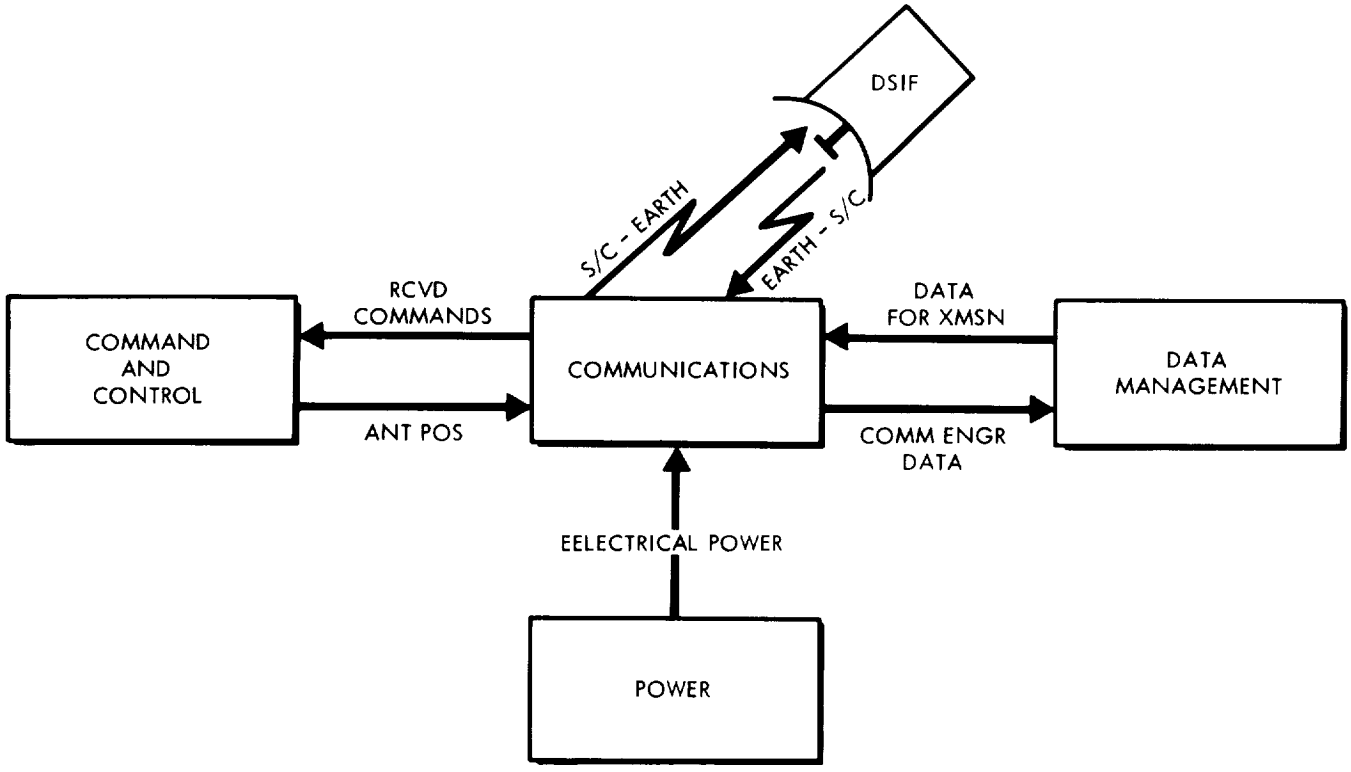

FIGURE 3.1-1

3.1.2 Identification of Trade-Offs

The trade-offs considered necessary for defining efficient systems are those between the various functional parameters, between the various physical parameters, and between the functional and physical parameters. The trade-offs to be made for the communications subsystem being considered in this study are shown diagrammatically in Figure 3.1-2. In this diagram, the antenna design is shown to be dependent

upon the spacecraft stabilization, the pointing accuracy which can be provided by the command and control subsystem, and the transmitter power. Transmitter design is a function of the type amplifier selected, the electrical power required, and the antenna design.

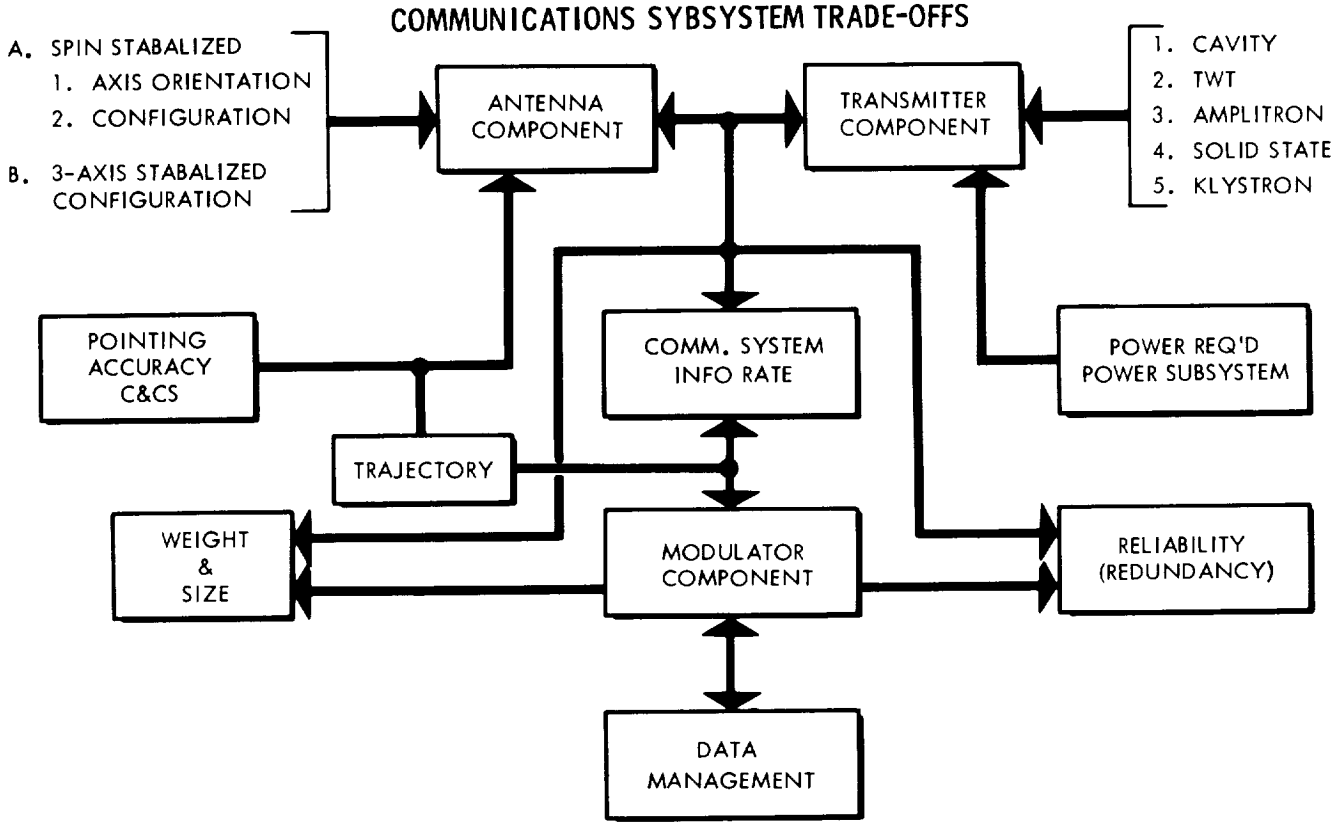

FIGURE 3.1-2

The information rate is dependent upon the effective radiated power (transmitter power multiplied by antenna gain) and the modulation scheme. Information rate is also dependent upon the coding technique and information storage capability of the data management subsystem. The spacecraft trajectory affects the entire subsystem because it both determines the length of the spacecraft Earth link and defines the antenna-positioning requirements. Finally, the weight, size, and reliability of the entire subsystem must be considered.

3.1.2.1 Antenna Problems and Considerations

Before specific problems are discussed, it is well to review possible antenna types. These fall into three major categories. Antennas, such as bicones, round waveguide slot arrays, or collinear arrays, produce toroidal patterns. Antennas which produce such patterns are used on spin-stabilized spacecraft and are always oriented normal to a given plane (approximately that of Earth's orbit), and there is no need for steering. The second category is that of pencil beam antennas. Such antennas are used on a spin-stabilized spacecraft that exhibits a properly oriented spin axis or on a three-axis stabilized spacecraft.

Finally, another category of antennas used on spin-stabilized spacecraft is that of electrically de-spun antennas. These antennas could be either arrays used in programmed scans or adaptive, self-focussing arrays. The use of a Luneberg lens in conjunction with multiple switched feeds, or some analogous device, is probably not practical but is not out of the question.

Since the antenna is physically located on the perimeter of the spacecraft, it will be susceptible to meteoroid damage. A discussion of the mechanics of the problem and of possible protective measures is presented in Appendix B. A solution of the problem is not considered unreasonable.

Consideration is now given to the relative merits of the use of various antenna types. Emphasis is placed on patterns, reliability, and other germane considerations. Very little emphasis is placed on costs, difficulty of construction, or difficulty of initial alignment. It is assumed that the alignment can be effected on the ground and that the cost and difficulty of construction is secondary in importance to reliability.

The first antennas to be discussed are those applicable to spin-stabilized spacecraft; the first of these is the biconical horn. Biconical antennas, being rotationally symmetric about an axis, naturally produce rotationally symmetric patterns. Perturbations, such as changes in the antenna surface shape, produce very little effect on this symmetric character. Bicones are quite rugged and can be confidently expected to survive a launch. On the other hand, there is a serious objection to using a bicone at the wavelength (13 centimeters) under consideration and for the gain and beamwidth desired (15 db and 3.6 degrees). The objection is that a biconical horn of even 180-inch diameter needs to be compensated by placing a lens in its mouth in order to obtain the desired gain and beamwidth (Reference 3.1-1). Such a compensated horn would be about 7 feet in height, as can be seen in Figure 3.1-3. Smaller diameter biconical horns exhibit even smaller maximum gain if they are uncompensated. In addition, circular polarization is difficult to obtain.

A collinear array, or any form of linear array of the same height as the compensated bicone, provides the same gain (Reference 3.1-2). However, for the case of the ordinary, simply fed collinear array (consisting of a line of end-fed halfwave dipoles separated by quarterwave sections), this gain is very difficult to obtain and is easily disturbed by vibrations, etc. The required gain is more easily obtained by using a broadside array instead. The problem of feeding such a broadside array without producing azimuthal variations in the pattern is difficult, but it could probably be solved by using cylindrical dipole elements and

running the feed line inside them. It is then necessary either to run perhaps 16 feed lines or to provide baluns and power dividers along the length of the array. Such an array is also susceptible to vibrations. Also, for the case of both the above array types, circular polarization is difficult to obtain.

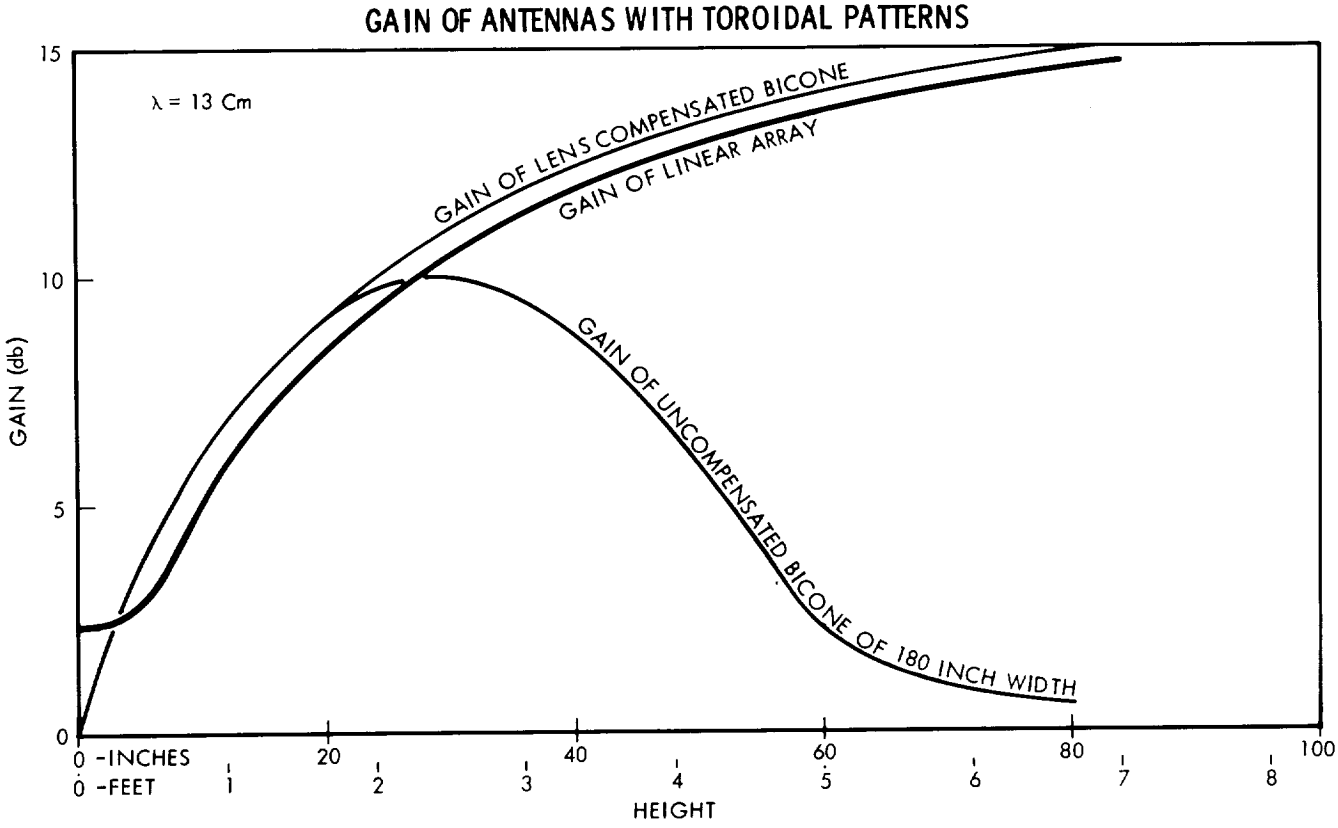

FIGURE 3.1-3

Most of the feed, ruggedness, and polarization problems are greatly simplified by use of a different design concept. Slots are cut in the wall of a circular waveguide and fed by waveguide mode fields. A sufficient number of slots, six or eight, cut around the circumference of the waveguide, produces pattern symmetry within any reasonable tolerance (Reference 3.1-3). Circular polarization is obtained by cutting cross-slots. Slot groups are used to form a linear array and phased properly by proper spacing (Reference 3.1-4). On the basis of the above considerations, it appears likely that a slotted waveguide comprises the most practical antenna for producing an azimuthally symmetric pattern under the circumstances. Such an antenna, which is 4 inches in diameter and 7 feet tall, produces a gain of 15 db. If less gain is acceptable, the height can be correspondingly reduced as shown in Figure 3.1-3.

No form of de-spun antenna, either mechanical or electrical, is considered to be practical. The former is impractical because of obvious mechanical difficulties experienced in the use of bearings, rotary joints, etc.; the latter because of more subtle difficulties

with timed switches (which affect reliability), accurate pointing, and many other problems. However, three possibilities present themselves. The simplest in concept is a pencil beam type array in which a clock and computer, or equivalent, are used to time the programmed beam scanning so that it points in the desired direction. Implementation of this concept is dependent on the use of not only a simple de-spin but also a changing de-spin to track the Earth in its orbit at different points in the spacecraft orbit. Such a setup seems impractical to build and program (though not impossible) and quite risky in view of the possibility of failure. In a more complicated concept, which might be called "crude electronic de-spin," a number of patterns are used. Each of these patterns covers one quadrant or one semicircle of azimuth. An example might be the use of four cardioid patterns. Such patterns can be obtained by using four collinear arrays, for example, or by use of a septated waveguide array, in which the waveguide is separated into four sections by walls and fed one section at a time (Reference 3.1-5). Simple switching is then used to select the pattern which provides the coverage of a full quadrant (for instance) at a time. The selected pattern is in the quadrant including Earth. The restriction of the radiated power to a segment of the full 360 degrees of azimuth thus produces additional gains on the order of 3 to 6 db. It should be possible to furnish a simple program that can be used to provide decisions on switching to one of the four patterns. Another concept which is really somewhat easier to implement is the concept of the adaptive or self-focussing array. Such an array works in the following way. Each individual element senses the phase of an incoming signal and sends out a transmitting signal with the opposite phase; consequently, a transmitted wave is produced. This wave is focussed on the origin of the received wave. Thus, in effect, such an antenna produces a beam in the direction of the transmitter of a received wave. A pilot pointing wave is required for such an antenna to operate, but this is no serious disadvantage. The main problem is that each individual element must receive (because of its own pattern gain) sufficient power for the phase of the incoming signal to be detected. It may be that a self-focussing or adaptive array would be more reliable than any other type if the individual elements could receive enough power. In the formulation of all the above de-spin concepts, it has been assumed that it was not feasible to de-spin anything but an array. It is felt that the case for such a statement is sufficiently well established that no other possibility will be discussed here. However, other possibilities, such as the use of Luneberg lenses in conjunction with multiple feed elements which can be switched in the proper sequence, do exist.

In regard to antennas for use on 3-axis stabilized spacecraft, it is clear that some form of reflector is the best choice. Reflectors are mechanically stable, simple to design and construct, almost invulnerable to meteoroids, and easy to make circularly polarized (by

providing a circularly polarized feed). It is difficult to name any important disadvantage. Reflectors can be designed to produce any reasonable gain consistent with the area which is specified, and no other antenna type of the same size can be used to better advantage. It is also easy to provide beam shaping by the use of reflectors.

3.1.2.2 Transmitter Amplifier Problems and Considerations

The type of transmitter amplifier which is considered as being compatible with DSIF at S-Band frequencies was limited to four types of vacuum tubes, plus solid state. Solid-state amplifiers in general have exhibited excellent reliability and stability in comparison to vacuum tube devices. The overall efficiency of a solid state S-Band amplifier is comparable to that of the better vacuum tube devices. However, the power level deemed necessary in this study cannot be achieved by the use of the present solid-state S-Band equipment.

Of the vacuum tube devices, the negative grid tube is probably the most familiar. The tube elements can be configured to exhibit an acceptable cathode-to-plate transit time at S-Band, e.g., the planar triode. The amplifier is then a class C power amplifier with cavity resonators. There is no problem in attaining the required power levels or in building the tube and cavity ruggedly enough to achieve stability. However, cavity amplifiers in the 10- to 20-watt range typically attain overall efficiencies in the order of 15 to 20 percent (Reference 3.1-6); however, one manufacturer claims an overall efficiency of 28 percent for the case of a 100-watt output. Unfortunately, operating these tubes under the conditions of maximum tube life results in roughly half the above stated efficiency.

The recently developed, electrostatically focussed klystron has demonstrated overall efficiencies of about 30 percent. The conventional intermediate power klystron has demonstrated a life of 5000 hours. However, because of the significant difference between the conventional and electrostatically focussed klystron, a long life for the latter cannot be assumed (Reference 3.1-7).

The traveling wave tube (TWT) has undergone considerable development work since the advent of space communications. Many reliable, efficient TWT's have been developed for space applications under NASA programs. Power levels of up to several hundred watts have been realized. It is not unreasonable to assume that an efficiency of 35 percent for the case of a 50-watt output can be readily attained.

The amplitron is a cross-field microwave tube. Its greatest attribute for space applications is its high efficiency which may run as high as 55 percent (Reference 3.1-7). Until recently, the amplitron was not considered suitable for space applications because of the large magnet needed as a part of the assembly. Recently, lightweight tubes have been developed. However, no reliability figures are available for the case of the lightweight tubes.

If it were necessary to provide a detailed transmitter amplifier design at this time, a TWT would be recommended because of the combination of reliability, efficiency, and power level. However, at the present pace of development, all microwave amplifiers should be surveyed before a design is finalized. In this study it is assumed that TWT's are used in the transmitter amplifier.

3.1.2.3 Modulation Systems

Presently, DSIF is designed to receive data from spacecraft by using coherent phase-shift-keying (PSK) modulation. A considerable amount has been written on this modulation scheme showing it to be one of the more efficient systems. In addition, synchronization is readily generated by using a pseudorandom noise sequence. To illustrate the system, the following example is presented. The DSIF is assumed to have the characteristics listed in Table 3.1-1 (Reference 3.1-10):

Table 3.1-1

DSIF ASSUMED CHARACTERISTICS

Antenna Gain	61 db
Receiver Sensitivity	-182 dbm ($40^{o}K$)
Receiver Threshold	-170 dbm ($2 B_{LO}$ = 12 cps)
	-165 dbm ($2 B_{LO}$ = 48 cps)
	-160 dbm ($2 B_{LO}$ = 152 cps)

($2 B_{LO}$ is the receiver loop noise bandwidth).

The spacecraft parameters listed in Table 3.1-2 are assumed.

Table 3.1-2

SPACECRAFT ASSUMED CHARACTERISTICS

Transmitter Power	45.5 dbm (35 watts)
Antenna Gain	30 db
Miscellaneous Losses	2 db
System Tolerances	6 db

The output of the transmitter is optimized so that half the power is in the sideband and half in the carrier. Therefore, the modulation loss is 3 db.

The normalized signal-to-noise ratio is found by use of the equation

$$S/N_O = P_T - P_M + G_T + G_R - L_S - \phi - L_M$$

where

P_T = Transmitter Power

P_M = Modulation Loss

G_T = Spacecraft Antenna Gain

G_R = Receiver Antenna Gain

L_S = Space Attenuation

ϕ = Normalized Receiver Noise Density

L_M = Miscellaneous Losses and Tolerances.

If the communications distance is 6 a.u., the space attentuation is 278 db. Thus, for this example,

$$S/N_O = 45.5 - 3 + 30 + 61 - 278 + 182 - 8$$

$$S/N_O = 29.5 \text{ db}$$

With PSK, a given value of ST/N_o (where T is the period of one bit) implies a given bit error probability (Reference 3.1-9). To maintain a bit error probability of 10^{-3},

$$ST/N_o = 6.8 \text{ db.}$$

At a bit rate of 67 bps,

$$S/N_o = 6.8 + 10 \log 67$$

$$S/N_o = 25.1 \text{ db.}$$

The difference between the actual and required S/N_o is called the "performance margin"; in this case, the margin is 4.4 db. The performance margin is important because it represents a safety factor that needed in order to overcome any unforeseen degradation of systems parameters. In addition to obtaining the necessary S/N_o ratio for an acceptable bit error probability, it is necessary to maintain a carrier signal level which will keep the phase loop locked. This required signal level is the receiver threshold.

The carrier power received is

$$P_R = P_T - P_M + G_T + G_R - L_S - L_M$$

where P_R is the received power and the other parameters are as previously defined. Then, in the example being considered,

$$P_R = 45.5 - 3 + 30 + 61 - 278 - 8$$

$$P_R = 152.5 \text{ dbm.}$$

In the case of a receiver loop bandwidth 2 B_{LO} of 152 cps, the receiver threshold is -160 dbm. Another performance margin can be mentioned here; this margin is 160 - 152.5 = 7.5 db. A performance margin is also needed here to account for unforseen degradations. Consequently, there are actually two performance margins to be considered relative to PSK modulation.

When information rates are greater than approximately 4 bps, holding a $ST/N_o = 6.8$ db to obtain a bit error probability of no more than 10^{-3} ensure that phase lock will be maintained. This fact is illustrated by letting T = 0.25. Then $S/N_o = 6.8 - 10 \log 0.25 = 12.8$ db. From the previous equation for S/N_o and P_R,

$$P_R = S/N_o + \phi$$

$$P_R = 12.8 - 182 = -169.2 \text{ dbm}$$

This level will be sufficient to maintain phase lock if a loop bandwidth of 12 cps is utilized. However, at bit rates lower than 4 bps, the maintaining of phase lock becomes a limiting factor.

In order to evaluate the limitations of PSK modulation at low data rates and 6 a.u. communications distance, consideration will be given to a spacecraft subsystem where transmitter power is 44 dbm (25 watts) and where antenna gain is 14 db. If the other spacecraft and DSIF characteristics listed previously are also assumed,

$$S/N_o = 44 - 3 + 14 + 61 - 278 + 182 - 8$$

$$S/N_o = 12 \text{ db.}$$

For an error probability of 10^{-3} in PSK, $ST/N_o = 6.8$ db, At one bit per second, T = 1 second = 0 db, and $S/N_o = 6.8$ db. This value leaves a performance margin of 12 - 6.8 = 5.2 db.

The received carrier power is

$$P_R = 44 - 3 + 14 + 61 - 278 - 8$$

$$P_R = -170 \text{ dbm.}$$

The performance margin here is zero for the case of $2B_{LO}$ of 12 cps and is not acceptable. However, if the loop noise bandwidth is reduced to 3 cps, a reduction which does not seem impractical for the 1973-1980 time period, the DSIF threshold is changed by 6 db to -176 dbm, and a 6-db performance margin is provided in the receiver lock threshold.

Because of the above mentioned limitations of PSK modulation at low data rates, other suggested modulation methods may be more efficient at low data rates. One such method has been presented by Goldstein and Kendall (Reference 3.1-8) and is called Multiple Frequency Shift Keying (MFS). The performance of this technique is evaluated below for comparison with PSK on the basis of using the same parameters as those used in the preceding example.

When MFS is used, all the transmitted energy contains information. Therefore, $P_M = 0$, and

$$S/N_o = 44 - 0 + 14 + 61 - 278 = 182 - 8$$

$$S/N_o = 15 \text{ db.}$$

Goldstein and Kendall have shown:

$$P_e = \frac{N-1}{2}\left[1 - \theta\left(S/N_o \quad \frac{T}{\pi} \quad \sqrt{\frac{2\,\tau\,max}{T}}\right)\right]$$

where

P_e = Probability of bit error

$N = 2^k$ where k = number of bits per word

T = The time length of transmission of one word

τ max = The period of truncation of the received signal

$$\theta(x) = \frac{2}{\sqrt{\pi}} \int_o^x e^{-y^2}\, dy \ .$$

In this study, data is considered to be transmitted by use of a seven-bit word for engineering data and a ten-bit word for scientific data. The MSF method would best be implemented by using a seven-bit word so that one word could be transmitted for engineering data and two words for scientific data. In the case of scientific data, the four extra bits could be used as a lable. Then to obtain one bit per second, the transmission time per word is seven seconds. In an overall receiver stability of 75 cps is assumed, $2\,\tau$ max is 0.013. Then, on the basis of a bit error probability of 10^{-3} and the approximation

$$1 - \theta(x) \cong \frac{e^{-x^2}}{x\sqrt{\pi}}$$

it can be shown that

$$(S/N_o) \quad \frac{T}{\pi}\sqrt{\frac{2\ \tau max}{T}} = 3.06$$

Then

$$S/N_o = \frac{3.06\,\pi\,\sqrt{75}}{\sqrt{7}} = 31.4$$

or

$$S/N_o = 15.0 \text{ db.}$$

thus the performance margin is 15 - 15 = 0 db.

Since S/N_o is a function of $1/\sqrt{T}$, the performance margin can be improved by increasing the transmission time if the word length remains constant. Doubling the transmission time will decrease the required S/N_o by 1.5 db. Consequently, reducing the bit rate to 1/8 bps will yield a performance margin of 4.5 db.

It may seem that another means of increasing the performance margin would be shortening the word length. A four-bit word could be readily implemented by using two words to transmit engineering data and three words to transmit scientific data. Analyzing this configuration yields a required S/N_o of 15.8 db to obtain an information rate of one bit per second.

The implementation of either MSF or PSK for bit rates less than 4 bps is contingent on some modification of the DSIF. If PSK is used, a narrower loop filter is necessary. In the case of MFS, a special detector is necessary. In addition, Doppler shift is another problem which may occur in using either method. Some method will have to be devised to provide a variable bias to the frequency of the ephemeris-controlled local oscillator to correspond with the Doppler rate. In PSK systems where loop noise bandwidth is 3 cps, the Doppler tracking rate capability is reduced by 6 db. The present rate capability of 4 cpsps at $2B_{LO}$ = 12 cps would then be reduced to 1 cpsps.

Therefore, Doppler rates present a problem in either case. Some other Doppler shift considerations for the communications subsystem are discussed in subsection 3.1.2.7.

Table 3.1-3 contains a comparison of the modulation schemes considered in this study.

Table 3.1-3

LOW DATA RATE MODULATION COMPARISON

System	Bit Rate	Margin	Considerations
PSK	1	Info., 5.2 db Rcvr. Threshold, 0 db	None
PSK	1	Info., 5.2 db Rcvr. Threshold, 6 db	$2\ B_{LO}$ = 3 cps
MSF	1	0 db	Note 1, 7-bit word
MSF	1	-0.8 db	Note 1, 4-bit word
MSF	1/8	4.5 db	Note 1, 7-bit word

Note 1: To implement MSF, a special detector system must be incorporated at DSIF.

On the basis of the foregoing analyses, PSK is recommended as the modulation method at all data rates > 1 bps. No problems in the use of this method are forecast at data rates of four bits per second and greater. At lower data rates, problems will occur in the use of either the PSK or MFS methods. Ways of overcoming these problems in either system have been presented. PSK is recommended rather than MSF in the interest of uniformity, a lesser amount of DSIF modification, and a higher data rate.

3.1.2.4 Earth System

Before examining the methods to be used in synthesizing a spacecraft communications subsystem, the characteristics of the Earth station should be defined.

For the purpose of this report, the full DSIF capability is assumed, i.e., a receiver noise temperature of 40°K, a receiving antenna gain of 61 db, a receiver frequency of 2295 mc, a transmitter power of 100 KW, a transmitting antenna gain of 51 db, and a transmitting frequency of 2113 mc. No attempt has been made to schedule communications with the spacecraft, and continuous communications capability is assumed except when the line-of-sight between Earth and the spacecraft is blocked. However, the scheduling of transmission times would be a minor item.

3.1.2.5 Antenna Positioning

The problem of positioning pencil beam antennas must be discussed before the discussion of the entire subsystem is continued. Since a pencil beam antenna, such as a parabolic reflector, transmits energy only in a very small solid angle, it is necessary to point the antenna very accurately. Figure 3.1-4 shows a curve of necessary pointing accuracy versus antenna gain. To point the antenna with such an accuracy is probably most easily and reliably done by command from the ground, because the use of an elaborate on-board antenna pointing system is eliminated. Pointing can be achieved by means of steering either the spacecraft or the antenna alone. Steering is accomplished by changing the antenna position in discrete angular increments within two planes of freedom. When the antenna beamwidth and the Earth's position relative to the sun are known, the magnitude of these increments can be preselected. An example of Earth-Sun position is shown in Figure 3.1-5.

ANTENNA POINTING ACCURACY

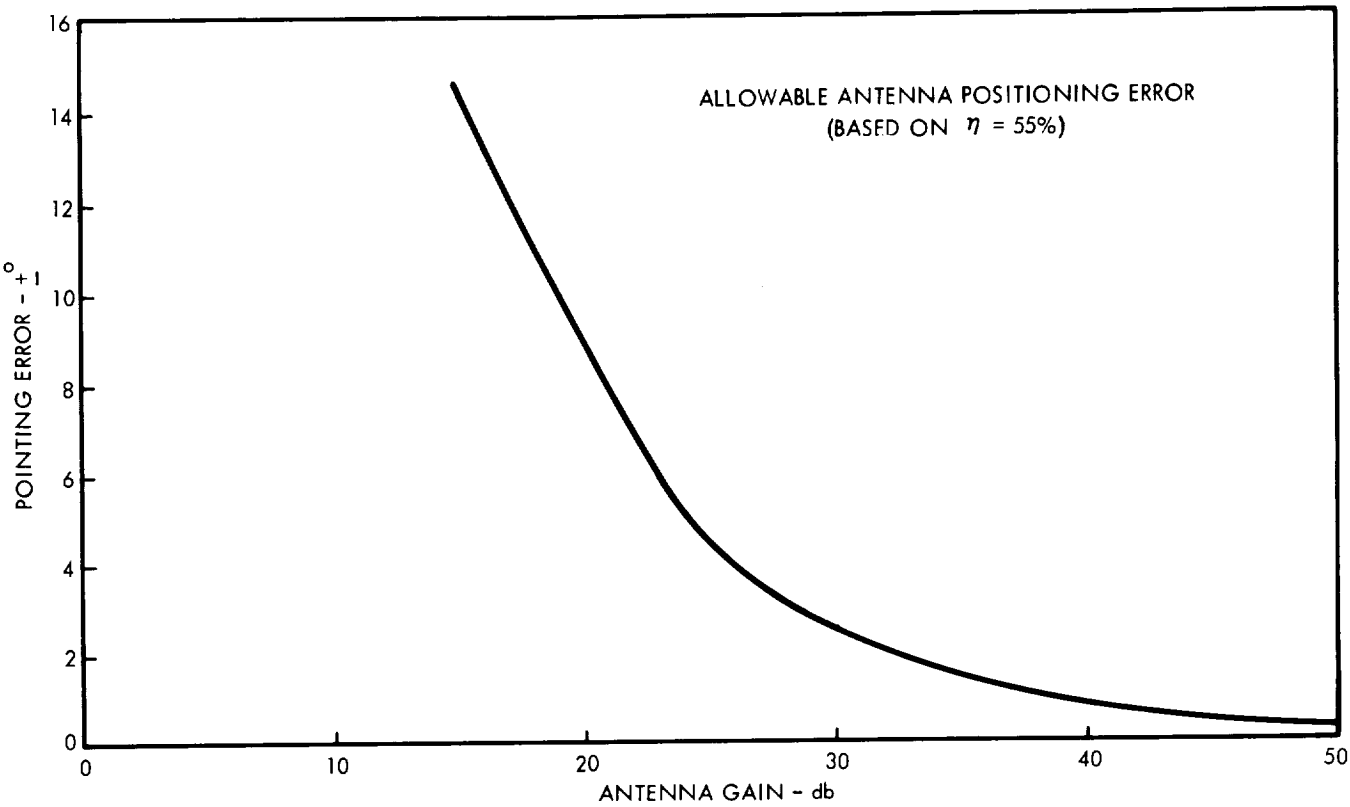

FIGURE 3.1-4

EARTH-SUN POSITION

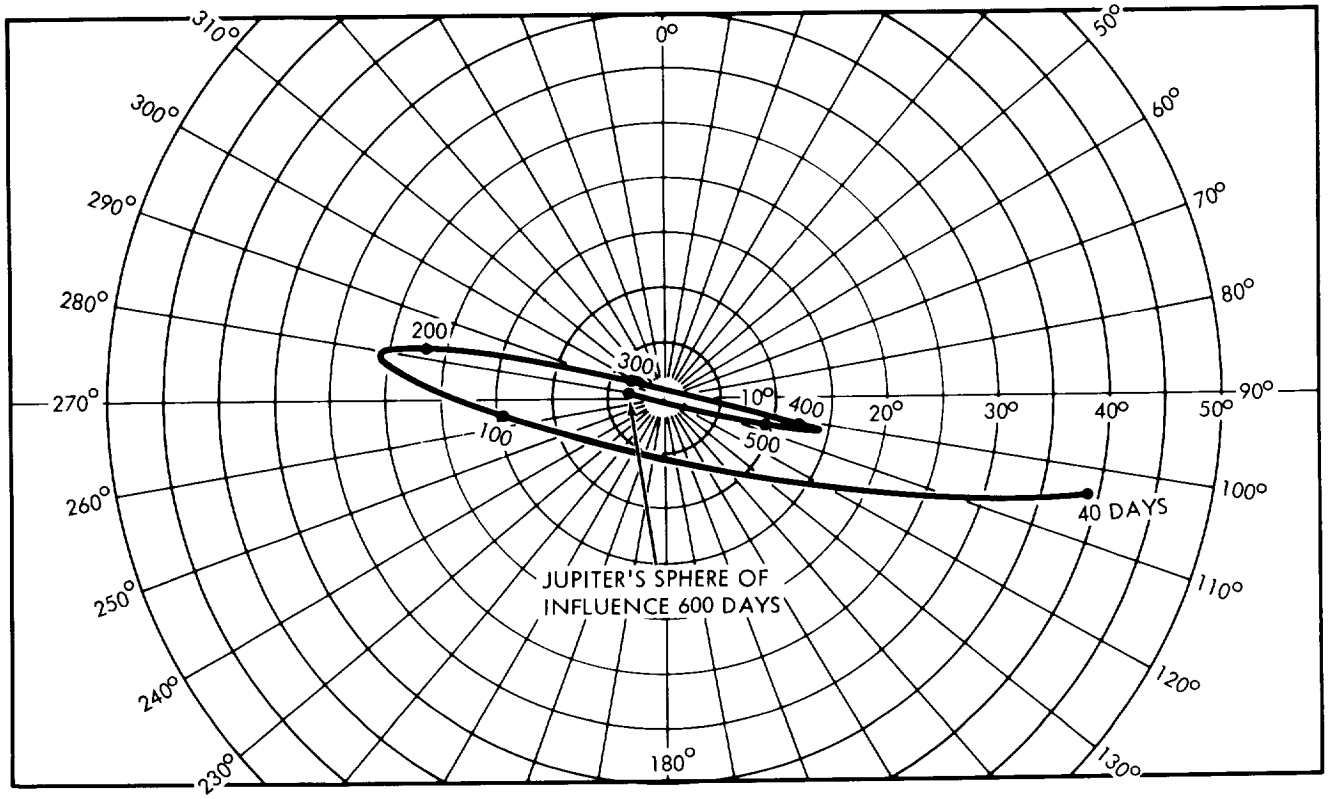

FIGURE 3.1-5

3.1.2.6 Spacecraft Subsystem

The spacecraft subsystem selection is basically dependent on tradeoffs between transmitter power, antenna gain, and information rate. To aid in these trade-offs. Figure 3.1-6 was conceived. In this figure, antenna gain is shown as a function of the information rate and the transmitter power which is necessary to maintain an error probability not greater than 0.001. Consequently, the signal-to-noise per unit bandwidth times (ST/N) must equal 6.8 db (Reference 3.1-9). The equation presented in paragraph 3.1.2.3 together with the DSIF parameters, was used to construct Figure 3.1-6.

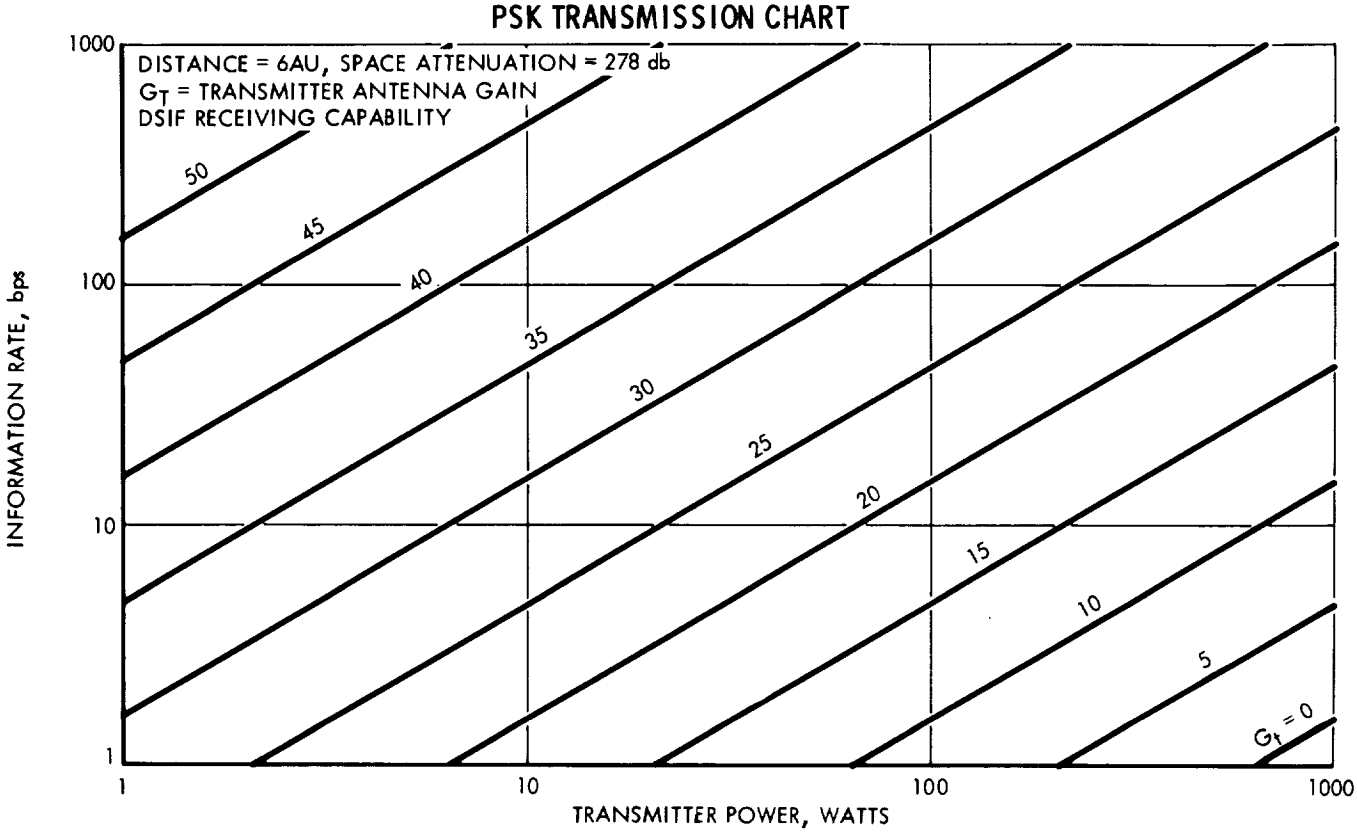

FIGURE 3.1-6

Antenna gain is considered first. Since increases in antenna gain increase the effective radiated power of the subsystem with no increase in electrical power input, the antenna gain is made as large as possible within physical and positioning limitations. After the attainable antenna gain is determined, it is necessary to choose either a bit rate or transmitter power. Because the transmitter power necessary to transmit all the required data in real time is generally prohibitive, it is always necessary to store data. Therefore, the transmitter power is chosen to be compatible with equipment limitations and the electrical power subsystem. This choice then determines the bit rate. The bandwidth is determined on the basis of the bit rate and modulation characteristics. Then by constructing a gain - loss chart, system operation will be confirmed.

3.1.2.7 Operational Considerations

Before specific recommendations for spacecraft subsystems are presented, two operational problems should be discussed. The first problem is that of high Doppler rates. To obtain the maximum DSIF threshold of -170 dbm, the Doppler rate must not exceed 4 cpsps. However, at a perijove altitude of one radius, Doppler rates on the order of 100 cpsps will be experienced from a posigrade pass. The loop bandwidth available within DSIF to track this Doppler rate is such that the threshold sensitivity must be -160 dbm which allows tracking rates up to 150 cpsps. The actual Doppler rate of the received signal is dependent upon the altitude of the perijove and the direction of the pass. In the case of a minimal capability spacecraft, it may be necessary to suspend telemetry, and DSIF may actually lose all communications with the spacecraft for several hours on either side of perijove. Curves of the expected Doppler rates for various passes are contained in Figure 3.1.7.

The second problem pertains to the considerations necessary for an occultation experiment. As indicated above, the Doppler rates at encounter allow a threshold sensitivity of -160 dbm. In order to make a meaningful occultation experiment, a performance margin of 10 db would be desirable. In addition, considerable signal attunuation and scattering can be expected from the Joivan atmosphere. A reasonable estimate of the attenuation and scattering degradation is in the order of 25 db. Therefore, the received signal level should be at least -125 dbm. At an encounter distance of 6 a.u., an effective radiated power of 100 dbm must be produced. This value is beyond the limits of the spacecraft considered in this study. However, an occultation experiment can still be attempted, but the success of such an experiment is questionable.

3.1.3 Conclusions

3.1.3.1 Antennas

Thin double walls, as discussed in Appendix B, are recommended for antenna construction because of light weight and invulnerability to meteoroid damage. Slotted waveguide antennas are used on spin-stabilized vehicles. The concept of using pencil beam antennas pointed along the spacecraft spin axis was eliminated because of the added complexity in continually controlling the spin axis orientation. This problem is discussed further in Section 1. The bicone antenna is more vulnerable to meteoroid damage than the slotted waveguide, and it also imposes the problem of manufacturing a precise compensating lens. Furthermore, circular polarization is readily

DOPPLER RATE AT ENCOUNTER WITH JUPITER

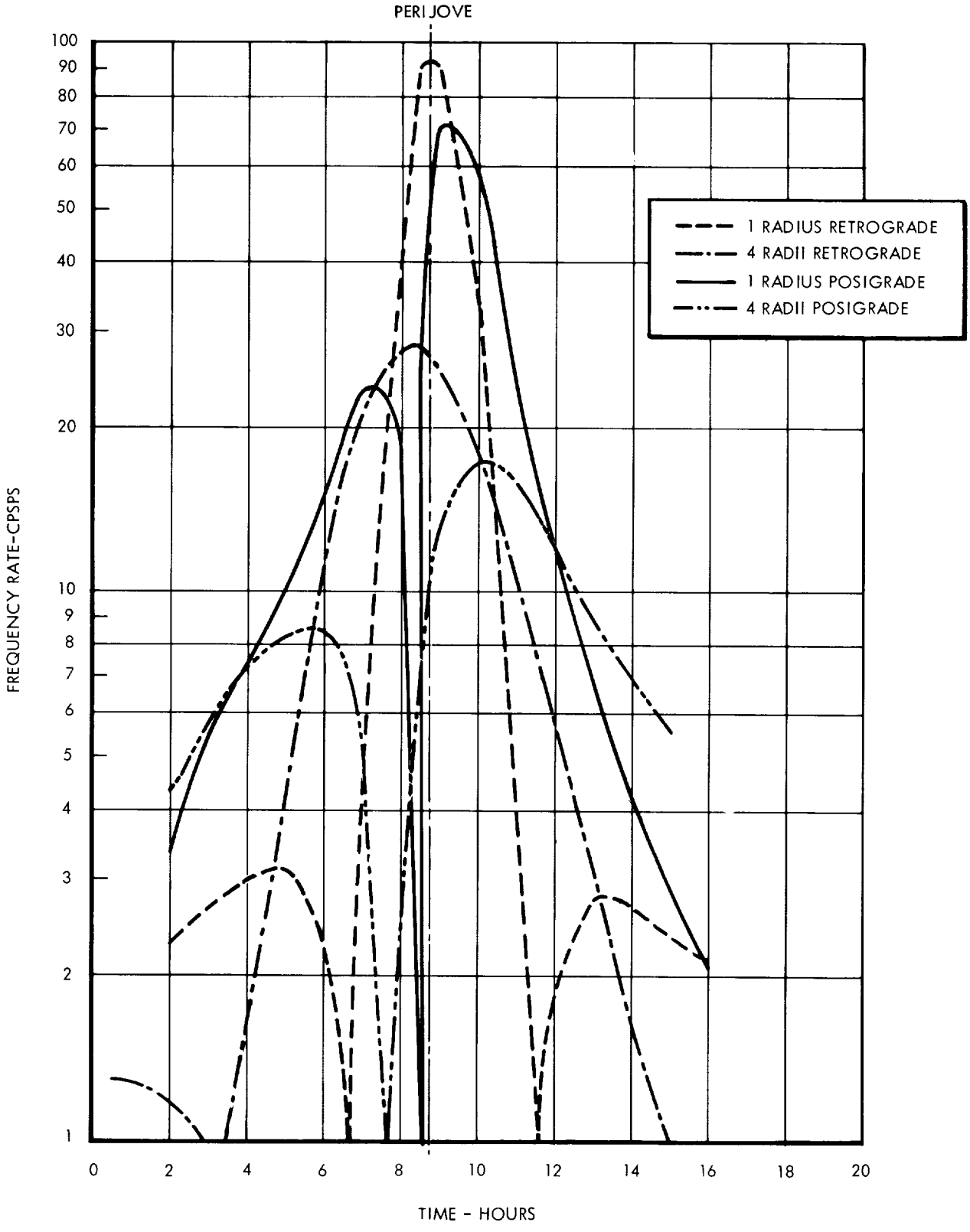

FIGURE 3.1-7

obtainable from the slotted waveguide while the bicone is basically a vertically polarized antenna.

It is recommended that parabolic, high-gain antennas with Cassegrainian feed be used in all three-axis stabilized vehicles to protect the feed point. Two horn-type feeds are felt to be necessary: one to provide a normal antenna pattern and one which is an "off-focal point" feed to spoil the beamwidth and thereby provide a broader beamwidth. This feedpoint is used so that a wide beamwidth is available for reacquisition, in the event that communication with the spacecraft is lost.

3.1.3.2 Transmitters

At this point in time, the transmitter is considered to be a traveling-wave tube. However, the developments in the other types of microwave tubes must be monitored. The transmitter consists of two amplifiers and two exciters, any combination of which can be selected to meet the reliability requirements of the spacecraft.

3.1.3.3 Modulation

PSK modulation with PN synchronization is recommended on the basis of the discussion contained in paragraphs 3.1.2.3. While this system falls very short of providing the theoretical maximum efficiency, it is the more efficient of the two systems investibated. It is also compatible with the present DSIF equipment. The synthesis of a new modulation system was not attempted.

3.1.3.4 Subsystem Configuration

A typical communications subsystem is shown in Figure 3.1-8. The interfaces between the communications subsystem and other subsystems are (1) antenna commands from command and control, (2) composite ground commands to command and control, (3) composite data from data management, (4) electrical power from the power subsystem, and (5) engineering data to data management. The operation of the communications subsystem is described below.

The automatic phase control receiver demodulates the signal received from the Earth. This signal is in the form A sin $(\omega_o t + \phi_c + \phi_r)$ where A = amplitude, $\omega_o t$ = carrier angular velocity, ϕ_c = command phase modulation, and ϕ_r = range phase modulation.

TYPICAL COMMUNICATIONS SUBSYSTEM

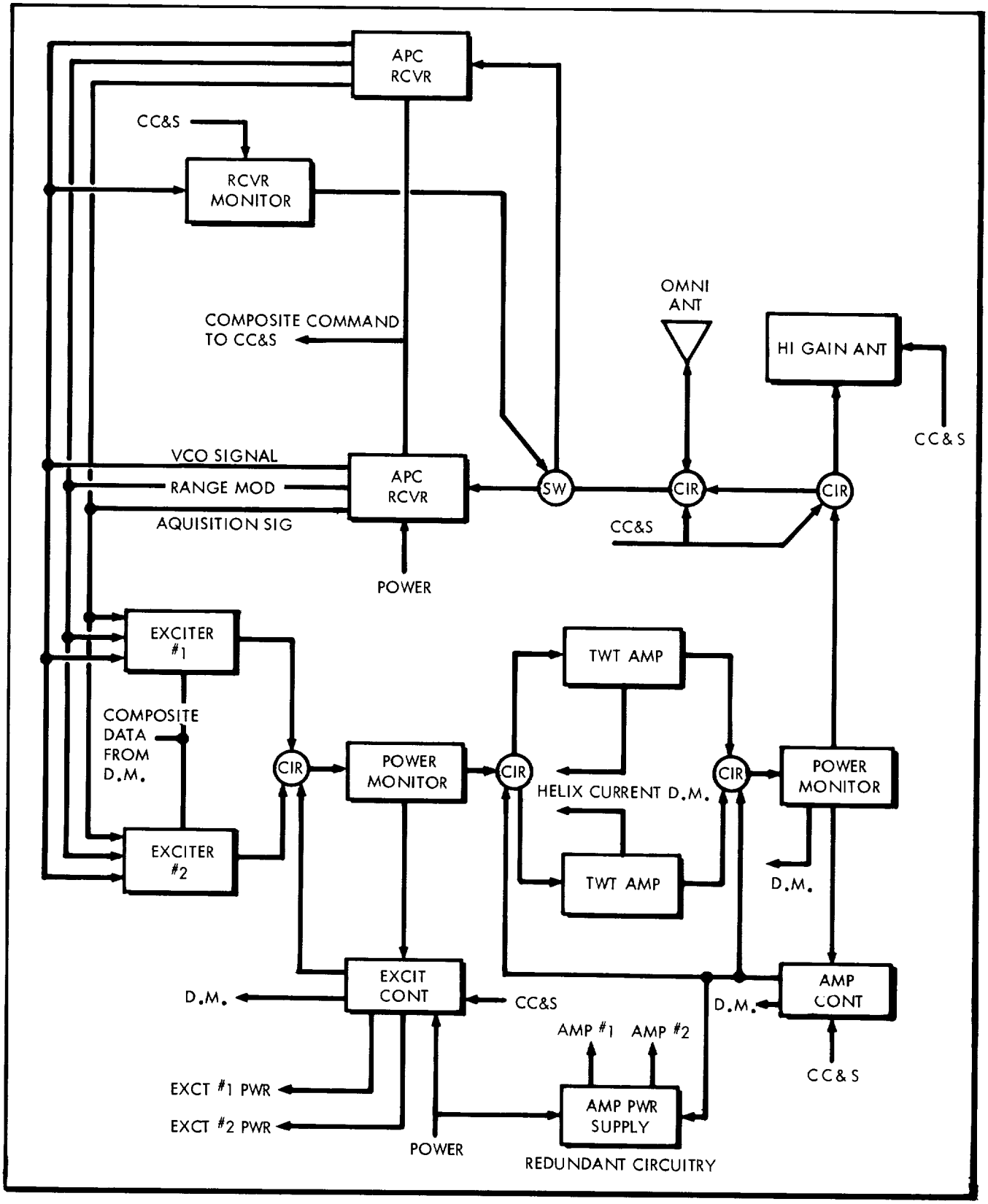

FIGURE 3.1-8

The general method of operation is for the spacecraft reciever to track the phase component of the received signal. This signal is locked to the received signal and provides two-way Doppler range tracking. The output from the receiver is a voltage controlled oscillator (VCO) signal that is translated at a known ratio and is used as an input signal to the exciters.

The exciter signal is then biphase modulated with digital data from the data management subsystem, amplified in a TWT amplifier, and radiated by the antenna. In the event the signal from the Earth is lost, the VCO is replaced by a crystal oscillator. Then the spacecraft radio transmitts back to Earth a non-coherent data signal that is referenced to the internal crystal oscillator. The receiver also demodulates ground commands and feeds them to the command and control subsystem. In addition, range interrogations are recognized and transponded.

To improve reliability, two exciters and two receivers are recommended. A reliability analysis or the communication subsystem is reported in subsection 3.13. The control circuit assigned the task of selecting the operational receiver monitors the output VCO signal voltage. Upon loss of the signal, the second receiver is automatically selected. However, if a phase-coherent signal from the Earth is not received within a pre-selected time (for example, 8 hours), the control circuit switches back to the other receiver. This approach will aid re-establishment of Earth tracking under adverse conditions.

The power output of the selected exciter and the selected TWT amplifier are monitored. If either of these units falls below a specified signal level, the built-in test control circuit automatically switches to the other unit. In this way, any combination of the two exciters and two TWT amplifiers can be used. This approach is considered to be necessary to satisfy the anticipated reliability requirements. In addition, redundant TWT power supplies are recommended. Another reliability consideration is incorporated in the high-gain antennas. This is the beam spoiling feature described in 3.1.3.1 which allows for re-acquisition of the spacecraft in case communications is lost because of an improperly-pointed antenna. A complete discussion of subsystem reliability is contained in subsection 3.13.

Except for the high-voltage power supply and the output TWT amplifiers, the circuits of the communication subsystem operate at a low power level. Where applicable, all circuitry is solid state. The temperature limits to be maintained are -54 to +95 degrees centigrade.

3.1.4 References

3.1-1. Jakes, W. C., Jr., "Bi-conical Horns," Antenna Engineering Handbook, New York: McGraw-Hill (1961), pages 10-13.

3.1-2. Southworth, C.G., "Arrays of Linear Elements," Antenna Engineering Handbook, New York: McGraw-Hill (1961), pages 5-14.

3.1-3. Galindo, V., and Green, K., "A Near Isotropic Circularly Polarized Antenna for Space Vehicles," Transactions of the Professional and Technical Group on Antennas and Propagation of the IEEE, Vol. AP-13, No. 6 November 1965), pages 872-878.

3.1-4. Silver, S., "Microwave Antenna and Design," Radiation Laboratory Series, Vol. 12. McGraw-Hill (1949), pages 10-11.

3.1-5. Blass, J., "Slot Antennas," Antenna Engineering Handbook. New York: McGraw-Hill (1961), pages 8-6.

3.1-6. Sill, D., Webb, J., and Fairley, D., "A Survey of RF Power Sources for Telemetry," Proc. Nat. Telemetering Conference, (May 1961).

3.1-7. Feldman, N., "Communication Satellite Output Devices," Micro-wave Journal, (December 1965).

3.1-8. Goldstein, R., and Kendall, W., Low Data Rate Telemetry, Symposium on Unmanned Exploration of the Solar System (February 8-10, 1965).

3.1-9. Springett, J., Telemetry and Command Techniques for Planetary Spacecraft, Technical Report No. 32-495, Pasadena, California, Jet Propulsion Laboratories (January 15, 1965).

3.1-10. System Capability and Development Schedule of the Deep Space Instrumentation Facility, 1964-68 (Revision 1), Technical Memorandum No. 33-83, Jet Propulsion Laboratory, Pasadena, California (April 24, 1964).

3.2 DATA MANAGEMENT

The data management subsystem of a Jupiter flyby spacecraft is used to perform the following two significant functions:

1. To provide an efficient interface to encode data from the scientific and engineering sensors and to transfer these data to the communications subsystem for subsequent transmission.

2. To provide an efficient method of detecting and decoding ground commands received by the communications subsystem and to transfer these commands to the appropriate instrument for execution.

The four elements of the data management subsystem shown in Figure 3.2-1 are the Data Automation Element (DAE), the Data Encoder Element (DEE), the Data Storage Element (DSE), and the Command Detector and Decoder Element (CDDE).

DATA MANAGEMENT SUBSYSTEM

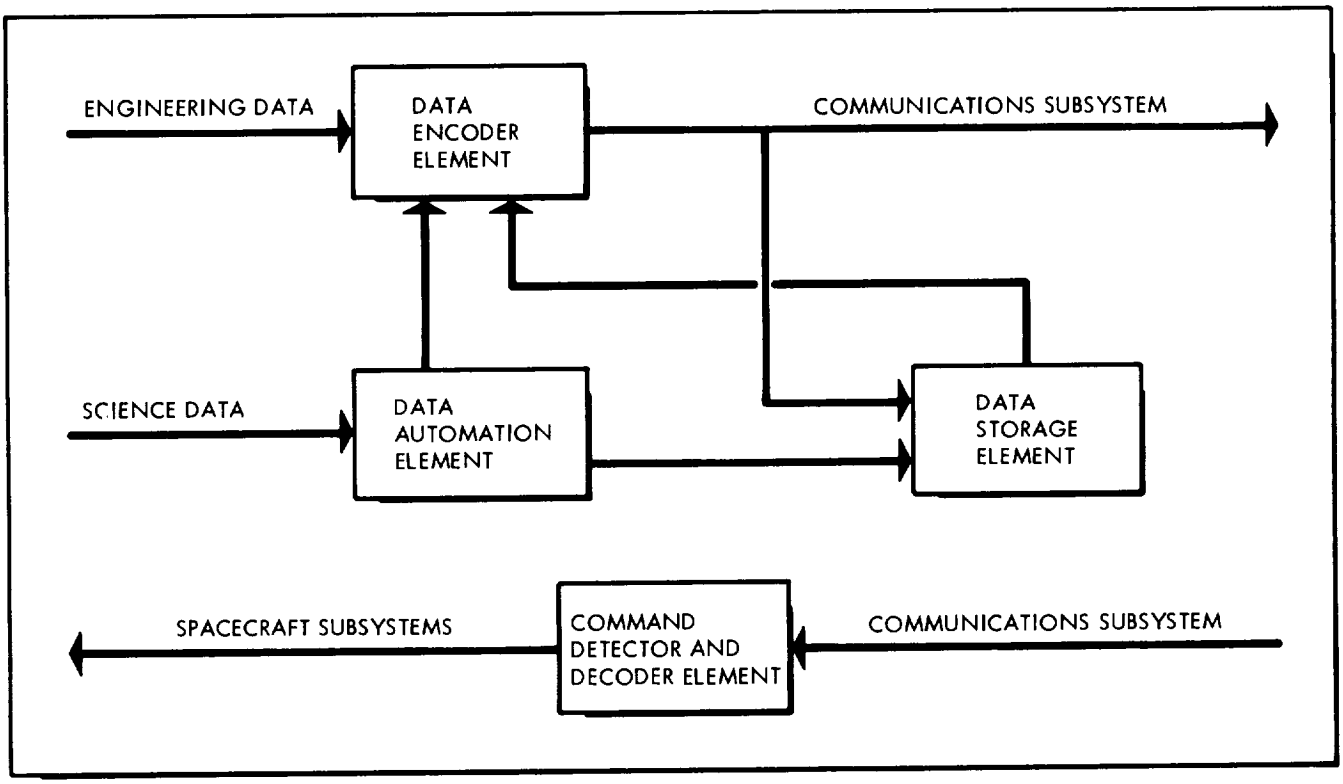

FIGURE 3.2-1

3.2.1 Functional Requirements

The elements contained in this subsystem are used to perform various functions. The specific functions supplied by each element are listed in the following paragraphs.

The data automation element is used to perform the following functions:

1. Control and synchronization of the scientific instruments within the DAE timing and format structure, so as to provide information on the instrument internal sequencing, and transmission of commands to the instruments as required

2. Provision of the necessary sampling rates, both simultaneous and variously sequential, to ensure that meaningful scientific data is obtained

3. Performance of the necessary conversions and encoding of the several forms of scientific data

4. Formatting of the scientific data

5. Buffering of the scientific data which are obtained at different and sporadic rates and subsequent transmission to the DEE and the DSE at the desired rates and in the desired modes

6. Issuance of commands which pertain to the operation of the science subsystem and reception of such commands from other subsystems aboard the spacecraft.

The data encoder element is used to perform the following functions:

1. Control and synchronization of the engineering measurement sensors within the DEE timing and format structure so as to provide information on the measurement internal sequencing

2. Provision of the necessary sampling rates to ensure that meaningful engineering data is obtained

3. Performance of the necessary conditioning, conversion, and encoding of the engineering analog signals and event pulses

4. Formatting and combination of the engineering data with serial binary data inputs from the DAE

5. Transference of serial binary data from the DSE to the communications subsystem

6. Provision of data compression for all data

7. Addition of the binary coded data to the synchronization code by means of modulo 2

8. Provision of the various command-selectable data transfer rates to the communications subsystem in order to facilitate the optimum use of the available communications capability throughout the mission

9. Provision of several command-selectable data modes to permit processing flexibility: Mode I - engineering data only; Mode II - engineering and science data; Mode III - science data only; and Mode IV - tape recorder data playback.

The data storage element is used to perform the following functions:

1. Provision of the required data storage capacity to store scientific data from the DAE and engineering data from the DEE

2. Provision of the capability to store data at the prescribed rates

3. Provision of the capability to read data at the prescribed rates.

The command detector and decoder element is used to perform the following functions:

1. Detection of commands in the form of a binary square wave subcarrier output from the spacecraft communications subsystem demodulator

2. Decoding of the digital commands, routing of discrete commands (DC) to spacecraft subsystems, and provision of quantitative commands (QC) to the CC&S.

3.2.2 Possible Concepts

In view of the types of data to be processed, the quantity of these data, and the transmission data rates available for each mission, several concepts must be investigated in order to provide optimum operation of the data management subsystem. One concept is to use the Mariner IV equipment and techniques to the greatest extent possible and to make only those modifications which are required because of differences in mission objectives. Use of this concept will satisfy mission requirements with the least

equipment development cost, but it will not result in any important improvement in capability. Another concept is to undertake a large-scale program directed to devising entirely new methods and designs for use in data management. The development cost will be high, but the possibility of lowering other costs and of accomplishing significantly more mission objectives is increased.

A third concept is a combination of the first two. Maximum use is made of Mariner designs, but at the same time, some development is undertaken. This development is concentrated in those areas which appear to offer the most opportunity for increasing the data management subsystem capability. In this way, capability can be improved without an unreasonably high development cost.

3.2.3 Analyses

The trade-off considerations are related to reliability, flexibility, efficiency, size, weight, and power. Because of the duration of a Jupiter flyby mission, reliability is considered the most important consideration. Flexibility and reliability can be achieved simultaneously by using interchangeable components which can replace each other in case of a malfunction. Although efficiency may be sacrificed in order to obtain greater reliability and flexibility, the significance of efficiency is still recognized. Weight, size, and power, though still important, are becoming less critical. Larger boosters and microminiaturization now permit greater latitude in the selection of equipment.

Several analyses were performed in order to select the most efficient data management subsystem for various Jupiter missions. A comparison was made between the engineering and science data-gathering requirements for the Jupiter flyby missions and the Mariner IV mission in order to assess the compatibility of the telemetry requirements for the two missions. In order to determine the applicability of data compression and data storage, another comparison was made between the data-gathering rates and the available transmission rates during the various mission phases. As expected, the results of this analysis indicated that the maximum data-gathering rates occur at Jupiter encounter, when the allowable transmission rates are minimum. It was also found that the data-gathering rate is considerably more than the transmission rate during this phase in all missions considered.

3.2.3.1 Data Compression

Data compression techniques were investigated in terms of the various types of data as a means of increasing the quantity of data which can be transmitted in real time. Results of a survey of the literature indicate that satisfactory data compression techniques are available for use in conjunction with both the engineering and the scientific measurements.

The fan method, developed and patented by Radiation, Incorporated, of Melbourne, Florida, seems to be applicable to all of the data types being considered for this mission, including television pictures (Reference 3.2-1). Figure 3.2-2 contains an illustration of the logical operations performed by means of this technique. Basically, the fan method is used to project an angle, or fan, from the last significant value and to determine if the current value falls within this angle. If the current value is located within these limits, the preceding point is discarded and the current value is stored until the following point has been tested. If the current value is located outside these bounds, the preceding value becomes the significant value, and it is transmitted.

Another much less complicated data compression scheme which can be used to replace the fan method is the zero order interpolator (References 3.2-2 and 3.2-3). The logical operations performed by use of this technique are shown in Figure 3.2-3. In the zero order interpolator, the current value is compared with the last significant value. If the difference between the two samples is less than the preset upper and lower tolerances, the current sample is considered insignificant and is dropped. If this difference exceeds the tolerances, the current sample becomes the significant value, and it is transmitted. The implementation of this technique is simpler than the fan method, but a comparison of their compression ratios indicates that engineering data, for example, can only be compressed 30:1 by use of the zero order interpolator while they can be compressed 150:1 by use of the fan method.

The quantile method of data compression seems to be applicable to certain types of data whose statistical properties are desired, such as particle count data (References 3.2-4, 3.2-5, and 3.2-6). The required equipment and the operations performed by use of this method of compression are shown in Figure 3.2-4. A counter is sampled periodically and reset to zero so that the number of counts accumulated since the last sampling time can be determined. A one is placed in the storage register corresponding to this count. At the end of the total count interval, the storage registers are added sequentially into the accumulator. The cumulative sum after each addition is compared with the value in the comparator which is currently being used. As soon as the sum equals or exceeds this comparator value, the comparator value is transferred to its corresponding quantile register, and the address of the current storage register and the comparison remainder are stored. After the accumulator is reset to zero, the addition of the storage registers is continued by comparing the sum with the next comparator value. This process is continued until all of the storage registers have been summed. The compressed data is then transferred, and a new total count interval is initiated by clearing the storage registers and accumulator and restarting with time equal to zero. A compression ratio of approximately 100-to-1 is expected in the data range considered.

Several techniques exist for compressing television picture data. Among these are the fan, stop-scan edge detection, block

FAN DATA COMPRESSION TECHNIQUE

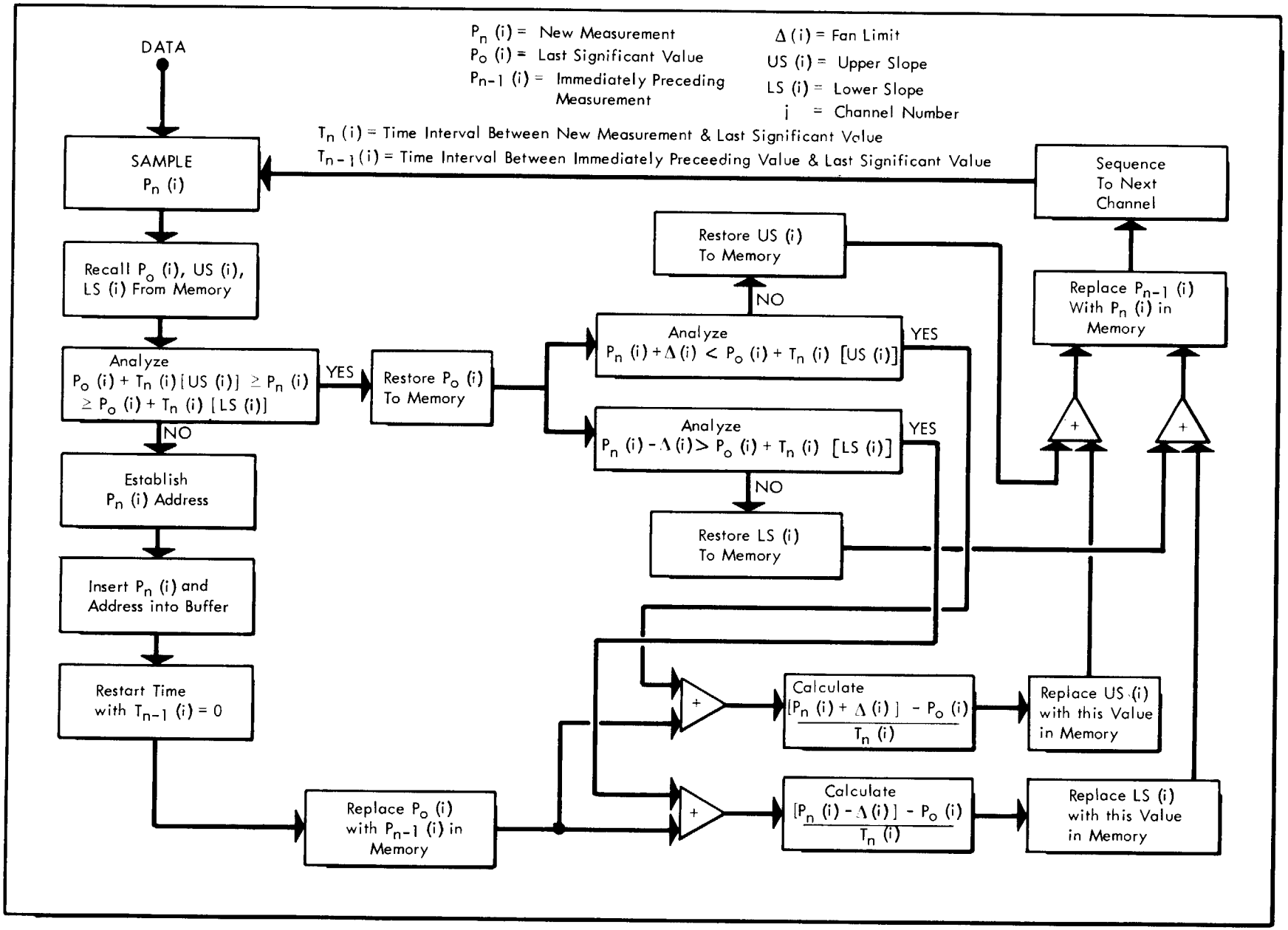

FIGURE 3.2-2

ZERO ORDER INTERPOLATOR DATA COMPRESSION TECHNIQUE

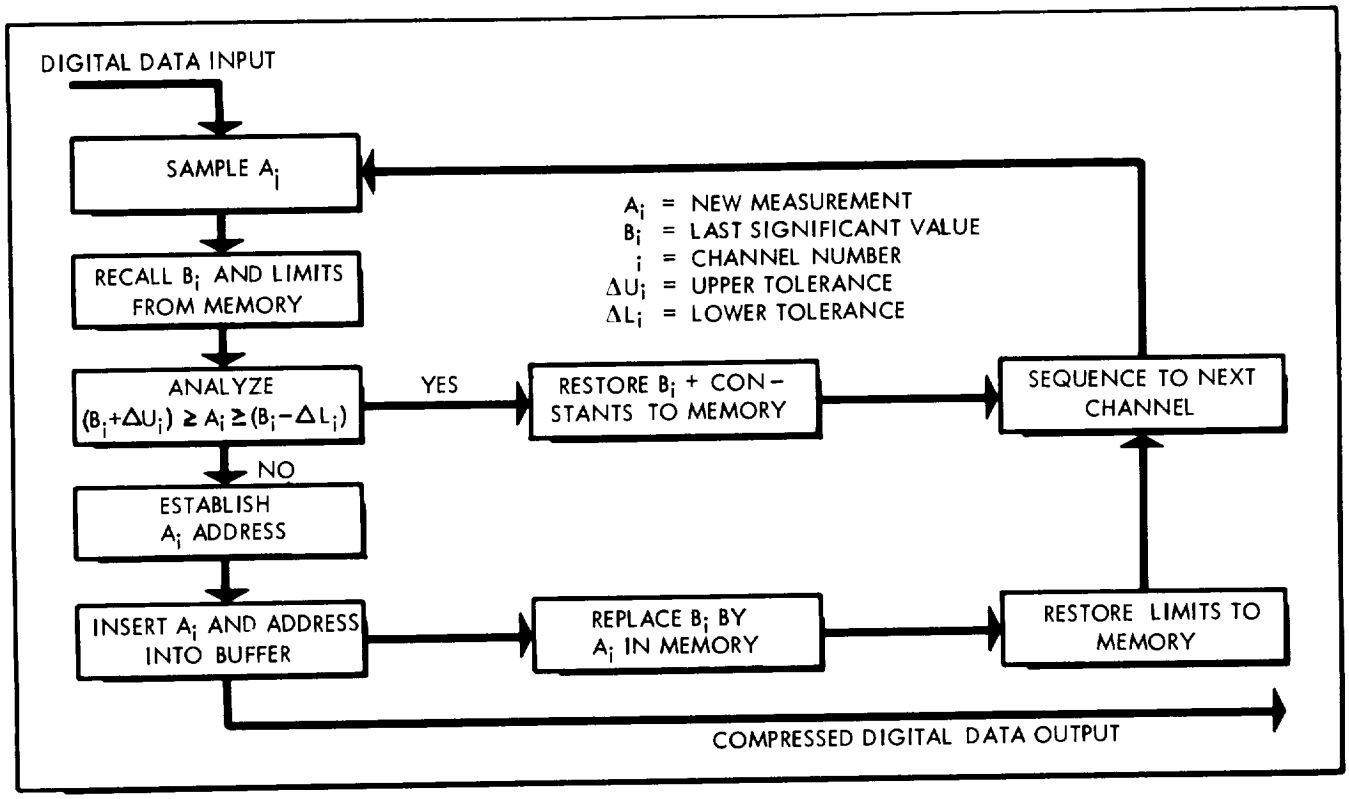

FIGURE 3.2-3

QUANTILE DATA COMPRESSION TECHNIQUE

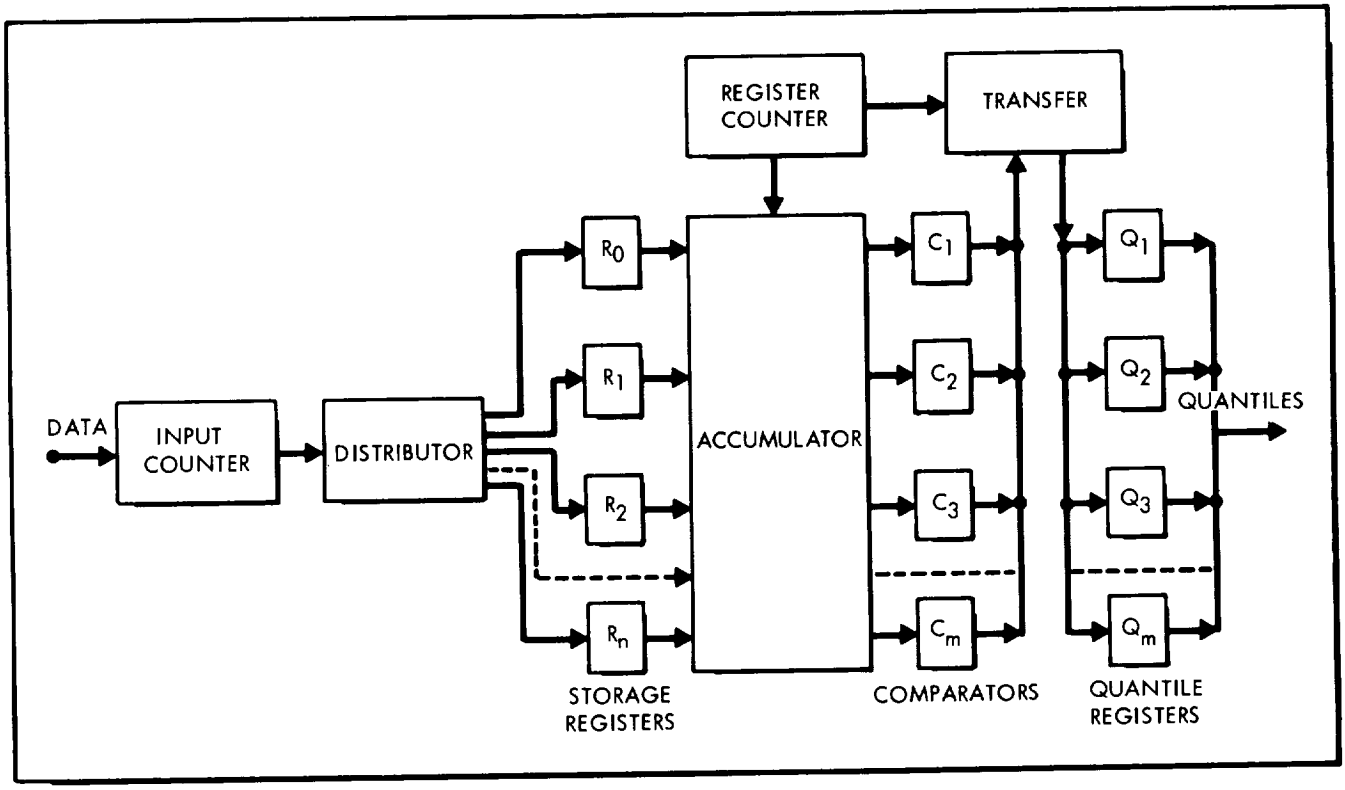

FIGURE 3.2-4

coding, self-adaptive prediction, high information delta modulation, improved gray scale, course-fine, and pseudo-random noise methods (References 3.2-7 through 3.2-13). The three techniques which seem to show the most promise are the fan method, the stop-scan edge detector, and the block coding.

In the stop-scan edge detection technique, shown in Figure 3.2-5, the television signal is separated into a low-frequency signal and a high-frequency signal. The low-frequency signal is used to perform a 2-bit delta modulation transformation, and the high-frequency signal is used to detect the location of picture edges (sudden changes in intensity) and to identify their intensity level. It is anticipated that a compression ratio of 10-to-1 can be obtained by use of the fan method and 5-to-1 by use of the stop-scan edge detector method.

In block coding the correlation between the elements of a television picture is determined, and a block of elements is coded according to its probability of occurrence. Several methods of achieving comma-free, variable-length code words are available. One of these methods has been developed by Fano (Reference 3.2-9). Compression ratios obtained by use of this technique are highly dependent on the data, and the results of specialized tests on pictures applicable to this mission are not available at this time.

STOP-SCAN EDGE DETECTOR DATA COMPRESSION TECHNIQUE

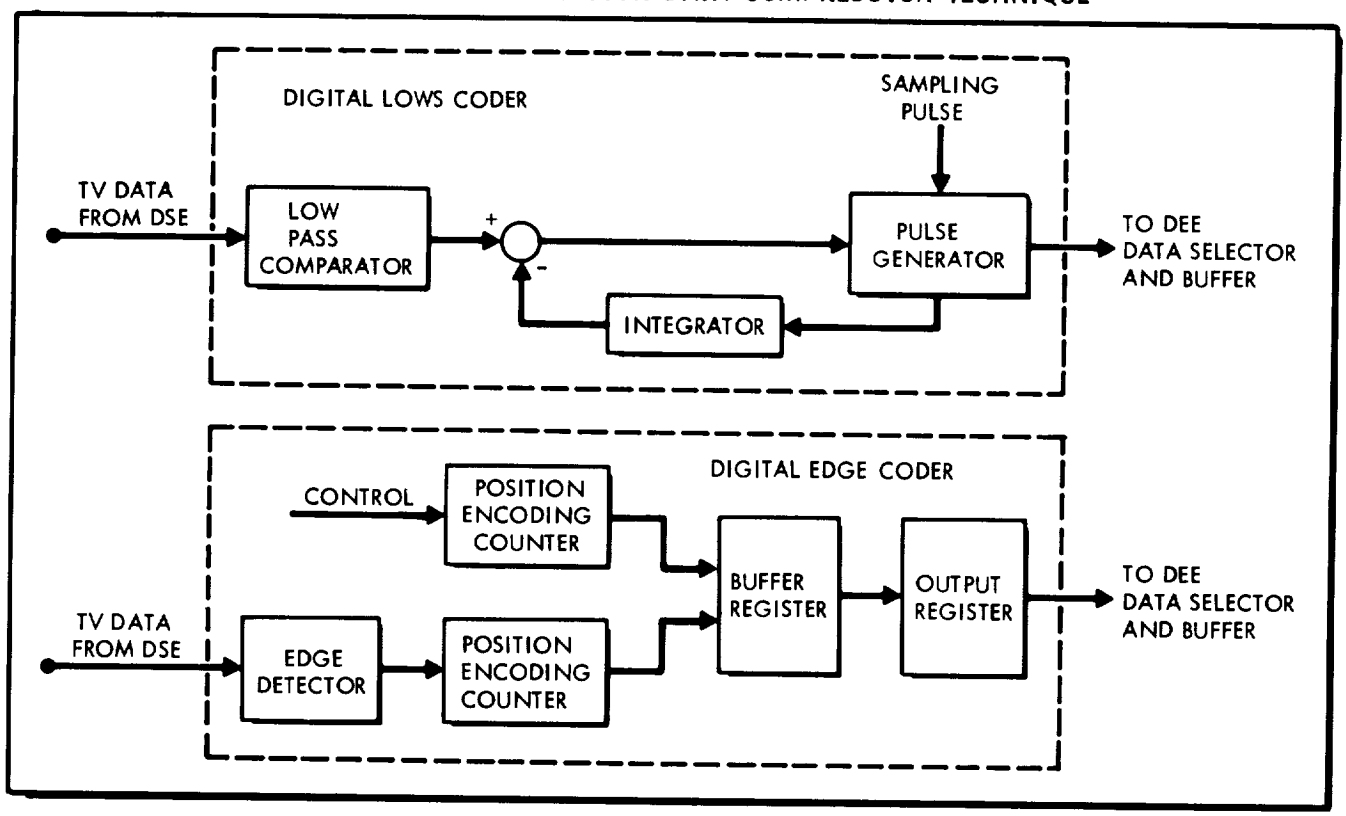

FIGURE 3.2-5

3.2.3.2 Data Storage

Storage of important data is required on a Jupiter flyby mission whenever the acquisition rate exceeds the transmission rate, whenever communications are interrupted as a result of radio interference from interplanetary disturbances or another body occludes the spacecraft from Earth, and whenever the rate of Doppler frequency change exceeds the receiver's tracking capability. Additionally, during those mission phases when the transmission rate is significantly greater than the data-gathering rate, data storage can be used to implement intermittent communications while a continuous data retrieval capability is maintained. This situation occurs during the cruise phase of all missions so that during the noncritical portions of this phase, the tracking stations and the control center can be released to perform other tasks. Mission success should not be degraded by the use of this procedure because of the long delay between the spacecraft transmission of telemetry and Earth reception of the data. This delay, more than twenty minutes at 2.5 AU, is such that real time telemetry has little value in correcting immediate spacecraft problems. Therefore, onboard diagnostic routines are required to handle these problems.

In terms of the concepts under investigation, the required data storage capacities vary from 23M bits to 300 M bits; the read-in rates vary from 37 bits per second to 150K bits per second; and the read-out rates fluctuate from 12 bits per second to 160K bits per second. Magnetic discs, magnetic core buffers, thin-film buffers, magnetic drums, and magnetic tape recorders were the devices considered for incorporation into the data management subsystem to satisfy these data storage requirements.

Standard magnetic discs are not believed to be applicable to a mission of this type because of the problem of maintaining a constant head-disc gap in the anticipated shock and vibration environment. Also, a special type of flexible mylar disc which had been developed to operate in this type environment is currently being phased out by the vendor in favor of solid-state memories. Magnetic core buffers have been used for data storage on the Vela, Pioneer, and Lunar Orbiter programs. Thin-film buffers are expected to offer size, weight, MTBF, power, and cost (mass production capability) advantages over the core buffers. Magnetic drums have been developed by several vendors in recent months to the extent that they provide significant size, weight, power, MTBF, and cost advantages over both types of buffer memories in the case of capacities greater than 10,000 bits. In current drums, there is only one moving part and it is operated on air bearings; this advance in design is responsible for the large increase in MTBF.

However, both buffers and drums are limited by their physical characteristics to storage capacities between 10^5 and 10^6 bits on missions of this type; therefore the DSE for all spacecraft concepts considered is a set of redundant magnetic tape recorders. Tape recorders which are similar to the one shown in Figure 3.2-6

DATA STORAGE ELEMENT

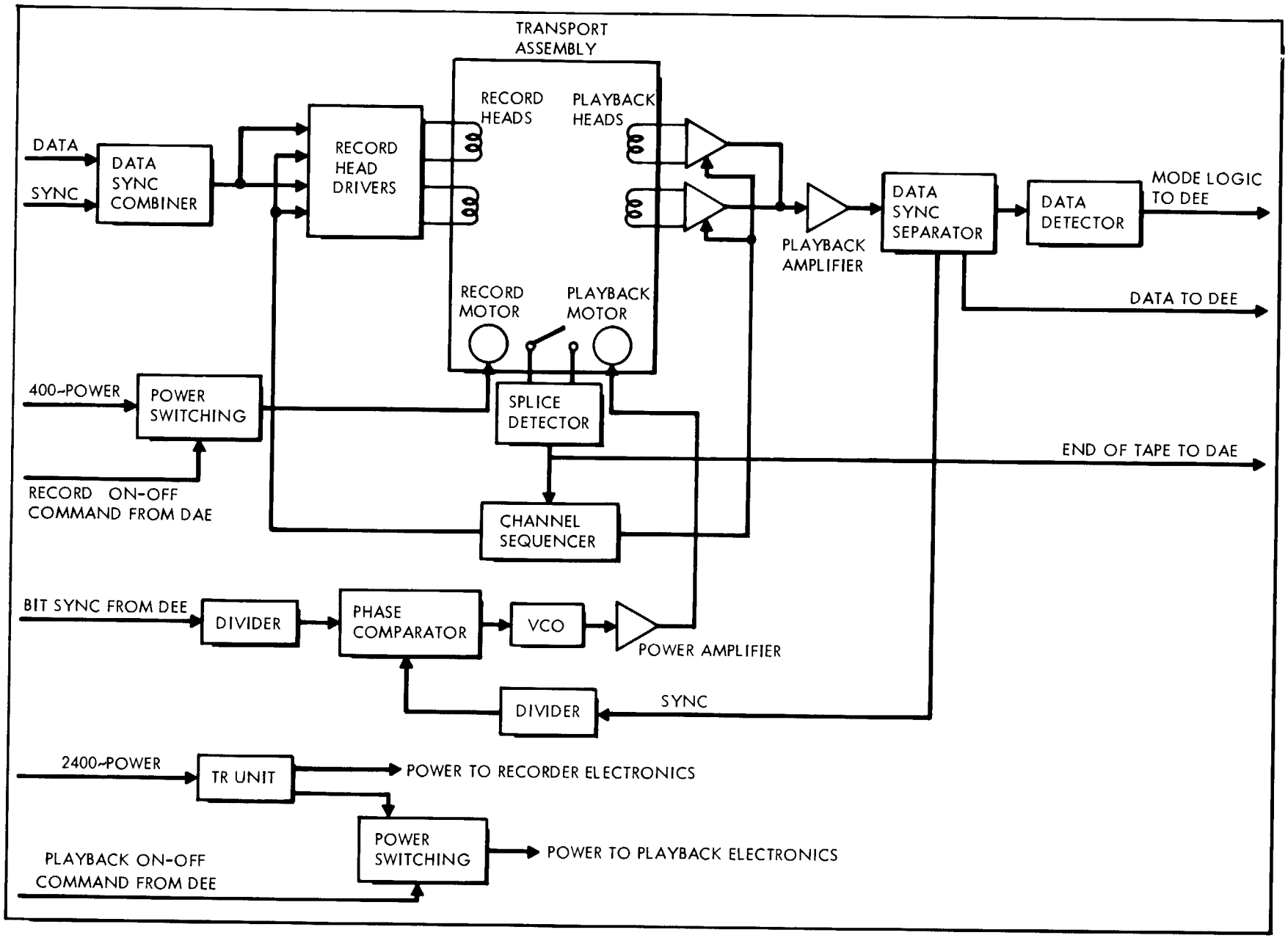

FIGURE 3.2-6

have been proved on Mariner and Tiros missions to be reliable and efficient devices for storing larger quantities of data. In the case of lower capacities, the increased reliability of buffers and drums indicates that they would be preferable to tape recorders. Even though drums seem to offer greater advantages than buffers, currently, advances in both types of devices are occurring so rapidly that this rating could well change within the next few months.

An additional reliability factor to be considered for the DSE during the encounter phase is the high magnetic fields of Jupiter. These fields, which are much stronger than those encountered near Earth, could introduce a large number of errors into the data if proper shielding is not provided. At the present time, though, it appears that satisfactory magnetic shielding can be supplied for any of the storage devices with negligible increase in size and weight.

3.2.3.3 Sychronization

A single-channel link containing both synchronization and data is believed appropriate for all of the design concepts being considered. The one-channel transmission link provides a better $[(S/T)/(N/B)]$ ratio than the two-channel link used on Mariner IV. This is true since all of the communications power can be concentrated into a single signal rather than being divided into two separate signals. A typical DEE which is used to provide four sampling rates of (1) 1/20 of the basic word time by the "100" decks, (2) 1/200 of the basic word time by the "200" decks, (3) 1/2000 of the basic word time by the "300" decks, and (4) 1/4000 of the basic word time by the "400" decks is shown in Figure 3.2-7. Data are combined with the sync code in the DEE as discussed below.

A 63-bit pseudonoise code, PN, used to supply both bit and word synchronization, is continuously produced by a pseudonoise generator. This code is modulo 2 added to the clock frequency, $2f_s$. This modulo-2 sum, PN $\oplus$ $2f_s$, is then modulo 2 added to the data, D, from the data selector and buffer, and this combination is transmitted. In order to provide for the transmission of data during prelaunch checkout and during boost, additional capability has been furnished to supply data to GSE and to the booster telemetry link.

The demodulator required on the ground to receive this telemetry data is shown in Figure 3.2-8. The following logical operations are performed by this demodulator to retrieve the data:

$$\pm \text{PN} \oplus 2f_s \oplus \text{PN}^* = \pm \text{PN} \oplus \text{PN} \oplus f_s \oplus 2f_s$$

$$= \pm f_s \angle 90^\circ$$

$$\pm f_s \angle 90^\circ \oplus f_s \angle 90^\circ = D$$

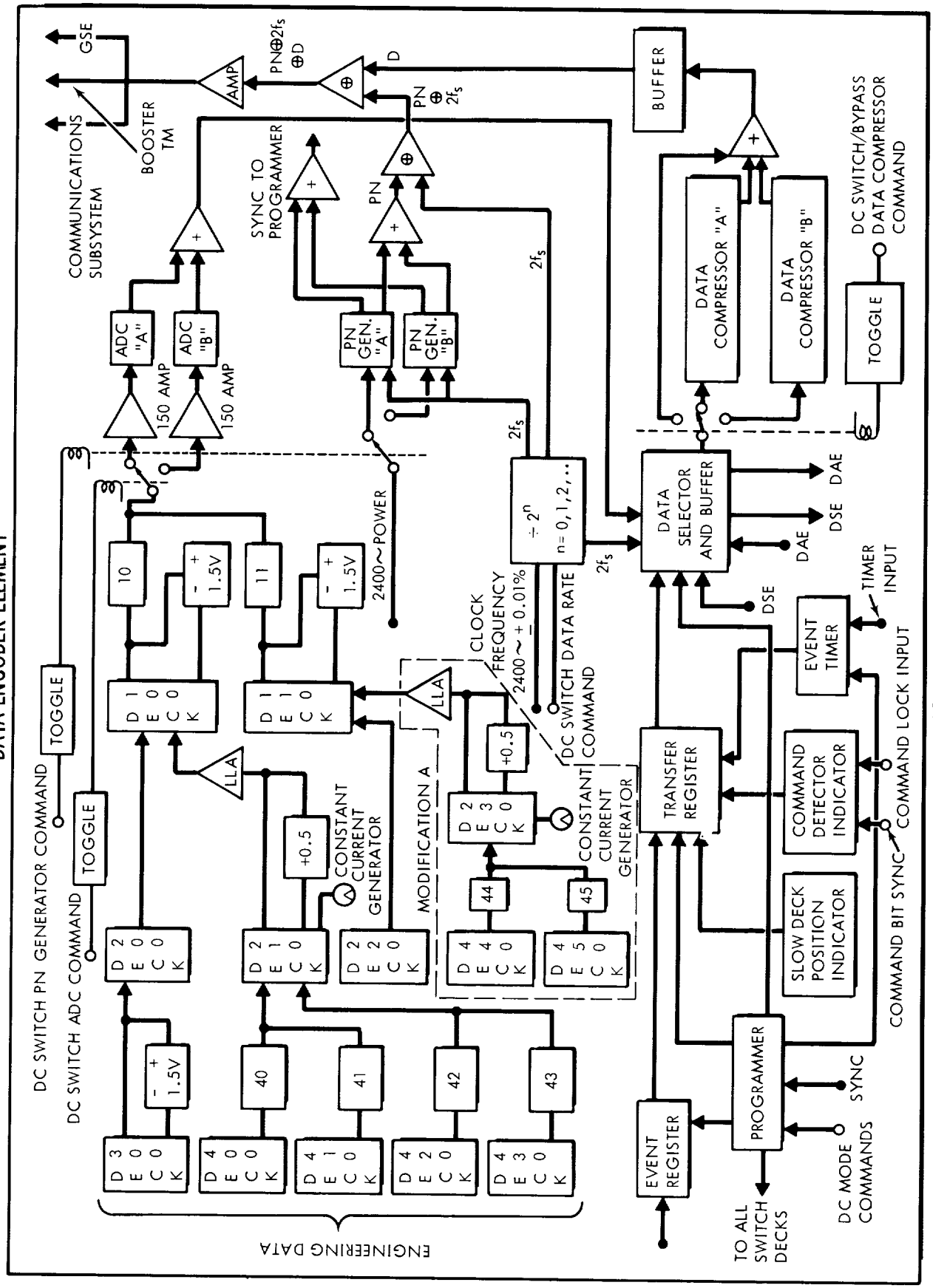
DATA ENCODER ELEMENT
COMMUNICATIONS SUBSYSTEM
BOOSTER TM
GSE
AMP
PN⊕2fs ⊕D
D
PN ⊕ 2fs
BUFFER
SYNC TO PROGRAMMER
PN
2fs
ADC "A"
ADC "B"
150 AMP
150 AMP
PN GEN. "A"
PN GEN. "B"
DATA COMPRESSOR "A"
DATA COMPRESSOR "B"
DC SWITCH/BYPASS DATA COMPRESSOR COMMAND
TOGGLE
2400~POWER
÷ 2^n n= 0, 1, 2, ..
DATA SELECTOR AND BUFFER
DAE
DSE DAE
DSE
TIMER INPUT
EVENT TIMER
CLOCK FREQUENCY 2400 ~ ± 0.01%
DC SWITCH DATA RATE COMMAND
LLA
MODIFICATION A
CONSTANT CURRENT GENERATOR
TRANSFER REGISTER
COMMAND DETECTOR INDICATOR
SLOW DECK POSITION INDICATOR
COMMAND LOCK INPUT
COMMAND BIT SYNC
DC SWITCH PN GENERATOR COMMAND
DC SWITCH ADC COMMAND
TOGGLE
CONSTANT CURRENT GENERATOR
ENGINEERING DATA
EVENT REGISTER
PROGRAMMER
SYNC
TO ALL SWITCH DECKS
DC MODE COMMANDS

FIGURE 3.2-7

GROUND TELEMETRY DEMODULATOR

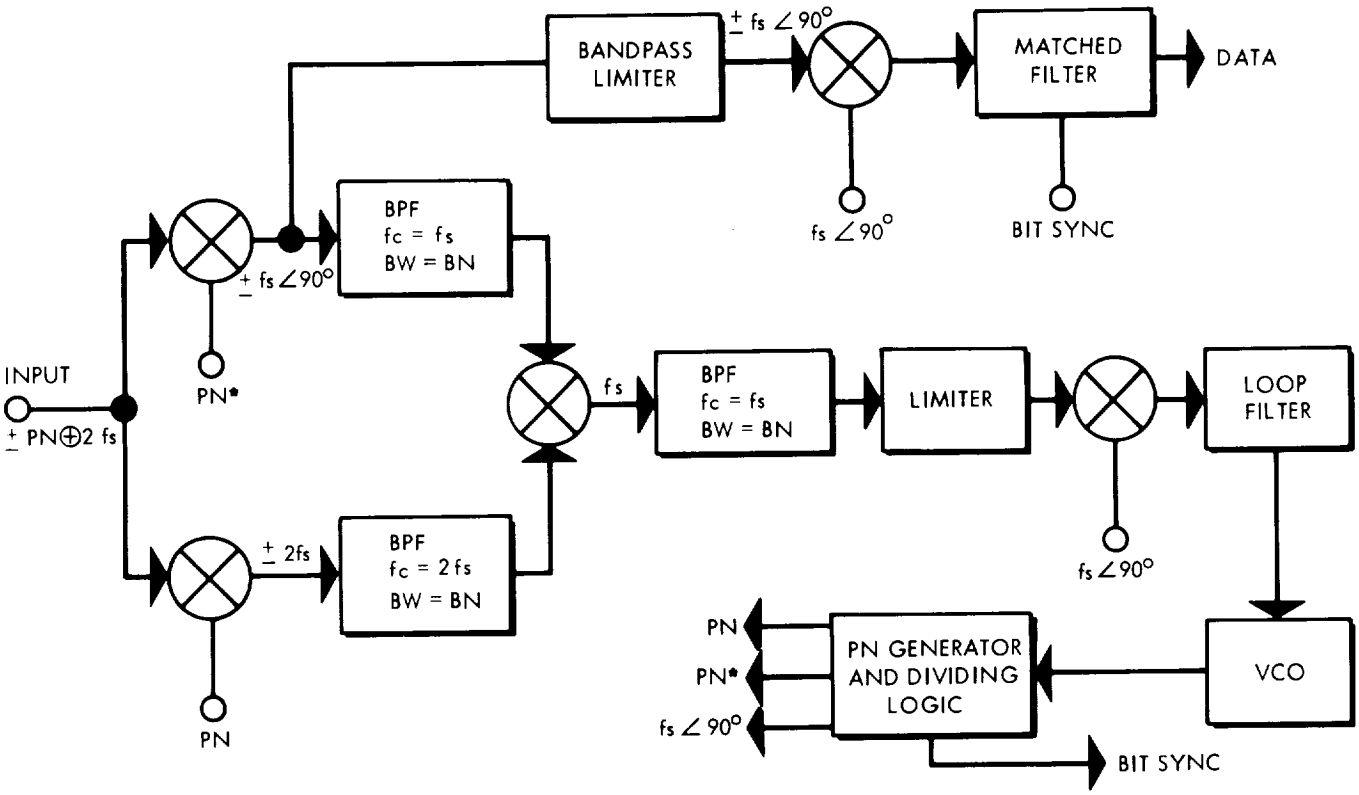

FIGURE 3.2-8

Synchronization is maintained by use of the following logical operations, which are performed by the phase-locked loop:

$$\pm \text{PN} \oplus 2f_s \oplus \text{PN}^* = \pm f_s \angle 90^\circ$$

$$\pm \text{PN} \oplus 2f_s \oplus \text{PN} = \pm 2f_s$$

$$\pm f_s \angle 90^\circ \oplus \pm 2f_s = f_s$$

$$f_s \oplus f_s \angle 90^\circ = 2f_s$$

$$2f_s \div 2 = f_s$$

$$\text{PN} \oplus f_s = \text{PN}^*$$

$$2f_s \oplus f_s = f_s \angle 90^\circ$$

A 7-bit analog-to-digital conversion is provided for engineering analog data; the conversion is accurate to one percent. The bit rates supplied in this operation are related to the clock frequency $2f_s$ by the following formula:

$$\text{Bit rate} = \frac{2f_s}{9}$$

where 9 is the number of PN bits being generated per data-word bit. This relationship permits bit rates to be changed by a simple division by two of the high-accuracy frequency sources supplied by the power subsystem (Reference 3.2-14).

3.2.3.4 Command

The only recommended modification of the Mariner IV CDDE for these spacecraft concepts is the use of a single-channel link for synchronization and command data. This link would resemble the one described earlier for telemetry transmission such that the detector of the CDDE operates similarly to the ground telemetry demodulator shown in Figure 3.2-8. The decoder that distinguishes which DC or QC has been transmitted is shown in Figure 3.2-9. The CDDE command word format is similar to that used for Mariner IV. The Mariner IV 26-bit command word is shown in Figure 3.2-10 (Reference 3.2-15).

3.2.3.5 Reliability

Reliability is enhanced through the use of flight-tested Mariner designs and by the incorporation of integrated circuits wherever possible. Redundancy is used for all elements in this subsystem and for the more critical components in each element, such as the analog-to-digital converters, PN generators, and data compressors. The capability to bypass data compression in the event of a malfunction is furnished to further increase the probability of reliable data handling. Whenever sets of redundant equipment are placed in series, separate switches, initiated by separate DC's, are provided to switch from one piece of equipment in a set to another in that same set. The various reliability analyses which were used to determine the designs for the four concepts are discussed in subsection 3.13.

3.2.4 Results

The comparison of telemetry requirements for the Jupiter and Mariner spacecraft indicates that in most instances the required measurements are either identical or very similar. Examination of the data-gathering quantities and rates related to Jupiter missions indicates that there is a definite need to provide for data storage and for the implementation of data compression techniques.

The storage of data, particularly during the critical phases of a mission (such as the encounter phase), increases the probability of obtaining reliable information. The stored data can also be used to fill in data gaps caused by interference, by receiver limitations, or by occlusion and to double check questionable data points received in real time. Whenever the rate of data acquisition exceeds the transmission rate, data storage can be used as a technique to provide a later replay of the important data at a rate compatible with the capability of the communications.

COMMAND DECODER SUBELEMENT

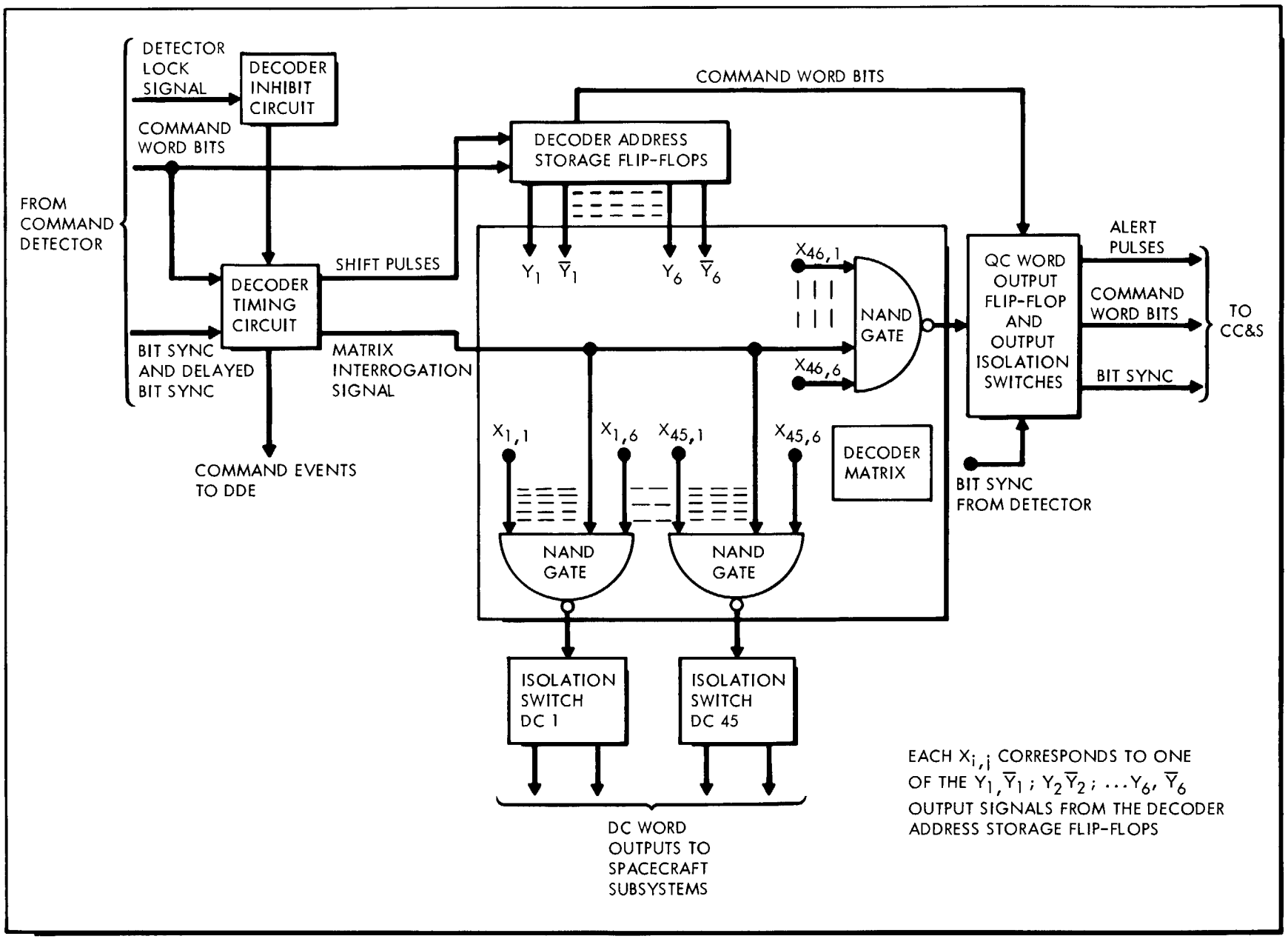

FIGURE 3.2-9

COMMAND WORD FORMAT

MARINER C COMMAND WORD FORMAT

COMMAND BIT NO.	1	2	3	4	5	6	7	8	9	10	11	12	13	14	15	16	17	18	19	20	21	22	23	24	25	26
COMMAND BIT IDENTIFICATION	COM-MAND DECODER START			COMMAND ADDRESS						ADDRESS PARITY See Note 1		BITS 12-26 HAVE NO SIGNIFICANCE IN DC'S. IN QC'S THEY FORM PART OF THE CC&S COMMAND. REFER TO QUANTITATIVE COMMAND FORMAT														
COMMAND BIT VALUE	1	1	0	VARIABLE								ZERO FOR DC'S; VARIABLE FOR QC'S														

QUANTITATIVE COMMAND (QC) FORMAT

COMMAND BIT NO.		1	2	3	4	5	6	7	8	9	10	11	12	13	14	15	16	17	18	19	20	21	22	23	24	25	26
CC&S COMMAND BIT NO.										1	2	3	4	5	6	7	8	9	10	11	12	13	14	15	16	17	18
CC&S COMMAND BIT IDENTIFICATION										CC&S ADDRESS See Note 2			Register Selector		See Note 3	TIME VALUE See Note 5											See Note 4
QC COMMAND BIT VALUES	PITCH TURN	1	1	0	0	1	1	0	0	0	1	1	1	0	ODD PARITY	VARIABLE											POLARITY
	ROLL TURN	1	1	0	0	1	1	0	0	0	0	0	0	1		VARIABLE											
	MOTOR BURN	1	1	0	0	1	1	0	0	0	1	0	1	1		VARIABLE											

1. COMMAND BIT NOS. 10 AND 11 ARE ADJUSTED TO ENSURE AGAINST SINGLE BIT ERRORS CAUSING AN INCORRECT COMMAND WORD OUTPUT.
2. COMMAND BIT NOS. 9–11 (CC&S COMMAND BIT NOS. 1–3) ARE NOT USED QUANTITATIVELY BY CC&S BUT ARE USED TO REMAIN COMPATIBLE WITH PREVIOUSLY DESIGNED HARDWARE (*MARINER R*).
3. COMMAND BIT NO. 14 (CC&S COMMAND BIT NO. 6) IS ADJUSTED IN QC'S TO GIVE AN ODD NUMBER OF *ONE* BITS IN COMMAND BIT NOS. 9–26 (CC&S BIT NOS. 1–18).
4. COMMAND BIT NO. 26 (CC&S COMMAND BIT NO. 18) MUST BE A *ONE* TO PRODUCE A CW (POSITIVE) SPACECRAFT ROTATION ABOUT THE SPECIFIED SPACECRAFT AXIS. A *ZERO* IN THIS BIT POSITION WILL RESULT IN A CCW (NEGATIVE) SPACECRAFT ROTATION ABOUT THE SPECIFIED SPACECRAFT AXIS. POLARITY BIT FOR MOTOR BURN COMMAND IS ALWAYS *ONE*.
5. COMMAND BIT NOS. 15–25 (CC&S COMMAND BIT NOS. 7–17) ARE A PSEUDO-BINARY CODE REPRESENTATION OF THE TURN OR MOTOR BURN DURATION.

FIGURE 3.2-10

Drums and buffers can be used to store small quantities of data (less than 10^5 to 10^6 bits) while magnetic tape recorders have proved to be the most efficient method of providing storage for larger quantities of data. In order to reduce power, weight, and size requirements, use of a television camera with a scan-converter tube is recommended. Through the use of a scan-converter tube, the data rate can be reduced to the extent that a lower-frequency recorder can be used to store television data instead of a larger, heavier video tape recorder which requires considerably more power. Intermittent communications are recommended as a good method of reducing mission support requirements.

Data compression is used to provide a method of obtaining the most efficient use of communications capability, and such compression will result in a reduction in ground processing time and cost. Because of the low transmission bit rates available on deep space probes, a choice of two undesirable alternatives usually develops: either data must be sampled at less than the optimum rate, or data must be stored and replayed later at a reduced bit rate. The data replay causes a loss of real time data during the playback interval. To overcome the undesirable effects of the alternative choices, data compression can be used to eliminate or reduce the difference between the desired and the available transmission bit rates. The advantage of greatly increased efficiency of communications provided by telemetry data compression is considered much more significant than its one major disadvantage:

the fact that the effect of an error in a received data point is amplified by the compression ratio. To reduce the effects of this undesirable feature, uncompressed data blocks can be transmitted at specified intervals or whenever data is obviously incorrect.

It was determined that a considerable number of integrated circuits can be incorporated into the data management subsystem. As a result, it is anticipated that reliability, flexibility, and efficiency can be greatly improved and that power, weight, and size requirements can be significantly reduced from those specified for current equipments without large-scale development.

3.2.5 Conclusions

Because of the extreme importance placed on reliability, it is recommended that the third concept discussed in paragraph 3.2.2 be implemented for all Jupiter spacecraft except the most advanced one. The probability of a successful mission will be greatly enhanced by the use of Mariner IV technology which has been thoroughly flight tested on a successful mission. Concentrated development of the Mariner IV technology is then recommended in three areas; at the present time, there are indications that these three areas have the most potential for increasing the value of a mission: (1) the maximum incorporation of integrated circuits, (2) data storage improvements, and (3) the implementation of data compression techniques.

3.2.6 References

3.2-1 Bryan, J. A. and Stumpe, J. W., "The Data Management Analyzer, A Laboratory Tool for Data Compression Analysis", 1965 PGAES Symposium Record, Miami Beach, Florida, November 2-4, 1965, pp. 11-A1 through 11-A13.

3.2-2 Morrison, W. L., Hogan, W. P., and Pentz, R. M., "Application of Data Compression to Flight Data Processing", Western Electronic Show and Convention Record, Los Angeles, California, August 25-28, 1964, Section 19.3.

3.2-3 Medlin, J. E., "Sampled Data Prediction for Telemetry Bandwidth Compression", Western Electronic Show and Convention Record, Los Angeles, California, August 25-28, 1964, Section 19.1.

3.2-4 JPL Technical Report No. 32-510, Jet Propulsion Laboratory, Pasadena, California, October 1, 1963.

3.2-5 JPL Technical Report No. 32-718, Jet Propulsion Laboratory, Pasadena, California, June 1, 1965.

3.2-6 JPL Technical Report No. 32-772, Jet Propulsion Laboratory, Pasadena, California, December 1, 1965.

3.2-7 Pratt, W. K., "Stop-Scan Edge Detection System for Interplanetary Television Transmission", 1962 PGSET Symposium Record, Miami Beach, Florida, October 2-4, 1962, Section 4.3.

3.2-8 Marggraff, W. A. and Klawa, R. F., Studies Related to Multi-Spectral Correlation: Error and Application Analyses of Satellite Television Camera Systems, General Dynamics/Convair, San Diego, California, December 15, 1965, pp. 20-31.

3.2-9 Fano, R. M., Transmission of Information, The MIT Press and John Wiley & Sons, Inc., New York, 1961.

3.2-10 Weber, D. R. and Wynhoff, F. J., "The Concept of Self-Adaptive Data Compression", 1962 PGSET Symposium Record, Miami Beach, Florida, October 2-4, 1962, Section 4.1.

3.2-11 Winkler, M. R., "Pictorial Transmission with HIDM" 1965 IEEE International Convention Record, New York, New York, March 22-26, 1965, part 1, pp. 285-291.

3.2-12 Bisignani, W. T., Richards, G. P., and Whelan, J. W., "The Improved Gray Scale and the Coarse-Fine PCM Systems, Two New Digital TV Bandwidth Reduction Techniques", Proceedings of the IEEE, New York, New York, March 1966, pp. 376-390.

3.2-13 Roberts, L. G., "Picture Coding Using Pseudo-Random Noise", IRE Transactions on Information Theory, New York, New York, February 1962, pp. 145-154.

3.2-14 JPL Technical Report No. 32-495, Jet Propulsion Laboratory, Pasadena, California, January 15, 1965, pp. 6-30.

3.2-15 JPL Space Programs Summary No. 37-29, Vol. II, Jet Propulsion Laboratory, Pasadena, California, September 30, 1964, pp. 37-42.

3.3 SPACECRAFT CONTROL

The spacecraft functions of interest in this section are (1) state estimation, (2) attitude determination, (3) prediction of terminal errors and steering, and (4) timing and sequencing of other spacecraft operations. These functions and the equipment required to perform them are referred to as "spacecraft control." Generally speaking, the implementation of control functions can be divided up many ways between systems on board the spacecraft and Earth-based tracking and data-processing facilities. It is possible to implement the entire control operation in a self-contained system on board the vehicle, or it is possible to perform a large part of the control from an Earth-based facility. Certain of the control functions, for example, the attitude sensing and vehicle maneuvering associated with guidance corrections or steering operations, are not suitable for any but "on board" control.

The choice of a control system for Jupiter flyby missions is based on a careful examination of (1) the operation and performance requirements, (2) the complexity and cost attendant to particular system concepts, and (3) the possibilities of using previously developed concepts such as those from the Mariner project.

Using these guidelines, a single basic control concept has been worked out for Jupiter flyby missions. This concept is characterized by several pertinent features. A group of optical sensors on board the vehicle is used to provide attitude reference. Earth-based facilities are used to determine the trajectory and to compute the required guidance corrections. A central computer and sequencer (CC&S) on the spacecraft provides master timing for all spacecraft systems and "translates" guidance commands into vehicle attitude changes and control signals for input to the midcourse propulsion system. The CC&S may also provide commands which are initiated from the Earth or an internally generated timing signal to an antenna positioning mechanism.

Variations in the detailed design of the spacecraft control subsystem are present in each of the spacecraft design concepts. Of particular interest are the control system variations which provide self-contained, terminal navigation and guidance. This mode of operation yields the best terminal accuracy but at a significant cost in terms of increased system complexity. Such a mode of operation is deemed appropriate for a spacecraft to achieve maximum scientific capability, because the meaningful

accomplishments of the scientific objectives is dependent on precise guidance and navigation.

Another variation in possible design concepts arises from the requirement for accurate orientation of a communications antenna. One concept is to steer the antenna mechanically while keeping the orientation of the spacecraft axes fixed in a particular inertial frame. The alternative is to fix the antenna to the spacecraft while changing the orientation of the spacecraft periodically. In both cases, the spacecraft control system must furnish angular control either to the antenna positioning device or the primary reference sensors. The steerable antenna approach has been adopted for the three-axis stabilized design concepts included in this study. This approach was selected because of (1) simplicity of on-board sensor control afforded by the steerable antenna and (2) the straightforward manner in which the antenna can be periodically moved. Additional discussion of this approach and the fixed-antenna approach will be found in subsection 3.3.3.

3.3.1 Spacecraft Control Operations

The functions of the spacecraft control system vary among the several design concepts. In order to illustrate the development of these concepts, the full list of control operations will be discussed individually with explanations of the traditional division of these functions between ground-based and on-board systems. The control operations are grouped into four functional categories: (1) attitude determination, (2) navigation, (3) guidance, and (4) timing and sequencing for other vehicle systems.

3.3.1.1 Attitude Determination

Expressed in the most basic terms, attitude determination is the process which permits the orientation of the vehicle body axes to be known in relation to or as a function of unit vectors which define some primary coordinate system. This primary coordinate system may be either the heliocentric inertial frame defined by the ecliptic and vernal equinox, some local vertical planetocentric frame, or some other convenient frame. The choice of a primary frame is based on the set of observables used in establishing the relationship between the primary frame and the vehicle axes. During the cruise phase of Jupiter missions, the trajectory is essentially heliocentric, and the convenient observables are the sun, stars, and, perhaps, planets; thus, the primary frame is the heliocentric inertial one, because the observables are known in that system. When the vehicle is in the near field of a planet, and its motion is essentially planetocentric, a planet local vertical coordinate frame offers some

attractive features from the standpoint of attitude control and orientation of scientific sensors. On the other hand, the change-over from the Sun to Jupiter as the primary attitude reference and the use of a local vertical orientation complicates the very important function of Earth to spacecraft communications. For this reason, the Sun-star system is the primary coordinate system considered for all phases of a Jupiter flyby mission. At times of planetary occultation of either the Sun or star, the spacecraft gyros are used for attitude control.

In the practical accomplishment of the attitude determination functions, it is not necessary that the transformation matrix relating the vehicle axes to the primary system be determined explicitly on board the spacecraft. The spacecraft can hold certain angular relationships with respect to the observables. Then, using the spacecraft position, the attitude transformation is explicitly determined at the Earth-based facility. Naturally, if the control philosophy calls for a self-contained operation, the entire attitude determination process can be mechanized in an on-board computer.

Once the attitude is determined, the vehicle can be accurately oriented for guidance maneuvers and other requirements. Also, pointing angles for antennas and other sensors can be determined.

3.3.1.2 Navigation

The control functions which come under the heading "navigation" have to do with obtaining the best estimate of the spacecraft trajectory. This best estimate is usually evolved from successive estimates of position and velocity. Over a period of time, this successive state estimation permits a definitive trajectory to be determined which is the basis of subsequent guidance maneuvers. Navigation, as used herein, implies only state estimation and must be distinguished from the broader usage of some authors in which navigation includes guidance or steering maneuvers as well as state estimation.

The navigation function can be accomplished from the Earth by the use of radar tracking, or it can be performed on board the spacecraft by the use of some type of angular measurements. In either case, the actual navigation process will probably involve the use of statistical filter methods. In this technique, navigational measurements are compared to computed values which correspond to the expected state, and these residuals are optimally weighted to derive an estimated state. Details of the navigation processes are contained in subsection 3.4.

3.3.1.3 Guidance

As stated previously, the objective of the navigation function is to determine as accurately as possible the spacecraft position and velocity, either for comparison with some design point value or to predict the state at some future time. In both cases, the information gained is used to compute a guidance correction. The guidance function includes those operations performed on the estimated vehicle position and velocity which lead to the determination of a required maneuver as well as those operations concerned with the control of the correction maneuver itself.

The vernier correction, typically performed sometime during the first 10 days of the mission, is designed to correct for velocity errors in the injection maneuver. Thus, the estimated velocity is compared to the nominal or design point velocity at this time, and the vector difference becomes the required correction. This required change in velocity is resolved into a spacecraft attitude maneuver and a required number of accelerometer pulses.

Somewhat different considerations enter into the synthesis of a terminal guidance maneuver. Computation of the correction depends on what component of the terminal error is to be corrected. Generally, this maneuver is designed to null some part of the terminal position error. The terminal error may consist of any or all of the following: (1) position components, (2) velocity components, and (3) time of arrival. A single impulsive change in velocity can correct only three components of the total error vector. Thus, three-dimensional position or velocity terminal errors are to be corrected, a midcourse velocity change is required for each. In practice, the terminal position error is expressed as a two-dimensional vector in a plane perpendicular to the approach hyperbola. This two-component position error alone, or the position error and the error in time of arrival, can be nulled with a single steering maneuver. Synthesis of the terminal correction is discussed further in subsection 3.4.

Having determined the required maneuver, the control system must implement the indicated velocity change. The vector velocity change expressed in the primary coordinate frame must be related to the vehicle body axes so that the vehicle can be aligned with this required velocity vector. The magnitude of the correction is monitored by an accelerometer. During the motor burn period, feedback from a system of gyros provides control to vanes in the rocket exhaust to maintain proper alignment.

3.3.1.4 Master Timing and Sequencing

In addition to all of the control operations identified or implied in the above discussions, certain timing and sequencing functions are also the responsibility of the spacecraft control system. A master frequency source in the control system provides the primary timing signal. Dividing circuits and other logic circuits are then used to generate signals for event sequencing throughout the spacecraft.

3.3.2 Design of the Central Computer and Sequencer

Control of the spacecraft systems is accomplished by the combined operation of the on-board central computer and sequencer (CC&S) and Earth-based facilities connected to the spacecraft through a radio command link. The CC&S furnishes the event signals required for automatic control and serves as a processor and sequencer for command data. The CC&S concepts considered are nearly identical with the exception of one which utilizes a computer in the more familiar sense for on-board navigation, guidance, and sensor control. It is felt that the self-contained system approach is justified only on vehicles with very sophisticated scientific payloads. In the other concepts studies, all sequencing of events is done through a simple timer which is a part of the CC&S. Events sequenced in this manner include the various steps involved with attitude acquisition or maneuvers, the steps involved with the encounter sequence, cycling the cruise science, and control of the high gain antenna. A block diagram of the basic CC&S concept is shown in Figure 3.3-1.

In the CC&S, command data and sync signals from the communications subsystem flow through the CC&S data encoder into the command data registers and sign flip-flops. An address matrix and encoder logic direct the serial data into the proper register or sign flip-flops. When the correct data have been stored, the maneuver sequence can begin. When the communication subsystem sends a maneuver-start pulse, the gyro power is turned on in the attitude control subsystem by the CC&S and the fine control mode is initiated. This consists of rate and angular control to the highest precision practical with the sensors concerned. After a certain interval, the actual maneuver begins with a roll turn sequence in which a one pulse per second pulse train drives the roll register as counter. During this same time, the control system commands a roll at some fixed rate. When the register overflows, the roll is stopped. The pitch turn and motor burn registers are pulsed in sequence in a similar manner. The fine limit cycle mode of attitude control is intended to provide a precision reference point from which to begin the maneuver. When the maneuver begins, the attitude system is decoupled from the optical sensors and is

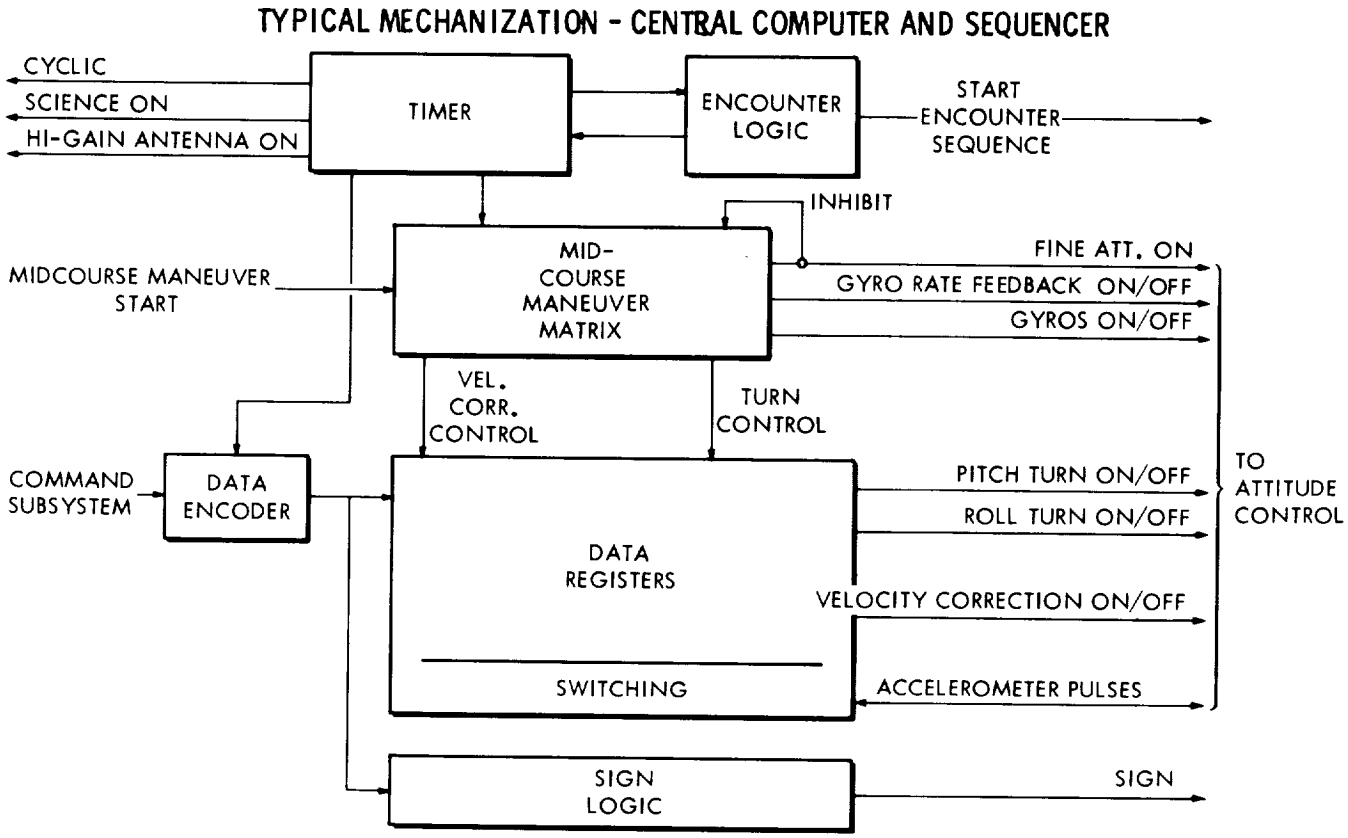

FIGURE 3.3-1

controlled by gyros and timed turns. After the velocity correction, the spacecraft is maneuvered back to the original orientation and the coarse limit cycle control mode is reestablished. When the cruise mode has been acquired, the inertial sensors are turned off.

The CC&S configuration planned for the self-contained system includes a digital computer for on board sensor control, terminal navigation, and guidance computation. These functions are additions to the master timing and sequencing functions which are required in all spacecraft configurations. The computer will determine a terminal steering correction based upon on-board determination of the deviation between the actual and the design point trajectories. The state estimation function required for the above is based on angular measurements made and processed on board the spacecraft. These navigational measurements are made with respect to the target planet and a suitable set of stars. Pointing control of the required sensors is based on the spacecraft attitude and expected position and the coordinates of the observables in the primary reference frame. In addition, the computer may be utilized to perform certain computations for the science payload, malfunction isolation, switching, data compression, and computation of antenna pointing angles.

3.3.3 Design of the Attitude Control Electronics

The various design concepts of the attitude control electronics exhibit basic similarities. The attitude electronics utilize signals from the Sun and star sensors to furnish attitude control inputs to a cold gas system or reaction wheels. Planet sensors are used to verify star acquisition and to provide auxiliary attitude information during certain phases of the flyby. There is a self-contained capability for acquisition of Sun and star references after an attitude acquisition command or after some inadvertent loss of the references. Turning rate signals are supplied by body-mounted gyros for rate control during timed turns, during the search sequences. Control signals for the subsystem originate from the central computer and sequencer. The basic attitude control electronics system concept is illustrated in Figure 3.3-2.

A signal from the CC&S timer initially starts the attitude acquisition sequence by turning on power to the attitude control electronics and the sensors. The search logic, located in the attitude control electronics, is designed so that star search begins only after Sun and Canopus acquisitions are checked by the Earth or Jupiter sensors. In each concept considered, there is also a roll override capability that can be activated through the command subsystem. The roll override signal is used for initiating another star search sequence. The CC&S may break the attitude acquisition sequence and restart the search sequence if required.

The gyros provide rate feedback for limiting turn rates during the search and maneuver sequences. Turns of any kind are accomplished by pulsing the gas jets (or utilizing reaction wheels). The attitude control electronics contain switching and compensation amplifiers for control of the gas jets. These amplifiers complete the turn control loop (amplifier output, gas jets, gyro rate feedback to amplifier). In the event of gyro failure, the control system can, on command, produce turns of a known rate so that open loop control is possible.

The attitude control electronics contain a turn command generator and logic for the maneuver mode. The turn command generator is a calibrated constant current source with two outputs, positive and negative. The turn command logic is driven by the CC&S so that the correct polarity current from this generator is switched to the appropriate gyro. The gyro is precessed at the calibrated rate. The control system seeks to null out movement between the gyro and the spacecraft. Therefore the gas jets pulse to turn the spacecraft so that there is no movement between the precessed gyro and the spacecraft. The calibrated turn continued until the calibrated current precessing the gyro is turned off.

TYPICAL ATTITUDE CONTROL ELECTRONICS

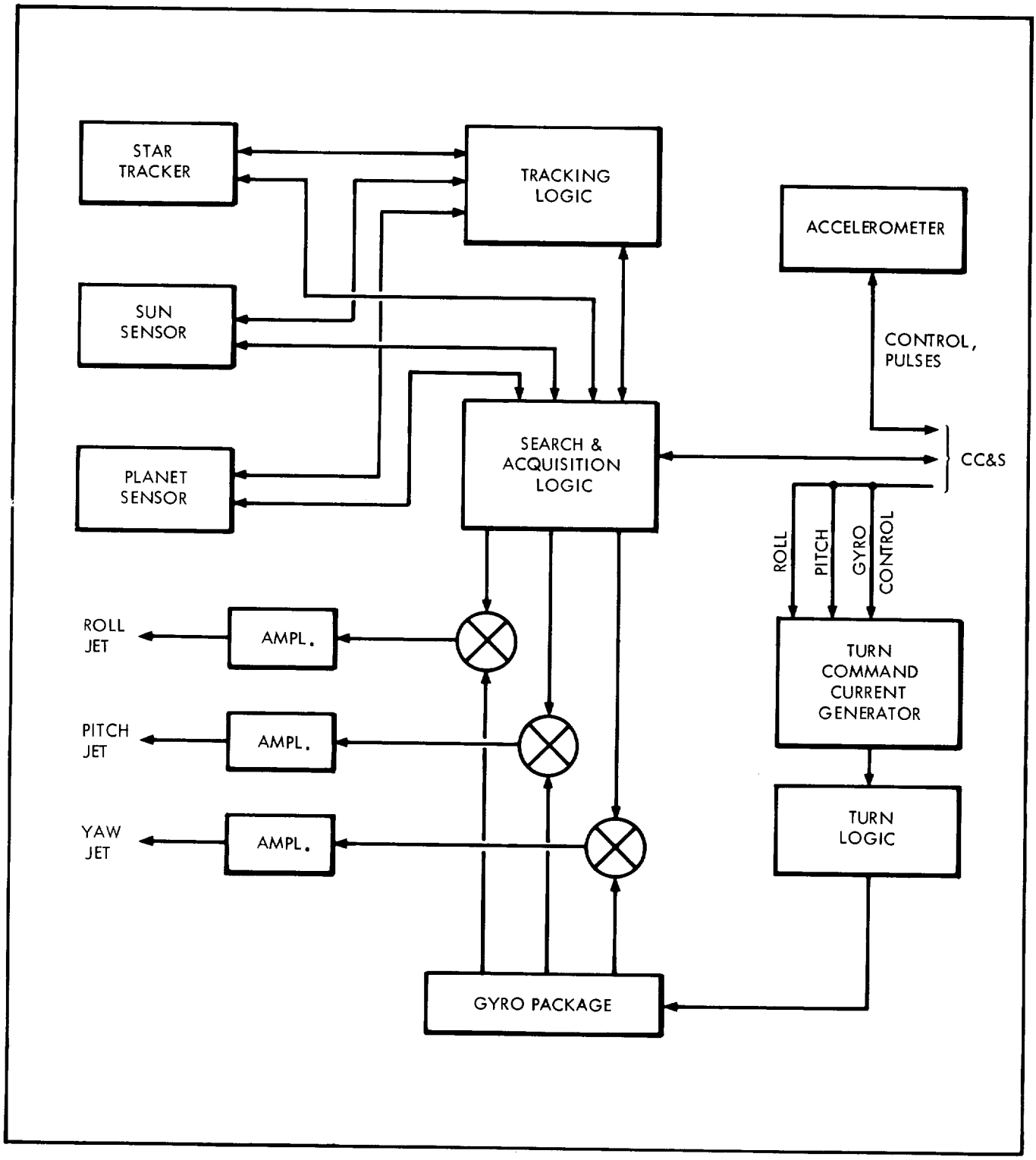

FIGURE 3.3-2

When the spacecraft is turned by the gas jets, attitude reference is lost. Rate feedback is used in the axes which are not being turned by command to prevent undesired spacecraft turning rates to build up during the maneuver. The search sequence is begun by the attitude control electronics each time a motor burn stop signal is received from the CC&S.

The fundamental concern of the attitude control system is to provide the necessary stability and proper orientation so that the primary function of scientific data gathering is enchanced. This responsibility includes concern for antenna pointing so that two way communications are maintained throughout the mission. One method of accomplishing this is to maintain a Sun pointing attitude during the cruise and encounter phases, and to require the high gain antenna be movable with respect to the spacecraft. The motion of the antenna is controllable by the CC&S. This allows the use of a very reliable attitude control logic which is entirely self-contained on board the spacecraft. Pointing calculations required to direct the antenna are done at Earth-based facilities, and commands are periodically relayed to the spacecraft to step the antenna to the desired position.

A second possibility for antenna pointing is to maintain the antenna fixed with respect to the spacecraft and to change the spacecraft axes orientation periodically in order to keep the antenna directed toward Earth. This can be done with certain modifications to the attitude sensors which permit the vehicle to be maneuvered with respect to the lines-of-sight connecting the spacecraft and the attitude references. In order to do this, the sensors must be pointable or must have wide enough fields of view to accommodate this quite severe angular motion. In any case, some computation is involved in determining either the sensor pointing angles or the bias signals which are required to offset the objectives in the sensor field of view. This computation can be done on Earth, as with the antenna pointing computations, and subsequently transmitted to the spacecraft. The steerable antenna approach is recommended because of the greater simplicity in the attitude sensor control logic.

3.3.4 Theory of Attitude Determination

As stated above, the process of attitude determination amounts to defining the relationship between the spacecraft principal axes and some primary coordinate frame. Usually the coordinates of some set of objects (stars, planets, etc.) are known in primary reference frame: thus, when the spacecraft attitude is determined, the directions to these objects can be reduced to a pair of angles at the spacecraft. In order to determine attitude, it is necessary to view

certain of these objects having known coordinates and relate unit vectors along these lines of sight to both the primary axis system and the vehicle axis system.

A single method of determining vehicle attitude in heliocentric space will be demonstrated in the following paragraphs. The primary frame in this case is a nonrotating one, centered at the Sun, and defined by the ecliptic and vernal equinox. With the vehicle's heliocentric position and the direction cosines of a single star known (see Figure 3.3-3), sensors on board the vehicle then must view these two objects and record their azimuth and elevation (as measured with respect to the vehicle axes). Next, unit vectors $\hat{r}$ in the direction of the sun and $\hat{s}$ in the direction of the star are defined. The star and Sun azimuths and elevations are denoted by A_s, E_s, A_r, E_r. The primary frame is defined by unit vectors $\hat{\alpha}_1$, $\hat{\alpha}_2$, and $\hat{\alpha}_3$. Assuming a vehicle position of x, y, z and star direction cosines of β_1, β_2, and β_3, then,

$$\hat{r} = -\frac{x}{R}\hat{i} - \frac{y}{R}\hat{j} - \frac{z}{R}\hat{k} \qquad R = \sqrt{x^2 + y^2 + z^2}$$

$$\hat{s} = \beta_1\hat{i} + \beta_2\hat{j} + \beta_3\hat{k}$$

Also,

$$\hat{r} = \ell_1\hat{\alpha}_1 + \ell_2\hat{\alpha}_2 + \ell_3\hat{\alpha}_3$$

$$\hat{s} = m_1\hat{\alpha}_1 + m_2\hat{\alpha}_2 + m_3\hat{\alpha}_3$$

where

$$\ell_1 = \cos E_r \cos A_r \qquad m_1 = \cos E_s \cos A_s$$

$$\ell_2 = \cos E_r \sin A_r \qquad m_2 = \cos E_s \sin A_s$$

$$\ell_3 = \sin E_r \qquad m_3 = \sin E_s$$

Next, $\hat{\rho}$ is defined as the unit vector obtained from the cross product of $\hat{r}$ and $\hat{s}$. Then,

$$\begin{vmatrix}\hat{r}\\ \hat{s}\\ \hat{\rho}\end{vmatrix} = M \begin{vmatrix}\hat{i}\\ \hat{j}\\ \hat{k}\end{vmatrix} \quad \text{or} \quad \begin{vmatrix}\hat{r}\\ \hat{s}\\ \hat{\rho}\end{vmatrix} = N \begin{vmatrix}\hat{\alpha}_1\\ \hat{\alpha}_2\\ \hat{\alpha}_3\end{vmatrix}$$

$$M \begin{vmatrix}\hat{i}\\ \hat{j}\\ \hat{k}\end{vmatrix} = N \begin{vmatrix}\hat{\alpha}_1\\ \hat{\alpha}_2\\ \hat{\alpha}_3\end{vmatrix} \quad \therefore \quad \begin{vmatrix}\hat{\alpha}_1\\ \hat{\alpha}_2\\ \hat{\alpha}_3\end{vmatrix} = N^{-1}M \begin{vmatrix}\hat{i}\\ \hat{j}\\ \hat{k}\end{vmatrix}$$

DETERMINATION OF SPACECRAFT HELIOCENTRIC ATTITUDE

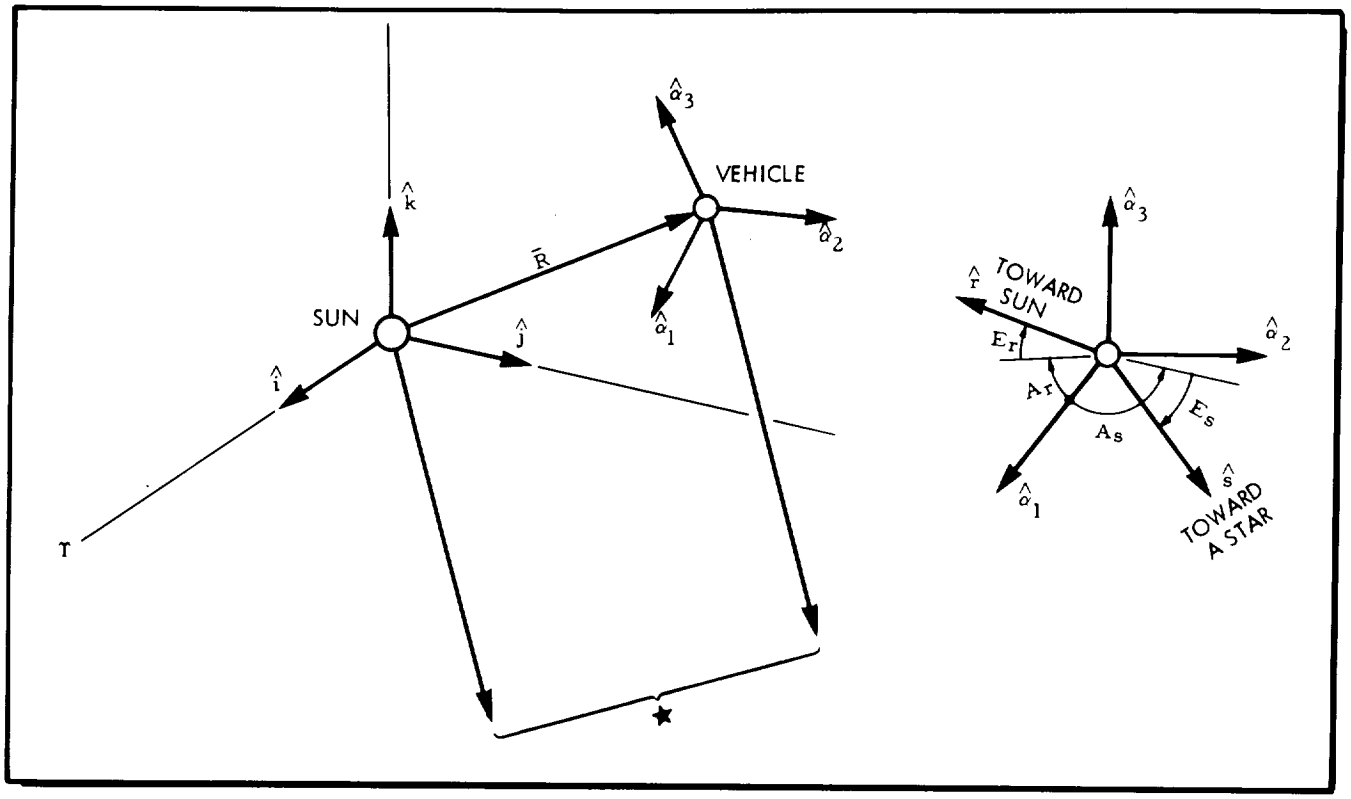

FIGURE 3.3-3

The transformation $C = N^{-1}M$ permits any vector given in the primary coordinate frame to be written as a vector in the frame $(\hat{a}_1, \hat{a}_2, \hat{a}_3)$. The angles this vector make with the spacecraft axes are immediately obtainable.

Except in the case of system concepts involving a fairly high level of on-board computation, the process described above would not be carried out on board the vehicle. These calculations would be performed at an Earth-based facility using the vehicle position and the knowledge that the Sun sensor and star tracker form certain angles with respect to the body axes.

The role of the control system on board the spacecraft is then to ensure that the sensor/spacecraft geometry remains fixed or is measured and relayed back to Earth as it changes. In carrying out this function, the attitude control subsystem comes into play. As the spacecraft drifts in attitude, error signals are produced in the sensors used to track the Sun and a star. These error signals are used by the attitude control system to counteract the vehicle motion and to keep the attitude within some allowable tolerance or dead band.

When it becomes necessary to reorient the vehicle (for example, prior to the vernier correction), commands are sent to the vehicle giving the duration of turns required (at fixed angular rates) to achieve the orientation. Rate sensing with body-mounted gyroscopes is used in the control system to accurately maintain the specified vehicle angular velocities. An alternate mechanization would involve commanding the angular amount of each turn required. In this case, the gyro rate signals are integrated, and the maneuver is terminated when the required total angle is achieved.

3.4 NAVIGATION AND GUIDANCE

3.4.1 The Guidance Requirement

In the years since the first artificial Earth satellites were orbited, the subject of space vehicle navigation and guidance has been the object of increasing amounts of research and development. The "state-of-the-art" in control system theory and technology can provide very accurate and sophisticated navigation and guidance system mechanizations. As has been mentioned before, navigation is concerned with determining the position and velocity of the vehicle so that the guidance function may be carried out more effectively. The guidance function is concerned with making corrections to the vehicle trajectory so that desired end conditions are met.

In the case of interplanetary missions between Earth and Jupiter, these functions are required to insure a reasonable probability of mission success. Starting with the fact that a satisfactory nominal trajectory has been chosen for the mission, the guidance functions begin during the launch and injection maneuvers. The booster control system attempts to place the space vehicle on the chosen trajectory. The deviation from the chosen trajectory near the target planet is largely dependent on errors in velocity near the departure planet. The degree of sensitivity of the terminal position to the initial velocity is dependent on the chosen trajectory, but for the typical Earth-Jupiter trajectories under consideration, this sensitivity is approximately 4000 km per 0.1 m/sec. Using figures of this type and the expected velocity dispersion at the end of the injection process, the RMS position error at the target is on the order of 5 to 6 Jupiter radii. This means that without any guidance correction after the injection maneuver, an aim point 10 to 12 Jupiter radii from the target must be chosen to give a 98 percent probability of not impacting the planet. Further, only very simple or crude experiments can be planned because of the large uncertainty in periapsis distance.

If a vernier correction is used to null the velocity error at a particular point early in the flight, an improvement of close to two orders of magnitude can be realized. If the allowable terminal error is less than 4000 km (one sigma), then the use of a second guidance correction later in the mission is indicated. To design for a second midcourse or terminal correction probably cannot be justified in view of the relatively simple scientific payloads under study for the early Jupiter flyby missions. To design for a second correction is to indicate that, in general, a higher terminal precision is required and/or the payload is important enough to warrant designing for an event having a low probability of occurrence. This event, that the effect of all the mission uncertainties will produce a terminal error large enough to negate the scientific objective, could occur if the vernier correction should be badly in error or if some astrophysical phenomena should produce an unexpected effect on the vehicle trajectory.

Navigation prior to the vernier correction is accomplished through earth-based tracking and orbit determination. Terminal navigation can be done in the same way, however, with understandably larger errors. The use of direct sighting on the target from the vehicle itself offers a means for improving the terminal navigation process.

3.4.2 Performance Analysis

The performance of the booster system is given in terms of a figure of merit (FOM) which amounts to the RMS velocity error or the square root of the expected quadratic velocity error. This number is valid for a period of time (~ 2 weeks) early in the flight and is typically interpreted as the RMS error in departure hyperbolic excess velocity or in the initial heliocentric velocity. Using the booster FOM, the 1σ position errors at Jupiter can be found in several ways. The position errors are usually given in the target plane which is a plane defined by unit vectors $\bar{r}$ and $\bar{t}$ perpendicular to a unit vector $\bar{s}$ along the approach asymptote. The impact parameter B is the distance in the target plane (the $\bar{r}$ and $\bar{t}$ plane) from the center of the planet to the approach asymptote. The position error at the target (in so far as the heliocentric trajectory is concerned) is ΔB or the error in the impact parameter.

The booster FOM can be used to find the RMS dispersion in the injection energy ΔC_3 or can be converted into RMS injection velocity errors ΔX_1, ΔX_2, ΔX_3. Either course of action will lead to an estimate of the error at the target resulting from booster dispersions, given that no corrections are made. By using first the error in injection Vis Viva ΔC_3, the analysis proceeds as follows:

$$\Delta C_3 = \left| V_\infty^2 - (V_\infty + \text{FOM})^2 \right| \approx \left| 2\ \text{FOM}\ V_\infty \right|$$

Setting FOM = 15 m/s and V_∞ = 10km/sec results in $\Delta C3 \cong 0.3\left(\frac{\text{km}}{\text{sec}}\right)^2$

$$\Delta B = \frac{\partial B}{\partial C_3}\ \Delta C_3$$

If a value of 1.4×10^6 km/(km/sec)^2 is used for the partial derivative, ΔB is found to be $\sim$420,000 km. A similar result is found by the use of the following expression:

$$B = \sqrt{\left(\frac{\partial B}{\partial \bar{X}_1}\ \Delta X_1\right)^2 + \left(\frac{\partial B}{\partial \bar{X}_2}\ \Delta \dot{X}_2\right)^2 + \left(\frac{\partial B}{\partial \bar{X}_3}\ \Delta \dot{X}_3\right)^2}$$

All necessary partial derivatives are generated by a digital computer program.

Because the vernier correction is designed to null the spacecraft initial velocity error, the magnitude of the velocity change capability to be provided is estimated from the booster FOM. The

vernier correction capability is usually 5 or more times the FOM. The determination of the actual required velocity will be covered in subsection 3.4.3.

An analysis similar to the one outlined above can be used to find the heliocentric error in the target plane which results from residual velocity error after application of ΔV to correct for the injection error V_ϵ (see Figure 3.4-1).

INJECTION AND VERNIER CORRECTION GEOMETRY

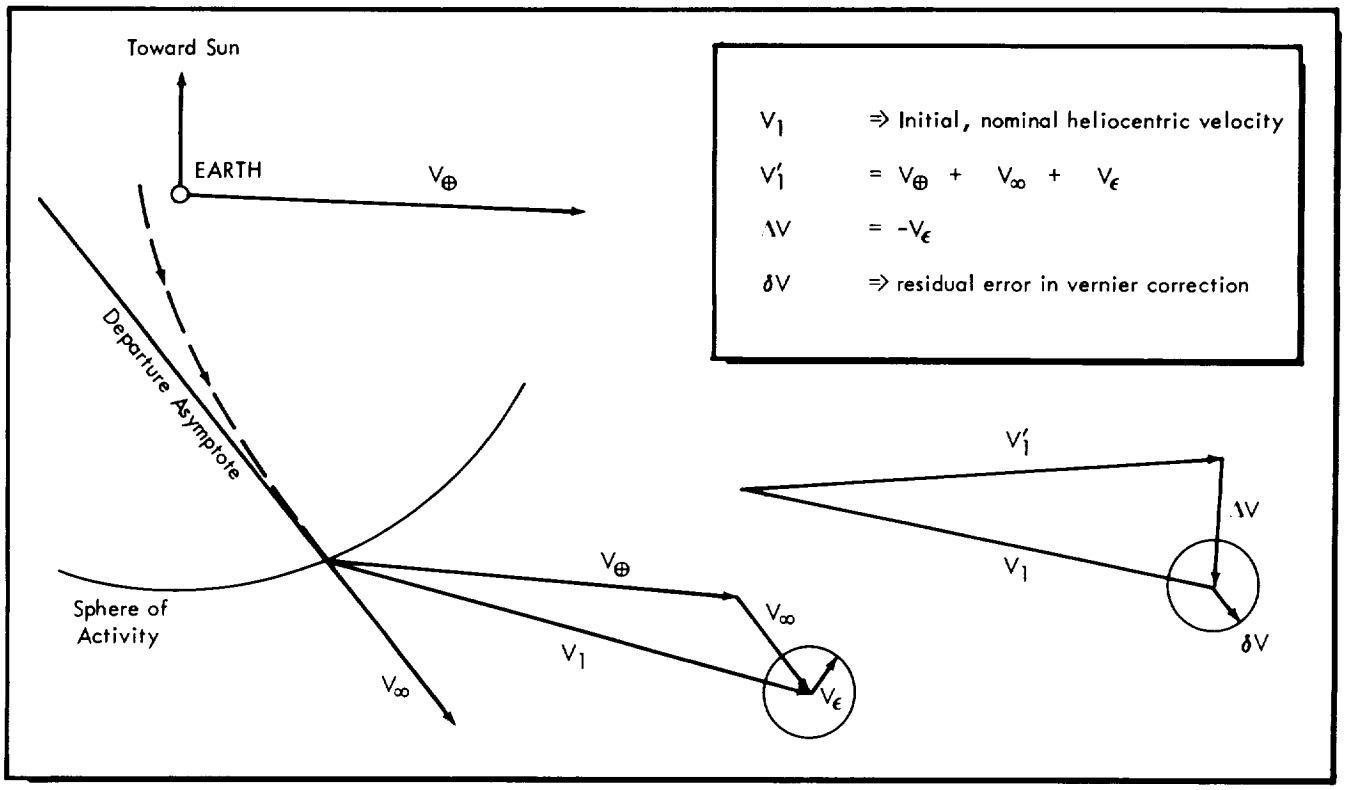

FIGURE 3.4-1

After the vernier maneuver, a residual error δV is left; this error is the result of several error sources. Principally, these are (1) error in the magnitude of ΔV, caused by thrust termination uncertainties, (2) spacecraft attitude control errors occurring prior to and during the vernier maneuver, and (3) orbit determination errors or errors in the estimation of V_ϵ. The individual velocity error components are represented as v_1, v_2, and v_3 respectively.

By using the expression $v_1 = \frac{\delta I}{W} g$, the error v_1 can be found from the spacecraft weight and the uncertainty in the vernier maneuver total impulse. For the vehicles under consideration, this error is approximately 0.06 m/sec. The one sigma value of v_2 will be approximately 0.0655 m/sec, using ΔV = 15 m/sec and a vehicle alignment accuracy of 0.25 degrees. The value of v_3 based on DSIF

projected capability should run about 0.005 m/sec (one sigma). Thus, the residual velocity error δV will be approximately 0.089 m/sec per axis (1σ). The error produced in the target plane due to this residual velocity error is found to be about 3800 km. The effect of Jupiter's gravity during the planetocentric phase of the flight will reduce the above RMS dispersion to approximately 2600 km at periapsis.

The velocity change capability to be designed into the system for terminal maneuvers can be estimated from the error ΔB. To correct for a given error, the ΔV requirement increases as the vehicle gets closer to the target. On the other hand, making the correction earlier will cause periapsis errors as a result of errors in the correction itself, to become larger. A more complete study of this trade-off is required in order to specify the optimum point for the terminal correction. In general, it should be made at a point where the required ΔV is very much greater than the expected velocity error in the guidance correction, and yet far enough away to produce the desired result with a reasonable ΔV expenditure. Assuming that the correction is made some 40-50 million km from Jupiter, the following ΔV estimate can be made. (See Figure 3.4-2.)

TERMINAL MANEUVER GEOMETRY

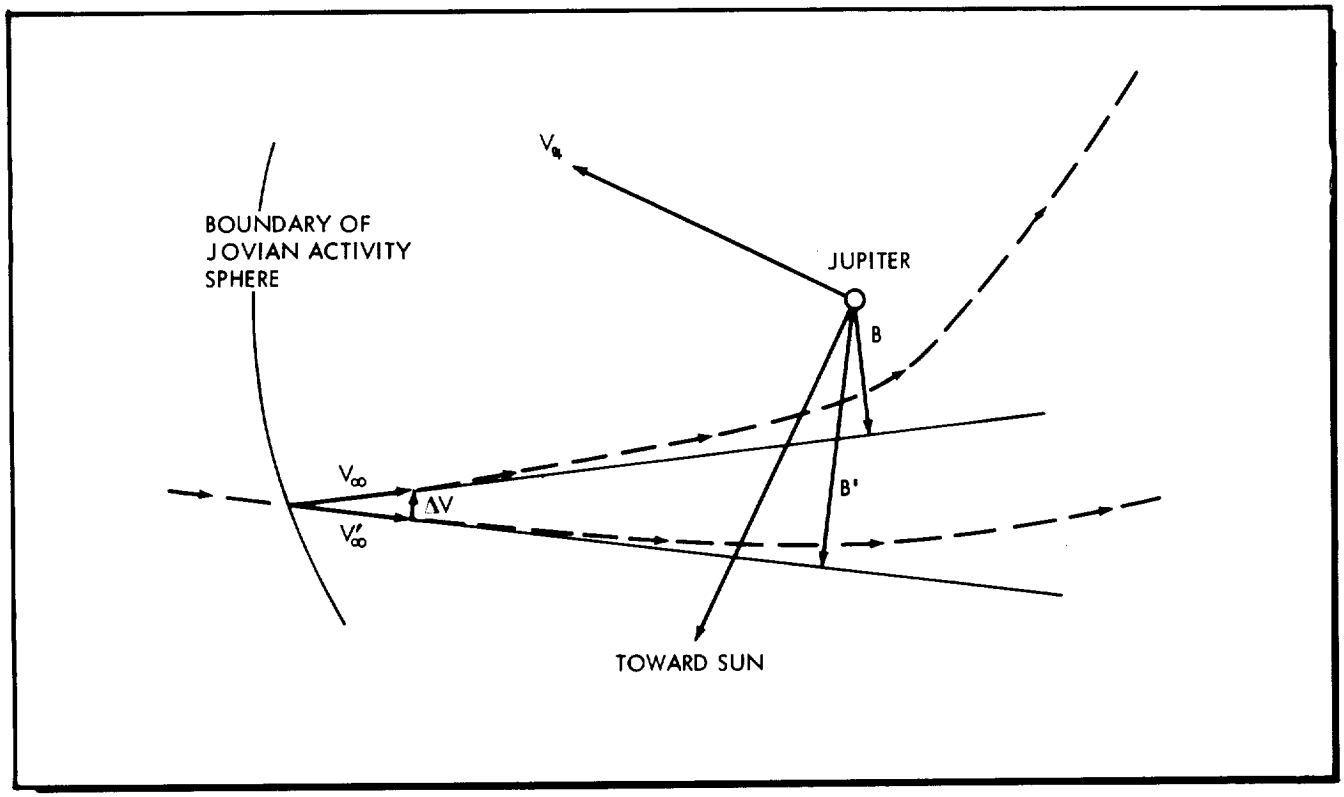

FIGURE 3.4-2

$$\Delta B \cong R \Delta \phi$$

$$\Delta \phi \cong \frac{\Delta V}{V_\infty}$$

$$\Delta B \cong R \frac{\Delta V}{V_\infty}$$

$$\frac{\partial B}{\partial V} \cong \frac{\Delta B}{\Delta V} \cong \frac{R}{V_\infty} \cong 3000 \quad \frac{km}{m/sec}$$

Using this value, a 5 sigma error in impact parameter can be corrected with a ΔV of less than 10 m/sec. An example can be used to show the effect of correction timing on the residual error in B. Assume that ΔB = 10,000 km and that the spacecraft has a correction capability of 15 m/sec. Further, assume that the RMS error in the terminal maneuver is approximately $\delta V = [\, 0.015 \ \Delta V + .1 \,]$ m/sec.

By postulating two points along the approach trajectory having different sensitivities of impact parameter to velocity changes orthogonal to the flight path, a reduction in residual error can be demonstrated which is the result of the timing of the terminal correction.

point #1

$$\frac{\partial B}{\partial V} = 3000 \quad \frac{km}{m/sec}$$

$$\Delta V = \frac{10,000}{3,000} = 3.33 \text{ m/sec}$$

$$\delta V = 0.15 \text{ m/sec}$$

$$\delta B = 450 \text{ km}$$

point #2

$$\frac{\partial B}{\partial V} = 1000 \quad \frac{km}{m/sec}$$

$$\Delta V = \frac{10,000}{1,000} = 10.0 \text{ m/sec}$$

$$\delta V = 0.25 \text{ m/sec}$$

$$\delta B = 250 \text{ km}$$

3.4.3 Guidance Analysis

The nominal trajectory is the trajectory, determined in advance, which satisfies the desired terminal position and velocity. The

guidance function is concerned with deriving one or more velocity corrections based on the difference between the best estimate of the actual position and velocity and the nominal trajectory position and velocity at this point. Applying these computed corrections, a new trajectory is gained which also nominally passes through the desired end state.

The terminal state is, generally speaking, very sensitive to initial errors in velocity. The proper choice of nominal trajectory can reduce this sensitivity somewhat, but the effect is still present. For this reason, a vernier correction is usually made early in the flight to correct for the injection velocity error. This should be made as soon as a good determination of the actual trajectory is available. Let the vector $\bar{\zeta}(t_i)$ represent the difference between the nominal state and the best estimate of the actual position and velocity, i.e.,

$$\bar{\zeta}(t_i) = \bar{X}(t_i) - X(t_i)$$

$X(t_i)$ = the best estimate of the actual state at time t_i

$X(t_i)$ = the nominal state at time t_i

Therefore, the vernier correction is found as follows:

First the column vector $\bar{\zeta}(t_i)$ is partitioned into position deviation and velocity deviation components.

$$\bar{\zeta}(t_i) = \begin{bmatrix} \bar{r}(t_i) \\ \hline \bar{v}(t_i) \end{bmatrix}$$

The vernier correction amounts to the negative of the velocity deviation existing at the time of the correction.

$$\overline{\Delta V} = -\bar{v}(t_i)$$

The computation of the terminal correction proceeds in a different manner. It is assumed that linear perturbation theory applies to the column vector $\bar{\zeta}(t_i)$. The linear perturbation equation

$$\frac{d\bar{\zeta}(t_i)}{dt} = F\bar{\zeta}(t_i)$$

has a solution of the following form:

$$\bar{\zeta}(t_i) = \emptyset(t_i, t_i\text{-}1)\bar{\zeta}(t_{i-1})$$

The state transition matrix $\emptyset$ is evaluated for the proper interval through integration of the perturbation equation. Using $\emptyset$, the expected terminal dispersion can be found.

$$\bar{\zeta}(t_f) = \emptyset(t_f, t_i)\ \bar{\zeta}(t_i)$$

Now by partitioning this matrix equation, the following is obtained:

$$\zeta(t_f) = \begin{bmatrix} \bar{r}(t_f) \\ \hline \bar{v}(t_f) \end{bmatrix} = \left[\begin{array}{c|c} \phi_{rr} & \phi_{rv} \\ \hline \phi_{vr} & \phi_{vv} \end{array}\right] \begin{bmatrix} \bar{r}(t_i) \\ \hline \bar{v}(t_i) \end{bmatrix}$$

The terminal deviation vector $\bar{\zeta}\ (t_f)$ is made up of six elements. A single velocity change can null three of these at the most. Consider the computation of $\overline{\Delta V}$ required at t_i to null the terminal position error $\bar{r}\ (t_f)$.

$$-\bar{r}(t_f) = \phi_{rv}\ \overline{\Delta V}$$

The elements of the three by three submatrix ϕ_{rv} have the form of partial derivatives of final position with respect to velocity components at t_i. Thus, we find

$$\overline{\Delta V} = \phi_{rv}^{-1} \left[-\bar{r}(t_f) \right]$$

As far as the guidance computation is concerned, all that remains is to translate this vector representation of ΔV (given in the primary coordinate frame) into attitude maneuver angles and a velocity change magnitude to be carried out by the spacecraft.

The terminal correction process described above is based on the use of an impulsive velocity change with three-dimensional freedom of the thrust vector orientation. Using a 50-pound thrust rocket, a velocity change of 10 meters per second can be made (in the intermediate and maximum payload vehicles) in something less than half a minute.

A second possibility for implementing the terminal maneuver involves the restriction of the thrust vector to the orbit plane and

the use of a considerably longer rocket thrust time and associated low thrust. This approach exhibits several attractive features. When the terminal maneuver is intended to correct errors only in the magnitude of the impact parameter, the velocity correction can be made in the plane of the trajectory. The hyperbolic approach trajectory is essentially rectilinear from the entrance into the activity sphere to a point very near periapsis. A change in the magnitude of the impact parameter can be effected by a change in the direction of the velocity vector, which causes an angular change in the approach asymptote. The angular rotation of the approach asymptote for the typical range of correction required is small and can be accomplished with a small ΔV applied normal to the spacecraft velocity vector and in the plane defined by the approach asymptote and the center of Jupiter. A further simplification can be achieved by using thrusters mounted perpendicular to the spacecraft longitudinal axis and pointing this axis toward Jupiter with a suitable sensor. The velocity correction is then made normal to the spacecraft/Jupiter line of sight. In this way a simple roll maneuver is all that is required to place the thrust direction in the proper plane. A star tracker is used to define the plane of the approach trajectory. A pair of rockets on opposite sides of the vehicle will usually limit the required roll to a small angle and allow the use of a single star tracker for control during corrections to increase or decrease the impact parameter. Estimation of the error in impact parameter is accomplished at a distance on the order of 50 million kilometers from Jupiter; at this distance the duration of the velocity change maneuver is not critical. Thus, the terminal correction thrusters could be much smaller in size, requiring that the maneuver itself occupy hours instead of minutes or seconds. This would eliminate the need for vane controls in the rocket exhaust. The small moments produced by the thrust-vector misalignments can be held by the attitude control system. The control signals would be generated by the Jupiter sensor pointed along the vehicle roll axis.

3.4.4 Self-Contained Terminal Navigation

For the sophisticated payloads, a terminal maneuver should be considered to compensate for the integrated effect of uncertainties in solar radiation pressure, solar plasma, meteoroid flux, the astronomical units, etc. or simply to improve the terminal precision over that obtainable with the vernier correction.

The nominal trajectory is the desired planetocentric trajectory at Jupiter. The reference trajectory is the best estimate of the spacecraft trajectory as it approaches Jupiter as determined by the DSIF. The objective of the terminal maneuver is to change the trajectory from the reference to a new trajectory which passes through the nominal or design point terminus.

In order to derive the most benefit from a terminal correction, the correction should be based on observations of the target planet. As the spacecraft approaches the planet, sensors will be used to search for and acquire the target planet. At this point, the operations

depend on whether the navigation and guidance computations are accomplished on Earth or on the spacecraft.

In the case of Earth-based navigation and guidance, the reference trajectory determined from Earth-based tracking can be improved (i.e., a better estimate is made) by using measurements made of the target planet from the spacecraft. These measurements are transmitted back to Earth with a time index. They may consist of stadiometric measurements, angular rate measurements, or measurements of the angular distance between Jupiter and the Sun, other stars, or one of Jupiter's moons. With the improved estimate of the reference trajectory, the terminal error can be predicted by a comparison of nominal and reference trajectories. The correction maneuver is computed and the proper commands sent to the spacecraft.

It is possible to design the spacecraft navigation and control system so that the terminal correction is computed on board. Essentially, this amounts to providing sufficient computer and sensor control functions so that Earth-based data processing is not required. To implement this, the same observations are made as in previous case, but they are used on board the spacecraft in a navigation routine in the central computer.

The terminal navigation phase, which precedes the terminal guidance maneuver, is initiated at a point some 60×10^6 km from Jupiter. Earth-based tracking and orbit determination has been engaged in the determination of the spacecraft position and velocity in heliocentric space. From this information and the knowledge of Jupiter's location with respect to the Earth, the position of the spacecraft with respect to Jupiter can be estimated. Tracking errors plus errors in Jupiter's ephemeris combine to produce an error in the knowledge of the spacecraft's planetocentric position and velocity. It is this error which is to be reduced by direct observations of Jupiter from the spacecraft and with on board trajectory determination and guidance computations based on these observations.

In the past several years researchers in the field of space navigation have applied the theory of statistical estimation to the problems of position and velocity estimation on board a space vehicle. The problem amounts to estimating the six components of the vehicle state vector from a sequence of angular measurements made on board the spacecraft with imperfect instruments. This problem and its solution has been formulated in the notation of modern control system theory, i.e., the state vector and state transition concepts. Although the spacecraft trajectory obeys nonlinear equations of motion, the state estimation process can be linearized by assuming the validity of a first order Taylor's expansion of the actual trajectory about the reference or nominal trajectory. From this, the state transition concept follows whereby the deviations from the reference state at one point may be written as linear functions of these deviations at a prior time.

The statistical filter is an estimator which makes an optimal estimate of this deviation vector based on a set of observations made from the spacecraft. This estimator minimizes the effects of the sensor noise. It can be proven that the best estimate of the deviation vector (in the least squares sense) is the conditional expectation of the deviation vector given the sequence of observables on which the estimate is to be based. The observables are the angular residuals obtained by comparison of measured angles from the actual but unknown spacecraft position and the computed angles based on the expected spacecraft position.

A concept of navigation has been developed which encompasses the statistical filter estimation method. The logic flow for this method of navigation is shown in Figure 3.4-3. The numbers appearing on this figure correspond to the sequence in which the operations are carried out.

STATE ESTIMATION FLOW DIAGRAM

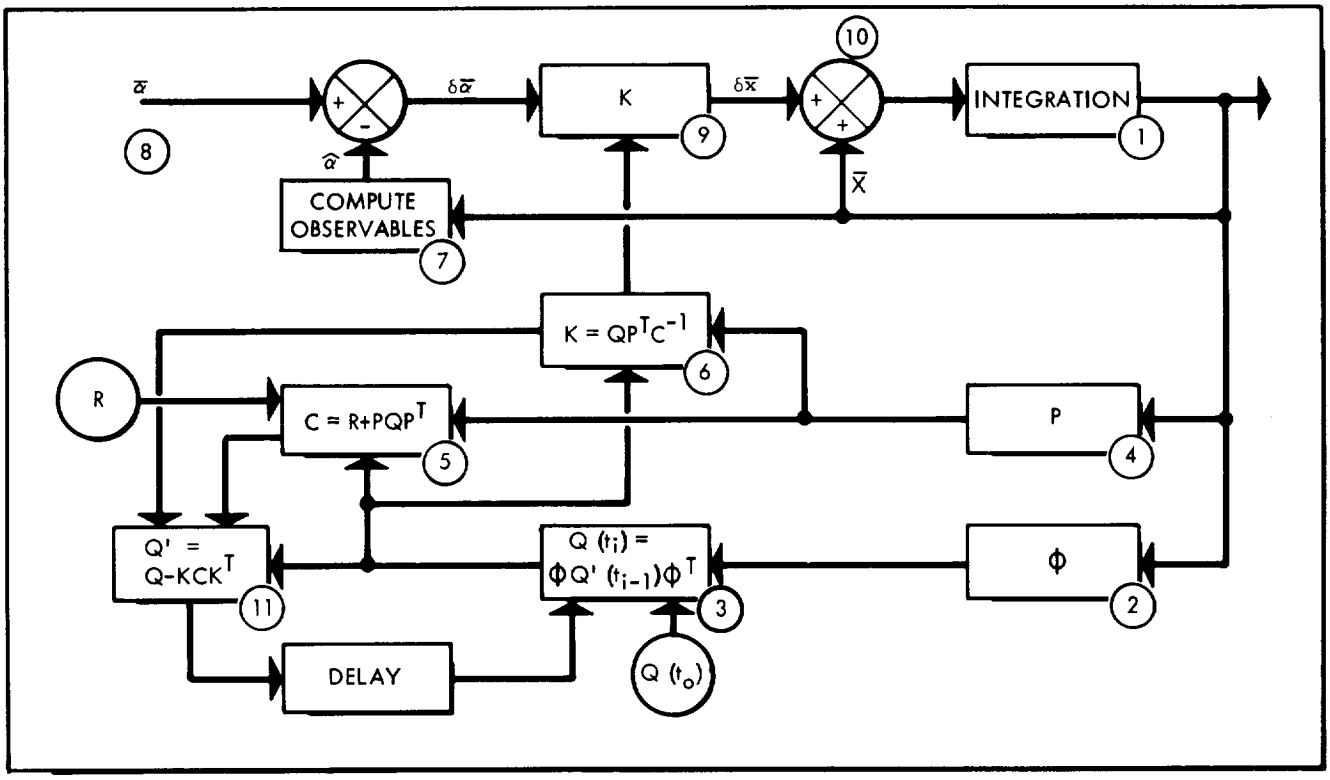

FIGURE 3.4-3

These operations are as follows:

Operation 1: In anticipation of the ith group of observations and the ith estimate of the spacecraft position and velocity, the navigation computer is used to integrate the equations of motion from the previous best estimated state to the time t_i.

Operation 2: The state transition matrix $\emptyset$, which links the state at t_{i-1} to the state at t_i, is evaluated.

Operation 3: The corrected covariance matrix of estimation errors at t_{i-1} is updated to t_i by the use of the $\emptyset$ matrix. The new matrix, $Q(t_i)$, reflects the state uncertainty just prior to the ith estimation.

Operation 4: The matrix P, which relates the angular residuals to the state, is evaluated.

Operation 5: The covariance matrix of the observation residuals C is formed with inputs $Q(t_i)$, $P(t_i)$ and R, the covariance matrix of sensor noise.

Operation 6: The optimum estimator K is computed.

Operation 7: The expected values of the observables (space angles) are computed on the basis of the reference position and velocity at the time of the ith estimation.

Operation 8: The observations are made from the spacecraft actual but unknown position. The actual values of the angles being measured are corrupted with sensor noise during the observation process, thus the sensor outputs are imperfect.

Operation 9: The computed space angles are subtracted from the observed angles. The angular residuals, including the noise component, are operated upon by the optimal estimator K.

Operation 10: The best estimate of the state is added to the reference position and velocity to form the initial condition for the next trajectory integration.

Operation 11: The covariance matrix of estimation error is corrected to reflect the ith estimation.

A computer simulation of this state estimation method was carried out in order to get a feel for its performance capability. Initial uncertainties were assumed in the planetocentric position and velocity of the spacecraft at a point 60 million km from Jupiter. These RMS errors were assumed to be 5000 km per axis and 0.2 meters/second per axis. Separate computer runs were made with instrument error standard deviations of 5, 10, and 30 arc seconds. The observables used were the Jovian angular diameter and the included angles between lines of sight from the spacecraft to Jupiter and from the spacecraft to 3 different stars. The results for two different observation rates are shown in Figures 3.4-4 and 3.4-5. The plots show the resultant total position error as a function of time.

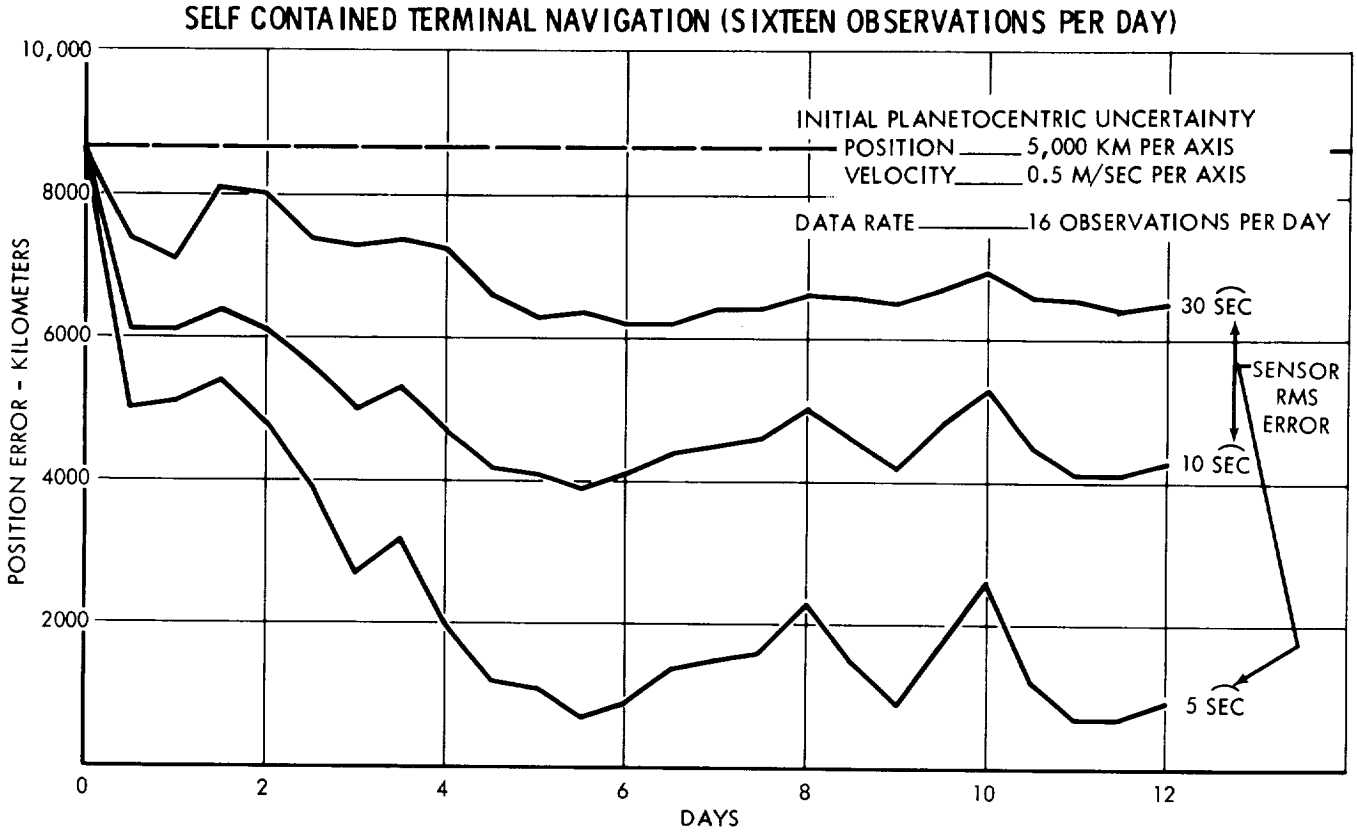

FIGURE 3.4-4

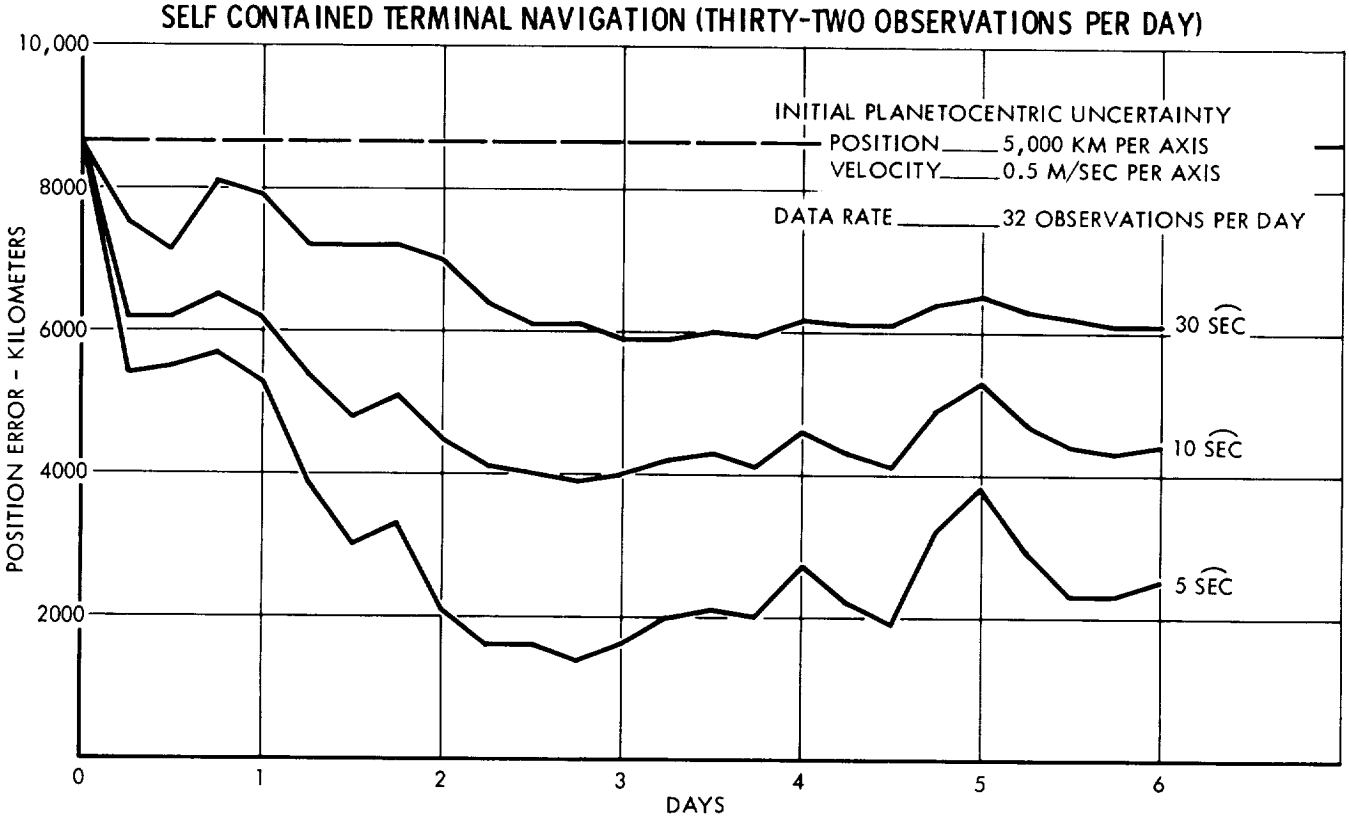

FIGURE 3.4-5

3.5 ATTITUDE CONTROL

The term "attitude control system" as used herein refers to the group of actuation devices and associated electronics which are employed to generate torques about the spacecraft axes for controlling the orientation to some desired condition. The generation of three-axis attitude error signals is considered part of the function of the spacecraft control system and is discussed in subsection 3.3.

There are many possible methods of achieving attitude control, any a succession of different modes of control will be needed on any specific mission. Many of the system requirements stem directly from the specific control objectives to be attained; consequently, guidance considerations are not entirely separable. The approach to the control problem will be limited or influenced to some degree by various design considerations, such as geometric and physical constraints (or preferences) arising from booster capabilities, equipment arrangements, and others. Also to be met are the usual requirements to accomplish maneuvers, perform scientific experiments, and overcome external disturbances. Communications requirements are critical in this application because of the long ranges involved; and the large antenna sizes under consideration create special problems in the design of the attitude control system. Reliability considerations are also of prime importance because of the extended period of time over which the system must operate.

In this section, attention is given to some general considerations and design criteria associated with the attitude control problem. The application of the results of this study to the design of an example spacecraft is also indicated.

3.5.1 Control Concepts

Attitude control concepts can be generally classified as either passive or active. Spin stabilization is the only passive method that is applicable to a Jupiter flyby spacecraft and that has been extensively implemented as a primary means of spacecraft control. A possible semipassive technique is one in which solar radiation pressure is used in conjunction with some active attitude control system. However, active attitude control by means of gas jets is the best known technique, and it has been utilized extensively in a wide variety of spacecraft.

The gas jet approach is relatively simple and reliable, and a great deal of development work has been done on this technique. Since mass expulsion is generally necessary in any attitude control problem where nonconservative external torques are involved, it is understandable that gas jet systems have received first priority. However, at the present time momentum storage devices, specifically, reaction wheels, are emerging from the development phase; and their capabilities are becoming better recognized. It was the intention herein to give due recognition to this possible approach since current state-of-the-art does not exclude it.

Spin stabilization is of interest in this study because of its inherent simplicity relative to the more complex concept of three-axis stabilization. However, there are several possible variations of this concept, which differ greatly in principle of operation. The selection of the spin axis orientation is one area where a primary difference can occur, especially in regard to the communications capabilities. In one approach, the spin axis (which is also the antenna axis) is maintained along the spacecraft-Sun line, and a parabolic reflector type of antenna is used. In an alternate approach, the spin axis is aligned approximately at right angles to the ecliptic plane; consequently, use must be made of toroidal-beam or despun antenna concepts. Although the first approach is superior with respect to communications, a continuously operating, active attitude control system is needed to precess the spin axis and maintain its desired orientation. Also, the relative movements of the Earth are such that a broad-beam antenna design must be used and some of the gain to be realized by the parabolic reflector are therefore compromised. These requirements are considered objectionable since they are inconsistent with the sought after simplicity ascribed to spin stabilization. Therefore, this concept was eliminated from further consideration, and the second approach was selected for analysis in this investigation.

Another area where a design choice is available in the implementation of the spin stabilization concept is that of the attitude control mode during the initial and final phases of the planetary flyby mission. It is necessary to provide some means of properly aligning the spin axis prior to spin-up. In addition, the capability to perform a vernier trajectory correction soon after injection is considered necessary in order to perform a meaningful flyby mission. One approach to this problem is to use the booster attitude control system to orient the spacecraft/booster combination in the desired attitude and spin up the spacecraft in the separation process. A precession type of gas jet system could be provided to make adjustments to the spin axis orientation. The required trajectory corrections would be made from the spinning spacecraft by using properly phased thrust pulses. An alternate concept is to delay spin up until after the trajectory correction has been applied. A conventional three-axis stabilization system is provided for control prior to this time. The latter concept is favored herein because it is regarded as less complex and is more consistent with the Mariner state-of-the-art. Accordingly, in keeping with the spin-stabilized concept evolved in this study, an interim gas jet attitude control system is postulated.

During the planetary encounter phase, the spinning spacecraft is limited insofar as the type of scientific experiments which can be performed. It would be preferable from the scientific standpoint to de-spin the spacecraft and reactivate the gas jet attitude control system to provide a three-axis stabilized platform from which to perform experiments. However, this concept was discarded because a significant reduction in the probability of mission success is associated with the approach. Consequently, in the spin-stabilized spacecraft design concept which is evolved in this study, the scientific

capability is limited to particles and fields, and it is governed by a philosophy of minimum spacecraft weight and subsystem capability.

An obvious conclusion of this study is that three-axis stabilization offers a greater capability for planetary investigations during the terminal encounter. There are many possible variations of the three-axis stabilization concept, also, but they were reduced to three basic cases that appear to offer some promise for the Jupiter flyby mission. These cases are described as follows:

1. Gas jets only

2. Reaction wheels, plus gas jets

3. Solar vanes (fixed), plus reaction wheels,plus gas jets.

Associated with each of these approaches is a different weight, power requirement, performance capability, reliability assessment, cost, etc.; and the selection of a final approach will depend upon an evaluation of the relative merits involved. In order to enable such a comparison, an example design is presented and analyzed at the end of this section. The results presented therein are considered together with reliability data in order to arrive at a final recommendation applicable to the concepts based on three-axis stabilization.

In all concepts of three-axis stabilization, a nominal Sun-pointing spacecraft attitude is to be maintained throughout the mission, including the planetary encounter phase. A design variation involves the question of whether or not a steerable antenna (Earth-pointing) is to be provided to improve the communications capabilities. An alternate approach to the idea of using a steerable antenna is to achieve the same effect with a fixed antenna by adding a variable bias to the Sun sensor output so that the null position of the spacecraft axis follows the approximate Earth location. Also involved is the option of providing a planet-pointing platform for the science package, as is required for some experiments. In general, these variations have only a secondary effect on the attitude-control problem, but there can be important distinctions involved when the reaction wheel system is considered.

3.5.2 Nominal Trajectory Characteristics

In order to assess the attitude control requirements, it is necessary to specify certain trajectory characteristics. However, because the results of an attitude control analysis are not especially sensitive to small variations in the trajectory, preliminary studies can be based on one representative case. The example chosen for this work corresponds to a 600-day mission with departure on 30 July 1976.

The variation of orbital radius with time is presented in Figure 3.5-1. The solar radiation pressure is also shown in this figure and is an inverse square function of orbital radius. The value of

the solar radiation pressure at the Earth's location (1 a.u.) was assumed to be 9.4×10^{-8} pounds per square foot (0.45 dynes per square meter), which is for the case of normal impingement upon a completely absorbing surface. The location of the Asteroid Belt, which extends from about 2.2 to 3.6 a.u. is indicated in the figure. These limits define a period which begins at about 150 days after launch and extends to about 330 days after launch, or approximately 180 days out of the total mission time of 600 days (30 percent).

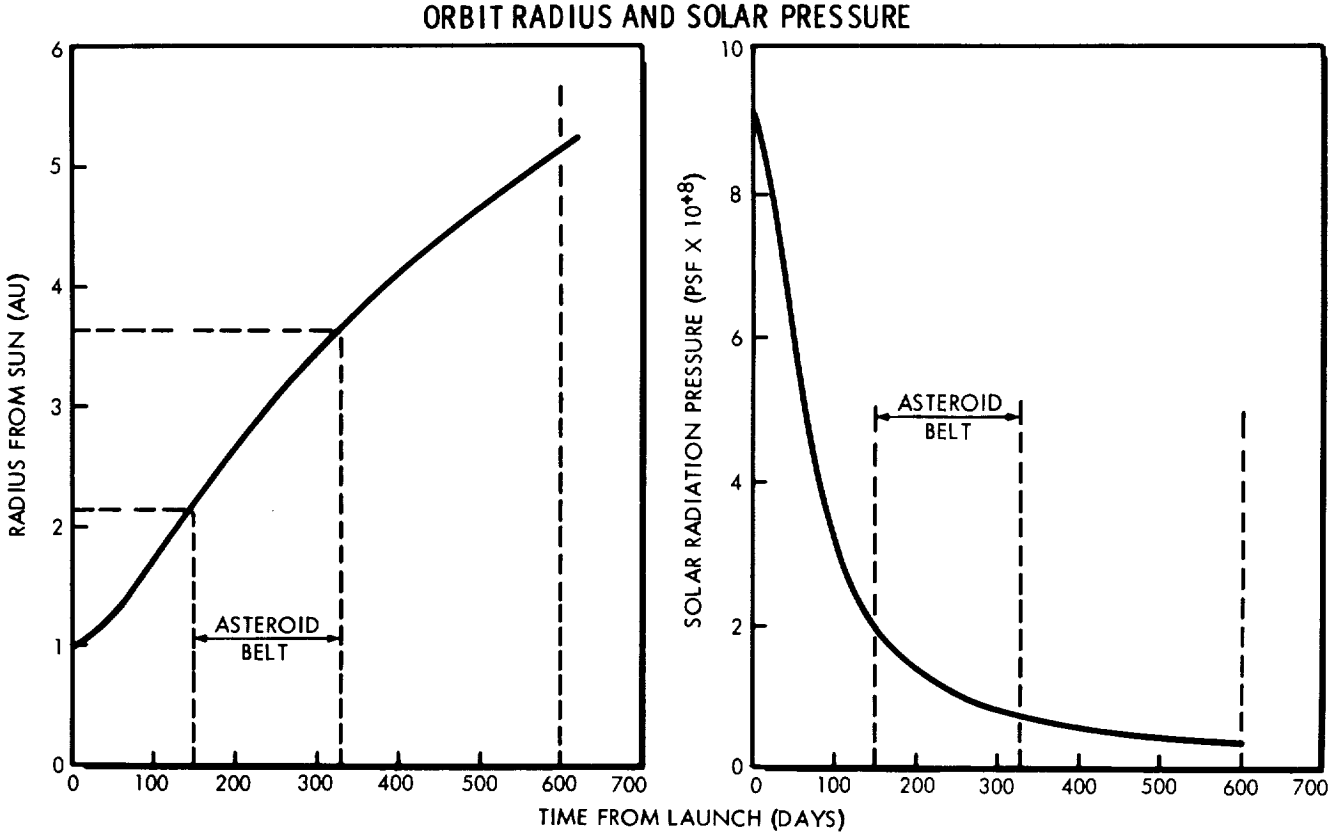

FIGURE 3.5-1

The variation of solar aspect angle along the trajectory is shown in Figure 3.5-2 for an Earth-pointing condition. This angle represents the amount of relative motion that must be provided between the antenna and the spacecraft if the antenna is to track Earth while the spacecraft body is maintained in the Sun-pointing attitude. If the antenna is fixed relative to the spacecraft, this angle represents the amount of spacecraft yaw angle required to keep the antenna locked on Earth. Both of these approaches are regarded as possible variations to the basic design concepts (B, C, and D). There will be differences in the net solar torques experienced in each case, and a different design philosophy may be used for coping with the problem.

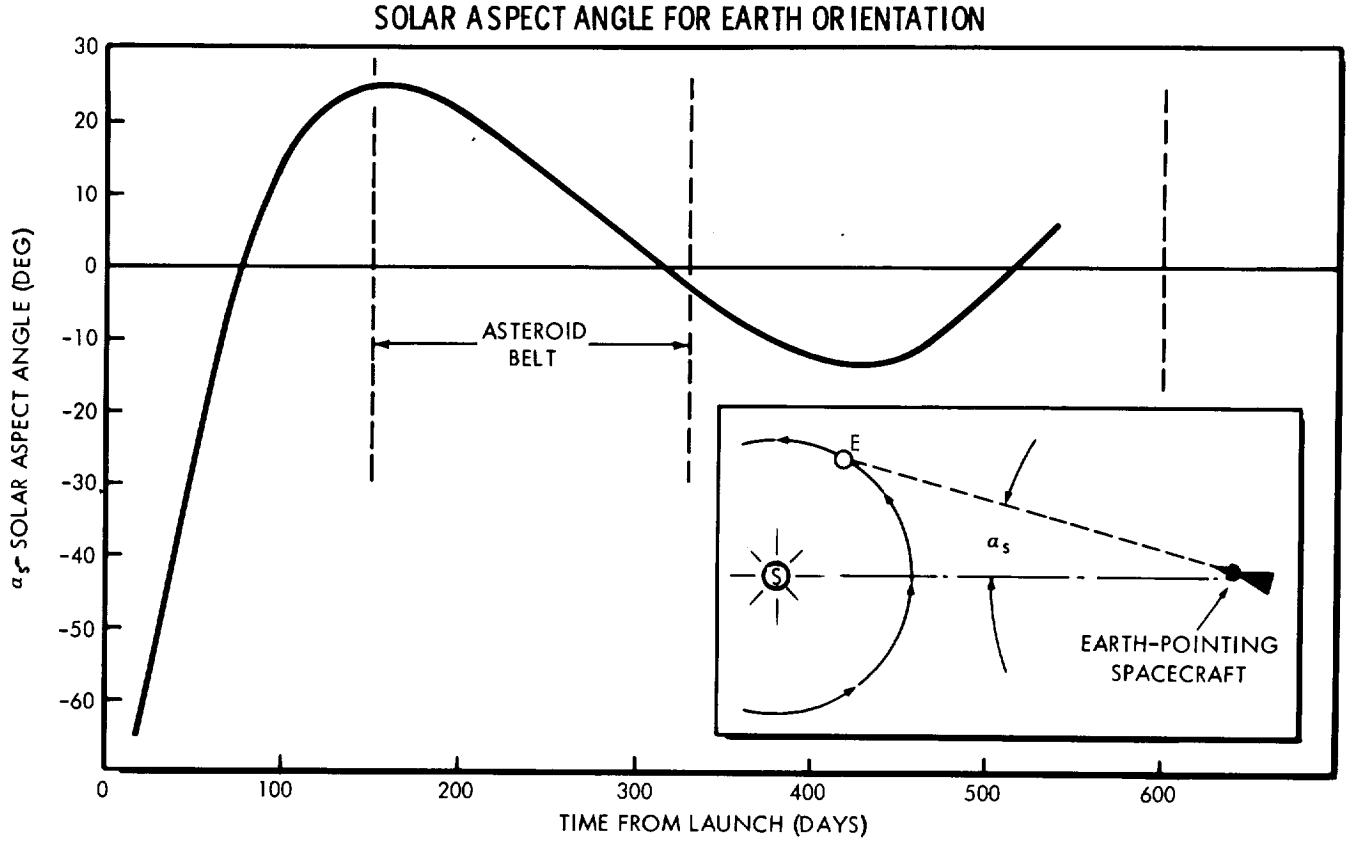

FIGURE 3.5-2

Finally, the meteoroid approach conditions relative to the spacecraft are presented in Figure 3.5-3. These results were computed under the assumption that the meteoroids move in circular orbits about the Sun, with characteristic velocities corresponding to local circular satellite velocity, so that the spacecraft velocity must be vectorially subtracted to yield the relative velocity vector. The approach angle of the meteoroids is shown for both Earth-pointing ($\bar{\alpha}$) and Sun-pointing ($\bar{\alpha}'$) conditions. In both cases, the approach is seen to be essentially from the rear. The average approach velocity in the Asteroid-Belt region is seen to be about 14.5 kilometers per second.

3.5.3 Considerations For Spin-Stabilization

Spin-stabilization is a simple approach to the problem of attitude control when only one axis of the spacecraft must be oriented in some inertial direction with relatively low accuracy. However, it is not generally possible to spin an arbitrary spacecraft and expect satisfactory results. As in any engineering problem, spin stabilization is circumscribed by certain minimum requirements, and there is a possibility of approaching optimum conditions by proper attention to the design parameters.

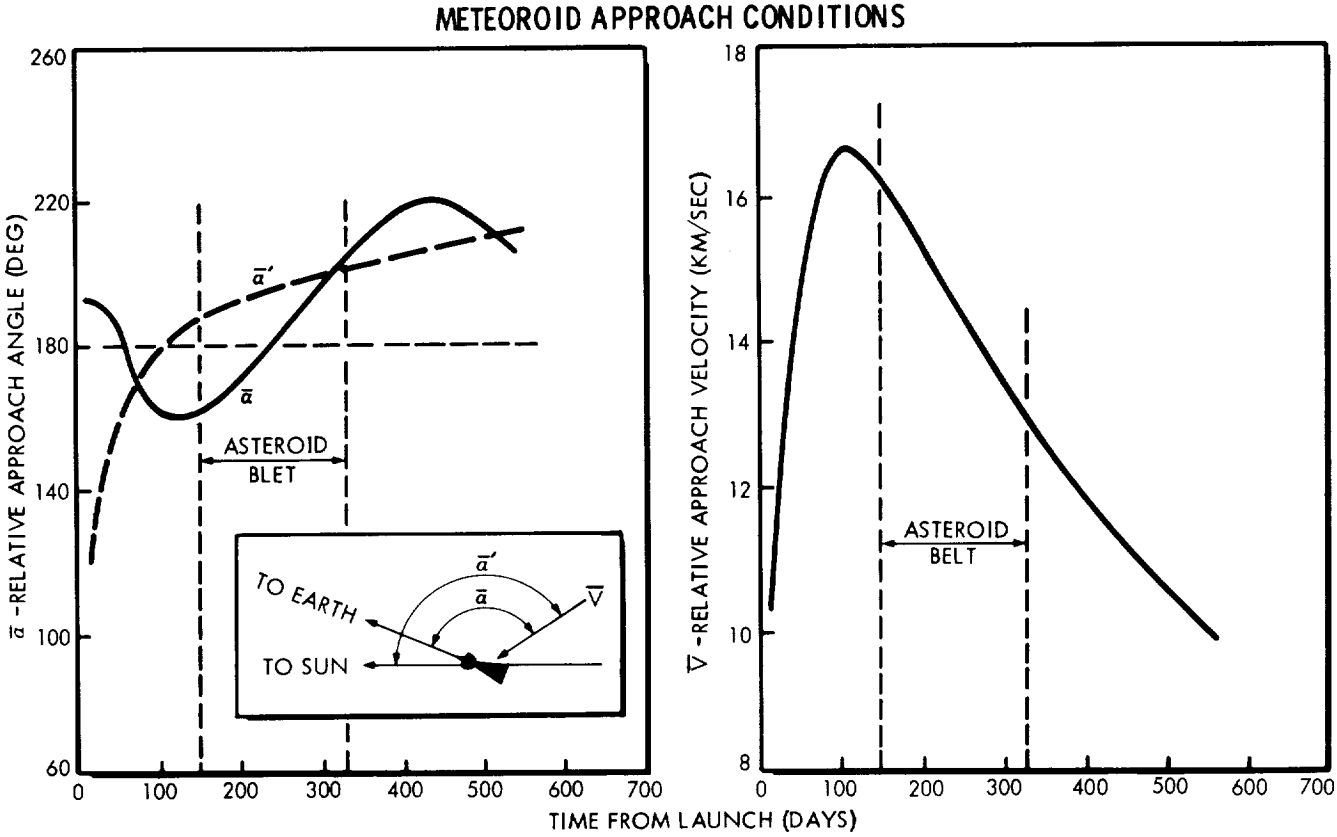

FIGURE 3.5-3

The stability of a spinning body is defined by its behavior under conditions of no external torques, and is related to the problem of nutation about the spin axis. This problem is described in many reports and textbooks, and is a function of the relative values of the moments of inertia. In the case of a nonrigid body (such as the spacecraft under consideration), it is necessary that the spin axis coincide with the principal axis of maximum moment of inertia. The vehicle would be either statically or dynamically unstable in any other spin condition. Satisfaction of this requirement leads to the use of disk-like configurations with the spin axis normal to the disk plane. By placing the maximum amount of mass near the periphery, the effect is to maximize the spin stability as well as the moment of inertia about the spin axis.

In the case of the symmetrical configurations of the type under consideration, two of the moments of inertia are essentially equal, and the spin stability is measured by the following factor:

$$K = \text{Spin stability factor} = \left[\frac{I_{spin}}{I_{normal}} - 1\right]$$

where: I_{spin} = Moment of Inertia about spin axis

I_{normal} = Moment of Inertia about axis normal to spin axis.

The condition of K = 0 corresponds to neutral stability and is obtained when all moments of inertia are equal. The maximum value of K is 1.0, and it corresponds to the case of a thin, flat disk which has a spin moment of inertia that is twice as large as that about the other two axes. A design objective was to achieve values of K = 0.4 or greater (i.e. $I_{spin} = 1.4\ I_{normal}$). This criterion was selected as a reasonable compromise for holding the steady-state nutation motion to the smallest value for a given spin rate. However, the solution of this problem involves much additional study, and it will be influenced by such factors as system damping, spin rocket burn time, thrust misalignment, manner of spin-up, etc.

The spin rate to be used for a given configuration will most likely be determined in terms of centrifugal force limitations. The spin moment of inertia must then be large enough to yield the required angular momentum for counteracting the precession resulting from external torques. The variation of spin rate with allowable centrifugal force level and radius arm is presented parametrically in Figure 3.5-4. For a 10-g limitation at a 35-inch radius arm, the allowable spin rate is only 100 RPM. A design value somewhat lower than this figure is more probable, but the final result will depend upon an analysis of the "g" tolerances due to structural strength and equipment operating limits.

SPIN-RATE LIMITATIONS

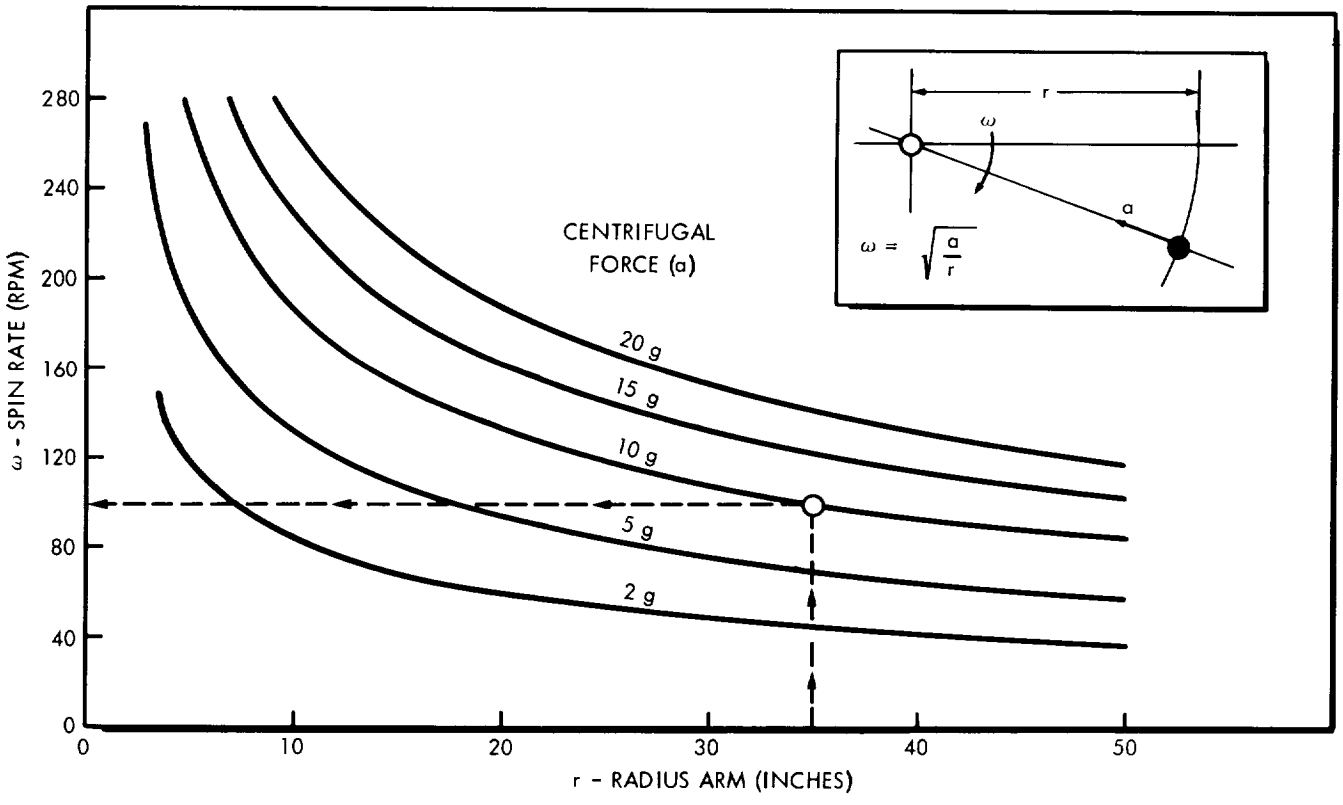

FIGURE 3.5-4

The spin rate in itself is not the fundamental quantity in spin stabilization; it is, rather, the angular momentum that is important. The angular momentum is defined as follows:

$$H = (I)\ (\omega)$$

where: H = Angular Momentum (ft-lb-sec)

I = Moment of Inertia (slug-ft^2)

ω = Spin Rate (rad/sec).

In the configuration arrangements under study, the value of H is maximized by locating the RTG units at the largest possible radius consistent with design limitations. The allowable spin rate would be reduced as the radius is increased (for a given "g" tolerance), but the moment of inertia contribution would increase faster. Under these assumptions, the contribution of the RTG units to H would increase as the 3/2 power of their radius arm. The attainable values of H are believed to be in the region of about 500 to 1000 foot-pound-seconds for the configuration studied.

In order to meet the objectives of the communications system, the precession of the spin axis caused by external torques must be held to the lowest possible value. The major part of the tolerable inaccuracy is expected to result from the effect of spin-up errors and errors associated with the inertially-fixed spin axis (which arise because of the slight difference between the plane of the ecliptic and the plane of the spacecraft's orbit). Because there is an upper limit to the amount of spin angular momentum that can be provided, design efforts to minimize the magnitude of the disturbance torques are important.

The most significant source of disturbance torque is the effect of solar radiation pressure. This problem can be reduced by designing a balanced configuration - that is, by making the moment-area zero about the axes normal to the spin axis. However, because of practical limitations and unknowns, a certain amount of unbalance is unavoidable. This small discrepancy can be important because of the long time period over which the resultant torque acts. An approximate analysis of this effect may be constructed by considering the analogy of the spinning spacecraft to a simple gyro, as indicated in Figure 3.5-5. By assuming that the moment vector is inertially fixed so that two-dimensional precession takes place, a simple expression for the precession angle, θ, is obtained. This expression involves the time integral of the solar pressure (K_1), which is evaluated from the data presented in Figure 3.5-1. The results are presented parametrically in Figure 3.5-6, in which the allowable moment-area unbalance is shown as a function of H and θ. In a typical example (H = 750 foot-pound-seconds; θ = .25 degree), the allowable value of unbalance is about 4 feet cubed. This corresponds to an area of one square foot at a moment arm of 4 feet. Although this allowable error is believed to be well within the tolerance, it indicates that the effect could become significant if the balance requirement is overlooked or if the value of H is not sufficiently high.

SPIN-AXIS PRECESSION DUE TO SOLAR PRESSURE

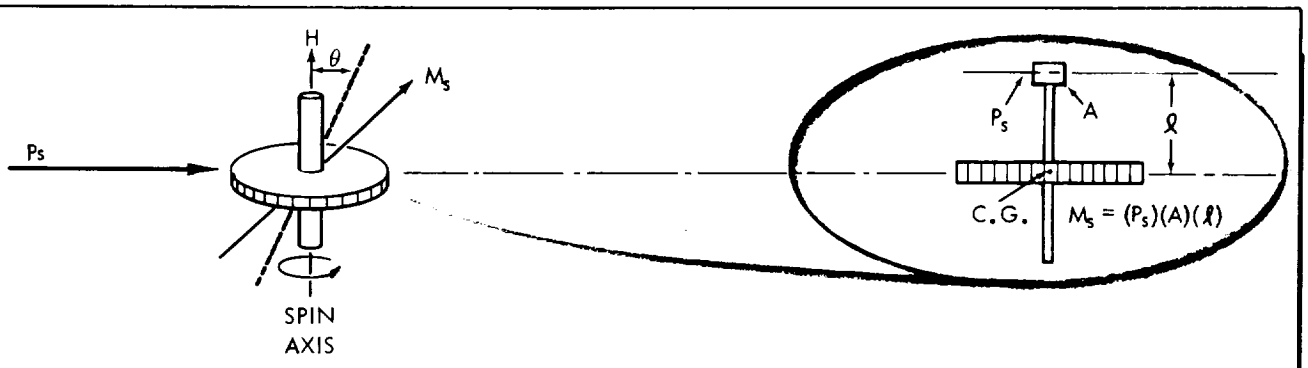

P_s	=	Solar Radiation Pressure (Lbs/Ft^2)
A	=	Net Unbalance Area (Ft^2)
ℓ	=	Moment Arm of A (Ft)
M_s	=	Moment of Solar Force about c.g. (Ft-Lb)
H	=	Spin Angular Momentum (Ft-Lb-Sec)
θ	=	Precession Angle (Rad)

PRECESSION EQ: $M_s = H\dot{\theta}$ or $\dot{\theta} = \left(\frac{M_s}{H}\right)$

INTEGRATING: $\theta = \int_0^{T_F} \left(\frac{M_s}{H}\right) dt = (K_1) \frac{(A)(\ell)}{H}$ (RAD)

WHERE: $K_1 = \int_0^{T_F} (P_s)\, dt = .90 \left(\frac{LB\text{-}SEC}{FT^2}\right)$

FIGURE 3.5-5

ALLOWABLE MOMENT - AREA UNBALANCE

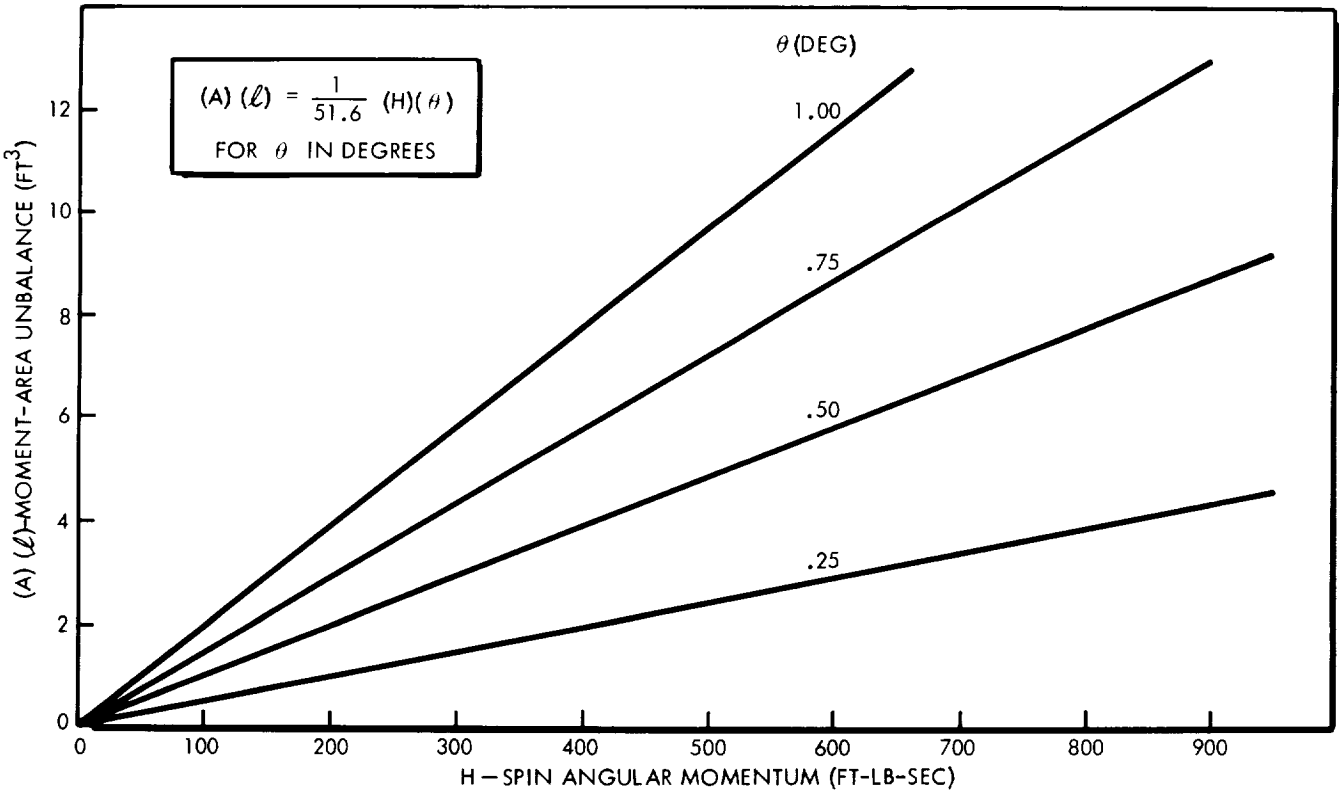

FIGURE 3.5-6

3.5.4 Considerations For Three-Axis Stabilization

Three-axis stabilization is required for the more ambitious missions in which orientation control must be used in order to accomplish navigation, data gathering, communications, and other functions in the most efficient manner. Although the disturbance torques in interplanetary space are few and relatively insignificant compared to ordinary measures, they can become important because of the long time periods over which they act. Therefore, the problem of three-axis stabilization is characterized by its delicacy, and the most important requirement is the achievement of long-term reliability.

According to present knowledge, the disturbance torques of primary importance in interplanetary space are due to solar radiation pressure and meteoroid impacts. The solar pressure is an electromagnetic phenomenon and may be thought of as the impingement of photons on a solid surface. The Sun also emits a stream of protons moving at velocities that are much less than the velocity of light, and they constitute the "solar wind". However, the pressure due to total momentum transfer of the solar wind is much smaller than the solar radiation pressure and may be ignored. The meteoroids are mass particles moving in orbits around the Sun and are of primary concern in the region of the Asteroid Belt which must be traversed in a Jupiter mission.

The disturbance torques due to solar pressure depend upon the solar aspect angle as well as the radiation intensity. The most significant instance where solar torques could become a basic design problem is in the case of the fixed-antenna, earth-pointing spacecraft which must experience the effect of the large aspect angles shown in Figure 3.5-2. For preliminary purposes, this problem may be treated in the manner indicated in Figure 3.5-7. The configuration may be envisioned as an equivalent sphere; consequently, the solar force becomes equal to the product of solar pressure and the spherical area. The design objective is to make the center of pressure of this solar force coincident with the center of gravity so that the torque is nominally zero in all attitudes of interest. However, this objective can only be approached in practice, and it is necessary to make allowances for a certain amount of error. Because of the symmetry of the configuration, it is assumed that both the center of gravity and center of pressure lie on the spacecraft centerline, but with a small offset, $\bar{X}$, between them. The solar torque is then a function of solar aspect angle, α_s, as well as solar radiation pressure, P_s. The magnitude of this torque is small in itself, and it is the time integral of the torque (angular momentum) that is important.

As indicated in Figure 3.5-7, the problem is expressed by the quantity, K_2, which may be evaluated from the trajectory data presented in Figures 3.5-1 and 3.5-2. The integrand of K_2 consists of both plus and minus area contributions because of the fact that α_s changes sign several times during the course of the trajectory.

TORQUE DUE TO SOLAR PRESSURE

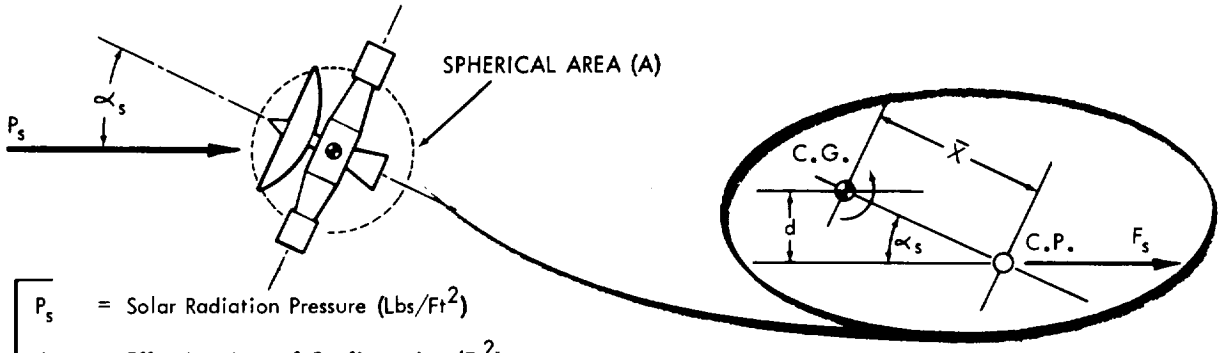

P_s = Solar Radiation Pressure (Lbs/Ft^2)

A = Effective Area of Configuration (Ft^2)

F_s = Net Solar Force = $(P_s)(A)$ (Lbs)

$\bar{X}$ = Offset Distance Between C.G. and C.P. (Ft)

d = Moment Arm of F_s = $(\bar{X})$ Sinds (Ft)

α_s = Solar Aspect Angle

M_s = Moment of F_s about C.G. (Ft-Lb)

H_s = Integrated Momentum Due to M_s (Ft-Lb-Sec)

BASIC EQUATIONS: $M_s = (F_s)(d) = (P_s)(A)(\bar{X}\ \mathrm{Sin}\alpha_s)$; $\dot{H}_s = M_s$

INTEGRATING: $$H_s = \int_o^{t_f} (M_s)\,dt = (K_2)\,(A)\,(\bar{X})$$

WHERE: $$K_2 = \int_o^{t_f} (P_s)(\mathrm{Sin}\alpha_s)\,dt = .30\ (\mathrm{PSF\text{-}SEC})$$

FIGURE 3.5-7

Since the results of this analysis are most applicable to the reaction wheel approach, the value of K_2 was chosen as the largest area segment, irrespective of sign. This value occurs during the first portion of the trajectory (up to about 75 days), and it is about three times larger than the next segment. The rapidly decreasing value of P_s is primarily responsible for this diminishing effect.

The variation of H_s with the parameters A and $\bar{X}$, according to the above result, is presented in Figure 3.5-8. In the case of a gas jet system on the limit cycle mode, this requirement would be insignificant and would be lost in the limit cycle impulse. However, in the case of a reaction wheel system, these results are very important, and they determine the momentum storage capacity required of the wheel if saturation is to be avoided. The value of H_s for a typical example is just within the range of a moderate-sized reaction wheel. This result indicates the importance of balancing the configuration to alleviate the solar torque effects when this type of attitude control problem is encountered.

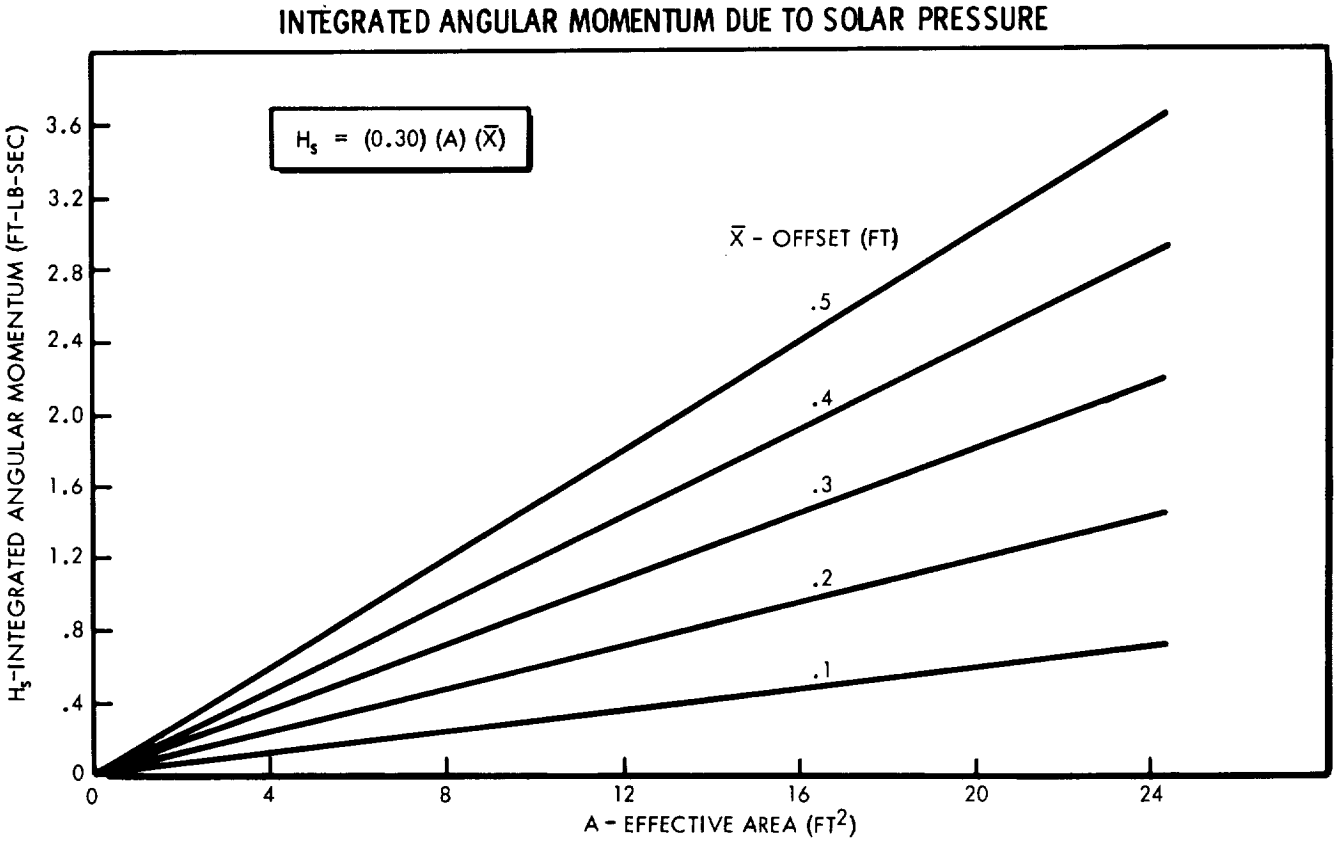

FIGURE 3.5-8

The meteoroid problem is uncertain because of the lack of direct data on the meteoroid flux and the existence of widely differing assessments of the problem. The impact of a meteoroid with a mass greater than some limiting value must be assumed to be catastrophic, but it is generally agreed that this is a low-probability occurrence. Of first interest in attitude-control considerations are the more numerous impacts of small particles which do not disable the spacecraft but do introduce disturbance torques. This problem is apparently most pronounced in the Asteroid Belt, but it is to be expected throughout the entire mission. Cometary debris constitute the most important source of interplanetary matter outside the Asteroid Belt.

Present estimates of meteoroid flux in the Asteroid Belt are based on extrapolations of the data available from observable objects, together with various theoretical guidelines. However, there is room for considerable disagreement, and the minimum and maximum estimates of the meteroid flux differ by many orders of magnitude. This problem is discussed in detail in subsection 3.10 where meteoroid protection requirements are considered. On the basis of using the most severe predictions presented there, the small-particle flux is predicted to be no greater than about 10^{-9} grams per square meter per second. These particles are assumed to be moving in circular orbits around the Sun; therefore, their average velocity in the Asteroid Belt region is about 17.5 kilometers per second.

The average density of this meteoroid "cloud" is then given as follows:

$$\rho = \text{Density} = \frac{\text{Mass Flow}}{\text{Velocity}} =$$

$$\frac{10^{-9}\ g/m^2\text{-sec}}{17.5 \times 10^3\ m/sec} = .57 \times 10^{-13} g/m^3$$

The spacecraft moves through this cloud at some velocity, $\overline{V}$, relative to the particles. This velocity was indicated in Figure 3.5-3 to be about 14.5 kilometers per second (average) for the Asteroid Belt region. If it is assumed that total momentum transfer occurs at impact, the pressure that would be experienced by a flat plate normal to $\vec{V}$ would be defined as follows:

$$\text{Pressure} = (\text{Mass Flow}) \times (\text{Velocity})$$

or

$$P = (\rho \overline{V}) \times (\overline{V}) = \rho (\overline{V})^2$$

This result is familiar to aerodynamicists and corresponds to the "dynamic pressure". It is seen that the pressure increases as the square of $\overline{V}$; therefore, the results may vary significantly with the particular trajectory. This effect is unlike the solar pressure, which is essentially unaffected by the motion of the spacecraft, because the impinging photons move at a velocity greatly in excess of the spacecraft velocity. On the basis of the figures presented above, the meteoroid pressure is as follows:

$$P = (.57 \times 10^{-13}\ g/m^3)\ (10^{-6}\ m^3/cm^3)\ (14.5 \times 10^5\ cm/sec)^2$$

$$= 1.22 \times 10^{-7}\ dynes/cm^2$$

$$= 1.22 \times 10^{-3}\ dynes/m^2$$

$$= 2.55 \times 10^{-10}\ lbs/ft^2$$

For comparison, the value of solar radiation pressure in the Asteroid Belt is about 1.1×10^{-8} pounds per square foot (see Figure 3.5-1). Thus, the solar radiation pressure is greater than the average meteoroid dynamic pressure by a factor of about 43.

On the basis of these results, the effect of micrometeoroids on the attitude control problem is small enough to be ignored. However, it should be noted that, if the meteoroid flux is revised upward several orders of magnitude, the reverse is true. It is likely that this situation will not be further clarified until the first probe is launched and actual measurements are undertaken. In the meantime, the designer should make whatever allowances are permissible without undue compromise and take comfort in the fact that the most reasonable estimates of the problem indicate no cause for concern.

Although the integrated effect of micrometeoroids is apparently unimportant, the effect of discrete, nondestructive impacts by particles of larger size constitutes an important criterion in the control system design. It is desired that the control system have the capability of responding to such an occurrence without losing the "lock" of its electromagnetic sensors (Sun sensors, Canopus startracker, and Jupiter sensor). This requirement constitutes a specification for the maximum control system torque capability that must be provided. It is assumed that the impact phenomenon is described by the case of simple momentum transfer, or

$$\text{Angular Impulse} = (\text{Linear Impulse}) \times (\text{Moment Arm})$$

$$= (\text{Mass}) \times (\text{Velocity}) \times (\text{Moment Arm})$$

In this problem, primary interest is centered on values of meteoroid mass in the region around 1/10 gram with an impact velocity of about 14.5 kilometers per second. In Figure 3.5-9, the variation of angular impulse, according to this formula, is shown as a parametric function of meteoroid mass and moment arm between the spacecraft center of gravity and the point of impact. The results were converted to engineering units for ease in use.

ANGULAR IMPULSE DUE TO METEOROID IMPACT

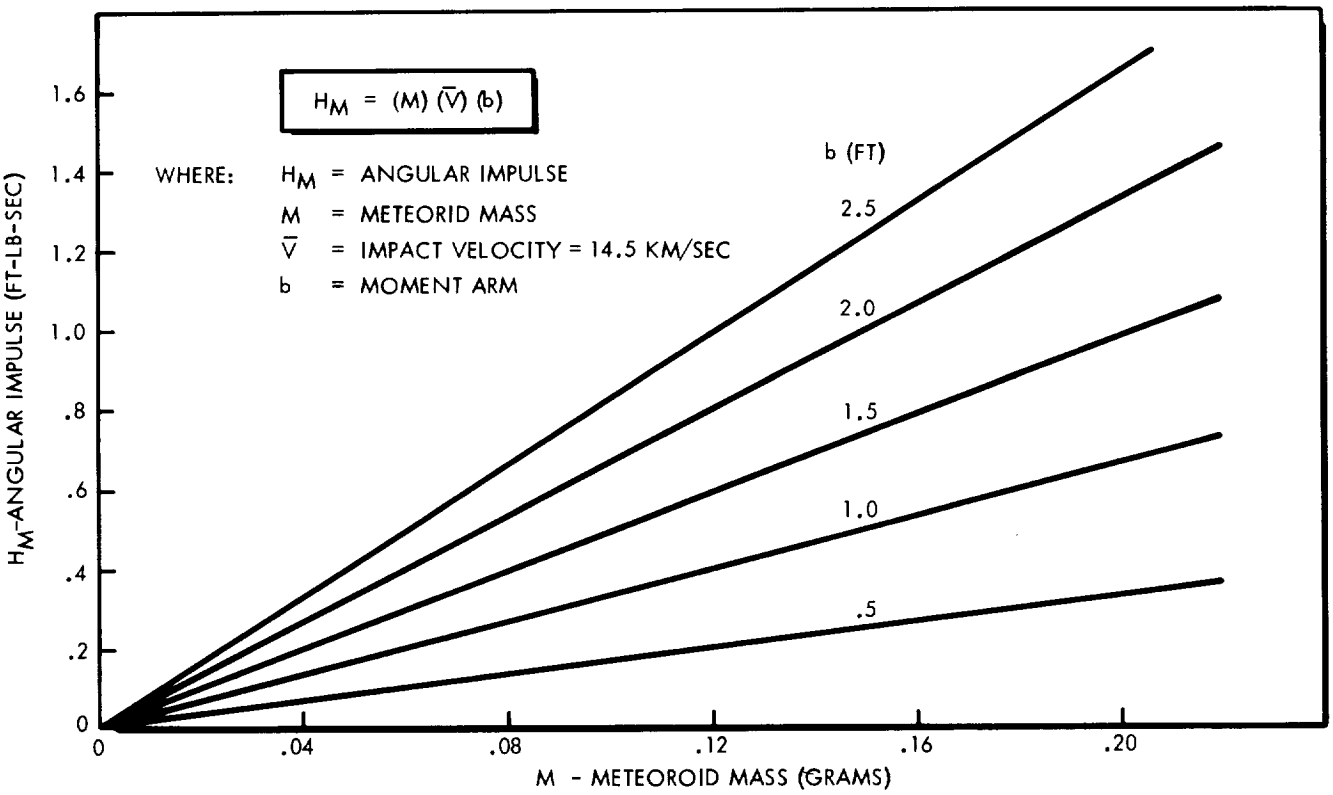

FIGURE 3.5-9

The meaning of the above result can be determined in terms of the maximum torque requirement by means of a simple response analysis. The meteoroid impulse introduces an initial angular rate which varies with the spacecraft moment of inertia. It is assumed that maximum control system torque will be commanded immediately after the disturbance and that this torque will be maintained until the angular rate is reduced to zero. The attitude excursion associated with this maneuver is not to exceed some specified limit, θ_F. The value of torque required to meet these conditions is found to be as follows:

$$T_{MAX} = \frac{H_M^2}{2\,(I)\,(\theta_F)}$$

where:

T_{MAX} = Maximum Torque (ft-lbs)

H_M = Angular Impulse (ft-lb-sec)

I = Moment of Inertia (slug-ft^2)

θ_F = Attitude Angle Limit (rad)

It is to be noted that the torque requirement varies with the square of the meteoroid angular impulse; the result is therefore sensitive to the particular assumptions made in regard to meteoroid mass and impact moment arm.

Another item of interest is the disturbance torque that is likely to be encountered in the vicinity of Jupiter as a result of interaction between Jupiter's magnetic field and that of the spacecraft. It was assumed in a preliminary estimate that the magnetic field of Jupiter is 10 Gauss with the spacecraft field set at 50×10^{-5} Gauss ($50\,\gamma$). The magnetic torque for a spacecraft volume of 1 cubic meter is thus calculated to be 5×10^5 Dyne-centimeters, or 0.04 foot-pounds. The maximum control torque capability to be provided is about three times greater than the above figure. This problem is not regarded as extremely critical, especially since the disturbance torque is only of short duration. However, because of the low margin of safety indicated above, the problem should be studied in more detail when a specific configuration is defined and its magnetic properties can be better determined.

3.5.5 Design Data for Gas Jet System

In this study, consideration was given only to the stored-gas type of mass expulsion system because of its superior reliability and performance capabilities for attitude control applications. The total impulse requirements computed for the various cases of interest are low enough so that monopropellant or bipropellant systems are not believed to be justifiable in view of the various compromises involved.

The weight requirements for a stored-gas system in which nitrogen is used, are analyzed in subsection 3.6, and curves are presented showing the variation of system weight with total impulse. Two basic system configurations are considered: (A) a single system employing one set of twelve jet nozzles and (B) a dual system using two sets of jet nozzles. Configuration A represents a minimum approach with no redundancy but some fail-safety protection afforded for each control axis by the use of four jet nozzles which normally operate to generate a torque couple. Configuration B represents a concept based on the use of redundancy, and it provides the capability of tolerating a stuck-open valve in one system. Configuration A is proposed for short-life systems, such as those required for the spin-stabilized approach, while Configuration B is proposed for long-life systems associated with the 3-axis stabilized approach. The referenced curves include an allowance for residuals and the redundant tank; the impulse ordinate therefore refers to the actual impulse requirement in both cases.

The total impulse requirement of a gas jet system is determined primarily by the fuel usage on the limit-cycle mode. Maneuvering requirements may influence the system design in other ways, but the amount of gas required to perform maneuvers is generally small. The characteristics of the idealized, symmetrical limit cycle are presented in Figure 3.5-10. On the basis of these relationships, the required impulse to support the limit cycle for each of the three control axes may be determined. The required system impulse is then the sum of these results multiplied by an appropriate factor of safety. The limit-cycle fuel requirement represents a conservative estimate of the overall requirements, unless unusually large external torques are expected.

LIMIT-CYCLE CHARACTERISTICS

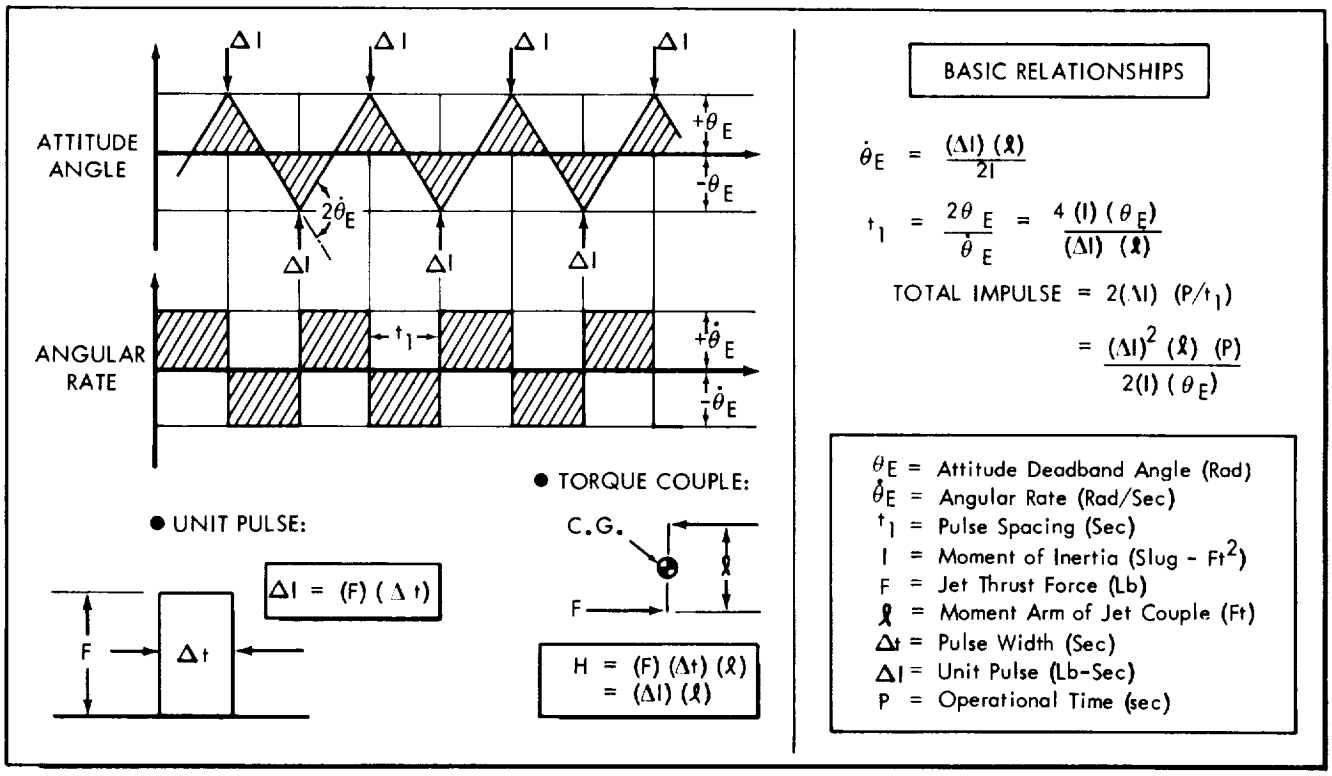

FIGURE 3.5-10

As noted in Figure 3.5-10, the limit-cycle impulse requirement is dependent upon a number of parameters which are under the control of the designer. The most important of these parameters is the unit pulse, ΔI, since it appears as a squared term in the impulse formula. Thus, the achievement of long lifetimes is dependent upon the use of small unit pulses in order to keep the fuel usage to a tolerable level. The requirements to perform maneuvers and develop a peak torque for other control purposes generally result in the specification of the jet thrust level, F, so that the unit pulse is dependent upon the pulse width, Δt, which is utilized. In the case of the solenoid-operated valves used on stored gas attitude control thrusters, it is possible to achieve very small pulse widths. However, in order to reduce valve power requirements and solenoid weight, and to reduce the gas leakage problem, it is not practical to plan on the lowest value. A pulse width of 0.02 second is used herein as a realistic lower limit.

The moments of inertia and jet moment arms depend upon the configuration approach, and the designer should seek to obtain optimum arrangements. The required lifetime and deadband angle are usually specified as part of the mission requirements.

3.5.6 Design Data For Reaction Wheel System

As the required lifetime of the attitude control system increases, the suitability of the gas jet approach diminishes, at least as a single mode of control. This decrease in suitability is due not only to the increased fuel weight required, but also to the greater number of pulses that must be demanded of the system hardware. One possible solution of this problem is the use of a reaction wheel system operating in conjunction with the gas jet system. In this approach, the limit cycle requirement of the gas jet system is removed, and the system would be operated mostly on a standby basis in addition to being used for occasional wheel desaturation. The reaction wheel provides a continuous control capability to a much finer degree than is possible under the gas jet, limit cycle concept. It is basically an electric motor with a high-inertia rotor, and designs of satisfactory reliability should be realizable. The bearing problem is a basic limiting factor, but the problems can be reduced by utilizing low RPM, brushless motors and hermetic sealing.

The reaction wheel system can be designed to give the same peak torque achievable with the limit-cycle gas system, but the peak power requirement will be larger. This feature may be prohibitive in instances where power is at a premium (i.e., in those systems in which batteries or solar panels are used), but it is not considered a serious drawback in the present concept. The reaction wheel system will probably require no overall increase in power capacity because the large capacity provided to meet the requirements for the communications and guidance systems is not needed continuously.

The determination of reaction wheel weight and power requirements can be accomplished by the use of generalized data presented in the literature. However, there is sufficient data available on actual designs to constitute a more realistic point of reference. The characteristics of eight designs representative of the type required in this application were used to construct the curves presented in Figure 3.5-11. The weight of a reaction wheel unit is primarily a function of its momentum storage capacity, and the power requirement is primarily a function of its maximum torque capability. The data points indicated in this figure bear out this generalization. Actually, a more accurate analysis of the problem would indicate that weight and power are each a function of the two basic parameters (momentum storage and maximum torque). All the data points in this figure correspond to sealed units with maximum speeds in the range from 900 to 1250 RPM. They range in size from a 6-inch diameter casing, 3 inches in thickness, to a 12-inch diameter casing, 5 inches in thickness. The data correspond to a single wheel only, and it is noted that three identical wheels will be required to accomplish 3-axis control. Provision should also be made for additional control electronics and power to accompany each wheel. An allowance of three pounds of electronics weight and one watt of power is recommended for each wheel control.

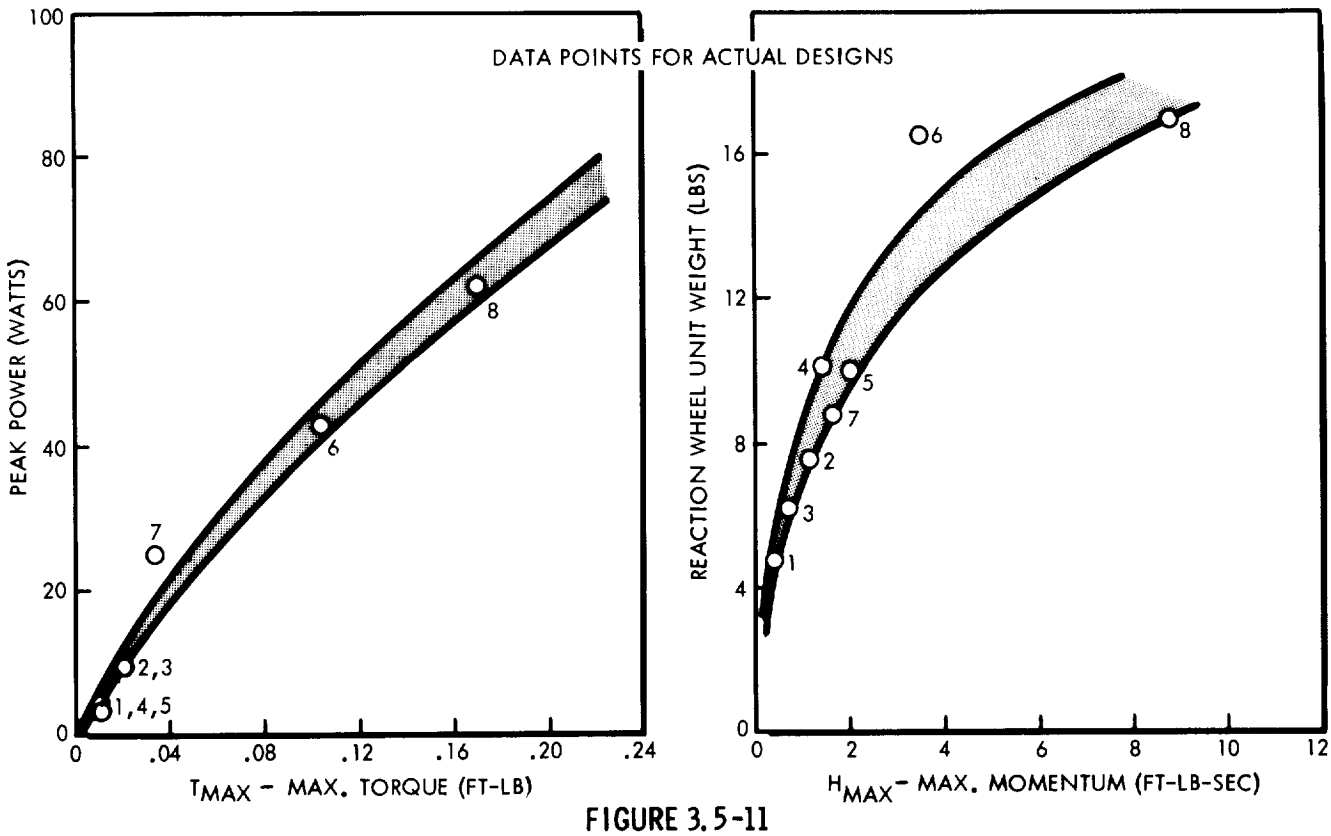

FIGURE 3.5-11

In some quarters, the fluid flywheel has been proposed as a substitute for the reaction wheel. Implementation of this concept is dependent on the circulation of a dense liquid (e.g., mercury) through a closed-circuit tube so that angular momentum is absorbed in the same manner as in the reaction wheel. The main advantage claimed is improved reliability because of the lack of moving parts; however, there is no apparent weight advantage to be realized. This idea is worth following, but it is considered novel at the present time and further development is needed. Reaction wheels are presently being used in a number of satellites and are in an advanced stage of development. Thus, they may be considered state-of-the-art equipment.

3.5.7 Use of Solar Torque for Control Purposes

As indicated previously, the most significant source of disturbance torque in interplanetary space is the solar radiation pressure, since the integrated effect of micrometeoroid impacts was found to be negligible in comparison. This fact suggests the idea of harnessing the solar torque and making it a useful part of the control concept. The solar torque realizable in this application is much too small to be of any interest as a primary means of control, but it has certain attractions as a long-term influence. It was shown earlier (Figure 3.5-8) that the integrated angular momentum caused by a typical solar unbalance condition was comparable to the momentum storage capability of a moderate-sized reaction wheel. Thus, the solar torque would appear to constitute a possible means of accomplishing reaction wheel desaturation.

The idea of utilizing solar torques for control purposes is not new. However, past proposals have usually involved movable surfaces of some sort which introduce the additional reliability problems associated with control servos. The Mariner IV spacecraft incorporated one manifestation of this approach, as an experiment. The concept pursued herein is somewhat different and is based upon the use of fixed solar vanes which provide a degree of static stability about the Sun-pointing attitude. Also, whereas the Mariner system was designed to operate in conjunction with gas jets on the limit cycle mode, the present idea is intended for the case where a reaction wheel system is employed.

The stabilizing contribution of a fixed solar vane may be determined by use of the process indicated in Figure 3.5-12. The force on the vane is a function of the solar radiation pressure, the aspect angle of the surface relative to the solar rays, and the reflective properties of the surface. The surface should be mirror-like to minimize absorption and provide maximum reflection of the incident radiation. For the ideal case of complete reflection, the force caused by the solar pressure is normal to the surface and varies as the sine squared of the aspect angle, as indicated in Figure 3.5-12. The factor of two in the formula accounts for the fact that the solar radiation pressure is defined for the case of complete absorption. The vane should be fixed

at the angle where the rate of change of moment with angular pertubations is maximized,so that maximum stability is obtained. A setting of 45 degrees is seen to be required under the given assumptions. However, a more realistic analysis which accounts for the proportion of absorbed radiation and an off-normal force direction would yield a modified result. Such an analysis could be undertaken once the design details of the vane construction are defined.

STABILITY CONTRIBUTION OF FIXED SOLAR VANES

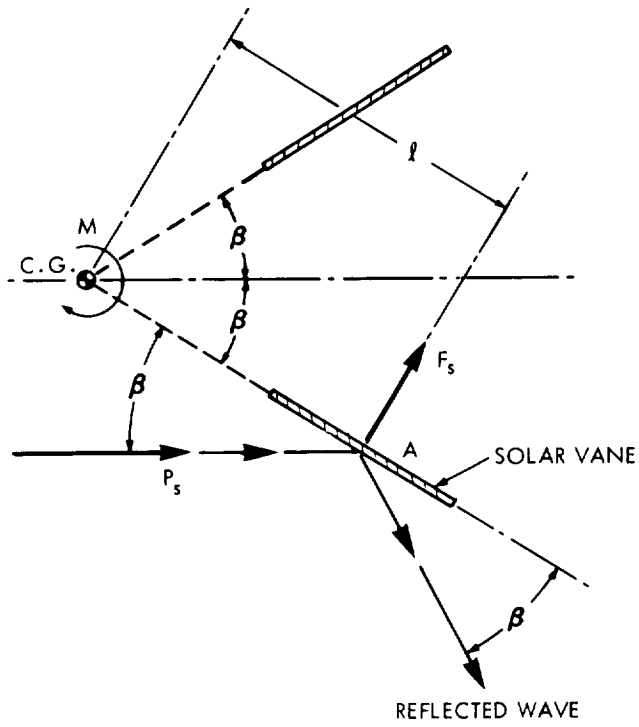

P_s = Solar Radiation pressure, for normal Impingement upon a completely absorbing surface (LBS/FT^2)

A = Area of one panel (FT^2)

β = Aspect angle relative to solar rays

F_s = Normal force on one panel (LB)

ℓ = Moment arm of F_s from C.G. (FT)

M = Moment of F_s about C.G. (FT-LB)

ASSUMING COMPLETE REFLECTION FROM SURFACE:

$$F_s = (2)\,(P_s)\,(A)\,(\sin^2\beta)$$

$$M = (F_s)\,(\ell)$$

$$\frac{dM}{d\beta} = (2)\,(P_s)\,(A)\,(\ell)\,(\sin 2\beta)$$

$$\left(\frac{dM}{d\beta}\right)_{max} = (2)\,(P_s)\,(A)\,(\ell) \quad @\ \beta = 45^\circ$$

(For One Panel Only)

FIGURE 3.5 - 12

Four vanes are to be provided in a symmetrical cruciform arrangement to yield two-axis stability about the Sun-pointing line, which lies along the spacecraft axis of symmetry. Control about the third axis (roll) is not included in this concept, but it may be necessary to provide some type of movable roll trim surface to account for misalignments of the vane settings. It should also be pointed out that the configuration will experience a steady-state solar force along the spacecraft-Sun line because of the vanes, and this force will affect the trajectory characteristics of the spacecraft.

The manner in which the solar stability is integrated into the control scheme is indicated by means of the system block diagram shown in Figure 3.5-13. The primary means of control is the reaction wheel, which is activated by attitude error signals provided by a Sun sensor. The boresight of the Sun sensor is along the spacecraft axis of symmetry so that zero attitude error corresponds very nearly to the point of zero solar torque. A tachometer is generally incorporated into the design of the wheel to measure reaction wheel speed, and it may be used to provide added damping in the feedback loop. However, the lag of the motor itself provides some degree of damping so that the tachometer feedback may not be necessary in all cases. Also included in the feedback loop is a low-gain term which is dependent upon the integral of wheel speed. There are various methods of mechanizing this idea, but it may be regarded as analogous to an automobile mileage indicator, or revolution counter, with the tachometer analogous to the speedometer.

BLOCK DIAGRAM FOR CONTROL SYSTEM UTILIZING SOLAR VANES

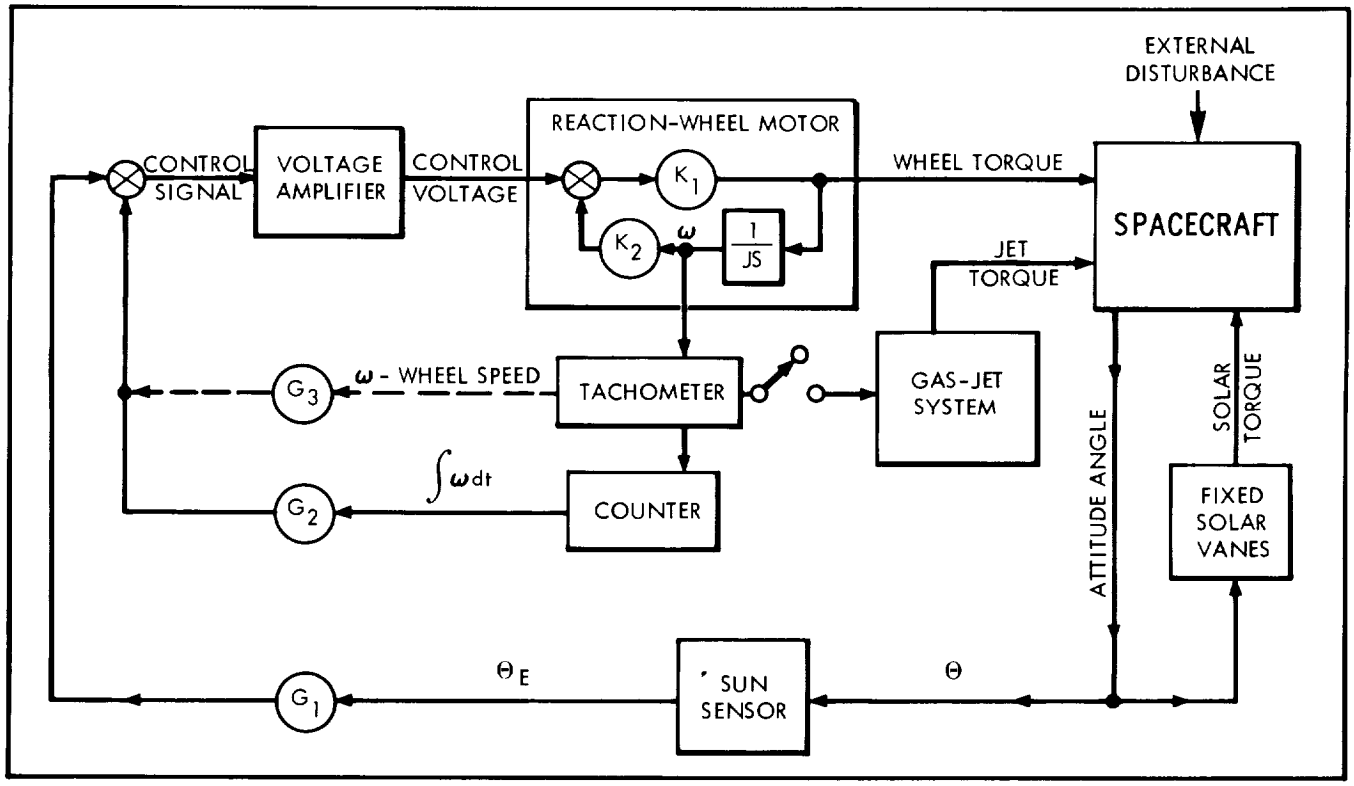

FIGURE 3.5-13

In the case of an external disturbance, such as a discrete meteoroid impact, the system responds first by absorbing the angular momentum in the reaction wheel. This response results in some specific wheel speed which is held by a steady-state error in attitude, θ. However, because of the associated solar stabilizing torque, the attitude error and wheel speed are gradually reduced until both approach zero. The integral feedback provides a bias voltage which permits the spacecraft to seek an off-null trim point (i.e. $\theta \neq o$) that may be caused by antenna deflections or vane misalignments. In the steady-state, the system approaches a condition of zero wheel speed with the spacecraft in its trim attitude.

The primary advantage claimed for this concept is that it permits the gas jet system to remain off during the long interplanetary cruise period since the jets are not required under normal conditions. The gas jet system may be sealed off by squib valves during this period to alleviate the problem of gas leakage through the thrusters. Parallel squib-operated flow lines may be incorporated in the gas supply line to permit the gas system to be reactivated or shut off during encounter and during the operation of other special functions, such as an emergency caused by a severe external disturbance that exceeds the limited capacity of the reaction wheel system.

There are also some disadvantages associated with the concept that may make it marginal for use on a Jupiter mission. The reaction wheel size to be employed in this system is determined basically by the degree of solar stability that is achievable with the solar vanes. Even in the case of the largest practical vane size, the optimum reaction wheel size is not as large as would be desired to accommodate discrete meteoroid hits of the magnitude presently considered for design purposes. However, the meteoroid problem is highly uncertain, and present assumptions may be overly conservative. It should be noted that disturbances related to solar activity would always be tolerable to the system because the magnitude of such a disturbance and the control capability would both vary together as the same function of distance from the sun. It is only the meteoroid problem, and other independent disturbances, that could affect the value of the concept.

3.5.8 Analysis of Example Case

The attitude control problem is closely related to the particular configuration under consideration because of the dependence upon moments of inertia, gas jet moment arms, and other

design features. Unless reference is made to some basic design, it is difficult to evaluate the relative merits of different control techniques without risking the omission of some very important trade-off aspects. Therefore, a typical spacecraft design is selected herein for use in comparing the three approaches to attitude control for the three-axis stabilized case. The spacecraft configuration is shown in Figure 3.5-14, and it is generally representative of the basic design concepts developed in this study.

EXAMPLE SPACECRAFT CONFIGURATION FOR ATTITUDE CONTROL SYSTEM COMPARISONS

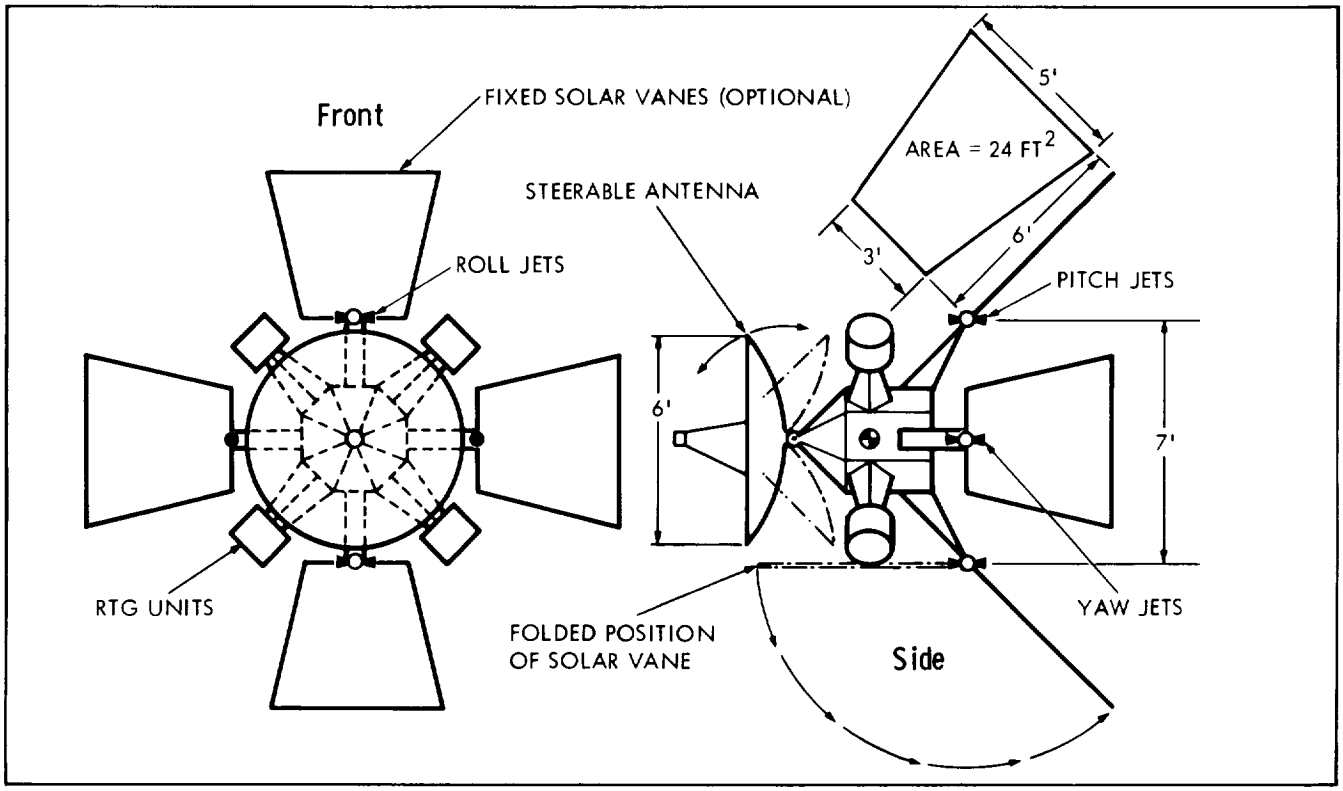

FIGURE 3.5-14

3.5.8.1 Physical Characteristics

The configuration incorporates a steerable antenna mounted on the front side of the central body, which constitutes the equipment bay. The RTG power units are mounted on radial booms to avoid excessive thermal and radiation problems in the equipment section. The gas jets are mounted on four additional booms placed at the rear of the spacecraft. In this arrangement, twelve gas jets (per system) are used to produce couples about each of the three control axes. The moment arm is identical in all cases and

is equal to 7 feet. The gas jets fire in the fore and aft direction to provide pitch and yaw control and in the circumfrential direction to provide roll control. The rear booms also serve as a mounting for the fixed solar vanes, which are optional and are used only in one control concept. The vanes would be in a forward folded position initially and would be permanently locked in the extended position after the spacecraft is separated from the booster. When provided, the reaction wheels would be located inside the spacecraft body.

The weight and moments of inertia for the configuration without solar vanes are estimated to be as follows:

Weight = 900 lbs

I_{ROLL} = 140 slug-ft^2

$I_{PITCH/YAW}$ = 120 slug-ft^2

The boom-mounted RTG units account for the major portion of the moments of inertia although they constitute only about a quarter of the total mass. The major part of the spacecraft mass is concentrated in the central body near the center of gravity. In general, it is favorable to obtain the largest possible moment of inertia as a design objective.

The solar vane size was determined on the basis of the largest practical size that could be accommodated on the configuration. It was estimated that a vane of this type could be constructed for a weight of about 0.6 pound per square foot. For the indicated size of 24 square feet, each vane would thus weigh about 15 pounds so that the total vane weight is about 60 pounds. With the addition of these vanes, the total weight and inertia become as follows:

Weight = 960 lbs

I_{ROLL} = 210 slug-ft^2

$I_{PITCH/YAW}$ = 215 slug-ft^2

Thus, although the weight is increased only about 7 percent, the roll inertia is increased about 50 percent and the pitch/yaw inertia is increased about 80 percent. The implications of this large inertia change are very significant in assessing the net penalty associated with the solar vane approach; and to overlook it leads to misleading results, as will be seen.

3.5.8.2 Gas Jet Approach

In this case, the gas jet system is the only means of control, and it is to be operated for the entire mission, starting at booster separation. Its basic mode of operation will be limit cycling,

and it represents an application of the Mariner IV control concept to a mission of longer duration.

The disturbance torques caused by solar radiation pressure will be small and due mostly to the asymmetry caused by antenna deflections. These torques pose no problem to the gas jet system, and they will be lost in the limit cycle impulse. The most important source of external disturbance torque to this system will be discrete meteoroid impacts, as described in paragraph 3.5.4. The problem of gas leakage must be reckoned with, but it is not indicated to be a serious problem insofar as fuel depletion or disturbance torques are concerned. However, the trajectory perturbations associated with gas leakage may be objectionable, and they can seriously affect the scientific value of the trajectory data insofar as the definition of environmental anamolies is concerned.

The basic design criterion for this system is the torque requirement to counteract the effect of a discrete meteoroid impact, but the approach must be somewhat arbitrary at present because of the uncertainty surrounding the meteoroid problem. As a preliminary estimate, a meteoroid mass of 1/10 gram at a moment arm of 3.0 feet is selected for design purposes. This case corresponds to a sudden angular impulse (H_M) of about 1.0 foot-pound-seconds according to Figure 3.5-9. The allowable excursion in attitude angle (θ_F) is chosen as 2.0 degrees. This criteria results in the following maximum torque requirement:

$$T_{MAX} = \frac{(H_M)^2}{(2)\ (I)\ (\theta_F)} =$$

$$\frac{(1.0)^2}{(2)\ (120)\ (0.0349)} = 0.12 \text{ ft-lbs}$$

It should be noted that this result varies with the square of H_M and is therefore sensitive to the particular assumptions made for meteoroid impulse. Therefore, the criterion should be regarded as somewhat flexible and subject to future modification.

The above requirement effectively sets the thrust level of the attitude control jets since the moment arm has been defined previously. However, the net result depends on the type of mechanization used in the pulse controller. It is possible to design the system so that the thruster valves are held open to provide continuous thrust when maximum torque is commanded. It is also possible that maximum torque will correspond to maximum pulse rate (i.e., minimum spacing between successive unit pulses) so that the discontinuous operation of the gas jets will reduce the effective thrust level. For present purposes, the latter case will be chosen in order to provide a conservative result. It is assumed that the interval between successive pulses is twice the pulse width so that the maximum torque is given as follows, by using the terminology of Figure 3.5-10:

$$T_{MAX} = \frac{1}{3} (F) (\ell)$$

$$\text{or } F = \left(\frac{3}{\ell}\right) T_{MAX}$$

By using the values for T_{MAX} and ℓ presented previously, the following value of F is obtained:

$$F = \frac{(3)(.12)}{(7.0)} = 0.05 \text{ lbs}$$

This thrust level is well above the minimum value attainable for a stored gas system. A reduction in thrust level is desirable to reduce the limit cycle fuel requirements and to improve the system reliability by lengthening the pulse spacing, but it compromises the system performance capability.

For the above thrust level, together with the minimum value of pulse width, the characteristics of the unit pulse become:

$$\Delta t = \text{Pulse Width} = 0.02 \text{ sec}$$

$$\Delta I = \text{Unit Pulse} = (F) (\Delta t) = 0.0010 \text{ lb-sec}$$

The fuel requirements for the system are defined primarily by the three-axis limit cycle, since maneuvering requirements and external torque requirements are negligible in comparison. The values of deadband angle and limit cycle time period were assumed to be:

θ_E = Deadband Angle = 0.5 degrees = 0.00873 Radians

P = Limit-cycle Time Period = 600 Days = 5.2×10^7 Sec

This value of deadband angle should be adequate to meet the expected pointing accuracy requirements and is well within the capabilities of typical sensors. The time period is simply the duration of the nominal mission. With this data, the characteristics of the limit cycle about each axis are computed by using the formulas presented in Figure 3.5-10, and the results are shown here in tabular form:

CONTROL AXIS	$\dot{\theta}_E$ (Deg/Minute)	t_1 (Minutes)	Impulse (lb-sec)
ROLL	.086	11.6	150
PITCH/YAW	.100	10.0	175

The total impulse required to sustain the three-axis limit cycle is thus determined as follows:

$$\text{LIMIT-CYCLE IMPULSE} = (1.5) [150 + (2) (175)] = 750 \text{ lb-sec}$$

The weight requirement for a stored gas system of this total impulse is obtained from Figure 3.6-10 for the hardware arrangement identified as Configuration B. This weight is found to be about 95 pounds, which includes gas, tankage, and hardware components. This system contains twice the amount of fuel necessary to meet the specified impulse and includes a redundant set of jet nozzles.

3.5.8.3 Reaction Wheel Approach

In this case, a reaction wheel system is the primary means of control during the long interplanetary cruise phase. A back-up gas jet system is to be provided also, and it functions during the vernier injection and planetary encounter phases and during emergency conditions when the capability of the reaction wheel system is exceeded. The reaction wheel size is chosen so that desaturation will not normally be required prior to encounter. Thus, the back-up gas jet system may be kept off to prevent gas leakage problems.

This approach is more sensitive to the effects of solar unbalance torques because the angular momentum introduced through this means must be stored in the reaction wheel. The problem of wheel saturation is to be avoided. This problem was previously analyzed in paragraph 3.5.4 for the case of a fixed antenna, Earth-pointing spacecraft. That case is more critical than the steerable antenna, Sun-pointing concept which is presently favored. However, since both cases are still regarded as definite possibilities, the latter is used as a conservative design estimate. If an effective area, A, of 20 square feet (corresponding to a 5 foot sphere) and an offset distance, $\overline{X}$, of 0.50 feet are assumed, the value of H_S indicated by Figure 3.5-8 is about 3.0 foot-pound-seconds. This angular impulse is only a third of that created by a meteoroid impact of the magnitude described earlier. For present design purposes, it is assumed that the reaction wheel should be capable of absorbing one meteoroid impact in addition to the solar disturbance. The required momentum storage capacity of the wheel is therefore:

$$H_{WHEEL} = H_S + H_M = 3.0 + 1.0 = 4.0 \text{ ft-lb-sec}$$

A wheel of this size weighs approximately 14 pounds, according to the data presented in Figure 3.5-11. The weight of a three-axis reaction wheel system, consisting of three wheels, plus associated electronics, is thus given as follows:

$$\text{Reaction Wheel System Weight} = (3) \quad [14 + 3] = 51 \text{ lbs}$$

It is desired that the back-up gas jet system be capable of handling the mission in the event the reaction wheel system fails; consequently, its design is subject to the same criterion previously described in paragraph 3.5.8.2. However, an important difference is that no redundancy in the system components or gas supply is now allowed since the reaction wheel system is regarded as a replacement

for this redundancy. The result of this philosophy is a significant reduction in the weight requirement for the gas jet system from that indicated previously. The back-up gas jet system is thus defined by the Configuration A curve in Figure 3.6-10, and a system weight of 45 pounds is obtained for the required impulse of 750 pound-seconds. Thus, the total weight of the reaction wheel/gas jet system is given as follows:

Total System Weight = 51 + 45 = 96 lbs

This result is almost identical to that obtained previously for the approach based on the use of gas jets only. Actually, a small weight advantage can be shown for either case by reasonable adjustments of the various parameters involved in the analysis. This condition merely means that weight should be eliminated as a basis for comparison of the two approaches.

The power required to operate the reaction wheel system is larger than that required for the gas jet system. The reaction wheel power varies directly with torque output, and peak power corresponds to peak torque. The power required to realize the peak torque output of 0.12 foot-pound (previously calculated in paragraph 3.5.8.2) is obtained from Figure 3.5-11 and is about 45 watts. However, this power is only required infrequently, and it will always be of short duration (30 to 40 seconds). The average operating power for the system is much less than the peak requirement and is dependent upon design details of the system, such as motor type, bearing friction, windage, etc. A figure of 12 watts is believed to be adequate for the three-axis, reaction wheel/gas jet control system.

3.5.8.4 Solar Vane Approach

In this case, consideration is given to the addition of fixed solar vanes to the reaction wheel/gas jet system described above. However, the presence of the vanes allows certain modifications of both the reaction wheel and gas jet systems, and these modifications tend to alleviate the weight penalty of the vanes themselves. This approach is limited to the case of a steerable antenna since the spacecraft axis of symmetry must be maintained in a near Sun-pointing attitude for the solar vanes to function properly. Variations in the precise trim point (attitude for zero solar torque) caused by antenna deflections or small asymmetries can be compensated for by the control logic.

Since the solar vanes function to accomplish continuous desaturation of the reaction wheels, the momentum storage requirements for the wheels can be relaxed. The basic requirement now is merely to absorb the effect of a meteoroid impact, which was previously set at 1.0 foot-pound-seconds. A wheel of this size weighs about 7 pounds, according to the data shown in Figure 3.5-11. Thus, the weight of the three-axis reaction wheel system becomes as follows:

Reaction Wheel System Weight = (3) [7 + 3] = 30 lbs

The modified values of moment of inertia must now be included in the calculations for sizing the gas jet system. First of all, the maximum torque requirement (T_{MAX}) discussed in paragraph 3.5.8.2 is seen to be reduced in direct proportion to inertia. The modified result is as follows:

$$T_{MAX} = (0.12)\left(\frac{120}{210}\right) = 0.07 \text{ ft-lbs}$$

This result allows a reduction in the thrust level from 0.05 pound to 0.03 pound, with a corresponding reduction in the unit pulse. By accounting for this effect, together with the modified moments of inertia, the limit-cycle calculations now yield the data shown here in tabular form:

CONTROL AXIS	$\dot{\theta}_E$ (Deg/Min)	t_1 (Minutes)	Impulse (Lb-Sec)
Roll	.0344	29.1	36
Pitch/Yaw	.0336	29.8	35

Thus, the total impulse requirement now becomes

$$\text{Limit Cycle Impulse} = (1.5)\left[36 + 2(35)\right] = 210 \text{ lb-sec}$$

This result represents a significant change from the previous figure of 750 pound-seconds, and it indicates the sensitivity of the problem to effects that might easily be overlooked. Actually, the above results must be adjusted somewhat because the value of pulse spacing, t_1, is now unrealistically large. An upper limit of about 20 minutes must be placed on t_1 to account for practical mechanization problems. One way of effecting the desired change is to reduce the value of deadband angle. Another way is to increase the thrust level so that a greater maximum torque capability is obtained. In any event, the net result is an increase in the limit-cycle impulse requirement to about 300 pound-seconds. The weight requirement for a system of this size of the Configuration A type is indicated by Figure 3.6-10 to be about 25 pounds.

The total weight of the attitude control system for this case is the sum of the weights of the solar vanes, reaction wheel system, and back-up gas jet system. By using the figures presented above, the system weight is found to be

Total System Weight = 60 + 30 + 25 = 115 lbs

This result is only about 20 pounds above the figure obtained for the other two approaches to attitude control. Also, because of the

reduction in maximum torque capability caused by the increased moment of inertia, the power requirements for the reaction wheel system are now reduced. The peak power requirement corresponding to a T_{MAX} of 0.07 foot-pounds is about 30 watts, compared to the earlier figure of 45 watts.

It should be noted that the reaction wheel size and solar vane size used above were determined independently by the application of separate criteria, and no consideration was given to the dynamic response characteristics of the combined system. Preliminary studies of this problem indicate that better results would be obtained if the reaction wheel size and power could be reduced somewhat to be more compatible with the degree of solar stability provided. This modification further reduces the weight and power requirements for the system, but some of the momentum storage capability of the wheel is sacrificed. An alternate approach is to increase the vane size, but this parameter is already near its practical upper limit.

3.5.8.5 Summary of Results

The previous analysis of the example case serves to illustrate the relative merits of the various approaches from the standpoint of weight and power requirements. These results may be summarized in tabular form as follows:

Type of System	System Weight (lbs)	Power Requirements (watts)	
		Peak	Continuous
Gas Jets	95	-	3
Reaction Wheels + Gas Jets	96	45	12
Solar Vanes + Reaction Wheels + Gas Jets	115	30	6

These figures do not include the basic attitude control electronics (except the increment required for the reaction wheels) or the sensors, since these are considered as part of the spacecraft control system and are common to all approaches. The figures for continuous power are estimates of the requirements for operating the jet thrusters and reaction wheels themselves, and they do not include the functions accomplished by the spacecraft control system.

3.5.9 Conclusions

When the above results are considered, together with the reliability comparisons presented in subsection 3.13, the gas jet system is seen to be the preferable control concept. For this reason, it is proposed for use on all three-axis stabilized design concepts presented herein.

The reaction wheel system is not out of the question, however, and it should not be categorically eliminated until more precise comparisons are made. The primary disadvantage of the reaction wheel system is the low reliability presently predicted for it. However, current research indicates that modified control techniques can result in improved reliability. These techniques are analogous to the limit-cycle approach employed for the gas jet system; their use should therefore result in improved reliability. Progress in this field should be followed closely before final conclusions are drawn. Also, there is a need to develop better methods for predicting the effect of variations of wheel speed, control technique, and other factors upon the reliability assessments of the reaction wheel.

The solar vane system also deserves further consideration although it is apparently marginal for the case of a Jupiter mission. It is perhaps more applicable for missions to Venus and Mercury. The level of solar torque is a little lower than would be desired along a Jupiter transfer trajectory.

3.6 PROPULSION

Two propulsion subsystems, one to perform midcourse correction and another for attitude control, are required to perform Jupiter flyby missions. Candidate subsystems have been investigated and the findings are reported herein.

3.6.1 Midcourse Propulsion Subsystem

The functional requirements of a Jupiter flyby spacecraft midcourse propulsion subsystem are similar in most respects to the functional requirements for the Mariner IV midcourse propulsion subsystem. Like its Mariner predecessor, the Jupiter flyby propulsion subsystem must be capable of providing (1) a desired velocity increment to the vehicle, and (2) two controlled-interval thrusts. The unit must be capable of repeatable ignition, operation, and shutdown in a hard vacuum and gravity-free environment, and meet space storage requirements with regard to materials compatibility, propellant stability, negligible fluids leakage, and avoidance of vacuum cold welding of movable component parts. In addition, it must be capable of maintaining proper orientation of the thrust vector during a propulsion maneuver so that trajectory errors arising from the maneuver itself are held to a minimum.

Several types of propulsion systems are theoretically capable of satisfying the functional requirements of the Jupiter flyby midcourse maneuver. Such types might be broadly categorized according to their primary energy source as electrical, nuclear, or chemical. Within each of these major categories, a great number of propulsion options exists. Typical electrical systems include the electrostatic (ion) engine, electrothermal (arcjet or resistojet) engine, and the electromagnetic (plasma) engine. Nuclear systems can be of the nuclear reactor or radioisotope-heated type. In the chemical category, optional systems include the cold gas, mono-, bi- and tri-propellant, hybrid, hypergolic subliming solids, and thixotropic gel systems.

Each of the above systems has its own peculiar advantages and disadvantages, and each has been evaluated on the basis of its applicability to the Jupiter flyby midcourse maneuver. The conclusion of this evaluation is that on the basis of current development status, proven performance, power required, simplicity, and cost, the monopropellant hydrazine and Earth-storable liquid bipropellant systems are the most suitable. Of these two systems, the monopropellant hydrazine unit is clearly superior both in

weight and simplicity for applications where the spacecraft mass is low and the velocity increments required are small. For applications where larger total impulses are involved, a bipropellant system offers potential weight and volume savings, but compromises simplicity. In comparing the weight of the two systems, it is interesting to note that the hydrazine propulsion systems aboard all Mariner and Ranger vehicles have, in each case, weighed less than 10 percent of the total payload. Viewed in this context, it is reasonable to inquire whether the weight savings obtained by the use of a bipropellant system can ever be justified in comparable Jupiter flyby vehicles when the overall reliability is impaired as a result. Although no intensive investigation of a bipropellant system has been performed in this study, recent comparisons at four selected design points between a conservative bipropellant unit (using IRFNA and MMH) and a hydrazine unit substantiate the marginal weight advantage and increased complexity characteristics of the bipropellant unit. A hydrazine propulsion system is therefore recommended for trajectory correction of all Jupiter flyby vehicles described in this report.

At this point, investigation of a basic gas-pressure-regulated hydrazine system is complete. A system configuration has been defined, analyses have been performed, and system sizing data have been generated. These efforts are reported in the subsections which follow.

3.6.1.1 Description of the Basic Hydrazine Subsystem

The basic hydrazine configuration described herein is shown schematically in Figure 3.6-1 together with an itemized listing of pertinent components and instrumentation. The configuration shown is based largely on the successful Mariner IV design with some notable exceptions discussed on the following pages.

The basic subsystem is a prepressurized, gas-pressure-regulated, constant-thrust device employing nitrogen as the pressurant and hydrazine as the propellant. During operation of the basic subsystem, nitrogen passes through a pressure regulator and displaces propellant from the propellant tank by the deformation of a Butyl rubber bladder. The hydrazine flows to the rocket motor where it is decomposed spontaneously into thrust gases upon contact with a Shell 405-type catalyst mounted in the chamber. Use of the Shell catalyst obviates the need for a hypergolic start slug (such as nitrogen tetroxide) and thereby eliminates the need for a slug control valve, storage tank, and supporting flow and sequencing circuitry.

SCHEMATIC DIAGRAM OF THE BASIC HYDRAZINE SUBSYSTEM

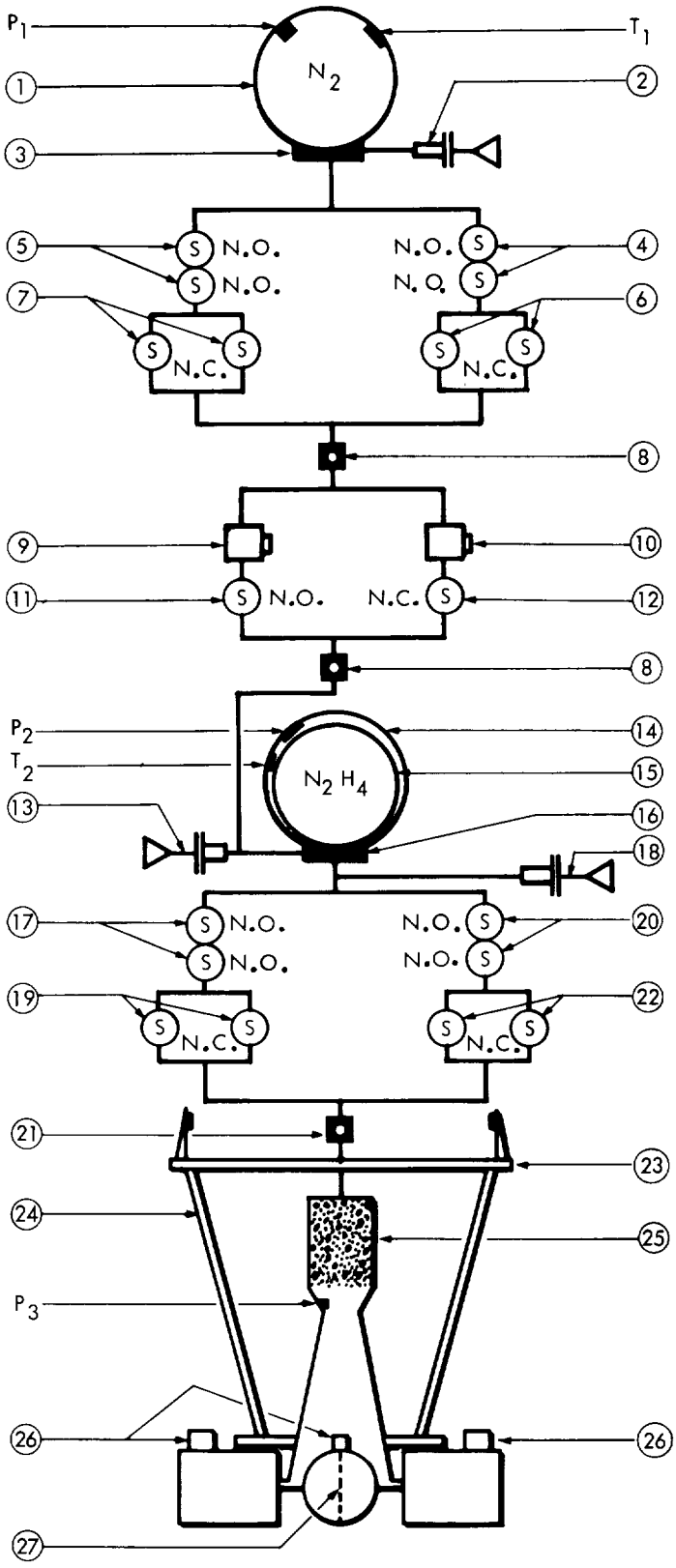

COMPONENTS

1	High pressure gas reservoir
2	N_2 fill port and closure valve
3	High pressur e reservoir manifold
4	N.O. squib valve, N_2 shutdown No. 2
5	N.O. squib valve, N_2 shutdown No. 1
6	N.C. squib valve, N_2 start No. 2
7	N.C. squib valve, N_2 start No. 1
8	Filter
9	Pressure regulator, primary
10	Pressure regulator, secondary
11	N.O. squib valve, primary reg. close
12	N.C. squib valve, secondary reg. start
13	Propellant prepressure, fill port
14	Propellant tank
15	Propellant bladder
16	Propellant tank manifold
17	N.O. squib valve, prop. shutdown No. 1
18	Propellant fill and drain port
19	N.C. squib valve, prop. start No. 1
20	N.O. squib valve, prop. shutdown No. 2
21	Filter
22	N.C. squib valve, prop. start No. 2
23	Thrust plate & tank support structure
24	Jet vane actuator support structure
25	Rocket motor and catalyst bed
26	Jet vane actuators (4)
27	Jet vanes (4)

INSTRUMENTATION

P_1	Nitrogen tank pressure
P_2	Propellant tank pressure
P_3	Thrust chamber pressure
T_1	Nitrogen tank temperature
T_2	Propellant tank temperature

FIGURE 3.6-1

In typical operation of the subsystem, the sequence of events involved in the initial rocket firing would be as follows (valve numbers coincide with those shown in Figure 3.6-1):

1. Upon the receipt of a start signal from the onboard computer, the normally closed, explosively actuated dual squib valves (7) and (19) are simultaneously activated, resulting in regulated pressurization of the hydrazine tank and a flow of hydrazine to the thrust chamber.

2. Catalytic decomposition of the hydrazine takes place in the chamber, and thrust is produced.

3. At a signal from the onboard computer to terminate rocket thrust, the normally open, explosively actuated dual squib valves (5) and (17) are simultaneously activated, resulting in isolation of the high pressure gas reservoir from the primary pressure regulator (9) and termination of propellant flow to the thrust chamber.

Should a second propulsion maneuver be required, the sequence of events if functionally the same. In this case, the normally closed dual squib valves (6) and (22) are activated in order to start thrusting, and the normally open dual squib valves (4) and (20) are activated to terminate thrust.

It should be noted that because the propellant tank is prepressurized only one start signal is required to commence the first maneuver. This signal activates valves (7) and (19) simultaneously, and the result is an almost immediate production of nominal thrust.

If the tank were not prepressurized, sequencing would be required to allow for regulator flow to increase the pressure in the tank up to the working level before the propellant start valve could be activated.

Provision is made in the basic design for two controlled-interval thrusts. This is accomplished by the inclusion of two full-on, full-off flow control channels in both the propellant pressurization and propellant feed subsystems. For each thrust application (start and shutdown), eight squib valves in redundant arrangements must be activated - four to accomplish engine start and four to accomplish engine shutdown.

The most significant difference between the Mariner IV midcourse propulsion system and the presently proposed Jupiter flyby design lies in the means employed to initiate hydrazine decomposition. In the basic subsystem presented here, the spontaneous Shell hydrazine catalyst is used in lieu of the JPL-type H-7 catalyst used on Ranger and Mariner. Use of the Shell catalyst eliminates the cumbersome start apparatus associated with the Ranger and Mariner systems, provides simplicity of operation, and results in a small reduction in system weight.

Additional differences between the basic propulsion system design and that of Mariner IV take the form of the following:

1. A redundant pressure regulator (10) (see Figure 3.6-1) and squib valves (11) and (12) are incorporated in the pressurization subsystem. The squib valves are used to transfer nitrogen gas regulation from the primary regulator (9) to regulator (10) in the event of primary regulator malfunction. Switch over is accomplished by a failure detection and implementation system driven by a signal voltage from the propellant tank pressure transducer.

2. Dual-redundant squib valves are incorporated in the propellant pressurization and propellant feed subsystems.

The use of dual-redundant squib valves in the subsystem now proposed is an outgrowth of a reliability analysis reported in subsection 3.13. Another possible configuration was initially considered in which the normally open and normally-closed squib valves were arranged in series within each of two parallel branches. Each branch was delegated to perform a separate propulsion maneuver, and the design implication at that time was that redundancy was provided for a first propulsion maneuver by the existence of a second manuever capability. Implied, of course, was the coexistence of a failure detection system which could accomplish automatic switchover from one valve branch to another in the event of a critical valve failure. The reliability of this arrangement consisting of the in-line squib valves combined with a failure detection and implementation system has been compared with the reliability of the arrangement consisting of dual-redundant valves which has no failure detection and implementation system. To accomplish this, a model of the failure detection apparatus which consistsof a pressure transducer, solid state switch, and power supply, was constructed. In typical operation, a threshold pressure (indicative of malfunction) is converted to transducer output

voltage which actuates the switch and causes current from the power supply to activate a backup squib. Representative failure rate data were used and the results, reported in subsection 3.13, support the selection of the dual-redundant valve arrangement with no failure detection provision. The use of dual-redundant squib valves, backed up by a failure detection system, was considered, but was rejected as an unnecessary complication.

A similar analysis was directed to comparing the reliability of a single pressure regulator scheme to that of redundant pressure regulators with a failure detection and switchover capability. The failure detection apparatus in this case was essentially the same as that described in the previous paragraph. Results of this analysis, also reported in subsection 3.13, indicate that the redundant regulator scheme with failure detection is more reliable than the single regulator scheme. This conclusion is qualified by the following comments.

In the analysis, regulator failure was interpreted to mean either a too-high or too-low regulated pressure condition. In the former condition, limited ullage volume and excessive regulator inflow could result in an overpressure condition, leading to tank rupture. In the second condition, limited ullage volume accompanied by low regulator inflow could result in propellant expulsion via a semi-blowdown method, with the attendant probability that chamber pressure would ultimately fall below a minimum level required for safe operation.

In light of the subsystem configuration depicted in Figure 3.6-1, both regulator malfunctions are potentially critical, and the use of a redundant regulator network appears warranted. It is significant to note, however, that by increasing the tank ullage volume, the probability of subsystem failure due to regulator malfunction would be greatly diminished. By so doing, the subsystem configuration as shown would approach the functional and dimensional character of an internally pressurized or blowdown system. The logical extension of this tactic, if it is feasible, would be the outright adoption of a nonregulated blowdown system and the elimination of an external pressure bottle, associated valving, and regulator. From the standpoint of reliability at least, the blowdown system is superior to the constant-gas-pressure regulated system, and it is somewhat lighter in weight. The primary objections to the blowdown system as compared to the pressure-regulated system arise from its increased envelope (for the same total impulse) and the occurrence of a decaying thrust level. This last objection, if serious enough, may be overcome by use of a liquid regulator in

the propellant feed circuit with a corresponding penalty in reliability and a slight increase in overall system weight.

The decision to use constant gas-pressure-regulation was made early in the study and was prompted mainly by the fact that this technique (1) enjoys a high state of development, (2) is applicable to both accelerometer and burn timer shutoff mechanisms, and (3) has been used with considerable success on both the Mariner and Ranger propulsion units. Moreover, it was felt that a subsystem of this type would provide a logical and conservative point of departure for future optimization and trade-off studies based on the detailed analysis of alternate pressurization techniques. Such studies should be directed to the analysis of hydrazine systems characterized by nonregulated blowdown pressurization, gas generator pressurization, and blowdown pressurization with liquid flow regulation.

A weight breakdown of the fixed hardware in the basic hydrazine subsystem is presented in Table 3.6-1. The term "fixed hardware" comprises those components whose weights are not drastically altered by changes in the total impulse required. Stated differently, the weight of a fixed hardware component is considered essentially constant for a given thrust level or for a particular design parameter such as operating pressure, line size, or rate of flow. The constituents of the subsystem whose weights are not fixed but vary with total impulse include the propellant, pressurant, bladder, and all tankage.

By using this technique of isolating subsystem elements into either fixed hardware or total impulse-variant categories, the subsystem sizing effort presented in the next paragraphs is greatly simplified. Weight estimates of all fixed hardware contained herein are obtained from in-house and Mariner IV experience and manufacturers' published data.

3.6.1.2 Parametric Analysis

A detailed parametric analysis of the monopropellant hydrazine subsystem is presented in Appendix D. This analysis forms the basis for the propulsion subsystem weight and volume data which are presented in subsection 3.6.1.3. Table 3.6-2 contains the nomenclature to be used and a summary of the primary equations that are developed in Appendix D.

Table 3.6-1 WEIGHT BREAKDOWN OF SUBSYSTEM FIXED HARDWARE

Item	Estimated Weight - lb
Nitrogen fill port and closure valve	0.10
High pressure reservoir manifold	0.50
Squib valves, nitrogen shutdown, No. 2	0.26
Squib valves, nitrogen shutdown, No. 1	0.26
Squib valves, nitrogen start, No. 2	0.26
Squib valves, nitrogen start, No. 1	0.26
Filter (2)	0.20
Pressure regulator, primary	1.20
Pressure regulator, secondary	1.20
Squib valve, primary regulator shutdown	0.13
Squib valve, secondary regulator start	0.13
Prepressurization fill port	0.10
Propellant tank manifold	1.10
Squib valves propellant shutdown, No. 1	0.26
Propellant fill and drain port	0.10
Squib valves, propellant start, No. 1	0.26
Squib valves, propellant shutdown, No. 2	0.26
Filter	0.15
Squib valves, propellant start, No. 2	0.26
Thrust plate and tank support structure	3.70
Jet vane actuator support structure	0.80
Rocket motor and catalyst bed	2.50
Jet vane actuators (4)	2.10
Jet vanes (4)	0.20
Cabling	2.10
Misc. mounting brackets, fasteners, etc.	1.30
Pressure (3) and temperature (2) transducers	1.15
Total Weight	20.84

Table 3.6-2 MIDCOURSE CORRECTION PROPULSION SUBSYSTEM - NOMENCLATURE AND EQUATION SUMMARY

Nomenclature

Symbol	Description	Units
W_{system}	Total weight of the subsystem	lb_m
W_H	Total weight of hydrazine required	lb_m
W_{H_1}	Expected hydrazine consumption	lb_m
W_{H_2}	Hydrazine contingency for I_{sp} degradation	lb_m
W_{H_3}	Hydrazine contingency for ΔV reserve	lb_m
W_{H_4}	Hydrazine contingency for bladder expulsion inefficiency	lb_m
$W_{S/C}$	Total weight of the spacecraft	lb_m
W_{H_T}	Weight of hydrazine tank	lb_m
W_{ACC}	Weight of tank accessories (welds, bosses, etc.)	lb_m
W_{weld}	Weight due to weldment	lb_m
W_{PG}	Weight of pressurant gas	lb_m
W_{PG_T}	Weight of pressurant gas tank	lb_m
W_B	Weight of expulsion bladder	lb_m
W_{COM}	Total weight of fixed hardware (i.e., valves, regulators, tubing, etc.)	lb_m
W_{PL}	Weight of nonpropulsive payload	lb_m
I_T	Total impulse required	$lb_f.sec$
I_{SP}	Specific impulse	$lb_f.sec/lb_m$
ΔV	Velocity increment required	ft/sec
g	Gravitational constant	$lb_m.ft/lb_f.sec^2$
α_H	Contingency factor for I_{SP} degradation	--
$(\frac{\delta\Delta V}{\Delta V})$	Contingency factor for ΔV reserve	--
ϵ	Bladder expulsion efficiency	--
P_D	Hydrazine or pressurant tank design pressure (at maximum anticipated temperature)	$lb_f/in.^2$
P_{PPG}	Initial pressure of the prepressurant gas in the hydrazine tank	$lb_f/in.^2$
P_T	Hydrazine tank working pressure	$lb_f/in.^2$
P_{PG_i}	Initial storage pressure of pressurant gas	$lb_f/in.^2$
P_{PG_f}	Final storage pressure of pressurant gas	$lb_f/in.^2$
V_H	Hydrazine volume (at 70°F)	$in.^3$
V_{H_T}	Hydrazine tank volume	$in.^3$
V_{UL}	Ullage volume	$in.^3$
V_B	Bladder material volume	in.
V_{PG}	Pressurant gas volume	$in.^3$
ΔV_{EXP}	Change in hydrazine volume due to thermal expansion	$in.^3/lb_m$
Δv	Change in hydrazine specific volume due to thermal expansion (to max. temp.)	$in.^3/lb_m$

Symbol	Description	Units
v_o	Hydrazine specific volume (at 70°F)	$in.^3/lb_m$
χ	Ullage factor = $\frac{V_{UL}}{V_H}$	--
(S.F.)	Design safety factor	--
T_{max}	Maximum anticipated temperature	°R
T_o	Initial temperature	°R
ρH	Hydrazine density (at 70°F)	$lb_m/in.^3$
ρmat	Density of tank material	$lb_m/in.^3$
ρB	Density of bladder material	$lb_m/in.^3$
σmat	Ultimate tensile strength of material	$lb_f/in.^2$
t_T	Nominal tank wall thickness	in.
t_W	Maximum thickness of weld buildup	in.
t_B	Bladder material thickness	in.
K_1	Arbitrary constant	--
θ	Taper angle of weld buildup	deg
ω	Width of weld buildup section	in.
D_B	Bladder diameter	in.
D	Tank diameter	in.
R	Pressurant gas constant	in. lb_f/lb_m °R
k	Ratio of specific heats of pressurant gas	--

Equation Summary

(1) $W_{System} = W_H + W_{H_T} + W_{PG} + W_{PG_T} + W_{COM} + W_B$

(2) $W_H = \frac{W_{S/C}}{\epsilon}\left[1 - e^{\frac{-\Delta V}{I_{SP_g}}}\right]\left\{1 + \alpha_H + \left(\frac{\delta\Delta V}{\Delta V}\right)\frac{\left(\frac{\Delta V}{I_{SP\ g}}\right)}{\left(e^{\frac{\Delta V}{I_{SP_{g_{-1}}}}}\right)}\right\}$

(11) $W_{H_T} = 1.5P_{PPG}\left(\frac{T_{MAX}}{T_o}\right)\left(\frac{\rho}{\sigma}\right)_{MAT}(S.F.)V_H\left\{\frac{1.02 + \chi}{1-\left(\frac{\Delta v}{v_o}\right)\frac{1}{\chi}}\right\}\left[1+\frac{22.7(S.F.)P_{PPG}\ T_{MAX}}{\left\{1-\left(\frac{\Delta v}{v_o}\right)\frac{1}{\chi}\right\}\ T_o\ \sigma_{MAT}}\right] + 0.35$

(12) $W_{PG} = \frac{P_T\ W_H}{RT_o\ \rho H}\left[\frac{k}{1 - (P_{PG_f}/P_{PG_i})}\right]$

(14) $W_{PG_T} = 1.5W_{PG}RT_{MAX}\left(\frac{\rho}{\sigma}\right)_{MAT}(S.F.)\left[1 + \frac{8.5(S.F.)P_{PG_i}\ T_{MAX}}{T_o\ \sigma_{MAT}}\right]+0.35$

(16) $W_B = 44.3(W_H)^{0.667}\ t_B\ \rho_B$

$W_{COM} = 20.84\ lb_m$

3.6.1.3 Subsystem Parametric Sizing

Parametric sizing of the basic hydrazine subsystem was undertaken to accomplish two main objectives: (1) to provide immediate support for spacecraft weight, packaging, and conceptual design studies and (2) to provide a format for the comparison of the basic hydrazine subsystem with any alternative propulsion concepts.

Sizing of the basic hydrazine subsystem proceeded in three discrete steps from the equations presented in subsection 3.6.1.2. First, a required weight of hydrazine was postulated, and, from the appropriate equations, the estimated weight of subsystem fixed hardware, and pertinent design data, a corresponding total subsystem weight was derived. This procedure was repeated for several values of required hydrazine weight and the results are depicted in the graphical plot in Figure 3.6-2. Appropriate equations and design data were treated in a similar manner to obtain the tank size information presented graphically in Figure 3.6-3.

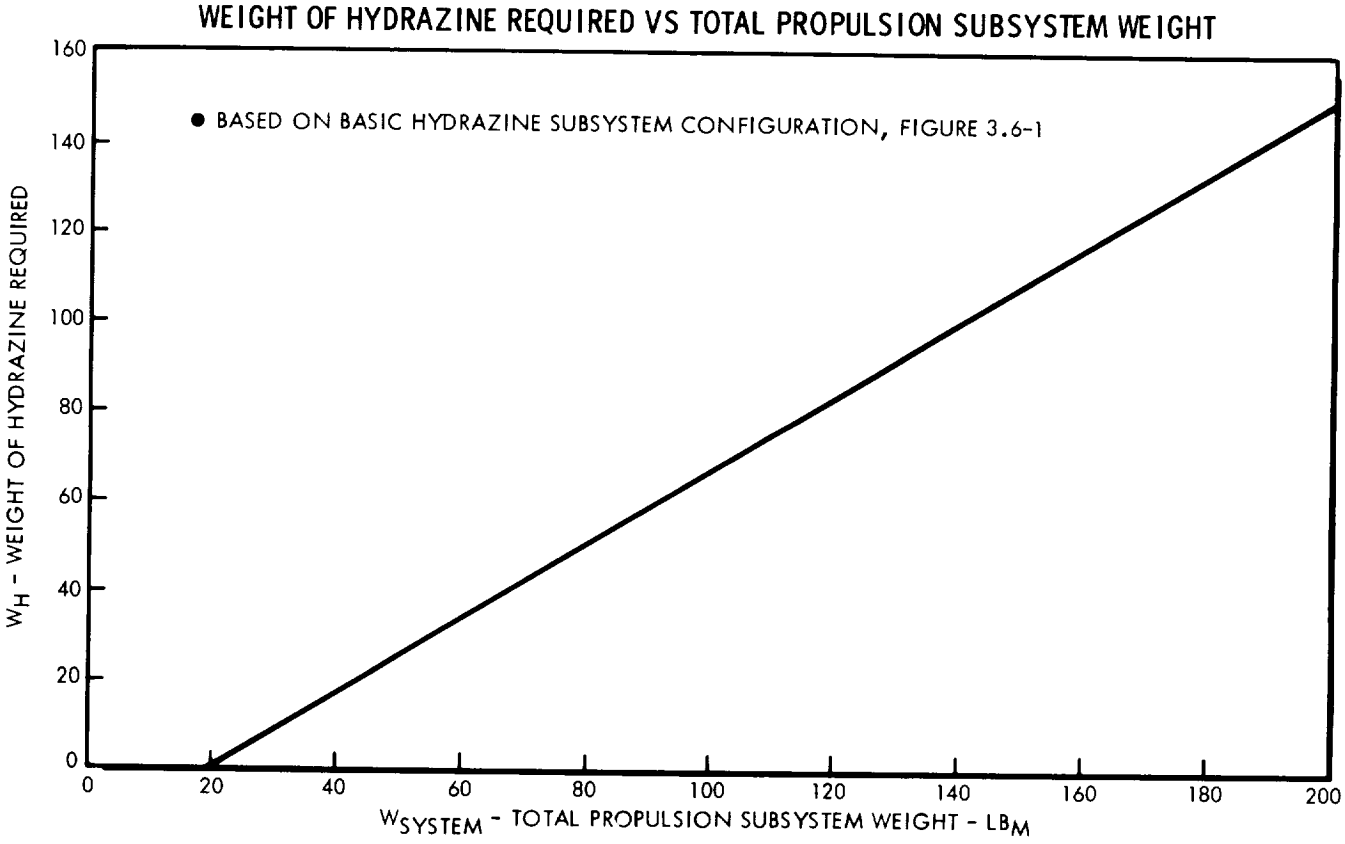

FIGURE 3.6-2

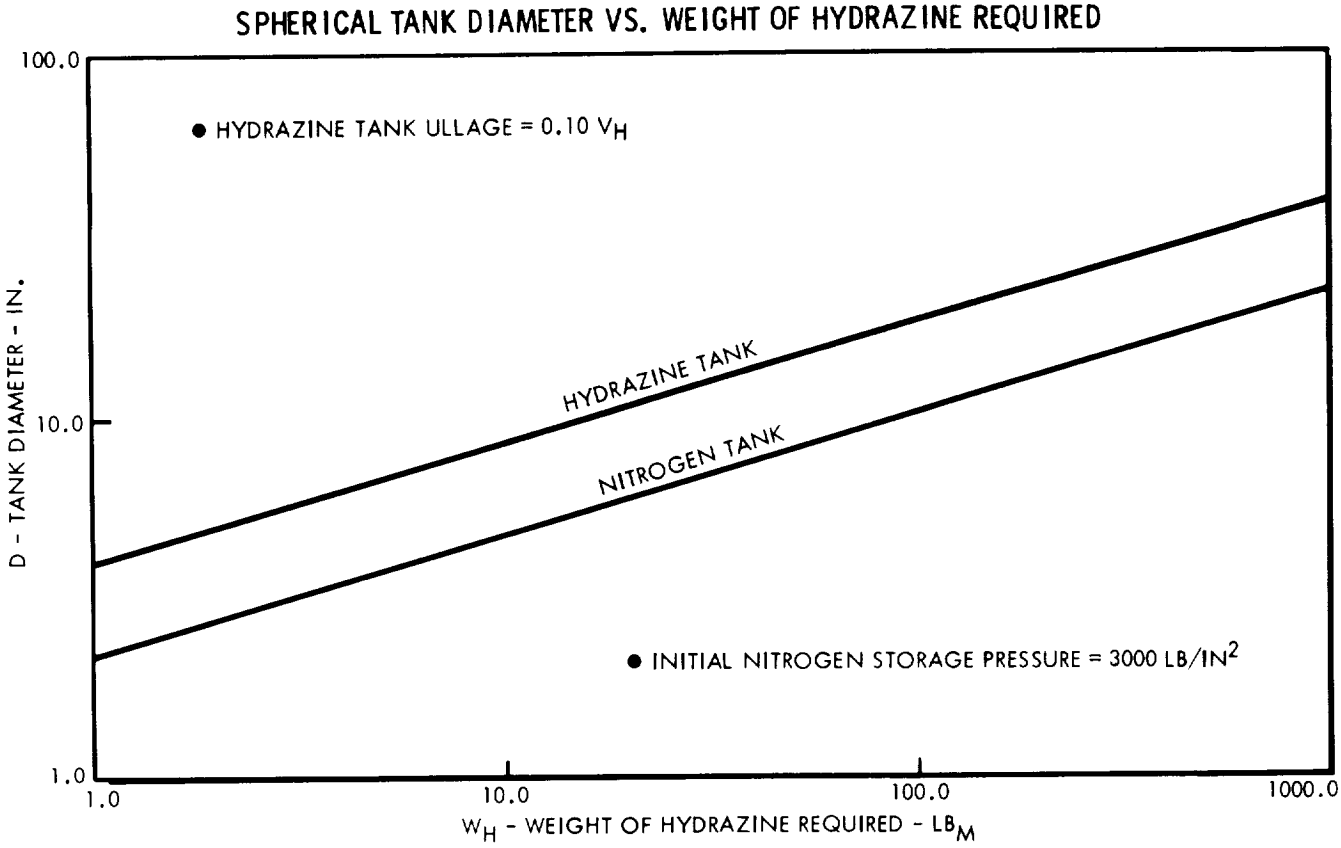

FIGURE 3.6-3

As the second step in sizing the hydrazine subsystem, the equation expressing the ratio of required hydrazine weight to total spacecraft weight was solved for a series of total velocity increments ranging from 100 to 500 feet per second. This equation, identified as equation (2) in the earlier analysis, is rewritten below.

$$\frac{W_H}{W_{S/C}} = \frac{1}{\epsilon}\left[1 - e^{\frac{-\Delta V}{I_{SP}g}}\right]\left\{1 + \alpha_H + \left(\frac{\delta\Delta V}{\Delta V}\right)\frac{\left(\frac{\Delta V}{I_{sp}\,g}\right)}{\left(e^{\frac{\Delta V}{I_{SP}g}} - 1\right)}\right\}$$

Next, total spacecraft weights ranging from 200 to 2000 pounds were assumed, so that the weight of hydrazine required to attain a particular velocity increment could be determined. With the required weight of hydrazine known, the total weight of the subsystem can be determined from Figure 3.6-2. By solving the relation

$$W_{PL} = W_{S/C} - W_{System}$$

the nonpropulsive payload is obtained.

The data obtained from this effort are presented graphically in Figures 3.6-4, 3.6-5, and 3.6-6 for the range of values investigated.

The design data presented in Table 3.6-3 were adopted for sizing of the basic hydrazine subsystem.

3.6.2 Attitude Control Propulsion Subsystem

The primary functional requirement of the attitude control propulsion subsystem is to provide control torques to the vehicle in response to processed information from the guidance and control computer. In order to achieve three-axis stabilization, the propulsion subsystem must be capable of imparting a control torque about either of the three vehicle-centered axes. When reaction jets are employed, this torque is accomplished by the simultaneous expulsion of mass from two opposing nozzles. Simultaneous operation of two opposing nozzles is required to assure a pure moment about any one axis; and two nozzle pairs are required for each axis to provide control capability in both the clockwise and counter-clockwise direction. Thus, a minimum of 12 nozzles is usually prescribed to obtain complete, pure-moment, three-axis control.

In addition to the requirements mentioned above, it is imperative that propellant leakage from the propulsion subsystem be held to a minimum. Propellant leakage is undesirable because it leads to a premature depletion of the propellant supply and could introduce range errors at encounter. Leakage not only represents an unscheduled loss of propellant, but it can impart a continuous disturbing torque to the vehicle, which accelerates propellant consumption even further. Because of the long durations associated with Jupiter flyby missions, propellant leakage must be regarded as a critical problem area and accommodated as such in the design and quality control phases of the attitude control propulsion subsystem development.

Numerous propulsion system concepts are technically capable of providing attitude control of space vehicles. Among these are systems which derive their exhaust kinetic energy from electrical, nuclear, or chemical sources or combinations of each. This idea is illustrated in Figure 3.6-7 and some typical attitude control concepts are identified. In the figure, the electrical and electrical/chemical devices, such as the ion engines, resistojet, arcjet, hydrolysis rocket, and plasma accelerator all require considerable use of onboard electrical power and at present are

Table 3.6-3 DESIGN DATA

GENERAL

Nominal thrust	50 lb_f
Propellant	Anhydrous Hydrazine
Specific impulse (area ratio 44:1)	233 lb_f.sec/lb_m
Pressurant	Nitrogen
Fixed hardware weight	20.84 lb_m
Thrust vector control	Jet vanes

MATERIALS

Propellant tank	Titanium Alloy 6AL-4V
Pressurant tank	Titanium Alloy 6AL-4V
Propellant bladder	Butyl rubber compound
Tank configurations	Spherical
Rocket nozzle	Haynes Alloy No. 25
Catalyst bed	Iridium on Alumina (Shell 405)

Constants

Symbol	Description	Assigned Value
α_H	I_{sp} Contingency Factor	0.05
$(\frac{\delta\Delta V}{\Delta V})$	ΔV reserve contingency factor	0.05
P_{PPG}	Pressure of prepressurant gas	270 $lb_f/in.^2$
P_T	Hydrazine tank working pressure	320 $lb_f/in.^2$
P_{PGi}	Initial nitrogen tank pressure	3000 $lb_f/in.^2$
P_{PG_f}	Final nitrogen tank pressure	600 $lb_f/in.^2$
P_D	Hydrazine tank design pressure(at maximum anticipated temperature)	513 $lb_f/in.^2$
P_D	Nitrogen tank design pressure (at maximum anticipated temperature)	3540 $lb_f/in.^2$
P_C	Chamber pressure	200 $lb_f/in.^2$
(S.F.)	Design safety factor	2.2
χ	Ullage factor (fraction of hydrazine volume)	0.10
T_{max}	Maximum anticipated temperature	165°F
T_o	Initial temperature	70°F
ϵ	Bladder expulsion efficiency	0.98
R	Nitrogen gas constant	660 in. lb_f/lb_m °R
ρ_{mat}	Density of tank material (Ti-6AL-4V)	0.16 $lb_m/in.^3$
σ_{mat}	U.T.S. of tank material (Ti-6AL-4V)	165000 $lb_f/in.^2$
v_o	Hydrazine specific volume at 70°F	27.70 $in.^3/lb_m$
Δv	Change in hydrazine specific volume due to thermal expansion (from 70°F to 165°F)	1.053 $in.^3/lb_m$
t_B	Bladder material thickness	0.030 in.
ρ_B	Density of bladder material	0.05 $lb_m/in.^3$

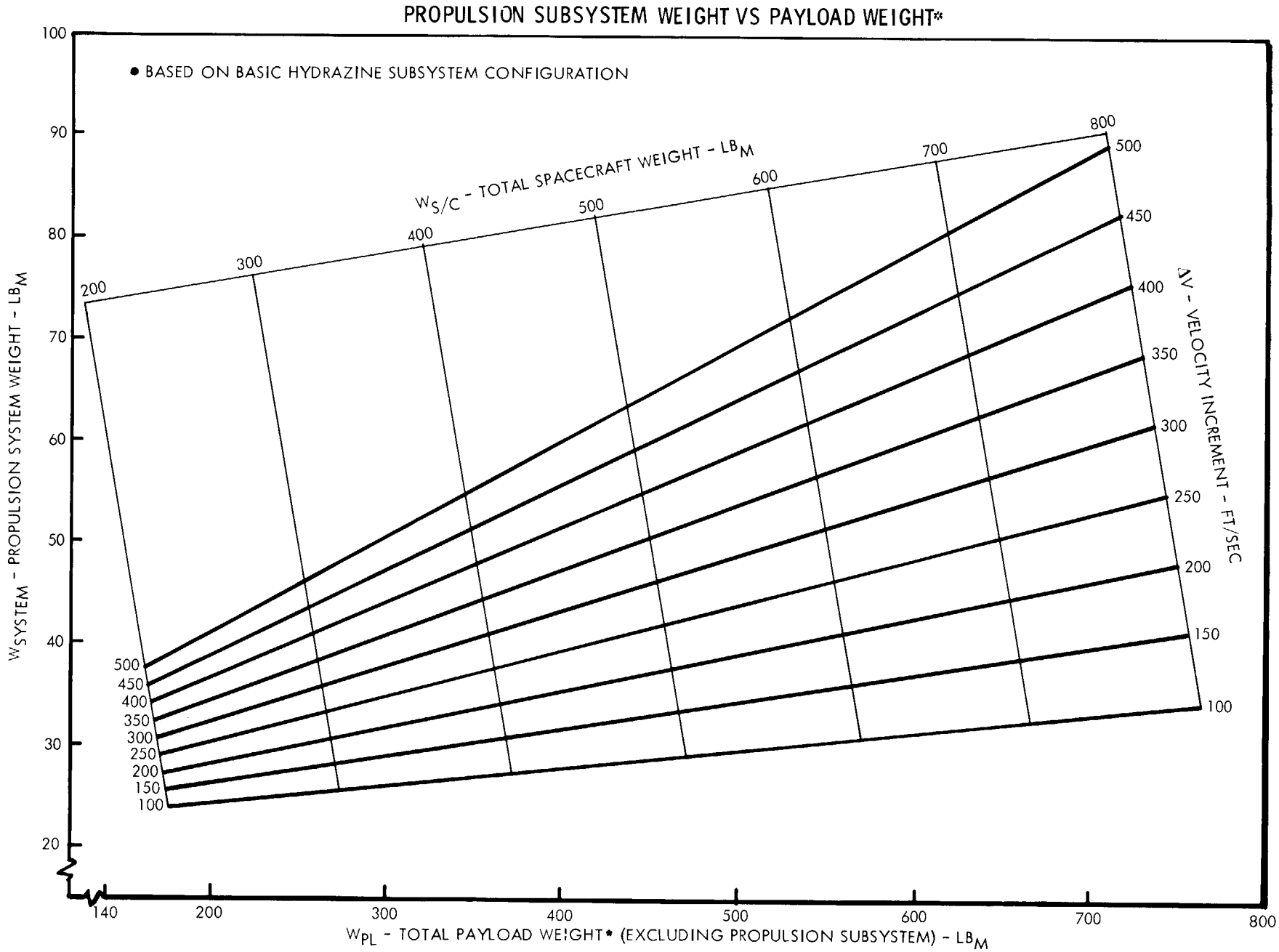
PROPULSION SUBSYSTEM WEIGHT VS PAYLOAD WEIGHT*
• BASED ON BASIC HYDRAZINE SUBSYSTEM CONFIGURATION
$W_{S/C}$ - TOTAL SPACECRAFT WEIGHT - LB_M
200
300
400
500
600
700
800
ΔV - VELOCITY INCREMENT - FT/SEC
500
450
400
350
300
250
200
150
100
W_{SYSTEM} - PROPULSION SYSTEM WEIGHT - LB_M
100
90
80
70
60
50
40
30
20
140
200
300
400
500
600
700
800
W_{PL} - TOTAL PAYLOAD WEIGHT* (EXCLUDING PROPULSION SUBSYSTEM) - LB_M

FIGURE 3.6-4

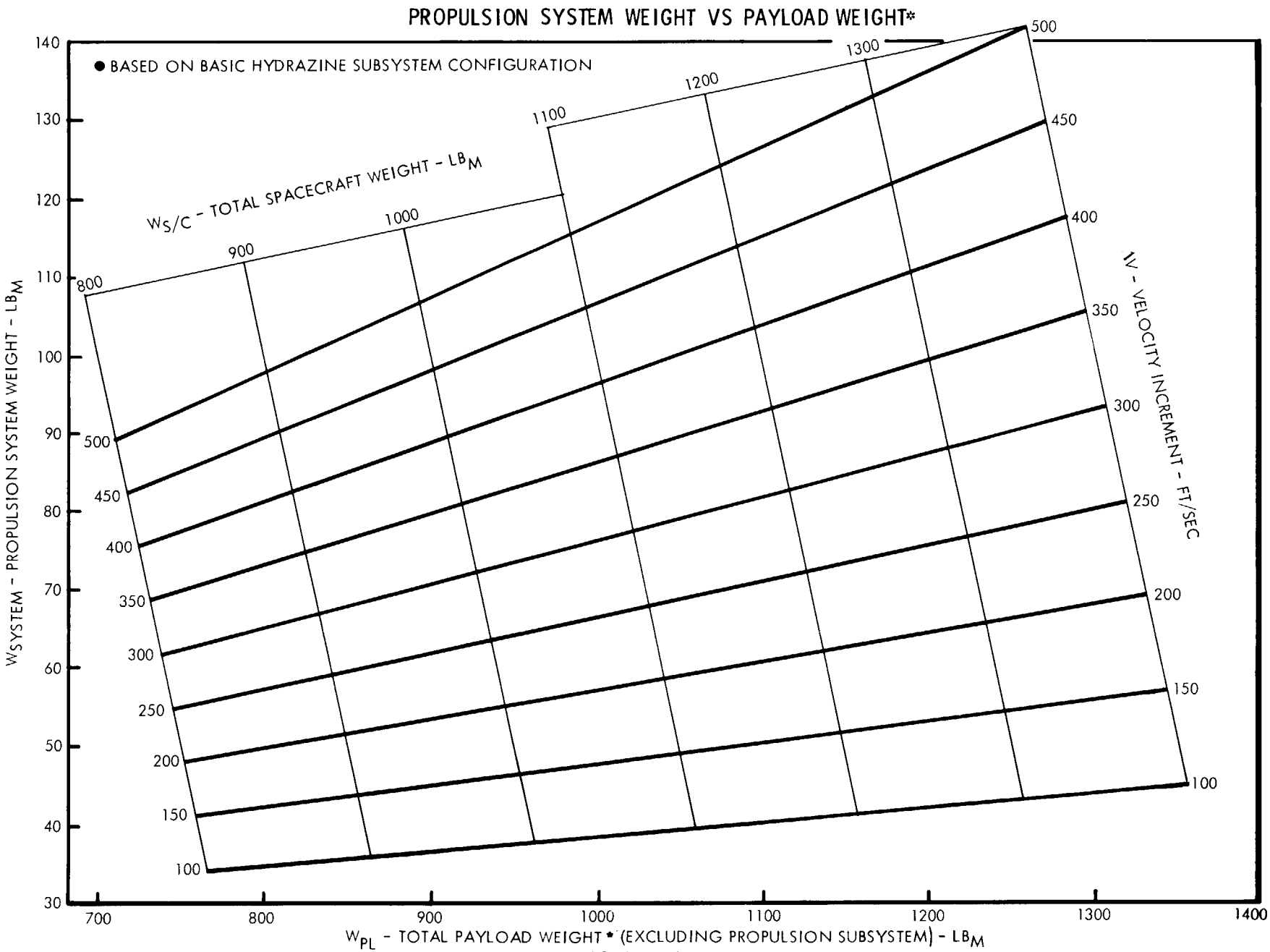
PROPULSION SYSTEM WEIGHT VS PAYLOAD WEIGHT*
● BASED ON BASIC HYDRAZINE SUBSYSTEM CONFIGURATION
$W_{S/C}$ - TOTAL SPACECRAFT WEIGHT - LB_M
800
900
1000
1100
1200
1300
500
450
400
350
300
250
200
150
100
ΔV - VELOCITY INCREMENT - FT/SEC
W_{SYSTEM} - PROPULSION SYSTEM WEIGHT - LB_M
140
130
120
110
100
90
80
70
60
50
40
30
700
800
900
1000
1100
1200
1300
1400
W_{PL} - TOTAL PAYLOAD WEIGHT * (EXCLUDING PROPULSION SUBSYSTEM) - LB_M

FIGURE 3.6-5

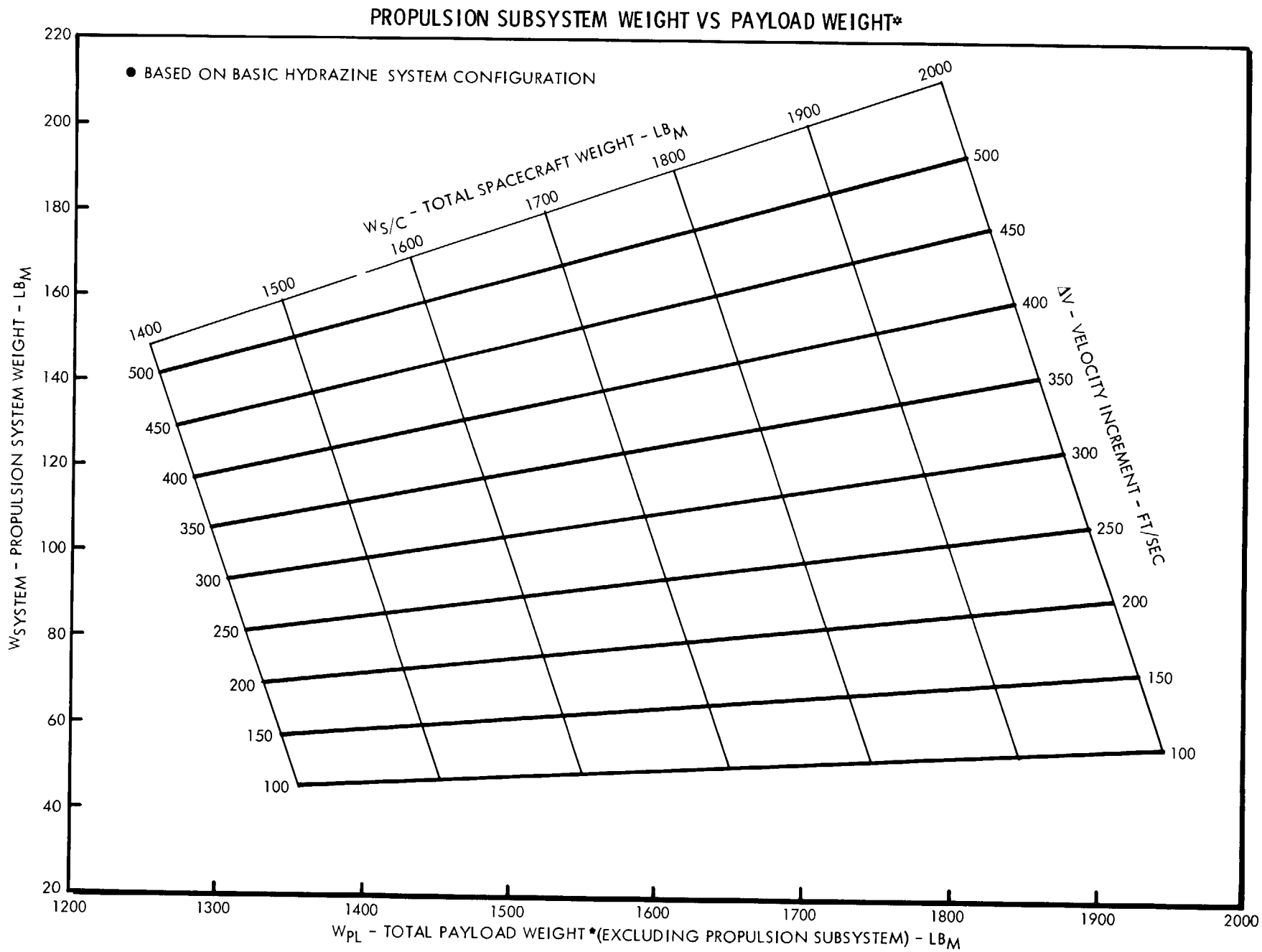
PROPULSION SUBSYSTEM WEIGHT VS PAYLOAD WEIGHT*
● BASED ON BASIC HYDRAZINE SYSTEM CONFIGURATION
$W_{S/C}$ - TOTAL SPACECRAFT WEIGHT - LB_M
1400
1500
1600
1700
1800
1900
2000
ΔV - VELOCITY INCREMENT - FT/SEC
500
450
400
350
300
250
200
150
100
W_{SYSTEM} - PROPULSION SYSTEM WEIGHT - LB_M
220
200
180
160
140
120
100
80
60
40
20
1200
1300
1400
1500
1600
1700
1800
1900
2000
W_{PL} - TOTAL PAYLOAD WEIGHT *(EXCLUDING PROPULSION SUBSYSTEM) - LB_M

FIGURE 3.6-6

PROPULSION SYSTEM CONCEPTS FOR SPACECRAFT ATTITUDE CONTROL

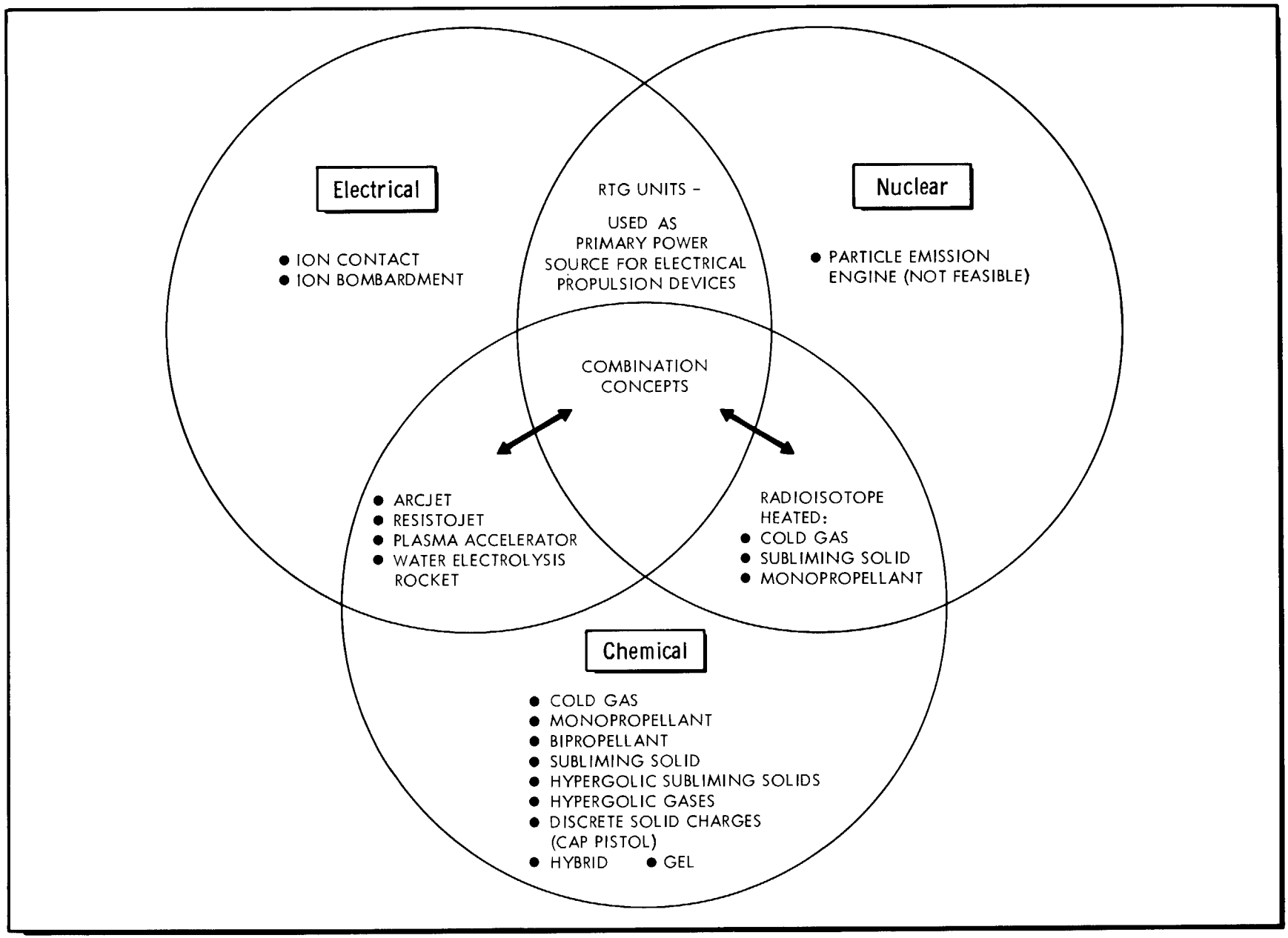

FIGURE 3.6-7

not as technically advanced or as simple as their chemical counterparts. Among the chemical devices, the bipropellant systems would be expected to pose some operational difficulties at the low thrust levels envisioned for attitude control of Jupiter flyby vehicles. The subliming solid systems appear promising for volume-limited situations, but these are unfortunately characterized by a tendency towards recondensation in flow channels and component volumes which compromises their reliability.

Among the remaining devices, the cold gas and monopropellant systems appear best suited for the Jupiter flyby mission by virtue of their innate reliability and adaptability to the requirements for rapid response, minimum impulse bit, and reproducible operation at low thrust levels. As a design option, either of these system types could be integrated with a radioisotope heat source or possibly the on board RTG units to improve system performance. For example, the cold gas system could be improved by heating the gas directly to increase the specific impulse. With a monopropellant system (such as hydrazine), performance could be improved by heating the catalyst bed to reduce I_{sp} losses due to start transients and assure uniform propellant decomposition. A number of design options in this area warrant further study.

In the interests of a simple and conservative design, however, the propulsion system selected for the attitude control of all Jupiter flyby vehicles is a cold gas system employing nitrogen as the propellant. This system is described and analyzed in the paragraphs which follow.

3.6.2.1 Description of the Cold Gas Propulsion System

In this study, two cold gas propulsion subsystem configurations are defined. These are illustrated in Figures 3.6-8 and 3.6-9. The first, identified as Configuration A, is typical of a system which is recommended to provide three-axis attitude control for short periods of time. As a result, the system is characterized by minimum redundancy.

The second configuration, identified as Configuration B, is typical of a system which is recommended for three-axis attitude control of Jupiter flyby vehicles for the entire duration of the mission. For such durations as these (400 to 800 days), it is felt that some operational redundancy is necessary in order to increase the probability of mission success. The redundant features provided in Configuration B include (1) a redundant propellant supply, that is, at least twice the nominal propellant

SCHEMATIC DIAGRAM OF COLD GAS PROPULSION SUBSYSTEM - CONFIGURATION A

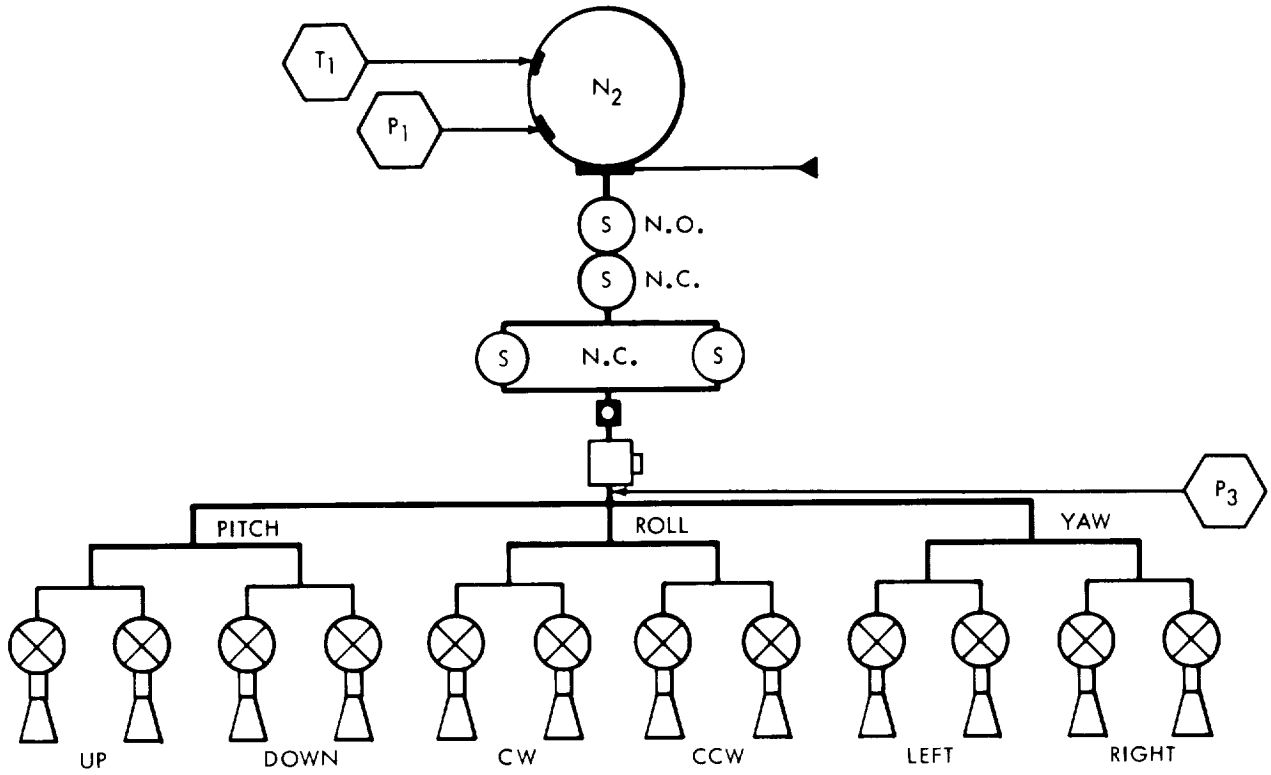

FIGURE 3.6-8

SCHEMATIC DIAGRAM OF COLD GAS PROPULSION SUBSYSTEM - CONFIGURATION B

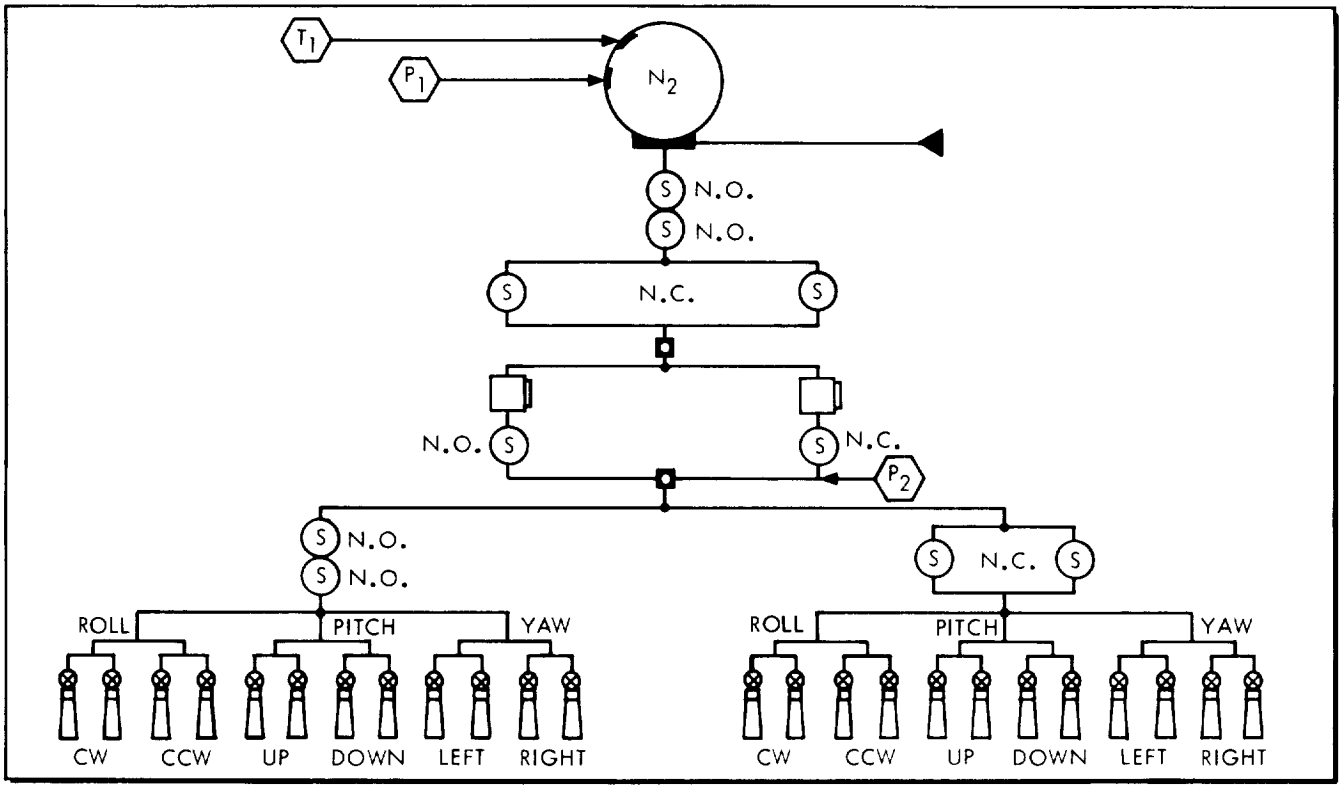

FIGURE 3.6-9

necessary to complete the mission is carried aboard, (2) a redundant gas pressure regulator, and (3) a redundant set of nozzle assemblies, each assembly consisting of a solenoid on-off valve and a rocket nozzle.

Two candidate design concepts have been considered for Configuration B in this analysis. The basic difference in the two concepts is in the number of propellant tanks employed, one or two. The results of a reliability analysis reported in subsection 3.13 coupled with practical considerations regarding implementation of failure detection led to the elimination of the two-tank system in favor of a one-tank system employing redundant squib valves. A redundant propellant supply, a redundant regulator network, and a redundant set of nozzles are included in the recommended design. No significant differences in weight exist between the two-tank and one-tank concepts when both are evaluated at comparable design points. This is attributed to the fact that, where spherical tanks are used, a one-tank system has very nearly the same weight as a two-tank system provided that both systems contain the same amount of propellant at the same storage pressure.

A questionable parameter in the weight estimates of Configuration B is the amount of redundant propellant required. In the present example, a factor of two is applied to the nominal propellant weight required. This is to accommodate uncertainties in leakage and unknown or unpredictable forces acting on the spacecraft. Further study is necessary to determine a more optimum propellant reserve for attitude control.

3.6.2.2 Weight Breakdown of Fixed Hardware

A common problem in predicting the weight of attitude control systems is the uncertainty associated with the weights of the fixed hardware components. Items such as solenoid valves, regulators, etc., which collectively form a significant portion of overall system weight, are found to vary considerably in weight from one manufacturer to another, even when each item is ostensibly capable of the same application. Recognizing this, it was decided to investigate a large sample of vendor's data for the purpose of isolating fixed hardware component weights into conservative (heavyweight) and optimistic (lightweight) categories. The results of this effort are tabulated below.

Weight Breakdown of Subsystem Fixed Hardware

	Configuration A	Configuration B
Conservative Estimate	16.80 lbm	33.40 lbm
Optimistic Estimate	6.90 lbm	14.80 lbm

This information was combined with the propellant and tank weight data developed in the following subsection to provide relationships for estimating overall system weight.

3.6.2.3 Parametric Analysis

A detailed parametric analysis of a cold gas attitude control propulsion subsystem is presented in Appendix E. This analysis forms the basis for the propulsion subsystem weight data which are presented in subsection 3.6.2.4. The nomenclature used and a summary of the primary equations which were developed are presented in Table 3.6-4.

3.6.2.4 Subsystem Sizing

The sizing of the two attitude control configurations A and B is accomplished by combining the fixed hardware weights of each configuration with the appropriate equation form developed in the preceding paragraph.

For Configuration A, which is nonredundant with respect to propellant supply, the basic equation (8) for subsystem weight is valid. Thus, in calculating the total subsystem weight,

$$W_{\substack{System \\ A}} = I_t \left[\frac{(1+\alpha_P)\left|1 + 1.5RT_{MAX}\left(\frac{\rho}{\sigma}\right)_{MAT}(S.F.)\right|}{I_{SP}\left|1 - \left(\frac{P_f}{P_i}\right)\left(\frac{T_i}{T_f}\right)\right|} \right] + W_{COM}$$

where W_{COM}, the weight of fixed hardware, is either 16.80 pounds (conservative estimate) or 6.90 pounds (optimistic estimate).

In the case of Configuration B, which is assumed to carry twice the nominal supply of propellant, the basic equation (8) is modified in the first term to read:

Table 3.6-4 ATTITUDE CONTROL PROPULSION SUBSYSTEM - NOMENCLATURE AND EQUATION SUMMARY

Nomenclature Symbol	Description	Units
W_{system}	Total Weight of the Subsystem	lbm
W_p	Total Weight of Propellant Required	lbm
W_t	Weight of Propellant Tank	lbm
W_{com}	Total Weight of Fixed Hardware (i.e., valves, regulators, tubing etc.)	lbm
W_{p1}	Expected Propellant Consumption	lbm
W_{p2}	Propellant Contingency for Isp Degradation	lbm
W_{p3}	Residual Propellant at Termination of Thrust Program	lbm
I_t	Total Impulse Required	lbf.sec
I_{sp}	Specific Impulse	lbf.sec/lbm
α_p	Contingency Factor for Isp Degradation	---
P_i	Initial Propellant Tank Pressure	$lbf/in.^2$
P_f	Final Propellant Tank Pressure	$lbf/in.^2$
P_D	Propellant Tank Design Pressure (at maximum anticipated temp.)	$lbf/in.^2$
T_{max}	Maximum Anticipated Temperature	^oR
T_i	Initial Propellant Temperature	^oR
T_f	Final Propellant Temperature	^oR
V_{tank}	Volume of Propellant Tank	$in.^3$
R	Propellant (gas) Constant	$in.\text{-}lbf/lbm\cdot{}^oR$
S.F.	Design Safety Factor	---
ρ_{mat}	Density of Tank Material	$lbm/in.^3$
σ_{mat}	U.T.S. of Tank Material	$lbf/in.^2$

Equation Summary

(1) $W_{System} = W_P + W_t + W_{COM}$

(3) $$W_P = \frac{I_t}{I_{sp}} \quad \frac{(1 + \alpha_p)}{1 - (\frac{P_f}{P_i})(\frac{T_f}{T_i})}$$

(7) $$W_t = 1.5\ W_p\ RT_{MAX}\ (\frac{\rho}{\sigma})_{MAT}\ (S.F.)$$

(8) $$W_{System} = I_t \left[\frac{(1 + \alpha_p)}{I_{sp}} \frac{\left| 1 + 1.5RT_{MAX} (\frac{\rho}{\sigma})_{MAT}(S.F.) \right|}{\left| 1 - (\frac{P_f}{P_i})(\frac{T_i}{T_f}) \right|} \right] + W_{COM}$$

$$W_{System_B} = 2I_t \left[\frac{(1 + \alpha_p) \left| 1 + 1.5\ RT_{MAX} \left(\frac{\rho}{\sigma}\right)_{MAT} (S.F.) \right|}{I_{sp} \left| 1 - \left(\frac{P_f}{P_i}\right) \left(\frac{T_i}{T_f}\right) \right|} \right] + W_{COM}$$

Where W_{COM} is estimated at 33.40 pounds (conservative) and 14.80 pounds (optimistic). Using the design data listed below, both of these equations were plotted as a function of the total impulse required for both the conservative and optimistic estimates of fixed hardware. These results appear in Figure 3.6-10.

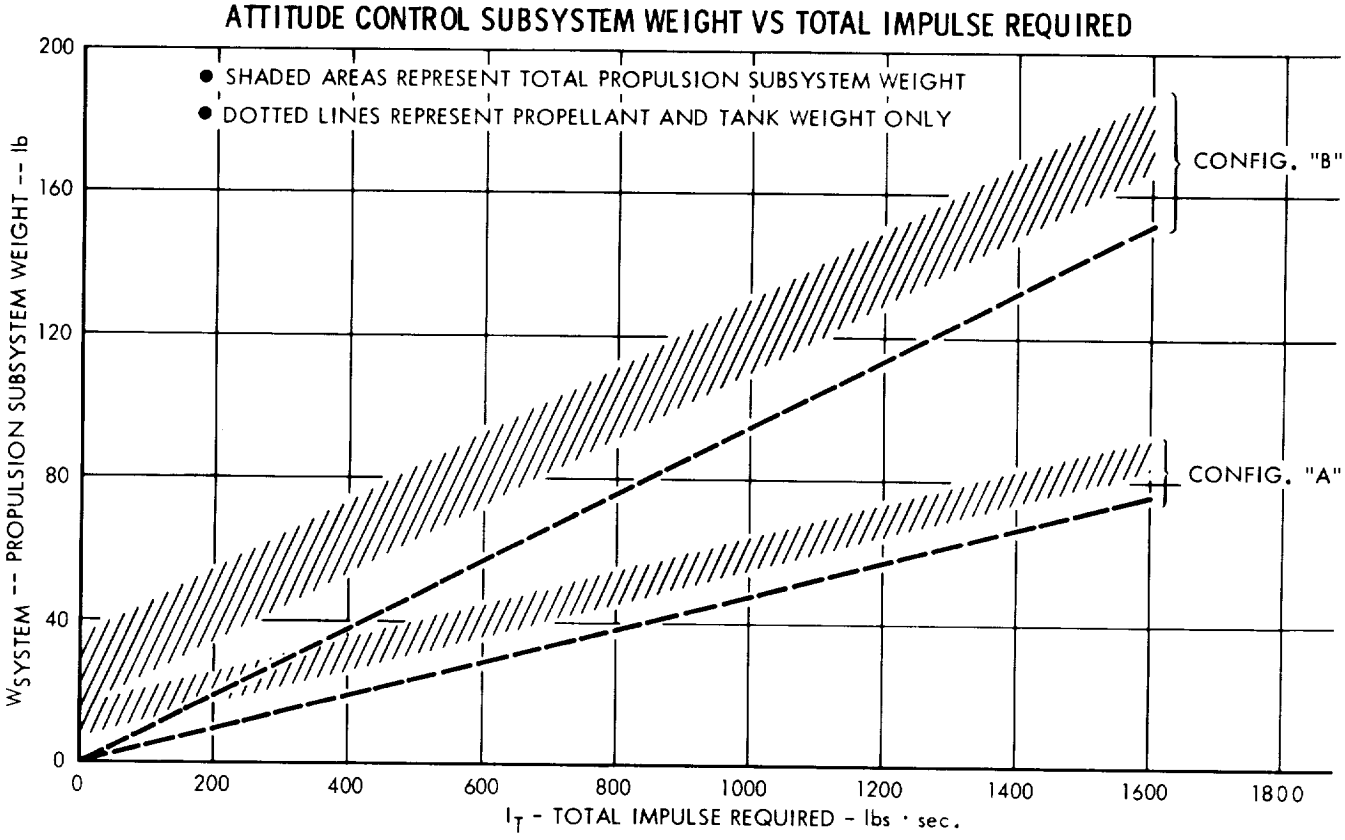

FIGURE 3.6-10

The design data listed in Table 3.6-5 have been adopted for sizing the attitude control propulsion subsystems.

Table 3.6-5 ATTITUDE CONTROL PROPULSION SUBSYSTEM - SIZING DESIGN DATA

General

Propellant	Nitrogen
Specific Impulse	56.0 lb_f. sec/lbm

Materials

Propellant Tank	Titanium Alloy 6 AL-4V
Configuration	Spherical

Constants

Symbol	Description	Assigned Value
α_p	Contingency Factor for Isp Degradation	0.10
P_i	Initial Propellant Tank Pressure	3000 lbf/in.^{2}
P_f	Final Propellant Tank Pressure	150 lb_f/in.^{2}
P_D	Propellant Tank Design Pressure (at maximum anticipated temperature)	3540 lb_f/in.^{2}
T_{max}	Maximum Anticipated Temperature	165^{o}F
T_i	Initial Propellant Temperature	70^{o}F
T_f	Final Propellant Temperature	70^{o}F
R	Propellant (Gas) Constant	660 in.lb_f/lbm^{o}R
S.F.	Design Safety Factor	2.2
ρ_{mat}	Density of Tank Material	0.16 lbm/in.^{3}
σ_{mat}	U.T.S. of Tank Material	165000 lb_f/in.^{2}

3.7 AUXILIARY ELECTRIC POWER

3.7.1 Scope and Requirements

The scope of the Jupiter flyby electrical power system study includes (1) the organization of applicable data on current power systems, (2) a projection from such data to that anticipated during the early 1970's, (3) coordination of various trade-off analyses which are expressed in terms of parametric system configurations, and (4) designation of specific design concepts. The objective is to define the major subsystem characteristics with sufficient accuracy to permit synthesis of meaningful spacecraft design concepts and evaluation of attendant missions. The requirements and constraints imposed upon the power subsystem by the Jupiter flyby mission profile include (1) temperature, vibration, atmospheric, and space vacuum environment of all the mission phases, (2) the volume and weight limitations of the launching system, (3) the power requirement profile, (4) the weight, volume, and reliability trade-offs, (5) the availability and cost considerations, and (6) interface coordination with other spacecraft systems. The last item includes the following: (1) structural aspects, (2) view angle restrictions of optical navigation devices, communications antennas, and thermal radiation, (3) vehicle inertial dimensions, and (4) nuclear irradiation effects.

3.7.2 Raw Power Generation

3.7.2.1 Energy Sources

Selection of the energy source and conversion process is the first consideration of the power system study. Mission durations in the 400- to 1000-day range immediately restrict considerations to solar, nuclear reactors, or radioisotopes thermal energy sources. Solar thermal energy intensity at Jupiter's orbit is approximately 4 percent of that at Earth's orbit, which is in the order of 5 watts per square foot. The low level negates any practical consideration of employing any form of currently envisioned solar energy collection system. Nuclear reactors have a minimum critical size and weight required to maintain a controlled nuclear reaction. The minimum weight is currently approximately 250 pounds. Reactor radiation effects further complicate the matter to the point of eliminating any consideration of nuclear reactors as an energy source for the subject application.

Isotopes alone remain as a candidate energy source. Isotope fuel selection is based on considerations of half-life, availability, cost, radiation characteristics, energy density, handling, and safety aspects. Strontium 90, Cesium 137, and possibly Promethium 147 can be used to meet the first three requirements. However, safety considerations, beta radiation effects on scientific instruments, shielding mass penalties, and lack of experience with their application combine to make their successful application extremely unlikely. Plutonium 238 and Currium 244 are long half-life alpha emitters. Of the two, Plutonium 238 is more favorable in terms of cost, availability, and safety; hence, it is recommended for this application.

3.7.2.2 Energy Converters

Candidate thermal-to-electric converters include thermionic, Rankine and Brayton dynamic, and thermoelectric. Thermionic systems, although they show great promise, are not sufficiently advanced to warrant consideration for use in the early 1970 time period. The dynamic systems are not competitive in terms of weight in the subkilowatt range. Information shown in Figure 3.7-1 (Reference 3.7-1) supports the conclusion that the RTG (Radioisotope-Thermalelectric-Generator) is best suited to provide power for the subject application.

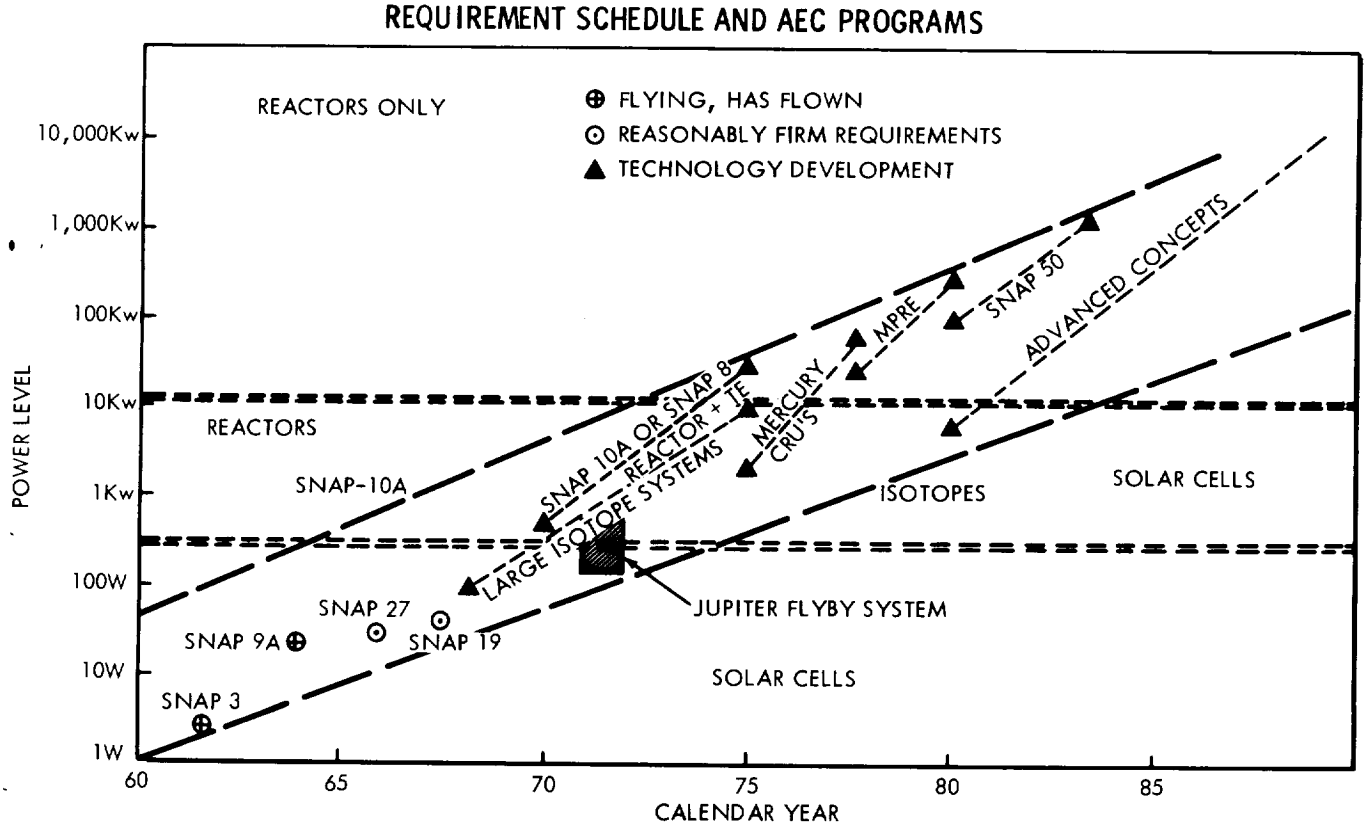

FIGURE 3.7-1

3.7.2.3 RTG Configuration

RTG's of the SNAP 9, 11, 17, and 19 are characterized by power densities of approximately one watt per pound, by hot and cold junction temperatures in the order of 1000 and 350°F, and by the application of lead-telluride (Pb-Te) thermocouples. The critical limitation on the availability of isotope fuel has favored efficiency optimization. It is generally agreed that higher power densities will be practical during the period anticipated for the Jupiter flyby missions. As is the case with all thermal energy converters, the increase of efficiency and power densities involve operation at higher temperatures. The major weight reduction occurs in the heat rejection system as a consequence of the fourth power function of radiated heat flux. To a lesser degree, the increase of temperature differential across the thermocouples results in a weight reduction as a consequence of increased conversion efficiency. Maximum operating temperatures are restricted by the development status of fuel forms, the fuel canister, the structure, and some forms of the thermocouple materials. The favorable figure-of-merit, Z, and industrial experience led to the utilization of Pb-Te couples in the "first generation" of RTG's. The low melting point and long term stability problems associated with the Pb-Te materials has favored the development of the more stable silicon-germanium (Si-Ge) couple materials. While the Si-Ge couples exhibit a less favorable figure-of-merit, they are capable of operation in the 2000°F temperature range.

The relative merits of the two couple systems are set forth with the aid of Figures 3.7-2 and 3.7-3. Properties of the couple are the following:

S = Seebeck voltage coefficients (volt/°C)

ρ = electrical resistivity (ohm-cm)

k = thermal conductivity

Z = figure-of-merit ($^{\circ}C^{-1}$)

$$= \frac{S^2}{\rho k} \qquad (1)$$

c_l = couple length in cm

c_a = couple cross-section in cm^2

THERMOCOUPLE THEORETICAL LOSS ANALYSIS DIAGRAM

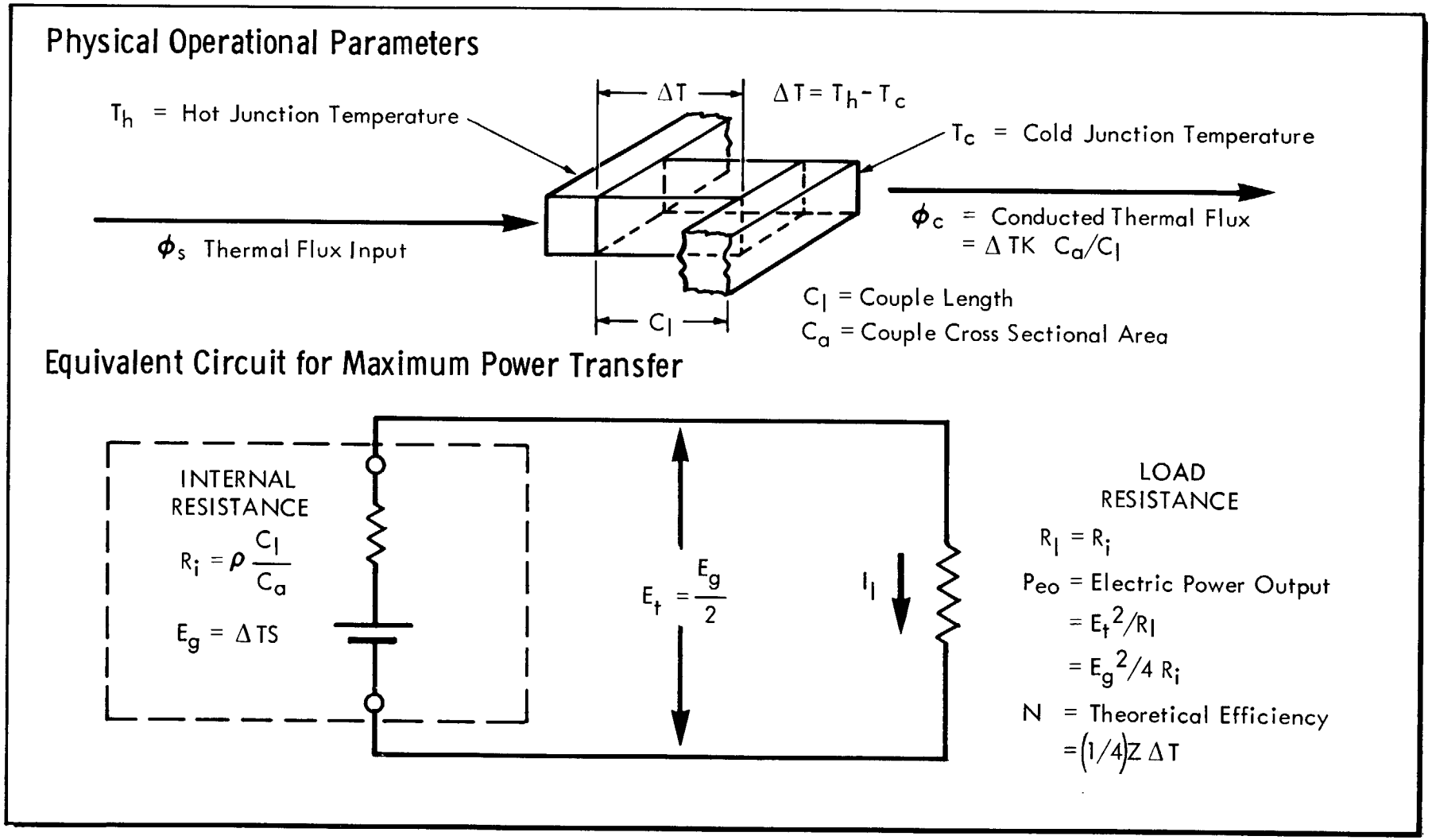

FIGURE 3.7-2

The physical operating parameters are

T_h = Hot junction temperature ^oC

T_c = Cold junction temperature ^oC

$\Delta T = T_h - T_c$ (2)

ϕ_s = Thermal flux input to couple (watts)

ϕ_c = Thermal flux conducted in watts

$\phi_c = k \Delta T \ Ca/Cl$ (3)

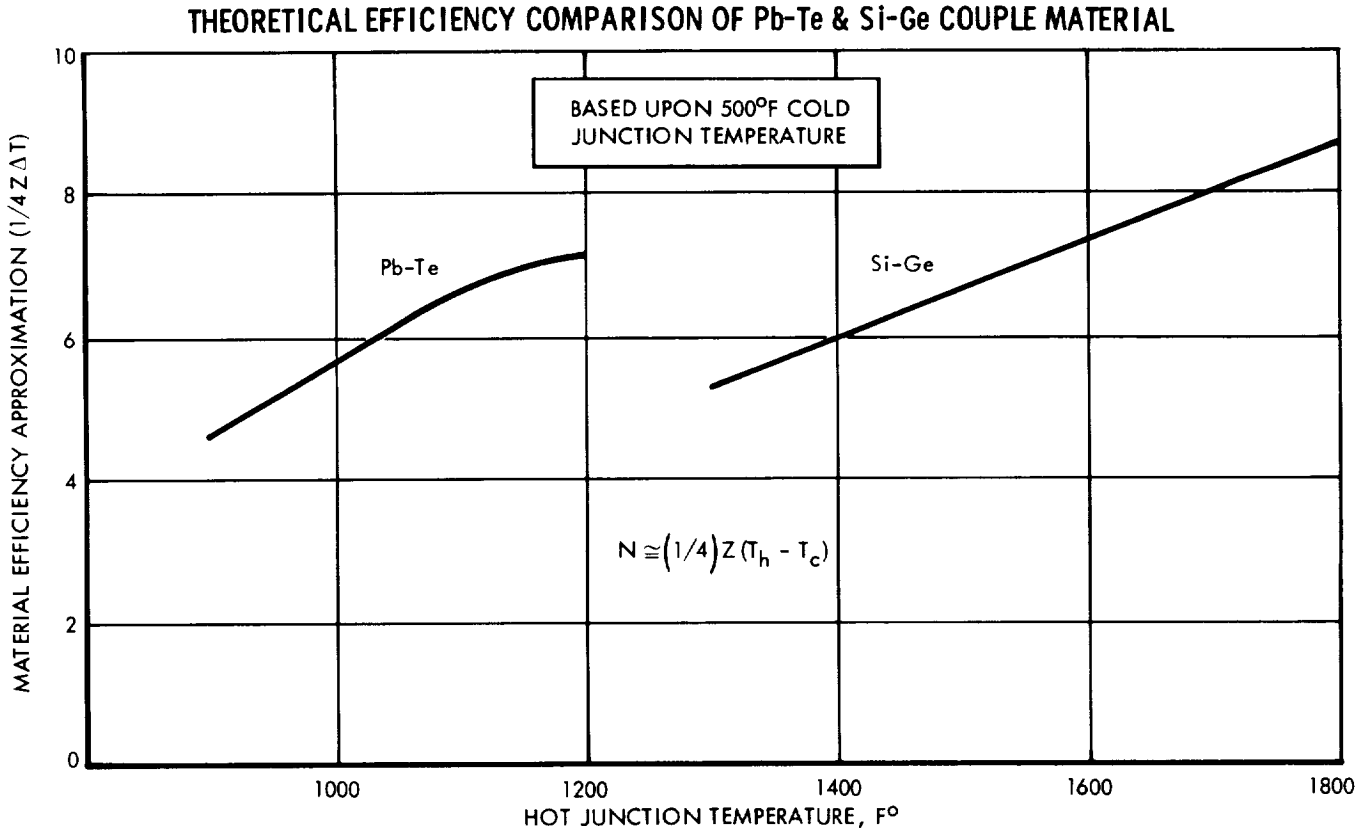

FIGURE 3.7-3

In the operation of the couple, the Seebeck voltage, Eg, causes a current, I_λ to flow through the load. The circuit resistance is made up of the internal couple resistance, interconnection resistance, and an external load resistance. As a simplifying assumption, the consideration of the interconnection resistance is initially omitted in the theoretical analysis. Maximum power transfer and efficiency occurs when the external and internal resistances are equal. Electric power output may then be expressed as

$$P_{eo} = E_t^2/R_l = \frac{E_g^2}{4R_i} = \frac{\Delta T^2 S^2}{4\rho c_l/c_a} \quad (4)$$

where

P_{eo} = electric watt output

P_{ei} = electric watt lost internally

$$P_{ei} = P_{eo} \quad (5)$$

E_g = Seebeck voltage

$$E_g = \Delta TS \quad (6)$$

R_l = load resistance

R_1 = couple resistance

$$R_l = R_i = c_1/c_a \quad (7)$$

Ideal couple efficiency (N) is therefore

$$N = \frac{P_{eo}}{\phi_c + P_{eo}+P_{ei}} = \left(\frac{\Delta T^2 S^2}{4\rho c_l/c_a}\right) \left(k\Delta T C_a/C = \frac{\Delta T^2 S^2}{2\rho C_l/C_a}\right) \quad (8)$$

$$= \left(\frac{\Delta TS^2}{4\rho}\right)\left(k+k\frac{\Delta TS^2}{2\rho k}\right)^{-1} = \frac{\Delta TZ}{4}\left(1+\frac{\Delta TZ}{2}\right)^{-1} \quad (9)$$

since

$$\frac{\Delta TZ}{2} \ll 1 \quad (11)$$

$$N \simeq \frac{\Delta TZ}{4}$$

Figure 3.7-3 is a plotted comparison of the efficiency approximation 1/4 $Z\Delta T$ for both P_b - T_e and S_i-G_e couples. The plot is based upon data from the General Electric Company and Radio Corporation of America (Reference 3.7-2 and 3.7-3). Delta T (T_h-T_c) data are based upon a rejection temperature of 500°F. Shunt heat flux loss, interconnection I^2R loss, and miss-match of the individual couples within the thermopile combine to distract from the achievement of the theoretical efficiencies.

However, the data in Figure 3.7-3 does illustrate the potential goals based upon the aforementioned figures-of-merit. Both Pb-Te and Si-Ge systems are characterized by problem areas. The Pb-Te limitation involves uncertain long-term stability, potential damage from transient overheating conditions, and the inability to make metalurgical hot-junction electrical connections. The data in Figure 3.7-3 indicates that hot-junction temperatures in the 1300°F range are required to produce a competitive Si-Ge system. While the Si-Ge system is reported to be capable of operation at temperatures well above that level, serious problems are involved in the development of a fuel system capable of operating at these temperatures and also meeting the various long-term safety requirements. At this time, the choice of Pb-Te or Si-Ge for a 1973 application rests upon the prediction of which of the two problem areas can best be solved. The very attractive possibility exists that a combination converter will be developed to combine both couples in thermal series with practical efficiencies of 10 percent or greater.

References 3.7-4 through 3.7-8 contain recently completed RTG studies. Reference 3.7-8 pertains to the SNAP 27 project performed by the General Electric Company. The work is considered to embody the most thorough current practical development. The study includes a projection analysis of a 100-watt RTG whose characteristics are given below:

1.	Specific Power Density	2 watts/pound
2.	Radiation temperature	500°F
3.	Physical Size	
	Diameter over fins	19 inches
	Length	0.02 inch/watt
4.	Thermocouple	
	Material	Lead-Teluride
	Open-circuit voltage	0.166 volt
	Max-power voltage	0.083 volt
5.	Overall efficiency	5 percent

The intensive research and development under way on all aspects of the RTG systems is resulting in significant advances. Hence, it is reasonable to assume that the systems to be flown in 1973 will be appreciably lighter than those available within the current state-of-art. For example, three years ago one watt per pound was the accepted density. Currently, 1.5 to 1.7 watts per pound is considered practical; therefore, the use of two watts per pound should be feasible during 1973. Degradation rates during operation of the advanced systems will be a function of several factors which cannot be predicted with any degree of accuracy at this time. On the basis of tests performed on SNAP 21 and 27 Pb-Te couples (Reference 3.7-10), it may be assumed that degradation within a properly constructed thermopile can be limited to a reasonable value. The specific degradation applied in the spacecraft configuration analysis is 10 percent over the 600-day period. A summary based on the criteria derived from the SNAP 27 developments and the foregoing assumptions is presented in Table 3.7-1. The data contained therein are employed in the spacecraft configuration analyses.

Table 3.7-1

60-, 80-, and 120- WATT RTG GEOMETRY

Rating, watts - initially	66	88	132
Rating, watts - after 2 years operation	60	80	120
RTG total weight, pounds	33	44	66
Nominal potential, volts	28	28	28
Number of groups, Ng	14	14	14
Series couples per group, Ns	24	24	24
Parallel strings per group, Np	2	2	3
Thermocouples per group	48	48	72
Total couples for RTG	672	672	1008
RTG nominal current	2.14	2.86	4.28
Couple nominal current	1.07	1.43	1.43
Couple nominal volts	0.083	0.083	0.083
Couple nominal watts	0.089	0.119	0.119

The General Electric Company is in the early phase of a contract study on a 250 watt Pu238-fueled RTG. The study will incorporate the results of development work on isotope heat source and the SNAP 27 as reported in References 3.7-9 and 3.7-10. At this time, General Electric anticipates that the use of the higher temperature fuel system will be feasible, and as a consequence, is considering the Si-Ge converters. The results of the effort will be applicable to Jupiter flyby spacecraft.

3.7.2.4 RTG Internal Interconnections

The RTG is composed of a large number of electrically independent, low-voltage power converters. The manner in which they may be interconnected to enhance overall reliability is described herein. Each thermocouple, when operated at a specific thermal environment, exhibits a linear voltage versus current relationship, as illustrated in Figure 3.7-4a. Maximum power output occurs when the internal and external impedances are balanced as illustrated in Figure 3.7-4b. The simplest RTG interconnector is a series string such as that illustrated in Figure 3.7-4c. However, one open couple or interconnection disables the entire RTG. The effect of open circuits can be minimized by a parallel interconnection, as illustrated in Figure 3.7-4d. However, in such a case the total output voltage is on the order of 0.1 volt at a current of several hundred amperes, and this produces an unmanageable power-conditioning task. A compromise which combines the advantages of both schemes is illustrated in Figure 3.7-4e. Here the couples are arranged in a number of groups, Ng, with the groups connected in series. Each group is composed of a number of parallel strings, N_p. The string consists of N_s couples connected in series.

The effects of open and shorted couples are illustrated by an analysis of the 120-watt RTG unit (see Figure 3.7-5c). As listed in Table 3.7-1, the proposed 120-watt unit is made up of 14 series-connected groups, each group of which is composed of 3 parallel strings of 24 couples; in each case, there is a total of 1008 couples for the complete RTG. Part a, Figure 3.7-5, is applicable to the individual couple. Part b illustrates the series string with 24 functional couples and a series string with 23 couples, representing the situation with one couple shorted. Part c applies to a fully functional group, a group with one string containing a shorted couple, and a group with one open-circuited string. Part d illustrates the performance of the complete RTG with all couples functioning properly and a situation in which 12 groups are functioning properly; one group contains a string

THERMOCOUPLE INTERCONNECTIONS

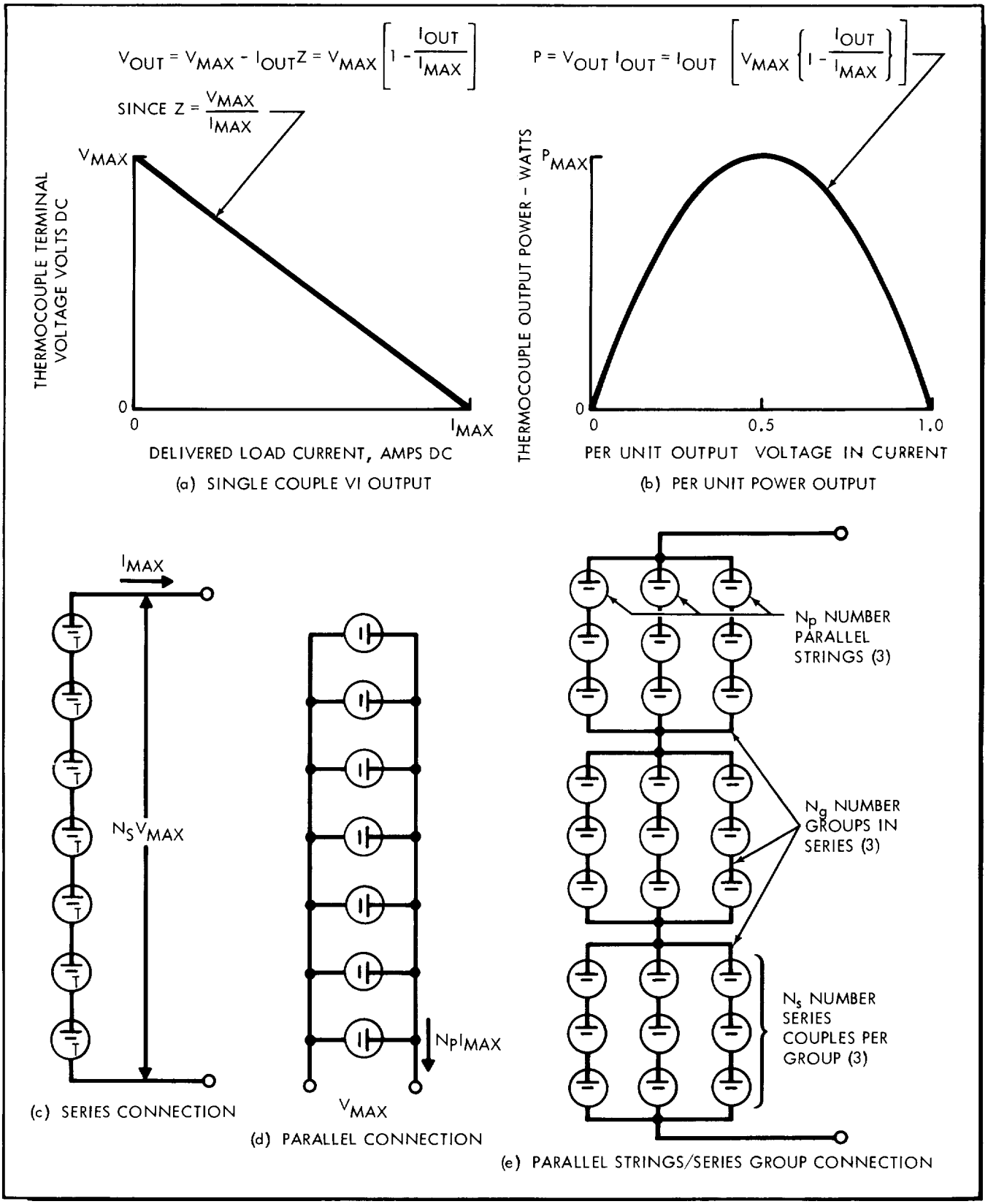

FIGURE 3.7-4

THERMOCOUPLE FAILURE EFFECTS

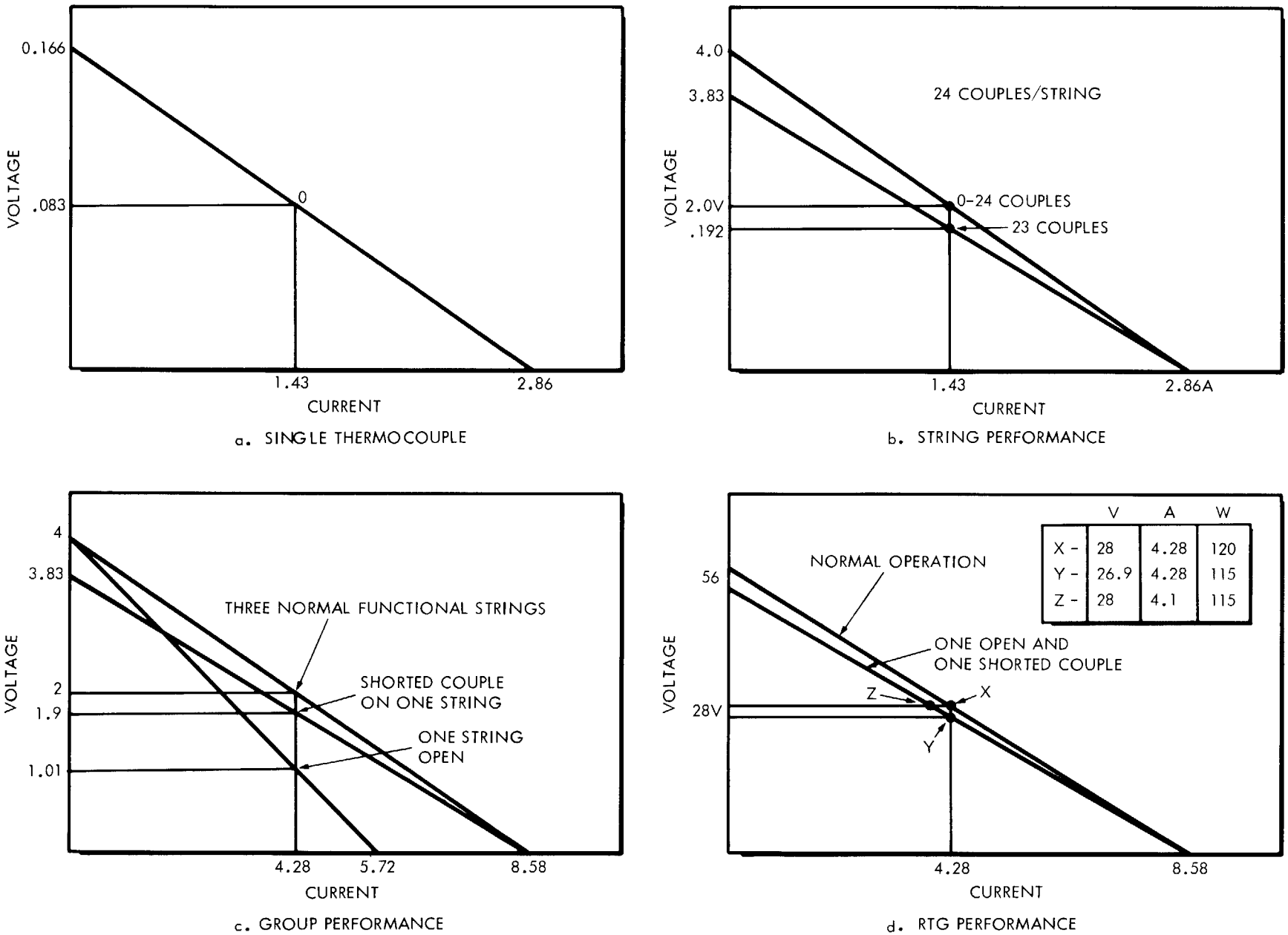

FIGURE 3.7-5

with a shorted couple, and one group has an open string. Note that with two such internal failures, the RTG maintains an output power of 95 percent normal.

3.7.3 Power Management System

3.7.3.1 Functions

The functions of a spacecraft power management system include conditioning, distribution, and control. The power conditioning system accepts raw electrical energy and converts it to ac or dc of the quality required by the utilization systems. The distribution system transmits power to each load device and minimizes spurious coupling effects. The control function includes a "switching action" which can be used to apply and interrupt power flow. Circuits are switched to obtain a more favorable diversity function and to remove faulty devices from the system.

Power conditioning and management functions are basically a combination of integrated switching operations. The devices available to perform the various functions are transistors, SCR's (silicon-controlled-rectifiers), and mechanically operated contacts. Of course, there are advantages and limitations in the use of each device. The transistor is fast, easily switched, and characterized by a moderately low forward voltage drop; and it is available in a wide variety of configurations. Its limitations include the continuous power drain required to maintain it in an "on" state and a sensitivity to overload currents and transient voltage abuse. The SCR is more rugged; it can be switched "on" more easily and its current and overload capability is high. Its limitations include a more complex turn-off action, a high forward voltage drop (0.5 to 1 volt), and a sensitivity to integrated radiation exposure. The mechanical contact results in a positive turn "on" and "off" capability with near-zero and infinite resistances in the respective states. However, the mechanical contact is physically large for its rating, is sensitive to mechanical vibration and shock, is a slow-speed device, and exhibits a lower reliability.

The assignment of the various devices to the specific power management functions will entail detail analyses of the application of the devices, the relative merit of each, and overall system performance goals. For purposes of this study, the transistor and SCR are considered to be interchangeable.

The overall power management function is arranged to provide the maximum assurance of success based upon total power system unit weight. Configuration optimization involves the judicious value assessment of partial versus total mission success and of light-weight system sophistication versus a rugged brute force approach. Three basic approaches to system configurations are illustrated in Figure 3.7-6: Nonredundant Single Channel System, Modular System Configuration, and Selective Redundancy.

SYSTEMS CONFIGURATIONS

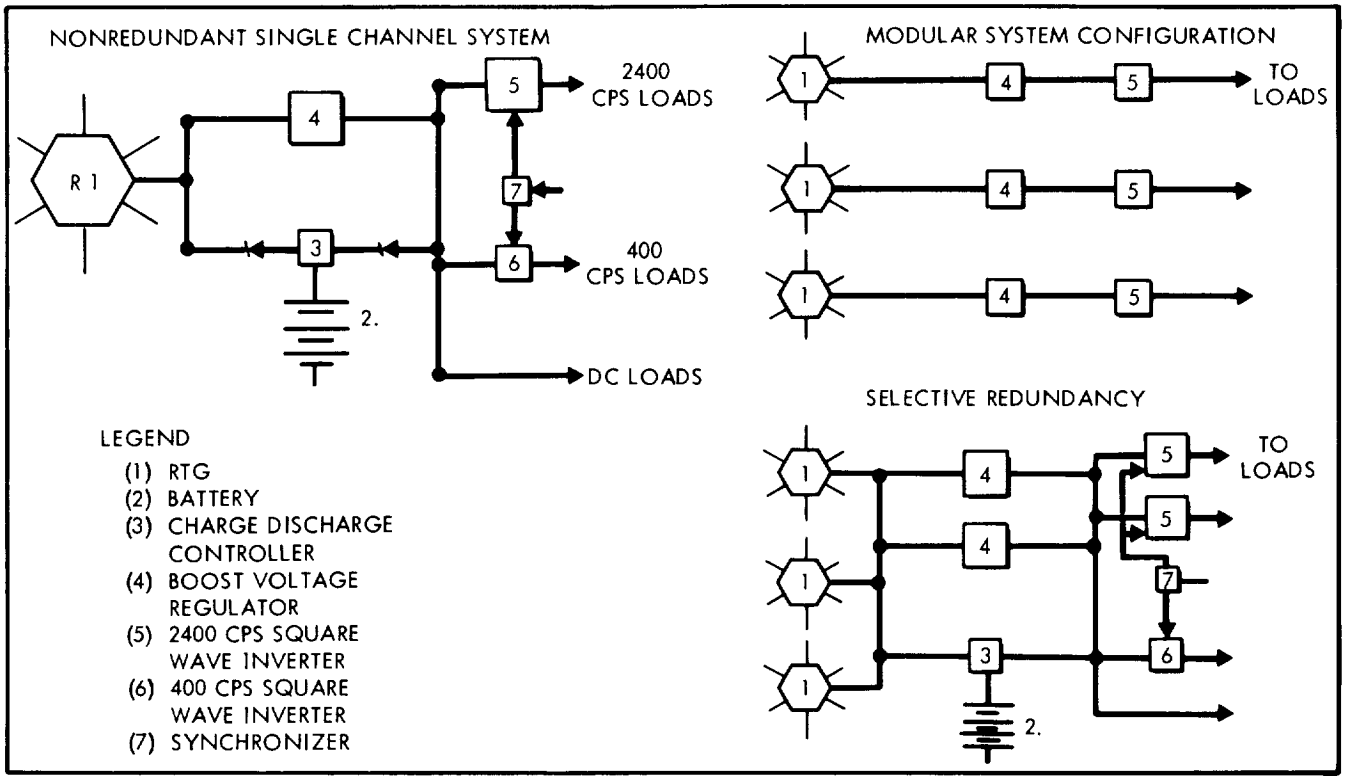

FIGURE 3.7-6

There are several advantages in the use of the Selective Redundancy approach. Reliability is enhanced because normal or partial performance may be continued after the failure of varying numbers of components. Growth capability is also enhanced. Component physical sizes and dimensions can be more readily adapted for convenience in the coordination of spacecraft interfaces. It is therefore concluded that the Selective Redundancy approach is best suited to the subject application.

3.7.3.2 Form of Conditional Power

After the raw power generation system has been designated, the selection of the most suitable form of power distribution is made. The choice rests essentially between ac and dc. The dc

system is the most simple. The possibility exists of arranging the utilization equipment to operate directly from the raw power source with a minimum amount of conditioning and loss. However, as the systems become more complex, as larger loads of various types are added, as the requirement for voltage boost functions are included, as motors are added to the system, and as the advantages of flexibility become greater, the merits of the ac system increase. Therefore, primary power is distributed as a 2400-cps square wave. Direct current is produced by transformer-rectifiers at the point of utilization. DC voltage regulation is achieved by high efficiency, phase-width control silicon-controlled rectifiers (SCR's) operating as both the rectifier and control element. A 400-cps supply is provided to operate gyros and synchros.

3.7.3.3 Inversion

The proposed power conditioning system is so arranged that no voltage regulation function is required of the 2400-cps inverters. Thus, an extremely simple inverter circuit can be used. By virtue of fewer parts and simpler operation, reliability is increased. The recommended inverter circuit was developed by the General Electric Company (Reference 3.7-11) and is illustrated in Figure 3.7-7. The SCR lends itself particularly well to the application because of its inherent ruggedness and simplicity of operation, Hence, the discussion herein is presented in terms of the SCR. However, a pair of transistors and a suitable passive network can be arranged to replace the SCR's if desired or if required because of the radiation environment.

The proposed circuit maintains a square-wave output under virtually all load conditions and does not create high voltage across the SCR's under lightly loaded or no-load conditions. A major advantage of the circuit is its ability to operate under lightly loaded or open-circuit conditions. In the circuit shown in Figure 3.7-7, the feed-back diodes prevent the voltage across either half of the primary winding from exceeding the supply voltage. These diodes not only maintain a square-wave output under all load conditions but permit the use of lower break-over voltage SCR's. The diodes also compensate for leading or lagging power load factors by feeding reactive power back into the supply. Consequently, the commutating capacitor C_2 can be much smaller since its value is dependent upon the maximum current to be commutated and it does not have to correct for the reactive load current. The RTG raw power source is complemented by the battery to reduce transient impedance. Capacitor C_1 is arranged to accept power from the raw power generation source as well as supply power to the inverter.

McMURRAY-BEDFORD INVERTER CIRCUIT

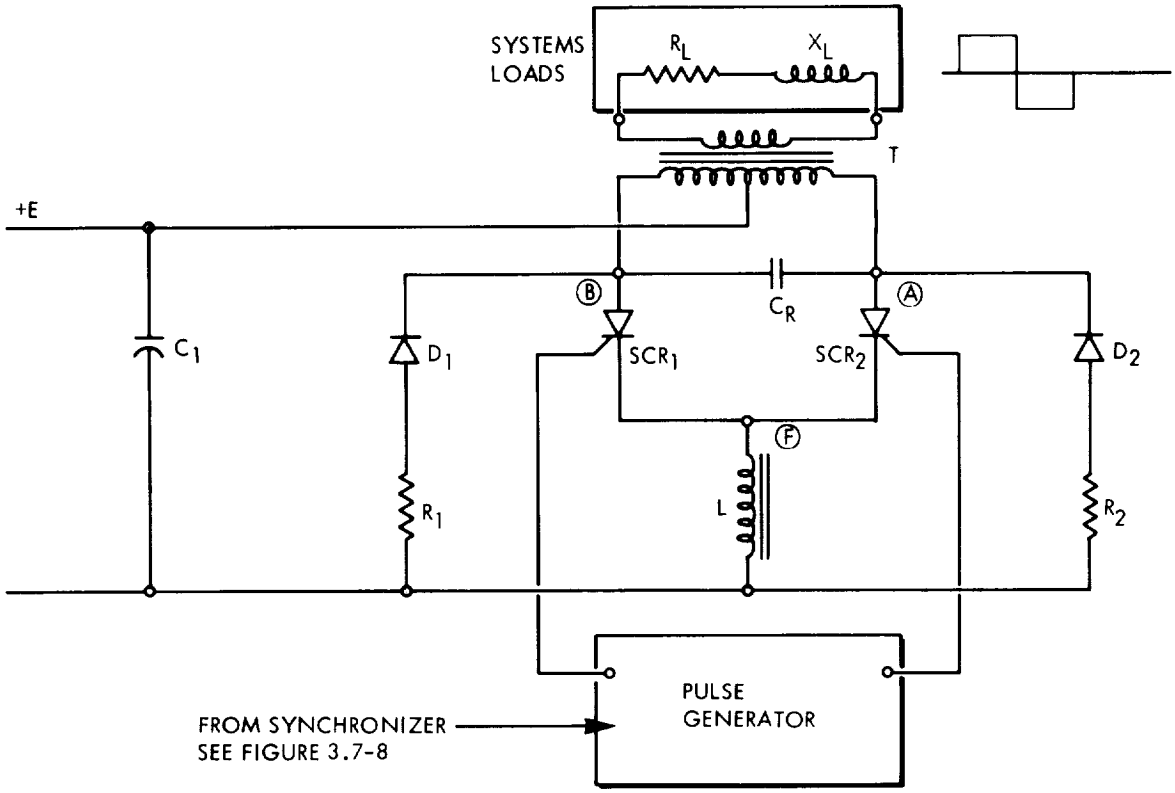

FIGURE 3.7-7

The series inductance L of Figure 3.7-7 is quite small (compared to that used in conventional parallel inverters) and is used because it will resonate with C_2 to create a short impulse to turn off the conducting SCR. The values of C and L are determined by the maximum current to be commutated, the dc supply voltage, and the turn-off time of the SCR's.

The operation of this inverter can best be understood by a detailed explanation of one complete cycle. Assume that SCR1 is conducting. The anode voltage of SCR2 and the right-hand side of capacitor C_2 will be at twice the supply voltage E because of the autotransformer action of T. When voltage is applied to the gate of SCR2, it will turn "on" and the top end of L, point "F", will rise momentarily to twice the supply voltage. Capacitor C is thereby connected directly across SCR1, and its voltage back-biases SCR1. The capacitor discharge through L is oscillatory, and when the anode of SCR2 goes below ground, diode D2 conducts and the oscillation is damped out by R2. C and L are used so that when the SCR is turned "off," it will be back-biased for a sufficient length of time to recover its blocking characteristics. With a purely resistive load, D2 and D1 conduct only during the commutation interval, and short turn-on pulses applied alternately to the gates would ensure proper operation.

With an inductive load, the operation of the inverter is more complex. Based on the assumption that SCR1 is conducting, turning "on" SCR2 will turn "off" SCR1, as described previously. An inductive load prevents the main load current from reversing instantaneously. Transformed load current must flow through diode D2 back into the dc supply until the load current reverses. During this feedback interval, the current through SCR2 will fall to zero and SCR2 will actually become back-biased so that it will have to be refired when the load current reverses. After being refired, SCR2 will continue conduction for the rest of the half cycle. SCR2 can be refired either by supplying another pulse at the proper time or, more easily, by maintaining gate drive for the full half cycle.

As illustrated in the Electric Power System Schematic Diagram of Figure 3.7-8, a signal from the power synchronizer controls the inverter square wave output to 2400 cps.

ELECTRIC POWER SYSTEM SCHEMATIC DIAGRAM

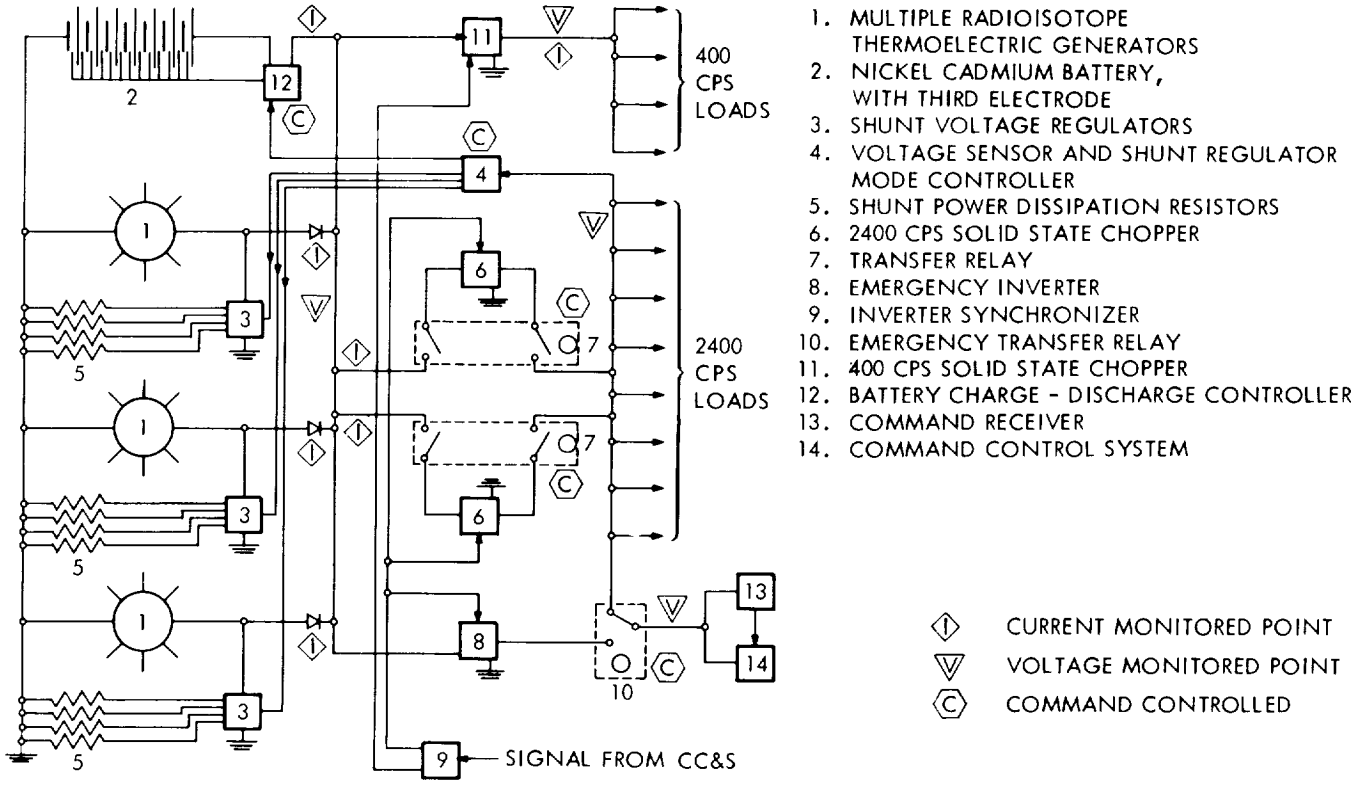

FIGURE 3.7-8

3.7.3.4 Voltage Regulation

The use of a shunt regulator for the purpose of voltage regulation is advantageous because at the end of its life, under maximum load conditions, the losses are essentially zero.

The shunt regulator draws the amount of extra current required to cause the excess voltage to be dropped across the internal resistance of the source in order to adjust the voltage to the desired point. The shunt regulator functions to maintain a constant load on the RTG. The continuous drain of a fixed level of electrical energy from the couples stabilizes the energy balance and temperature.

When operated in conjunction with an RTG, the shunt regulator is inherently more efficient and reliable than any form of series regulator. Under all operating modes, the series regulator is characterized by some forward voltage drop and energy loss. Most failures are catastrophic. The proposed shunt regulator consists of a large number of independent shunt resistors. By the incorporation of current limiters, the operation of the system will not be adversely affected by failures occurring within any combination of several shunt elements. Further, when the system is fully loaded, all shunt elements will be "off" and the regulator will become 100-percent efficient.

In the Power System Schematic Diagram, Figure 3.7-8, a shunt regulation system consisting of three separate parts is depicted. The shunt power dissipation resistors, Item 5, are shown relative to each RTG. Each group of resistors is rated to accept the full output of the RTG. Item 3, the switching unit, is arranged to switch individual resistors on and off the line. The resistors are sized to permit a step regulation function to maintain voltage within tolerances. The transistor switches of Item 3 are arranged to operate in the saturated mode in order (1) to decrease the heat rejection requirement, (2) to reduce the temperature, and (3) to prolong life. Items 3 and 5 are operated separately with each RTG in such a manner that a failure within one unit will not impair the operation of the full raw power generation system.

Item 4 is used to sense voltage on the 2400-cps bus and to produce signals to each switching unit to maintain voltage at the 2400-cps bus within tolerance. Thus, there is no requirement for the inversion unit to include regulation functions.

Item 4 can serve also as a mode-of-operation selector. To prevent the occurrence of instability between the separate voltage controllers, one RTG control unit is selected as the master voltage controller. The remaining units are operated in a slave mode as a function of both output current and bus voltage. A command link permits the selection of a mode for each of the RTG units.

3.7.4 Energy Storage

An energy storage system can be arranged to supply power to accommodate peak loads, and thus the size of the prime power source can be significantly smaller than that required to meet the peak power demand. Peak loads can be considered in three categories. The first category includes loads which are characterized by brief, high-power surges resulting from a small energy requirement at any time throughout the entire mission period. The second category includes repetitive loads which might occur during such events as data transmission cycles. The last category pertains to spike-type power surges with durations in the millisecond range. Such surges may occur at regular intervals throughout the mission as a consequence of switching and commutation events which take place within the load systems. The RTG has no transient overload capability. As illustrated in Figure 3.7-2, it can be represented as a power source with a fixed internal voltage and unit internal resistance. Hence, current load spikes are reflected as voltage notches. In case of a transient overload, the battery serves as a filter by reducing the system transient impendance.

Table 3.7-2 is an excerpt from an Eagle-Picher Company brochure. Typical energy densities and the major applications of the four types of high-energy density batteries employed in the space program are depicted.

Functionally, the use of a battery is desirable. However, because of the contribution it makes to the "parts population," the reliability of a system required to operate over a prolonged period is seriously degraded. Hence, analytical investigations and laboratory analyses of the operation of an integrated systems mock-up are required to define the best composition of an energy storage system as well as the manner in which the system should be applied, if at all.

The proposed system configuration includes a nickel-cadmium battery. The nickel-cadmium battery is capable of the greatest number of change-discharge cycles and the longest wet stand of all batteries. Hence, although it represents a "worst case" contingency it is recommended until (1) further investigations verify that one of the higher energy density batteries is capable of meeting the mission requirements or (2) it is proved that the nonmagnetic characteristics of the zinc-silver oxide on the silver-cadmium batteries are required. The supervision of the condition of the battery over the long mission period is a matter which will require extensive study. Overcharge produces high

TABLE 3.7-2

BATTERY SYSTEM CHARACTERISTICS

BATTERY SYSTEM	OPERATING TEMPERATURE °F NORMAL	W/HEATER	TYPICAL ENERGY DENSITY Whr/lb	Whr/Cu in	MAJOR APPLICATION
Silver-Zinc Primary	-40° to 130°	-65° to 130°	50-100	3.5-7.5	Where long dry shell-life, maximum energy, and close voltage regulation is required - For extremely high continuous pulse rates of discharge - Life limited to one to two months.
Silver-Zinc Secondary	-40° to 110°	-65° to 110°	30-80	2.0-4.5	Where maximum energy density and voltage regulation is required throughout a cycle life period of 6 to 8 months.
Silver-Cadmium Secondary	-40° to 110°	-65° to 120°	15-40	1.0-2.8	Where maximum energy density is required throughout a cycle life period of 6 to 36 months.
Nickel-Cadmium Secondary	-65° to 120°	-65° to 120°	10-25	0.8-1.5	Where reliable cycling capability is required over a period measured in years.

pressure and over-temperature and reduces life. Low-depth discharge cycles result ultimately in reduced capacity because of the "memory effect". In the System Configuration Schematic, Figure 3.7-8, a charge-discharge controller with a command control link is depicted. The operational details must be developed as the system requirements become better defined. The minimum requirements for the controller are as follows (1) to function normally by floating the battery on the system, (2) to provide a voltage boost toward the battery during periodic heavy-charge cycles, and (3) to function as a boost toward the load to produce an occasional high-depth discharge. Under all battery operational modes, the discharge voltage must be coordinated below the shunt regulator control point.

3.7.5 Recommended Configuration

The application of principles set forth above evolved into the recommended system configuration as shown in Figure 3.7-8.

3.7.5.1 Operation

The currents for the raw power generator and inverter are monitored by the data management system. Raw-power and conditioned-power bus voltages are monitored in a similar manner. Command control functions include (1) the turn-on and turn-off of loads individually and in groups, (2) the operational mode selection of individual RTG shunt voltage regulators, (3) the function selection of the battery charge-discharge controller, and (4) the application and removal of the redundant 2400-cps inverters.

The command receiver and control system is normally powered from the main 2400-cps load bus. However, a transfer switch is provided so that a shift from the essential command functions to the emergency bus occurs automatically upon a failure of the normal source. Command override is provided for the transfer function. The proposed method of voltage control is described in subsection 3.7.3.4.

3.7.5.2 Efficiency

As stated in subsection 3.7.3.4, the shunt regulator is used to consume only the surplus power required to reduce the voltage to the desired point. Hence, losses occurring under light load situations are not included in the consideration of efficiency.

The component efficiencies are as follows: (1) blocking diode on RTG output, 96 percent, (2) inverter switching elements, 96 percent, (3) inverter transformation and control, 92 percent, (4) distribution, 97 percent, and (5) control elements, 98 percent. The total system efficiency is therefore the product of component efficiencies, i.e., 80.5 percent.

3.7.6 References

3.7-1 "The Nuclear Space Power Program," Paper presented by Dr. J. D. Lafleur and R. T. Carpenter, 12th Nuclear Science Symposium, 18 October 1964. (Unclassified)

3.7-2 Private communication from General Electric Company, Missile and Space Division, J. W. Millard, Manager Isotope Application, 15 April 1966. (Unclassified)

3.7-3 "Silicon-Germanium Thermoelectric Power-Generating Devices," R. L. Klem and A.G.F. Dingwall, Radio Corporation of America, presented at the International Conference on Energetics, University of Rochester, Publication No. ST-2953, August 1965.

3.7-4 "Design Study for an Advanced RTG Power Supply, "General Atomics/GA-500, July 17, 1964. (Confidential)

3.7-5 "Advanced SR-90 Space Power Supply Study," Martin Company, MND-3393, August 1964. (Confidential)

3.7-6 "Engineering Study of an Advanced 250 Watt, SR-90 Fueled Thermoelectric Power Supply, "Hittman Associates, HIT-143, August 14, 1964. (Confidential)

3.7-7 "Advanced Space RTG Study, "General Electric Co., GEMS-NS-107, August 1964. (Confidential)

3.7-8 40-Watt PU-238 Power Supply Engineering Study, General Electric Company, GEMS-NS-111, January 1965. (Confidential)

3.7-9 "Preliminary Design and Safety Studies of Large Radioistope Heat Sources for Space Power," General Electric Company, GE Document No. 655D4408 GEMS-3526-1, 31 July 1965, (Confidential-Restricted)

3.7-10 "SNAP-27, Quarterly Report No. 1," General Electric Company GEMS-3535-1, 28 January 1966.

3.7-11 "Voltage Regulation and Power Stability in Unconventional Electrical Generating Systems, Quarterly Progress Report No. 3, General Electric Company, ASTIA No. 282718.

3.7-12 "Technical Data on Eagle-Picher Customized Batteries," Eagle-Picher Company, Couples Department, Joplin, Missouri, 1965.

3.8 THERMAL CONTROL

The thermal control requirements of a Jupiter flyby spacecraft vary significantly with variations in the spacecraft configuration, and in many cases, the final section of the thermal control concepts will depend on specific details of the spacecraft design. The thermal control analysis reported herein is designed to accommodate these requirements for versatility. The approach has been to conduct parametric analyses on configurations typical of Jupiter flyby spacecraft, to identify basic thermal control concepts, and, subsequently, to recommend approaches for thermal control of specific spacecraft design concepts.

3.8.1 Component Thermal Control Requirements

Requirements for thermal control of the spacecraft equipment involve primarily the operating and storage temperature limits and the dissipation of waste heat. An environmental (cold plate) operating temperature range of 14° to 100° is suitable for most components. Some components are capable of operating over a wider range of temperature limits and will tolerate a broader range of nonoperating temperates. On the other hand, the temperature of the propellant for the midcourse propulsion system (hydrazine) should not be allowed to drop below 40°F. The final layout of equipment requires a consideration of the temperature limits of individual components for optimum placement. Summaries of the operating and nonoperating temperature limits, nominal power dissipation, and mass of the components in each spacecraft design concept considered in this study are presented in Section 5.

The heat dissipation of components with large power requirements is an important consideration in providing sufficient heat flow paths from these components to the heat sink (radiating surface). With the exception of the communication transmitter, the power dissipation of the individual components is generally small.

3.8.2 Mission Considerations

The Jupiter flyby mission has several distinct phases in terms of the thermal environment. These are prelaunch, launch, Earth orbit, cruise, and Jovian encounter. During prelaunch, the payload compartment is usually supplied with conditioned cooling air. It is assumed in this study that the necessary cooling air will be available.

During the launch phase of the mission, a potential problem area is the dissipation of excess heat, particularly from the RTG's. The radioisotopes are unmodulated and will dissipate a significant amount of heat. The payload compartment which is aerodynamically heated, cannot be expected to serve as a heat sink. Additionally, provisions for cooling the payload are not usually available from the spacecraft during this time. Thus, until the payload fairing is separated, the RTG's either will have to depend on thermal transients or an auxiliary cooler must be incorporated.

The Earth orbital phase of the mission may present a particular problem for thermal control of the spacecraft equipment components. Because of the length of this phase (up to 1 - 1/2 hours), the thermal transients cannot be expected to maintain the equipment temperature limits unassisted. For this study, a 105 nautical mile circular, noon orbit is assumed in order to ascertain the maximum expected Earth radiation and reflected solar radiation heating rates.

Soon after the Earth escape rockets are fired, the spacecraft leaves the Earth's thermal sphere of influence. During the cruise phase of the mission, the only sources of radiative heating of the equipment components are the RTG's and the Sun. RTG heating is essentially constant because of the long half-life of the plutonium fuel. Intensity of the solar radiation, however, varies from 134 watts per square foot at 1 a.u. near Earth to approximately 5.8 watts per square foot in the vicinity of Jupiter.

At Jovian encounter, the spacecraft passes within a few planet radii of Jupiter. The mean planet radiation temperature, which is estimated at -190°F, is so low, however, that the thermal radiation can be neglected in thermal control considerations. Heating from planet reflected solar radiation is also low because of the low level of incident solar radiation. Planet encounter is not analyzed in this study as a separate mission phase because of its similarity to the thermal environment in the latter portions of the cruise phase.

Some of the characteristics of the mission pertinent to thermal analysis are shown in Figure 3.8-1. It should be noted that the data for the three parameters shown are not applicable to the same trajectory. The data selected represent the worst anticipated thermal problem in each mission phase. In the case of distance from Earth during departure, a slow Earth departure trajectory has been selected. A nominal heliocentric transfer is used for solar distance data, and a relatively slow trajectory for Jupiter encounter was selected for data on distance from Jupiter.

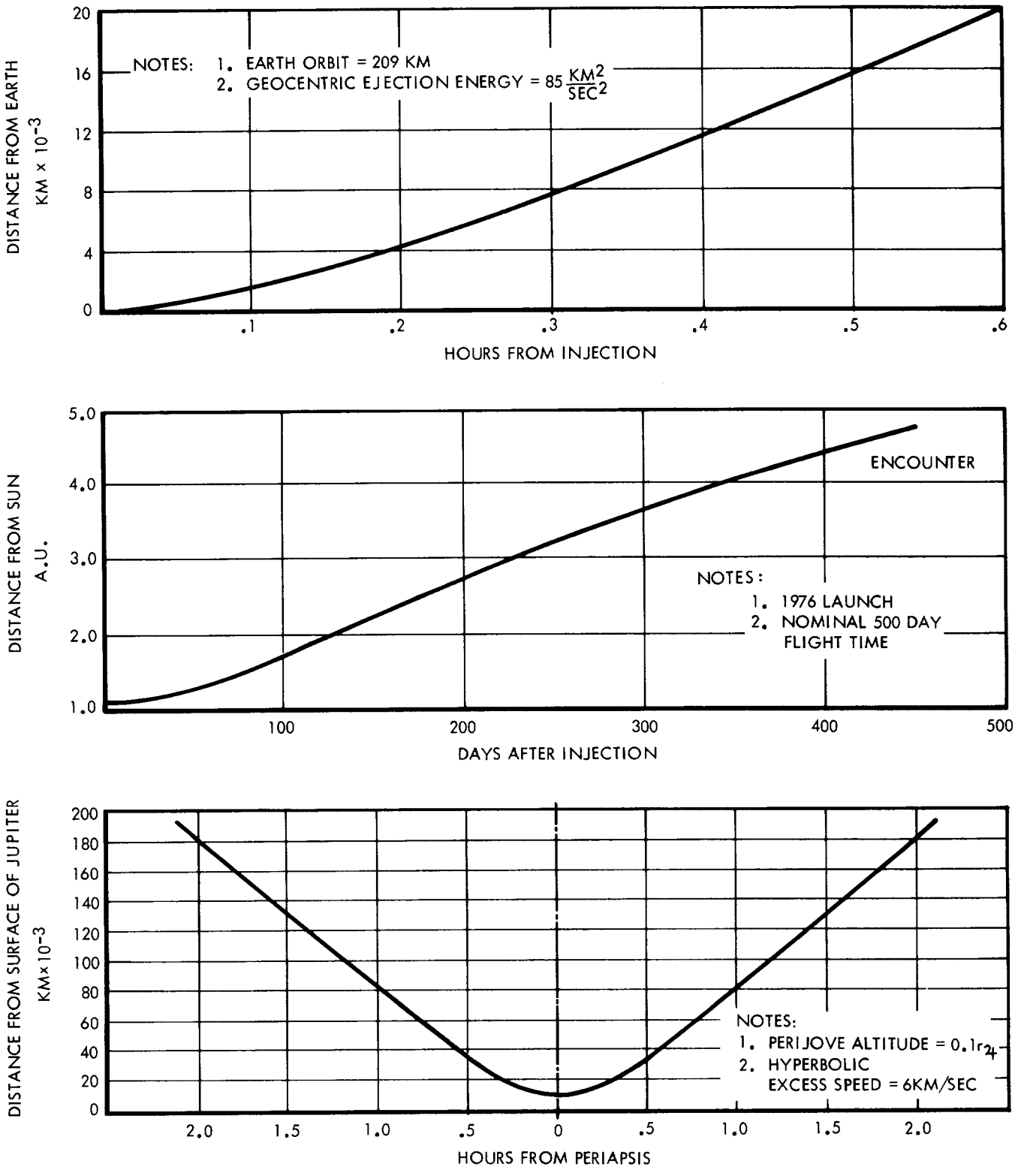
DISTANCE FROM EARTH KM x 10⁻³
20
16
12
8
4
0
NOTES: 1. EARTH ORBIT = 209 KM
2. GEOCENTRIC EJECTION ENERGY = 85 KM²/SEC²
.1
.2
.3
.4
.5
.6
HOURS FROM INJECTION
DISTANCE FROM SUN A.U.
5.0
4.0
3.0
2.0
1.0
ENCOUNTER
NOTES:
1. 1976 LAUNCH
2. NOMINAL 500 DAY FLIGHT TIME
100
200
300
400
500
DAYS AFTER INJECTION
DISTANCE FROM SURFACE OF JUPITER KMx10⁻³
200
180
160
140
120
100
80
60
40
20
0
NOTES:
1. PERIJOVE ALTITUDE = 0.1r_J
2. HYPERBOLIC EXCESS SPEED = 6KM/SEC
2.0
1.5
1.0
.5
0
.5
1.0
1.5
2.0
HOURS FROM PERIAPSIS

FIGURE 3.8-1

3.8.3 Design Considerations

The spacecraft may be divided into three distinct areas for thermal design purposes. These are (1) the RTG's, (2) equipment located in the central equipment bus, and (3) components located on extensions from the spacecraft.

An analysis of the design variations of the RTG's was considered beyond the scope of this study. Therefore, a ground rule was established to define RTG exterior surface temperature and size. The surface temperature is considered to be 510°F, and the size-capacity relations are those discussed in subsection 3.7.

Thermal control of the components in the central equipment bus depends on an overall thermal balance and local temperature variations between components. The sources of heat to be dissipated by the bus are (1) waste heat dissipated by electronic components, (2) radiant heating from the space environment (which includes planetary heating near Earth), and (3) heating from the RTG's.

The waste heat dissipated by the components varies somewhat during the mission. This variation is due to components being turned on and off or placed on a standby status. When a shunt resistor voltage control is used in the power conditioning equipment, the power not required by the components is dissipated in shunt resistors. Assuming the shunt resistors can be located in the equipment bus, the total power dissipation from components and shunt resistors is essentially constant. The major problem then becomes the balancing of the heat dissipation between groups of thermally connected components. Equipment power density, component temperature limits, and time variations must be considered.

Space environmental heating will vary from a maximum in Earth orbit to a minimum during cruise near Jovian encounter. Except for about the first hour, the only appreciable environmental heating during cruise is solar radiation. This presents a problem since the solar intensity at encounter is only about 4 percent of the near-Earth value. Appropriate design can minimize the effect of variable solar heating for the three-axis stabilized, solar oriented spacecraft concepts by insulating the surface facing the Sun. For spin-stabilized spacecraft with spin axis perpendicular to the spacecraft-Sun vector, only the sides are exposed to a significant degree of solar radiation.

Here, too, solar heating can be virtually eliminated by insulating the sides of the spacecraft.

Radiant heating in Earth orbit is more difficult to control. In addition to direct solar energy, radiation from the Earth and reflected solar radiation are significant heat inputs. During this phase of the mission, the spacecraft is fixed with respect to the launch vehicle which will probably be oriented along the velocity vector. This means that the spacecraft receives significant incident energy on virtually all surfaces. Thermal control will depend on orientation of the heat dissipating surfaces and possibly on thermal transients.

The modes of heating from the RTG's are conduction through the supports and thermal radiation. Conduction through the supports can be minimized by appropriate design and selection of materials. Thermal radiation exchange between the RTG's and the equipment bus is determined by geometry, surface coating properties, insulation, and, when present, radiation shields.

Depending on spacecraft design, RTG heating can be either a hindrance to thermal control or a help in stabilizing temperatures. Since the capability of surfaces exposed to RTG heating to reject heat is greatly reduced, heat dissipation surfaces either must be located on surfaces not exposed to RTG heating or thermal shields must be employed to block the thermal radiation from the RTG's. However, RTG heating can also be used to keep surface temperatures from dropping too low under low power conditions. The simplest method of accomplishing this is to apply high emittance coatings to the surfaces "seeing" the RTG's. By proper selection of geometry, the heat absorbed from the RTG's is equal to the heat dissipated by the surface at the design temperature and as a result no net heating of the surface exists. As the temperature drops, the net heat absorbed from the RTG's increases. There are many variations to this basic concept, but it generally requires a close proximity of the RTG to the spacecraft. A trade-off study between the radiation effects and the advantages of this thermal control concept would be required to justify the concept.

A more accurate control of RTG heating can be achieved by the use of louvers. In this concept, the RTG's have to be close enough to the surface so that the heat exchange is always from the RTG to the equipment bus surface. Louvers are then used to control the net amount of heat absorbed by the bus. The geometry

required to obtain heating from the RTG's is best described by the geometrical view factor F_{i-j} where i refers to the bus surface and j refers to the RTG (F_{i-j} is the ratio of energy impinging on surface j to the energy emitted by surface i). A view factor of 0.1 or greater is required to obtain appreciable heating. Performance of an RTG-louver heating system is shown in Figure 3.8-2.

Heat dissipation from the spacecraft equipment bus will be accomplished by the use of radiating surfaces to which the components are mounted. The amount of heat dissipated can be controlled by adding louvers. The estimated performance of a practical louver design was determined from the work of Plamondon (Reference 3.8-1) and from analyses conducted for this study. Figure 3.8-3 is a presentation of louver performance. It was constructed for preliminary sizing of louver areas not exposed to solar irradiation.

Location of the heat dissipation surfaces is important in minimizing the variation in effective radiation sink temperature during the mission. If the surface is exposed to solar radiation during the near-Earth portion of the mission (solar distance near 1 a.u.), solar heating becomes a problem. This problem is amplified in Earth orbit where the surface may also receive heating from planetary and reflected radiation. The amount of heat absorbed from the RTG's is also affected by location of the heat dissipation surface.

The recommended location of the heat dissipation surfaces is on a side or sides of the bus not "seen" by the Sun. This is possible on all spacecraft concepts considered since all have a constant orientation with respect to the Sun. Although thermal shields can be used to considerably reduce heating from the RTG's, it is normally desirable to locate the heat dissipation surface so that it is not seen by the RTG. The feasibility of complying with this latter restriction depends on detailed layout requirements of the bus equipment. The effects of Earth orbital environment on specific surface location could not be thoroughly evaluated in this study because of the dependence on design details. Such factors as thermal transients and upper stage design must be analyzed before a firm configuration can be selected.

Local temperature variations on the heat dissipation surfaces result primarily from nonuniform component heating. These can be minimized by placement of the components so that the specific power dissipation (watts/ft^2) is as uniform as possible and by using high thermal conductivity materials in the mounting plate. The TWT amplifier presents a particular problem in component placement because of its relatively small size and high power dissipation. It dissipates about 20 percent of the total component heat generation. This unit should be mounted directly in good thermal contact with the base plate of a heat dissipation surface (heat sink) of sufficient area to dissipate the required heat.

CONTROLLED HEAT ABSORBTION FROM RTG

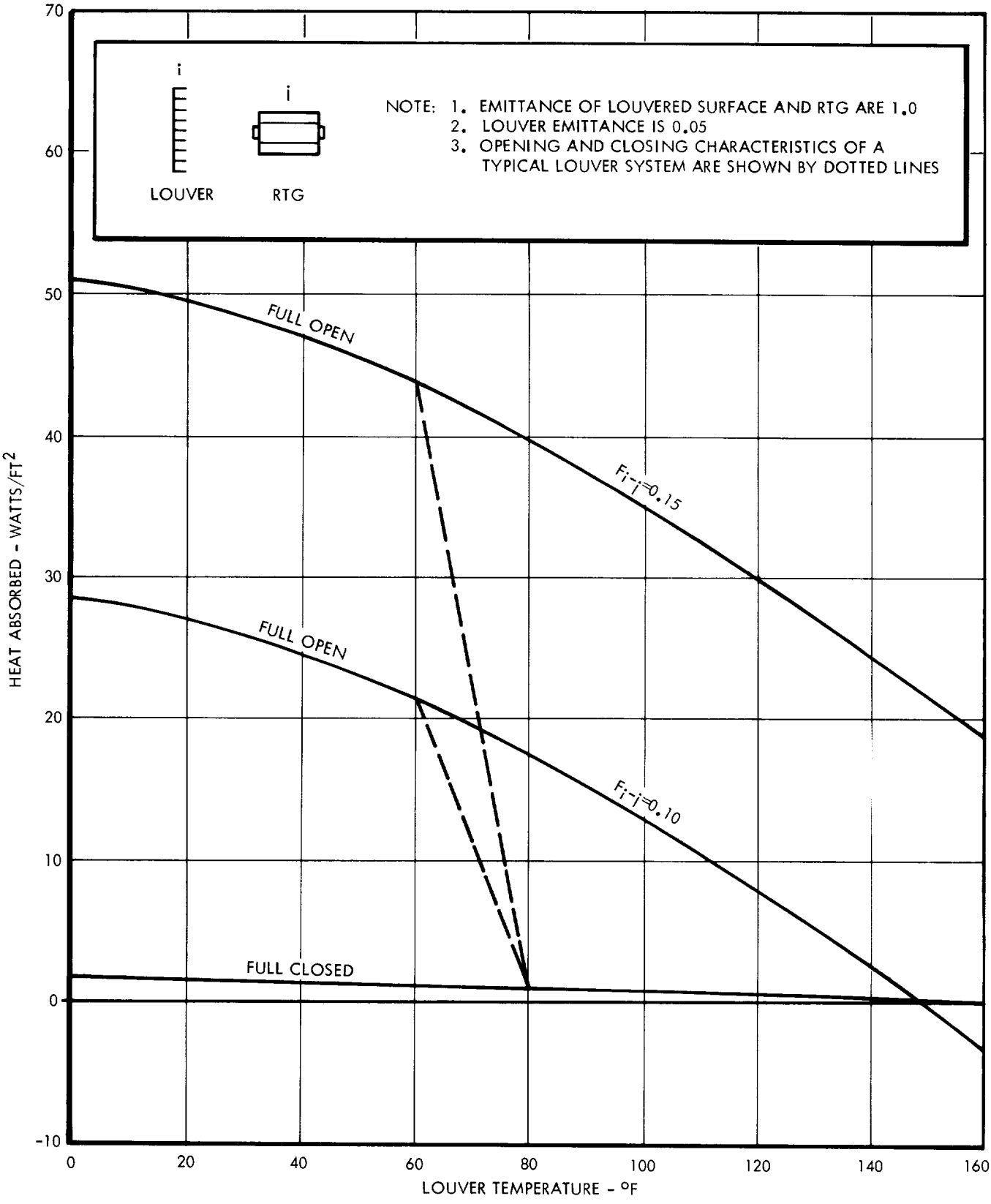

FIGURE 3.8-2

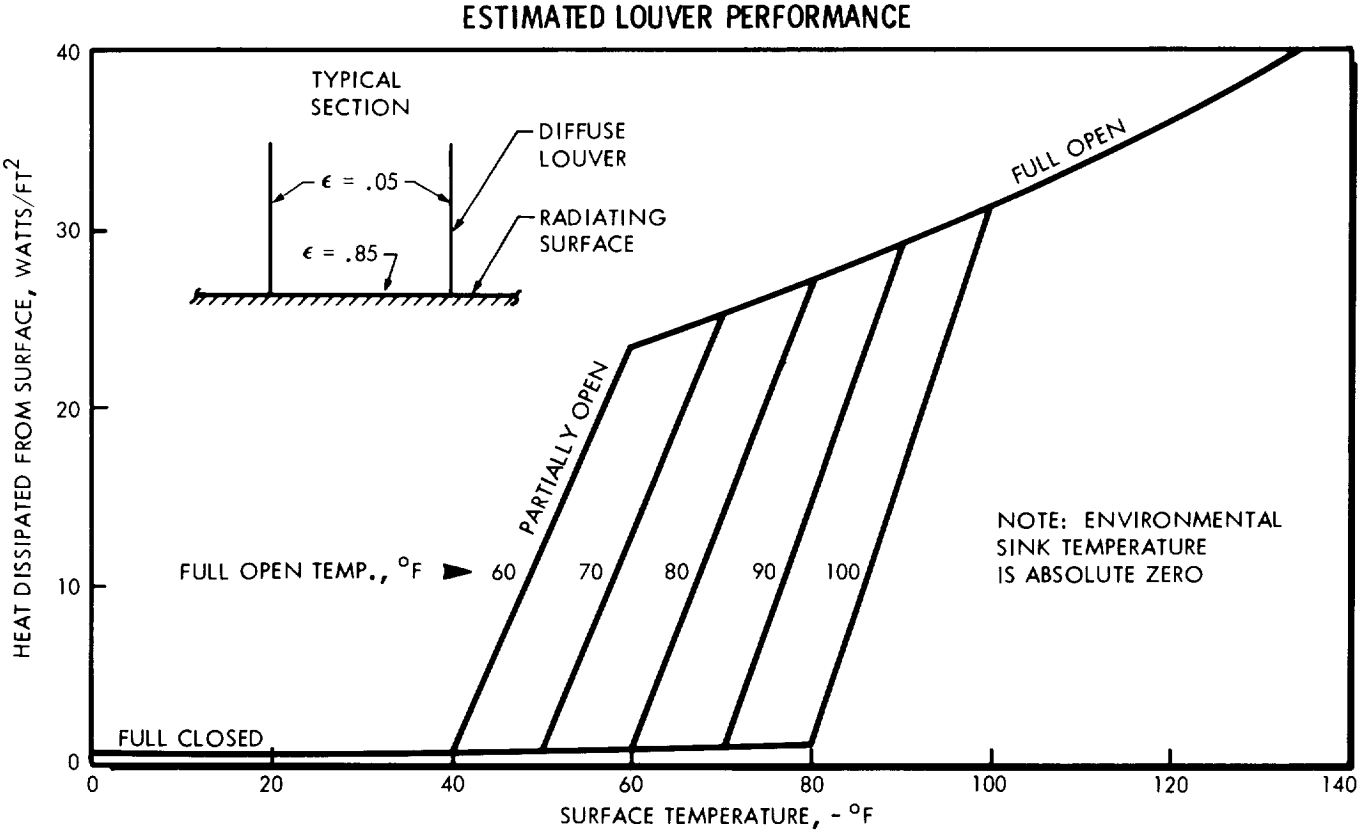

FIGURE 3.8-3

The temperature of extended components is determined by the thermal radiation environment. Heat sources that materially affect these component temperatures, besides power dissipation, are (1) space thermal environment, primarily the Sun, (2) the RTG's, and (3) the spacecraft bus. These components are mostly sensors for the scientific equipment and generally have rather wide temperature limits. An exception is the suggested Rubidium magnetometer sensor which requires a temperature between 32° and 122°F. Such items require a self-contained thermal control function. This may include auxiliary heaters and solar shields to alleviate the extremes in temperature. The effect of power dissipation on extended component temperatures is shown in Figure 3.8-4. The data are based on characteristics associated with spacecraft design concept A (described in subsection 5.1), but they are considered representative.

Additional spacecraft mass for thermal control provisions results primarily from additional thickness of heat dissipation (equipment mounting) surfaces required for high thermal conduction and from use of louvers. Other items, such as coatings, thermal shields, and insulation are relatively light.

Other factors affecting thermal design are the requirements for flexibility, serviceability, and reliability. Thermal design

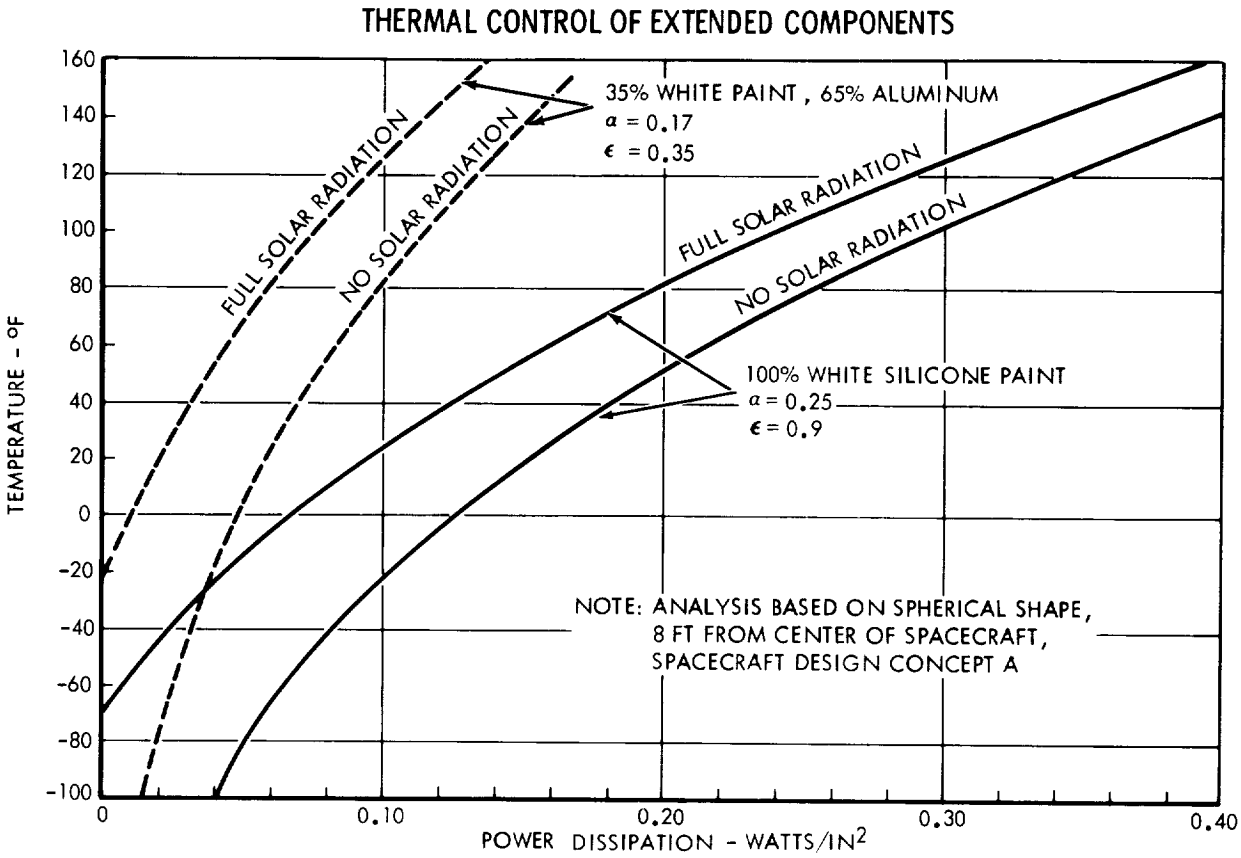

FIGURE 3.8-4

must be flexible enough to accommodate design and component changes which may occur at any time prior to launch date. One technique for achieving this flexibility is to control heat dissipation by changing the ratio of low emittance-to-high emittance coatings. Another method is to mount the equipment in separate compartments so that each compartment is designed to be thermally independent. The modular equipment mounting concept also enables easy service and prelaunch checkout.

Reliability of the thermal control function is closely associated with predictability of performance. A number of previous spacecraft have reportedly failed because component operating temperature limits were exceeded. The recommended approach is to use passive techniques (geometry, conduction, insulation, radiative coatings, etc.) for thermal control to the greatest extent possible so long as a sufficient level of confidence can be maintained in the predictability of their performance. These techniques will be supplemented by semiactive components such as louvers and electrical heater circuits to more accurately control operational temperatures.

3.8.4 Equipment Bus Thermal Control Concepts

3.8.4.1 Isothermal Module

One concept for thermal control of the equipment bus is termed the "isothermal module." In this concept, the vehicle

surface is made of a highly conductive material, such as aluminum, so that the temperature variations over the surface are small. Such a concept is particularly applicable to small spacecraft where the requirement for increased wall thickness to provide high conduction does not impose prohibitively high mass penalties. This concept permits the designer to take advantage of the constant heating from the RTG's as a temperature stabilizing effect over the entire mission. The amount of heating by the RTG's can be controlled (1) by proper selection of coatings and/or louvers on the sides of the spacecraft exposed to the RTG's, (2) by insulation of spacecraft surfaces, and (3) by shielding the RTG's from the spacecraft. Correspondingly, heat dissipation and temperature control can be achieved by selection of proper coatings on the surfaces not seen by the RTG's and by the use of louvered surfaces.

Initial analyses have been conducted to establish the feasibility of applying the isothermal module concept to the spin-stabilized Jupiter flyby spacecraft evolved in this study. Although this concept is used as a reference, the results are expected to be applicable to other concepts as well. The basic configuration, illustrated in Figure 5.1-1, consists of a central equipment bay with RTG units around the periphery. The central equipment bay can be characterized thermally by two regions: (1) the side surfaces and (2) the upper and lower surfaces (perpendicular to the spin axis). Since the spin axis is oriented nominally perpendicular to the solar vector, the sides are the primary surfaces affected by solar radiation. These sides also receive heating from the RTG's. The upper and lower surfaces receive very little heating from the Sun and RTG's and are a logical location for thermal control louvers.

Considering the three characteristic surface areas - louvered area, unlouvered area on top and bottom, and side area - there is an indefinite number of combinations of surface properties and insulation applications that can be evaluated for thermal control. The approach selected for this analysis was to assume initially no insulation on the spacecraft surfaces, to use the louver area provided by initial configuration development, and then to analyze the effect of various surface properties on the other two surface areas.

In order to make the analysis more realistic, the coating properties are assumed to be those of a mosaic of low emittance aluminum and white silicone paint. This combination yields a wide range of emittances while retaining a low solar absorptance For a particular mosaic on the sides of the spacecraft, the heat rejected from the spacecraft can be calculated as a function of emittance of the upper and lower surfaces. The heat rejected with louvers full open is shown in Figure 3.8-5 for a range of mosaic properties.

If the voltage regulator shunt resistors are designed to dissipate heat within the central bay, the total component heat dissipation will remain essentially constant. Considering the design

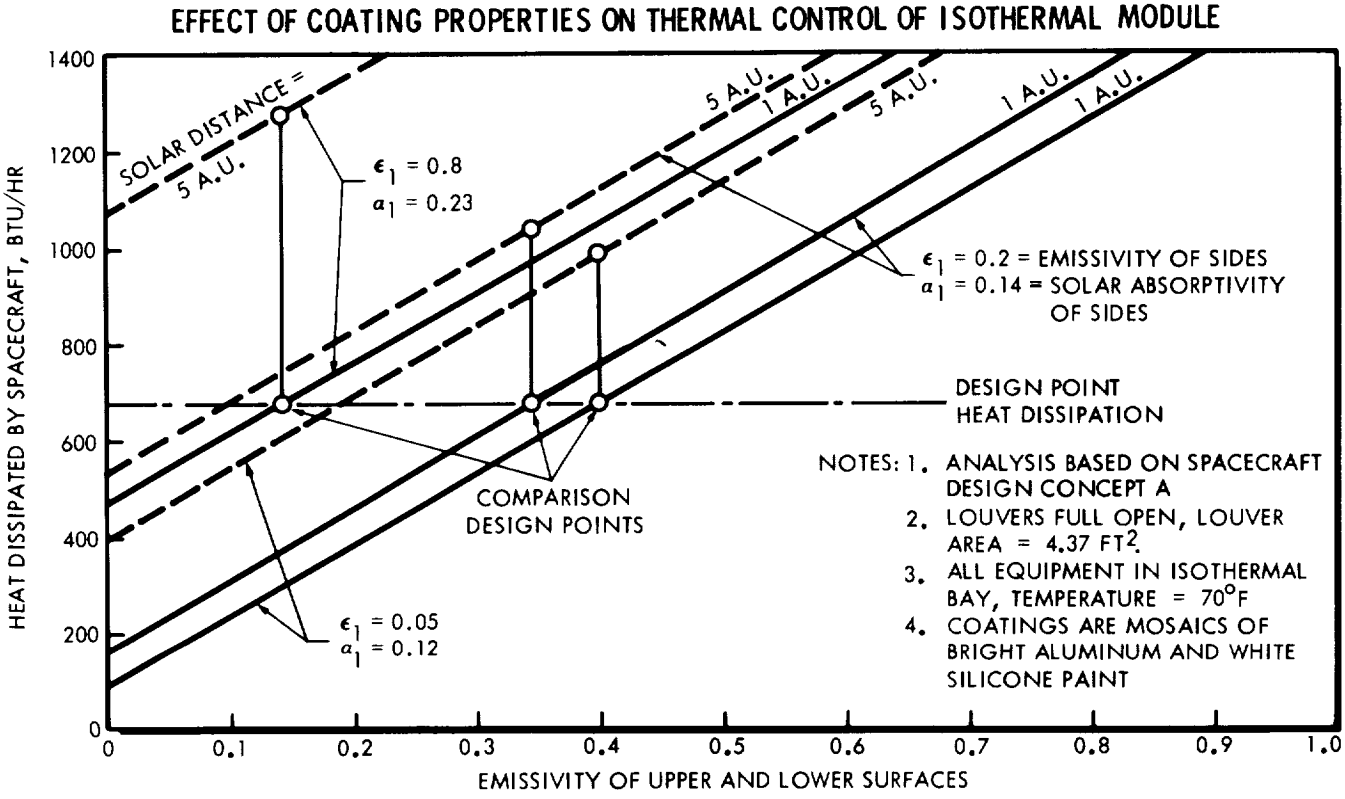

FIGURE 3.8-5

point to be the louver full-open position at a solar distance of 1 a.u., the variation in heat dissipation capability for a mission is indicated by performance at 5 a.u. It is noted from Figure 3.8-5 that as the side surface emittance decreases (lower percentage of white silicone paint), the variation in heat dissipation also decreases thereby requiring less control by louvers. The capability of Mariner-type louvers to control the heat dissipation is illustrated in Figure 3.8-6 with a side wall coating of low emittance aluminum only.

The trend of decreasing louver requirements with decreasing emittance suggests the possible advantages of insulating the side-wall surfaces. The capability of the louvers to control heat dissipation with the sides fully insulated (negligible heat flow) is illustrated in Figure 3.8-7.

Another consideration in the use of low emittance and low solar absorptance surfaces is the sensitivity of these properties to surface condition. The effect of deviation from the nominal, or predicted, value of emittance on heat dissipation from the spacecraft is shown in Figure 3.8-8. Similarly, the effect of deviation in solar absorptance is shown in Figure 3.8-9. A maximum expected deviation is difficult to predict accurately, but it is not expected to be more than about 0.02 with proper handling procedures. Such a deviation results in a significant error in predicted heat dissipation, but the louvers can be designed to accommodate it. If the

EFFECT OF SOLAR DISTANCE ON THERMAL CONTROL OF ISOTHERMAL MODULE DESIGN WITH NO SIDEWALL INSULATION

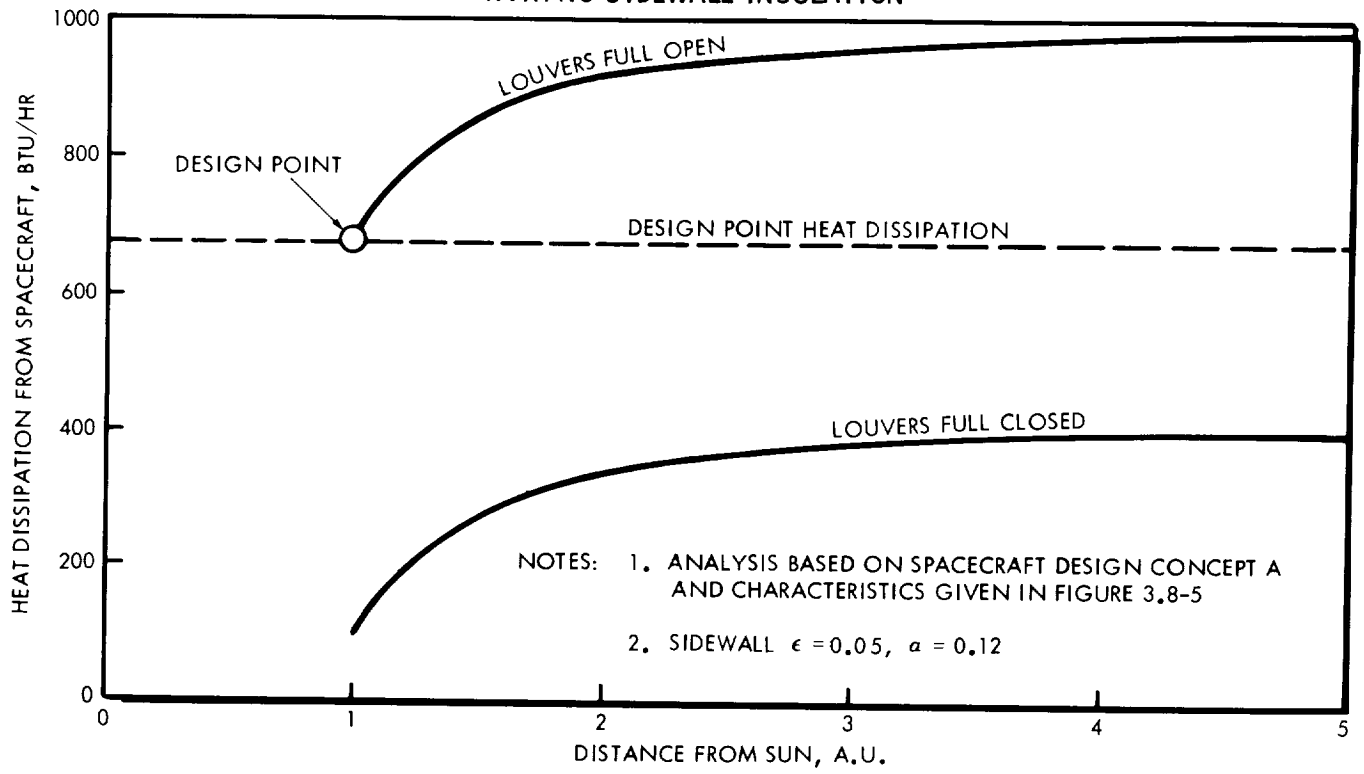

FIGURE 3.8-6

EFFECT OF SOLAR DISTANCE ON THERMAL CONTROL OF ISOTHERMAL MODULE DESIGN WITH SIDEWALL INSULATION

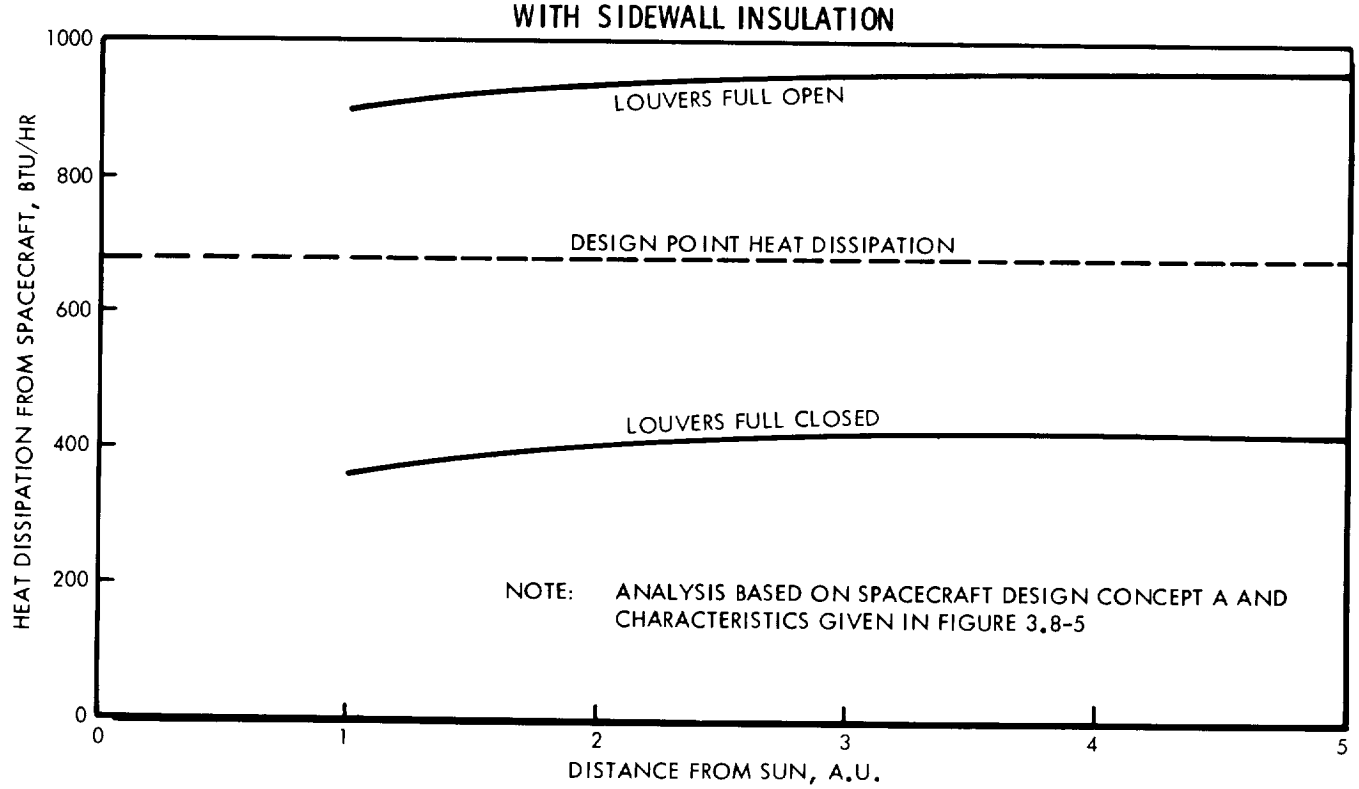

FIGURE 3.8-7

EFFECT OF DEVIATION FROM NOMINAL VALUE OF EMISSIVITY ON HEAT BALANCE

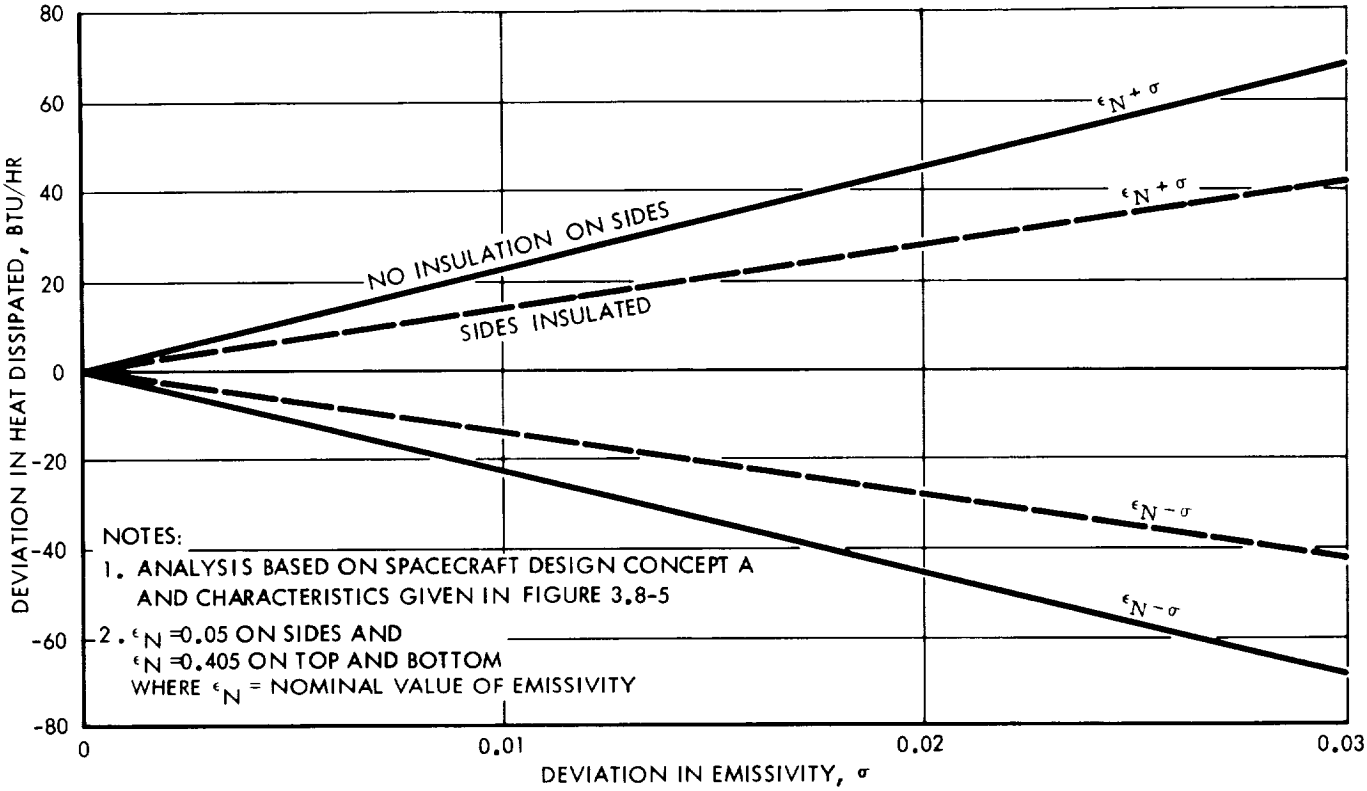

FIGURE 3.8-8

EFFECT OF DEVIATION FROM NOMINAL VALUE OF SOLAR ABSORPTIVITY ON SOLAR HEATING

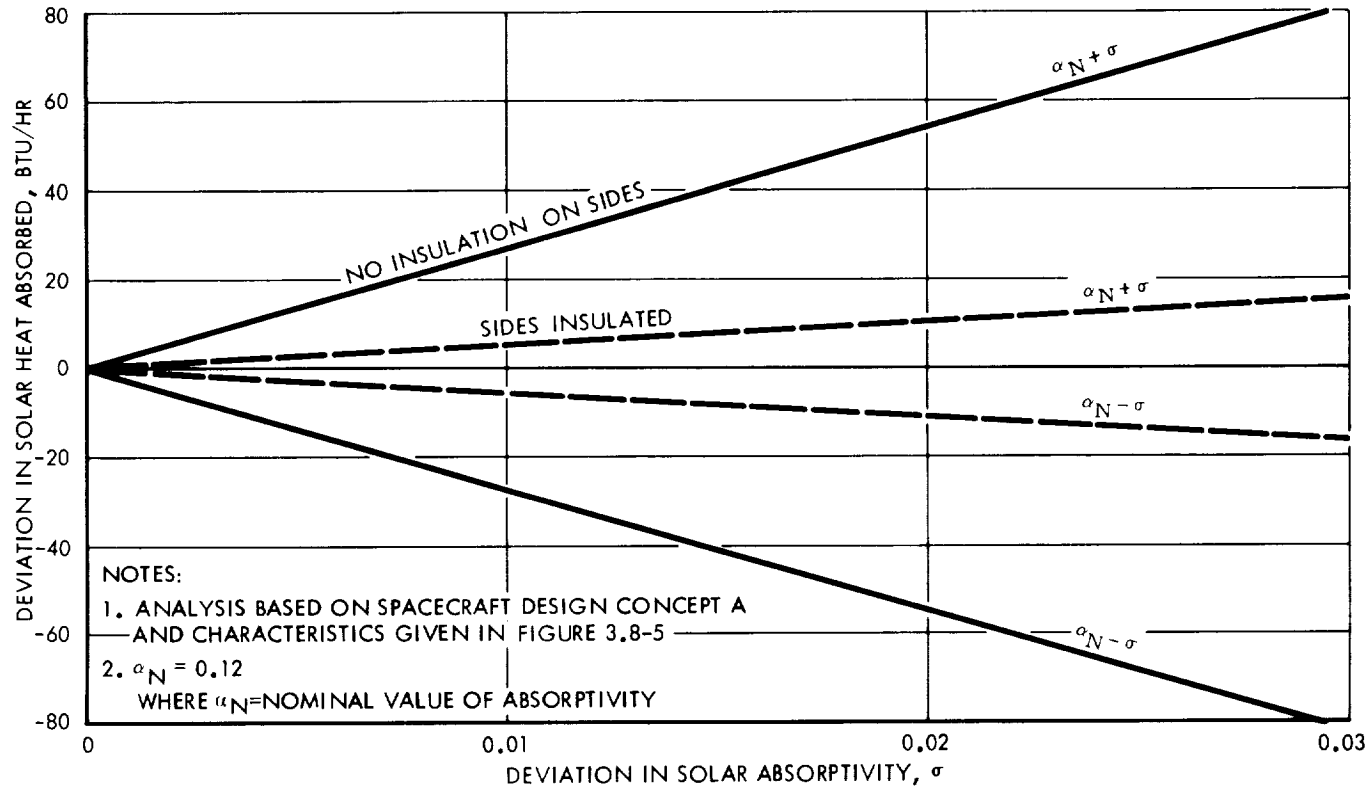

FIGURE 3.8-9

sides of the spacecraft are insulated, the deviation in absorbed solar energy is considerably reduced.

On the basis of thermal control capability, it appears that the spacecraft sides should be insulated where an isothermal module concept is utilized. Sidewall insulation also reduces environmental problems during the launch phase of the mission.

3.8.4.2 Modular Concept

The modular concept of bus equipment temperature control is investigated primarily because it is a possible means of improving design flexibility and serviceability. In this concept, the components are arranged in thermally isolated (or semi-isolated) equipment compartments. Hence, less protection is required for the compartments housing components with wide operating temperature limits.

The equipment compartments or modules provide design flexibility, particularly for thermal design, in that each compartment can be modified essentially independently of the other compartments. Even last minute changes in heat load can be accommodated by adjusting radiative coating properties or louver area.

Serviceability is enhanced since the heat dissipation surfaces to which the equipment is mounted can be made to swing out intact. Components are then serviced or interchanged without disturbing the thermal control.

On the other hand, the modular concept presents some peculiar problems in equipment design and layout. A certain amount of mass and geometrical symmetry is desirable in the spacecraft for structural loading, propulsive maneuvers, and attitude control. This means the compartments should be of similar size or at least paired. Volume and mounting area of the components must be compatible with the compartments available.

The two thermal control parameters which must be compatible with the compartments are component temperature limits and total power dissipation. Maximum latitude in operating temperatures can be achieved if components with similar temperature limits are grouped together. In some cases, this approach conflicts with the goal of keeping components of each subsystem together which would be desirable for checkout and service. The same problem is encountered with balancing total compartment power dissipation.

Feasibility of the modular concept was evaluated by conducting a preliminary analysis of component groupings for each of spacecraft design concepts A through D which are described in detail in section 5. Only the thermal constraints of power dissipation and temperature limits were considered. To indicate the results, potential group arrangements for the four spacecraft design concepts are summarized in Table 3.8-1. In each case, four compartment areas are identified for the spacecraft components. The

Table 3.8-1

POTENTIAL MODULAR GROUP ARRANGEMENT OF COMPONENTS

AREA AND COMPONENTS	NOMINAL TEMPERATURE LIMITS OF AREA °F	SPACECRAFT DESIGN SPACECRAFT DESIGN CONCEPT	HEAT DISSIPATED DURING EACH OPERATIONAL MODE WATTS							
			PRELAUNCH	BOOST & PARK ORBIT	ACQUISITION	CRUISE-SPIN STABILIZED	CRUISE-3-AXIS STABILIZED	NAVIGATION	MANEUVER	ENCOUNTER
1. Communication Amplifier	-65 to 203	A	45	10	45	45	45	*	45	45
		B	45	10	45	*	45	*	45	45
		C	85	15	85	*	85	*	85	85
		D	110	30	110	*	110	110	110	110
2. Communication Control Communication Receiver Communication Exciter Gyros Gyro Electronics	-65 to 200	A	40	40	40	30	40	*	60	30
		B	40	40	40	*	40	*	60	40
		C	50	50	50	*	50	*	70	50
		D	55	55	55	*	55	55	75	61
3. Power Conditioning Equipment	-30 to 160	A	37	19	40	30	37	*	47	32
		B	40	20	41	*	40	*	50	41
		C	63	42	60	*	55	*	67	63
		D	83	30	71	*	69	114	80	86
4. Encoder DAE Tape Recorder Command Detector & Decoder CC&S Sun Sensors Canopus Tracker Earth Sensor Batteries	10 to 100	A	36	35	57	24	49	*	65	23
		B	34	30	52	*	40	*	59	43
		C	36	35	57	*	42	*	64	47
		D	34	26	51	*	43	59	46	43

* NOT APPLICABLE

NOTES:
(1) SCIENCE COMPONENTS ARE NOT INCLUDED BECAUSE OF THE UNCERTAINTY OF THEIR LOCATION.
(2) SHUNT RESISTORS SHOULD BE EQUALLY DISTRIBUTED AMONG AREAS.

components, nominal operating temperature limits, and power dissipation of each area are identified. Science subsystem components are not included because of the uncertainty as to their location on the spacecraft. Other specific groupings are possible and are possibly more desirable from other design considerations. These groupings do indicate, however, that the modular approach is feasible on the basis of thermal control requirements.

3.8.5 Conclusions and Recommendations

Both the isothermal module and modular concepts of bus thermal control appear to be feasible. Firm selection of the thermal control design for Jupiter flyby spacecraft requires an amount of analysis beyond the scope of this study. Guidelines for such a design have been identified, however, and the thermal control design information of four specific spacecraft design concepts are described in Section 5.

Selection of the modular or isothermal approaches depends partially on the requirements for detailed equipment arrangement. If the requirements for mass and geometric similarity can be met, the modular approach is desirable from the standpoints of spacecraft serviceability and flexibility of thermal design.

The advantages of using heating from the RTG's to stabilize spacecraft temperatures must be determined by an analysis of thermal control performance for a complete mission, including prelaunch and launch. For surfaces not needed for heat dissipation, a trade-off exists between (1) the use of insulation to minimize the effects of the varying space thermal environment or (2) the use of high emittance coatings to absorb heat from the RTG's. RTG heating should only be used if it is shown to materially reduce other thermal control penalties or enhance spacecraft reliability.

The location and specifications for insulation and radiative control coatings also require a detailed analysis of the spacecraft design. Although considerable variations in detailed thermal design are possible, the effects on spacecraft design will be largely limited to structural details. They are not expected to require major changes in the basic configuration.

Thermal control of components extended from the spacecraft will probably be integrated with component design. It is anticipated that adequate thermal control of these components can be achieved by insulation, radiative control coatings, electrical power dissipation, and possibly solar shields.

A flow of cooling air is required through the spacecraft compartment during prelaunch. The primary cooling load is the RTG's. The heat capacity of the spacecraft was found to be sufficient to prevent overheating during boost. The thermal environment in Earth orbit has to be considered in thermal control design, but it is not expected to pose a severe problem.

3.8.6 Reference

3.8-1 Plamondon, J. A., "Analysis of Movable Louvers for Temperature Control," Journal of Spacecraft and Rockets, September-October, 1964.

3.9 RADIATION PROTECTION

Because the Jupiter flyby spacecraft will be subjected to particulate and electromagnetic radiation from various sources, some knowledge of the effects of these radiations on spacecraft equipment operation is a prerequisite to the synthesis of a spacecraft design concept which minimizes the effects of the radiation environment through configuration selection and/or the use of shielding. Predictions of the effects of radiation are dependent upon (1) knowledge of the radiation environment, (2) descriptions of the equipment, and (3) availability of data and procedures for ascertaining equipment performance in the predicted environment. Uncertainties and deficiencies in any of these areas are necessarily reflected in uncertainties and inaccuracies in the predicted requirements for configuration restrictions and the need for shielding. The approach therefore is to state as concisely as possible what is currently known in each of these three areas as it applies to Jupiter flyby spacecraft.

3.9.1 Description of the Radiation Environments

The radiation environments of interest in this study can be identified as (1) galactic cosmic, (2) solar, (3) Earth-trapped, (4) Jupiter-trapped, and (5) RTG emissions.

The following subsections discuss these environments in the preceding order.

3.9.1.1 Galactic Cosmic Radiation

The galactic cosmic radiation in interplanetary space within the solar system is predominantly composed of protons typically having energies of several Bev. Less than 10 percent of the total flux is made up of helium and heavier nuclei. The cosmic proton flux varies between approximate minimum and maximum values of 1.5 proton/cm^2-second to 4 proton/cm^2-second. Peak values are observed during periods of low solar activity. Estimates of the integral energy spectra for various particle components of galactic cosmic radiation are shown in Figure 3.9-1. These estimates are based on data presented in Reference 3.9-1. Although not indicated, energies range up to 10^{20} ev in rapidly decreasing numbers of particles. Although the radiation is assumed to be relatively constant throughout the solar system, it is subject to variations due to local magnetic influences and material absorption.

3.9.1.2 Solar Radiation

The radiation of interest emanating from the Sun can be categorized as (1) solar wind, (2) nonrelativistic flares, and (3) relativistic flares (velocities near the speed of light). The solar wind (plasma) is composed of ionized hydrogen gas.

INTEGRAL SPECTRA OF GALACTIC COSMIC RADIATION

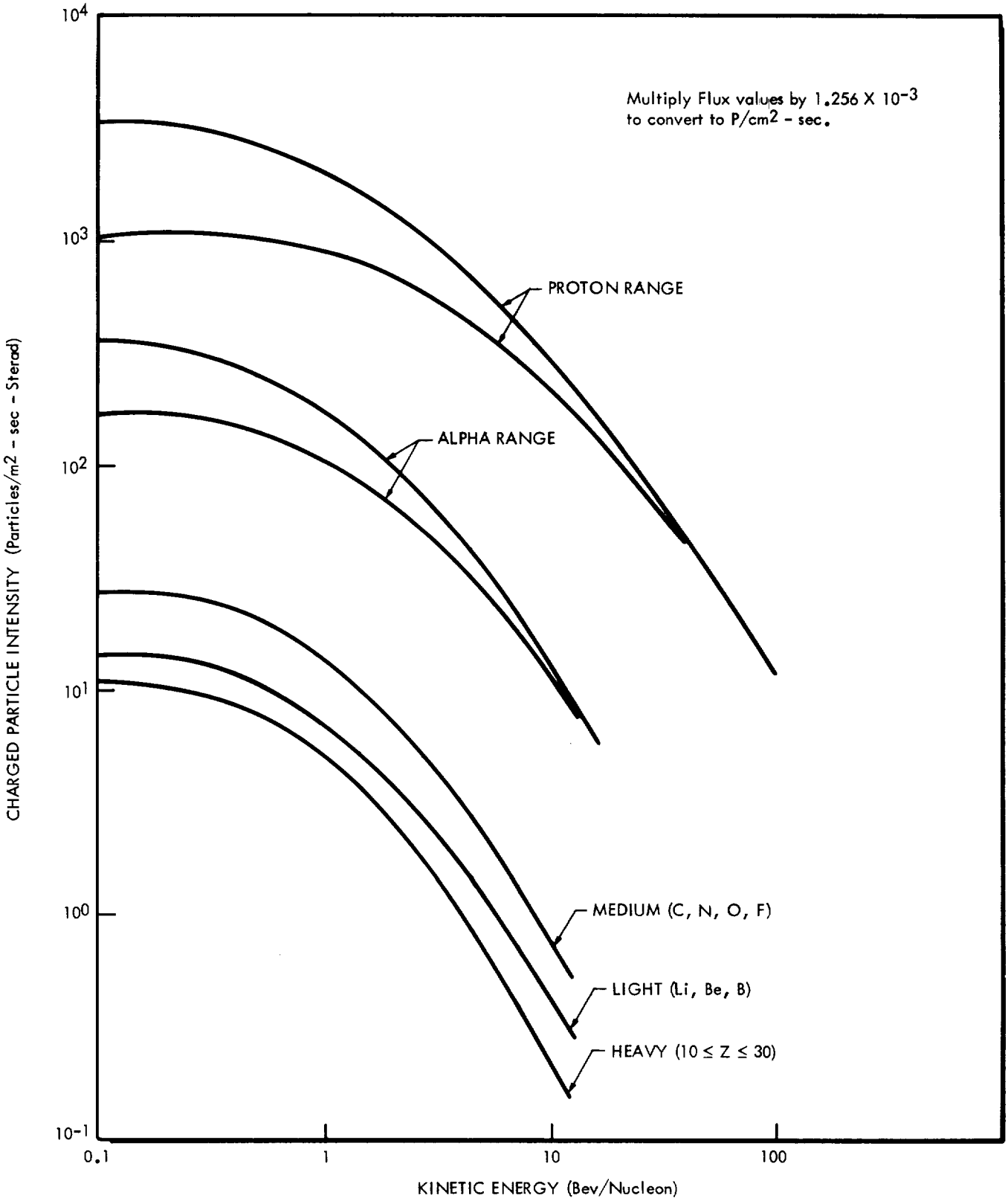

FIGURE 3.9-1

Estimates of proton intensities in the vicinity of the Earth range from 10^8 protons/cm^2-second (E ~ 1 Kev) for quiet Sun to 10^{12} protons/cm^2-second (E ~ 10 Kev) for active Sun. The solar wind intensities are assumed to vary as the inverse square of the distance from the Sun.

Intensities of nonrelativistic flares have exceeded 10^6 particles/cm^2-second with proton energies ranging from 10 to 500 Mev. An example of a severe nonrelativistic flare is depicted in Figure 3.9-2 as taken from Reference 3.9-1. Although the low-energy component has not been measured, observed geomagnetic and auroral effects indicate fluxes as high as 10^{10} P/cm^2-second.

Relativistic flares are not common; only six were recorded between March 1942 and May 1960. The largest, recorded in 1956, reached estimated peak intensities of 10^5 particles/cm^2-second for all energies and 10^3 proton/cm^2-second for E >1 Bev. An estimate on the spectral shape of this flare is presented in Figure 3.9-3.

In general the occurrence of solar flares seems to follow the solar activity cycle. Flares usually occur in the vicinity of Sun spots, so that the greater the number of Sun spots the greater the probability of a flare. The particles ejected move away from the Sun at speeds approaching the velocity of light. Thus, after a flare becomes visible there are only a few hours, at most, before the corpuscular radiation arrives in the vicinity of the observer. Solar flares may last hours or several days. The decay of intensity typically follows an inverse time-squared relationship from the value at one hour after onset of the event. Although it is known that relativistic flares occur more frequently during the rise or fall of the solar-activity curve and that the maxima and minima of the activity curve are relatively free of flares, no satisfactory method of flare prediction has been developed.

In the absence of any reliable method of solar-flare prediction, the past two solar cycles (18 and 19) have been projected to serve as a model of the solar flares of solar cycles 21 and 22 spanning the Jupiter flyby time interval of this study (see Figure 3.9-4). The minimum solar activity time for the 18th cycle was matched to the minimum for the 22nd cycle, and with this area as the reference, the 21st and 22nd cycles were plotted. The major solar flares are placed on the new cycles in the same positions which they occupied on the previous cycles. Records of major solar flares have been kept only for cycles 18 and 19. Since measurement techniques were being developed during this period (and still are under development), some of the smaller flares may have been missed during this time, particularly during the early portion of cycle 18. During cycle 19, a great amount of solar activity was recorded and many large flares were observed. Much data were taken on solar activity during the IGY (1958) with

ENERGY SPECTRUM OF A SEVERE NONRELATIVISTIC FLARE

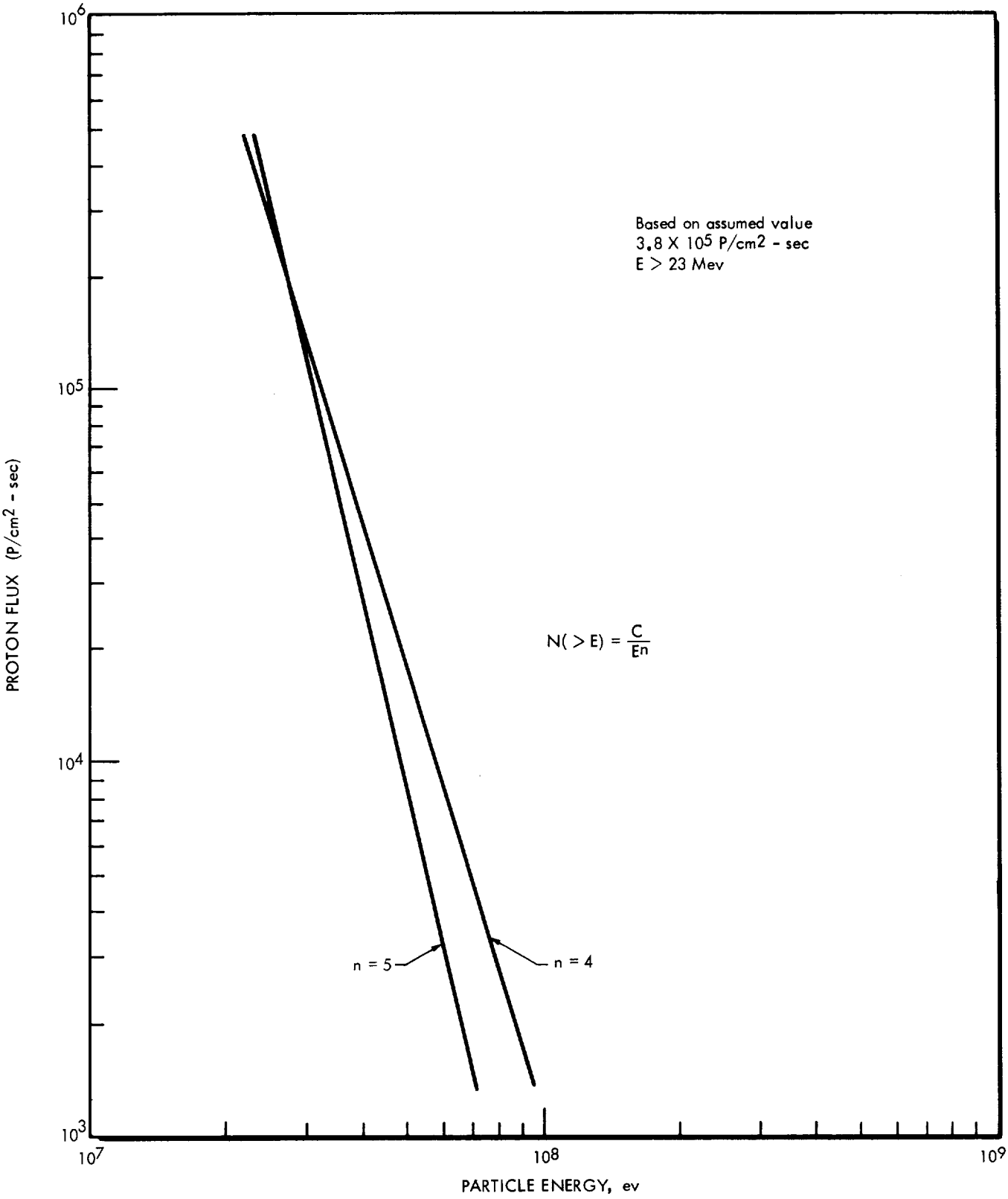

FIGURE 3.9-2

ENERGY SPECTRUM OF A TYPICAL RELATIVISTIC FLARE

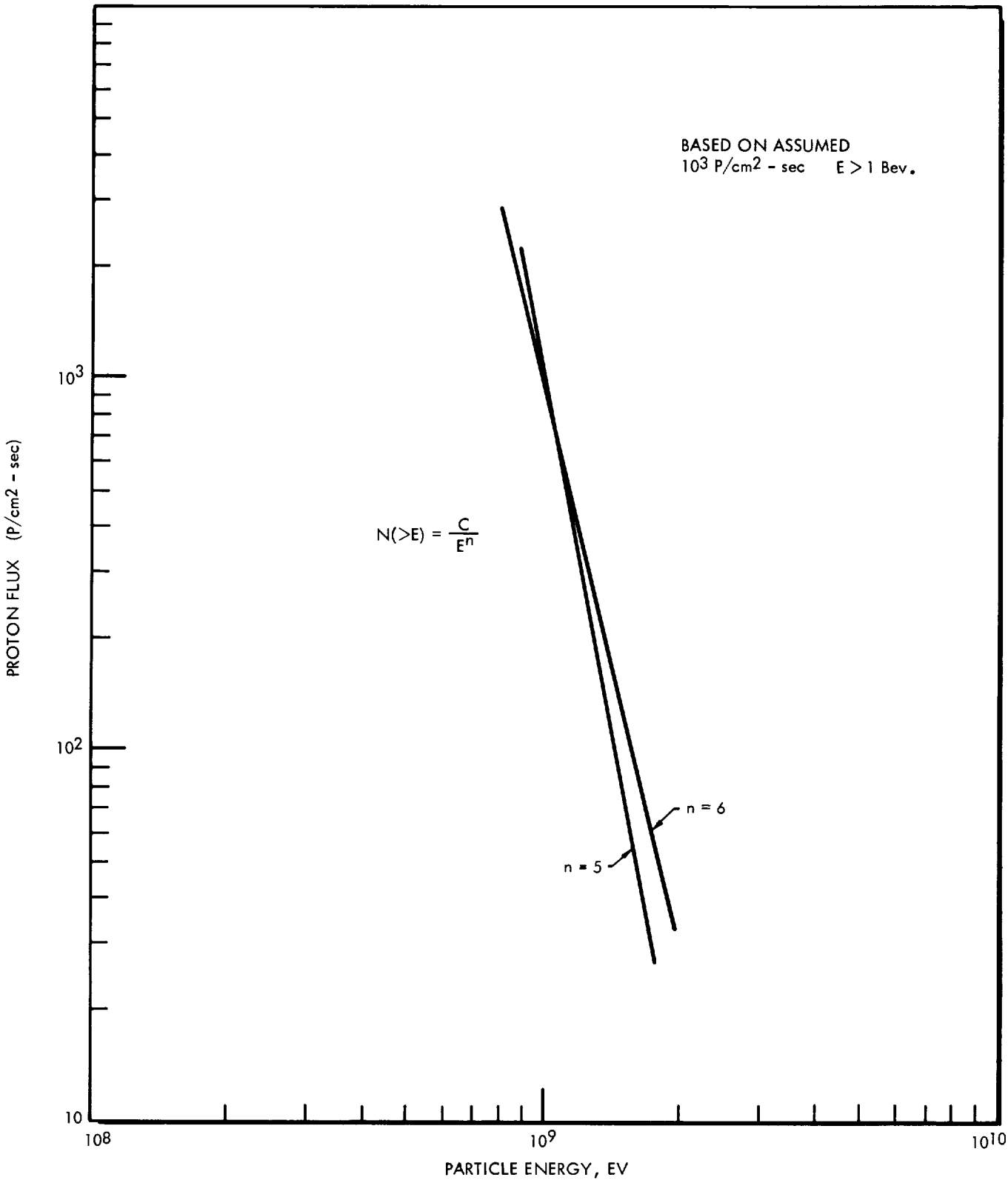

FIGURE 3.9-3

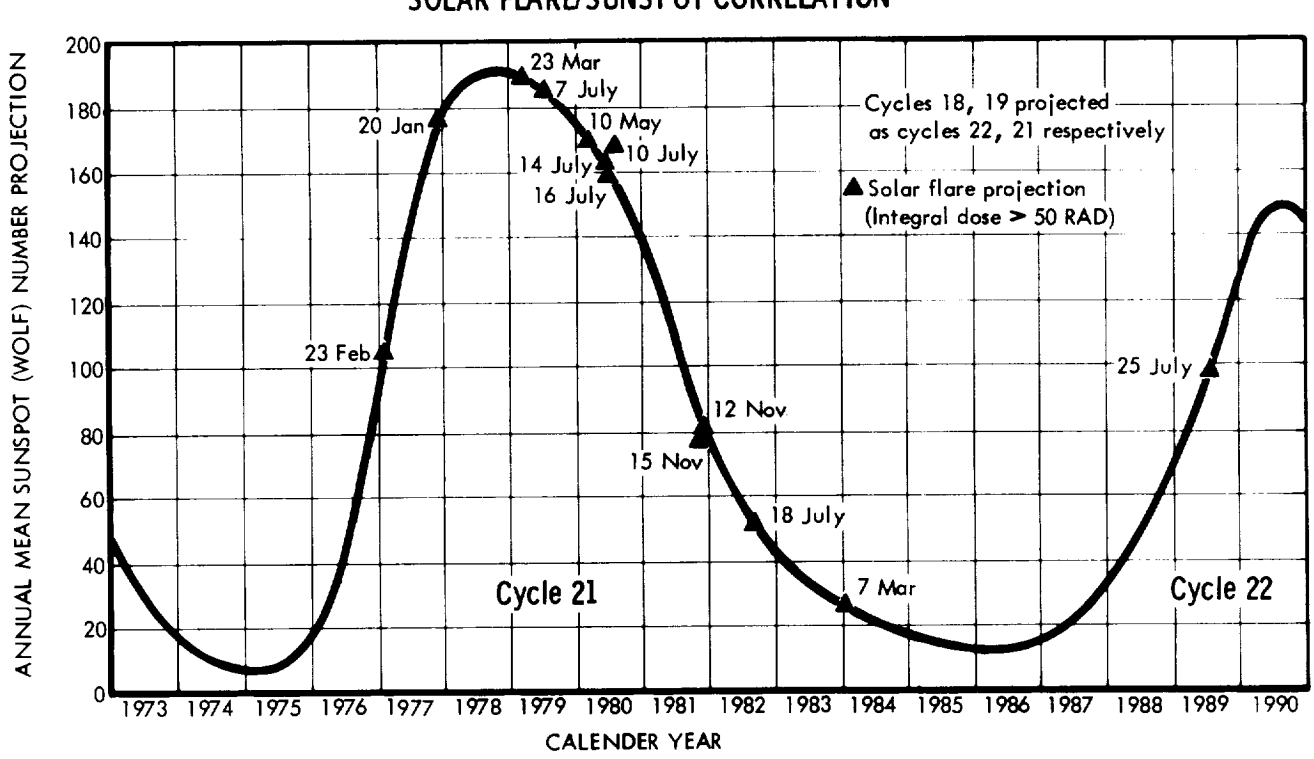

FIGURE 3.9-4

particular emphasis on solar flares. At best, Figure 3.9-4 reflects some feeling for the frequency of flares to be expected during the time period of interest. Estimates of how this relates to radiation incident on the spacecraft is an additional complication discussed below.

The question of how the flare radiation varies with distance from the Sun has not been fully answered. It is known that flare radiation is ejected from a relatively small area of the Sun and some flares eject particles which fail to arrive in the vicinity of the Earth. The particles which do hit the Earth come predominantly from the western limb of the Sun; thus, it seems that the particular area of space in which a body lies determines at least to some extent whether, and possibly how much, of the ejected radiation will be incident on the vehicle. This observation indicates that possibly some mechanism exists which confines the particles to a particular volume which moves through space as a unit. It has been suggested that a confining mechanism might be a "frozen-in" magnetic field. The charged particles are trapped by this magnetic field and follow it through space. Another indication of the frozen-in magnetic field is the fact that at the outset the particles are unidirectional, however, as the particles continue to arrive in the vicinity of the Earth the flux becomes isotropic. This suggests a spiraling flow around magnetic lines

of force. However, this effect could be caused by the Earth's magnetic field since these observations have been made near the Earth. If the frozen-magnetic-field concept is valid, the variation in intensity with distance may be difficult to estimate. The particles continue to arrive at the Earth for several hours after the visible evidence of the flare is no longer detectable. This suggests that the particles may be stored by some means as they travel through space. All of these points indicate that there may not be a general inverse distance-squared or distance-cubed decrease in intensity.

It is readily seen that uncertainties in event frequency, event intensity, and particle transport phenomena make prediction of solar radiation incident in the spacecraft highly speculative.

3.9.1.3 Earth-Trapped Radiation

Since the primary purpose of discussing the Earth-trapped radiation is to provide a basis for developing estimates of Jupiter-trapped radiation, only the natural components of the radiation are discussed.

The Earth-trapped radiation consists of two apparent belts. The location of peak intensities depends upon particle type and energy specified; the inner belt peaks at something less than 2 Earth radii and the outer belt at more than 3.5 Earth radii at the geomagnetic equator. Integral flux profiles for several energies of electrons and protons are presented in Figure 3.9-5 (Reference 3.9-2). Based on observations of the decay of electrons introduced into the Van Allen belts, inner-belt electrons are observed to have lifetimes of a year or more while outer-belt electrons have lives on the order of several days. The long lifetimes of the inner-belt electrons suggest that the source of these electrons may be the interaction between cosmic rays and atoms of the atmosphere. One product of these reactions is albedo neutrons; these neutrons decay producing electrons and energetic protons. These particles are captured by the magnetic field of the Earth forming the inner belt. The outer belt is thought to be supplied by solar corpuscular radiation.

Several Earth radii beyond the Earth's magnetopause, a collisionless magnetohydrodynamic shock wave has been observed. This shock wave is the result of an interaction between the Sun's and Earth's magnetic fields. In the transition region between this shock wave and the Earth's magnetosphere, electron fluxes of 10^{10} electrons/cm^2-second ($1 \leq E \leq 10$ kev) and proton fluxes of 10^7 protons/cm^2-second ($E > 2$ kev) exist. The particles in this region appear to be accelerated and have a random motion; they come from the solar plasma; and they are considered a potential source of outer-belt protons which are pumped into the belt during magnetic storms (Reference 3.9-3).

EARTH TRAPPED RADIATION

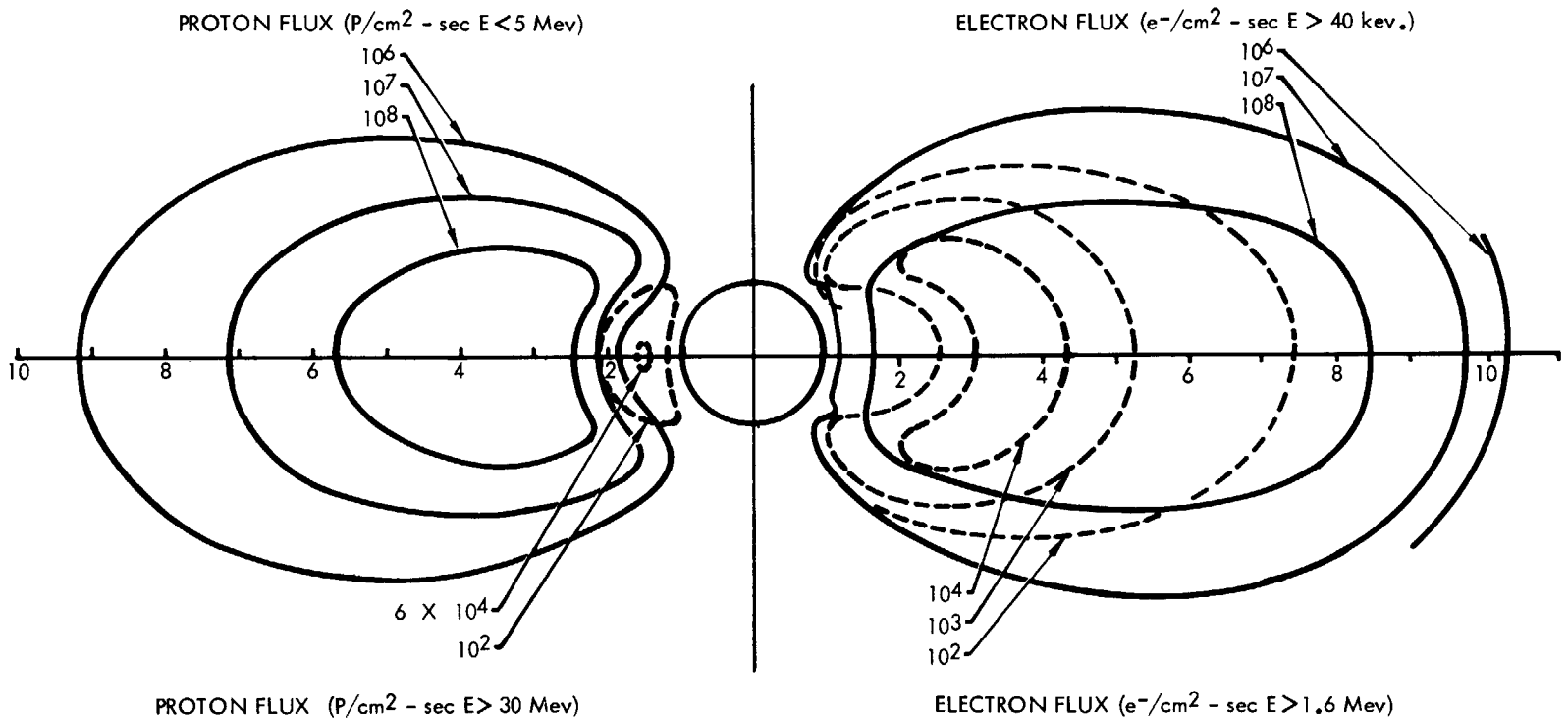

Radial distance in earth radii R_E (R_E = 3440 n.mi.)

FIGURE 3. 9-5

3.9.1.4 Jupiter-Trapped Radiation

Radio-frequency radiation from the planet Jupiter was discovered in the late 1950's. At first the radiation was thought to be of a thermal nature, however, the intensity seemed too high and the radiation was found to be coming from a much larger area than the planetary disc. Several theories have been proposed to explain this observation. One of the more probable is that of synchrotron radiation (Reference 3.9-4) in which it is suggested that the radiation may be coming from relativistic electrons trapped in a Jovian magnetic field. Results of polarization measurements of the radiation (Reference 3.9-5) have added further evidence of synchrotron radiation. The synchrotron radiation theory has been questioned because of the large number and energy requirements of the relativistic electrons necessary to produce the measured radio intensity. However, a mechanism is discussed in Reference 3.9-6 in which it is shown that the electrons obtainable from the solar corpuscular radiation are sufficient in number and may be accelerated to the necessary relativistic energies to produce synchrotron radiation. The area of greatest intensity of electrons as implied by radio-energy intensity measurements appears to be at about 3 Jupiter radii. Polarization measurements indicate that the planet's magnetic poles do not coincide with the axis of rotation. The two axes seem to be about 10 degrees apart.

Assuming the radiation belts of Jupiter follow the Earth-type configuration, the potential existence of an inner belt in which high energy protons are present is recognized. However, there are some arguments against this assumption (Reference 3.9-6). One argument is that the albedo-neutron source may not be powerful enough to be a source of supply. The albedo neutrons produced in the Earth's vicinity come largely from spallation of heavy nuclei in the atmosphere. The atmosphere of Jupiter appears to be composed principally of light elements. The direction of the collision products of the light nuclei would be peaked in the direction of the incoming particle, and thus would be directed mainly toward the planet itself rather than toward the radiation-zone. Additionally, the high magnetic field thought necessary for the maintenance of the high intensity belt would reduce greatly the cosmic ray particles penetrating through to the atmosphere. No direct evidence for or against a high-intensity proton inner belt was found during this study.

The following conclusions were drawn as a result of a review of References 3.9-4 through 3.9-10. Most observers believe the magnetic field around the planet to be from 0.1 to 10 gauss at a distance of 3 Jupiter radii. The most probable value is about 1 gauss. At this field strength, most observers feel the radio-frequency radiation, if produced by synchrotron radiation, would be produced mainly by electrons in the energy range 1 to 100 Mev. The differential energy spectrum for the radiation is probably of the form $N(E)dE = KE^{-\gamma} dE$ with $\gamma \simeq 1$ which would account for

the rather uniform intensity in the range of frequencies observed. Higher values of γ would be expected if a thick shell of lower energy radiation existed around the high energy radiating fields. To explain observations for an assumed value of 1 gauss at 3 R_j an average electron density in the vicinity of Jupiter on the order of 10^{-3} e-/cm^3 over 10 planetary volumes is required. This compared to an electron density on the order of 10^{-6} in the Earth's field suggests an electron flux scaling factor of 10^3 for estimating Jupiter's environment.

Based on the above discussion, the following criteria were employed in estimating the electron fluxes in the vicinity of Jupiter:

Jupiter magnetic field	1 gauss at 3 R_j
Electron energy range	$1 < E < 100$ Mev
Electron energy spectra	$\gamma = 1.02$ $\gamma = 2$
Electron flux intensity	$\frac{\text{Flux } (1 < E < 100 \text{ at } R_j = 3)}{\text{Flux } (E > 1 \text{ Mev at } R_e = 3.6)} = 10^3$

The selection of Earth flux energy range and distance reflected in the last item above is based on data reported in Reference 2 on Explorer 6 and 12 flights. From this data it was determined that the Earth's electron flux ($E > 1$ Mev) was approximately 2×10^6 e$^-$/cm^2-second and that the peak intensity occurred at approximately 3.6 R_e. This value correlates well with the data presented in Figure 3.9-5. To provide an estimate of electron intensity variation as a function of R_j, the iso-flux lines for electrons ($E > 1.6$) from the flux map of Figure 3.9-5 were employed. It was assumed that the ratio of electron flux at Jupiter to the electron flux at Earth was proportional to the ratio of magnetic field intensities at the respective peak value points which was determined by solving

$$\frac{M(3\ R_j)}{M(3.6\ R_E)} = \frac{1}{9.90 \times 10^{-3}} = 1.01 \times 10^3$$

Magnetic field data employed for Earth were taken from Reference 3.9-11 and those for Jupiter from values developed by Davis and Chang for Jupiter. The procedure was as follows. The Earth's magnetic field intensity at intersection of the geomagnetic equator and the iso-flux line was determined. The above ratio was then employed to determine the magnetic field strength required at Jupiter to maintain the ratio constant. The distance in Jupiter radii at which this field strength occurred was then determined.

The Jupiter peak flux was reduced by the same fraction as the Earth peak flux (Figure 3.9-5) and plotted at this point. The Earth's peak flux ($E > 1.6$) was determined (from the data of Reference 3.9-10) to be approximately 2×10^5.

The results of these calculations are presented in Figures 3.9-6 through 3.9-9. The energy spectra for $\gamma = 1.02$ and $\gamma = 2$ are shown in Figure 3.9-6. The flux distribution as a function of energy and planetary radii out from Jupiter center is presented in Figures 3.9-7 and 3.9-8. Although the curves given are extended out to about 5.3 R_j, the radiation zones extend further out in space. The Earth's zones at lower electron energies are found throughout the magnetosphere; Jupiter's radiation may also reach this limit which, as previously indicated, is approximately 50 R_j. An iso-flux map of the Jupiter-trapped radiation is shown in Figure 3.9-9.

3.9.1.5 Radiation from the RTG

The concensus for isotope selection for the RTG is Pu^{238}. Many considerations including availability, safety, operating temperature, and power density, support the selection of this isotope. In the absence of final decisions on the exact characteristics of the unit a set of conservative criteria must be established to describe the radiation environment associated with these units. Presently, planned operating temperatures and current technology indicate the use of PuO_2. Though PuN appears to have greater potential from the standpoint of both power density (6.17 w/cm^3) and neutron production (4×10^3 n/gm), its availability in the immediate future is limited by current technology. However, it should be seriously considered as a desirable alternate which might be available at some point in the 1973 to 1980 time period. For purposes of this discussion, the PuO_2 form will be assumed in defining the radiation environment. The characteristics of PuO_2 fuel of interest here are given in Table 3.9-1.

Assuming an overall efficiency of 5%, the PuO_2 quantities and activities for the proposed units are as follows.

Unit	UO_2(gm)	Activity (d/sec)
60 W_e (1200 W_{th})	3070	1.39×10^{15}
80 W_e (1600 W_{th})	4100	1.86×10^{15}
120 W_e (2400 W_{th})	6150	2.78×10^{15}

Conservatively assuming a point source, the following results for a 120 W_e unit are obtained for radiation at 1 meter.

INTEGRATED ELECTRON FLUX VS. ENERGY

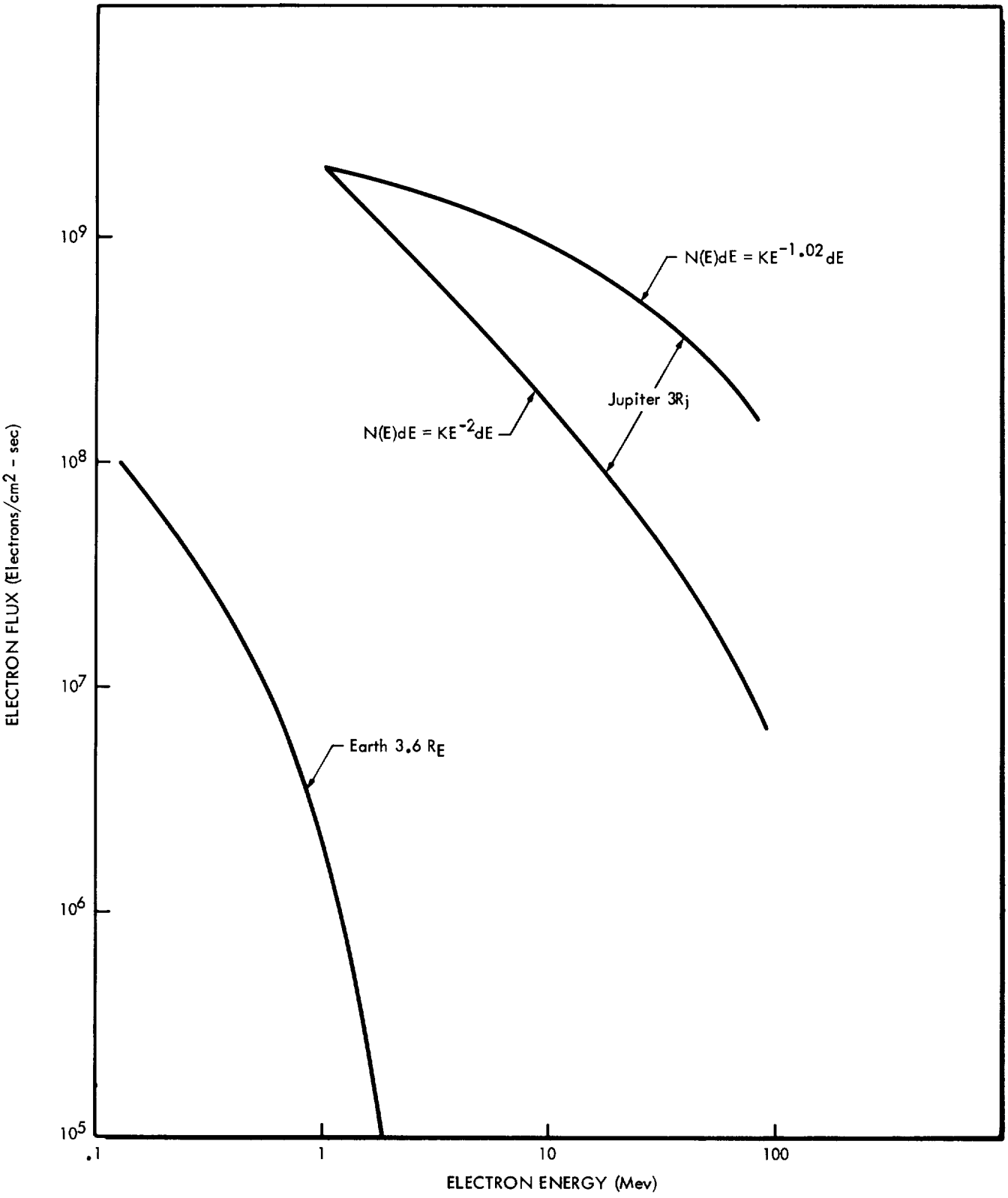

FIGURE 3.9-6

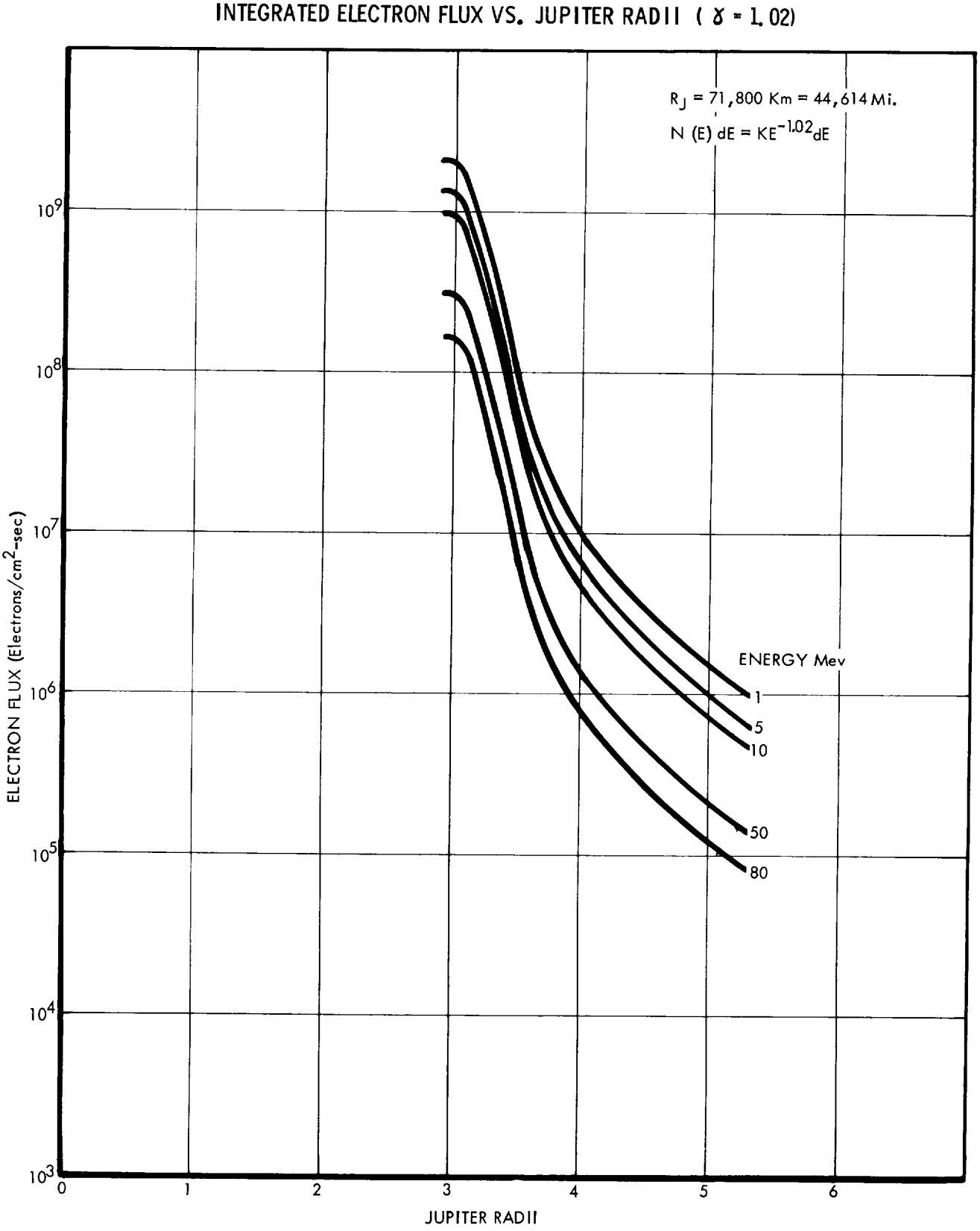
INTEGRATED ELECTRON FLUX VS. JUPITER RADII (γ = 1.02)
R_J = 71,800 Km = 44,614 Mi.
N (E) dE = $KE^{-1.02}dE$
ELECTRON FLUX (Electrons/cm^2-sec)
10^9
10^8
10^7
10^6
10^5
10^4
10^3
ENERGY Mev
1
5
10
50
80
0
1
2
3
4
5
6
JUPITER RADII

FIGURE 3.9-7

INTEGRATED ELECTRON FLUX VS. JUPITER RADII ($\gamma = 2$)

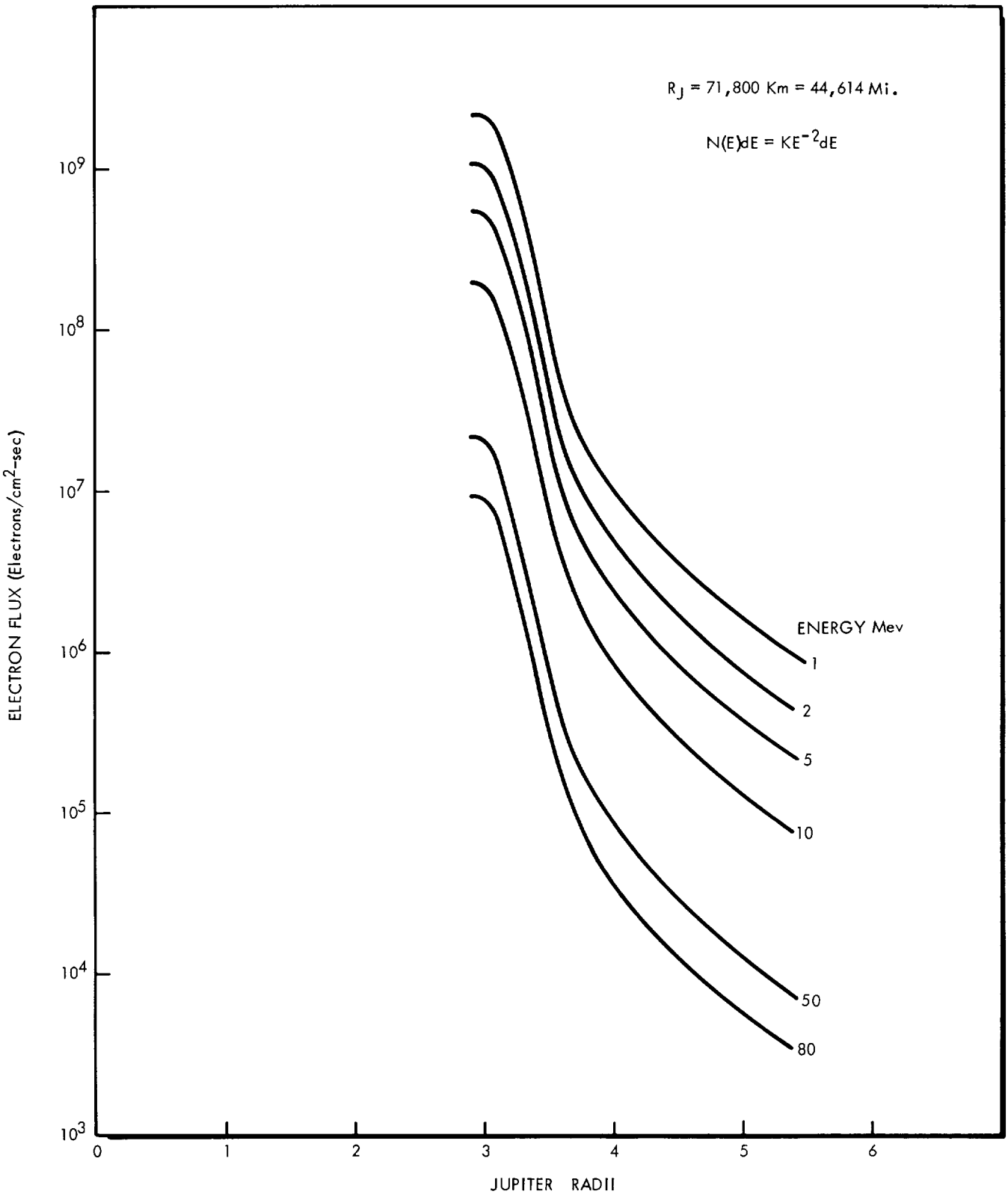

FIGURE 3.9-8

JUPITER TRAPPED RADIATION ISO-FLUX MAP

RADIAL DISTANCE IN JUPITER RADII (R_J)

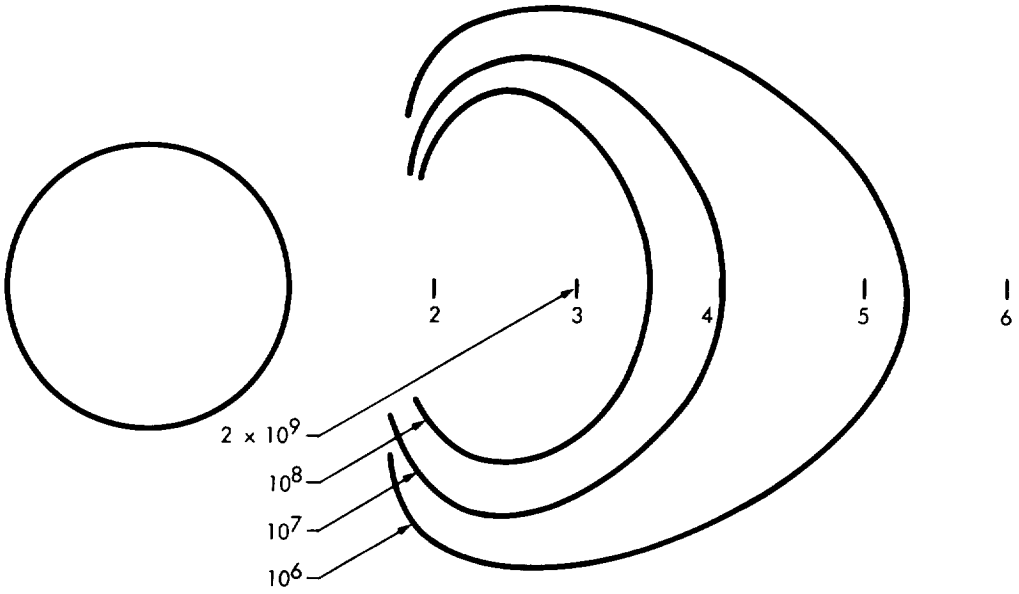

ELECTRON FLUX [Electrons/cm^2-sec (E > 1 Mev)]

FIGURE 3.9-9

For neutron flux,

$$\phi_{(\alpha,\ n)} = \frac{(5 \times 10^4\ n/gm)(6150\ gm)}{4\ R^2}$$

$$= \frac{3.08 \times 10^8}{12.56 \times 10^4}$$

$$= 2.45 \times 10^3\ n/cm^2\text{-sec}$$

$$\phi_{(fission)} = \frac{(3.3)(6150)}{4\ R^2}$$

$$= 1.62 \times 10^2\ n/cm^2\text{-sec}$$

$$\phi_{TOTAL} = 2.6 \times 10^3\ n/cm^2\text{-sec}.$$

Table 3.9-1

Characteristics of UO_2 *

Half Life (α Decay-years)		86.4 years
Activity (α)	(Disintegrations/sec-gm)	4.52×10^{11}
	(curies/gm)	12.2
Power Density	(watts/cm^3)	3.9
	(watts/gm)	0.39
Neutron Production (n/sec-gm)		
	(α , n)	5×10^4
	(fission)	3.3×10^3
	Total	5.33×10^4

Gamma Ray Production** (α Decay)

Mev	γ/disintegration
0.044	3.8×10^{-4}
0.099	8×10^{-5}
0.15	1×10^{-5}
0.203	4×10^{-8}
0.760	5×10^{-7}
0.875	2×10^{-7}

* 70% By Weight U^{238}

** Other Gamma radiation is present as a result of fission and impurities. Some more penetrating high energy components can become important if shielding by orders of magnitude is required.

In order to provide a feeling for the attenuation afforded by RTG structure, attenuation factors were developed for a unit similar in design to those proposed. In these rough calculations, neutron flux was reduced only about 25%; this would lead to a, perhaps, more realistic value of 2×10^3 n/cm^2-sec at 1 meter.

Employing the value of 2.78×10^{15} d/sec and the values listed in Table 3.9-1, the gamma fluxes for a point source are presented below for the RTG unattenuated and attenuated case at 1 meter.

E(MEV)	UNATTENUATED γ/cm^2-sec	ATTENUATION FACTOR	MR/HR = 1.86×10^{-3} EI
0.044	8.42×10^6	5×10^{-8}	3.44×10^{-5}
0.099	1.78×10^6	3.3×10^{-4}	1.08×10^{-1}
0.15	2.22×10^5	8.8×10^{-4}	5.5×10^{-2}
0.203	8.88×10^2	2.13×10^{-3}	7.16×10^{-4}
0.760	1.11×10^4	4.58×10^{-1}	7.2
0.875	4.44×10^3	4.82×10^{-1}	3.48
		TOTAL	10.84

Figures 3.9-10, 3.9-11, and 3.9-12 are shown to provide a basis for rough shield weight estimates. The calculation of shield weight depends on separation distance (source to unit), shield location, and shield geometry factors which are variable within the limits of vehicle configuration. To obtain shield thicknesses, the values in gm/cm^2 are divided by the density values shown. Both neutron and gamma shield materials are presented on each figure so that the gamma removal effectiveness of a neutron shield (or the neutron removal effectiveness of a gamma shield) can be estimated by reference from one to the other.

These attenuation curves must be used with caution. In Figure 3.9-12 gamma build-up has not been included, since it should not be important for the energies treated and an attenuation by less than a factor of 10.

The attenuation plots of Figure 3.9-10 are for neutrons of 16 Mev, and attenuation for 2-Mev neutrons is depicted in Figure 3.9-11. This is done because of the likelihood of a 2 Mev neutron being more characteristic of the neutrons coming from the RTG. Although no experimental data could be found on the spectrum of neutrons produced by the oxygen absorption of particles in the RTG, on a theoretical basis, the spectrum can be expected to be of the form shown in Figure 3.9-13. As shown in Figures 3.9-10

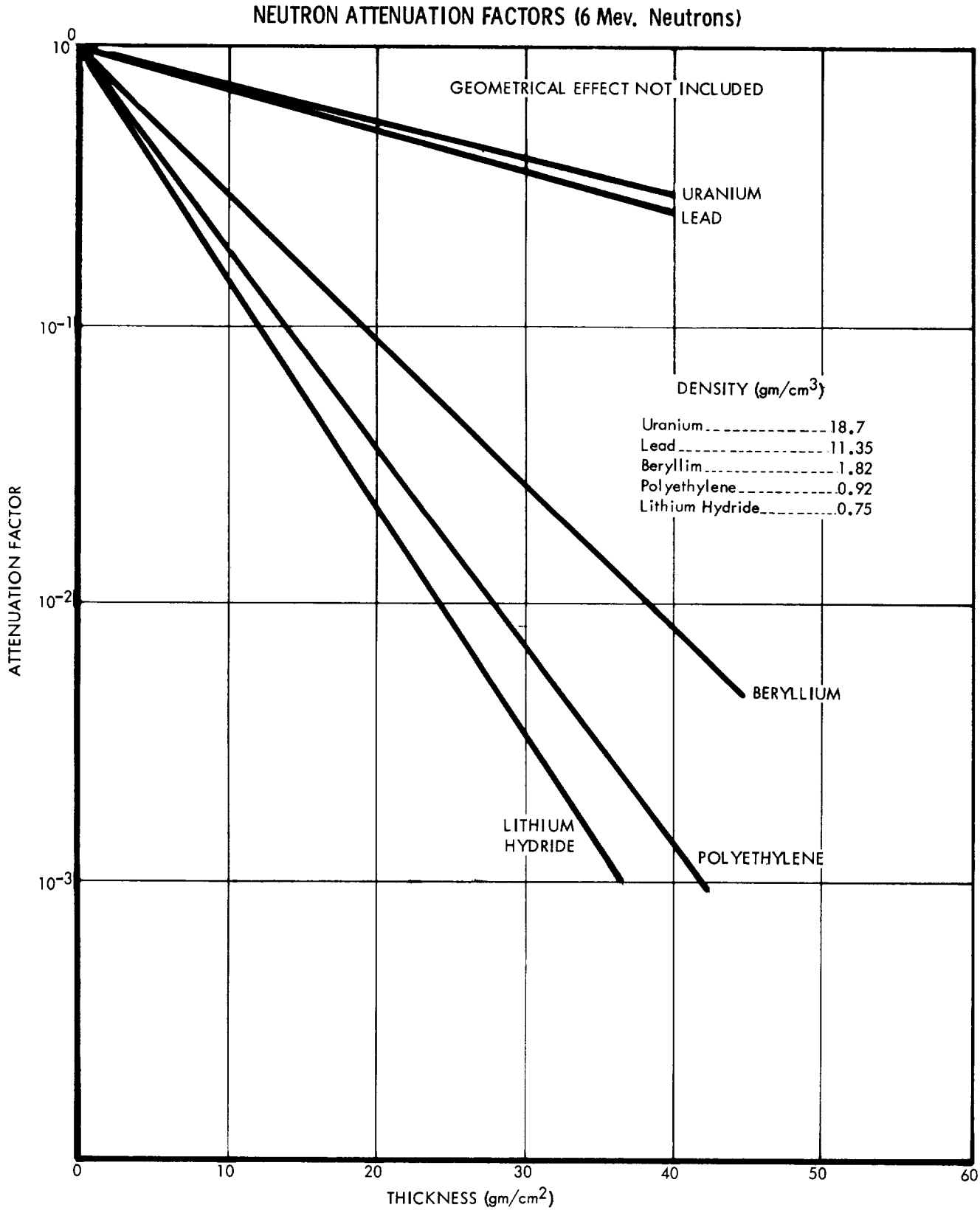
NEUTRON ATTENUATION FACTORS (6 Mev. Neutrons)
GEOMETRICAL EFFECT NOT INCLUDED
URANIUM
LEAD
DENSITY (gm/cm3)
Uranium 18.7
Lead 11.35
Beryllim 1.82
Polyethylene 0.92
Lithium Hydride 0.75
BERYLLIUM
LITHIUM HYDRIDE
POLYETHYLENE
ATTENUATION FACTOR
THICKNESS (gm/cm2)
10^0
10^-1
10^-2
10^-3
0
10
20
30
40
50
60

FIGURE 3. 9-10

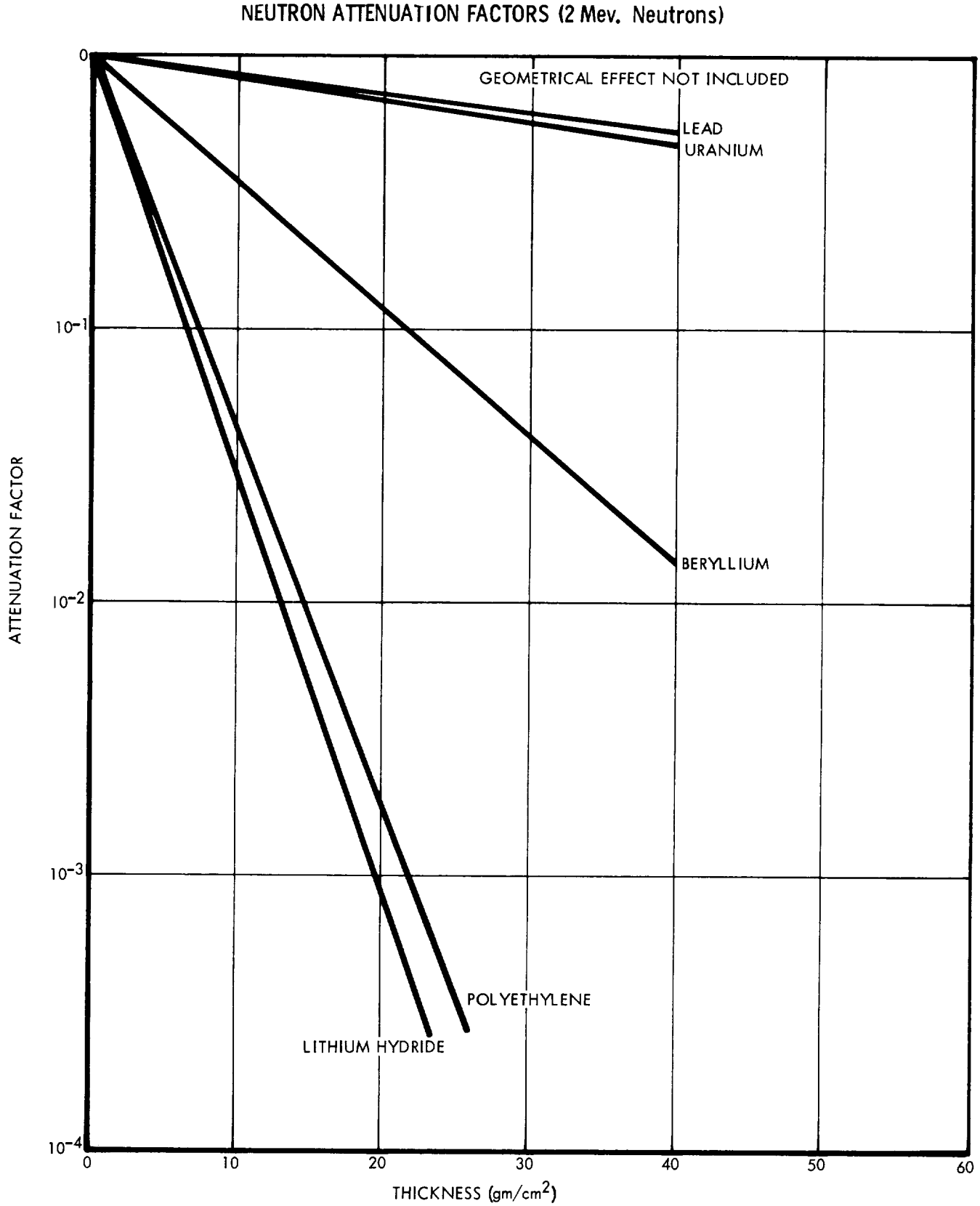
NEUTRON ATTENUATION FACTORS (2 Mev. Neutrons)
GEOMETRICAL EFFECT NOT INCLUDED
LEAD
URANIUM
BERYLLIUM
POLYETHYLENE
LITHIUM HYDRIDE
ATTENUATION FACTOR
0
10^{-1}
10^{-2}
10^{-3}
10^{-4}
0
10
20
30
40
50
60
THICKNESS (gm/cm^2)

FIGURE 3. 9-11

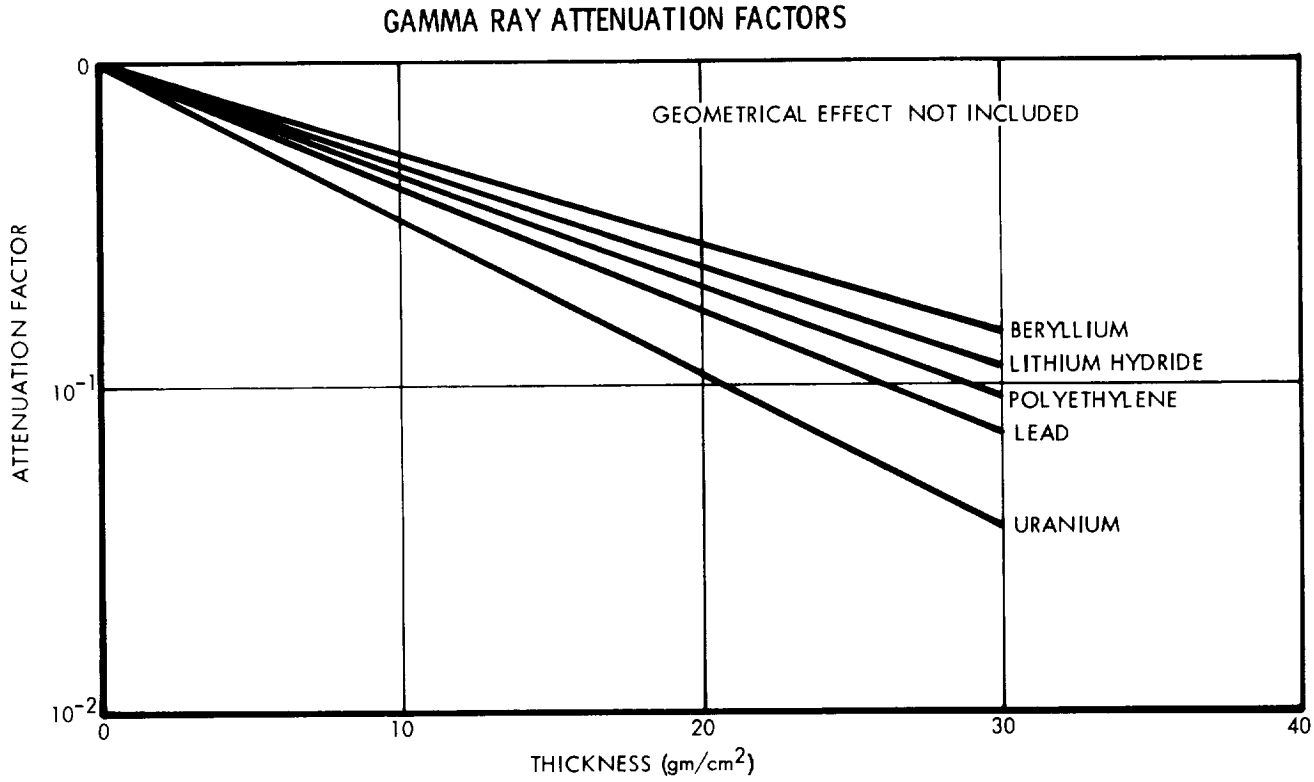

FIGURE 3.9-12

and 3.9-11, attenuation factors for the two neutron energies differ markedly and are most significant for polyethylene and LiH. Thus, if a 6 Mev monoenergetic neutron source is assumed for the RTG, significant errors in estimates of shielding requirements can result. The heavy dependence of shield weight estimates on the assumed neutron energy spectrum is readily apparent and indicates the need for accurate neutron source terms.

3.9.2 Radiation Effects on Vehicle Equipment

Ideally a radiation effects analysis involves a detailed examination of equipment operating principles, materials, and parts. Applicable radiation effects data are then applied to identify radiation sensitive areas, make recommendations on radiation hardening, identify shield requirements, identify configuration restrictions, and identify test and development requirements. Present limitations on knowledge of equipment characteristics, applicable radiation effects data, and the scope of the study precludes the possibility of such a detailed analysis. It is necessary, therefore, to identify the most important radiation problem areas and emphasize these areas to the limit of the study scope. Certainly all of the environments identified will not present a problem. Each is briefly considered to permit identification of the areas on which emphasis is required.

RTG APPROXIMATE NEUTRON SPECTRUM

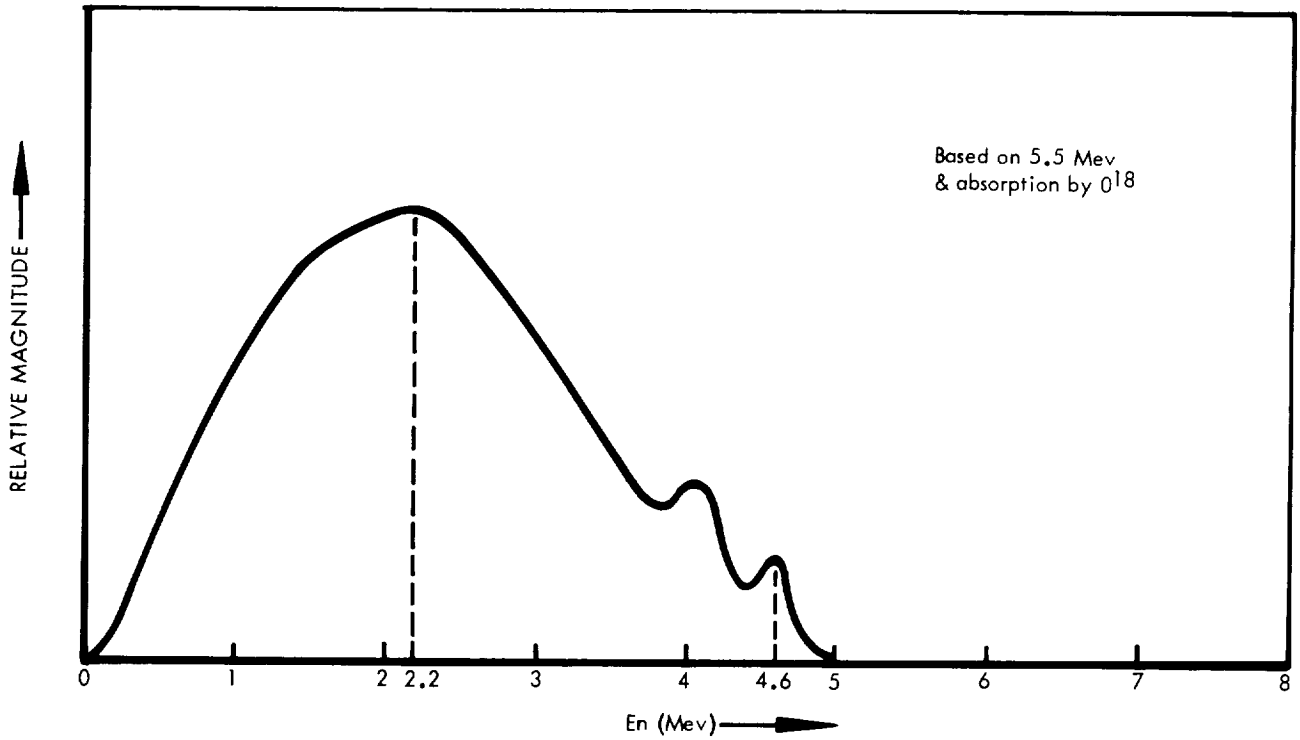

FIGURE 3.9-13

The galactic cosmic radiation is not of sufficient intensity to be considered a problem in equipment damage.

The solar radiation is composed of two components, the solar flare and the solar wind particles. The frequency, radiation intensity, and duration of flares are of a magnitude which does not represent a serious hazard to the equipment of the spacecraft, with the possible exception of the low energy component. The low energy component of flares and the low energy solar wind is of concern because it could damage the thermal control coatings.

The Earth-trapped radiation is not considered a problem since the duration of transit through the field is short.

Jupiter's trapped radiation belts are of sufficient magnitudes and energies to cause spacecraft equipment damage and they are of most serious concern. Extensive use is made of semiconductor circuits in equipment design. The obvious sensitivity of semiconductors to radiation requires some consideration. Other areas which are considered important enough to require some attention include control sensors, scientific sensors, and data storage equipment. Ultimately, the equipment designs will have to be evaluated and qualified in a radiation environment. This requirement dictates the consideration of the need for simulating application environments in such tests.

Neutron and gamma radiation from the RTG's suggest three areas of potential concern - integrated neutron flux damage to semiconductors, interference with radiation detection instruments, and nuclear safety.

Discussions relative to the radiation source and related areas of concern follow.

3.9.2.1 Solar Radiation Effects

The low energy component of solar flares and the low-energy solar wind have been demonstrated to be a potential problem with regard to spacecraft thermal control coatings. The low-energy particles are heavily absorbed in these coatings.

The extent of damage to thermal control surfaces by particulate and electromagnetic radiation has not been fully investigated; however, the results of several investigations on the effects of space radiation on thermal control coatings have recently become available. In addition, some data on the effects of reactor radiation on some selected coatings have also been generated. While the effects of radiation vary considerably with the types of coating material, it has been shown in solar-wind simulations that an integrated flux of 10^{16} protons/cm^2 (1-10 kev range) is an apparent threshold of damage. At higher proton energies (50-400 kev), significant reduction of solar reflectance with a corresponding increase in solar absorptance has been produced at 2×10^{13} p/cm^2. It is concluded from this that the selection of thermal control coatings for the Jupiter flyby vehicle will be influenced by the radiation environment in transit.

If vehicle coatings are not sufficiently radiation stable, the apparently large fluxes of electrons in the Jovian radiation field could also produce a serious alternation of thermal-control properties during transit of the radiation field. Some selected radiation-effects data are discussed briefly in the following paragraphs.

Miller and Campbell (Reference 3.9-13) irradiated several thermal control paints with protons at four specific energies between 50 and 400 kev (simulating the high fluxes of protons having energies below 1 Mev in the outer radiation belt and in solar-flare events). Typical results (Table 3.9-2) show that a loss in reflectivity in the 0.400 to 0.433 micron spectral range takes place at integrated fluxes as low as 10^{13} p/cm^2, a fluence that could in an intense solar flare be reached in as little as 10 to 100 seconds near the Earth. The loss in reflectivy is minor from about 0.6 to 1.3 microns, the upper limit of the measurements. However, the spectral range below 0.6 micron contains approximately 33 percent of the solar energy. Conclusions drawn by Miller and Campbell are (1) that the amount of degradation is nearly linear with absorbed energy (kinetic

energy of the protons times their integrated flux), and (2) in the range of fluxes investigated (from 1 x 10^{10} to 1 x 10^{12} p/cm^2-sec), the damage is nearly independent of flux, indicating the possibility of extrapolating the results to fluxes encountered in space. The first conclusion is valid only for some limited proton-energy range; since the penetrating power of protons increases with energy, more energy will be deposited below the surface or in the substrate as the energy increases. The calculated range for a 400 kev proton is about 4.0 microns.

Table 3.9-2

Effects of Proton Irradiation on the Reflectivity of Thermal Control Coatings*

Coating	Proton Fluence (p/cm^2)**	Percent Decrease in Reflectivity at Proton Energy of 50 kev	100 kev	200 kev	400 kev
ZnS-Epoxy	2 x 10^{13}	10.8	18.4	36.4	15.8
	2 x 10^{14}	48.1	70.6	--	50.4
ZnO-Methyl Silicone	2 x 10^{13}	6.0	7.0	25.6	11.2
	2.4 x 10^{14}	34.0	32.3	53.4	46.0
TiO_2-Methyl Silicone	2 x 10^{13}	2.5	--	--	0.5
	5 x 10^{14}	28.4	--	--	21.7
ZnO-K_2SiO_3	2 x 10^{13}	2.0	3.5	6.5	10.8
	2.5 x 10^{14}	38.9	27.8	37.8	46.5
TiO_2-K_2SiO_3	2 x 10^{13}	1.2	2.3	2.8	4.4
	2 x 10^{14}	2.9	5.9	7.8	11.7

* Data from Reference 3.9-13 (Miller, NRL)
** Irradiation rate of 2 x 10^{11} p/cm^2-sec

Gillette, et.al. (Reference 3.9-14) have studied the effects of protons and alpha particles expected during a 230-day Earth-to-Mars mission on the thermal properties of spacecraft coatings. A solar-wind simulator was used to produce 1- to 9-kev protons and 2- to 16-kev alpha particles. Low-emittance anodic-coated aluminum began to show an increase in solar absorptance at 10^{16} p/cm^2 and had increased by 92 percent at 10^{17} p/cm^2 solar absorptance. High-emittance anodic-coated aluminum also exhibited a slight change at 10^{16} p/cm^2 but was not exposed to high levels. Zinc oxide/potassium silicate coatings were essentially unaffected at a fluence of 10^{14} p/cm^2, but at an exposure of 10^{16} p/cm^2 solar absorptance had increased by 83 percent. Zinc oxide/LTV-602 coatings had an increase in solar absorptance of 39 percent after 5 x 10^{15} p/cm^2.

Irradiation of these coatings with alpha particles appeared to give similar results; the threshold for the onset of damage was at somewhat higher fluences.

In a study by Breuch (Reference 3.9-15), 100-kev proton bombardment of white Kemacryl, thermatrol, and Fuller Gloss White paints resulted in increased solar absorptance at fluences of around 10^{15} p/cm^2. The increase in solar absorptance at 3-4 x 10^{15} p/cm^2 was of the order of 100 percent. Irradiation of the same materials with 0.8 Mev electrons produced a slight increase in solar absorptance at an integrated flux of 6 x 10^{14} e^-/cm^2.

In each of the above experiments, the specimens were irradiated in vacuo but measurements (reflectance) were taken in air. There is some evidence (Reference 3.9-16) that the exposures to air may, for some coatings, result in a return to more nearly their original conditions, so caution must be used in applying this type of data. Two programs now in progress at the Fort Worth Division of General Dynamics may help to enlighten this area - irradiations of thermal control coatings by electrons and by reactor radiation are to be carried out in vacuo with the specimens maintained in vacuo through measurement of spectral reflectivity.

3.9.2.2 Jupiter-Trapped Radiation Effects

There is strong evidence that the Jupiter flyby spacecraft equipment will be subjected to severe environmental stresses at encounter. Without a doubt, semiconductor devices, in particular SCR's and transistors, and the circuits and subsystems in which they are employed could be subjected to permanent damage and, hence, comprise an area of major concern. Optical glass, one of the more radiation sensitive materials, is another area of concern because of color center formation which results in darkening of the glass and loss of transmission.

Data from a test conducted by Jet Propulsion Laboratory (Reference 3.9-26) in which Mariner IV subsystems were irradiated by monoenergetic electrons indicate malfunction threshold fluxes of some subsystems are as low as 10^9 e/cm^2-sec of 2 Mev electrons. These malfunctions were of a transient-radiation-effects type; however, such malfunctions, even though temporary, would cause loss of control and data during the most important segment of the mission. Malfunctions of the type observed are induced by ionization currents and induced voltages in low signal level-high impedance circuitry. Additionally, of perhaps greater importance in some cases, induced scintillation and Cerenkov radiation in clear sensor covers and optical elements and the transient response of devices for sensing radiation from the IR to UV frequencies can produce serious errors in equipment operation. The problem areas noted above warrant further consideration; these areas are discussed more fully in the paragraphs which follow.

Semiconductors - There are considerable data on the effects of neutron irradiation on semiconductors and a smattering of data from electron and proton irradiations. No attempt is made to delve into these data in detail, but some "threshold" flux levels are used to illustrate possible problem areas.

Silicon-controlled rectifiers are perhaps the most radiation sensitive of the semiconductor devices. Data obtained in reactor irradiations (Reference 3.9-17) show that several units failed completely at an exposure of 4.8×10^{12} n/cm^2 and all other units were severely damaged at the same exposure level. The conservative threshold for SCR's is often set at 10^{11} n/cm^2.

It is also well established that a fast neutron exposure of 10^{12} n/cm^2 will cause a degradation of performance in some types of transistors. However, the effects in transistors varies widely with type, construction, and frequency range and also depends upon the performance parameters of interest. As a general rule, the thinner base, higher frequency, and smaller junction-area devices usually have the better radiation resistance, and germanium devices are better than silicon devices. Thatcher, et al. (Reference 3.9-17) gives the following approximate exposure levels for serious damage to several categories of transistors: audio - 3×10^{13} n/cm^2, power - 10^{13} n/cm^2, high-level switching - 10^{14} n/cm^2, high frequency - 2×10^{14} n/cm^2, low-level switching - 2×10^{14} n/cm^2.

Proton effects in semiconductor devices have been found at flux levels between 10^{11} and 10^{12} p/cm^2. Brown, for example, in Reference 3.9-18 reports approximate thresholds for a number of transistor types exposed to 10 Mev Protons; these thresholds range upward from 2×10^{11} p/cm^2. It was also shown in this work that the transistor case can provide a high degree of protection, illustrating the importance of considering proton energy and inherent shielding when evaluating proton effects. In another investigation using 40-Mev protons, thresholds were found to be in the range between 10^{11} and 2×10^{12} p/cm^2. Exposures with 240-Mev protons did not appear to be quite as damaging as those with the lower energy protons. Also the high frequency transistors were less seriously affected than the lower frequency transistors.

On the basis of the number of displacements produced per collision, electrons are considerably less damaging than protons. The minimum electron energy required to produce a displacement in silicon is about 200 kev; as electron energy increases the recoil atoms can produce secondary displacements of rather high density. However, electrons dissipate the greater part of their energy by ionization, and hence are effective in producing transient radiation effects. Unshielded silicon solar cells (p/n type) when irradiated with electrons in the energy range of 1 to 2 Mev were found to decrease in short-circuit current at around 10^{13} e/cm^2. Since electrons of this energy are rather easily shielded (1 gm/cm^2 Al), a damage threshold for enclosed transistors can be expected to be somewhat higher. Based on very limited data, a value of 10^{14} e/cm^2 appears to be realistic.

The purpose of the foregoing cursory look at the neutron and charged-particle thresholds of semiconductor devices is to place the radiation-effects problems associated with the Jupiter flyby spacecraft in somewhat better perspective.

The major uncertainty as to possible radiation effects to the spacecraft is, of course, the magnitude and types of particles and the particle energies associated with the theorized Jovian radiation belt. If the estimate of the electron flux of energy greater than 1 Mev (2×10^9 e/cm^2-sec at 3 R_j) is anywhere near reality, it offers a strong indication that a severe problem will be encountered. Exposure to an average flux of 2×10^9 e/cm^2-sec for 10^4 seconds ($\sim$3 hours) would approach permanent damage thresholds for some semiconductor devices.

Optical Glass - Darkening can occur in some glasses at rather low exposure levels so the choice of optical materials, such as lenses or windows, for the Jupiter flyby spacecraft should be made with this fact in mind.

The effect of gamma rays on glasses has been investigated quite extensively, and it has been determined that ordinary crown and flint optical glasses begin to discolor appreciably at dosages of about 10^6 ergs/gm(C). Electrons and protons are very effective in producing ionization and, hence, color centers. Charged particle effects have not been extensively investigated, but enough data are available to define the approximate exposure level at which detrimental effects might be expected. A study of the effects of 1.2 and 0.30 Mev electrons on the optical transmission properties of several transparent materials has been conducted by Haynes and Miller (Reference 3.9-19). Spectral transmission in the range of 0.25 to 2.7 microns and wide-band transmission in the range of 0.40 to 1.2 microns was measured after exposure to electrons at a rate of approximately 1.9×10^{11} e/cm^2-sec. Some of the results are summarized in Table 3.9-3. Of the materials investigated, only two - a fused quartz (one of several brands) and a heat-resistant glass (Feurex) - showed appreciable loss of transmission below 10^{15} e/cm^2. Transmission of all the materials was degraded mainly in the ultraviolet and visible region. It was also noted that ultraviolet light may bleach discolored materials.

In another investigation (Reference 3.9-20), several materials were irradiated with 0.75 Mev electrons with resulting discolorations ranging from light brown to deep brown at 1×10^{14} e/cm^2.

In an irradiation with 0.5 to 160 Mev protons, Gegas, et al., (Reference 3.9-21) found that Corning-type 1723 glass suffered a large loss in transmission at an exposure of 1×10^{13} p/cm^2. It is not known if this is typical of optical-type glass exposed to proton irradiation.

Table 3.9-3

Effects of 1.2 Mev Electrons on the Transmission of Some Optical Materials

Material	Dose (e/cm^2)	Wide-Band Transmission Loss - %	Spectral Transmission
Sapphire	2.7×10^{15}	0	Negligible loss
Sapphire	1.0×10^{17}	0	Slight loss in UV; darkened slightly
Synthetic Fused Silica	1.0×10^{15}	0	Some loss in UV
Synthetic Fused Silica	1.0×10^{16}	0	Sharp loss below 0.4 micron
Fused Quartz	2.7×10^{15}	0.8 to 58.9*	Loss below 1.0 micron; absorption band at 0.55 micron
Silica Glass	2.7×10^{15}	7.6	Considerable loss below 1.0 micron
Soda-Lime Glass	1.7×10^{15}	26.0	Sharp loss below 0.8 micron; some loss above 0.8 micron
Borosilicate Glass	2.2×10^{14}	--	Large loss below 1.0 micron
	2.7×10^{15}	25.2	Large loss below 1.0 micron

* Depending upon particular material type

In another investigation, a number of infrared window materials were irradiated with 1 Mev electrons and 10 Mev and 26 Mev protons (Reference 3.9-22). In the electron experiments Engelhard Suprasil fused silica, Engelhard Infrasil fused quartz, Corning 7940 fused silica, General Electric-type 151 fused silica, General Electric-type 101 fused quartz, Kodak Irtran 2 (ZnS), Linde sapphire, Valpey silicon, and Valpey germanium were exposed in steps to integrated electron fluxes of 10^3 e/cm^2, 10^{14} e/cm^2, and 10^{15} e/cm^2. Spectral transmission (0.4 to 40 microns) was measured before and after each irradiation.

Only two of the materials tested showed any change in transmission after irradiation to 10^{13} e/cm^2. In the Infrasil, a loss in transmission was noted below 1 micron; at 10^{15} e/cm^2 it had a smokey-grey coloration and about 14 percent transmission at 0.55 micron, above 1 micron transmission was unaffected. General Electric 101 quartz showed a similar absorption band but the coloration was not uniform. The other materials were essentially unaffected at an exposure of 10^{15} e/cm^2.

Proton irradiations of Suprasil fused silica, Infrasil fused quartz, sapphire, Irtran 2, silicon, and germanium were carried

out at levels of 10^{11} p/cm^2 and 10^{12} p/cm^2. Except for the Infrasil quartz, none of the materials showed any change in transmission characteristics with either 10 Mev or 26 Mev proton irradiation. The Infrasil exhibited the same absorption band as in the electron experiments and on a total energy basis the absorption was almost the same.

It should be pointed out that a number of radiation-resistant or stabilized glasses have been developed. Cerium oxide is the most common additive; the cerium ion is a powerful electron acceptor and it removes radiation-created free electrons that would otherwise form color centers. Several basic types of glass, including borosilicate crown, barium crown, and flint glasses, when formulated with cerium are usable at exposure levels at least one hundred times higher than the unprotected glasses (at least for gamma radiation). Cerium oxide will, however, produce a yellow color in glass so the quantity added must be governed by this consideration.

Scintillation and Cerenkov Radiation in Optical Materials - The only direct experimental results on scintillation and Cerenkov effects uncovered in this study were in the same investigation previously discussed for permanent damage of optical materials (Reference 3.9-22). In that study, luminescence of the optical materials was determined as a function of electron flux level. Average electron energy was 0.9 Mev and fluxes ranged from 3×10^9 e/cm^2-sec to 3×10^{11} e/cm^2-sec. With the exception of germanium, all of the materials showed electron-induced luminescence. In most cases the luminescence signal was approximately a linear function of incident flux. Luminescence was also observed in 20-Mev proton irradiations at levels between 10^{12} p/cm^2-sec and 10^{13} p/cm^2-sec. While the spectral characteristics of the fluorescence was primarily in the visible range, there was considerable detectable luminescence beyond one micron. Signal-to-noise ratios obtained with a filter having a cut-on (50% transmission) wave length of 1.1 microns were as follows: sapphire - 13, Irtran - 2 to 25, quartz - 8 to 10, silicon - 4. Germanium does not transmit below 1.7 microns so lack of observed luminescence in this material is likely due to self-absorption.

Low energy electrons are capable of producing scintillation whereas the production of Cerenkov radiation requires that the velocity of the charged particle exceed the velocity of light in the medium. That is

$$v = \frac{3 \times 10^{10} \text{ cm/sec}}{\text{Index of Refraction}}$$

This indicates that electrons having energies in the tenth's of Mev can produce Cerenkov radiation in glass. To obtain some feeling for production of Cerenkov radiation in optical elements and transparent covers, estimates were made of radiation production in the

visible portion of the spectrum. A value of approximately 650 ev/cm was determined for energy emission rates in the 2 to 100 Mev range of energies. The ranges of 2, 20, and 100 Mev electrons in glass are approximately 0.4, 3, and 10 cm. Assuming a lens penetration on the order of 0.2 cm (2 Mev electron degraded to~1 Mev) with the above energy emission rate and assuming an electron current of $\sim 10^9$ e^-/cm^2-sec, the light emission in a lens is computed as follows:

$$I = \left(\frac{dE}{dx}\right) \Delta x \phi$$

$$= (650)\ (.2)10^9$$

$$= 1.3 \times 10^{11}\ ev/cm^2\text{-sec}$$

$$= 2.1 \times 10^{-8}\ watts/cm^2$$

The above result is well above star irradiance levels which are typically on the order of 10^{-13} to 10^{-12} watts/cm^2. The above calculation is very approximate and can be expected to be conservative for the lower energy electrons, but the higher energy electrons in thick lenses are considerably underestimated.

Sun Sensors - A Sun sensor employing silicon solar cells would be subject to degradation of performance because of radiation damage to the solar cells. It is well established that electron and proton bombardment of solar cells decreases the minority-carrier lifetime; the consequence is a decrease in short-circuit current and, therefore, a loss in efficiency. The radiation effects problem with solar cells, or with any type of Sun, star, or planet sensor for that matter, is accented by the fact that the device must of necessity be more or less openly exposed in order to perform its function. Furthermore, the successful performance of the function is obviously critical to the entire mission.

Sun sensors of the nulling type, such as those using four silicon solar cells, might well withstand an appreciable degradation in efficiency and still function properly. However, it would appear that a critical consideration would be the possible imbalance of the device resulting from the relative changes in efficiency of the four nulling cells. This could conceivably create a situation in which the device signaled the controls for improper orientation.

As with all semiconductor devices, the radiation sensitivity of photovoltaic cells varies with the type of cell. Silicon n/p cells exhibit somewhat better radiation tolerance than silicon p/n cells. Gallium arsenide, a relatively wide-band-gap semiconductor, appears to be more radiation stable than either type of silicon cell. There is reason to expect, therefore, that improved solar cells will become available in the future, but the entire area of detectors - including windows, shields, and associated electronics - operating in the ultraviolet, visible, or infrared

spectral range will require detailed investigation to provide the most radiation-stable devices for the Jupiter flyby mission.

Star Tracker - The primary areas of interest in a star tracker are the light-sensitive tubes employed and the optical elements. Under exposure to radiation, light-sensitive tubes will exhibit both permanent and transient effects. The permanent effect most probably produced at the lowest integrated flux level will be coloration of glass envelopes, as discussed previously. Of perhaps more significance to the Jupiter flyby mission will be dark current and leakage current effects produced by high fluxes of electrons, protons, and bremsstrahlung; characteristic X-rays; and visible radiations produced in the absorption of the primary particles. The amount of data available on light-sensitive tubes is not extensive, but the summary given in Reference 3.9-23 shows that ionization induced currents are produced in photomultiplier tubes at rather low radiation exposure rates. This dark current has been ascribed to (1) luminescence induced in the glass envelope, (2) increased current leakage through the insulation of the tube base, and (3) increased electron density in the vicinity of the first few dynodes which could be caused by recoil electrons ejected from the cathodes or the tube elements. All of these effects, and perhaps others as well, can be expected in the high-level electron fields of Jupiter.

As has been previously illustrated, Cerenkov radiation alone in optical elements can be expected to render the tracker inoperative in electron fields of the magnitude anticipated at Jupiter. Malfunctions of the star tracker were experienced in the Mariner IV tests in electron fields over 10^9 e^-/cm^2-sec (E $\approx$ 2.7 Mev). Although no reference is made to the possibility of Cerenkov radiation in optical elements causing the malfunction, a rough analysis indicates that this might explain the behavior of the star tracker in that test. Using an irradiance value for Canopus of 1.633×10^{-12} watts/cm^2, it is seen that the value previously computed of 2.1×10^{-8} watts/cm^2 (which would be representative of visible light emission of lenses under the test conditions) is approximately 10,000 times greater. Allowing for optical magnification of the star light by a typical value on the order of 10^3, this ratio is reduced to 10. Further, because the Cerenkov radiation is not entirely directed into the sensing light path and other geometric factors enter into the determination of the light intensity falling on the light-sensitive device, a further reduction of this ratio can be expected. In the Mariner IV test, star indications were observed with the simulated star source out of the field of view and an apparent star intensity of 6 times Canopus brightness at a flux of 4×10^9 e^-/cm^2-sec. Although the above approximations are rough, it seems highly probable that more detailed analysis or further experiment with the exact equipment would tend to substantiate Cerenkov radiation in the optical elements as the source of the observed behavior.

Radiation Damage Correlation - The sparsity of data under high intensity-high energy electron irradiation dictates the eventual need for extensive evaluation and qualification tests of materials, parts, and equipments. Of major concern in the specification of these tests is the simulation of the anticipated nuclear environment. The geometry of the irradiated sample is extremely important in trying to correlate the damage done by incident electrons having different energies. The following discussion is intended to afford some insight into the difficulty of specifying test environments that will yield data truly representative of the response of various materials, parts, and equipments in the anticipated environment. Energies of 2 and 20 Mev have been selected for discussion; the difficulties of simulation illustrated are typical of even wider spreads in energy between experiment and application. Consideration is given to geometries ranging from thin samples (e.g., thermal control coatings) to complex subassemblies.

When the sample is extremely thin so that electrons with either of the energies above lose only small fractions of their original energies, then the number of ionizations caused by the 20-Mev electrons themselves will be only slightly higher than those caused directly by the 2-Mev electrons. The higher energy electrons will lose an equal amount of energy through bremsstrahlung radiation in medium-weight materials, however, and some fraction of these photons will interact with electrons of the sample to produce additional ionization. Even when all of the photons are absorbed in the thin sample, one would only expect to get, as an upper limit, something like twice as much ionization from the 20-Mev electrons as from the 2-Mev ones, where radiation losses can essentially be neglected.

The cross section for producing displaced atoms with electrons saturates slightly above 2 Mev for medium-weight materials, so that about 1.5 times as many primary atoms will be displaced by the 20-Mev electrons in thin samples as by the 2-Mev ones. Moreover, the primary atoms from the higher energy electrons will have about 3 times as much energy, on the average, as those from the lower energy electrons and will produce about 2.7 times as many secondary displacements. Therefore, the 20-Mev electrons will be about 4 times as effective in producing atomic displacements as will the 2-Mev electrons, and the higher energy electrons should be more damaging in all thin samples.

If the sample is just thick enough to stop the 2-Mev electrons while allowing the 20-Mev ones to pass through with a good fraction of their original energy, then ionization by the lower energy electrons will probably be greater, since the energy loss through ionization increases drastically as the electrons are slowed down to an energy below half a Mev. The number of displacements caused by the 20-Mev electrons will not change very much even if they lose several Mev in passing through the sample, but slight energy losses by the 2-Mev electrons will shift the value of their displacement cross sections from the edge of the

plateau of the cross section curve to its rapidly falling face, and, at the same time, the average energy of the primary displacements that do occur will be reduced as the electron traverses the material. Hence, the effectiveness of the 2-Mev electron in producing displacements in the thicker sample will be greatly reduced when averages are taken over the path of the electron in the material. Thus, as the sample thickness approaches the range of the 2-Mev electrons, the low energy electrons may become more ionizing than the higher energy electrons, but may only produce 1/20th as many displaced atoms. The function and class of the target sample would have to be known to evaluate which of the electrons would be more damaging in this case.

Finally, if the sample thickness approaches the range of the 20-Mev electrons, then the higher energy electrons should cause much more ionization, both through the higher energy loss of the electrons to ionization and through the greater absorption of the electromagnetic radiation which they produce. In this case, it is necessary to average over the paths of both electrons to determine the number of atomic displacements which they produce, but the higher energy electron still is much more effective in this respect. The high-energy photons which the 20-Mev electrons produce also produce a number of displacements themselves to add to the effectiveness of this process. Hence, it seems that the 20-Mev electrons are always more effective than the 2-Mev electrons in producing displacements, by factors of from 4 to perhaps 20 or so, depending on the sample geometry.

It appears that either of the electron groups might be more effective in producing ion pairs depending on the geometry of the sample, but this is somewhat obscured by the effectiveness of the electromagnetic radiation in producing ionizations. Of course, if one is interested in a bulky sample or a whole spacecraft, then certainly the higher energy electrons would be more ionizing en masse, but their relative effectiveness on a small, critical component is difficult to judge.

The correlation of damage produced by electrons of two different energies is critically dependent on the class, function, and shape of the individual samples even when the energy and intensity of the incident electrons are known. If the samples are enclosed within an outer container, then the correlation is further complicated by the container which will present the sample with electrons and photons having wide distributions in energy. For example, one might select a container with a thickness greater than the range of all electrons, so that no damage could be done by the incident electrons, but now the photons produced in the container would be focused toward its interior. These photons, in turn, could produce high energy electrons in the sample to cause ionizations directly, and these electrons could then displace atoms of the sample. Hence, in effect, the photons would serve to transport energy from one electron to another over distances which the electron could not travel. Thus, the whole problem of correlating radiation damage is complicated by cascading random

interactions in various sample-container configurations. Educated speculations about the relative effects of particles with various energies can be made but to accurately correlate damage on a firm basis, a Monte Carlo radiation-energy transfer computer program, such as the one outlined in Reference 3.9-24, is required.

3.9.2.3 RTG Radiation Effects

Semiconductors - For a 600-day mission and at a distance of 1 meter from an RTG, an item of equipment would receive approximately 10^{10} n/cm^2. The threshold established in short term tests for some of the more sensitive devices is most often considered to be 10^{11} n/cm^2. The possibility of this threshold being decreased in a long-term, low-flux radiation environment has been little explored. The data from the 10,000-hour tests just completed by Battelle for the Jet Propulsion Laboratory could possibly shed light in this area but were not available for this study. In any case, the likelihood of having to place equipment in a neutron field which would result in permanent damage is remote. A factor of three advantage can be expected from a more typical separation distance of 5 feet. The possibility of damage from the RTG should be kept in mind, but it should not constitute a requirement for shielding or represent a serious restriction on configuration selection.

Radiation Detection Instruments - Although the methods for detection of radiation have been previously discussed in subsection 2.1, a brief discussion from a slightly different point of view seems warranted here. The detectors of interest are gas ionization, scintillation, Cerenkov, solid state, and charge collection.

Gas ionization devices are based on the sensing of radiation induced ionization in a gas subjected to an electric field. Three types of instruments operate on this principle. Characteristics of these instruments very by virtue of the variations in the ionized gas characteristics as a function of applied voltage. The devices are referred to as ionization chambers, proportional counters, and Geiger counters. The ionization current-voltage characteristics of these devices are illustrated in Figure 3.9-14.

The ionization chamber operates in a region referred to as the saturation region, region A. The current produced in this region by an ionizing event is proportional to the amount of ionization produced by the event with little loss due to recombination and little multiplication of gas ions produced. The pulse heights are proportional to particle energy deposited. Circuitry can be designed to operate in an individual pulse-sensing mode or integrating mode.

The proportional counter is operated in region B. In this region the applied voltage is high enough that sufficient energy is imparted to the initial ions to produce secondary ionizations

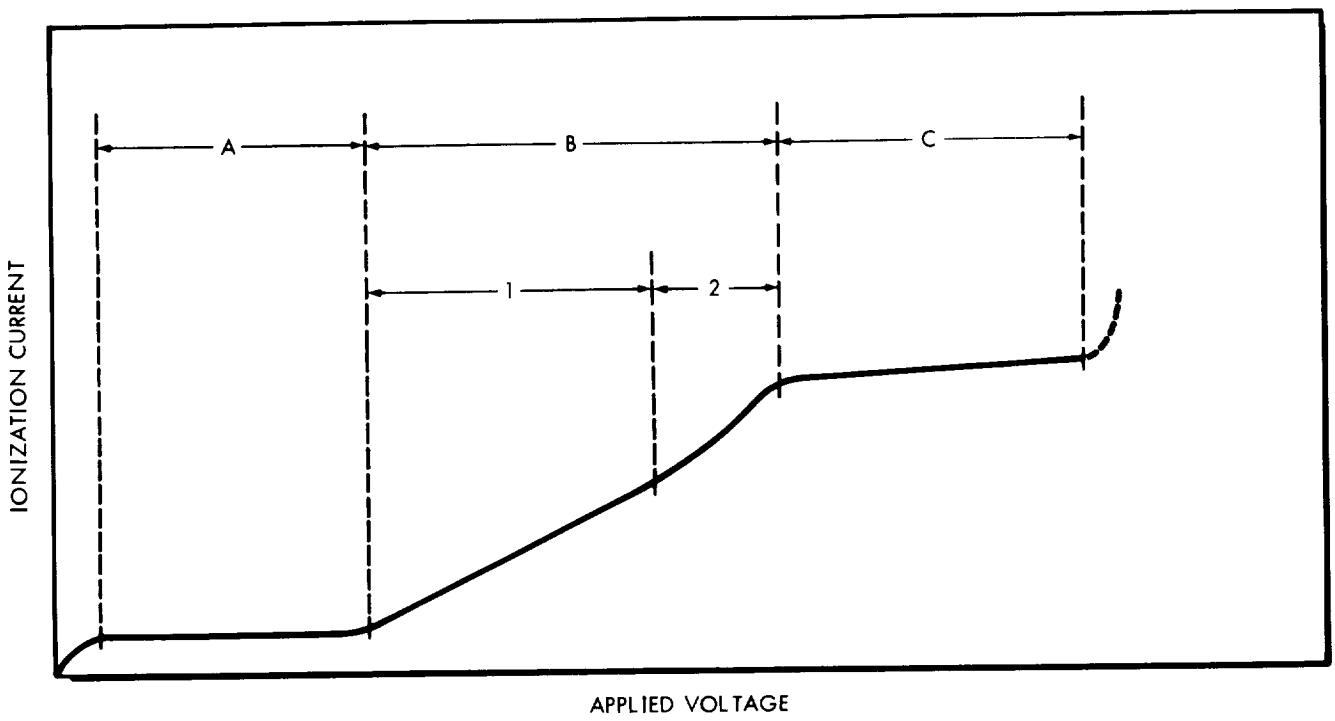

FIGURE 3.9-14

(avalanche process) effectively amplifying the initial event. In region B1 the multiplication is independent of the size of the initial event, however, in region B2 the multiplication becomes dependent on the energy deposited in the initial event and, hence, the output can be interpreted in terms of energy deposited. The recovery time when operating in this region is very rapid, and the device can be employed in high intensity fields.

The Geiger tube operates in region C. The output pulse in this region is of the same height and independent of the energy deposited in the initial event. To return the device to a non-conducting mode after a discharging event requires voltage reduction or the addition of a quenching gas to the primary gas. (The second method is more commonly used.) The quenching time limits the count rate to which these devices are effective. This time interval is such that limiting count rates are on the order of 10,000 to 40,000 counts/sec.

In a scintillation instrument, the light pulse produced in the deposition of radiation energy in a luminescent material is sensed and interpreted to provide information about the character of the radiation. The intensity of the pulse is proportional to the energy deposited.

The Cerenkov detector is based on the sensing of light emitted by charged particles entering the sensing material; the charged

particles have velocities which exceed the velocity of light in the material. The methods of detecting the emitted light are similar to those employed in the scintillation counter, most often employing photo-multiplier tubes.

The solid-state detectors involve the detection of radiation-induced ionization in the depletion region of a reverse biased semiconductor junction. The pulse is proportional to the energy deposited by the traversing radiation.

The charge collection devices provide detection of low-energy charged particle fields by the trapping of ions (Farady Cage) and the measurement of the resulting currents. Collector polarity and entrance grid potentials are varied for energy and charge discrimination. A device called an electrostatic analyzer employs an electrostatic field to deflect the incident charged particles into the collection region. The energy and charge-to-mass ratio of the detected particle is related to the electric field strength used.

Of concern in this study is the sensitivity of these instruments to the neutron and gamma fields of the RTG units. The sensitivity of these instruments is very much a function of individual instrument design. The type, energy, and intensity of radiation being measured also must be considered to determine the significance of instrument response to the RTG environment.

The measurement of interplanetary and planetary charged particle types, intensities, energies, and angular distributions are required. The characteristics of these charged particles dictate the selection of methods and sensitive media for this measurement. Angular distribution is largely accomplished by selective shielding and/or coincidence counting. Particle type and energy discrimination is accomplished through relative response of detector materials, pulse height analysis and biasing, coincidence gating, material shielding, magnetic fields, and electric fields. Since neutrons and gamma radiation are not of primary scientific interest, much can be done in the design of detectors to reduce the detector sensitivity to RTG emanations without seriously degrading the effectiveness of the detector in charged particle measurements. Of course, all of the methods described are sensitive to some degree to neutrons and gammas. The significance of this sensitivity can only be judged by comparing the relative sensitivity of the instrument to the radiation being measured. The neutron and gamma response becomes important only when it can not be discriminated from the radiation being measured. This latter observation has led to an emphasis being placed on ionization chamber and Geiger tube responses to interplanetary radiation and, in particular, galactic cosmic radiation. The relative intensities and/or energies of planetary trapped and solar flare radiation seems to afford the possibility of discriminating out the RTG environment.

Charge collection systems for solar wind measurements appear to be relatively insensitive to RTG radiation, at least for instruments having thresholds of $\sim 10^6$ P/cm^2-second. No further consideration of RTG radiations is deemed necessary in this discussion; however, should charge collection instruments having lower thresholds be used to measure fields of lower intensity in close proximity to an RTG, this matter will require further consideration.

In order to estimate the effects of the RTG neutrons and gammas on the measurement of cosmic radiation obtained from ion chambers and GM tubes, it was necessary to identify probable characteristics of each type of instrument. These characteristics are presented in Table 3.9-4. Also indicated are nuclear properties of materials pertinent to the estimates of effects. The ionization chamber is a Neher-type, and the GM tube is similar to the Electronic Optical Nuclear Corporation 6213 used on Mariner IV.

Table 3.9-4

Detector Characteristics and Nuclear Properties

DETECTORS

Ionization Chamber

Diameter - 3 in.

Wall - 20 Mil Aluminum

Gas - Argon (94#/in^2)

GM Tube

Effective Cathode Dimensions - 0.093 in. D x 0.300 in. long

Cathode Material - 28% Cr - 72% Fe

Cathode Thickness - 0.125 in.

Gas Assumed - $\sim$ 1 Atmos. - Ne + 0.1% Cl

NUCLEAR PROPERTIES*

	Ar^{40}	Al^{27}	Cl^{35}	Ne^{20}	Fe^{56}	Cr^{52}
Tel.	1.8b(3)	--	1.7b	900 mb(1.5b)	--	--
Tn,p	440mb(200)	20 mb(-)	170mb(60)	--	--	--
Tn,x	320mb(40)	--	60mb(-)	275mb(60)	--	--

* Initial values are for 5-Mev neutrons and the bracketed values are for 2-Mev neutrons. Dashes indicate zero cross sections or insignificant values for these estimates.

Neutron Sensitivity of Ionization Chamber - Neutron interaction rates, R, follow the relationship

$$R = \frac{\rho N}{A} \sigma \phi$$

where ρ = Density of media
N = Avagadro's number
σ = Microscopic cross section
A = Media atomic weight
ϕ = Neutron flux.

The reaction rates per unit neutron flux in the argon gas are as follows:

$$\frac{R}{\phi} = \frac{(0.0108)(6.03 \times 10^{23})}{40} \sigma$$

$$= 1.75 \times 10^{20} \sigma$$

	5 Mev (events/cm^3-sec-ϕ)	2 Mev (events/cm^2-sec-ϕ)
Elastic Collision	3.15×10^{-4}	5.25×10^{-4}
n,p	7.7×10^{-5}	3.5×10^{-5}
n,α	5.6×10^{-5}	7×10^{-6}

The average energy transferred to the argon atom in elastic collision is:

$$E_{avg} = E_n \left[1 - 0.5(1 + \alpha) \right]$$

when:

$$\alpha = \left(\frac{A - 1}{A + 1}\right)^2 = \left(\frac{39}{41}\right)^2 = 0.9$$

$$E_{avg} = 0.05\ E_n$$

$$E_{avg} = 0.25 \text{ Mev } (E_n = 5 \text{ Mev})$$

$$E_{avg} = 0.10 \text{ Mev } (E_n = 2 \text{ Mev}).$$

For this instrument, 1.55×10^2 Mev/cm^3-sec is equivalent to 1 r/hr. Therefore, the neutron flux required to produce 1 mr/hr (which is the lower limit from the expected cosmic ray flux) from 5 Mev neutron elastic collisions and assuming total absorption of recoil energy is:

$$\phi = \frac{0.155}{(3.15 \times 10^{-4})(0.25)}$$

$$= 1.97 \times 10^3 \text{ n/cm}^2\text{-sec}.$$

The contribution of the n,p reaction in the aluminum wall of the chamber is estimated as follows:

$$\frac{R}{\emptyset} = \frac{\rho VN}{A}\sigma$$

$$= \frac{(2.7)(9.413)(0.603)(0.020)}{27}$$

$$= 0.011 \text{ events/sec-}\emptyset$$

The protons emitted have energies from 1.8 to 3.2 Mev. The range of a 3-Mev proton is on the order of 0.002 cm in aluminum, which is only 1/25 the thickness of the aluminum wall. Even assuming half the protons produced in this thickness arrive in the chamber, only 0.2 particle arrives in the chamber per 10^3 n/cm^2-sec. Clearly the chamber response from this source is negligible.

Gamma Response Ionization Chamber - The gamma radiation from the RTG was previously computed to be 10.8 mr/hr at 1 meter. At 3.25 meters, the field produces a response of 1 mr/hr in the ionization chamber.

Neutron Response of the GM Tube - The same calculational procedure is employed for the detector gas to calculate neutron reaction rates as in the ionization chamber with the inclusion of detector active volume, assuming each event produces a count. Only neon is considered since the quantities and cross sections of chlorine will make relatively small contributions.

$$\frac{R}{\emptyset} = \frac{\rho VN}{A}\sigma$$

$$= \frac{(9 \times 10^{-4})(3.33 \times 10^{-2})(6.03 \times 10^{23})}{20.2} T$$

$$= 9 \times 10^{17}\sigma$$

The resultant count rate per unit flux for elastic collisions and n,α reactions in the gas for 5-Mev neutrons is 1.06×10^{-6}, and for 2-Mev neutrons it is 1.45×10^{-6} counts/sec-$\emptyset$. Fluxes well above those expected would be required to approach a cosmic background of 0.6 c/sec.

Gamma Response of GM Tube - For estimates of gamma sensitivity, values presented in the Electronic Optical Nuclear Corporation catalog for device type 6213 are used. Values for the number of secondary electrons which emerge into the detector sensitive volume per 1000 photons/cm^2 range from 0.48 at an energy of 0.08 Mev to 2.85 at an energy of 1 Mev. The cathode area seen by the incident flux must be multiplied by these values to give detector response. The worst case for the unidirectional flux of the RTG

is for the flux to be perpendicular to the axis of the detector. The cathode area is then 0.18 cm^2. The response for the various gamma energies at 1 meter is calculated as follows:

$$C = \frac{eAI}{10^3} = 1.8 \times 10^{-4}\ eI$$

e = Secondary electron production per 10^3 γ/cm^2-sec

A = Cathode area

I = Gamma flux at 1 meter.

The values are tabulated below:

E (Mev)	Count Rate (c/sec)
0.044	Nil
0.099	0.0677
0.15	0.0268
0.203	Nil
0.760	2.02
0.875	0.963
TOTAL	3.08 c/sec

At 2.24 meters the count rate is of the order of cosmic ray background count, 0.6 c/sec for this instrument.

Summarizing the preceding results, it appears likely that separation of the above instruments from the source affords reduction of detector response without shielding to the level of cosmic background, which represents the minimum radiation fields to be encountered. It is felt that variations in cosmic radiation levels can be evaluated under these conditions. Other phenomena such as the detection of ~ 40 Kev electrons from the Sun reported by Van Allen and Krimigis (Reference 3.9-25) can still be observed. Furthermore, these instruments should not be relied upon as the primary means of cosmic radiation measurement. A solid-state telescope could be effectively employed. The methods of pulse height biasing and analysis, together with coincidence gating techniques generally used, render the instrument relatively insensitive to the radiation from the RTG.

3.9.3 RTG Safety Considerations

The radioisotopes of the RTG can represent a serious health hazard if not properly controlled. Safety criteria are established

to minimize the potential health hazards during fabrication, shipping, installation, checkout, launch, and operational phases. In general, these criteria are established by the agency developing the RTG. The criteria of particular interest to the user are those which dictate procedures during the prelaunch, launch, and operational phases. In general, shipment is governed by 49 CFR 71-78 and Bureau of Explosives regulations. The received container will have dose rates not exceeding 200 mrem/hr at the surface and 10 mrem/hr at 1 meter. Container temperatures will not exceed 180°F on accessible surfaces and 350°F for surfaces in contact with a floor or wall. During operations prior to launch, personnel doses will not exceed 1-1/4 rem/quarter. Absolute containment of the fuel is currently the objective during all phases of the mission and after launch vehicle malfunctions. Fuel containment on Earth is based on the objective of 10 half-life confinement of the isotope.

From a radiation safety point-of-view, no unusual procedural requirements are evident during the prelaunch phase for normal operations. The possibilities of thermal problems will dominate. Access to the launch area after a destructive launch system malfunction (fire or explosion) during the prelaunch or early launch phase must not precede an area radiation survey, even though the RTG unit is designed to survive credible incidents. In launch aborts, launch trajectories which do not result in unfavorable impact points for the RTG's should be selected.

3.9.4 Conclusions and Recommendations

Conclusions and recommendations of the study are discussed relative to operational, configuration, and equipment performance considerations. During prelaunch operations, normal compliance with the standard Health Physics practices will provide adequate protection to the personnel working with and around the RTG's. In the selection of launch trajectory, consideration should be given to potential RTG impact points in the event of launch abort. The predicted steep rate of change of Jupiter radiation intensity with increasing planetary radii suggests an analysis of the scientific compromise involved in moving the point of closest approach to greater distances from Jupiter. The estimated radiation rate at 4 Jupiter radii is 1/200 that at 3 Jupiter radii. Consideration of this involves a trade-off between scientific investigations and equipment performance.

With regards to spacecraft configuration selection, the effect of the RTG environment on several radiation detectors is of primary concern. First consideration should be given to providing the maximum equipment separation distance possible within the limits of practical possibilities. How far these limits are stretched depends on the value of scientific information sacrificed and the penalties associated with increased system weight if shielding is required. Analyses in the previous subsection indicate that separation distances (from a single 120 W_e unit)

of 10 feet for the ionization chamber and 6 feet for the GM tube result in levels of instrument response associated with cosmic background. If these conditions are achieved, it is believed that no serious loss of scientific information would ensue. It is pointed out again that the radiation source term which was employed in the calculations is conservative. The expected neutron spectrum is softer than assumed. More important, self-absorption of the gamma radiation is likely to be appreciable. This is especially true if the radiation detector is located along the axis of a cylindrical RTG. Further advantage is to be expected if spacecraft equipments lie between the source and detector. All things considered, radiation shielding of the RTG does not seem to be warranted at this time. Certainly before configuration penalties or the inclusion of shielding are specified, a more detailed analysis as well as experimentation is required to ascertain the exact nature of radiation detector response in the anticipated environment.

Based on the radiation effects analysis, it is concluded that serious radiation-induced degradation of equipment performance can be expected unless particular attention is given this area during the selection of spacecraft subsystem operating principles, materials, and parts. Particular attention will be required in connection with thermal control coatings; IR, visible, and UV detector materials; covers and optical elements; high-impedance, low-signal-level circuitry; and semiconductor devices in general.

The most serious difficulties are encountered in penetrating Jupiter's radiation belts. Shielding against the high energy radiation of Jupiter is not a satisfactory solution. Radiation resistant equipment design is required to ensure mission success. It is recommended that a radiation effects program be initiated prior to hardware procurement to ensure the availability of equipment with maximum possible radiation resistance. The program should be directed towards the timely acquisition of information for use in the preparation of specifications by the procuring agency and for use in the design and development of equipment. Specifications which place restrictions on the use of operating principles, materials, and parts are required at the time of equipment acquisition. Additionally, they are required to identify requirements for evaluation and qualifications tests.

A suggested approach is to use the Mariner IV design and the Jupiter flyby equipment requirements as a baseline. Detailed analyses of the Mariner IV equipment applicable to the Jupiter flyby mission and the equipment unique to Jupiter spacecraft will identify radiation sensitive areas and specify those operating principles, materials, and parts which afford the greatest potential for radiation resistance. Data deficiencies and development requirements will be identified at the same time.

An experimental program is required to provide the data necessary to select a radiation-resistant design approach. The

experimental program will involve the development of test techniques which provide the basis for preparation of test specifications. The intent of the experimental program is not to develop hardware but to provide the background and data which are required to design and develop the hardware. As such a program progresses, it will provide increasing resolution of the best design approach and, eventually, will result in the preparation of specifications to control and direct the activities of the contractor in the acquisition phase.

3.8.5 References

3.9-1 Space Radiation Guide, TDR No. AMRL-TDR-62-86, August 1962.

3.9-2 Space Materials Handbook, Technical Documentary Report No. ML-TDR-64-40, March 1964.

3.9-3 "Earth's Radiation Environment," Wilmot N. Hess, Manager, Theoretical Division, Goddard Space Flight Center, NASA, Space/Aeronautics, November 1964.

3.9-4 Chang, D. B. and L. Davis, Jr., "Synchrotron Radiation as the Source of Jupiter's Polarized Decimeter Radiation," Astrophysical Journal, 136, 1962, p. 567.

3.9-5 Morris, D., and G. L. Berge, "Measurements of the Polarization and Angular Extent of the Decimeter Radiation from Jupiter," Astrophysical Journal, 136, 1962, p. 276.

3.9-6 Chang, D. B., "Synchrotron Radiation as the Source of the Polarized Decimeter Radiation from Jupiter," Boeing Research Report D1-82-0129, (1962).

3.9-7 Cladis, J. B. et al., "Energy Spectrum and Angular Distribution of Electrons Trapped in the Geomagnetic Field," Journal of Geophysical Research, 66, (August, 1961) p. 2297.

3.9-8 Roberts, J. A., and M. M. Komesaroff, "Observations of Jupiter's Radio Spectrum and Polarization in the Range from 6 cm to 100 cm," Icarus, 4, 1965, p. 127.

3.9-9 Berge, G. L., "An Interferometic Study of Jupiter at 10 and 2/cm," Radio Science, Volume 69D, No. 12, (December 1966).

3.9-10 Roberts, J. A., "Radio Emission from the Planets," Planetary and Space Science, 11 (1963) p. 221.

3.9-11 Space Physics, University of California Engineering and Physical Sciences Extension Series, Edited by D. P. Le Galley and A. Rosen, John Wiley & Sons, Inc.

3.9-12 Foster, K. W., Gamma Shielding Requirements for Plutonium - 238 and Polonium - 210 (Revised), AEC Research and Development Report MLM-1315.

3.9-13 Miller, R. A., and Campbell, J. J., Effects of Low Energy Protons on Thermal Control Coatings, Paper presented at the AIAA Thermophysics Specialist Conference, Monterey, California, 13-15 September 1965.

3.9-14 Gillette, R. B., Brown, R. R., Seiler, R. F., and Sheldon, W. R., Effects of Protons and Alpha Particles on Thermal Properties of Spacecraft and Solar Concentrator Coatings, Paper presented at the AIAA Thermophysics Specialist Conference, Monterey California, 13-15 September 1965.

3.9-15 Breuch, R. A., Exploratory Trapped-Particle-Plus Ultraviolet Effects on the Optical Properties of Spacecraft Thermal Control Coatings, Paper presented at the AIAA Thermophysics Specialist Conference, Monterey, California, 13-15 September 1965.

3.9-16 Jorgenson, G. V., Effects of Simulated Solar-Wind Bombardment on Spacecraft Thermal Control Surfaces, Paper presented at the AIAA Thermophysics Specialist Conference, Monterey, California, 13-15 September 1965.

3.9-17 Thatcher, R. K. et al., The Effects of Nuclear Radiation on Electronic Components, Including Semiconductors, REIC Report No. 36, 1 October 1964.

3.9-18 Brown, R. R., Experimental Techniques of Proton Accelerator Bombardment for Simulating Permanent Space Radiation Damage to Transistors and Diodes, Boeing Co.

3.9-19 Haynes, G. A., and Miller, W. E., Effects of 1.2 and 0.30 Mev Electrons on the Optical Transmission Properties of Several Transparent Materials, Langley Research Center Report, NASA, TN D-2620, March 1965.

3.9-20 Solar Cell Shield Materials, General Electric, Missile and Space Vehicle Department, GE, 137-108, 15 May 1961.

3.9-21 Gegas, G., Euband, N.M., and Gruber, D. E., Interim Report on the Apollo Window Materials Radiation Testing Program, North American Aviation, Atomics International, A1-Memo-9366, 5 February 1964.

3.9-22 Downing, R. G., Snively, F. T., and Van Atta, W. K., Investigation of Charged Particle Effects on Infrared Optical Materials, Air Force Materials Laboratory Report AFML-TR-65-261, November 1965.

3.9-23 REIC Report No. 36, The Effects of Nuclear Radiation on Electronic Components, Including Semiconductors.

3.9-24 Radiation Effects Technology for Military Space Missions Requiring Nuclear Electric Power, AFWL TR-66-36 (GD/FW FZK 280) February 1966.

3.9-25 Van Allen, J. A., and Krimigis, S. M., Impulsive Emission of 40 Kev Electrons from the Sun, Journal of Geophysical Research, Vol. 70, December 1, 1965 (p. 5737).

3.9-26 Anspaugh, Bruce E., "Electron Radiation Testing of Mariner IV Electronic Subsystems," Presentation at the Space Radiation Effects Meeting - Langley Research Center - Hampten, Virginia - November 18-19, 1965.

3.10 METEOROID PENETRATION PROTECTION

In this study, the basic method of providing protection against meteoroid penetration is to provide armor-type shielding that will prevent such penetration. Meteoroid environment and hypervelocity impact data have been collected and analyzed in an effort to provide spacecraft design information pertaining to the protection of the spacecraft subsystems from meteoroid damage. It is well known that this type of information will be questionable because of the nature of its origin. Two factors contribute to the uncertainty of the penetration analysis: (1) the lack of a physical description of impacts between appropriately sized particles and targets at velocities of interest and (2) the lack of data on the number and size of meteoroids in space, particularly outside the immediate vicinity of Earth. The first uncertainty is the result of present-day incapabilities to accelerate particles of mass 0.1 to 1 gram to velocities of 10 km/sec and greater. The latter uncertainty results from the absence of in situ measurements of the meteoroid population in space or the lack of a significant statistical sample.

Because of these unknowns and the scope of the task, the meteoroid penetration protection analysis is based on information contained in existing literature. A consensus is used when the resulting design requirements are affected only a little by differences of opinion. Both conservative and liberal viewpoints are considered in matters which significantly affect the penetration requirements.

3.10.1 Basic Relationships

Although laboratory verified descriptions of hypervelocity impact in the momentum range of interest are not available, several theoretical descriptions have been postulated in the form of mathematical equations (Reference 3.10-1). All have merit, but none yield significantly different results. The hypervelocity impact equation predicted by Herrmann and Jones (Reference 3.10-1) has been selected for use in the analysis, i.e.,

$$(1) \quad t_T = 1.119 \; \rho_T^{-2/3} \; \rho_P^{1/3} \; m^{1/3} \; \ell n\left(1 + \frac{\rho_P^{2/3} \; \rho_T^{1/3} \; V^2}{39.23 \; H_T}\right)$$

where t_T (meters) is the maximum thickness of a target having a density ρ_T (g/m^3) and Brinell hardness H_T (g/m^2) that will be penetrated by a particle of mass m (grams) and density ρ_P (g/m^3) that is moving at a velocity V (m/sec) relative to the target.

A relationship such as the one described in equation (1) provides a means of obtaining the thickness of a specific shielding material that will prevent penetration by a meteoroid of a particular mass, density, and relative velocity. The analysis is then applied to the determination of these unknowns--mass, density, and velocity. The selection of a worst-case set of values for these meteoroid parameters would constitute a design point, and such a selection must be made for any ultimate design application. The usual approach (Reference 3.10-2) is to delay the decision at this point and bring in another meaningful consideration, namely, the effect that the amount of spacecraft exposed area and the length of time it is in the meteoroid environment has on the realization of meteoroid impacts.

The analysis used herein defines a meteoroid flux for a given portion of space, i.e., the expected number of meteoroids of mass m or greater passing through a unit area of the particular region of space in unit time. This flux $\emptyset$ is expressed as (e.g., Reference 3.10-2)

$$(2) \quad \emptyset = \alpha m^{-\beta} = \frac{\text{number of particles of mass m or greater}}{m^2\text{-sec}}$$

where α and β are constants. Thus, if the flux is multiplied by the spacecraft exposed area and the spacecraft flight time in the particular region, the number of expected impacts, I, on the spacecraft of particles having mass m or greater will be the result, i.e.,

$$(3) \quad I = \emptyset AT = \text{number of impacts of particles having mass m or greater}$$

where A is the spacecraft exposed area and T is staytime.

If equation (1) is solved for m, and m is substituted into equation (2), and the resulting $\emptyset$ is subsequently included in

equation (3), the expected number of penetrations N of spacecraft exposed area A during time T will be determined, i.e.,

$$(4) \quad N = \alpha \left[\frac{t_T \rho_T^{2/3}}{1.119 \rho_P^{1/3} \ell n\left(1 + \frac{\rho_P^{2/3} \rho_T^{1/3} V^2}{39.23 H_T}\right)} \right]^{-3\beta} AT.$$

The parameter N will be used as a basic measure of the meteoroid hazard to spacecraft. It is noted that the parameter "probability of penetration" (or "probability of no penetration") will not be employed, because it is felt that the use of this parameter only complicates further an already complicated picture. If its use is required in calculating the probability of mission success, such a number can be obtained at a later date; but N is considered a more meaningful design parameter.

Reflecting on the number of meteoroid environment parameters that appear in equation (4), it becomes apparent that a completely parametric analysis is prohibitively large, and that any uncertainty in these parameters is increased by orders of magnitude in the ultimate answer. On these grounds, "average" values of the parameters α, β, ρ_P, and V are defined for each of four meteoroid environments. These values and their origins are discussed in the following subsection.

3.10.2 Meteoroid Environments

The portion of space through which a Jupiter spacecraft must pass is considered to present four different meteoroid environments, namely, the near-Earth, interplanetary, asteroid, and near-Jupiter. As implied, these refer to different regions of the spacecraft trajectory. In this study, the interplanetary region is considered to extend from Earth to Jupiter, and the asteroid environment is superimposed at its appropriate limits.

3.10.2.1 Near-Earth

The meteoroid flux intensity and gradient adopted for this region were presented by Alexander, et. al. in Reference 3.10-6. To complete the near-Earth criteria, the meteoroid density and velocity presented by Whipple (Reference 3.10-3) and Volkoff's suggested extent of the near-Earth region (Reference 3.10-2) are used. The particle flow direction in the near-Earth region is generally assumed to be isotropic.

METEOROID VELOCITY DETERMINATION

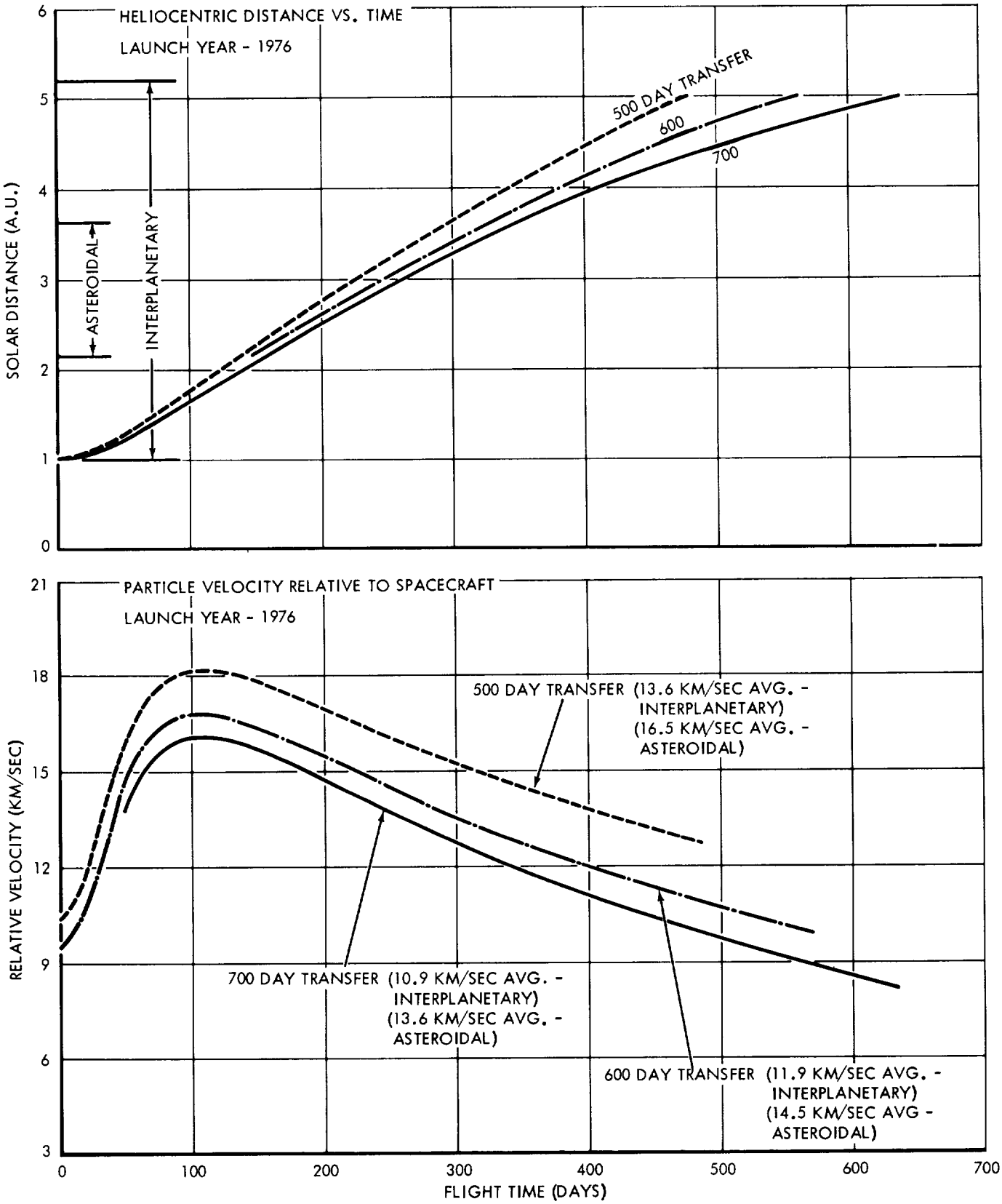

FIGURE 3. 10-1

The summation of the near-Earth parameters is as follows:

1. The near-Earth region starts at a geocentric distance of 1.0 Earth radius (6436 km) and extends to 65.0 Earth radii (414,115 km).

2. The near-Earth flux intensity, α, and flux gradient, β, are $\alpha = 10^{-17}$ and $\beta = 1.70$.

3. Particle density is 0.433 g/cc.

4. Particle velocity relative to the spacecraft is 22 km/sec.

3.10.2.2 Interplanetary

The interplanetary region is considered to extend from near-Earth to near-Jupiter. This region actually consists of both cometary and asteroidal debris. The cometary debris exists through the entire region (1.0 to 5.2 a.u.) whereas the asteroidal debris primarily exists in a region from approximately 2.15 to 3.65 a.u. from the Sun. Because of this difference and differences in particle flux density, the cometary flux and the asteroidal flux are considered separately and denoted as the interplanetary region and asteroidal region, respectively. The meteoroid penetration hazards from each type of particle are combined at a later point in the analysis.

The cometary debris in the interplanetary region is assumed to have the same density as the near-Earth flux. The meteoroid flux intensity and gradient are based on data from the Pegasus satellites, the Mariner II and Mariner IV space probes, and the corrected "Watson law" as reviewed by Whipple (References 3.10-3 and 3.10-7).

In order to obtain an average relative particle velocity, all particles were assumed to move in direct circular orbits. Relative velocities at regular time intervals were then calculated from trajectory data for 500-, 600-, and 700-day transfers in 1976. The variation in relative velocity and heliocentric distance with time for these trajectories is shown in Figure 3.10-1. The average relative particle velocity for each trajectory was obtained and the arithmetic mean of these three averages is the value used in the subject analysis.

The summation of the interplanetary parameters is as follows:

1. The interplanetary region extends from 1.0 a.u. to 5.2 a.u.

2. The interplanetary flux intensity, α, and flux gradient, β, are $\alpha = 10^{-13.3}$ and $\beta = 1.00$.

3. Particle density is 0.443 g/cc.

4. Relative particle velocity is 12.1 km/sec.

3.10.2.3 Asteroidal

The most logical studies of the hazards to spacecraft in the Asteroid Belt are based on extrapolations of data points obtained from visual observations (References 3.10-4 and 3.10-5). Objects in the Asteroid Belt that have an absolute photographic magnitude greater than 18 can be observed from Earth, and extrapolations of these data can be done on various theoretical grounds (Reference 3.10-4). It is felt that the most extreme environment that could possibly be postulated corresponds to an α of 10^{-9} and a β of 1.0, and a nominal environment corresponds to an α of 10^{-15} and a β of 0.67. Both of these environments are considered in the parametric analysis of protection requirements.

In most of the literature surveyed, the Asteroid Belt is defined as having the shape of a torus with a major radius of approximately 2.90 a.u. and a minor radius of approximately 0.75 a.u. There is also general agreement that the particle densities range from 1.0 to 7.0 g/cc with 3.0 to 3.5 g/cc generally used as average. Some uncertainty exists as to whether asteroidal particles travel in circular orbits, but relative velocities will be determined here as they were in the case of the interplanetary region (see Figure 3.10-1).

The summation of the asteroidal parameters is as follows:

1. The asteroidal region extends from 2.15 to 3.65 a.u.

2. Two asteroidal flux intensities and flux gradients and considered. They are $\alpha = 10^{-15}$, $\beta = 0.667$, and $\alpha = 10^{-9}$ and $\beta = 1.0$.

3. Particle density is 3.0 g/cc.

4. Relative particle velocity is 14.9 km/sec.

3.10.2.4 Near-Jupiter

Very little information is available on the meteoroid environment in the vicinity of Jupiter. The environment employed here is based on postulations that the particle flux intensity is approximately 3 orders of magnitude more dense near-Jupiter than near-Earth, which would correspond to an α of 10^{-14}. The increased flux intensity is attributed to the increased gravitation field of Jupiter. The flux gradient, β, is considered the same as the flux gradient near-Earth, or 1.70. The debris is considered to be mostly cometary with a density of 0.433 g/cc; however, there is some speculation that the density may be slightly higher near Jupiter because of the contribution made by asteroidal material. Jupiter's meteoric debris is believed to extend to the planet's tidal radius which is approximately equal to 400 Jupiter radii.

Generally, particle impact velocity in the vicinity of a planet is assumed to be the larger of the planet's escape velocity or heliocentric velocity. In the case of Jupiter, the escape velocity at the surface is 61 km/sec and is the larger. However, because on a flyby mission the spacecraft is in the near-surface area for only a short span of the total Jupiter influence time, an average relative particle velocity of 41 km/sec is assumed for the entire near-Jupiter region. This is approximately equal to averaging the escape and heliocentric velocities. The particle flow direction in the near-Jupiter region is assumed to be isotropic.

The following is a summation of the near-Jupiter parameters:

1. The near-Jupiter region extends from the surface (69,892 km) to 400 Jupiter radii (27,956,800 km).

2. The near-Jupiter flux intensity, α, and flux gradient, β, are $\alpha = 10^{-14}$ and $\beta = 1.70$.

3. Particle density is 0.443 g/cc.

4. Relative particle velocity is 41 km/sec.

3.10.2.5 Environment Summary

The meteoroid environment that is used in the penetration protection requirements analysis is summarized in Figure 3.10-2.

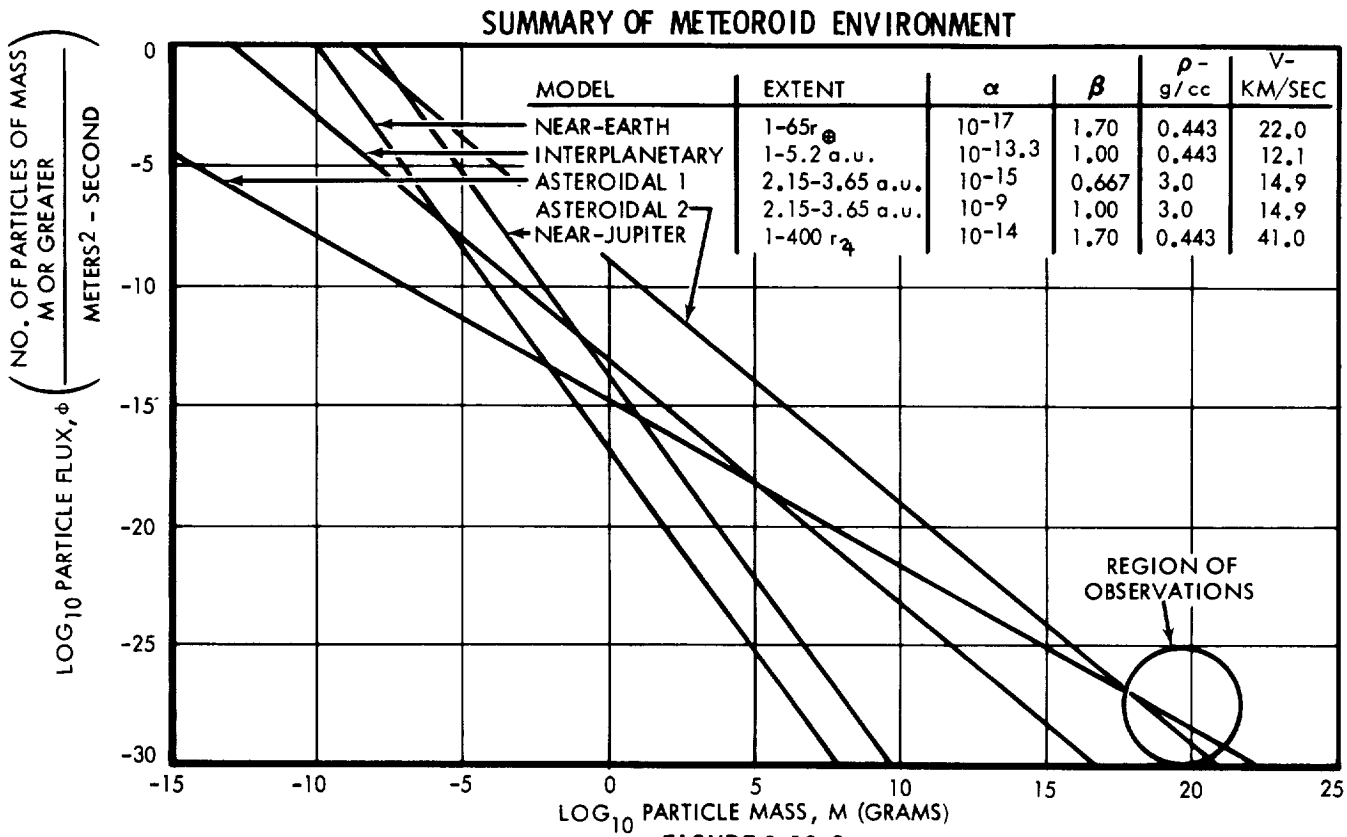

FIGURE 3.10-2

3.10.3 Parametric Analysis

The results of combining the meteoroid model for the various regions with the hypervelocity penetration equation are shown in Figures 3.10-3 through 3.10-7. The data are presented in the form of the exposed area-time product vs. number of penetrations for various thicknesses of aluminum. Only aluminum has been considered in the parametric analysis, however, other materials have merit. Titanium for instance will show a slightly lighter structure for the same penetration protection, but the fabrication processes are considerably more complicated than those for aluminum.

In addition to the armor-type protection, various other types of protection have been proposed. The most notable of these are the so-called "bumper shields." Bumper shields consist of two metal sheets separated by a specified space which may or may not contain a filler material. By proper selection of sheet thicknesses, separation distances, and filler material, claims of up to 80 percent weight savings over the armor-type systems have been made. For purposes of this study, these systems are not considered, because

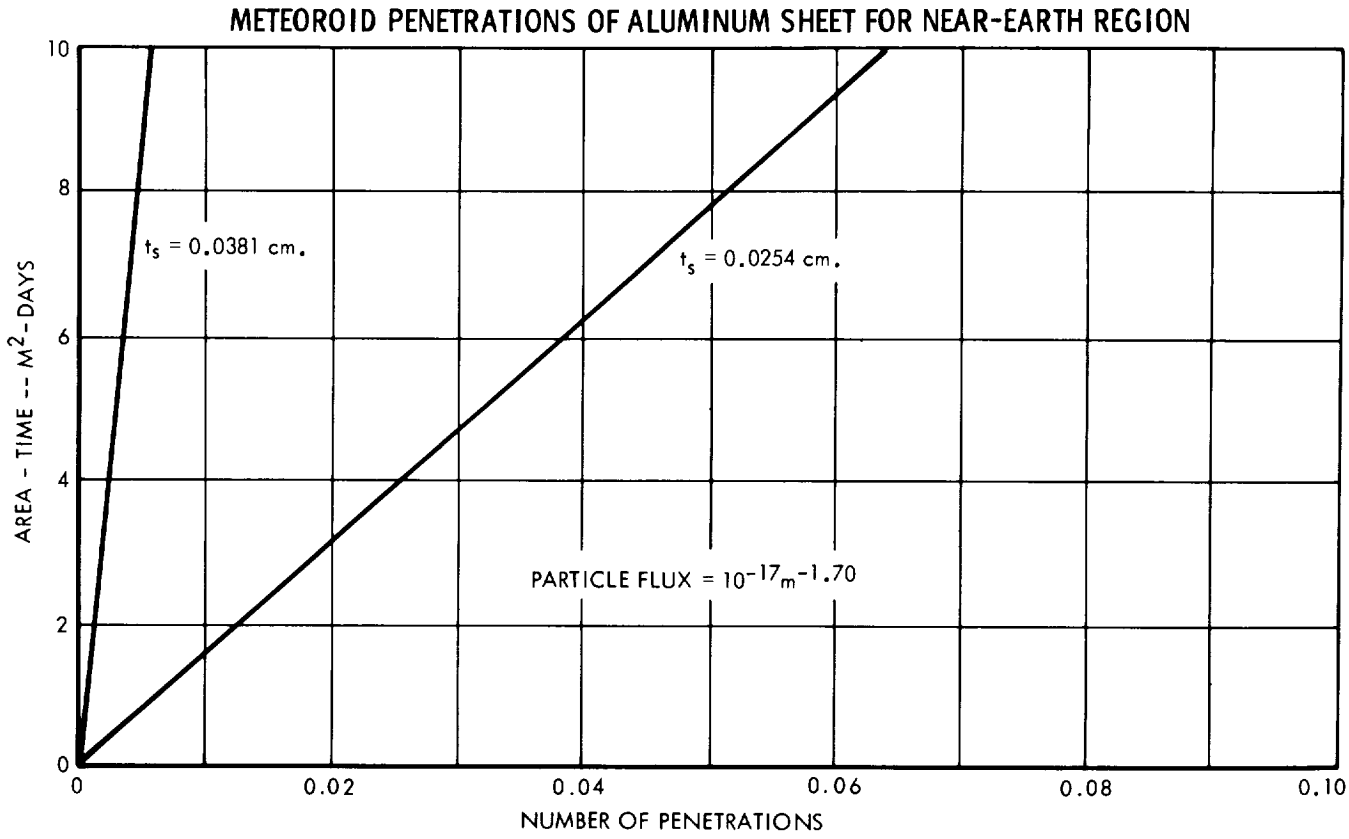

FIGURE 3. 10-3

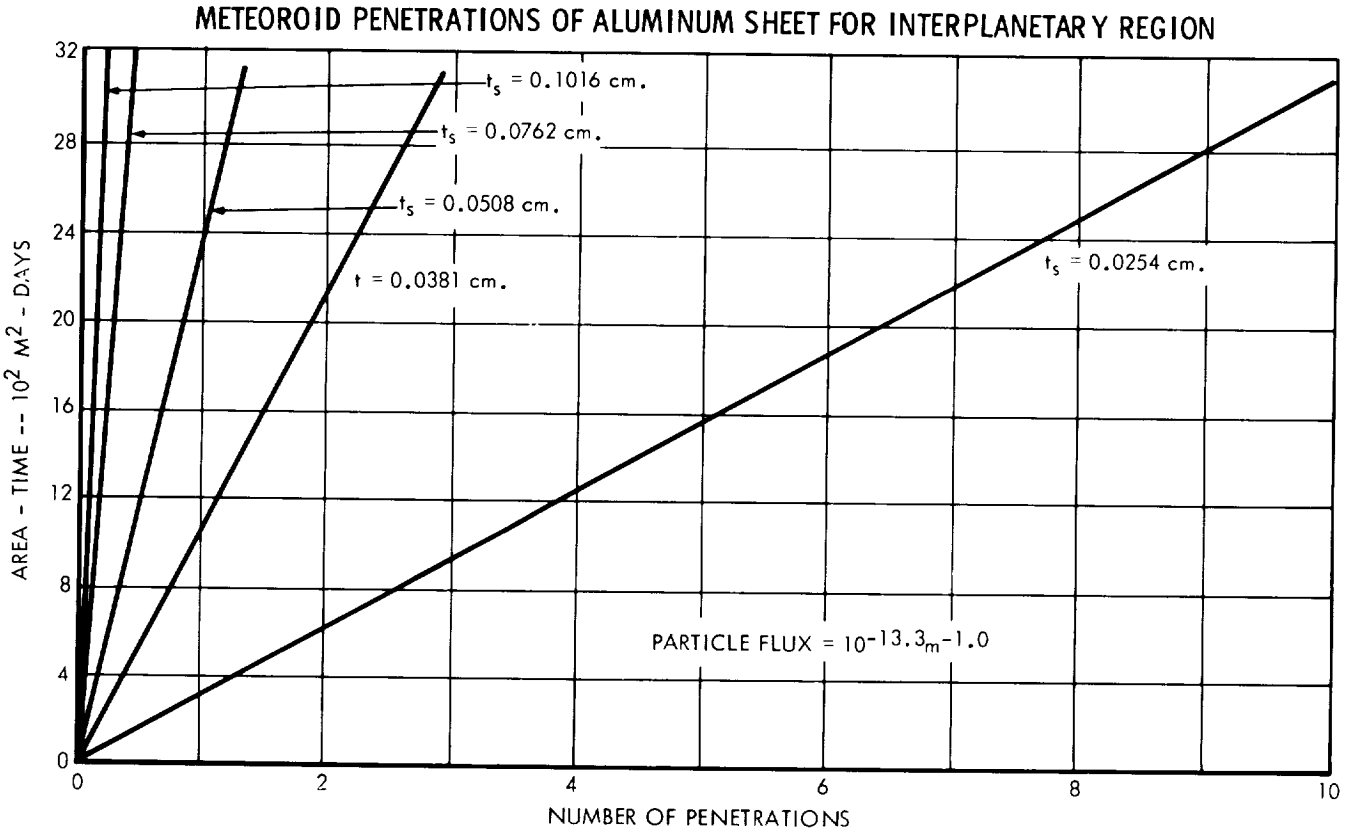

FIGURE 3. 10-4

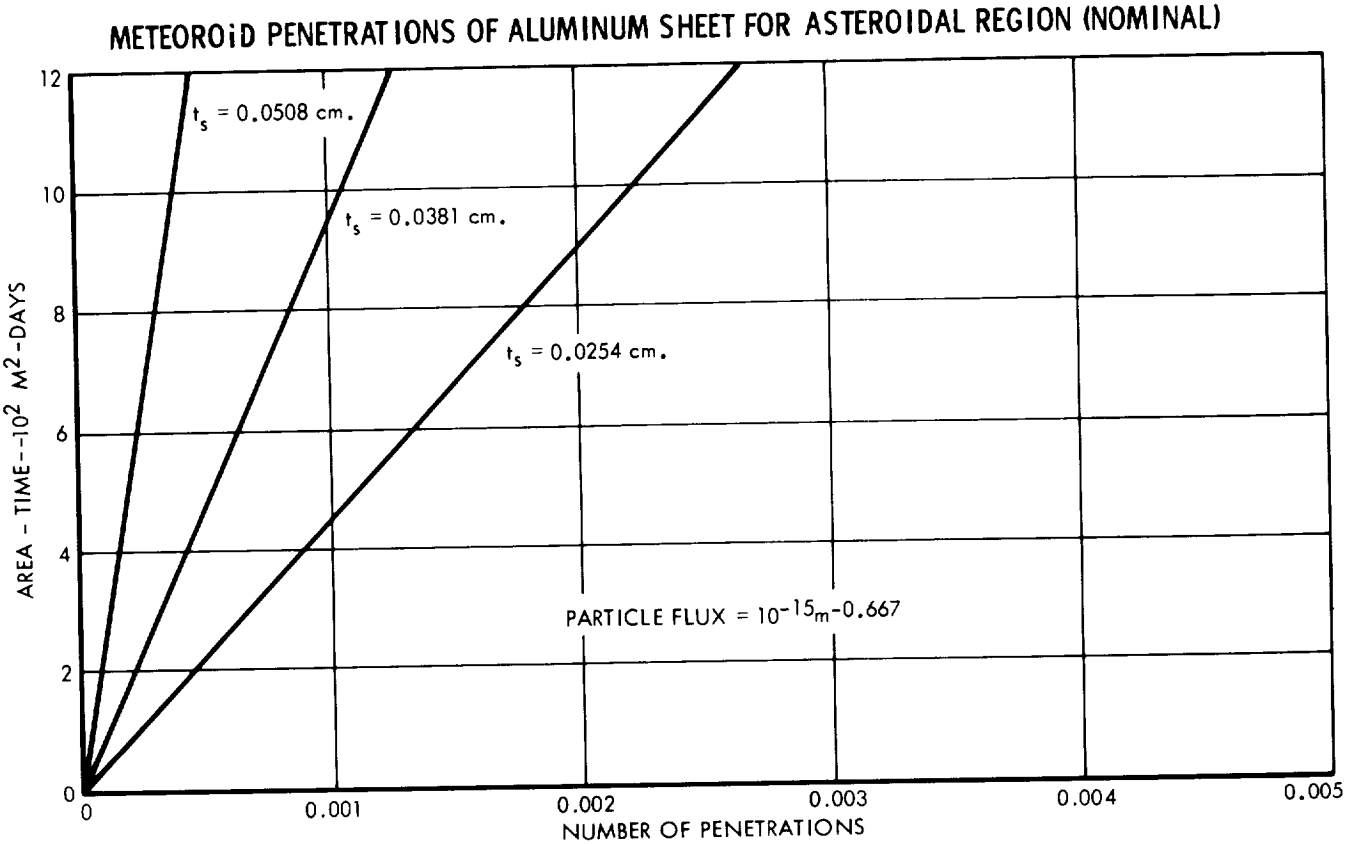

FIGURE 3. 10-5

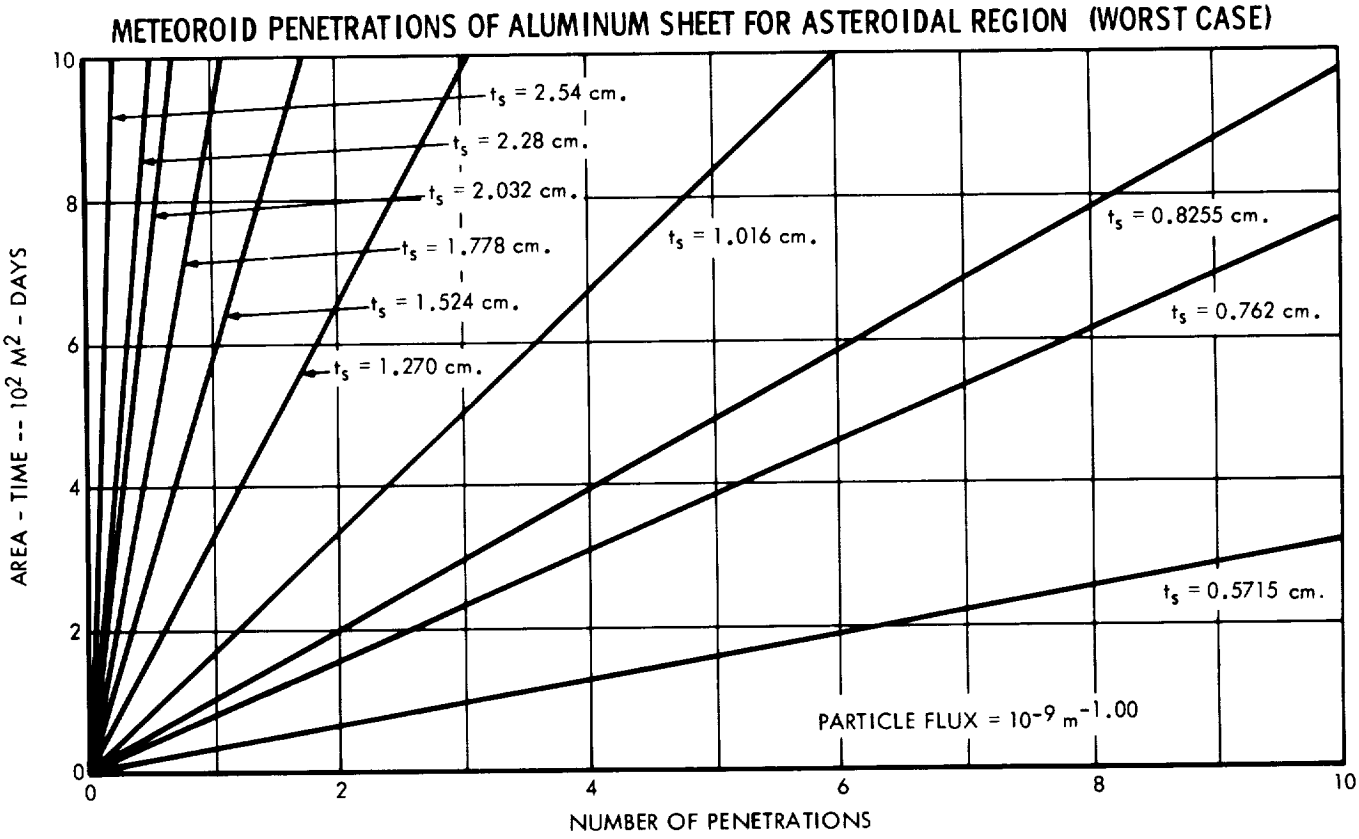

FIGURE 3. 10-6

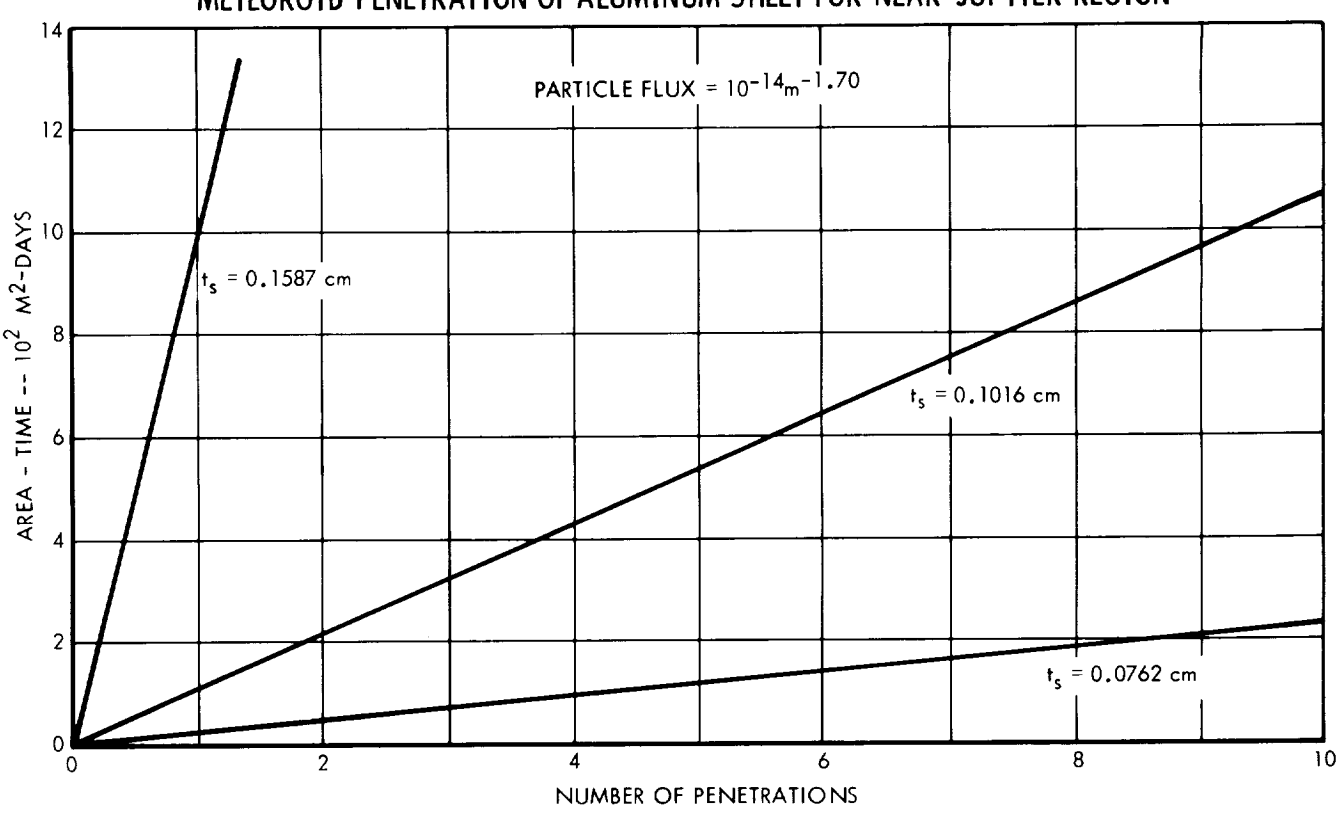

FIGURE 3.10-7

their exact worth has not been universally evaluated. However, the general approach to the analysis presented here is such that much of the data can be applied to the design of bumper shields if desired. In any case, it is not expected that the incorporation of a bumper shield system would have a greatly different effect on the overall spacecraft design from that of the armor shield.

3.10.4 Design Approach

Examination of the preceding data indicates several considerations which are pertinent to the design of the meteoroid penetration protection of Jupiter flyby spacecraft. These considerations and the design approach used in incorporating them are the subject of the ensuing discussion.

In the interplanetary and asteroidal regions, only a portion of the surface area of a three-axis stabilized spacecraft is exposed to meteoroid impact (see Figure 3.5-3). This conclusion

is based on the assumption that the meteoroids in the interplanetary/asteroidal regions are traveling in direct, heliocentric circular orbits. In the near-Jupiter region, the entire surface area is exposed to meteoroid impact, because the meteoroid activity is assumed to be isotropic.

If the nominal asteroidal flux is postulated, the contribution of the near-Jupiter flux to the total meteoroid hazard far exceeds the combined contribution of the near-Earth, interplanetary, and asteroidal fluxes. Therefore, the total spacecraft surface area requires equal protection. If the worst-case asteroidal flux is assumed, the asteroidal flux presents a much greater hazard to spacecraft than the combined near-Earth, interplanetary, and near-Jupiter fluxes. Thus, the portion of a spacecraft which is exposed to asteroid impact requires a different degree of protection than that portion which is not exposed. The unexposed area requires protection as dictated by the near-Jupiter flux.

In this study, the area of a particular three-axis stabilized spacecraft which is exposed in the interplanetary/asteroidal region is determined by computing the total surface area projected on a plane perpendicular to the ecliptic plane as the meteoroid incidence angle relative to the spacecraft's solar-oriented axis traverses its limits. Because the meteoroid impact area varies with heliocentric radius, the largest instantaneous projected area through a particular region is used to determine the damage in that region. Curves of meteoroid incidence angle and instantaneous exposed area versus heliocentric radius for a specific mission are obtained in the design process.

For spin-stabilized vehicles with the spin axis normal to the ecliptic, all portions of the spacecraft require equal protection for all fluxes. The exposed area used in determining the interplanetary/asteroidal meteoroid damage is that projected on a plane parallel to the spin axis. In the near-Jupiter region, the total spacecraft surface area is considered to be exposed to meteoroid impacts.

The limits of the various regions defined in the meteoroid models dictate the time of exposure of a spacecraft in these regions during a particular mission. The near-Earth exposure time is arbitrarily taken as 0.5 of a day for all missions. The near-Jupiter exposure time is based on the time spent in the 400 Jupiter radii influence zone as stated in the meteoroid environment model. In this analysis, the times spent in this sphere of influence for both the inbound and outbound phases of encounter

trajectories are used. Times spent in the various meteoroid regions for missions launched in 1976 and having nominal flight times of 400, 500, 600, and 700 days are shown below.

Nominal Flight Time (Days)	Exposed Time (Days)			
	Near-Earth	Inter-planetary	Asteroidal	Near-Jupiter
400	0.5	390	137	36.7
500	0.5	485	164	50.0
600	0.5	565	190	63.3
700	0.5	640	205	75.0

Design data are obtained by using the area-time product for a particular spacecraft and mission and the appropriate protection requirements curve.

3.10.5 Reference

3.10-1 Procedings of the Fifth Symposium on Hypervelocity Impact, Vo. 1- Part 2, April 1962.

3.10-2 Volkoff, John J., Protection Requirements for the Resistance of Meteoroid Penetration Damage of Interplanetary Spacecraft Systems, Technical Report No. 32-410, 1 July 1964.

3.10-3 Whipple, Fred L., "On Meteoroid and Penetration," The Journal of the Astronautical Sciences, Vol. X, No. 3, Fall 1963.

3.10-4 "Advanced Pioneed-Synthesis of System Concepts for a Mission to 10 AU," ASS Symposium on Unmanned Space Exploration, 1965, General Electric Co.

3.10-5 Bradford, D., and Martin, C. O., "Meteroid Environment", North American Space and Information Systems Division Report SID 64-1-2, July 1963.

3.10-6 Alexander, W. M., McCracken, C. W., Secretan, L., and Berg, O. E., "Rocket, Satellite, and Space-Probe Measurements of Interplanetary Dust," Trans. Amer. Geophys. Union 43 (1962), pp. 351-360.

3.10-7 Watson, F. G., "Between the Planets", Harvard University Press, Cambridge, Mass., 1932.

3.11 SPACECRAFT CONFIGURATION

Configuration design of the Jupiter flyby spacecraft is influenced primarily by launch vehicle constraints, trajectory constraints, and the integration requirements associated with the various spacecraft systems. The shroud dynamic envelope geometry, payload weight limitations, and adapter interface requirements comprise the major launch vehicle constraints considered in this study. Trajectory constraints, which are of particular importance in the encounter phase of the mission, exert considerable influence on certain spacecraft design concepts. The time relationships related to the Earth-spacecraft-Jupiter and Sun-spacecraft-Jupiter angles are very significant in this respect. The various systems integration problems also have a major effect on the ultimate configuration of the spacecraft. Systems of primary concern are the scientific instrumentation, communications antenna, RTG power supply, environmental control, attitude control, and midcourse propulsion. Other systems, which have indirect effects, are not discussed in this subsection.

3.11.1 Launch Vehicle Constraints

3.11.1.1 Shroud Dynamic Envelope

Definition of the shroud geometry of the launch vehicles considered in this study is based on data presented in the Jet Propulsion Laboratory "Future Mission Study Launch Vehicle Guidelines" (Reference 3.11-1). First priority is given to the minimum allowable spatial limitations specified, but certain modifications to the basic envelope, which are discussed in the referenced document, are also considered in this study. These include an increase in the shroud constant section length and the possibility of increased diameters (i.e. hammer head designs) for certain launch vehicles.

3.11.1.2 Payload Weights

Payload weight capabilities of the various candidate launch vehicles are specified in Reference 3.11-1. Appropriate modifications have been made to change the data into a form which is convenient for application in the study. The resulting payload capabilities of the subject launch vehicles are presented in subsection 2.3.2 in terms of gross weight. In order to determine allowable net spacecraft weight, the weight of the spacecraft-to-vehicle adapter must be subtracted from the values specified in the data. Adapter weight is estimated to be 6.5 percent of the spacecraft weight. In addition to the payload weight limitations, constraints on the center-of-gravity location of the spacecraft are outlined in Reference 3.11-1. This particular restriction appears applicable only to the Saturn IB/Centaur/HEKS and Atlas SLV 3x/Centaur/HEKS vehicles.

3.11.1.3 Adapter Interface Requirements

Basic spacecraft adapter relationships are presented in Figure 3.11-1 for the particular launch vehicles of interest. The payload adapter is designed to transfer load over a uniformly distributed path to the booster/adapter interface. Specific requirements, such as restrictions on the allowable load path beyond this interface for various launch vehicles and conditions, are outlined in Reference 3.11-1.

SPACECRAFT-TO-ADAPTER INTERFACE REQUIREMENTS

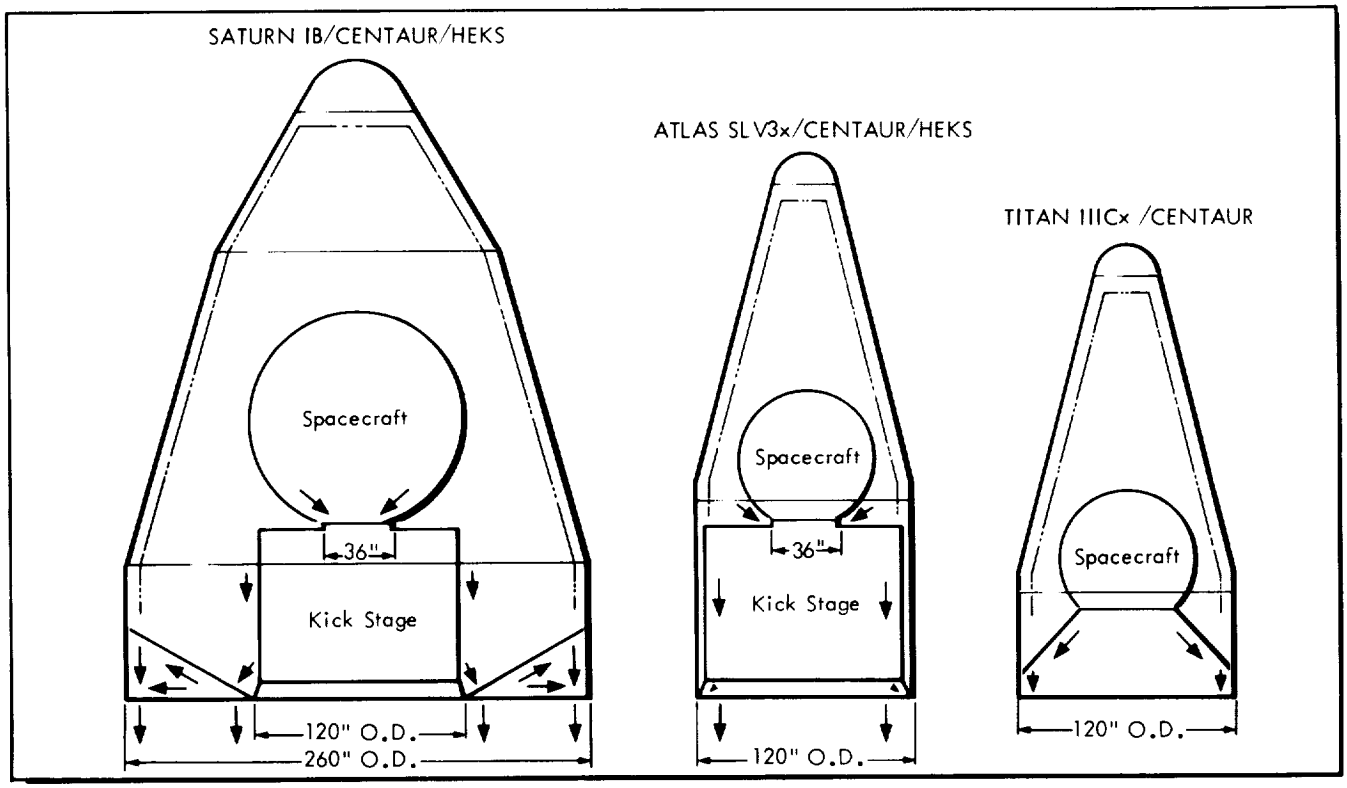

FIGURE 3.11-1

3.11.2 Trajectory Constraints

The geometry of the Jupiter flyby trajectory coupled with the various system and instrument orientation requirements constitutes a significant influence on the spacecraft configuration design. This is particularly true with respect to the encounter phase of the mission for the case of three-axis stabilized spacecraft which contain scientific sensors that are required to point at Jupiter. For instance, the combination of a Sun-pointing spacecraft attitude, Jupiter-pointing scientific sensors, and an Earth-pointed communications antenna (at encounter) requires that certain compromises be made to achieve a satisfactory integrated system arrangement. A fixed spacecraft-antenna relationship with scanning science instruments or a fixed spacecraft

science arrangement with a steerable antenna are likely alternatives. Examples of the variation in the Earth-spacecraft-Jupiter angle during typical encounter trajectories are shown in Figures 3.11-2, 3.11-3, and 3.11-4. These figures represent data for a 500 day mission launched in 1976 (Reference 3.11-2) and for retrograde encounters of 0 degrees, 45 degrees, and 90 degrees inclination, respectively. The actual angle (ψ) which is plotted in these curves with respect to time is the projection of the Earth-spacecraft-Jupiter angle (ϕ) on the plane of the encounter trajectory as shown in the inset in each figure. The magnitude and rate of angular change shown in the curves are indicative of the range of operation which is required for a system designed to provide the proper Earth-spacecraft-Jupiter pointing relationship throughout the encounter.

The heliocentric portions of Jupiter flyby trajectories are such that considerable excursion of the Sun-spacecraft-Earth angle occurs during a given mission. For a three-axis stabilized spacecraft which is Sun oriented, the utilization of a directional antenna for Earth communications requires that a steering system be employed to provide the desired pointing capability. Depending on the type of communications antenna employed, spin stabilized spacecraft are generally limited by trajectory considerations, to equatorial encounters with Jupiter.

3.11.3 Spacecraft Systems Integration

The major systems which influence the configuration design of the spacecraft are (1) scientific instrumentation, (2) communications antenna, (3) RTG power, (4) attitude control, (5) propulsion, and (6) environmental control. The primary configuration design requirements associated with each particular system are presented in this subsection. The data management and spacecraft control subsystems do not exert direct influence on the basic physical characteristics of the vehicle configuration and therefore are not discussed here.

3.11.3.1 Scientific Instrumentation

A major problem in integrating the science into the spacecraft configuration involves proper placement of the various scientific instruments on the vehicle. This problem is particularly acute for instruments which must be pointed in certain directions without interference. For encounter science instruments, such as television cameras, radiometers, and photometers, a requirement to look at the target planet without interference from other spacecraft elements in the field of view of the sensors is paramount. Alternatives to provide proper spacecraft orientation associated with these instruments are (1) orientation of the spacecraft to the planet with fixed sensors or (2) the incorporation of a scan platform which allows the sensors to track the planet.

TYPICAL ENCOUNTER GEOMETRIES, 0° INCLINATION

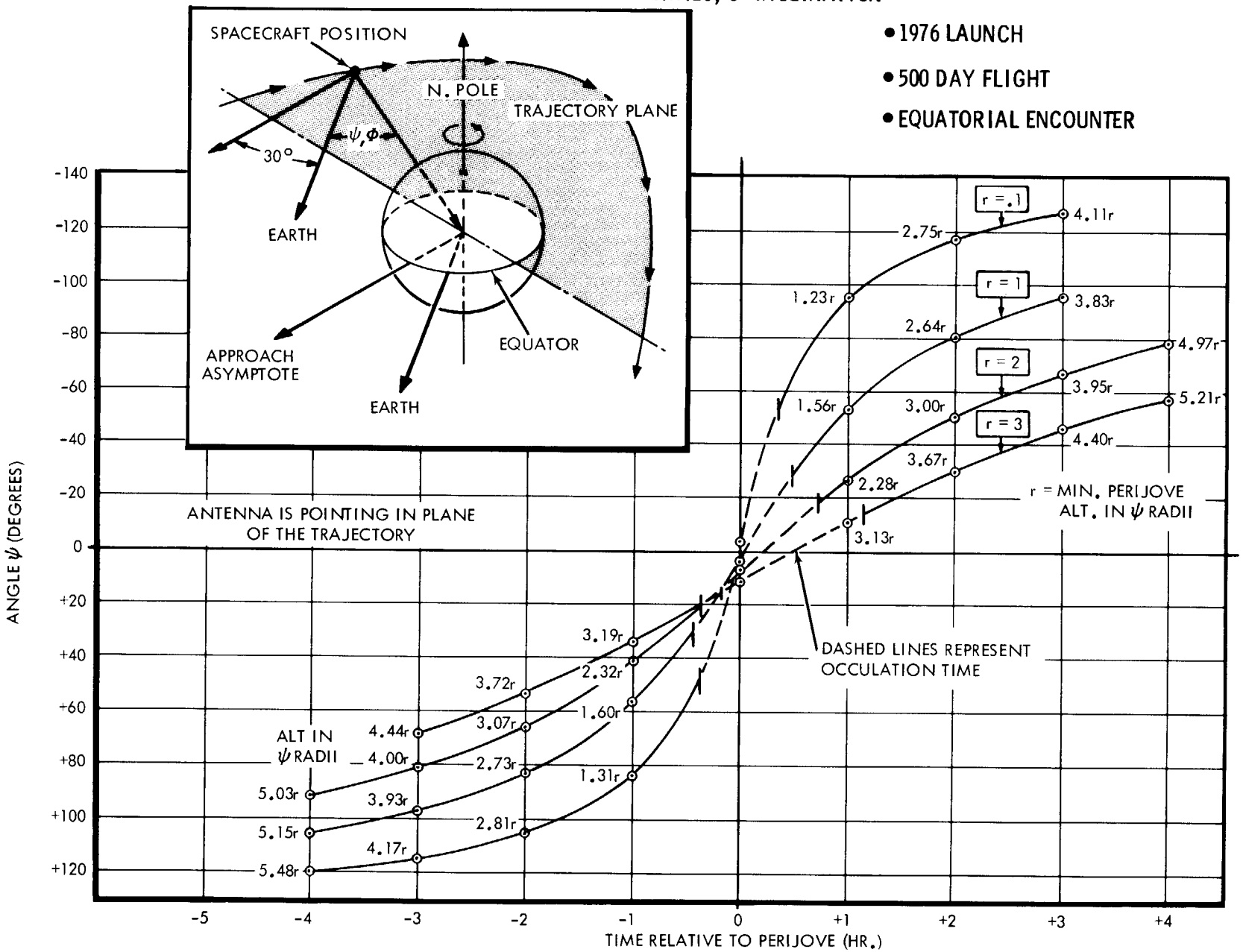

FIGURE 3.11-2

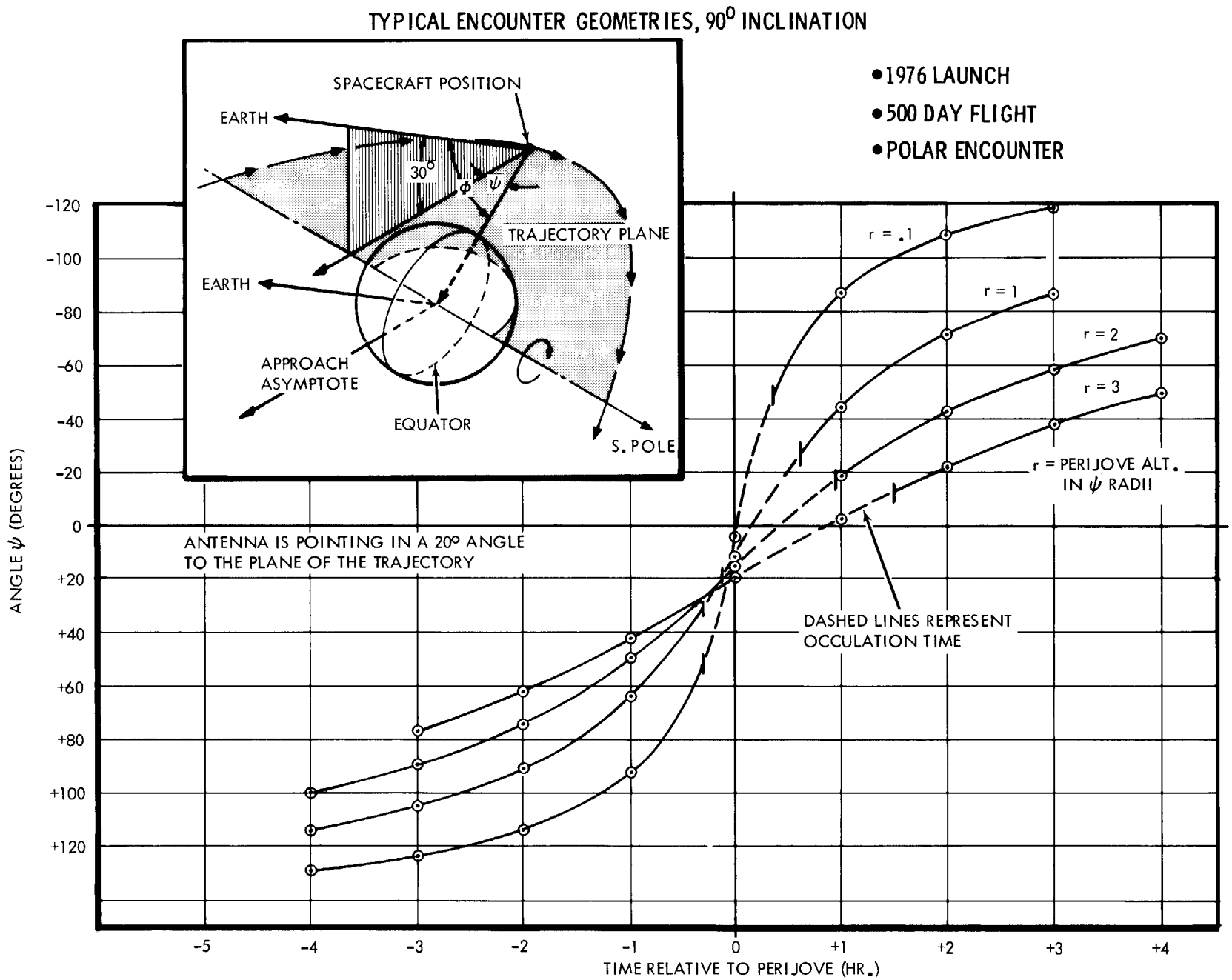
TYPICAL ENCOUNTER GEOMETRIES, 90° INCLINATION
SPACECRAFT POSITION
EARTH
30°
Φ
ψ
TRAJECTORY PLANE
EARTH
APPROACH ASYMPTOTE
EQUATOR
S. POLE
•1976 LAUNCH
•500 DAY FLIGHT
•POLAR ENCOUNTER
r = .1
r = 1
r = 2
r = 3
r = PERIJOVE ALT. IN ψ RADII
ANTENNA IS POINTING IN A 20° ANGLE TO THE PLANE OF THE TRAJECTORY
DASHED LINES REPRESENT OCCULATION TIME
ANGLE ψ (DEGREES)
-120
-100
-80
-60
-40
-20
0
+20
+40
+60
+80
+100
+120
-5
-4
-3
-2
-1
0
+1
+2
+3
+4
TIME RELATIVE TO PERIJOVE (HR.)

FIGURE 3. 11-3

TYPICAL ENCOUNTER GEOMETRIES, 45° INCLINATION

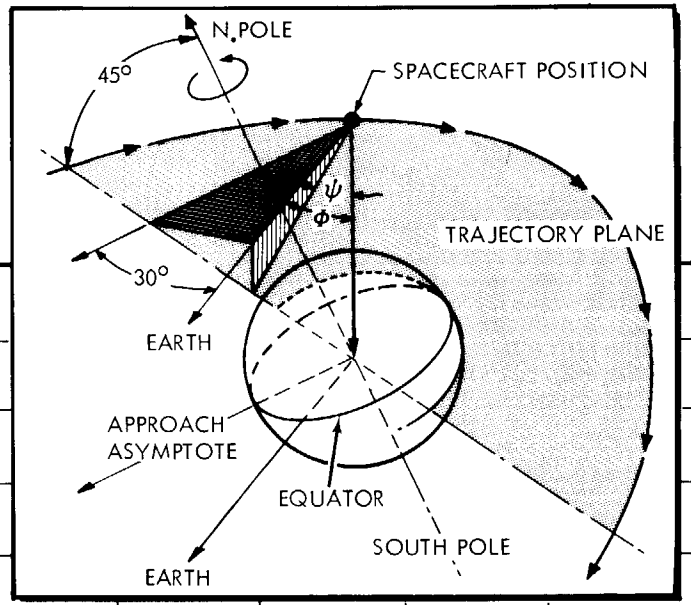

- 1976 LAUNCH
- 500 DAY FLIGHT
- 45° ENCOUNTER

FIGURE 3.11-4

In general, the placement of the cruise science instrumentation is less critical with respect to the effects on overall configuration than the encounter sensors. Here again, the look-angle problem exists, but the requirements for accurate directional pointing are not as stringent, and in many cases, nonexistent. For instance, the plasma probe must be pointed toward the Sun and can be a fixed installation on Sun oriented spacecraft designs. Cosmic dust detectors and energetic particle counters have specific orientation requirements related to the suspected nature and origin of the phenomena being measured. Instruments such as the ion chamber and the magnetometer require separation and/or shielding from the main spacecraft body, in some cases, to minimize the effects of the spacecraft on the measurements to be taken.

3.11.3.2 Communications Antenna

Perhaps the most prominent feature which characterizes a spacecraft designed to perform a Jupiter flyby mission is the primary communications antenna. The extreme communication distances require that large directional antennas be utilized to provide adequate information return rates.

The parabolic dish antennas utilized in three-axis stabilized vehicle configuration studies range from 4 to 10 feet in diameter. On spacecraft which are Sun oriented throughout the trajectory, antennas of this size require pointing to allow continuous communication between the Earth and the spacecraft. When pointing is achieved by steering the antenna with respect to the spacecraft, the configuration must allow for the antenna movement.

The Earth-spacecraft-Jupiter relationship, as discussed in subsection 3.11.2, has a primary effect on planetary sensor and antenna pointing during planetary encounter. These combined requirements can be accomplished by two basic concept arrangements which allow for a continuously Earth-pointing antenna as shown in Figure 3.11-5.

The centrally mounted concept provides a symmetrical spacecraft configuration which involves a simple launch packaging arrangement and results in minimum disturbing torques on the spacecraft. However, the placement of various sensors to accommodate the required look angles is a definite problem. The offset spacecraft concept affords an easy solution to the Earth-spacecraft-Jupiter angle problem. But, in addition to launch packaging and disturbing torque considerations, the change from a Sun oriented to a Jupiter oriented attitude prior to the encounter sequence is not desirable. In this study, the centrally mounted concept for antenna location is adopted.

3.11.3.3 RTG Power

The utilization of RTG systems to supply auxiliary power for the spacecraft presents a significant integration problem in

DIRECTIONAL ANTENNA - SPACECRAFT LOCATION ALTERNATIVES

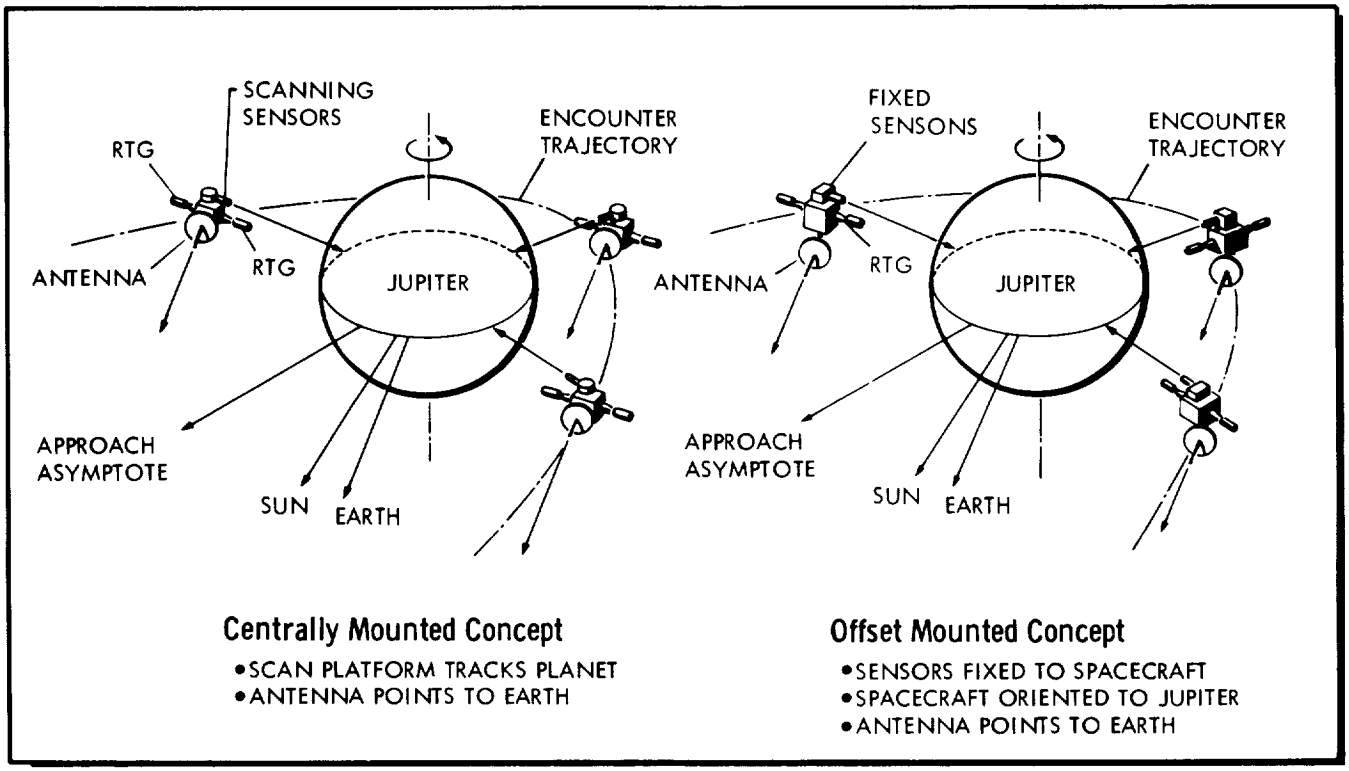

FIGURE 3.11-5

spacecraft configuration design. Environmental considerations require that the RTG units be placed some distance away from the main spacecraft equipment compartment. The shroud envelope presents a limitation on how far away the units can be placed and not require deployment. Increased separation distance is possible by resorting to hinged booms, which are deployed after spacecraft separation. However, an assessment of the resulting weight and reliability effects is an important step in considering such an alternative.

The effects on structural launch loads, center-of-gravity location, and spacecraft moments of inertia are also important considerations in the placement of the RTG units. The utilization of multiple RTG units, rather than a single unit of higher power, suggests a configuration with equal distribution of the elements about the spacecraft body. This contributes to a symmetrical distribution pattern with respect to launch loads and the thermal environment. Accessibility for installation of the RTG fuel elements before launch is also a necessary feature.

The placement of the RTG units is particularly important on a spin stabilized spacecraft design from the standpoint of attitude control stability. This is discussed further in the following subsection.

3.11.3.4 Attitude Control

In the case of attitude control by spin stabilization, the vehicle mass distribution and the effects of solar torques on the precession of the spin axis are important considerations for the configuration design. The effect of solar torques can be minimized by proper arrangement of equipment on the spacecraft to provide a balanced moment-area condition about axes normal to the spin axis. The placement of the RTG units has a considerable effect on the stability of a spin stabilized spacecraft. For adequate stability, multiple units should be placed in the nominal plane of the spacecraft center of mass. In addition, the distance the units are located from the spin axis has an important bearing on vehicle stability. The effect of varying the RTG radial positions of a typical spin-stabilized spacecraft is shown in Figure 3.11-6.

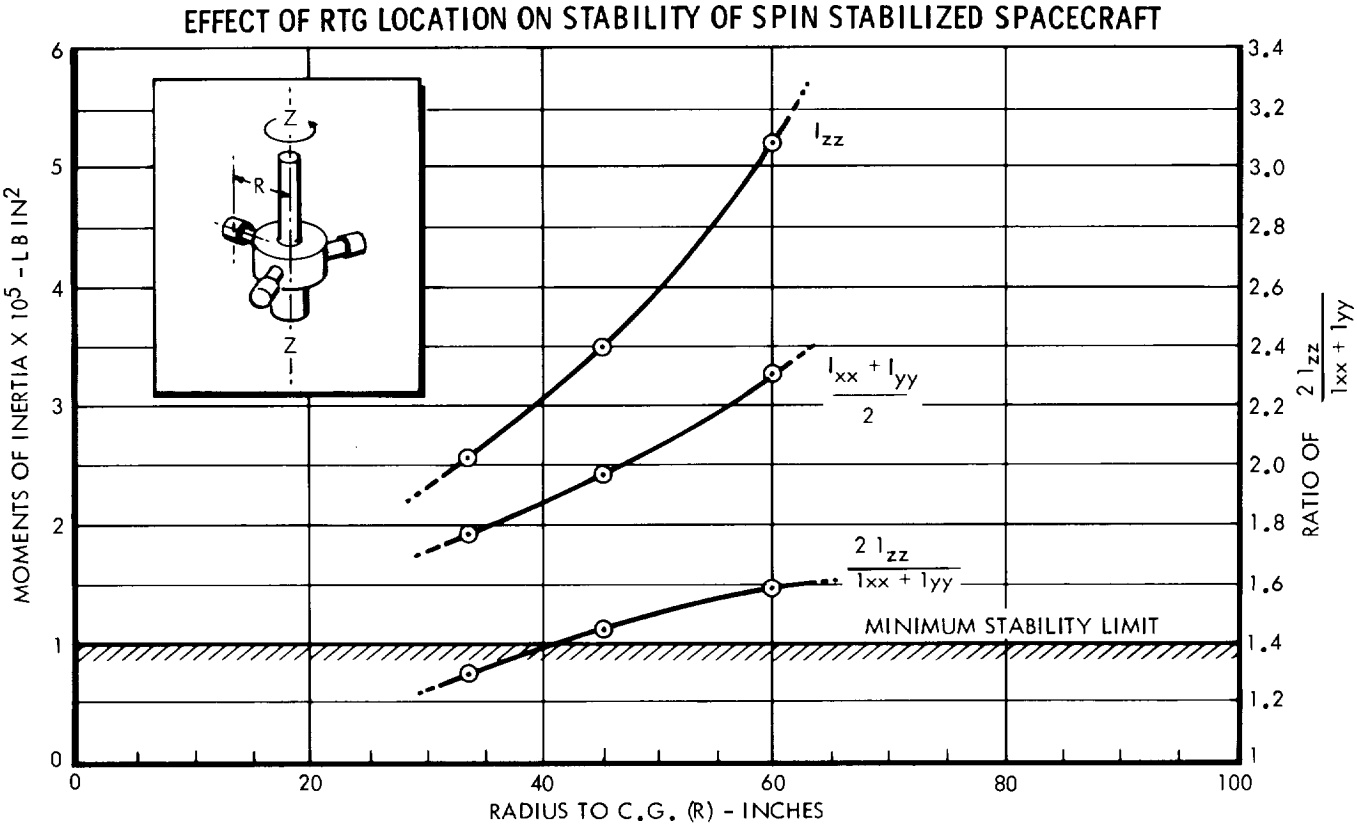

FIGURE 3.11-6

In spacecraft designs which utilize three-axis stabilization for the entire mission, several variations are of special interest from the configuration design standpoint. One such concept is the simple cold gas reaction system. The primary consideration here is the proper placement of the jets to provide maximum efficiency with minimum weight.

Another approach to attitude control is to use fixed solar vanes as a means of supplementing a basic gas jet system (see subsection 3.5 for detailed discussion). Two cases are presented which have certain configuration design implications. In one case, proper arrangement of equipment plus the use of appropriately placed fixed solar vanes provides a vehicle which is "neutrally stable" with respect to solar torques. This then minimizes the drain on the gas jet system. Implementing an arrangement such as this requires extensive testing and even minor changes in the spacecraft configuration, which are inherent in any development program, can cause great problems.

In the other case, fixed solar vanes are arranged to provide positive stability so that the vehicle seeks a natural trim point to compensate for any change in disturbing torques. To implement this design, the antenna must be located in a central location on the spacecraft, and the solar vanes must extend aft. Large areas and long moment arms are required to implement the concept, and this presents a packaging problem for the launch condition. The look angle problem also requires careful examination to eliminate any interference of the vanes with the myriad of sensors on board.

3.11.3.5 Propulsion

The most significant configuration design factors with respect to the propulsion system are thrust vector direction, spacecraft center-of-gravity location, propellant thermal control, and impingement of ejected material from the thrust unit. It is desirable to locate the attitude control propellant as close as possible to the spacecraft center of gravity to minimize the uncertainties in attitude control propellant usage prior to the midcourse correction. Impingement of the ejected material from the thruster presents a potential compatibility problem with respect to the various sensors which are located in the near vicinity.

3.11.3.6 Environmental Control

The primary aspects of environmental control which affect spacecraft configuration are thermal control and radiation protection. Primary configuration problems of thermal control design are (1) the placement of louvers with respect to the RTG units and (2) the appropriate arrangement of internal equipment to provide good temperature control conditions. Several important considerations are significant with respect to louver location. First of all, for a Sun-pointing spacecraft attitude, thermal control louvers should either look out the side or aft surfaces of the main spacecraft body section. A location on the aft portion of the vehicle presents a potential problem during the orbital coasting period if the spacecraft is attached to the injection stage for a very long time. In this case, the louvers can see the injection stage, and therefore, the efficiency of heat rejection from the spacecraft body may be compromised.

On the other hand, if the location of the RTG units is around the spacecraft periphery, placement of the thermal control louvers on the side of the spacecraft poses a potential thermal interference problem. In this case, the view factors between the louvers and the RTG units can be adjusted by proper louver hinge orientation to minimize any detrimental effects between the two systems. Another consideration with respect to the thermal control problem is that the internal equipment should be arranged to provide proper heat transfer between the louver system and the equipment. This requirement coupled with the requirement that the equipment be accessible for maintenance and checkout on the launch pad is an important factor in the spacecraft configuration design.

A primary consideration in evolving a spacecraft configuration is the RTG nuclear radiation effects on certain scientific sensors. The particular instruments affected most are ion chambers and Geiger-Mueller tubes. This problem can be attacked by either increasing the separation distance of the RTG unit from the spacecraft, by providing shielding, or by proper placement of the particular sensor with respect to the RTG units. Increased separation distance between the sensors and the RTG units can be accomplished with hinged booms, but the attendant reliability and weight penalties are trade-offs that must be considered. Results of the studies discussed in subsection 3.9 indicate that by proper location of the sensitive sensors with respect to the RTG units, shielding and increased separation distances are not necessary.

3.11.4 References

3.11-1 "Launch Vehicle Future Missions Study Guideline," Jet Propulsion Laboratory Technical Direction Memorandum No. 1, Contract 951285, 7 January 1965.

3.11-2 "Earth-Jupiter Heliocentric Transfer Trajectory Data," Fort Worth Division of General Dynamics Report MR-A-2001, 13 December 1965.

3.12 STRUCTURAL AND MECHANICAL DESIGN

Two basic areas of importance in the design of the spacecraft involve the structural and mechanical systems. Significant structural design items include the basic equipment compartment, support of the RTG units, and the construction of large parabolic antennas. Major mechanical systems consist of the antenna drive, scan platform actuation, deployment of special sensors, and thermal control louver installation. In addition to a general discussion of these considerations, a method for estimating spacecraft structural/mechanical weights is presented for use in this study.

3.12.1 Structural Systems

3.12.1.1 Basic Equipment Compartment

The basic equipment compartment, which forms the core of the spacecraft, has three primary functions. These are (1) to form a protective enclosure to house the basic electronic and propulsion equipment, (2) to provide the primary structural load path for the transmission of launch loads to the booster interface, and (3) to serve as the basic platform for the mounting of external sensors and other equipment. A major factor in the design of the equipment compartment is the spacecraft adapter interface which is discussed in subsection 3.11.1. Another significant influence which is exerted on the equipment compartment design concerns the size and type of antenna employed and its location on the spacecraft. Spacecraft with large diameter parabolic antennas, which are centrally located on the forward end of the compartment, require that portions of the periphery of this compartment be extended outside the antenna envelope so that sensors which require particular viewing angles of the Sun can be accommodated. The attitude control jets and the omni-directional antennas also require clearances beyond the antenna for proper operation.

Packaging of the equipment inside the compartment is also a significant design problem. Internal elements should be arranged in a compact manner with appropriate attention to the requirements of accessibility and adequate routing provisions. Thermal control considerations also influence the arrangement of the equipment inside the compartment. The proper grouping of various equipment according to temperature limitations is desirable from the standpoint of optimization of thermal control characteristics, but not necessarily from a weight distribution aspect. To obtain the most efficient thermal control characteristics, equipment should be mounted to the skin panels which are fitted with louver installations.

In general, the major portion of the electronics equipment can be placed around the periphery of the basic enclosure, thus leaving the core section for the storage of midcourse and attitude control propellants. A centralized location for these tanks provides an arrangement which is advantageous with respect to thermal control, meteoroid protection, and the effects of center-of-gravity shift.

The basic structure of the equipment compartment is of stressed skin construction; longerons join with the shear panels to comprise the complete enclosure. The shear panels act as the chassis for the electrical equipment mounting and as the heat sink for the external louver assemblies, which are independently attached. This arrangement also provides a certain amount of intrinsic meteoroid shielding capability.

3.12.1.2 RTG Support

The support of multiple RTG units on the spacecraft is provided by lightweight tubular truss structures. The RTG units are fixed to the truss members and project radially from the spacecraft body at the maximum separation distance available within the limits of the payload fairing. The truss arrangement allows a lightweight support with a minimum of thermal conduction between the RTG unit and the spacecraft.

3.12.1.3 Antenna Construction

The high-gain parabolic antennas examined during the study range in size from approximately 5 to 10 feet in diameter. The smaller antenna reflectors are fabricated of aluminum honeycomb structures. This type of construction has been used successfully on Mariner IV and appears practical for application to the Jupiter spacecraft also. Construction of the proper curvature is reasonably simple with the use of the bonded honeycomb structure. The composite configuration forms a lightweight and reasonably stiff type structure which is compatible with the environmental conditions present at launch. Antenna feeds are generally suspended from the dish by lightweight truss structures made of RF-transparent fiberglass tubular members. During launch operations gimballed antennas must be clamped to the bus by temporary members which support the antenna during this phase. These members are released after injection by pyrotechnic devices after their function has been served. The larger antennas employ wire mesh construction. The mesh is stretched over concentric ring frames attached to ribs which radiate from the central hub of the dish. This arrangement, especially on the very large antennas, is considered less likely to be damaged in normal handling operations.

3.12.2 Mechanical Systems

3.12.2.1 Antenna Drive

To allow proper orientation of high gain antennas, gimballed systems of both one and two degrees of freedom are employed. Actuation systems for these antennas are provided by a sychronous motor drive arrangement which is controlled by command from the CC&S or Earth. The movable antenna is arranged so that it is driven to discrete pointing positions at various times during the mission to accommodate the specific orientation requirements associated with the flight trajectory. The most significant problem in the design of the mechanical system results from the long term storage requirement inherent in the Jupiter mission. Consideration is given to a backup system which would automatically drive the antenna to the encounter position in case of a failure in the normal mode of the actuation mechanism. This would result in the loss of considerable interplanetary data but the encounter data could be obtained.

3.12.2.2 Scan Platform

Two types of scan platforms are considered for this study. For minimal-type missions, a single degree of scan freedom is utilized. In this case the scan platform mounted sensors are actually fixed at the time of the encounter maneuver, and the one degree of freedom allows for orientation corrections required by off-nominal trajectory conditions. This is the type of platform employed on Mariner IV and is considered adequate for spacecraft designs with minimal encounter science complements.

Scan platforms employing motion in two degrees of freedom are required for the more sophisticated science subsystems. These vehicles carry several sensors which require Jupiter tracking and even scanning. This scan platform arrangement requires as much as 270 degrees rotational capability in the plane of the encounter, depending on the perijove altitude, inclination angle, and the length of the encounter sequence (see Figures 3.11-2, 3.11-3, and 3.11-4). Addition of a maximum of ± 30 degree movement which is vertical to the encounter trajectory plane gives full coverage for a perijove pass of one Jupiter radius altitude.

The scan platform utilizes a gimballed arrangement which is actuated by a synchronous motor drive system. On spacecraft arrangements where more than one platform is employed, a slave drive coupling system is suggested so that either drive assembly can drive both platforms in case of a failure in the other. Scan platform tracking

is controlled by the Jupiter sensor which is mounted along with the scientific sensors on the platform.

3.12.2.3 Sensor Deployment

Certain sensors require special consideration from the standpoint of spacecraft separation distance. Two of these are the magnetometer and the ion chamber experiements. A typical mechanism which has been developed to provide this extension capability is the DeHavilland Storable Tubular Extendible Member (STEM) system.

EXTENSION DEVICE FOR PROVIDING SENSOR - SPACECRAFT SEPARATION

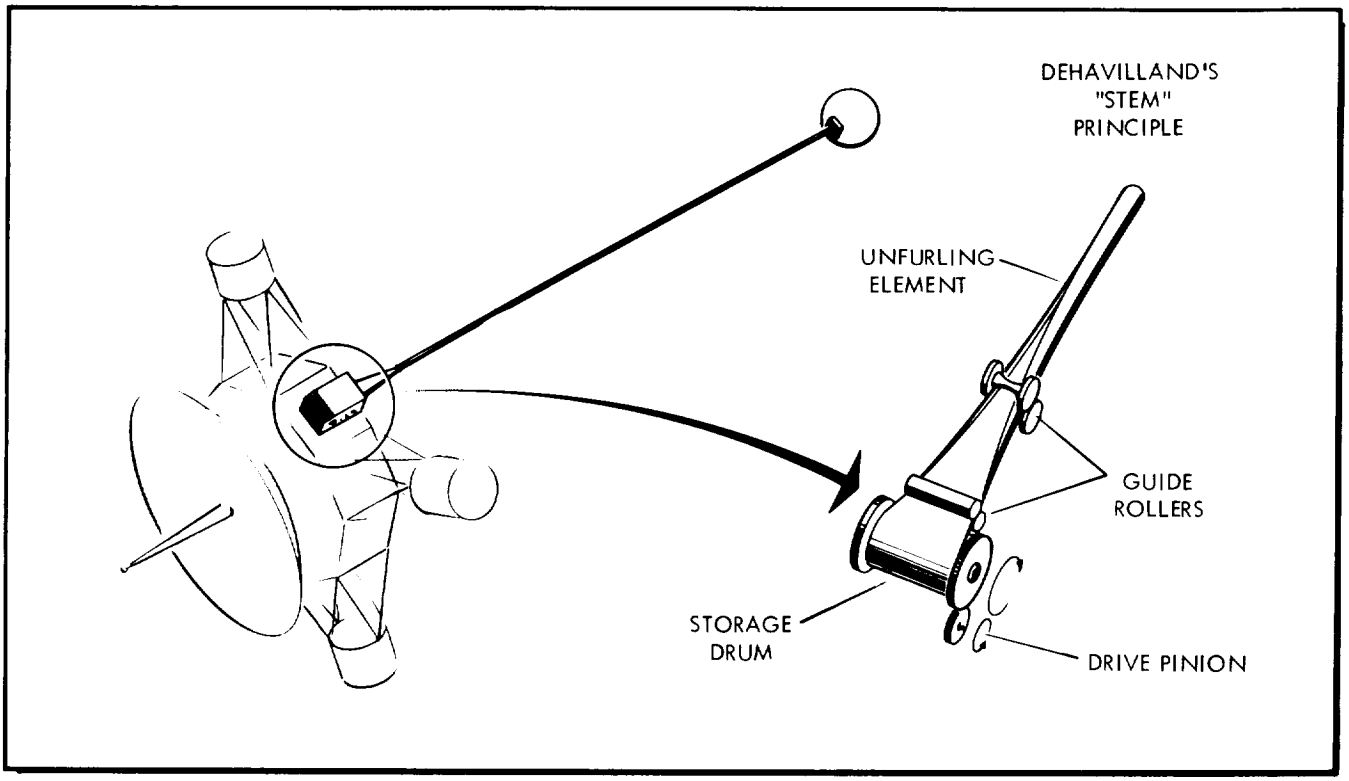

FIGURE 3.12-1

The principle involved in the system and a potential application are illustrated in Figure 3.12-1. This mechanism allows for a compact arrangement during the launch condition where the instrument can be clamped to the spacecraft body and isolated from vibration during this operational phase. The sensor instruments are then released by the activation of a pyrotechnic device. This allows the tubular member to be driven to its full extension by an electric motor. These devices have been utilized on previous spacecraft and are considered a reliable means of providing large separation distances for a minimum expenditure of weight.

3.12.2.4 Thermal Control Louvers

The thermal control louver systems are of the same type which were employed on the Mariner IV spacecraft. The louvers are driven by spirally wound bimetallic elements which are located in a housing in the center of each louver array. The driving elements are insulated and shielded to provide thermal radiation coupling to the face temperature of the skin panel which forms the chassis for the internal equipment.

3.12.3 Weight Estimation

In order to obtain total spacecraft weight, it is necessary to specify the weight of the structural/mechanical systems. This weight can be specified either by an exhaustive structural and mechanical design or by an estimation procedure. For this study, an in-depth structural and mechanical analysis is not considered compatible with the study objectives.

Weight estimates can be obtained in several ways. Parametric data based on launch environment, length of moment arms, types of mechanical provisions, etc., can be used to obtain relationships for estimating structural and mechanical weights. This method is not considered to offer any significant improvement in the estimation of weight over the method used in this study.

In this study, structural/mechanical weight is estimated for each of the spacecraft design concepts using the data presented in Figure 3.12-2. This estimating relationship is based on historical data relating spacecraft structural/mechanical weight to total weight for a number of unmanned space probes and satellites. It reflects the expected nonlinear increase in structural weight with total spacecraft weight.

The meteoroid protection provided for each of the spacecraft design concepts can be designed to provide an efficient structural system. Thus, armor-type meteoroid protection is considered to be an integral part of the structural system. In tabulating the various subsystem weights for each design concept, the structural/mechanical and meteoroid protection weights are considered together, and this weight is obtained from Figure 3.12-2 as described above. This assumes that the meteoroid protection is a completely efficient structure, therefore the resulting weight is an optimistic estimate.

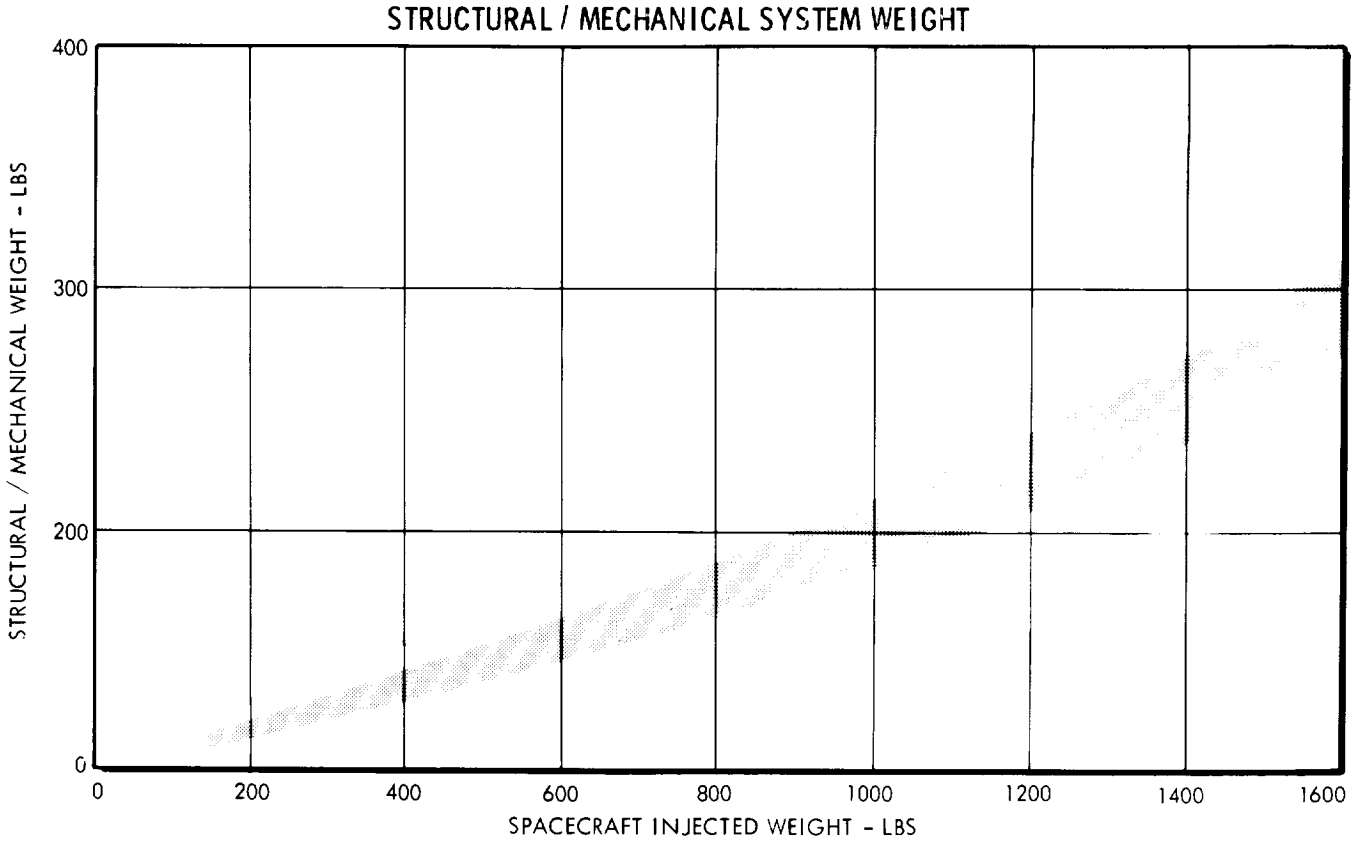

FIGURE 3.12-2

It is obvious that the degree of optimism is heavily dependent on the amount of protection being provided. That is, if a heavy armor is recommended, the assumption is not justified, but for armor which contributes somewhat less than half the total structural/mechanical and meteoroid protection weight, the assumption is considered a good one.

3.13 SUBSYSTEMS RELIABILITY

The purposes of the subsystems reliability study have been to determine the predicted reliability of the different spacecraft subsystems and to use these predictions to aid in selecting the recommended subsystem design. The major efforts reported in this study are (1) determination of the achievable reliability levels of the subsystem equipments, (2) prediction of subsystem reliability based upon the achievable reliability levels of the equipment, and (3) performance of technical evaluations, trade-offs, and investigations of possible reliability problem areas utilizing the equipment and subsystem level reliability predictions.

In this section only the reliability investigations that were accomplished on the various subsystem configurations are reported. These investigations were closely coordinated with the design of the spacecraft subsystems. Probability-of-mission-success evaluations for entire spacecraft design concepts are contained in Section 5.

3.13.1 Subsystem Predicted Reliability

Reliability analyses were performed on the following subsystems: (1) communications, (2) data management, (3) spacecraft control, (4) attitude control propulsion, (5) propulsion, (6) auxiliary electrical power, and (7) science.

In these analyses, subsystem reliability is defined as the probability that a completely checked out subsystem will successfully perform its designated functions for the required subsystem operational phases of a 600-day Jupiter flyby mission. Subsystem reliability can be described in general equation form as follows:

$$R_{sub} = \prod_{i=1}^{n} R_i$$

where R_{sub} = subsystem reliability for a specified mission and R_i = probability of satisfactory operation of subsystem function i.

A mission can be successfully accomplished when a subsystem operates (1) with no failure of any equipment within the subsystem or (2) with equipment failure that does not impair successful mission completion because of redundancy or alternate modes of function operation. For example, if a function can be performed by either of two equipments that are active throughout the mission, the probability of satisfactory operation of this function can be written as

$$R_i = (R_{i.1}) + (R_{i.2})(R_{i.3}) - (R_{i.1})(R_{i.2})(R_{i.3})$$

where

R_i = probability of satisfactory operation of subsystem function i

$R_{i.1}$ = probability of satisfactory operation of the primary equipment which provides function i

$R_{i.2}$ = probability of satisfactory operation of the backup equipment which provides function i upon failure of the primary equipment

$R_{i.3}$ = probability of a successful switching operation from the primary to the backup equipment.

The achievable reliability for each equipment contained within a subsystem was determined using (1) a build up of failure rates when an equipment design was available or (2) reliability estimates from similar equipment designs and best engineering judgment, when the particular Jupiter flyby equipment design was not available.

3.13.2 Subsystems Reliability Analyses

3.13.2.1 Communication Subsystem

A minimum hardware concept of the communication subsystem is depicted in the block diagram of Figure 3.13-1. This configuration contains only the minimum hardware necessary to perform all the required functions. All of the equipments are in series and there are no redundancies nor any alternate modes of equipment operation. The satisfactory completion of the 600 day Jupiter flyby mission is dependent upon the communication subsystem performing its designated function continuously throughout the 600 days. The reliability of this communication subsystem configuration for the 600 day mission was calculated to be 0.14 utilizing the set of equations described previously and the predicted meantime-between-failure (MTBF) of each subsystem equipment contained in Figure 3.13-1.

The low reliability of this configuration is due to the long mission time of 600 days. The major contributors to this low reliability are the receiver, the exciter, and the TWT amplifier. To increase the reliability of the subsystem, configurations which contain redundancies in these equipment areas have been investigated. Three of these configurations are illustrated in Figure 3.13-2. Each of these subsystem configurations contains backup equipment in selected areas. Each of the backup equipments is in an inactive state until failure of the primary equipment occurs. The backup equipment is then activated to furnish the required function.

The configuration shown at the top of Figure 3.13-2 has redundant exciters, redundant TWT amplifiers, a series receiver, and a series TWT amplifier power supply. The predicted reliability of this communication configuration is 0.23. The second configuration contains redundant exciters, redundant TWT amplifiers, redundant TWT amplifier power supplies, and redundant receivers. The predicted reliability of this configuration is 0.45. The third configuration is equipped with redundant exciters, redundant TWT amplifiers, redundant TWT amplifier power supplies, and three redundant receivers. The predicted reliability of this configuration is 0.51.

A SERIES COMMUNICATION SUBSYSTEM CONFIGURATION

RELIABILITY BLOCK DIAGRAM AND EQUIPMENT MTBF's

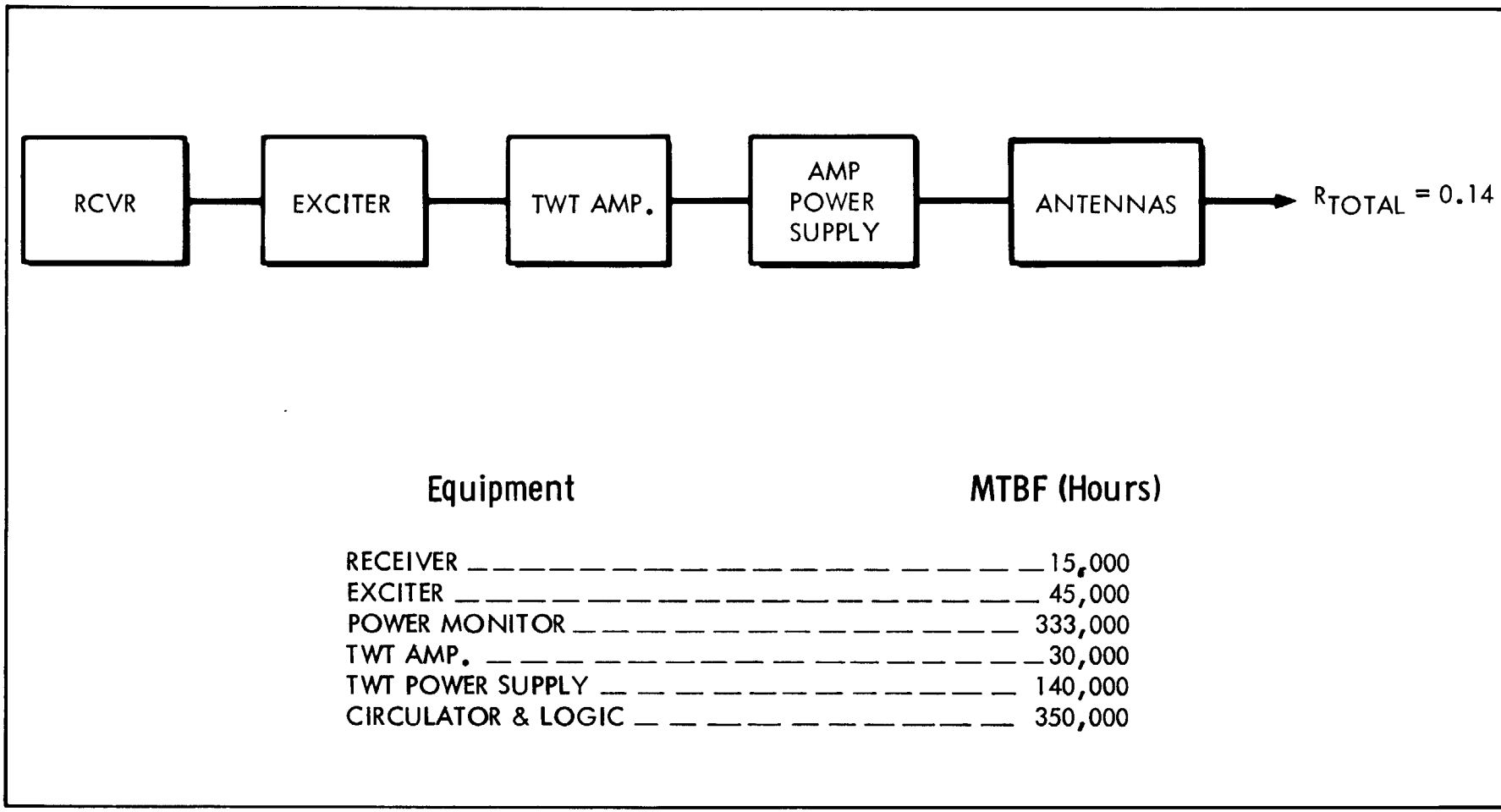

Equipment	MTBF (Hours)
RECEIVER	15,000
EXCITER	45,000
POWER MONITOR	333,000
TWT AMP.	30,000
TWT POWER SUPPLY	140,000
CIRCULATOR & LOGIC	350,000

FIGURE 3.13-1

COMMUNICATION SUBSYSTEM

RELIABILITY BLOCK DIAGRAM - THREE CONFIGURATIONS

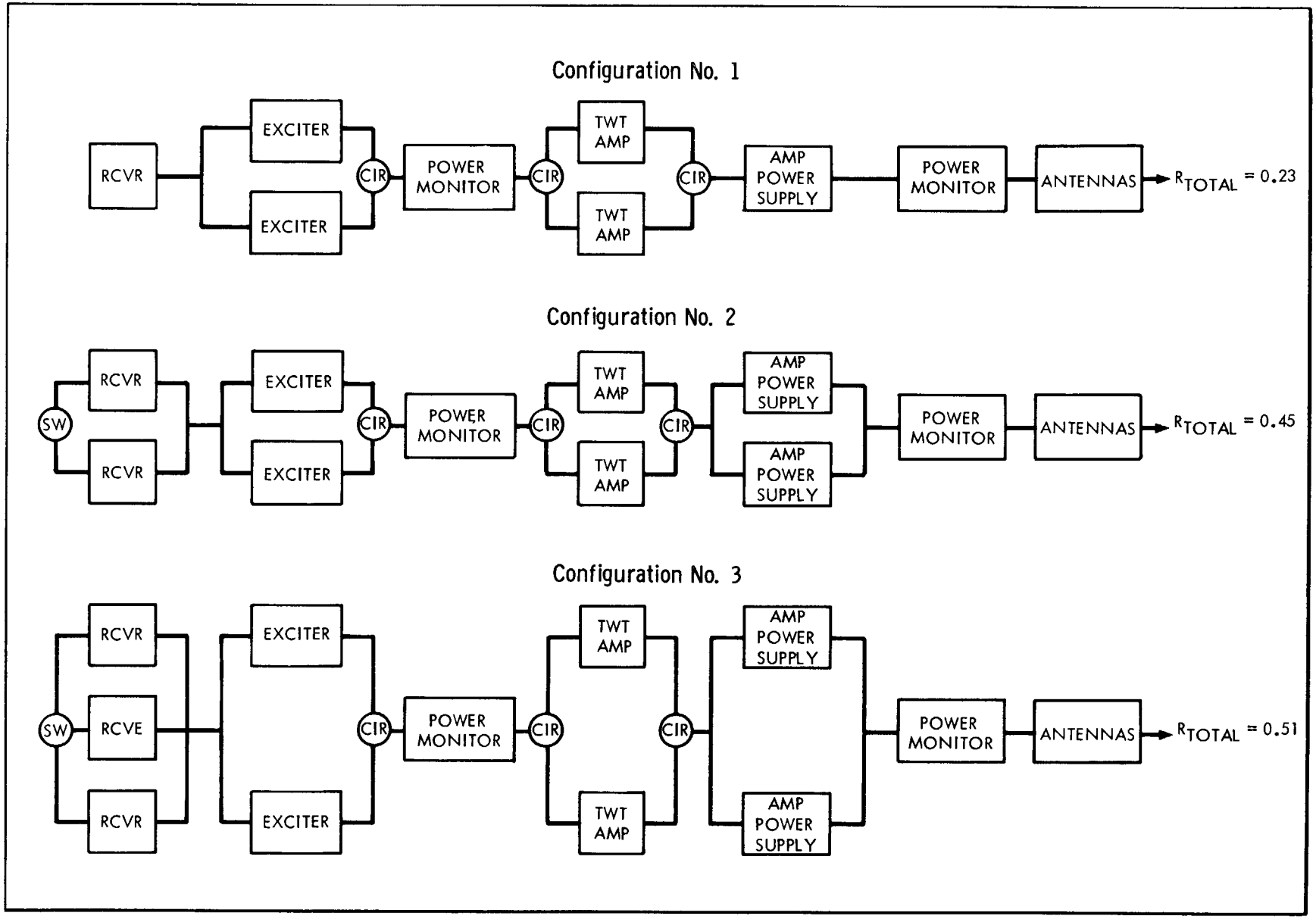

FIGURE 3.13-2

It is apparent that some redundancy of equipment, at least in the critical equipment areas mentioned, will be required to obtain adequate reliability for subsystem mission success.

3.13.2.2 Data Management Subsystem

The data management subsystem consists of the data encoder element (DEE), the data storage element (DSE), the data automation element (DAE), and the command detector and decoder element (CDDE). The reliability analysis for each of these elements is presented separately in the following paragraphs. Mariner IV design and reliability information is used in these analyses when applicable.

Data Encoder Element - The satisfactory completion of the 600 day Jupiter flyby mission is dependent upon the data encoder element performing its designated functions continuously throughout the 600 days. One DEE configuration is shown in Figure 3.13-3. The predicted reliability of this configuration is 0.04. The reliability of the subsystem is increased in configurations which contain redundancies in certain equipment areas have been investigated. Three of these configurations are shown in Figure 3.13-4. Each of the backup equipments is in an inactive state until failure of the primary equipment occurs. The backup equipment is then activated and furnishes the required function.

DATA ENCODER ELEMENT

RELIABILITY BLOCK DIAGRAM AND SUBELEMENT MTBF's

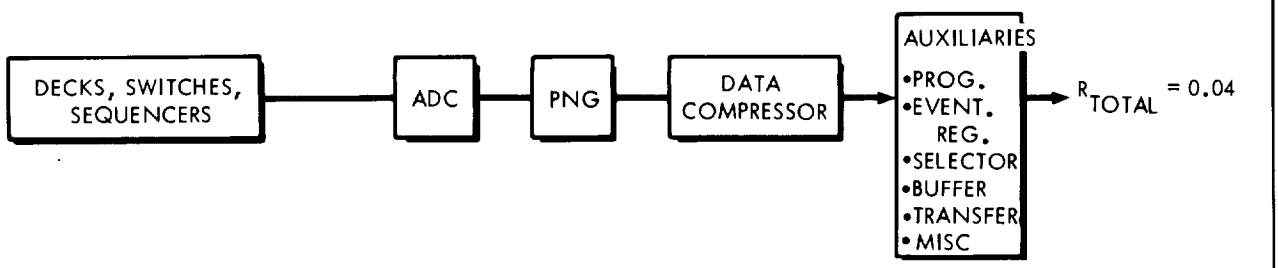

Subelement	MTBF (Hours)
AUXILIARIES	6,000
PNG	60,000
ADC	110,000
DATA COMP.	30,000
DECKS, ETC.	2,000

FIGURE 3.13-3

DATA ENCODER ELEMENT

RELIABILITY BLOCK DIAGRAM - THREE CONFIGURATIONS

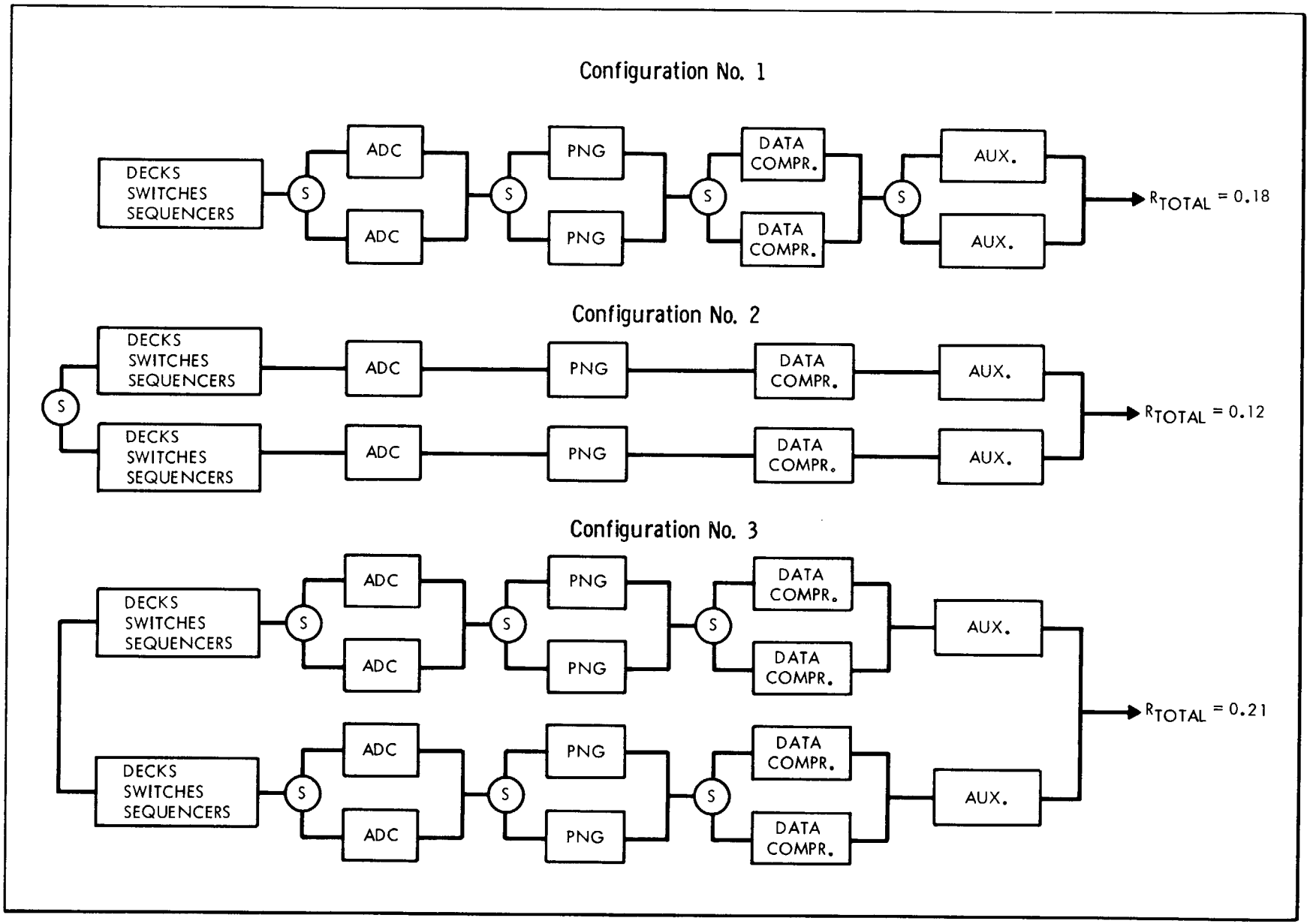

FIGURE 3.13-4

Data Storage Element - Several different types of data storage methods were investigated, but because of considerations other than reliability (e.g., weight, power, and size), redundant tape recorders will be utilized. The estimated MTBF of a single tape recorder is 6000 hours. Satisfactory completion of the 600 day Jupiter flyby mission is dependent upon the DSE performing its function upon command throughout the 600 days. This function can be accomplished by any one of the two recorders. If it is assumed that the redundant recorder DSE is active only during certain phases of the 600 day flight, accumulating 50 days of operating time, the predicted reliability of the DSE is 0.95.

Command Detector and Decoder Element - Results of a reliability analysis of the CDDE are depicted in Figure 3.13-5. The CDDE provides earth controlled commands to other subsystems. Configuration 1 consists of only the minimum hardware required to furnish these commands, i.e., the detector and decoder circuits and the discrete output circuits for each command. The predicted reliability of an earth controlled command at the end of 600 days ranges from 0.17 to 0.19 depending upon command complexity. The detector and encoder circuits are assumed to be active throughout the mission.

Configuration 2 contains complete redundancy of all functions. Both detector and decoder circuits are assumed to be active throughout the mission and the commands can be initiated by either one of the circuits. The predicted reliability of an earth controlled command at the end of 600 days ranges from 0.32 to 0.35, again depending upon command complexity.

COMMAND DETECTOR AND ENCODER ELEMENT
RELIABILITY BLOCK DIAGRAM AND SUBELEMENT MTBF's

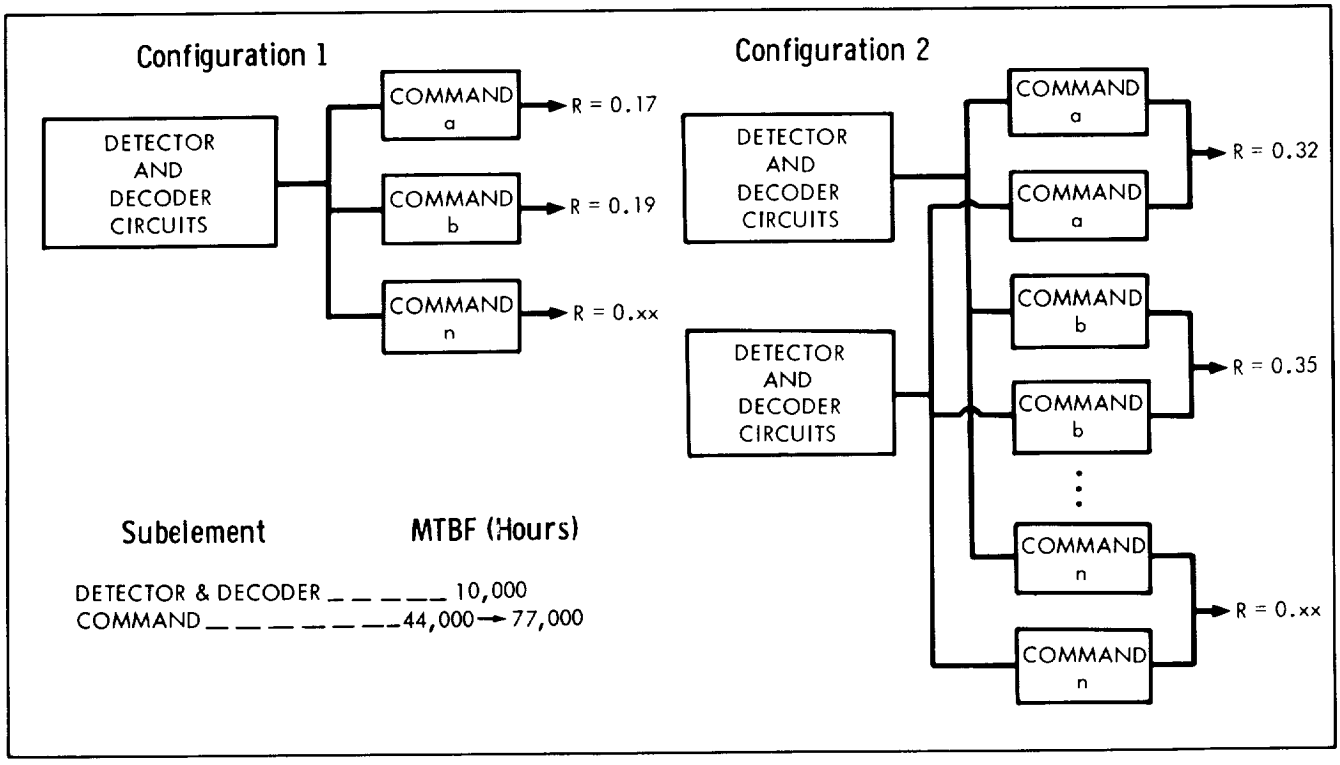

FIGURE 3.13-5

Data Automation Element - Two concepts of a DAE design were investigated. One concept is a design in which the real-time and non-real-time sequencer are combined into a single sequencer. The second concept contains both a real-time section and a non-real-time section. The satisfactory completion of the mission is dependent upon the DAE performing its designated function continuously throughout the 600 days.

A reliability block diagram of a combined real-time and non-real-time sequencer configuration is presented in Figure 3.13-6. The predicted reliability of this configuration is 0.13. Because of the low predicted reliability, a total redundant configuration of the combined sequences DAE was investigated. The predicted reliability of this redundant configuration is 0.32.

A reliability block diagram of the two section DAE is shown in Figure 3.13-7. The predicted reliability for this type DAE is 0.06. Because of the low predicted reliability, a total redundant configuration of the two section DAE was investigated. The predicted reliability for this redundant configuration is 0.17.

3.13.2.3 Spacecraft Control Subsystem

Three spacecraft control system concepts were examined in the analysis under discussion. Design and reliability data from the Mariner IV spacecraft have been utilized in the analyses

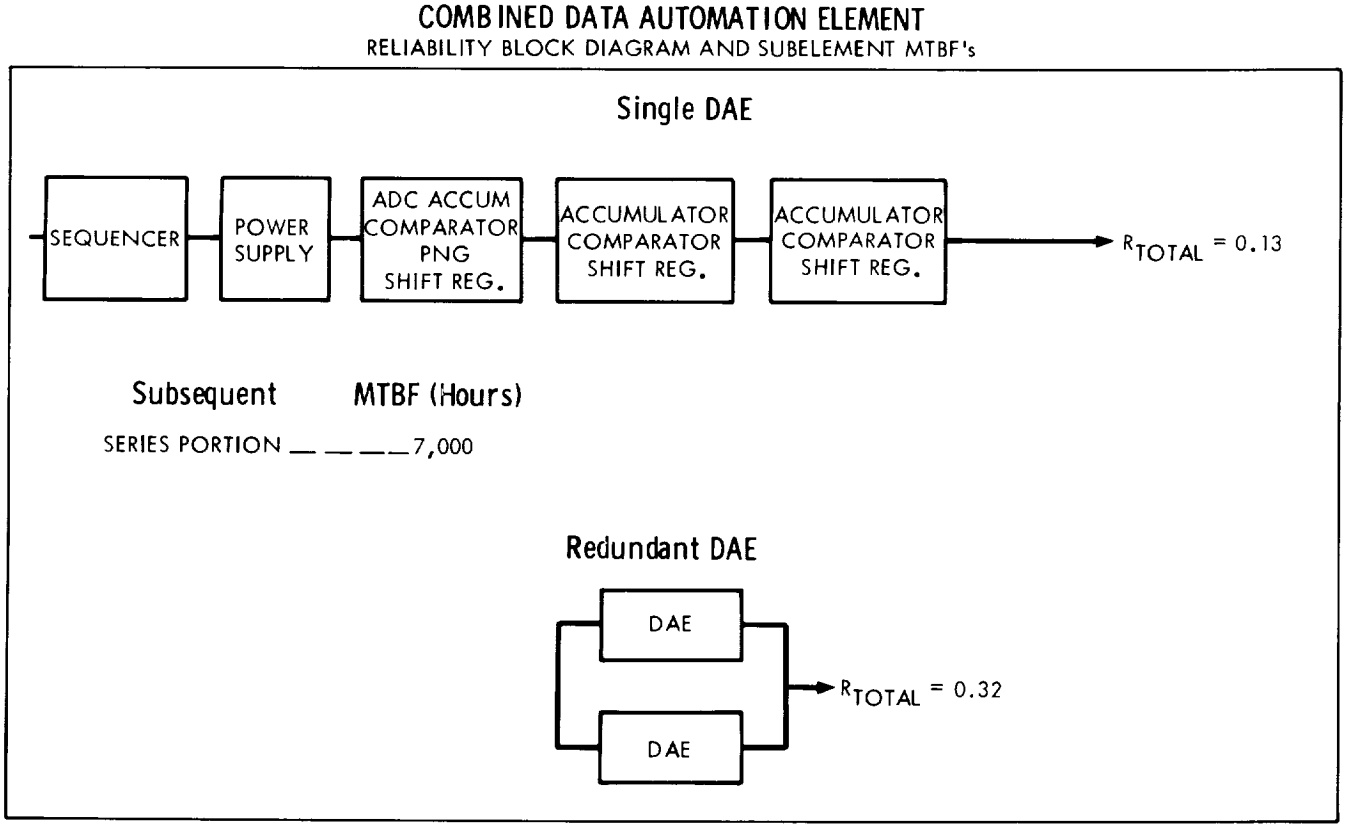

FIGURE 3.13-6

A TWO SECTION DATA AUTOMATION ELEMENT

RELIABILITY BLOCK DIAGRAM AND SUBELEMENT MTBF's

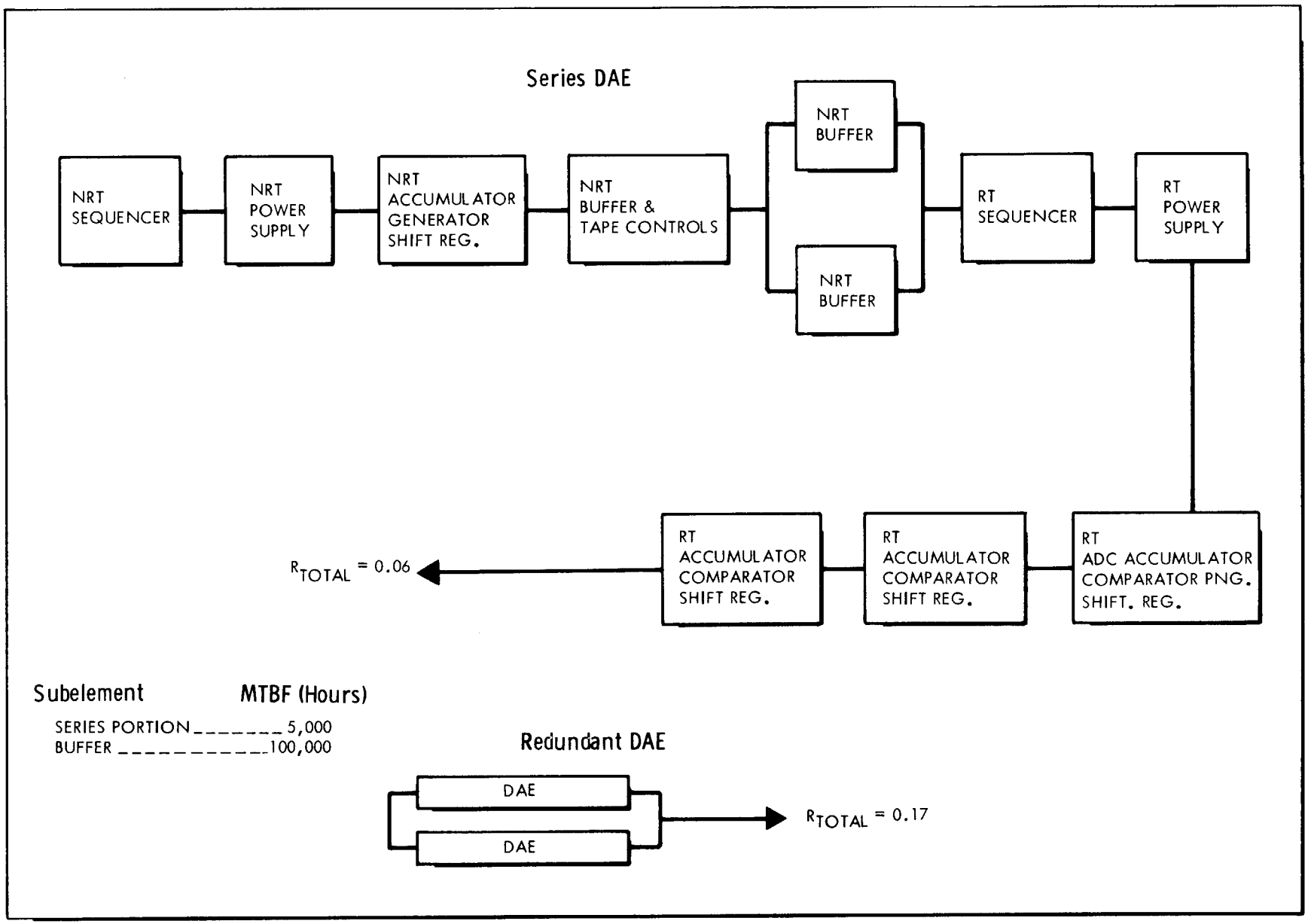

FIGURE 3. 13-7

of the equipment comprising the spacecraft control subsystem. Concept 1 is summarized in Figure 3.13-8, which contains a reliability block diagram, a list of the equipment MTBF's, and the estimated operating time of the equipment. For purposes of the analysis, it is assumed that all the subsystems equipment, except the central computer and sequencer, are required to operate for the first 14 days of the 600 day flight; after that time an equipment failure will not constitute a flight failure. The predicted reliability of this spacecraft control subsystem is 0.30. A reliability block diagram of the central computer and sequencer portion of the subsystem is shown in Figure 3.13-9. The functions to be performed by the different parts of the equipment are also noted on the figure.

SPACECRAFT CONTROL SUBSYSTEM ONE

RELIABILITY BLOCK DIAGRAM, EQUIPMENT MTBF's, AND EQUIPMENT OPERATING TIMES

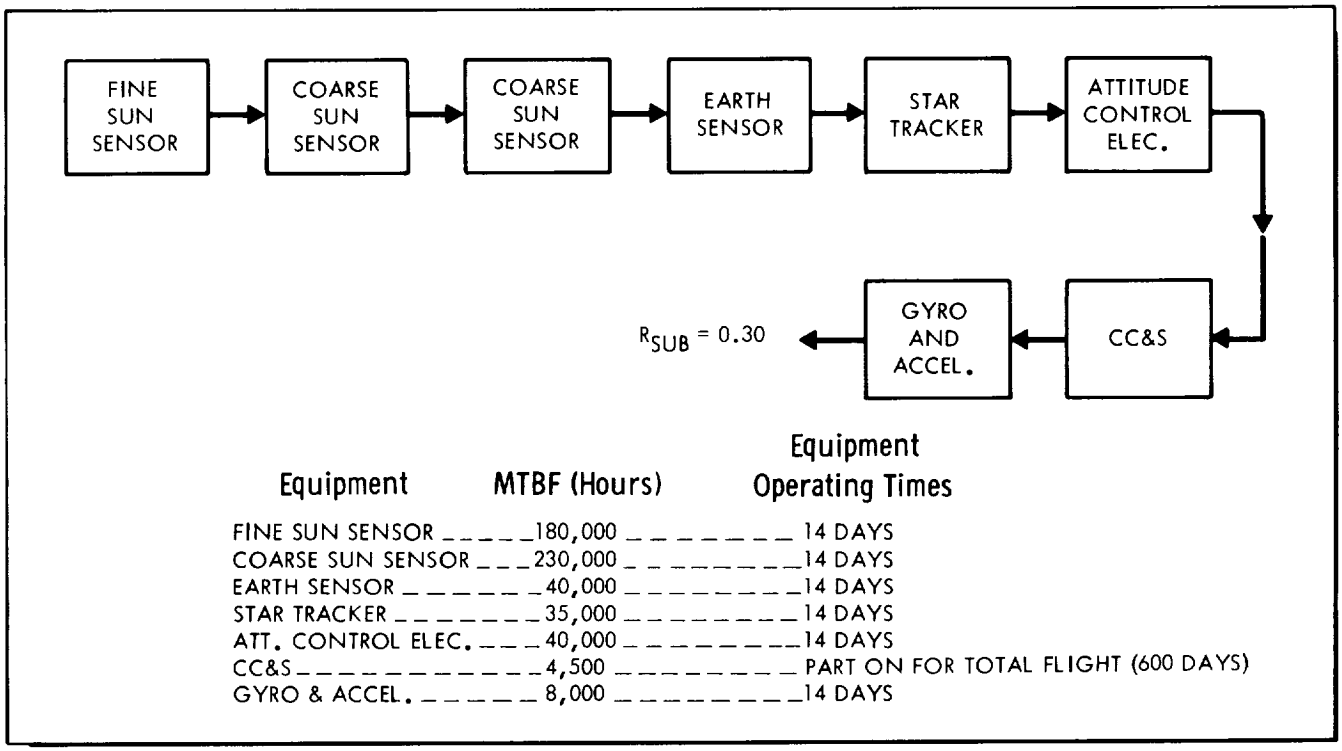

Equipment	MTBF (Hours)	Equipment Operating Times
FINE SUN SENSOR	180,000	14 DAYS
COARSE SUN SENSOR	230,000	14 DAYS
EARTH SENSOR	40,000	14 DAYS
STAR TRACKER	35,000	14 DAYS
ATT. CONTROL ELEC.	40,000	14 DAYS
CC&S	4,500	PART ON FOR TOTAL FLIGHT (600 DAYS)
GYRO & ACCEL.	8,000	14 DAYS

FIGURE 3.13-8

Concept 2 of the spacecraft control subsystem is summarized in Figure 3.13-10. The predicted reliability of this subsystem is 0.13. The diagram of the central computer and sequencer shown in Figure 3.13-9 is also considered applicable to this concept.

Concept 3, summarized in Figure 3.13-11, has a predicted reliability of 0.21. Each of the back-up equipments in this configuration is in an inactive state until failure of the primary equipment occurs. The back-up equipment is then activated to furnish the required function.

CENTRAL COMPUTER AND SEQUENCER

RELIABILITY BLOCK DIAGRAM

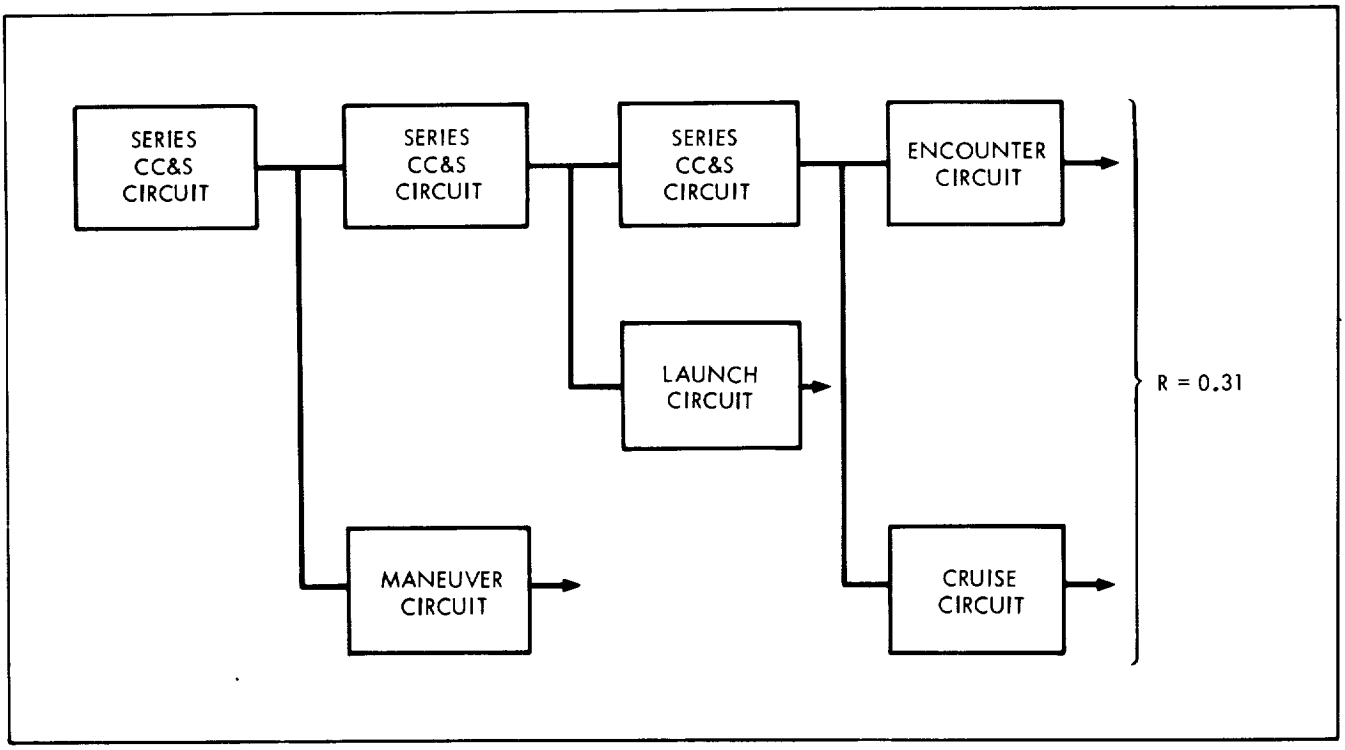

FIGURE 3.13-9

SPACECRAFT CONTROL SUBSYSTEM TWO

RELIABILITY BLOCK DIAGRAM, EQUIPMENT MTBF's, AND EQUIPMENT OPERATING TIMES

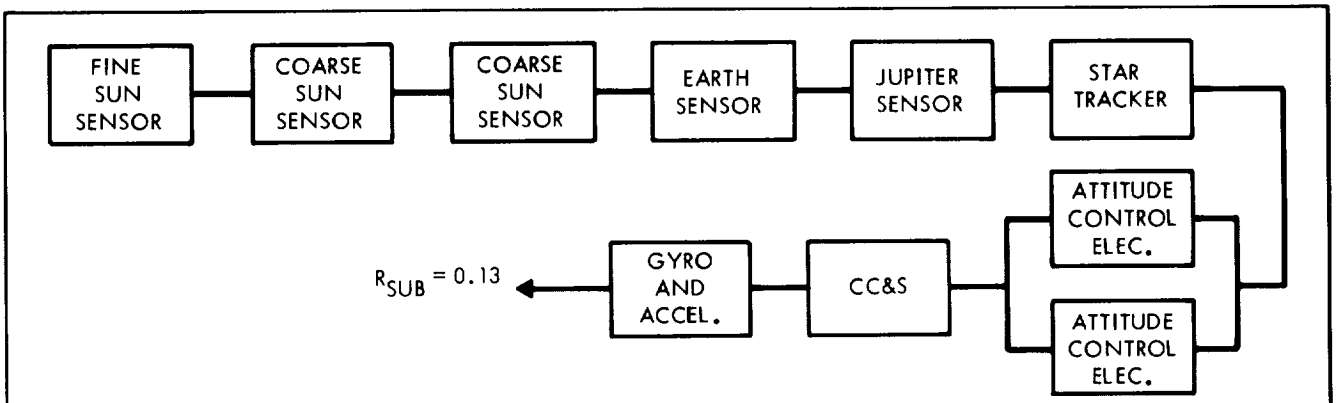

Equipment	MTBF (Hours)	Operating Times
FINE SUN SENSOR	40,000	OFF FIRST 7 DAYS - ON 1 HOUR
COARSE SUN SENSOR	230,000	TOTAL FLIGHT (600 DAYS)
EARTH SENSOR	40,000	ONE DAY
JUPITER SENSOR	40,000	OFF TO ENCOUNTER - 12 HR, ON TO ENCOUNTER
STAR TRACKER	35,000	TOTAL FLIGHT (600 DAYS)
ATT. CONT. ELEC.	40,000	TOTAL FLIGHT (600 DAYS)
CC&S	4,500	TOTAL FLIGHT (600 DAYS)
GYRO & ACCEL.	8,000	GYROS ON-TOTAL OF 9 HRS. ACCEL. OFF - 1ST 7 DAYS - ON 1.5 HRS.

FIGURE 3.13-10

SPACECRAFT CONTROL SUBSYSTEM THREE

RELIABILITY BLOCK DIAGRAM, EQUIPMENT MTBF's, AND EQUIPMENT OPERATING TIMES

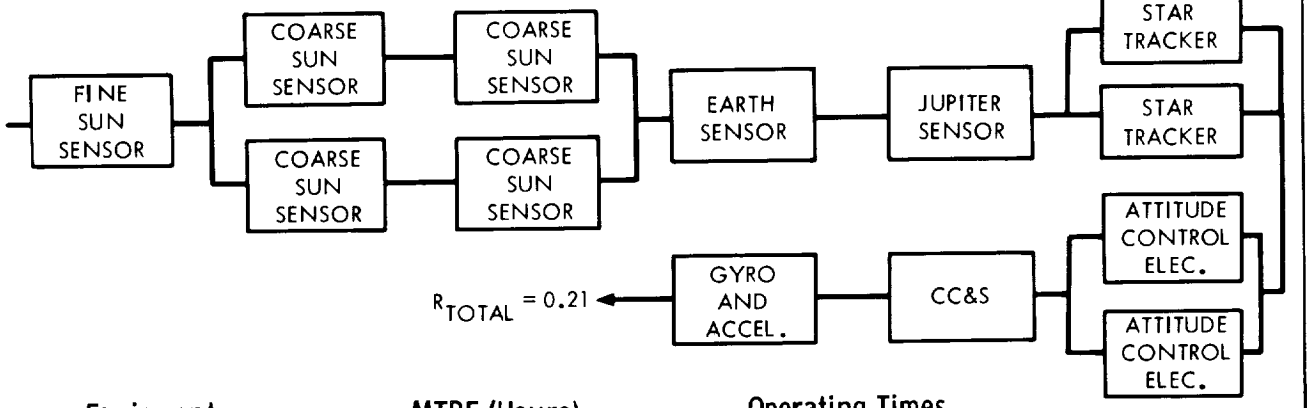

Equipment	MTBF (Hours)	Operating Times
FINE SUN SENSOR	40,000	OFF 1ST 7 DAYS - ON 1 HOUR.
COARSE SUN SENSOR	230,000	TOTAL FLIGHT (600 DAYS)
EARTH SENSOR	40,000	ON ONE DAY
JUPITER SENSOR	40,000	OFF TO ENCOUNTER - 12 HRS, ON TO ENCOUNTER
STAR TRACKER	35,000	TOTAL FLIGHT (600 DAYS)
ATT. CONT. ELEC.	40,000	TOTAL FLIGHT (600 DAYS)
CC&S	4,500	TOTAL FLIGHT (600 DAYS)
GYRO & ACCEL.	8,000	GYROS- ON TOTAL 9 HRS. ACCEL - ON TOTAL 1.5 HRS.

FIGURE 3.13-11

3.13.2.4 Attitude Control Propulsion Subsystem

The different types of attitude control propulsion subsystems considered are a single cold gas subsystem, a redundant cold gas subsystem, and a subsystem consisting of a combination of reaction wheels and a single cold gas system.

A reliability block diagram of a single cold gas propulsion subsystem and the probabilities associated with this subsystem are presented in Figure 3.13-12. For purposes of this analysis, it was assumed that this attitude control subsystem is shut down at the end of spacecraft spin up which occurs at 14 days and any malfunction after this time would not result in a flight failure. The predicted reliability of this design concept is 0.990. This reliability prediction is based on frequency rates of 1530 actuations per month per roll jet and 2190 actuations per month per pitch/yaw jet.

Investigations were accomplished on two redundant cold gas subsystem designs. These subsystems are summarized in Figures 3.13-13 and 3.13-14. The predicted reliability of the dual cold gas subsystem shown in Figure 3.13-13 is 0.983. The predicted reliability of the cold gas subsystem shown in Figure 3.13-14 is 0.984. These reliability predictions are based on a frequency rate of 1080 actuations per month per roll jet, 1275 actuations per month per pitch/yaw jet, and a usage factor of 20 months.

SINGLE-COLD GAS ATTITUDE CONTROL SUBSYSTEM
RELIABILITY BLOCK DIAGRAM AND EQUIPMENT PROBABILITIES

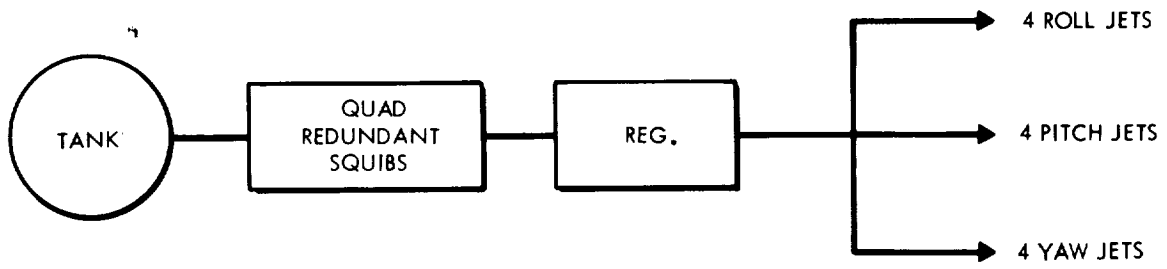

Equipment	Probability
TANK	.999800
SQUIB	.999896
REGULATOR	.999556
SINGLE ROLL JET	.999465
SINGLE PITCH/YAW JET	.999233

FIGURE 3. 13-12

DUAL COLD GAS ATTITUDE CONTROL SUBSYSTEM ONE
RELIABILITY BLOCK DIAGRAM AND EQUIPMENT PROBABILITIES

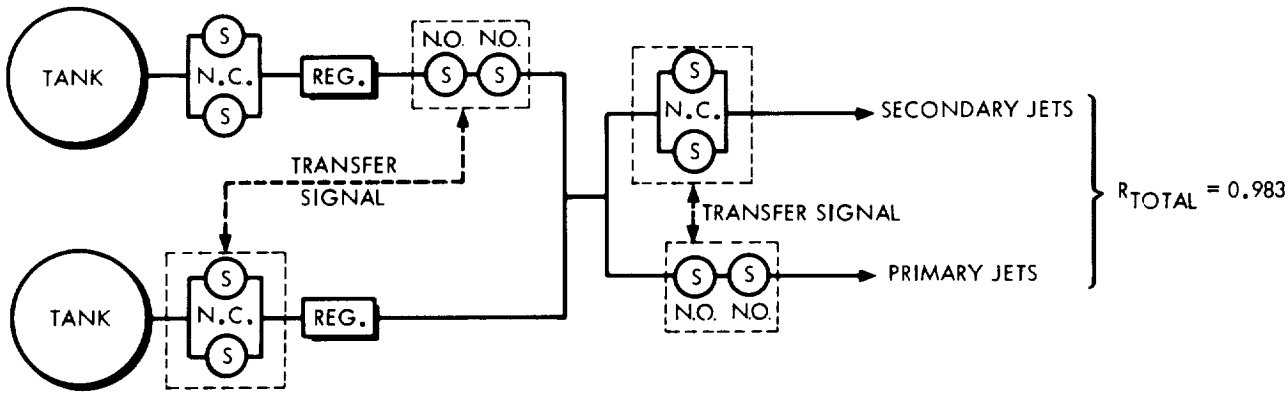

Equipment	Probability
TANK	.9998
SQUIB	.999896
REGULAR	.9567
SINGLE ROLL JET	.98488
SINGLE PITCH/YAW JET	.98215

FIGURE 3. 13-13

DUAL COLD GAS ATTITUDE CONTROL SUBSYSTEM TWO

RELIABILITY BLOCK DIAGRAM

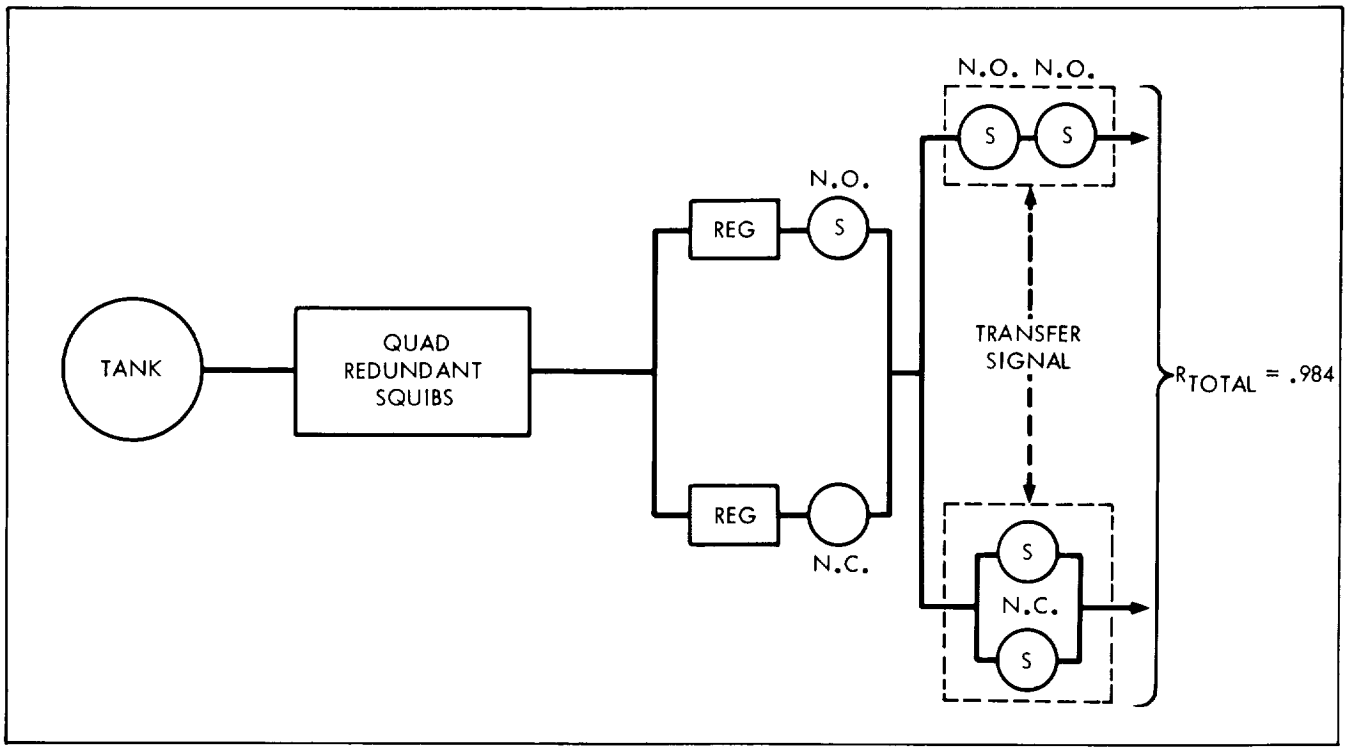

FIGURE 3.13-14

An attitude control subsystem configuration consisting of three reaction wheels and a single cold gas system was investigated. The predicted MTBF for a single reaction wheel with associated electronics is 47,000 hours. Based on the assumption that all three reaction wheels must operate throughout the flight of 600 days, the predicted subsystems reliability for a three reaction wheel configuration is 0.395. If a three reaction wheel configuration is used in redundancy with a single cold gas subsystem, the predicted subsystem reliability is 0.867. This reliability prediction is based on the assumption that the cold gas system is used throughout the mission for wheel desaturation and to aid spacecraft control.

Dual and single tank design configurations were investigated for purposes of trade-off. The tank configurations and associated reliabilities are presented in Figure 3.13-15. The predicted reliabilities for the various tank configurations are 0.999899 for the dual tank and 0.9998 for the single tank with redundant squibs.

3.13.2.5 Midcourse Propulsion Subsystem

The reliability analysis is based on the assumption that two maneuvers will be necessary for satisfactory completion of the mission.

VARIOUS ATTITUDE CONTROL TANK CONFIGURATIONS
RELIABILITY BLOCK DIAGRAM AND RELIABILITY PROBABILITIES

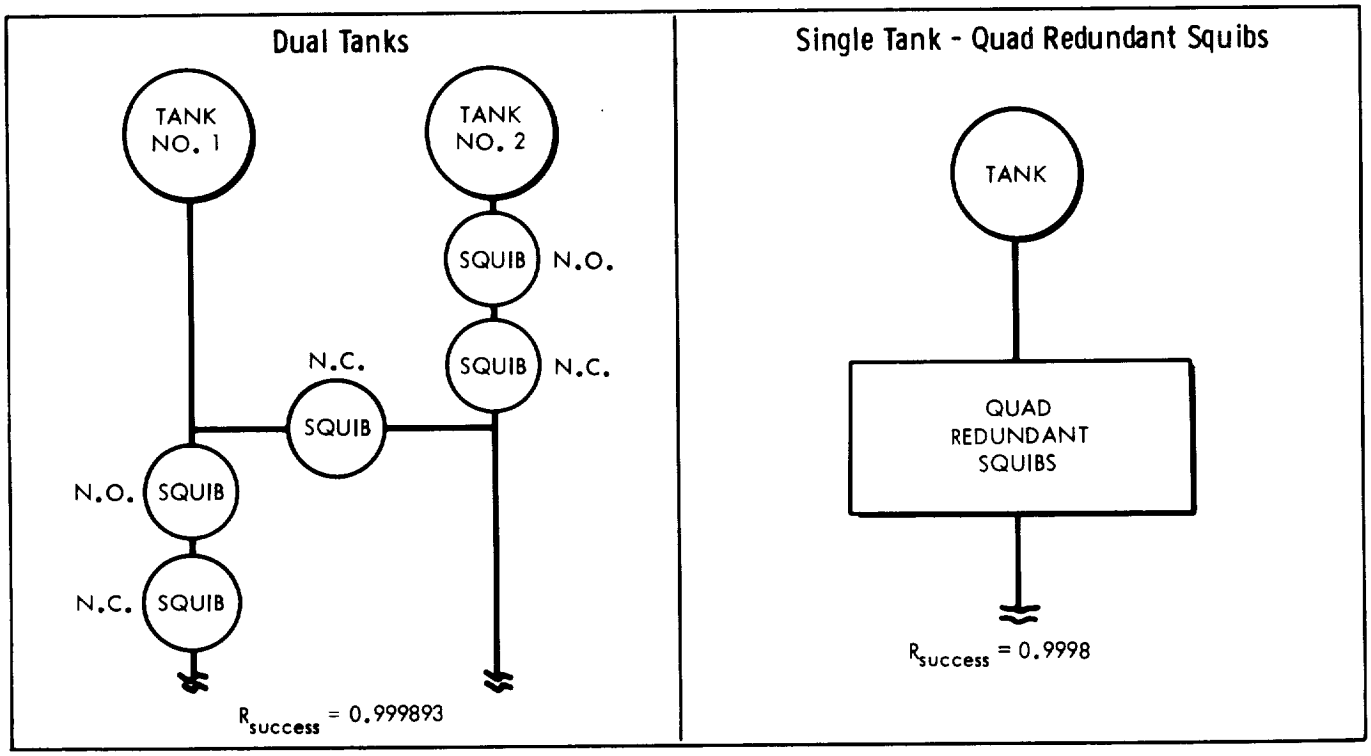

FIGURE 3.13-15

A reliability block diagram of the propulsion along with the equipment probabilities is presented in Figure 3.13-16. The design variations in the subsystem considered for this analysis were the use of series control squibs as opposed to the use of quad redundant control squibs and the use of a series regulator with no failure detection as opposed to the use of redundant regulators with failure detection. Both configurations are shown in Figure 3.13-17. The predicted reliability for a propulsion subsystem with a series control squib design is 0.9969; for a propulsion subsystem with a redundant control squib design, the predicted reliability is 0.9978.

Two different regulator configurations are depicted in Figure 3.13-18. The reliability of the total propulsion subsystem with the two different regulator configurations and quad redundant control squibs is 0.9572 for a configuration containing a series regulator with no failure detection circuit,and 0.9977 for a configuration containing redundant regulators with a failure detection circuit.

3.13.2.6 Auxiliary Electrical Subsystem

Two auxiliary electrical subsystem configurations, one comprised of three RTG's and one of four RTG's, were analyzed. The satisfactory completion of the 600 day mission is dependent upon

PROPULSION SUBSYSTEM

RELIABILITY BLOCK DIAGRAM AND EQUIPMENT PROBABILITIES

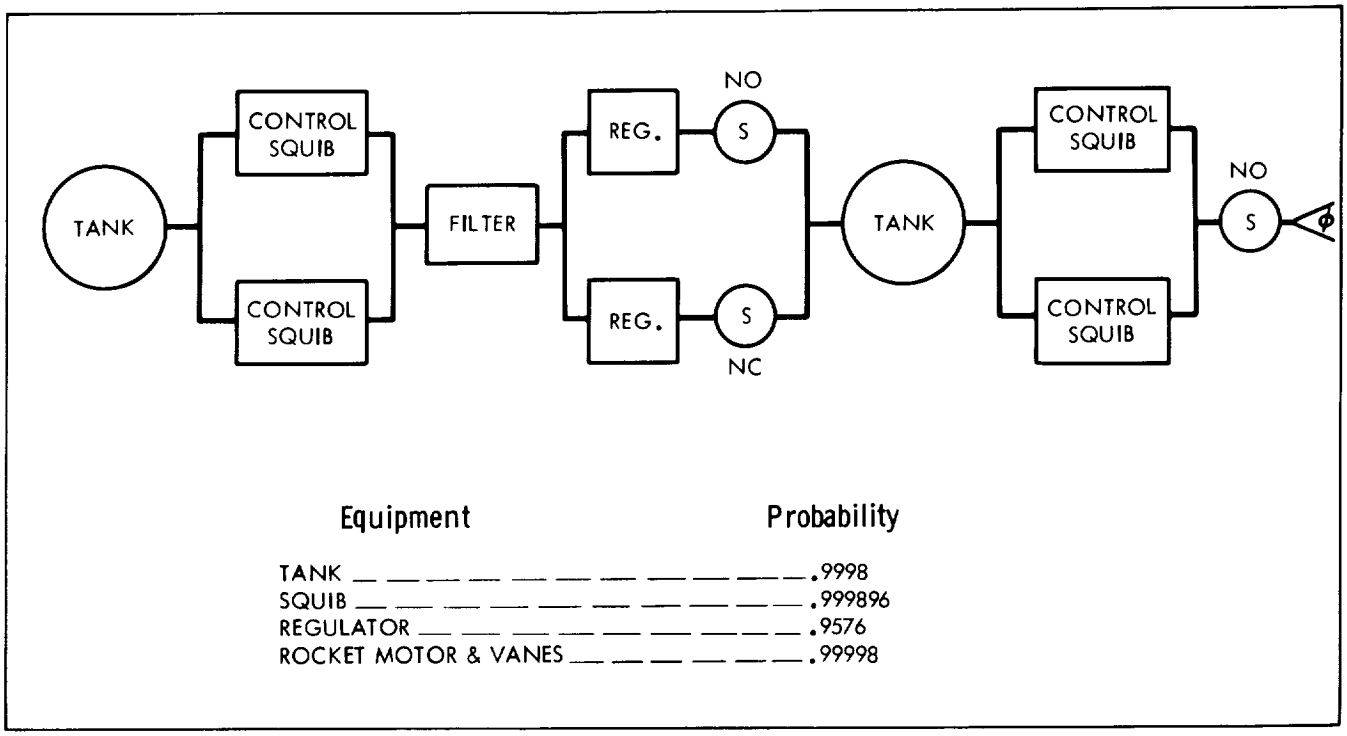

Equipment	Probability
TANK	.9998
SQUIB	.999896
REGULATOR	.9576
ROCKET MOTOR & VANES	.99998

FIGURE 3.13-16

CONTROL SQUIB CONFIGURATIONS FOR PROPULSION SYSTEM

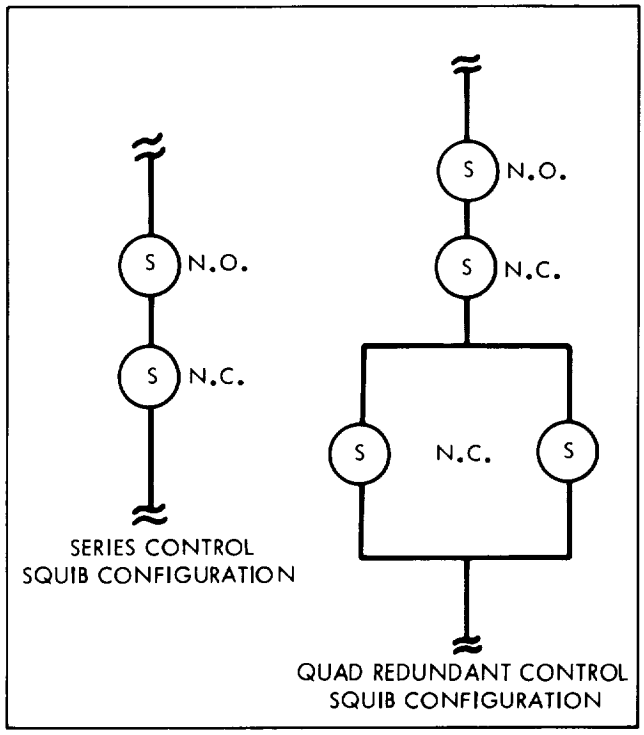

FIGURE 3.13-17

REGULATOR CONFIGURATIONS FOR THE PROPULSION SUBSYSTEM

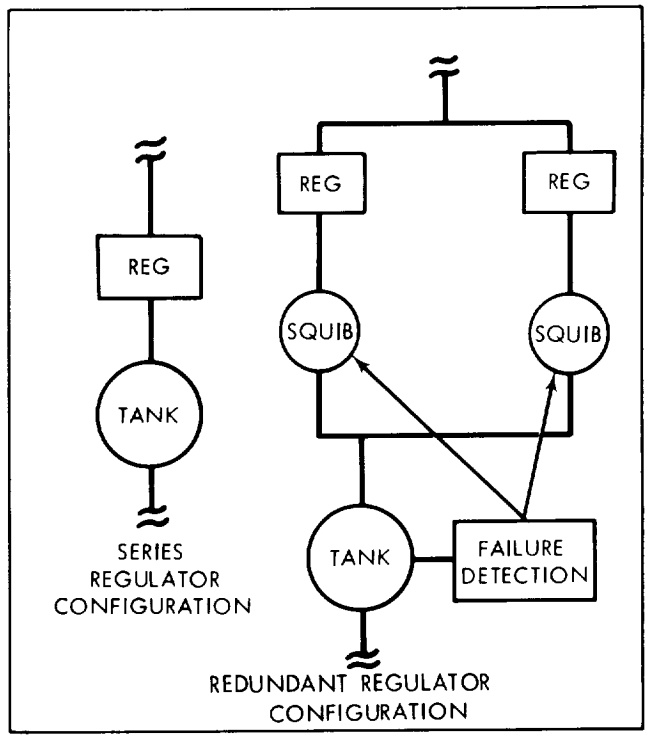

FIGURE 3.13-18

ELECTRICAL POWER SUBSYSTEM

RELIABILITY BLOCK DIAGRAM AND EQUIPMENT MTBF's

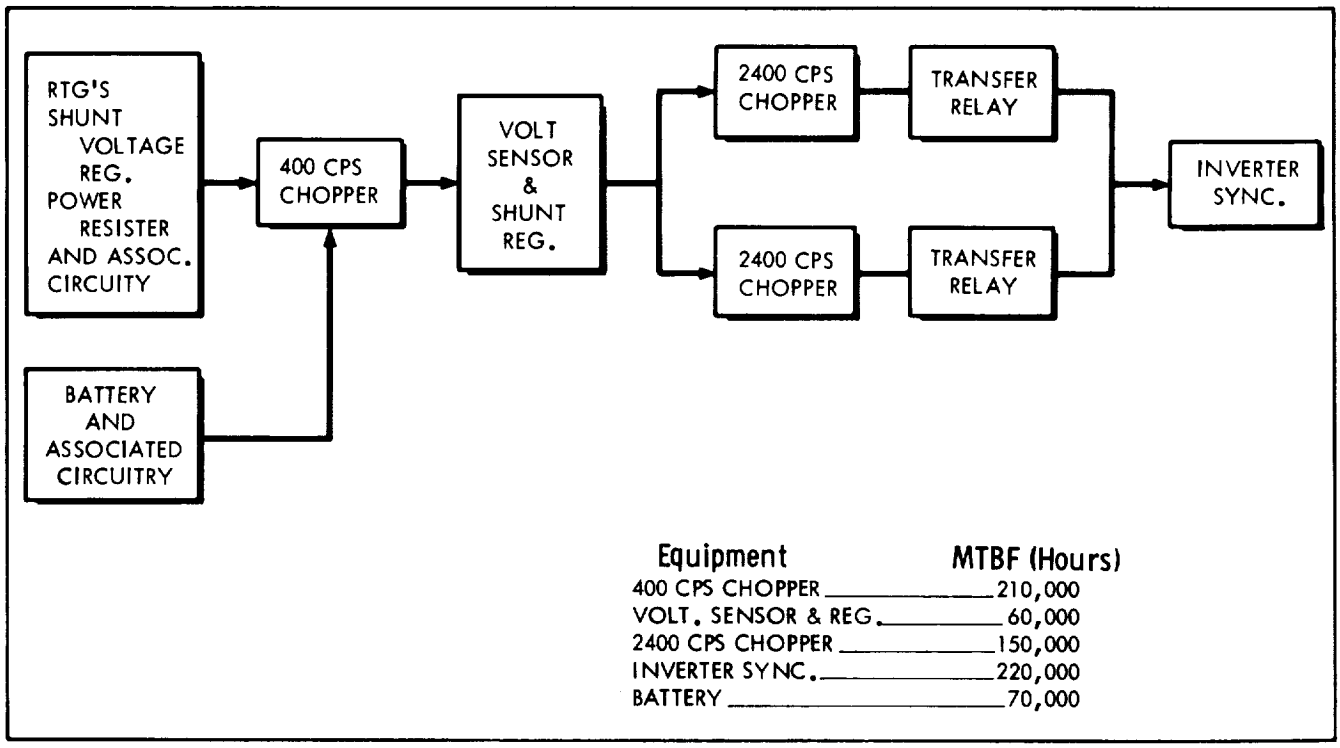

FIGURE 3.13-19

the auxiliary electrical subsystem supplying the electrical power requirements of the spacecraft throughout the mission.

The auxiliary electrical subsystem is summarized in Figure 3.13-19. In determining the reliability of the three RTG subsystem, the following assumptions have been made: (1) the reliability of the RTG's is approximately one (based on the discussion of subsection 3.7), (2) the subsystem can operate successfully with 2 of 3 of the shunt-voltage regulators operating, (3) the shunt-voltage regulators are active throughout the mission, (4) the subsystem can operate successfully with either of the two 2400 cps choppers. The predicted reliability of the three RTG subsystem is 0.71 when the reliability of battery is not included in the subsystem predictions and 0.47 when the reliability of the battery is included.

Reliability estimates of the four RTG subsystems are based on the following assumptions: (1) the reliability of the RTG's is approximately unity (based on the discussion of paragraph 3.7), (2) the subsystem can operate successfully with 3 of 4 of the shunt-voltage regulators operating, (3) the shunt-voltage regulators are active throughout the mission, and (4) the subsystem can operate successfully with either of the two 2400 cps choppers. The predicted reliability of this subsystem is 0.717 when the reliability of the battery is not included in the subsystem prediction and 0.472 when the reliability of the battery is included.

3.13.2.7 Science Subsystem

No subsystem reliability trade-off studies were performed on the scientific instruments to be carried on a Jupiter flyby mission. Predictions of mean-time-between-failure of the scientific instruments are listed in Table 3.13-1. Because of the lack of design information on many of these instruments, the MTBF's of these instruments are based upon known instrument designs and the best engineering judgment.

Table 3.13-1

MEAN-TIME-BETWEEN-FAILURES FOR SCIENTIFIC INSTRUMENTS

Scientific Instrument	MTBF
Extended Magnetometer	15,000
Energetic Particle Detector	40,000
Cosmic Dust Detector	40,000
Visible Photometer	50,000
TV Camera I	6,500
Plasma Probe	15,000
Microwave Radiometer	4,000
IR Radiometer	20,000
ION Chamber	35,000
IR Spectrometer	6,000
High Energy Proton Directional Monitor	25,000
Cosmic Ray Spectrum Analyzer	10,000
Expanded Photometer	20,000
UV Visible Spectrometer	5,000
Medium Energy Proton Directional Monitor	35,000
Bistatic Radar	7,000
Radio Noise Detector	20,000
Null Radio Seeker	20,000
Radar Altimeter	4,000
TV Camera II	3,500

SECTION 4

SPACECRART CONCEPT EVALUATION

This section contains a discussion of the guidelines, assumptions, approach, and general analyses employed in evaluating each of the four spacecraft design concepts synthesized in the study. The evaluation comprises four categories. These are (1) mission performance, (2) probability of mission success, (3) development requirements, and (4) cost. The results of these efforts, i.e., the specific evaluations of each design concept, are reported in Section 5.

4.1 Mission Performance Analysis

Mission performance data are obtained by use of adjusted launch vehicle performance curves and the mission maps of injection energy requirements which are contained in Appendix A. Adjustments to the launch vehicle performance curves (explained in subsection 2.3.1), are made to account for (1) a launch from AMR at an azimuth of 114 degrees and (2) the jettisoning of the payload fairing at 350,000 feet.

The adjusted launch vehicle performance curve for a particular spacecraft/launch vehicle combination is used to determine the maximum injection energy, C_3, attainable with that combination. The locus of these points on the injection energy mission map of a particular launch year defines the mission performance envelope for the specified spacecraft/launch vehicle combination. Intersections of these envelopes with Jupiter arrival dates define constant-arrival-date launch window widths, or launch periods, for the spacecraft/launch vehicle combination. The performance capability of the combination is measured in terms of launch window width for specified arrival dates.

In Section 5, the mission performance capabilities of each of the four spacecraft design concepts in combination with applicable launch vehicles is summarized. The Jupiter arrival dates selected for performance summary definitions are those corresponding to the appropriate western quadrature, opposition, and eastern quadrature date for each launch opportunity from 1973 to 1980.

4.2 PROBABILITY OF MISSION SUCCESS

One of the parameters used for spacecraft concept evaluation is the probability of mission success. In this study, the probability of mission success is defined as the probability that a completely checked out spacecraft will successfully obtain the required information and relay the information to the DSIF. Information lost because of booster failure, shroud separation, etc., is not included.

4.2.1 Approach

The probability of mission success can be described in general equation form as follows:

$$P_S = \prod_{j=1}^{n} R_{sub_j}$$

where

P_S = probability of satisfactory operation of all spacecraft functions required for mission success

R_{sub_j} = probability of satisfactory operation of all subsystem j functions.

The predictive results based on the solution of the probability of mission success equations for each spacecraft design concept are included in Section 5. The success-failure criteria and the equipment operational requirements used in the development of the equations for each concept are presented generally below.

1. The complete scientific data gathering function is required through the encounter phase of the mission.

2. The communication receiving and transmitting function is required through the encounter playback phase of the mission.

3. The data encoder function is required through the encounter playback phase of the mission.

4. The data storage element function is required for the encounter and encounter playback phases of the mission.

5. The data automation function is required as needed to support science and engineering data accumulation through the encounter playback phase of the mission.

6. The following equipments are required to function as needed: the fine Sun sensor, the course Sun sensor, the star tracker, the gyros, the accelerometer, and the Jupiter sensor.

7. The CC&S and the CDDE functions are required as needed through the midcourse maneuver. After midcourse maneuver, at least one of either the CC&S or the CDDE functions is required through the encounter playback phase of the mission.

8. The attitude control function is required through the encounter playback phase of the mission.

9. The midcourse propulsion function is required through the midcourse maneuver.

10. The electrical power function to satisfy spacecraft power requirements is required through the encounter playback phase of the mission.

Other required functions which are specifically applicable to the individual design concepts are delineated for each concept in Section 5. Also, the detail mission sequence and mission objectives for each concept are presented in that section. Nominal missions and associated flight times are selected for obtaining the probability of mission success for each spacecraft design concept. The equipment MTBF's which are utilized in the computations for the individual concepts are listed in Section 5.

4.2.2 Discussion of Results

As was expected, the probability of total mission success as defined above and based on the reliability predictions used is very low for all design concepts. In fact, it is less than one percent. The exact evaluations obtained are not quoted, since the number of significant places used in the calculations is not compatible with results of this magnitude.

In considering the import of these results, it is emphasized that the defined conditions for achieving total mission success are very stringent and do not allow for any form of degraded

mission performance. In order to evaluate this consideration, three different probabilities of partial mission success are presented for each concept in Section 5. One is the probability of successful operation of all equipment, except the science instruments, for all required functions throughout the total mission. The other two probabilities are based on successful completion of the first half of the mission by the total spacecraft and by the spacecraft less science.

The first probability indicates the definite effect of the science complement on mission success and also allows quick calculation of the probability of successfully performing any one of the individual experiments. The last two probabilities offer points of reference, because the equipment operating times are near those for the Mariner IV systems.

One of the objectives of this study is to identify the spacecraft systems which need reliability improvement efforts. For example, the equipment comprising the data management subsystem has been found to generally possess the lowest reliability of any other spacecraft subsystem. One exception to this is the data management concept presented in subsection 5.4.2.3. This concept exhibits a high reliability, but it also represents an extensive development program. In keeping with the objective of identifying reliability problem areas on the subsystem level, the probabilities of total mission success and half-mission success are presented in Section 5 for the four systems which are the largest contributors to the low probability of mission success of each spacecraft design concept.

4.3 DEVELOPMENT REQUIREMENTS

This section contains a description of the general approach used in defining the development requirements associated with the Jupiter flyby spacecraft. The major pacing items having the most uncertainties in each spacecraft development plan are (1) the RTG power subsystem, (2) the scientific payloads, and (3) the series of integrated, interrelated spacecraft test requirements. The problems associated with the RTG power subsystem and the scientific payloads are discussed in subsections 4.3.2 and 4.3.3 respectively. A composite Program Implementation Network of the test requirements was prepared in PERT form (subsection 4.3.4) and analyzed using ASD PERT III x 80 program. An explanation of the general network used for all spacecraft design concepts is included herein. Individual spacecraft schedules are presented in section 5.

As part of the network development, the number of major test articles and their approximate configurations were defined. Therefore, another output of this analysis is an estimate of the procurement quantities associated with each concept. These quantities are also used for costing purposes as explained in subsection 4.4.

In constructing the overall Program Implementation Networks, only the spacecraft development activities and events are included. An analysis of the proposed launch vehicle, its integration, and the development of any necessary HEKS's is not considered appropriate to this study. However, events and times signifiying when launch vehicle procurement should be initiated and when the vehicles and the associated launch facilities should be available is included in the networks. Mission support facilities such as the DSIF are treated in the same manner.

Each of the various subsystems have been reviewed to determine (1) present status - availability, volume, weight, and performance; (2) problem areas with respect to development and testing; (3) possible interface problems with other systems on the spacecraft; (4) development needs, times, schedules; and (5) test requirements, schedules, facilities. The following classifications were made to establish the state-of-the-art.

(1) Breadboard

(2) Prototype

(3) Flying model

(4) Flying model, repackaged.

Since development of RTG's is a common requirement for each Jupiter flyby spacecraft design concept, its development is discussed in this section. The variations within spacecraft design concepts, namely the fuel procurement problems, are discussed in section 5.

4.3.1 Special Test and Mission Vehicle Requirements

To facilitate understanding of the material which follows, a synopsis of the test and mission vehicles planned into each of the Program Implementation Networks is given in Table 4.3-1. These configurations are similar to those used in the Ranger, Mariner R, and Mariner IV programs.

4.3.2 Radioisotope Thermoelectric Generator Development

4.3.2.1 Present Status of RTG

Since Pu 238 fueled, thermoelectric generators have been used successfully on board orbiting satellites, it can be stated that a prototype for the Jupiter flyby RTG exists. None of the materials, other than the fuel, are in short supply or require extraordinary consideration here. As to the fuel requirements, the following assumptions are made:

(1) No Pu 238 is required for the prototype models or for the first thermal control tests. Here, simulation by heater coils can be used.

(2) No fueled RTG's will be required for the launch environment test model (LETM) because, as specified elsewhere, the RTG will undergo component testing far in excess of the LETM requirements.

(3) Only flying models will be fueled with Pu 238.

(4) Fuel from the flying model used in the Special Test Model (STM) test will be transferred to the model used for the final Thermal Control Model (TCM) tests.

(5) All Pu 238 will be recovered and returned to the supplier with the exception of that used in the launched units and the material lost by radioactive decay.

4.3.2.2 RTG Problem Areas and Interfaces

The problem areas of the RTG power subsystem are (1) production and procurement of Pu 238 fuel, (2) radiation background from RTG

Table 4.3-1
SUMMARY OF SPACECRAFT HARDWARE REQUIREMENTS

SPACECRAFT	UTILIZATION	CONFIGURATION
Special Test Vehicles		
.System Test Model (STM)	Model will be used for testing subsystem interface compatability, RF interference, and general functional testing including hot fire tests and will likely undergo considerable modifications. The same model will later be used for flight acceptance (FA) testing of components, subassemblies and subsystems arriving for later test vehicles and mission spacecraft.	All first article subsystems are required during initial tests. However, RTG units can be removed and used on the TCM and some testing can be accomplished prior to receiving fueled RTG's. A considerable amount of redesign can be expected to emanate from these tests.
.Thermal Control Model (TCM)	This model will initially be placed in a space thermal-vacuum simulator for heat balances and control development. Later it will be used for Type Approval (TA) testing with overstressed environments to simulate an accelerated life test.	This test article will initially contain dummy subsystem heat sources and evolve into the flight configuration with all changes emanating from STM tests incorporated. Since this test must be accomplished after STM tests and the resulting modifications are incorporated, the STM RTG units can be used.
.Launch Environment Test Model (LETM)	Test of launch vibration, acoustical noise and shock environments.	This model can use dummy RTG units, otherwise the configuration should be the one established by the STM and TCM testing. Spacecraft can be considered "operational" after these tests are successfully completed.
Mission Spacecraft		
.Primary Mission (PMV)	Will be first launched	Complete Flight Qualified Vehicle
.Back-up Mission (BUV)	Will be launched on turnaround basis	Complete Flight Qualified Vehicle
.Proof Test Model (PTM)	Used at Mission Control as a diagnostic aid.	Complete Flight Qualified Vehicle

(interface aspects), (3) thermal balance of integrated spacecraft (interface aspects), (4) realistic life-testing and reliability-determination, and (5) internal pressure generation.

The number of RTG units and the total Pu 238 fuel required to meet spacecraft electrical power requirements of 240 and 480 watts (rating at end of mission) in the RDT&E phases of the program are listed in Table 4.3-2.

Table 4.3-2
RTG THERMAL WATT REQUIREMENTS FOR
240 AND 480 ELECTRICAL WATT POWER SYSTEM

End of Mission Power Capacity	240	480
Initial Electrical Watts/Unit	66	132
Number of Units/Spacecraft	4	4
Spacecraft Requiring Fueled Units		
Special Test Vehicles (STM & TCM)	1	1
Operational Spacecraft (PMV & BUV)	2	2
Total Fueled Spacecraft	3	3
Spacecraft x Units/Spacecraft	12	12
Total Thermal Watts Required at 5% Efficiency	15,800	31,600

NOTES: (1) STM & TCM use same fueled units.

(2) STM & TCM fuel used for PTM and for spare; fuel remaining in these 4 RTG's will be recovered.

Several factors affect the availability of Pu 238 fuel. The most important of these are (1) production capacity set by Np 237 and reactor space availability, (2) possible demands by other space programs, (3) necessary lag-time between order and final delivery, (4) shelf-life (determined by the growth of gamma radiation background and the normal decay of Pu 238), and (5) cost of the fuel (doubling production is estimated to quadruple costs).

Alan Streb, in Reference 4.3-1, indicates that 20,000 thermal watts of Pu 238 can be produced per year around 1970 (see Figure 4.3-1). A spacecraft requiring 480 watts of electrical power would require the total production for 1966, 1967 and 1968. In view of other probable priorities, it is not likely that this amount of fuel can be procured without accelerated production. The need for much more planning and coordination is indicated in this area.

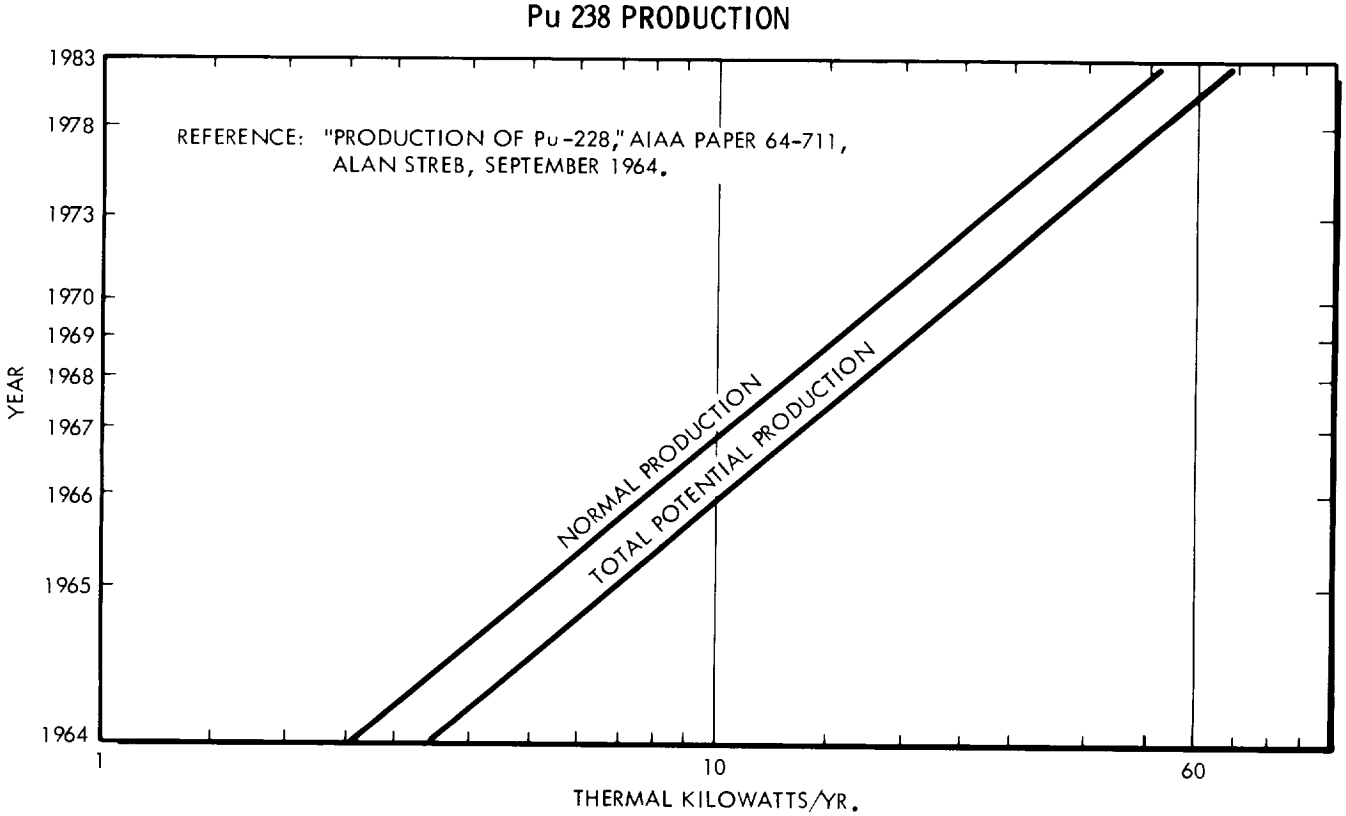

FIGURE 4.3-1

Streb (Reference 4.3-1) also estimates that five years would be required for final delivery of a 4000 watt system. Certainly, a 40,000 watt system will require as much time. Shelf-life of an RTG for the Jupiter probe will most likely be set by the growth of Tl^{208}. This substance greatly increases the gamma radiation background of the RTG and consequently increases the RTG's effect on radiation measuring instruments on the probe.

4.3.2.5 Test Requirements

The developmental tests established for the RTG are required to verify the capability of the subsystem to withstand the stress levels and environments encountered by the spacecraft.

Component-Level Tests - Components of the RTG subsystem will be subjected to structural strength tests, corrosion tests, and temperature and radiation tests. In some cases the parameter values are dependent upon the launch vehicle selected.

(1) Structural Strength Tests

Internal pressures to 40,000 psi

Drop and shock to 200 gravity units

Vibration from 100 to 400 cps over a 20 decibel range for 5 minutes

Thermal shock from +350°F to -300°F (drop into liquid nitrogen) with an internal pressure of 5000 psi

Explosive atmosphere - standard gasoline and air test

Leak test - requirements not known. Probably about 0.1% per day decrease in internal pressure

Acoustic noise - 120 db of 20 cps to 4800 cps for 30 minutes

Magnetic fields - Up to 10 gauss for 6 days.

(2) Corrosion Tests

Humidity test - 95% humidity at 160°F in air for 10 days

Water immersion test - immersion in salt water for one month

Sand/dust test - 0.1 g/ft^3 of dust at 100 ft/min velocity for 12 hours

Oxygen atmosphere test - 48 hours at 160°F in 100% oxygen.

(3) Temperature and Nuclear Radiation Tests

10^{12} proton/cm^2 sec for 10 hours in vacuum. Measurement of reflectivity of thermal control coatings before and after and during operation of the unit

Exposure to a 2000°F temperature for 5 minutes.

Explanations of tests - Over the life of the RTG's the peak pressure is estimated to be around 30-40,000 psi. In order to prevent bursting and the resulting contamination the RTG must be able to withstand the maximum internal pressure that will be generated by the fuel decay process. Drop and shock test values represent abort conditions which the RTG's must be able to withstand to avoid contamination. Vibration levels are consistent with launch vehicle characteristics plus some safety factor. Thermal shock values are those that might occur if an oxygen-fueled launch vehicle exploded and the RTG's were suddenly subjected to the cryogenicly stored fuel temperature. Leak test limits are set by the size of a hole which could release a significant amount of radioactive material. Acoustic noise specifications meet launch vehicle performance.

Humidity tests, sand/dust, and oxygen atmosphere tests are accelerated corrosion tests for determining the effects of normal handling in the pre-assembly stage. The water immersion test is designed to estimate the condition of an RTG recovered from the ocean after an abort.

The nuclear radiation test is designed to prove the thermal control surfaces and electrical equipment. The high temperature test is applied to verify that the RTG units can withstand re-entry into the Earth's atmosphere in case of an abort.

Except for the radiation effects tests, the component level tests will be accomplished in existing facilities.

Integrated Systems Tests for the RTG - Hazards, high costs, legal accounting, and a long lead-time for procurement are some of the factors that affect RTG fuel use. These factors cannot, however, be allowed to delay the integrated systems tests (see Figure 4.3-2). Some tests such as thermal control and other special systems tests require very long times (a minimum of 6 months and a maximum of 18 months) and should be started as soon as possible. By using simulated fuel, the integrated systems testing can be started about five months after go-ahead.

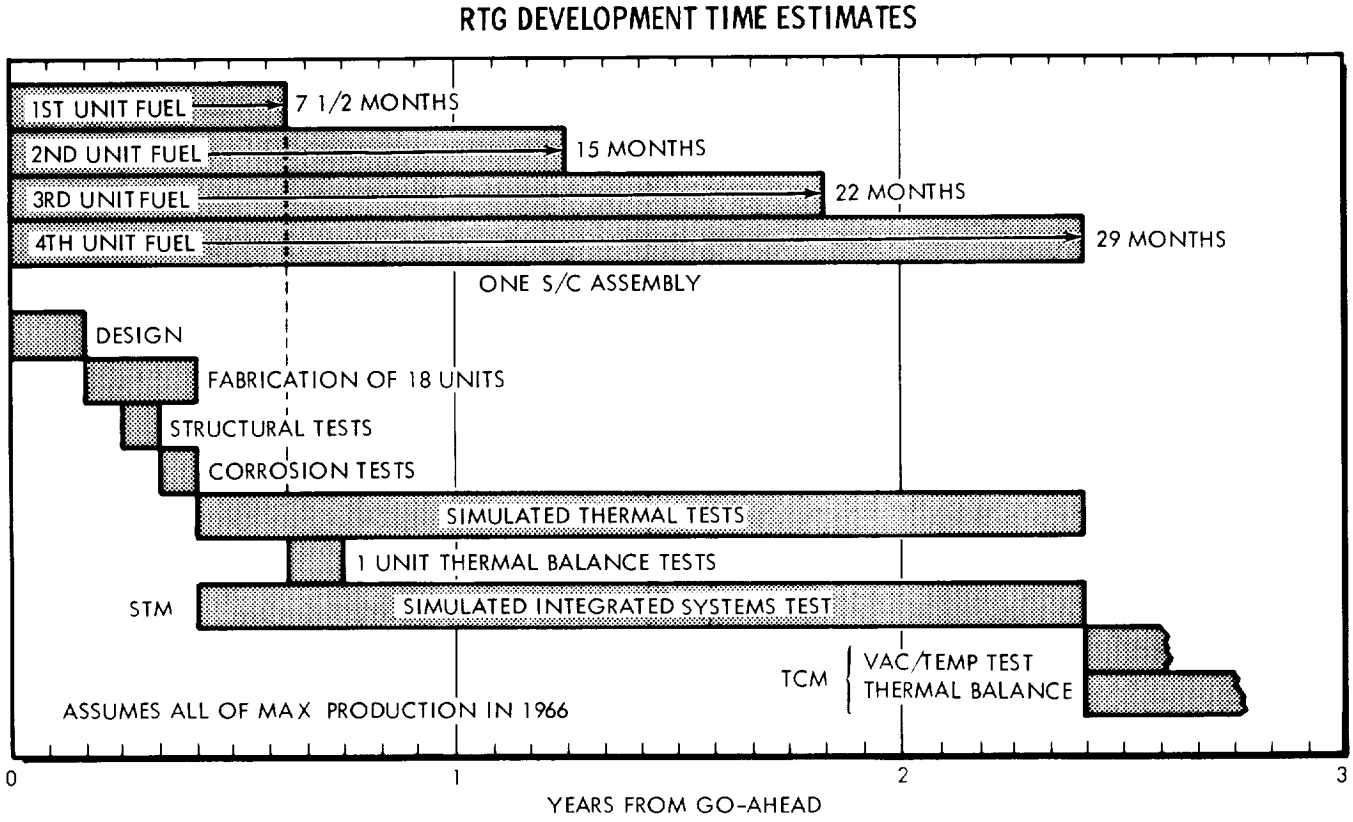

FIGURE 4.3-2

Interface problems are created by interactions of systems. The interface problems associated with the RTG arise mainly from the thermal and nuclear radiation environment of the subsystem. The nuclear radiation background from the RTG affects the instrumentation designed to measure the radiation fields in interplanetary and planetary space. Some of this background radiation is due to impurities in the fuel, and since radiation absorption and scattering processes are not accurately known, the resulting uncertainties must be resolved during the STM and TCM tests using fueled RTG's.

Jupiter is believed to have trapped radiation belts with intensities maybe a thousand times greater than those bound in the Earth's Van Allen belts. This belt may extend beyond 5 Jupiter radii. Such intense radiation is almost certain to be harmful to thermal control coatings, to thermal and electrical insulation, and to temperature control sensors associated with the RTG's. Radiation-effects testing, in vacuum, and with temperature control, requires at least six months of time.

4.3.2.6 Summary

The pacing item in the RTG development and testing program appears to be the Pu 238 procurement rate. This is shown clearly in Figure 4.3-2, Pu 238 production schedule (Figure 4.3-2). While much component testing can be accomplished by simulating the Pu 238 with electrical heaters, it is recommended that the final STM and TCM tests be made with RTG's. The reasoning which leads to this recommendation is outlined below.

Only in the integrated spacecraft is it possible to measure the thermal balances with flight-acceptable accuracy. Heat transfer factors, such as the pressure forcing two surfaces together are not always controllable. Corrosion can be a serious problem when thermal balance is involved. Whenever two dissimilar materials are in contact, corrosion is a possibility.

The radiation background of the Pu 238 RTG's is very unlikely to be known to better than a 20 percent confidence level. This is due to impurities, uncertainties in reaction and absorption cross sections, geometrical effects in radiation scattering, etc. If the background due to the RTG's is of the same order of magnitude as the phenomena to be measured in interplanetary space, special calibrations (prelaunch tests) are required on the completed spacecraft in a simulated interplanetary environment.

4.3.3 Science Subsystem

4.3.3.1 State-of-the-Art

Instrumentation state-of-the-art has been classified as breadboard, prototype, flying model, and flying model - re-packaged and on-board spacecraft. In terms of RDT&E time and effort, the four stages are estimated to constitute 30, 40, 20 and 10 percent of the total, respectively. These amounts may vary considerably on individual items.

The instrument systems considered to be applicable to Jupiter flyby missions (subsection 2.1) are listed in Table 4.3-3 and the SOA for each proposed system is rated. The ratings are based on the following assumptions:

(1) Any instrument whose specifications are not significantly different from those of a model already operated in space flight, such as on Mariner IV, is considered to be in the flying model phase.

(2) None of the equipment is assumed to be in the flying model, repackaged and on-board, condition, i.e., all require integration.

(3) Changes in size, power required, or weight of more than 10 percent from the specifications of instruments which have already operated in flight reduce the SOA to the prototype stage.

(4) Integration of the individual systems into a complete spacecraft is equivalent to repackaging.

(5) In a few instances, such as the TV-II camera, a changed specification results in the instrument being placed in the breadboard stage.

Table 4.3-3
SCIENTIFIC INSTRUMENT STATE-OF-THE-ART

SCIENTIFIC INSTRUMENT	SOA RATING
Extended Magnetometer	Flying
Cosmic Dust Detector	Flying
Energetic Particle Detector	Flying
Visible Photometer	Flying
Expanded Photometer	Prototype
Television Camera I	Prototype
Television Camera II	Breadboard
Plasma Probe	Flying
Microwave Radiometer	Prototype
Infrared Radiometer	Flying
Ion Chamber	Flying
Infrared Spectrometer	Prototype
High Energy Proton Directional Monitor	Prototype
Cosmic Ray Spectrum Analyzer	Breadboard
UV-Visible Spectrometer	Prototype
Medium Energy Proton Directional Monitor	Flying
Bistatic Radar	Breadboard
Radio Noise Dectertor	Prototype
Null Radio Seeker	Not Known
Radar Altimeter	Not Known

NOTE: References 4.3-2, 4.3-3, and 4.3-4 were used in making many of these ratings.

Development programs for space flight instrumentation have always centered on weight and volume reduction. A ten percent or greater change in size or weight specifications calls for a new model.

4.3.3.2 Development and Testing of Scientific Payloads

On the component level, some of the instruments in the breadboard stage may be expected to require several years of development time. This likelihood is due to the extreme environments (temperature, nuclear radiation, magnetic fields, vibration, etc.) and operation time. Estimates of development time for the five science packages considered in this study have been made and are listed below:

Spin-stabilized package - Three to five months

Minimal package - The prototype TV camera raises requirements to six to nine months

Intermediate 1 and 2 packages - One to two years will be needed because of the prototype models

Full package - From two to four years of development time is indicated by the 1000 line TV camera, the bistatic radar, and the cosmic ray spectrum analyzer.

Component level testing is not expected to reveal any unexpected or unusual requirements that might constitute problems. Similarly, testing facilities are not expected to present a problem. Too many units and too much time would be required to establish reliability by testing complete instruments for operation times in excess of 600 days. Therefore, reliabilities of the subsystems will be based on the reliabilities of the subsystem parts.

Specific tests for the components of the individual systems will probably be similar to those listed given for the RTG components. The time required should not exceed a few months.

The time required to develop and test the scientific instrumentation for the Special Test Model and the Temperature Control Model tests may be quite long. Factors which contribute to this situation are

(1) Thermal balance over a wide environmental temperature range

(2) Nuclear radiation background produced by the RTG's

(3) Nuclear radiation effects (dependent upon shielding, orientation, etc.)

(4) Magnetic field effects caused by equipment and spacecraft structure

(5) Vibration resonances due to structures and balance of the spacecraft

(6) Configuration requirements of directional sensors

(7) Possibility of late "freezing" of the scientific payload, as in the Mariner IV program.

4.3.4 Program Implementation Network and Schedule Preparation

4.3.4.1 Summary of Approach Used

The PERT diagram shown in Figure 4.3-3 was prepared for use in determining the many interacting and constraining activities and events required from program go-ahead to launch. Table 4.3-4 is a list of the abbreviations used in the network. The same network is used for each spacecraft design concept, because the events at the level of detail identified do not vary substantially with the different design concepts. Discussions in subsection 4.3.4.2 indicate where potential variations exist. Individual time estimates of the activities necessary to reach each event are presented for each of the concepts in section 5.

In making the time estimates, standard PERT procedures are used, i.e., three estimates are made: optimistic, most likely, and pessimistic. These estimates are based on historical data and engineering judgment.

The first task of the ASD PERT III analysis was to determine the critical path through the network. From this information, time can be counted backward from an assumed launch period to determine the start date that will allow each spacecraft to meet the launch date. Secondly, the available slack times are determined for the non-constraining events; i.e., those not in the critical path. From these data, time line charts are constructed for each concept to summarize the constraints, key milestones, and the total span-times. It should be noted that, in some cases, funding commitments can be delayed on some activities not in the constraining path. However, any decision to delay an activity must be weighed against the possibility that the need dates might not be met, and a schedule slippage would result.

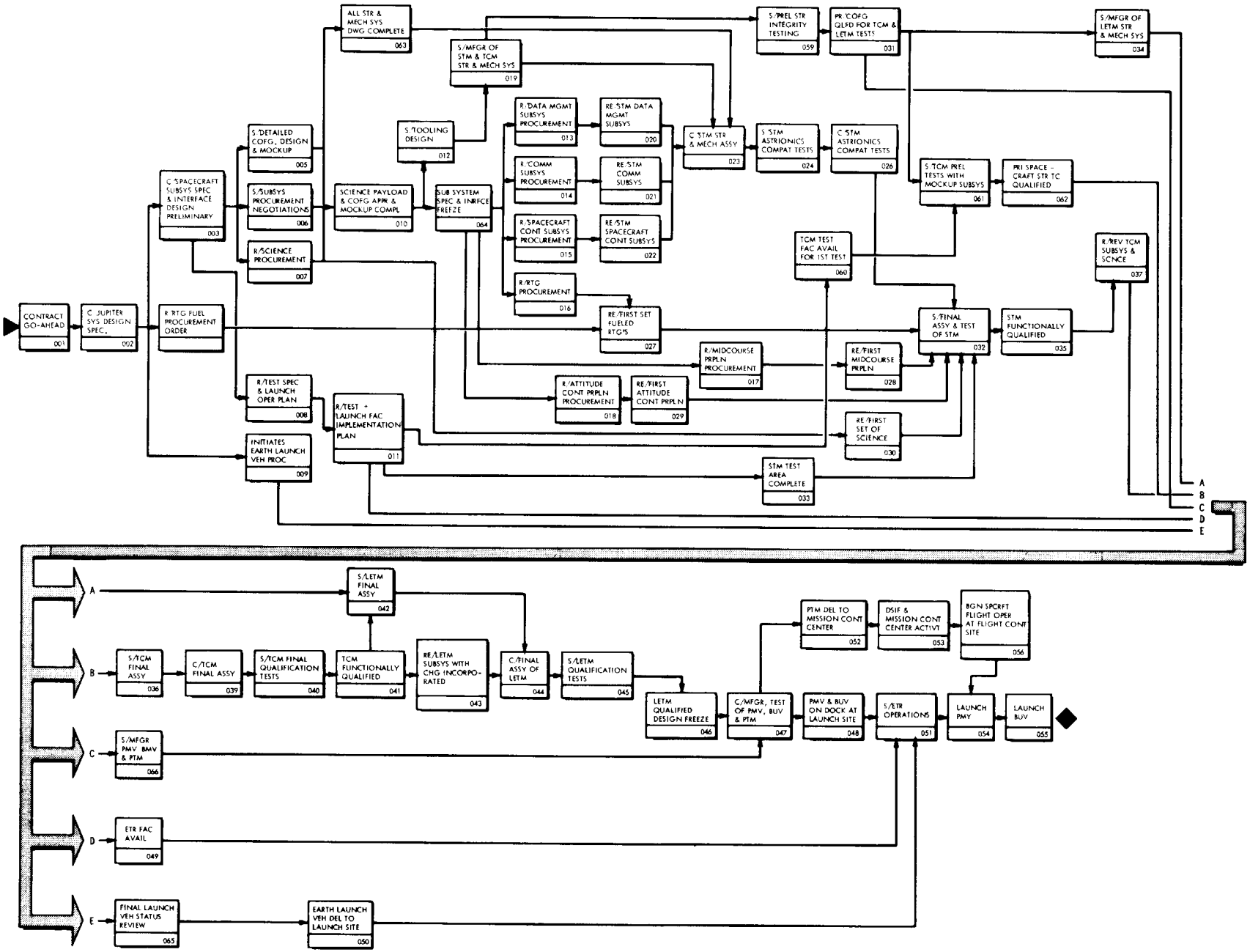

FIGURE 4.3-3 PROGRAM IMPLEMENTATION NETWORK

Table 4.3-4
ABBREVIATIONS USED ON FIGURE 4.3-3

ACTVT	Activated
APPR	Approved
ASSY	Assembly
AVAIL	Available
BGN	Begin
BUV	Backup Mission Vehicle
COFG	Configuration
COMM	Communication
COMPAT	Compatibility
COMPL	Complete
CONT	Control
DEL	Delivery/-ed/
DSGN	Design
DWG	Drawing
ETR	Eastern Test Range
FAC	Facilities
FLT	Flight
IMPLMTN	Implementation
INRFCE	Interface
INC	Incorporates
LETM	Launch Environmental Test Model
MCKUP	Mockup
MECH	Mechanical
MFGR	Manufacture
OPER	Operation/-al/
PMV	Primary Mission Vehicle
PREL	Preliminary
PRI	Primary
PROC	Procurement
PRPLN	Propulsion Subsystem
PTM	Proof Test Model
PYLD	Payload
QLFD	Qualified
R/	Release
RE/	Received
REV	Revised
RTG	Radioisotope Thermo-electric Generator
S/	Start
SCNCE	Scientific Payload
SPEC	Specification/-s/
SPCRFT	Spacecraft
STE	Site
STM	System Test Model
STR	Structure/-al/
VEH	Vehicle
SUBSYS	Subsystem/-s/
SYS	System
TC	Temperature Control
TCM	Temperature Control Model

An attempt is made to achieve better estimates of the probability of making the specified launch date than the standard PERT network analysis yields. This is done for two reasons: (1) the standard PERT analysis gives a point probability of making the schedule and (2) the PERT is believed to be biased too heavily toward the "most likely" time estimate (Reference 4.3-5). Therefore, the estimates along the critical paths of each concept are convoluted to obtain an estimate of the probability of meeting the schedule.

4.3.4.2 Program Implementation Network

The major events of the Program Implementation Network (Figure 4.3-3) and the philosophy followed in developing the network are discussed briefly in the following paragraphs. The network and the discussion are presented to illustrate the evolution of the program from go-ahead to launch.

From events 001 to 002, the design of the complete Jupiter flyby system is accomplished. This includes preparation of launch vehicle specifications and interface designs, launch facility needs and interface specifications, DSIF facilities, etc. When this system design phase is completed, procurement of long lead items such as the launch vehicle and RTG fuel can be initiated.

Also, after event 002, a preliminary spacecraft design can be accomplished, and the science payload defined to some extent (completion signified by event 003). Procurement and/or buildup of the instruments can then proceed as indicated by event 007. In parallel with the initial science procurement, the spacecraft detail configuration design can be accomplished, and the subsystem specifications finalized. This initial, parallel effort has been recommended because of the many early interactions that will likely exist between the spacecraft configuration and subsystem during definition of the science payload. It is recognized that this interaction will exist to some degree probably until somewhere near launch, but early, planned-in flexibility can make incorporation of changes at a late date much easier.

Also, using the data available at event 003, some preliminary subsystem procurement negotiations can be made and potential sources selected. In addition the preparation of test procedures and operational plans can be initiated.

Event 010 signifies that the spacecraft configuration and science has been approved and subsystem development can proceed. At this time, complete subsystem functional specifications and interface designs can be finalized and procurement action initiated as indicated by events 13-18 (detail networks for the subsystems have not been considered in this study). Also at event 010 the tool design necessary for manufacturing the composite spacecraft can be initiated.

Event 024 signifies the start of the integrated system tests. At this point the Systems Test Model (STM) structure, data management, communications, and the spacecraft control subsystems are assembled for what has been called an astrionics compatibility test. These tests have the external interfaces mocked up for a more realistic simulation. The science subsystem is not included in these preliminary tests because a gradual buildup of compatibility among subsystem interfaces results in a subsequent narrowing down of the problem areas. However, simple science packages, might be included in the tests without causing undue complications.

After the astrionics compatibility tests are complete, the other subsystems, namely, the RTG and midcourse and attitude control propulsion, are qualified along with the science. The entire spacecraft is functionally qualified as signified by event 035. Although fueled RTG's are shown as a constraint at the beginning of this test, much work can be accomplished using an external power source. However, because of the potential radiation effects problem (see subsection 4.3.2.5), an actual unit is deemed necessary before the complete spacecraft can be functionally qualified.

The procurement times for Pu 238 RTG fuel is estimated as follows. The production rates are assumed as shown in Figure 4.3-1. The optimistic time is obtained using the assumption that one-half of the accumulated, accelerated production is available at program go-ahead. The pessimistic estimate represents one-fourth of accumulated present production. The nominal is the average between the pessimistic and optimistic estimates. Only RTG's for the PMV, BUV, and PTM spacecraft are considered to be fueled before the first launch. As discussed in Section 5, some flexibility and further study is needed in this area.

After the STM assembly is functionally qualified using Type Approval (TA) components, the STM is used for acceptance testing of the Flight Article (FA) for both the remaining test vehicles and flight vehicle as well.

Almost in parallel with the STM manufacture and test, a Temperature Control Model (TCM) and its ensuing testing effort is evolving. At event 059, a series of preliminary structure tests begins in order to verify that the structure and mechanical designs are sound. Because of the structural changes which will evolve from this effort, the thermal testing is held up until event 031 is reached. At this point the primary structure and mechanical subsystem are considered functionally qualified.

Simulated heat sources and heat flow paths such as electrical wiring are then added to the structure, and the TCM tests begin as shown by event 061. These tests proceed to event 062. During this testing effort, the many unknown temperature control problems are solved as they are encountered, and designs are revised accordingly. One particular problem to be resolved is in achieving the desired flexibility in placement of the louvers to handle different scientific payloads. Finally, at event 036, a temperature control test is conducted on a complete vehicle. This is again the same vehicle except for a full complement of live subsystems with the changes emanating from the STM tests incorporated. However, it is assumed that the STM RTG units are reused for these tests. Although the subsystems are temperature-qualified at the component level before these tests, the tests on the composite vehicle will uncover the interface problems that subassembly level testing cannot. In particular, the effects and control of the RTG heat source.

A minimum of 200 hours in the vacuum-thermal simulation chamber is an estimate for the thermal balance control tests. The Ranger spacecraft, for example, are reported to have required 750 hours of time in the simulation chamber. Each run of several hours requires several weeks of setup and analysis. In addition, there will likely be problems in scheduling the use of simulation chambers. This scheduling problem can be serious because of the "test and fix" technique that must be employed. Due consideration should be given to detailed planning of chamber utilization between events 008 and 011.

Event 041 signifies the point where the TCM configuration is accepted as being qualified for the mission environment. During these tests, changes are continually integrated into the spacecraft design, and at event 042, the launch environmental tests discussed in the following paragraphs are begun.

The manufacture of the Launch Environmental Test Model (LETM) starts after event 031, which has been defined as the point where the primary structure and mechanical subsystems are deemed qualified for flight. The major purpose of the LETM is to qualify the complete spacecraft for all expected vibration, shock, and acoustic environments. The most serious, of course, being the launch environment. Since none of the launch vehicles considered at the present time have been flown and no firm programs exist for their integration and test (with the exception of the Saturn V), some extrapolation of data and wind tunnel testing will likely be necessary to establish the qualification test levels. This same data

are required for the detail design activity between events 005 and 063, the structural testing effort between events 059 and 031, and to set subsystem specifications. Therefore, if wind tunnel testing is required, it should be scheduled soon after event 002.

The configuration of the LETM should incorporate all the changes emanating from the preliminary structure testing (events 061 to 062), the STM tests, and the TCM tests. Once it is functionally qualified and the changes incorporated into the overall spacecraft design, the design is frozen at event 046. The manufacture of the Primary Mission Vehicle (PMV), the Back-up Mission Vehicle (BUV), and the PTM can then be completed (event 047). It should be noted that the manufacture of these vehicles is actually initiated at event 066 after the primary structure and mechanical systems are qualified (event 031). Changes can be made from the parallel testing effort at appropriate times between events 047 and 066.

After complete checkout at the manufacturing sites, the PMV and BUV are shipped to the launch site (events 047 to 048). Approximately at this same time, the launch vehicle component parts should also be available at the launch site and the launch operations will commence at event 051. This is not a single event as shown and will actually be a gradual buildup of activity. For the purpose of this analysis, a single event is considered adequate.

Parallel with the preparation at the launch site, the PTM that is to be used as a diagnostic aid during the actual mission is shipped to the mission control center (probably Goldstone), placed into operation, and the inflight mission ground support operations begin at event 056.

At event 054, the PMV is launched, and assuming a 2 week turnaround time, the BUV is launched as shown by event 055. Obviously, to achieve this turnaround time, the BUV and its launch vehicle would have to be in a near launch status. What impact this will have on the launch facilities is not known, but the effects should be defined and any corrective action planned between events 008 and 011. The rather arbitrary launch period of 20 days adopted for this study dictated the 14-day turnaround time.

In the above discussion, an attempt has been made to explain the major activities, constraints, and interactions associated with the development and launch of a Jupiter flyby spacecraft. Admittedly, more remains to be done before a detail implementation plan can be developed. As the program progresses beyond the conceptual stage, better time estimates and more detail can be added to the plan. In addition, test descriptions and operational activities can be detailed more completely.

4.3.5 Referances

4.3-1 Streb, Alan J., "Radioisotope Power Systems for Manned Space Stations," AIAA Paper No. 64-711, September 1964.

4.3-2 Fawcett, W. G., Schutz, F. L., Sloan, R. K., and Trostle, H. G., Astronautics & Aeronautics, October 1965, "Scientific Exploration with Mariner IV."

4.3-3 "Mariner C Information for Future Mission Studies," Jet Propulsion Laboratory Engineering Planning Document 296, 15 Apri1 1965.

4.3-4 Design Data Information System, Jet Propulsion Laboratory, 1 October 1965.

4.3-5 Hartley, H. O., and Wortham, "Assessment and Correction of Deficiencies on PERT," Institute of Statistics, Texas A&M University, College Station, Texas.

4.4 COST ANALYSIS

The objective of the cost analysis presented in this subsection is to provide a plausible and consistent cost evaluation of (1) costs in terms of spacecraft subsystems parameters and (2) cost estimates based on the concept design point.

4.4.1 Subsystem Cost Methodology

The cost methodology used in the assessment of the Jupiter flyby spacecraft subsystems is directed toward determining a range of values for each set of cost estimating parameters. Although no formal cost methodology is presently available, the method used herein has been developed from a combination of two independent approaches to the costing problem, (1) the cost estimating technology that developed at the Fort Worth Division of General Dynamics for previous space system studies and (2) the techniques which have been recently published in the Air Force Systems Command Space Planners Guide, Reference 4.4-1.

Before the cost estimating relationships (CER's) presented in the Space Planners Guide were used, the applicable CER's were evaluated by comparing derived estimates with available cost data on similar spacecraft subsystems and with results obtained from the use of in-house CER's. The costs derived in the evaluation of the Space Planners Guide CER's were found to be highly correlated with the costs of the respective subsystems of various existing, unmanned spacecraft.

Cost estimating relationships are used in the analysis of the following representative major cost items: the design, test, and evaluation (D,T,&E) costs, the unit costs of the spacecraft subsystem hardware, the costs of operational support equipment (OSE), tooling and special equipment costs, system integration costs, and ground test hardware costs. The methods used to determine each of these cost items are discussed in the following paragraphs.

4.4.1.1 Science Subsystem

One of the most significant and sensitive cost elements among the spacecraft subsystems is the cost of the science subsystem. In this study, the general approach used to develop the cost of the science subsystem is based upon subsystem cost as a function of weight. In this approach, the state-of-the-art development of each instrumentation component is estimated (Subsection 4.3.1), and the percent of the total cost to completion is used to determine an equivalent weight to completion. When the equivalent weight value is known, the D,T,&E costs can be derived by use of the cost estimating relationship provided for the science subsystem in Figure 4.4-1. In the CER for unit costs, which is also shown in this figure, the total subsystem weight is used to obtain the estimated cost.

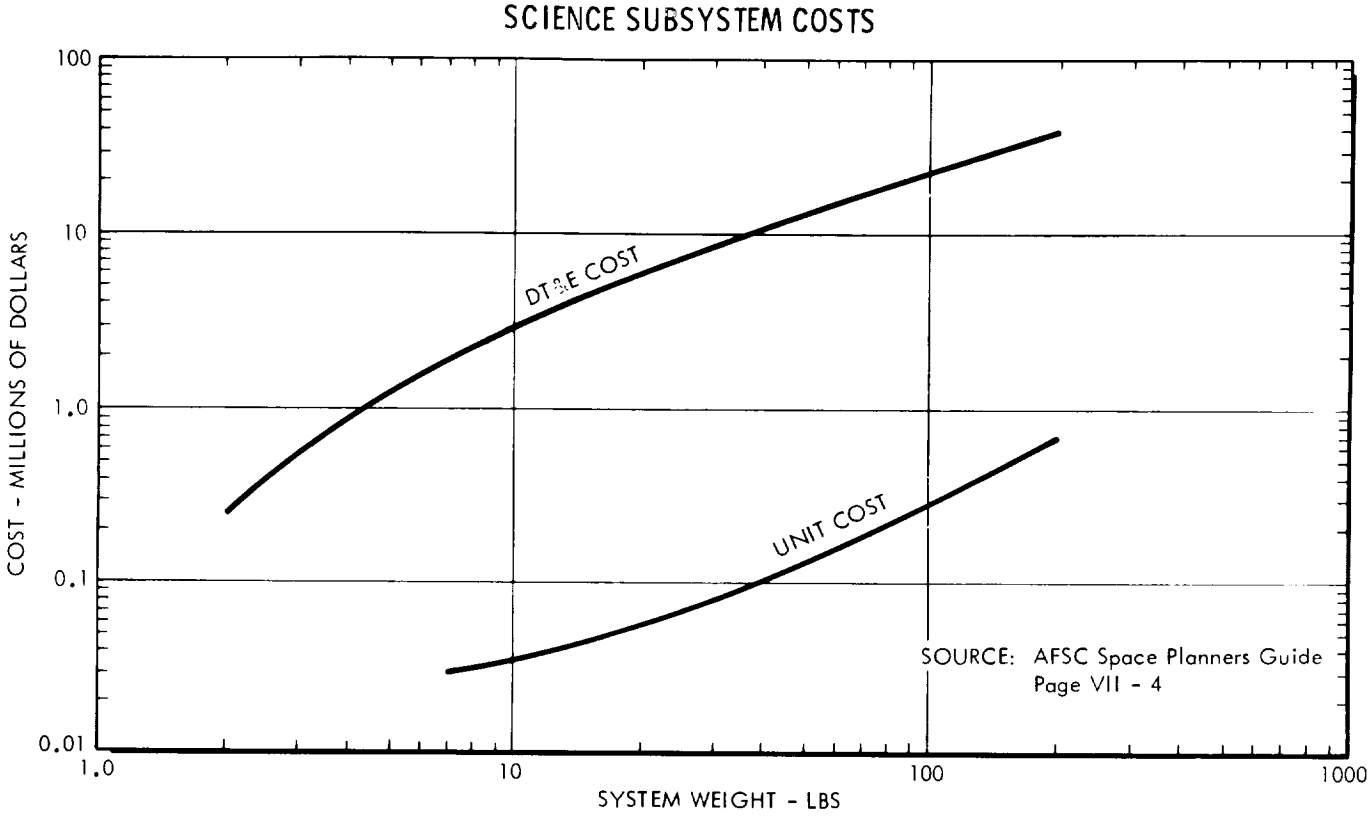

FIGURE 4.4-1

4.4.1.2 Electrical Power Subsystem

Another costly subsystem to develop for a Jupiter flyby spacecraft is the electrical power subsystem, particularly the radioisotope thermoelectric generators (RTG). The costs of the Pu 238 fuel source are potentially more costly than the development costs. This cost is a "sunk cost" in the sense that it is not recoverable once the spacecraft has been injected into escape velocity. There is a considerable amount of uncertainty in regard to the cost of manufacturing the Pu 238 fuel. Although there are a number of alternatives in supplying Pu 238, a concensus among unclassified sources generally estimates the range to lie between $500 and $3000 per thermal watt.

Since the cost of the Pu 238 radioisotope is relatively expensive and the isotope has such a long half-life (approximately 90 years), it is believed that it is reasonable to assume that the using agency should be charged a "rent" for the use of this resource when the isotopes are to be recovered, as in development tests. The rent could possibly be based on the pro rata depletion of the fuel during the time it was in use. For example, in Figure 4.4-2, it is shown that the relative fuel half-life remaining after a five-year development program is approximately 0.96; thus rent for the use of fuel would be four percent of the imputed fuel cost. Fuel costs are discussed further in subsection 4.4.3.1.

The cost estimating relationships used for the D,T,&E and unit costs of the RTG, fuel capsule, and power conditioning equipment are depicted in Figure 4.4.3.

4.4.1.3 Communications and Data Management Subsystems

Among the communications subsystems comprising the available historical cost data, it was found that the components making up the data management subsystem (i.e., encoder, command, and data storage) are generally included as part of communications. Therefore, the communications and data handling subsystem design, test, and evaluation and unit costs were derived by aggregating the weights of two subsystems (see Figure 4.4-4).

4.4.1.4 Spacecraft Control Subsystem

The costs for the spacecraft control subsystem are made up of two basic costing elements, (1) the sensors used for attitude reference and navigation and (2) the computer (CC&S) and electronics. The costs of the primary sensing instruments are determined by using the CER's shown in Figure 4.4-1 since these sensors are in a class similar to that of the sensors in the science subsystem.

The costs of the CC&S and attitude electronics are derived from a Space Planners Guide CER (Figure 4.4-5) representing several components which include the computer, the buffer and tape storage, switching and multiplexing, analog-digital-analog conversion, and signal conditioning. Since some of these components are considered a part of the data management subsystem in this study, it is possible that the spacecraft control subsystem development costs are overstated by an amount equal to costs that are understated for the communications and data handling subsystems. However, on the basis of the sources that were available, the cost breakout of these components is not possible.

4.4.1.5 Structure, Mechanical Devices, Thermal Control, Radiation Shielding and Meteoroid Shielding

The costs of the spacecraft structure also include the subsystem costs of the mechanical devices, thermal control, meteoroid shielding, and radiation shielding since these are closely, if not inseparably, related to the structure. The costs for the spacecraft structure are derived from the cost estimating relationship presented in Figure 4.4-6.

4.4.1.6 Midcourse Propulsion Subsystem

The DT&E and unit costs of the midcourse propulsion subsystem are determined on the basis of the expected engine thrust in a vacuum. The cost estimating relationships used for obtaining the costs are shown in Figure 4.4-7.

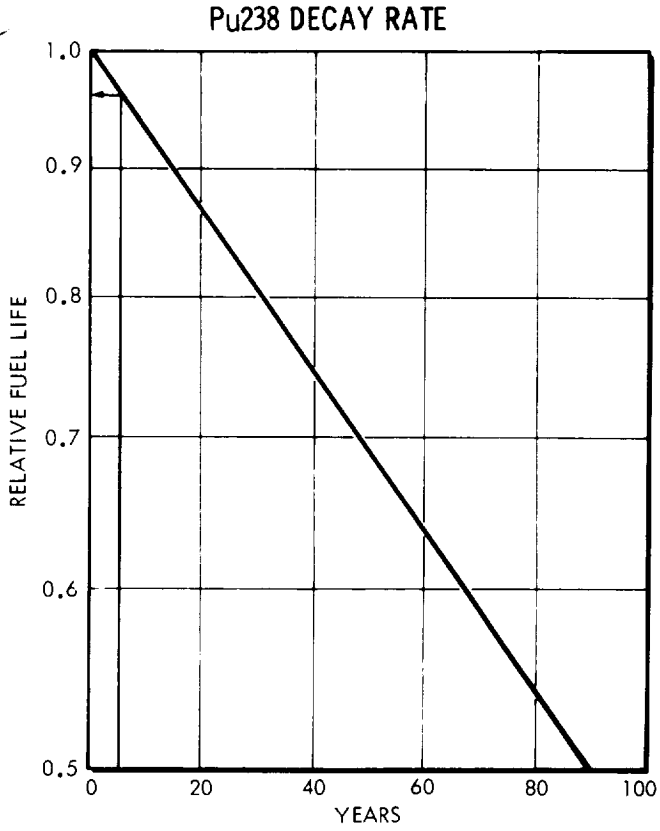

FIGURE 4.4-2

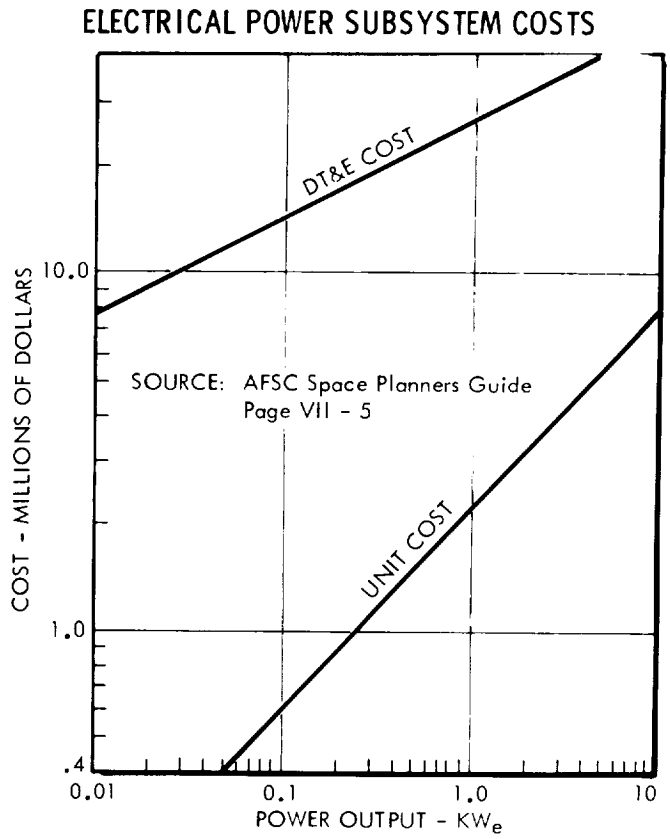

FIGURE 4.4-3

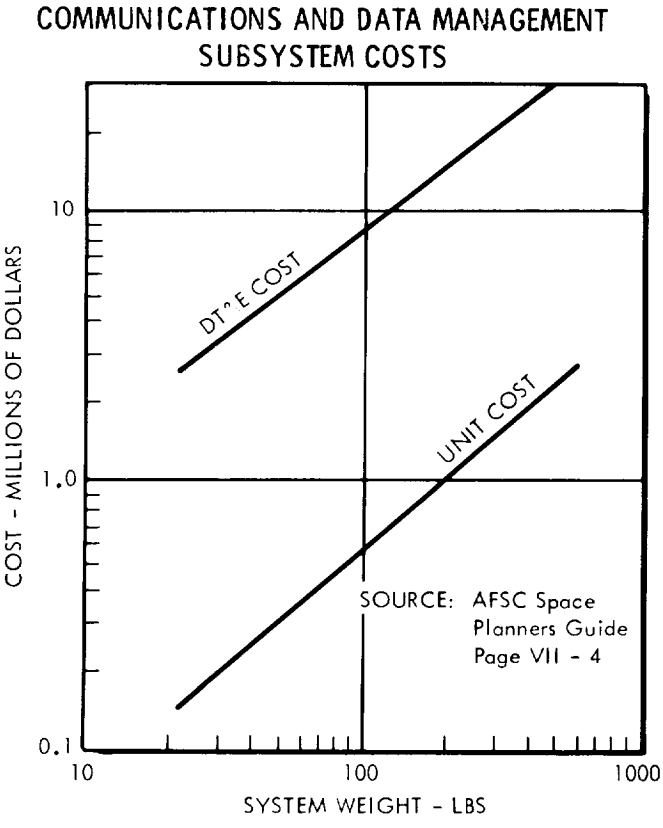

FIGURE 4.4-4

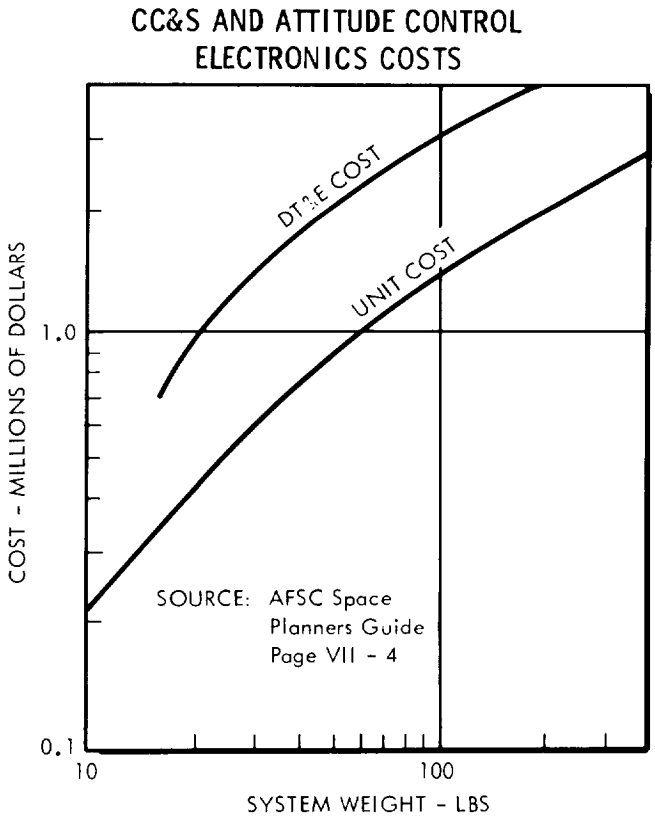

FIGURE 4.4-5

4.4.1.7 Attitude Control Propulsion Subsystem

The final subsystem CER is the attitude control propulsion subsystem costs, as shown in Figure 4.4-8. The costs of the sensor and electronic portion of attitude control are discussed under the spacecraft control subsystem (subsection 4.4.1.4).

4.4.2 Nonsubsystem Cost Estimating Relationships

In addition to the subsystems costs, there are other major cost items for which cost estimating relationships were developed or adapted for use in this study. Among these cost items are costs that are incurred during the development program for operational support equipment, tooling and special equipment, system integration, and ground test subsystems.

4.4.2.1 Operational Support Equipment

One of the more difficult costs to estimate with regard to an unmanned spacecraft program is the cost of the operational support equipment. In the past, equipment that has been used in the development of the subsystems and the spacecraft as a whole has also been used as operational support equipment. Therefore, the costs of this equipment may be mingled with the development costs of the subsystems (e.g., the electrical power subsystem). In the Space Planners Guide, the CER that is believed to provide the best approximation of costs for operational support equipment is that provided for aerospace ground equipment (AGE). This CER is depicted in Figure 4.4-9.

4.4.2.2 Tooling and Special Equipment

Cost items that are often neglected in the conceptual phases of a program are the estimates related to tooling and special equipment. Although tooling costs may be estimated by means of a relatively straight-forward approach, it is difficult to generalize about such items as special equipment. However, historical data can be used to demonstrate a general relationship between spacecraft dry weight and the cost of tooling and special equipment. The CER shown in Figure 4-4-9 was based on the Space Planners Guide.

4.4.2.3 System Integration

Another cost that is difficult to pinpoint is the cost incurred in integrating the spacecraft subsystems into an operable system. As in the case of the operational support equipment costs, the integration tasks and their costs are difficult to isolate from the development of subsystems and other items unless specific contract information and other historical cost data are available. The CER for estimating the integration costs is shown in Figure 4.4-9 as a function of dry weight of the spacecraft.

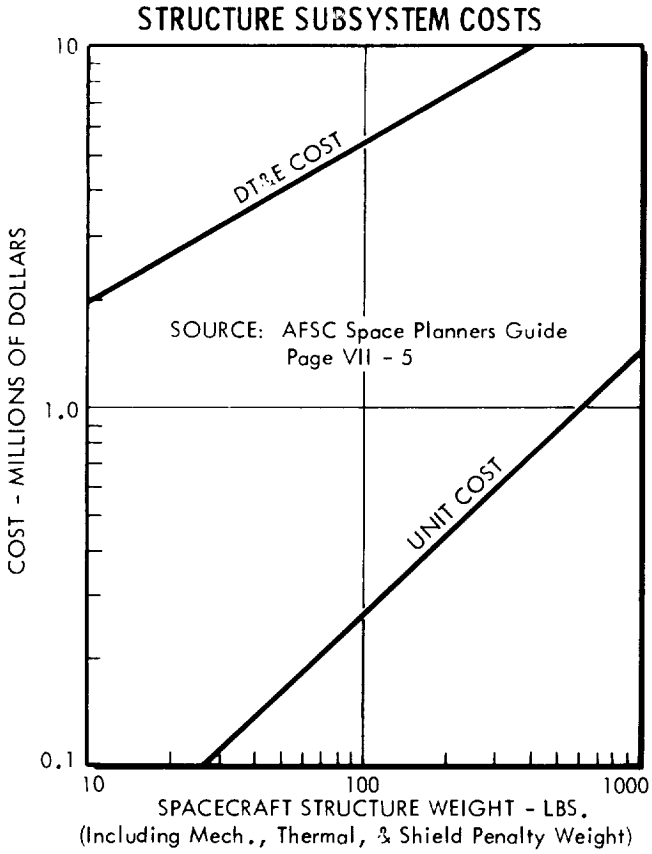

FIGURE 4.4-6

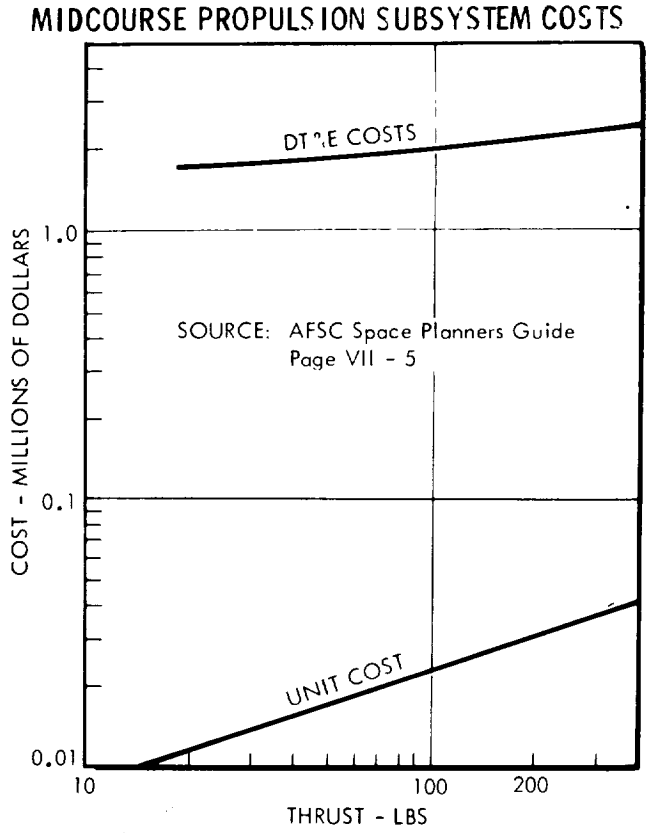

FIGURE 4.4-7

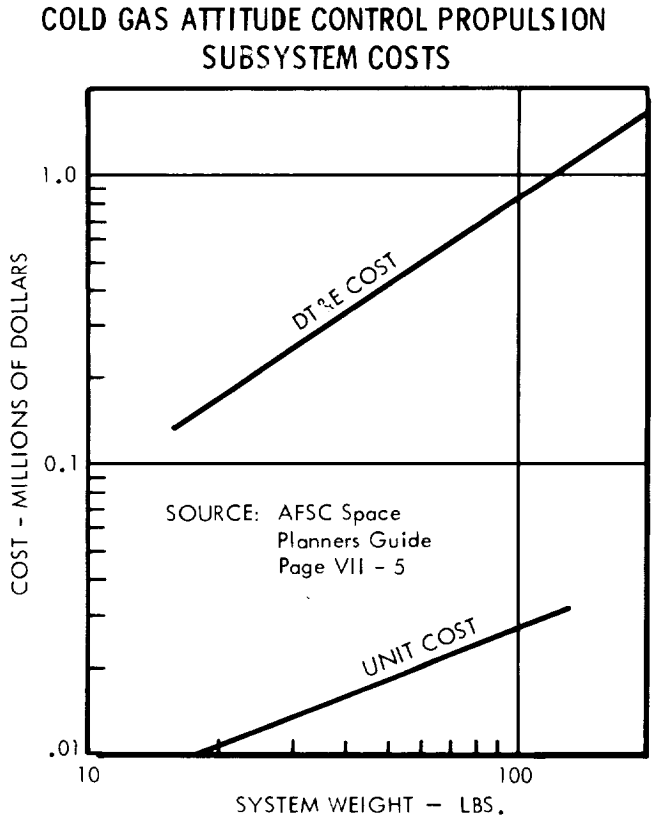

FIGURE 4.4-8

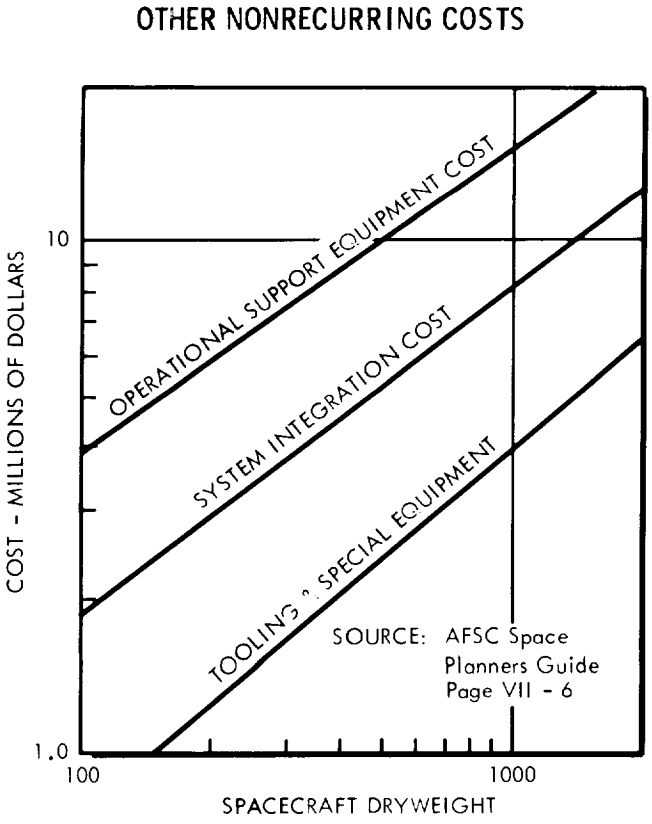

FIGURE 4.4-9

4.4.2.4 Ground Test Subsystems

The costs of the ground test subsystems are obtained by multiplying the unit cost estimate used for each subsystem by the number of units to be used in testing. Unit costs are determined by entering the appropriate CER with the desired specific value of the cost estimating variable. The quantities of test hardware are determined in the analysis of development requirements (subsection 4.3). There is no learning curve applied to the unit costs since the nature of this type of program is such that a learning curve effect can seldom be demonstrated on the basis of the small quantities that are involved.

4.4.3 Operational Cost Methodology

Certain major costs are incurred before and during the operational flight of the spacecraft, and they recur in the case of some items with each additional flight. Among these operational costs are recurring spacecraft costs, spacecraft spares, deep space net support, spacecraft operations support, launch vehicles, and launch vehicle operations.

4.4.3.1 Recurring Spacecraft Costs

The costs of the operational spacecraft for a Jupiter flyby mission are presented in this category. The recurring spacecraft costs are computed by summing the unit costs that are derived from the CER's used for each subsystem. Added to the total of the unit costs is the cost for spacecraft checkout and assembly. The CER used for spacecraft checkout and assembly is presented in Figure 4.4-10. A final item to be included in this category is the cost of the RTG fuel. Since the cost of Pu 238 may range from $500 to $3000 per thermal watt, the RTG fuel cost is a major part of the total recurring spacecraft cost. In Figure 4.4-11, the total fuel cost for electrical power outputs of interest is shown in terms of varying costs of fuel.

4.4.3.2 Spares Costs

The cost of spares for the operational phases of a Jupiter flyby mission are based on the assumption that two sets of spares are required. The spares include two of each subsystem with the exception of the RTG and the structure. Since there are generally two, three, or four RTG units on each spacecraft, only two units are set aside as spares.

There are no structure subsystem spares included in the cost. Spares costs are computed in the same manner as recurring spacecraft costs except that the costs for checkout and assembly and for RTG fuel are not included.

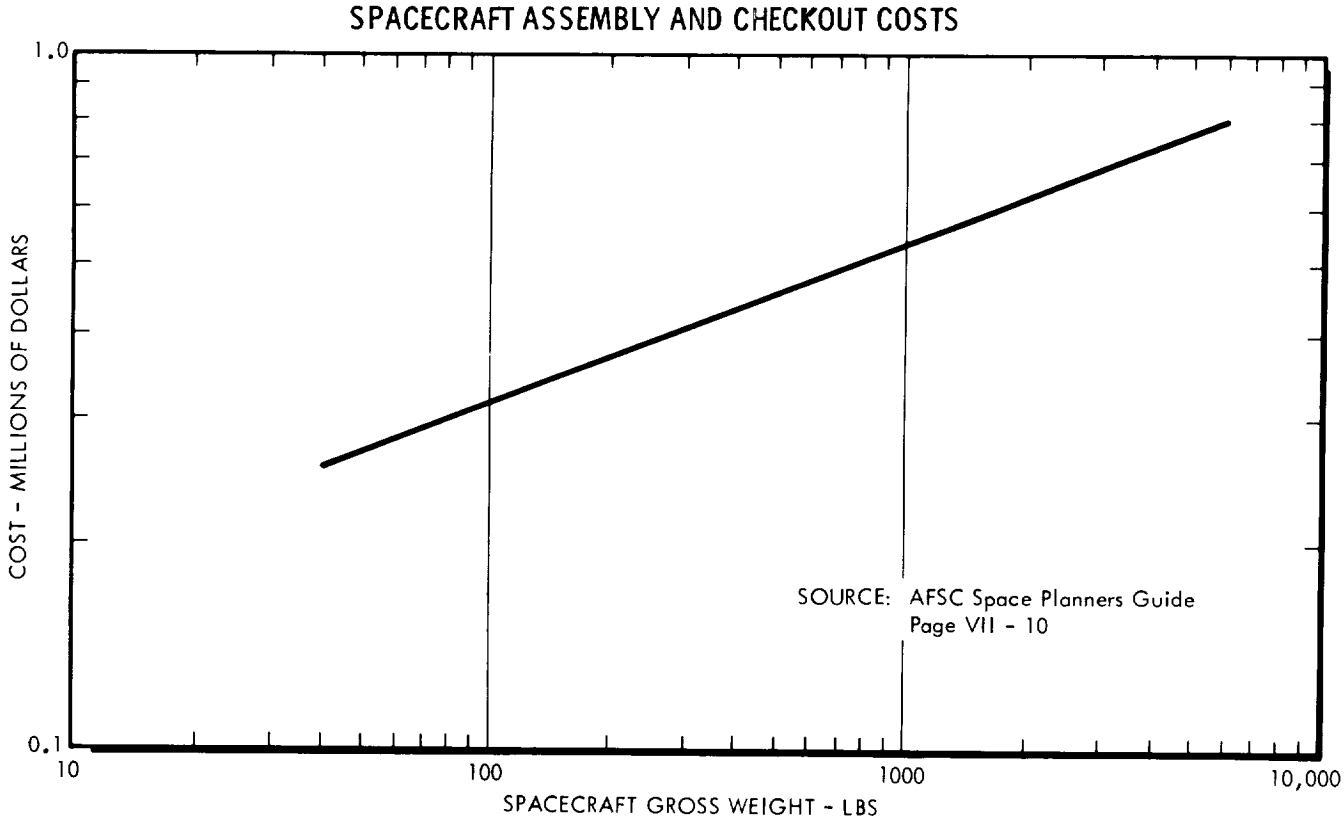

FIGURE 4.4-10

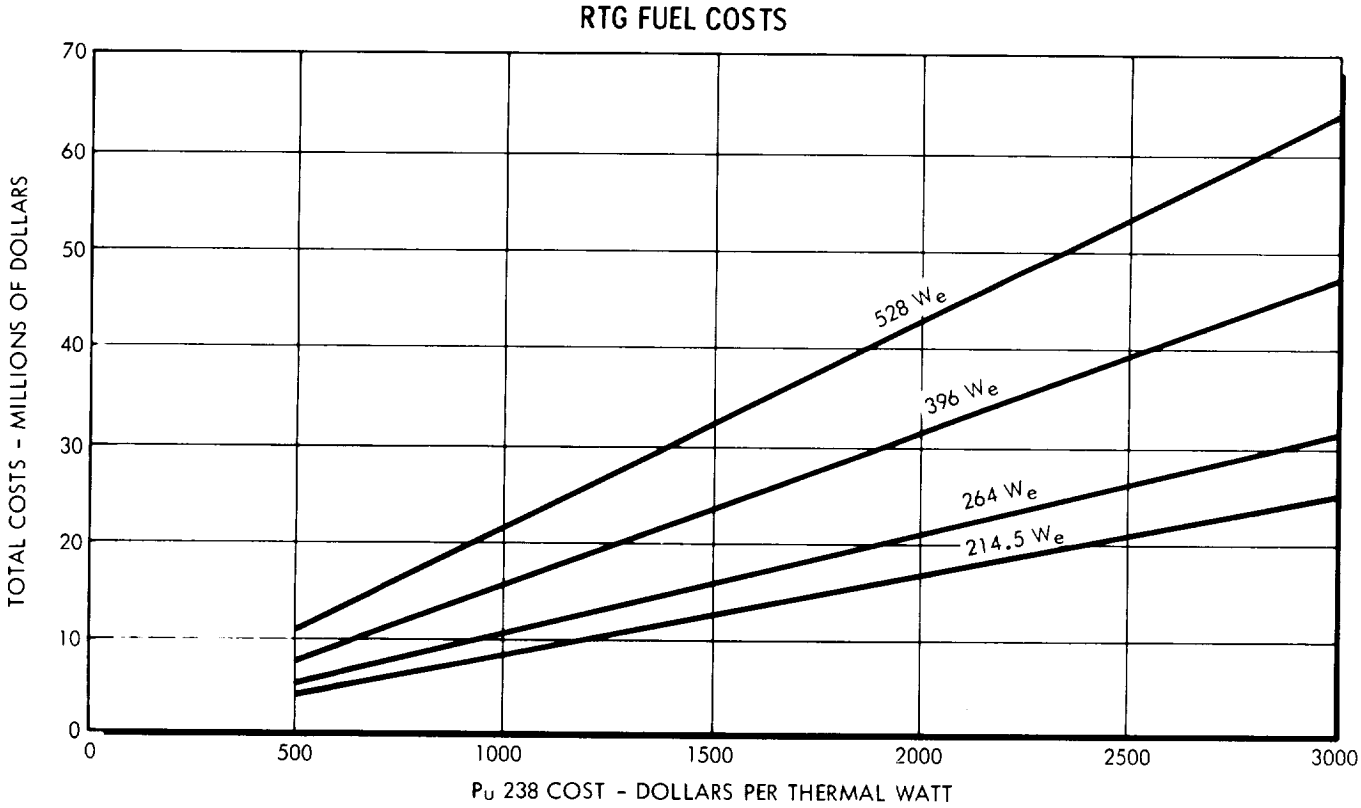

FIGURE 4.4-11

4.4.3.3 Deep Space Net Support

A significant cost that is incurred during the operations phase of a Jupiter flyby mission is the cost allocated for Deep Space Net support. On the basis of the cost data related to Mariner IV, a CER was developed to relate cost to mission flight time (see Figure 4.4-12).

4.4.3.4 Spacecraft Operations

In general, the spacecraft operations cost item covers a number of the activities that are carried on during the mission at the Space Flight Operations Facilities and in laboratories. The specific activities represented in this category include spaceflight operations, system analysis, spacecraft support analysis, film reports, technical documentation, and computing. The CER presented in Figure 4.4-12 was developed for obtaining spacecraft operations costs by estimating cost as a function of the length of the mission.

4.4.3.5 Launch Vehicle Costs

The launch vehicle hardware costs are based on the assumption that the vehicle is available and that no development is required. Included in the costs of the launch vehicle are costs

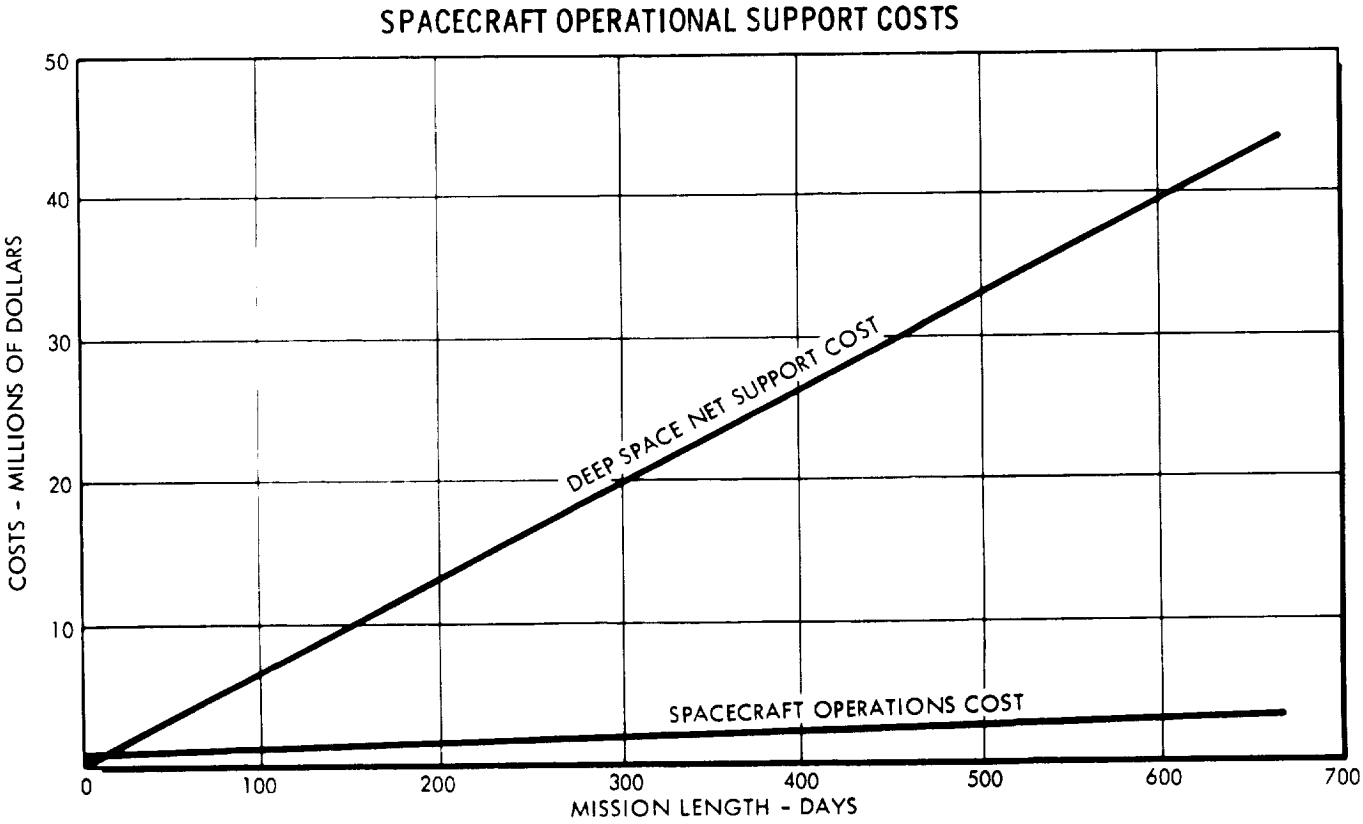

FIGURE 4.4-12

for all stages of the vehicle, including the upper stages, such as the Centaur and HEKS. Also included are the costs of vehicle adapters and aerodynamic shrouds.

The costs for the launch vehicle were determined from CER's developed by the Fort Worth Division. The costs for the four most likely launch vehicle candidates are listed in Table 4.4-1.

Table 4.4-1

LAUNCH VEHICLE COSTS
(Cumulative Average Cost in Millions of 1965 Dollars)

LV Type / Cost Elements	Atlas SLV 3x/ Centaur HEKS		Titan III Cx/ Centaur		Saturn 1B/ Centaur HEKS		Saturn V	
	Cum. No.	Cost	Cum. No.	Cost	Cum. No.	Cost	Cum. No.	Cost
Basic Vehicle	20	2.50	20	14.90	10	22.5	10	62.50
Centaur	22	6.32	22	6.32	22	6.32	-	
HEKS	10	1.72	-		10	1.72	-	
Adapter & Shroud	10	0.16	22	0.19	10	0.26	10	0.27
TOTAL		10.70		21.41		30.80		62.77

4.4.3.6 Launch Operations Costs

A second cost that is associated directly with launch vehicles is the launch operations cost. This cost is incurred during the prelaunch and boost phases. The cost includes the launch vehicle transportation, assembly, check, propellant, technical direction, and the direct launch costs. This cost is estimated by using actual NASA launch operations cost data.

4.4.4 Reference

4.4-1 U. S. Air Force Systems Command, Space Planners Guide, 1 July 1965.

SECTION 5

SPACECRAFT DESIGN CONCEPTS

This section contains the design details of four Jupiter flyby spacecraft concepts as evolved during the Jupiter Flyby Mission Study. Specifically, design concepts of the science, communications, data management, spacecraft control, attitude control, propulsion, and electrical power subsystems are described for each spacecraft. Consideration is given to the thermal control, radiation protection, and meteoroid protection of each spacecraft and the configuration, structural, and mechanical characteristics of the design concepts are delineated. Estimations of the reliability of the various subsystem equipments are listed. Finally, the spacecraft design concepts are evaluated in terms of performance, probability of mission success, development requirements, and cost.

At the beginning of the study, it was apparent that several spacecraft design concepts and many variations of these design concepts are possible candidates for a feasibility study. Thus, it was necessary to make decisions as to which design concepts should be pursued, and these decisions resulted in the four spacecraft described in this section. Detailed discussions of the alternative spacecraft design concepts and the reasoning used in eliminating them from consideration are presented in subsection 1.4 and are not repeated here. Rather, the four spacecraft are presented on their own merits without general comparison to other design philosophies.

In short, the spacecraft design concepts described in this section are believed to cover a range of alternate design concepts for accomplishing the mission objectives outlined in subsection 1.1. The concepts are felt to represent feasible designs and are considered to be competitive with any other design concept of equal mission capability.

5.1 SPACECRAFT DESIGN CONCEPT A

In this section, a spin-stabilized Jupiter flyby spacecraft, denoted as Design Concept A, is described.

5.1.1 Design Summary

A configuration of Spacecraft Design Concept A is illustrated in Figure 5.1-1. The concept is governed by a philosophy of spin-stabilization, and its scientific capability is limited. The injected weight of the spacecraft is approximately 530 pounds. When the Atlas SLV3x/Centaur/HEKS booster is used, potential Earth-Jupiter flight times range upwards from 460 days for missions in the 1973-1980 time period. Use of the Titan IIICx/Centaur makes possible flight times equal to or greater than approximately 490 days for missions in the 1973-1980 time period. Significant flight events for a nominal mission are detailed in Table 5.1-1.

SPACECRAFT DESIGN CONCEPT A CONFIGURATION

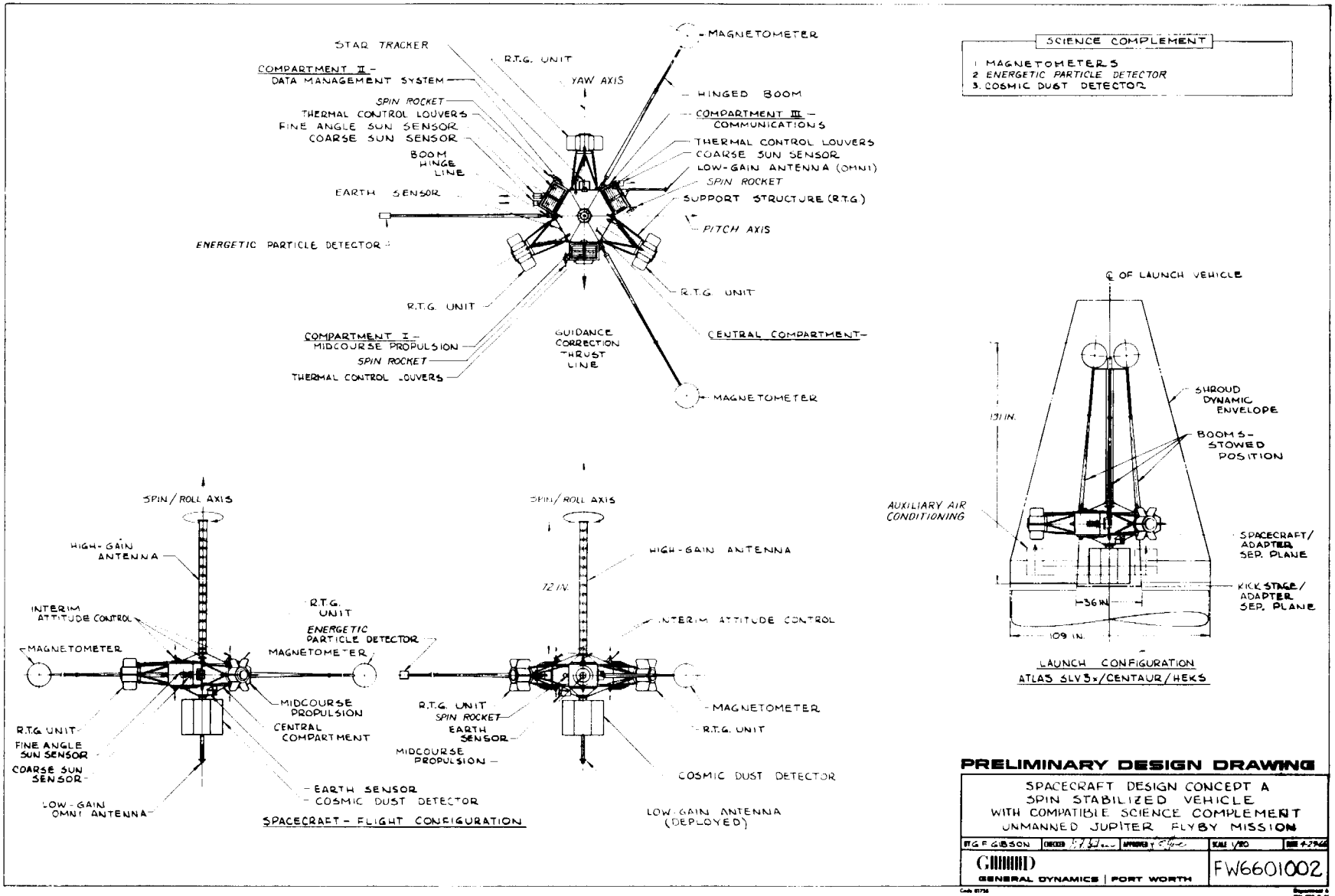

FIGURE 5.1-1

Table 5.1-1
SEQUENCE OF SIGNIFICANT FLIGHT EVENTS FOR SPACECRAFT DESIGN CONCEPT A

Notes: The mission characteristics are a 1976 launch, Atlas/Centaur/HEKS launch vehicle, 497 day flight time, posigrade equatorial pass, and 1.0 Jupiter radius nominal perijove altitude. The CC&S is the primary control for all spacecraft events except where noted. Backup via ground command is implied for all events.

No.	Event	Nominal Time
1	Install RTG units and activate auxiliary cooling system	L - 1 day
2	Update CC&S master clock and sequence timer	L - 3 min.
3	Turn on gyros, DEE, and CDDE	L - 2 min.
4	Liftoff	L
5	Atlas booster engine cutoff	
6	Payload fairing separation	
7	Atlas sustainer engine cutoff	
8	Atlas vernier engine cutoff	
9	First Centaur ignition	
10	First Centaur cutoff (begin orbital coast)	
11	Second Centaur ignition (end orbital coast)	
12	Second Centaur cutoff	
13	High Energy Kick Stage (HEKS) ignition	
14	HEKS cutoff (Injection)	I = L + 120 min.
15	Spacecraft - HEKS separation	I + 2 min.
	a. Pyrotechnics armed	
	b. Omni antennas deployed	
	c. Transmitter power up	
	d. Begin communication with omni antennas at data transmission rate of 33 bps.	
16	Initial Sun acquisition	I + 10 min.
	a. Turn on attitude control system	
	b. Turn on coarse Sun sensor	
	c. Activate gas-jet system	
	d. Begin Sun acquisition sequence	
17	Sun acquired	I + (10 - 20) min.
18	Activate cruise science	I + 20 min.
	a. Deploy magnetometers	
	b. Turn on DAE	
	c. Turn on cruise science	
19	Canopus acquisition	I + 100 min.
	a. Turn on Canopus sensor	
	b. Set sensor cone angle	
	c. Begin roll turn	
	d. Receive acquisition signal	
	e. Turn on Earth sensor	
	f. Verify Canopus acquisition (continue roll search if Earth not acquired)	

No.	Event	Nominal Time
20	Canopus acquired	I + (100 -130) min.
	a. Gyros turned off	
21	Prepare for midcourse maneuver	M - 60 min.
	a. Transmit and verify roll-turn duration and polarity	
	b. Transmit and verify pitch-turn duration and polarity	
	c. Transmit and verify velocity increment	
22	Begin midcourse maneuver sequence	M = I + (1 - 7) days
	a. Turn on fine Sun sensor	
	b. Acquire Sun with fine Sun sensor	
	c. Turn on gyros	
	d. Turn on accelerometer	
23	Execute roll turn	M + 60 min.
	a. Switch out error signals from Earth, Sun, and Canopus sensors	
	b. Set proper polarity	
	c. Roll turn started	
	d. Roll turn stopped	M+ (60 - 65) min.
24	Execute pitch turn	M + 75 min.
	a. Set proper polarity	
	b. Pitch turn started	
	c. Pitch turn stopped	M + (75 - 80) min.
25	Execute motor burn	M + 90 min.
	a. Command motor ignition	
	b. Command motor shutoff	M +(90 - 91.5)min.
26	Sun reacquisition	M + 93 min.
	a. Turn off accelerometer	
	b. Switch in error signal from coarse Sun sensor	
	c. Execute pitch turn with opposite polarity	
	d. Execute roll turn with opposite polarity	
	e. Begin Sun acquisition sequence	
27	Sun reacquired	M + (93 - 98) min.
28	Canopus reacquisition	M + 99 min.
	a. Switch in error signal from Canopus sensor	
	b. Begin pitch turn	
	c. Receive acquisition signal	
	d. Switch in signal from Earth sensor	
	e. Verify Canopus acquisition	

Table 5.1-1 (Continued)

No.	Event	Nominal Time
29	Canopus reacquired	M + (99 - 104) min.
30	Execute spin-up maneuver	M + (110-120) min.
	a. Orient roll axis to proper angle	
	b. Verify orientation	
	c. Initiate spin-up with roll (gas) jets	
	d. Damp wobble of spin axis with pitch and yaw gyros	
	e. Command spin rocket burn	
	f. Turn off gyros	
31	Switch transmitter to medium-gain antenna	I + 30 days
32	Switch transmitter to high-gain antenna	I + 70 days
33	Switch data transmission rate from 33 to 17 bps	I + 120 days
34	Switch data transmission rate from 17 to 8 bps	I + 140 days
35	Swtich data transmission rate from 8 to 4 bps	I + 170 days
36	Swtich data transmission rate from 4 to 2 bps	I + 200 days
37	Swtich data transmission rate from 2 to 1 bps	I + 260 days
38	Turn on DSE	E - 480 min.
39	Loss of communications (due to DSIF receiver limitations)	E - 450 min.
40	Begin encounter data acquisition mode (approximately 280,000 km from planet surface)	E - 180 min.
41	Perijove passage (one Jupiter radius altitude)	E = I + 497 days
42	Begin Sun occultation (0^{o} cone)	E + 22 min.
43	Begin Earth occultation (0^{o} cone)	E + 25 min.
44	End Sun occultation (0^{o} cone)	E + 90 min.
45	End Earth occultation (0^{o} cone)	E + 94 min.
46	End encounter data acquisition mode (approximately 280,000 km from planet surface)	E + 180 min.
47	Regain communications	E + 330 min.
	a. Turn off DSE	
48	Transmit command to initiate encounter data playback	E + 2 days
	a. DSE turned on (cyclic transmission of one hour real time data to five hours of non-real time data)	
49	End data playback	E + 22 days
	a. Turn off DSE	
50	Return to cruise mode	E + 22 days

The development time for the spacecraft is estimated to be 5 years. Total program cost for two Atlas SLV3x/Centaur/HEKS launched spacecraft is estimated to be $151 million. For two Titan IIICx/Centaur launched spacecraft, this cost is estimated to be $178 million.

The salient characteristics of the spacecraft are (1) interim three-axis, reaction jet stabilization, (2) spin-stabilization, (3) a science capability on the order of 20 pounds and 10 watts, (4) a slotted waveguide antenna and a 25-watt transmitter, (5) data compression and tape storage, (6) Mariner IV-type midcourse propulsion, (7) Plutonium 238 radioisotope thermoelectric generators, and (8) armor-type meteoroid protection. The spacecraft performance is indicated by the following: (1) A one-bit-per-second information rate at 6 a.u. communications distance, (2) data storage for 22M bits, (3) a vernier correction capability of 60 m/sec, and (4) 195 watts of available electrical power.

The three-axis stabilization system provides spacecraft attitude control between the times of spacecraft injection and completion of the vernier correction. All science equipment is turned on prior to the maneuver and operates throughout the mission. The spacecraft is spun up by solid-propellant rocket motors following the correction. The high/medium gain slotted waveguide antenna provides the primary communications downlink. Omni antennas are available for two-way communications during near-Earth operation and for command capability throughout the mission. The data management subsystem compresses and stores scientific and engineering data in addition to converting data to a telemetry signal. The spacecraft is expected to pass by the planet Jupiter within approximately 2600 km of any selected periapsis. The spacecraft weight is summarized in Table 5.1-2.

Table 5.1-2

SPACECRAFT DESIGN CONCEPT A - WEIGHT SUMMARY

Subsystem	Weight, lbs
Science	13
Communications	65
Data Management	34
Spacecraft Control	45
Attitude Control Propulsion	25
Spin Rockets	6
Midcourse Propulsion	41
Electrical Power	197
Structural/Mechanical and Meteoroid Protection	94
Thermal Control	11
Total Spacecraft	531
Adapter (0.065 x Spacecraft Weight)	35
Launch Weight	566

5.1.2 Subsystem Design Information

5.1.2.1 Science

The design philosophy of Spacecraft Design Concept A is such that the following limitations are imposed on the scientific capability provided through use of the design:

1. Planetary instruments which must be pointed at Jupiter are not compatible with spin-stabilization.

2. The communications subsystem applicable to spin-stabilization limits data rate and consequently limits the number of scientific instruments. It also restricts encounter trajectories to essentially equatorial flybys.

The scientific experiment package selected for Design Concept A is originally defined in Table 2.1-8, and the instruments are listed again in Figure 5.1-1. Details of the instruments are discussed in subsection 2.1. The total weight of this package is 13 pounds.

5.1.2.2 Communications

An examination of candidate high gain antennas for spin-stabilized spacecraft (subsection 3.1.2.1) has led to the selection of a slotted waveguide antenna for use in the communications subsystem of Design Concept A. The gain of this antenna is limited by the beamwidth that can be tolerated by the vehicle trajectory and by the amount of wobble about the spin axis. The physical length of the antenna is also a limitation. An antenna yielding 14 db gain is approximately 6 feet tall. Such an antenna has a 4 degree beamwidth and, except in the early part of the flight, this beamwidth falls within the above limitations. Prior to injection, the omnidirectional turnstile antennas are used for communications. After injection and during approximately the first 100 days of cruise, the Earth does not fall within the 4 degree beamwidth of the high gain antenna. However, a shutter arrangement may be incorporated so that a portion of the slots on the high gain antenna can be closed. This reduces the gain by 4 db and widens the beamwidth to 11.4 degrees. The omni antennas are used for receiving during the entire mission.

The recommended configuration of the communications subsystem is essentially that shown in Figure 3.1-8. The amplifiers are 25 watt TWT's, and the high gain antenna is a slotted waveguide with 14 db gain and a 4 degree beamwidth. With this antenna, the gain can be reduced to 11 db with a subsequent increase in the beamwidth to 11.4 degrees. Using this system, the gain-loss chart shown in Table 5.1-3 is applicable at a 6 a.u. communications distance.

Table 5.1-3

DESIGN CONCEPT A - GAIN-LOSS CHART

	Gain	Loss
Transmitter Power	44 dbm	
Modulation		3 db
S/C Ant Gain	14 db	
Space Attenuation		278 db
Rcvr Ant Gain	61 db	
Rcvr Sens ($40^{o}K$)		-182 dbm
Misc Loss		2 db
System Tolerances		6 db
TOTALS	119 db	107 db

$S/N_0 = 119 - 107 = 12$ db.

Therefore, at 6 a.u. the information performance margin at 1 bps is 5.2 db. However, the information threshold performance margin is 0 db (see subsection 3.1.2.3). The phase-lock threshold performance margin can be increased by decreasing the loop bandwidth of DSIF, and this DSIF modification is assumed for this concept.

As discussed in subsection 3.1.2.7, it is probable that the Doppler rate of the spacecraft-Earth signal during encounter will be too high for DSIF to track the signal using the 170 dbm receiver threshold. Since the threshold cannot be increased and phase-lock maintained, it is assumed that communication is suspended for approximately 13 hours during encounter. The exact time period depends on the direction and perijove of the encounter trajectory, but some period of communication interruption is expected for any acceptable flyby trajectory.

For each applicable antenna configuration, gain-loss charts can be constructed to determine allowable information rates for various communications distances. An antenna and information rate schedule is shown in Table 5.1-4 as a function of communications distance. The actual times of switching antennas and information rates are dependent upon the trajectory chosen.

Table 5.1-4

DESIGN CONCEPT A -
ANTENNA AND INFORMATION RATE SCHEDULE

Communications Distance (a.u.)	Antenna	Info Rate (bps)
0-0.2	Omni	33
0.2-0.5	Med Gain	33
0.5-1.1	Hi Gain	33
1.1-1.5	Hi Gain	17
1.5-2.2	Hi Gain	8
2.2-3	Hi Gain	4
3-4.2	Hi Gain	2
4.2-6.0	Hi Gain	1

The number and weight of the components of the communications subsystem are shown in Table 5.1-5. The recommended numbers of components are based on a reliability analysis of the communications subsystem. Although the proposed configuration is not necessarily optimum with respect to reliability, it is considered to be an appropriate compromise between reliability, weight, and power considerations.

Table 5.1-5

DESIGN CONCEPT A - COMMUNICATIONS SUBSYSTEM WEIGHT

Component (no.)	Weight, lbs
Amplifier (2)	4
Power Monitor (2)	2
Circulator (5)	5
Exciter (2)	7
APC Receiver (2)	18
Rcvr Monitor	1
Exciter Control	2
Amp Control	2
Omni Ant (2)	4
SWG Ant	6
Power Supply, HV (2)	10
Cabling, etc.	4
TOTAL	65

5.1.2.3 Data Management

The elements and the functional requirements of the data management subsystem are discussed in general terms in subsection 3.2. It is expected that the subject mission can be accomplished so that a minimum of modification of equipment used for the Mariner IV mission is required. Data storage is required during the cruise (both near-Earth and interplanetary) and the encounter phases of the mission. A magnetic tape recorder is employed for this purpose.

The available transmission rates for various portions of the mission have been identified in Table 5.1-4. The anticipated raw and compressed data bit rates for the different phases of the mission are listed in Table 5.1-6. The large difference between the anticipated raw data rates and the available transmission rates is an indication of the need for data compression.

The raw data rates shown in Table 5.1-6 were obtained by estimating the optimum sampling interval (Nyquist rate) of each data source. On the basis of data from previous missions and on scientific opinions as to expected variations in the data, calculations were made to obtain the compressed data rates by using the fan method. It should be noted that these compressed data rates are average values and that the instantaneous rates can vary from zero to maximum values which approach the raw data rates. It is significant that, for the interplanetary portion of the cruise phase, the total compressed data-gathering rate is much lower than the available transmission rate. This surplus communications capability can be used advantageously during routine intervals of this portion of the mission to implement intermittent communications.

Table 5.1-6

DESIGN CONCEPT A - ANTICIPATED DATA BIT RATES

TYPE	NEAR EARTH			INTERPLANETARY			ENCOUNTER		
	Raw	Compressed (Fan)		Raw	Compressed (Fan)		Raw	Compressed (Fan)	
1. Engineering	33.3	(150:1)	0.2	33.3	(150:1)	0.2	33.3	(150:1)	0.2
2. Magnetometer	300.0	(10:1)	30.0	0.2	(10:1)	≈ 0.0	300.0	(10:1)	30.0
3. Cosmic Dust Detector	0.1	(1000:1)	≈ 0.0	0.1	(1000:1)	≈ 0.0	0.1	(1000:1)	≈ 0.0
4. Energetic Particle Detector	0.3	(3:1)	0.1	0.3	(3:1)	0.1	1.7	(3:1)	0.6
5. Housekeeping	30.0	(30:1)	1.0	3.0	(30:1)	0.1	30.0	(30:1)	1.0
TOTAL	363.7	(11:1)	31.3	36.9	(92:1)	0.4	365.1	(11:1)	31.8

The fan method appears to be the most applicable data compression technique in the case of both the engineering and the scientific data. The zero order interpolator method, for which less complex equipment is required, is also a possibility, but the data compression ratio is significantly lower than that of the fan method. Although applicable, the quantile method is not recommended for use in conjunction with the energetic particle detector data because a more reliable, efficient, and economical design can be obtained by using one generalized compression technique for all data. The fan method can be used to compress data from all of the engineering and scientific sensors and should yield a high compression ratio for data from the magnetometers, which provide the greatest quantity of scientific data.

Data storage of important sensor measurements is required whenever the data acquisition rate exceeds the data transmission rate, whenever Earth-spacecraft communication is involuntarily interrupted, or whenever intermittent communication is employed. Data is compressed after storage to increase the reliability of data retrieval. By using this procedure, stored data can be transmitted uncompressed in the event of a complete data compression failure. Several environments and mission situations must be studied in order to calculate the required storage capacity.

During the near-Earth portion of the mission, the only data storage requirement results from a condition in which the data becomes so dynamic that the data compression devices cannot reduce the data-acquisition rate below the available data-transmission rate. It is assumed that for this portion of the mission the dynamic data condition will not exist for more than one hour before a readout of the DSE can be accomplished. The required storage capacity for this mission period is then calculated to be 1.31M bits.

To determine the required storage capacity for the interplanetary portion of the cruise phase, consideration must be given to two conditions: dynamic data, and intermittent communications. The dynamic data condition is assumed to exist for no more than six hours, and it is doubtful that intermittent communication will be employed without a station contact at least once a week for readout. The required storage capacities under these circumstances are 800K and 22.4M bits, respectively.

In the case of Concept A, a unique situation occurs which determines the required storage capacity for the encounter phase. This situation is caused by a rate of Doppler frequency change that exceeds the ground receivers' tracking capability to the extent that communication capability is lost. The time period of this communications loss varies nominally between 5 and 13 hours as a function of the perijove altitude and the encounter flight path. Since the final trajectory has not been selected at this time, the maximum period of 13 hours, which includes the entire 6-hour encounter phase, has been assumed. Another half-hour of

storage time is added to the 13-hour interval to account for any uncertainty in this estimate. This extra period is necessary because between 35 and 45 minutes will be required for a transmitted command to initiate tape recorder operation after the loss of communications. Therefore, it is considered essential that this command be transmitted well before the time of anticipated communications loss in order to prevent a corresponding data loss. The required storage capacity in this instance is 8.88M bits.

Since the maximum required storage capacity is 22.4M bits and, under most conditions, the required capacity is in excess of 1.0M bits, a tape recorder is recommended for use as the DSE. However, if the configuration or mission requirements are modified by future studies in such a way that the maximum required storage capacity is reduced to less than 1.0M bits, the possible use of either a drum or buffer as the DSE should be considered.

Further calculations were made to determine whether the time required to transmit the data stored during encounter would be so excessive that the possibility of retrieving such data would be endangered. If it is assumed that continuous tracking station coverage is provided, that one hour of real time data is transmitted for every five hours of non-real time data, and that two complete readouts are required, the transmission of the stored encounter data in a compressed format at the one-bit-per-second rate will require slightly less than 20 days. This time interval is considered acceptable.

The specific functional requirements which are recommended for the elements of the data management subsystem are as follows: The DAE of the data management subsystem encodes and buffers science data and inputs them to the DEE and the DSE at specified rates compatible with the selected transmission rates. The DEE provides four interdependent commutator rates for approximately 90 analog measurements. The sampling speeds of these commutators are determined by the six command-selectable data-transfer rates of 1, 2, 4, 8, 17, and 33 bits per second. The DSE is used to provide data storage for 22.4M bits of information at read-in rates of 37 and 370 bits per second and at readout rates up to 3100 bits per second as a function of the selected transmission rate and the average compression ratio. In the following paragraphs, each element of the data management subsystem is discussed in detail.

The basic differences between the DAE recommended for this mission (see Figure 5.1-2) and the DAE used on Mariner IV are (1) the combination of the real time and non-real time sequencer into a single sequencer and (2) a magnetometer data comparator for automatic selection of the magnetometer to be used. The combination of the two sequencers into a single unit is possible because all science sensors are operated throughout the mission. In order to provide a means of automatic switching between the high-range and the low-range magnetometers, the comparator is included to provide a means of continuously monitoring the difference between magnetometer current readings and preset switchover tolerances.

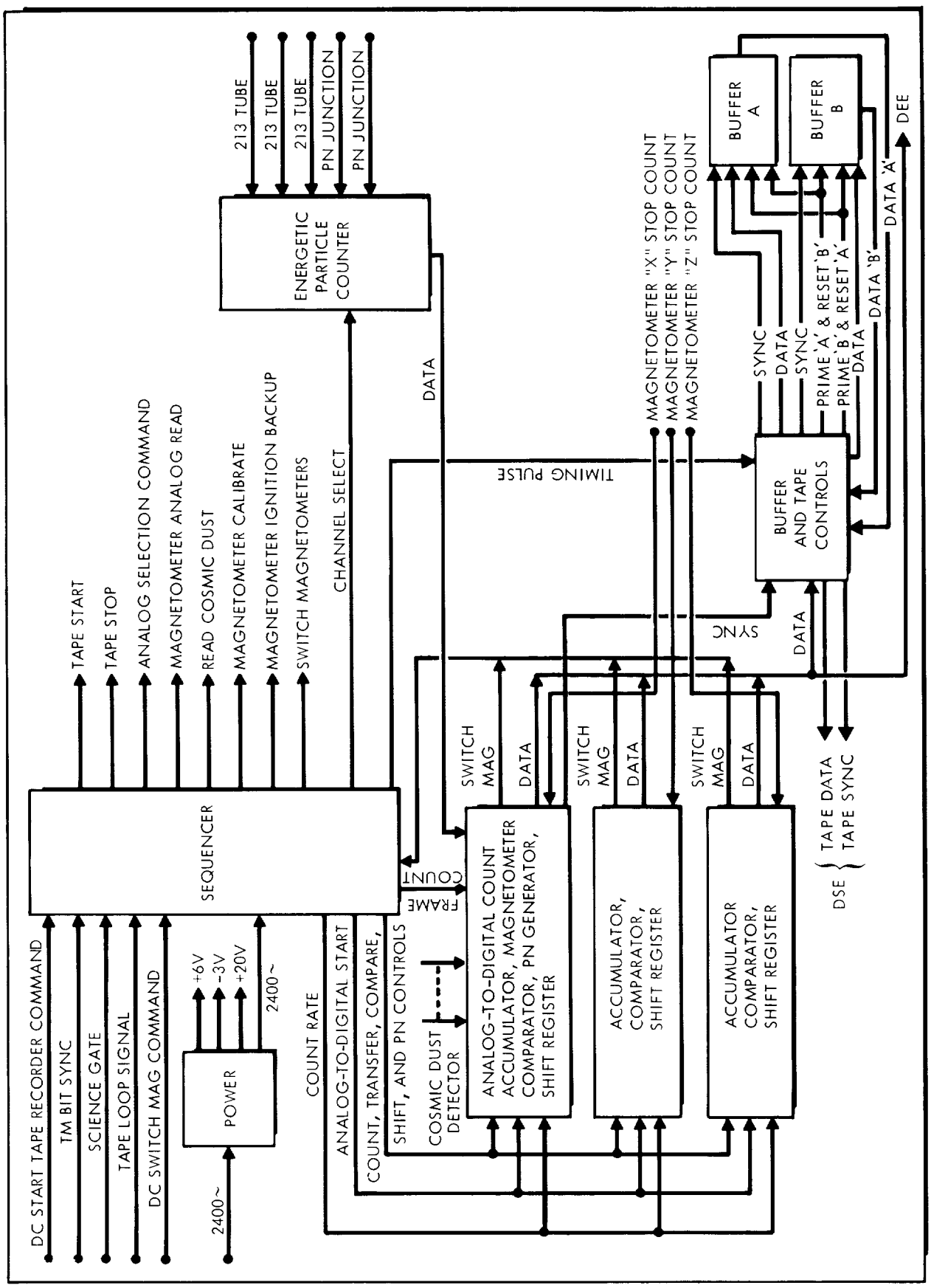
DESIGN CONCEPT A DATA AUTOMATION ELEMENT
DC START TAPE RECORDER COMMAND
TM BIT SYNC
SCIENCE GATE
TAPE LOOP SIGNAL
DC SWITCH MAG COMMAND
2400~
+6V
-3V
+20V
2400~
POWER
SEQUENCER
TAPE START
TAPE STOP
ANALOG SELECTION COMMAND
MAGNETOMETER ANALOG READ
READ COSMIC DUST
MAGNETOMETER CALIBRATE
MAGNETOMETER IGNITION BACKUP
SWITCH MAGNETOMETERS
CHANNEL SELECT
213 TUBE
213 TUBE
213 TUBE
PN JUNCTION
PN JUNCTION
ENERGETIC PARTICLE COUNTER
DATA
COUNT RATE
ANALOG-TO-DIGITAL START
COUNT, TRANSFER, COMPARE,
SHIFT, AND PN CONTROLS
COSMIC DUST DETECTOR
FRAME COUNT
SWITCH MAG
DATA
ANALOG-TO-DIGITAL COUNT ACCUMULATOR, MAGNETOMETER COMPARATOR, PN GENERATOR, SHIFT REGISTER
ACCUMULATOR, COMPARATOR, SHIFT REGISTER
ACCUMULATOR COMPARATOR, SHIFT REGISTER
TIMING PULSE
SYNC
DATA
MAGNETOMETER "X" STOP COUNT
MAGNETOMETER "Y" STOP COUNT
MAGNETOMETER "Z" STOP COUNT
BUFFER AND TAPE CONTROLS
SYNC
DATA
SYNC
PRIME 'A' & RESET 'B'
PRIME 'B' & RESET 'A'
DATA
DATA 'B'
DATA 'A'
BUFFER A
BUFFER B
DEE
DSE
TAPE DATA
TAPE SYNC

FIGURE 5.1-2

Basically, data from the cosmic dust detector and the energetic particle detector enter the DAE as digital inputs while data from the magnetometers enter the DAE as pulsewidth inputs. Pulsewidth representation of the magnetometer data is used rather than analog because of the long distance between the sensor and the DAE. Three count accumulators are provided so that data from all three magnetometer axes can be sampled simultaneously. Moreover, unless the ground command override has been used, the magnetometer data are compared with the preset tolerances to determine whether it is necessary to switch instruments. After the scientific data has been encoded and put in format, it is sent to the DEE and, when required, to the DSE.

The primary differences between the Spacecraft Design Concept A DEE (Figure 3.2-7 without modification A) and the Mariner IV DEE are that (1) data compression is included for the engineering and scientific measurements and (2) a single-channel, synchronization data link is used to replace the Mariner IV two-channel data link.

Analog data are conditioned, multiplexed, and converted into digital format before being transferred to the data selector. In the data selector, these data are combined with digital inputs from the event-registers and the DAE and, when specified, are sent to the DSE for playback at a later time. Next, these data are compressed, modulated, and temporarily stored in a buffer prior to their transfer to the communications subsystem.

This buffer is provided with an overflow sensing capability so that whenever the data-gathering rate exceeds the transmission rate for a long enough time period that the buffer is filled, no more data is accepted by the buffer until a sufficient quantity of data has been transmitted. This sensing will also automatically initiate data storage if the DSE is not already operating.

During data playback, the previously described functions are continued except that the stored DSE data is substituted for the real-time data by the data selector; therefore, only the stored data is processed further by the data compressor and modulator in subsequent transmission. The capability to bypass data compression devices has been provided to enable operation if a malfunction occurs and to permit transmission of uncompressed data blocks for the purpose of verifying data compression accuracy.

The DSE (see Figure 3.2-6) is a 22.4M-bit-capacity magnetic tape recorder which can accept engineering data inputs from the DEE and scientific data inputs from the DAE. All playback is implemented through the DEE. Except for the incorporation of a single-channel command data link, the CDDE (see subsection 3.2.3.4) is functionally identical to the Mariner IV CDDE. The use of approximately 45 DC's and 3 QC's should be adequate to accomplish the mission objectives.

The number and weight of the components of the data management subsystem are shown in Table 5.1-7. The recommended numbers of components are based on a reliability analysis of the data management subsystem. Although the proposed configuration is not necessarily optimum with respect to reliability, it is considered to be an appropriate compromise between reliability, weight, and power considerations.

Table 5.1-7

DESIGN CONCEPT A - DATA MANAGEMENT SUBSYSTEM WEIGHT

Component (no.)		Weight, lbs
DEE	(2)	14
DAE	(2)	8
DSE	(2)	8
CDDE	(2)	4
	TOTAL	34

5.1.2.4 Spacecraft Control

The function of the spacecraft control subsystem for the spin-stabilized Jupiter flyby vehicle is to perform master timing and sequencing for other vehicle subsystems, to sense vehicle attitude, to control vehicle maneuvers in anticipation of the vernier correction, and to control the thrust duration of the correction itself. In addition, the control subsystem properly orients the vehicle spin axis prior to spin up and acts to null angular rates about axes other than the spin axis during the initial phase of spin up. The roll channel of the cold gas attitude control system is used to begin the initial phase of spin up. While the roll rate is increasing, wobble of the spin axis is sensed with rate gyros and nulled through the attitude control subsystem.

The fundamental objective in the Concept A configuration is the achievement of a very high probability of mission success in conjunction with relatively low cost and low system complexity. To meet this basic objective, the specific functions of the control subsystem are established to reflect high reliance on available Earth-based facilities. Thus, the orbit determination and the determination of the vernier correction are implemented by means of Earth-based tracking and data processing. In so far as the vernier correction is concerned, the function of the on board control system is to orient the thrust vector and measure the velocity change.

The selection of a control system for Concept A is necessarily dependent upon the choice of a terminal control concept. Basically,

two concepts are considered - one requires despin prior to encounter, the other does not. To despin and stabilize about three axes for the Jupiter encounter provides a more satisfactory platform from which to gather the encounter scientific data and from which to point a suitable antenna toward Earth for transmission of this information. The drawbacks to this approach are the requirements for (1) the despin mechanism, (2) attitude sensing and control equipment which must now function through the encounter phase, and (3) antenna pointing during encounter and post-encounter phases. If the scientific payload is such that three-axis attitude control is not a requirement during encounter, then despin and control mechanisms are not required to operate after the initial spin up. The spacecraft attitude control system and the control electronics are then very light in weight and require only moderate reliability because there are only 10 to 14 days between injection and spin up. Because of considerations such as these, the capability for despin maneuver is not included in the spin-stabilized vehicle configuration.

The guidance and attitude control system proposed for the spin-stabilized vehicle consists of the sensors, attitude jets, and the electronics needed to stabilize the vehicle, carry out the vernier correction, and properly orient the spin axis prior to spin up (see Figure 3.3-2). Spin axis orientation and spin rate are chosen to provide the proper communications geometry throughout the flight and to hold this orientation within some tolerance against expected en route disturbance. These basic functions are completed in 1 to 7 days following the injection maneuver. When spin up is complete, no further use of the attitude control system is anticipated. The central computer and sequencer (CC&S), shown in Figure 3.3-1, will continue to perform in its capacity as master timer and sequencer for other spacecraft systems.

The general operations of the spacecraft control subsystem have been indicated in Table 5.1-1. The first operation following injection of the spacecraft into the transfer trajectory is to stabilize the craft with respect to the Sun and a star in anticipation of the vernier correction. The three orthogonal gyros which have been running for some time begin to feed rate signals to the attitude control electronics and the coarse Sun sensors are turned on.

The above sequence is initiated by a signal from the CC&S. Pitch and yaw rates will be reduced to 0.5 deg/min through a loop involving the gyros and the pitch and yaw thrusters. Signals from the coarse Sun sensor are used to null the vehicle roll rate, leaving the Sun in the plane of the pitch and roll axes. Error signals from the Sun sensors are then applied to the yaw channel to position the vehicle pitch axis directly toward the Sun. The remaining task is to pitch about the Sun/vehicle line to orient the roll axis approximately normal to the ecliptic. This is controlled by setting a star tracker to the declination of a suitable star (traditionally Canopus) and pitching slowly until the star

tracker indicates that it has acquired the star. A feedback loop including the star tracker and the pitch thrusters refines the vehicle attitude.

As a check on the star tracker, an Earth sensor is oriented so that, if the attitude is right, it will view the Earth and produce a suitable signal. If the Earth is not directly in view of the Earth sensor, then the star tracker has acquired the wrong star and the star acquisition sequence must be repeated.

A coarse limit cycle operation is maintained from this point until time for the vernier correction. On the basis of tracking and orbit determination, a vernier correction is computed to reduce the injection velocity errors. The correction velocity vector is reduced to a vehicle roll and pitch sequence and to a magnitude described by so many accelerometer pulses. The correction and the time at which it is to be made are transmitted to the spacecraft.

Prior to the correction, the gyros are turned on and the attitude control is switched to a fine limit cycle. The roll and pitch maneuvers are timed, while the gyros and attitude thrusters control the angular rates. At the proper time, the vernier engine is turned on, and accelerometer pulses which measure the velocity change are used to control the magnitude change of the velocity. During motor burn, rate error signals are sent to the propulsion unit thrust vector control vanes to keep the line of thrust constant in space. At the end of the vernier maneuver, the attitude control system reacquires the Sun and a star for attitude reference much as it did at the end of the injection.

Prior to spin up, the fine attitude control is established, and the roll axis is oriented in the direction which it is to hold throughout the mission. It appears to be desirable to begin the spin up with the roll attitude jets while the pitch and yaw gyros and jets are used to damp out any wobble of the spin axis. At this point the spin jets are fired.

As discussed in subsection 3.4, the vernier correction performed prior to spin up is expected to yield a terminal position accuracy of better than 0.1 Jupiter radii.

The number and weight of the components of the spacecraft control subsystem are shown in Table 5.1-8. The recommended numbers of components are based on a reliability analysis of the spacecraft control subsystem. Although the proposed configuration is not necessarily optimum with respect to reliability, it is considered to be an appropriate compromise between reliability, weight, and power considerations.

Table 5.1-8

DESIGN CONCEPT A - CONTROL SUBSYSTEM WEIGHT

Component (no.)	Weight, lbs
Fine Sun Sensor	1
Coarse Sun Sensor (2)	2
Earth Sensor	6
Star Tracker	10
Attitude Control Electronics	10
CC&S	12
Gyros & Accelerometers	4
TOTAL	45

5.1.2.5 Attitude Control

A gas jet attitude control subsystem is required on Design Concept A to accomplish the various functions occurring between injection and spin-up. During this period of about two weeks, the spacecraft is maintained in a three-axis stabilized attitude on a limit-cycle mode. The functions to be accomplished during this period have been described in the previous subsection. After spin-up, all control functions are terminated, and the stabilization becomes completely passive. Spin stability is designed into the configuration through a favorable inertia distribution, with nutation damping provided either by natural structural flexure or specially designed dampers, as required. The effect of solar torques on the precession of the spin axis is minimized to a tolerable level by balancing the moment-area about the axes normal to the spin axis.

Except for the spin-up function, the control functions associated with the gas jet system are similar to those encountered in the initial phases of the Mariner IV mission. Therefore, the same general philosophy is being applied in the attitude control system design. The system utilizes stored nitrogen gas to feed 12 jets. These jets are operated in pairs to produce a couple about each of the three spacecraft axes.

Since the lifetime of the system is fairly short, the size of the unit pulse is not a critical consideration. The gas usage on the limit-cycle mode can be kept within reasonable bounds even for a fairly large unit pulse, especially since there is no stringent requirement on the deadband angle. The design of the gas jet system is thus determined as a compromise between the desire to keep the total system impulse to a minimum level and to provide maximum control torque to accommodate the spin-up functions. In order to analyze this problem, the following estimates of moments of inertia and gas jet moment arms are utilized:

$$I_{ROLL} = 100 \text{ slug-ft}^2$$

$I_{PITCH/YAW} = 70$ slug-ft^2

Jet moment arms = 33 in. = 2.75 ft.

The roll axis corresponds to the spin axis, which is made the axis of maximum inertia to meet the stability criteria described in subsection 3.5.3. The pitch and yaw axes are assumed to have identical moments of inertia, although there may actually be a slight difference involved. The moment arm for all gas jets is the same, and it refers to the distance between matching jets in the couple (i.e., the quantity, ℓ , defined in Figure 3.5-10). It is assumed that the gas jets are all identical in design.

For the limit-cycle calculations, the following values of deadband angle and limit-cycle time period are postulated:

θ_E = Deadband angle = 1 degree = 0.01745 radian

P = Limit-cycle time period = 2 weeks = 1.2×10^6 sec.

This value of deadband angle is fairly large because the spacecraft is not subject to any stringent attitude requirements during the major part of the control period. However, it is considered that the deadband is switched out, or reduced, when maximum accuracy is required during the thrusting and spin-up maneuvers. During these periods, the spacecraft can be controlled to the sensor threshold, if desired.

The pulse width of the gas jets is set at 0.02 second, which is considered to be the minimum practical value for a stored gas system. It is desirable to make the thrust level as high as possible without causing excessive fuel usage on the limit cycle mode. After some iteration, the following design point is selected:

F = Jet thrust force = 0.30 lb

Δt = Pulse width = 0.02 sec

ΔI = Unit pulse = (F) (Δt) = 0.006 lb-sec.

This thrust level is considerably above the minimum value (about 0.005 lb) that is attainable for a stored gas system, but it is below the maximum achievable value (1 to 5 lbs). For these design points, the characteristics of the limit cycle about each axis are computed by use of the formulas presented in Figure 3.5-10, with the following results:

Control Axis	$\dot{\theta}E$ (deg/min)	t_1 (min)	Impulse (lb-sec)
Roll	0.283	7.06	34
Pitch/Yaw	0.405	4.93	49

Thus, the total impulse required for the three-axis limit cycle is obtained as follows:

$$\text{Limit-Cycle Impulse} = (1.5)\ \left[34 + 2(49)\right] = 200 \text{ lb-sec.}$$

The factor of safety of 1.5 is considered adequate to account for variations in the unit pulse and other deviations from the idealized assumptions used in the limit-cycle analysis. The total system impulse is obtained by adding to the above figure an allowance for maneuvering and initiation of spin up as follows:

3-Axis Limit Cycle	200 lb-sec
Maneuvering Allowance	25 lb-sec
Spin-up Allowance	75 lb-sec
TOTAL	300 lb-sec

From the data presented in Section 3.6.2, a stored gas system of the Configuration A-type and capable of producing the required impulse indicated above weighs about 25 pounds.

Large attitude changes may be required to accommodate the vernier correction. These maneuvers are governed by the inertial reference unit (body-mounted gyros operating in conjunction with a computer) on a rate-command mode. If it is assumed that a maximum rate of 1.0 degree per second is utilized, a 180-degree attitude change requires about 3 minutes to accomplish. The impulse required to achieve this rate about the roll axis (worst case) is defined as follows:

$$\text{Angular Impulse} = (I)\ (\dot{\theta})$$

$$= (100) \times \frac{1.0}{57.3} = 1.745 \text{ ft-lb-sec}$$

The number of pulse pairs required to obtain this result is:

$$\text{No. of Pulse pairs} = \frac{(I)\ (\dot{\theta})}{(2)(\Delta I)\ (\ell)} = \frac{1.745}{(2)(.006)(2.75)} = 53$$

If a spacing of two pulse widths between pulses (i.e., maximum pulse rate) is assumed, the time required to achieve this rate is about 3.2 seconds. The amount of gas used in this process is very small, corresponding to only 0.64 pound-second of impulse. The number of pulses required is indicative of the accuracy to which the commanded rate can be maintained by the control system. For the above case, this result is 1/53 or about 1.9 percent. This accuracy is approximately equivalent to the rate gyro resolution.

For the spin-up process, it is assumed that the roll-jet valves are held open so that maximum continuous roll acceleration is applied. It is further assumed that the gas jets are required to achieve a spin rate of 1.0 radian per second, which is about 10 rpm. This moderate initial rate reduces the effects of misalignments in the more efficient spin rockets, which are subsequently utilized to achieve final spin rate. The time required to attain this initial rate by means of the gas jets is computed as follows:

$$\text{Thrust time} = \frac{\text{Angular momentum}}{\text{Control torque}} = \frac{(I)(\dot{\theta})}{(F)(\ell)}$$

$$= \frac{(100)\ (1.0)}{(0.30)(2.75)} = 121 \text{ sec.} = 2.0 \text{ min.}$$

During this time, the spacecraft completes about 10 revolutions. The amount of gas impulse required for this operation is:

$$\text{Gas impulse} = (2) \times (0.30) \times (121) \quad 75 \text{ lb-sec.}$$

This value corresponds to that used earlier to determine the total system impulse requirement. Under the present concept, the attitude control system is permanently shut down after spin up by positive action squibs, which prevents the possibility of gas leakage.

For a maximum spin rate of 72 rpm (or about 7.5 radians per second), the spin angular momentum is approximately 750 foot-pound-seconds in the case of the assumed inertias. The precession due to solar radiation pressure, indicated by Figure 3.5-6, is only about 0.25 degree when the moment-area unbalance is as high as 4 feet cubed. A preliminary analysis of attitude control sensor errors and spin rocket thrusting errors indicates the expected error in spin axis orientation will be on the order of 0.5 degree. These figures indicate that precession is well within the tolerable limits relative to the communications requirements. However, it is not known what damping torques (magnetic fields or unknown phenomena) will act on the spacecraft to reduce its spin rate during the mission. If future studies indicate a problem in this regard, it may be necessary to incorporate corrective measures such as additional spin rockets to provide a mid-course spin boost.

5.1.2.6 Propulsion

The midcourse propulsion subsystem of Concept A is the basic hydrazine system described in subsection 3.6.1. The system design has the capability of imparting a total velocity increment of 60 meters per second (200 fps) to a spacecraft mass of about 531 pounds. This corresponds to approximately a 5 σ design criteria for a launch vehicle FOM of 10-15 m/sec. Table 5.1-9 contains a summary of the components and weight of the midcourse propulsion system.

Table 5.1-9

DESIGN CONCEPT A - MIDCOURSE PROPULSION SUBSYSTEM WEIGHT

Component		Weight, lbs
Hydrazine		16.0
Hydrazine tank		1.3
Nitrogen		0.71
Nitrogen tank		1.73
Bladder		0.42
Fixed hardware		20.84
	TOTAL	41.0
Hydrazine Tank Diameter	9.8 in.	
Nitrogen Tank Diameter	5.4 in.	

The attitude control propulsion subsystem considered for Concept A is the one identified and described as Configuration A in subsection 3.6.2. In subsection 5.1.2.5, the need for a 300 lb-sec total impulse capability is indicated. As shown in Figure 3.6-10, the total system weight is estimated to be 25 pounds; this weight includes gas, tankage, and components.

The rockets for spacecraft spin-up are small, solid propellant thrusters. The approximate required impulse is 75 lb-sec. Based on manufacturer's data, the weight of the rockets is estimated as being 1 to 2 pounds. The placement of the rockets on the periphery of the vehicle is necessary, in Figure 5.1-1 they are shown mounted on the equipment compartments. A total weight of 6 pounds is estimated for the rockets, mountings, and thermal control provisions.

5.1.2.7 Auxiliary Electric Power

The auxiliary electric power arrangement for Design Concept A is illustrated by the schematic diagram in Figure 3.7-8. A profile of subsystem loads is presented in Table 5.1-10. The critical load occurs in the cruise, three-axis stabilized period when the surplus power capacity is approximately 4 percent. During the acquisition and maneuver periods, the total load exceeds the capacity of the RTG by 9 and 49 watts, respectively. If the duration of these periods is 0.5 and 1.5 hours, the battery will experience a discharge of 1.1 and 17.5 percent during the respective periods. The specific components, the total number used, and the weights are listed in Table 5.1-11. The RTG capacities indicated therein represent the end-of-life capability. In Table 5.1-10, degradation in RTG capacity is accounted for by an indication of the variation in capacity as a function of time.

Table 5.1-10

DESIGN CONCEPT A - ELECTRIC POWER LOADS

	Prelaunch	Boost & Park Orbit	Acquisition	Cruise	Cruise, 3-Axis Stabilized	Maneuver	Encounter
Encoder	6	6	6	6	6	6	6
DAE	3	3	3	3	3	3	3
Tape Recorder	1	0	0	2	2	1	1
Command Detector & Decoder	3	3	3	3	3	3	3
CC&S	12	12	12	10	10	12	10
Control Gyro Electronics	5	5	5	0	5	15	0
A/C Electronics	11	11	11	0	9	23	0
Gyro 400 cps Power	5	5	5	0	5	15	0
Sun Sensors	0	0	2	0	2	3	0
Canopus Tracker	0	0	10	0	7	7	0
Earth Sensor	0	0	10	0	7	7	0
Communication Control	10	10	10	10	10	10	10
Communication Receiver	10	10	10	10	10	10	10
Communication Exciter	10	10	10	10	10	10	10
Communication Amplifier	70	10	70	70	70	70	70
Magnetometer	7	0	7	7	7	7	7
Energetic Particle Detector	0.4	0	0.4	0.4	0.4	0.4	0.4
Cosmic Dust Detector	0.2	0	0.2	0.2	0.2	0.2	0.2
Total Power Requirement	153.6	85	173.6	131.6	159.6	205.6	130.6
Raw Power Input to Power Cond.	191	104	214	162	197	253	163
Power Input to Shunt Reg. & Bat.	24	110	0	43	8	0	32
Power From RTG (3 - 65W)	214	214	205	205	205	205	195
Power From Battery	0	0	9	0	0	48	0
Watt-hour From Battery	0	0	4.5	0	0	73.5	0
Battery % Discharge	0	0	1.1	0	0	17.5	0

Table 5.1-11

DESIGN CONCEPT A - ELECTRIC POWER SUBSYSTEM WEIGHT

Component (no.)	Rating	Weight, lbs
Radioisotope Thermalelectric Generator (3)	65 watt, 28 volt	108.00
3 Electrode Ni-Cd Battery	15 ampere-hour	21.00
Shunt Volt. Reg. Switch (3)	Eight .5a channels	1.80
Volt. Reg. Mode Controller	Signal Device	.75
Shunt Dissipation Resistors (3)	112 watts	6.00
Main 2400 cps Inverter (2)	10 ampere input	4.00
Transfer Relay (2)	10 ampere dpst	1.00
Emergency 2400 cps Inverter	2 ampere input	.50
Inverter Synchronizer	Signal device	.50
Emergency Transfer Unit	5 ampere spdt	.50
400 cps Inverter	2 ampere input	4.00
Battery Charge-Discharge Controller	2 amp. chg, 5 amp discharge	9.00
Power Distribution and Wiring		40.00
	TOTAL	197.05

5.1.2.8 Thermal Control

In Spacecraft Design Concept A, the equipment bus is divided into four compartments: a central equipment bay and three extended equipment compartments. The central bay houses the midcourse propellant and other low power dissipation items. The temperature of this bay is controlled by insulation, coatings, and heat exchange with the RTG's and the outer equipment compartments. The three outer compartments are equipped with louvers on the upper and lower surfaces to provide a greater range of thermal control (see launch configuration, Figure 5.1-1). The sides of these compartments are insulated to minimize the effects of solar heating. The heat dissipated from electrical components will be distributed as uniformly as possible throughout the spacecraft by proper placement of components. Component thermal design information for Concept A is summarized in Table 5.1-12.

A detailed analysis of the thermal control requirements of components mounted on extensions from the spacecraft was not attempted in this study. The thermal control required depends on the specific component design and will probably be an integral part of the components. Thermal control of these items may require the use of insulation, coatings, heaters, and solar shields. A trade-off regarding spin rocket location exists between rocket performance and rocket thermal control. Total impulse required of the rocket is decreased by increasing the moment arm. From

Table 5.1-12

DESIGN CONCEPT A - THERMAL CONTROL INFORMATION

SUBSYSTEM AND COMPONENTS	TEMPERATURE LIMITS, °F OPERATING MIN	OPERATING MAX	NONOPERATING MIN	NONOPERATING MAX	HEAT DISSIPATION WATTS	WEIGHT, LBS.
Science Subsystem						
Extended Magnetometer						
Electronics	-13	167	NA	NA	7.0	5.0
Helium Sensor	-13	167	NA	NA	NA	1.5
Rubidium Sensor	32	122	NA	NA	NA	1.5
Energetic Particle Detector	14	122	NA	NA	0.4	2.5
Cosmic Dust Detector						
Electronics	-40	212	NA	NA	0.2	2.0
Sensor	-148	392	NA	NA	NA	0.5
Spacecraft Control						
Central Computer & Sequencer	0	125	NA	NA	10.0	12.0
Fine Sun Sensor	0	120	-58	212	1.0	1.0
Coarse Sun Sensors	0	120	-58	212	2.0	2.0
Earth Sensor	-10	125	-58	212	7.0	6.0
Star Tracker	-10	125	-58	212	10.0	10.0
Gyros	-65	250	-65	250	29.0	2.0
Accelerometer	10	100	-31	185	1.0	2.0
Attitude Control Electronics	10	100	-31	185	15N*/20P*	10.0
Midcourse Propulsion						
Thruster Assembly	NA	1500	70	NA	NA	2.5
Hydrazine Propellant & Tank	40	100	40	100	NA	16.3
Nitrogen Pressurization System	40	100	40	100	NA	20.0
Nitrogen and Tank	40	165	40	165	NA	2.4
Auxiliary Electric Power						
RTG Units	510	510	NA	NA	NA	120.0
Shunt Voltage Regulator	-30	160	NA	NA	6.0	1.8
Shunt Power Dissipation Resistors	-30	160	NA	NA	**	6.0
NI-CD-3 Electrode Battery	0	120	-65	120	**	21.0
Charge-Discharge Controller	-30	160	NA	NA	5.0	9.0
Voltage Regulator Mode Controller	-30	160	NA	NA	4.0	0.8
2400 cps Inverter	-30	160	NA	NA	23.0	4.0
Transfer Relay	-30	160	NA	NA	NA	1.0
400 cps Chopper & Regulator	-30	160	NA	NA	5.0	4.0
Emergency 2400 cps Inverter	-30	160	-65	160	NA	0.5
Inverter Synchronizer	-30	160	NA	NA	3.0	0.5
Power Distribution & Wiring	-65	160	-65	160	7.0	40.0
Diodes	-65	160	NA	NA	10.0	NA
Emergency Transfer Unit	-30	160	-65	160	NA	0.5
Communications						
TWT Amplifier	-65	203	NA	NA	45.0	4.0
Power Monitor	-65	203	NA	NA	NA	2.0
Circulator	-65	203	NA	NA	NA	5.0
Exciter	-65	203	NA	NA	10.0	7.0
Exciter Control	-65	203	NA	NA	5.0	2.0
APC Receiver	-65	203	NA	NA	10.0	9.0
Amplifier Control	-65	203	NA	NA	5.0	2.0
Power Supply	-65	203	NA	NA	12.0	7.0
Data Management						
Data Encoder Element	14	176	NA	NA	6.0	7.5
Data Storage Element	14	176	-55	185	1.0	5.0
Command Detector & Decoder Element	14	176	NA	NA	2.0	4.0
Data Automation Encoder	14	176	-55	257	2.0	4.0

*N Denotes nominal value
P Denotes peak value
** Dependent on operational requirements

this viewpoint, it would be desirable to mount the spin rockets on the outer surface of the RTG's. This location poses a severe thermal problem since the RTG's operate with a surface temperature of 510°F, considerably higher than the spin rocket limit. A compromise location on the equipment compartments is shown in Figure 5.1-1. Good thermal contact is maintained between the rocket cases and the equipment compartments to minimize rocket-to-rocket temperature variations. A suitable moment arm is also maintained.

The RTG heating through the supports is held to a low value by the use of low conductivity materials. Suitable materials include stainless steel, titanium, and glass-reinforced composites.

Cooling air is required during prelaunch to dissipate the heat from the RTG's and electronic equipment. The RTG heat is the major cooling load and amounts to about 14,600 BTU/hr. By cooling the components and RTG's to somewhat below the upper temperature limits during prelaunch, no cooling is required during launch. Thermal transients are sufficient to prevent overheating until Earth orbit is achieved. Then heat is dissipated by radiation as during the cruise phase of the mission. The thermal environment in Earth orbit does not cause overheating for this design concept.

The thermal control weight requirement is estimated to be 11 pounds. This is based on 6 pounds for insulation, shielding, etc., and 4.38 square feet of louvers at 1.12 lbs/sq.ft. It is noted that some of the spacecraft surface skin acts as cold plates, and the skin therefore has minimum thickness requirements. It appears that the structural and meteoroid protection requirements dictate thicknesses which amply meet the thermal control requirements, thus this weight is not considered a part of thermal control.

5.1.2.9 Radiation Protection

The general problem of nuclear radiation protection for Jupiter flyby spacecraft is discussed in subsection 3.9. The conclusion reported therein is that no specific design penalties should be incorporated for radiation protection. The judicious selection of radiation resistant components for the various subsystems and the proper placement of scientific instruments which are sensitive to RTG radiation is the recommended approach to radiation protection. Design Concept A reflects these design considerations to the extent possible in a conceptual design. This is particularly manifested in the spacecraft configuration. Based on the results presented in subsection 3.9, no radiation shielding is included in the design concept.

5.1.2.10 Meteoroid Protection

The data for a nominal 600 day mission used in assessing the meteoroid protection requirements for Concept A are summarized

in Table 5.1-13. The spacecraft exposed area in the interplanetary and asteroidal regions is determined as discussed in subsection 3.10.4, and the near-Earth and near-Jupiter exposed area is the total surface area of the spacecraft equipment compartment.

Table 5.1-13

DESIGN CONCEPT A - METEOROID PROTECTION ANALYSIS DATA

Region	Exposed Area(m^2)	Time (Days)	Area x Time (m^2-Days)
Near-Earth	2.79	0.5	2
Interplanetary	1.34	565	758
Asteroidal	1.34	190	255
Near-Jupiter	2.79	63.3	177

These data are combined with the data presented in subsection 3.10.3 to provide the design data shown in Figure 5.1-3. The two curves indicate the magnitude of difference in the protection requirements for the two asteroidal flux models. If a spacecraft aluminum skin thickness of 0.2 centimeter is used, the weight of the skin is approximately 30 pounds. This gives an expectation of essentially zero penetrations for the nominal asteroidal flux. On the other hand, if a criteria of one penetration during the mission is established, and the spacecraft is designed for the worst case of asteroidal flux, the resulting aluminum sheet thickness is 1.14 centimeters, and the weight is 195 pounds.

The meteroid protection system provided for Concept A consists of a complete covering of the spacecraft with 0.2 centimeter of aluminum. The choice of this design point is obviously arbitrary, but it is felt that it represents an adequate protection system with very little penalty. It does not appear desirable to accept the penalties imposed by the worst case asteroidal flux without in situ measurements of the actual environment.

As indicated in subsection 3.12, the armor-type meteoroid protection is considered to be an integral part of the spacecraft structure, and for nominal protection measures, the weight is assumed to be completely chargeable to the structure. Therefore, the meteoroid protection weight is not listed separately in the Design Concept A weight summary (Table 5.1-2), but is included in the estimate of structural/mechanical weight.

5.1.2.11 Configuration

The spacecraft configuration, shown in Figure 5.1-1, is characterized by four primary elements: (1) the central equipment compartment, (2) three truss-mounted RTG units, (3) a

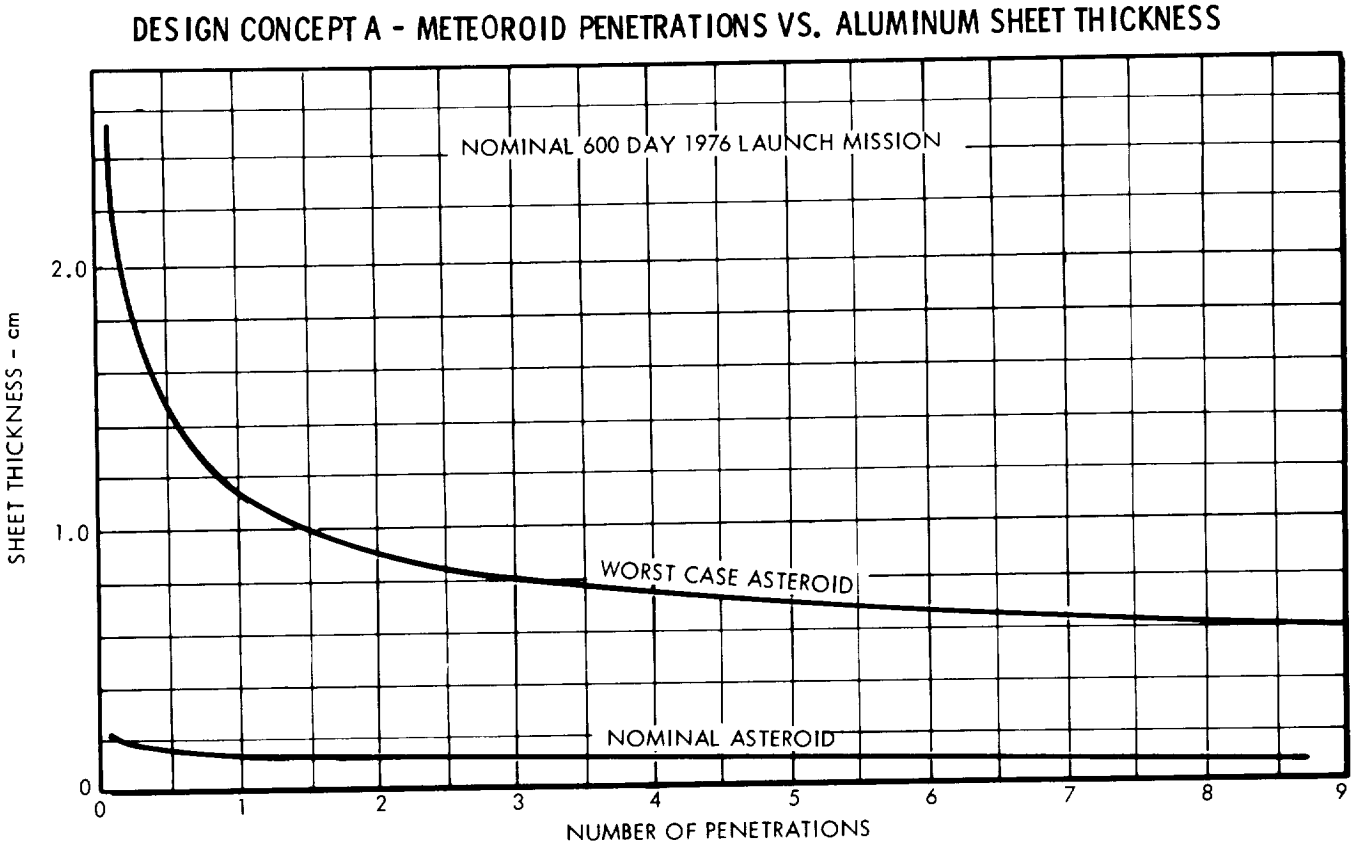

FIGURE 5.1-3

slotted wave guide communications antenna, and (4) three scientific sensors mounted on long deployable booms.

The central equipment compartment is a hexagonal-shaped enclosure. Three RTG units are mounted on truss supports projecting radially from the compartment and equally spaced at 120-degree intervals around the sides. Additional equipment compartments are attached to the center compartment between each of the RTG units. The center compartment houses the midcourse and attitude control propellant, the power conditioning, and the electrical cabling and routing. Data handling, communications, and midcourse thruster installation systems are located in each of the respective outer compartments. Thermal control louvers are located in the upper and lower surfaces of the outer compartments and are directed away from the Sun once the spacecraft is oriented. The high-gain communications antenna projects from the top of the center compartment along the spin axis; it is a cylindrical slotted wave guide type antenna which is 6 feet in length.

The thrust line of the midcourse propulsion system, which is located in one of the outer equipment compartments, is aligned perpendicular to the spin axis in such a manner that it is nominally in line with the spacecraft center-of-gravity. The central

location of the propellants and the careful attention to equipment placement within the spacecraft provide for minimum error in center of gravity location which is essential in this concept.

Two magnetometers of different dynamic ranges and the energetic particle detector are mounted on deployable booms which are clustered around the high-gain antenna during the launch phase. The cosmic dust detector is located on the lower portion of the spacecraft body in such a manner that the detector plates are arranged concentric to the spin axis to provide a potential 360^{o} view angle for detecting cosmic dust particles. The size of the detector is selected to offset the moment-area of the high-gain antenna. Mounted on the body of the spacecraft is an attitude control system which is a cold gas system providing interim three-axis control and initial spin-up rotation. The actual spin-up maneuver is conducted initially by the interim system and brought up to final rotational speed by the action of three solid-propellant rocket thrusters. These are mounted about the spacecraft body on the three outer compartments. As shown in Figure 5.1-1, the spacecraft is attached to the adapter structure mounted on the Atlas SLV 3x/Centaur/HEKS launch vehicle.

5.1.2.12 Structural and Mechanical Design

The central equipment compartment provides the core structure for Spacecraft Design Concept A. The central hex structure is built up of two frames held together by means of longerons, and closure is formed by skin panels completely surrounding the compartment. In order to provide meteoroid protection, the skin panels are 0.2 centimeter thick. They also are an integral part of the structure.

The lower section of the compartment is arranged with six pads which mate with the adapter interface, and primary launch loads are directed through the central compartment to the booster. Separation is provided by means of a spring loaded mechanism. This mechanism is activated upon the release of a hold down strap which is used to attach the spacecraft to the adapter during launch.

The three outer compartments are rectangular in construction and designed so that the upper and lower panels are removable for access to the internal equipment. The internal equipment is mounted to these panels, and thermal control louver assemblies are independently mounted on the external surfaces.

The central portion of the main compartment houses the propellant tanks which are mounted about a central column attached to the center box by means of a truss assembly. The center column supports (1) the main antenna which projects vertically upward and (2) the cosmic dust detector which projects vertically downward along the spin axis.

The thrust unit is housed in one of the outer compartments, and thrust loads are transmitted to a face plate which carries the loads into the box structure. An additional conical cover provides protection for the thruster nozzle and the associated control valve equipment.

The three booms which support the sensors are hinged from the outer compartments and latched to a plate on top of the slotted wave guide antenna. The booms are unlatched by means of a pyrotechnic device, and a spring-loaded mechanism is employed to move the booms to their final position in the nominal plane of the center of gravity. Each of the outer compartments is attached by four fasteners to the center compartment for quick and easy removal as a unit. The RTG units are supported on welded aluminum tubular truss assemblies which provide for (1) ease of assembly and (2) sufficient accessibility for installation of the fuel elements prior to lift off.

Structural and mechanical system weight (including meteoroid protection) for Design Concept A is estimated at 94 pounds on the basis of the average value derived from the relationship shown in Figure 3.12-2 for the case of a spacecraft injected weight of 531 pounds.

5.1.2.13 Subsystems Reliability

Table 5.1-14 contains the equipment mean-time-between-failure (MTBF) for Spacecraft Design Concept A. The science MTBF's are listed in Table 3.13-1. These MTBF's were determined using (1) a buildup of failure rates when an equipment design was available and (2) reliability estimates from similar equipment design and best engineering judgment when the equipment design was not available. For subsystem configurations containing redundant equipment, the MTBF listed in the table is for each of the redundant equipments. These equipment MTBF's are used to derive probability of mission success in subsection 5.1.4.

Table 5.1-14

SPACECRAFT DESIGN CONCEPT A - EQUIPMENT MTBF

SUBSYSTEM EQUIPMENT	MTBF (Hours)
Communications Subsystem	
Receiver	15,000
Exciter	45,000
TWT Amplifier	30,000
Circulator and Logic	350,000
TWT P/S	140,000
Power Monitor	333,000

Table 5.1-14
(Continued)

SUBSYSTEM EQUIPMENT	MTBF (Hours)
Data Management Subsystem	
Data Encoder Element	1,300
Data Storage Element	6,000
Command Det & Decoder Element	
Detector & Decoder	10,000
Commands	44,000 - 77,000
Data Automation Element	7,000
Spacecraft Control Subsystem	
Fine Sun Sensor	180,000
Coarse Sun Sensor	230,000
Earth Sensor	40,000
Star Tracker	35,000
Attitude Control Electronics	40,000
CC&S	4,500
Gyro and Accelerometer	8,000
Propulsion Subsystem	
Tank	0.9998*
Squib	0.999896*
Regulator	0.999556*
Rocket Motor and Vanes	0.99998*
Attitude Control Subsystem	
Tank	0.9998*
Squib	0.999896*
Regulator	0.999556*
Single Roll Jet	0.999465*
Single Pitch/Yaw Jet	0.999233*
Auxiliary Electrical Subsystem	
400 cps Chopper	210,000
Voltage Sensor and Regulator	60,000
2400 cps Chopper	150,000
Inverter Sync	220,000
Battery	70,000

* Probability of operations as required

5.1.3 Mission Performance

Mission performance envelopes, similar to that shown in Figure 5.1-4, were prepared for the Titan IIICx/Centaur and Atlas SLV3x/Centaur/HEKS launch vehicles, in combination with Spacecraft Design Concept A, for the launch years 1973 through 1980. From these envelopes, performance capabilities for Concept A were defined in terms of the width of the launch window or launch period, corresponding to the dates of western quadrature, opposition, and eastern quadrature. Arrival on the dates of these events requires Earth-to-Jupiter flight times of approximately 420 days, 510 days, and 600 days, in that order.

SPACECRAFT DESIGN CONCEPT A - MISSION PERFORMANCE ENVELOPE

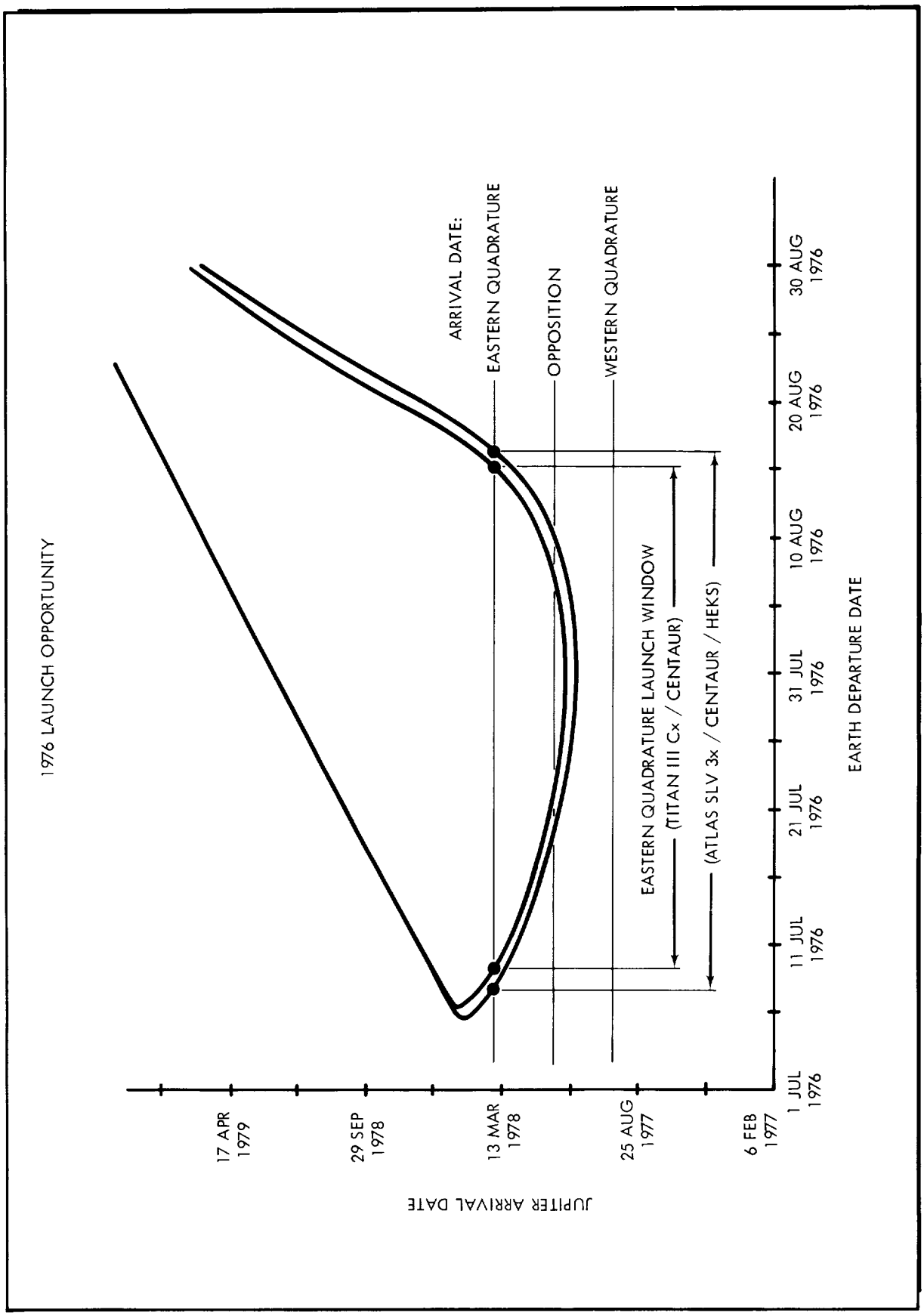

FIGURE 5.1-4

The mass of Concept A is below that mass at which the performance crossover between the Titan IIICx/Centaur and Atlas SLV3x/Centaur/HEKS takes place. The resultant effect is that the Atlas SLV3x/Centaur/HEKS launch vehicle provides slightly superior performance. As can be seen in Figure 5.1-5, neither launch vehicle is capable of injecting the spacecraft with sufficient energy to arrive at the time of western quadrature (approximately 420 days flight time).

Data denoted by dashes in Figure 5.1-5 represent the interval of the launch window in which magnitude of the departure asymptote declination is greater than 36 degrees. This upper limit on declination is explained in subsection 2.2.1.

5.1.4 Probability of Mission Success

The approach and guidelines employed in this study to evaluate the probability of mission success for Design Concept A are discussed in subsection 4.2. The results indicated therein are based on the mission described by the sequence of events in Table 5.1-1. It should be noted that the three-axis attitude stabilization function is required only through the time of spacecraft spin-up. The MTBF's utilized in this analysis are listed in Table 5.1-14.

The probabilities of mission success for both total and half missions are presented in Table 5.1-15. The probabilities of successful operation in the case of the communications, auxiliary electrical power, data management, and science subsystems are presented in Table 5.1-16.

Table 5.1-15

DESIGN CONCEPT A - PROBABILITY OF MISSION SUCCESS

Configuration	Probability of Mission Success: Total Mission (517 days)	Probability of Mission Success: Half Mission (259 days)
Spacecraft Less Science Instruments	0.02	0.20
Total Spacecraft	less than 0.01	0.10

Table 5.1-16

DESIGN CONCEPT A - SUBSYSTEMS PROBABILITY OF MISSION SUCCESS

Subsystem	Probability of Mission Success: Total Mission (517 days)	Probability of Mission Success: Half Mission (259 days)
Communications	0.58	0.82
Auxiliary Electrical Power	0.49	0.68
Data Management	0.07	0.39
Science	0.23	0.48

SPACECRAFT DESIGN CONCEPT A — LAUNCH VEHICLE MISSION PERFORMANCE SUMMARY CHART

(a) Titan III Cx / Centaur Launch Vehicle

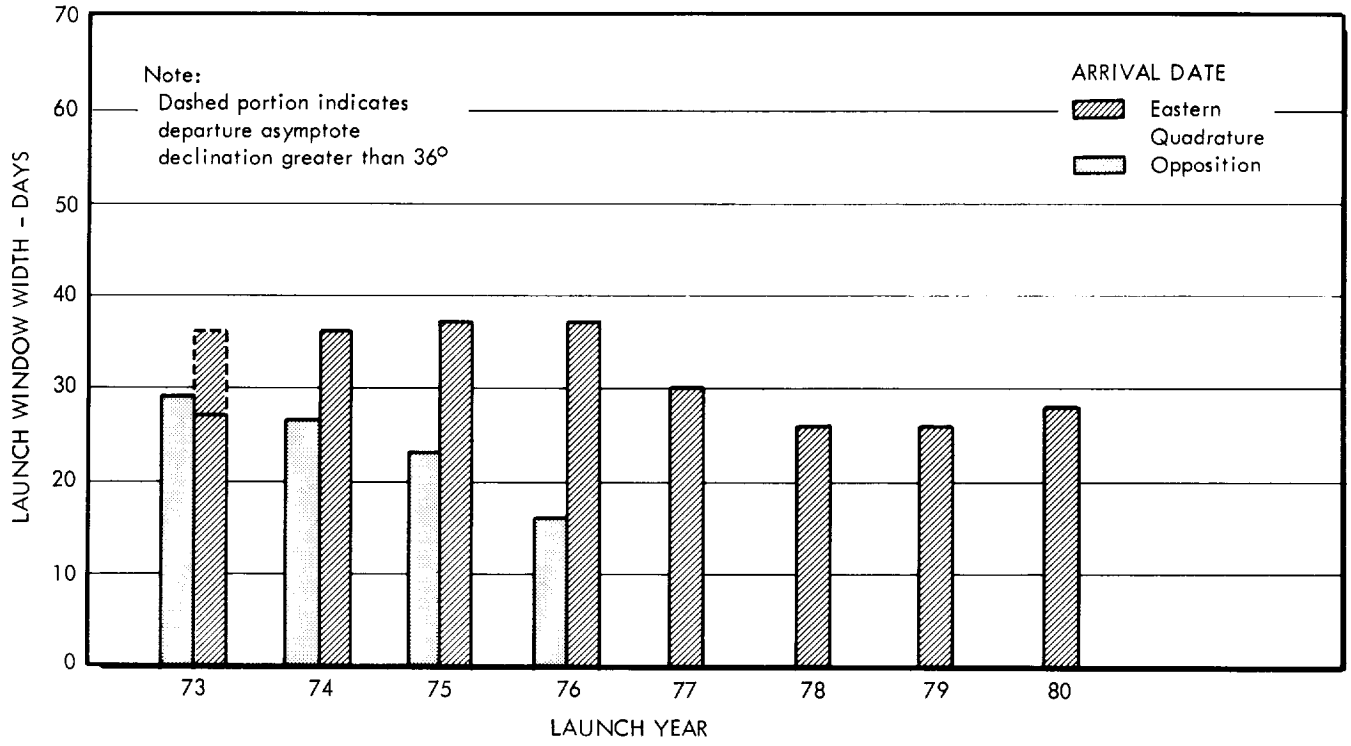

(b) Atlas SLV 3x / Centaur / HEKS Launch Vehicle

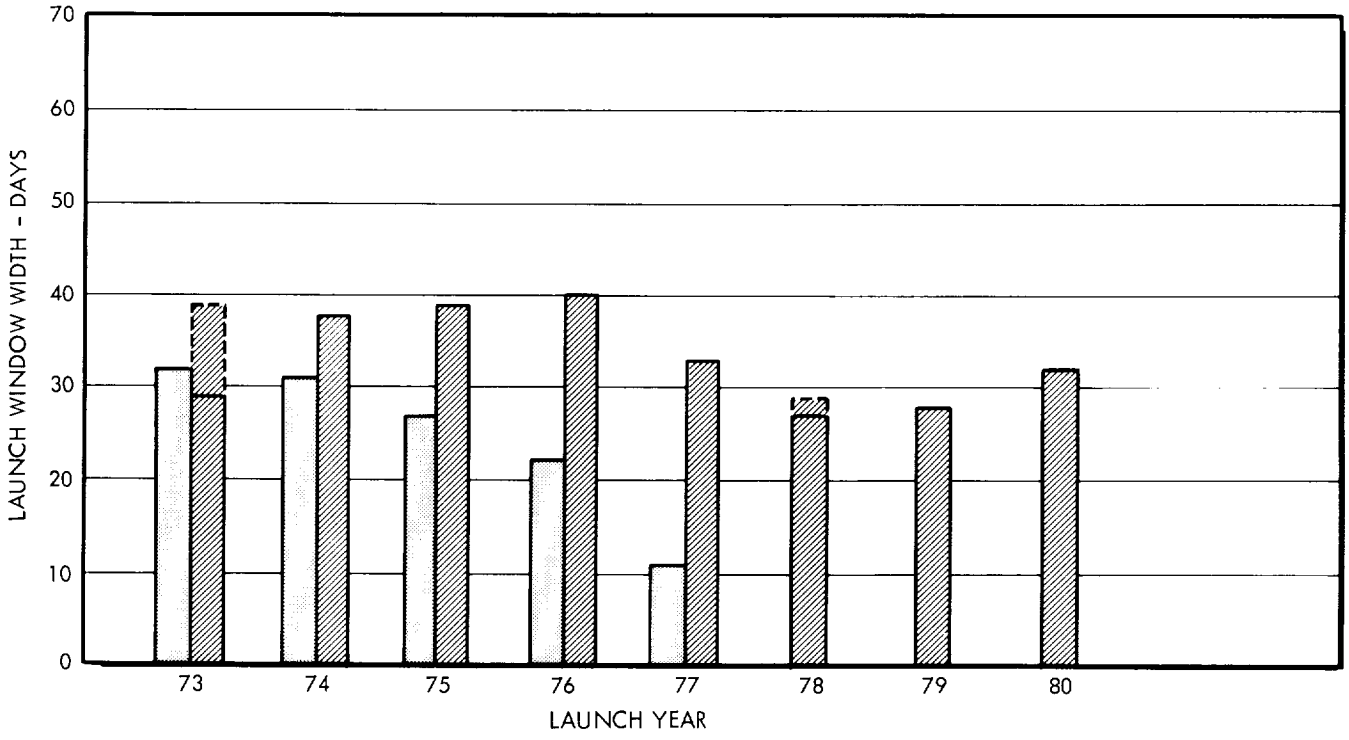

FIGURE 5. 1-5

5.1.5 Development Requirements

Optimistic, most likely, and pessimistic time estimates for completing each of the activities occurring between the events listed in the Program Implementation Network (see Figure 4.3-3) are shown in Table 5.1-17. In making the ASD PERT analysis, a program go-ahead date of 1 January 1968 was assumed with target launch dates of 28 March 1973 and 11 April 1973 for the primary mission vehicle and the back-up mission vehicle, respectively.

The essential results of the network analysis are presented in Table 5.1-18. The "Expected Date" column can be interpreted to mean that if the program were actually started 1 January 1968, the event dates shown could be achieved with a launch of the PMV in September 1972. The go-ahead date of 15 July 1968 shown in the "Latest Date" column is the latest possible start time to make a 28 March 1973 launch. It should be noted that the "Slack Times," "Standard Deviations," and "Probability of Meeting the Schedule" columns shown in the table are based on the go-ahead date of 1 January 1968.

The time line chart shown in Figure 5.1-6 was constructed by establishing the critical path through the network using the Latest Date column of Table 5.1-18. As shown by the chart, the total program span time is approximately 4 years and 8 months. The critical path can be traced by starting at the BUV launch (event 055) and following the critical predecessors back to event 001, contract go-ahead. As can be seen from the time line chart, the most critical subsystem development is the RTG. The fuel for this first unit can be obtained in less time (using the assumptions made in subsection 4.3) than the RTG unit per se can be developed. This, in turn, constrains the STM testing effort; however, completion of the PMV and BUV and, hence, their delivery to the launch site are constrained by the Pu 238 production rate. Obviously, if this span time can in some way be shortened, the total program span time would be much less. It is suggested that substantial effort be devoted to a more detailed analysis of the Pu 238 production problem, and the apportionment of this fuel among the various potential customers.

The results of the schedule confidence analysis of Spacecraft Design Concept A is shown in Figure 5.1-7. There is a probability of 0.6 that the program span time will be less than the 4 years 8 months shown in Figure 5.1-6. Similar probabilities can also be obtained from this figure.

5.1.6 Cost Results

Presented in Table 5.1-19 is a summary of the items that comprise the total program costs for Spacecraft Design Concept A, assuming two operational flights. The costs presented in Table 5.1-20 are the recurring spacecraft costs for two flights. The total cost increment for a third flight is given in Table 5.1-21. These results are based on the discussion in subsection 4.4.

Table 5.1-17
DESIGN CONCEPT A - PERT III INPUT ACTIVITY TIME ESTIMATES

TC	SP SCH OPT	BEG EVENT LC	END EVENT LC	OPT TIME	MEAN TIME	PESS TIME	SCH DATE ACT DATE / 1 / 2 / 3 / 4	EVENT TITLE /ACTIVITY TITLE
3			00.000.001				1.01.68	CONTRACT GO-AHEAD
1		00.000.001	00.000.002	2.0	4.0	12.0		C/JUPITER SYS DESIGN SPEC
1		00.000.002	00.000.003	4.0	8.0	12.0		C/SPCFT PREL SUBSYS + INRFCE SPEC
1		00.000.002	00.000.004	1.0	1.0	2.0		R/RTG FUEL PROCUREMENT ORDER
1		00.000.003	00.000.005					S/DETAILED CONFG DSGN + MOCKUP
1		00.000.003	00.000.006					S/SUBSYS PROCUREMENT NEGOTIATIONS
1		00.000.003	00.000.007	8.0	12.0	14.0		R/SCNCE PROCUREMENT
1		00.000.003	00.000.008	3.0	6.0	12.0		R/TEST SPEC + LAUNCH OPER PLAN
1		00.000.002	00.000.009	2.0	2.0	4.0		INITIATES EARTH LAUNCH VEH PROC
1		00.000.005	00.000.010	2.0	4.0	6.0		SCNCE PYLD, CONFG APPR + MCKUP COMPL
1		00.000.006	00.000.010					SCNCE PYLD, CONFG APPR + MCKUP COMPL
1		00.000.007	00.000.010	2.0	4.0	6.0		SCNCE PYLD, CONFG APPR + MCKUP COMPL
1		00.000.008	00.000.011	16.0	26.0	37.0		R/TEST + LAUNCH + FAC IMPLMTN PLAN
1		00.000.010	00.000.012	2.0	4.0	8.0		S/TOOLING DSGN
1		00.000.064	00.000.013					R/DATA MGMT SUBSYS PROCUREMENT
1		00.000.064	00.000.014					R/COMM SUBSYS PROCUREMENT
1		00.000.064	00.000.015					R/SPACECRAFT CONT SUBSYS PROC
1		00.000.064	00.000.016					R/RTG PROCUREMENT
1		00.000.064	00.000.017					R/MIDCOURSE PRPLN PROCUREMENT
1		00.000.064	00.000.018					R/ATTITUDE CONT PRPLN PROCUREMENT
1		00.000.012	00.000.019	2.0	4.0	6.0		S/MFGR OF STM + TCM STR + MECH SYS
1		00.000.013	00.000.020	26.0	52.0	104.0		RE/STM DATA MGMT SUBSYS
1		00.000.014	00.000.021	26.0	37.0	52.0		RE/STM COMM SUBSYS
1		00.000.015	00.000.022	26.0	64.0	130.0		RE/STM SPACECRAFT CONT SUBSYS
1		00.000.019	00.000.023	26.0	41.0	52.0		C/STM STR + MECH ASSY
1		00.000.020	00.000.023	1.0	1.0	2.0		C/STM STR + MECH ASSY
1		00.000.021	00.000.023	1.0	1.0	2.0		C/STM STR + MECH ASSY
1		00.000.022	00.000.023	1.0	1.0	2.0		C/STM STR + MECH ASSY
1		00.000.063	00.000.023					C/STM STR + MECH ASSY
1		00.000.023	00.000.024	1.0	2.0	3.0		S/STM ASTRIONICS COMPAT TESTS
1		00.000.024	00.000.026	2.0	4.0	6.0		C/STM ASTRIONICS COMPAT TESTS
* 1		00.000.004	00.000.027	12.0	36.0	48.0		RE/FIRST SET FUELED RTGS
1		00.000.016	00.000.027	64.0	78.0	208.0		RE/FIRST FUELED RTGS
1		00.000.017	00.000.028	29.0	52.0	104.0		RE/FIRST MIDCOURSE PRPLN
1		00.000.018	00.000.029	29.0	52.0	104.0		RE/FIRST ATTITUDE CONT PRPLN
1		00.000.007	00.000.030	12.0	20.0	52.0		RE/FIRST SET OF SCNCE
1		00.000.059	00.000.031	8.0	16.0	26.0		PRI CONFG QLFD FOR TCM + LETM TESTS
1		00.000.026	00.000.032					S/FINAL ASSY + TEST OF STM
1		00.000.027	00.000.032					S/FINAL ASSY + TEST OF STM
1		00.000.028	00.000.032					S/FINAL ASSY + TEST OF STM
1		00.000.029	00.000.032					S/FINAL ASSY + TEST OF STM
1		00.000.030	00.000.032					S/FINAL ASSY + TEST OF STM
1		00.000.033	00.000.032					S/FINAL ASSY + TEST OF STM
1		00.000.011	00.000.033					STM TEST AREA COMPL
1		00.000.031	00.000.034	1.0	2.0	6.0		S/MFGR OF LETM STR + MECH SYS
1		00.000.032	00.000.035	4.0	8.0	26.0		STM FUNCTIONALLY QLFD
1		00.000.037	00.000.036					S/TCM FINAL ASSY
1		00.000.062	00.000.036					S/TCM FINAL ASSY
1		00.000.035	00.000.037	4.0	4.0	26.0		R/REV TCM SUBSYS + SCNCE
1		00.000.036	00.000.039	2.0	4.0	6.0		C/TCM FINAL ASSY
1		00.000.039	00.000.040	2.0	2.0	4.0		S/TCM FINAL QUALIFICATION TESTS
1		00.000.040	00.000.041	2.0	4.0	8.0		TCM FUNCTIONALLY QLFD
1		00.000.034	00.000.042	12.0	12.0	26.0		S/LETM FINAL ASSY
1		00.000.041	00.000.042	1.0	1.0	2.0		S/LETM FINAL ASSY
1		00.000.041	00.000.043					RE/LETM SUBSYS WITH CHG INC
1		00.000.042	00.000.044	2.0	4.0	8.0		C/FINAL ASSY OF LETM
1		00.000.043	00.000.044	2.0	2.0	3.0		C/FINAL ASSY OF LETM
1		00.000.044	00.000.045	1.0	1.0	1.0		S/LETM QUALIFICATION TESTS
1		00.000.045	00.000.046	3.0	4.0	8.0		LETM QLFD DSGN FREEZE
1		00.000.046	00.000.047					C/MFGR, TEST OF PMV, BUV + PTM
1		00.000.066	00.000.047	12.0	12.0	26.0		C/MFGR, TEST OF PMV, BUV + PTM
* 1		00.000.067	00.000.047					C/MFG,TST OF PMV,BUV PTM
1		00.000.047	00.000.048	1.0	1.0	2.0		PMV + BUV ON DOCK AT LAUNCH SITE
1		00.000.011	00.000.049					ETR FAC AVAIL
1		00.000.065	00.000.050	4.0	4.0	6.0		EARTH LAUNCH VEH DEL TO LAUNCH SITE
1		00.000.048	00.000.051					S/ETR OPERATIONS
1		00.000.049	00.000.051					S/ETR OPERATIONS
1		00.000.050	00.000.051					S/ETR OPERATIONS
1		00.000.047	00.000.052	1.0	1.0	2.0		PTM DEL TO MISSION CONT CENTER
1		00.000.052	00.000.053	2.0	4.0	6.0		DSIF + MISSION CONT CENTER ACTVT
1		00.000.051	00.000.054	10.0	12.0	16.0	3.28.73	LAUNCH PMV
1		00.000.056	00.000.054	4.0	4.0	4.0	3.28.73	LAUNCH PMV
1		00.000.054	00.000.055	1.0	2.0	2.0	4.11.73	LAUNCH BUV
1		00.000.053	00.000.056					BGN SPCRFT FLT OPER AT FLT CONT STE
1		00.000.019	00.000.059	26.0	41.0	52.0		S/PREL STR INTEGRITY TESTING
1		00.000.011	00.000.060					TCM TEST FAC AVAIL FOR FIRST TEST
1		00.000.031	00.000.061	1.0	2.0	6.0		S/TCM PREL TESTS WITH MCKUP SUBSYS
1		00.000.060	00.000.061					S/TCM PREL TESTS WITH MCKUP SUBSYS
1		00.000.061	00.000.062	37.0	52.0	104.0		PRI SPCRFT STR TC QLFD
1		00.000.005	00.000.063	20.0	26.0	29.0		ALL STR + MECH SYS DWG COMPLETE
1		00.000.010	00.000.064	2.0	2.0	3.0		SUBSYS SPEC + INRFCE FREEZE
1		00.000.009	00.000.065					FINAL LAUNCH VEH STATUS REVIEW
1		00.000.031	00.000.066	2.0	3.0	6.0		S/MFGR PMV, BMV + PTM
* 1		00.000.027	00.000.067	56.0	104.0	152.0		RE/PMV+BUV RTG FUEL

Table 5.1-18
DESIGN CONCEPT A - PERT III EVENT SCHEDULE REPORT

EVENT TITLE	EVENT NO.	L C	CRITICAL PREDECESSOR	L C	S P	ACTUAL DATE	EXPECTED DATE	LATEST DATE	SCHEDULED DATE	SLACK TIME	STD DEV	PROB SCD	PROB POS	PROB SL
CONTRACT GO-AHEAD	CO-000-001						02JAN68	15JUL68		27.8	.0			.84
C/JUPITER SYS DESIGN SPEC	00-000-002		00-000-001				05FEB68	19AUG68		27.8	1.7			.84
C/SPCFT PREL SUBSYS + INRFCE SPEC	00-000-003		00-000-002				01APR68	14OCT68		27.8	2.1			.84
RE/FIRST SET FUELED RTGS	00-000-027		00-000-016				16JUN70	28DEC70		27.8	24.1			.84
S/ETR OPERATIONS	00-000-051		00-000-048				22JUN72	02JAN73		27.8	28.9			.84
R/RTG PROCUREMENT	00-000-016		00-000-064				05AUG68	17FEB69		27.8	2.4			.84
R/SCNCE PROCUREMENT	00-000-007		00-000-003				24JUN68	03JAN69		27.8	2.3			.84
C/MFGR, TEST OF PMV, BUV + PTM	00-000-047		00-000-067				13JUN72	26DEC72		27.8	28.9			.84
RE/PMV+BUV RTG FUEL	00-000-067		00-000-027				13JUN72	26DEC72		27.8	28.9			.84
SCNCE PYLD, CDFG APPR + MCKUP COMPL	00-000-010		00-000-007				22JUL68	31JAN69		27.8	2.4			.84
PMV + BUV ON DOCK AT LAUNCH SITE	00-000-048		00-000-047				22JUN72	02JAN73		27.8	28.9			.84
SUBSYS SPEC + INRFCE FREEZE	00-000-064		00-000-010				05AUG68	17FEB69		27.8	2.4			.84
LAUNCH PMV	00-000-054		00-000-051				18SEP72	30MAR73	28MAR73	27.8	28.9	.84		.84
LAUNCH BUV	00-000-055		00-000-054				29SEP72	11APR73	11APR73	27.8	28.9	.84		.84
BGN SPCRFT FLT OPER AT FLT CONT STE	00-000-056		00-000-053				20JUL72	02MAR73		32.1	28.9			.87
PTM DEL TO MISSION CONT CENTER	00-000-052		00-000-047				22JUN72	02FEB73		32.1	28.9			.87
DSIF + MISSION CONT CENTER ACTVT	CO-000-053		00-000-052				20JUL72	02MAR73		32.1	28.9			.87
S/DETAILED CDFG DSGN + MOCKUP	00-000-005		00-000-003				01APR68	03JAN69		39.5	2.1			.92
S/SUBSYS PROCUREMENT NEGOTIATIONS	CO-000-006		00-000-003				01APR68	31JAN69		43.5	2.1			.93
S/MFGR OF STM + TCM STR + MECH SYS	00-000-019		00-000-012				16SEP68	28APR70		84.1	2.7			1.00
S/TOOLING DSGN	00-000-012		00-000-010				19AUG68	31MAR70		84.1	2.6			1.00
S/PREL STR INTEGRITY TESTING	00-000-059		00-000-019				25JUN69	04FEB71		84.1	5.1			1.00
S/TCM PREL TESTS WITH MCKUP SUBSYS	00-000-061		CO-000-031				04NOV69	15JUN71		84.1	6.0			1.00
LETM QLFD DSGN FREEZE	00-000-046		00-000-045				17MAY71	26DEC72		84.1	12.7			1.00
S/LETM QUALIFICATION TESTS	00-000-045		00-000-044				15APR71	24NOV72		84.1	12.7			1.00
PRI SPCRFT STR TC QLFD	00-000-062		00-000-061				16DEC70	27JUL72		84.1	12.7			1.00
C/FINAL ASSY OF LETM	CO-000-044		00-000-042				08APR71	17NOV72		84.1	12.7			1.00
S/TCM FINAL ASSY	00-000-036		00-000-062				16DEC70	27JUL72		84.1	12.7			1.00
S/LETM FINAL ASSY	CO-000-042		CO-000-041				09MAR71	17OCT72		84.1	12.7			1.00
PRI COFG QLFD FOR TCM + LETM TESTS	00-000-031		00-000-059				17OCT69	31MAY71		84.1	5.9			1.00
C/TCM FINAL ASSY	CO-000-039		00-000-036				13JAN71	24AUG72		84.1	12.7			1.00
TCM FUNCTIONALLY QLFD	CO-000-041		00-000-040				01MAR71	09OCT72		84.1	12.7			1.00
S/TCM FINAL QUALIFICATION TESTS	00-000-040		00-000-039				29JAN71	11SEP72		84.1	12.7			1.00
RE/LETM SUBSYS WITH CHG INC	00-000-043		00-000-041				01MAR71	01NOV72		87.4	12.7			1.00
STM FUNCTIONALLY QLFD	CO-000-035		00-000-032				28AUG70	05JUN72		92.2	24.4			1.00
R/REV TCM SUBSYS + SCNCE	00-000-037		00-000-035				20OCT70	27JUL72		92.2	24.7			1.00
S/FINAL ASSY + TEST OF STM	00-000-032		00-000-027				16JUN70	23MAR72		92.2	24.1			1.00
C/STM STR + MECH ASSY	00-000-023		00-000-022				08DEC69	10FEB72		113.6	17.5			1.00
S/STM ASTRIONICS COMPAT TESTS	CO-000-024		00-000-023				22DEC69	24FEB72		113.6	17.5			1.00
R/SPACECRAFT CONT SUBSYS PROC	00-000-015		CO-000-064				05AUG68	09OCT70		113.6	2.4			1.00
C/STM ASTRIONICS COMPAT TESTS	00-000-026		00-000-024				19JAN70	23MAR72		113.6	17.5			1.00
RE/STM SPACECRAFT CONT SUBSYS	00-000-022		00-000-015				28NOV69	01FEB72		113.6	17.5			1.00
R/RTG FUEL PROCUREMENT ORDER	00-000-004		00-000-002				13FEB68	04MAY70		115.8	1.7			1.00
RE/STM DATA MGMT SUBSYS	00-000-020		00-000-013				02SEP69	01FEB72		126.0	13.2			1.00
R/DATA MGMT SUBSYS PROCUREMENT	00-000-013		00-000-064				05AUG68	04JAN71		126.0	2.4			1.00
RE/FIRST MIDCOURSE PRPLN	CO-000-028		00-000-017				08SEP69	23MAR72		132.7	12.7			1.00
R/MIDCOURSE PRPLN PROCUREMENT	00-000-017		CO-000-064				05AUG68	19FEB71		132.7	2.4			1.00
R/ATTITUDE CONT PRPLN PROCUREMENT	00-000-018		CO-000-064				05AUG68	19FEB71		132.7	2.4			1.00
RE/FIRST ATTITUDE CONT PRPLN	CO-000-029		00-000-018				08SEP69	23MAR72		132.7	12.7			1.00
R/TEST + LAUNCH + FAC IMPLMTN PLAN	00-000-011		00-000-008				18NOV68	15JUN71		134.5	4.4			1.00
TCM TEST FAC AVAIL FOR FIRST TEST	00-000-060		00-000-011				18NOV68	15JUN71		134.5	4.4			1.00
R/TEST SPEC + LAUNCH OPER PLAN	00-000-008		00-000-003				17MAY68	14DEC70		134.5	2.6			1.00
S/MFGR OF LETM STR + MECH SYS	00-000-034		00-000-031				04NOV69	10JUL72		139.8	6.0			1.00
R/COMM SUBSYS PROCUREMENT	00-000-014		00-000-064				05AUG68	14MAY71		144.6	2.4			1.00
RE/STM COMM SUBSYS	00-000-021		00-000-014				25APR69	01FEB72		144.6	4.9			1.00
S/MFGR PMV, BMV + PTM	00-000-066		00-000-031				10NOV69	18SEP72		148.8	5.9			1.00
RE/FIRST SET OF SCNCE	00-000-030		00-000-007				09DEC68	23MAR72		171.7	7.1			1.00
STM TEST AREA COMPL	00-000-033		00-000-011				18NOV68	23MAR72		174.7	4.4			1.00
ALL STR + MECH SYS DWG COMPLETE	00-000-063		00-000-005				27SEP68	10FEB72		175.9	2.6			1.00
ETR FAC AVAIL	00-000-049		00-000-011				18NOV68	02JAN73		215.5	4.4			1.00
FINAL LAUNCH VEH STATUS REVIEW	00-000-065		00-000-009				21FEB68	04DEC72		249.6	1.7			1.00
EARTH LAUNCH VEH DEL TO LAUNCH SITE	00-000-050		00-000-065				22MAR68	02JAN73		249.6	1.7			1.00
INITIATES EARTH LAUNCH VEH PROC	00-000-009		00-000-002				21FEB68	04DEC72		249.6	1.7			1.00

DESIGN CONCEPT A — TIME LINE CHART

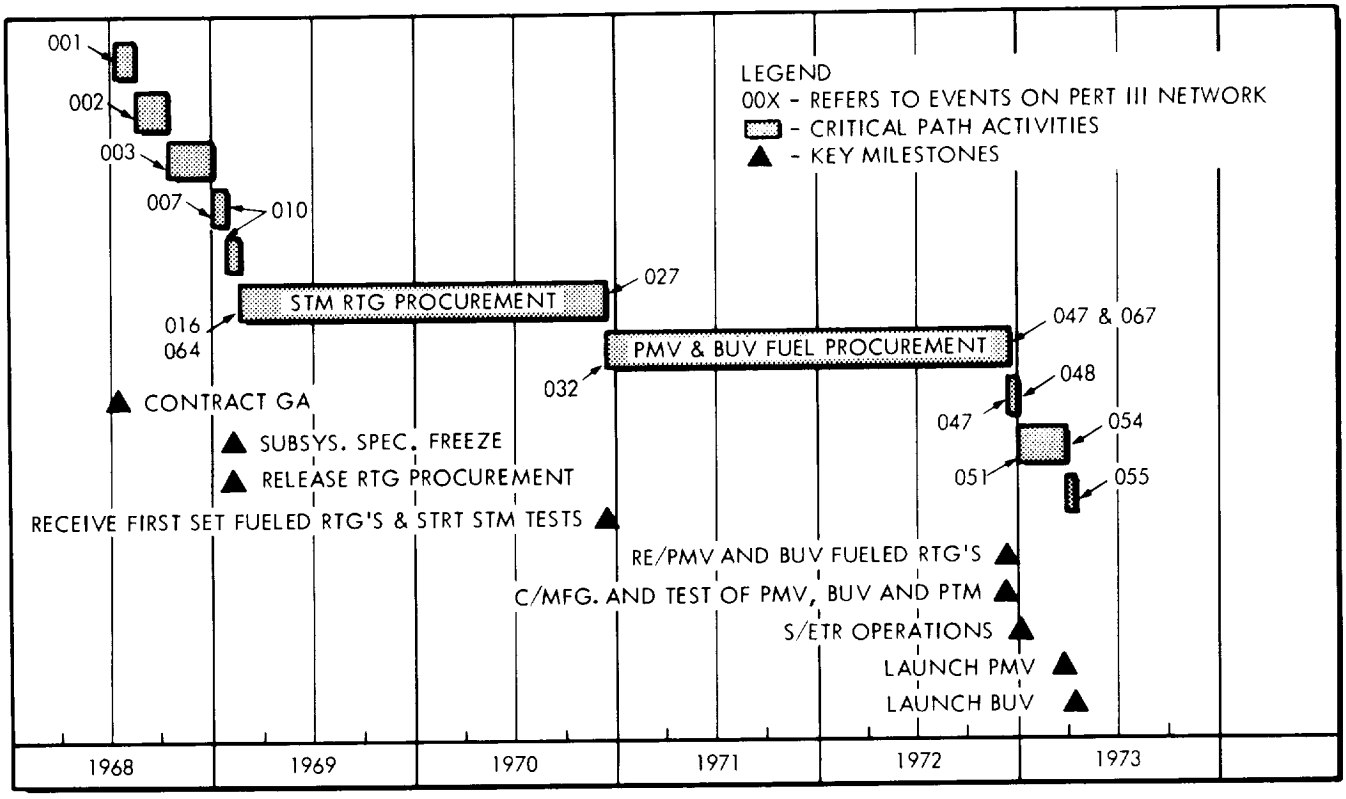

FIGURE 5.1-6

DESIGN CONCEPT A - SCHEDULE CONFIDENCE

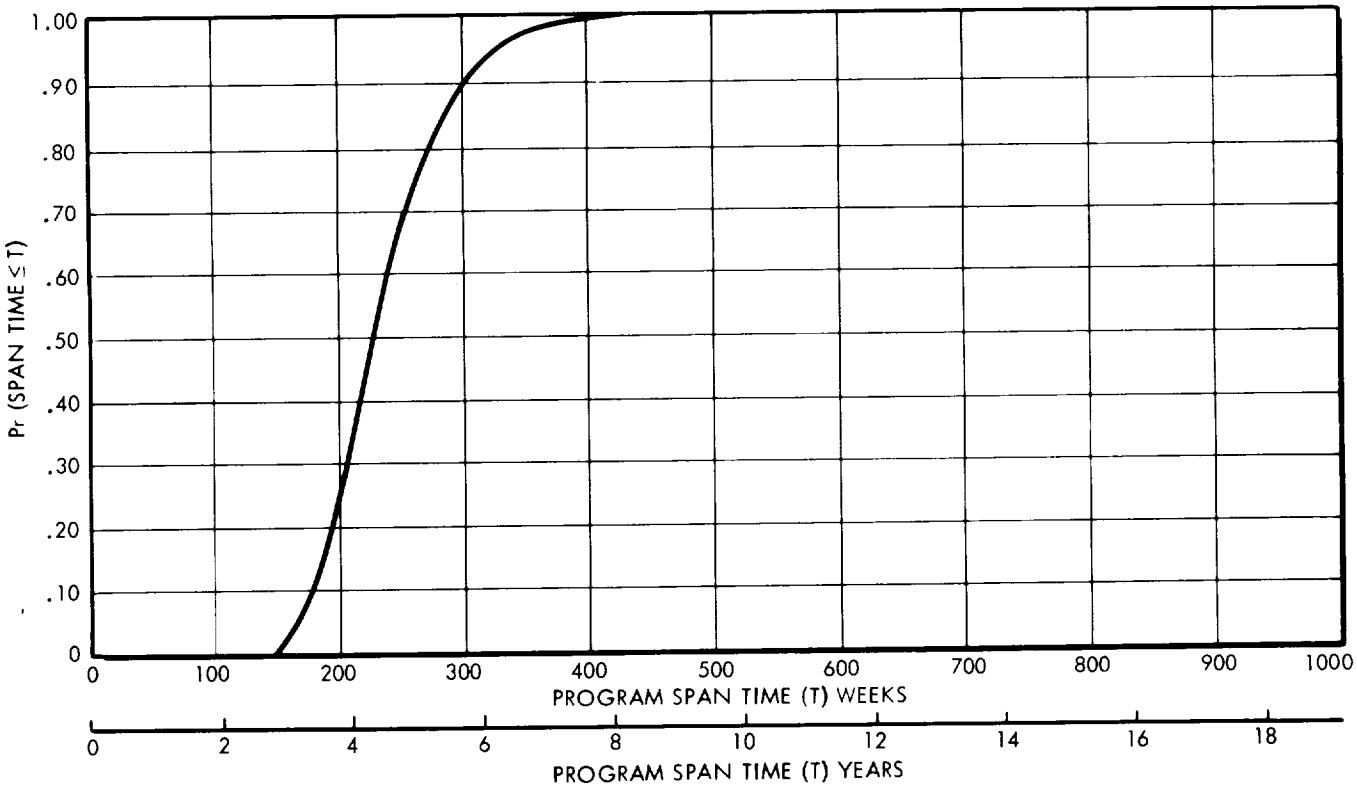

FIGURE 5.1-7

Table 5.1-19

DESIGN CONCEPT A - SUMMARY OF PROGRAM COSTS

(In Millions of 1965 Dollars)

COST CATEGORIES	LAUNCH VEHICLE TYPE	
	Atlas SLV3x/ Centaur/HEKS	Titan IIICx/ Centaur
NONRECURRING		
Science	0.65	
Communications & Data Mgt	8.00	
Spacecraft Control	7.75	
Attitude Control	0.25	
Midcourse Propulsion	1.90	
Electrical Power	13.20	
Structural, Mech, Therm, & Shield	4.62	
Subtotal Subsystems, DT&E	36.37	
Operational Support Equip	10.00	
Tooling & Special Equip	2.30	
System Integration	5.00	
Ground Test Hardware	9.90	
Total Nonrecurring Costs	63.57	63.57
RECURRING (2 Launches)		
Recurring Spacecraft	19.39	19.39
Spacecraft Spares (2 Sets)	2.32	2.32
Deep Space Net Support	30.00	32.00
Spacecraft Operations	2.82	2.95
Launch Vehicles	21.40	42.82
Launch Operations	11.20	14.80
Total Recurring Costs	87.13	114.28
TOTAL PROGRAM COSTS	150.70	177.85

Table 5.1-20

DESIGN CONCEPT A - RECURRING SPACECRAFT COSTS FOR TWO FLIGHTS

(In Millions of 1965 Dollars)

COST CATEGORY	
Science	0.08
Communications & Data Mgt	0.98
Spacecraft Control	0.90
Attitude Control	0.03
Midcourse Propulsion	0.08
Electrical Power	3.12
Structure, Mech, Ther, & Shield	0.41
Spacecraft Checkout & Assembly	0.92
Subtotal Spacecraft Cost	6.52
RTG Fuel Cost @ $\$1500/W_t$	12.87
Total Spacecraft	19.39

Table 5.1-21

DESIGN CONCEPT A - COST INCREMENT FOR A THIRD FLIGHT

(In Millions of 1965 Dollars)

	Atlas SLV3x/ Centaur/HEKS	Titan IIICx/ Centaur
Recurring Spacecraft	$ 9.70	$ 9.70
Launch Vehicle	10.70	21.41
Launch Operations	5.60	7.40
TOTAL	$ 26.00	$ 38.51
TOTAL*	$ 23.66	$ 36.17

* The total cost increment for a third flight assuming that one of the ground test models is used.

5.2 SPACECRAFT DESIGN CONCEPT B

Spacecraft Concept B, which is a three-axis stabilized, minimal scientific capability Jupiter flyby vehicle, is described in this subsection.

5.2.1 Design Summary

A configuration of Spacecraft Design Concept B is illustrated in Figure 5.2-1. The design philosophy for this concept is to provide minimal capability and complexity in the science package. As a result, the supporting subsystems also exhibit these characteristics. The injected weight of the spacecraft is approximately 720 pounds. Flight times of 500-600 days are possible with the Atlas SLV3x/Centaur/HEKS or the Titan IIICx/Centaur for most launch opportunities in the time period 1973-1980. Significant flight events for a nominal mission are detailed in Table 5.2-1.

A time period of 5.5 years is estimated for the development of the spacecraft. If two spacecraft are launched with Atlas SLV3x/Centaur/HEKS launch vehicles, total program cost is estimated to be $179 million. Total program cost for two Titan IIICx/Centaur launched spacecraft is estimated to be $204 million.

The salient characteristics of the spacecraft are (1) a science capability of approximately 40 pounds and 25 watts, (2) a steerable, 27 db gain antenna and a 25-watt transmitter, (3) data compression and tape storage, (4) three-axis stabilization using a reaction jet system, (5) Mariner IV-type midcourse propulsion, (6) Pu 238 RTG's, and (7) armor-type meteoroid protection. The spacecraft performance is indicated by the following: (1) a 17-bit per second information rate at 6 a.u. communications distance, (2) data storage for 48 M bits, (3) a vernier correction capability of 60 m/sec, and (4) 240 watts of available electrical power.

Following injection into a transfer trajectory, the spacecraft acquires three-axis stabilization using the Sun and Canopus as primary references. The cruise science is turned on. A vernier correction is executed utilizing computations and commands transmitted from Earth. The primary communications downlink is the high gain parabolic antenna. Omni antennas are provided for two-way communications during the early part of the mission and for uplink communications throughout the mission. The high gain antenna is pointed at the Earth by periodically changing its position relative to the spacecraft axes. During encounter, occultation of both of the primary attitude references by Jupiter is a good possibility. Therefore, the spacecraft attitude is inertially controlled during part of the encounter phase. Encounter data is stored on tape. The expected deviation from the nominal periapsis altitude is 2600 km. Following occultation, cruise attitude references are reacquired, and the encounter data are played back. The spacecraft then returns to cruise mode operations.

SPACECRAFT DESIGN CONCEPT B CONFIGURATION

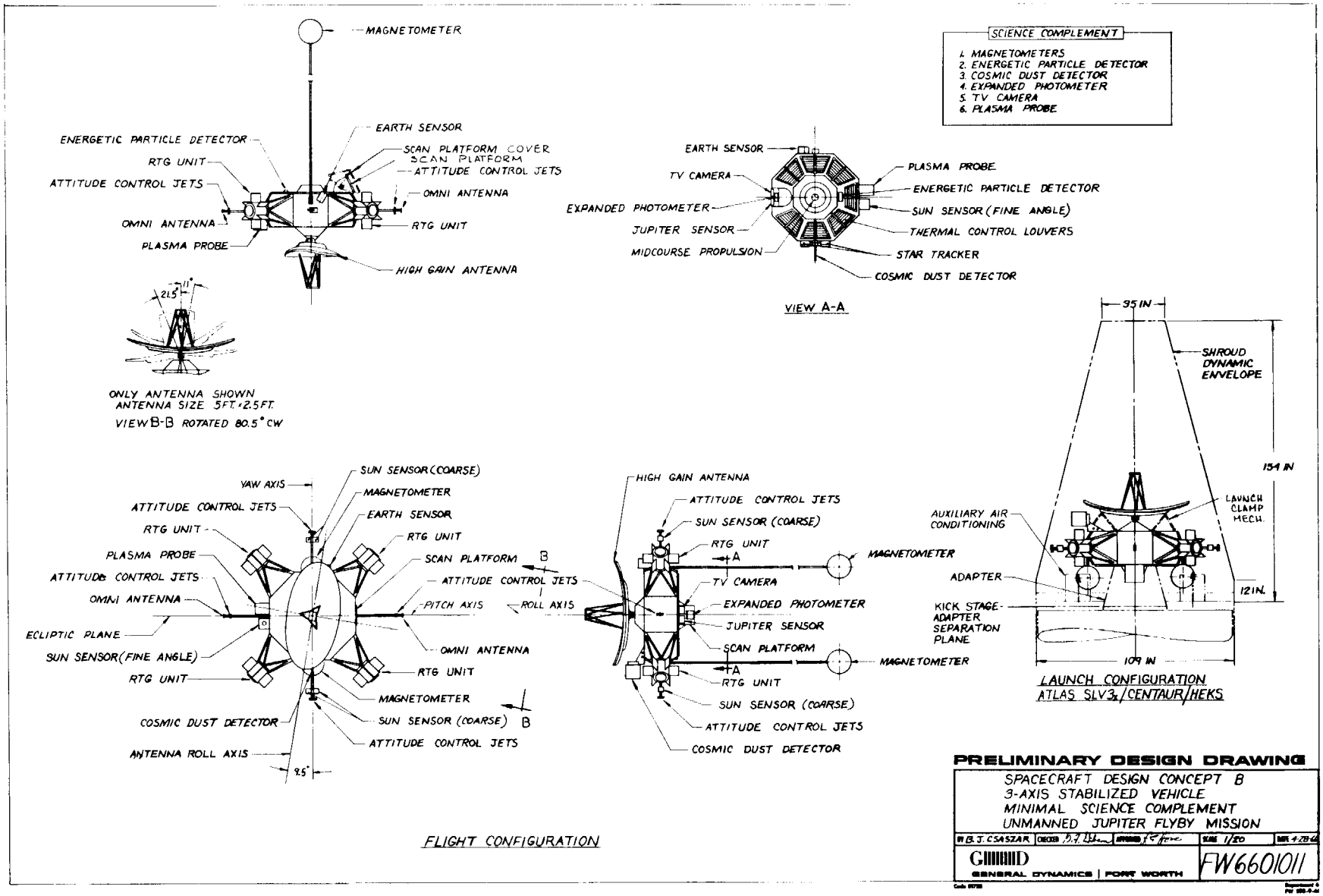

FIGURE 5.2-1

Table 5.2-1
SEQUENCE OF SIGNIFICANT FLIGHT EVENTS FOR SPACECRAFT DESIGN CONCEPT B

Notes: The mission characteristics are a 1976 launch, Atlas/Centaur/HEKS launch vehicle, 582 day flight time, posigrade equatorial pass, and 1.0 Jupiter radius nominal perijove altitude. The CC&S is the primary control for all spacecraft events except where noted. Backup via ground command is implied for all events.

No.	Event	Nominal Time
1	Install RTG units and activate auxiliary cooling system	L - 1 day
2	Update CC&S master clock and sequence timer	L - 3 min.
3	Turn on gyros, DEE, and CDDE	L - 2 min.
4	Liftoff	L
5	Atlas booster engine cutoff	
6	Payload fairing separation	
7	Atlas sustainer engine cutoff	
8	Atlas vernier engine cutoff	
9	First Centaur ignition	
10	First Centaur cutoff (begin orbital coast)	
11	Second Centaur ignition (end orbital coast)	
12	Second Centaur cutoff	
13	High Energy Kick Stage (HEKS) ignition	
14	HEKS cutoff (Injection)	I = L + 120 min.
15	Spacecraft - HEKS separation	I + 2 min.
	a. Pyrotechnics armed	
	b. Transmitter power up	
	c. Begin communication with omni antennas at data transmission rate of 33 bps	
16	Initial Sun acquisition	I + 10 min.
	a. Turn on attitude control system	
	b. Turn on coarse Sun sensor	
	c. Activate gas-jet system	
	d. Begin Sun acquisition sequence	
17	Sun acquired	I + (10 - 20) min.
18	Activate cruise science	I + 20 min.
	a. Deploy magnetometers	
	b. Turn on DAE	
	c. Turn on cruise science	
19	Canopus acquisition	I + 100 min.
	a. Turn on Canopus sensor	
	b. Set sensor cone angle	
	c. Begin roll turn	
	d. Receive acquisition signal	
	e. Turn on Earth sensor	
	f. Verify Canopus acquisition (continue roll search if Earth not acquired)	
20	Canopus acquired	I + (100 - 130) min.
	a. Gyros turned off	
21	Prepare for midcourse maneuver	M - 60 min.
	a. Transmit and verify pitch-turn duration and polarity	
	b. Transmit and verify roll-turn duration and polarity	
	c. Transmit and verify velocity increment	
22	Begin midcourse maneuver sequence	M = I + (1 - 7)days
	a. Turn on fine Sun sensor	
	b. Acquire Sun with fine Sun sensor	
	c. Turn on gyros	
	d. Turn on accelerometer	
23	Execute pitch turn	M + 60 min.
	a. Switch out error signals from Earth, Sun, and Canopus sensors	
	b. Set proper polarity	
	c. Pitch turn started	
	d. Pitch turn stopped	M + (60 - 65) min.
24	Execute roll turn	M + 75 min.
	a. Set proper polarity	
	b. Roll turn started	
	c. Roll turn stopped	M + (75 - 80) min.
25	Execute motor burn	M + 90 min.
	a. Command motor ignition	
	b. Command motor shutoff	M + (90 - 91.5) min.
26	Sun reacquisition	M + 93 min.
	a. Turn off accelerometer	
	b. Switch in error signal from coarse Sun sensor	
	c. Execute roll turn with opposite polarity	
	d. Execute pitch turn with opposite polarity	
	e. Begin Sun acquisition sequence	
27	Sun reacquired	M + (93 - 98) min.
28	Canopus reacquisition	M + 99 min.
	a. Switch in error signal from Canopus sensor	
	b. Begin roll turn	
	c. Receive acquisition signal	
	d. Switch in signal from Earth sensor	
	e. Verify Canopus acquisition	

Table 5.2-1 (Continued)

No.	Event	Nominal Time
29	Canopus reacquired	M + (99 - 104) min.
	a. Gyros turned off	
30	Switch data transmission rate from 33 to 17 bps	I + 32 days
31	Activate high-gain antenna	I + 60 days
	a. Unlock antenna	
	b. Drive to position 1	
	c. Switch transmitter to high-gain antenna	
	d. Switch data transmission rate from 17 to 133 bps	
32	Drive high-gain antenna to position 2	I + 65 days
33	Drive high-gain antenna to position 3	I + 80 days
34	Drive high-gain antenna to position 4	I + 88 days
35	Drive high-gain antenna to position 5	I + 105 days
36	Switch data transmission rate from 133 to 67 bps	I + 182 days
37	Drive high-gain antenna to position 4	I + 230 days
38	Switch data transmission rate from 67 to 33 bps	I + 232 days
39	Drive high-gain antenna to position 3	I + 270 days
40	Drive high-gain antenna to position 2	I + 310 days
41	Drive high-gain antenna to position 1	I + 360 days
42	Drive high-gain antenna to position 2	I + 480 days
43	Drive high-gain antenna to position 3	I + 520 days
44	Drive high-gain antenna to position 4	I + 570 days
45	Transmit and verify required scan platform orientation angle	E - 2 days
46	Scan platform orientation	E - 1 day
	a. Remove encounter science instrument cover	
	b. Activate scan platform drive	
	c. Position scan platform	
	d. Turn on Jupiter sensor Verify sensor operation	

No.	Event	Nominal Time
47	Turn on Gyros	E - 360 min.
48	Jupiter acquired	E - 210 min.
49	Begin encounter sequence	E - 180 min.
	a. Turn on DSE	
	b. Turn on encounter science	
50	Begin TV picture recording	E - 80 min.
51	TV turned off	E - 30 min.
52	Perijove passage (one Jupiter radius altitude)	E = I + 582 days
53	Switch to inertial attitude control mode	E + 10 min.
	a. Switch out error signal from Sun sensor	
	b. Uncage pitch and yaw gyros	
54	Begin Earth occultation (0^{o} cone)	E + 18 min.
55	Begin Sun occultation (0^{o} cone)	E + 30 min.
56	End Earth occultation (0^{o} cone)	E + 84 min.
57	End Sun occultation (0^{o} cone)	E + 102 min.
58	End encounter sequence	E + 180 min.
	a. Turn off encounter science	
	b. Turn off DSE	
59	Switch to Sun-reference attitude control mode	E + 190 min.
	a. Acquire Sun	
	b. Turn off gyros	
60	Transmit command to initiate encounter data playback	E + 2 days
	a. DSE turned on (cyclic transmission of one hour real time data to five hours of non-real time data)	
61	End data playback	E + 6 days
	a. Turn off DSE	
62	Return to cruise mode	E + 6 days
63	Switch data transmission rate from 33 to 17 bps	E + 12 days

A weight summary for Design Concept B is given in Table 5.2-2.

Table 5.2-2

SPACECRAFT DESIGN CONCEPT B WEIGHT SUMMARY

Subsystem	Weight, lbs.
Science	37
Communications	75
Data Management	39
Spacecraft Control	68
Attitude Control Propulsion	80
Midcourse Propulsion	47
Electrical Power	222
Structural/Mechanical and Meteroid Protection	138
Thermal Control	11
Total Spacecraft	717
Adapter (0.065 x Spacecraft Weight)	47
Launch Weight	764

5.2.2 Subsystem Design Information

5.2.2.1 Science

In Spacecraft Design Concept B, provision is made for a scientific instrument complement of minimal capability. A definition of the minimal scientific experiment package is presented in Table 2.1-8, and the instruments are listed again in Figure 5.2-1. The individual instruments are described in subsection 2.1. The total weight of this package is 37 pounds.

Several design features related to Concept B represent direct responses to the science subsystem requirements. These design features and the associated requirements are discussed in some of the subsections which follow, particularly, in those subsections related to data management (data automation element), radiation protection, configuration (pointing geometries), and structural and mechanical design (scan platform implementation and sensor deployment).

5.2.2.2 Communications

The communications subsystem recommended for Design Concept B is essentially the subsystem shown in Figure 3.1-8. The TWT amplifiers have a power output of 25 watts which is considered consistent with the amount of data to be returned by the Concept B spacecraft. For simplicity, the steering mechanism of the high gain antenna is limited to one degree of freedom. With only one degree of freedom, the antenna's beam must be specially shaped to allow continuous communications. Since the Earth's position with respect to the Sun is a function of the trajectory chosen, the

shape of the antenna reflector must be tailored to each specific mission. Examples of possible antenna beams and pointing requirements for three trajectories are shown in Figures 5.2-2, 5.2-3 and 5.2-4. The antenna positions shown in Figure 5.2-2 are representative of those obtained with the antenna arrangement shown in Figure 5.2-1. The antenna has a 6 degree x 12 degree beam and the major axis is aligned with the Earth's path. A circular pattern with an 8 degree beamwidth is shown in Figure 5.2-3. The positions shown in Figure 5.2-4 are those of an antenna with a 6 degree x 12 degree beam and with the minor axis generally along the Earth's path. Each of these antennas yields 27 db of gain.

ANTENNA POSITIONING EXAMPLE - 1976, 600 DAY MISSION

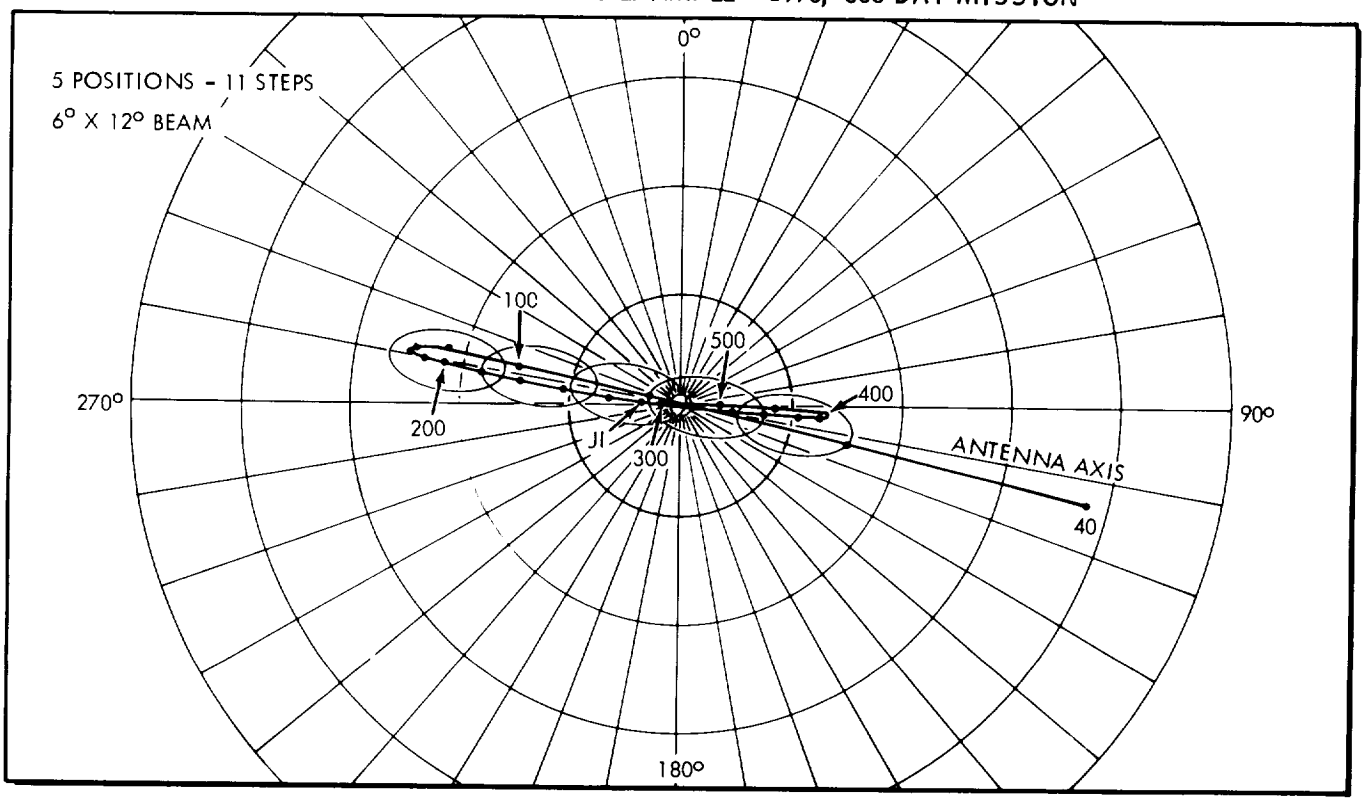

FIGURE 5.2-2

ANTENNA POSITIONING EXAMPLE - 1975, 600 DAY MISSION

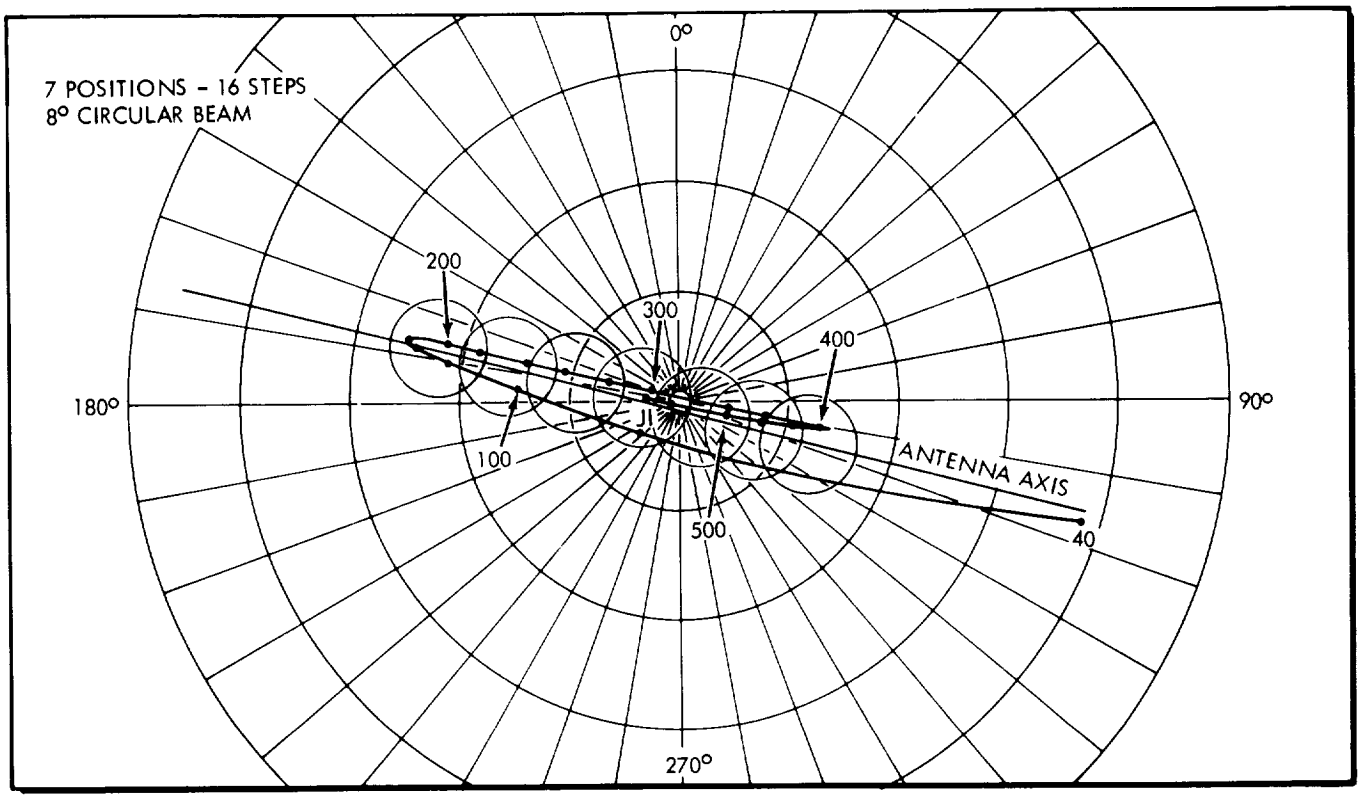

FIGURE 5. 2-3

ANTENNA POSITIONING EXAMPLE - 1974, 600 DAY MISSION

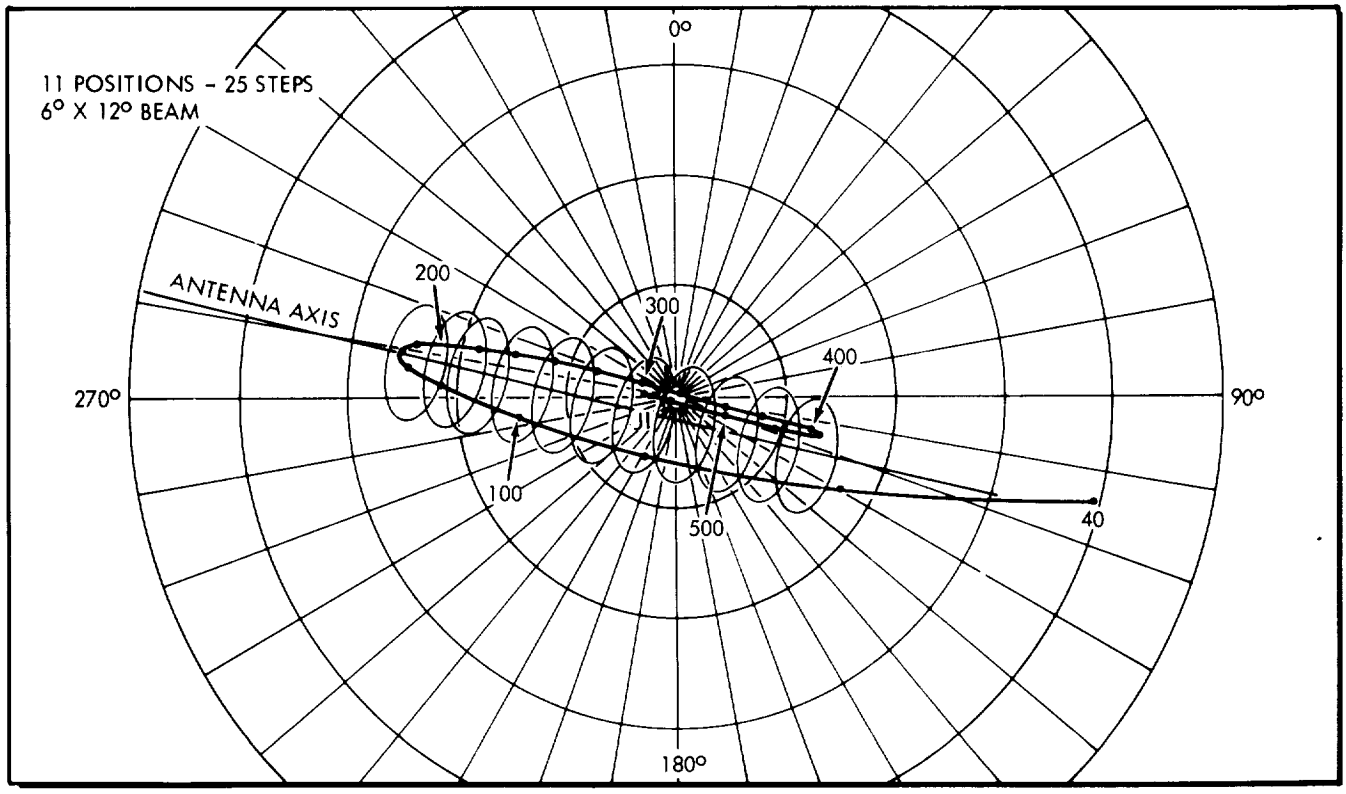

FIGURE 5. 2-4

The gain-loss chart shown in Table 5.2-3 is applicable for a subsystem using a 25 watt amplifier and a 27 db antenna at a 6 a.u. communications distance.

Table 5.2-3

DESIGN CONCEPT B - GAIN-LOSS CHART

	Gain	Loss
Transmitter Power	44 dbm	
Modulation		3 db
S/C Ant Gain	27 db	
Space Attenuation		278 db
Rcvr Ant Gain	61 db	
Rcvr Sens (40^{o} K)		-182 dbm
Misc. Losses		2 db
System Tolerances		6 db
	132	107

$S/N_o = 132 - 107 = 25$ db

Then, assuming a bit rate of 17 bps,

$ST/N_o = 25 - 10 \log 17 = 12.7.$

The information performance margin is 12.7 - 6.8 = 5.9 db. The phase-lock performance margin is not critical since the information rate is greater than 4 bps (see 3.1.2.3).

By use of similar gain-loss calculations, the antenna and information rate schedule shown in Table 5.2-4 can be derived.

Table 5.2-4

DESIGN CONCEPT B - ANTENNA AND INFORMATION RATE SCHEDULE

Communications Distance (a.u.)	Antenna	Info Rate (bps)
0-0.2	Omni	33
0.2-2.5	Parabola	133
2.5-3.5	Parabola	67
3.5-5	Parabola	33
5-6	Parabola	17

The number and weight of the components of the communications sybsystem are shown in Table 5.2-5. The recommended numbers of components are based on a reliability analysis of the communications subsystem. Although the proposed configuration is not necessarily optimum with respect to reliability, it is considered to be an appropriate compromise between reliability, weight, and power considerations.

Table 5.2-5

DESIGN CONCEPT B - COMMUNICATIONS SUBSYSTEM WEIGHT

Component (no.)	Weight, lbs
Amplifier (2)	4
Circulator (6)	6
Power Monitor (2)	2
Exciter (2)	7
APC Receiver (2)	18
Exciter Control	2
Amp Control	2
Omni Ant (2)	4
Parabolic Ant	15
Power Supply-HV (2)	10
Cabling, etc.	4
Rcvr Monitor	1
TOTAL	75

5.2.2.3 Data Management

The elements and the functional requirements of the data management subsystem have been discussed in general terms in subsection 3.2. A tape recorder is employed to implement data storage during the cruise and encounter phases.

The transmission rates available in various portions of the mission have been presented previously in Table 5.2-4, and the anticipated raw and compressed data bit rates for Design Concept B are presented in Table 5.2-6. On the basis of the information contained in these tables, it is indicated that data compression is required.

The fan method or the zero-order interpolator technique can be applied in order to compress the engineering or the scientific data; however, a significantly higher data compression ratio can be achieved by use of the fan method. It is recommended that one generalized data compression technique be selected for use with both types of data so that a more reliable, efficient, and economical design can be obtained.

Table 5.2-6

DESIGN CONCEPT B - ANTICIPATED DATA BIT RATES

Type	Near Earth			Interplanetary			Encounter (No TV)			Encounter (TV)		
	Raw	Compressed (Fan)		Raw	Compressed (Fan)		Raw	Compressed (Fan)		Raw	Compressed (Fan)	
1. Engineering	33.3	(150:1)	0.2	33.3	(150:1)	0.2	33.3	(150:1)	0.2	33.3	(150:1)	0.2
2. Magnetometer	300.0	(10:1)	30.0	0.2	(10:1)	≈ 0.0	300.0	(10:1)	30.0	300.0	(10:1)	30.0
3. Cosmic Dust Detector	0.1	(1000:1)	≈ 0.0	0.1	(1000:1)	≈ 0.0	0.1	(1000:1)	≈ 0.0	0.1	(1000:1)	≈ 0.0
4. Energetic Particle Detector	0.3	(3:1)	0.1	0.3	(3:1)	0.1	1.7	(3:1)	0.6	1.7	(3:1)	0.6
5. Photometer	-----	----------		----	----------		0.2	(4:1)	0.1	0.2	(4:1)	0.1
6. Plasma Probe	0.1	(1:1)	0.1	0.1	(1:1)	0.1	0.1	(1:1)	0.1	0.1	(1:1)	0.1
7. Television	-----	----------		----	----------		-----	----------		20000.0	(10:1)	2000.0
8. Housekeeping	30.0	(30:1)	1.0	3.0	(30:1)	0.1	30.0	(30:1)	1.0	600.0	(10:1)	60.0
TOTAL	363.8	(11:1)	31.4	37.0	(74:1)	0.5	365.4	(11:1)	32.0	20945.4	(10:1)	2091.0

In the case of Design Concept B, the quantity of data generated by the television pictures determines the required data storage capacity. The estimated data storage capacity required for dynamic data handling in the near-Earth environment is 1.31M bits; to meet similar requirements related to the interplanetary environment and those related to intermittent communications, 800K bits and 22.4M bits, respectively, are needed. To meet overall requirements for the entire encounter phase, which includes Jupiter occlusion and dynamic data handling, 47.9M bits are needed. This quantity includes the capacity necessary to store the television pictures. Data from the entire encounter phase are stored to provide a further increase in reliability in obtaining all of the important data acquired during this phase. Assumptions based on the data storage requirements outlined in subsection 5.1.2.3 were applied in these calculations.

It is recommended that a tape recorder with a 47.9M bit capacity be used as the DSE. All of the encounter data can be stored therein, and the storage requirements for the other mission phases can also be accommodated. If the conditions described in subsection 5.1.2.3 are assumed, and if encounter occurs at less than 5 AU so that the 33-bit-per-second rate can be used, the time interval required for data transmission will be slightly less than 4 days.

Specific functional requirements which are recommended for the elements of the data management subsystem are as follows: The DAE encodes and buffers scientific data for input to the DEE and the DSE at specified rates compatible with the selected transmission rates. The DEE (Figure 3.2-7 without modification A) accepts data from the engineering sensors, from the DAE, and from the DSE, and it transfers this data to the communications subsystem at rates of 17, 33, 67, and 133 bits per second. The DSE (Figure 3.2-6) provides storage for 47.9M bits of information at recording rates of 37, 370, and 31K bits per second and at playback rates of up to 9.9K bits per second as a function of the selected transmission rate and the average compression ratio.

The basic difference between the DAE recommended for a Jupiter flyby mission (Figure 5.2-5) and the DAE used on Mariner IV is in the use of a magnetometer data comparator to provide automatic selection of the particular magnetometer to be operated. The method of processing plasma probe and visible photometer data is similar to that used in processing magnetometer data (refer to subsection 5.1.2.3).

The basic modifications of the Mariner IV DEE which have been incorporated in the Concept B DEE (Figure 3.2-7 without modification A) comprise data compression devices and an increase in the number of available data transfer rates. Greater storage capacity and multiple record and playback rates are the main modifications required in the DSE used for Mariner IV; the changes required in the CDDE will result in an increase in the number of DC's from 29 to 50 and the use of a single-channel command transmission link.

DESIGN CONCEPT B DATA AUTOMATION ELEMENT

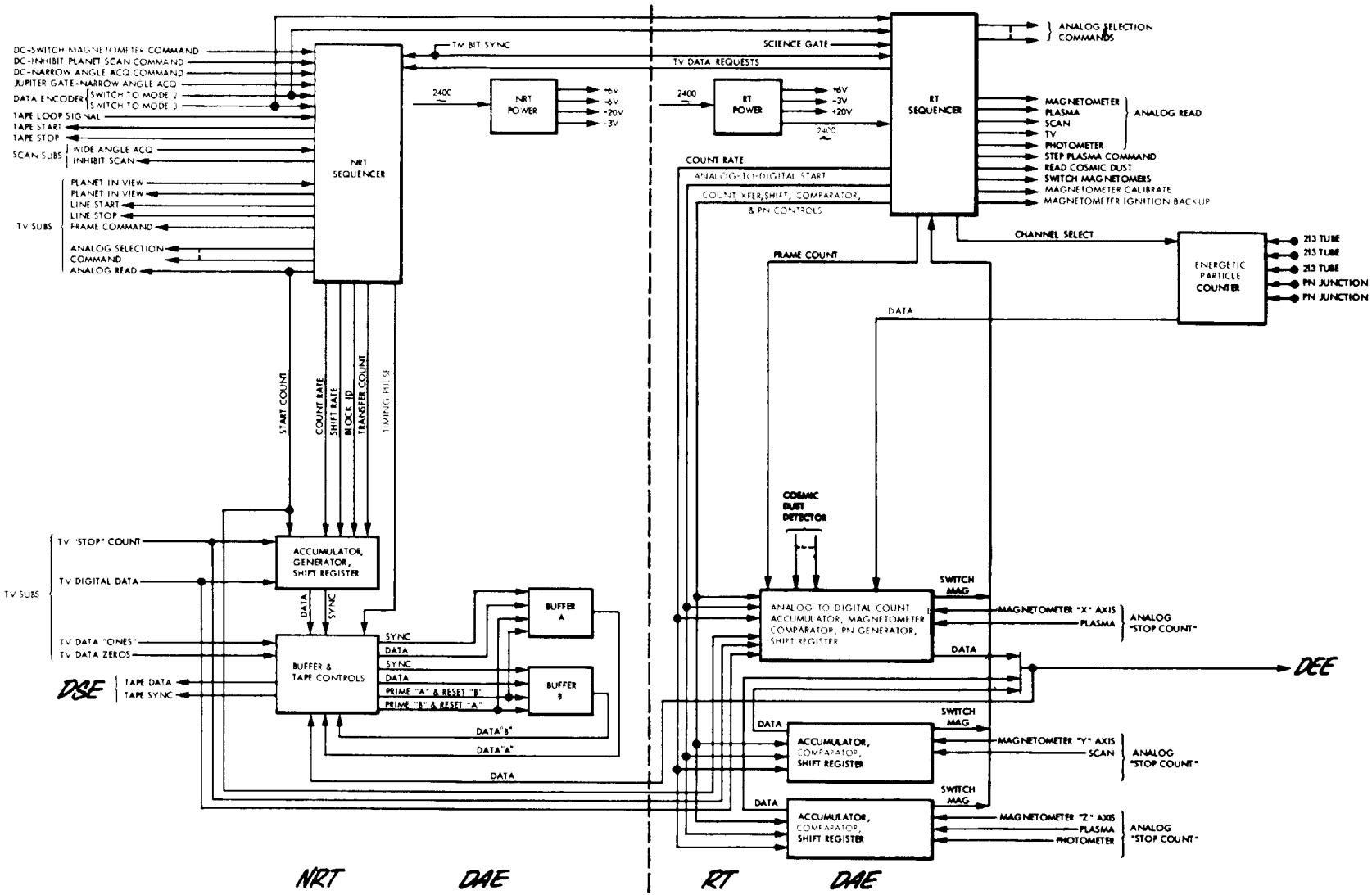

FIG. 5.2-5

Redundant units are provided in the case of each element and the critical components in each element.

The number and weight of the components of the data management subsystem are shown in Table 5.2-7. The recommended numbers of components are based on a reliability analysis of the data management subsystem. Although the proposed configuration is not necessarily optimum with respect to reliability, it is considered to be an appropriate compromise between reliability, weight, and power considerations.

Table 5.2-7

DESIGN CONCEPT B - DATA MANAGEMENT SUBSYSTEM WEIGHT

Component (no.)		Weight, lbs
DEE	(2)	14
DAE	(2)	12
DSE	(2)	9
CDDE	(2)	4
	TOTAL	39

5.2.2.4 Spacecraft Control

The functions of the Design Concept B spacecraft control system are identical to those outlined for Design Concept A through the execution of the vernier correction maneuver. In Concept B, three-axis stabilization is reestablished following the maneuver and is maintained for the duration of the mission. The attitude references are the Sun and the star Canopus. During the occultation of either or both of these references at Jupiter, upon involuntary loss of the references, or upon failure of these sensor systems, an inertial mode is used to provide control.

The experiments to be performed at Jupiter require only a 6000 km to 8000 km accuracy in periapsis distance. Analysis shows that this accuracy can be achieved with a single vernier correction which is based on tracking and commands from Earth-based facilities.

Since a Sun-pointing attitude is to be maintained throughout the mission, a one degree-of-freedom scan platform (Mariner IV type) is included. This platform contains all experiments which require a Jupiter pointing orientation. The pointing angle for this platform is computed on Earth and transmitted to the spacecraft. The platform remains fixed during Jupiter passage. Mounted on the scan platform is a Jupiter sensor which can be used to turn the experiments on and off or, in case of an orientation command failure, to search for the planet.

The recommended central computer and sequencer (CC&S) for Design Concept B is illustrated in Figure 3.3-1. The proposed attitude control electronics are shown in Figure 3.3-2. In addition to the sequence of events listed in Table 5.2-1, a sequence of events for the operation of the control subsystem is narrated below.

The sequence timer in the CC&S is started before lift-off. The gyros are supplied with power. Following injection, the sequence timer activates the attitude control system which implements three-axis attitude stabilization. This is initiated by supplying the Sun sensors with power. The gyros are uncaged, and the Sun search begins. When the Sun sensor indicates Sun acquisition, the acquisition signal turns on the star tracker power and a search signal to the roll switching amplifier. The spacecraft rolls about the Sun axis until a star is acquired by the star tracker. If the star acquired is not Canopus, the Earth gate interrupts the star acquisition and initiates another search. When Canopus is acquired, the Earth gate sends a no-interrupt signal, the star tracker continues to track Canopus, and the Earth sensor begins tracking Earth. The gyros are caged and turned off.

The gyros, having been warmed up prior to attitude acquisition, are used for supplying control system rate feedback to limit turning rates in the Sun and star search sequences. The turn jets also emit calibrated amounts of gas in a series of very short pulses to obtain the torque for turn execution. The number of gas pulses emitted are preset so that the spacecraft turns at the limiting rate set by the gyros. This mechanization serves as a back-up in the event of a failure of a gyro. This back-up capability is especially important in the maneuver sequence.

The next event depends upon telemetered Earth commands. Earth tracking stations track the spacecraft, and the data obtained are used to calculate the trajectory of the spacecraft, its position, and the parameters required for the midcourse correction maneuver. After these parameters are determined, the data are transmitted to the spacecraft where they are stored in the CC&S registers. The data consist of pitch (one pulse equals one second of pitch turn at a calibrated rate), roll (one pulse equals one second of roll turn at a calibrated rate), and velocity correction (one pulse equals one pulse from a calibrated accelerometer output).

At the appropriate time, the command for execution of the midcourse maneuver is sent from Earth. The CC&S sequence timer then controls the maneuver sequence. The attitude control system receives a fine attitude acquisition signal. This causes the Sun and Canopus sensor deadbands to narrow so that attitude is kept within narrower limits. Power to the gyros is turned on to warm up the gyros, and the sequence timer starts the roll maneuver, allowing time for the gyros to warm-up. The roll gyro is uncaged so that rate feedback is provided in that channel. The spacecraft is moved in pitch in a similar manner.

The start-thrust signal from the sequence timer turns on the rocket motor, and the overflow pulse from the velocity register turns off the rocket motor. The velocity register receives a pulse train from the accelerometer, which measures the ΔV correction. Roll, pitch, and yaw gyros remain uncaged and send rate signals to thrust vector control vanes in the rocket motor. The vanes deflect exhaust gases to obtain sufficient torques to oppose moments caused by uneven motor burn or other causes. This is necessary, because the gas jets do not generate enough torque to oppose attitude perturbations caused by uneven motor burning. At the end of the velocity correction, roll and pitch turns are executed in reverse order with opposite polarity. The sequence timer then commands acquisition of coarse attitude in a manner similar to that used in the post-injection attitude acquisition.

Use of the high gain antenna begins at a preset time. The antenna is reoriented periodically on command from the CC&S. Antenna pointing commands can be computed on Earth and transmitted to the spacecraft as a back-up mode if necessary.

The Earth sensor is turned off when the Earth signal is too weak to permit tracking. At a point prior to encounter, the Jupiter sensor is turned on in connection with orientation of the scan platform to a position compatible with the spacecraft trajectory. This angle is computed on Earth and transmitted to the spacecraft. Ihus, the Jupiter sensor line of sight is preset so that Jupiter acquisition should occur at a known time. If Jupiter is not acquired, the scan platform can operate in a search mode using the Jupiter sensor to indicate proper positions.

The encounter experiments which do not require a particular orientation with respect to Jupiter are turned on and off by the sequence timer at preselected times independent of the Jupiter sensor. For most encounter trajectories, either or both of the attitude references, the Sun and Canopus, will be occluded. For this reason, the sequence timer switches out the primary reference control signals at a preselected time, and the spacecraft attitude is controlled with the inertial system. Following the occultation period, the Sun and Canopus are reacquired just as they were acquired following injection. After communications with Earth have been reestablished, a command from Earth initiates playback of the encounter data. When playback is finished, the spacecraft operates in the cruise mode.

Analyses, which are presented in subsection 3.4, show that the vernier correction will place the spacecraft on a trajectory having an error in the impact parameter of approximately 4000 km RMS. Coarse attitude control throughout the mission will hold vehicle orientation to within ± 0.5 degree. The fine mode of attitude control allows the spacecraft axes to be held close to the threshold accuracy of the sensors and control system combination, which is on the order of $\pm$ 0.1 degree.

The number and weight of the components of the spacecraft control subsystem are shown in Table 5.2-8. The recommended numbers of components are based on a reliability analysis of the spacecraft control subsystem. Although the proposed configuration is not necessarily optimum with respect to reliability, it is considered to be an appropriate compromise between reliability, weight, and power considerations.

Table 5.2-8

DESIGN CONCEPT B - SPACECRAFT CONTROL SUBSYSTEM WEIGHT

Component (no.)	Weight, lbs
Fine Sun Sensor	1
Coarse Sun Sensors (4)	4
Earth Sensor	6
Jupiter Sensor	6
Canopus Star Tracker (2)	12
Attitude Control Electronics	20
CC&S	12
Gyros (6) and Accelerometers (1)	7
TOTAL	68

5.2.2.5 Attitude Control

Three-axis attitude control for Design Concept B is to be accomplished by a stored gas reaction jet system designed to operate for the entire mission, starting at booster separation. The basic functions to be performed prior to and including the time of the vernier trajectory correction are the same as those for Design Concept A, and the same general approach is used. Any differences involved are due mostly to the reduced capabilities of the gas jet system, since a smaller unit pulse must now be utilized to accommodate the long term limit-cycle mode of operation.

The system requirements are determined in the same manner indicated in the example case of subsection 3.5.8. The results are seen to be dependent upon a number of parameters that can only be estimated at present. For present purposes, a total impulse of 600 pound-seconds is selected to determine the system weight requirement. This weight is about 80 pounds for the Configuration B attitude control propulsion arrangement (see Figure 3.6-10).

5.2.2.6 Propulsion

The midcourse propulsion subsystem considered for Design Concept B is the basic hydrazine system described in subsection 3.6.1.

This subsystem has the capability of imparting a total velocity increment of 60 meters per second (200 fps) to a spacecraft mass of about 717 pounds. This corresponds to approximately a 5 σ design criteria for a launch vehicle FOM of 10-15 m/sec. The components and weight of the midcourse propulsion subsystem are summarized in Table 5.2-9.

Table 5.2-9

DESIGN CONCEPT B - MIDCOURSE PROPULSION WEIGHT

Component	Weight, lbs
Hydrazine	21.0
Hydrazine Tank	1.6
Nitrogen	0.93
Nitrogen Tank	2.12
Bladder	0.51
Fixed Hardware	20.84
TOTAL	47.0
Hydrazine Tank Diameter	10.8 in.
Nitrogen Tank Diameter	6.0 in.

The attitude control propulsion system utilized in Concept B is the one identified and described as Configuration B in subsection 3.6.2. In subsection 5.2.2.5, a need for 600 lb-sec total impulse capability is indicated. From Figure 3.6-10, the total system weight is estimated to be 80 pounds. This figure includes gas, tankage, and components.

5.2.2.7 Auxiliary Electrical Power

The auxiliary electric power arrangement for Design Concept B is illustrated by the schematic diagram in Figure 3.7-8. A profile of subsystem loads is presented in Table 5.2-10. The critical load occurs during the encounter period when the surplus capacity is approximately 10 percent. During the maneuver period, the load exceeds the capacity of the RTG by 10 watts. On the basis of an anticipated 1.5-hour duration, the event will produce a discharge of 4 percent in the battery. The specific components, the total numbers used, and the weights are listed in Table 5.2-11. The RTG capacities indicated therein represent end-of-life capabilities. The degradation in the capacities of the RTG as a function of time is indicated in Table 5.2-10.

Table 5.2-10

DESIGN CONCEPT B - ELECTRIC POWER LOADS

	Pre-Launch	Boost & Park Orbit	Acquisition	Cruise	Maneuver	Encounter
Encoder	4	4	4	4	4	4
DAE	3	0	3	3	3	3
Tape Recorder	1	0	0	2	2	1
Command Detector & Decoder	3	3	3	3	3	3
CC&S	12	12	12	10	12	12
Control Gyro Electronics	5	5	5	5	15	5
Attitude Control Electronics	11	11	11	9	25	11
Gyro 400 cps Power	5	5	5	5	15	5
Sun Sensors			2	2	3	2
Canopus Tracker			10	7	7	7
Earth Sensor			10	0	0	0
Communication Control	10	10	10	10	10	10
Communication Receiver	10	10	10	10	10	10
Communication Exciter	10	10	10	10	10	10
Communication Amplifier	70	10	70	70	70	70
Extended Magnetometer	7	0	7	7	7	7
Energetic Particle Detector	0.4	0	0.4	0.4	0.4	0.4
Cosmic Dust Detector	0.2	0	0.2	0.2	0.2	0.2
Expanded Photometer	1.5	0	0	0	0	1.5
TV Camera (TV-I)	10.0	0	0	0	0	10.0
Plasma Probe	2.5	0	2.5	2.5	2.5	2.5
Total Power Required	165.6	80.0	175.1	160.1	206.1	174.6
Raw Power Input to Power Cond.	206	100	217	200	256	216
Power Input to Shunt Reg & Bat.	48	164	35	46	0	24
Power From RTG (4-60W)	264	264	252	246	246	240
Power From Battery	0	0	0	0	10	0
Watt-hour from Battery	0	0	0	0	15	0
Battery % Discharge	0	0	0	0	4%	0

Table 5.2-11

DESIGN CONCEPT B - ELECTRIC POWER SUBSYSTEM WEIGHT

Component (no.)	Rating	Weight, lbs
Radioisotope Thermoelectric Generator (4)	60 watts, 28v	132.00
3 Electrode Ni-Cd Battery	15 ampere hour	21.00
Shunt Volt. Reg. Switch (4)	Six 0.5a channels	1.80
Volt. Reg. Mode Controller	Signal Device	.75
Shunt Dissipation Resistors (4)	84 watts	6.00
Main 2400 cps Inverter (2)	10 ampere inputs	4.00
Transfer Relay (2)	10 ampere dpst	1.00
Emergency 2400 cps Inverter	2 ampere input	0.50
Inverter Synchronizer	Signal Device	0.50
Emergency Transfer Unit	5 ampere spdt	0.50
400 cps Inverter	2 ampere input	4.00
Battery Charge-Discharge Controller	2 amp. chg. 5 amp disc.	9.00
Power Distribution and Wiring		41.00
	TOTAL	222.05

5.2.2.8 Thermal Control

The equipment bus of Spacecraft Design Concept B is basically designed as a single unit having a "pancake" shape. The upper flat surface (see configuration, Figure 5.2-1) is nominally solar oriented. Thermal control louvers are located on the lower surface. The equipment within the bus can either be installed in an "isothermal" structure or arranged in semiisolated equipment compartments. Equipment arrangement in the compartments should follow the guidelines shown in Table 3.8-1. Component thermal design information for Concept B is shown in Table 5.2-12.

The upper surface of the bus will be insulated to minimize the variation in heating by the Sun. Temperature control of the outer surfaces can be obtained by insulation or by RTG heating. The insulation approach is preferred for thermal control since it minimizes the effects of varying space thermal environment of the total mission from prelaunch heating to the cold thermal environment of cruise at large solar distances.

Requirements for thermal control during launch for extended components, RTG supports, ground cooling, and the entire spacecraft are similar to those of Design Concept A (subsection 5.1.2.8).

Table 5.2-12

DESIGN CONCEPT B - THERMAL CONTROL INFORMATION

SUBSYSTEM AND COMPONENTS	TEMPERATURE LIMITS, °F OPERATING MIN	OPERATING MAX	NONOPERATING MIN	NONOPERATING MAX	HEAT DISSIPATION WATTS	WEIGHT, LBS.
Science Subsystem						
Extended Magnetometer						
Electronics	-13	167	NA	NA	7.0	5.0
Helium Sensor	-13	167	NA	NA	NA	1.5
Rudidium Sensor	32	122	NA	NA	NA	1.5
Energetic Particle Detector	14	122	NA	NA	0.4	2.5
Cosmic Dust Detector						
Electronics	-40	212	NA	NA	0.2	2.5
Sensor	-148	392	NA	NA	NA	0.5
Expanded Photometer	-4	104	-58	212	1.5	2.0
TV Camera						
Electronics	14	158	-40	257	10.0	NA
Optics	-4	104	-58	212	NA	NA
Plasma Probe	14	176	NA	NA	2.5	7.0
Spacecraft Control						
Central Computer & Sequencer	0	125	-31	185	10.0	12.0
Coarse Sun Sensors	0	120	-58	212	2.0	2.0
Fine Sun Sensor	0	120	-58	212	1.0	12.0
Earth Sensor	-10	125	-58	212	7.0	6.0
Jupiter Sensor	-10	125	-58	212	7.0	6.0
Canopus Star Tracker	-65	200	-58	212	10.0	10.0
Gyros (3)	-65	250	-65	250	29.0	2.0
Accelerometer	10	100	-31	185	1.0	2.0
Attitude Control Electronics	10	100	-31	185	15N*/20P*	20.0
Midcourse Propulsion						
Thruster Assembly	NA	1500	70	NA	NA	2.5
Hydrazine Prop ellant & Tank	40	100	40	100	NA	22.5
Nitrogen Pressurization System	40	100	40	100	NA	20.0
Nitrogen and Tank	40	165	40	165	NA	3.1
Auxiliary Electric Power						
RTG Units	510	510	NA	NA	NA	120.0
Shunt Voltage Regulators	-30	160	NA	NA	6.0	1.0
Shunt Power Dissipation Resistors	-30	160	NA	NA	**	6.0
NI-CD-3 Electrode Battery	-65	120	-65	120	**	21.0
Charge-Discharge Controller	-30	160	NA	NA	5.0	9.0
Voltage Sensor & Regulator Mode Control	-30	160	NA	NA	4.0	0.8
2400 cps Inverter	-30	160	NA	NA	29.0	4.0
Transfer Relay	-30	160	NA	NA	NA	1.0
400 cps Inverter & Regulator	-30	160	NA	NA	5.0	4.0
Emergency 2400 cps Inverter	-30	160	-65	160	NA	0.5
Inverter Synchronizer	-30	160	NA	NA	3.0	0.5
Power Distribution and Wiring	-65	160	-65	160	7.0	41.0
Diodes	-65	160	NA	NA	10.0	NA
Emergency Transfer Unit	-30	160	-65	160	NA	0.5
Communications						
TWT Amplifier	-65	203	NA	NA	45.0	4.0
Power Monitor	-65	203	NA	NA	NA	2.0
Circulator	-65	203	NA	NA	NA	6.0
Exciter	-65	203	NA	NA	10.0	7.0
Exciter Control	-65	203	NA	NA	5.0	2.0
APC Receiver	-65	203	NA	NA	10.0	9.0
Amplifier Control	-65	203	NA	NA	5.0	2.0
Power Supply	-65	203	NA	NA	10.0	7.0
Data Management						
Data Encoder Element	14	176	-55	257	6.0	7.5
Data Automation Element	14	176	NA	NA	2.0	6.0
Data Storage Element	14	176	-55	185	4.0	5.0
Command Detector & Decoder Element	14	176	NA	NA	2.0	4.0

*N Denotes nominal value
P Denotes peak value
** Dependent on operational requirements

The thermal control weight requirement is estimated to be 11 pounds. This is based on 5 pounds for insulation, shielding, etc., and 5.50 square feet of louvers at 1.12 lbs/sq.ft. It is noted that some of the spacecraft surface skin acts as cold plates, and the skin therefore has minimum thickness requirements. It appears that the structural and meteoroid protection requirements dictate thicknesses which amply meet the thermal control requirements, thus this weight is not considered a part of thermal control.

5.2.2.9 Radiation Protection

The general problem of nuclear radiation protection for Jupiter flyby spacecraft is discussed in subsection 3.9. The conclusion reported therein is that no specific design penalties should be incorporated for radiation protection. The judicious selection of radiation resistant components for the various subsystems and the proper placement of scientific instruments which are sensitive to RTG radiation is the recommended approach to radiation protection. Design Concept B reflects these design considerations to the extent possible in a conceptual design. This is particularly manifested in the spacecraft configuration. Based on the results presented in subsection 3.9, no radiation shielding is included in the design concept.

5.2.2.10 Meteoroid Protection

The data for a nominal 600 day mission used in assessing the meteoroid protection requirements for Concept B are summarized in Table 5.2-13. The spacecraft exposed area in the interplanetary and asteroidal regions is determined as discussed in subsection 3.10.4. The results of this analysis are shown in Figure 5.2-6. The near-Earth and near-Jupiter exposed area is the total surface area of the spacecraft equipment compartment.

Table 5.2-13

DESIGN CONCEPT B - METEOROID PROTECTION ANALYSIS DATA

Region	Exposed Area (m^2)	Time (Days)	Area x Time (m^2-Days)
Near-Earth	4.33	0.5	2
Interplanetary	1.36	565	770
Asteroidal	1.36	190	259
Near-Jupiter	4.33	63.3	274

These data are combined with the data presented in subsection 3.10.3 to provide the design data shown in Figure 5.2-6. The two curves indicate the magnitude of difference in the protection

METEOROID IMPACT CONDITIONS

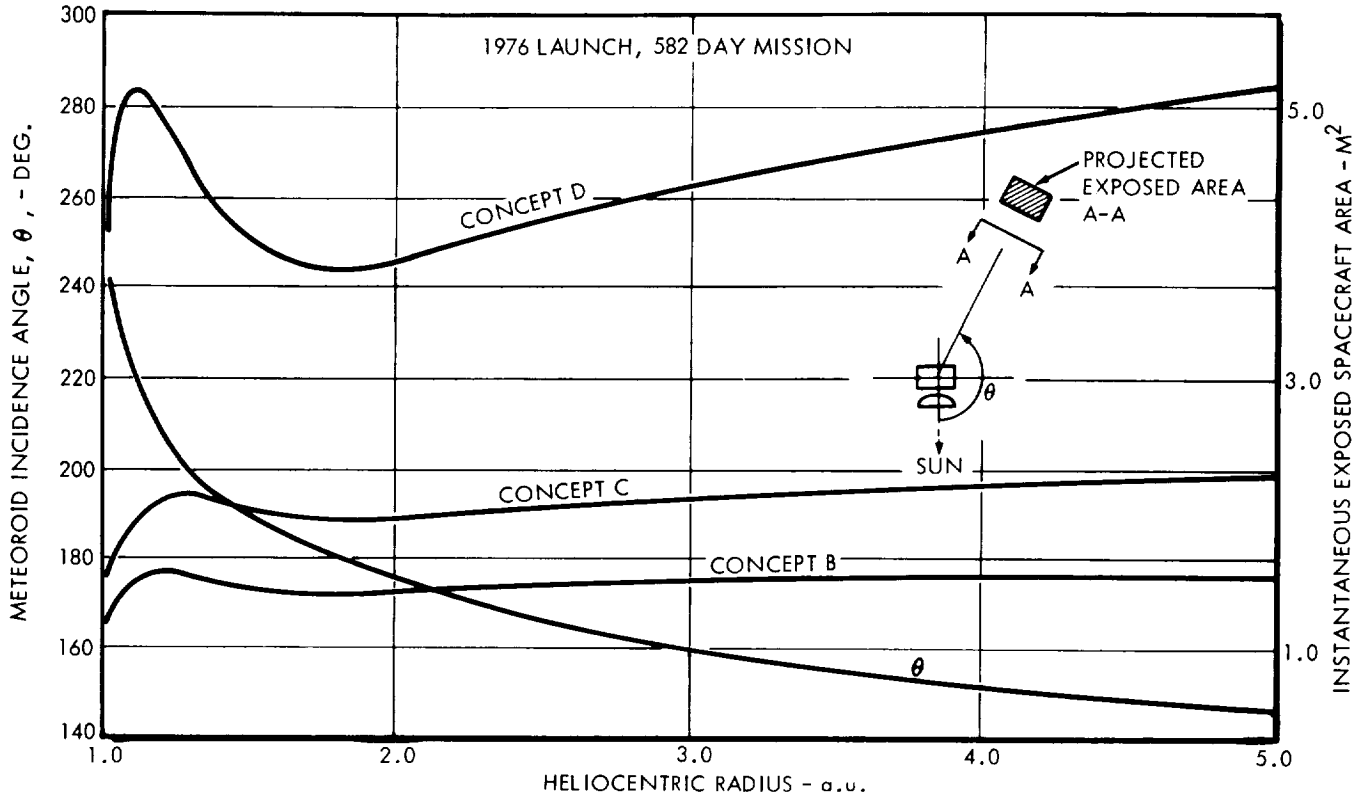

FIGURE 5.2-6A

DESIGN CONCEPT B - METEOROID PENETRATIONS VS. ALUMINUM SHEET THICKNESS

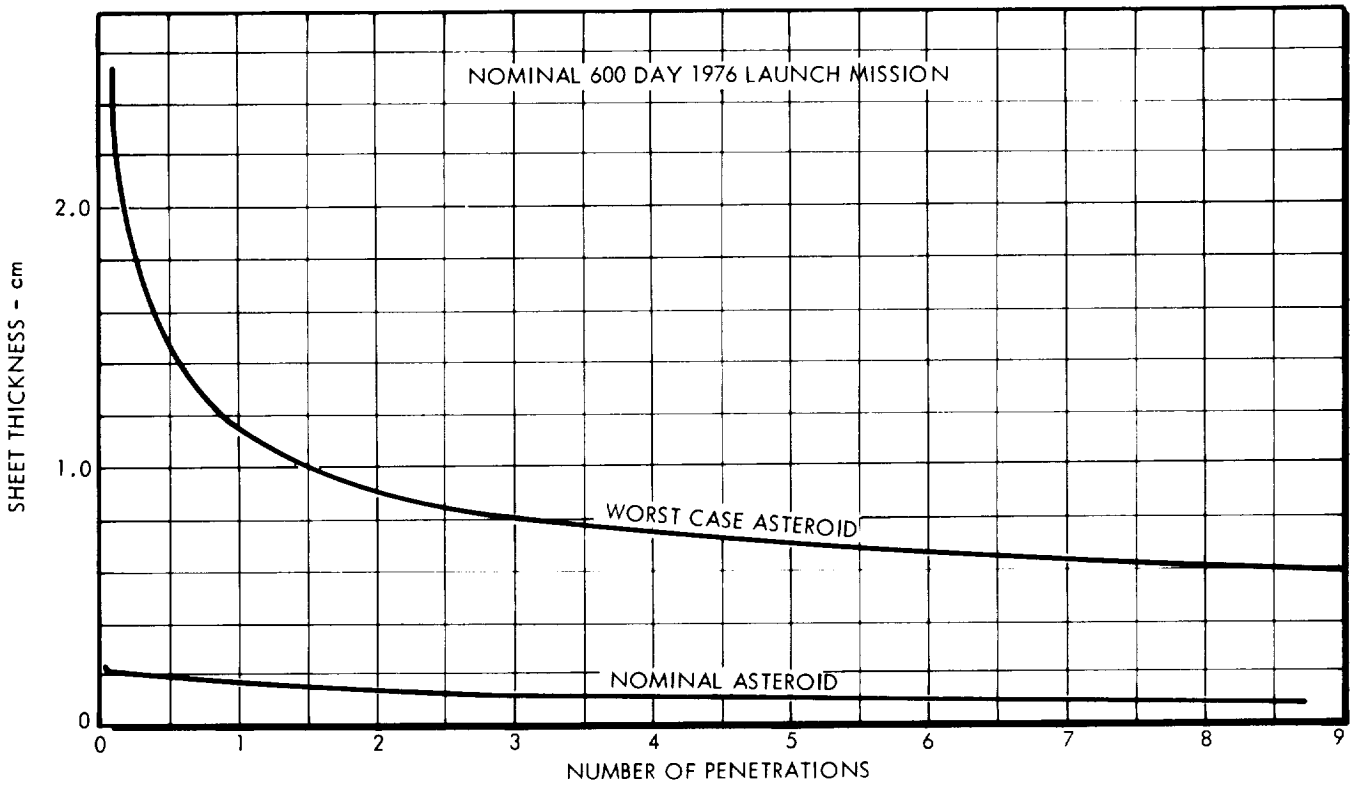

FIGURE 5.2-6B

requirements for the two asteroidal flux models. As outlined in subsection 3.10.4, meteoroid protection requirements for the nominal asteroidal flux condition are the same for all portions of the spacecraft equipment compartment. For the worst case asteroidal flux, the protection requirements for the back and sides of the compartment are dictated by the worst case curve while the front of the spacecraft needs only the protection necessary to meet the requirements shown by the nominal curve.

If 0.2 centimeter of aluminum is provided for protection of the complete compartment, the expected number of penetrations is essentially zero based on the nominal asteroidal flux. The total skin weight in that case is 53 pounds. For the worst case asteroidal flux and a criteria of one penetration, a skin thickness of 1.14 centimeters is required for the back and sides, and a thickness of 0.2 centimeter is selected for the front panels. The resulting skin weight is 235 pounds.

The meteroid protection system is provided, and it consists of a complete covering of the spacecraft with 0.2 centimeter of aluminum. The choice of this design point is obviously arbitrary, but it is felt that it represents an adequate protection system with very little penalty. It does not appear desirable to accept the penalties imposed by the worst case asteroidal flux without in situ measurements of the actual flux.

As indicated in subsection 3.12, the armor-type meteoroid protection is considered to be an integral part of the spacecraft structure; and, for nominal protection measures, the weight is assumed to be completely chargeable to the structure. Therefore, the meteoroid protection weight is not listed separately in Table 5.2-2, but is included in the structural/mechanical weight estimate.

5.2.2.11 Configuration

The configuration of Design Concept B is shown in Figure 5.2-1. The spacecraft is basically composed of (1) an equipment compartment, (2) four RTG units, (3) a parabolic high-gain antenna, (4) scan platform mounted encounter science, and (5) various cruise sensors located about the spacecraft.

The central compartment is an octagon shaped enclosure of the same dimensions and shape as the basic Mariner IV package. The equipment compartment incorporates a series of thermal control louvers on the aft section. The midcourse propulsion system is mounted in the center of the octagonal enclosure with the thrust vector directed aft along the spacecraft roll axis. The propellant tankage for the attitude control and propulsion system is centrally located within the basic compartment and the electronic subsystems are spaced around the periphery. This equipment

is attached to the aft skin of the spacecraft such that maximum effectiveness can be gained from louver systems attached thereon.

Four RTG units are equally spaced 90° about the octagon, and support for the RTG's is provided by tubular truss assemblies which project radially from the periphery of the spacecraft. An elliptical shaped, parabolic antenna is centrally mounted on the forward face of the equipment section with the 5 foot major axis canted 9.5 degrees from the yaw axis. The antenna dimensions and orientation are tailored to the particular trajectory shown in Figure 5.2-2.

The encounter science sensors are mounted on a Mariner IV type scan platform which projects aft from the main equipment compartment and is oriented such that the sensors are directed to the side. The view angles for these sensors are aligned along a line which forms an angle of approximately 70 degrees from the thrust vector. The scan platform is provided with a one degree-of-freedom scan capability to compensate for errors in the inclination of the encounter trajectory. The remaining science and attitude reference sensors are positioned about the spacecraft beyond the boundary of antenna movement such that the required look angle of each individual sensor is accommodated.

A boom extends from the spacecraft body between each RTG unit to support the attitude control jets. An omnidirectional antenna is provided on each side of the spacecraft along the pitch axis to allow for complete communications coverage prior to attitude acquisition.

5.2.2.12 Structural and Mechanical Design

The central compartment forms the core of the spacecraft structural system and transmits spacecraft launch loads to the booster interface. The enclosure is of the same basic construction as the Mariner IV spacecraft compartment except that the propellant tankage for the attitude control and mid-course propulsion is mounted centrally inside the compartment with a thruster installation which is directed aft rather than to the side.

The RTG units are mounted on truss assemblies of lightweight construction which are arranged about the spacecraft to provide a symetrical loading condition during launch. The scientific sensors and attitude control sensors are mounted exterior to the basic spacecraft structure, and all loads resulting from these elements are transmitted into the skins of the octagonal enclosure. The enclosure is covered with 0.2-centimeter aluminum plate.

The high-gain antenna is equipped with a gimbal mechanism which provides an angular movement of 32.5 degrees in one degree of freedom about a line parallel to the antenna major axis. The antenna is designed so that five discrete positions of the gimbal

can provide full Earth coverage during the particular mission shown in Figure 5.2-2. This is a nominal case as discussed in subsection 5.2.2.2. The antenna actuation is provided by a synchronous motor drive system which is activated by the CC&S or backup command from the Earth. The antenna is locked to the spacecraft during the launch period and released by a pyrotechnic device prior to beginning its operation.

The magnetometers are locked to the spacecraft during launch and extended following launch by means of a STEM mechanism. The scan platform is provided with a one-degree-of-freedom scan capability to compensate for potential errors in the inclination of the encounter trajectory. The platform is rotated by a synchronous motor system which provides an operating angle of 180 degrees.

The structural and mechanical weight, including meteoroid protection, is estimated from Figure 3.12-2 to be 138 pounds for a spacecraft injected weight of 717 pounds.

5.2.2.13 Subsystems Reliability

Table 5.2-14 contains the equipment mean-time-between-failure (MTBF) for Spacecraft Design Concept B. The science MTBF's are listed in Table 3.13-1. These MTBF's were determined using (1) a buildup of failure rates when an equipment design was available and (2) reliability estimates from similar equipment design and best engineering judgment when the equipment design was not available. For subsystem configurations containing redundant equipment, the MTBF listed in the table is for each of the redundant equipments. These equipment MTBF's are used to derive probability of mission success in subsection 5.2.4.

Table 5.2-14

SPACECRAFT DESIGN CONCEPT B - EQUIPMENT MTBF

SUBSYSTEM EQUIPMENT	MTBF (Hours)
Communications Subsystem	
Receiver	15,000
Exciter	45,000
TWT Amplifier	30,000
Circulator and Logic	350,000
TWT P/S	140,000
Power Monitor	333,000
Data Management Subsystem	
Data Encoder Element	1,300
Data Storage Element	6,000
Command Det & Decoder Element	
Detector & Decoder	10,000
Commands	44,000 - 77,000
Data Automation Element	5,000

Table 5.2-14
(Continued)

SUBSYSTEM EQUIPMENT	MTBF (Hours)
Spacecraft Control Subsystem	
Fine Sun Sensor	40,000
Coarse Sun Sensor	230,000
Earth Sensor	40,000
Star Tracker	35,000
Attitude Control Electronics	40,000
CC&S	4,500
Gyro and Accelerometer	8,000
Jupiter Sensor	40,000
Propulsion Subsystem	
Tank	0.9998*
Squib	0.999896*
Regulator	0.999556*
Rocket Motor and Vanes	0.99998*
Attitude Control Subsystem	
Tank	0.9998*
Squib	0.999896*
Regulator	0.9587*
Single Roll Jet	0.9794*
Single Pitch/Yaw Jet	0.9756*
Auxiliary Electrical Subsystem	
400 cps Chopper	210,000
Voltage Sensor and Regulator	60,000
2400 cps Chopper	150,000
Inverter Sync	220,000
Battery	70,000

* Probability of operating as required

5.2.3 Mission Performance

Mission performance envelopes, such as that shown in Figure 5.2-7 for the 1976 launch opportunity, were prepared for the launch years 1973 through 1980. These were used to derive the mission performance obtainable by Spacecraft Design Concept B in combination with the Titan IIICx/Centaur and Atlas SLV3x/Centaur/HEKS launch vehicles. Performance data for Design Concept B are defined in terms of the width of the launch window, or launch period, corresponding to the dates of western quadrature, opposition, and eastern quadrature. Arrival on the date of these events corresponds to an Earth-to-Jupiter flight time of approximately 420 days, 510 days, and 600 days, in that order.

As contrasted with the case of Concept A, the Titan IIICx/Centaur launch vehicle provides better performance than the Atlas SLV3x/Centaur/HEKS for Concept B because of the increased weight

SPACECRAFT DESIGN CONCEPT B - MISSION PERFORMANCE ENVELOPE

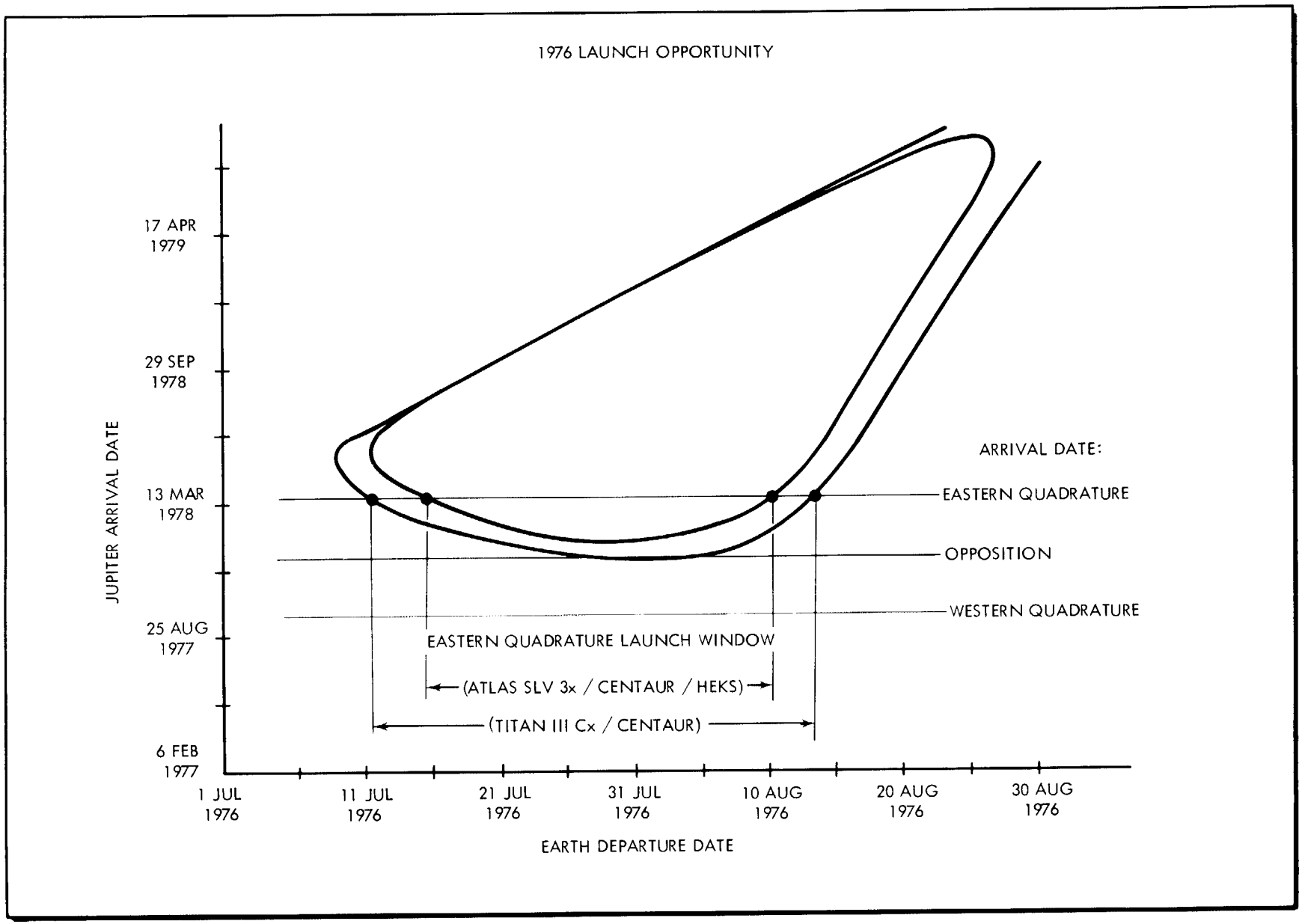

FIGURE 5. 2-7

of this spacecraft. As can be seen in Figure 5.2-8, the Titan IIICx/Centaur provides three launch opportunities for arriving at the time of opposition (approximately 510 days flight time), and only two launch opportunities are available with the Atlas SLV3x/Centaur/HEKS vehicle.

The data denoted by dashes in Figure 5.2-8 represent the interval of the launch window in which the departure asymptote declination is greater than 36 degrees. This specification of an upper limit of 36 degrees on the magnitude of the departure asymptote declination is explained in subsection 2.2.1.

5.2.4 Probability of Mission Success

The approach and guidelines employed in this study to evaluate the probability of mission success for Design Concept B are discussed in subsection 4.2. The results indicated therein are based on a mission described by the sequence of events in Table 5.2-1. The MTBF's utilized in this analysis are listed in Table 5.2-14.

The probabilities of mission success for both total and half missions are presented in Table 5.2-15. The probabilities of successful operation in the case of the communications, auxiliary electrical power, data management, and science subsystems are presented in Table 5.2-16.

Table 5.2-15

DESIGN CONCEPT B - PROBABILITY OF MISSION SUCCESS

	PROBABILITY OF MISSION SUCCESS	
CONFIGURATION	Total Mission (586 days)	Half Mission (293 days)
Spacecraft - Less Science Instruments	less than 0.01	0.11
Total Spacecraft	less than 0.01	0.05

Table 5.2-16

DESIGN CONCEPT B - SUBSYSTEMS PROBABILITY OF MISSION SUCCESS

	PROBABILITY OF MISSION SUCCESS	
SPACECRAFT SUBSYSTEM	Total Mission (586 days)	Half Mission (293 days)
Communication	0.52	0.76
Auxiliary Electrical Power	0.45	0.68
Data Management	0.02	0.25
Science	0.13	0.48

SPACECRAFT DESIGN CONCEPT B — LAUNCH VEHICLE MISSION PERFORMANCE SUMMARY CHART

(a) Titan III Cx / Centaur Launch Vehicle

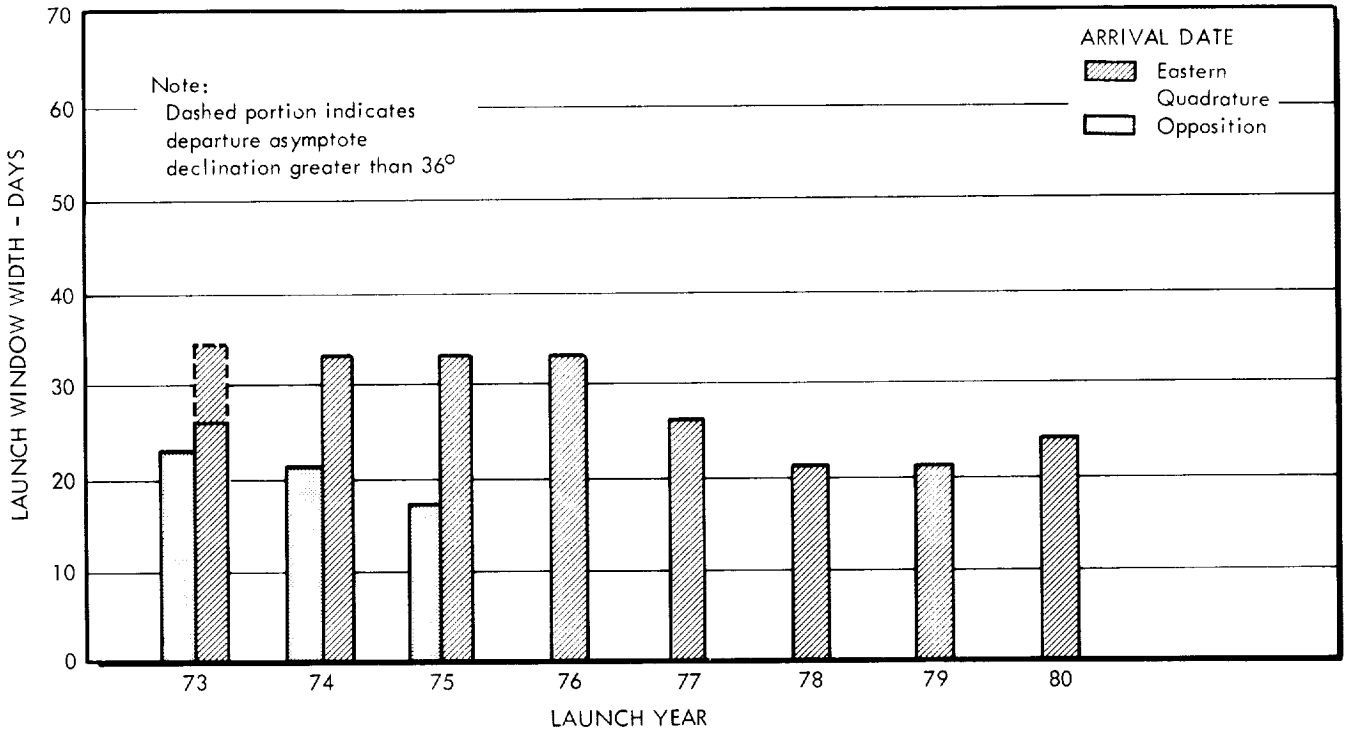

(b) Atlas SLV 3x / Centaur / HEKS Launch Vehicle

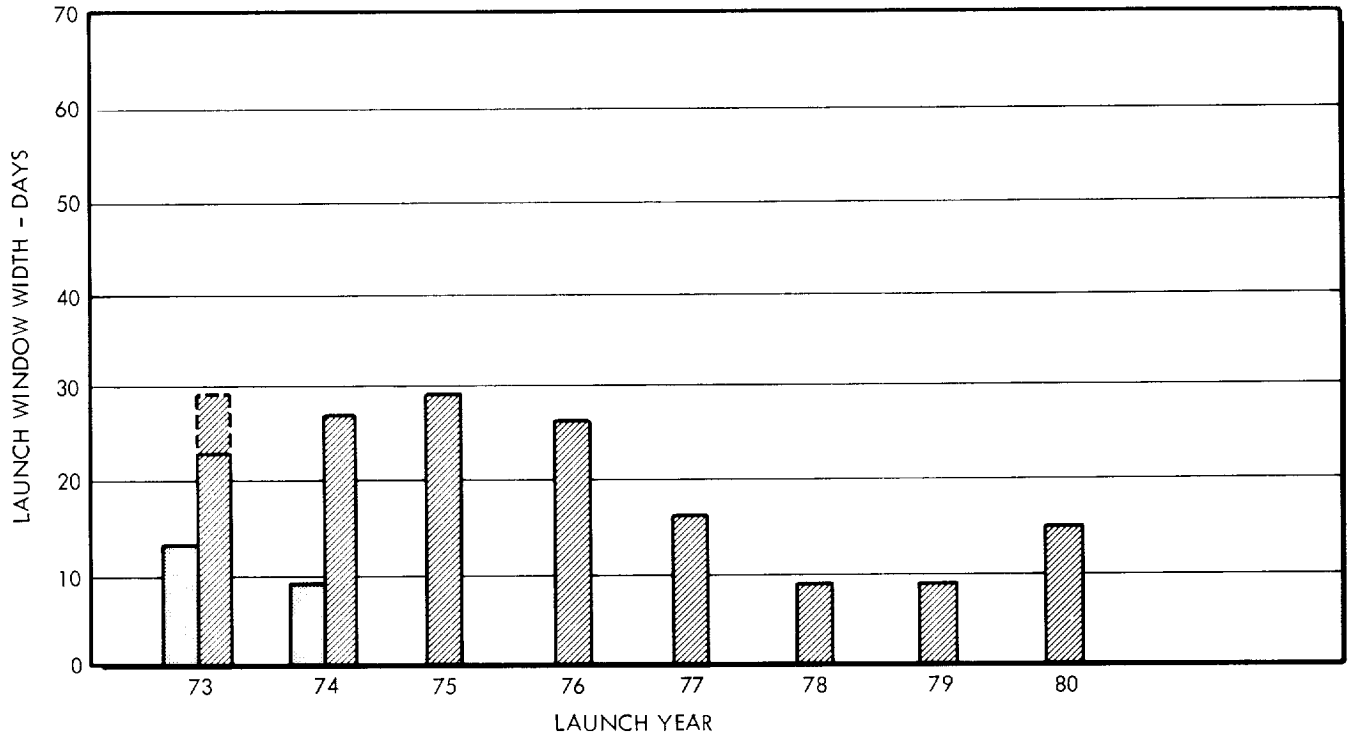

FIGURE 5. 2-8

5.2.5 Development Requirements

Time estimates for each of the activities between the events shown in the Program Implementation Plan (see Figure 4.3-3) are given in Table 5.2-17 for Design Concept B. Using the same techniques explained in subsection 5.1.5 for Design Concept A, i.e., tracing the critical path from Table 5.2-18, the go-ahead date necessary to make a PMV launch on 13 May 1974 is 26 December 1968. (This launch date was selected only for purposes of the analysis.) This represents a total span time of 5 years 5 months.

From the time line of Figure 5.2-9, it is evident that the major constraints on the program are the development of the RTG and the procurement of the Pu 238 for the PMV and BUV. As shown in Figure 5,2-10, the probability that the program will be less than that shown in the time line chart is 0.63.

5.2.6 Cost Results

Presented in Table 5.2-19 is a summary of the items that comprise the total program costs for Spacecraft Design Concept B, assuming two operational flights. The costs presented in Table 5.2-20 are the recurring spacecraft costs for two flights. The total cost increment for a third flight is given in Table 5.2-21. These results are based on the discussion in subsection 4.4.

Table 5.2-17
DESIGN CONCEPT B - PERT III INPUT ACTIVITY TIME ESTIMATES

TC	SP SCH OPT	BEG EVENT LC	END EVENT LC	OPT TIME	MEAN TIME	PESS TIME	SCH DATE / 1 / 2 / 3 / 4	ACT DATE	EVENT TITLE /ACTIVITY TITLE
3			00.000.001				1.01.70		CONTRACT GO-AHEAD
1		00.000.001	00.000.002	4.0	6.0	16.0			C/JUPITER SYS DESIGN SPEC
1		00.000.002	00.000.003	12.0	26.0	52.0			C/SPCFT PREL SUBSYS + INRFCE SPEC
1		00.000.002	00.000.004	1.0	1.0	2.0			R/RTG FUEL PROCUREMENT ORDER
1		00.000.003	00.000.005						S/DETAILED CONFG DSGN + MOCKUP
1		00.000.003	00.000.006						S/SUBSYS PROCUREMENT NEGOTIATIONS
1		00.000.003	00.000.007	16.0	26.0	52.0			R/SCNCE PROCUREMENT
1		00.000.003	00.000.008	3.0	6.0	12.0			R/TEST SPEC + LAUNCH OPER PLAN
1		00.000.002	00.000.009	2.0	2.0	4.0			INITIATES EARTH LAUNCH VEH PROC
1		00.000.005	00.000.010	16.0	26.0	37.0			SCNCE PYLD, CONFG APPR + MCKUP COMPL
1		00.000.006	00.000.010						SCNCE PYLD, CONFG APPR + MCKUP COMPL
1		00.000.007	00.000.010	16.0	26.0	37.0			SCNCE PYLD, CONFG APPR + MCKUP COMPL
1		00.000.008	00.000.011	26.0	41.0	64.0			R/TEST + LAUNCH + FAC IMPLMTN PLAN
1		00.000.010	00.000.012	4.0	6.0	18.0			S/TOOLING DSGN
1		00.000.064	00.000.013						R/DATA MGMT SUBSYS PROCUREMENT
1		00.000.064	00.000.014						R/COMM SUBSYS PROCUREMENT
1		00.000.064	00.000.015						R/SPACECRAFT CONT SUBSYS PROC
1		00.000.064	00.000.016						R/RTG PROCUREMENT
1		00.000.064	00.000.017						R/MIDCOURSE PRPLN PROCUREMENT
1		00.000.064	00.000.018						R/ATTITUDE CONT PRPLN PROCUREMENT
1		00.000.012	00.000.019	4.0	8.0	12.0			S/MFGR OF STM + TCM STR + MECH SYS
1		00.000.013	00.000.020	104.0	260.0	520.0			RE/STM DATA MGMT SUBSYS
1		00.000.014	00.000.021	26.0	37.0	52.0			RE/STM COMM SUBSYS
1		00.000.015	00.000.022	104.0	312.0	520.0			RE/STM SPACECRAFT CONT SUBSYS
1		00.000.019	00.000.023	41.0	64.0	156.0			C/STM STR + MECH ASSY
1		00.000.020	00.000.023	1.0	1.0	2.0			C/STM STR + MECH ASSY
1		00.000.021	00.000.023	1.0	1.0	2.0			C/STM STR + MECH ASSY
1		00.000.022	00.000.023	1.0	1.0	2.0			C/STM STR + MECH ASSY
1		00.000.063	00.000.023						C/STM STR + MECH ASSY
1		00.000.023	00.000.024	3.0	4.0	6.0			S/STM ASTRIONICS COMPAT TESTS
1		00.000.024	00.000.026	8.0	12.0	52.0			C/STM ASTRIONICS COMPAT TESTS
• 1		00.000.004	00.000.027	36.0	72.0	110.0			RE/FIRST SET FUELED RTGS
1		00.000.016	00.000.027	64.0	78.0	208.0			RE/FIRST FUELED RTGS
1		00.000.017	00.000.028	29.0	52.0	104.0			RE/FIRST MIDCOURSE PRPLN
1		00.000.018	00.000.029	29.0	52.0	104.0			RE/FIRST ATTITUDE CONT PRPLN
1		00.000.007	00.000.030	104.0	208.0	416.0			RE/FIRST SET OF SCNCE
1		00.000.059	00.000.031	12.0	26.0	64.0			PRI CONFG QLFD FOR TCM + LETM TESTS
1		00.000.026	00.000.032						S/FINAL ASSY + TEST OF STM
1		00.000.027	00.000.032						S/FINAL ASSY + TEST OF STM
1		00.000.028	00.000.032						S/FINAL ASSY + TEST OF STM
1		00.000.029	00.000.032						S/FINAL ASSY + TEST OF STM
1		00.000.030	00.000.032						S/FINAL ASSY + TEST OF STM
1		00.000.033	00.000.032						S/FINAL ASSY + TEST OF STM
1		00.000.011	00.000.033						STM TEST AREA COMPL
1		00.000.031	00.000.034	1.0	2.0	6.0			S/MFGR OF LETM STR + MECH SYS
1		00.000.032	00.000.035	26.0	26.0	208.0			STM FUNCTIONALLY QLFD
1		00.000.037	00.000.036						S/TCM FINAL ASSY
1		00.000.062	00.000.036						S/TCM FINAL ASSY
1		00.000.035	00.000.037	4.0	4.0	26.0			R/REV TCM SUBSYS + SCNCE
1		00.000.036	00.000.039	4.0	8.0	12.0			C/TCM FINAL ASSY
1		00.000.039	00.000.040	2.0	2.0	4.0			S/TCM FINAL QUALIFICATION TESTS
1		00.000.040	00.000.041	4.0	8.0	26.0			TCM FUNCTIONALLY QLFD
1		00.000.034	00.000.042	20.0	29.0	156.0			S/LETM FINAL ASSY
1		00.000.041	00.000.042	1.0	1.0	2.0			S/LETM FINAL ASSY
1		00.000.041	00.000.043						RE/LETM SUBSYS WITH CHG INC
1		00.000.042	00.000.044	2.0	4.0	8.0			C/FINAL ASSY OF LETM
1		00.000.043	00.000.044	2.0	2.0	3.0			C/FINAL ASSY OF LETM
1		00.000.044	00.000.045	1.0	1.0	1.0			S/LETM QUALIFICATION TESTS
1		00.000.045	00.000.046	3.0	4.0	8.0			LETM QLFD DSGN FREEZE
1		00.000.046	00.000.047						C/MFGR, TEST OF PMV, BUV + PTM
1		00.000.066	00.000.047	20.0	29.0	156.0			C/MFGR, TEST OF PMV, BUV + PTM
• 1		00.000.067	00.000.047						C/MFG,TST OF PMV,BUV PTM
1		00.000.047	00.000.048	1.0	1.0	2.0			PMV + BUV ON DOCK AT LAUNCH SITE
1		00.000.011	00.000.049						ETR FAC AVAIL
1		00.000.065	00.000.050	4.0	4.0	6.0			EARTH LAUNCH VEH DEL TO LAUNCH SITE
1		00.000.048	00.000.051						S/ETR OPERATIONS
1		00.000.049	00.000.051						S/ETR OPERATIONS
1		00.000.050	00.000.051						S/ETR OPERATIONS
1		00.000.047	00.000.052	1.0	1.0	2.0			PTM DEL TO MISSION CONT CENTER
1		00.000.052	00.000.053	4.0	8.0	10.0			DSIF + MISSION CONT CENTER ACTVT
1		00.000.051	00.000.054	12.0	16.0	26.0	11.23.80		LAUNCH PMV
1		00.000.056	00.000.054	4.0	4.0	4.0	11.23.80		LAUNCH PMV
1		00.000.054	00.000.055	1.0	1.0	2.0	11.30.80		LAUNCH BUV
1		00.000.053	00.000.056						BGN SPCRFT FLT OPER AT FLT CONT STE
1		00.000.019	00.000.059	41.0	64.0	156.0			S/PREL STR INTEGRITY TESTING
1		00.000.011	00.000.060						TCM TEST FAC AVAIL FOR FIRST TEST
1		00.000.031	00.000.061	1.0	2.0	6.0			S/TCM PREL TESTS WITH MCKUP SUBSYS
1		00.000.060	00.000.061						S/TCM PREL TESTS WITH MCKUP SUBSYS
1		00.000.061	00.000.062	37.0	52.0	156.0			PRI SPCRFT STR TC QLFD
1		00.000.005	00.000.063	37.0	52.0	104.0			ALL STR + MECH SYS DWG COMPLETE
1		00.000.010	00.000.064	4.0	6.0	12.0			SUBSYS SPEC + INRFCE FREEZE
1		00.000.009	00.000.065						FINAL LAUNCH VEH STATUS REVIEW
1		00.000.031	00.000.066	2.0	3.0	6.0			S/MFGR PMV, BMV + PTM
• 1		00.000.027	00.000.067	108.0	184.0	240.0			RE/PMV+BUV RTG FUEL

BLANK PAGE

DESIGN CONCEPT B - TIME LINE CHART

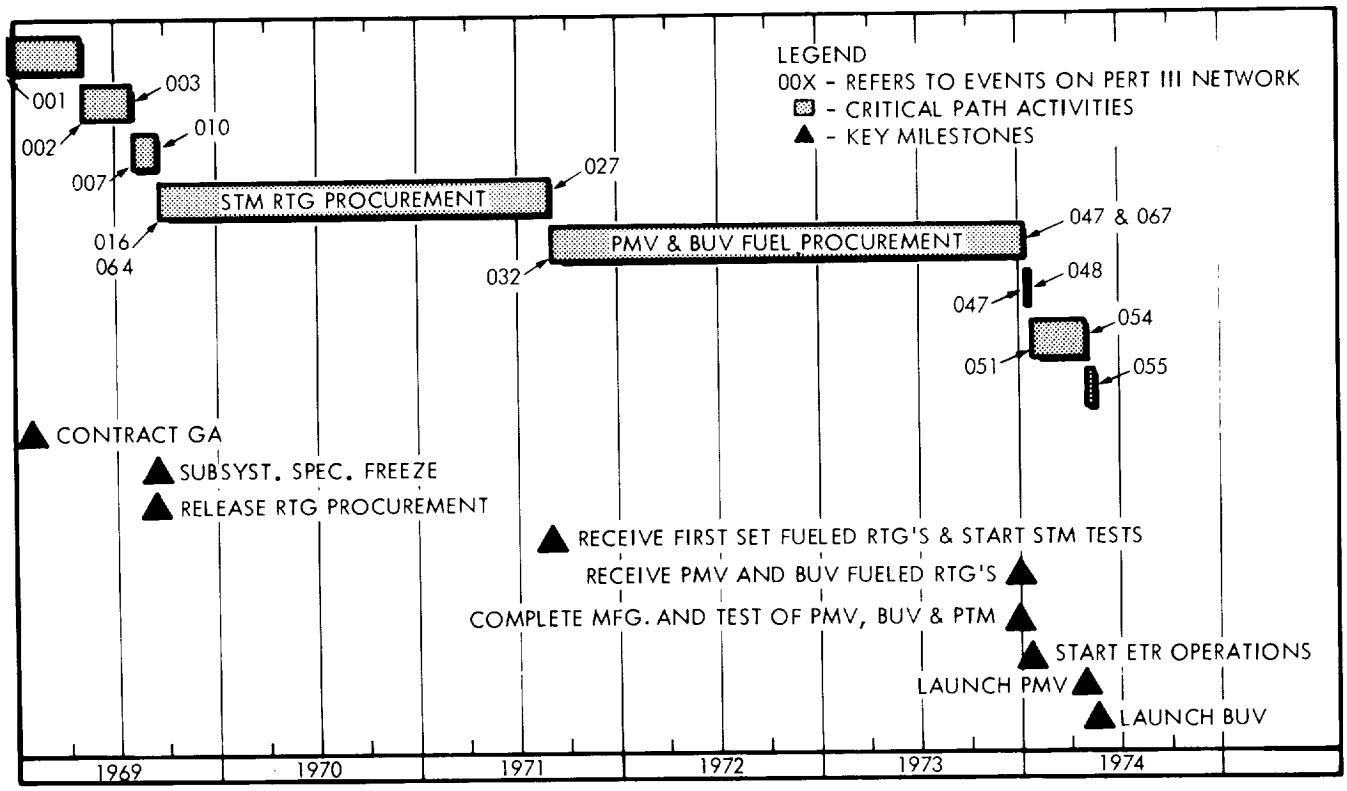

FIGURE 5.2-9

DESIGN CONCEPT B - SCHEDULE CONFIDENCE

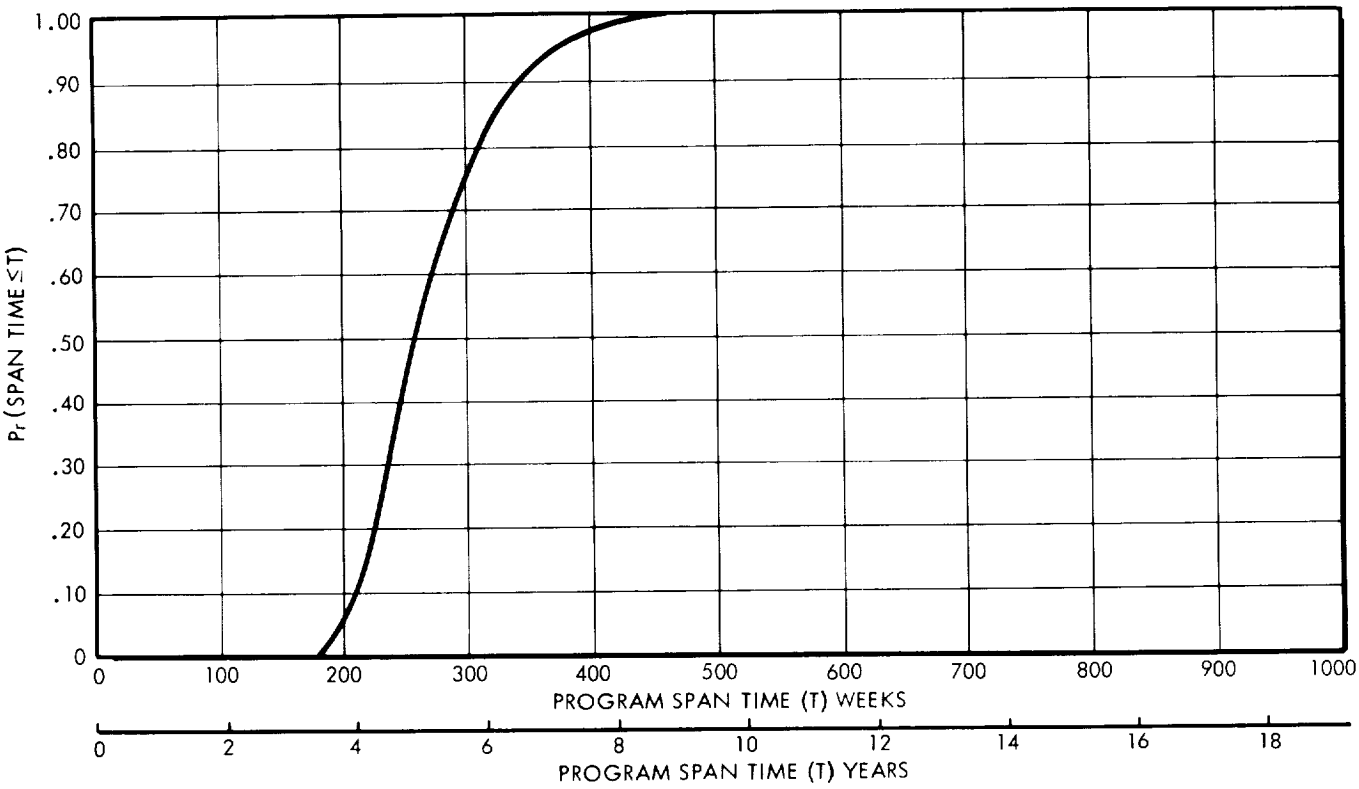

FIGURE 5.2-10

Table 5.2-19

DESIGN CONCEPT B - SUMMARY OF JUPITER FLYBY PROGRAM COSTS
(In Millions of 1965 Dollars)

COST CATEGORIES	LAUNCH VEHICLE TYPE	
	Atlas SLV3x/ Centaur/ HEKS	Titan IIICx/ Centaur
NONRECURRING		
Science	4.80	
Communications & Data Mgt	9.10	
Spacecraft Control	9.80	
Attitude Control	0.88	
Midcourse Propulsion	1.90	
Electrical Power	13.00	
Structural, Mech, Therm & Shield	6.00	
Subtotal Subsystems, DT&E	45.48	
Operational Support Equip	12.30	
Tooling & Special Equip	3.00	
System Integration	6.50	
Ground Test Hardware	11.65	
TOTAL NONRECURRING COSTS	78.93	78.93
RECURRING (2 Launches)		
Recurring Spacecraft	23.31	23.31
Spacecraft Spares (2 Sets)	2.38	2.38
Deep Space Net Support	38.10	38.10
Spacecraft Operations	3.32	3.32
Launch Vehicles	21.40	42.82
Launch Operations	11.20	14.80
TOTAL RECURRING COSTS	99.71	124.73
TOTAL PROGRAM COSTS	178.64	203.66

Table 5.2-20

DESIGN CONCEPT B - RECURRING SPACECRAFT COSTS FOR TWO FLIGHTS

(In Millions of 1965 Dollars)

COST CATEGORY	
Science	0.18
Communications & Data Mgt.	1.12
Spacecraft Control	1.24
Attitude Control	0.05
Midcourse Propulsion	0.08
Electrical Power	3.20
Structure, Mech, Therm, & Shield	0.62
Spacecraft Checkout & Assembly	0.98
Subtotal Spacecraft Cost	7.47
RTG Fuel Cost @ \$1500/W_t	15.84
Total Spacecraft	23.31

Table 5.2-21

DESIGN CONCEPT B - COST INCREMENT FOR A THIRD FLIGHT

(In Millions of 1965 Dollars)

	Atlas SLV3x/ Centaur/HEKS	Titan IIICx/ Centaur
Recurring Spacecraft	\$ 11.65	\$ 11.65
Launch Vehicle	10.70	21.41
Launch Operations	5.60	7.40
TOTAL	\$ 27.95	\$ 40.46
TOTAL*	\$ 25.20	\$ 37.71

* The total cost increment for a third flight assuming that one of the ground test models is used.

5.3 SPACECRAFT DESIGN CONCEPT C

A three-axis stabilized Jupiter flyby spacecraft of intermediate scientific capability, which is referred to as Design Concept C, is described in this subsection.

5.3.1 Design Summary

A configuration of Spacecraft Design Concept C is illustrated in Figure 5.3-1. The concept design philosophy is one of intermediacy in the scientific capability. That is, the capabilities of the subsystem design concept are somewhere between the most capable and least capable of the candidate concepts. The injected weight of the spacecraft is approximately 1060 pounds. Flight times upward from 520 days are possible during the period 1973-1980 when the Titan IIICx/Centaur is used. Dual launches using Saturn IB/Centaur/HEKS are possible with flight times of 430-480 days. Significant flight events for a nominal mission are detailed in Table 5.3-1.

The estimated development time for the spacecraft is 6 years. The total program cost for two Titan IIICx/Centaur launched spacecraft is estimated to be $236 million. For two spacecraft launched by one Saturn IB/Centaur/HEKS, the total program cost is estimated to be $209 million.

The salient characteristics of Design Concept C are (1) a science capability of approximately 115 pounds and 45 watts, (2) a steerable, 30 db gain antenna and a 35-watt transmitter, (3) data compression and tape storage, (4) three-axis attitude stabilization implemented by gas jets, (5) Mariner IV-type midcourse propulsion, (6) Pu 238 RTG's, and (7) armor-type meteoroid protection. The spacecraft performance is indicated by the following: (1) a 67 bit per second information rate at 6 a.u communications distance, (2) data storage for 49 M bits, (3) a vernier correction capability of 90 m/sec, and (4) 360 watts of available electric power.

Following spacecraft injection, three-axis attitude stabilization is acquired. Cruise science is then activated. Approximately one week following injection, a vernier correction maneuver is executed. The capability is provided to make a second correction during later portions of the mission if required. The parabolic antenna provides the primary communications downlink, and it is pointed at Earth by means of a mechanical steering device. Omni antennas are used for near-Earth communications and for command

SPACECRAFT DESIGN CONCEPT C CONFIGURATION

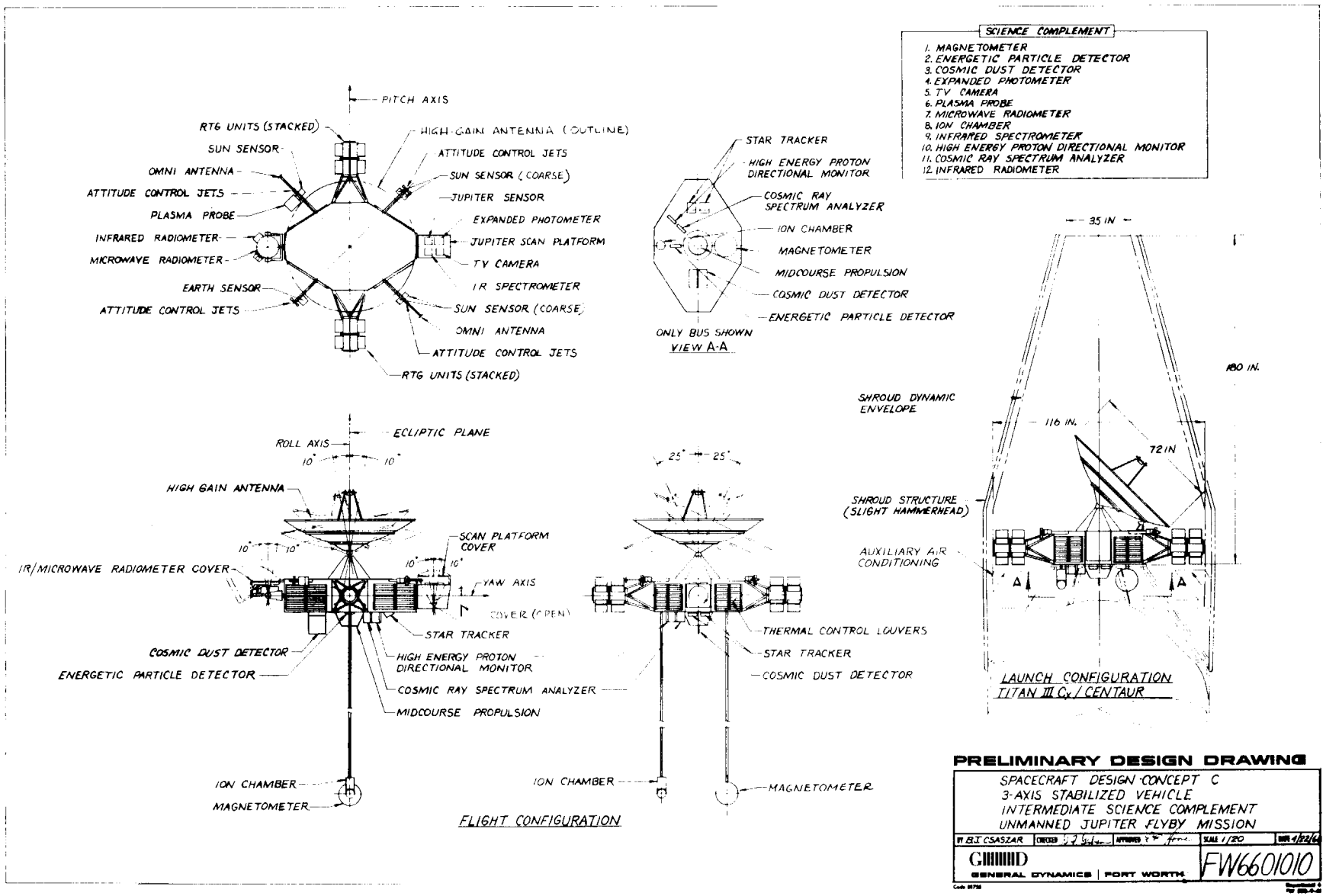

FIGURE 5.3-1

Table 5.3-1

SEQUENCE OF SIGNIFICANT FLIGHT EVENTS FOR SPACECRAFT DESIGN CONCEPT C

Notes: The mission characteristics are a 1976 launch, Titan III Cx/Centaur launch vehicle, 582 day flight time, posigrade equatorial pass, and 1.0 Jupiter radius nominal perijove altitude. The CC&S is the primary control for all spacecraft events except where noted. Backup via ground command is implied for all events.

No.	Event	Nominal Time
1	Install RTG units and activate auxiliary cooling system	L - 1 day
2	Update CC&S master clock and sequence timer	L - 3 min.
3	Turn on gyros, DEE, and CDDE	L - 2 min.
4	Stage 0 ignition	
5	Liftoff	L
6	Stage I ignition	
7	Stage 0 burnout	
8	Jettison Stage 0	
9	Jettison payload fairing	
10	Stage I cutoff	
11	Stage II ignition	
12	Jettison Stage I	
13	Stage II cutoff	
14	Jettison Stage II	
15	First Centaur ignition	
16	First Centaur cutoff (being orbital coast)	
17	Jettison Centaur insulation panels	
18	Second Centaur ignition (end orbital coast)	
19	Second Centaur cutoff (injection)	I = L + 120 min.
20	Spacecraft - Centaur separation	I + 2 min.
	a. Pyrotechnics armed	
	b. Transmitter power up	
	c. Begin communication with omni antenna at data transmission rate of 33 bps.	
21	Initial Sun acquisition	I + 10 min.
	a. Turn on attitude control system	
	b. Turn on coarse Sun sensor	
	c. Activate gas-jet system	
	d. Begin Sun acquisition sequence	
22	Sun acquired	I + (10 - 20) min.
	a. Gyros turned off	
23	Activate cruise science	I + 20 min.
	a. Deploy magnetometer and ion chamber	
	b. Turn on DAE	
	c. Turn on cruise science	
24	Canopus acquisition	I + 100 min.
	a. Turn on Canopus sensor	
	b. Set sensor cone angle	
	c. Begin roll turn	
	d. Receive acquisition signal	
	e. Turn on Earth sensor	
	f. Verify Canopus acquisition (continue roll search if Earth not acquired)	
25	Canopus acquired	I + (100-130) min.
26	Prepare for midcourse maneuver	M - 60 min.
	a. Transmit and verify pitch-turn duration and polarity	
	b. Transmit and verify roll-turn duration and polarity	
	c. Transmit and verify velocity increment	
27	Begin midcourse maneuver sequence	M = I + (1-7) days
	a. Turn on fine Sun sensor	
	b. Acquire Sun with fine Sun sensor	
	c. Turn on gyros	
	d. Turn on accelerometer	
28	Execute pitch turn	M + 60 min.
	a. Switch out error signals from Earth, Sun, and Canopus sensors	
	b. Set proper polarity	
	c. Pitch turn started	
	d. Pitch turn stopped	M + (60 - 65) min.
29	Execute roll turn	M + 75 min.
	a. Set proper polarity	
	b. Roll turn started	
	c. Roll turn stopped	M + (75 - 80) min.
30	Execute motor burn	M + 90 min.
	a. Command motor burn	
	b. Command motor shutoff	M + (90 - 92) min.
31	Sun reacquisition	M + 94 min.
	a. Turn off accelerometer	
	b. Switch in error signal from	
	c. Execute roll turn with opposite polarity	
	d. Execute pitch turn with opposite polarity	
	e. Begin Sun acquisition sequence	
32	Sun reacquired	M + (94 - 99) min.
33	Canopus reacquisition	M + 100 min.
	a. Switch in error signal from Canopus sensor	
	b. Begin roll turn	

Table 5.3-1 (Continued)

No.	Event	Nominal Time
	c. Receive acquisition signal	
	d. Switch in signal from Earth sensor	
	e. Verify Canopus acquisition	
34	Canopus reacquired	M + (100 - 105)min.
	a. Gyros turned off	
35	Switch data transmission rate from 33 to 17 bps	I + 35 days
36	Activate high-gain antenna	I + 40 days
	a. Unlock antenna	
	b. Drive antenna to position 1	
	c. Switch transmitter to high-gain antenna	
	d. Switch data transmission rate from 17 to 267 bps	
37	Drive high-gain antenna to position 2 (periodic update of antenna pointing angles initiated by CC&S command throughout mission with Earth-based backup command capability provided - 28 position changes required)	I + 42 days
38	Switch data transmission rate from 267 to 133 bps (CC&S command with Earth based backup command typical for all bit rate change events)	I + 212 days
39	Switch data transmission rate from 133 to 67 bps	I + 262 days
40	Transmit and verify required scan platform orientation angle	E - 2 days
41	Scan platform orientation	E - 1 day
	a. Remove encounter science instrument cover	
	b. Activate scan platform drive	
	c. Position scan platform	
	d. Turn on Jupiter sensor	
	e. Verify sensor operation	

No.	Event	Nominal Time
42	Begin Jupiter search (if Jupiter not acquired)	E - 1 day
	a. Cycle scan platform	
43	Jupiter acquired	E - 1 day
	a. Begin Jupiter tracking	
44	Turn on gyros	E - 360 min.
45	Begin encounter sequence	E - 180 min.
	a. Turn on DSE	
	b. Turn on encounter science	
46	Begin TV picture recording sequence	E - 80 min.
47	TV turned off	E - 30 min.
48	Perijove passage (one Jupiter radius altitude)	E - I + 582 days
49	Switch to inertial attitude control mode	E + 10 min.
	a. Switch out error signal from Sun sensor	
	b. Uncage pitch and yaw gyros	
50	Begin Earth occultation (0° cone)	E + 18 min.
51	Begin Sun occultation (0° cone)	E + 30 min.
52	End Earth occultation (0° cone)	E + 84 min.
53	End Sun occultation (0° cone)	E + 102 min.
54	End encounter sequence	E + 180 min.
	a. Turn off encounter science	
	b. Turn off DSE	
55	Switch to Sun reference attitude control mode	E + 190 min.
	a. Acquire Sun	
	b. Turn off gyros	
	c. Turn off Jupiter sensor	
	d. Deactivate scan platform	
56	Transmit command to initiate encounter data playback	E + 2 days
	a. DSE turned on (cyclic transmission of one hour real time data to five hours of non-real time data)	
57	End data playback	E + 4 days
	a. Turn off DSE	
58	Return to cruise mode	E + 4 days

capability throughout the mission. Spacecraft attitude is held during Sun and Canopus occultations at encounter by use of inertial control. Data are stored intermittently throughout the mission and during encounter. The expected error in periapsis altitude is approximately 2600 km. Playback of the television picture is accomplished following encounter and after reacquisition of the primary attitude references. The spacecraft then assumes its cruise mode of operation.

A weight summary of Spacecraft Design Concept C is presented in Table 5.3-2.

Table 5.3-2

SPACECRAFT DESIGN CONCEPT C - WEIGHT SUMMARY

Subsystem	Weight, lbs.
Science	115
Communications	88
Data Management	69
Spacecraft Control	68
Attitude Control Propulsion	95
Midcourse Propulsion	78
Electrical Power	326
Structural/Mechanical and Meteoroid Protection	202
Thermal Control	17
Total Spacecraft	1058
Adapter (0.065 x Spacecraft Weight)	69
Launch Weight	1127

5.3.2 Subsystem Design Information

5.3.2.1 Science

In Spacecraft Design Concept C, provision is made for a scientific instrument complement of intermediate capability. A definition of this experiment package (Intermediate Scientific Experiment Package - 2) is present in Table 2.1-8, and the instruments are listed again in Figure 5.3-1. The individual instruments are described in subsection 2.1. The total weight of this package is 115 pounds.

Several design features related to Concept C represent direct responses to the science subsystem requirements. These design features and the associated requirements are discussed in some of the paragraphs which follow, particularly in those related to data management (data automation element), radiation protection, configuration (pointing geometries), and structural and mechanical design (scan platform implementation and sensor deployment).

5.3.2.2 Communications

The communications subsystem recommended for Design Concept C is configured in the manner shown in Figure 3.1-8. In order to obtain a data rate compatible with the amount of data gathered, the transmitter power is 35 watts and the high-gain antenna is a 6 foot reflector with a gain of 30 db. The antenna strains device has 2 degrees of freedom to accommodate the narrow beam width, and the antenna should be circular.

With this configuration, the gain-loss chart shown in Table 5.3-3 is applicable at 6 a.u. communications distance.

Table 5.3-3

DESIGN CONCEPT C - GAIN-LOSS CHART

	Gain	Loss
Transmitter Power	45.5 dbm	
Modulation		3 db
S/C Ant Gain	30 db	
Space Attenuation		278 db
Rcvr Ant Gain	61 db	
Rcvr Sens ($40^{o}K$)		-182 dbm
Misc Loss		2 db
System Tolerances		6 db
TOTALS	136.5 db	107 db

S/N_O = 136.5 - 107 = 29.5 db
Then, with an information rate of 67 bps,

ST/N_O= 29.5 - 10 log 67 = 11 db. This results in an information performance margin of 11 - 5.8 = 5.2 db.

By means of similar gain-loss charts, the transmission schedule for Concept C (Table 5.3-4) can be derived.

Table 5.3-4

DESIGN CONCEPT C - ANTENNA AND INFORMATION RATE SCHEDULE

Communications Distance (a.u.)	Antenna	Info Rate (bps)
0-0.2	Omni	33
0.2-3	Parabola	267
3-4	Parabola	133
4-6	Parabola	67

The number and weight of the components of the communications subsystem are shown in Table 5.3-5. The recommended numbers of components are based on a reliability analysis of the communications subsystem. Although the proposed configuration is not necessarily optimum with respect to reliability, it is considered to be an appropriate compromise between reliability, weight, and power considerations.

Table 5.3-5

DESIGN CONCEPT C - COMMUNICATIONS SUBSYSTEM WEIGHT

Component (no.)	Weight, lbs
Amplifier (2)	6
Power Monitor (2)	2
Circulator (6)	6
Exciter (2)	9
APC Receiver (2)	18
Revr Monitor	1
Exciter Control	2
Amp Control	2
Omni Ant (2)	4
Parabolic Ant	20
Power Supply-HV (2)	14
Cabling, etc.	4
TOTAL	88

5.3.2.3 Data Management

The elements and functional requirements of the data management subsystem have been discussed in general terms in subsection 3.2. The available transmission rates in various portions of the mission have been presented previously in Table 5.3-4; the anticipated raw and compressed data bit rates are presented in Table 5.3-6. Data compression by means of the fan method or the zero-order interpolator is used (1) to permit real-time transmission of all data, except the television pictures, throughout the mission and (2) to allow intermittent communications.

The television pictures determine the required storage capacity. On the basis of the assumptions outlined in subsection 5.1.2.3, the near-Earth storage capacity required for the dynamic data handling is 1.31M bits; the interplanetary storage capacities necessary for such handling and for the implementation of intermittent communications are 820K bits and 23.0M bits, respectively; and the encounter capacity required to store all of the important data, including the television pictures, is 48.7M bits. A tape recorder with a capacity of 48.7M bits is therefore recommended for use as the DSE. Slightly more than two days are required to transmitt the encounter data by using the available 67-bit-per second transmission rate. Few changes are required in the data management subsystem elements used for Mariner IV. The DAE shown in Figure 5.3-2 processes the microwave radiometer, the infrared radiometer, the high-range interferometer spectrometer, the high-energy proton directional monitor, and the cosmic ray spectrum analyzer, and the method of processing is similar to that used for the magnetometer measurements described for Concepts A and B. Likewise, the method of processing ion chamber data is similar to that used for processing the energetic particle detector data. The DEE is capable of processing approximately 110 analog measurements, as indicated by modification A in Figure 3.2-7. Also, provisions for data compression and for data-transmission rates of 17, 33, 67, 133, and 267 bits per second are included. The capacity of the DSE (Figure 3.2-6) is 48.7 bits; read-in rates of 41, 410, and 21K bits per second and readout rates of up to 20K bits per second are provided. The number of DC's for Concept C is 60.

The number of weight of the components of the data management subsystem are shown in Table 5.3-7. The recommended numbers of components are based on a reliability analysis of the data management subsystem. Although the proposed configuration is not necessarily optimum with respect to reliability, it is considered to be an appropriate compromise between reliability, weight, and power considerations.

Table 5.3-6

DESIGN CONCEPT C - ANTICIPATED DATA BIT RATES

TYPE	NEAR EARTH		INTERPLANETARY		ENCOUNTER(NO TV)		ENCOUNTER (TV)	
	RAW	COMPRESSED(FAN)	RAW	COMPRESSED(FAN)	RAW	COMPRESSED(FAN)	RAW	COMPRESSED(FAN)
1. Engineering	33.3	(150:1) 0.2	33.3	(150:1) 0.2	33.3	(150:1) 0.2	33.3	(150:1) 0.2
2. Magnetometer	300.0	(10:1) 30.0	0.2	(10:1) ≈ 0.0	300.0	(10:1) 30.0	300.0	(10:1) 30.0
3. Cosmic Dust Detector	0.1	(1000:1) ≈ 0.0	0.1	(1000:1 ≈ 0.0	0.1	(1000:1) ≈ 0.0	0.1	(1000:1) ≈ 0.0
4. Energetic Particle Detector	0.4	(3:1) 0.1	0.4	(3:1) 0.1	2.0	(3:1) 0.7	2.0	(3:1) 0.7
5. Expanded Photometer					0.8	(4:1) 0.2	0.8	(4:1) 0.2
6. Plasma Probe	0.1	(1:1) 0.1	0.1	(1:1) 0.1	0.1	(1:1) 0.1	0.1	(1:1) 0.1
7. Microwave Radiometer					1.3	(2:1) 0.7	1.3	(2:1) 0.7
8. Infrared Radiometer					0.7	(2:1) 0.4	0.7	(2:1) 0.4
9. Ion Chamber	0.1	(10:1) ≈ 0.0	0.1	(10:1) ≈ 0.0	0.3	(10:1) ≈ 0.0	0.3	(10:1) ≈ 0.0
10. High-Range Interferometer Spectrometer					33.3	(2:1) 16.7	33.3	(2:1) 16.7
11. High-Energy Proton Directional Monitor	0.1	(10:1) ≈ 0.0	0.1	(10:1) ≈ 0.0	0.4	(10:1) ≈ 0.0	0.4	(10:1) ≈ 0.0
12. Cosmic Ray Spectrum Analyzer	0.2	(10:1) ≈ 0.0	0.2	(10:1) ≈ 0.0	0.5	(10:1) 0.1	0.5	(10:1) 0.1
13. Television							20000.0	(10:1) 2000.0
14. Housekeeping	30.0	(30:1) 1.0	3.0	(30:1) 0.1	30.0	(30.1) 1.0	600.0	(10:1) 60.0
TOTAL	364.3	31.4	37.5	0.5	402.8	50.1	20972.8	2109.1

DESIGN CONCEPT C DATA AUTOMATION ELEMENT

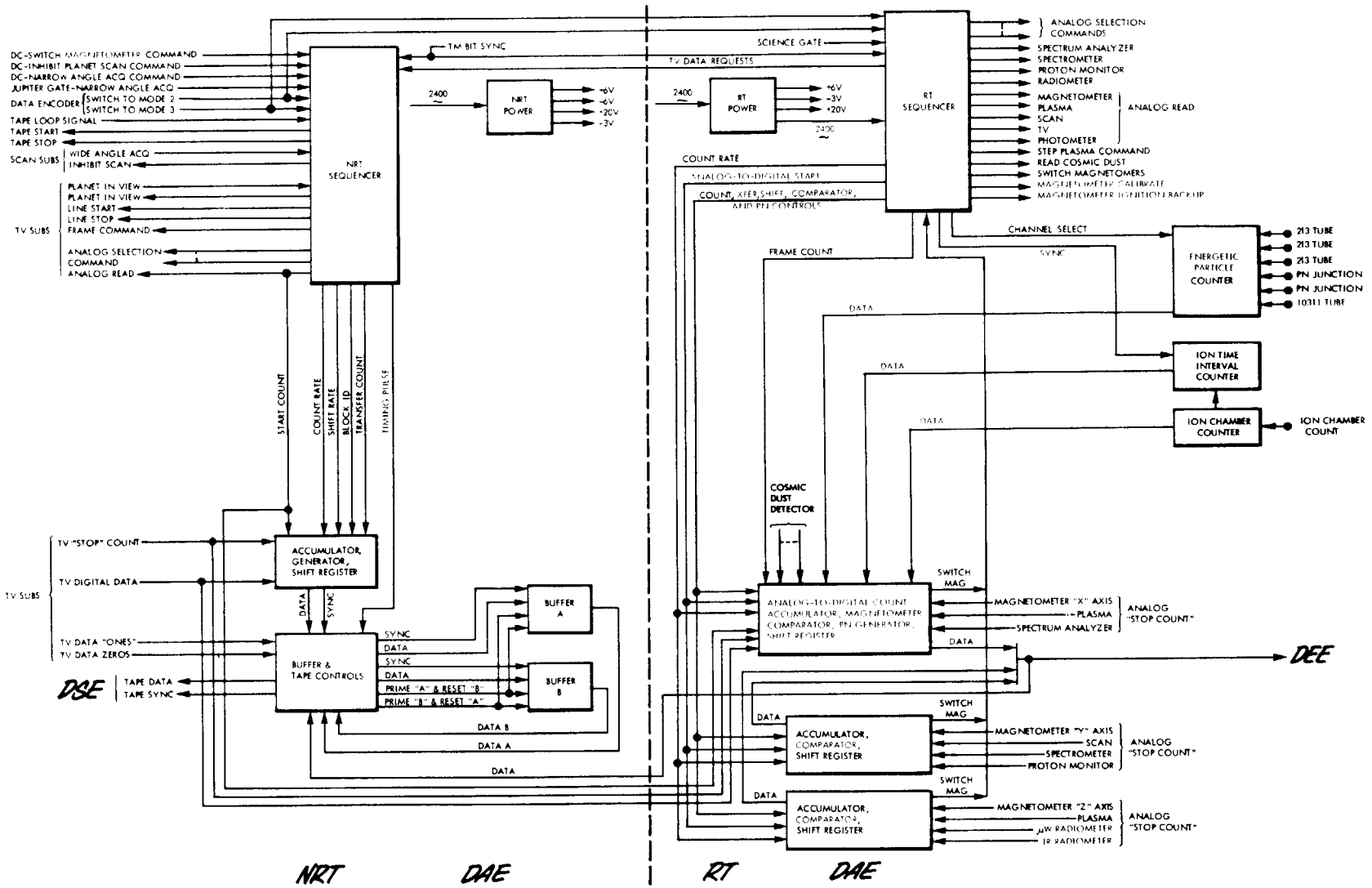

FIG. 5.3-2

Table 5.3-7

DESIGN CONCEPT C - DATA MANAGEMENT SUBSYSTEM WEIGHT

Component (no.)		Weight, lbs
DEE	(3)	27.0
DAE	(3)	19.5
DSE	(3)	13.5
CDDE	(3)	9.0
	TOTAL	69.0

5.3.2.4 Spacecraft Control

The function of the spacecraft control subsystem for Design Concept C is essentially the same as the one for Design Concept B. The most prominent difference is that provision is made for a terminal correction in the case that the vernier correction does not provide the required accuracy. As with Design Concept B, the references used in the stellar attitude control mode are the Sun and Canopus with an inertial mode provided for use during Sun acquisition, spacecraft maneuvers, and occultation of either of the stellar references. The inertial mode also serves as a back-up in case of failure of the primary control system. The navigation and control computations of trajectory determination, maneuver commands, pointing angles for the high gain antenna (two degrees-of-freedom), and scan platform orientation angle are performed by Earth-based facilities with the resultant commands and information subsequently transmitted to the spacecraft.

If no terminal maneuver is necessary, the sequence of events to be accomplished by Concept C is identical to the one for Design Concept B to the level of detail of this description. The sequence of events necessary to accomplish the terminal maneuver is (1) computation of the required roll and pitch turn magnitudes, roll and pitch turn polarities, and velocity increment, (2) transmission and verification of these commands; (3) begin maneuver command; (4) switch to fine attitude control mode; (5) turn on gyros and accelerometer; (6) switch to inertial control; (7) execute pitch turn; (8) execute roll turn; (9) execute motor burn; (10) reacquire Sun; and (11) reacquire Canopus.

The validity of Canopus reacquisition after the terminal maneuver is checked through the acquisition of Jupiter. This is accomplished by positioning the scan platform as an Earth-commanded angle during Sun reacquisition. The Jupiter sensor is

then slewed through an Earth-commanded angle to normal to the plane of scan platform movement. When the Canopus sensor signals acquisition of a star, the Jupiter sensor is turned on, and Jupiter acquisition should be immediate. If Jupiter is not acquired, the roll search is continued. The general configurations of the CC&S and the attitude control electronics are shown in Figures 3.3-1 and 3.3-2. The number and weight of the components of the spacecraft control subsystem are shown in Table 5.3-8. The recommended numbers of components are based on a reliability analysis of the spacecraft control subsystem. Although the proposed configuration is not necessarily optimum with respect to reliability, it is considered to be an appropriate compromise between reliability, weight, and power considerations.

Table 5.3-8

DESIGN CONCEPT C - SPACECRAFT CONTROL SUBSYSTEM WEIGHT

Component (no.)	Weight, lbs
Fine Sun Sensor	1
Coarse Sun Sensors (4)	4
Earth Sensor	6
Star Tracker (2)	12
Jupiter Tracker	6
CC&S	12
Attitude Control Electronics	20
Gyros (6) and Accelerometers	7
TOTAL	68

5.3.2.5 Attitude Control - The attitude control concept for Spacecraft Design Concept C is identical to that for Concept B. The only differences involved are those resulting from modifications to the physical parameters, such as moments of inertia, moment arms, etc. This case is closely approximated by the example design analyzed in subsection 3.5.8, and the analysis presented there is considered applicable. A system impulse of 750 pound-seconds is selected for a design point, with a corresponding weight requirementof about 95 pounds.

5.3.2.6 Propulsion

The midcourse propulsion subsystem for Design Concept C is the basic hydrazine system described in subsection 3.6.1. It has the capability of imparting a total velocity increment of 90 meters per second (300 fps) to the spacecraft mass of about 1058 pounds. This corresponds to approximately a 5 σ design criteria

for a launch vehicle FOM of 10-15 m/sec and a added capability for a possible second maneuver. Table 5.3-9 contains a summary of the components and weight of the midcourse propulsion system.

Table 5.3-9

DESIGN CONCEPT C - MIDCOURSE PROPULSION SUBSYSTEM WEIGHT

Components	Weight, lbs
Hydrazine	47.0
Hydrazine Tank	3.1
Nitrogen	2.1
Nitrogen Tank	4.2
Bladder	0.86
Fixed Hardware	20.84
Total	78.1
Hydrazine Tank Diameter	14.0 in.
Nitrogen Tank Diameter	7.7 in.

The attitude control propulsion system considered for Concept C is the one identified and described as Configuration B in subsection 3.6.2 The estimated weight of the system necessary to meet the projected 750 pound-second impulse requirements of Spacecraft Design Concept C is 95 pounds (see Figure 3.6-10).

5.3.2.7 Auxiliary Electric Power

The auxiliary power arrangement for Design Concept C is illustrated by the schematic diagram in Figure 3.7-8. A profile of subsystem loads is presented in Table 5.3-10. The maximum continuous load occurs during the encounter period when the surplus capacity is approximately 10 percent. During the maneuver period the load is slightly greater, but its duration is less than two hours. The specific list of components, the numbers used, and the weights are listed in Table 5.3-11. The RTG rating is based upon the end-of-life capacity. The degradation in the capacity of the RTG or a junction of time is indicated in Table 5.3-10.

Table 5.3-10

DESIGN CONCEPT C - ELECTRIC POWER LOADS

	Pre-Launch	Boost & Park Orbit	Acquisition	Cruise	Maneuver	Encounter
Encoder	5	5	5	5	5	5
DAE	4	4	4	4	4	6
Tape Recorder	1	0	0	2	2	1
Command Detector & Decoder	3	3	3	3	3	3
CC&S	12	12	12	10	12	12
Control Gyro Electronics	5	5	5	5	15	5
Attitude Control Electronics	11	11	11	9	25	11
Gyro 400 cps Power	5	5	5	5	15	5
Sun Sensors			2	2	3	2
Canopus Tracker			10	7	7	7
Earth Sensor			10	0	7	0
Communication Control	10	10	10	10	10	10
Communication Receiver	10	10	10	10	10	10
Communication Exciter	20	20	20	20	20	20
Communication Amplifier	120	15	120	120	120	120
Extended Magnetometer	7.0	0	7.0	7.0	7.0	7.0
Energetic Particle Detector	0.4	0	0.4	0.4	0.4	0.4
Cosmic Dust Detector	0.2	0	0.2	0.2	0.2	0.2
Expanded Photometer	5.0	0	0	0	0	5.0
TV Camera (TV-I)	10.0	0	0	0	0	10.0
Plasma Probe	2.5	0	2.5	2.5	2.5	2.5
Microwave Radiometer	6.0	0	0	0	0	6.0
Infrared Radiometer	3.0	0	0	0	0	3.0
Ion Chamber	0.5	0	0.5	0.5	0.5	0.5
Infrared Spectrometer	5.0	0	0	0	0	5.0
High Energy P. Direct. Monitor	0.6	0	0.6	0.6	0.6	0.6
Cosmic Ray Spectrum Analyzer	2.0	0	2.0	2.0	2.0	2.0
Total Power Requirement	248.2	172	240.2	225.2	271.2	259.2
Raw Power Input to Power Cond.	311	214	300	280	338	322
Power Input to Shunt Reg. & Bat.	85	182	78	89	31	38
Power From RTG (4-90W)	396	396	378	369	369	360

Table 5.3-11

DESIGN CONCEPT C - ELECTRIC POWER SUBSYSTEM WEIGHT

Component (no.)	Rating	Weight, lbs
Radioisotope Thermoelectric Generator (4)	90 watt, 28 volt	200.00
3 Electrode Ni-Cd Battery	20 ampere hour	28.00
Shunt Volt. Reg. Switch (4)	Eight .5a Channels	1.60
Volt. Reg. Mode Controller	Signal Device	.75
Shunt Dissipation Resistors (4)	112 Watt	12.00
Main 2400-cps Inverter (2)	15 ampere input	6.00
Transfer Relay (2)	15 ampere dpst	1.00
Emergency 2400-cps Inverter	2 ampere input	.50
Inverter Synchronizer	Signal device	.50
Emergency Transfer Unit	5 ampere spdt	.50
400-cps Inverter	2 ampere input	4.00
Battery Charge-Discharge Controller	3 amp chg, 7.5 amp. disc.	12.00
Power Distribution and Wiring		59.00
	Total	325.85

5.3.2.8 Thermal Control

The equipment bus of Spacecraft Design Concept C is basically a flat octagon with two appendages on opposite sides as shown in Figure 5.3-1. The central part of the bus houses the propellants for midcourse correction and attitude control. There is very little power dissipated in this region, and the temperature is controlled largely by the surrounding equipment compartments.

Four louvered equipment compartments surround the propulsion tankage. The louvers are located on the sides of the spacecraft and receive some incident energy from the RTG's. If necessary, radiation shields may be employed to reduce RTG heating. A guide to equipment arrangement is shown in Table 3.8-1, and component thermal design infromation for this concept is shown in Table 5.3-12.

The appendages house the gimbaling devices for the planet-oriented science subsystem platforms. The gimbal equipment is expected to dissipate a small amount of heat. Temperature of this equipment is controlled primarily by adjacent equipment bays. The exposed surfaces of the appendages are insulated or coated with a low emittance material.

Table 5.3-12

DESIGN CONCEPT C - THERMAL CONTROL INFORMATION

SUBSYSTEM AND COMPONENTS	TEMPERATURE LIMITS, °F OPERATING MIN	OPERATING MAX	NONOPERATING MIN	NONOPERATING MAX	HEAT DISSIPTATION WATTS	WEIGHT, LBS,
Science Subsystem						
Extended Magnetometer						
Electronics	-13	167	NA	NA	7.0	5.0
Helium Sensor	-13	167	NA	NA	NA	1.5
Rubidium Sensor	32	122	NA	NA	NA	1.5
Energetic Particle Detector	14	122	NA	NA	0.4	2.5
Cosmic Dust Detector						
Electronics	-40	212	NA	NA	0.2	2.0
Sensor	-148	392	NA	NA	NA	0.5
Expanded Photometer	-4	104	-58	212	5.0	6.0
TV Camera						
Electronics	14	158	-40	257	10.0	15.0
Optics	-4	104	-58	212	NA	NA
Plasma Probe	14	176	NA	NA	2.5	7.0
Microwave Radiometer	-20	150	-58	212	6.0	28.0
Infrared Radiometer	-4	104	-58	212	3.0	5.0
Ion Chamber	-22	158	NA	NA	0.5	3.0
Infrared Spectrometer	-4	104	-58	176	5.0	16.0
High Energy Proton Directional Monitor	14	122	NA	NA	0.6	4.0
Cosmic Ray Spectrum Analyzer						
Electronics	-22	167	-22	167	2.0	18.0
Sensor	-22	122	-22	122	NA	NA
Spacecraft Control						
Central Computer & Sequencer	0	124	-31	185	15.0	12.0
Wide Angle Sum Sensor	0	120	-58	212	2.0	2.0
Fine Angle Sum Sensor	0	120	-58	212	1.0	1.0
Earth Sensor	-10	125	-58	212	7.0	6.0
Jupiter Sensor	-10	125	-58	212	7.0	6.0
Star Trackers	-10	125	-58	212	7.0	6.0
Gyros	-65	250	-65	250	29.0	2.0
Accelerometer	10	100	-31	185	1.0	2.0
Attitude Control Electronics	10	100	-31	185	15N*/20P*	20.0
Midcourse Propulsion						
Thruster Assembly	NA	1500	70	NA	NA	2.5
Hydrazine Propellant and Tank	40	100	40	100	NA	43.8
Nitrogen Pressurization System	40	100	40	100	NA	20.0
Nitrogen and Tank	40	165	40	165	NA	5.6
Auxiliary Electric Power						
RTG Units	510	510	NA	NA	NA	160.0
Shunt Voltage Regulator	-30	160	NA	NA	13.0	1.6
Shunt Power Dissipation Resistors	-30	160	-65	160	**	12.0
NI-CD-3 Electrode Battery	-65	120	-65	120	**	28.0
Charge-Discharge Controller	-30	160	NA	NA	10.0	12.0
Voltage Sensor & Regulator Mode Control	-30	160	NA	NA	7.0	0.75
2400 cps Inverter	-30	160	NA	NA	38.0	6.0
Transfer Relay	-30	160	NA	NA	NA	1.0
400 cps Inverter & Regulator	-30	160	NA	NA	5.0	4.0
Emergency 2400 cps Inverter	-30	160	-65	160	NA	0.5
Inverter Synchronizer	-30	160	NA	NA	5.0	0.5
Power Distribution	-65	160	-65	160	10.0	59.0
Diodes	-65	160	NA	NA	15.0	NA
Emergency Transfer Unit	-30	160	-65	160	NA	0.5
Communications						
TWT Amplifier	-65	203	NA	NA	85.0	6.0
Power Monitor	-65	203	NA	NA	NA	2.0
Circulator	-65	203	NA	NA	NA	6.0
Exciter	-65	203	NA	NA	20.0	9.0
Exciter Control	-65	203	NA	NA	5.0	2.0
APC Receiver	-65	203	NA	NA	5.0	9.0
Amplifier Control	-65	203	NA	NA	5.0	2.0
Power Supply	-65	203	NA	NA	10.0	9.0
Data Management						
Data Encoder Element	14	176	NA	NA	7.0	9.0
Data Storage Element	14	176	-55	185	4.0	12.0
Command Detector & Decoder	14	176	NA	NA	2.0	6.0
Data Automation Encoder	14	176	-55	257	4.0	8.0

*N Denotes nomincal value
P Denotes peak value for short duration
** Dependent on operational requirements

The upper surface (launch position) and the exposed portions of the lower surface are insulated. It is possible that the lower surface can be covered with a low emittance coating in lieu of insulation.

Thermal control of the Jupiter scan platforms at large solar distances presents a problem since there is no power dissipation until encounter at which time the experiments are turned on. The entire platforms are enclosed in an insulated cover which is jettisoned when the experiments are to be used. A low level of continuous power dissipation is required to prevent the temperature from becoming too low.

As in the concepts discussed previously, the components mounted on extensions from the spacecraft require their own peculiar thermal design. The magnetometers and the ion chamber normally are shielded from the Sun by the equipment bus. The variations in solar energy should, therefore, have a negligible effect on the temperature of these units. Conductive heating from the RTG's poses no problem when low thermal conductivity materials are used for the supporting structure.

A larger amount of cooling air is required to dissipate the heat from the RTG's and electronic equipment during prelaunch of Concept C than for Spacecraft Design Concepts A and B. This is due to the larger electrical power load. The RTG, which is the source of the major cooling load, dissipates about 27,000 BTU/hour. This higher power dissipation does not interfere with the method of using heat capacity to limit temperature during launch.

The thermal control wieght requirement is estimated to be 17 pounds. This is based on 6 pounds for insulation, shielding, etc., and 9.72 square feet of louvers at 1.12 lbs/sq.ft. It is noted that some of the spacecraft surface skin acts as cold plates, and the skin therefore has minimum thickness requirements. It appears that the structural and meteroroid protection requirements dictate thicknesses which amply meet the thermal control requirements, thus this weight is not considered a part of thermal control.

5.3.2.9 Radiation Protection

The general problem of nuclear radiation protection for Jupiter flyby spacecraft is discussed in subsection 3.9. The conclusion reported therein is that no specific design penalties should be incroporated for radiation protection. The judicious selection of radiation resistant components for the various subsystems together with the proper placement of scientific instruments which are sensitive

to RTG radiation, is the recommended approach to radiation protection. Design Concept C reflects these design considerations to the extent possible in a conceptual design. This is particularly manifested in the spacecraft configuration. Based on the results presented in subsection 3.9, no radiation shielding is included in the design concept.

5.3.2.10 Meteoroid Protection

The data for a nominal 600-day mission used in assessing the meteroid protection requirements for Concept C are summarized in Table 5.3-13. The spacecraft exposed area in the interplanetary and asteroidal regions is determined as discussed in subsection 3.10.4 (See Figure 5.2-5). The near-Earth and near-Jupiter exposed area is the total surface area of the spacecraft equipment compartment.

Table 5.3-13

DESIGN CONCEPT C - METEOROID PROTECTION ANALYSIS DATA

Region	Exposed Area (m^2)	Time (Days)	Area x Time (m^2-Days)
Near-Earth	6.23	0.5	3
Interplanetary	2.23	565	1260
Asteroidal	2.23	190	424
Near-Jupiter	6.23	63.3	395

These data are combined with the data presented in subsection 3.10.3 to provide the design data shown in Figure 5.3-3. The two curves indicate the magnitude of difference in the protection requirements for the two asteroidal flux models. Using the criteria outlined in subsection 5.2.2.10, the nominal asteriodal flux indicates a skin thickness of 0.2-centimeter and an associated skin weight of 76 pounds. The worst case asteriodal flux requires a 1.34-centimeter skin thickness on the front. The protection system weight then is 355 pounds.

The meteroid protection system is provided for Concept C consists of a complete covering of the spacecraft with 0.2 centimeter of aluminum. The choice of this design point is obviously arbitrary, but is is felt that it represents an adequate protection system with very little penalty. It does not appear desirable to accept the penalties imposed by the worst case of asteroidal flux without in situ measurements of the actual flux.

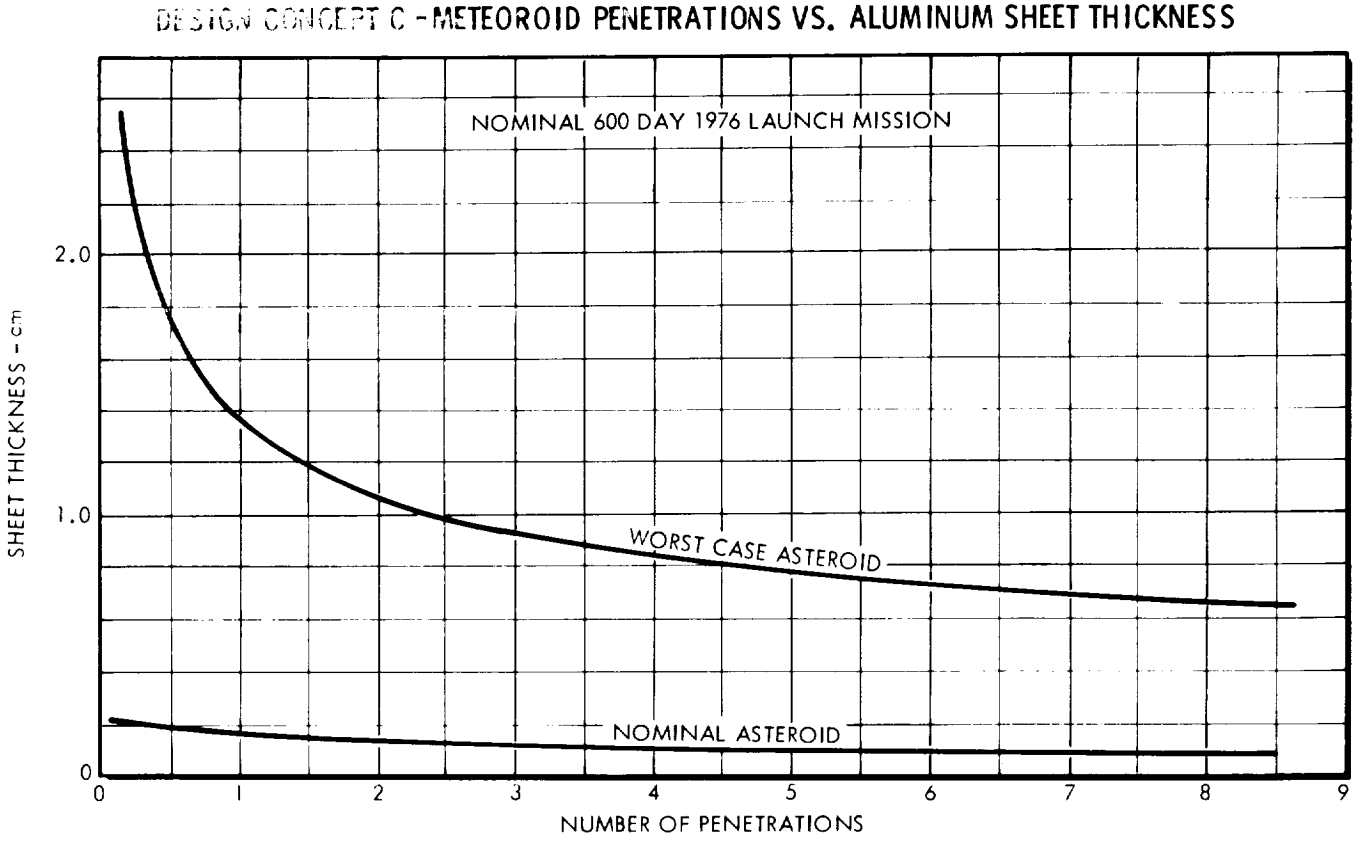

FIGURE 5.3-3

As indicated in subsection 3.12, the armor-type meteoriod protection is considered to be an integral part of the spacecraft structure, and for nominal protection measures, the weight is assumed to be completely charageable to the structure. Therefore, the meteoroid protection weight is not listed separately in Table 5.3-2, but is included in the structural/mechanical weight estimate.

5.3.2.11 Configuration

The Design Concept C Configuration is shown in Figure 5.3-1. Its primary features are (1) an equipment compartment, (2) four RTG units, (3) a 6-foot-diameter high-gain antenna, (4) a dual scan platform which accommodates the encounter science, and (5) the cruise science instruments which are located about the spacecraft body.

The equipment compartment is a polygon-shaped enclosure which is 6 feet long and 4 feet across at its maximum width. The basic electronic equipment and the midcourse and attitude control propellant tankage are housed in this package which forms the nucleus of the spacecraft. The equipment compartment is arranged in such a manner that the midcourse propulsion system is partially buried in the center of the vehicle and the thrust vector is directed aft.

A pair of RTG units are stacked on either side of the vehicle along the pitch axis. The power elements are mounted on tubular truss assemblies which project from the spacecraft body so that the RTG units extend beyond the periphery of the antenna. The antenna is a 6-foot parabolic dish which is located on the forward face of the equipment section.

Thermal control of the equipment and propellant systems is provided by means of louver systems which are mounted on the sides of the spacecraft. The electronic equipment is attached to the surface structure, and the louver systems are independently attached on the outer face. The entire assembly is removable for quick access during mating and pre-launch operations.

A scan platform is provided on either side of the spacecraft along the yaw axis in such a manner that the pointing requirements of the encounter sensors can be accommodated without interference from the primary antenna. Two-axis gimbal systems provide full tracking capability for each of these platforms.

Attitude control jets are placed on booms which extend from the four sides of the spacecraft adjacent to the scan platform and RTG unit installations. The booms are also used to provide support for the Sun and Earth sensors so that proper look angles can be provided without interference from the large antenna. A slight modification in the nose shroud of the Titan IIICx/Centaur to allow the spacecraft to clear the dynamic envelope in the launch configuration. This is necessary to allow the RTG units to extend beyond the antenna periphery and still retain the fixed RTG support feature.

5.3.2.12 Structural and Mechanical Design

Structural design of the equipment compartment is similar to that of Concepts A and B with the exception that the bus shape is slightly different. The equipment compartment skin is 0.2-centimeter aluminum plate.

The spacecraft antenna is gimballed from the forward face of the spacecraft equipment compartment and is capable of two degrees of freedom movement. The drive system is the same as that of the Concept B antenna with the exception of the increased requirements associated with the extra degree of freedom. The scan platforms are independently driven but coupled so that in case of failure of either system, the remaining drive unit will have the capability to drive both platforms. The magnetometers and ion chamber experiments are extended through the use of the STEM system.

On the basis of the relationships shown in Figure 3.12-2 the structural/mechanical and meteoroid protection weight is estimated to be 202 pounds for the case of an inserted spacecraft weight of 1058 pounds.

5.3.2.13 Subsystems Reliability

Table 5.3-14 contains the equipment mean-time-between-failure (MTBF) for Spacecraft Design Concept C. The science MTBF's are listed in Table 3.13-1. These MTBF's were determined using (1) a buildup of failure rates when an equipment design was available and (2) reliability estimates from similar equipment design and best engineering judgement when the equipment design was not available. For subsystem configurations containing redundant equipment, the MTBF listed in the table is for each of the redundant equipments. These equipment MTBF's are used to derive probability of mission success in subsection 5.3.4.

Table 5.3-14

SPACECRAFT DESIGN CONCEPT C - EQUIPMENT MTBF

SUBSYSTEM EQUIPMENT	MTBF (Hours)
Communications Subsystem	
Receiver	15,000
Exciter	45,000
TWT Amplifier	30,000
Circulator and Logic	350,000
TWT P/S	140,000
Power Monitor	333,000
Data Management Subsystem	
Data Encoder Element	1,300
Data Storage Element	6,000
Command Det & Decoder Element	
Detector & Decoder	10,000
Commands	44,000-77,000
Data Automation Element	5,000
Spacecraft Control Subsystem	
Fine Sun Sensor	180,000
Coarse Sun Sensor	230,000
Earth Sensor	40,000
Star Tracker	35,000
Attitude Control Electronics	40,000

Table 5.3-14 (Cont'd)

SUBSYSTEM EQUIPMENT	MTBF(Hours)
CC&S	4,500
Gyro and Accelerometer	8,000
Jupiter Tracker	40,000
Propulsion Subsystem	
Tank	0.9998*
Squib	0.999896*
Regulator	0.999556*
Rocket Motor and Vanes	0.99998*
Attitude Control Subsystem	
Tank	0.9998*
Squib	0.999896*
Regulator	0.9587*
Single Roll Jet	0.9794*
Single Pitch/Yaw Jet	0.9750*
Auxiliary Electrical Subsystem	
400 cps Chopper	210,000
Voltage Sensor and Regulator	60,000
2400 cps Chopper	150,000
Inverter Sync	220,000
Battery	70,000

* Probability of operating as required

5.3.3 Mission Performance

Mission performance envelopes such as that shown in Figure 5.3-4 were prepared for Spacecraft Design Concept C in combination with the Titan IIICx/Centaur launch vehicle. These data are used to derive the mission performance data presented in Figure 5.3-5(a) in terms of the width of the launch window, or launch period, corresponding to the dates of western quadrature, opposition, and eastern quadrature. Arrival on the dates of these events requires Earth-to-Jupiter flight times of approximately 420 days, 510 days, and 600 days, in that order.

SPACECRAFT DESIGN CONCEPT C - MISSION PERFORMANCE ENVELOPE

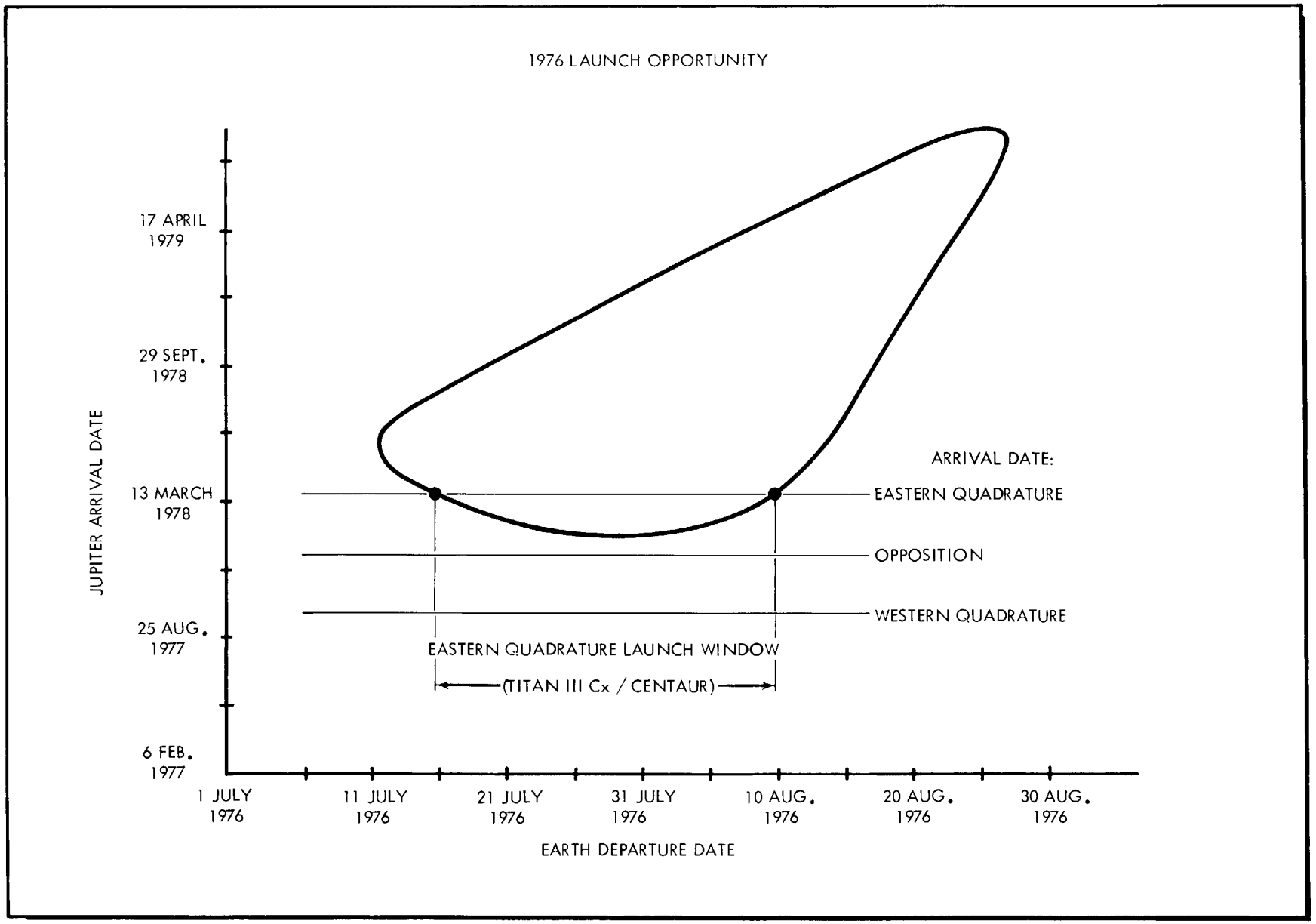

FIGURE 5.3-4

SPACECRAFT DESIGN CONCEPT C — LAUNCH VEHICLE MISSION PERFORMANCE SUMMARY CHART

(a) Titan III Cx / Centaur Launch Vehicle

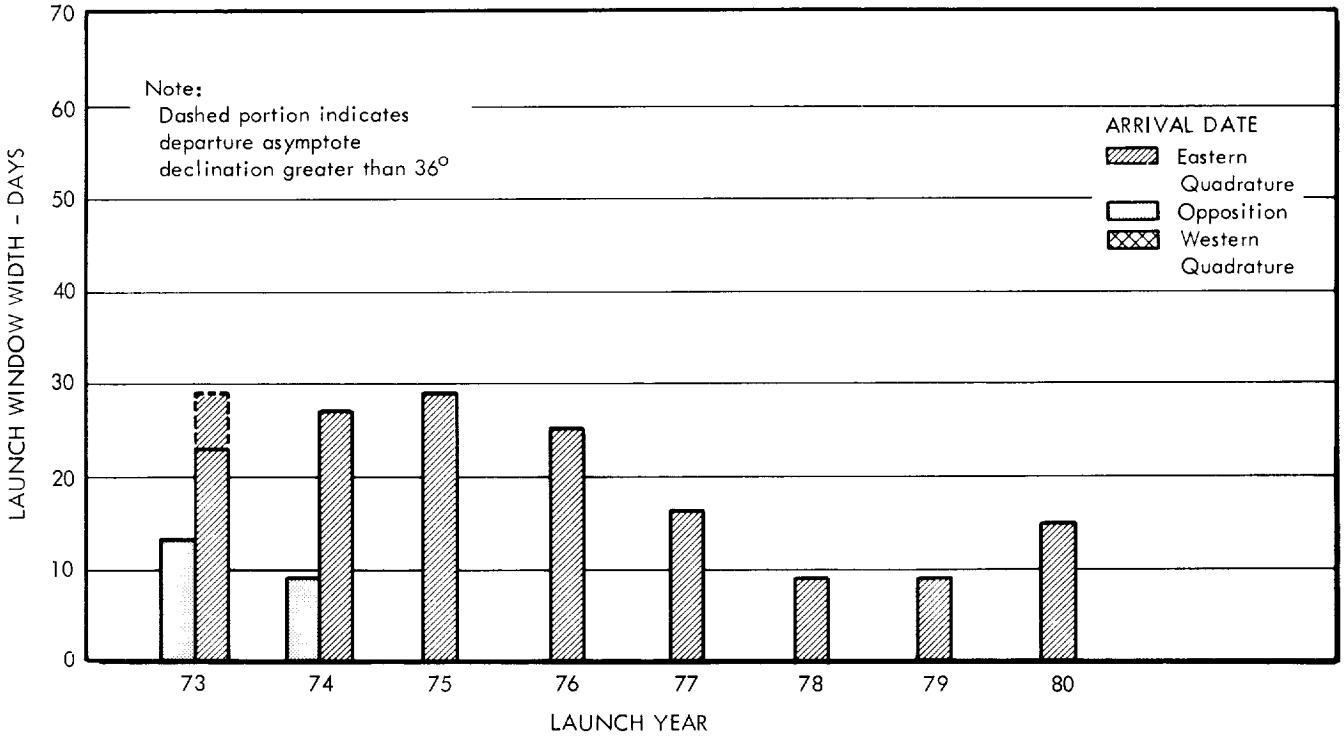

(b) Saturn IB / Centaur / HEKS Launch Vehicle

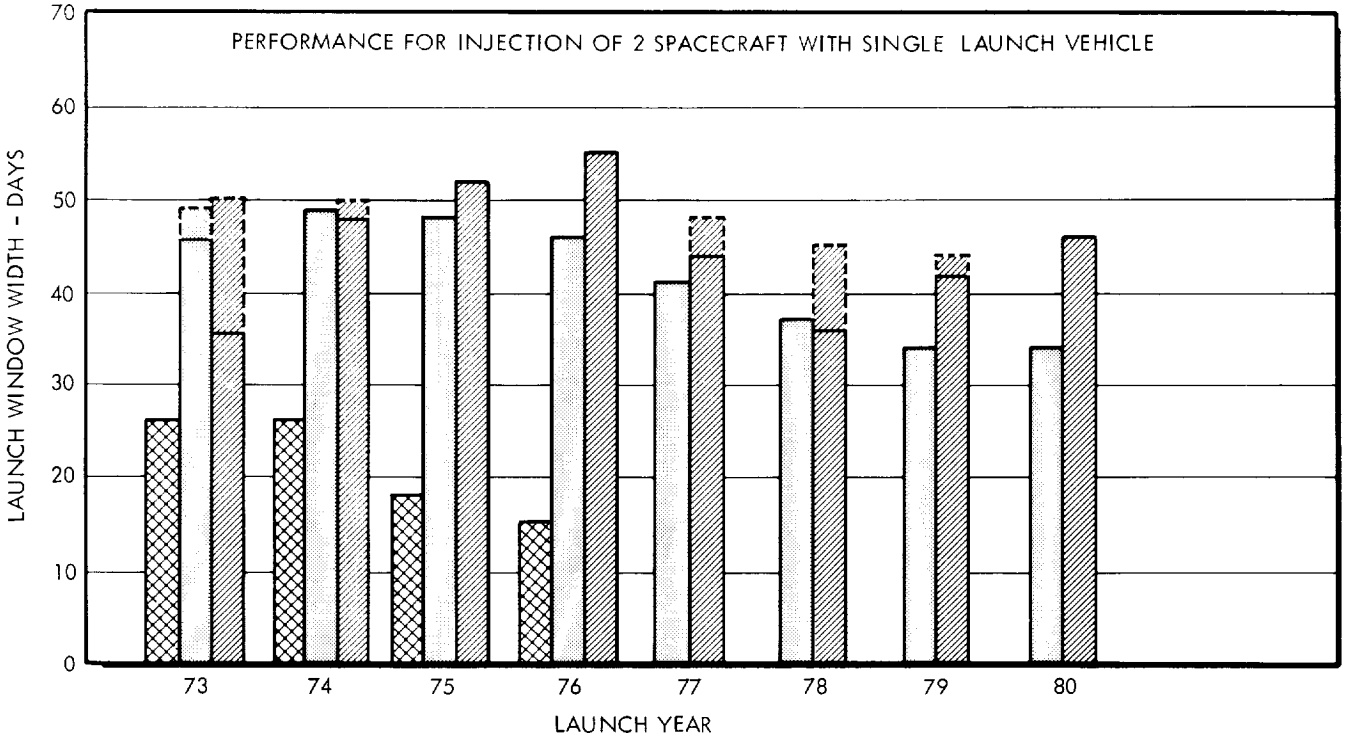

FIGURE 5.3-5

The Atlas SLV3x/Centaur/HEKS launch vehicle does not have the capability of injecting Concept C with sufficient energy for arrival on the three dates considered. It does provide sufficient performance for marginal launch opportunities in 1975 and perhaps in 1976 with flight times of about 800 days.

In addition to the evaluation of the Titan IIICx/Centaur, the mission performance of the Saturn IB/Centaur/HEKS launch vehicle in combination with two Concept C spacecraft was evaluated. The results are summarized in Figure 5.3-5(b). Spacecraft adapter mass for the dual launch configuration was estimated as 6.5 percent of the total injected spacecraft mass.

The data denoted by dashes in Figure 5.3-5 represents the interval of the launch window in which the magnitude of the departure asymptote declination is greater than 36 degrees. The reasons for this upper limit on the magnitude of asymptote declination are given in subsection 2.2.1

5.3.4 Probability of Mission Success

The approach and guidelines employed in this study to evaluate the probability of mission success for Design Concept C are discussed in subsection 4.2. The results indicated therein are based on a mission described by the sequence of events in Table 5.3-1. The MTBF's utilized in this analysis are listed in Table 5.3-14.

The probabilities of mission success for both total and half missions are presented in Table 5.3-15. The probabilities of successful operation in the case of the communications, auxiliary electrical power, data management, and science subsystems are presented in Table 5.3-16.

Table 5.3-15

DESIGN CONCEPT C - PROBABILITY OF MISSION SUCCESS

Configuration	Probability of Mission Success	
	Total Mission (586 days)	Half Mission (293 days)
Spacecraft Less Science Instruments	0.01	0.21
Total Spacecraft	less than 0.01	0.05

Table 5.3-16

DESIGN CONCEPT C - SUBSYSTEMS PROBABILITY OF MISSION SUCCESS

Subsystem	Probability of Mission Success: Total Mission (586 days)	Probability of Mission Success: Half Mission (293 days)
Communication	0.52	0.76
Auxiliary Electrical Power	0.45	0.68
Data Management	0.09	0.47
Science	less than 0.01	0.26

5.3.5 Development Requirements

The time estimates associated with the Program Implementation Network (see Figure 4.3-3) used for Design Concept C are printed in Table 5.3-17. From Table 5.3-18, it can be seen that the program should have a go-ahead date of October 1970 for a PMV launch date of 16 July 1976. This results in a total span time of 5 years 9 months as shown in Figure 5.3-6. As with Design Concepts A and B, the RTG development and Pu 238 fuel procurement are the major constraints. Estimates of the fuel procurement times are based on an assumed go-ahead date of 1 January 1970 with no production available from the preceding years. The probability that this span time will be less than the 5 years 9 months as shown on the time line chart is 0.6 (Figure 5.3-7).

5.3.6 Cost Results

Presented in Table 5.3-19 is a summary of the items that comprise the total program costs for Spacecraft Design Concept C, assuming two operational flights. The Saturn IB/Centaur/HEKS costs are based on a single launch of two spacecraft. The costs presented in Table 5.3-20 are the recurring spacecraft costs for two flights. The total cost increment for a third flight is given in Table 5.3-21. These results are based on the discussion in subsection 4.4.

Table 5.3-17
DESIGN CONCEPT C - PERT III INPUT ACTIVITY TIME ESTIMATES

TC	SP SCH OPT	REG EVENT LC	END EVENT LC	OPT TIME	MEAN TIME	PESS TIME	SCH DATE ACT DATE / 1 / 2 / 3 / 4	EVENT TITLE /ACTIVITY TITLE
3			00.000.001				1.01.70	CONTRACT GO-AHEAD
1		00.000.001	00.000.002	2.0	4.0	12.0		C/JUPITER SYS DESIGN SPEC
1		00.000.002	00.000.003	8.0	12.0	26.0		C/SPCFT PREL SUBSYS + INRFCE SPEC
1		00.000.002	00.000.004	1.0	1.0	2.0		R/RTG FUEL PROCUREMENT ORDER
1		00.000.003	00.000.005					S/DETAILED CDFG DSGN + MOCKUP
1		00.000.003	00.000.006					S/SUBSYS PROCUREMENT NEGOTIATIONS
1		00.000.003	00.000.007	12.0	16.0	18.0		R/SCNCE PROCUREMENT
1		00.000.003	00.000.008	3.0	6.0	12.0		R/TEST SPEC + LAUNCH OPER PLAN
1		00.000.002	00.000.009	2.0	2.0	4.0		INITIATES EARTH LAUNCH VEH PROC
1		00.000.005	00.000.010	2.4	6.0	8.0		SCNCF PYLD, CDFG APPR + MCKUP COMPL
1		00.000.006	00.000.010					SCNCE PYLD, CDFG APPR + MCKUP COMPL
1		00.000.007	00.000.010	2.4	6.0	8.0		SCNCE PYLD, CDFG APPR + MCKUP COMPL
1		00.000.008	00.000.011	16.0	33.0	41.0		R/TEST + LAUNCH + FAC IMPLMTN PLAN
1		00.000.010	00.000.012	2.0	4.0	8.0		S/TOOLING DSGN
1		00.000.064	00.000.013					R/DATA MGMT SUBSYS PROCUREMENT
1		00.000.064	00.000.014					R/COMM SUBSYS PROCUREMENT
1		00.000.064	00.000.015					R/SPACECRAFT CONT SUBSYS PROC
1		00.000.064	00.000.016					R/RTG PROCUREMENT
1		00.000.064	00.000.017					R/MIDCOURSE PRPLN PROCUREMENT
1		00.000.064	00.000.018					R/ATTITUDE CONT PRPLN PROCUREMENT
1		00.000.012	00.000.019	2.0	4.0	6.0		S/MFGR OF STM + TCM STR + MECH SYS
1		00.000.013	00.000.020	29.0	52.0	104.0		RE/STM DATA MGMT SUBSYS
1		00.000.014	00.000.021	26.0	37.0	52.0		RE/STM COMM SUBSYS
1		00.000.015	00.000.022	29.0	64.0	130.0		RE/STM SPACECRAFT CONT SUBSYS
1		00.000.019	00.000.023	41.0	52.0	78.0		C/STM STR + MECH ASSY
1		00.000.020	00.000.023	1.0	1.0	2.0		C/STM STR + MECH ASSY
1		00.000.021	00.000.023	1.0	1.0	2.0		C/STM STR + MECH ASSY
1		00.000.022	00.000.023	1.0	1.0	2.0		C/STM STR + MECH ASSY
1		00.000.063	00.000.023					C/STM STR + MECH ASSY
1		00.000.023	00.000.024	1.0	2.0	3.0		S/STM ASTRIONICS COMPAT TESTS
1		00.000.024	00.000.026	2.0	8.0	12.0		C/STM ASTRIONICS COMPAT TESTS
* 1		00.000.004	00.000.027	48.0	52.0	76.0		RE/FIRST SET FUELED RTGS
1		00.000.016	00.000.027	64.0	78.0	208.0		RE/FIRST FUELED RTGS
1		00.000.017	00.000.028	29.0	52.0	104.0		RE/FIRST MIDCOURSE PRPLN
1		00.000.018	00.000.029	29.0	52.0	104.0		RE/FIRST ATTITUDE CONT PRPLN
1		00.000.007	00.000.030	52.0	104.0	208.0		RE/FIRST SET OF SCNCE
1		00.000.059	00.000.031	8.0	16.0	26.0		PRI CDFG QLFD FOR TCM + LETM TESTS
1		00.000.026	00.000.032					S/FINAL ASSY + TEST OF STM
1		00.000.027	00.000.032					S/FINAL ASSY + TEST OF STM
1		00.000.028	00.000.032					S/FINAL ASSY + TEST OF STM
1		00.000.029	00.000.032					S/FINAL ASSY + TEST OF STM
1		00.000.030	00.000.032					S/FINAL ASSY + TEST OF STM
1		00.000.033	00.000.032					S/FINAL ASSY + TEST OF STM
1		00.000.011	00.000.033					STM TEST AREA COMPL
1		00.000.031	00.000.034	1.0	2.0	6.0		S/MFGR OF LETM STR + MECH SYS
1		00.000.032	00.000.035	12.0	16.0	52.0		STM FUNCTIONALLY QLFD
1		00.000.037	00.000.036					S/TCM FINAL ASSY
1		00.000.062	00.000.036					S/TCM FINAL ASSY
1		00.000.035	00.000.037	4.0	4.0	26.0		R/REV TCM SUBSYS + SCNCE
1		00.000.036	00.000.039	2.0	4.0	6.0		C/TCM FINAL ASSY
1		00.000.039	00.000.040	2.0	2.0	4.0		S/TCM FINAL QUALIFICATION TESTS
1		00.000.040	00.000.041	2.0	4.0	8.0		TCM FUNCTIONALLY QLFD
1		00.000.034	00.000.042	12.0	16.0	37.0		S/LETM FINAL ASSY
1		00.000.041	00.000.042	1.0	1.0	2.0		S/LETM FINAL ASSY
1		00.000.041	00.000.043					RE/LETM SUBSYS WITH CHG INC
1		00.000.042	00.000.044	2.0	4.0	8.0		C/FINAL ASSY OF LETM
1		00.000.043	00.000.044	2.0	2.0	3.0		C/FINAL ASSY OF LETM
1		00.000.044	00.000.045	1.0	1.0	1.0		S/LETM QUALIFICATION TESTS
1		00.000.045	00.000.046	3.0	4.0	8.0		LETM QLFD DSGN FREEZE
1		00.000.046	00.000.047					C/MFGR, TEST OF PMV, BUV + PTM
1		00.000.066	00.000.047	12.0	16.0	37.0		C/MFGR, TEST OF PMV, BUV + PTM
* 1		00.000.067	00.000.047					C/MFG,TST OF PMV,BUV PTM
1		00.000.047	00.000.048	1.0	1.0	2.0		PMV + BUV ON DOCK AT LAUNCH SITE
1		00.000.011	00.000.049					ETR FAC AVAIL
1		00.000.065	00.000.050	4.0	4.0	6.0		EARTH LAUNCH VEH DEL TO LAUNCH SITE
1		00.000.048	00.000.051					S/ETR OPERATIONS
1		00.000.049	00.000.051					S/ETR OPERATIONS
1		00.000.050	00.000.051					S/ETR OPERATIONS
1		00.000.047	00.000.052	1.0	1.0	2.0		PTM DEL TO MISSION CONT CENTER
1		00.000.052	00.000.053	2.0	4.0	6.0		DSIF + MISSION CONT CENTER ACTVT
1		00.000.051	00.000.054	10.0	14.0	20.0	7.17.76	LAUNCH PMV
1		00.000.056	00.000.054	4.0	4.0	4.0	7.17.76	LAUNCH PMV
1		00.000.054	00.000.055	1.0	1.0	2.0	7.24.76	LAUNCH BUV
1		00.000.053	00.000.056					BGN SPCRFT FLT OPER AT FLT CONT STE
1		00.000.019	00.000.059	41.0	52.0	78.0		S/PREL STR INTEGRITY TESTING
1		00.000.011	00.000.060					TCM TEST FAC AVAIL FOR FIRST TEST
1		00.000.031	00.000.061	1.0	2.0	6.0		S/TCM PREL TESTS WITH MCKUP SUBSYS
1		00.000.060	00.000.061					S/TCM PREL TESTS WITH MCKUP SUBSYS
1		00.000.061	00.000.062	37.0	52.0	104.0		PRI SPCRFT STR TC QLFD
1		00.000.005	00.000.063	29.0	33.0	41.0		ALL STR + MECH SYS DWG COMPLETE
1		00.000.010	00.000.064	2.0	2.0	3.0		SUBSYS SPEC + INRFCE FREEZE
1		00.000.009	00.000.065					FINAL LAUNCH VEH STATUS REVIEW
1		00.000.031	00.000.066	2.0	3.0	6.0		S/MFGR PMV, BMV + PTM
* 1		00.000.027	00.000.067	84.0	144.0	200.0		RE/PMV+BUV RTG FUEL

Table 5.3-18
DESIGN CONCEPT C - PERT III EVENT SCHEDULE REPORT

EVENT TITLE	EVENT NO.	L C	CRITICAL PREDECESSOR	L C	S P	ACTUAL DATE	EXPECTED DATE	LATEST DATE	SCHEDULED DATE	SLACK TIME	STD DEV	PROB SCD	PROB POS SL
CONTRACT GO-AHEAD	00-000-001						02JAN70	27OCT70		42.7	.0		.92
C/JUPITER SYS DESIGN SPEC	00-000-002		00-000-001				05FEB70	01DEC70		42.7	1.7		.92
C/SPCFT PREL SUBSYS + INRFCE SPEC	00-000-003		00-000-002				12MAY70	08MAR71		42.7	3.4		.92
PMV + BUV ON DOCK AT LAUNCH SITE	00-000-048		00-000-047				13JUN75	08APR76		42.7	31.0		.92
RE/FIRST SET FUELED RTGS	00-000-027		00-000-016				04SEP72	02JUL73		42.7	24.3		.92
C/MFGR, TEST OF PMV, BUV + PTM	00-000-047		00-000-067				04JUN75	29MAR76		42.7	31.0		.92
R/SCNCE PROCUREMENT	00-000-007		00-000-003				31AUG70	25JUN71		42.7	3.5		.92
LAUNCH BUV	00-000-055		00-000-054				29SEP75	24JUL76	24JUL76	42.7	31.0	.92	.92
RE/PMV+BUV RTG FUEL	00-000-067		00-000-027				04JUN75	29MAR76		42.7	31.0		.92
SCNCE PYLD, CDFG APPR + MCKUP COMPL	00-000-010		00-000-007				09OCT70	04AUG71		42.7	3.6		.92
LAUNCH PMV	00-000-054		00-000-051				22SEP75	16JUL76	17JUL76	42.7	31.0	.92	.92
R/RTG PROCUREMENT	00-000-016		00-000-064				26OCT70	19AUG71		42.7	3.6		.92
SUBSYS SPEC + INRFCE FREEZE	00-000-064		00-000-010				26OCT70	19AUG71		42.7	3.6		.92
S/ETR OPERATIONS	00-000-051		00-000-048				13JUN75	08APR76		42.7	31.0		.92
PTM DEL TO MISSION CONT CENTER	00-000-052		00-000-047				13JUN75	22MAY76		49.0	31.0		.95
DSIF + MISSION CONT CENTER ACTVT	00-000-053		00-000-052				11JUL75	18JUN76		49.0	31.0		.95
BGN SPCRFT FLT OPER AT FLT CONT STE	00-000-056		00-000-053				11JUL75	18JUN76		49.0	31.0		.95
S/DETAILED CDFG DSGN + MOCKUP	00-000-005		00-000-003				12MAY70	25JUN71		58.4	3.4		.97
S/SUBSYS PROCUREMENT NEGOTIATIONS	00-000-026		00-000-003				12MAY70	04AUG71		64.1	3.4		.98
R/RTG FUEL PROCUREMENT ORDER	00-000-004		00-000-002				13FEB70	08JUN72		120.8	1.7		1.00
S/PREL STR INTEGRITY TESTING	00-000-059		00-000-019				22DEC71	09MAY74		124.1	7.3		1.00
LETM QLFD DSGN FREEZE	00-000-046		00-000-045				12NOV73	29MAR76		124.1	13.7		1.00
S/LETM QUALIFICATION TESTS	00-000-045		00-000-044				11OCT73	29FEB76		124.1	13.7		1.00
C/FINAL ASSY OF LETM	00-000-044		00-000-042				04OCT73	22FEB76		124.1	13.7		1.00
TCM FUNCTIONALLY QLFD	00-000-041		00-000-040				27AUG73	12JAN76		124.1	13.7		1.00
S/MFGR OF STM + TCM STR + MECH SYS	00-000-019		00-000-012				07DEC70	23APR73		124.1	3.8		1.00
S/TCM PREL TESTS WITH MCKUP SUBSYS	00-000-061		00-000-031				02MAY72	18SEP74		124.1	7.9		1.00
S/TOOLING DSGN	00-000-012		00-000-010				09NOV70	26MAR73		124.1	3.7		1.00
S/TCM FINAL QUALIFICATION TESTS	00-000-040		00-000-039				27JUL73	15DEC75		124.1	13.7		1.00
PRI CDFG QLFD FOR TCM + LETM TESTS	00-000-031		00-000-059				14APR72	02SEP74		124.1	7.9		1.00
C/TCM FINAL ASSY	00-000-039		00-000-036				11JUL73	27NOV75		124.1	13.7		1.00
PRI SPCRFT STR TO QLFD	00-000-062		00-000-061				13JUN73	30OCT75		124.1	13.7		1.00
S/LETM FINAL ASSY	00-000-042		00-000-041				04SEP73	22JAN76		124.1	13.7		1.00
S/TCM FINAL ASSY	00-000-036		00-000-062				13JUN73	30OCT75		124.1	13.7		1.00
RE/LETM SUBSYS WITH CHG INC	00-000-043		00-000-041				27AUG73	04FEB76		127.4	13.7		1.00
R/REV TCM SUBSYS + SCNCE	00-000-037		00-000-035				18MAY73	30OCT75		127.9	27.3		1.00
S/FINAL ASSY + TEST OF STM	00-000-032		00-000-030				27OCT72	10APR75		127.9	26.2		1.00
RE/FIRST SET OF SCNCE	00-000-030		00-000-007				27OCT72	10APR75		127.9	26.2		1.00
STM FUNCTIONALLY QLFD	00-000-035		00-000-032				26MAR73	08SEP75		127.9	27.0		1.00
R/SPACECRAFT CONT SUBSYS PROC	00-000-015		00-000-064				26OCT70	26SEP73		152.6	3.6		1.00
C/STM ASTRIONICS COMPAT TESTS	00-000-026		00-000-024				08MAY72	10APR75		152.6	17.3		1.00
S/STM ASTRIONICS COMPAT TESTS	00-000-024		00-000-023				14MAR72	17FEB75		152.6	17.2		1.00
C/STM STR + MECH ASSY	00-000-023		00-000-022				29FEB72	03FEB75		152.6	17.2		1.00
RE/STM SPACECRAFT CONT SUBSYS	00-000-022		00-000-015				21FEB72	24JAN75		152.6	17.2		1.00
R/DATA MGMT SUBSYS PROCUREMENT	00-000-013		00-000-064				26OCT70	24DEC73		165.0	3.6		1.00
RE/STM DATA MGMT SUBSYS	00-000-020		00-000-013				26NOV71	24JAN75		165.0	13.0		1.00
S/MFGR OF LETM STR + MECH SYS	00-000-034		00-000-031				02MAY72	11SEP75		175.3	7.9		1.00
R/MIDCOURSE PRPLN PROCUREMENT	00-000-017		00-000-064				26OCT70	08MAR74		175.9	3.6		1.00
RE/FIRST MIDCOURSE PRPLN	00-000-028		00-000-017				26NOV71	10APR75		175.9	13.0		1.00
R/ATTITUDE CONT PRPLN PROCUREMENT	00-000-018		00-000-064				26OCT70	08MAR74		175.9	3.6		1.00
RE/FIRST ATTITUDE CONT PRPLN	00-000-029		00-000-018				26NOV71	10APR75		175.9	13.0		1.00
R/COMM SUBSYS PROCUREMENT	00-000-014		00-000-064				26OCT70	06MAY74		184.1	3.6		1.00
RE/STM COMM SUBSYS	00-000-021		00-000-014				15JUL71	24JAN75		184.1	5.6		1.00
S/MFGR PMV, BMV + PTM	00-000-066		00-000-031				08MAY72	19NOV75		184.3	7.9		1.00
R/TEST SPEC + LAUNCH OPER PLAN	00-000-008		00-000-003				26JUN70	11FEB74		189.1	3.7		1.00
TCM TEST FAC AVAIL FOR FIRST TEST	00-000-060		00-000-011				02FEB71	18SEP74		189.1	5.6		1.00
R/TEST + LAUNCH + FAC IMPLMTN PLAN	00-000-011		00-000-008				02FEB71	18SEP74		189.1	5.6		1.00
ALL STR + MECH SYS DWG COMPLETE	00-000-063		00-000-005				04JAN71	03FEB75		212.9	3.9		1.00
STM TEST AREA COMPL	00-000-033		00-000-011				02FEB71	10APR75		218.3	5.6		1.00
ETR FAC AVAIL	00-000-049		00-000-011				02FEB71	08APR76		270.1	5.6		1.00
FINAL LAUNCH VEH STATUS REVIEW	00-000-065		00-000-009				23FEB70	08MAR76		315.2	1.7		1.00
EARTH LAUNCH VEH DEL TO LAUNCH SITE	00-000-050		00-000-065				23MAR70	08APR76		315.2	1.7		1.00
INITIATES EARTH LAUNCH VEH PROC	00-000-009		00-000-002				23FEB70	08MAR76		315.2	1.7		1.00

DESIGN CONCEPT C - TIME LINE CHART

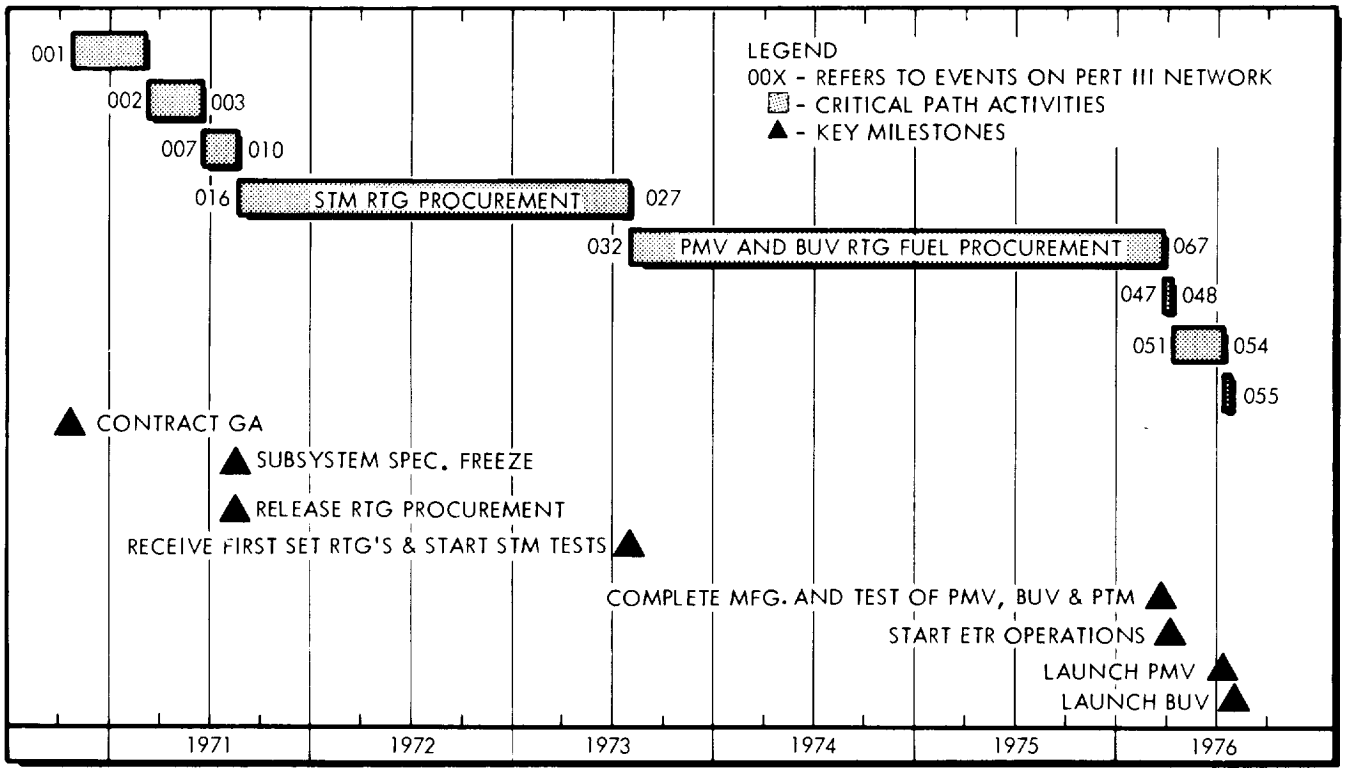

FIGURE 5.3-6

DESIGN CONCEPT C - SCHEDULE CONFIDENCE

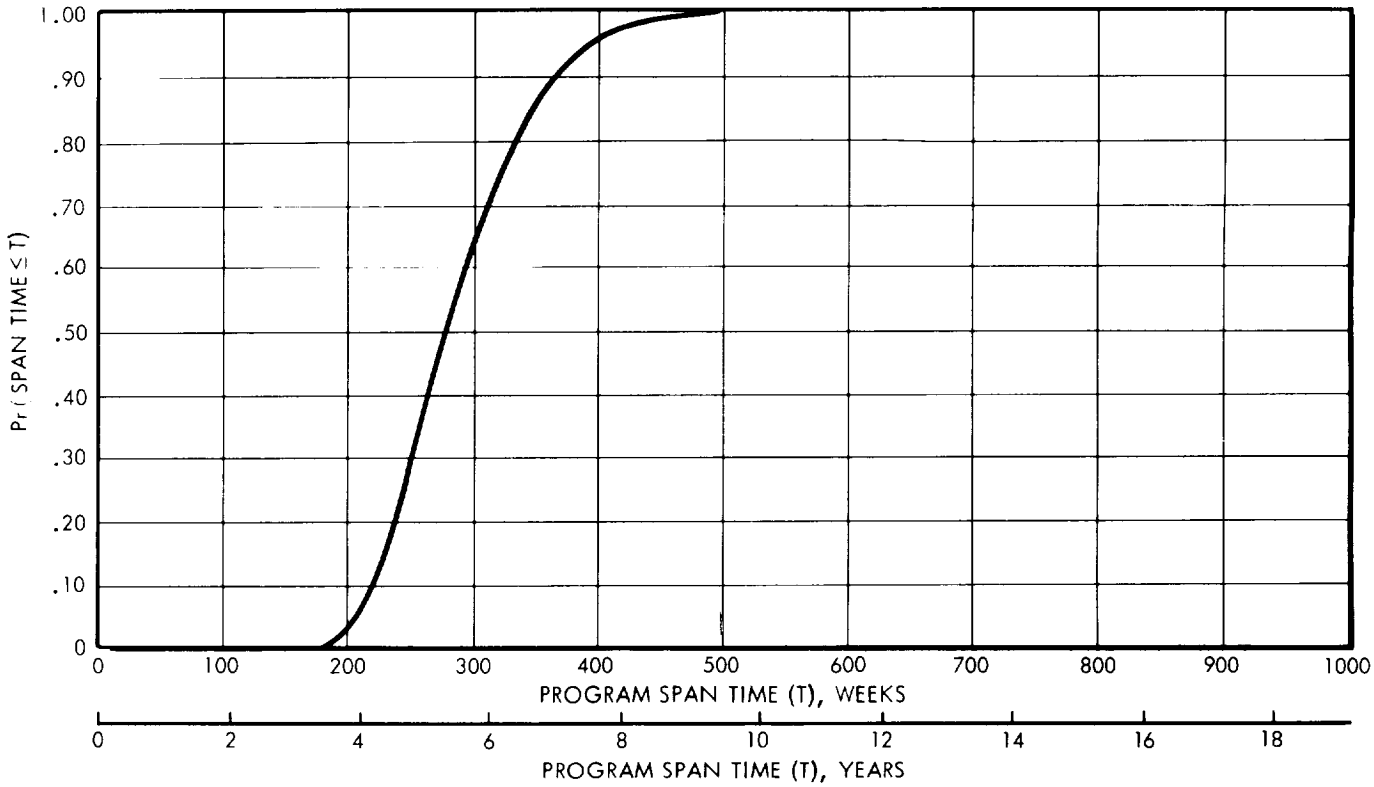

FIGURE 5.3-7

Table 5.3-19

DESIGN CONCEPT C - SUMMARY OF JUPITER FLYBY PROGRAM COSTS
(In Millions of 1965 Dollars)

COST CATEGORIES	LAUNCH VEHICLE TYPE	
	TITAN IIICx/ CENTAUR	SATURN IB/ CENTAUR/HEKS*
NONRECURRING		
Science	16.40	
Communication & Data Mgt	11.90	
Spacecraft Control	8.90	
Attitude Control	1.08	
Midcourse Propulsion	1.90	
Electrical Power	14.50	
Structural, Mech, Therm, & Shield	6.95	
Subtotal Subsystems, DT&E	61.63	
Operational Support Equip	14.30	
Tooling & Special Equip	3.80	
System Integration	7.60	
Ground Test Hardware	17.48	
Total Nonrecurring Costs	104.81	104.81
RECURRING (2 Launches)		
Recurring Spacecraft	33.38	33.38
Spacecraft Spares (2 Sets)	3.54	3.54
Deep Space Net Support	34.00	26.80
Spacecraft Operations	3.07	2.60
Launch Vehicles	42.82	30.80
Launch Operations	14.80	6.50
Total Recurring Costs	131.61	103.62
TOTAL PROGRAM COSTS	236.42	208.43

* Assuming a single launch with dual payload.

Table 5.3-20

DESIGN CONCEPT C - RECURRING SPACECRAFT COSTS FOR TWO FLIGHTS

(In Millions of 1965 Dollars)

COST CATEGORY	
Science	0.70
Communications & Data Mgt	1.52
Spacecraft Control	1.24
Attitude Control	0.06
Midcourse Propulsion	0.08
Electrical Power	4.16
Structure, Mech, Therm, & Shield	0.80
Spacecraft Checkout & Assembly	1.06
Subtotal Spacecraft Cost	9.62
RTG Fuel Cost @ $\$1500/W_t$	23.76
Total Spacecraft	33.38

Table 5.3-21

DESIGN CONCEPT C - COST INCREMENT FOR A THIRD FLIGHT

(In Millions of 1965 Dollars)

	Titan IIICx/ Centaur	Saturn IB/ Centaur/HEKS**
Recurring Spacecraft	$16.69	$33.38
Launch Vehicle	21.41	30.80
Launch Operations	7.40	6.50
Total	$45.50	$70.68
Total*	$41.75	$66.93

* The total cost increment for a third flight assuming that one of the ground test models is used.

** Assuming a single launch vehicle with dual payload.

5.4 SPACECRAFT DESIGN CONCEPT D

In this subsection, a Jupiter flyby spacecraft is described which has "full" scientific capability and is denoted as Design Concept D.

5.4.1 Design Summary

A configuration of Design Concept D is illustrated in Figure 5.4-1. The design philosophy is one of maximum scientific capability in scientific instrumentation. The injected weight of the spacecraft is approximately 1500 pounds. Use of the Saturn IB/Centaur/HEKS makes possible 400-day missions launched in any of the years 1973-1980. A dual launch of the spacecraft by a Saturn V also allows 400-day missions in any year. Significant flight events for a nominal mission are detailed in Table 5.4-1.

The development of the spacecraft is estimated to require 10.5 years. The total program cost for two spacecraft using the Saturn IB/Centaur/HEKS launch vehicle is estimated to be $288 million. Total program cost for a dual launch with the Saturn V is estimated to be $284 million.

The salient characteristics of the spacecraft are (1) a science capability on the order of 200 pounds and 85 watts, (2) a steerable, 35 db gain antenna and a 50-watt transmitter, (3) data compression and tape storage, (4) an on board, self-contained spacecraft control system, (5) three-axis stabilization implemented by gas jets, (6) Mariner-IV type midcourse propulsion, (7) Pu 238 RTG's, and (8) armor-type meteoroid protection. The spacecraft performance is indicated by the following: (1) a 133 bit per second information rate at 6 a.u. communications distance, (2) data storage for 292 M bits, (3) a trajectory correction capability of 90 m/sec, and (4) 480 watts of available electric power.

Following spacecraft injection, spacecraft attitude is stabilized by use of the Sun and Canopus as primary references. Cruise science is turned on. A vernier correction is made using Earth-based navigation, computation, and command facilities. The parabolic antenna is the primary communications downlink. Omni antennas are used for two-way communications during early portions of the mission and for uplink communications throughout the mission. The parabolic antenna is mechanically positioned by means of angular computations made on board the spacecraft. If necessary, a terminal trajectory correction is made by use of navigation measurements, computations, and commands generated on board. Encounter

SPACECRAFT DESIGN CONCEPT D CONFIGURATION

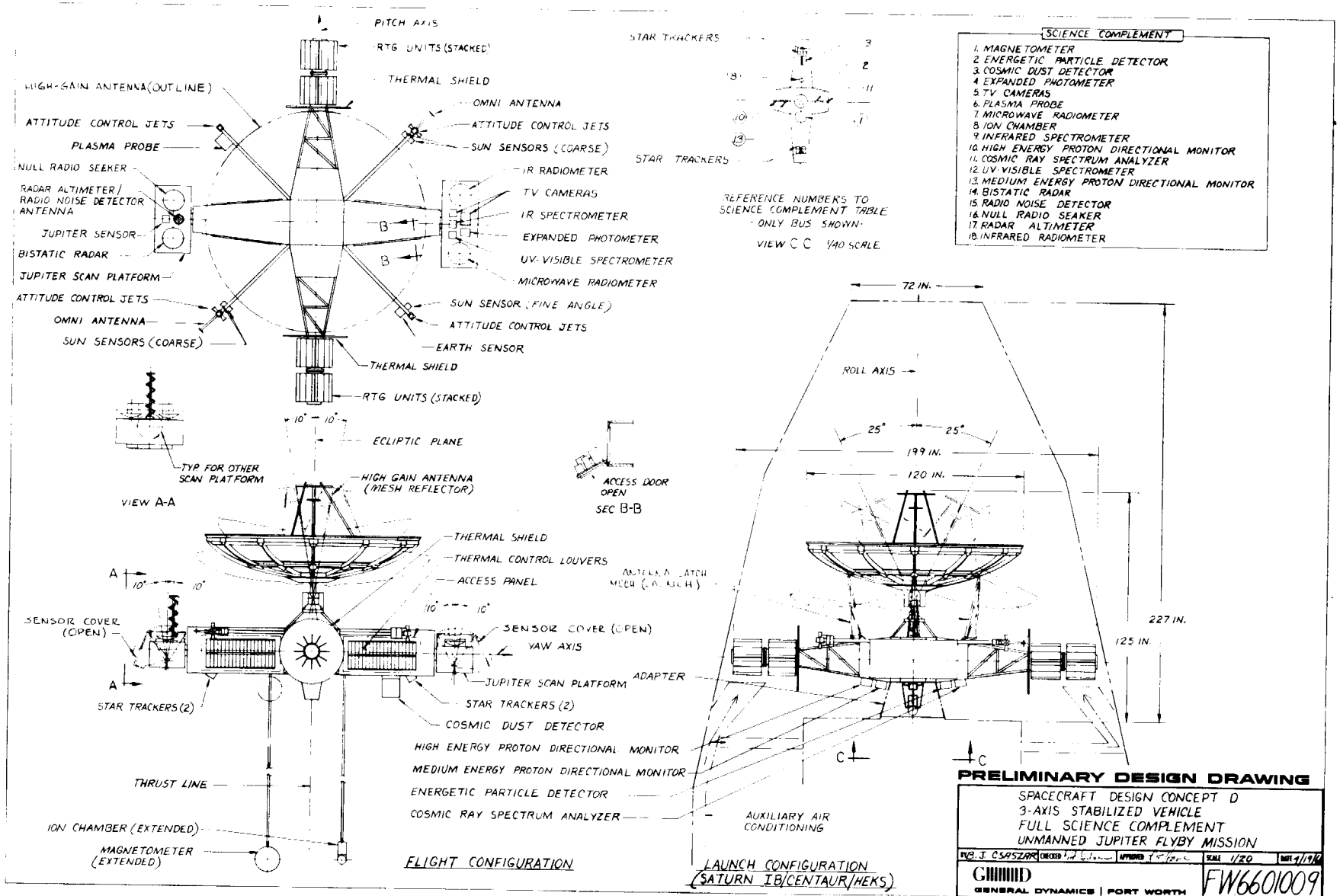

FIGURE 5.4-1

Table 5.4-1
SEQUENCE OF SIGNIFICANT FLIGHT EVENTS FOR SPACECRAFT DESIGN CONCEPT D

Notes: The mission characteristics are a 1976 launch, Saturn IB/Centaur/HEKS launch vehicle, 412 day flight time, posigrade equatorial pass, and 1.0 Jupiter radius nominal perijove altitude. The spacecraft computer is the primary control for all spacecraft events except where noted. Backup via ground command is implied for all events.

No.	Event	Nominal Time
1	Install RTG units and activate auxiliary cooling system	L - 1 day
2	Update CC&S master clock and sequence timer	L - 3 min.
3	Turn on gyros, DEE, and CDDE	L - 2 min.
4	Liftoff	L
5	Cutoff inboard S-1B engines	
6	Cutoff outboard S-1B engines	
7	S-IB retro-motor ignition	
8	S-IVB ullage motor ignition	
9	Jettison S-IB stage	
10	Jettison S-IVB ullage rockets	
11	Jettison Centaur - spacecraft shroud	
12	S-IVB/IU retro-motor ignition	
13	Centaur ullage motor ignition	
14	Jettison S-IVB/IU	
15	First Centaur ignition	
16	First Centaur cutoff (begin orbital coast)	
17	Second Centaur ignition (end orbital coast)	
18	Second Centaur cutoff	
19	High Energy Kick Stage (HEKS) ignition	
20	HEKS cutoff (Injection)	I = L + 120 min.
21	Spacecraft - HEKS separation	I + 2 min.
	a. Pyrotechnics armed	
	b. Transmitter power up	
	c. Begin communication with omni antenna at data transmission rate of 33 bps	
22	Initial Sun acquisition	I + 10 min.
	a. Turn on attitude control system	
	b. Turn on coarse Sun sensor	
	c. Activate gas-jet system	
	d. Begin Sun acquisition sequence	
23	Sun acquired	I + (10 - 20) min.
	a. Gyros turned off	
24	Activate cruise science	I + 20 min.
	a. Deploy magnetometer and ion chamber	
	b. Turn on cruise science	
25	Canopus acquisition	I + 100 min.
	a. Turn on Canopus sensor	
	b. Set sensor cone angle	
	c. Begin roll turn	
	d. Receive acquisition signal	
	e. Turn on Earth sensor	
	f. Verify Canopus acquisition (continue roll search if Earth not acquired)	
26	Canopus acquired	I + (100-130) min.
27	Prepare for midcourse maneuver	M - 60 min.
	a. Transmit and verify pitch-turn duration and polarity	
	b. Transmit and verify roll-turn duration and polarity	
	c. Transmit and verify velocity increment	
28	Begin midcourse maneuver sequence	M = I + (1-7)days
	a. Turn on fine Sun sensor	
	b. Acquire Sun with fine Sun sensor	
	c. Turn on gyros	
	d. Turn on accelerometer	
29	Execute pitch turn	M + 60 min.
	a. Switch out error signals from Earth, Sun, and Canopus sensors	
	b. Set proper polarity	
	c. Pitch turn started	
	d. Pitch turn stopped	M + (60 - 65) min.
30	Execute roll turn	M + 75 min.
	a. Set proper polarity	
	b. Roll turn started	
	c. Roll turn stopped	M + (75 - 80) min.
31	Execute motor burn	M + 90 min.
	a. Command motor burn	
	b. Command motor shutoff	M + (90 - 93.5) min
32	Sun reacquisition	M + 95 min.
	a. Turn off accelerometer	
	b. Switch in error signal from coarse Sun sensor	
	c. Execute roll turn with opposite polarity	
	d. Execute pitch turn with opposite polarity	
	e. Begin Sun acquisition sequence	
33	Sun reacquired	M + (95 - 100)min.

Table 5.4-1 (Continued)

No.	Event	Nominal Time
34	Canopus reacquisition	M + 101 min.
	a. Switch in error signal from Canopus sensor	
	b. Begin roll turn	
	c. Receive acquisition signal	
	d. Switch in signal from Earth sensor	
	e. Verify Canopus acquisition	
35	Canopus reacquired	M + (101-106) min.
	a. Gyros turned off	
36	Switch data transmission rate from 33 to 17 bps	I + 31 days
37	Activate high-gain antenna	I + 46 days
	a. Unlock antenna	
	b. Drive antenna to position 1	
	c. Switch transmitter to high-gain antenna	
	d. Switch data transmission rate from 17 to 2133 bps	
38	Drive high-gain antenna to position 2 (periodic update of antenna pointing angles initiated by CC&S command throughout mission with Earth-based backup command capability provided - 37 position changes required)	I + 48 days
39	Switch data transmission rate from 2133 to 1067 bps (CC&S command with Earth based backup command typical for all bit rate change events)	I + 91 days
40	Switch data transmission rate from 1067 to 533 bps	I + 176 days
41	Switch data transmission rate from 533 to 267 bps	I + 216 days
42	Switch data transmission rate from 267 to 133 bps	I + 296 days
43	Prepare for terminal navigation and maneuver	I + 370 days
	a. Transmit and verify required scan platform angle and Jupiter sensor slew angle	
44	Begin Jupiter acquisition sequence	I + 372 days
	a. Remove Jupiter sensor cover	
	b. Turn on Jupiter sensor	
	c. Activate scan platform drive	
	d. Begin Jupiter search	
45	Jupiter acquired	I + 372 days
46	Begin navigation measures	I + 372 days
	a. Turn on star trackers 1 and 2	
	b. Acquire stars 1 and 2	
47	Terminal correction data computed and transmitted to Earth for verification	I + 392 days
48	Begin terminal maneuver sequence	T = I + 393 days
49	Repeat events 28 through 35	
50	End terminal maneuver sequence	T + (60-360) min.
51	Prepare for encounter sequence	E - 360 min.
	a. Remove encounter sicence covers	
	b. Turn on gyros	
52	Begin encounter sequence	
	a. Turn on DSE	
	b. Turn on encounter science	
	c. Activate individual encounter science instrument scanning operations	
53	Begin TV picture recording sequence	E - 80 min.
54	TV turned off	E - 30 min.
55	Perijove passage (one Jupiter radius altitude)	E = I + 412 days
56	Switch to inertial attitude control mode	E + 10 min.
	a. Switch out error signal from Sun sensor	
	b. Uncage pitch and raw gyros	
57	Begin Sun occultation (0^{o} cone)	E + 28 min.
58	Begin Earth occultation (0^{o} cone)	E + 45 min.
59	End Sun occultation (0^{o} cone)	E + 96 min.
60	End Earth occultation (0^{o} cone)	E + 122 min.
61	End encounter sequence	E + 180 min.
	a. Turn off encounter science	
	b. Turn off DSE	
62	Switch to Sun reference attitude control mode	E + 190 min.
	a. Acquire Sun	
	b. Turn off gyros	
	c. Turn off Jupiter sensor	
	d. Deactivate scan platform	
63	Transmit command to initiate encounter data playback	E + 2 days
	a. DSE turned on (cyclic transmission of one hour real time data to five hours of non-real time data)	
64	End data playback	E + 8.5 days
	a. Turn off DSE	
65	Return to cruise mode	E + 8.5 days

attitude during Sun and Canopus occultations is controlled inertially. The expected periapsis miss distance at Jupiter is 200 km. Data storage is implemented intermittently during cruise and continuously during encounter. Playback of encounter data is performed following reacquisition of primary attitude references. Following playback, the spacecraft reverts to its cruise mode of operation.

The weight of Spacecraft Design Concept D is summarized in Table 5.4-2.

Table 5.4-2

SPACECRAFT DESIGN CONCEPT D - WEIGHT SUMMARY

Subsystem	Weight, lbs.
Science	203
Communications	98
Data Management	90
Spacecraft Control	135
Attitude Control Propulsion	110
Midcourse Propulsion	106
Electrical Power	437
Structural/Mechanical and Meteoroid Protection	375
Thermal Control	27
Total Spacecraft	1581
Adapter (0.065 x spacecraft weight)	103
Launch Weight	1684

5.4.2 Subsystem Design Information

5.4.2.1 Science

In Spacecraft Design Concept D, provision is made for a scientific instrument complement of full capability. A definition of the full experiment package is presented in Table 2.1-8, and the instruments are listed again in Figure 5.4-1. The individual instruments are described in subsection 2.1. The total weight of this package is 203 pounds.

Several design features related to Concept D represent direct responses to the science subsystem requirements. These design

features and the associated requirements are discussed in some of the subsections which follow, particularly, in those subsections related to data management (data automation element), radiation protection, configuration (pointing geometries), and structural and mechanical design (scan platform implementation and sensor deployment).

5.4.2.2 Communications

The communications subsystem recommended for Design Concept D has been configured in accordance with Figure 3.1-8. A power output of 50 watts and an antenna gain of 33 db is commensurate with the amount of data to be gathered and transmitted by this spacecraft. The antenna utilizes a 10-foot circular dish with 2 degrees of freedom to facilitate pointing of the narrow beam.

A gain-loss chart for a communications distance of 6 a.u. is presented in Table 5.4-3.

Table 5.4-3

DESIGN CONCEPT D - GAIN-LOSS CHART

	GAIN	LOSS
Transmitter Power	47 dbm	
Modulation		3 db
S/C Ant Gain	35 db	
Space Attenuation		278 db
Rcvr Ant Gain	61 db	
Rcvr Sens ($40^{o}K$)		-182 dbm
Misc Loss		2 db
System Tolerances		6 db
	143 db	107 db

S/N_o = 143 - 107 = 36 db, then, at a bit rate of 133 bps,
ST/N_o = 36 - 10 log 133 = 14.5 db.
So the information performance margin is 14.5 - 6.8 = 7.7 db.

By use of similar gain-loss charts, the schedule shown on Table 5.4-4 has been derived.

Table 5.4-4

DESIGN CONCEPT D - ANTENNA AND INFORMATION RATE SCHEDULE

Communication Distance (a.u.)	Antenna	Info Rate (bps)
0-0.2	Omni	33
0.2-0.75	Parabola	2133
0.75-2.5	Parabola	1067
2.5-3.5	Parabola	533
3.5-5	Parabola	267
5-6	Parabola	133

The number and weight of the components of the communications subsystem are shown in Table 5.4-5. The recommended numbers of components are based on a reliability analysis of the communications subsystem. Although the proposed configuration is not necessarily optimum with respect to reliability, it is considered to be an appropriate compromise between reliability, weight, and power considerations.

Table 5.4-5

DESIGN CONCEPT D - COMMUNICATIONS SUBSYSTEM WEIGHT

Component (no.)	Weight, lbs
Amplifier (2)	8
Power Monitor (2)	2
Circulator (6)	6
Exciter (2)	10
APC Receiver (2)	18
Exciter Control	2
Rcvr Monitor	1
Amp Control	2
Omni Ant (2)	4
Parabolic Ant	25
Power Supply, HV (2)	16
Cabling, etc.	4
TOTAL	98

5.4.2.3 Data Management

In the case of Concept D, two modifications of the data management subsystem elements and functional requirements discussed in subsection 3.2 have been made: i.e., the integration of the DAE and DEE into a single element and the use of the central digital computer for variable-rate, low-capacity buffer storage and for storing control instructions for the DEE, DSE, and CDDE. The proposed design exhibits considerable flexibility.

A telemetry command word to be used for each scientific and engineering measurement is supplied by the CC&S portion of the central digital computer (discussed in the next subsection) and is 12 bits in length. One bit is used to indicate direct or indirect addressing; four bits are used to specify the sampling rate; five bits are used to indicate the converted word length; and two bits are used to specify the routing. Four interchangeable tape recorders are provided in the DSE to permit processing flexibility throughout the mission. Figure 5.4-2 is an illustration of one such arrangement (Reference 5.4-1). Scientific and engineering data are temporarily stored in the central digital computer memory while similar previously stored data are being placed on Tape Recorder A. Meanwhile, the same procedure is used for storing the television data on tape recorder C, and previously recorded data is being transferred from tape recorder B to the communications subsystem for transmission. Tape recorder D is redundant in this arrangement.

Other arrangements permit data to be routed simultaneously to the communications subsystem for real-time transmission and to a tape recorder for playback later. The use of this procedure will further increase the reliability of receiving important data (e.g., data from an encounter). Additionally, it is planned to record redundant and modified sets of command words for the CC&S at the beginning of the tape in each tape recorder as well as to provide the capability of modifying these words by ground command through four redundant CDDE's. In this way, sampling rates can be modified on the basis of mission performance, and useless measurements from malfunctioning equipment or limited-use equipment can be deleted.

DESIGN CONCEPT D DATA ENCODER AND DATA STORAGE ELEMENT INTERFACE

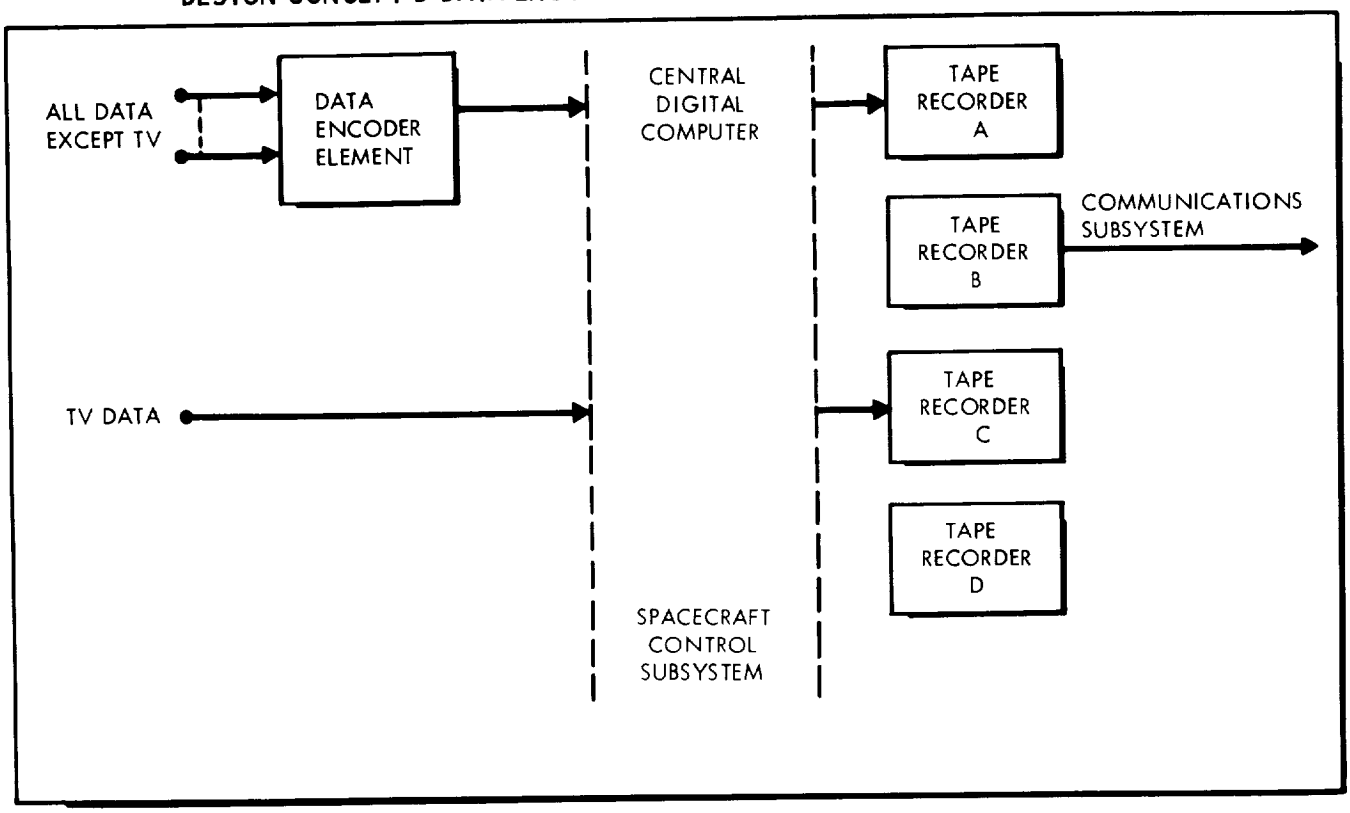

FIGURE 5.4-2

The available transmission rates in various portions of the mission have been presented previously in Table 5.4.4. The anticipated raw and compressed data bit rates for the different phases of the mission are presented in Table 5.4-6. Data compression is used (1) to provide real-time transmission of all data, excluding television pictures and (2) to permit intermittent communications.

The maximum required data storage capacity for Concept D is 292M bits. With this capacity, all of the encounter data, including the television pictures from both cameras can be stored. Slightly less than 6½ days are required to transmit the encounter data at the 133-bit-per-second transmission rate.

The following specific functional requirements which are recommended for elements of the data management subsystem are as follows: The DEE is able to process 300 analog and digital measurements at sampling intervals between 0.01 to 4096 seconds and to transfer these measurements to the communications subsystem

Table 5.4-6

ANTICIPATED DATA BIT RATES (BITS PER SECOND) FOR DESIGN CONCEPT D

TYPE	NEAR EARTH			INTERPLANETARY			ENCOUNTER (No TV)			ENCOUNTER (TV)		
	RAW	COMPRESSED	(FAN)	RAW	COMPRESSED	(FAN)	RAW	COMPRESSED	(FAN)	RAW	COMPRESSED	(FAN)
1. ENG	33.3	(150:1)	0.2	33.3	(150:1)	0.2	33.3	(150:1)	0.2	33.3	(150:1)	0.2
2. MAG	300.3	(10:1)	30.0	0.2	(10:1)	≈ 0.0	300.0	(10:1)	30.0	300.0	(10:1)	30.0
3. CDD	0.1	(1000:1)	≈ 0.0	0.1	(1000:1)	≈ 0.0	0.1	(1000:1)	≈ 0.0	0.1	(1000:1)	≈ 0.0
4. EDD*	0.4	(3:1)	0.1	0.4	(3:1)	0.1	2.0	(3:1)	0.7	2.0	(3:1)	0.7
5. EX PHO*	--	--	--	--	--	--	0.8	(4:1)	0.2	0.8	(4:1)	0.2
6. PP	0.1	(1:1)	0.1	0.1	(1:1)	0.1	0.1	(1:1)	0.1	0.1	(1:1)	0.1
7. MR	--	--	--	--	--	--	1.3	(2:1)	0.7	1.3	(2:1)	0.7
8. IRR	--	--	--	--	--	--	0.7	(2:1)	0.4	0.7	(2:1)	0.4
9. IC*	0.1	(10:1)	≈ 0.0	0.1	(10:1)	≈ 0.0	0.3	(10:1)	≈ 0.0	0.3	(10:1)	≈ 0.0
10. IRS	--	--	--	--	--	--	33.3	(2:1)	16.7	33.3	(2:1)	16.7
11. HEPDM	0.1	(10:1)	≈ 0.0	0.1	(10:1)	≈ 0.0	0.4	(10:1)	≈ 0.0	0.4	(10:1)	≈ 0.0
12. CRSA	0.2	(10:1)	≈ 0.0	0.2	(10:1)	≈ 0.0	0.5	(16:1)	0.1	0.5	(10:1)	0.1
13. UV-VS	--	--	--	--	--	--	66.7	(2:1)	33.3	66.7	(2:1)	33.3
14. MEPDM	0.4	(10:1)	≈ 0.0	0.4	(10:1)	≈ 0.0	2.0	(10:1)	0.2	2.0	(10:1)	0.2
15. BR	--	--	--	--	--	--	0.3	(3:1)	0.1	0.3	(3:1)	0.1
16. RND	--	--	--	--	--	--	0.6	(3:1)	0.2	0.6	(3:1)	0.2
17. NRS	--	--	--	--	--	--	0.3	(3:1)	0.1	0.3	(3:1)	0.1
18. RA	--	--	--	--	--	--	0.3	(3:1)	0.1	0.3	(3:1)	0.1
19. TV	--	--	--	--	--	--	--	--	--	145000.0	(10:1)	14500.0
20. HK	30.0	(30:1)	1.0	3.0	(30:1)	0.1	30.0	(30:1)	1.0	4000.0	(10:1)	400.0
TOTAL	364.7	(11.6:1)	31.4	37.9	(75.8:1)	0.5	473.0	(5.63:1)	84.1	149443.0	(9.98:1)	14983.1

at rates of 17, 33, 133, 267, 533, 1067, and 2133 bits per second. Word lengths of up to 31 bits per channel are accommodated. Data from the science sensors, which are unique to this concept, are processed by a method similar to that used for the magnetometer data. The capacity of each tape recorder is 300M bits.

The number and weight of the components of the data management subsystem are shown in Table 5.4-7. The recommended numbers of components are based on a reliability analysis of the data management subsystem. Although the proposed configuration is not necessarily optimum, with respect to reliability, it is considered to be an appropriate compromise between reliability, weight, and power considerations.

Table 5.4-7

DESIGN CONCEPT D - DATA MANAGEMENT SUBSYSTEM WEIGHT

Component (no.)	Weight, lbs.
DEE (2)	46
DSE (4)	28
CDDE (4)	16
TOTAL	90

5.4.2.4 Spacecraft Control

In the Design Concept D spacecraft control subsystem, consideration is given to the performance of any or all of the following tasks: (1) attitude control computations, (2) sensor control, (3) event sequencing, (4) navigation computations, (5) guidance computations for midcourse and/or terminal maneuvers, (6) execution of midcourse and/or terminal maneuvers, (7) malfunction isolation, (8) malfunction mode switching decisions, (9) computations necessary for antenna pointing, and (10) compression of data prior to transmittal. Since the spacecraft design concept, as postulated, is not severely limited by weight, most of these tasks may be performed on board the spacecraft. Considerations which influence the decision as to which tasks are to be performed on board are (1) the availability of adequate sensors for navigation measurements, (2) accuracy of

measurements made by Earth-based equipment, (3) capability of the spacecraft to house a computer large enough to perform the navigation and/or guidance computations (considering all aspects of systems integration), (4) selection, (5) provisions, if any, to be made for alternate operational modes in case of malfunction, and (6) the effect of each added function on the probability of mission success.

The considerations and functions enumerated must be weighed with respect to their relationship to the requirements of the mission. The basic requirement of any mission is a high probability of mission success. This probability is to be made as large as possible under the constraints imposed upon the design philosophy under consideration. The success of a spacecraft concept having maximum capability is heavily dependent on the following aspects of spacecraft control: (1) the miss distance at the target planet must be kept within the prescribed limits, (2) the encounter trajectory of the spacecraft and its orientation with respect to the target planet must be controlled, and (3) the recorded data must be transmitted back to Earth. Naturally, these three aspects are interrelated. The first and second are dependent on the accuracy of midcourse and terminal corrections. These, in turn, are largely dependent on the accuracy with which spacecraft attitude can be determined and controlled. If accurate determination of attitude is required, then the probability of successful data transmission is enhanced. Although data transmission per se is not a function of the spacecraft control subsystem, the computation of pointing angles for the antenna is. These pointing angles, in conjunction with accurate attitude determination and control, permit more accurate pointing of the antenna; thus, higher antenna gain may be used, and higher data rates are possible. This improves the probability of data recovery.

Another factor which greatly influences the accuracy with which trajectory corrections can be made is the accuracy of the computed corrections. In order to determine the magnitude and direction of the corrections, the position and velocity of the spacecraft must be known. These are obtained by processing the Earth-based tracking data or the measurements made on-board the spacecraft. In the latter case, accurate attitude determination and control are required for pointing the sensors which make the on-board measurements.

Thus, it is seen that, other than such reliability oriented measures as redundance and choice of high-reliability components, the foremost requirement of a complex on board spacecraft control subsystem is accurate attitude determination.

Most of the functions considered for incorporation in the Concept D spacecraft can be carried out either on Earth or on board the spacecraft; however, some must be performed on board if they are included at all. These functions are sensor control, maneuver execution, and data compression. Of the remaining functions, the attitude control computations, event sequencing, and malfunction isolation can be implemented on board a spacecraft with no problems when the spacecraft contains a computer capable of performing a modest amount of computation. It is proposed, therefore, that these functions be performed on board the craft.

The navigation and guidance computations, malfunction mode switching, and the antenna pointing computations are still to be considered. Of these, malfunction mode switching presents the fewest problems. The chief reason for performing this function on Earth is simply that more consideration can be given to the selection of alternate modes. However, an automatic system in which there is a provision for override commands can be used to accomplish the same purpose. Therefore, this function is included in the list of funtions which are to be performed on board.

In light of the previous discussion, four alternative philosophies of spacecraft control can be outlined:

1. Navigation and guidance computations and antenna pointing computations done on Earth

2. Navigation and guidance computations performed on Earth, and antenna pointing computations performed on board the spacecraft

3. Navigation and guidance computations and antenna pointing computations done on board the spacecraft with back-up computations done on Earth

4. A combination of concepts 2 and 3. That is, all antenna pointing computations performed on board, and the navigation and guidance computations for the midcourse (vernier) correction (if any) performance on Earth.

Note that all other functions are to be accomplished on board the spacecraft, and override commands are provided from Earth when they are necessary or more expedient. From the following examination of the advantages and disadvantages of each of these philosophies will come a recommended subsystem for the Spacecraft Concept D.

The first philosophy offers three distinct advantages: (1) the spacecraft is less complex; consequently, the probability that the subsystem will operate during the entire mission is increased; (2) the peak power required is low compared to that required in philosophies 3 and 4; therefore a smaller load is placed on the power subsystem; and (3) proven components and techniques can be used; thus the probability of subsystem operation for the duration of the mission is enhanced. Also, no appreciable state-of-the art advances are required. A factor which is of somewhat unknown importance is the smaller system weight. This system weighs 50 to 60 pounds less than the next smallest competitive system. This variation is principally caused by differences in computer size and the absence of the requirement for additional sensors.

However, there is a significant problem with this philosophy. It is expected that the vernier correction will place the spacecraft on a trajectory which exhibits a standard deviation of approximately 4000 km from the desired impact parameter. In the estimation of this standard deviation, no uncertainties in astrophysical phenomena were considered. Such perturbations as solar pressure, meteoroid impacts, and uncertainties in the knowledge of the Jovian gravitational field could easily increase this deviation beyond the tolerances imposed by the scientific payload. Compensation for these unknown effects can best be made by means of a provision for a terminal correction. Thus, not only can miss distance be more accurately controlled, but a high degree of control over the orientation of the trajectory with respect to the target planet can be exercised.

The above consideration of planetary control is not a completely obvious one. If on board control is not provided, such parameters as antenna pointing angles and maneuver commands must be transmitted over vast distances so that there is the attendant uncertainty of reception and verification. Added restrictions are placed on the selection of launch windows so that the Earth is in a favorable position for tracking and maneuver command generation and transmission. Also, the maneuver must be timed so that a DSIF station which has command capability, probably Goldstone, is in position to track and transmit the commands. Another significant consideration is spacecraft navigation during the terminal portion of the mission. The generation of spacecraft steering commands for the terminal correction is dependent on the determination of spacecraft position and velocity with respect to the target planet which is, in turn, dependent on tracking accuracy and on accurate knowledge of the astronomical unit. These parameters are discussed further in subsection 3.4.

The second design concept is very similar to the first and has essentially the same advantages and disadvantages. The difference is that the added complexity of antenna pointing angle computation capability must be added to the computer. This modification proves advantageous in that spacecraft-Earth communications are no longer as dependent on the Earth-based computations. The effects of a slight increase in complexity is not expected to be a significant factor in the probability of mission success.

The third concept includes almost all of the features of self-contained interplanetary navigation and control theory. Since a completely self-contained system is employed, many of the disadvantages previously enumerated are dispensed with. In this concept, the potential for more accurate navigation information is provided; therefore, more accurate guidance commands can be computed and possibly more important, the spacecraft location is determined to a degree of accuracy compatible with the requirements of the science. The spacecraft becomes essentially independent of the long communication link to Earth during the terminal phase of the mission. This concept imposes fewer restrictions on the selection of launch windows, and it allows both the vernier and terminal corrections

to be made at or near the optimum times. The navigation and guidance technique employed in this concept was discussed in subsection 3.4.4.

The disadvantages attendant to this concept are few, but they are of considerable importance. The first of these is the inevitable increase in complexity of the subsystem. The computer itself can be designed for high reliability or can be made somewhat failure tolerant, but the reliability of the associated equipment necessary to make adequate stellar measurements can only be estimated at present. These instruments do not have an "off the shelf" availability; thus, new instrument designs are required to make this concept feasible. If highly reliable, suitable instruments can be developed, this concept should have a high probability of successfully performing the mission objectives. Even if reliability remains questionable, a backup mode is readily available, i.e., measurements and computations are made by Earth-based equipment, and the associated maneuver commands are transmitted to the spacecraft control subsystem. Another disadvantage is that a relatively large amount of power, approximately 200 to 250 watts is required to operate this subsystem. However, this power requirement only occurs for short periods of time over a 10 to 20 day time span prior to each correction. The control system power requirement for the other portions of the mission would be approximately 40 to 50 watts.

The fourth concept is a hybrid system which is composed of the more attractive features of concepts 2 and 3. Since Earth-based tracking and computations are used to make the vernier correction, the advantage of using the DSIF in the region of its maximum accuracy is gained. The inaccuracy in the knowledge of the astronomical unit is not a factor in this correction, because the velocity of the spacecraft relative to the earth is the dominant parameter in this computation. The accuracy of the self-contained system in the terminal phase is retained. Although the power drain is still high for this concept, it occurs only during one period of the mission. The disadvantages of using this concept are (1) the system is still complex; (2) although the power requirement has been reduced, this requirement is still large; and (3) advanced sensor designs and control concepts must be developed in order to implement the concept.

On the basis of the arguments presented in the preceding paragraphs, the logical choice for the Spacecraft Design Concept D control system is the hybrid philosophy. This philosophy employs the most successful of present techniques, yet allows for the expected improvements of the 1973 to 1980 time period. There is some risk involved in the area of sensor development, but the gain in navigation and guidance accuracy in the terminal mission phase obtained with this technique is appreciable and is necessary to fully realize the scientific capability of the spacecraft.

The performance of a system similar to the recommended system was discussed in subsections 3.4.2 and 3.4.4. The analysis and data presented in those subsections show that one vernier correction places the spacecraft on a trajectory which is expected to deviate 3000 to 7000 km from the nominal trajectory at perijove. Also, Earth-based orbit determination results in an approximate RMS error in spacecraft location of 8000 km. The self-contained terminal navigation coupled with a single terminal correction is expected to reduce these deviations by approximately an order of magnitude each. This places the spacecraft within tolerable miss distance and orbit determination limits for scientific experimentation.

The primary attitude control references for this concept are the Sun and Canopus. An inertial mode is used during Sun acquisition, maneuver execution, the occultation of either of the stellar references, and for back-up in case of failure of the stellar mode.

A scan platform capable of movement in a single plane is a part of the design. A Jupiter tracker is mounted on this platform so that it can be slewed in a plane normal to the plane of scan platform movement. Scan platform and Jupiter sensor slew commands are computed on board the spacecraft, with the stipulation that these commands can be over-ridden by Earth-computed commands. With the these computational differences, the reacquisition of the stellar references after the execution of the terminal maneuver is accomplished as described for Concept C.

The sequence of operations of the spacecraft control subsystem is composed of several sub-sequences. These

sub-sequences are (1) pre-launch, (2) acquire stellar attitude (Sun and Canopus), (3) execute maneuver, and (4) execute navigation measurements. The first three sub-sequences are essentially the same as those discussed for Design Concepts B and C. The execution of navigation measurements is described in the following paragraphs.

The Jupiter tracker first acquires Jupiter. Acquisition of a desired star and verification of the acquisition is then performed. Acquisition is accomplished under the control of the computer, which selects the star and computes its elevation and azimuth angles with respect to the spacecraft. Acquisition of the desired star is verified by the sampling of the actual elevation and azimuth and brightness of the acquired star and a comparison of these parameters with known values. The included angle between the lines of sight to the star and Jupiter is computed. The navigation measurements are made without loss of the spacecraft Sun-Canopus oriented attitude. The star tracker used to track Canopus continues to operate in the normal mode during the measurement cycle. The four star trackers available in this configuration are mounted so that two will be capable of tracking stars above the ecliptic, and two are used as redundant Canopus trackers. It is possible that the redundant Canopus tracker can be used in the navigation process to track stars below the ecliptic, but no definite plans have been made to use southern hemisphere stars.

The measurement cycle is repeated until the required number of measurements has been made. The computer processes each measurement in turn, using a statistical filter method to estimate the spacecraft position and velocity on the basis of an optimal weighting of the measurement residuals. The required steering command is computed from the current estimate of the spacecraft state (see subsection 3.4.4).

The most critical component of the control system is the computer. For this reason, the computer must be made as reliable as possible. Fortunately, there are techniques which improve the probability of successful computer operation for the duration of the mission. The computer can be made to be self-organizing and/or to possess redundant logic, circuitry, and critical components.

The computer must be capable of performing the navigation computations and handling some part of the data management load. The navigation task includes the management of the sensing devices, the selection and acquisition of the stars and/or planets to be observed, and the processing of the acquired data. The filtering process entails the manipulation and inversion of matrices which may be as large as 6 x 6, although the size of these arrays should be kept as small as is consistent with optimality considerations and the time available for data processing.

For this computational load, a computer with a 8192 word memory is required. However, if a data management task is postulated, an additional 8192 words of memory is a nominal estimate of the requirements. If the navigation task should require more than 8192 words, a part of all of the additional 8192 words for data management can be used since little or no data compression is required during the 20-day period of terminal navigation. Also, more than the 8192 words added for the data management task can be used at encounter (or any period of maximum data gethering), since the task of terminal navigation has been accomplished and only sensor control and other functions which impose few requirements on the computer have to be accomplished at this time. A typical computer for this application weighs 45 pounds, requires 15 watts of power for cruise operation, and has a 190 watt peak power requirement.

The number and weight of the components of the spacecraft control subsystem are shown in Table 5.4-8. The recommended numbers of components are based on a reliability analysis of the spacecraft control subsystem. Although the proposed configuration is not necessarily optimum with respect to reliability, it is considered to be an appropriate compromise between reliability, weight, and power considerations.

Table 5.4-8

DESIGN CONCEPT D - SPACECRAFT CONTROL SUBSYSTEM WEIGHT

Component (no.)	Weight, lb
Fine Angle Sun Sensor	1
Coarse Sun Sensors (4)	4
Earth Sensor	6
Startrackers (4)	40
Jupiter Sensor	6
Computer	45
Attitude Control Electronics	20
Gyros (6)	6
Accelerometer	1
Jupiter Moon Tracker *	6
TOTAL	135

* Optional

5.4.2.5 Attitude Control

For Design Concept D, there is no basic change in the attitude control philosophy for that used in Concepts B and C. Therefore, the only recommended change in the system is an increase in the system impulse to reflect the required increase in control capabilities. A total design impulse of 900 pound-seconds is selected, corresponding to attitude control propulsion system weight of 110 pounds.

5.4.2.6 Propulsion

The midcourse propulsion subsystem considered for Concept D is the basic hydrazine system described in subsection 3.6.1. The subsystem is designed to impart a total velocity increment of 90 meters per second (300 fps) to a spacecraft mass of about 1580 pounds. This corresponds to approximately a 5σ design criteria for a launch vehicle FOM of 10-15 m/sec and includes the required capability for the terminal correction. Table 5.4-9 contains a summary of the components and weight of the midcourse propulsion subsystem.

Table 5.4-9

DESIGN CONCEPT D - MIDCOURSE PROPULSION SUBSYSTEM WEIGHT

Component	Weight, lbs
Hydrazine	70.0
Hydrazine Tank	4.4
Nitrogen	3.1
Nitrogen Tank	6.13
Bladder	1.13
Fixed Hardware	20.94
TOTAL	105.60
Hydrazine Tank Diameter	18.3 in.
Nitrogen Tank Diameter	8.8 in.

The attitude control propulsion system of Concept D is the one defined as Configuration B in subsection 3.6.2. As stated in subsection 5.4.2.5, 900 pound-seconds is estimated to be the total impulse required. The weight of the attitude control system obtained from Figure 3.6-10, is 110 pounds.

5.4.2.7 Auxiliary Electric Power

The auxiliary electric power arrangement for Design Concept D is illustrated by the schematic diagram in Figure 3.7-8. Table 5.4-10 contains a list of individual and total loads in the case of each of the mission phases. A maximum load of 466 watts occurs during the operation of the navigation computer. The computer is operated over a 21-day period on a maximum duty cycle of 10 minutes on and 50 minutes off. During the 10-minute-on period, the battery supplies 64 watts which is equivalent to 11 watt-hours or 8.5 percent of the battery capacity. On the basis of a total charge-discharge efficiency of 60 percent, the average system load is 384 watts during the 50-minute charge period. During the encounter period, when the maximum long-duration load occurs, a surplus capacity of 8.4 percent is available.

In Table 5.2-11, the specific components included in the arrangement are listed. The RTG capacities indicated therein

Table 5.4-10

DESIGN CONCEPT D - ELECTRIC POWER LOADS

	Pre-Launch	Boost & Park Orbit	Acquisition	Cruise	Navigation	Maneuver	Encounter
Data Encoder	15	10	10	10	10	10	15
Tape Recorder	4	4	4	4	4	4	4
Command Detector & Decoder	3	0	3	3	3	3	3
CC&S	12	12	12	10	200	12	12
Control Gyro Electronics	5	5	5	5	5	15	5
Attitude Control Electronics	11	11	11	9	11	25	11
Gyro 400 cps Power	5	5	5	5	5	15	5
Sun Sensors	0	0	2	2	2	3	2
Canopus Tracker	0	0	10	7	7	7	7
Earth Sensor	0	0	10	7	0	7	0
Communication - Control	10	10	10	10	10	10	10
Communication - Receiver	10	10	10	10	10	10	10
Communication - Exciter	25	25	25	25	25	25	25
Communication - Amplifier	160	30	160	160	160	160	160
Extended Magnetometer	7	0	7	7	7	7	7
Energetic Particle Detector	0.4	0	0.4	0.4	0.4	0.4	0.4
Cosmic Dust Detector	0.2	0	0.2	0.2	0.2	0.2	0.2
Expanded Photometer	5	0	0	0	0	0	5
TV Camera (TV-II)	20	0	0	0	0	0	20
Plasma Probe	2.5	0	2.5	2.5	2.5	2.5	2.5
Microwave Radiometer	6	0	0	0	0	0	6
Infrared Radiometer	3	0	0	0	0	0	3
Ion Chamber	0.5	0	0.5	0.5	0.5	0.5	0.5
Infrared Spectrometer	5	0	0	0	0	0	5
High Energy Proton Directi Mon	0.6	0	0.6	0.6	0.6	0.6	0.6
Cosmic Ray Spectrum Analyzer	2	0	2	2	2	2	2
UV - Visible Spectrometer	10	0	0	0	0	0	10
Medium Energy Proton Mon.	1	0	1	1	1	1	1
Bistatic Radar	8	0	0	0	0	0	8
Radio Noise Detector	2	0	0	0	0	0	2
Null Radio Seeker	2	0	0	0	0	0	2
Radar Altimeter	10	0	0	0	0	0	10
Total Power Requirements	345.2	122	291.2	281.2	466.2	320.2	354.2
Raw Power Input to Cond.	428	151.5	362	350	580	400	440
Power Input to Shunt Reg. & But.	100	376.5	142	166	0	100	40
Power from RTG (4-120 W)	528	528	504	516	516	500	480
Power from Battery	0	0	0	0	64	0	0
Watt-Hour from Battery	0	0	0	0	11	0	0
Battery % Discharge	0	0	0	0	8.5	0	0

represent end-of-life values. The degradation of the capacities of the RTG as a function of time is indicated in Table 5.4-10.

Table 5.4-11

DESIGN CONCEPT D - ELECTRIC POWER SUBSYSTEM WEIGHT

Component	Rating	Weight, lbs.
Radioisotope Thermoelectric Generator (4)	120W, 28V	264.00
3 Electrode Ni-CD Battery	20 ampere-hour	42.00
Shunt Volt. Reg. Switch (4)	Ten .5a channels	3.60
Volt. Reg. Mode Controller	Signals Device	.75
Shunt Dissipation Resistors	140 watt	12.00
Main 2400 cps Inverter (2)	20 amperes input	8.00
Transfer Relay (2)	20 ampere dpst	1.00
Emergency 2400 cps Inverter	2 ampere input	.50
Inverter Synchronizer	Signal Device	.50
Emergency Transfer Unit	5 ampere spdt	.50
400 cps Inverter	2 ampere input	4.00
Battery Charge-Discharge Controller	5 a chg.; 10 a dischg.	16.00
Power Distribution and Wiring		84.30
TOTAL		437.15

5.4.2.8 Thermal Control

In Design Concept D, the equipment bus consists of a cross structure. The central portion and the short arms, shown in Figure 5.4-1, house the propulsion system tankage. Thermal control of this region is achieved by insulation of the exposed surfaces, by heat exchange with adjacent equipment areas, and by conduction through the RTG supports. RTG heating is needed because of the size of the exposed area. Even with a good insulation, enough heat is dissipated from the exposed surfaces so that a heat source is required. Design of the RTG supporting structure to supply the proper heat will require extensive analysis and testing.

The larger compartment arms of the bus contain the majority of electronic equipment. This equipment is mounted to four louvered plates which can be pivoted outward for easy access. Consideration should be given the group arrangements shown in Table 3.8-1 in locating the equipment. The upper and lower surfaces (launch configuration) are insulated or possibly covered with a low emittance surface. Heating of the louvered surfaces by the RTG's is reduced by employing thermal shields. Component thermal design data are shown in Table 5.4-12.

The Jupiter scan platforms present a thermal design problem (reference subsection 5.3.2.8). Insulated covers, RTG heating, and power dissipation are expected to provide thermal control.

Thermal control of components mounted on extensions, prelaunch cooling air, and spacecraft components during launch will be handled in the manner discussed for Design Concept C. Prelaunch cooling load from the RTG's will be about 36,000 BTU/hour.

The thermal control weight requirement is estimated to be 27 pounds. This number is based on 10 pounds for insulation, shielding, etc, and 16.4 square feet of louvers at 1.12 lbs/sq. ft. It is noted that some of the spacecraft surface skin acts as cold plates, and the skin therefore has minimum thickness requirements. It appears that the structural and meteoroid protection requirements dictate thicknesses which amply meet the thermal control requirements; thus this weight is not considered a part of thermal control.

5.4.2.9 Radiation Protection

The general problem of nuclear radiation protection for Jupiter flyby spacecraft is discussed in subsection 3.9. The conclusion reported therein is that no specific design penalties should be incorporated for radiation protection. The judicious selection of radiation resistant components for the various subsystems and the proper placement of scientific instruments which are sensitive to RTG radiation is the recommended approach to radiation protection. Design Concept D reflects these design considerations to the extent possible in a conceptual design. This is particularly manifested in the spacecraft configuration. Based on the results presented in subsection 3.9, no radiation shielding is included in the design concept.

Table 5.4-12

DESIGN CONCEPT D - THERMAL CONTROL INFORMATION

SUBSYSTEM AND COMPONENTS	TEMPERATURE LIMITS, °F OPERATING MIN	OPERATING MAX	NONOPERATING MIN	NONOPERATING MAX	HEAT DISSIPATION WATTS	WEIGHT, LBS.
Science Subsystem						
Extended Magnetometer						30.0
Electronics	-13	167	NA	NA	7.0	NA
Helium Sensor	-13	167	NA	NA	NA	NA
Rubidium Sensor	32	122	NA	NA	NA	1.5
Energetic Particle Detector	14	122	NA	NA	0.4	1.5
Cosmic Dust Detector						2.5
Electronics	-40	212	NA	NA	0.2	2.0
Sensor	-148	392	NA	NA	NA	0.5
Expanded Photometer	-4	104	-58	212	5.0	6.0
TV Camera						30.0
Electronics	14	158	-40	257	20.0	NA
Optics	-4	104	-58	212	NA	NA
Plasma Probe	14	176	NA	NA	2.5	7.0
Microwave Radiometer	-20	150	-58	212	NA	28.0
Ion Chamber	-22	158	NA	NA	0.5	13.0
Infrared Spectrometer	-4	104	-58	176	5.0	16.0
High Energy Protron Directional Monitor	14	122	NA	NA	0.6	4.0
Medium Energy Protron Directional Monitor	14	122	NA	NA	1.0	3.0
Cosmic Ray Spectrum Analyzer						18.0
Electronics	-22	167	-22	167	2.0	NA
Sensor	-22	122	-22	122	NA	NA
Infrared Radiometer	-4	104	-58	212	3.0	5.0
Ultra Violet Visible Spectrometer	-4	104	-40	257	10.0	20.0
Bistatic Radar	-20	150	-40	257	8.0	15.0
Radio Noise Detector	-20	150	-40	257	2.0	5.0
Radar Altimeter	-20	150	-40	257	2.0	5.0
Null Radio Seeker	-20	150	-40	257	10.0	25.0
Spacecraft Control						
Central Computer & Sequencer	0	125	-31	185	10.N*/190.P*	45.0
Wide Angle Sun Sensor	0	120	-58	212	2.0	2.0
Fine Angle Sun Sensor	0	120	-58	212	1.0	1.0
Earth Sensor	-10	125	-58	212	7.0	6.0
Jupiter Sensor	-10	125	-58	212	7.0	6.0
Star Trackers	-65	200	-58	212	7.0	6.0
Gyros	-65	250	-65	250	29.0	2.0
Accelerometer	10	100	-31	185	1.0	2.0
Attitude Control Electronics	0	104	-31	185	15.N*/20.P*	20.0
Midcourse Propulsion						
Thruster Assembly	NA	1500	70	NA	NA	2.5
Hydrazine Propellant and Tank	40	100	40	100	NA	60.0
Nitrogen Pressurization System	40	100	40	100	NA	20.0
Nitrogen and Tank	40	165	40	165	NA	7.5
Auxiliary Electric Power						
RTG Units	510	510	NA	NA	NA	240.0
Shunt Voltage Regulators	-30	160	NA	NA	20.0	3.6
Shunt Power Dissipation Resistors	-30	160	-65	160	**	12.0
NI-CD-3 Electrode Battery	-65	120	-65	120	**	42.0
Charge-Discharge Controller	-30	160	NA	NA	10.0	16.0
Voltage Sensor & Regulator Mode Control	-30	160	NA	NA	10.0	1.0
2400 cps Inverter	-30	160	NA	NA	58.0	8.0
Transfer Relay	-30	160	NA	NA	NA	1.0
400 cps Inverter & Regulator	-30	160	NA	NA	5.0	4.0
Emergency 2400 cps Inverter	-30	160	-65	160	NA	0.5
Inverter Synchronizer	-30	160	NA	NA	NA	0.5
Power Distribution	-65	160	NA	NA	15.0	84.3
Diodes	-65	160	NA	NA	19.0	NA
Emergency Transfer Relay	-30	160	-65	160	NA	0.5
Communications						
TWT Amplifier	-65	203	NA	NA	110.0	8.0
Power Monitor	-65	203	NA	NA	NA	2.0
Circulator	-65	203	NA	NA	NA	6.0
Exciter	-65	203	NA	NA	25.0	10.0
Exciter Control	-65	203	NA	NA	5.0	2.0
APC Receiver	-65	203	NA	NA	10.0	9.0
Amplifier Control	-65	203	NA	NA	5.0	2.0
Power Supply	-65	203	NA	NA	12.0	10.0
Data Management						
Data Encoder Element	14	176	NA	NA	15.0	40.0
Data Storage Element	14	176	-55	185	4.0	24.0
Command Detector & Decoder Element	14	176	NA	NA	1.5	12.0

*N Denotes nominal value
P Denotes peak value for short duration
** Dependent on operational requirements

5.4.2.10 Meteoroid Protection

The data for a nominal 600-day mission is used in assessing the meteoroid hazard to Concept D are summarized in Table 5.4-13. The spacecraft exposed area (Figure 5.2-5) in the interplanetary and asteroidal regions is determined as discussed in subsection 3.10.4. The near-Earth and near-Jupiter exposed area is the total surface area of the spacecraft equipment compartment.

Table 5.4-13

DESIGN CONCEPT D - METEOROID PROTECTION
ANALYSIS DATA

Region	Exposed Area (m^2)	Time (Days)	Area X Time (m^2-Days)
Near-Earth	16.25	0.5	8
Interplanetary	5.4	565	3050
Asteroidal	5.4	190	1020
Near-Jupiter	16.25	63.3	1030

These data are combined with the data presented in subsection 3.10.3 to provide the design data shown in Figure 5.4-3. The two curves indicate the magnitude of difference in the protection requirements for the two asteroidal flux models. Criteria for comparitive designs are discussed in subsection 5.2.2.10. For these criteria, the nominal asteroidal flux requires a 0.2-centimeter covering of the complete equipment compartment. This amount of protection weighs 198 pounds. If the worst case asteroidal flux is assumed, the required skin thickness on the back and sides of the spacecraft is 1.79 centimeters and on the front is 0.2 centimeter. The weight of this protection system is 1220 pounds.

The meteroid protection system provided for Design Con-Cept D consists of a complete covering of the spacecraft with 0.2 centimeters of aluminum. The choice of this design point is obviously arbitrary, but it is fact that it represents an adequate protection system with very little penalty. It does not appear desirable to accept the penalties imposed by the worst case asteroidal flux without in situ measurements of the actual flux.

DESIGN CONCEPT D - METEOROID PENETRATIONS VS. ALUMINUM SHEET THICKNESS

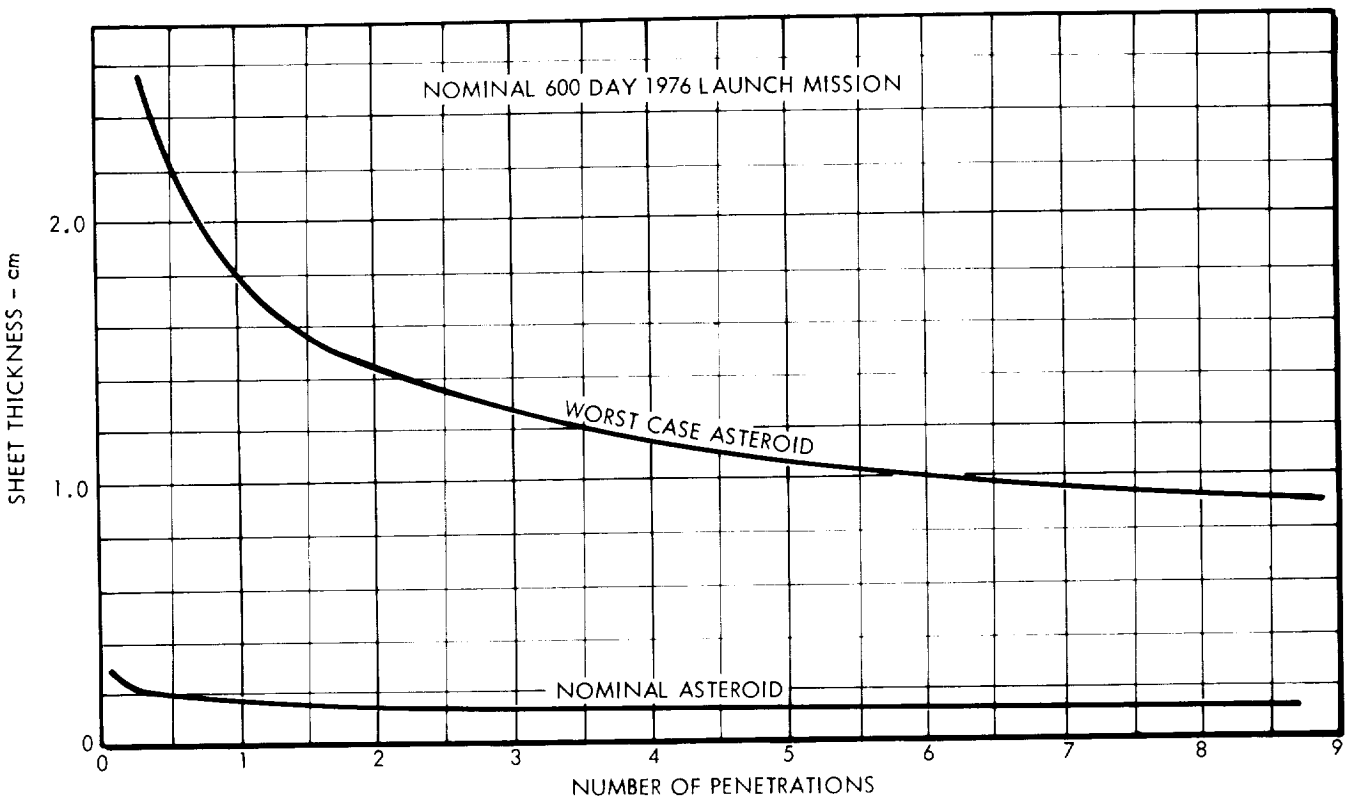

FIGURE 5.4-3

As indicated in subsection 3.12, the armor-type meteroid protection is considered to be an integral part of the spacecraft structure, and, for nominal protection measures, the weight is assumed to be completely chargeable to the structure. Therefore, the meteoroid protection weight is not listed separately in Table 5.4-2, but is included in the structural/mechanical weight estimate.

5.4.2.11 Configuration

The configuration of Design Concept D, shown in Figure 5.4-1, exhibits considerable resemblance to the Concept C configuration. Two basic differences are that (1) the high-gain antenna of Design Concept D is 10 feet in diameter and construction is of a wire mesh and rib arrangement, and (2) the equipment compartment of Concept D is more elongated to allow for clearance of the antenna by the scan platforms. The resultant enclosure is essentially cruciform in shape.

The inclusion of the extra sensors which make up the "full" science complement involves more complexity in the scan platform systems. Two extra dish antennas and a helical antenna are added as a result of the inclusion of the null radio seeker, radio altimeter, radio noise detector, and the bistatic radar instruments.

5.4.2.12 Structural and Mechanical Design

Most of the structural and mechanical features of Design Concept C also apply to Concept D. The major difference is in degree of complexity involved. For instance, the cruciform structure of the equipment compartment involves different geometry and less compactness as an enclosure; consequently the structural and thermal characteristics of Concept D are somewhat different from those of Concept C. The increased science instrumentation of Concept D entails more mechanical design complexity, particularly if all the added antennas require conflicting pointing angle requirements.

The weight of the spacecraft structural and mechanical provisions including meteroid protection is estimated to be 375 pounds for an injected spacecraft weight of 1581 pounds.

5.4.2.13 Subsystems Reliability

Table 5.4-14 contains the equipment mean-time-between-failure (MTBF) for Spacecraft Design Concept D. The science MTBF's are listed in Table 3.13-1. These MTBF's were determined using: (1) a buildup of failure rates when an equipment design was available and (2) reliability estimates from similar equipment design and best engineering judgment when the equipment design was not available. For subsystem configurations containing redundant equipment, the MTBF listed in the table is for each of the redundant equipments. These equipment MTBF's are used to derive probability of mission success in subsection 5.4.4.

Table 5.4-14

SPACECRAFT DESIGN CONCEPT D - EQUIPMENT MTBF

SUBSYSTEM EQUIPMENT	MTBF (Hours)
Communications Subsystem	
Receiver	15,000
Exciter	45,000
TWT Amplifier	30,000
Circulator and Logic	350,000
TWT P/S	140,000
Power Monitor	333,000
Data Management Subsystem	
Data Encoder Element	-
Data Storage Element	6,000
Command Det & Decoder Element	
Detector & Decoder	10,000
Commands	44,000 - 77,000
Spacecraft Control Subsystem	
Fine Sun Sensor	180,000
Course Sun Sensor	230,000
Earth Sensor	40,000
Star Tracker	35,000
Attitude Control Electronics	40,000
CC&S	4,500
Gyro and Accecelerometer	8,000
Jupiter Tracker	40,000
Propulsion Subsystem	
Tank	0.9998*
Squib	0.999896*
Regulator	0.9704*
Rocket Motor & Vanes	0.99996*
Attitude Control Subsystem	
Tank	0.9998*
Squib	0.999896*
Regulator	0.9704*
Single Roll Jet	0.9850*
Single Pitch/Yaw Jet	0.9823*

Auxiliary Electrical Subsystem	
400 cps Chopper	210,000
Voltage Sensor and Regulator	60,000
2400 cps Chopper	150,000
Inverter Sync	220,000
Battery	70,000

* Probability of operating as required

5.4.3 Mission Performance

Mission performance envelopes such as that shown in Figure 5.4-4 were utilized to derive the mission performance data for the Spacecraft Design Concept D and the Saturn IB/Centaur/HEKS launch vehicle combination. The performance data shown in Figures 5.4-5 and 5.4-6 are defined in terms of the width of the launch window, or launch period corresponding to the dates of arrival at western quadrature, opposition, and eastern quadrature. Arrival on the dates of these events requires Earth-to-Jupiter flight times of approximately 420 days, 510 days, and 600 days, in that order.

As shown in Figure 5.4-5(b), the performance capabilities of the Saturn IB/Centaur/HEKS launch vehicle are more than adequate, providing sufficient launch window width in all years for missions with arrival dates from western quadrature through eastern quadrature. The performance data for the Titan IIICx/Centaur are given in Figure 5.4-5(a), but as can be seen, this vehicle offers only marginal capability.

Mission performance summary charts for multi-spacecraft injection by the Saturn IB/Centaur/HEKS and Saturn V launch vehicles are presented in Figure 5.4-6. The spacecraft adapter mass of multi-spacecraft systems was obtained by taking 6.5 percent of the total injected spacecraft mass.

The data denoted by dashes in Figures 5.4-5 and 5.4-6 represent the interval of the launch window in which the magnitude of the departure asymptote declination is greater than 36 degrees. This upper limit on declination is explained in subsection 2.2.1.

SPACECRAFT DESIGN CONCEPT D - MISSION PERFORMANCE ENVELOPE

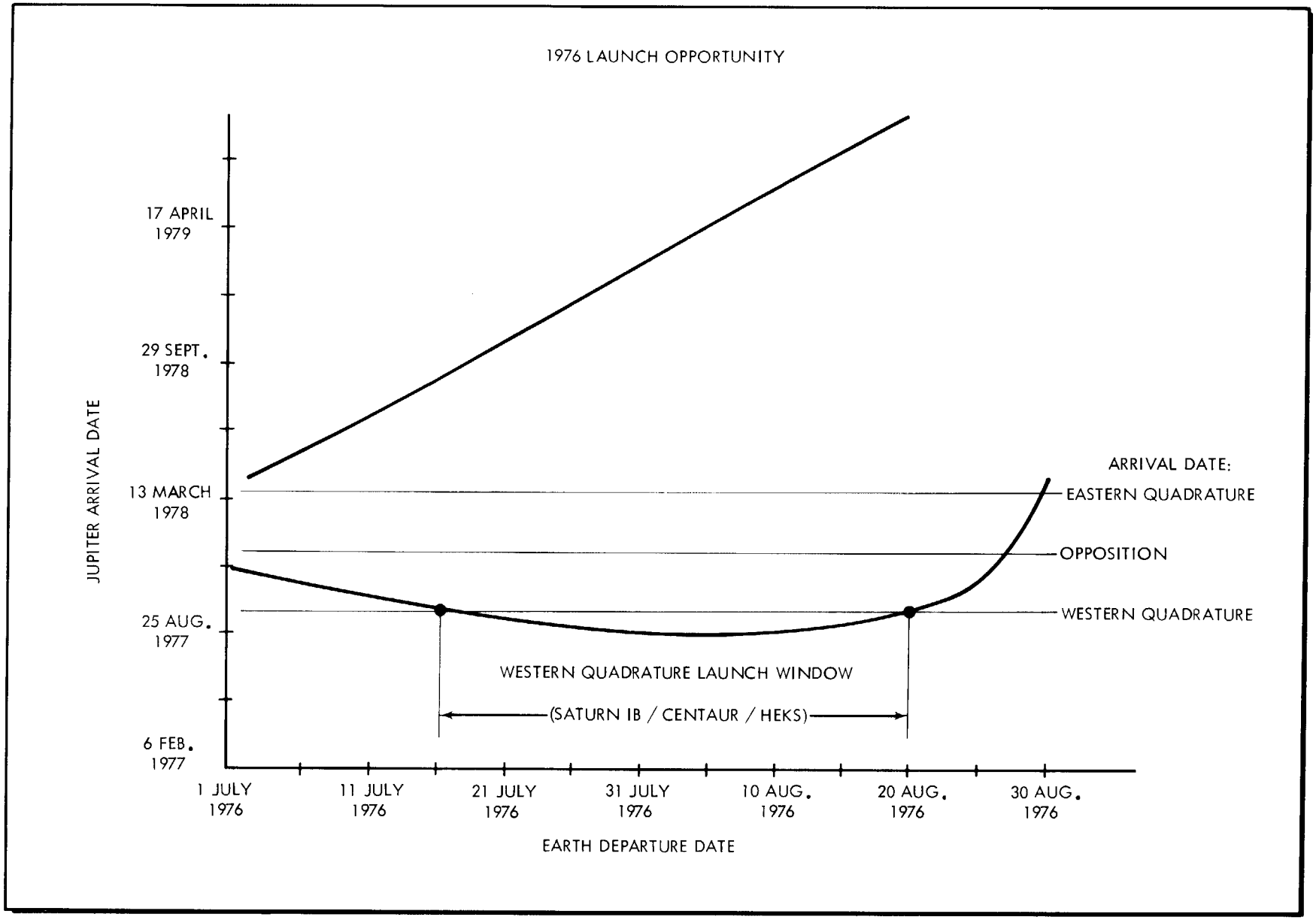

FIGURE 5.4-4

SPACECRAFT DESIGN CONCEPT D — LAUNCH VEHICLE MISSION PERFORMANCE SUMMARY CHART I

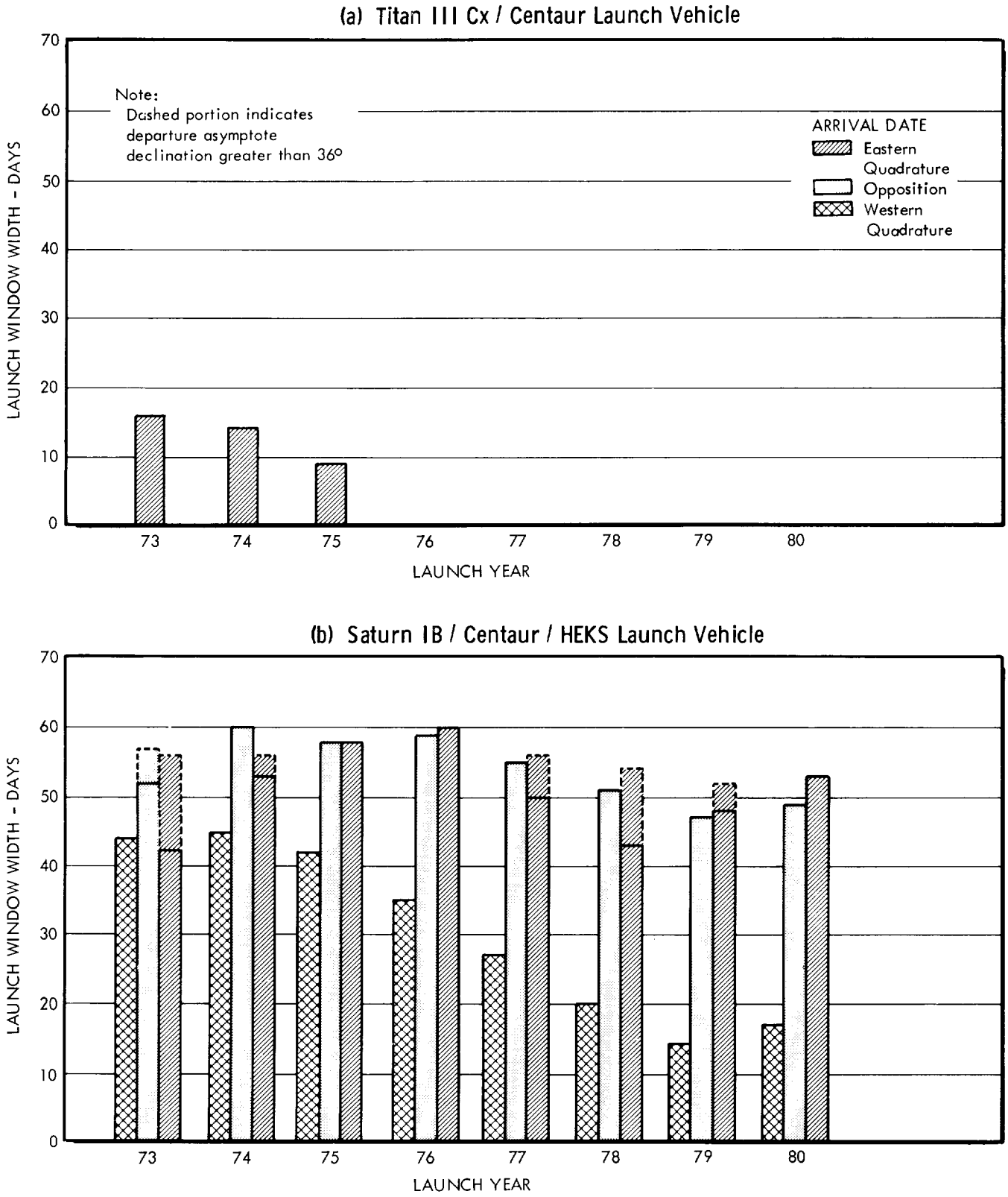

FIGURE 5.4-5

SPACECRAFT DESIGN CONCEPT D — LAUNCH VEHICLE MISSION PERFORMANCE SUMMARY CHART II

(a) Saturn IB / Centaur / HEKS Launch Vehicle

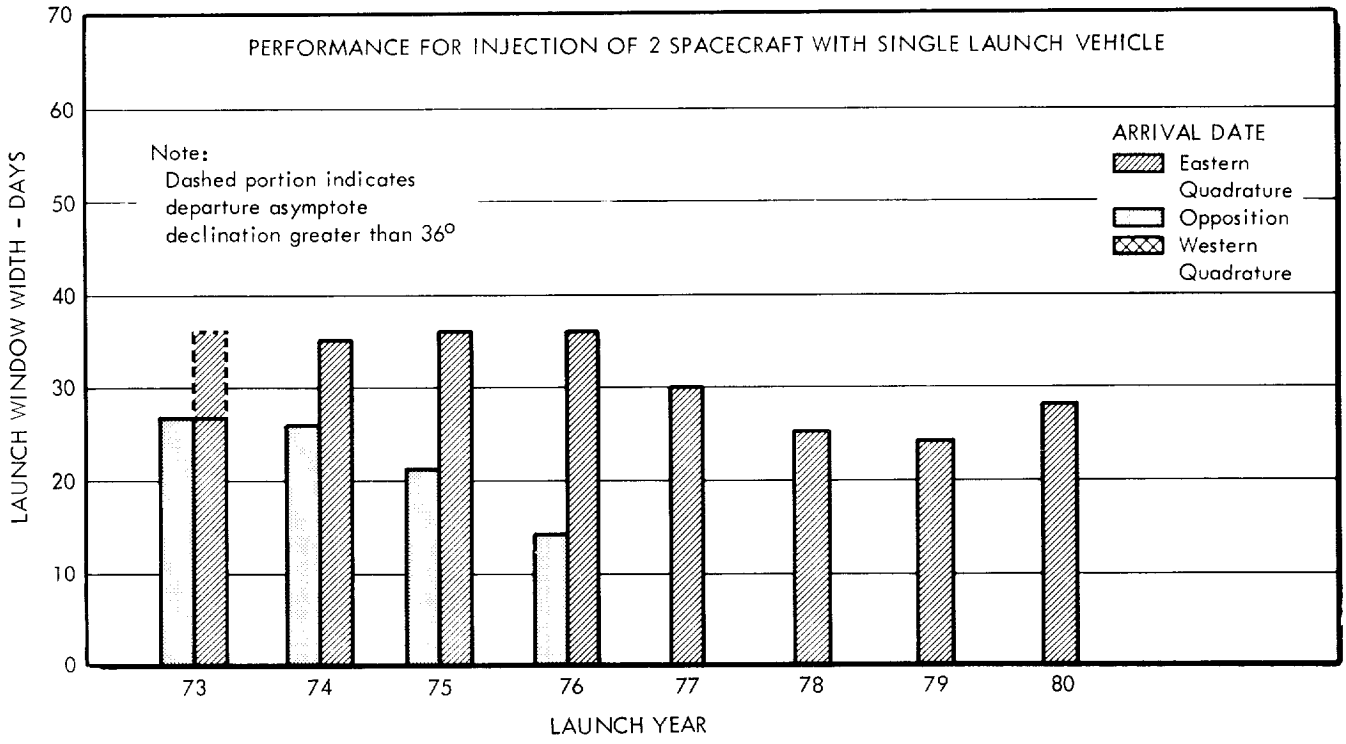

(b) Saturn V Launch Vehicle

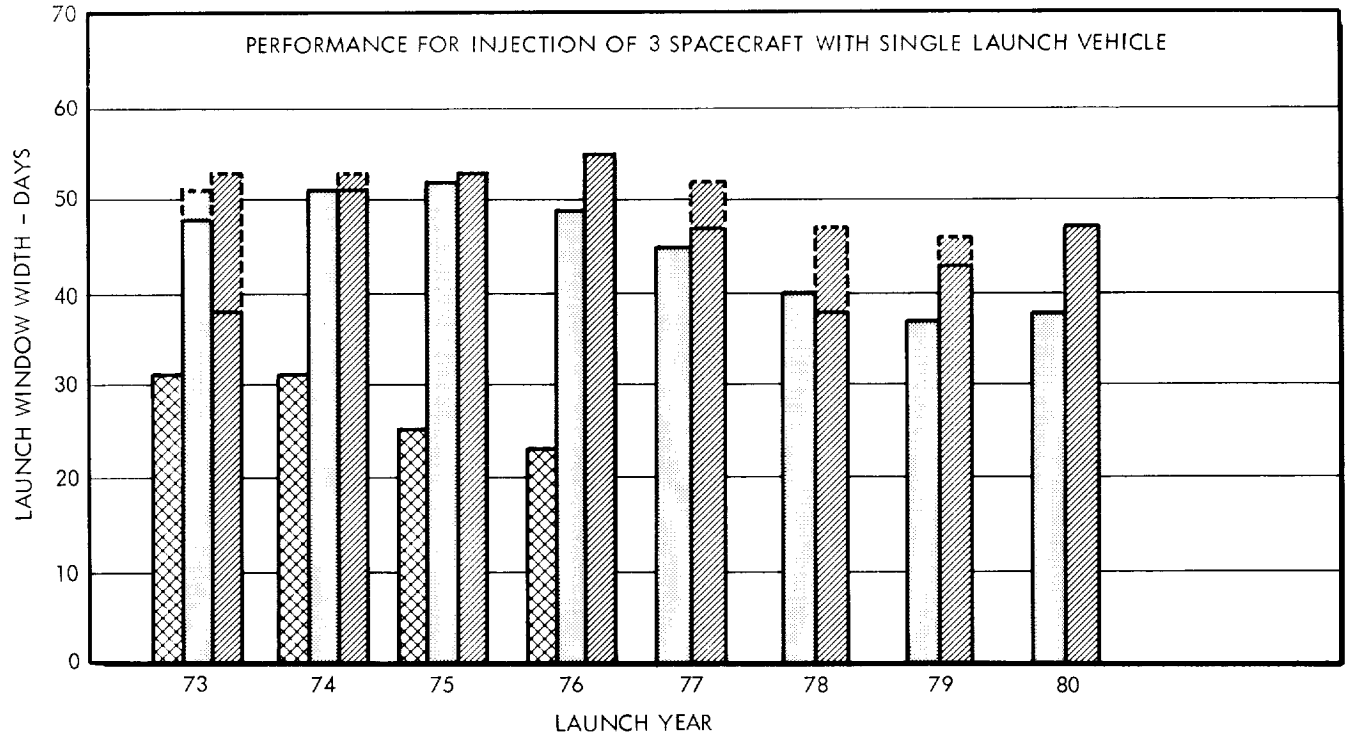

FIGURE 5.4-6

5.4.4 Probability of Mission Success

The approach and guidelines employed in this study to evaluate the probability of mission success for Design Concept D are discussed in subsection 4.2. The results indicated therein are based on the mission described by the sequence of events in Table 5.4-1. It should be noted that the spacecraft computer replaces the CC&S, and the computer function is required through the encounter playback phase. Also, the data automation function is included in the DEE function. The MTBF's utilized in this analysis are listed in Table 5.4-14.

The probabilities of mission success for both total and half missions are presented in Table 5.4-15. The probabilities of successful operation in the case of the communications, auxiliary electrical power, spacecraft control, and science subsystems are presented in Table 5.4-16. The fact that the probabilities of mission success exhibited by Concept D are somewhat higher than those for Concepts A through C is directly attributable to (1) the shorter mission time and (2) the improved reliability of the Data Management Subsystem.

Table 5.4-15

DESIGN CONCEPT D - PROBABILITY OF MISSION SUCCESS

CONFIGURATION	PROBABILITY OF MISSION SUCCESS	
	TOTAL MISSION (418 Days)	HALF MISSION (209 Days)
Spacecraft Less Science Instruments	0.14	0.49
Total Spacecraft	less than 0.01	0.10

Table 5.4-16

DESIGN CONCEPT D - SUBSYSTEMS PROBABILITY OF MISSION SUCCESS

SPACECRAFT SUBSYSTEM	PROBABILITY OF MISSION SUCCESS TOTAL MISSION (418 Days)	HALF MISSION (208 Days)
Communication	0.64	0.85
Auxiliary Electrical Power	0.57	0.73
S/C Control	0.61	0.84
Science	0.01	0.21

5.4.5 Development Requirements

The total time span for development of Design Concept D, derived from Tables 5.4-17 and 5.4-18, is 10 years 5 months. From the time line chart shown in Figure 5.4-7, it can be seen that the major program constraints are the spacecraft control

DESIGN CONCEPT D - TIME LINE CHART

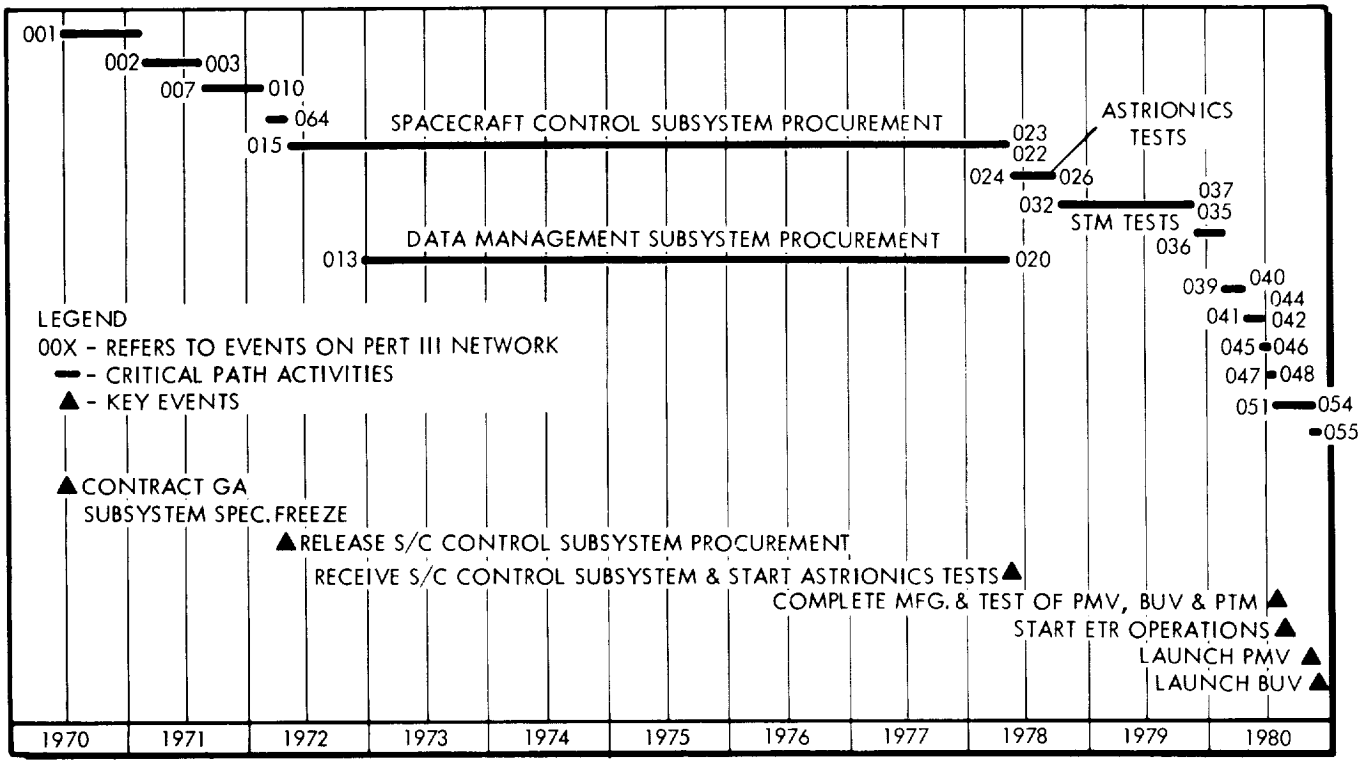

FIGURE 5.4-7

Table 5.4-17
DESIGN CONCEPT D - PERT III INPUT ACTIVITY TIME ESTIMATES

TC	SP	SCH OPT	BEG EVENT LC	END EVENT LC	OPT TIME	MEAN TIME	PESS TIME	SCH DATE / 1 / 2 / 3 / 4	ACT DATE	EVENT TITLE /ACTIVITY TITLE
3				00.000.001					1.01.68	CONTRACT GO-AHEAD
1			00.000.001	00.000.002	2.0	4.0	12.0			C/JUPITER SYS DESIGN SPEC
1			00.000.002	00.000.003	8.0	12.0	20.0			C/SPCFT PREL SUBSYS + INRFCE SPEC
1			00.000.002	00.000.004	1.0	1.0	2.0			R/RTG FUEL PROCUREMENT ORDER
1			00.000.003	00.000.005						S/DETAILED CDFG DSGN + MOCKUP
1			00.000.003	00.000.006						S/SUBSYS PROCUREMENT NEGOTIATIONS
1			00.000.003	00.000.007	8.0	14.0	16.0			R/SCNCE PROCUREMENT
1			00.000.003	00.000.008	3.0	6.0	12.0			R/TEST SPEC + LAUNCH OPER PLAN
1			00.000.002	00.000.009	2.0	2.0	4.0			INITIATES EARTH LAUNCH VEH PROC
1			00.000.005	00.000.010	2.4	6.0	8.0			SCNCE PYLD, CDFG APPR + MCKUP COMPL
1			00.000.006	00.000.010						SCNCE PYLD, CDFG APPR + MCKUP COMPL
1			00.000.007	00.000.010	2.4	6.0	8.0			SCNCE PYLD, CDFG APPR + MCKUP COMPL
1			00.000.008	00.000.011	16.0	26.0	37.0			R/TEST + LAUNCH + FAC IMPLMTN PLAN
1			00.000.010	00.000.012	2.0	4.0	8.0			S/TOOLING DSGN
1			00.000.064	00.000.013						R/DATA MGMT SUBSYS PROCUREMENT
1			00.000.064	00.000.014						R/COMM SUBSYS PROCUREMENT
1			00.000.064	00.000.015						R/SPACECRAFT CONT SUBSYS PROC
1			00.000.064	00.000.016						R/RTG PROCUREMENT
1			00.000.064	00.000.017						R/MIDCOURSE PRPLN PROCUREMENT
1			00.000.064	00.000.018						R/ATTITUDE CONT PRPLN PROCUREMENT
1			00.000.012	00.000.019	2.0	4.0	6.0			S/MFGR OF STM + TCM STR + MECH SYS
1			00.000.013	00.000.020	29.0	52.0	104.0			RE/STM DATA MGMT SUBSYS
1			00.000.014	00.000.021	26.0	37.0	52.0			RE/STM COMM SUBSYS
1			00.000.015	00.000.022	29.0	64.0	130.0			RE/STM SPACECRAFT CONT SUBSYS
1			00.000.019	00.000.023	41.0	52.0	78.0			C/STM STR + MECH ASSY
1			00.000.020	00.000.023	1.0	1.0	2.0			C/STM STR + MECH ASSY
1			00.000.021	00.000.023	1.0	1.0	2.0			C/STM STR + MECH ASSY
1			00.000.022	00.000.023	1.0	1.0	2.0			C/STM STR + MECH ASSY
1			00.000.063	00.000.023						C/STM STR + MECH ASSY
1			00.000.023	00.000.024	1.0	2.0	3.0			S/STM ASTRIONICS COMPAT TESTS
1			00.000.024	00.000.026	2.0	8.0	6.0			C/STM ASTRIONICS COMPAT TESTS
* 1			00.000.004	00.000.027	40.0	56.0	72.0			RE/FIRST SET FUELED RTGS
1			00.000.016	00.000.027	64.0	78.0	208.0			RE/FIRST FUELED RTGS
1			00.000.017	00.000.028	29.0	52.0	104.0			RE/FIRST MIDCOURSE PRPLN
1			00.000.018	00.000.029	29.0	52.0	104.0			RE/FIRST ATTITUDE CONT PRPLN
1			00.000.007	00.000.030	26.0	37.0	104.0			RE/FIRST SET OF SCNCE
1			00.000.059	00.000.031	8.0	16.0	26.0			PRI CDFG QLFD FOR TCM + LETM TESTS
1			00.000.026	00.000.032						S/FINAL ASSY + TEST OF STM
1			00.000.027	00.000.032						S/FINAL ASSY + TEST OF STM
1			00.000.028	00.000.032						S/FINAL ASSY + TEST OF STM
1			00.000.029	00.000.032						S/FINAL ASSY + TEST OF STM
1			00.000.030	00.000.032						S/FINAL ASSY + TEST OF STM
1			00.000.033	00.000.032						S/FINAL ASSY + TEST OF STM
1			00.000.011	00.000.033						STM TEST AREA COMPL
1			00.000.031	00.000.034	1.0	2.0	6.0			S/MFGR OF LETM STR + MECH SYS
1			00.000.032	00.000.035	12.0	12.0	52.0			STM FUNCTIONALLY QLFD
1			00.000.037	00.000.036						S/TCM FINAL ASSY
1			00.000.062	00.000.036						S/TCM FINAL ASSY
1			00.000.035	00.000.037	4.0	4.0	26.0			R/REV TCM SUBSYS + SCNCE
1			00.000.036	00.000.039	2.0	4.0	6.0			C/TCM FINAL ASSY
1			00.000.039	00.000.040	2.0	2.0	4.0			S/TCM FINAL QUALIFICATION TESTS
1			00.000.040	00.000.041	2.0	4.0	8.0			TCM FUNCTIONALLY QLFD
1			00.000.034	00.000.042	12.0	14.0	37.0			S/LETM FINAL ASSY
1			00.000.041	00.000.042	1.0	1.0	2.0			S/LETM FINAL ASSY
1			00.000.041	00.000.043						RE/LETM SUBSYS WITH CHG INC
1			00.000.042	00.000.044	2.0	4.0	8.0			C/FINAL ASSY OF LETM
1			00.000.043	00.000.044	2.0	2.0	3.0			C/FINAL ASSY OF LETM
1			00.000.044	00.000.045	1.0	1.0	1.0			S/LETM QUALIFICATION TESTS
1			00.000.045	00.000.046	3.0	4.0	8.0			LETM QLFD DSGN FREEZE
1			00.000.046	00.000.047						C/MFGR, TEST OF PMV, BUV + PTM
1			00.000.066	00.000.047	12.0	14.0	37.0			C/MFGR, TEST OF PMV, BUV + PTM
* 1			00.000.067	00.000.047						C/MFG,TST OF PMV,BUV PTM
1			00.000.047	00.000.048	1.0	1.0	2.0			PMV + BUV ON DOCK AT LAUNCH SITE
1			00.000.011	00.000.049						ETR FAC AVAIL
1			00.000.065	00.000.050	4.0	4.0	6.0			EARTH LAUNCH VEH DEL TO LAUNCH SITE
1			00.000.048	00.000.051						S/ETR OPERATIONS
1			00.000.049	00.000.051						S/ETR OPERATIONS
1			00.000.050	00.000.051						S/ETR OPERATIONS
1			00.000.047	00.000.052	1.0	1.0	2.0			PTM DEL TO MISSION CONT CENTER
1			00.000.052	00.000.053	2.0	4.0	6.0			DSIF + MISSION CONT CENTER ACTVT
1			00.000.051	00.000.054	10.0	14.0	16.0	5.04.74		LAUNCH PMV
1			00.000.056	00.000.054	4.0	4.0	4.0	5.04.74		LAUNCH PMV
1			00.000.054	00.000.055	1.0	1.0	2.0	5.11.74		LAUNCH BUV
1			00.000.053	00.000.056						BGN SPCRFT FLT OPER AT FLT CONT STE
1			00.000.019	00.000.059	41.0	52.0	78.0			S/PREL STR INTEGRITY TESTING
1			00.000.011	00.000.060						TCM TEST FAC AVAIL FOR FIRST TEST
1			00.000.031	00.000.061	1.0	2.0	6.0			S/TCM PREL TESTS WITH MCKUP SUBSYS
1			00.000.060	00.000.061						S/TCM PREL TESTS WITH MCKUP SUBSYS
1			00.000.061	00.000.062	37.0	52.0	104.0			PRI SPCRFT STR TC QLFD
1			00.000.005	00.000.063	29.0	33.0	41.0			ALL STR + MECH SYS DWG COMPLETE
1			00.000.010	00.000.064	2.0	2.0	3.0			SUBSYS SPEC + INRFCE FREEZE
1			00.000.009	00.000.065						FINAL LAUNCH VEH STATUS REVIEW
1			00.000.031	00.000.066	2.0	3.0	6.0			S/MFGR PMV, BMV + PTM
* 1			00.000.027	00.000.067	84.0	128.0	172.0			RE/PMV+BUV RTG FUEL

Table 5.4-18
DESIGN CONCEPT D - PERT III EVENT SCHEDULE REPORT

EVENT TITLE	EVENT NO.	L C	CRITICAL PREDECESSOR	L C	S P	ACTUAL DATE	EXPECTED DATE	LATEST DATE	SCHEDULED DATE	SLACK TIME	STD DEV	PROB SCD	PROB POS SL
CONTRACT GO-AHEAD	00-000-001						02JAN68	26DEC68		51.4	.0		.97
C/JUPITER SYS DESIGN SPEC	00-000-002		00-000-001				05FEB68	30JAN69		51.4	1.7		.97
C/SPCFT PREL SUBSYS + INRFCE SPEC	00-000-003		00-000-002				06MAY68	29APR69		51.4	2.6		.97
PMV + BUV ON DOCK AT LAUNCH SITE	00-000-048		00-000-047				01FEB73	28JAN74		51.4	28.3		.97
RE/FIRST SET FUELED RTGS	00-000-027		00-000-016				11AUG70	06AUG71		51.4	24.2		.97
C/MFGR, TEST OF PMV, BUV + PTM	00-000-047		00-000-067				23JAN73	18JAN74		51.4	28.3		.97
R/SCNCE PROCUREMENT	00-000-007		00-000-003				05AUG68	31JUL69		51.4	2.9		.97
LAUNCH BUV	00-000-055		00-000-054				16MAY73	13MAY74	13MAY74	51.4	28.3	.97	.97
RE/PMV+BUV RTG FUEL	00-000-067		00-000-027				23JAN73	18JAN74		51.4	28.3		.97
SCNCE PYLD, CDFG APPR + MCKUP COMPL	00-000-010		00-000-007				16SEP68	09SEP69		51.4	3.0		.97
LAUNCH PMV	00-000-054		00-000-051				08MAY73	03MAY74	06MAY74	51.4	28.3	.97	.97
R/RTG PROCUREMENT	00-000-016		00-000-064				30SEP68	24SEP69		51.4	3.0		.97
SUBSYS SPEC + INRFCE FREEZE	00-000-064		00-000-010				30SEP68	24SEP69		51.4	3.0		.97
S/ETR OPERATIONS	00-000-051		00-000-048				01FEB73	28JAN74		51.4	28.3		.97
PTM DEL TO MISSION CONT CENTER	00-000-052		00-000-047				01FEB73	08MAR74		57.1	28.3		.98
DSIF + MISSION CONT CENTER ACTVT	00-000-053		00-000-052				01MAR73	05APR74		57.1	28.3		.98
BGN SPCRFT FLT OPER AT FLT CONT STE	00-000-056		00-000-053				01MAR73	05APR74		57.1	28.3		.98
S/DETAILED CDFG DSGN + MOCKUP	00-000-005		00-000-003				06MAY68	31JUL69		64.7	2.6		.99
S/SUBSYS PROCUREMENT NEGOTIATIONS	00-000-006		00-000-003				06MAY68	09SEP69		70.4	2.6		.99
S/TCM PREL TESTS WITH MCKUP SUBSYS	00-000-061		00-000-031				08APR70	10JUL72		117.5	7.6		1.00
S/PREL STR INTEGRITY TESTING	00-000-059		00-000-019				28NOV69	28FEB72		117.5	7.0		1.00
S/LETM QUALIFICATION TESTS	00-000-045		00-000-044				17SEP71	18DEC73		117.5	13.5		1.00
C/FINAL ASSY OF LETM	00-000-044		00-000-042				10SEP71	11DEC73		117.5	13.5		1.00
C/TCM FINAL ASSY	00-000-039		00-000-036				18JUN71	17SEP73		117.5	13.5		1.00
S/LETM FINAL ASSY	00-000-042		00-000-041				11AUG71	12NOV73		117.5	13.5		1.00
S/MFGR OF STM + TCM STR + MECH SYS	00-000-019		00-000-012				12NOV68	12FEB71		117.5	3.3		1.00
S/TCM FINAL ASSY	00-000-036		00-000-062				21MAY71	20AUG73		117.5	13.5		1.00
S/TOOLING DSGN	00-000-012		00-000-010				14OCT68	15JAN71		117.5	3.2		1.00
PRI SPCRFT STR TC QLFD	00-000-062		00-000-061				21MAY71	20AUG73		117.5	13.5		1.00
PRI CDFG QLFD FOR TCM + LETM TESTS	00-000-031		00-000-059				23MAR70	21JUN72		117.5	7.6		1.00
TCM FUNCTIONALLY QLFD	00-000-041		00-000-040				03AUG71	02NOV73		117.5	13.5		1.00
S/TCM FINAL QUALIFICATION TESTS	00-000-040		00-000-039				05JUL71	03OCT73		117.5	13.5		1.00
LETM QLFD DSGN FREEZE	00-000-046		00-000-045				19OCT71	18JAN74		117.5	13.5		1.00
RE/LETM SUBSYS WITH CHG INC	00-000-043		00-000-041				03AUG71	26NOV73		120.8	13.5		1.00
R/RTG FUEL PROCUREMENT ORDER	00-000-004		00-000-002				13FEB68	10JUL70		125.4	1.7		1.00
R/REV TCM SUBSYS + SCNCE	00-000-037		00-000-035				12FEB71	20AUG73		131.4	25.4		1.00
STM FUNCTIONALLY QLFD	00-000-035		00-000-032				21DEC70	27JUN73		131.4	25.1		1.00
S/FINAL ASSY + TEST OF STM	00-000-032		00-000-027				11AUG70	16FEB73		131.4	24.2		1.00
R/SPACECRAFT CONT SUBSYS PROC	00-000-015		00-000-064				30SEP68	03AUG71		148.3	3.0		1.00
C/STM ASTRIONICS COMPAT TESTS	00-000-026		00-000-024				15APR70	16FEB73		148.3	17.1		1.00
S/STM ASTRIONICS COMPAT TESTS	00-000-024		00-000-023				18FEB70	22DEC72		148.3	17.1		1.00
C/STM STR + MECH ASSY	00-000-023		00-000-022				04FEB70	08DEC72		148.3	17.1		1.00
RE/STM SPACECRAFT CONT SUBSYS	00-000-022		00-000-015				27JAN70	30NOV72		148.3	17.1		1.00
R/DATA MGMT SUBSYS PROCUREMENT	00-000-013		00-000-064				30SEP68	29OCT71		160.7	3.0		1.00
RE/STM DATA MGMT SUBSYS	00-000-020		00-000-013				03NOV69	30NOV72		160.7	12.9		1.00
S/MFGR OF LETM STR + MECH SYS	00-000-034		00-000-031				08APR70	11JUL73		170.0	7.6		1.00
RE/FIRST ATTITUDE CONT PRPLN	00-000-029		00-000-018				03NOV69	16FEB73		171.9	12.9		1.00
R/ATTITUDE CONT PRPLN PROCUREMENT	00-000-018		00-000-064				30SEP68	17JAN72		171.9	3.0		1.00
RE/FIRST MIDCOURSE PRPLN	00-000-028		00-000-017				03NOV69	16FEB73		171.9	12.9		1.00
R/MIDCOURSE PRPLN PROCUREMENT	00-000-017		00-000-064				30SEP68	17JAN72		171.9	3.0		1.00
S/MFGR PMV, BMV + PTM	00-000-066		00-000-031				14APR70	18SEP73		179.0	7.6		1.00
RE/STM COMM SUBSYS	00-000-021		00-000-014				20JUN69	30NOV72		179.8	5.2		1.00
R/COMM SUBSYS PROCUREMENT	00-000-014		00-000-064				30SEP68	13MAR72		179.8	3.0		1.00
R/TEST SPEC + LAUNCH OPER PLAN	00-000-008		00-000-003				18JUN68	07JAN72		185.4	3.0		1.00
R/TEST + LAUNCH + FAC IMPLMTN PLAN	00-000-011		00-000-008				19DEC68	10JUL72		185.4	4.6		1.00
TCM TEST FAC AVAIL FOR FIRST TEST	00-000-060		00-000-011				19DEC68	10JUL72		185.4	4.6		1.00
RE/FIRST SET OF SCNCE	00-000-030		00-000-007				25JUN69	16FEB73		190.3	13.3		1.00
ALL STR + MECH SYS DWG COMPLETE	00-000-063		00-000-005				26DEC68	08DEC72		206.2	3.3		1.00
STM TEST AREA COMPL	00-000-033		00-000-011				19DEC68	16FEB73		217.2	4.6		1.00
ETR FAC AVAIL	00-000-049		00-000-011				19DEC68	28JAN74		266.4	4.6		1.00
FINAL LAUNCH VEH STATUS REVIEW	00-000-065		00-000-009				21FEB68	28DEC73		305.2	1.7		1.00
EARTH LAUNCH VEH DEL TO LAUNCH SITE	00-000-050		00-000-065				22MAR68	28JAN74		305.2	1.7		1.00
INITIATES EARTH LAUNCH VEH PROC	00-000-009		00-000-002				21FEB68	28DEC73		305.2	1.7		1.00

and data management subsystems. For a launch date of 23 November 1980, the program should have a go-ahead in June 1970. Figure 5.4-8 reflects a probability of 0.65 that the total program development time will be less than that shown on the time line chart.

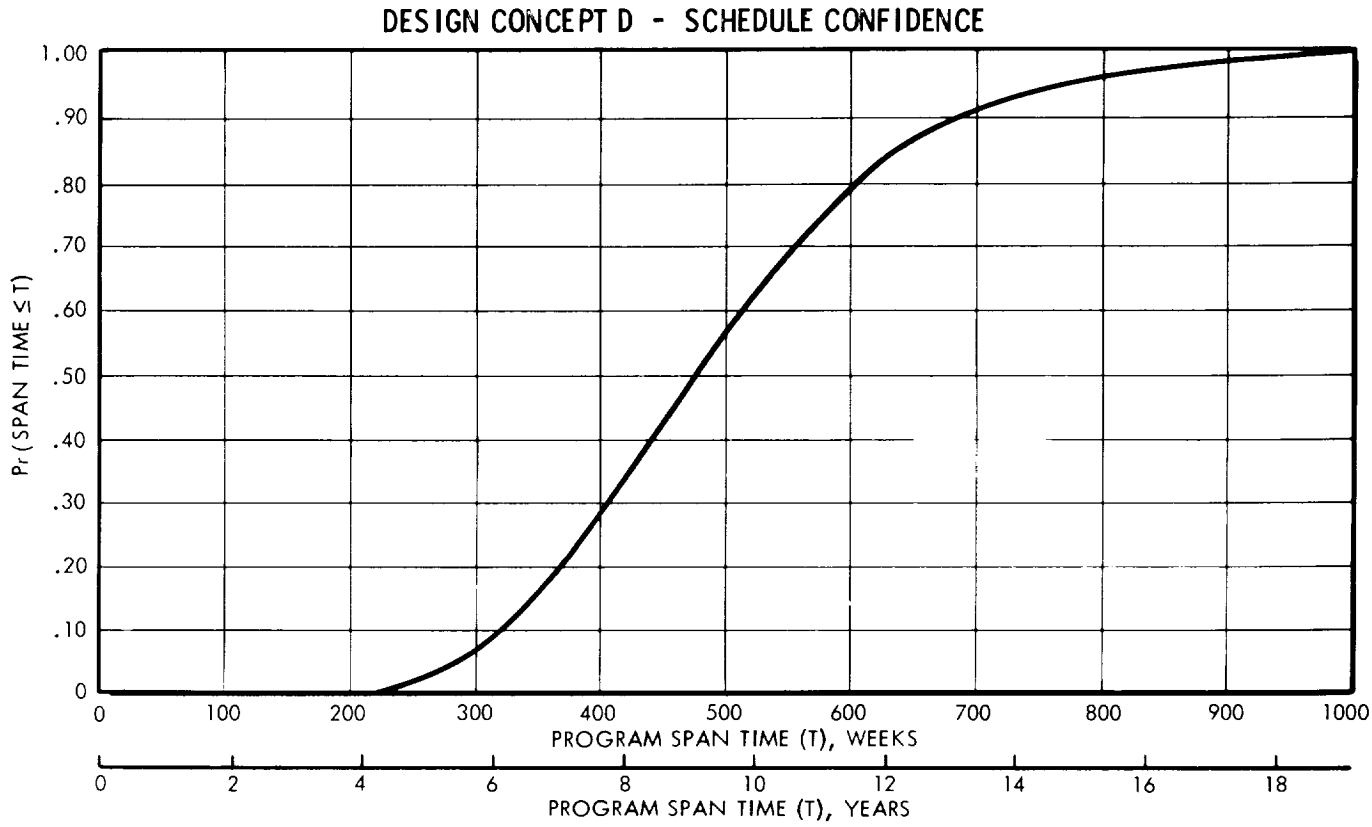

FIGURE 5.4-8

5.4.6 Cost Results

Presented in Table 5.4-19 is a summary of the items that comprise the total program costs for Spacecraft Design Concept D, assuming two operational flights. The Saturn V costs are based on a single launch of two spacecraft. The costs presented in Table 5.4-20 are the recurring spacecraft costs for two flights. The total cost increment for a third flight is given in Table 5.4-21. These results are based on the discussion in subsection 4.4.

Table 5.4-19

DESIGN CONCEPT D - SUMMARY OF JUPITER FLYBY PROGRAM COSTS

(In Millions of 1965 Dollars)

COST CATEGORIES	LAUNCH VEHICLE TYPE	
	SATURN IB/ CENTAUR/ HEKS	SATURN V*
NONRECURRING		
Science	24.00	
Communications & Data Mgt	13.80	
Spacecraft Control	14.50	
Attitude Control	1.24	
Midcourse Propulsion	1.90	
Electrical Power	15.65	
Structural, Mech., Therm., & Shield	7.65	
Subtotal Subsystems, DT&E	78.74	
Operational Support Equip	18.00	
Tooling & Special Equip	4.80	
System Integration	9.70	
Ground Test Hardware	23.18	
Total Nonrecurring Costs	134.42	134.42
RECURRING (2 Launches)		
Recurring Spacecraft	44.41	44.41
Spacecraft Spares (2 Sets)	5.27	5.27
Deep Space Net Support	26.80	26.80
Spacecraft Operations	2.60	2.60
Launch Vehicles	61.60	62.77
Launch Operations	13.00	7.50
Total Recurring Costs	153.68	136.35
TOTAL PROGRAM COSTS	288.10	283.77

* Assuming a Single Launch Vehicle With Dual Payload

Table 5.4-20

RECURRING SPACECRAFT COSTS FOR TWO FLIGHTS
(In Millions of 1965 Dollars)

COST CATEGORY	DESIGN CONCEPT D
Science	1.40
Communications & Data Mgt.	1.82
Spacecraft Control	2.06
Attitude Control	0.07
Midcourse Propulsion	0.08
Electrical Power	5.20
Structure, Mech., Therm. & Shield	0.96
Spacecraft Checkout & Assembly	1.14
Subtotal Spacecraft Cost	12.73
RTG Fuel Cost @ \$1500/W_t	31.68
Total Spacecraft	44.41

Table 5.4-21

DESIGN CONCEPT A - COST INCREMENT FOR A THIRD FLIGHT
(In Millions of 1965 Dollars)

	Saturn IB/ Centaur/HEKS	Saturn V**
Recurring Spacecraft	\$22.20	\$44.41
Launch Vehicles	30.80	62.77
Launch Operations	6.50	7.50
Total	\$59.30	\$114.68
Total*	\$54.17	\$109.55

* The total cost increment for a third flight assuming that one of the ground test models is used.

** Assuming a single launch vehicle with dual payload.

5.4.7 Reference

5.4-1 Tooley, J. R., and Sarrafian, G. P., "A Programmable Spacecraft Data Handling System," 1964 PGSET Symposium Record, Las Vegas, Nevada, October 6-9, 1964, pp 2-C-1 through 2-C-12.

APPENDIX A

MISSION MAPS

The basic working charts which were used to determine mission requirements are the hybrid digital/contour mission maps which are shown in Figures A-1 through A-16. Although only four trajectory parameters (geocentric injection energy, departure asymptote declination, and departure and arrival hyperbolic excess speeds) are shown in these high-resolution maps, low-resolution maps of 11 other mission parameters that are adequate for most mission planning purposes have been published in Reference 2.2-1. The parameters contained herein are those for which high-resolution maps were deemed necessary.

In the first set of maps (Figures A-1 through A-8), only injection-energy contours were drawn. Since the digital values of the trajectory parameters are retained in this type of display, asymptote declination contours (or additional energy contours) can be drawn on the map for any desired value of the parameter. For reference, the injection energy contours were transferred from the first set of maps (Figures A-1 through A-8) to the second set of maps (Figures A-9 through A-16). Because injection energy is directly related to hyperbolic excess speeds, the injection energy contours which were transferred to the hyperbolic excess speed maps also represent contours of constant departure hyperbolic excess speed, albeit the contours do not represent round-number values of hyperbolic excess speed. The dashed contours on Figures A-9 through A-16 represent constant values of the arrival hyperbolic excess speed.

For convenience, curves of communication distance and Earth elongation angle as functions of Jupiter arrival date are included in Figures A-1 through A-8. In like manner, interplanetary flight times have been indicated in the margins of Figures A-9 through A-16.

The trajectory data contained in Figures A-1 through A-16 are based on heliocentric conic calculations and mean planet orbit elements. As pointed out in paragraph 2.2.2, the Jupiter arrival dates corresponding to heliocentric conic trajectory computations can be in error by as much as 20 days. To obtain more accurate arrival dates and flight times, the corrections described in the cited paragraph should be applied.

INJECTION ENERGY AND ASYMPTOTE DECLINATION MISSION MAP, 1973 LAUNCH

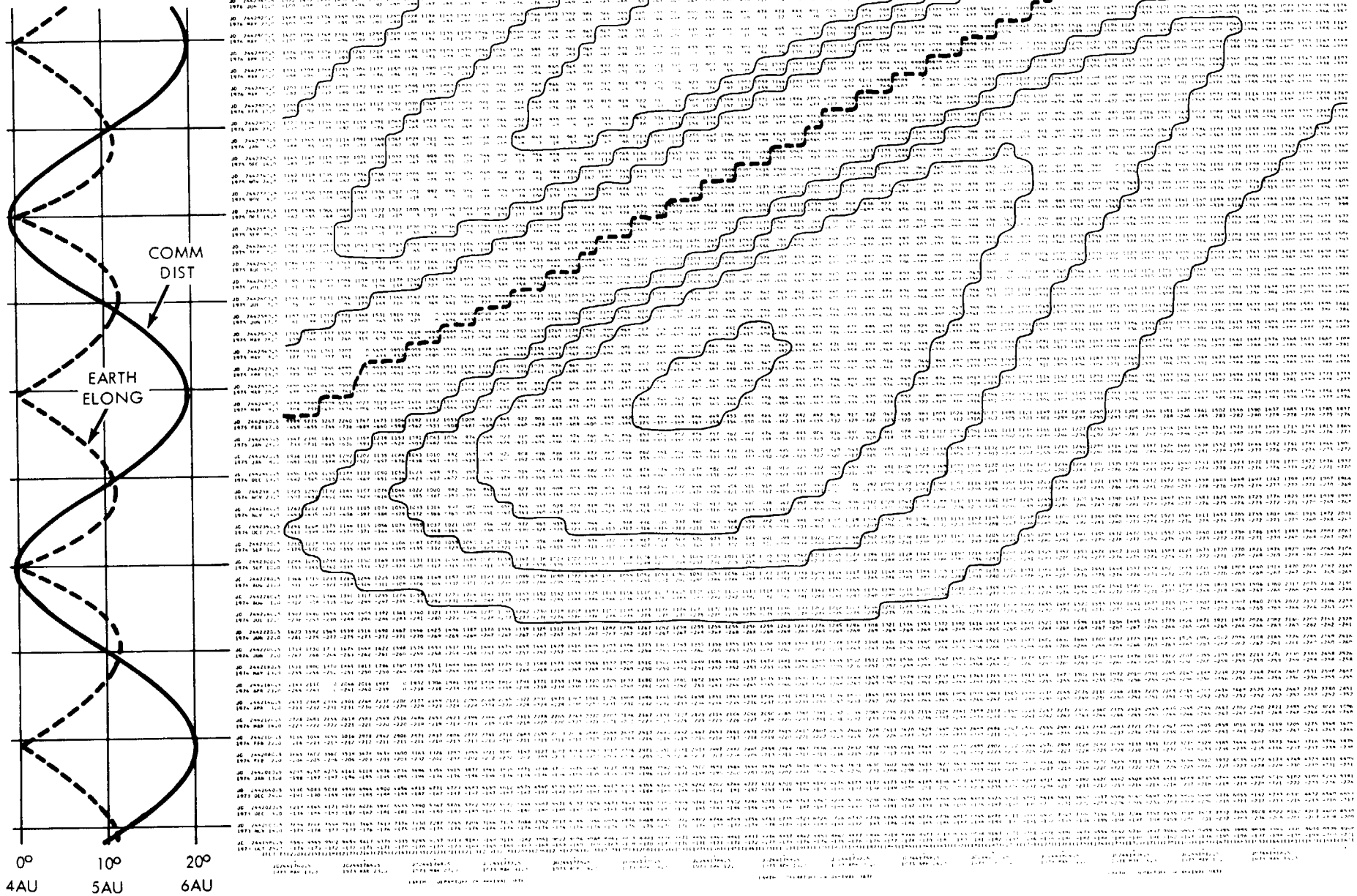

FIGURE A-1

INJECTION ENERGY AND ASYMPTOTE DECLINATION MISSION MAP, 1974 LAUNCH

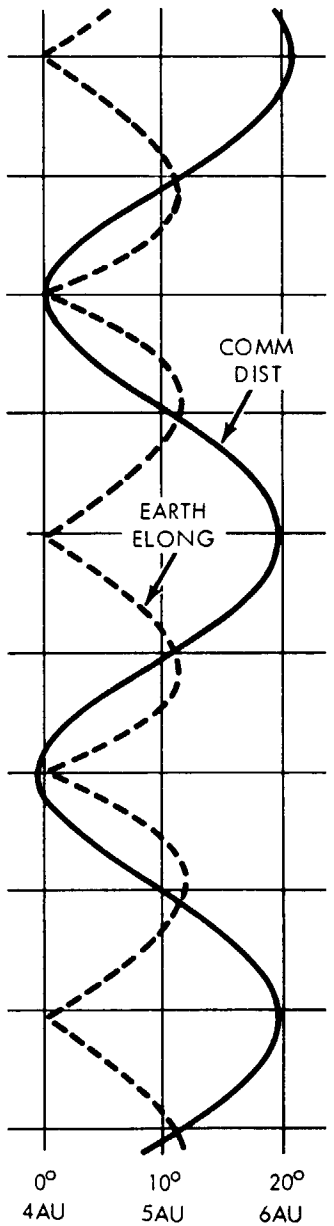

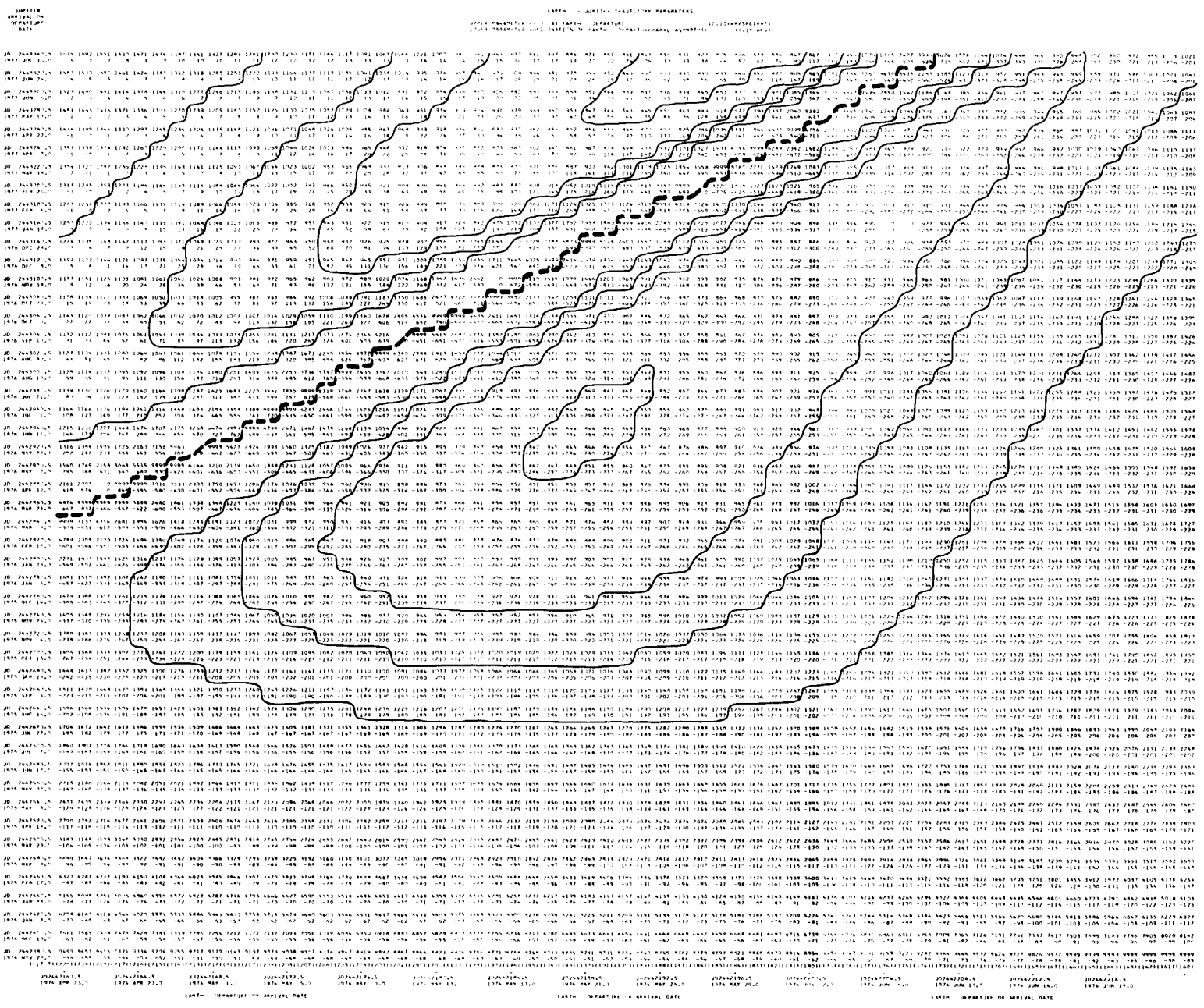

FIGURE A-2

INJECTION ENERGY AND ASYMPTOTE DECLINATION MISSION MAP, 1975 LAUNCH

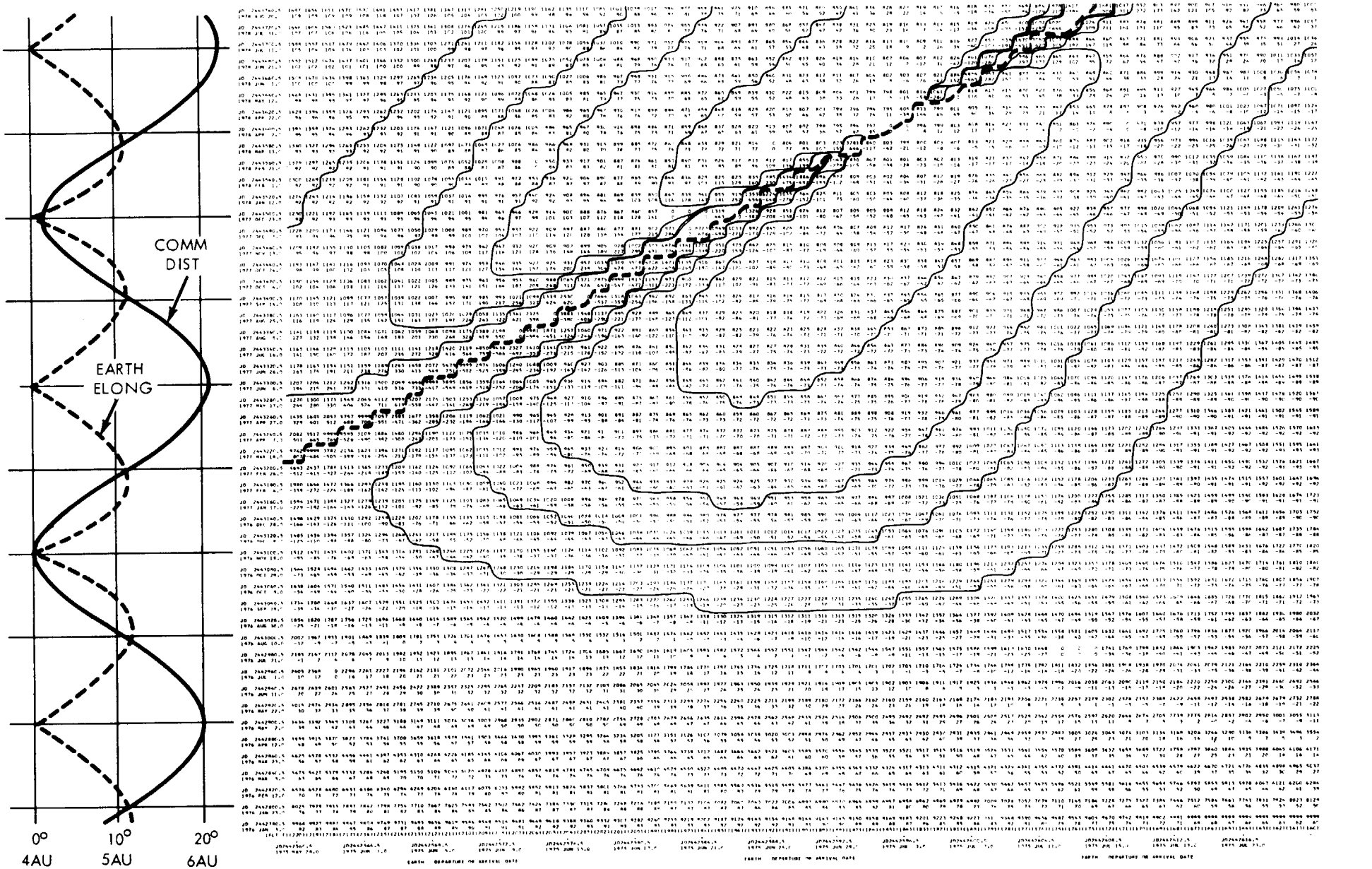

FIGURE A-3

INJECTION ENERGY AND ASYMPTOTE DECLINATION MISSION MAP, 1976 LAUNCH

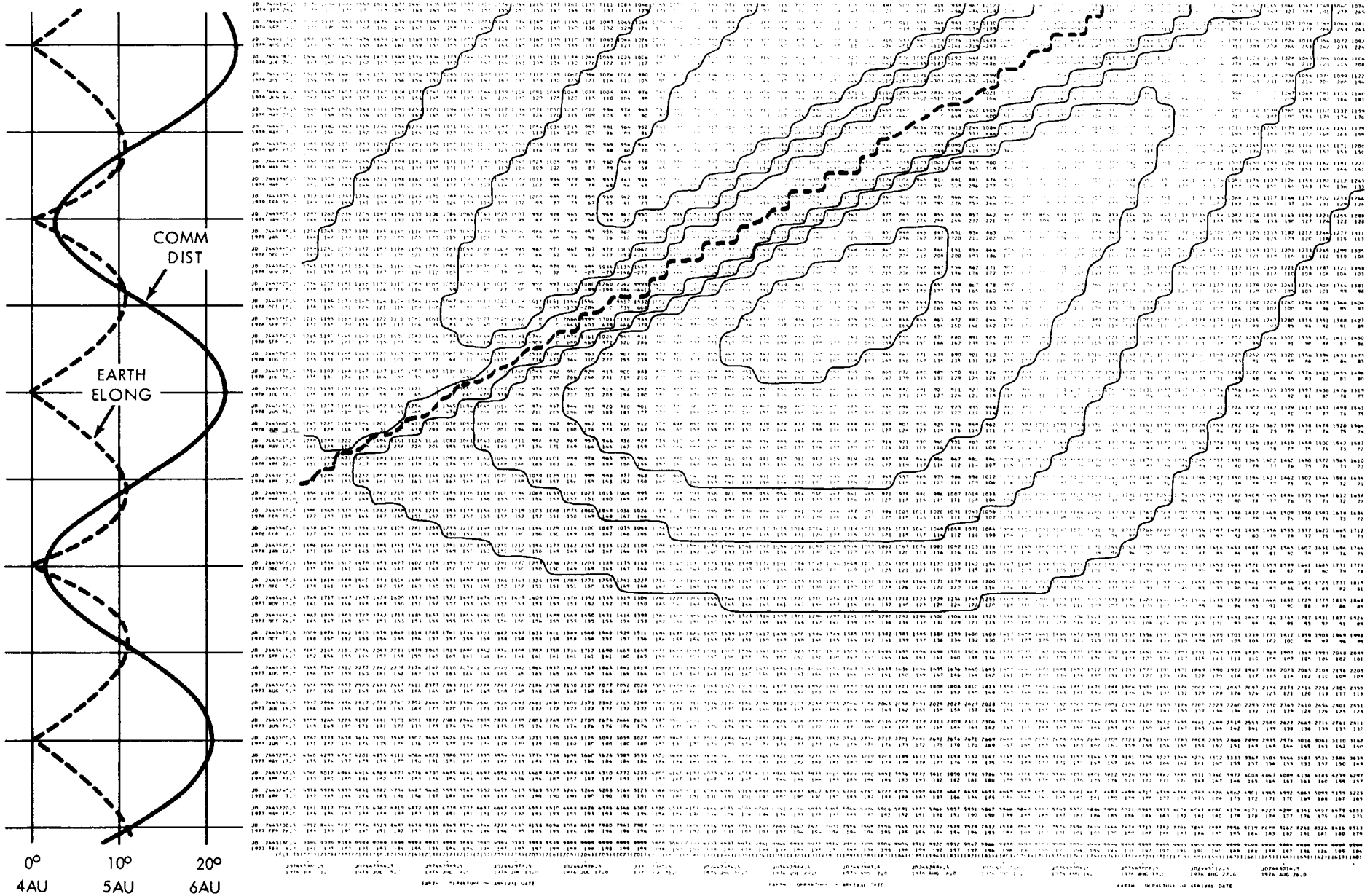

FIGURE A-4

INJECTION ENERGY AND ASYMPTOTE DECLINATION MISSION MAP, 1977 LAUNCH

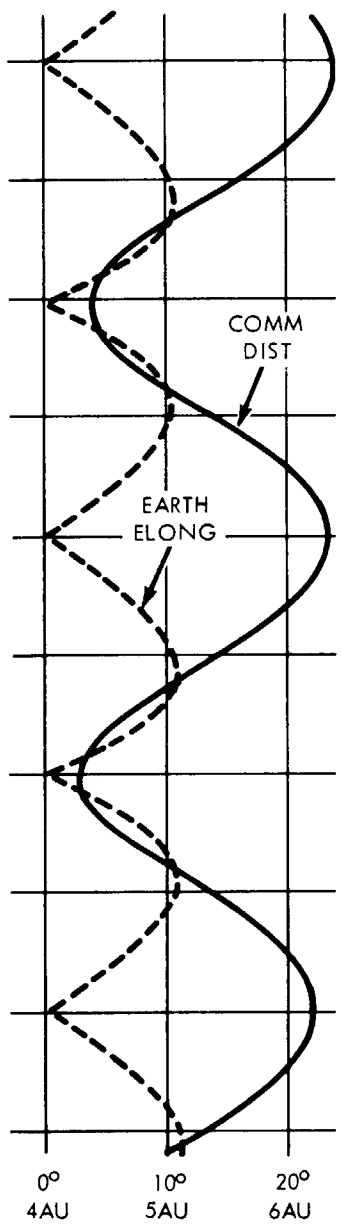

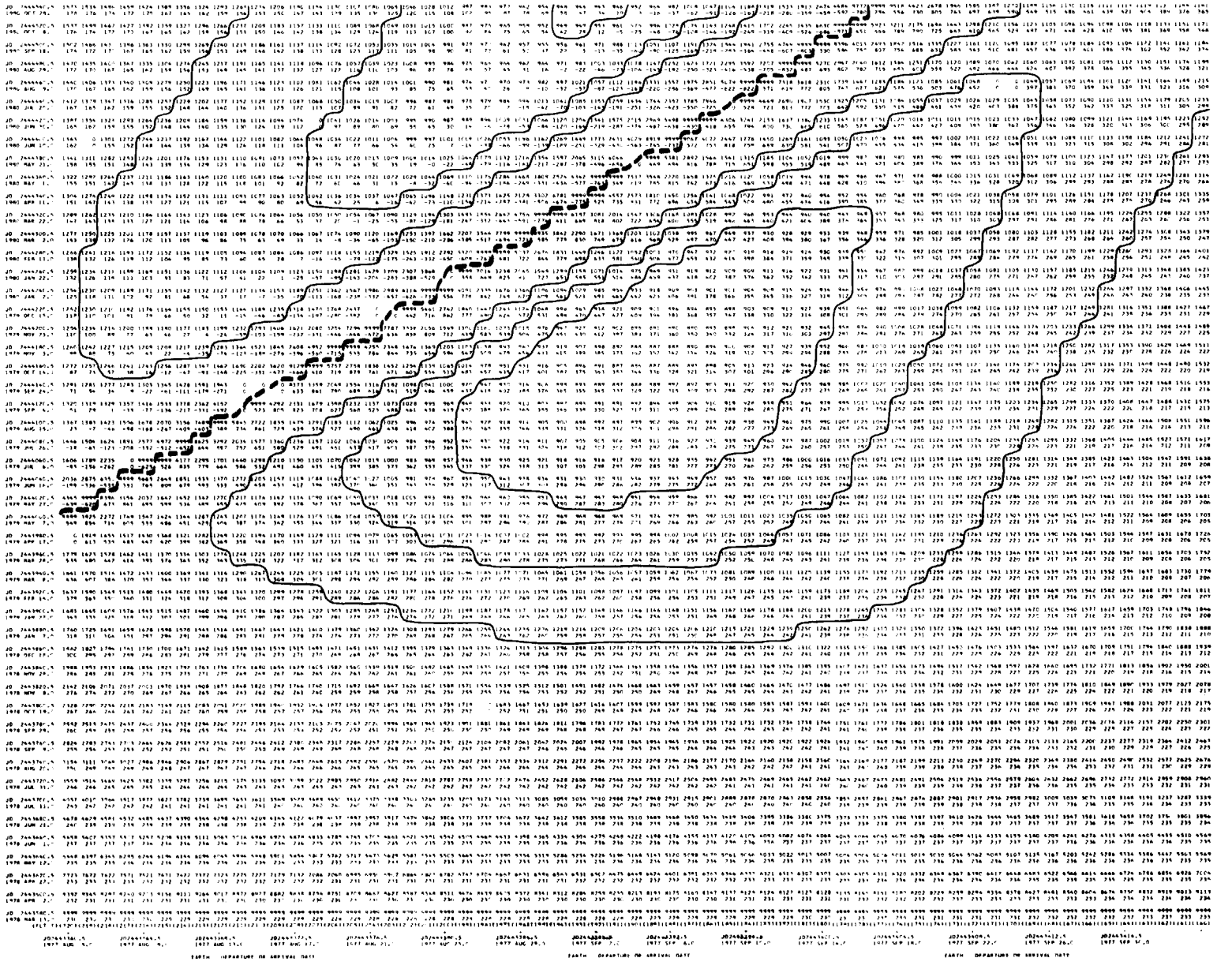

FIGURE A-5

INJECTION ENERGY AND ASYMPTOTE DECLINATION MISSION MAP, 1978 LAUNCH

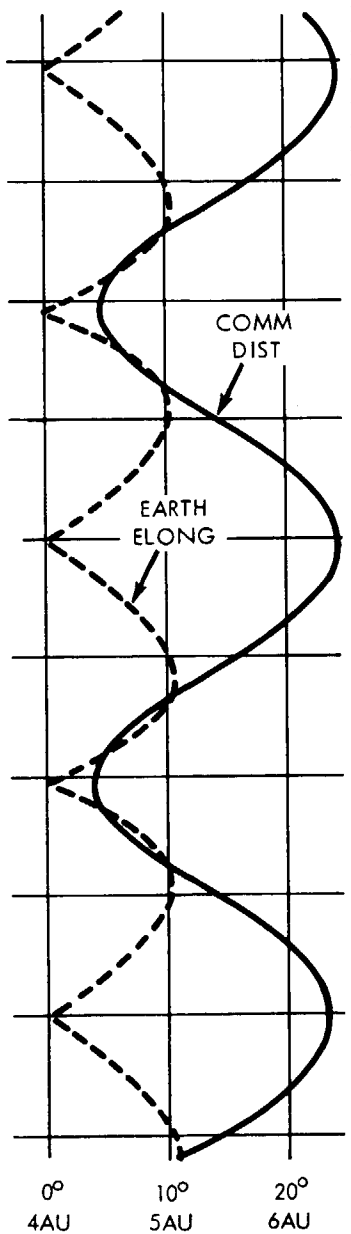

FIGURE A-6

INJECTION ENERGY AND ASYMPTOTE DECLINATION MISSION MAP, 1979 LAUNCH

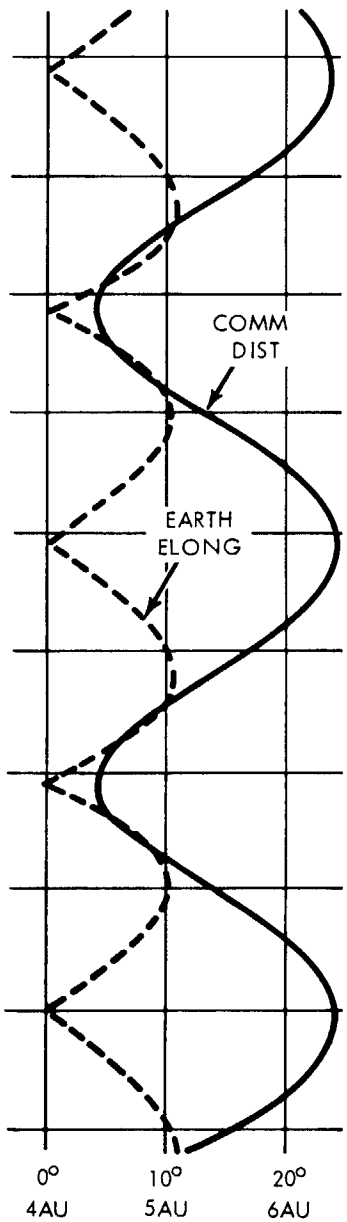

FIGURE A-7

INJECTION ENERGY AND ASYMPTOTE DECLINATION MISSION MAP, 1980 LAUNCH

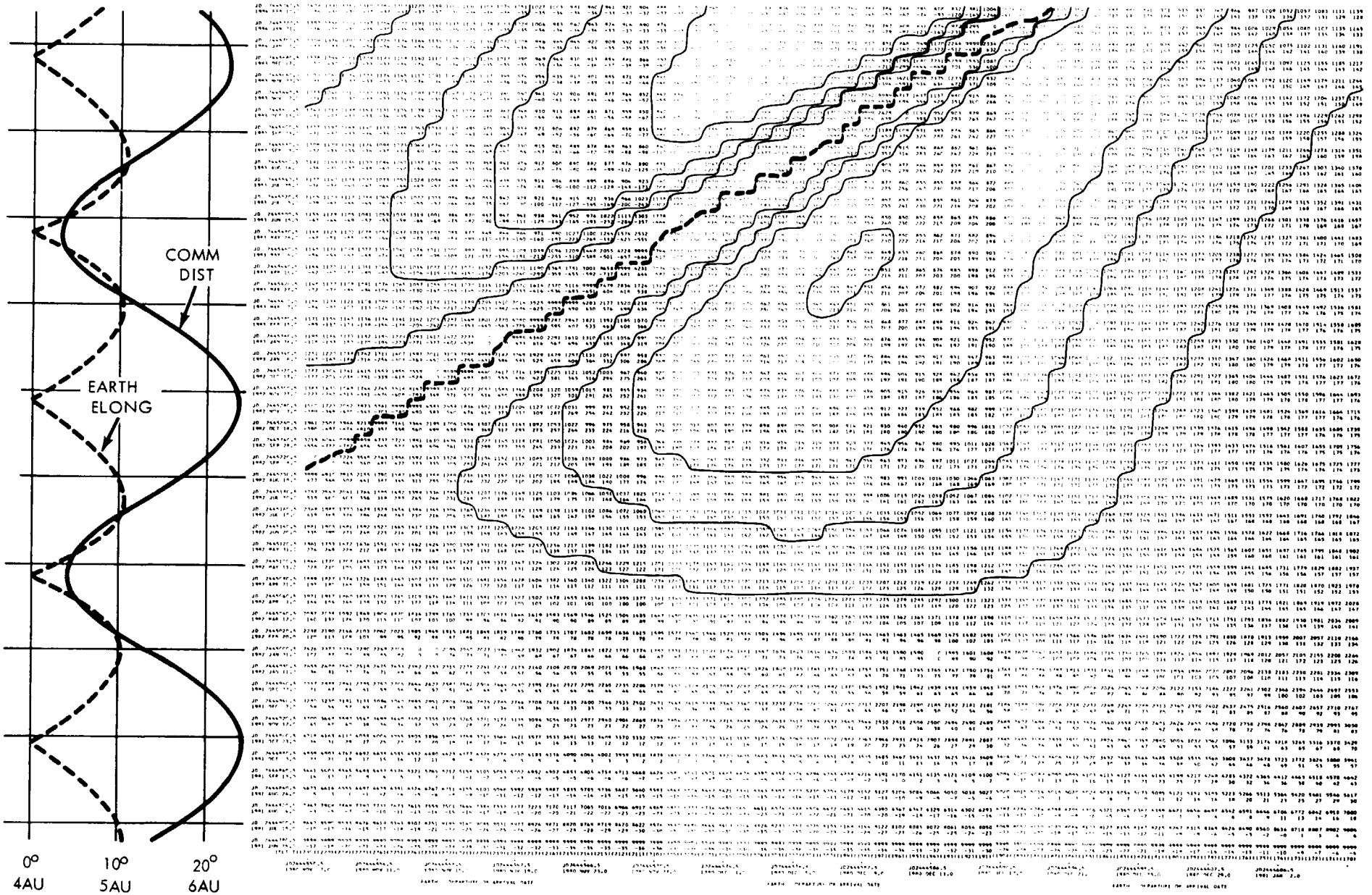

FIGURE A-8

HYPERBOLIC EXCESS SPEED MISSION MAP, 1973 LAUNCH

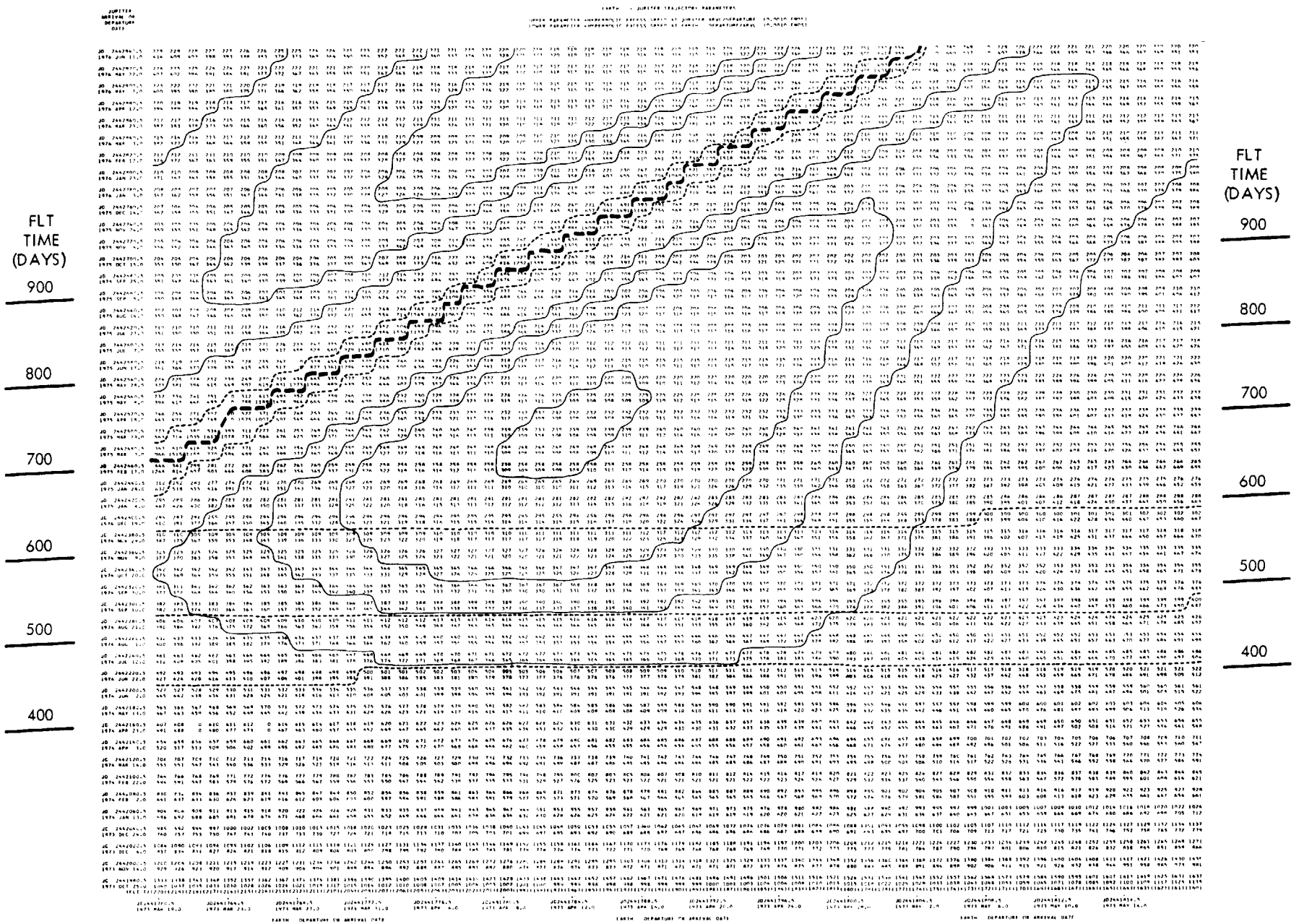

FIGURE A-9

HYPERBOLIC EXCESS SPEED MISSION MAP, 1974 LAUNCH

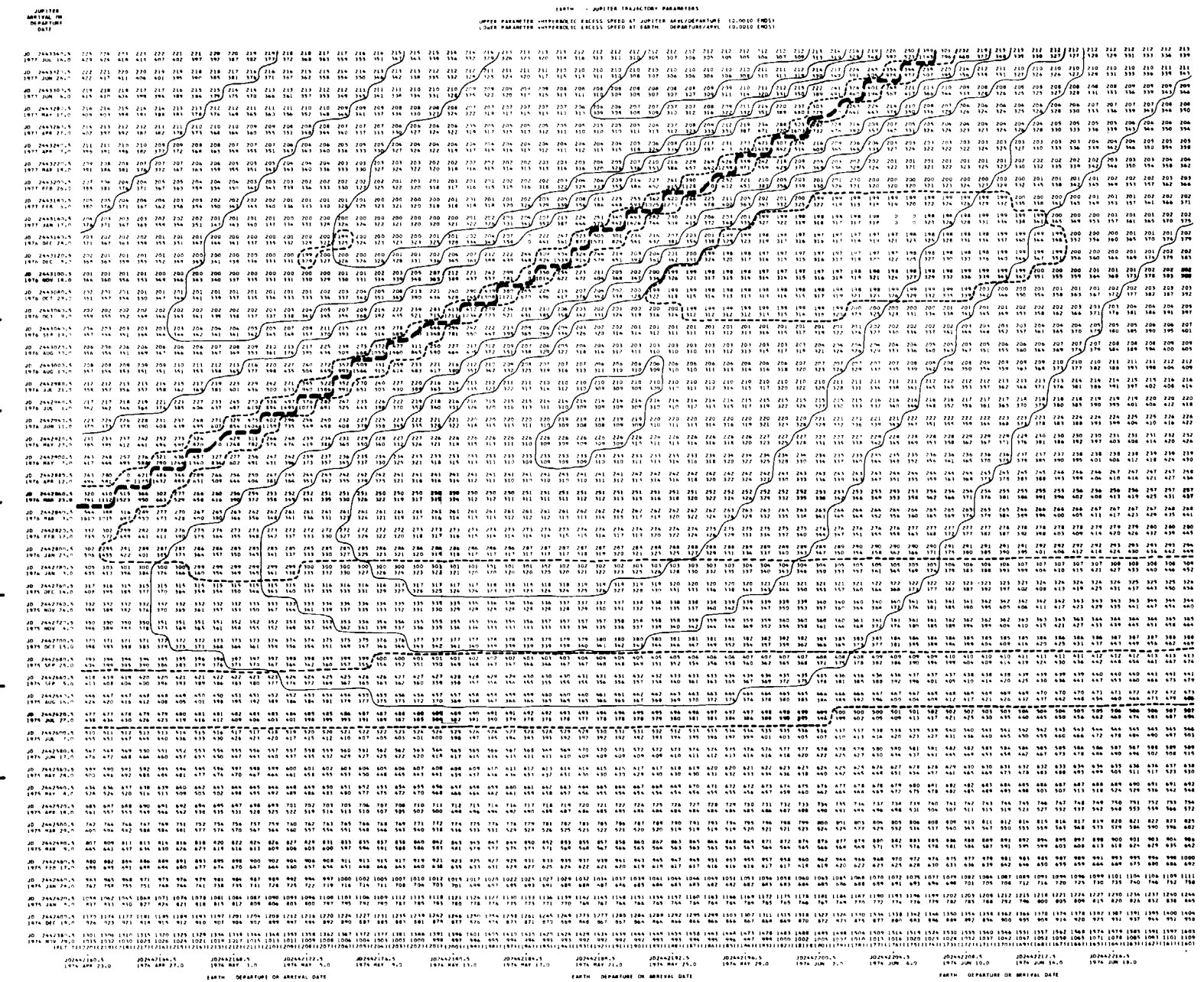

FIGURE A-10

HYPERBOLIC EXCESS SPEED MISSION MAP, 1975 LAUNCH

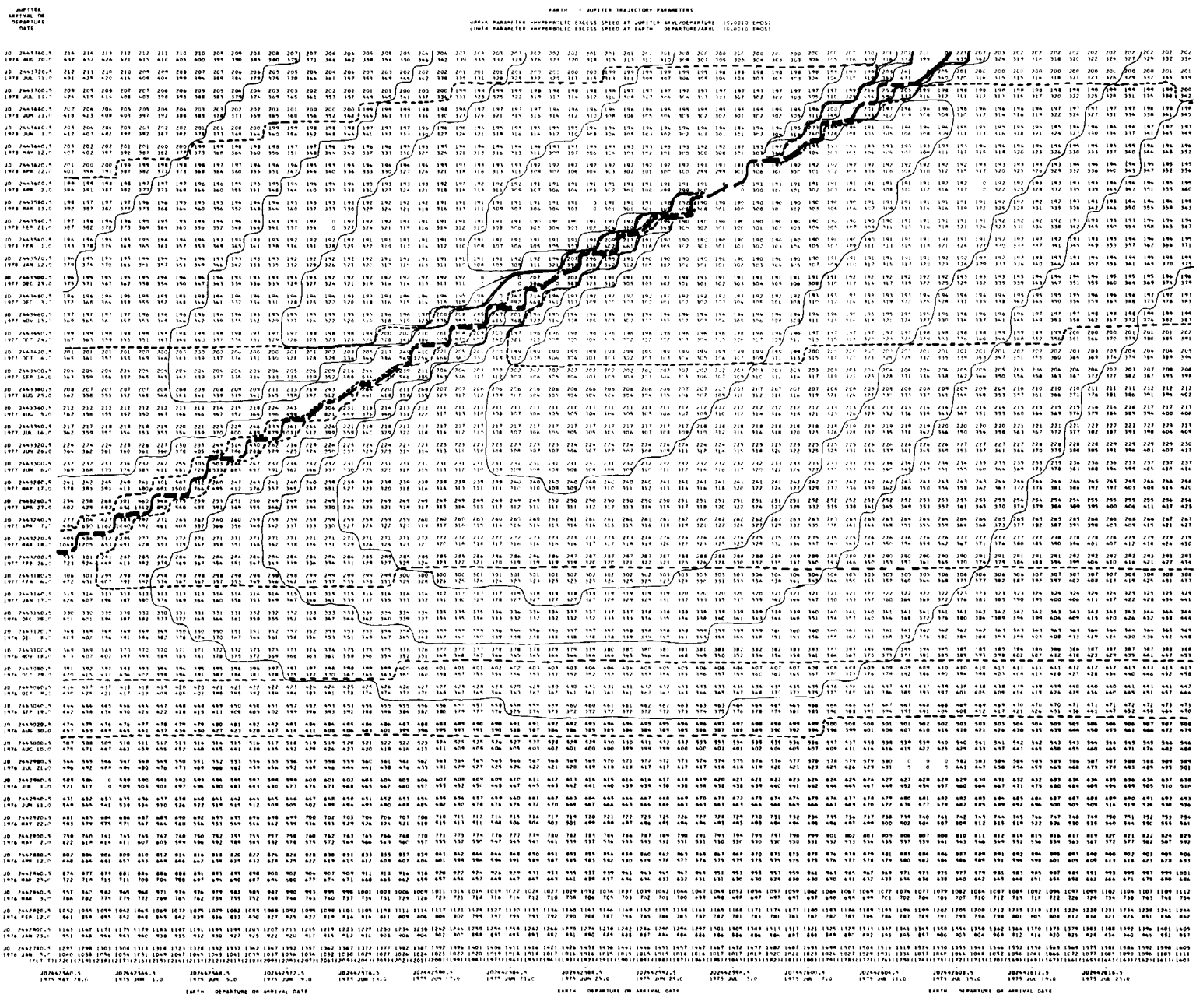

FIGURE A-11

HYPERBOLIC EXCESS SPEED MISSION MAP, 1976 LAUNCH

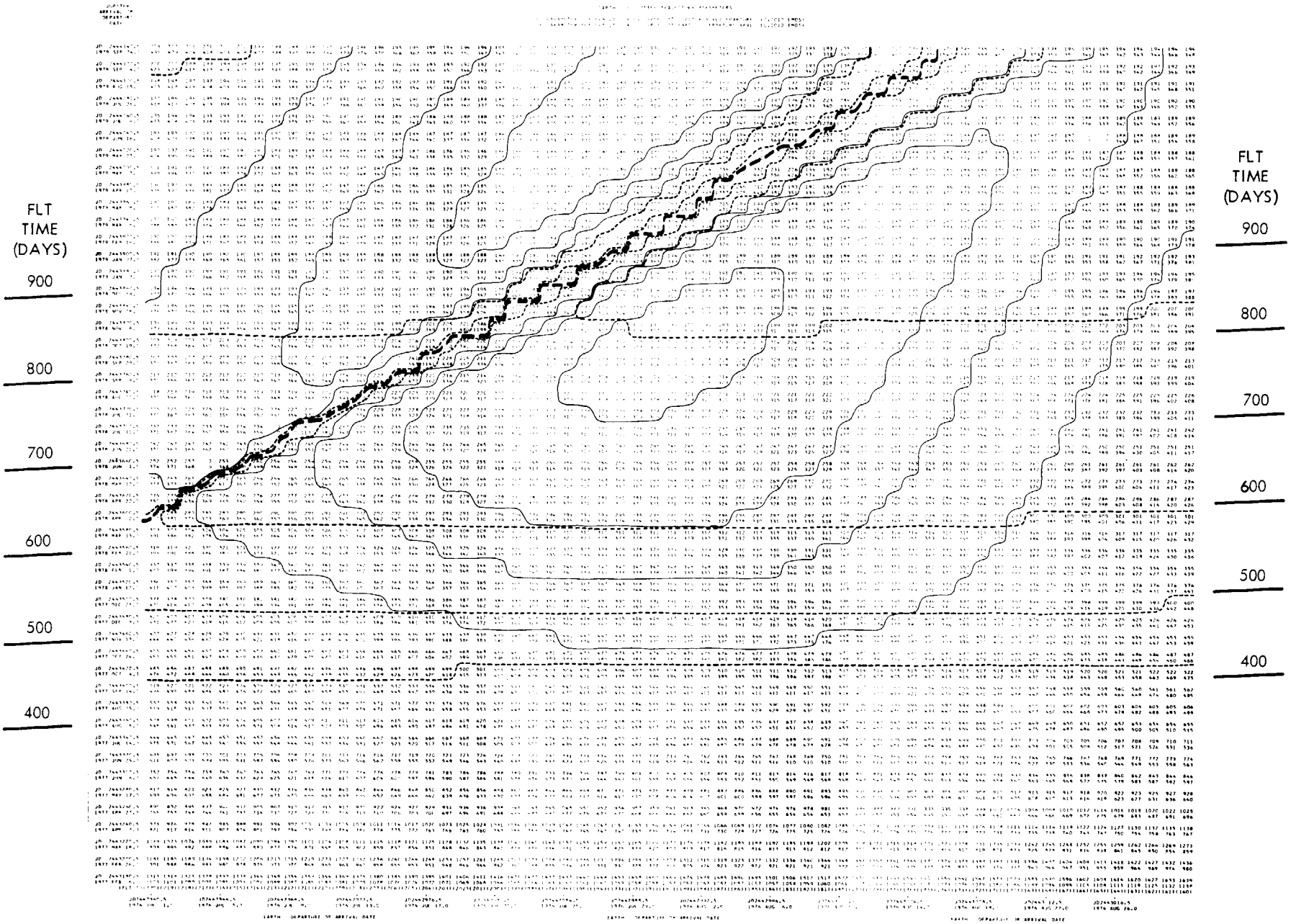

FIGURE A-12

HYPERBOLIC EXCESS SPEED MISSION MAP, 1977 LAUNCH

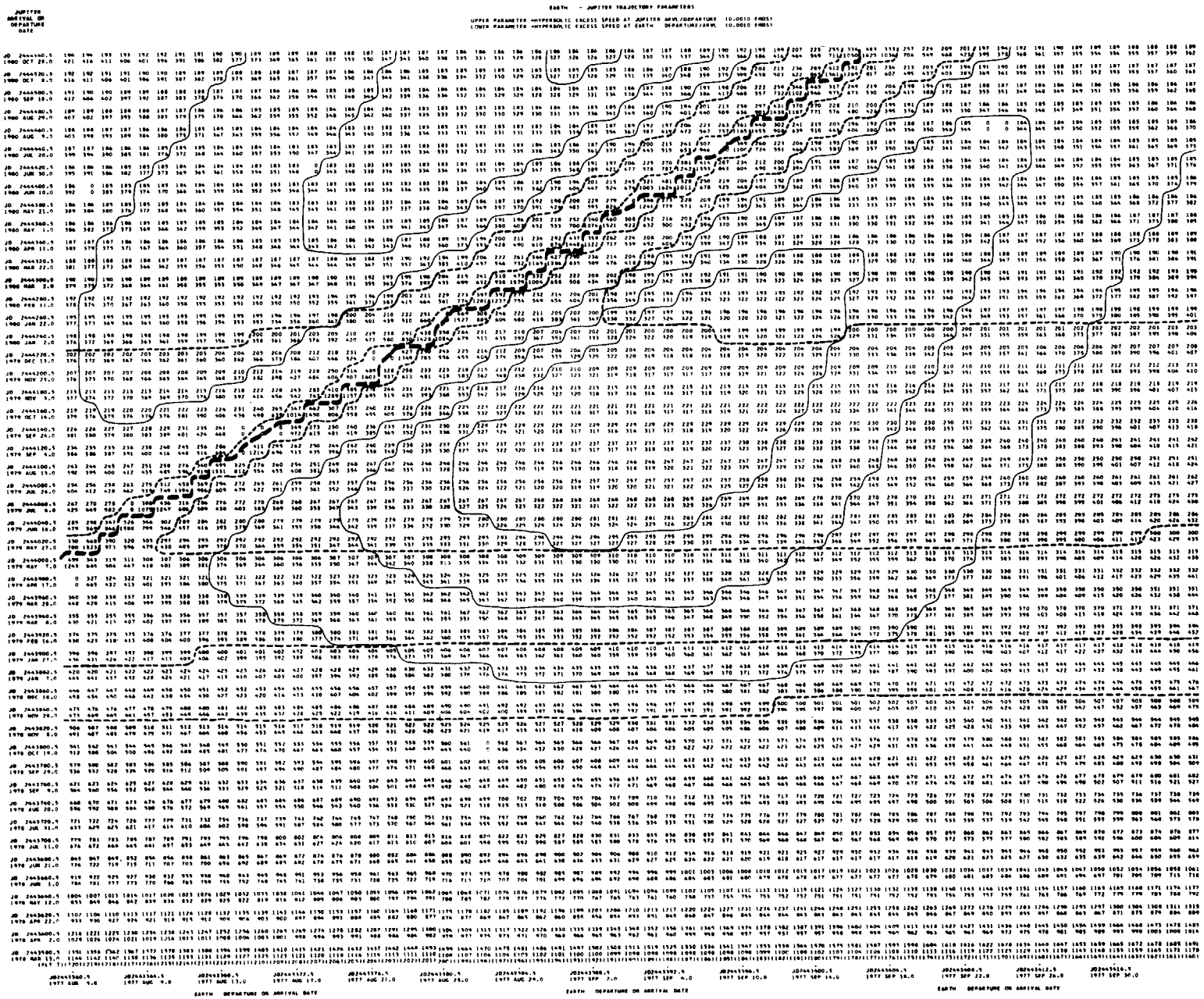

FIGURE A-13

HYPERBOLIC EXCESS SPEED MISSION MAP, 1978 LAUNCH

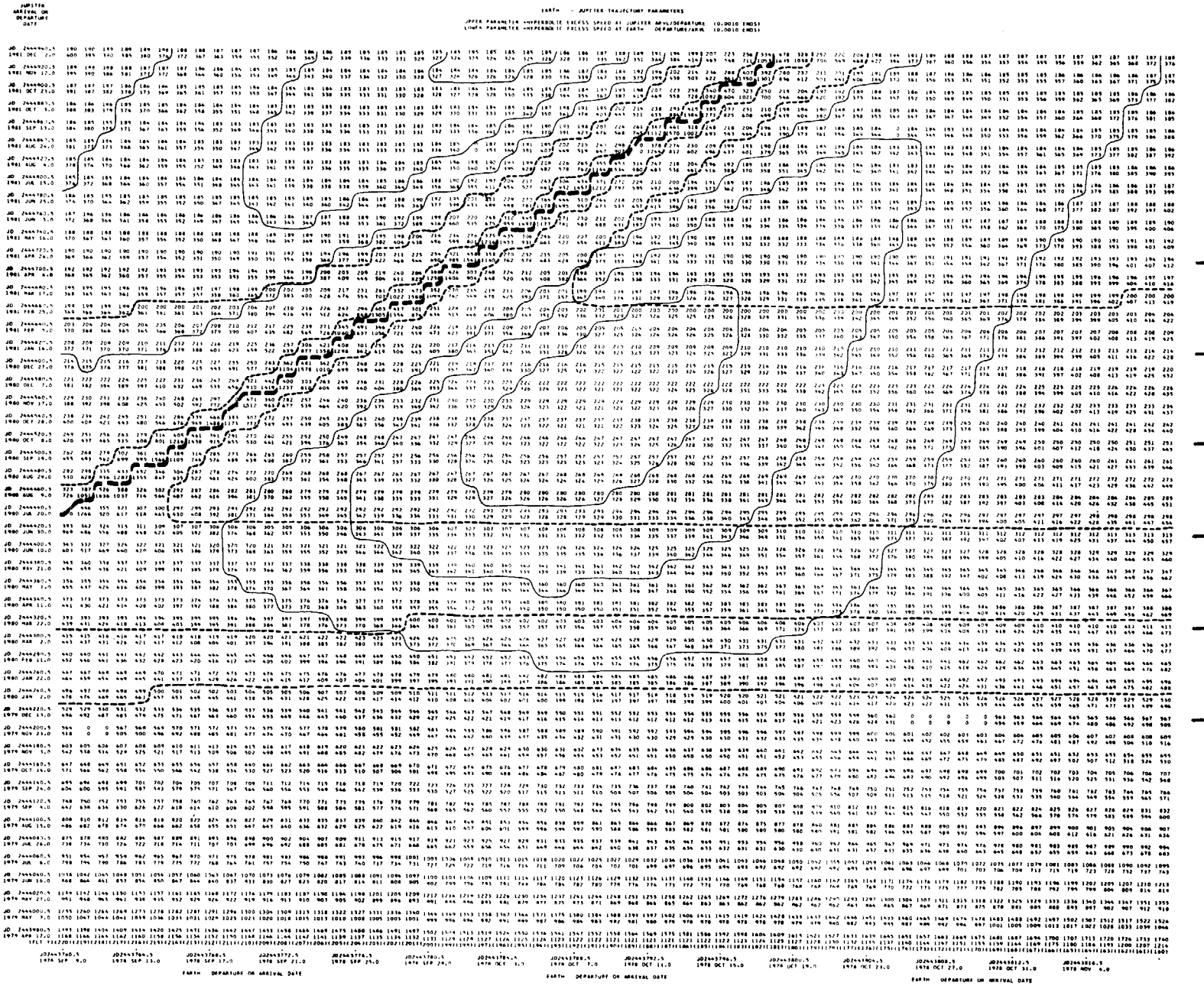

FIGURE A-14

HYPERBOLIC EXCESS SPEED MISSION MAP, 1979 LAUNCH

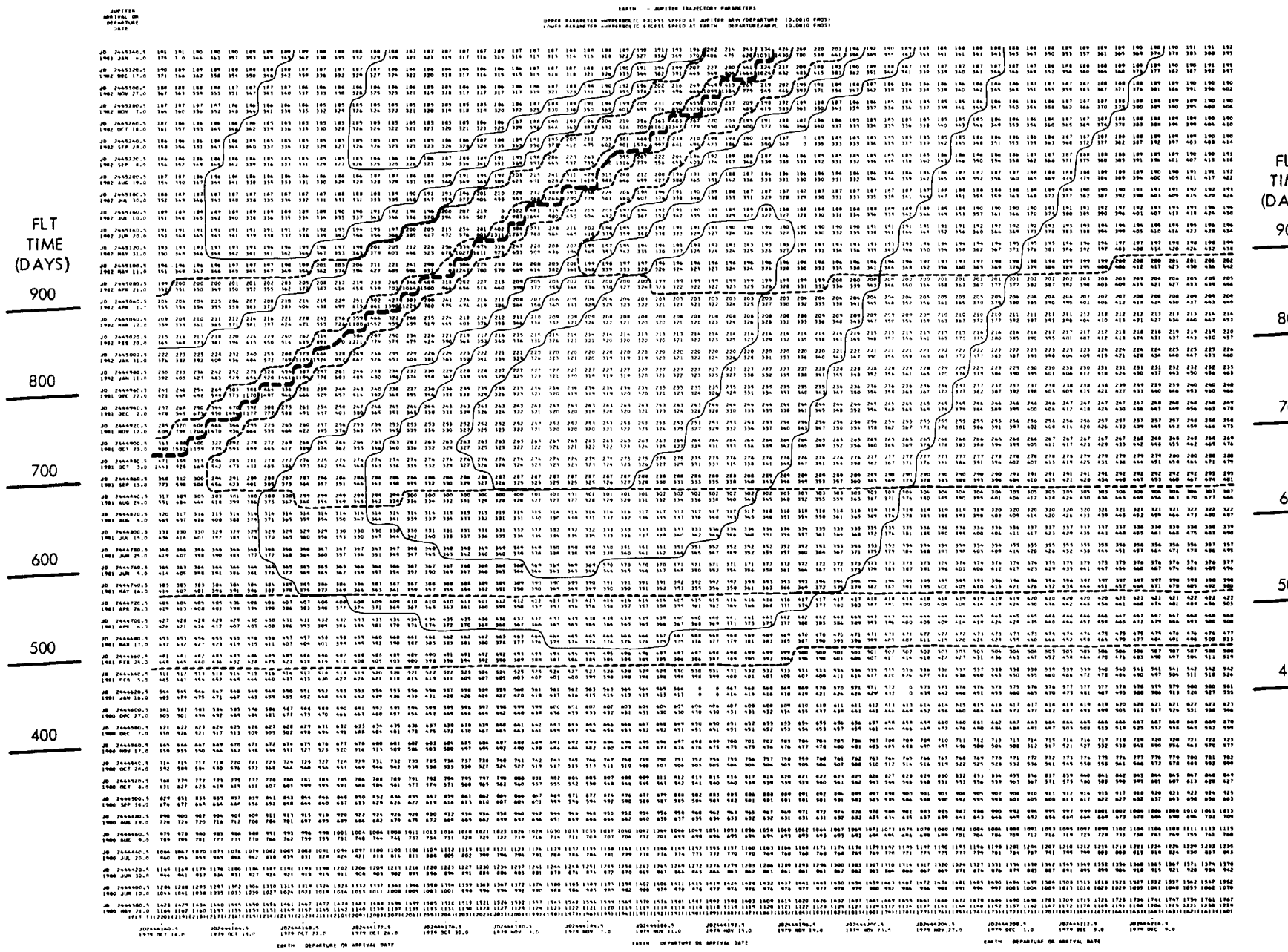

FIGURE A-15

HYPERBOLIC EXCESS SPEED MISSION MAP, 1980 LAUNCH

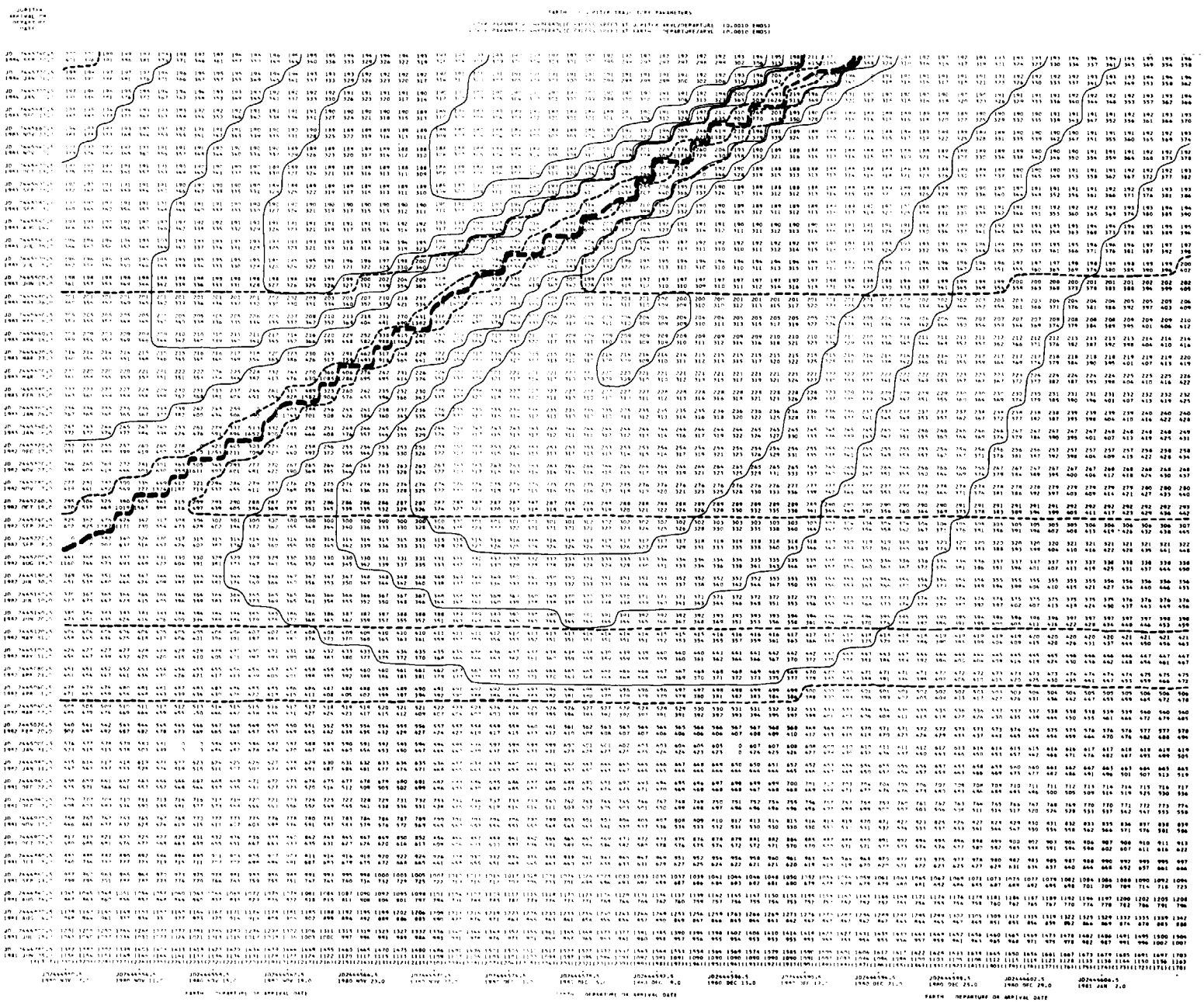

FIGURE A-16

APPENDIX B

TARGETING CHARTS

Three sets of digital/contour targeting charts are contained in this appendix, one set for each of three Earth-Jupiter trajectories having approximately optimal launch dates in 1976 and nominal interplanetary flight times of 582, 498, and 413 days. The charts are essentially self-explanatory. The B·T axis is normal to the approach asymptote and parallel to the ecliptic plane. The following definitions apply to the abbreviations used in the figure titles:

Abbreviations	Definition
PEH	Post-Encounter Heliocentric
CPJ	Canopus-Probe - Near Limb of Jupiter Angle
EPJ	Earth-Probe - Near Limb of Jupiter Angle
SPJ	Sun-Probe - Near Limb of Jupiter Angle

The 10 degree value for CPJ and SPJ appearing in some charts represents the half-angle which was assumed for the appropriate sensors' fields of view in this study. The Earth (solar) immersion and emersion latitudes, respectively, are the latitudes at which the spacecraft-Earth (-Sun) line touches Jupiter's surface upon entry into and departure from the occultation zone. A spherical model of Jupiter was used in the trajectory computations. Since Jupiter's oblateness is actually very pronounced, the occultation data should be regarded as only approximate.

582-DAY FLIGHT TARGETING CHART: TIME IN CPJ ≤ 10° ZONE

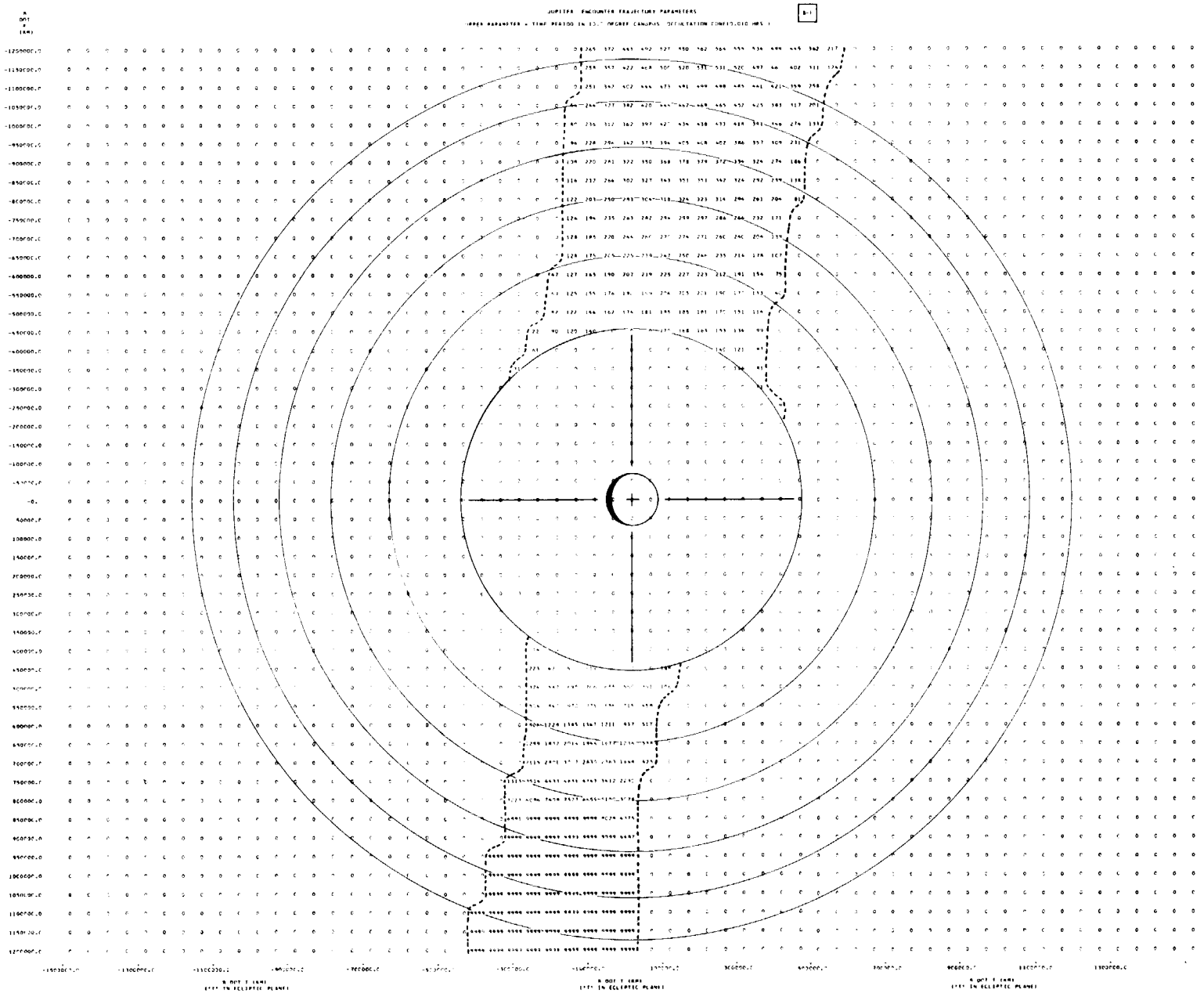

FIGURE B-1

582-DAY FLIGHT TARGETING CHART: TIME IN SPJ ≤ 10⁰ ZONE

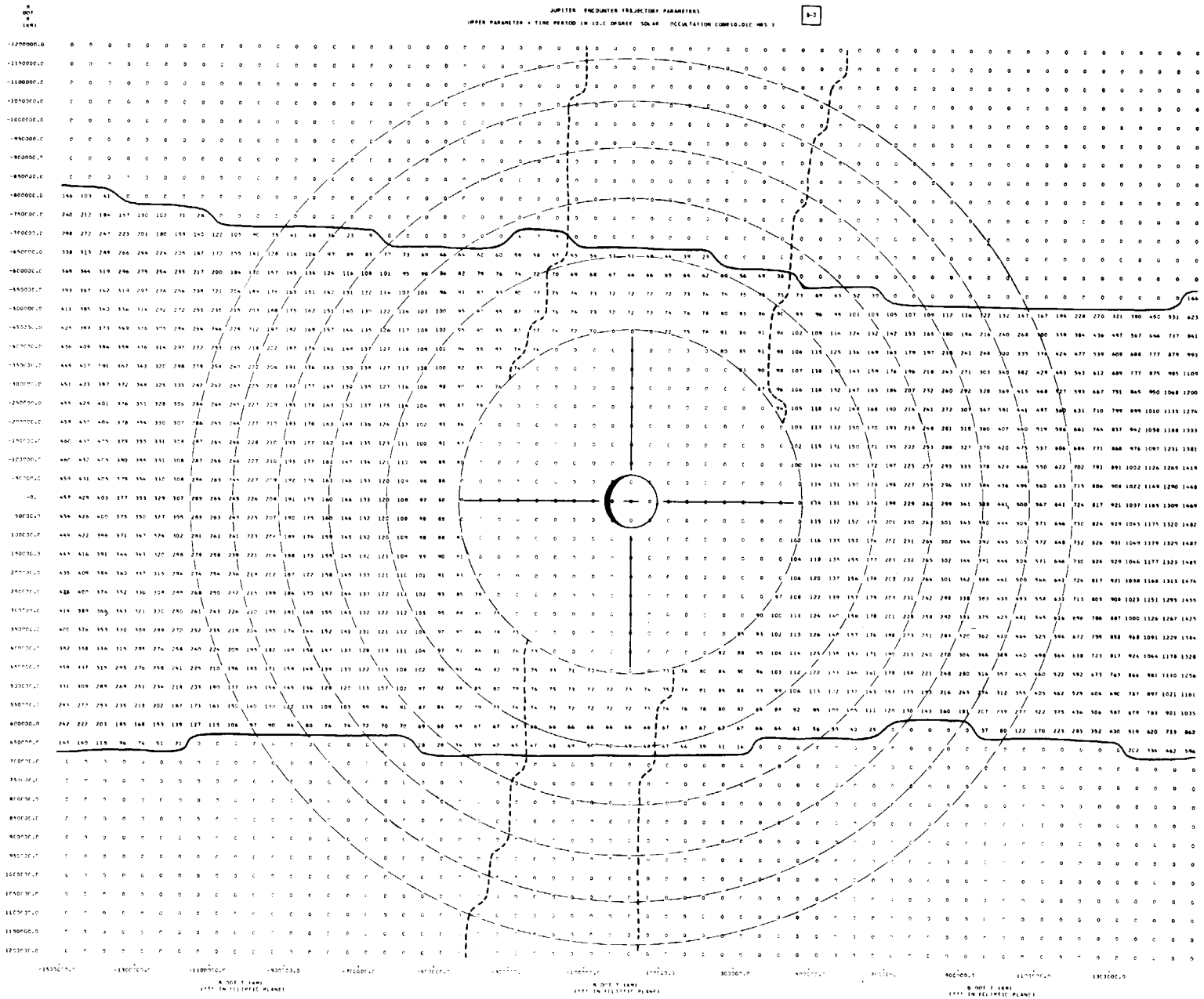

FIGURE B-2

582-DAY FLIGHT TARGETING CHART: TIME IN SPJ ≤ 0° ZONE

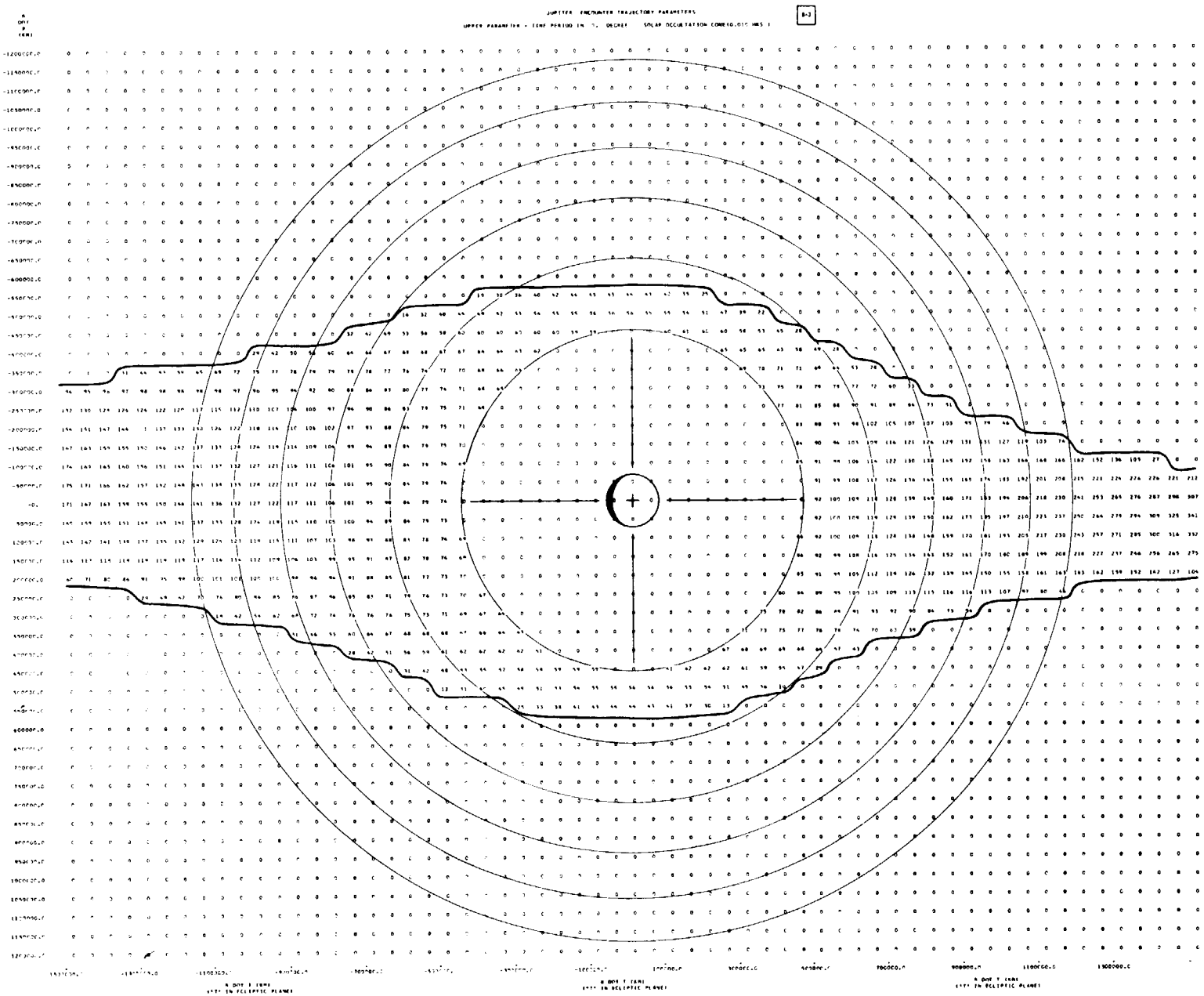

FIGURE B-3

582-DAY FLIGHT TARGETING CHART: TIME IN EPJ ≤ 0° ZONE

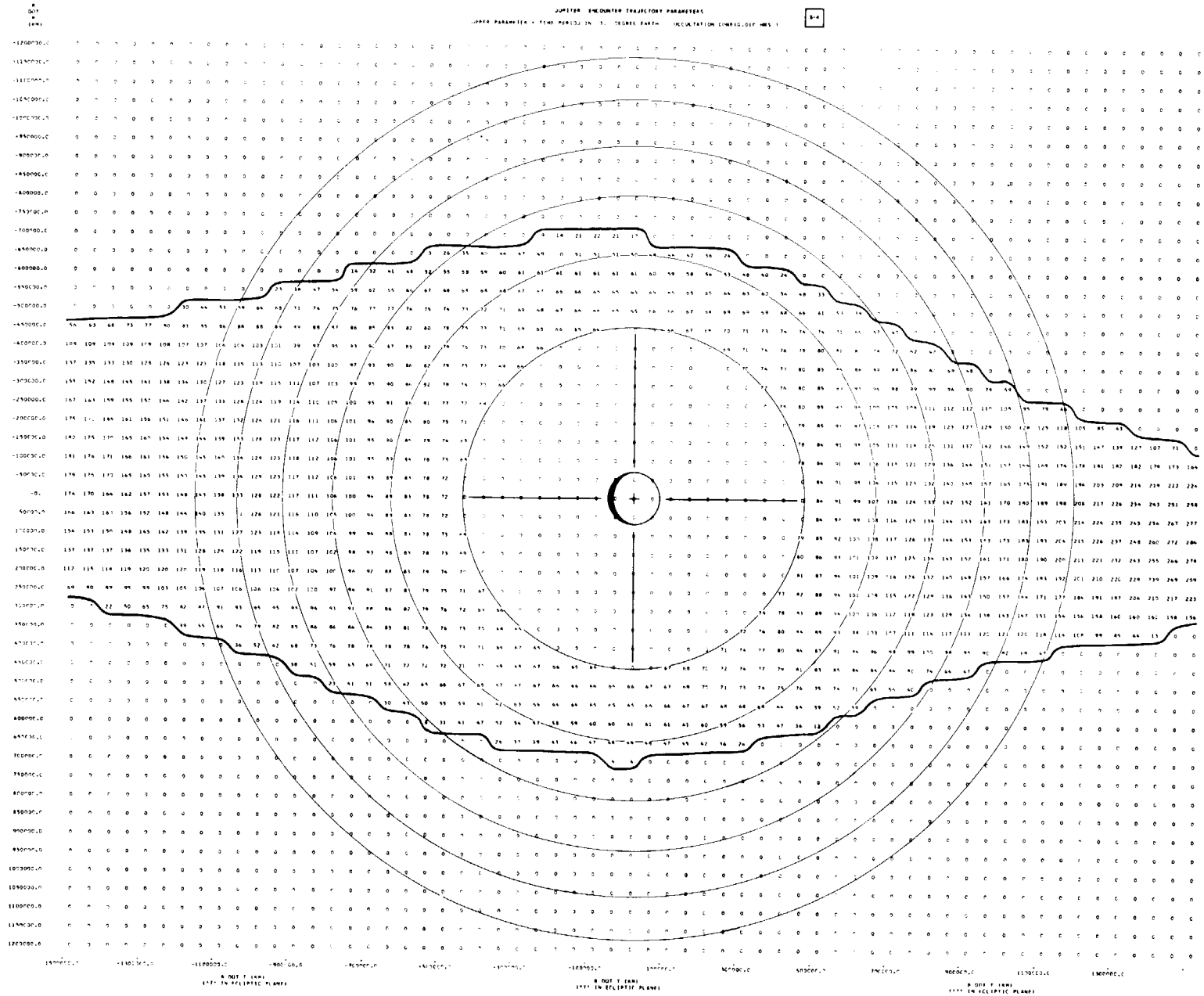

FIGURE B-4

582-DAY FLIGHT TARGETING CHART: SOLAR IMMERSION AND EMERSION LATITUDES

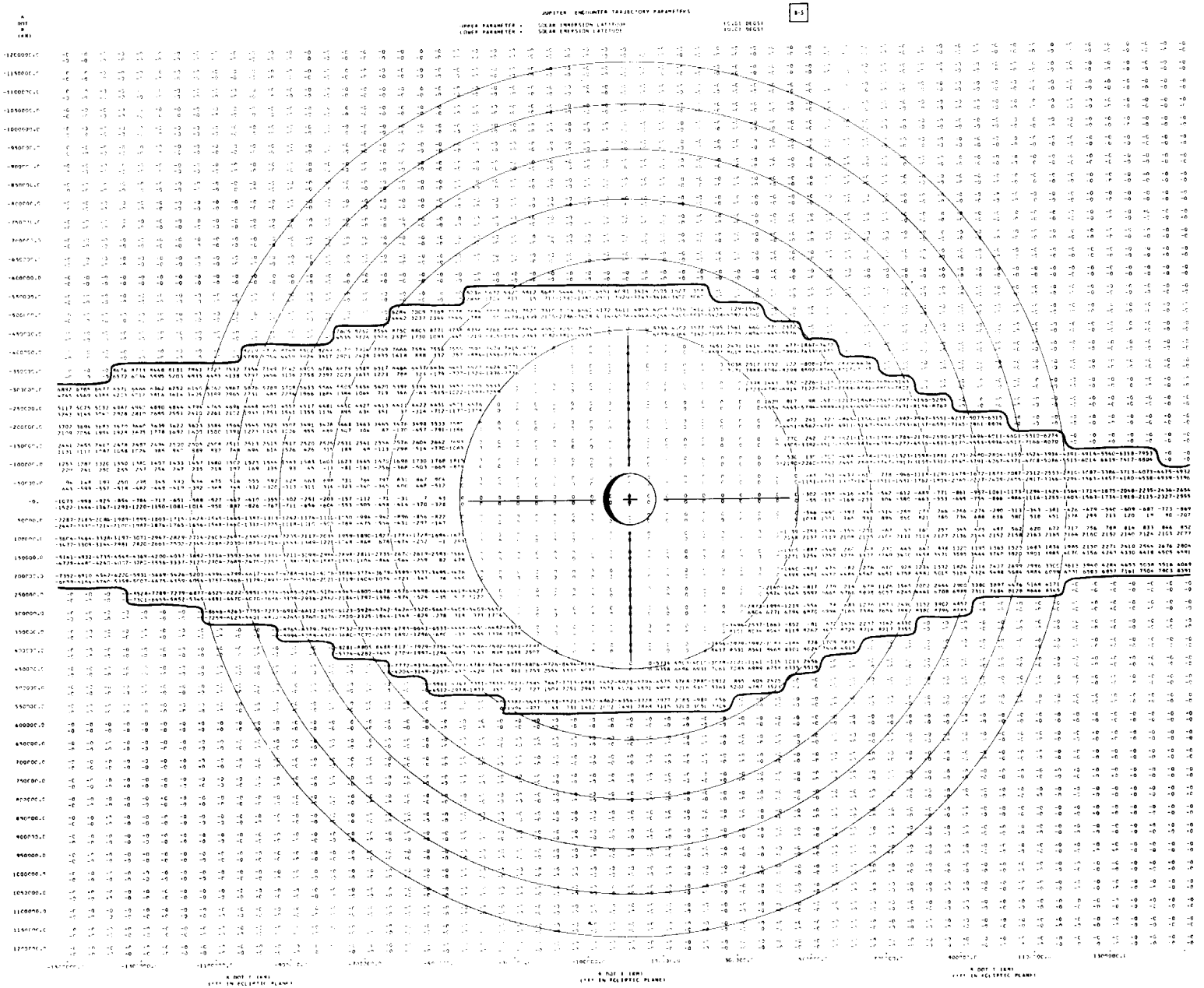

FIGURE B-5

582-DAY FLIGHT TARGETING CHART: EARTH IMMERSION AND EMERSION LATITUDES

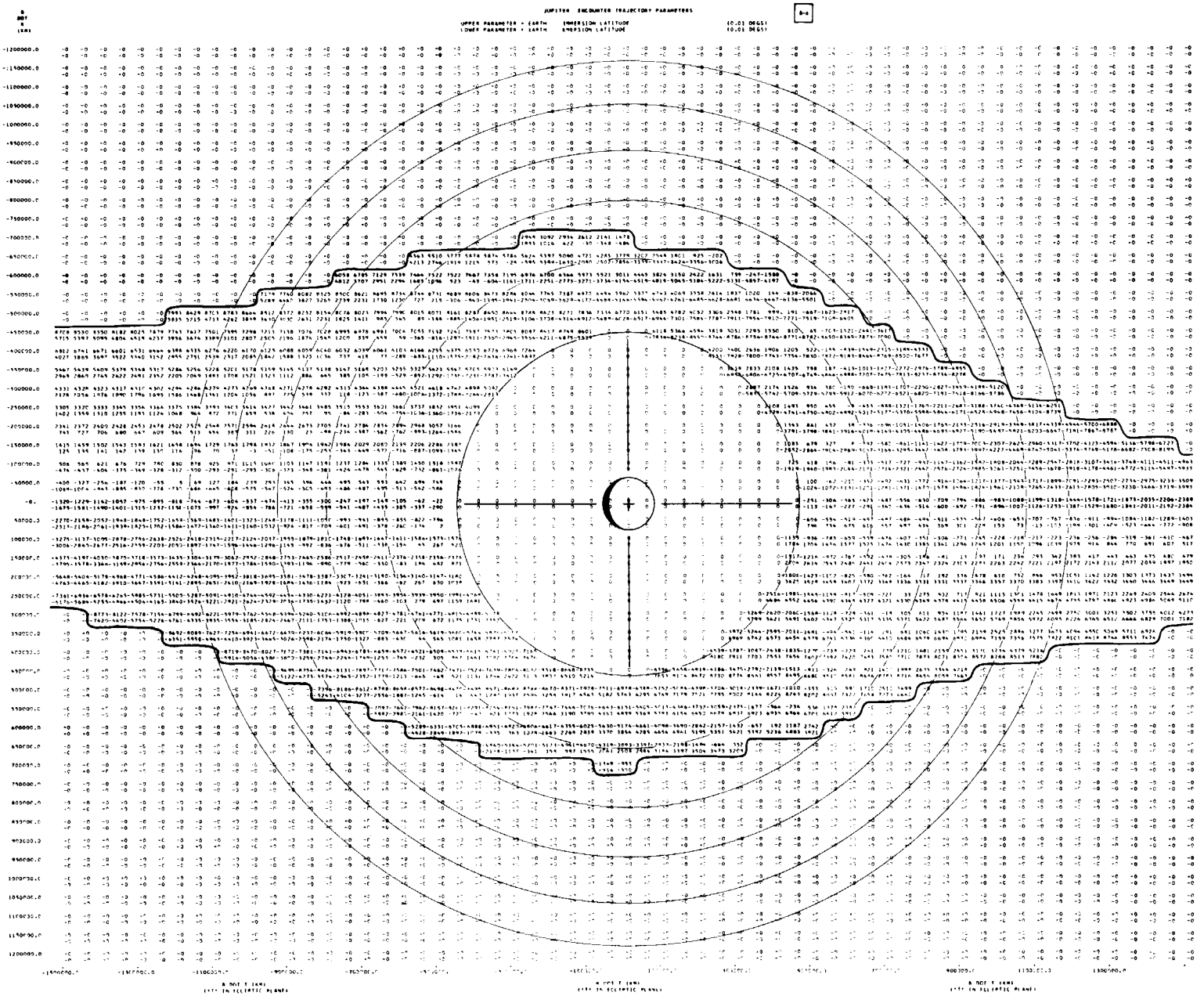

FIGURE B-6

582-DAY FLIGHT TARGETING CHART: ECCENTRICITY AND INCLINATION OF PEH TRAJECTORY

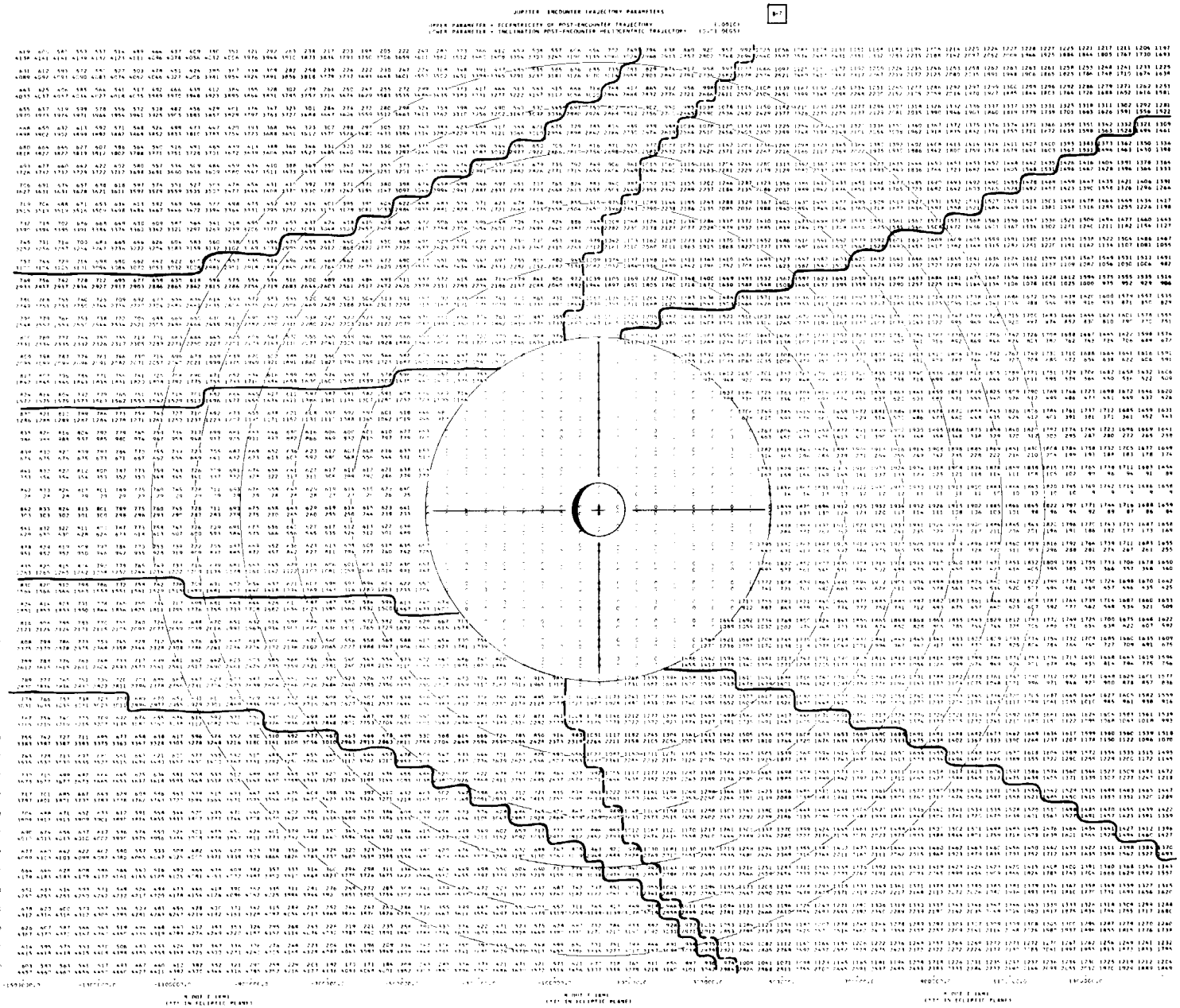

FIGURE B-7

582-DAY FLIGHT TARGETING CHART: PERIHELION AND APHELION DISTANCES OF PEH TRAJECTORY

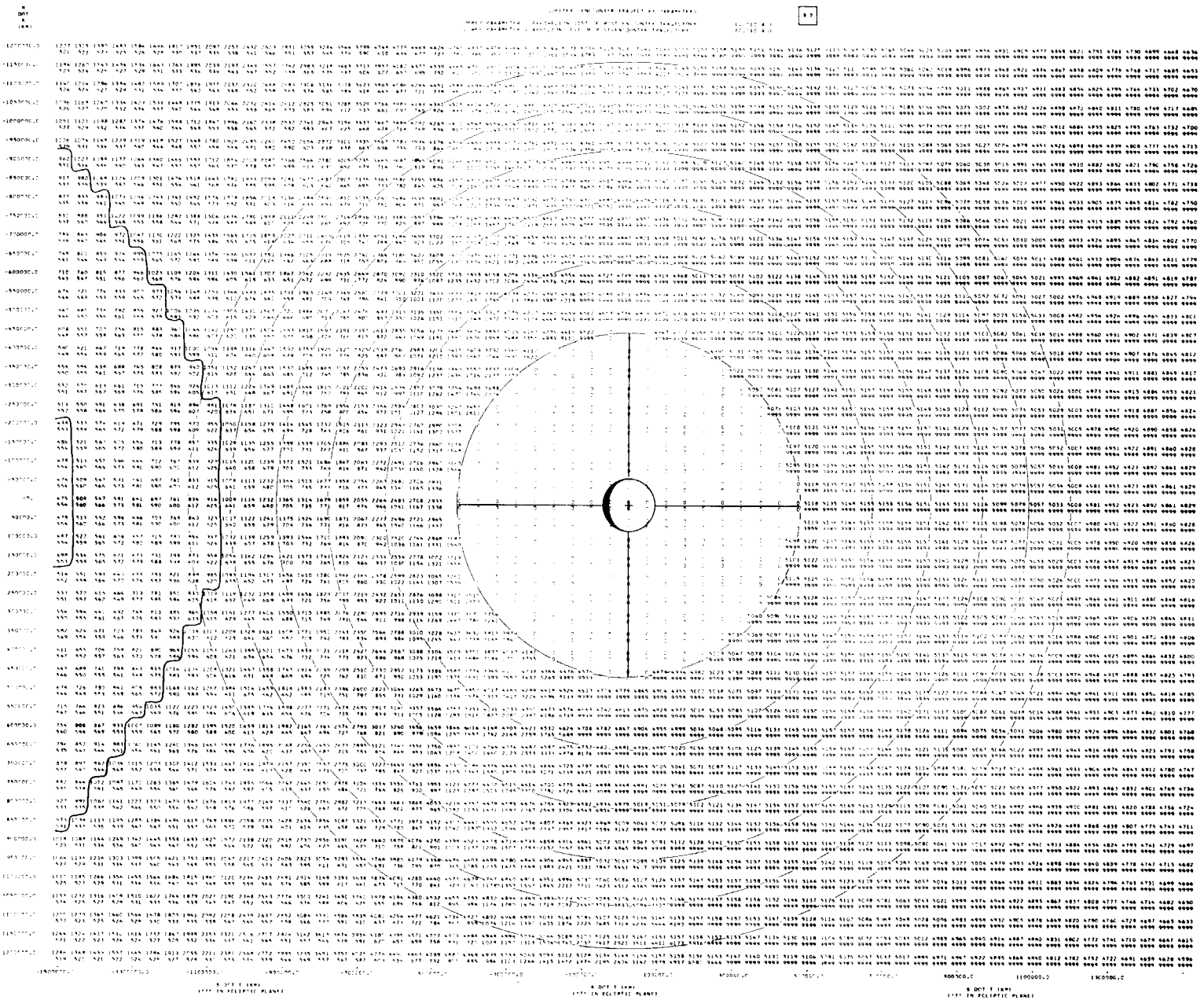

FIGURE B-8

498-DAY FLIGHT TARGETING CHART: TIME IN CPJ ≤ 10° ZONE

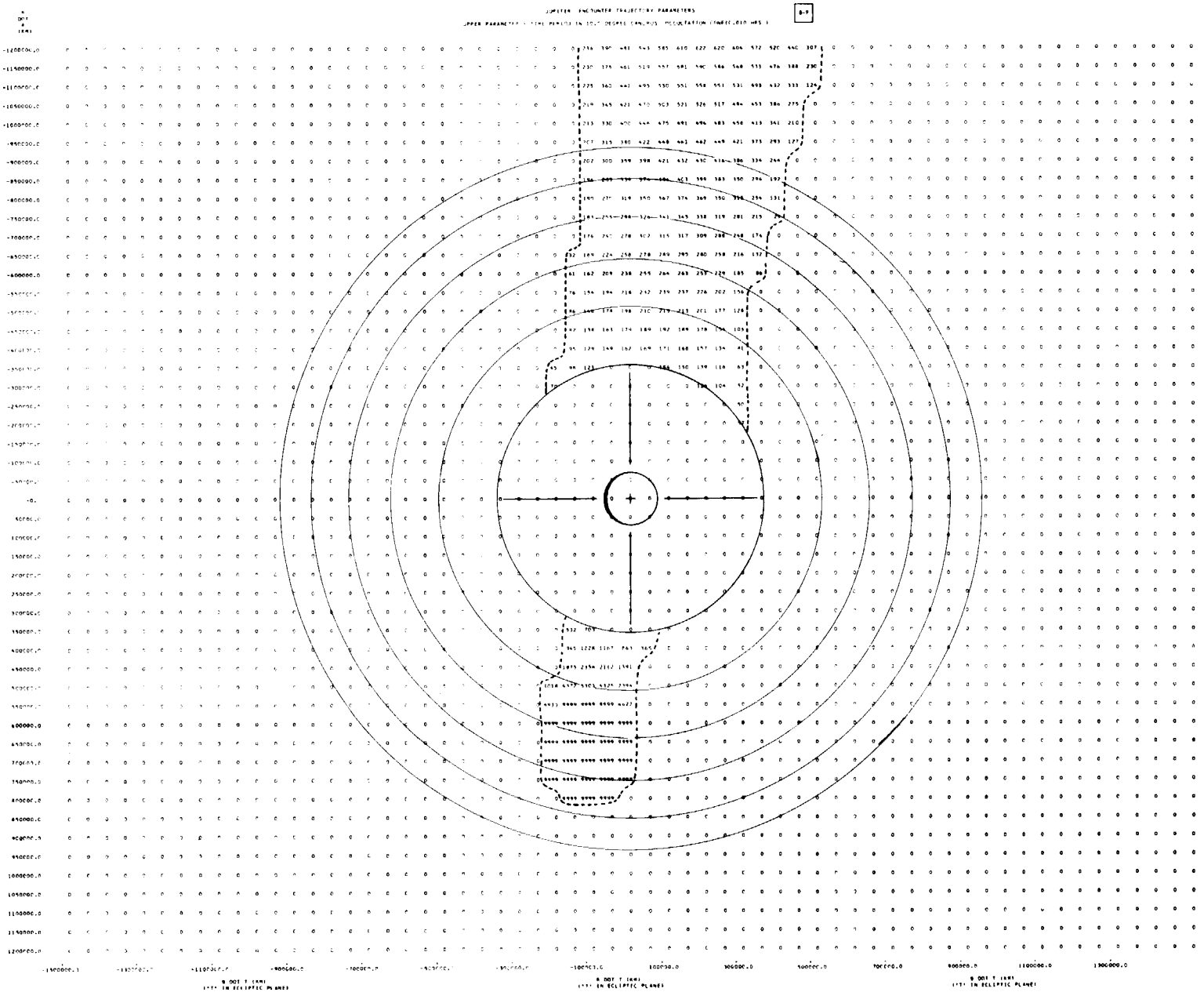

FIGURE B-9

498-DAY FLIGHT TARGETING CHART: TIME IN SPJ ≤ 10° ZONE

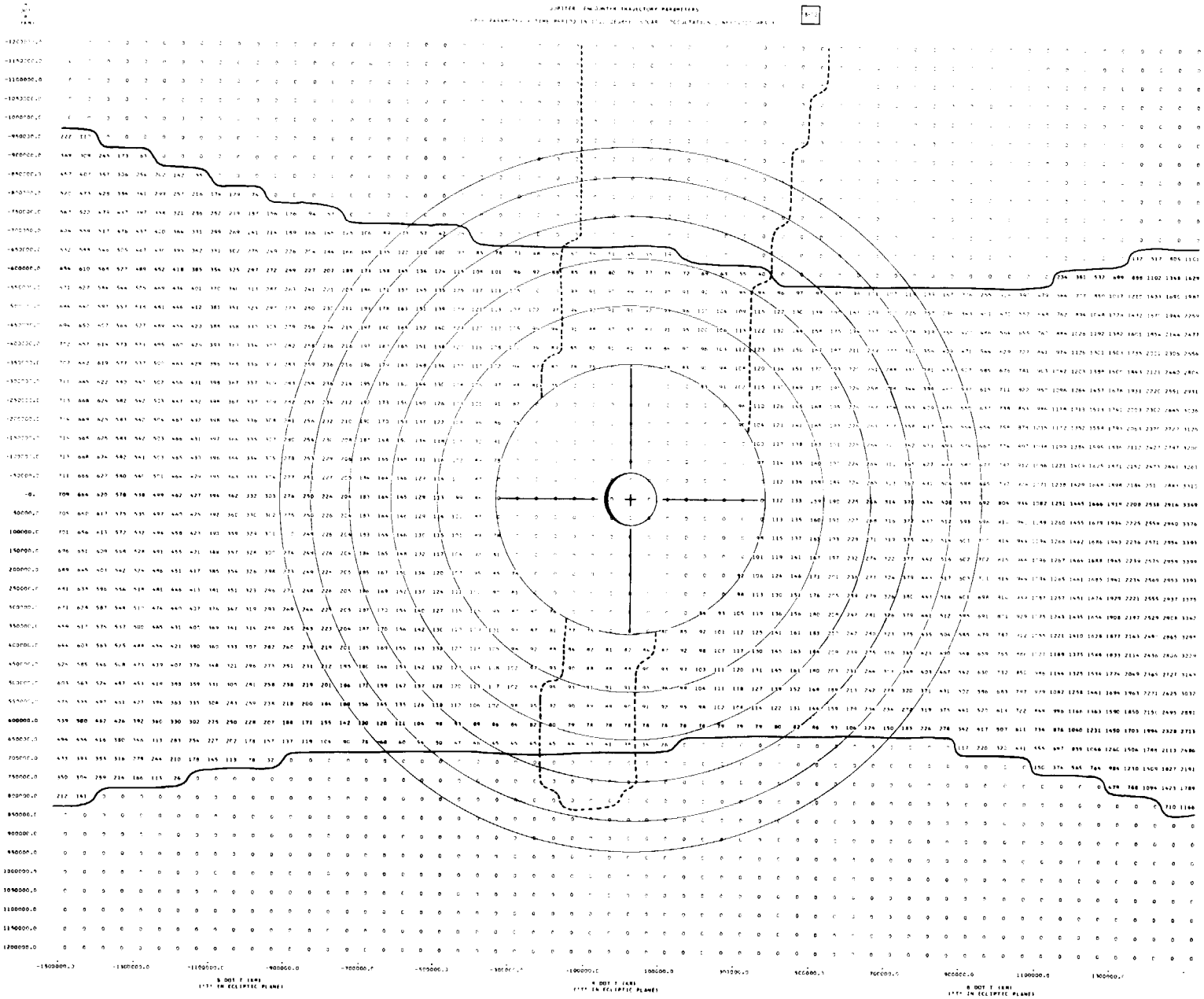

FIGURE B-10

498-DAY FLIGHT TARGETING CHART: TIME IN SPJ ≤ 0° ZONE

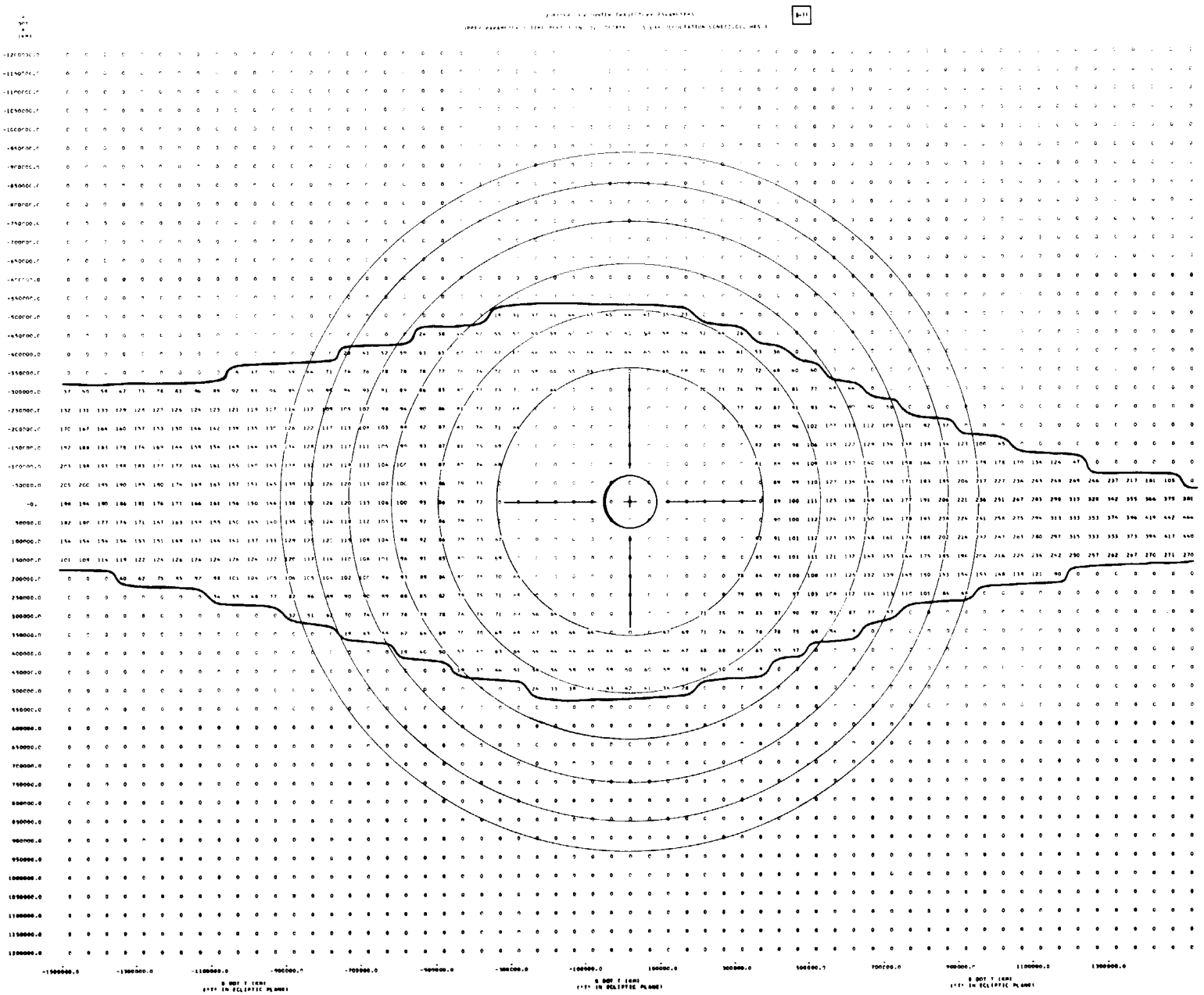

FIGURE B-11

498-DAY FLIGHT TARGETING CHART: TIME IN EPJ ≤ 00 ZONE

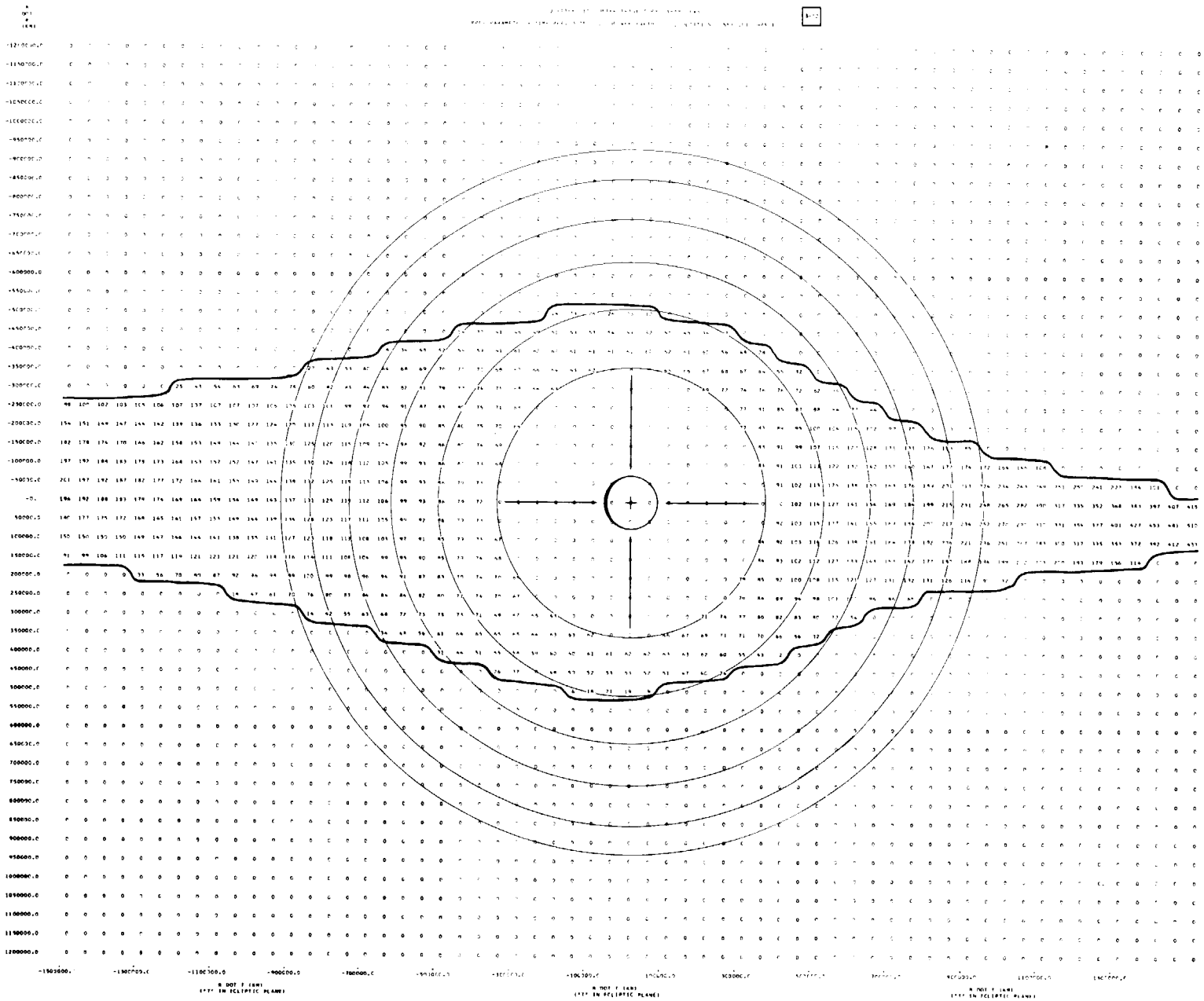

FIGURE B-12

498-DAY FLIGHT TARGETING CHART: SOLAR IMMERSION AND EMERSION LATITUDES

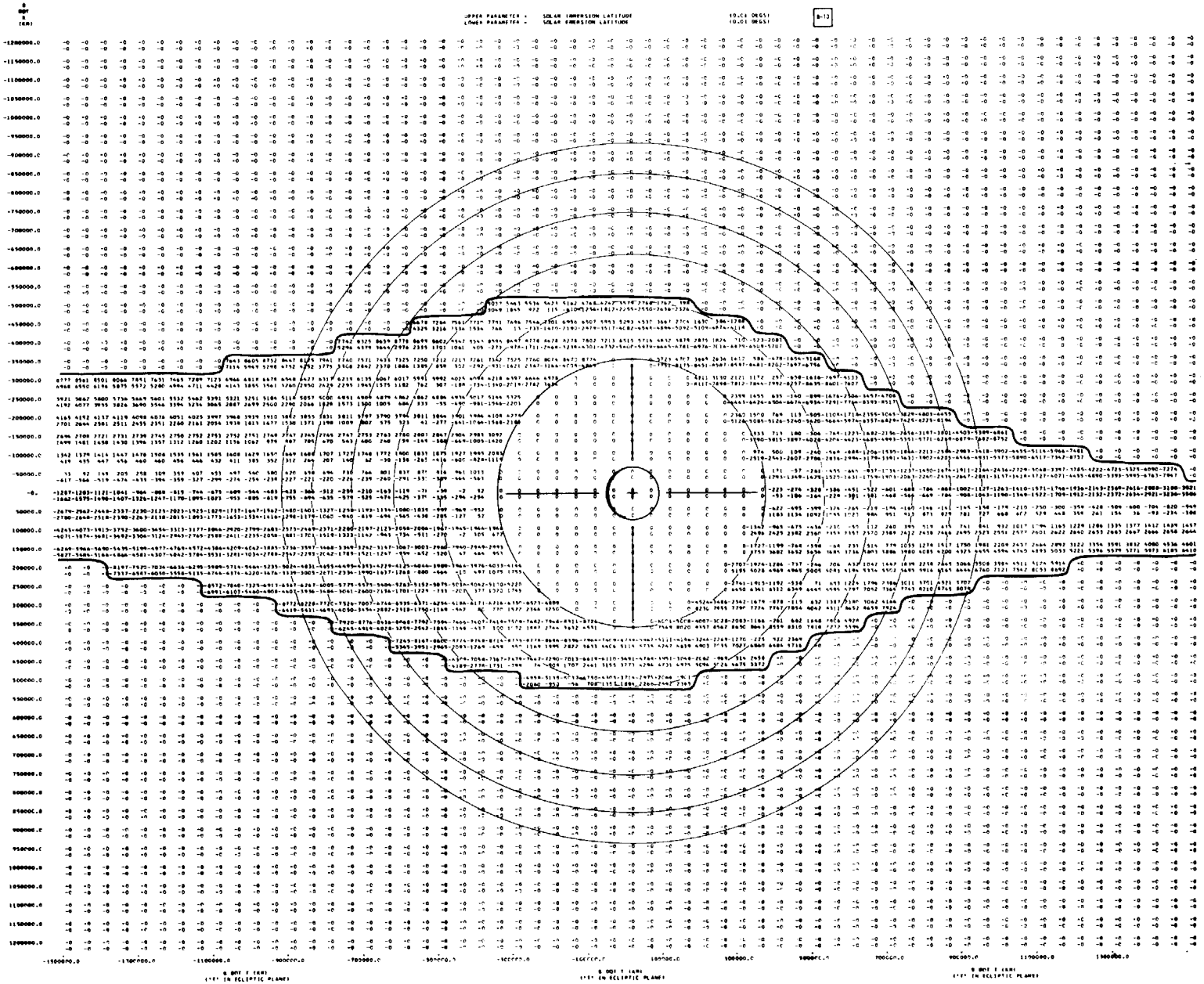

FIGURE B-13

498-DAY FLIGHT TARGETING CHART: EARTH IMMERSION AND EMERSION LATITUDES

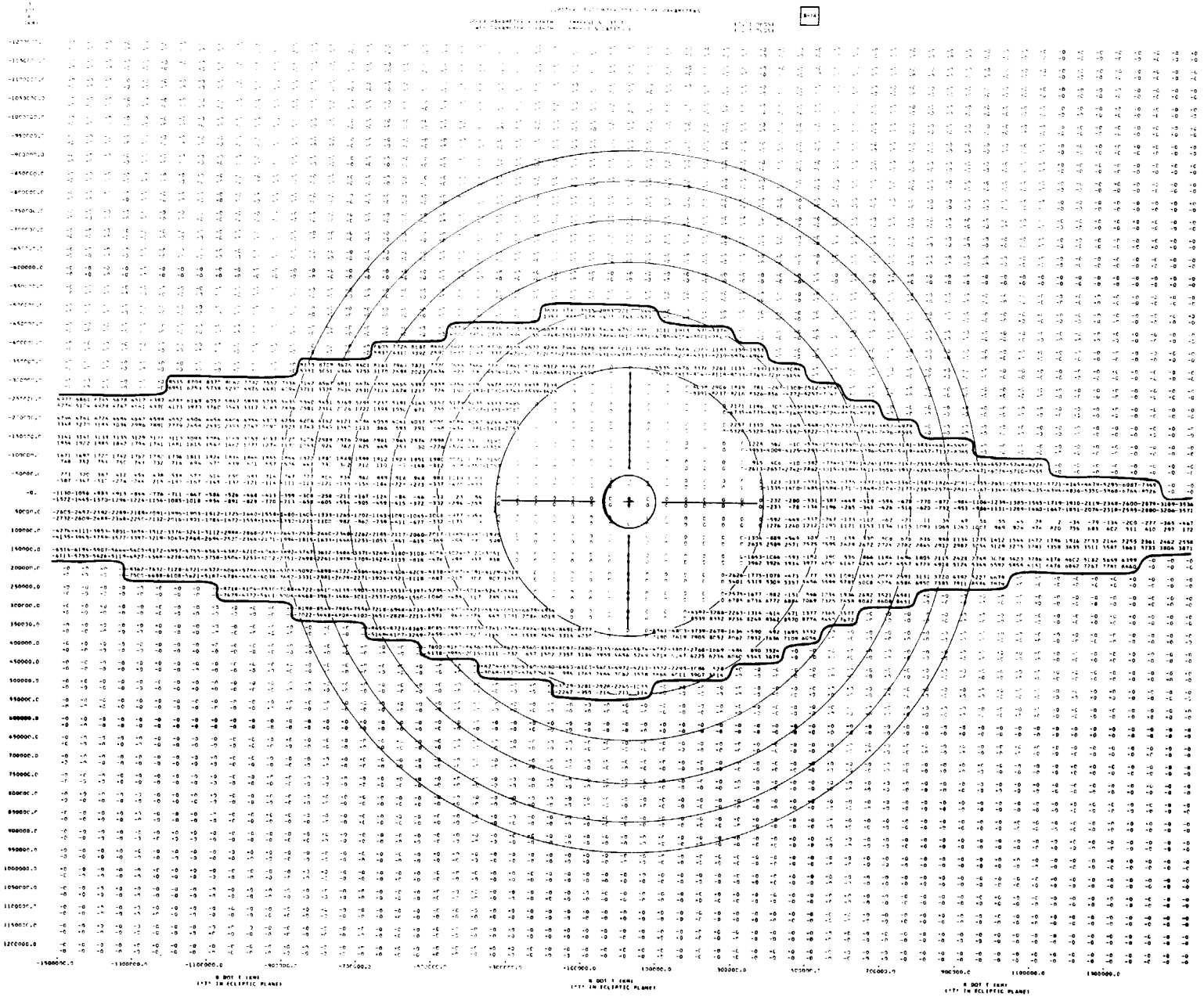

FIGURE B-14

498-DAY FLIGHT TARGETING CHART: ECCENTRICITY AND INCLINATION OF PEH TRAJECTORY

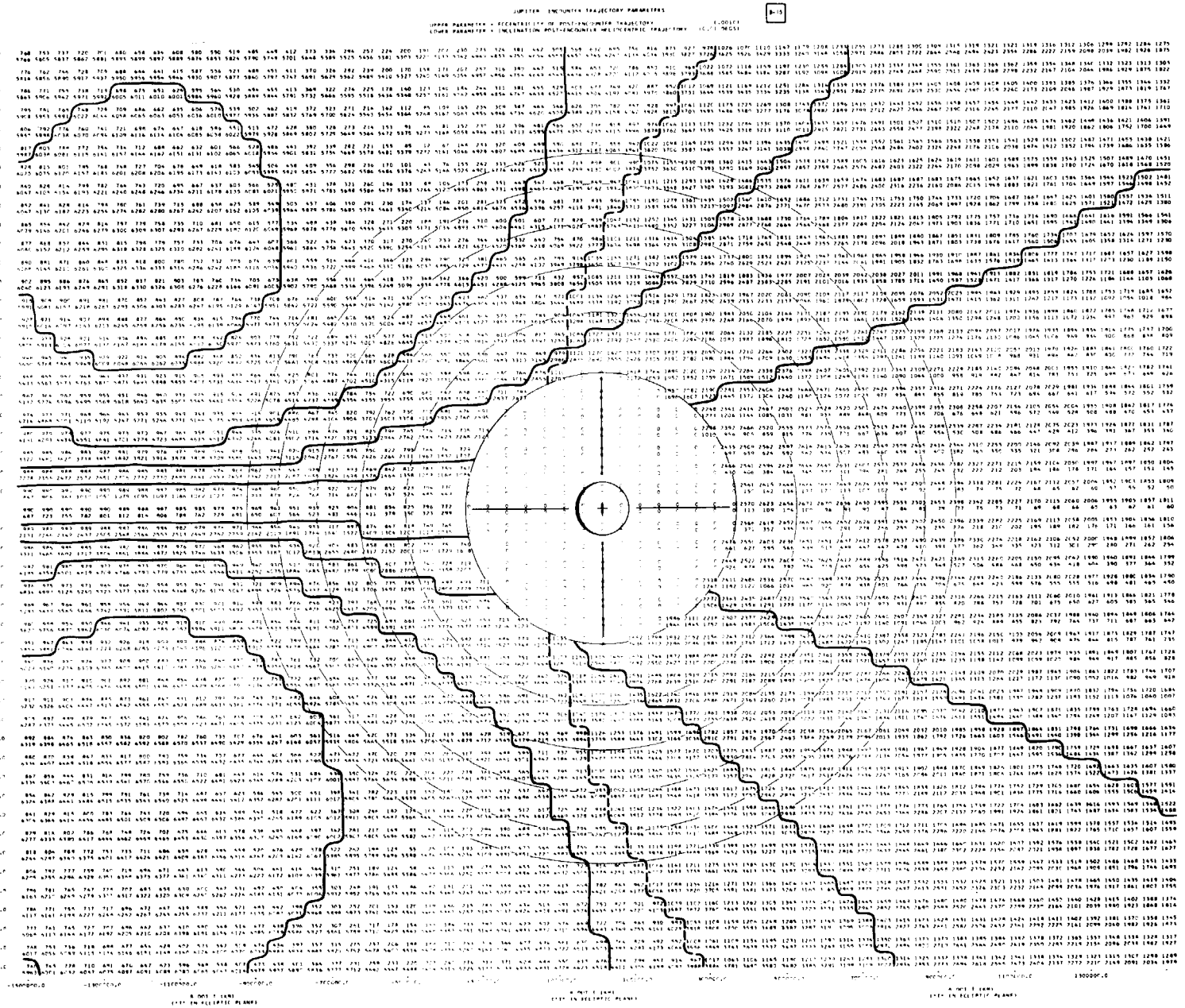

FIGURE B-15

498-DAY FLIGHT TARGETING CHART: PERIHELION AND APHELION DISTANCES OF PEH TRAJECTORY

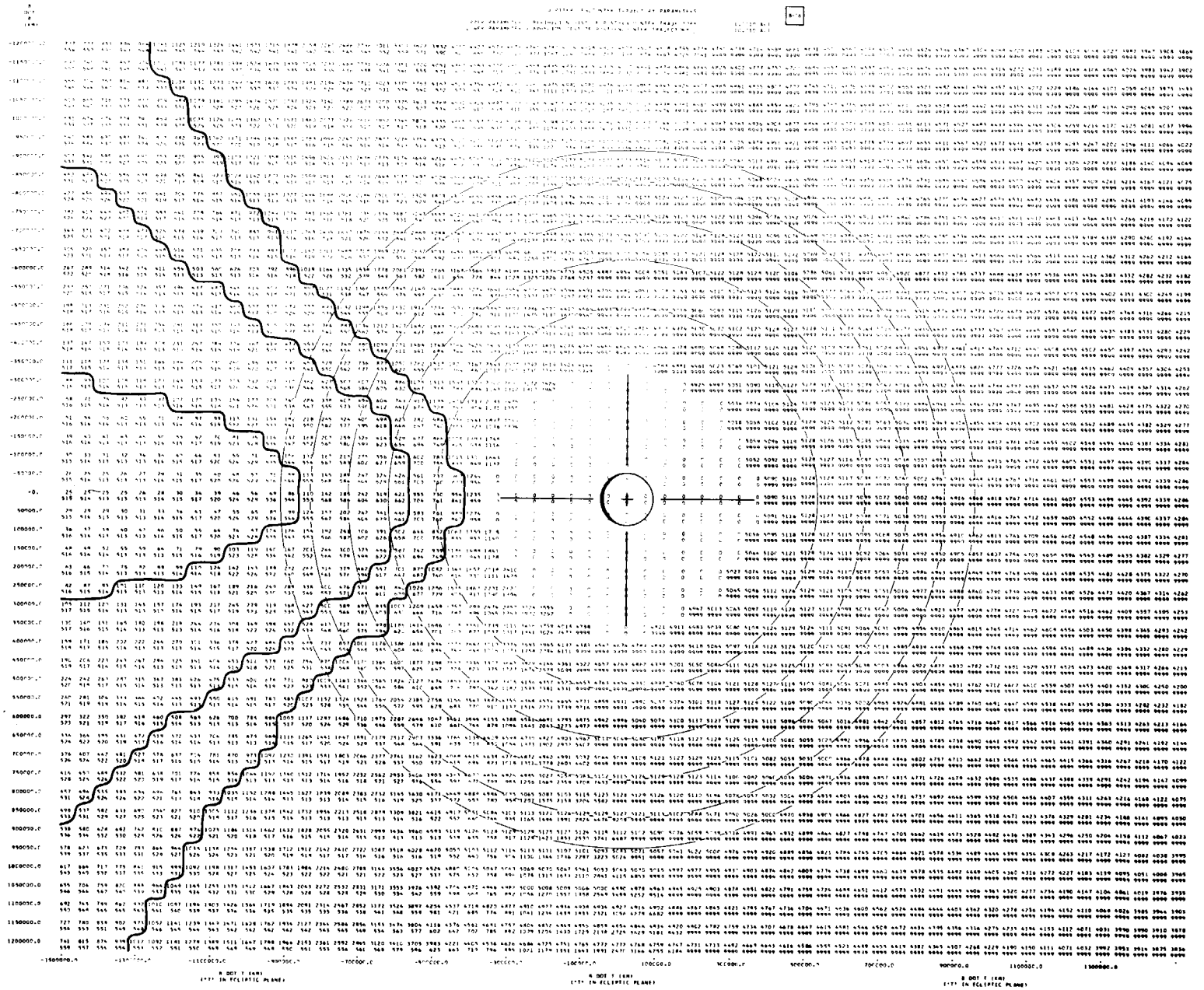

FIGURE B-16

413-DAY FLIGHT TARGETING CHART: TIME IN CPJ ≤ 10⁰ ZONE AND TIME IN SPJ ≤ 10⁰ ZONE

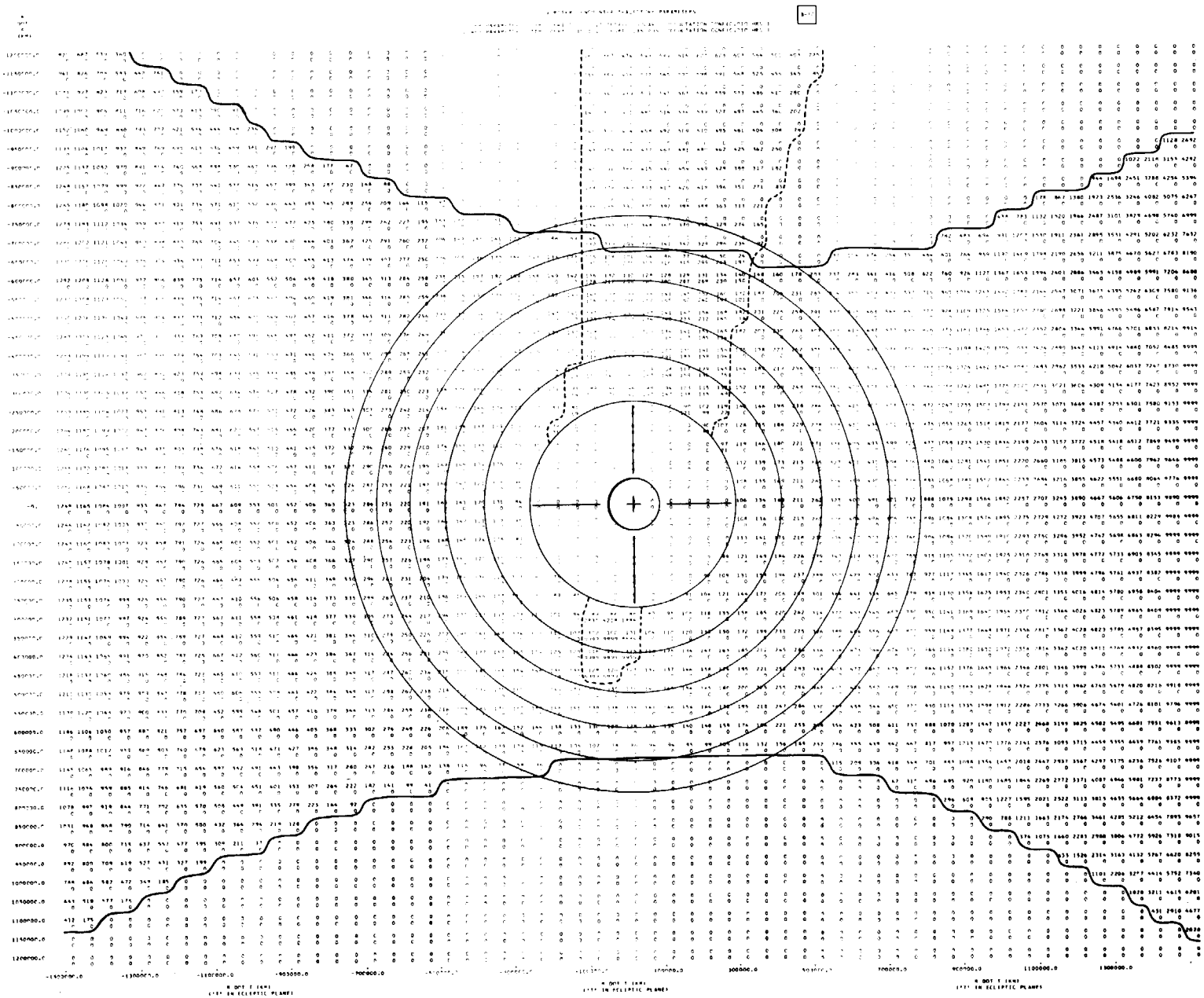

FIGURE B-17

413-DAY FLIGHT TARGETING CHART: TIME IN SPJ ≤ 0° ZONE AND TIME IN EPJ ≤ 0° ZONE

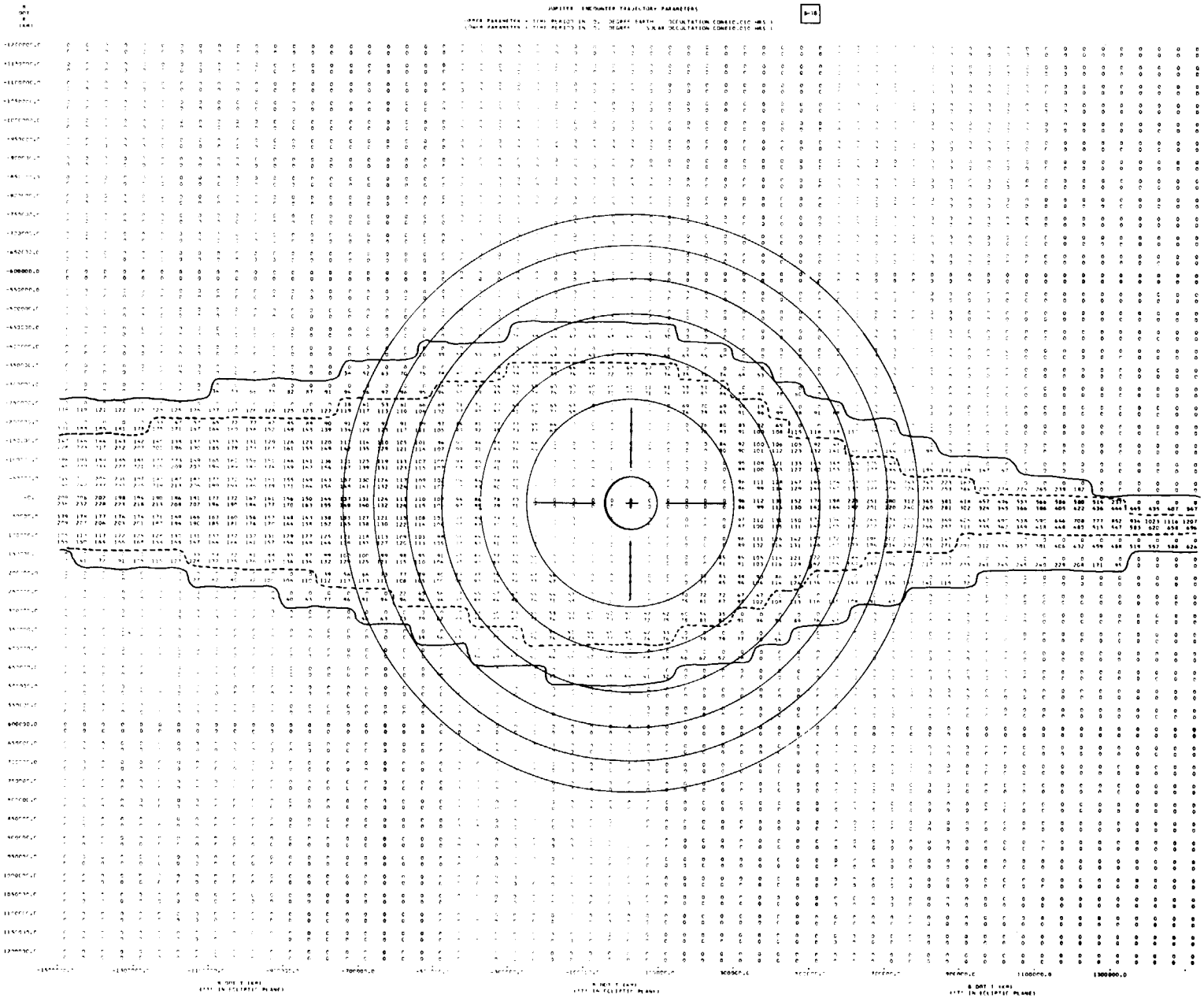

FIGURE B-18

413-DAY FLIGHT TARGETING CHART: SOLAR IMMERSION AND EMERSION LATITUDES

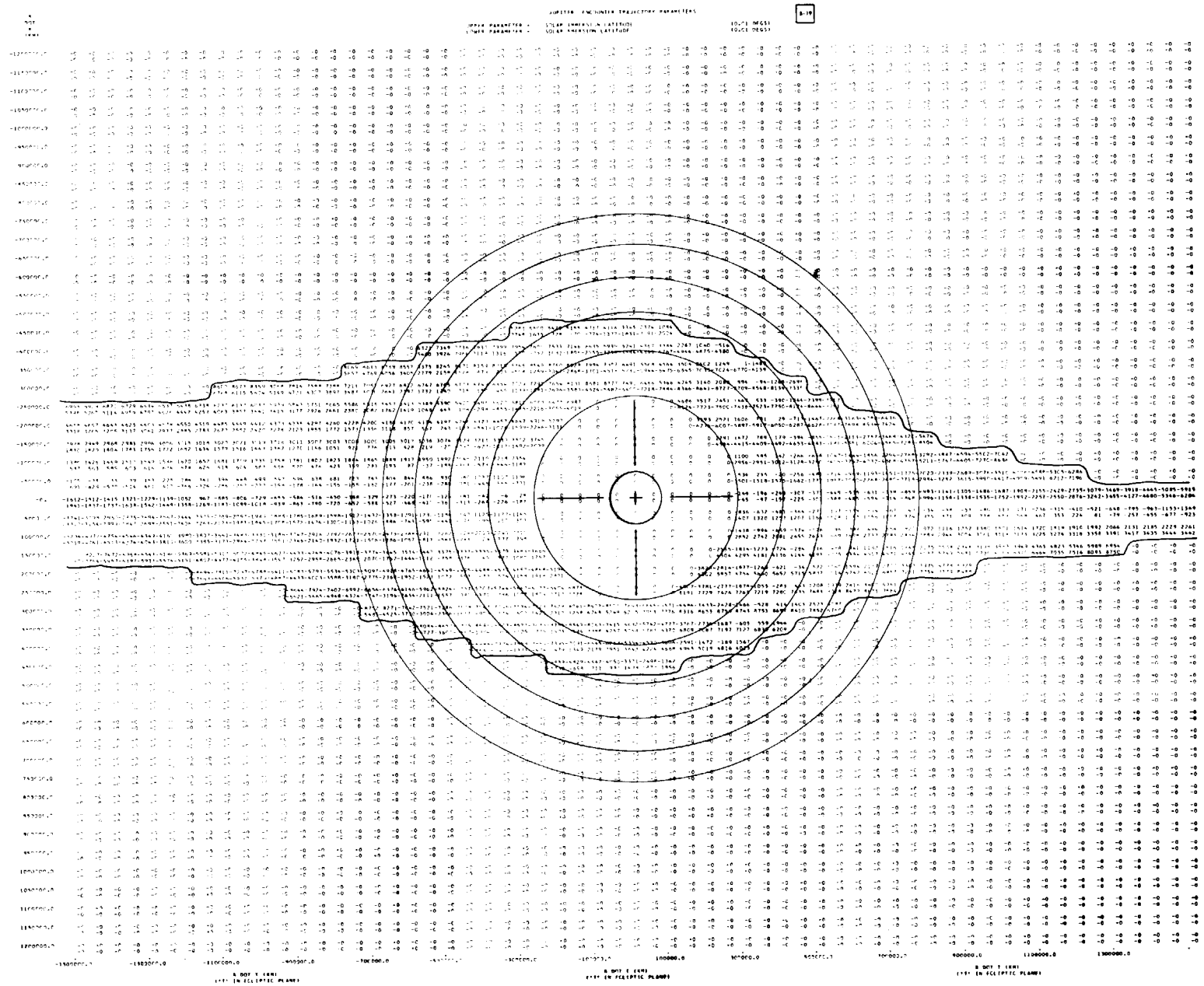

FIGURE B-19

413-DAY FLIGHT TARGETING CHART: EARTH IMMERSION AND EMERSION LATITUDE

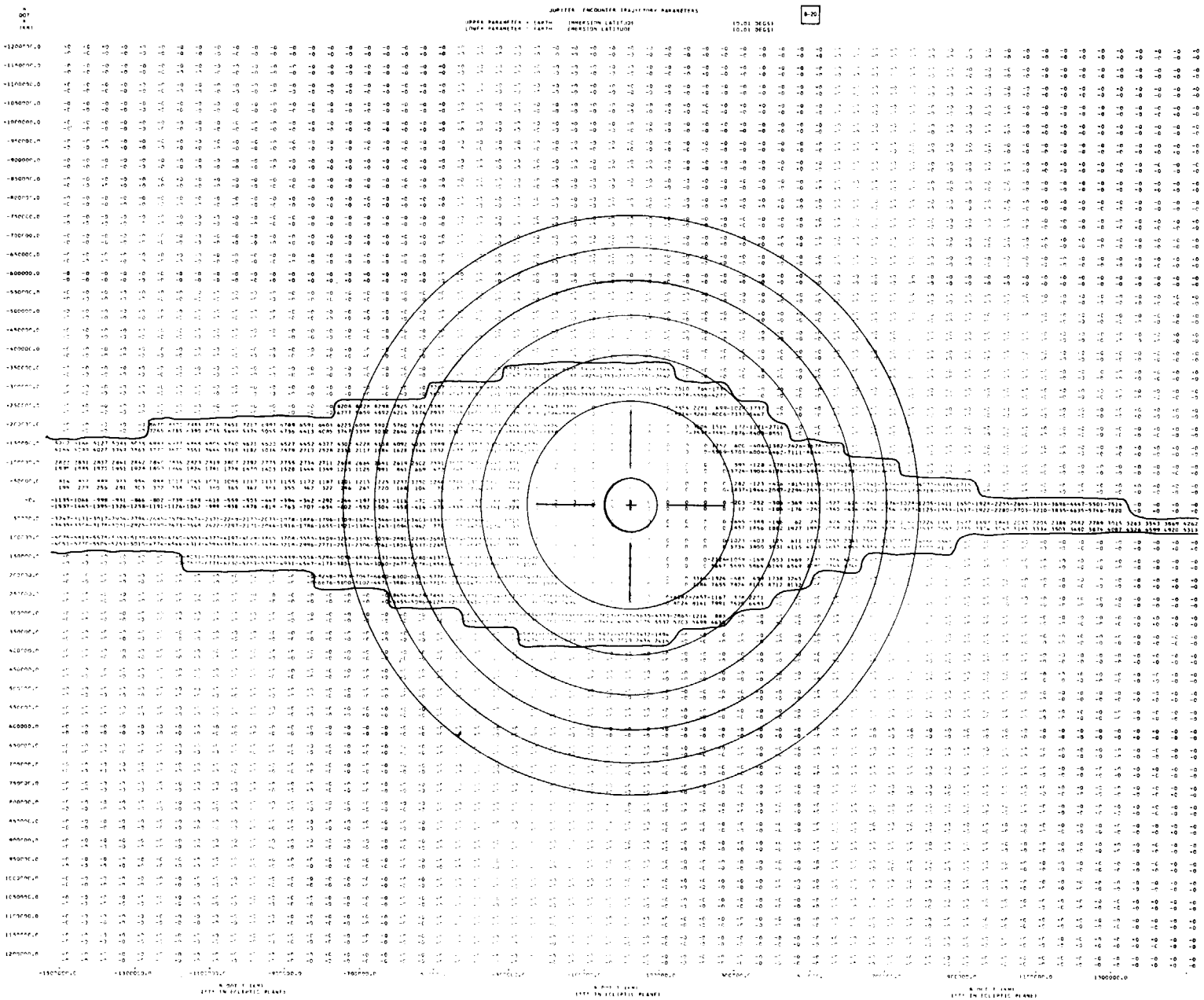

FIGURE B-20

413-DAY FLIGHT TARGETING CHART: ECCENTRICITY AND INCLINATION OF PEH TRAJECTORY

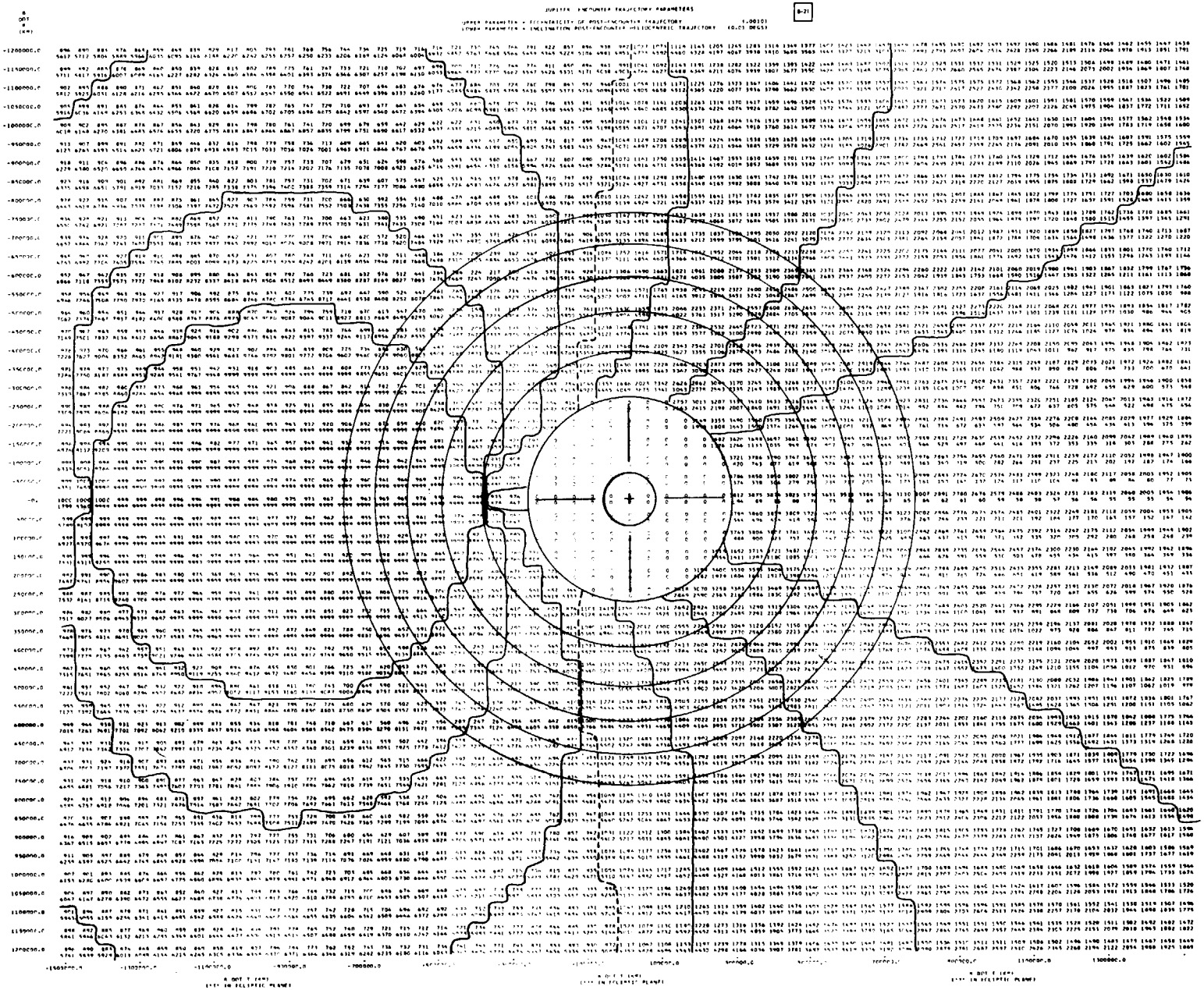

FIGURE B-21

413-DAY FLIGHT TARGETING CHART: PERIHELION AND APHELION DISTANCES OF PEH TRAJECTORY

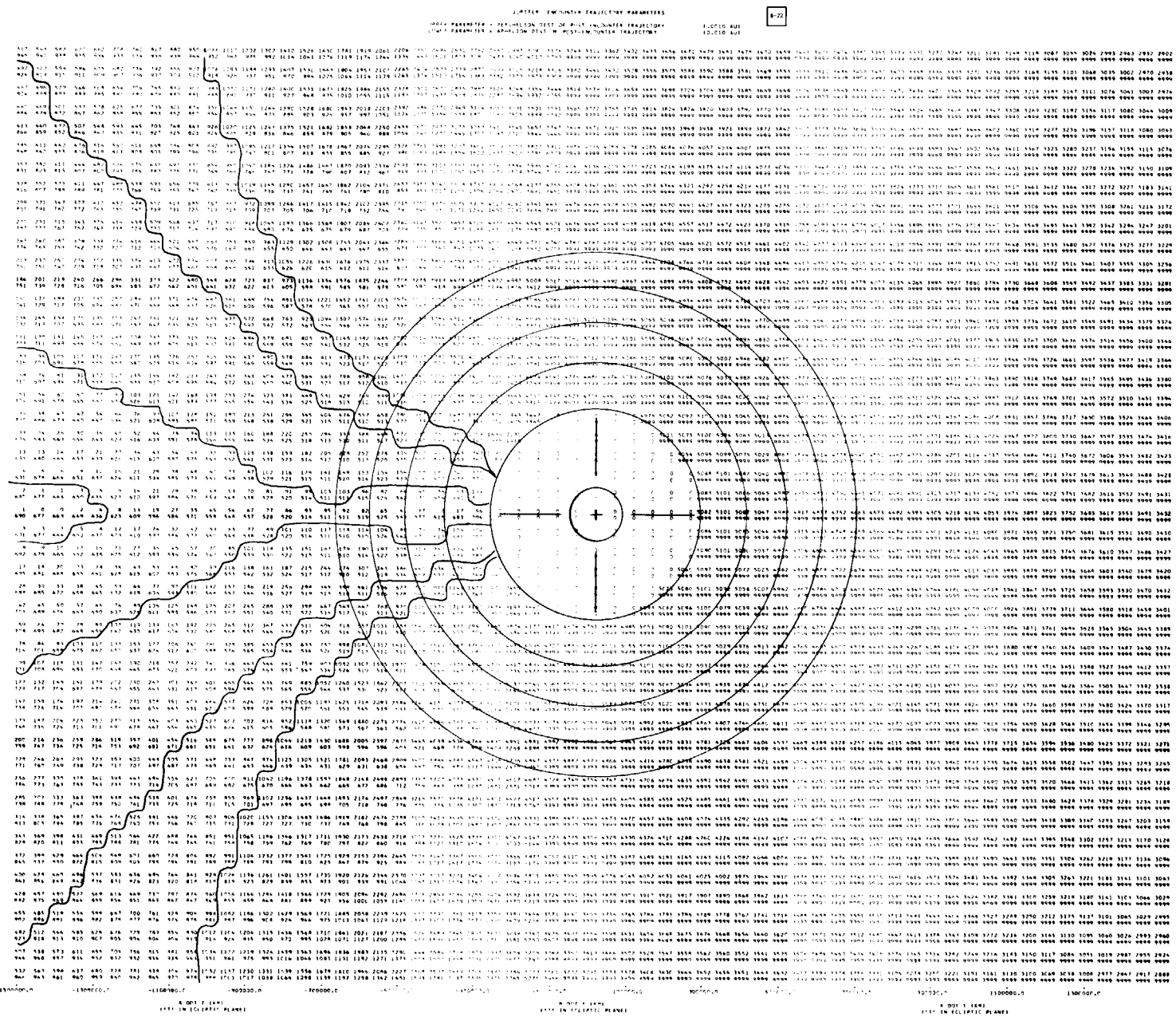

FIGURE B-22

APPENDIX C

METEOROID DAMAGE TO SPACECRAFT ANTENNAS

The following considerations are a part of the treatment of the overall problems of meteoroid damage to spacecraft antennas: (1) the types of damage which may be expected to occur, (2) the effect of each of these types of damage, (3) possible forms of protection, and (4) the effects of each of these forms of protection on the performance of the antenna.

The types of damage which seem most likely are (1) sandblasting or surface roughening due to very small particles, and (2) small holes or small deformations (Reference C-1) of not more than 2/10 wavelength (2.6 centimeter) but of sufficient size to be classed as a hole or deformation instead of surface roughness. The effect of holes and deformations is similar if the deformations are of appreciable depth. There are other types of damage that are less probable but still important enough to warrant consideration. Slits which are thin but of an appreciable wavelength (larger than 1.25 inches) must be considered separately and are of the same class as long thin deformations. There is also the possibility of large holes or deformations of appreciable size in both dimensions with respect to a wavelength. It will be useful to speak generally of the effects of these different kinds of damage before attempting to discuss the specific impact upon the performances of the individual antennas to be considered.

Sandblasting, which causes surface roughness, chiefly affects the conductivity of the material. The skin effect causes currents to be confined to a very thin layer of conductor close to the surface, and the primary effect of surface roughness is to lengthen the conducting path, thus increasing surface resistance and resulting in losses (Reference C-2). Such an effect is important when the operation of the antenna depends upon wave conduction over a surface and is of relatively little importance when the primary function of the surface is that of a reflector or radiating element. Small holes or deformations are individually the least effective in producing noticeable changes in antenna operation. The effects of these tend to vary as the fourth power of the "radius" or largest dimension of the hole or deformation (expressed in wavelengths), and therefore would be quite small unless a great many holes were produced (Reference C-3). Therefore, it appears desirable to allow small holes to be produced rather than to attempt to stop a meteoroid with a consequent widening of the affected area. Slits and

large holes (or long and/or large deformations) can be discussed in similar ways. Their primary effect is to act as "negative" or at least differently phased sources of approximately the same strength of feed distribution. Thus, a round hole tends to produce a pattern similar to that of a parabola of the same size, and a long slit tends to produce a pattern similar to a line source of the same size (Reference C-3). The same can be said of the corresponding deformation. It is also possible for two parallel or nearly parallel slits to produce interferometer patterns with many sharp lobes.

The forms of protection against meteoroids which are considered possible are (1) conductor sheets, (2) foamed structures, (3) covering conductors with non-conducting alyer, (4) metal coverings (shielding), (5) thin walls, and (6) double walls. The purpose of the first four types of protection listed is obviously to attempt to avoid as much as possible meteoroids striking the surface of all or to minimize the damage if a strike occurs. Thin walls would minimize damage by allowing the meteoroid to penetrate freely so that the smallest possible hole results. Double walls would be of primary advantage in minimized the effect of small holes in one or the other of the walls or of slits (which even if they occurred in both walls would tend to be displaced from each other).

The effect of these different forms of protection can also be discussed generally. It will almost never be possible to use metal shielding, because such shielding will affect the performance of the antennas. Essentially, thick or thin walls used as conductors are electrically identical at the proposed frequency, almost down to the point of transluscence. The limiting factor in this case will be a mechanical one. Double layers need to be kept close (to within approximately 1/4 inch), and the selection of separating material is not critical. It is important to achieve low loss in any covering material which will be in the antenna fields, particularly in the area close to feed points where efficiency will be materially affected. High dielectric materials can change patterns appreciably due to diffraction effects, and when these materials are used as coverings for conductors, they should be kept as thin as possible. Coverings thinner than 0.125 inch would generally be permissible. Low-loss materials, such as glasses, should be used. Low dielectric materials, such as foams, are ordinarily low loss also, and their thickness is not important. Foams can be used as fillers, inside a bicone for example, and can be used in such a way that efficiency or radiation patterns will not be noticeably affected. These overall considerations can now be applied to the types of antennas considered for the spacecraft.

In the case of a biconical horn antenna, the primary meteoroid damage problem from the standpoint of the effect on the operation of the antenna would be sandblasting. Sandblasting would increase surface resistance. Since the action of the bicone is that of a waveguide, considerations applying to waveguides are important for this antenna (Reference C-4). The losses in the wall resistance that are caused by the currents induced by the guided waves produce attenuation. This attenuation may possibly rise to quite large values, perhaps of the order of magnitude between 1 and 10 db. It would therefore be important in the case of a biconical antenna to protect the inner surfaces between the cones from such effects, particularly near the feed region, where currents are large. On the other hand, a few small holes would be of little consequence, and even large holes would not be likely to cause more difficulties than slight perturbations in the radiation patterns. A meteoroid strike which seriously damages the feed region would knock the antenna out of action. It would probably suffice to think of a a spherical area of about a six-inch radius about the apices of the cone as the feed region. It is not permissible to use dielectric between the cones in this region because the high field strength there would induce loss in the dielectric. Holes of any appreciable size in the cones in this region might also seriously affect the radiation pattern. Therefore, the following methods of protecting the biconical antenna seem most appropriate.

The regions between the cones should be foamed to prevent sandblasting on the inner surfaces, except near the feed region which should be left empty. This foam could also be used to form a lens to obtain the desired gain as discussed below. The outer region (inside each of the cones themselves) may be protected by foam or not as desired, but the small portion inside each of the cones near the feed region should be filled with a fairly dense material (perhaps even made of solid metal) in order to avoid holes which would affect the radiation pattern. The remainder of the conducting cones should probably be made of very thin material so that hole sizes would be minimized. Double-wall construction might be advisable when the effect of long slits along the circumference of the cone on the radiation patterns might be fairly important.

The next type of antenna to be considered is the round waveguide type with an array of radiating slots cut through its walls. Of the possible types of damage for such an antenna, sandblasting is the least important because it affects only the outer surface. That surface plays little role in the operation of the antenna. Holes are the most serious, particularly large holes, although holes smaller than 0.5 inches in diameter, will not have an important effect. Larger holes would radiate and thus produce

side-lobes and some side effect on the main lobe of the pattern, but the radiation would be unlikely to produce important effects on the pattern. The most important effect of large holes would be to induce reflections in the waveguide. Such reflections could result in a mismatch and a consequent reduction in the power reaching the original radiating slots and a disruption of the pattern symmetry. Slits stretched around the circumference of the waveguide would also have a significant effect. This effect could be minimized by double wall construction if desired. The wall(s) should probably be thin in order to minimize the size of the holes, but not so thin as to increase the probability of deformations which would obviously affect the reflections in the waveguide. These same problems would exist with deformations produced by some cause other than meteoroids.

The next type of antenna to be discussed is the collinear array type. Such an array consists of dipole elements fed by transmission lines. About the only kind of damage which could matter would be a meteoroid strike which actually clipped one of the lead wires. This would put out a portion of the array completely, and large reductions in the gain would be caused by increasing beamwidth. Significant deformation of a portion of the array (further than 2 inches) would also seriously effect the operation of the antenna. It is probable that any meteoroid large enough to produce a hole in a waveguide would be capable of clipping a lead.

The next type of antenna to be discussed is reflector or parabolic type. Aside from the feed element of the parabola, (which must be protected at all costs) such an antenna is almost invulnerable to meteoroid strikes. Sandblasting affects primarily the conductivity of the surface, and this conductivity is of almost no importance within very wide ranges. Holes produce effects which are easily approximated by thinking of them as "negative patterns." Thus, a large hole would tend to produce a lobe in the same direction as the main lobe, but somewhat wider. Such a lobe would not be much noticed on the pattern. Only if it took a significant portion of the energy from the main lobe and spread it in other directions would the effect be appreciable. This would not happen until a significant fraction of the dish surface was removed. Thus, a 10 percent removal of the dish surface would produce on a 1 db reduction in gain. Probably the most serious possible effect of meteoroids could come from slits. Slits would act as negative line sources which produce maximum beams in the main lobe direction. If two of these line sources were approximately parallel and separated by an appreciable distance, say a foot, they would produce an interferometer pattern which could cause ripples in the main lobe.

This could seriously effect the energy density in the portion of the main lobe which actually intercepts the Earth, perhaps by as much as 3 db. While this possibility seems quite remote, it could be eliminated almost entirely by the use of a double-walled construction because slits in the back and front faces would not be aligned.

The final types of antennas to be discussed are the electrically de-spun types. Because of the great variety of such antennas, it would certainly be possible to choose the design of the elements in such an array that meteoroid damage would be unlikely. In any case, such an array would have most of its leads, etc., interior to a well shielded region, perhaps covered by a fairly thick material sphere. In any case, it is unlikely that more than one element at a time would be removed by a meteoroid strike, and this would not be a serious problem. It is therefore not felt necessary to discuss the protection of de-spun arrays.

REFERENCES

C-1. Eichelberger, R. J. and Gehring, J. W. "Effects of Meteoroid Impacts on Space Vehicles", American Rocket Society, Space Flight Report to the Nation/New York Coliseum, 9 October, 1961.

C-2. "Skin Effect," Reference Data for Radio Engineers, 4th ed., American Book--Stratford Press, Inc., New York, New York, 1959, pp. 128-132.

C-3. Mack, R. B. and Blacksmith, P., Jr. "Some Thoughts on Scattering Cross Sections in the Resonance Region", The Modification of Electromagnetic Scattering Cross Sections in the Resonant Region, A Symposium Record, Vol. I., September 1964, AD 606106, pp. 1-9.

C-4. Schelkunoff, S., Advanced Antenna Theory, Wiley, New York, 1952., pp. 39-54.

APPENDIX D

PARAMETRIC ANALYSIS OF THE BASIC HYDRAZINE PROPULSION SUBSYSTEM

The weight of the monopropellant hydrazine system considered in this study is represented by the following equation:

$$(1)\quad W_{system} = W_H + W_{H_T} + W_{PG} + W_{PG_T} + W_B + W_{COM}$$

In the equation above, the last term, W_{COM}, represents fixed hardware, i.e., the sum of the weights of components such as valves, regulators, tubing, catalyst bed and nozzle assembly, etc., whose individual weights do not vary appreciably with total impulse. For a given thrust level, this term may be predicted from manufacturer's weight data in conjunction with an itemized listing of the system's components. The remaining five terms, however, vary directly with the total impulse requirement, or more exactly, with the weight of propellant contained within the system. Equations for these five terms are developed in the analysis which follows.

The weight of hydrazine contained within the system may be obtained from the sum of the following equations:

$$W_{H_1} = \frac{I_T}{I_{SP}} = W_{S/C}\left[1 - e^{\frac{-\Delta V}{I_{SP} g}}\right]$$ expected hydrazine consumption

$$W_{H_2} = \alpha_H W_{H_1}$$ contingency for I_{sp} degradation

$$W_{H_3} = W_{H_1}\left(\frac{\delta\Delta V}{\Delta V}\right)\frac{\left(\frac{\Delta V}{I_{SP} g}\right)}{\left(e^{\frac{\Delta V}{I_{SP} g}} - 1\right)}$$ contingency for ΔV reserve (ref. JPL TR 32-26)

$$W_{H_4} = \left(\frac{1-\epsilon}{\epsilon}\right)\left(W_{H_1} + W_{H_2} + W_{H_3}\right)$$ contingency for bladder expulsion inefficiency

Combining these four equations and rearranging gives:

$$(2)\quad W_H = \frac{W_{s/c}}{\epsilon}\left[1 - e^{\frac{-\Delta V}{I_{sp} g}}\right]\left\{1 + \alpha_H + \left(\frac{\delta \Delta V}{\Delta V}\right)\frac{\left(\frac{\Delta V}{I_{sp} g}\right)}{\left(e^{\frac{\Delta V}{I_{sp} g}} - 1\right)}\right\}$$

The weight of a spherical hydrazine tank whose wall thickness is small compared to the tank radius, is given by:

$$(3)\quad W_{H_T} = 1.5\, P_D V_{H_T} \left(\frac{\rho}{\sigma}\right)_{MAT} (S.F.) + W_{ACC}$$

In this equation, the first term on the right-hand side represents the weight of the tank shell as determined from thin-wall stress theory. The use of this term presumes no overriding minimum gauge wall thickness considerations, which is a valid presumption for the tank diameters, design pressures, and material strengths anticipated in this study. The second term of this equation represents the weight of tank accessories such as welds, bosses, fittings, etc., which are often responsible for a significant portion of the overall delivered tank weight. This last term, unfortunately, is more difficult to describe mathematically since it is influenced by a variety of factors such as manufacturing techniques, materials, and peculiarities of the particular tank design. Nevertheless, an attempt was made to account for the weight of tank welds and fittings (and thus bring tank estimates more in line with existing hardware) by adopting the following simplified model.

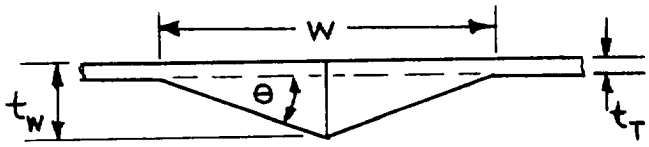

Girth Weld Cross Section

In the figure to the left,

W = width of weld buildup section

t_T = nominal tank wall thickness

t_W = max. thickness of weld buildup

θ = taper angle of buildup

. Tank curvature is neglected

. Filler material density = parent material density

Weight increase due to weldment = $\left(\frac{\text{weight buildup}}{\text{linear inch}}\right)$ x(tank circumference)

Letting:

$$t_w = K_1 t_T \qquad \text{where } K_1 \text{ is some constant}$$

$$t_T = \left(\frac{P_D\ D}{2\,\sigma_{mat}}\right)(S.F.)$$

then:

$$\text{TAN}\ \theta = \frac{(t_w - t_T}{\left(\frac{w}{2}\right)}$$

and,

$$w = \frac{2(t_w - t_T)}{\text{TAN}\ \theta}$$

The weight of the weld buildup per linear inch is:

$$\frac{\rho_{mat} w}{2}\ (t_w - t_T) = \frac{\rho_{mat}\ (K_1 - 1)^2}{\text{TAN}\ \theta}\ (t_T)^2$$

Multiplying by the circumference gives:

$$W_{weld} = \frac{\rho_{mat}\ (K_1 - 1)^2}{\text{TAN}\ \theta}\left(\frac{P_D\ D}{2\,\sigma_{mat}}\right)^2\ (S.F.)^2\ \pi D$$

Since $\frac{\pi D^3}{6}$ is the tank volume, the last equation may be written:

$$W_{weld} = \frac{1.5\ (K_1 - 1)^2}{\text{TAN}\ \theta}\ P_D^{\,2}\ V_{H_T}\left(\frac{\rho}{\sigma^2}\right)_{mat}\ (S.F.)^2$$

Substituting typical values, i.e., $K_1 = 3.0$, $\theta = 10^\circ$ gives:

$$(4)\quad W_{weld} = 1.5\ (22.7) P_D^{\,2}\ V_{H_T}\left(\frac{\rho}{\sigma^2}\right)_{mat}\ (S.F.)^2$$

It remains now to account for the effects due to bosses, tank outlet cut-out, and buildup at the tank outlet. For these effects, an arbitrary fixed weight of 0.35 pound is assumed. The weight of tank accessories thus becomes

$$(5)\quad W_{acc} = 1.5(22.7) P_D^{\,2}\ V_{H_T}\left(\frac{\rho}{\sigma^2}\right)_{mat}\ (S.F.)^2 + 0.35$$

Substituting Eq. (5) into Eq. (3) gives

$$(6)\quad W_{H_T} = 1.5\ P_D\ V_{H_T}\left(\frac{\rho}{\sigma}\right)_{mat}\ (S.F.)\left[1.0 + \frac{22.7\ P_D\ (S.F.)}{\sigma_{mat}}\right] + 0.35$$

The volume of the prepressurized hydrazine tank may be written as

$$(7)\quad V_{H_T} = V_H + V_B + V_{UL}$$

From previous studies, the volume of the bladder material, V_B, is conservatively estimated at 2 percent of the propellant volume, i.e., $V_B = 0.02\ V_H$. The ullage volue, V_{UL}, in a prepressurized system (with no pressure relief provision) must be ample enough to accommodate the thermal expansion of the propellant due to temperature increases, without incurring an intolerable rise in pressure in the tank due to the compression of the prepressurant gas. With an increase in temperature, the gas pressure rise in the tank is the result of (1) gas pressure increase as a result of the increase in gas temperature, and (2) gas pressure increase as a result of the reduction of the original ullage volume by an amount equivalent to the volume increase of the propellant. The ideal gas law provides an expression for the increased tank pressure in such a situation.

$$(8)\quad P_D = P_{PPG}\left(\frac{V_{UL}}{V_{UL} - \Delta V_{EXP}}\right)\left(\frac{T_{MAX}}{T_O}\right)$$

Expressing the ullage volume as a fractional part of the propellant volume gives

$$V_{UL} = \chi V_H$$

so that Eq. (8) may be written

$$(9)\quad P_D = P_{PPG}\left\{\frac{1}{1 - \left(\frac{\Delta V}{V_o}\right)\frac{1}{\chi}}\right\}\left(\frac{T_{MAX}}{T_O}\right)$$

Eq. (7) may be rewritten as

$$(10)\quad V_{H_T} = (1.02 + \chi)V_H$$

When Eqs. (9) and (10) are substituted in the previously derived Eq. (6) for the hydrazine tank weight, the result is

$$(11)\quad W_{H_T} = 1.5\ P_{PPG}\left(\frac{T_{MAX}}{T_O}\right)\left(\frac{\rho}{\sigma}\right)_{mat}(S.F)V_H\left\{\frac{1.02 + \chi}{1 - \left(\frac{\Delta V}{V_o}\right)\frac{1}{\chi}}\right\}\left[1.0 + \frac{22.7(S.F.)(P_{PPG})\left(\frac{T_{MAX}}{T_O}\right)}{\left\{1 - \left(\frac{\Delta V}{V_o}\right)\frac{1}{\chi}\right\}\sigma_{mat}}\right] + 0.35$$

This last equation is plotted in modified form in Figure C-1 wherein representative design values are used. From the curve it can be seen

RATIO OF HYDRAZINE TANK WEIGHT TO HYDRAZINE VOLUME VERSUS ULLAGE FACTOR

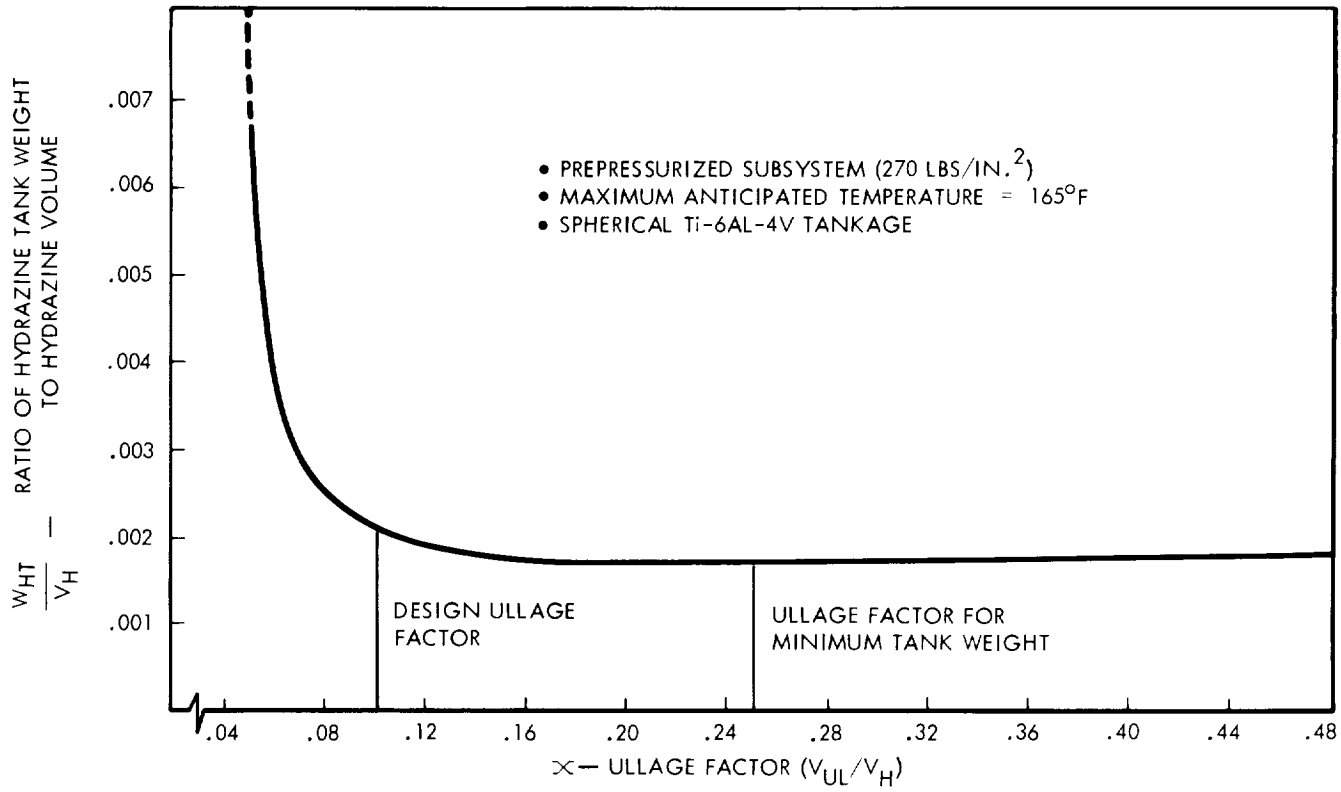

FIGURE D-1

that no appreciable savings in tank weight are attainable beyond an ullage factor of approximately 0.10. For this reason, and for the sake of reasonable tank volumes, an ullage factor of 0.10 was used in all subsequent system design calculations.

The weight of pressurant gas required for propellant expulsion may be conservatively estimated by an energy and mass balance analysis which assumed an adiabatic process and negligible line residuals. For a given weight of propellant, W_H, the weight of pressurant required becomes:

$$(12)\quad W_{PG} = \frac{P_T\, W_H}{R\, T_O\, \rho_H} \left\{ \frac{k}{1 - (P_{PG_f}/P_{PG_i})} \right\}$$

The weight of a spherical pressurant tank is given by the expression:

$$W_{PG_T} = 1.5\, P_D\, V_{PG} \left(\frac{\rho}{\sigma}\right)_{mat} (S.F.) + W_{ACC}$$

where, as before, W_{ACC} equals the weight of weldment plus the weight effect of bosses, cut-outs, fittings, etc. An argument similar to that used for determining propellant tank weight (Eq. (6)) but using $K_1 = 2.2$ gives

$$(13)\quad W_{PG_T} = 1.5\, P_D\, V_{PG} \left(\frac{\rho}{\sigma}\right)_{mat} (S.F.) \left[1.0 + \frac{8.5\, P_{PG_i} (S.F.) T_{max}}{\sigma_{mat}(T_o)} \right] + 0.35$$

which may be rewritten as

$$(14)\quad W_{PG_T} = 1.5\ W_{PG}\ R\ T_{MAX}\left(\frac{\rho}{\sigma}\right)_{mat}\ (S.F.)\left[1.0 + \frac{8.5\ P_{PG_i}\left(\frac{T_{MAX}}{T_O}\right)\ (S.F.)}{\sigma_{mat}}\right] + 0.35$$

The weight of the bladder (assumed to be essentially spherical) may be estimated from the following analysis

$$W_B = \pi D_B^2\ t_B\ \rho_B$$

$$(15)\quad W_B = 4.84\ (V_H)^{.667}(t_B)(\rho_B)$$

or alternately

$$(16)\quad W_B = 44.3\ (W_H)^{.667}(t_B)(\rho_B).$$

APPENDIX E

PARAMETRIC ANALYSIS OF A COLD GAS ATTITUDE CONTROL PROPULSION SUBSYSTEM

The weight of a typical cold gas attitude control subsystem may be represented by the following equation:

(1) $W_{system} = W_P + W_T + W_{com}$

In this equation, only the terms W_P and W_T vary appreciably with changes in the total impulse required. Expressions for these terms are derived in the treatment which follows. (Wcom, which represents the total weight of the subsystem fixed hardware, was obtained empirically and was reported in subsection 3.6.2.4.)

The weight of propellant required may be obtained from the sum of the following equations:

(a) $W_{p_1} = \frac{I_t}{I_{sp}}$ Expected Propellant Consumption

(b) $W_{p_2} = \alpha_p \, W_{p_1}$ Contingency for Isp Degradation

(c) $W_{p_3} = P_f \frac{V_{tank}}{RT_f}$ Residual Propellant at Termination of Thrust Program

The propellant tank volume may be approximated from the ideal gas law as

(2) $V_{tank} = \frac{W_p R T_i}{P_i}$ (neglects compressibility effects)

So that, Equation (c) above may be re-written as

$$W_{p_3} = \left(\frac{P_f}{P_i}\right) \left(\frac{T_i}{T_f}\right) W_p$$

Combining equations (a), (b), and (c) and rearranging them in order to derive the total weight of propellant required gives

(3) $$W_p = \left(\frac{I_t}{I_{sp}}\right) \frac{(1+\alpha_p)}{\left\{1 - \left(\frac{P_f}{P_i}\right)\left(\frac{T_i}{T_f}\right)\right\}}$$

The weight of a spherical propellant tank with a wall thickness that is small compared to the tank radius is given by the following equation:

(4) $$W_T = 1.5\ P_D\ V_{tank} \left(\frac{\rho}{\sigma}\right)_{mat} (S.F.)$$

(For the sake of brevity, the weight contribution of welds, fittings, etc. is neglected.)

The tank design pressure P_D, is defined as the pressure which would occur if the gas at the initial condition was heated to the maximum anticipated temperature. In a constant volume situation, this is:

(5) $$P_D = P_i \left(\frac{T_{MAX}}{T_i}\right)$$

Substituting equation (5) into (4) yields:

(6) $$W_T = 1.5\ P_i\ V_{TANK} \left(\frac{T_{MAX}}{T_i}\right)\left(\frac{\rho}{\sigma}\right)_{MAT} (S.F.)$$

which may be rewritten as:

(7) $$W_T = 1.5\ W_P\ R\ T_{MAX} \left(\frac{\rho}{\sigma}\right)_{MAT} (S.F.)$$

Combining equations (3) and (7) into (1) and rearranging for the total subsystem weight results in

(8) $$W_{SYSTEM} = I_T \left[\frac{(1+\alpha_p)\left\{1.0 + 1.5\ R\ T_{MAX}\left(\frac{\rho}{\sigma}\right)_{MAT} (S.F.)\right\}}{I_{sp}\left\{1 - \left(\frac{P_f}{P_i}\right)\left(\frac{T_i}{T_f}\right)\right\}}\right] + W_{COM}$$

Equation (8) is a linear equation of the slope-intercept form with the slope represented by the bracketed [ ] quantity. For a given I_T and W_{com}, the subsystem weight will be a minimum for that propellant and tank material combination which yields a minimum slope value.